

# **Mirror-Symmetry Breaking in Photoswitchable Liquid Crystalline Materials**

Kumulative Habilitationsschrift

zur Erlangung des akademischen Grades

Dr. rer. nat. habil.

vorgelegt der

Naturwissenschaftlichen Fakultät II - Chemie, Physik und Mathematik

der Martin-Luther-Universität Halle-Wittenberg

von

Dr. rer. nat. Mohamed Alaasar

Gutachter:

1. Prof. Dr. René Csuk (Martin-Luther-University, Halle-Wittenberg)
2. Prof. Dr. Matthias Lehmann (University of Würzburg)
3. Prof. Dr. Metin Tülü (Yıldız Technical University, Istanbul)

Halle (Saale), verteidigt am 01.12.2023.

## Contents

Preamble .....	1
Preliminary remark.....	3
List of publications summarized in the work (attachments).....	3
1. Introduction .....	5
1.1. Bent-core molecules.....	7
1.1.1. Designing bent-core mesogens.....	8
1.1.2. Polar phases of bent-core mesogens.....	9
1.1.3. Chirality and mirror symmetry breaking in polar mesophases of bent-core molecules	11
1.1.4. Development of tilt and polar order .....	12
1.1.5. Bent-core molecules involving azobenzene units .....	13
1.2. Polycatenar liquid crystals.....	14
1.2.1. Bicontinuous cubic phase (Cub <sub>bi</sub> ).....	14
2. Objectives.....	16
3. Photo-responsive bent-core liquid crystals.....	17
3.1. 4-Cyanoresorcinol derived BCLCs .....	17
3.1.1. Previous work .....	17
3.1.2. Compounds and synthesis .....	18
3.1.3. Cybotaxis in the nematic phases.....	20
3.1.4. Development of polar order and tilt.....	23
3.1.5. Mirror symmetry breaking in fluid smectic phases.....	23
3.1.6. Effect of changing F position and using different substituents.....	25
3.1.7. Effect of replacing one azo group by ester group.....	26
3.1.8. Isothermal photo-switching of chirality and polarity.....	27
3.2. Other 4-substituents at the resorcinol bent unit .....	30
3.2.1. Synthesis.....	30
3.2.2. Dark Conglomerate formation.....	31
4. Photo-responsive polycatenars.....	36
4.1. Overview.....	36
4.1.1 Synthesis.....	37
4.2. Isothermal photo switching of chirality with nonpolarized light.....	39
4.3. From meso-structures to conglomerates formation in liquid and liquid crystalline ... networks	42
4.4. Synclinic-anticlinic transitions and spontaneous helix formation.....	45
4.5. Supramolecular polycatenars forming chiral cubic and Iso <sub>1</sub> <sup>[*]</sup> phases .....	47
4.6. Nematic polycatenars and their investigation on photo switching properties and optical storage devices	50
5. Combination of structural features of polycatenars with mesogenic dimers and bent-core mesogens	51
6. Summary and conclusions.....	54
7. References .....	56

## **Preamble**

The focus of this work is the design and investigations of different classes of photoswitchable nanostructured self-assembled materials to understand the fundamental factors leading to the macroscopic chirality in soft matter systems of achiral molecules. This is a contemporary research topic with great importance for the general understanding of spontaneous mirror symmetry breaking and has an impact on the discussion around the emergence of uniform chirality in biological systems and technological applications. This thesis deals with two different classes of liquid crystalline materials. The first part is devoted to bent-core liquid crystals (BCLCs), while the second one is focusing on multichain (polycatenars) liquid crystalline materials.

I hope that the overview of the two classes, highlighting different types of interesting liquid crystalline phases observed in each type, could stimulate interesting new research ideas.

My research would not have been possible without the help from many collaborators. My entrance into the field of liquid crystals would have been very much more difficult without the generous and open attitudes of friends and colleagues from these communities that I have come to know in the last few years. Prof. Dr. Carsten Tschierske was the one who got me interested in bent-core liquid crystals. I came to know Prof. Tschierske from his very interesting publications in the field of liquid crystals. I owe a great deal of my understanding about these materials to him. I started my postdoctoral research in Germany by spending a few months in his group at Martin-Luther university through DAAD fellowship. Although it was very short, this stay was most rewarding, the pleasant atmosphere in this lab inspiring to many new ideas. Also, a long-lasting friendship with several colleagues in Tschierske's group started, with whom I am still interacting actively. Later I got the Alexander von Humboldt fellowship to pursue my postdoctoral research again in the Tschierske's group for additional two years from 2012 to 2014. My stay as a post-doc in Tschierske's group at the University of Halle was a period of fascinating research, during which I came to know other research groups and collaborators inside and outside Germany. Therefore, for my achievements in the field of liquid crystals I am much indebted to Prof. Tschierske for his support and for a very pleasant working environment in his working group. Based on the fruitful cooperation between me and other collaborators it was possible to carry out extensive characterization of many interesting materials using several techniques such as X-ray diffraction (XRD) with synchrotron source, second harmonic generation, DFT calculations, etc. This results in establishing long standing cooperation channels and publishing the results in high reputation peer reviewed journals.

Moreover, based on the experience I gained during my work I was able to get my own funded DFG project which is recently extended for additional three years.

I would like to thank the DFG for financial support of my current position in Halle. I would like also to express my deep thanks to Prof. René Csuk for his continuous support.

I am also grateful to my parents, my wife Samaa Aladawy and my children for their endless encouragement and support.

Halle, February 2023

Mohamed Alaasar

mohamed.alaasar@chemie.uni-halle.de

## Preliminary remark

The cumulative form was chosen to present the results. The selected most important publications with me as the first and as a corresponding author [AA*n*] are attached and contain the experimental data as well as the detailed discussion of the respective results. In the text part of the work, the essential results are briefly presented, the focus is on the classification of the individual works in a larger context. The original publications are organized according to their appearance in the discussion and are attached as appendices; corresponding references to the relevant publication can be found in the text. Other publications which I co-authored with collaborators [A*n*] are included in the general references [*n*]. Publications [A*n*] contain more detailed XRD and other physical studies, which were performed with my materials by the collaborating scientists.

## List of publications summarized in the work (attachments)

- Pub. AA1** A liquid crystalline phase with uniform tilt, local polar order, superstructural chirality and capability of symmetry breaking. M. Alaasar, M. Prehm, M. Nagaraj, J. K. Vij, C. Tschierske. *Adv. Mater.* **2013**, *25*, 2186.
- Pub. AA2** 4-Cyanoresorcinol based bent-core mesogens with azobenzene wings – emergence of sterically stabilised polar order in liquid crystalline phases. M. Alaasar, M. Prehm, K. May, A. Eremin, C. Tschierske. *Adv. Funct. Mater.* **2014**, *24*, 1703.
- Pub. AA3** Development of polar order in the liquid crystal phases of 4-cyanoresorcinol based bent-core mesogen with fluorinated azobenzene wings. M. Alaasar, M. Prehm, M.-G. Tamba, N. Sebastián, A. Eremin, C. Tschierske, *Chem. Phys. Chem.* **2016**, *17*, 278.
- Pub. AA4** Development of polar order by liquid crystal self-assembly of weakly bent molecules. M. Alaasar, M. Prehm, S. Poppe, C. Tschierske. *Chem. Eur. J.* **2017**, *23*, 5541.
- Pub. AA5** Polar order, mirror symmetry breaking, and photoswitching of chirality and polarity in functional bent-core mesogens. M. Alaasar, M. Prehm, S. Belau, N. Sebastián, M. Kurachkina, A. Eremin, C. Chen, F. Liu, C. Tschierske. *Chem. Eur. J.* **2019**, *25*, 6362.
- Pub. AA6** New azobenzene containing bent-core liquid crystals based on disubstituted resorcinol. M. Alaasar, M. Prehm, C. Tschierske. *Liq. Cryst.* **2014**, *41*, 126.
- Pub. AA7** Cybotactic nematic phases of photoisomerisable hockey-stick liquid crystals. M. Alaasar, S. Poppe, C. Tschierske. *Liq. Cryst.* **2017**, *44*, 729.
- Pub. AA8** Cluster phases of 4-cyanoresorcinol derived hockey-stick liquid crystals. M. Alaasar, A. Eremin, S. Poppe, C. Kerzig, C. Klopp, C. Tschierske. *J. Mater. Chem. C* **2017**, *5*, 8454.
- Pub. AA9** Influence of halogen substituent on the mesomorphic properties of five-ring banana-shaped molecules with azobenzene wings. M. Alaasar, M. Prehm, C. Tschierske. *Liq. Cryst.* **2013**, *40*, 656.
- Pub. AA10** A new room temperature dark conglomerate mesophase formed by bent-core molecules combining 4-iodoresorcinol with azobenzene units. M. Alaasar, M. Prehm, C. Tschierske. *Chem. Comm.* **2013**, *49*, 11062.
- Pub. AA11** Dark conglomerate phases of azobenzene derived bent-core mesogens – Relations between molecular structure and mirror symmetry breaking in soft matter. M. Alaasar, M. Prehm, M. Brautzsch, C. Tschierske, *Soft Matter* **2014**, *10*, 7285.
- Pub. AA12** 4-Methylresorcinol based bent-core mesogens with azobenzene wings – A new class of compounds with dark conglomerate phases. M. Alaasar, M. Prehm, M. Brautzsch, C. Tschierske. *J. Mater. Chem. C* **2014**, *2*, 5487.

- Pub. AA13** Helical nano-crystallite (HNC) phases – chirality synchronization of achiral bent-core mesogens in a new type of dark conglomerates. M. Alaasar, M. Prehm, C. Tschierske. *Chem. Eur. J.* **2016**, *22*, 6583.
- Pub. AA14** Mirror symmetry breaking in fluorinated bent-core mesogens. M. Alaasar, M. Prehm, C. Tschierske. *RSC Advances* **2016**, *6*, 82890.
- Pub. AA15** Spontaneous mirror symmetry breaking in liquid phases of photoisomerizable achiral molecules. M. Alaasar, M. Prehm, Y. Cao, F. Liu, C. Tschierske, *Angew. Chem. Int. Ed.* **2016**, *55*, 312.
- Pub. AA16** Isothermal chirality switching in liquid-crystalline azobenzene compounds with non-polarized light. M. Alaasar, S. Poppe, Q. Dong, F. Liu, C. Tschierske. *Angew. Chem.* **2017**, *129*, 10941.
- Pub. AA17** Y-shaped tricatener azobenzenes – Functional liquid crystals with synclinic-anticlinic transitions and spontaneous helix formation. M. Alaasar, S. Poppe, Y. Cao, C. Chen, F. Liu, C. Zhu, C. Tschierske. *J. Mater. Chem. C* **2020**, *8*, 12902.
- Pub. AA18** Switching chirophilic self-assembly: From meso-structures to conglomerates in liquid and liquid crystalline network phases of achiral polycatenar compounds. M. Alaasar, Y. Cao, Y. Liu, F. Liu, C. Tschierske. *Chem. Eur. J.* **2022**, e202201857.
- Pub. AA19** Mirror symmetry breaking in cubic phases and isotropic liquids driven by hydrogen bonding. M. Alaasar, S. Poppe, Q. Dong, F. Liu, C. Tschierske. *Chem. Comm.* **2016**, *52*, 13869.
- Pub. AA20** Controlling ambidextrous mirror symmetry breaking in photosensitive supramolecular polycatenars by alkyl-chain engineering. M. Alaasar, X. Cai, F. Kraus, M. Giese, F. Liu, C. Tschierske. *J. Mol. Liq.* **2022**, *351*, 118597.
- Pub. AA21** Controlling liquid and liquid crystalline network formation by core-fluorination of hydrogen bonded supramolecular polycatenars. M. Alaasar, J.-C. Schmidt, X. Cai, F. Liu, C. Tschierske, *J. Mol. Liq.* **2021**, *332*, 115870.
- Pub. AA22** Photoresponsive halogen bonded polycatenar liquid crystals. M. Alaasar, S. Poppe, C. Tschierske. *J. Mol. Liq.* **2019**, *277*, 233.
- Pub. AA23** Mirror symmetry breaking and network formation in achiral polycatenars with thioether tail. M. Alaasar, A. F. Darweesh, X. Cai, F. Liu, C. Tschierske. *Chem. Eur. J.* **2021**, *27*, 14921.
- Pub. AA24** Cybotactic nematic phases with wide ranges in photoresponsive polycatenars. M. Alaasar, S. Poppe. *Liq. Cryst.* **2020**, *47*, 939.
- Pub. AA25** Non-symmetric ether-linked liquid crystalline dimers with a highly polar end group. M. Alaasar, C. Tschierske. *Liq. Cryst.* **2017**, *44*, 387.
- Pub. AA26** Transition from lamellar to nanostructure mesophases in azobenzene-based hockey-stick polycatenars. M. Alaasar, X. Cai, Y. Cao, F. Liu. *New J. Chem.* **2022**, *46*, 15871.
- Pub. AA27** Hockey-stick polycatenars: Network formation and transition from one dimensional to three-dimensional liquid crystalline phases. M. Alaasar, S. Poppe. *J. Mol. Liq.* **2022**, *351*, 118613.
- Pub. AA28** Nematic phases driven by hydrogen-bonding in liquid crystalline nonsymmetric dimers. M. Alaasar, C. Tschierske. *Liq. Cryst.* **2019**, *46*, 124.
- Pub. AA29** Azobenzene-based supramolecular liquid crystals: The role of core fluorination. M. Alaasar, J.-C. Schmidt, A. F. Darweesh, C. Tschierske. *J. Mol. Liq.* **2020**, *310*, 113252.
- Pub. AA30** Hydrogen-bonded supramolecular complexes formed between isophthalic acid and pyridine-based derivatives. M. Alaasar, C. Tschierske, M. Prehm. *Liq. Cryst.* **2011**, *38*, 925.

## 1. Introduction

Since the initial discovery of Reinitzer [31] – and subsequent early pioneering work of Vorländer [32] – the occasional existence of an intermediate state of matter between the crystalline solid and the isotropic liquid phases has been established and nowadays developed into a large research area with significant technological applications. This state of matter is called *Liquid Crystal* (LC) or mesophase. Liquid crystalline materials combine between order and mobility on a molecular level. According to their modes of formation LCs can be divided in two main groups, the thermotropic and lyotropic LCs.[33] Thermotropic substances show mesophases as a function of temperature, while lyotropic systems are solutions having liquid crystalline behaviour depending on the temperature and concentration of the solution. The scope of this thesis is thermotropic systems.

Due to its fascinating properties, LCs triggered numerous scientists. It resulted in a rapid development of liquid crystal displays (LCDs) which have totally replaced cathode ray tube displays. This results in revolutionizing of our daily life by mobile and communication devices.[34] Besides LCDs, there are other promising application fields such as organic semiconductor for photovoltaics,[35] steerable antennas in SATCOM and 5G communication systems,[36] responsive materials for biosensor applications,[37] active matter [37] and photonic applications.[38,39] So one can claim that without the liquid crystalline materials, many things of modern life would not exist.

The shape anisotropy of the molecules is very important for the formation of liquid crystalline materials. Therefore, many examples of elongated, rod-like (so called calamitic) molecules have been produced since the birth of the LCs research (Figure 1a). Most of them contained rigid aromatic cores substituted in terminal para positions with flexible moieties (alkyl- or alkoxy-chains), leading to both order and mobility at the same time. The rigid parts align in a preferred direction and due to the high mobility of the flexible part, its configuration can be changed by external stimuli e.g. electric or magnetic.[40] LCs phases are not limited to molecules with rigid and flexible part, but more generally appear in molecules composed of two incompatible parts. For example, amphiphilic mesogens composed of hydrophilic and hydrophobic segments are known to exhibit distinct nanometer-scale order on a one-dimensional, two dimensional, or three-dimensional periodic lattice.[40] Likewise, the segregation of fluorinated and nonfluorinated segments can stabilize or induce LC phases. Overall, the degree of order of the LC phases is affected by several factors such as the rigidity, mobility, anisometricity, nano-segregation and specific intermolecular interactions (e.g.

hydrogen-bonding or halogen-bonding). This leads to orientational long-range order in the different types of LC phases such as nematic, smectic and columnar phases (Figure 2).

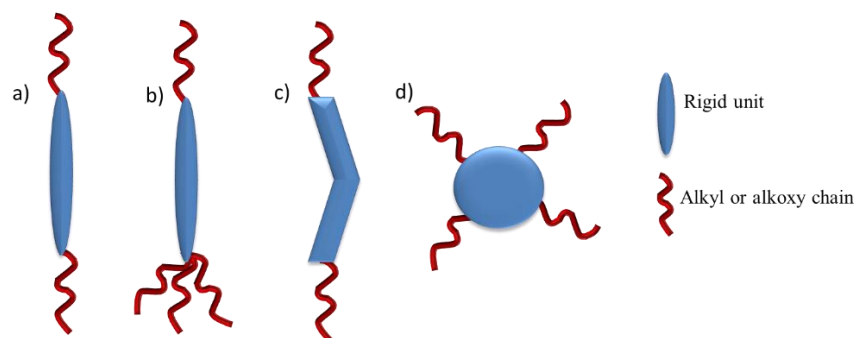


**Figure 1.** Different molecular geometries that can form liquid-crystalline phases: a) rod-like (calamitic); b) multichain (polycatenar); c) bent-core and d) disc-like (discotic) shape.

While discotic molecules mostly form columnar [41] and nematic [42] phases, calamitic mesogens prefer layer structures (smectic phases), nematic [43] and cubic [44] phases. The smectic phase is characterized by high positional and orientational long-range order (Figure 2b,c). Variation of the molecular arrangement inside the layers result in various mesophase types. The most important mesophase types are shown in Figure 2. So, these can be either orthogonal (smectic A, SmA, Figure 2b,) or tilted to the layer plane (smectic C, SmC, Figure 2c).

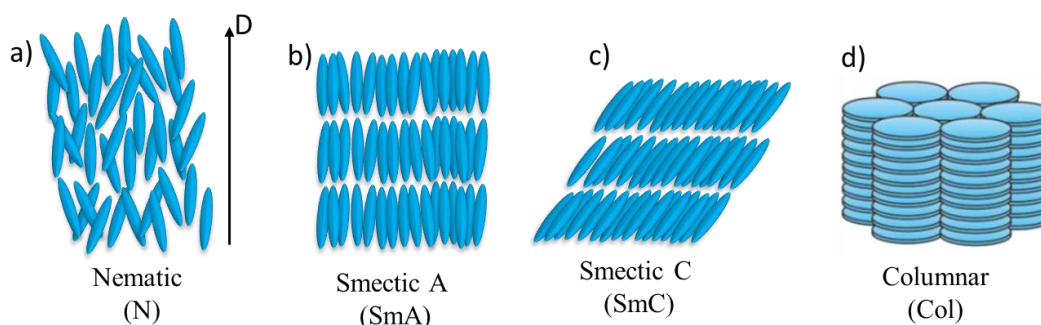


**Figure 2.** Examples of different types of liquid crystalline phases.

Due the long-range order N, Sm and Col mesophases show birefringence and these birefringent phases are used to characterize LC phases. Figure 3 show representative examples for textures observed in different types of LC phases. By using polarized optical microscopy (POM) between crossed polarizers, e.g. in the nematic phase a schlieren texture with four brush declinations is observed (Figure 3a), while in the SmA phase a fan-shaped texture is observed (Figure 3b). More detailed characterization of LCs could be performed using different methods



including X-scattering, calorimetric studies of the phase transitions and electrooptical investigations.[33]

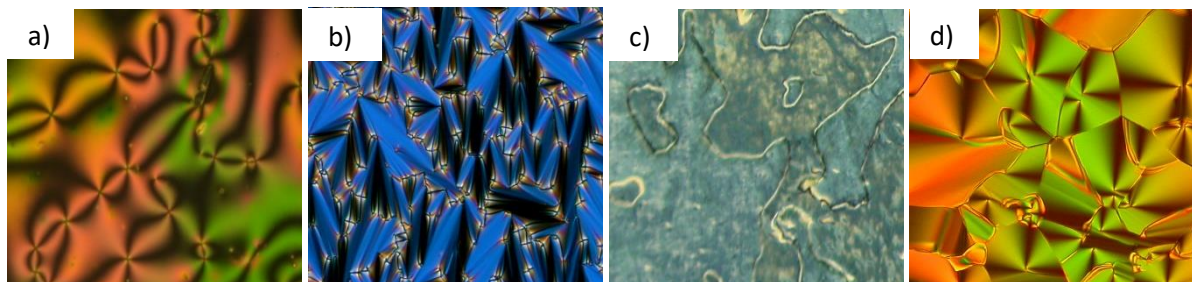


**Figure 3.** Representative textures for different types of liquid crystal phases: a) nematic (N); b) smectic A (SmA); c) smectic C (SmC) and hexagonal columnar phase ( $Col_{hex}$ ). a, c, d) In a homeotropic alignment and b) in a planar alignment.

The simplest and best studied LC phase is the nematic phase (abbreviated N). In the N phase, there is no positional long-range order but the molecules orient themselves to each other so that their long axis point on average in one direction (the director,  $D$ , Figure 2a).[45] The N phase has much in common with ordinary liquids, the phase is fluid, the molecules are moving rather free, rotation around the short and long axes are possible. Nevertheless, exciting versions of N phases have been discovered in the recent years, among them the twist-bend nematic ( $N_{TB}$ ) phase which is spontaneously chiral [46-61] and the ferroelectric nematic ( $N_F$ ) phase being spontaneously polar.[62-70]

Besides the classic rod-like and disc-like molecules, dimers, oligomers, dendrimers, polycatenars and polyphilic mesogens and specially the class of the so-called bent-core mesogens have been developed.

### 1.1. Bent-core molecules

Bent-core mesogens represent a special class of LC compounds having a curved rigid unit and for this reason they show special characteristics. The first bent-core mesogens were synthesized and described by Vorländer in 1929 in Halle. The synthesized nonlinear molecules were derived from resorcinol and isophthalic acid, however due to their high transition temperatures the special features of their LC behaviour stayed for many years undiscovered.[71,72] Later investigations of these non-linear materials by Pelzl, Wirth and Weissflog proved that they exhibit LC phases that were typically observed for bent-core mesogens,[73] which were firstly reported by Niori et al. in 1996. Therein, the formation of polar smectic LC phases by achiral molecules was reported for the first time.[74] Previously, polar order was assumed to require the reduction of the phase symmetry of tilted smectic (SmC) phases by uniform chirality induced by permanent molecular chirality of the involved molecules.[75-79]

### 1.1.1. Designing bent-core mesogens

As the name suggests, bent-core (BC) mesogenic compounds have a bent molecular core. This core is formed by a rigid unit, which usually consists in most cases of five to six benzene rings, which are directly or covalently linked to each other through various bridging groups Y, Z (COO, OOC, N=N, single bond). Other examples of BCLCs with smaller [80] or larger [81,82] rigid units are also known.[83,84,85]

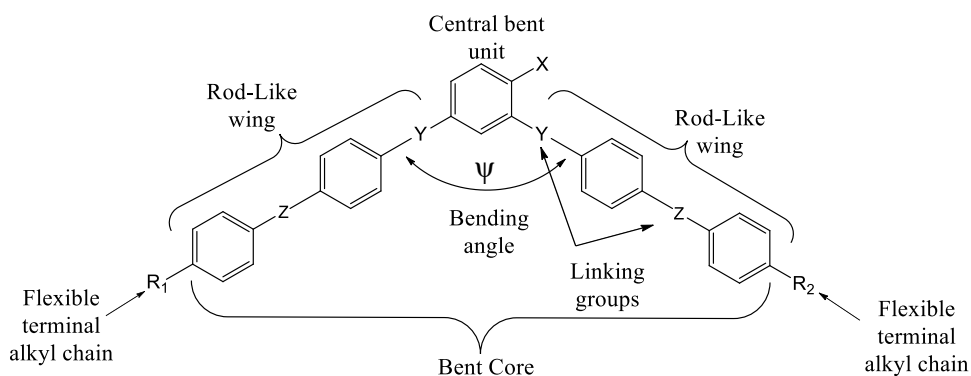


**Figure 4.** General structure of bent-core mesogens.

As can be seen from **Figure 4**, to design the curved shape of a bent-core mesogen a central core unit is required to induce the bending angle ( $\psi$ ) of the mesogen. When using resorcinol ( $X = H$ ) the bending angle is  $\sim 120^\circ$ , which could be also obtained with other bent-core units such as 3,4'-disubstituted biphenyl [86,87] and 2,6-disubstituted pyridine moieties.[88,89] Other central core units have been used to vary the bending angle such as cyclic urea [90] and 5-ring heteroaromatic system (1,3,4-oxadiazole).[91] Another successful tool to influence the bend angle is the introduction of a lateral substituent ( $X$ ) at the central core unit, especially if placed beside one or both of the linking units Y (see Figure 4). Halogens ( $X = F, Cl, Br, I$ ) and cyano group ( $X = CN$ ) have been applied and found to be very effective in varying the bending angle which in turn results in the observation of interesting LC phases as will be discussed later.[92,93,94]

To reach the liquid crystalline state, the rigid unit must be connected terminally to flexible segments, usually *n*-alkyl or *n*-alkoxy chains. These terminal chains inhibit the crystallization and simultaneously raise the molecular mobility. The segregation of the rigid cores and the flexible chains results in a preferred arrangement of the bent-core mesogens in layered structures.

### 1.1.2. Polar phases of bent-core mesogens

Bent-core mesogens are capable of producing conventional nonpolar LC phases such as nematic and smectic phases as well as polar LC phases. The formation of a permanent polar vector is only possible through the restriction of the freedom of rotation around the long axis of the molecule, which is the case due to the bent shape of the molecule.

For rod-shaped mesogens ( $D_{\infty h}$ -Symmetry) there is a possibility of free rotation of the molecules around their long axis (Figure 5a). Therefore, no polarization could be observed in the mesophase since these molecules have no preferred polar direction. Under electric field these calamitic mesogens tend to orient themselves to a limited extent. In the case of bent-core molecules, the rotation of molecules is inhibited and this leads to a reduced symmetry of the system ( $C_{2v}$ -symmetry) and thus the molecules have a polar direction, which is a result of the parallel arrangement of the uniformly bended molecules within a smectic layer (Figure 5c).[83] The polar direction is perpendicular to the long axis of the molecule and parallel to the layer plane (Figure 5b). Polar mesophases are denoted by the letter P. A distinction of different polar mesophases is possible through the application of an electrical field because the molecules align themselves along the field lines and thus create a macroscopic polar direction.

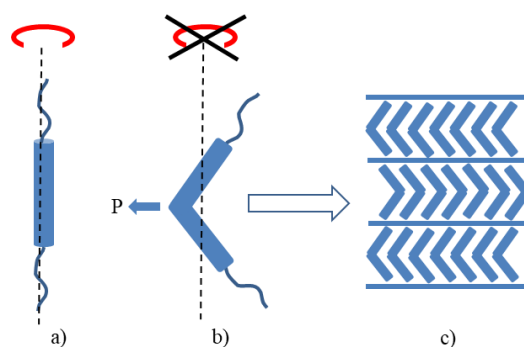


**Figure 5.** a) Calamitic and b) bent-core molecule. c) Due to restricted rotation of bent core molecules around their long axis they form this preferred parallel arrangements and layered structures.

There are two distinguishable ways for the polar smectic layers to be organized. Either the direction of the polar order in adjacent layers can be parallel which is designated as ferroelectric (FE) or antiparallel, designated as antiferroelectric (AF), as shown in **Figure 6**. The FE state ( $SmP_F$ ) represents a macroscopic polar structure whereas the AF structure ( $SmP_A$ ) is macroscopic apolar and usually more stable than the FE states.

The FE state represents an arrangement with anticlinic interlayer interfaces (state (2) and (3), Fig. 6), i.e., the alkyl chains cannot align parallel at the interlayer interfaces. Therefore, the FE state is destabilised by the inhibition of out-of plane interlayer fluctuations in this

structure. These interlayer fluctuations are possible in the AF state, which represents an arrangement with synclinic interlayer interfaces (state (1), Fig. 6).[83]

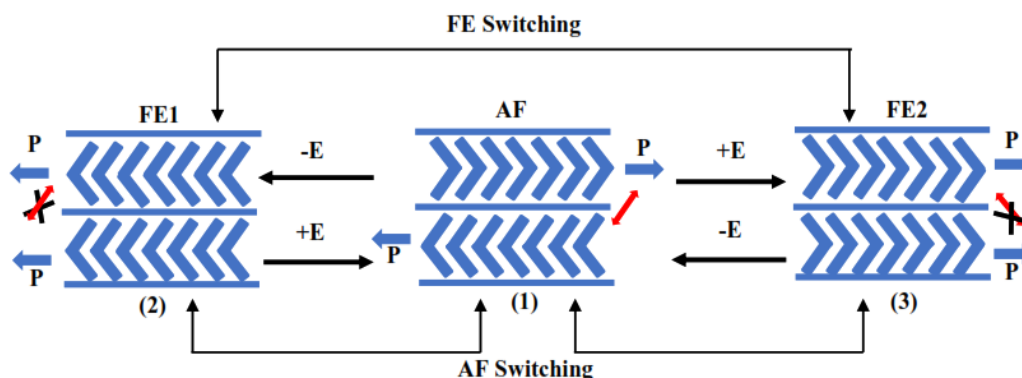


**Figure 6.** Switching behaviour of polar smectic phases in bent-core mesogens under an electric field. The different states can be antiferroelectric (AF, antipolar) or ferroelectric (FE, synpolar). The red arrows indicate the out-of-plane interlayer fluctuations.

For most polar smectic phases of bent-core molecules the ground state is AF. Because there is only a small energy barrier between the two different states (AF and FE), the FE state can be induced by alignment under an applied electric field and stabilized by polar surface interactions. Typical switching current curves obtained for the AF and FE phases of a bent-core compound under a triangular-wave field is shown in **Figure 7**.

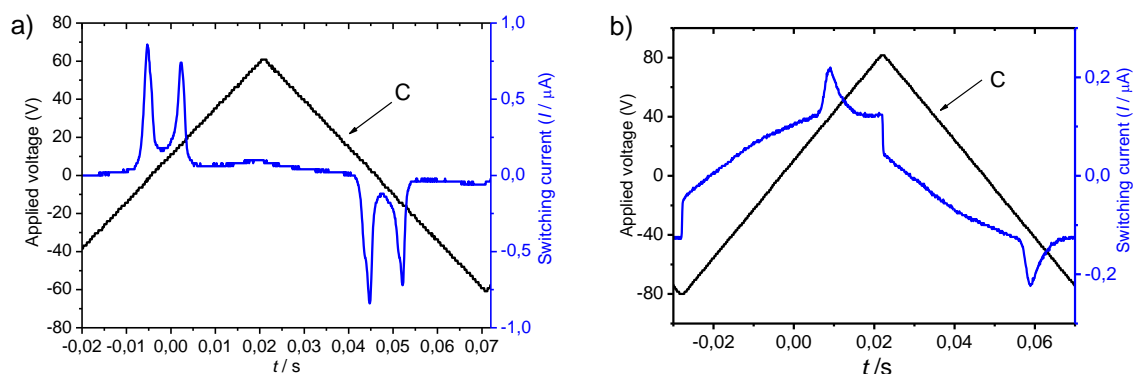


**Figure 7.** Switching current response curves obtained on applying a triangular wave voltage in: a) an AF mesophase and b) in FE mesophase. The letter C Refers to the triangular waveform for comparison.

The AF switching is characterized by the occurrence of two separate polarization peaks in each half period of the applied triangular voltage ( $FE1 \leftrightarrow AF \leftrightarrow FE2$ , Fig. 7a), while the FE switching is characterized by the occurrence of one polarization peak ( $FE1 \leftrightarrow FE2$  Fig. 7b). Most of the LC phases exhibited by BCLCs could display polar electric response and depending on the shape of the current switching curves they are subdivided.

Beside the polar switching, there are additional differences of BCLCs compared to the mesophases exhibited by classical rod-like mesogens. For example, the X-ray diffraction

pattern of polar smectic phases are characterised by numerous harmonics of the layer reflection. Typically, reflections up to the 3rd or even up to the 6th order can be found in BCLCs, which indicate very well-defined layers with sharp interfaces. In smectic phases of rod-like molecules these interfaces are much more diffuse. Mostly, only the 1st order reflection and in some cases also the 2nd or 3rd order, can be found in the smectic LC phases (though hexatic phases can show more).

In addition, the enthalpy values for the clearing transition i.e. the transition between a polar smectic phase and the isotropic liquid state are in the range of  $\Delta H = 15\text{--}25 \text{ kJ mol}^{-1}$ , which is significantly larger than the values found for conventional smectic phases of rod-like mesogens ( $\Delta H = 1\text{--}10 \text{ kJ mol}^{-1}$ ).[83]

### 1.1.3. Chirality and mirror symmetry breaking in polar mesophases of bent-core molecules

The SmC phases, found very frequently for BCLCs are characterized by inclination of the molecules within the layers. If the tilt direction in the adjacent layers is identical, the phase is a synclinic phase ( $\text{SmC}_s$ ). In case of opposite tilt direction between adjacent layers, the phase is anticlinic ( $\text{SmC}_a$ ). Therefore, beside the non-polar SmC phase this tilt organization results in four different types of polar SmC phases:  $\text{SmC}_s\text{P}_F$ ,  $\text{SmC}_s\text{P}_A$ ,  $\text{SmC}_a\text{P}_F$  and  $\text{SmC}_a\text{P}_A$  (Figure 8b).

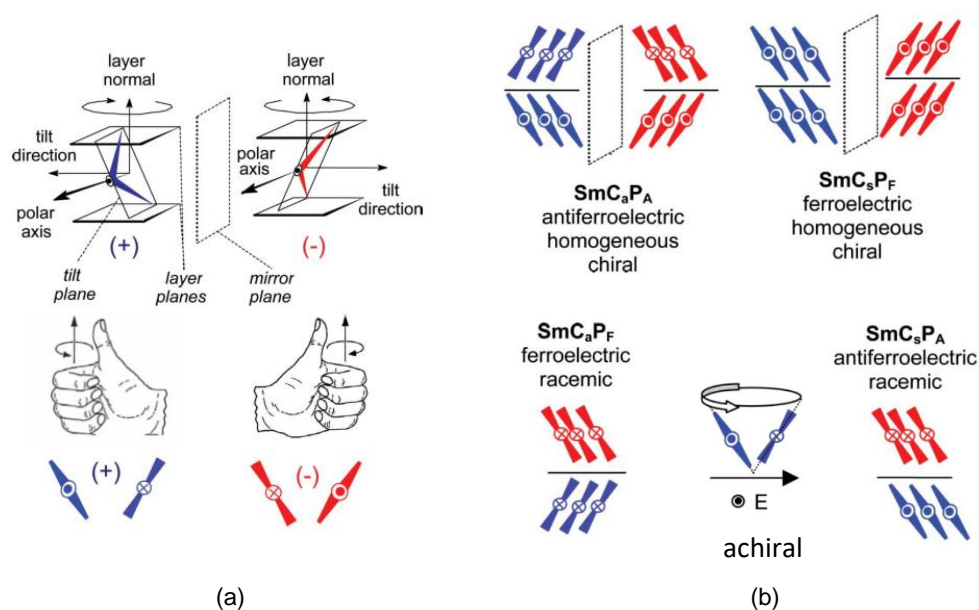


**Figure 8.** Different polar SmC phases. a) Layer normal, tilt direction and the polar axis define either a right-handed coordinate system (+) shown in blue, whereas in the mirror image these vectors define a left-handed system (-), shown in red. b) Polar SmC phases, which can be chiral or achiral depending on the orientation of the molecules. Mesogens with a dot in the middle point towards the viewer, crosses away. The blue and red colours indicate (+) and (-) enantiomers.[83]

Because of the tilt, these phases are biaxial. The tilt direction, layer normal and polar direction form a right-handed (+) or left-handed (-) coordinate system (Figure 8a). Both resemble each other like image and mirror image, whereby a chirality is generated in these

mesophase. Thus, chirality is induced in LC phases of achiral molecules through the combination of polar order and molecular tilt (Figure 8a).[83,95] Therefore,  $\text{SmC}_a\text{P}_A$  and  $\text{SmC}_s\text{P}_F$  mesophases show chirality of the mesophase because molecules of adjacent layers share the same sense of chirality, leading to the formation of two enantiomeric forms (Figure 8b). With the help of an electric field, it is possible to switch between different chiralities. To retain the tilt direction, the switching process must be carried out by rotating the molecules around their long axis. If the molecules rotate on a cone, which is usually the case, the chirality is reversed (Figure 8b). For the other two SmC phases i.e. the  $\text{SmC}_a\text{P}_F$  and  $\text{SmC}_s\text{P}_A$  phases, the molecules of adjacent layers show a different sense of chirality, leading to achiral structures.[83]

#### *1.1.4. Development of tilt and polar order*

In the SmA phases of BCLCs the bent-core mesogens are arranged on average orthogonal in the layers, therefore they are achiral. The simple uniaxial SmA and the biaxial  $\text{SmA}_b$  phase can be easily distinguished by POM if there is no polar order, because SmA is optically uniaxial and  $\text{SmA}_b$  is biaxial. Samulski et al. reported in 1998 a biaxial SmA phase ( $\text{SmA}_b$ ) for oxadiazole derivatives.[96] Biaxiality in a  $\text{SmA}_b$  phase results from freezing of the free rotation around the long axis of the molecule. Polar SmA phases are rare, since the onset of a polar order is usually accompanied by a tilt and thus a phase transformation of SmA to SmC often takes place.[97,98] Special  $\text{SmC}_a$  phases with small anticlinic tilt are difficult to distinguish from the  $\text{SmA}_b$  phases.

As described above, according to the polar order in neighbouring layers the polar  $\text{SmA}_b$  phases are subdivided to  $\text{SmAP}_A$  and  $\text{SmAP}_F$  phases. The latter phase was reported for the first time for a bent-core mesogen by Reddy et al. in 2011.[99] Based on theoretical considerations, Pocięcha et al. reported three additional SmA phases that exhibit local polar order.[100] Later the  $\text{SmAP}_R$  phase was reported, in which the polar director is randomly distributed in the layers.[101,102,103,104] In this case polar order can be induced by applying an electric field of appropriate strength.

The  $\text{SmAP}_\alpha$  phase shows a helicoidally modulated polarization with a short pitch. A repeating bilayer structure characterizes the  $\text{SmAP}_2$  phase, which has not yet been confirmed in the literature for any bent-core mesogen. Gomola et al. describes a phase assigned as  $\text{SmAP}_{AR}$  phase with local antiferroelectric order.[105] Electro-optical investigations and simulations by Panarin et al. indicate that the reported  $\text{SmAP}_{AR}$  phase could agree with the theoretically predicted  $\text{SmAP}_\alpha$  phase.[106]

Because of their properties in an electric field, bent-core mesogens offer a variety of applications such as electro-optical switches. Thus, by using e.g. SmAP<sub>R</sub> phases, biaxiality can be achieved by applying an electric field. This could enable the use of the SmAP<sub>R</sub> phase forming material in LCD applications with very short switching times.[107,108] For the chiral SmC<sub>a</sub>P<sub>A</sub> and SmC<sub>s</sub>P<sub>F</sub> phases, under an electric field, there is a change between the transparent state of the SmC<sub>a</sub>P<sub>A</sub> phase and the non-transparent (opaque) state of the SmC<sub>s</sub>P<sub>F</sub> phase. This offers possibilities to use such systems as optical switches.[109] In addition due to the non-centro symmetric structure of the synpolar smectic phases, BCLCs could be used as materials for non-linear optics (NLO).[110]

#### 1.1.5. Bent-core molecules involving azobenzene units

Azobenzene-based molecules were among the first recognised liquid-crystalline materials.[111] Initially because of their photosensitive nature they were considered to not be used in LCDs industry. However, today the same phenomenon (*cis-trans* photoisomerization) is the basis of their applications. Therefore, azobenzene derivatives are well known for potential applications in photonics such as optical data storage,[112,113] photochemical molecular switches,[114,115] polarization holography[116] and nonlinear optics.[117,118] Combining photoswitchable azobenzenes with liquid crystalline ferroelectrics or chiral phases provides access to potential new multifunctional materials where polar response can be modulated by light.

Pioneering work in the field of azo-containing bent-core mesogens has been done by Prasad *et al.*[119-121] but as mentioned earlier the first BCLC derived from isophthalic acid as the central core unit was synthesized by Vorländer in 1929 in Halle.[71] Indeed this material represent the first example of azobenzene-based BCLC (compound **Azo1**, **Figure 9**). Later the first examples of azobenzene containing BCLCs with a central resorcinol unit were reported by Prasad *et al.* in 2001 (compounds **Azo2/n** with  $n \geq 12$ ).[120,122]

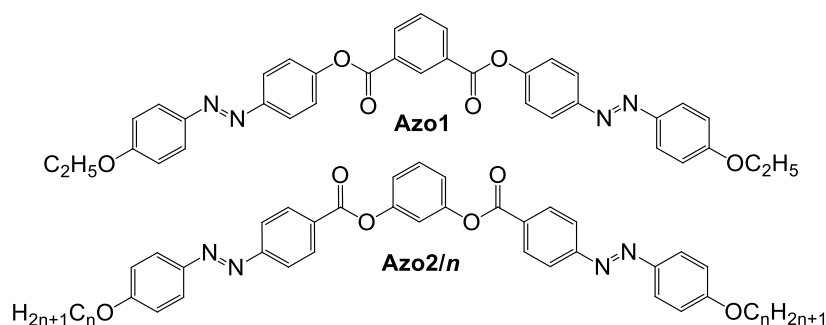


**Figure 9.** Chemical structure of the first example of azobenzene containing bent-core molecule (**Azo1**) synthesized by Vorländer [71] and the materials synthesized by Prasad (**Azo2/n**).[120,122]

A detailed overview over known azobenzene containing BCLCs up to 2016 is given in my review in the journal of Liquid Crystals in reference [A123].

## 1.2. Polycatenar liquid crystals

Polycatenar LCs are materials in which the rod-like structure is ‘decorated’ with more than two terminal flexible chains (mutli-chain compounds).[124] They are named according to the number of the terminal chains, e.g. tetracatenar mesogens have four terminal chains, hexacatenars six chains and so on. A stepwise variation of the terminal chains in number, length, and substitution pattern on the aromatic backbone leads to a successive change in the volume of this molecular segment, whereby the interfaces become progressively more curved and thus a bridge was built between the lamellar structures of conventional calamitic and the columnar phases of discotic molecules.[125,126] The most interesting LC phase observed in recent years for polycatenar systems is the bicontinuous cubic phase ( $Cub_{bi}$ ). Therefore, in the following a short introduction about this phase and its history is given.

### 1.2.1. Bicontinuous cubic phase ( $Cub_{bi}$ )

Among the most complex LC phases there are the bicontinuous cubic phases ( $Cub_{bi}$ ), which occur as intermediate phases at the transition from lamellar (1D) to columnar (2D) mesophases (**Figure 10**).[127,128]

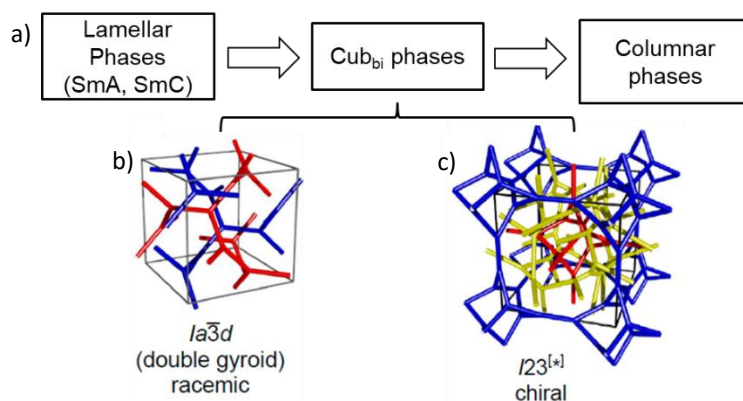


**Figure 10.** a) Transition from lamellar to columnar phases via bicontinuous cubic ( $Cub_{bi}$ ) phases by increasing interface curvature between the nano-segregated compartments, as observed for polycatenar compounds, b) the double gyroid  $Cub_{bi}$  phase with  $Ia\bar{3}d$  symmetry ( $Cub_{bi}/Ia\bar{3}d$ ) and c) the triple network  $Cub_{bi}$  phase with  $I23$  symmetry ( $Cub_{bi}/I23$ ). Both b) and c) show cubic phases with three-way network junctions.

These  $Cub_{bi}$  phases with a 3D lattice represent networks of branched columns. Bicontinuous means that there is a continuum and additional continuous networks, independent of the actual number of these networks. The networks are distinguished by the valence of their junctions (mostly three, but also four and six [129]) and the number of networks per unit cell



(in most cases two [129,130], but in some cases also one [131,132] or three [133]). The continuum is, in most cases, either formed by a solvent in the lyotropic systems, or by flexible chains in the solvent-free thermotropic systems. The fluidity of solvents or chains contributes significantly to the mobility and to the segregation of networks and continuum.

Thermotropic  $Cub_{bi}$  phases, which will be in the focus of this thesis, are rarely observed for polycatenar rod-like mesogens or those combining long chains with polar core units. The first organic molecules reported to have such phase are 4'-*n*-alkoxy-3'-nitrobiphenyl-4-carboxylic acids **ANBC-*n*** (Figure 11a) with  $X=NO_2$ , [134] and the dibenzoyldiazines (**BANH-*n***, Figure 11b). [135]

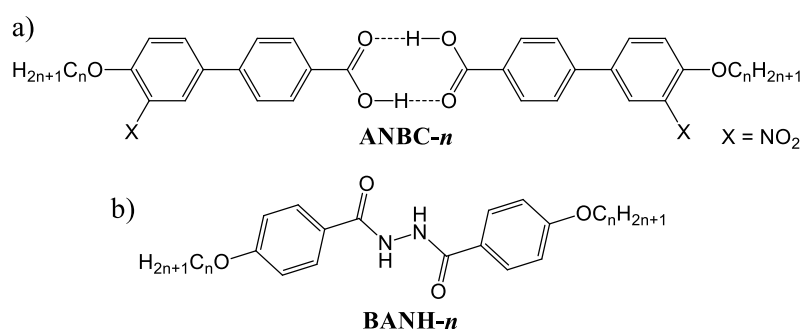


**Figure 11.** The first examples of bicontinuous cubic ( $Cub_{bi}$ ) phase forming materials. [134,135]

Because of their cubic symmetry both types of  $Cub_{bi}$  phases are optically isotropic like ordinary liquids. Cubic phases are very viscous due to their 3D-structure and thus could be distinguished from the ordinary liquids. Also, each type of  $Cub_{bi}$  phase has a characteristic X-ray diffraction (XRD) pattern with several sharp signals in the small angle region, while for the isotropic liquid there is only a diffuse small angle scattering. [133,136] Figure 10b,c shows the two common cases of networks with three-way junctions, namely the double gyroid ( $Ia\bar{3}d$ ) and the more complex triple network  $I23$  phase. The double gyroid  $Cub_{bi}/Ia\bar{3}d$  phase consists of two infinite networks with three-way junctions with opposite chirality sense (Fig. 10b), and thus, this phase is an achiral racemate or meso-form and optically inactive. [127,125, A136,137] The second type of  $Cub_{bi}$  with three-way junctions has more complex structure and a larger lattice parameter compared to the  $Ia\bar{3}d$  phase. It was initially supposed to have  $Im\bar{3}m$  space group, [138] but more recently after the discovery of the inherent chirality [138] it was proved to have  $I23$  space group involving three networks. [133] Because they do not show any linear birefringence their optical activity could easily be detected by optical investigations under POM.

Because  $Cub_{bi}$  phases contain nano-segregated networks of one component in the continuum of the other component, they can build continuous conduction channels in all three

spatial dimensions.[139] The junctions in these cubic phases provide abundant transport routes for ions, electrons or holes. Thus, these 3D Networks minimize distortions induced by structural defects in lamellar (1D) and columnar structures (2D), as recently demonstrated for ion carrying ionic amphiphiles.[140] This makes  $Cub_{bi}$  phase involving  $\pi$ -conjugated units excellent candidates for organic semiconductors.[141]

An especially exciting feature of specifically designed polycatenars is their ability to show mirror symmetry breaking in the isotropic liquid state assigned as  $(Iso_1^{[*]})$ .[138] The discovery of  $Iso_1^{[*]}$  phase is one of the most exciting achievements in recent years representing a new step in complexity of mesophase structure and is of fundamental interest for basic science and also has wide prospects for technological applications.[142] All polycatenars reported to date which show this phase are non-symmetric molecules having the terminal chains non-symmetrically distributed at both ends.[125,137,138,143] The  $Iso_1^{[*]}$  phase could be observed on heating the chiral  $I23$  phase, where the helical organization is retained in local clusters even during the transition to the isotropic liquid state, leading to a liquid polyamorphism involving a mirror symmetry broken liquid ( $Iso_1^{[*]}$ ). It could be also formed during cooling from an achiral cybotactic isotropic liquid phase ( $Iso_1$ ) leading to the development of helical networks. At the  $Iso_1$ - $Iso_1^{[*]}$  transition the chirality synchronization between the networks becomes long range, but without formation of a long-range cubic lattice. Further cooling of  $Iso_1^{[*]}$  leads to the achiral  $Cub_{bi}/Ia\bar{3}d$  or a chiral  $Cub_{bi}/I23$  depending on the aliphatic chain lengths. In the recent years such phases were found for numerous polycatenar mesogens,[136,138,141] as well as for so-called double-swallow-tailed compounds.[126,144,A16]

## 2. Objectives

In the present work two different classes of photoresponsive functional materials have been synthesised and investigated in detail. The materials are azobenzene-based liquid crystals either in the form of bent-core mesogens or multichain rod-like molecules (polycatenars) or combination of both. This aims to combine the optical properties and stimuli responsive characteristics of LCs with photoisomerizable azobenzene units in single molecules, which in turn could lead to potentially fascinating multifunctional materials with novel and/or enhanced properties for fundamental studies as well as for practical applications.

Besides polar ordered phases an additional goal was to get mirror-symmetry broken LC phases from photoisomerizable achiral molecules. Mirror symmetry breaking was observed in new types of fluid smectic and dark conglomerate phases of bent-core LCs as well as in isotropic liquids and bicontinuous cubic mesophases of polycatenars. Because the synthesized materials are photoswitchable fine tuning of the molecular structure leads to photoresponsive

LCs exhibiting a fast and reversible photo-induced change of the mode of the switching between ferroelectric-like and antiferroelectric-like states as well as a light-induced switching between achiral and chiral LC phases. Also, structure property relationships were investigated in detail and design rules for interesting chiral LC phases were successfully established in the course of the work.

### 3. Photo-responsive bent-core liquid crystals

The work on azobenzene based resorcinolbisbenzoates by Prasad *et al* initially lead to nonpolar and achiral rectangular columnar phases (so called B1-phases).[119] Therefore, I decided to investigate the influence of different substituents at the resorcinol unit on the self-assembly of azobenzene based BCLCs. During the presented work several BCLCs related to compounds **Azo2/n (Figure 9)** were synthesized and investigated in detail. The substitution patterns were varied from the highly polar cyano group (CN) to different halogen groups (I, Br, Cl, F) in addition to the methyl group (CH<sub>3</sub>). The substituents were in all cases located adjacent to one of the COO linking groups. In few cases double substitutions were also used. The side wings were identical in most compounds, but also different side arms were used. Also, the lengths of the side arms were kept constant or two different lengths were used. In the latter case the obtained materials are named as hockey-stick LCs, where one arm is relatively long and the other one is short. The effect of lateral substitution of the side arms was also investigated. Moreover, several BCLCs involving different linking units (mostly N=N + COO) in the distinct wings were also synthesized.

This modification of molecular structure leads to a wide variety of new and interesting LC phases and phase sequences as will be discussed in the following sections, which are derived by the kind of substituent at the resorcinol unit.

#### 3.1. 4-Cyanoresorcinol derived BCLCs (Pub. AA1-AA5, AA8)

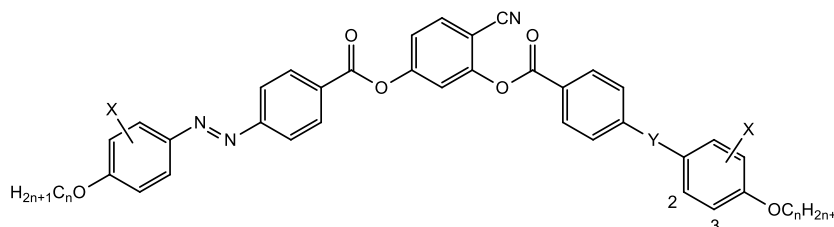
##### 3.1.1. Previous work

The first examples of 4-cyanoresorcinol based BCLCs have been synthesized and investigated by Weissflog's group in Halle. The focus of his work was on Schiff base derived materials. The LC phases of his materials were conventional LC phases of rod-like molecules such as N, SmA and SmC phases in addition to the polar SmCP<sub>A</sub> phase.[145,146,147,148,149,150] Also, the effect of peripheral core-fluorination was investigated, where based on X-ray studies and optical investigations a non-tilted single layer biaxial SmAP<sub>A</sub> phase was reported for the first time.[150] Further work was focused on the uniaxial-biaxial smectic phase transition in thin films [151] and in bulk state[152]. The bending angle ( $\psi$ ) between the two Schiff base arms

was carefully investigated with NMR studies and was found to be larger than 120° (typically observed for resorcinol based BCLCs) and its value ~ 136° which raises to 143 °C with increasing temperature.[153] This large value of  $\psi$  is due to a combination of dipole compensation between C=O and CN, steric and stereoelectronic interactions around the COO group in 3-position. This results in molecules with an effective average shape at the border line between classical rod-like and bent-core molecules. Therefore, non-polar and polar LC phases are observed for 4-cyanoresorcinol derived BCLCs.[148] This large value of the bending angle is also the reason for the observation of nematic phases in 4-cyanoresorcinol-based BCLCs,[148,150] which are rare for other bent-core mesogens with a typical bend angle of ~120°.[119-121] Later Tschierske's group reported several examples of such BCLCs with interesting LC phases.[101,106,154,155]

### 3.1.2. Compounds and synthesis

The first azobenzene-based BCLC derived from 4-cyanoresorcinol was reported in 2013 (compound **AA16** with  $n = 16$ , **Scheme 1**),[in Pub. AA1] and later a full series of this type of molecules was published in 2014 (compounds **AA $n$** , **Scheme 1**).[in Pub. AA2] Additional related molecules (see **Scheme 1**) with symmetric or non-symmetric wings were also published over several scientific papers in [AA3-AA5] and proved to show new LC phases and interesting phase behaviour.

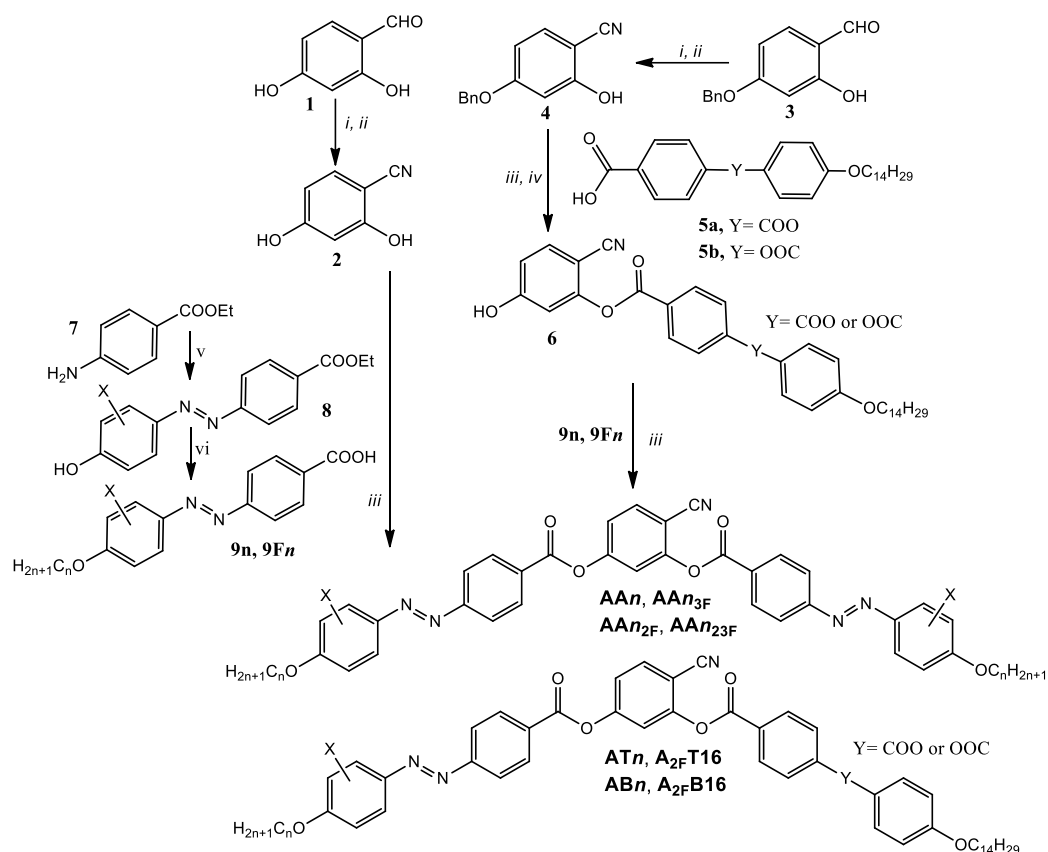


Compound	X	Y	Publications
<b>AA<math>n</math></b>	H	N=N	AA1, AA2
<b>AA<math>n</math>3F</b>	3-F	N=N	AA3, AA4
<b>AA<math>n</math>2F</b>	2-F	N=N	AA4
<b>AA<math>n</math>23F</b>	2,3-F	N=N	AA4
<b>AT<math>n</math></b>	H	COO	AA5
<b>AB<math>n</math></b>	H	OOC	AA5
<b>A2FT16</b>	3-F	COO	AA5
<b>A2FB16</b>	3-F	OOC	AA5

**Scheme 1.** Molecular structures of 4-cyanoresorcinol derived BCLCs reported in Pub. AA1-AA5 and their codes. The numbers (2 and 3) in the chemical structure indicate the position of the substituent X. The type of the rod-like

arm is indicated by the letters in the compound abbreviations: **A** = azobenzene, **B** = phenylbenzoate and **T** = phenylterephthalate. The fluorinated compounds have additional **F** in their abbreviations.

The synthesis of the 4-cyanoresorcinol based BCLCs under discussion is shown in **Scheme 2** and described in detail in the supplementary information of publications AA1-AA5.



**Scheme 2.** Synthesis of the 4-cyanoresorcinol based bent-core materials. Reagents and conditions: i: 1.  $\text{H}_2\text{NOH}$ , 2.  $\text{Ac}_2\text{O}$ ; ii:  $\text{NaOH}/\text{H}_2\text{O}$ ; iii: 1.  $\text{SOCl}_2$ ,  $80^\circ\text{C}$ , 1 h., 2. removal of excess  $\text{SOCl}_2$  under pressure, 3. **2** (0.5 equ) or **6** (1.0 equ),  $\text{DCM}$ , pyridine,  $50^\circ\text{C}$ , 6 hrs.; iv:  $\text{H}_2/\text{Pd}/\text{C}$ ; v: 1.  $\text{NaNO}_2$ ,  $\text{HCl}$ ,  $\text{H}_2\text{O}$ ,  $0-5^\circ\text{C}$ , 2. Phenol or substituted phenol,  $\text{NaOH}$ , 3.  $\text{NaHCO}_3$ ; vi: 1.  $\text{C}_n\text{H}_{2n+1}\text{Br}$ ,  $\text{KI}$ ,  $\text{K}_2\text{CO}_3$ , 2-butanone, reflux 18 hrs., 2.  $\text{EtOH}$ ,  $\text{KOH}$ , reflux, 1 h., 3.  $\text{HCl}/\text{H}_2\text{O}$ ,  $0-5^\circ\text{C}$ . [AA1-AA5]

The synthesis starts from commercially available materials either 2,4-dihydroxybenzaldehyde (**1**) for symmetric molecules or 4-benzyloxy-2-hydroxybenzaldehyde (**3**) for non-symmetric molecules.

The synthesis of the side arms without azobenzene units and combining two different core units **5** were performed as follows: 4-(4-Tetradecyloxyphenoxycarbonyl)benzoic acid (**5a**) was prepared starting with the esterification of 4-*n*-tetradecyloxyphenol with 4-formylbenzoic acid followed by oxidation using sodium chlorite as oxidizing agent, [A156] while the isomeric 4-(4-tetradecyloxybenzoyloxy)benzoic acid (**5b**) was prepared by the esterification of 4-tetradecyloxybenzoic acid with benzyl-4-hydroxybenzoate followed by catalytic hydrogenation. [157]

The synthesis of the azobenzene-based side arm (**9n** and **9Fn**) is accomplished in four steps starting from diazotization of ethyl 4-aminobenzoate (**7**) and coupling of the resulting diazonium salt with phenol or substituted phenols followed by alkylation of the obtained intermediate (**8**) with the appropriate alkyl halide, then basic hydrolysis of the resulting esters and a final step of acidification to get the desired benzoic acids (**9n**, **9Fn**, Scheme 2).

Though the synthesis of the final materials is straight forward and uses well established procedures, it requires experience to obtain sufficiently pure and long-time stable products. Especially, it must be considered that the CN group increases the reactivity of the adjacent COO groups (especially in position 3) against nucleophilic attack. Such ‘active esters’ are prone to acyl group transfer, scrambling the COO groups in a process known as transesterification in the molecules not only during synthesis, but also during chromatography and recrystallization (purification), storage and even during investigation in the mesophases. For this reason, the use of dicyclohexylcarbodiimide (DCC) with 4-dimethylaminopyridine (DMAP) as a catalyst,[158] for the esterification reaction between 4-cyanoresorcinol and benzoic acid derivatives is not recommended. Tiny traces of DCC or DMAP catalyse the transesterification. To overcome this problem, neat thionyl chloride (SOCl<sub>2</sub>) was used to first activate the benzoic acids (**5**, **9** or **9Fn**) by converting it to the corresponding benzoyl chloride, followed by careful removal of SOCl<sub>2</sub>, then adding the appropriate phenols with triethylamine and a catalytic amount of pyridine in a second step. This synthetic route usually leads to long term stable pure products.

### 3.1.3. Cybotaxis in the nematic phases

(Pub. AA1, AA2, AA6-AA8, AA23)

The nematic phases of BCLCs are of special interest due to their potential biaxiality and polar order.[159,160,161] The main characteristic feature of these N phases is the formation of local smectic clusters, known as cybotaxis. This phenomenon was assumed for a long time to be a pre-transitional state,[162] but research with BCLCs, especially those derived from 4-cyanoresorcinol,[154] and oxadiazoles,[163,164,165] has shown that cybotaxis in the nematic phases of these BC molecules is a general feature.

For BC mesogens, the usually observed cybotactic nematic (N<sub>Cyb</sub>) phase type is the skewed cybotactic nematic phase composed of synclitic tilted smectic (SmC<sub>s</sub>) clusters known as N<sub>Cybc</sub>. [154,163,AA6] Another type of (N<sub>Cyb</sub>) composed of non-tilted SmA clusters (N<sub>Cyba</sub>) could be also formed by BCLCs but it is rarely observed.[159,166]

As reported in Pub. [AA1 and AA2], for the synthesized azobenzene-based BCLCs with nonfluorinated side arms (**AA<sub>n</sub>**, **Figure12a**) the N<sub>Cybc</sub> phase was observed for all homologues except the one with longest terminal chains ( $n = 18$ ). In the temperature range of the N<sub>Cybc</sub>

phases of all **AA $n$**  materials the XRD patterns of magnetically aligned samples ( $B \sim 1\text{T}$ ) show a diffuse scattering in the wide-angle region (WAXS) centred at the equator (Figure 13a), while in the small-angle region (SAXS) a dumbbell-like shape scattering is observed (Figure 13b), which is typically observed for such  $N_{\text{Cybc}}$  phases.

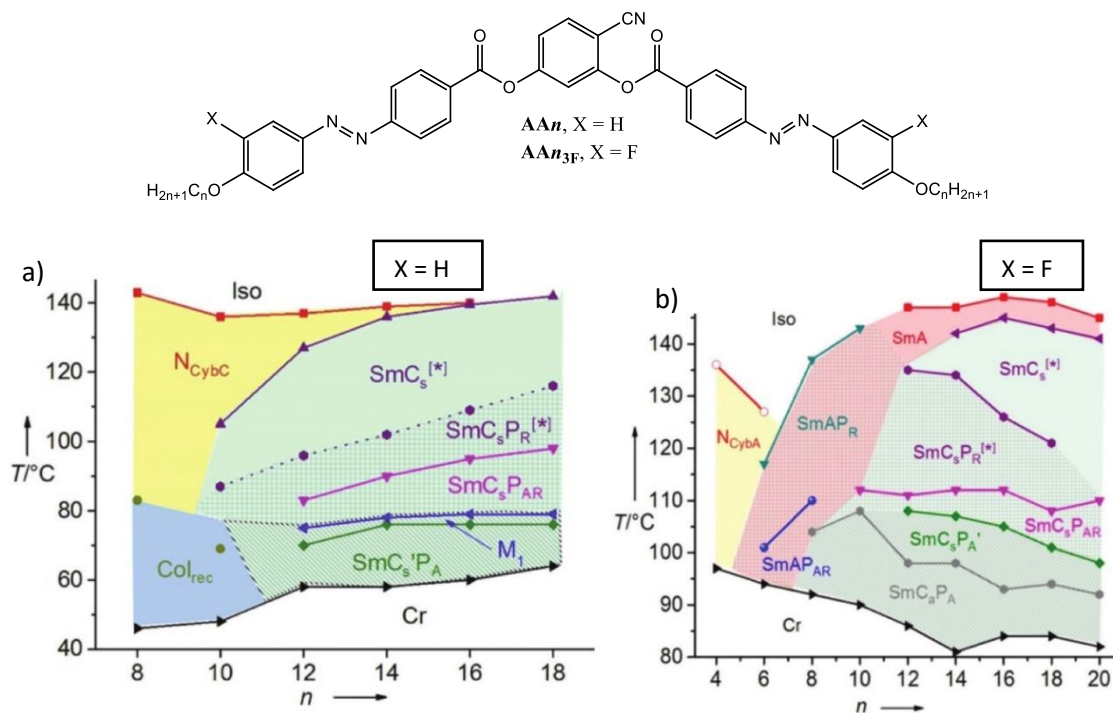


**Figure 12.** Chemical structures and phase behaviour of 4-cyanoresorcinol derived azobenzene-based BCLCs with symmetric side arms depending on terminal chain length as a function of temperature: a) Non fluorinated BCLCs (**AA $n$** , X=H)[AA1, AA2] and b) Fluorinated BCLCs (**AA $n_{3F}$** , X= F).[AA3, AA4]

Due to the unique combination of high polarity and low polarizability, and its conformational and steric effects,[167] fluorination of the aromatic core is considered as a powerful tool for tailoring the LC properties for modern LC technologies[168-171] and BCLCs for new applications.[172-177] Therefore, peripheral fluorination of the aromatic core of compounds **AA $n$**  at the ortho position next to the alkoxy chain was also performed, as described in Pub. [AA3, AA4]. This results in compounds **AA $n_{3F}$**  with two identical fluorinated wings and leads to the replacement of the  $N_{\text{Cybc}}$  phases by the less common  $N_{\text{Cyba}}$  phases, which are observed only for the shorter derivatives with  $n = 4$  and  $6$  (Figure 12b). Moreover, the nematic phase is suppressed for  $n > 6$  and the smectic phases of the **AA $n_{3F}$**  materials are also different from those of **AA $n$**  compounds as can be seen from Fig. 12a,b and as will be discussed later.

The  $N_{\text{Cybc}}$  phase was also reported for other related BCLCs derived from 4,6-dichlororesorcinol instead of 4-cyanoresorcinol.[AA6] It was also found for hockey-stick (HS) molecules derived from 4-bromoresorcinol.[AA7] Moreover, the type of the  $N_{\text{Cybc}}$  phases was

successfully controlled in 4-cyanoresorcinol-based HS materials by changing the position of the cyano group in the bent-core unit, where  $N_{CybA}$  phase was observed if the CN group is located close to the short side arm and changed to  $N_{CybC}$  phase if the CN group was shifted to the other side to be in the same side of the long arm.[AA8]

It should be noted that the main reason for cybotaxis is not the bend molecular shape, but the extended aromatic core with  $\geq 5$  benzene rings used as building blocks for BCLCs in most cases. This provides a significant source of nano-scale segregation from the flexible terminal chains, which increases with chain length elongation.[161,178] Therefore, wide range of the  $N_{CybC}$  phase was also reported for azobenzene-based polycatenars having four terminal chains and extend rod-like aromatic backbone as reported in Pub. [AA23].

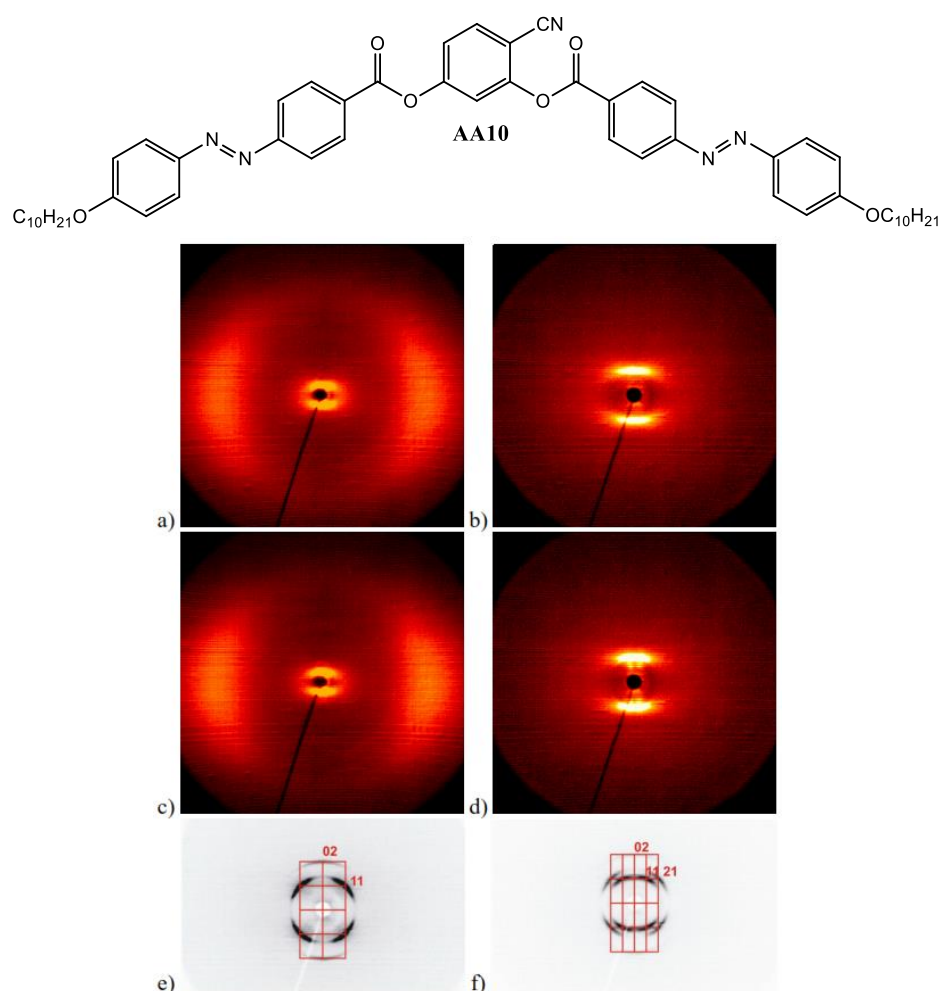


**Figure 13.** XRD investigation of an aligned sample of compound **AA10**: a) wide angle and b) small angle scattering of the  $N_{CybC}$  phase at  $T = 130$  °C; c) wide angle and d) small angle scattering of the  $SmCsPR^{[*]}$  phase at  $T = 90$  °C; e) small angle scattering with reciprocal lattice and indexation of the centred rectangular columnar phase  $Col_{rec1}$  ( $B_{1rev}$  phase) at  $T = 70$  °C and f) of the non-centred rectangular columnar phase  $Col_{rec2}$  at  $T = 60$  °C.[AA2]



### 3.1.4. Development of polar order and tilt

(Pub. AA1-AA4)

As shown in Fig. 12a and outlined in Pub. [AA1,AA2] compounds **AA $n$**  with relatively electron rich side arms have a strong tendency for uniform tilt ( $\sim 30^\circ$ ) and exhibit exclusively synclinc tilted  $N_{Cybc}$  and  $SmC_s$  phases in addition to  $Col_{rec}$  for the shorter two homologues (with  $n = 8$  and 10) as the lower temperature LC phases as indicated from the optical textures and XRD investigations (Fig.13c-f).[AA2] On the other hand, the related fluorinated analogues **AA $n_{3F}$**  with reduced electron deficient wings due to the electron withdrawing effect of the fluorine atoms, exhibit a reduced tilt ( $\sim 15\text{--}20^\circ$ ) as reported in Pub. [AA3,AA4]. This leads to the formation of  $N_{CybA}$  and  $SmA$  phases for the short chain homologues of **AA $n_{3F}$**  series. The  $SmA$  phases of the fluorinated materials represent uniaxial orthogonal phases. The  $SmA$  phase for all compounds with  $n \geq 12$  is a low permittivity paraelectric phase as no polarization peak could be recorded in its temperature range, while the  $SmA$  phases exhibited by shorter homologues represent high permittivity paraelectric  $SmA$  phases with randomized polar order with one polarization peak ( $SmAP_R$ ) or two polarization peaks ( $SmAP_{AR}$ ). Moreover, there is an additional transition from synclinc to anticlinc tilt in the titled polar antiferroelectric  $SmCP_A$  phases at lowest temperature (Fig. 12b). In both series of compounds with  $X = H$  or  $F$ , on growing the terminal chain length the synclinc tilt becomes more dominating (i.e. the order parameter along the tilt axis is increased), though the tilt angle itself does not change significantly. The effect of changing the position of the  $F$  atoms to inner 2-positions, using double 2,3-fluorination, or using other larger groups was also investigated in detail in Pub. [AA4] and will be discussed later (section 3.1.6.).

### 3.1.5. Mirror symmetry breaking in fluid smectic phases

(Pub. AA1-5, AA8)

Mirror symmetry breaking by conglomerate formation was occasionally observed in the nematic phases of BCLCs ( $N^*$ ).[179] This was also found for the  $N_{Cybc}$  phases of some 4-cyanoresorcinol based BCLCs [180] and shown to be due to twisted states developing between the cell surfaces.[165,181] Though this surface supported mode of mirror symmetry breaking would not require any source of chirality, it is assumed to be supported by the pronounced transient helicity of bent-core molecules.

Conglomerate formation by surface supported mirror symmetry breaking is for the first time reported in the paraelectric  $SmC_s$  phase observed in compounds **AA $n$**  ( $X=H$ )[AA1,AA2] and **AA $n_{3F}$**  ( $X= F$ ).[AA3,AA4] The chiral  $SmC_s$  phases designated as  $SmC_s^{[*]}$  and  $SmC_sPR^{[*]}$ , where the star in brackets stands for the conglomerate structure and subscript  $R$  stands for randomized polar order in these high permittivity paraelectric LC phases.

As described in Pub. AA1 and Pub. AA2 and shown in **Figure 14a-c** under slightly uncrossed polarizers dark and bright domains can be distinguished which invert their brightness by inverting the direction of the analyzer, confirming chiral conglomerates formation. Rotation of the sample between crossed polarizers (Fig. 14d,e) does not lead to any change of the brightness of the texture, meaning that simple tilt domains can be excluded and formation of a conglomerate of optical active domains is observed. The chiral domains are lost at the transition to the  $\text{SmC}_s\text{P}_{\text{AR}}$ , which is racemic due to the synclinic and antipolar organization of the molecules (see Section 1.1.3).

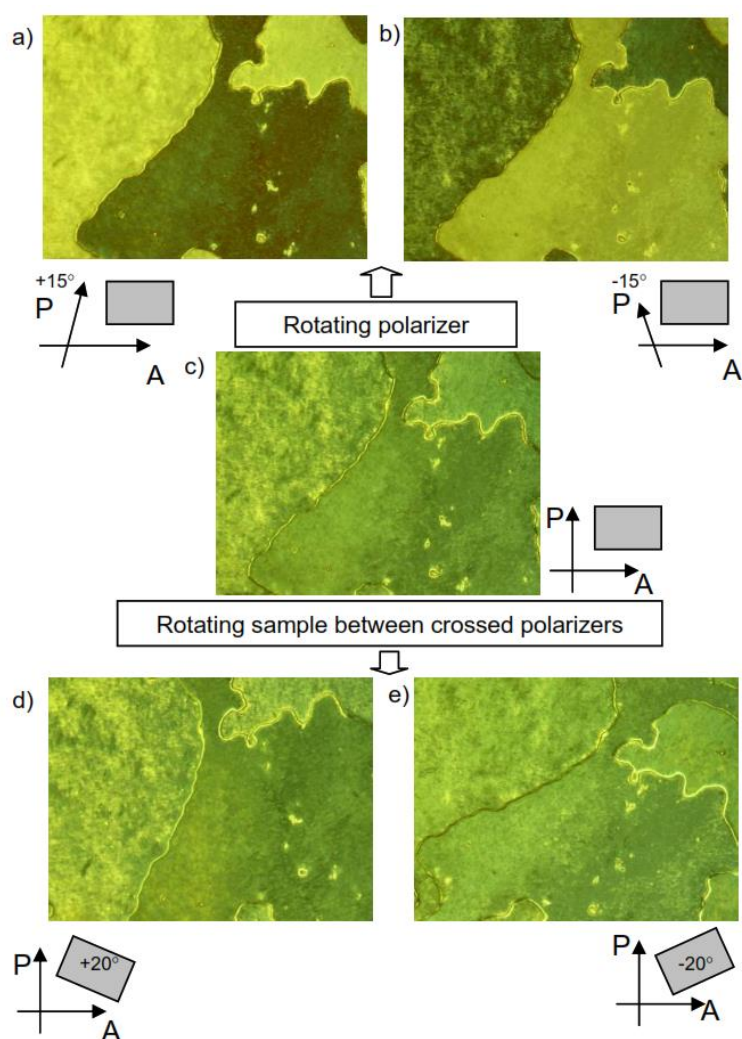


**Figure 14.** Textures of the  $\text{SmC}_s^{[*]}$  phase of compound **AA14** at  $T = 130\text{ °C}$  between glass slides (homeotropic alignment): c) between crossed polarizers and a, b) between slightly uncrossed polarizers, showing dark and bright domains, indicating the presence of areas with opposite chirality sense; d,e) show the texture between crossed polarizers, but after rotation of the sample by  $20^\circ$  either clockwise or anticlockwise; the birefringence does not change which confirms chirality as origin of the effects seen in a-c); there is no change of the textures at the transition to the  $\text{SmC}_s\text{P}_{\text{R}}^{[*]}$  phase.[AA2]

That conglomerates formation in the  $\text{SmC}_s^{[*]}$  and  $\text{SmC}_s\text{P}_{\text{R}}^{[*]}$  phases cannot be observed in freely suspended films or in thick samples [AA2] indicates that the mirror symmetry breaking in these materials is surface supported, similar to that observed in the  $\text{N}_{\text{Cybc}}$  phases.[179]

However, conglomerate formation is more easily reproduced than in the  $N^{[*]}$  phases. This is presumably a result of the enhanced cooperativity provided by the quasi-infinite layers in comparison to the cybotactic clusters. In Pub. AA2 it is also shown that, there is a relation between the appearance of a broad single peak in the current response curves and conglomerate formation. The formation of the  $SmC_sP_R^{[*]}$  phases is accompanied with the observation of a single broad current peak under the triangular wave electric field, similar to this one shown in Fig. 7b, whereas  $SmC_s$  phases without this peak do not show chiral domains. This means that also a growing coherence length of polar order has a stabilizing effect on conglomerate formation.

### 3.1.6. Effect of changing $F$ position and using different substituents (Pub. AA4)

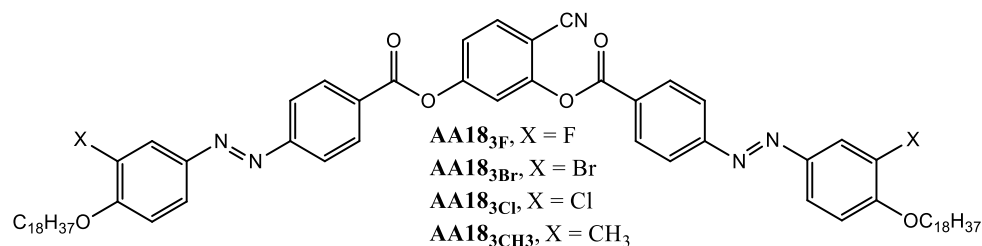
Pub. AA4 deals with the effect of partial core fluorination on the LC phases. Shifting the position of fluorine atom at the outer benzene ring from the peripheral ortho positions in  $AA_n3F$  to the inner meta positions with respect to the terminal alkoxy chains leads to compounds  $AA_n2F$  (Scheme 1 with  $n = 8-16$ ). This modification results in reducing the melting and clearing temperatures. Moreover, only LC phases with tilted organization ( $N_{CybC}$  phases and  $SmC_s$  phases) were observed instead of the orthogonal  $SmA$  phases. Neither chiral domain formation nor any polarization current peaks and optical response under applied electric field could be found in  $AA_n2F$  materials. Therefore, introducing  $F$  substitution in inner positions favours tilt, reduces mesophase stability and removes polar order. This is attributed to the unfavourable steric effect of fluorine in this inside-directed position.

Using double fluorine substitution at ortho and meta positions (series  $AA_n23F$ , Scheme 1) leads to higher transition temperatures compared to series  $AA_n2F$ , but lower if compared with the series  $AA_n3F$ . The nematic phase is totally removed and the  $SmA$  phase appears only as a metastable phase for  $n = 10$ , which is replaced by the chiral non-polar  $SmC_s^{[*]}$  phase for all derivatives with  $n \geq 12$ .

Replacing fluorine (crystal volume  $cv = 12.8 \text{ nm}^3$ ) [182] in  $AA183F$  (with  $n = 18$ ) by the larger and less polar bromine atom ( $cv = 33.0 \text{ nm}^3$ ) retains a phase sequence of Iso- $SmA$ - $SmC_s^{[*]}$ - $SmC_sP_{AR}$  without the observation of  $SmCP_A$  phase before crystallization and reduces the phase transition temperatures. [AA4]

As shown in Pub. [AA4], keeping the chain length fixed with  $n = 18$  and replacing the  $F$  atom by the non-polar  $CH_3$  group ( $cv = 31.7 \text{ nm}^3$ , compound  $AA183CH_3$ ) with similar volume compared to  $Br$  further reduces the LC phase stability considerably, removes the non-tilted  $SmA$  phase and removes polar order completely, leaving only a nematic ( $N_{CybC}$ ) and a nonpolar

and nonchiral SmC phase. This is mainly attributed to the unfavorable reduction of core-core interactions by the non-polar and electron donating CH<sub>3</sub> group.



These systematic investigations provided fundamental insights into the general understanding of the development of polar order in soft matter and the unusual phenomena associated with the formation and growth of polar domains, as for example, spontaneous mirror symmetry breaking and electric field induced tilt by a non-classical electroclinic effect, and the relations of these phenomena to the molecular structure.

### 3.1.7. Effect of replacing one azo group by ester group (Pub. AA5)

Additional structural modifications were done in Pub. [AA5] by replacing one of the azobenzene side arms by a terephthalate-based side arm (**AT<sub>n</sub>**, **Figure 15a**) or a benzoate-based wing having the direction of one ester group inverted (**AB<sub>n</sub>**, **Figure 15b**).[AA5] Moreover, the effect of core fluorination was also investigated in one selected example from each series (**A<sub>2F</sub>T16** and **A<sub>2F</sub>B16**, Fig. 15a,b).[AA5]

As can be seen from Fig. 15, Compounds **AT<sub>n</sub>** have phase sequences like those exhibited by the fluorinated **AA<sub>n3F</sub>** materials (compare Figures 15a and 12b). This also applies if we compare the phase sequence of the non-fluorinated **AA<sub>n</sub>** (Fig. 12b) compounds with that of **AB<sub>n</sub>** series (Fig. 15a). The main difference is that the compounds having one azobenzene wing replaced by the electron rich phenyl benzoate wing (**AB<sub>n</sub>**) display lower phase stability as only monotropic phases were observed compared to **AA<sub>n</sub>** series.[AA1,AA2] On the other hand, compounds **AT<sub>n</sub>** involving the electron deficit phenyl terephthalate wing show much higher isotropization temperatures, a smaller tilt and have a SmA high temperature phase, which is more comparable to the fluorinated materials discussed above (**AA<sub>n3F</sub>**).[AA3,AA4] Complete details are given in Pub. [AA5].

Also, the liquid crystalline behaviour of related 4-cyanoresorcinol BCLCs materials without azo units either with symmetric or non-symmetric side arms (phenylbenzoate or phenylterephthalate) are described in detail in references.[A156, A183, A184,A185]

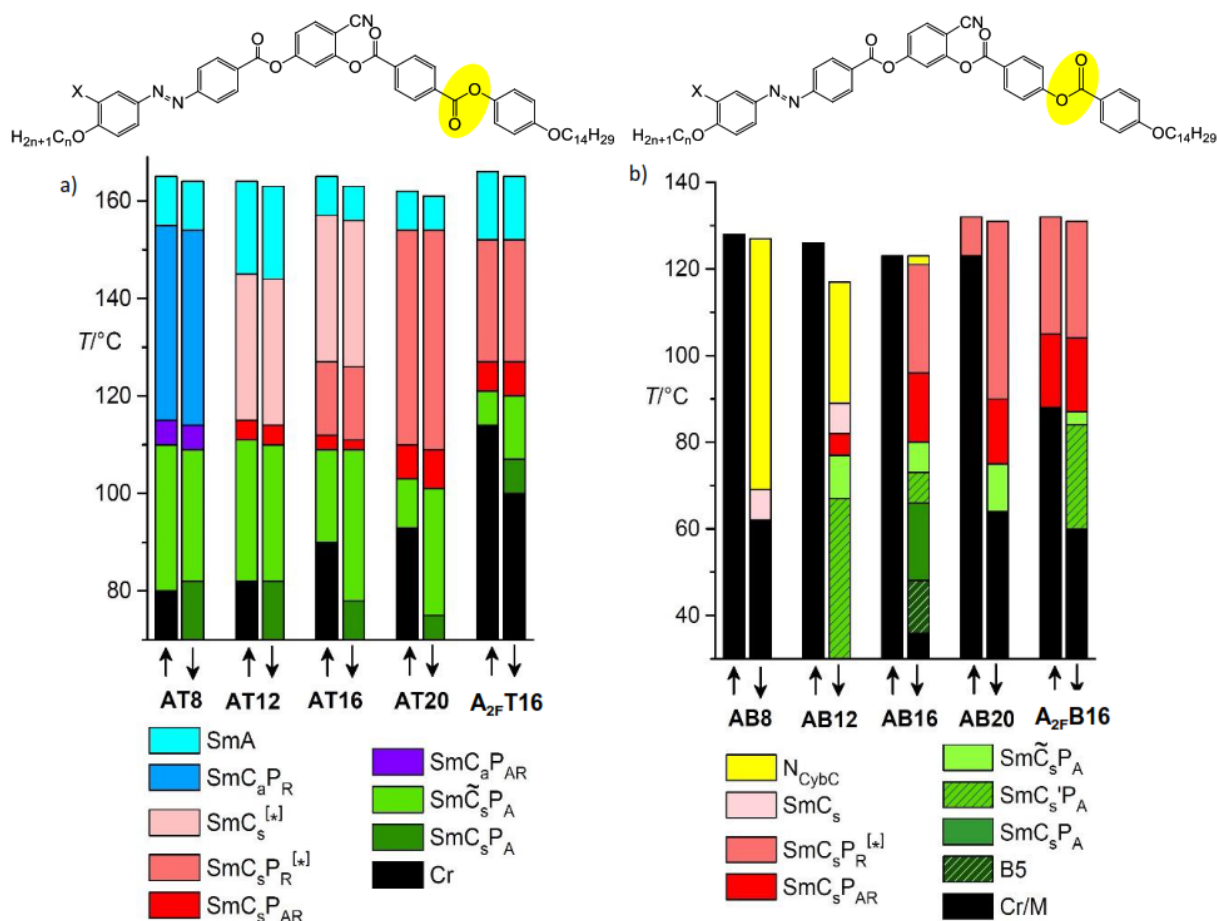


**Figure 15.** Chemical structures and phase behaviour of 4-cyanoresorcinol derived azobenzene-based BCLCs with non-symmetric side arms depending on terminal chain length as a function of temperature: a) Terephthalate-based materials (**AT<sub>n</sub>**, **A<sub>2F</sub>T<sub>16</sub>**) and b) Benzoate-based materials (**AB<sub>n</sub>**, **A<sub>2F</sub>B<sub>16</sub>**).[AA5]

### 3.1.8. Isothermal photo-switching of chirality and polarity

(Pub. AA5)

All previous attempts of photoinduced switching involving azobenzene based BCLCs were focused on a transition from a LC phase such as the antiferroelectric SmCP<sub>A</sub> or the helical superstructure B<sub>7</sub> phase [95] to the isotropic liquid state,[186,187,188,A189] whereas with **AT<sub>n</sub>** and **AB<sub>n</sub>** compounds it was possible for the first time to report an isothermal photo switching of the mode of switching under an electric field as well as an on/off switching of superstructural chirality.[AA5]

For this purpose compound **AB<sub>16</sub>**, placed in a 6 μm ITO cell on a temperature controlled heating stage, was illuminated in the antiferroelectric (AF) state close to the SmC<sub>s</sub>P<sub>AR</sub>-SmC<sub>s</sub>P<sub>R</sub><sup>[\*]</sup> transition temperature, by UV light (wavelength= 405 nm) for 2 s. As shown in **Figure 16**, the AF-like double peak switching changes into a ferroelectric (FE)-like single peak switching and relaxes back almost immediately to the AF-like mode after switching off the light source (< 3 s). Therefore, this allows for the first time a photoinduced change of the mode of the switching.

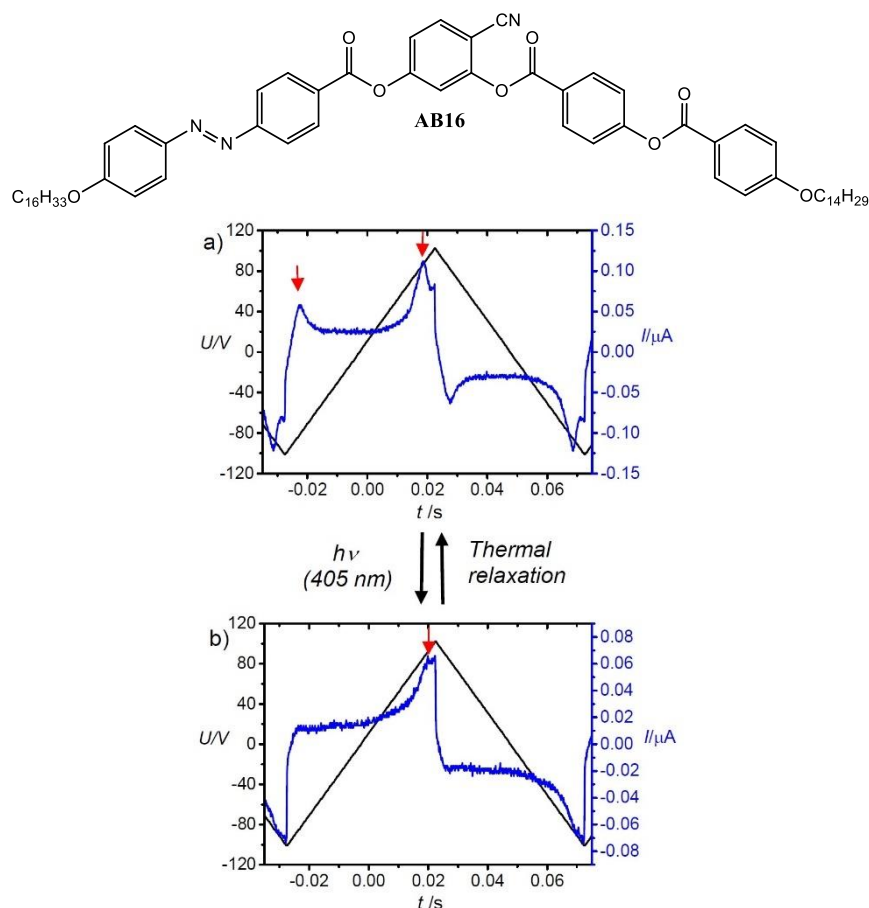


**Figure 16.** Reversible isothermal switching between a) antiferroelectric-like and b) ferroelectric-like switching in the paraelectric SmC phase range as recorded for compound **AB16** at  $T = 101\text{ }^{\circ}\text{C}$  in a  $6\text{ }\mu\text{m}$  ITO cell.[AA5]

For the second case, reported in Pub. [AA5], the chiral  $\text{SmC}_s^{[*]}$  phase of **AT16** (Figure 17a, b) was successfully switched to the achiral SmA phase under light irradiation (405 nm, 5  $\text{mW}/\text{mm}^2$ , Figure 17a-c). The transition to a SmA phase is evident from the optical isotropic appearance in homeotropic alignment, accompanied by the formation of birefringent defects (Maltese crosses, see inset in Fig. 17c). Also, this process is fast and reversible ( $< 3\text{ s}$ ). After switching off the light, the chiral domains almost immediately (within  $< 3\text{ s}$ ) reform (Fig. 17c-e). However, there appears to be no chiral memory, meaning that the positions of the chiral domains change during the switching process (Fig. 17a,b $\rightarrow$ d,e). This is attributed to the fluidity of these smectic phases, leading to movement of the material, but it also shows that the chirality in these phases is unlikely to be based exclusively on a chiral surface effect. The change of molecular shape from a rather well-defined bent shape to a more non-specific one by *trans* $\rightarrow$ *cis* photoisomerization leads to a decrease in the packing density and a reduction of the coherence length of polar order below a critical value, thus the polar order.

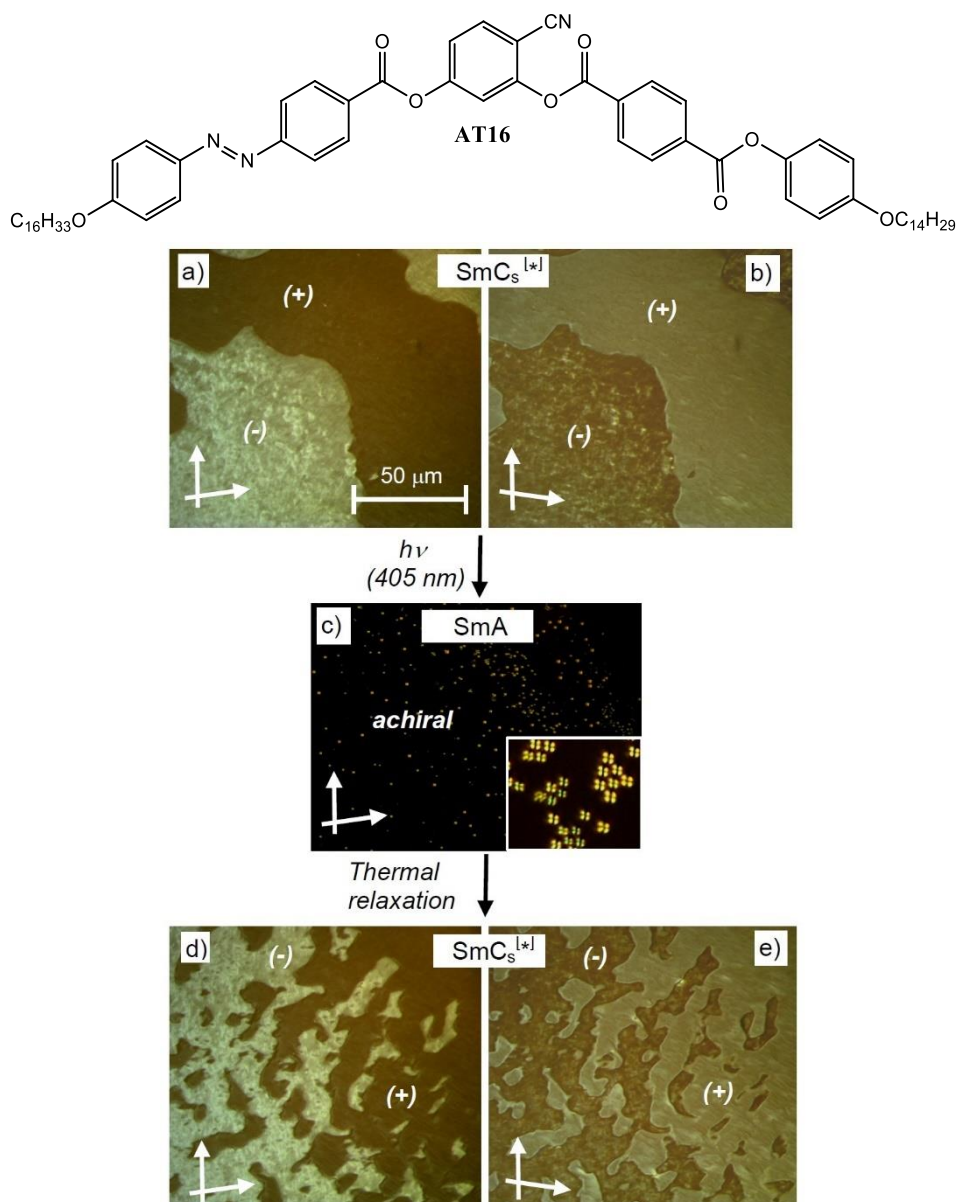


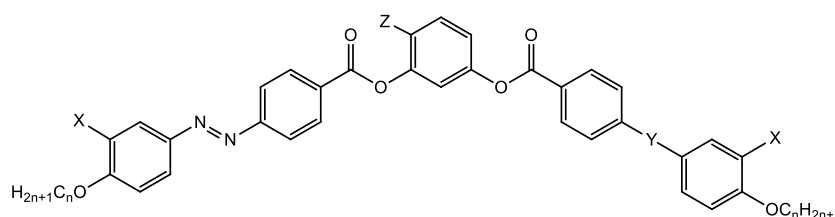
**Figure 17.** Reversible isothermal photo-on-off switching of chirality as observed for **AT16** at  $T = 152$  °C in a homeotropic cell (ca. 10  $\mu m$ ); the inset in c) shows an enlarged region, indicating that the small spots in c) represent Maltese crosses as typical for defects in homotropic  $SmA$  phases.[AA5]

The reduced packing density and polar order is also responsible for the observed photoinduced on-off switching of chirality. A related on-off switching of this kind of superstructural chirality in fluid LCs was only reported in Pub. [AA16] for a sawtooth shaped polycatenar molecule (as will be discussed later in section 4.2.) and for the  $N_{TB}$ -N transition in mesogenic dimers.[190] However, there were no reports of photoinduced chirality switching in any fluid conglomerate type phase of achiral BCLCs.

### 3.2. Other 4-substituents at the resorcinol bent unit

(Pub AA9-AA14)

The first examples of azobenzene-based BCLC derived from 4-substituted resorcinol using different substitution patterns ranging from halogen atoms (I, Br, Cl, F) with different polarities to the non-polar methyl (CH<sub>3</sub>) group were also reported (Scheme 3). In Pub. [AA9-AA14] this was done in a systematic study and leads to a better understanding and new insights about the formation of dark conglomerate (DC) phases, which will be discussed in the following section.



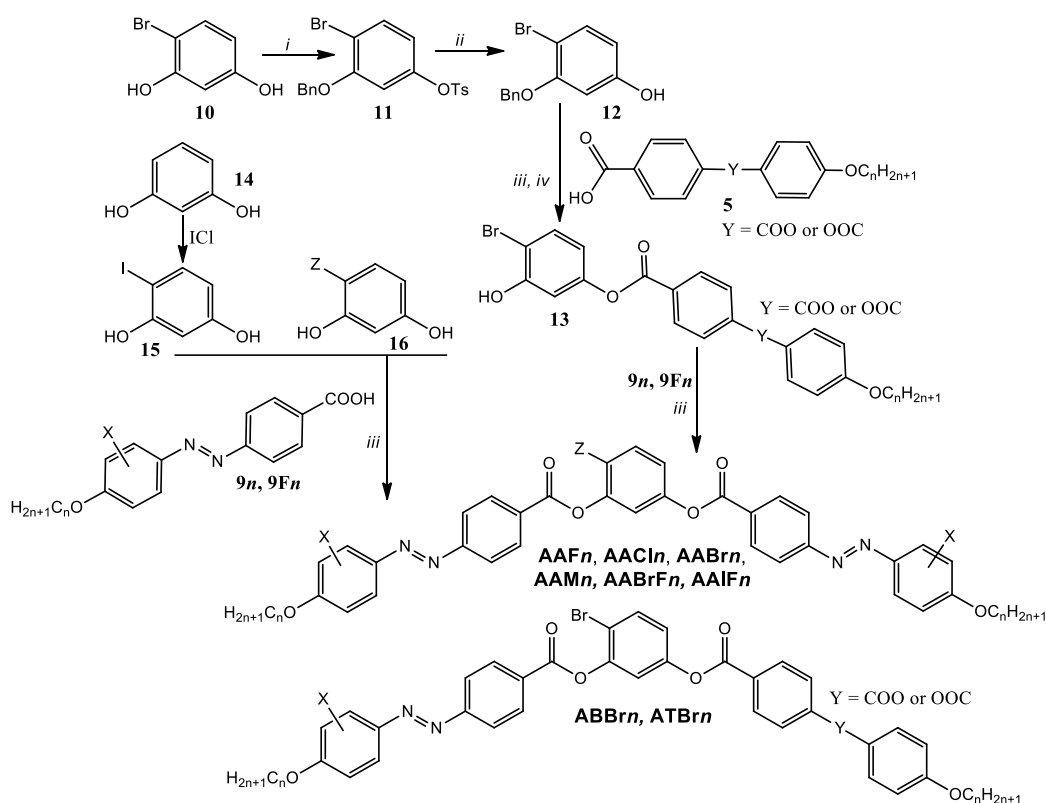
Compound	X	Y	Z	Publications
<b>AAFn</b>	H	N=N	F	AA9
<b>AACln</b>	H	N=N	Cl	AA9
<b>AABrn</b>	H	N=N	Br	AA9
<b>AAIFn</b>	F	N=N	I	AA10
<b>AABrFn</b>	F	N=N	Br	AA11
<b>AAMn</b>	H	N=N	CH <sub>3</sub>	AA12
<b>ABBrn</b>	H	OOC	Br	AA13
<b>ATBrn</b>	H	COO	Br	AA13

**Scheme 3.** Molecular structures of the 4-substituted resorcinol derived BCLCs and their codes.

#### 3.2.1. Synthesis

The synthesis of the 4-substituted resorcinol BCLCs is shown in **Scheme 4**. The synthesis of these compounds starts from commercially available 4-bromoresorcinol (**10**), 4-chlororesorcinol (**16**, Z = Cl), 4-fluororesorcinol (**16**, Z = F) and 4-methylresorcinol (**16**, Z = CH<sub>3</sub>) core units or by synthesizing the 4-iodoresorcinol (**15**) or the protected 4-bromoresorcinol (**12**) as shown in Scheme 4. The synthesis of the final compounds was done in analogous way to that described before for the 4-cyanoresorcinol derived BCLCs (Scheme 2). All synthetic details are described in the corresponding supporting information of Pub. [AA9-AA14].





**Scheme 4.** Synthesis of the 4-substituted resorcinol bent-core materials. Reagents and conditions: *i*: 1. TsCl, K<sub>2</sub>CO<sub>3</sub>, acetone, reflux, 16 hrs, 2. Benzylbromide, reflux, 16 hrs.; *ii*: NaOH, CH<sub>3</sub>OH, reflux, 12 hrs.; *iii*: 1. SOCl<sub>2</sub>, 80 °C, 1 h., 2. removal of excess SOCl<sub>2</sub> under pressure, 3. **10** or **13** or **15** or **16**, DCM, pyridine, 50 °C, 6 hrs; *iv*: H<sub>2</sub>/Pd/C, THF, 48 hrs., 25 °C.[AA9-AA14]

### 3.2.2. Dark Conglomerate formation

An interesting mesophase which could be exhibited by bent core mesogen is the so-called dark conglomerate (DC) phase, representing a mirror symmetry broken mesophase, occurring as an intermediate state between the long-range ordered crystalline or LC state and the disordered liquid. The common feature of all DC phases of BCLCs is their homeotropic appearance i.e. absence of any birefringence under crossed polarizers (**Figure 18b**) due to the distortion of the long-range periodic order. In most cases chiral domains with significant optical activity could be observed by slight rotation of one of the analyzers from the crossed positions in these DC phases (**Figure 18a,c**), though the involved molecules themselves are achiral.

There are two distinct major types of DC phases, the first one is the sponge phase representing a deformed smectic LC phase with sponge like structure and the second type is the helical nano-filament (HNF known also as B4) phases,[87-89,95,191-204] where the molecules are organized in stacks of twisted ribbons forming arrays of helical nano-scale filaments.[205-209,210,215] A major difference between these two types is provided by the local molecular order. In the sponge phases there is a lamellar organization in layers, where the individual

molecules have no fixed positions; hence, these are considered as truly liquid crystalline phases. In contrast, there is crystal-like packing of the polyaromatic cores in the individual nano-scale filaments forming the HNF phases, representing robust glassy solids. Further modifications and intermediate structures between these two types have been also reported.[216-221] For example, there are liquid crystalline DC phases composed of ribbons (modulated DC phases)[222,223] and also sponge-like structures involving hexatic and possibly crystal-like order.[224]

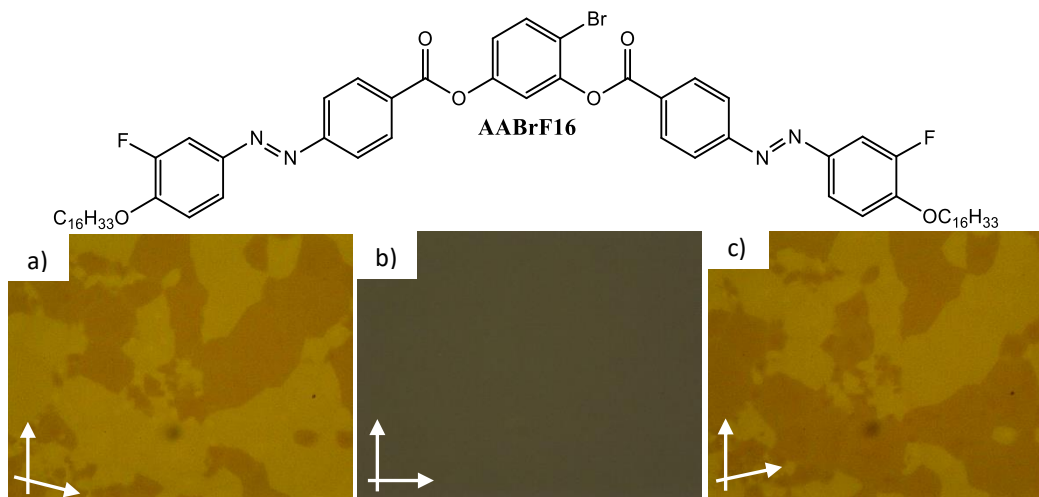


**Figure 18.** Textures of compound **AABrF16** (with  $n = 16$ ) on cooling at  $T = 60$  °C: b) between crossed polarizers; a) after rotating one polarizer by  $7^\circ$  from the crossed position in clock-wise direction and c) in anticlockwise direction, showing dark and bright domains, indicating the presence of areas with opposite chirality sense.[AA11]

In Pub. [AA9-AA14] a third major type of DC phases located between the sponge-like and HNF phases was reported for the azobenzene-based BCLCs derived from 4-substituted resorcinol bent core units (**Scheme 3**). This new class of DC phases are composed of helical nano-crystallite and therefore designated as helical nano-crystallite phases (HNC). Depending on the type of the substituent ( $Z$ ) on the central core different subtypes of these HNC phases were reported but all of them have the same fundamental structure (see Figure 19).

In all cases the formation of HNC phases requires the presence of a bulky substituent at 4-position in the central core units. Therefore, HNC phases were observed in all 4-iodoresorcinol ( $Z = I$ ), 4-bromoresorcinol ( $Z = Br$ ) and 4-methylresorcinol ( $Z = CH_3$ ) derivatives having azobenzene wings, compounds **AAIF $n$** , **AABr $n$** , **AABrF $n$** , **ABB $r$  $n$** , **ATBr $n$**  and **AAM $n$** , respectively (Scheme 4).[AA9-AA13] Peripheral core fluorination was found to induce or suppress HNC phase formation for the complete homologues series depending on the nature of the substituent  $Z$ . In case of 4-iodoresorcinol or 4-bromoresorcinol it induces the HNC, while it suppresses its formation in case of 4-methylresorcinol. In the latter case the azobenzene-based wings were replaced by ester-based arms for some selected examples. This modification

resulted in total removal of the HNC phases and the formation of different types of polar SmC phases depending on the direction the ester groups in the side arms.[AA12]

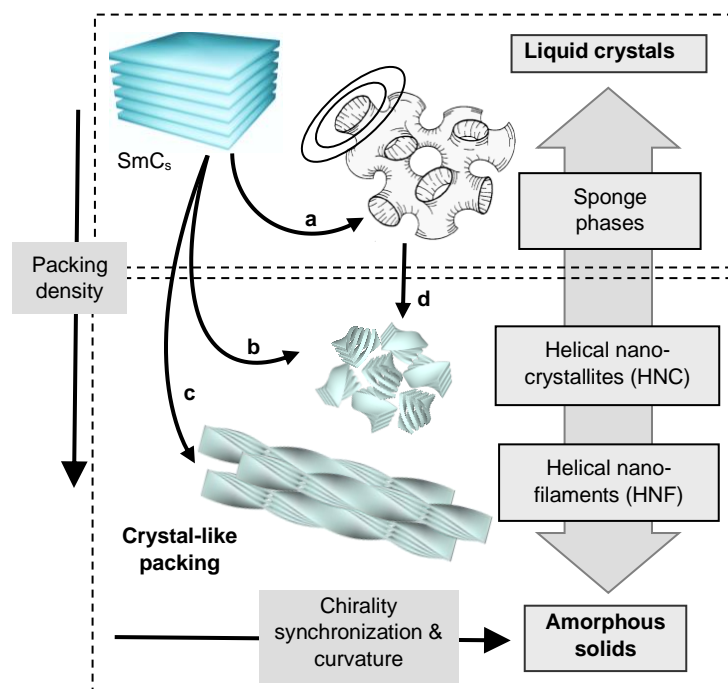


**Figure 19.** The distinct types of dark conglomerate phases (DC phases) formed by BCLCs ranging from isotropic LCs to amorphous solids and their development with increasing average packing density of the involved molecules.[AA13]

Thus, obviously the formation of these HNC requires a rigid side arm with trans double bonds in the linking units such as azobenzene-based or Schiff base containing wings. The more flexible COO linking appears to disfavor formation of crystalline nanofilaments. Therefore, the focus of the work was mainly the azobenzene containing materials.

Replacing the bulky substituent at the apex of the bent-core molecule ( $Z = \text{I, Br, CH}_3$ ) with a smaller halogen group ( $Z = \text{F or Cl}$ ) removes the HNC and instead N, B6 phases or even crystalline materials were observed depending on the nature of the side arms. The B6 phase is characterized by a focal-conic fan-shaped texture with the extinction crosses parallel to polariser and analyser. By shearing this texture no homeotropic alignment with pseudoisotropic texture or schlieren texture could be achieved.[AA9,119,163] Therefore, for symmetrically nonfluorinated side arms with  $Z = \text{F}$ , only crystalline materials were obtained except for the longest derivative with  $n = 16$ , which displays a modulated SmC phase.[AA9] Using the chlorine atom ( $Z = \text{Cl}$ ) induces the formation of N, SmC or B6 phases depending on the nature of the side arms and the direction of the Cl atom with respect to the azobenzene-side arm in case of nonsymmetric bent-core mesogens.[AA9, AA13] Moreover, the presence of Cl group induces the formation of the paraelectric  $\text{SmC}_s^{[*]}$  phase in a short range before the formation of the antiferroelectric  $\text{SmC}_s\text{P}_{\text{AR}}$  phase.[AA13, AA14]

The effect of replacing one of the azobenzene wings with ester-based wing in case of 4-bromoresorcinol derived BCLCs was also investigated (compounds **ABBrn** and **ATBrn**, Scheme 3).[AA13] It was found that the direction of the ester group plays an important rule on the formation of the HNC phases. Therefore, using a phenyl benzoate wing (compounds **ABBrn**, Scheme 3) mainly stabilizes the conglomerate phases, while inverting the direction of the ester unit i.e. replacing the benzoate unit with a terephthalate one suppress the formation of the HNC phases and induces smectic phases, which were found to be polar phases.[AA13]

The effect of double core fluorination on the formation of HNC and polar LC phases was also investigated in detail using different 4-bromoresorcinol or 4-chlororesorcinol units and symmetrically difluorinated azobenzene-based wings and the results are given in Pub. [AA14].

From XRD investigations, there are clear difference in the XRD patterns of the methyl substituted and the halogen substituted BCLCs (see **Figure 20a**), indicating that the HNC phases of compounds **AAMn** are different from those of **AABrFn** and **AAIFn**. The presence of only lower harmonics (up to the 4<sup>th</sup>) of the layer reflections (5<sup>th</sup> and 6<sup>th</sup> order harmonics of the layer reflections has been reported for typical B4 phases, see for example Fig. 20b [207]) and the significantly increased broadness of the wide-angle scatterings indicates a stronger distortion of layer structures and filament formation in the case of the halogen substituted compounds.

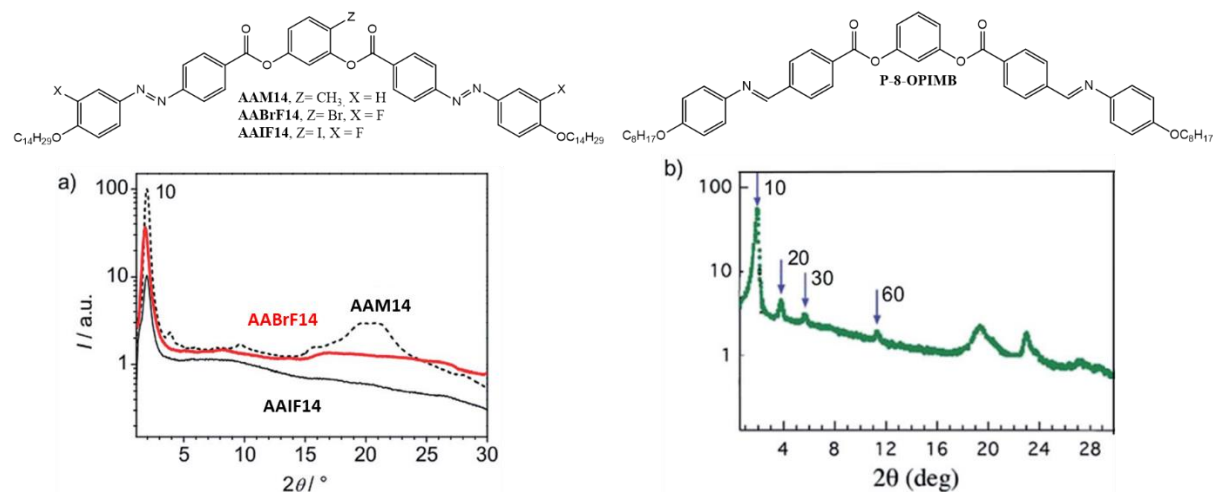


**Figure 20.** a) Comparison of the  $2\theta$ -scans of the HNC phases of compounds **AABrF14**, **AAIF14** and **AAM14** and (b) typical  $2\theta$ -scans of a HNF phase (B4 phase) of a benzylideneaniline based bent-core mesogen (P-8-OPIMB).[ AA11,207]

The missing of HNC phases in 4-cyanoresorcinol derived materials discussed before (Scheme 1) compared to the materials discussed in this section (Scheme 3) was understood based on the DFT calculations as reported in Pub. AA11. From the DFT calculations it appears

that the 4-CN group reduces the molecular bend (larger opening angle  $\psi$ ), but induces a relatively large twist  $\alpha$  between the  $\pi$ -planes of the wings ( $\alpha = 86^\circ$ , Figure 21).[AA11] This obviously retains flat layers and supports the development of a heliconical twist between the layers by the twist between the alkyl end-chain orientations, thus supporting the formation of the heliconical phases, namely the short pitch  $\text{Sm}(\text{CP})^{\text{hel}}$  phase [A156,A183,A185] and the surface stabilized long pitch heliconical states in the  $\text{N}^{[*]}$  and  $\text{SmC}_s\text{P}_R^{[*]}$  phases.[179,A1,AError! Bookmark not defined.] However, this twist  $\alpha$  obviously does not produce a sufficient transversal twist of the layers themselves, required for the formation of HNC phases. This transversal twist obviously requires a stronger molecular bend, i.e. an opening angle  $\psi$  close to  $120^\circ$ . In addition, the bulkiness of the halogens and  $\text{CH}_3$  provide significant layer distortion, destabilizing the layers and allowing an easier layer deformation, which support HNC phases formation.

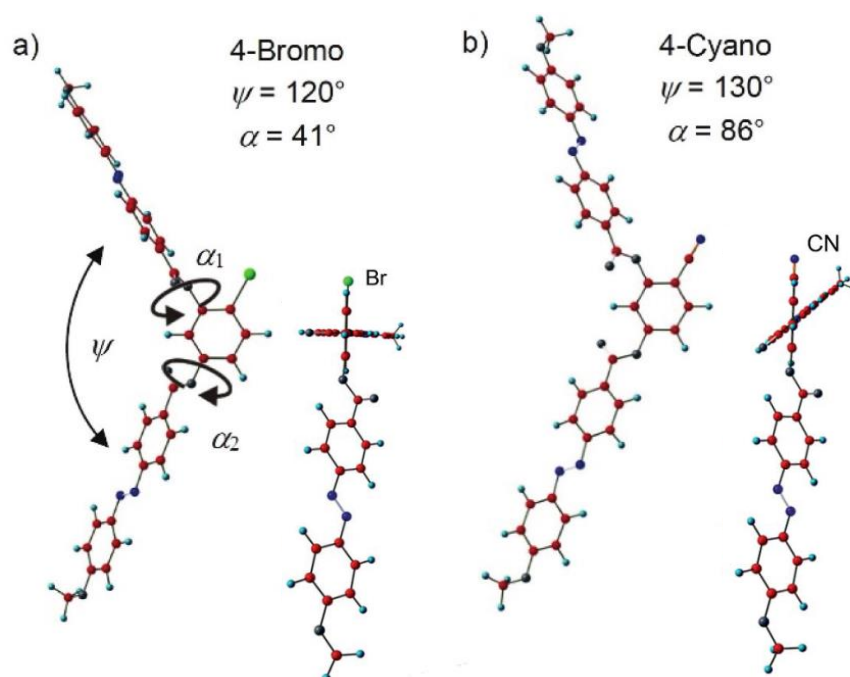


**Figure 21.** Energy minimum conformations obtained by DFT calculations for (a) the 4-bromo- and (b) 4-cyanoazobenzene based BCLCs with azobenzene wings.[ AA11]

Therefore, this systematic study in Pub. AA13 contributes to the understanding of DC phase formation by achiral bent-core systems and provides important guidelines for the molecular design of new materials forming mirror-symmetry broken HNC phases. The most important results could be understood from **Figure 19**, with growing packing density there are at least three distinct major types of DC phases, (i) the fluid sponge phases, (ii) the HNC phases and (iii) the HNF phases.

In the sponge phases chirality synchronization takes place before crystalline packing is achieved and thus is based on a dynamic route of mirror symmetry breaking (route **a**, Fig.

19).[143] In the HNC and HNF phases macroscopic chirality develops together with the evolving crystal-like packing of the molecules (routes **b**, **c**, Fig. 19). In the HNC phases considered here, layer deformation develops simultaneously with the emergence of crystal-like core packing, but alternatively, this process could also take place in two separate steps by crystallization of previously formed sponge phases (route **a+d**, Fig. 19).[224] It is proposed that all three sources of chirality, conformational molecular chirality, supramolecular helical twist and superstructural layer chirality contribute cooperatively to the mirror symmetry breaking in soft matter systems formed by BCLCs.[143]

As mentioned before, the subject of azobenzene-based containing BCLCs was reviewed in 2016 in reference [A123]. Moreover, in cooperation with other co-workers detailed photoisomerization studies for some selected series of the discussed azobenzene-based BCLCs were performed to study the effect of the substituent at the apex as well as peripheral substitution on the photo switching process.[A225] In the same work the possibility of using some selected examples of such BCLCs in optical storage devices was also investigated and the results are given in reference [A225].

#### 4. Photo-responsive polycatenars

(Pub AA15-AA30)

##### 4.1. Overview

The surprising first experimental observation of spontaneous mirror symmetry breaking in the isotropic liquid phase ( $\text{Iso}_1^{[*]}$ ) of achiral polycatenar molecule was reported in 2014 for the bithiophene based compound **Th6/6**, **Figure 22**).[226]

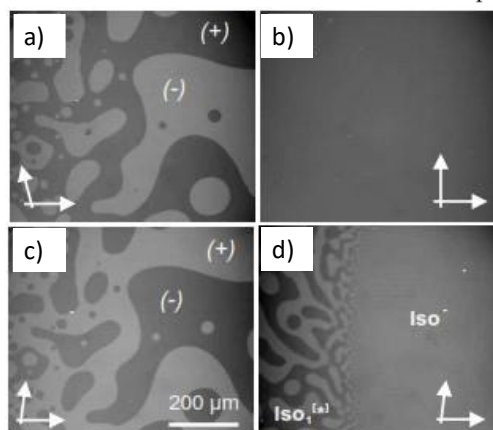
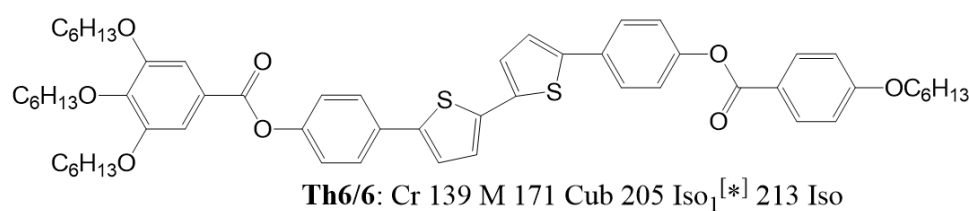


**Figure 22.** Chemical structure and phase transition temperatures of the first reported polycatenar compound (**Th6/6**) showing mirror symmetry breaking in the isotropic liquid ( $\text{Iso}_1^{[*]}$ ); a-c) chiral domains in the  $\text{Iso}_1^{[*]}$  phase;

a), c) between polarizers slightly uncrossed in opposite directions, b) between crossed polarizers and d) Iso-Iso<sub>1</sub><sup>[\*]</sup> transition on cooling showing the formation of chiral domains at the phase transition at  $T = 213$  °C.[226]

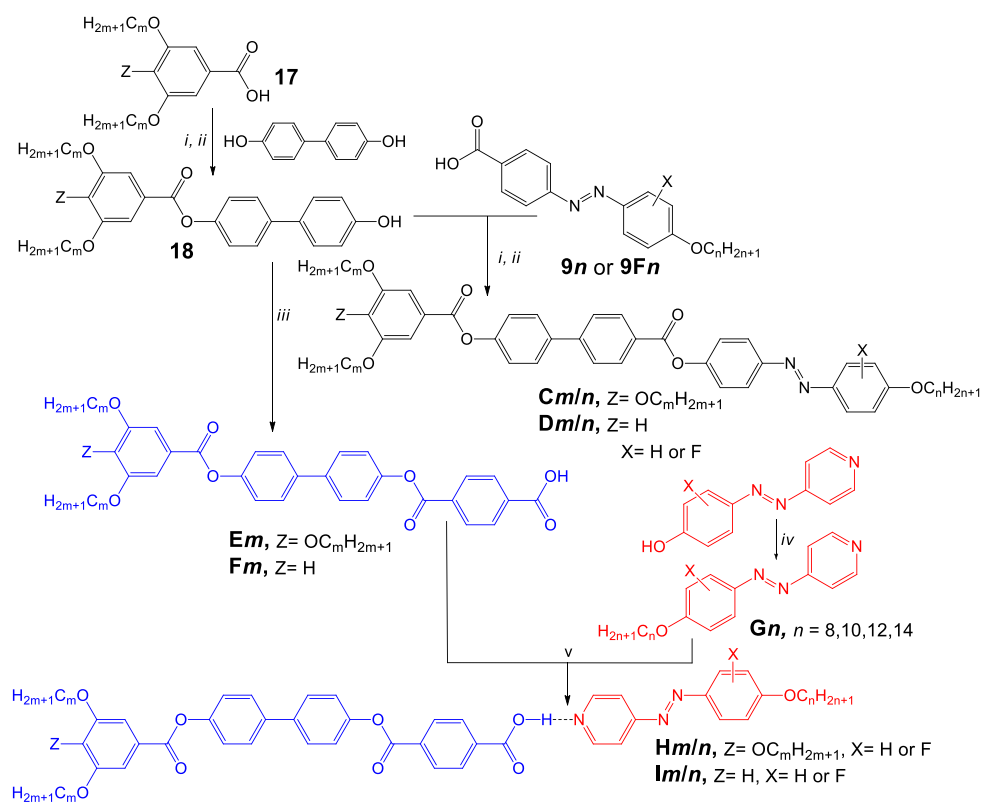
Formation of this Iso<sub>1</sub><sup>[\*]</sup> phase obviously requires a locally twisted cluster structure of the liquid, providing cooperativity and acting as a template for chirality synchronization.[226,143] The few examples known to display Iso<sub>1</sub><sup>[\*]</sup> phases were in most cases metastable, with only few exceptions, meaning that they could only be detected on cooling. Moreover, they were found at high temperatures around  $\sim 210$  °C, where the decomposition becomes an issue, thus making their investigation and application difficult.

Therefore, the focus was to design new polycatenar materials capable of displaying Iso<sub>1</sub><sup>[\*]</sup> phases at reasonable temperature to make their investigations easier. Another target was to produce materials which could be applied for optical storage devices and other potential application, and therefore the azobenzene unit was incorporated into the molecular structures of the target materials as reported in Pub. AA15-AA27. Moreover, different intermolecular interactions such as hydrogen or halogen bonding were used to obtain azobenzene-based supramolecular polycatenars (Pub. AA19-AA22). This resulted not only in wide ranges of Iso<sub>1</sub><sup>[\*]</sup> phases but also in interesting new liquid crystalline phases and phase sequences. The results of this work will be the focus of the following sections.

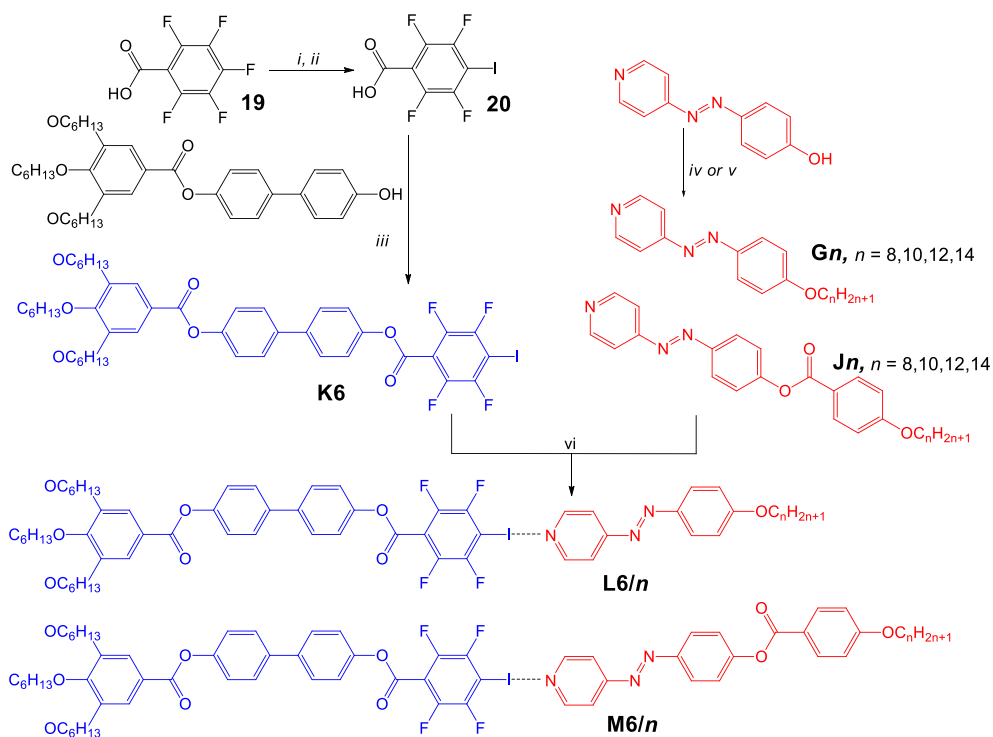
#### 4.1.1 Synthesis

The synthesis of the azobenzene-based polycatenars either having four (**Cm/n**) or three terminal (**Dm/n**) chains is shown in **Scheme 5**. [Pub. AA15-AA18] The synthesis starts from the multichain benzoic acids by an acylation reaction with 4,4'-dihydroxybiphenyl to get the mono ester compounds **18** which then were used in another acylation reaction with the benzoic acids **9n** and **9Fn**.

The supramolecular polycatenars constructed by intermolecular interaction either hydrogen (**Hm/n** and **Im/n**) or halogen bonding (**L6/n** and **M6/n**), respectively were synthesized according to the synthetic routes shown in **Scheme 5** and **6**. The hydrogen-bonded supramolecules **Hm/n** and **Im/n** were constructed using multichain benzoic acid derivatives **Em** and **Fm** as the proton donors and the azopyridine derivatives **Gn** as the proton acceptors (Scheme 5). [Pub. AA19-AA21] The halogen-bonded supramolecules **L6/n** and **M6/n** were synthesized according to scheme 6 using the same azopyridines **Gn** or with additional benzene ring (**Jn**) as the halogen bond acceptors [Pub. AA22] and the 4-iodotetrafluorobenzoates **K6**. All synthesis details are given in the corresponding publications and described in their supporting information. [AA15-AA22]



**Scheme 5.** Synthesis of the tetracatenars **Cm/n**, tricatensars **Dm/n** and the supramolecular hydrogen-bonded polycatenars **Hm/n** and **Im/n**. Reagents and conditions: i. SOCl<sub>2</sub>, DMF, reflux, 1 h.; ii. Et<sub>3</sub>N, dry pyridine, DCM, reflux 6 hrs.; iii. 1. 4-Formylbenzoic acid, DCC, DMAP, DCM, stirring 48 hrs., 2. NaOCl<sub>2</sub>, NaH<sub>2</sub>PO<sub>4</sub>, resorcinol, stirring overnight; iv. BrC<sub>n</sub>H<sub>2n+1</sub>, KI, K<sub>2</sub>CO<sub>3</sub>, DMF, stirring, 50 °C, 48 h; v. Melting with stirring. [AA15-AA18, AA19-AA21]

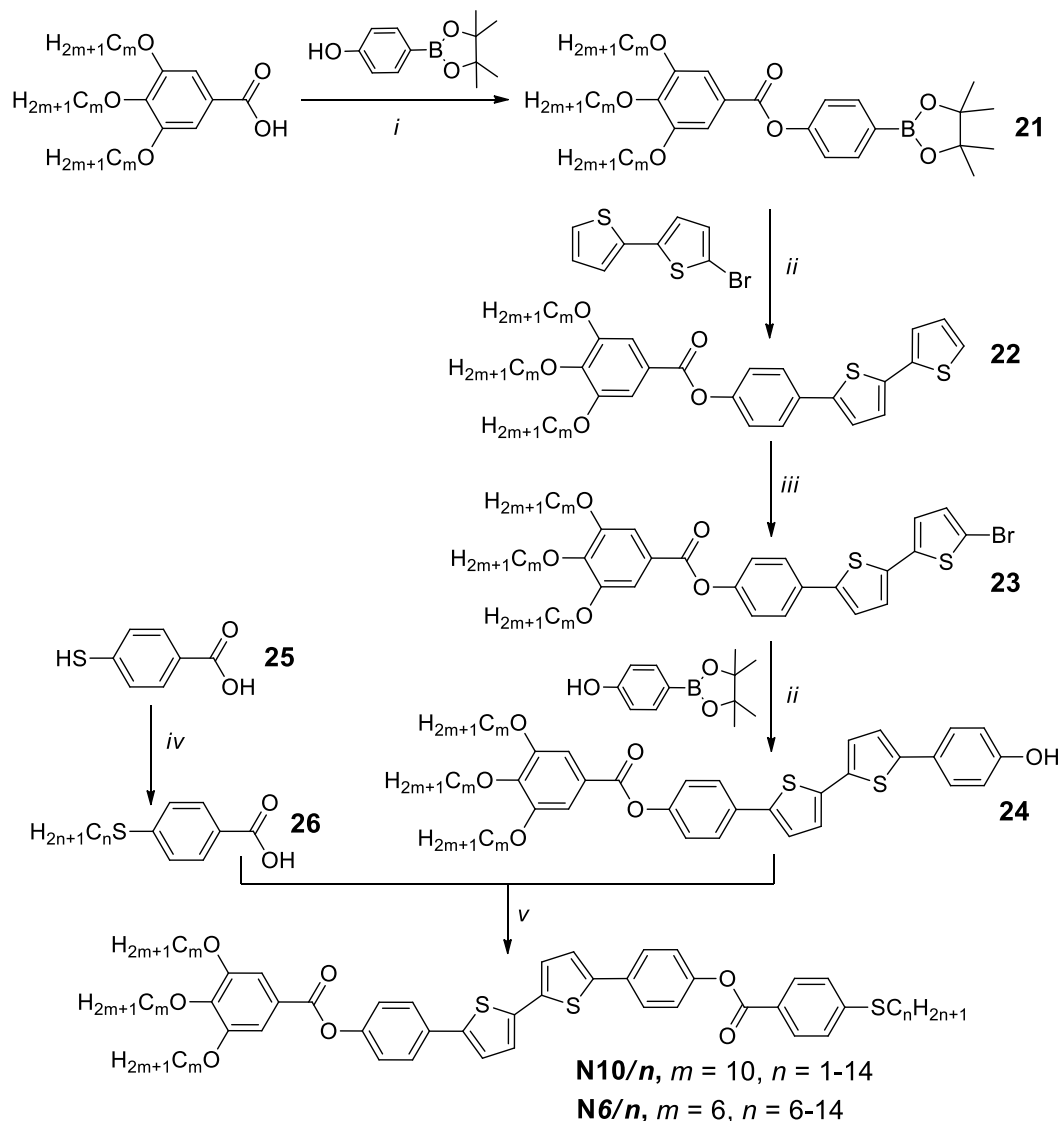


**Scheme 6.** Synthesis of the supramolecular halogen-bonded polycatenars **L6/n** and **M6/n**. Reagents and conditions: i. Zn/NH<sub>3</sub> aq.; ii. *n*-BuLi, I<sub>2</sub>; iii. DCC, DMAP, DCM, stirring, rt., 24 h; iv. For **Gn** compounds:



BrC<sub>n</sub>H<sub>2n+1</sub>, KI, K<sub>2</sub>CO<sub>3</sub>, DMF, stirring, 50 °C, 48 h; v. For **Jn** compounds: 4-*n*-alkoxybenzoic acids, DCC, DMAP, DCM, stirring, rt., 48 h; vi. Melting with stirring.[AA22]

Related polycatenars **Nm/n** without azobenzene unit but derived from a bithiophene core and terminated with thioalkyl chains were synthesized as described in Pub. AA23 and shown in **Scheme 7**.



**Scheme 7.** Synthesis of bithiophene-based polycatenars without azobenzene unit. Reagents and conditions: i. DCC, DMAP, DCM, RT, stirring; ii. [Pd(PPh<sub>3</sub>)<sub>4</sub>], THF/sat. NaHCO<sub>3</sub>-solution, reflux; iii. NBS, THF, RT, absence of light; iv. 1. Absolute EtOH, KOH, H<sub>2n+1</sub>C<sub>n</sub>Br, 2. NaOH solution, reflux, 3. H<sup>+</sup>; v. 1. SOCl<sub>2</sub>, 2. Triethylamine, pyridine, DCM, reflux.[AA23]

#### 4.2. Isothermal photo switching of chirality with nonpolarized light

Compound **C6/8**, reported in Pub. AA15 (**Scheme 5**), represents the first example of azobenzene-based polycatenar exhibiting mirror-symmetry breaking in the isotropic liquid phase (Iso<sub>1</sub><sup>[\*]</sup>), in this case occurring beside tetragonal (Tet) liquid crystalline phase as indicated

from the optical texture investigations (Figure 23 a-c). The Tet phase observed in this material is a 3D non-cubic LC network phase characterized by high viscosity and high birefringence. It was found that the Iso<sub>1</sub><sup>[\*]</sup> phase occurs at lower temperature compared to that of the bithiophene-based material TH6/6 (Figure 22) and therefore, its investigation with XRD was possible (Fig. 23d).[AA15]

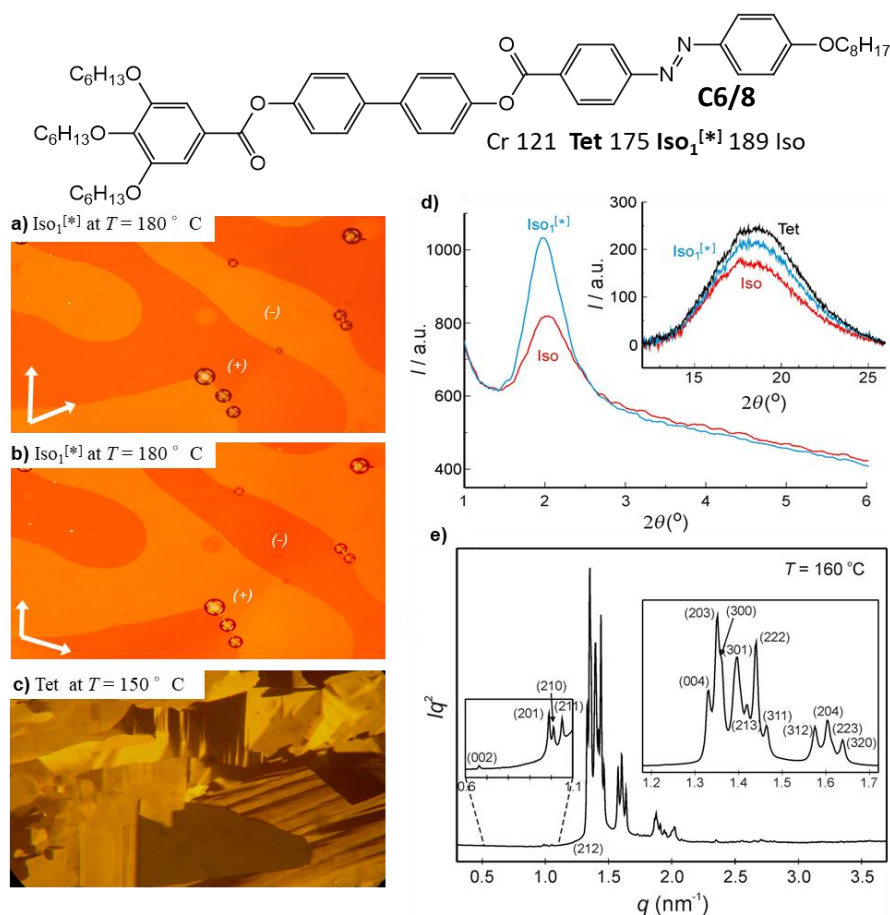


**Figure 23.** Chemical structure and transition temperatures of the first example of azobenzene-based polycatenar (**C6/8**) exhibiting Iso<sub>1</sub><sup>[\*]</sup> phase. a) and b) Textures of the Iso<sub>1</sub><sup>[\*]</sup> phase at T = 180 °C under slightly uncrossed polarizers either in clockwise or anticlockwise directions; c) texture of the Tet phase T = 150 °C; d) small-angle and wide-angle (inset) XRD diffractograms at different temperatures for the achiral Iso phase at T = 195 °C, the chiral Iso<sub>1</sub><sup>[\*]</sup> phase at T = 180 °C, and Tet phase at T = 170 °C; e) SAXS diffractogram of the Tet phase at T = 160 °C with indexation.[AA15]

XRD investigation of the Iso and Iso<sub>1</sub><sup>[\*]</sup> phases of compound **C6/8** shown in both Iso phases a diffuse small- and wide-angle scattering (Fig. 23d). The position of the maximum of the small angle scattering is at  $d = 4.3\text{-}4.4$  nm, corresponding approximately to the molecular length ( $d/L_{\text{mol}} = 0.87\text{-}0.90$ ). This indicates that the Iso<sub>1</sub><sup>[\*]</sup> phase has a cybotactic structure. The clusters appear to have a helical or a twisted lamellar local structure acting as template for helical molecular packing with long range chirality synchronization. At the Iso<sub>1</sub><sup>[\*]</sup>-Tet transition the local clusters fuse to a long-range 3D structure forming the tetragonal lattice. Whether the chirality is retained or lost at the transition to the Tet phase is difficult to decide

because of the high linear birefringence observed in the Tet phase. However, a related Tet phase exhibited by another azobenzene-based tetracatenar analogue was recently investigated in details with resonant soft X-ray scattering (RSoXS) and its exact structure was successfully solved as described in ref. A227 and as will be discussed later (see section 4.3).

In Pub. AA15 it is shown, how the type of LC phases as well as the range of Iso<sub>1</sub><sup>[\*]</sup> phase observed in compound **C6/8** were successfully controlled by aromatic core fluorination either in outer or inner positions of the rod-like backbone or by double fluorination.[AA15]

As described in Pub. AA15, the photoisomerization of **C6/8** was investigated in solution but it was difficult to measure in the bulk state i.e. in the LC phase, which is attributed to the kinetic hindrance of the three-dimensional structure of the Tet phase. To overcome this problem, compound **D6/8** with Z = H (**Scheme 5**) i.e. with one terminal chain less at the crowded end compared to compound **C6/8** was designed and synthesized. This slight modification results in removing the 3D Tet phases and the observation of the Iso<sub>1</sub><sup>[\*]</sup> phase beside a fluid lamellar LC (SmA) phase. This allowed the demonstration of the first report of a fast and reversible photoinduced switching between an achiral LC phase (SmA) and a mirror symmetry broken isotropic liquid (Iso<sub>1</sub><sup>[\*]</sup>) with non-polarized light (**Figure 24**) as outlined in detail in Pub. AA16.

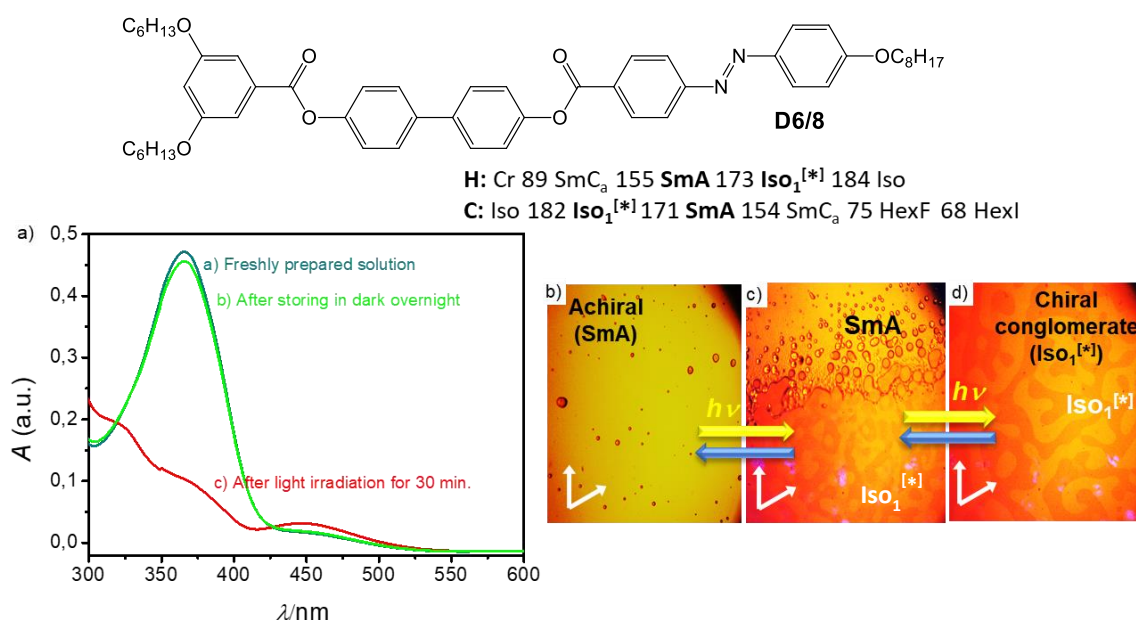


**Figure 24.** Chemical structure and transition temperatures of compound **D6/8**. a) UV-vis spectra of **D6/8** dissolved in chloroform at 25°C. b-d) Isothermal photo induced SmA-to-Iso<sub>1</sub><sup>[\*]</sup> transition observed for **D6/8** under slightly uncrossed polarizers at  $T = 168$  °C: b) SmA phase before illumination with non-polarized 405 nm laser light (5 mW/mm<sup>2</sup>); c) during SmA-to-Iso<sub>1</sub><sup>[\*]</sup> transition upon starting of illumination and d) Iso<sub>1</sub><sup>[\*]</sup> phase as observed during illumination. The reverse sequence is obtained immediately after switching off the light source.[AA16]

### 4.3. From meso-structures to conglomerate formation in liquid and liquid crystalline networks

The  $Cub_{bi}/Ia\bar{3}d$  phase is one of the nature's most symmetric and complex structures, the electron density map of which was established long time ago.[228] It is composed of two enantiomorphous helical networks and therefore represents an achiral meso-structure (**Figure 25a,b**), i.e. there is enantiophilic coupling between the networks. Using compound **C10/18** and utilizing small-angle X-ray scattering, resonant soft X-ray (RSoXS) scattering at the carbon K edge and model-dependent tensor-based scattering theory, Yu Cai et al. elucidate the morphology and investigated the molecular packing in the double gyroid phases formed by **C10/18**. [A136] The study revealed that, the spatial variation of molecular orientation through the channel junctions in the double gyroid phase can be either continuous in the case of anisotropic channels or discontinuous in the case of isotropic channels depending on the molecular structure and shape. Only the anisotropic channels lead to a helical organization of the rod-like polycatenar molecules along these channels, whereas flexible molecules assume a randomized organization. [A136]

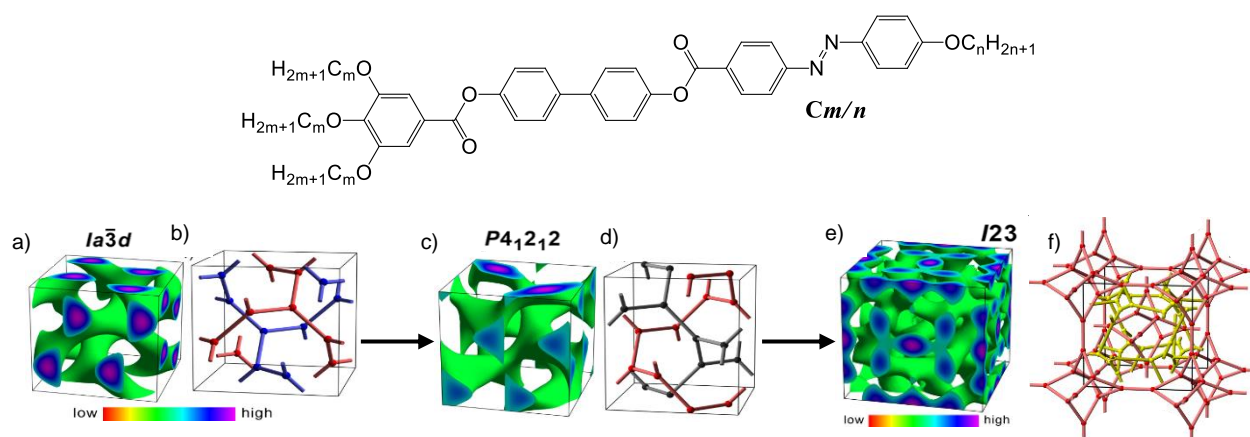


**Figure 25.** Helical network 3D phases formed by compounds **Cm/n**: a, c, e) the reconstructed 3D electron maps in the achiral double gyroid  $Cub_{bi}$  with  $Ia\bar{3}d$  space group; in  $Tet_{bi}$  phase and in the chiral triple network  $Cub_{bi}$  with space group  $I23^{[*]}$  phase, respectively; b, d, f) corresponding schematic presentations of their network structures; in b) there are two enantiomorphous networks with opposite helicity (blue/red), in d) one of the networks (grey) has a reduced coherence length of helix sense and in f) there are two similar networks (red) and the third one is different (yellow). [AA18]

On the other hand, the  $I23$  phase being composed of three networks (Fig. 25e,f) is always chiral and typically forms a conglomerate of chiral domains ( $Cub_{bi}^{[*]}/I23$ ) meaning that the network coupling becomes enantiophobic. [133] The detailed investigation performed by Yu Cai et al. for compound **C10/18** using different XRD techniques leads to the discovery of a new bicontinuous tetragonal LC ( $Tet_{bi}$ ) phase and its structure was successfully solved and shown to form a pair of chiral  $P4_12_12$  and  $P4_32_12$  space groups (Figure. 25c,d) as described in ref. [A227]. The tetragonal phase is in this case observed as an intermediate phase at the transition

from enantiophilic self-assembly in the achiral  $Ia\bar{3}d$  phase to enantiophobic one in the chiral  $I23$  phase. At this transition one of the enantiomorphic networks in the  $Ia\bar{3}d$  meso-structure is racemized in the  $Tet_{bi}$  phase, which synchronizes its chirality at the transition to the  $I23$  phase. These findings could help to understand the exact structure of the Tet phase mentioned above for compound **C6/8** [AA15] and other unsolved Tet-phases which are currently under investigation.

Pub. AA18 reports the synthesis and investigation of a complete series of compounds **C10/n**, having  $m = 10$  and  $n = 5-20$ . Depending on the chain length and temperature these achiral polycatenars self-assemble into a series of liquid crystalline helical network phases (**Figure 26**). Whereas the chiral  $Iso_1^{[*]}$  and  $Cub_{bi}^{[*]}/I23$  were found for the short chain compounds, non-cubic and achiral cubic phases dominate for the long chain compounds. Among them a nanoscale conglomerate with  $I23$  lattice, a tetragonal phase ( $Tet_{bi}$ ) with  $P4_12_12$  and  $P4_32_12$  space groups combining a chirality synchronized and a non-synchronized achiral network like that reported for **C10/18**, [A227] an achiral double network *meso*-structure with  $Ia\bar{3}d$  lattice and an achiral percolated isotropic liquid mesophase ( $Iso_1$ ).

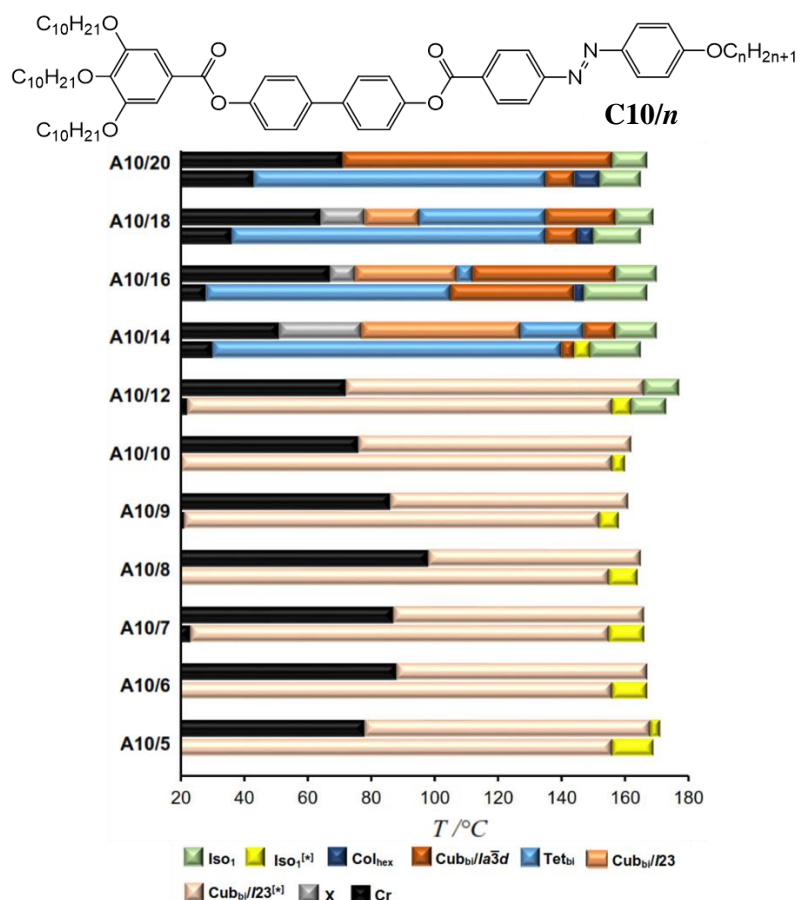


**Figure 26.** Chemical structure and bar diagram of the tetracatenars (**C10/n**) showing the mesophases and phase transition temperatures on cooling (lower bars) and on heating (upper bars). [AA18]

This sequence is attributed to a decreasing strength of chirality synchronization between the networks, combined with a change of the preferred interhelical network interaction from enantiophobic to enantiophilic with growing chain length. This work provided an understanding of spontaneous mirror symmetry breaking and the factors leading to chirality synchronization in these achiral materials. Moreover, these nanostructured phases exist over wide temperature ranges which is of interest for potential applications requiring fast charge transfer.[141]

Pub. AA23 reports 5,5'-diphenyl-2,2'-bithiophene based polycatenars (**Nn/m**) with a fork-like triple alkoxyated end and a thioether chain with variable length at the monosubstituted apex (for the synthesis, see **Scheme 7**). The effect of the thioalkyl chain length on the development of helical and mirror symmetry broken soft matter network phases was investigated and compared to the related analogues terminated with alkoxy chains.[138,226] In these materials also helical self-assembly of the  $\pi$ -conjugated rods in networks occurs, leading to broad temperature range (> 200 K) of bicontinuous cubic network phases. Full details are given in Pub. AA23.

Comparing some of compounds **Nn/m** with their related alkoxy-substituted derivatives (**Figure 27**) indicate that the same phase types and phase sequences are observed in both cases. However, replacing S by O increases the Iso<sub>1</sub><sup>[\*]</sup> ranges on the expense of the Cub<sub>bi</sub> phases. For the pair **N10/1**, **Th10/1** an increased stability of the cubic phase is observed by replacing O by S, whereas for the materials with longer chains ( $n = 6, 10$ ) this order is reversed.

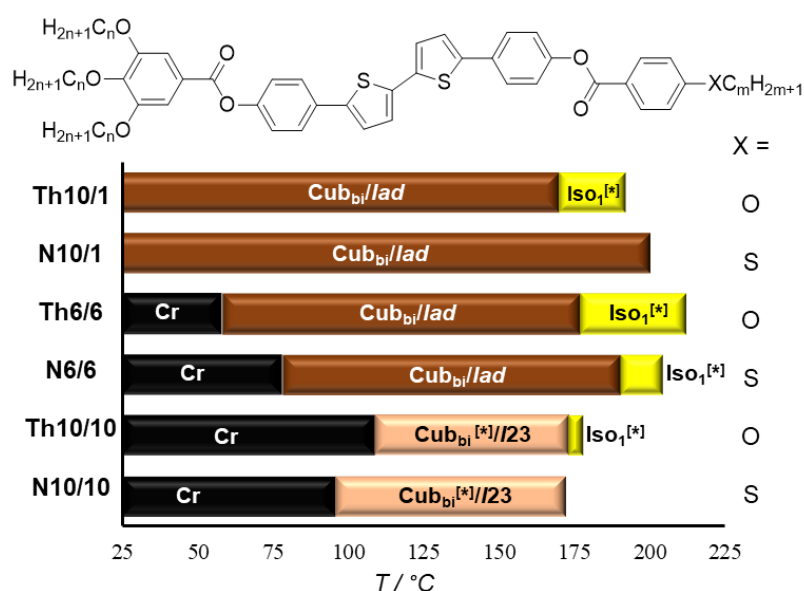


**Figure 27.** Phase transitions of the polycatenar compounds **N10/1**, [AA23] **N10/10**, [AA23] **N6/6** [AA23] and their related analogues **B10/1**, [138] **B10/10** [138] and **B6/6** [226] as observed on cooling (DSC with rate 10 K min<sup>-1</sup>).

The main effects of replacing ether by thioether linkages are a decreased C-S-C bonding angle ( $99^\circ$ ) compared to C-O-C ( $114^\circ$ ),[229] a changed molecular shape from almost rod-like to more bent and an increased C-S bond length (1.82 nm) compared to C-O (1.45 nm).[229] The latter decreases the rotational barrier around the C-S bonds compared to the C-O bonds (O-CH<sub>3</sub>: 11.3 kJ mol<sup>-1</sup>; S-CH<sub>3</sub>: 8.4 kJ mol<sup>-1</sup>) and thus increases conformational chain mobility.[230,231] Increased conformational chain disorder of arylthioethers is also supported by the decreased conjugation of S with the benzene ring if compared with related aryloethers.[232] Moreover, the reduced electronegativity of S compared to O leads to reduced dipolar intermolecular interactions whereas its larger electric polarizability provides stronger dispersion forces between the thioethers. In cases where the conformation is biased, as in heterocycles, a strong mesophase stabilizing effect of S compared to O of about 20 K per S was observed.[233] In contrast, the enhanced conformational flexibility around the C-S bonds reduces the stability of LC phases if an alkyl chain is attached to a core unit via a thioether linkage.[234,235] The increased stability of the LC phases can be attributed to the increased attractive dispersion forces provided by the larger sulphur. For the longer chain this stabilizing effect of S is compensated by its mesophase destabilizing effect due to the increased conformational chain mobility and therefore the effect of replacing O by S is reversed for the longer homologues. The increased chain mobility is likely to also contribute to the reduced melting points and reduced crystallization tendency of the thioethers and widens the Cub<sub>bi</sub> ranges in all cases.[AA23,138,226]

#### 4.4. Synclincic-anticlincic transitions and spontaneous helix formation

Another interesting series of Y-shaped achiral azobenzene-based tricaténars (compounds **D6/n**, Scheme 5) with a 3,5-disubstitution pattern at one end was reported in Pub. AA17.

As mentioned before (section 4.2), it was possible with one member from this series (compound **D6/8**) to photo switch between chiral and achiral states.[AA16] However, this was not the only interesting point with these materials, where it was found that they provide a rich variety of distinct modes of LC self-assembly, including hexatic phases (HexF<sub>s</sub>, HexI<sub>s</sub>, HexB), synclincic (SmC<sub>s</sub>) and the rarely observed anticlincic tilted smectic C phases (SmC<sub>a</sub>), achiral Cub<sub>bi</sub>/*Ia3d*, and chiral (Iso<sub>1</sub><sup>[\*]</sup>) as well as achiral (Iso<sub>1</sub>) isotropic liquid network phases (**Figure 28**). An additional uniaxial tilted smectic phase is observed at the transition between anticlincic and synclincic tilt correlation in compounds **D6/n** and was investigated by soft resonant X-ray scattering by Chenhui Zhu.[AA17]

Especially notable were the broad regions of the SmC<sub>a</sub> phases achieved with these achiral compounds, providing a new design concept for anticlincic smectics, eventually leading

to practically important orthoconic LCs.[236] Moreover, the phase transitions from smectic to hexatic phases is associated with a change of the layer correlation from anticlinic to synclinic on cooling, which is opposite to the usually observed  $\text{SmC}_s$  to  $\text{SmC}_a$  transitions.[AA17]

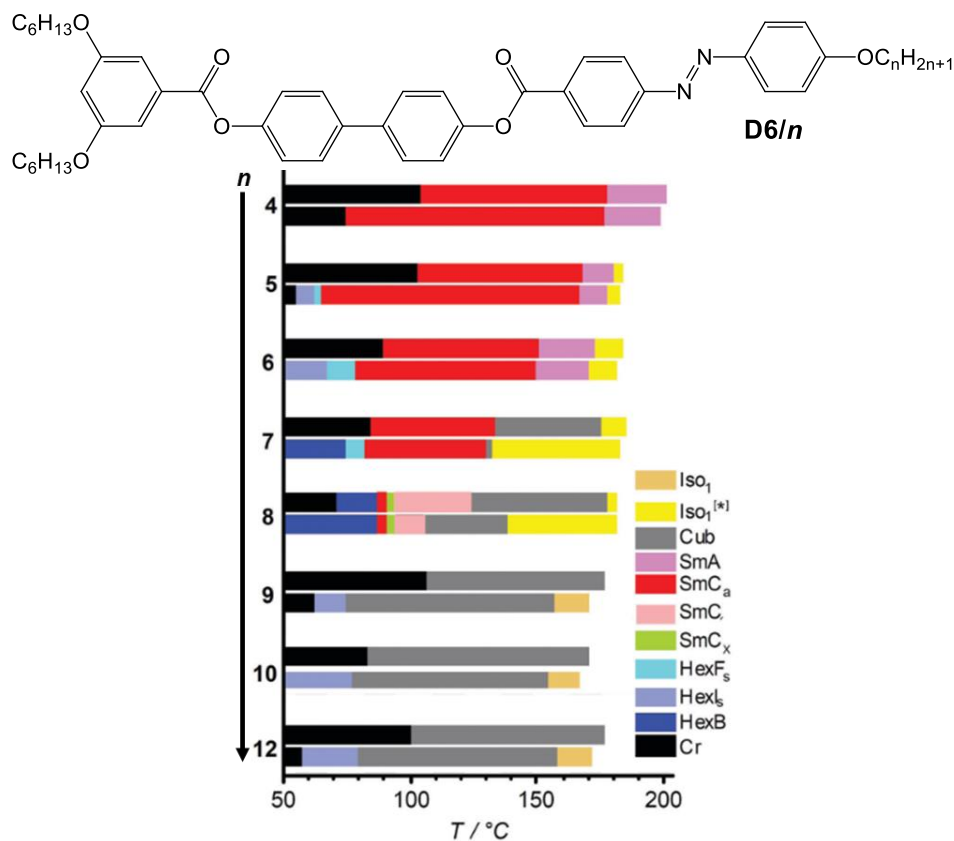


**Figure 28.** Chemical structure and bar diagram of compounds **D6/n** showing the mesophases and phase transitions on heating (upper bars) and on cooling (lower bars); Cub = achiral  $\text{Cub}_{\text{bi}}/\text{Ia}3d$ . [Pub. AA17]

Another remarkable feature of these compounds is the formation of  $\text{Iso}_1^{[*]}$  phase for compounds with medium alkyl chain length ( $n = 5-8$ ). Upon further chain elongation ( $n \geq 9$ ) only the achiral  $\text{Iso}_1$  phase was observed (**Figure 28**). Development of these  $\text{Iso}_1/\text{Iso}_1^{[*]}$  phases (**Figure 29**) is explained by dynamic network formation after crossing a critical connectivity of the helical aggregates if a homogeneously chiral local network structure can develop in the  $\text{Iso}_1^{[*]}$  phase (e.g.  $I23$  like structure). If the critical network density is not achieved or an achiral network structure (e.g.  $\text{Ia}3d$ , Fig. 29e) is preferred, then the network liquid is achiral ( $\text{Iso}_1$ ).

An efficient way to stabilize the  $\text{Cub}_{\text{bi}}$  phases in these materials was the peripheral fluorination of the aromatic core. This effect of core fluorination is opposite to central core fluorination of symmetric polycatenars which is known to give only smectic phases.[237] Therefore, this work provides a new concept for the design of technological interesting LC materials with anticlinic smectic C phases ( $\text{SmC}_a$ ) and spontaneously emerging chirality in self-assembled systems. More details are explained in Pub. AA17.



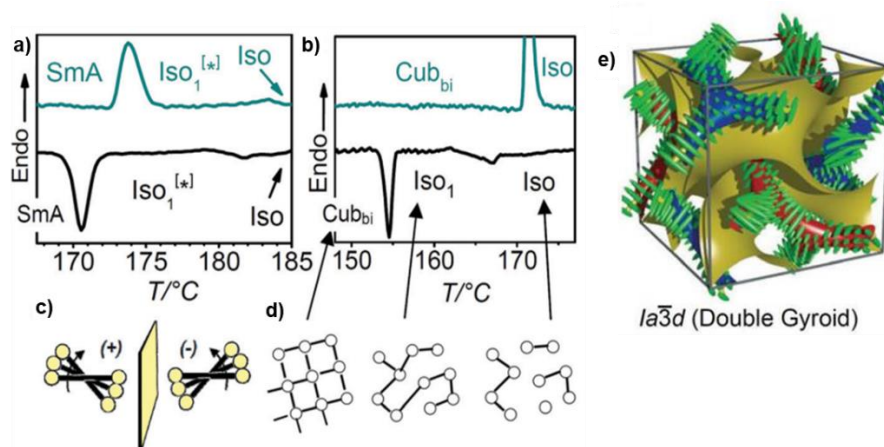


**Figure 29.** Expanded sections of the DSC traces of compound **D6/6** showing (a) the Iso-Iso<sub>1</sub><sup>[\*]</sup> transition on heating and cooling and (b) the Iso-Iso<sub>1</sub> transition of compound **D6/10**; (c) shows the origin of the helical superstructure due to the clashing of the bulky end chains of the rod-like molecules; (d) illustrates the development of the networks (from right to left); (e) shows the helical structures in the *Ia3d* phase (with opposite helix sense in blue and red networks and three way junctions; the minimal surface separating the networks is shown in yellow), assumed to represent the local structures in the chiral Iso<sub>1</sub><sup>[\*]</sup> and the achiral Iso<sub>1</sub> phase, respectively.[AA17]

#### 4.5. Supramolecular polycatenars forming chiral cubic and Iso<sub>1</sub><sup>[\*]</sup> phases

In Pub. AA19 hydrogen bonding was used as intermolecular interaction to design the first examples of the azobenzene-based supramolecular polycatenars (**H6/n**, X=H Scheme 5). The supramolecules were designed using azopyridines with one variable terminal chain (**Gn**) as the proton-acceptors and a taper shaped benzoic acid derivative with three terminal chains as the hydrogen bond-donor (**E6**). These supramolecules displayed the chiral Iso<sub>1</sub><sup>[\*]</sup> phase in addition to the two different versions of the bicontinuous cubic phases i.e. the achiral double gyroid (*Cub<sub>bi</sub>/Ia3d*) and the chiral triple network cubic (*Cub<sub>bi</sub><sup>[\*]</sup>/I23*) phase in relatively wide temperature ranges.

In a more recent work (Pub. AA20) the formation of mirror-symmetry broken *Cub<sub>bi</sub><sup>[\*]</sup>/I23* and Iso<sub>1</sub><sup>[\*]</sup> phases was successfully controlled by alkyl chain engineering). For this purpose, three series of supramolecular photo-switchable polycatenars formed by intermolecular hydrogen bonding interaction were designed and synthesized (**Hm/n** and **Im/n**, Scheme 5). In all of them the same azopyridines (**Gn**) were used as the proton acceptors, while the proton donors were either the taper shaped benzoic acid derivative **E10** with longer terminal chains compared to **E6** or Y-shaped benzoic acid derivatives having only two terminal chains (**Fm**).[AA20] The Iso<sub>1</sub><sup>[\*]</sup> phase is observed only adjacent to the *I23* cubic phase, which means that it is likely to be composed of a local *I23*-like structure. In addition to the chiral *Cub<sub>bi</sub><sup>[\*]</sup>/I23* phases, the achiral *Cub<sub>bi</sub>/Ia3d* phases as well as *Col<sub>hex</sub>* phases were observed depending on the length of the terminal alkyl chains.

More interesting, with these supramolecules it was possible to report the first case of fast and reversible photo switching by UV irradiation between the chiral  $\text{Cub}_{\text{bi}}^{[*]}/I23$  and the achiral  $\text{Cub}_{\text{bi}}/Ia3d$  phases as well as between  $\text{Cub}_{\text{bi}}^{[*]}/I23$  and a chiral crystalline ( $\text{Cr}^{[*]}$ ) phase (**Figure 30**).[AA20] This could lead to interesting perspectives for chirality switching and phase modulation by interaction with non-polarized light, which in turn could be used to improve the materials properties to be applied in optical shutters and other optical, electronic, or mechanical modulation devices.

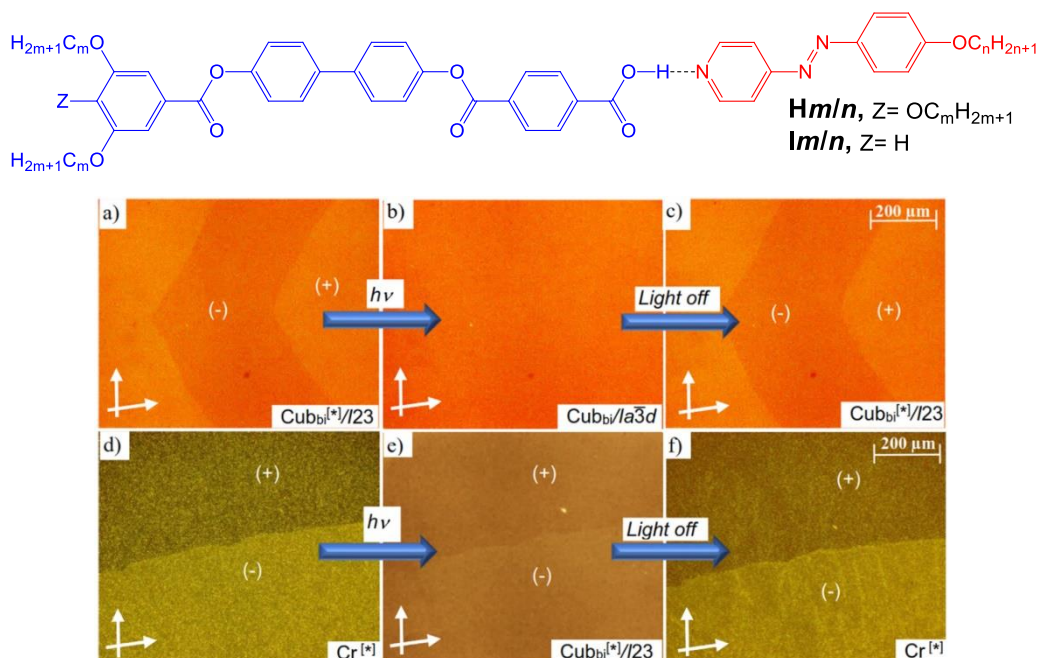


**Figure 30.** (a-c) Reversible isothermal photo-off-on switching of chirality at  $T = 150\text{ }^{\circ}\text{C}$  and (d-f) switching between the  $\text{Cr}^{[*]}$  and the  $\text{Cub}_{\text{bi}}^{[*]}/I23$  phase by retaining chirality at  $T = 70\text{ }^{\circ}\text{C}$  as observed for **H10/8** in a homeotropic cell.[Pub. AA20]

Related supramolecules but designed with halogen bonding interaction instead of the hydrogen bonding are reported in Pub. AA22 (complexes **L6/n** and **M6/n**, **Scheme 6**). For these supramolecules, no 3D cubic or tetragonal phases were observed in contrast to those observed in the hydrogen-bonded supramolecules or in the covalently bonded materials discussed before. Instead, wide ranges of SmA phases were exhibited by the halogen-bonded materials, which for one supramolecule was found to be the widest among all previously reported supramolecular perfluoroarylhalide/pyridine based halogen-bonded LCs.[AA22,238,239] Moreover, a fast and reversible photoisomerization process in the bulk state between the lamellar SmA phase and the isotropic liquid was successfully achieved.

The absence of the  $\text{Cub}_{\text{bi}}$  phases in all **L6/n** and **M6/n** supramolecules is attributed to the large size of the four lateral fluorine atoms present in the halogen bond donor (**K6**) used to design these materials. The thus increased cross sectional area of the fluorinated aromatic cores

leads to a reduction of the interface curvature between aromatics and aliphatics and this is responsible of the formation of only lamellar phases rather than bicontinuous cubic phases with curved interfaces.[AA22]

It should be mentioned at this point that the hydrogen-bonding interaction was also used to design nematogenic supramolecular dimers [AA28] as well as bent-shaped supramolecules [AA30]. The details for these studies are given in references AA28 and AA30.

In Pub. AA21 the design, synthesis, and investigation of fluorinated supramolecular azobenzene-based polycatenars formed by intermolecular hydrogen-bonding between the taper shaped benzoic acid (**E6**) and a variety of fluorinated azopyridine derivatives (supramolecules **H6/n**, X=F, Scheme 5) were reported. The effect of core fluorination at different positions of the aromatic core on the development of soft matter network phases was investigated and compared to the parent nonfluorinated supramolecules.[AA19] Depending on the position of the fluorine substitution, helical network formation was observed in the  $\text{Iso}_1^{[*]}$  and in the  $\text{Cub}_{\text{bi}}^{[*]}/I23$  phase (**Figure 31**).

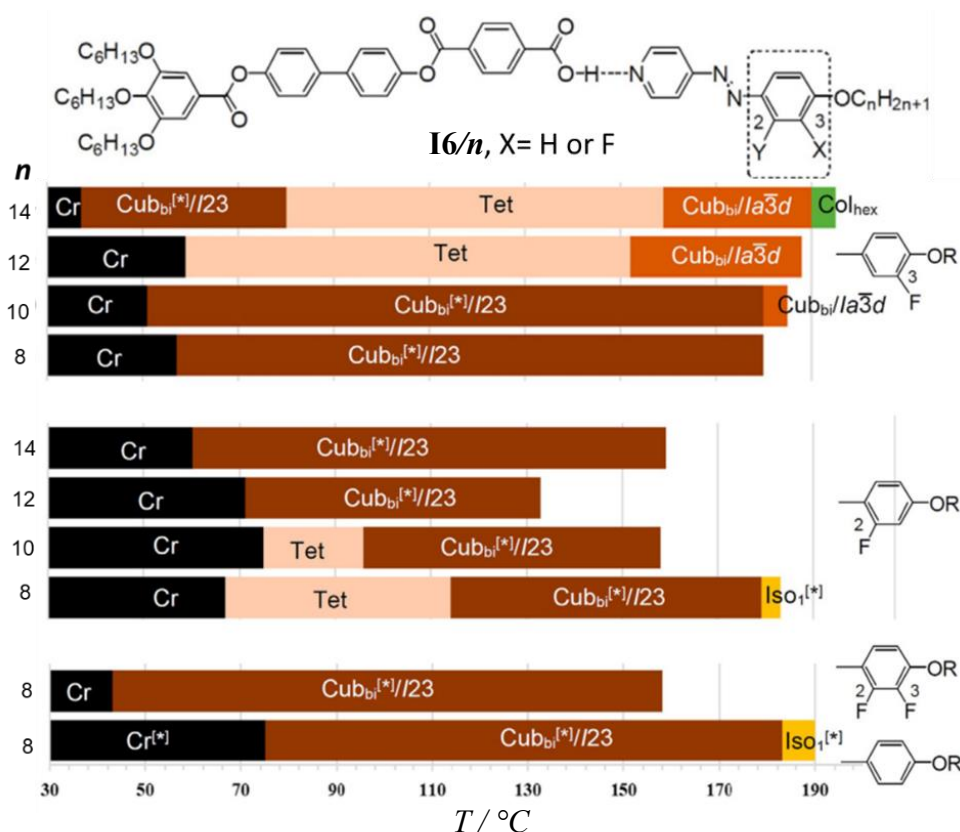


**Figure 31.** Phase transitions of the fluorinated hydrogen-bonded supramolecules as observed by DSC on cooling with  $10 \text{ K min}^{-1}$ . [AA21]

The  $\text{Iso}_1^{[*]}$  phase is found for complexes with short chains and without peripheral fluorine and it occurs besides the  $\text{Cub}_{\text{bi}}^{[*]}/I23$  phase, and therefore, a local  $I23$ -like network

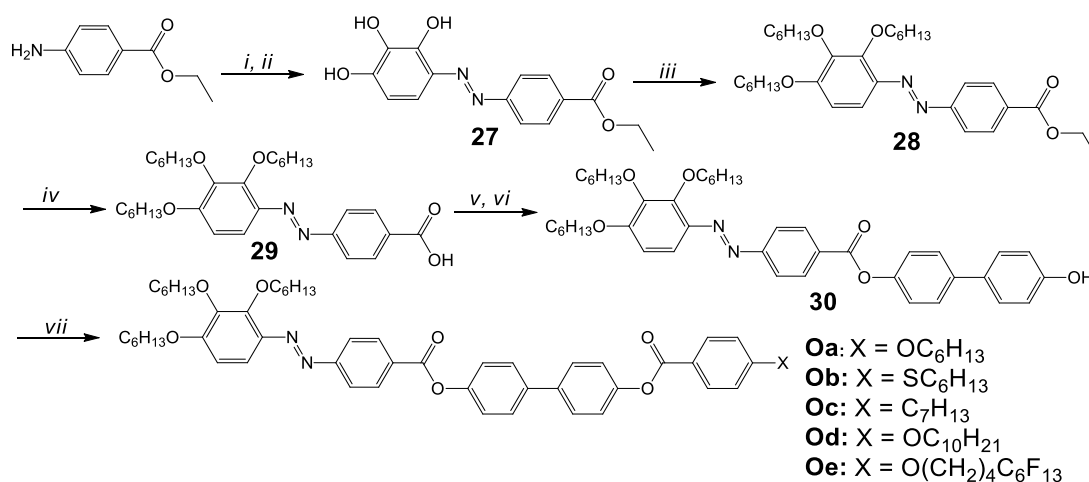
structure is proposed. Moreover, the reported materials represent the first examples of hydrogen-bonded supramolecular complexes exhibiting 3D tetragonal phases (Tet) over relatively wide temperatures ranges and in different phase sequences, in most cases representing deformed versions of the  $I23$  lattice, appearing as intermediate phases at the  $Ia3d$ - $I23$  transitions in the overall sequence  $Ia3d$ -(Tet)- $I23$ -Tet- $Ia3d$ - $Col_{hex}$ .

Interestingly, the type of the Tet phase is changing by changing the position of the fluorine substitution as indicated from the optical texture and the lattice parameters calculated from the XRD measurements. The formation of these Tet phases is assumed to be the result of the combined action of minimizing steric frustration and optimizing helix packing in chirality synchronized helical network structures. Overall, this report provided guidelines for the application of core fluorination at different positions as a powerful tool for controlling spontaneous helical self-assembly in supramolecular liquid and liquid crystalline materials.

It should be noted here, that the role of aromatic core fluorination was investigated in details for simple supramolecular rod-like molecules designed by hydrogen-bonding interaction in another work.[AA29]

#### 4.6. Nematic polycatenars and their investigation on photo switching properties and optical storage devices

In another study [A24,A240] the positions of the three alkyl chains at the trisubstituted end of polycatenars were changed to give compound (**Oa-e**). These materials were synthesized as outlined in **Scheme 8** and investigated in detail.



**Scheme 8.** Synthesis of the polycatenars **Oa-e**. Reagents and conditions: i. NaNO<sub>2</sub>, HCl; ii. NaOH, 1,2,3-trihydroxybenzene; iii. BrC<sub>6</sub>H<sub>13</sub>, KI, K<sub>2</sub>CO<sub>3</sub>, DMF, stirring, 80 °C, 48 h; iv. NaOH, stirring, 85 °C, for 4 h then H<sup>+</sup>; v. SOCl<sub>2</sub>, few drops of DMF, stirring, 80 °C, 1h; vi. 4,4'-dihydroxybiphenyl, pyridine, stirring, 100 °C, 12 h; vii. DCC, DMAP, DCM, stirring, 48 h.[A24]

Though these compounds cannot be directly compared with the previously discussed polycatenars (**Cn/6**),[AA15] the shift of one of the terminal hexyloxy chains into the 2-position

distorts the core-chain segregation and provides a significant steric distortion. Therefore, these compounds form exclusively nematic LC phases with cybotactic clusters ( $N_{CybC}$ ) in wide temperature ranges beside SmC phases in some cases.[A24] Moreover, they have the advantage of the incorporation of the azo units in their structures. Therefore, they were selected for further investigations.

Besides the three hexyloxy chains at one terminus of the polycatenars **Oa-e** a variable single chain at the other terminus, which was varied with  $-OC_6H_{13}$ ,  $-SC_6H_{13}$ ,  $-C_7H_{13}$ ,  $-OC_{10}H_{21}$  and  $-O(CH_2)_4C_6F_{13}$  chains was used. The effect of variation of terminal chains on the LC-phases, the photo-switching properties of these azobenzene-based materials upon light irradiation and their kinetic reactions were investigated in ref. [A240]. Surprisingly, trans-cis conversion in solutions takes around 85 seconds, while relaxing back i.e. cis-trans conversion takes  $\sim$  30-60 minutes depending on the type of the terminal chain. On the other hand, irrespective of the nature of the terminal chain all of them exhibit fast thermal back relaxation time. The potential of one selected example in optical storage device was elucidated (**Figure 32**) confirming the possibility of using such photoswitchable polycatenars in optical shutters and other optical devices.

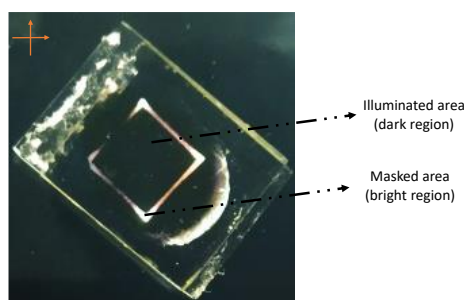


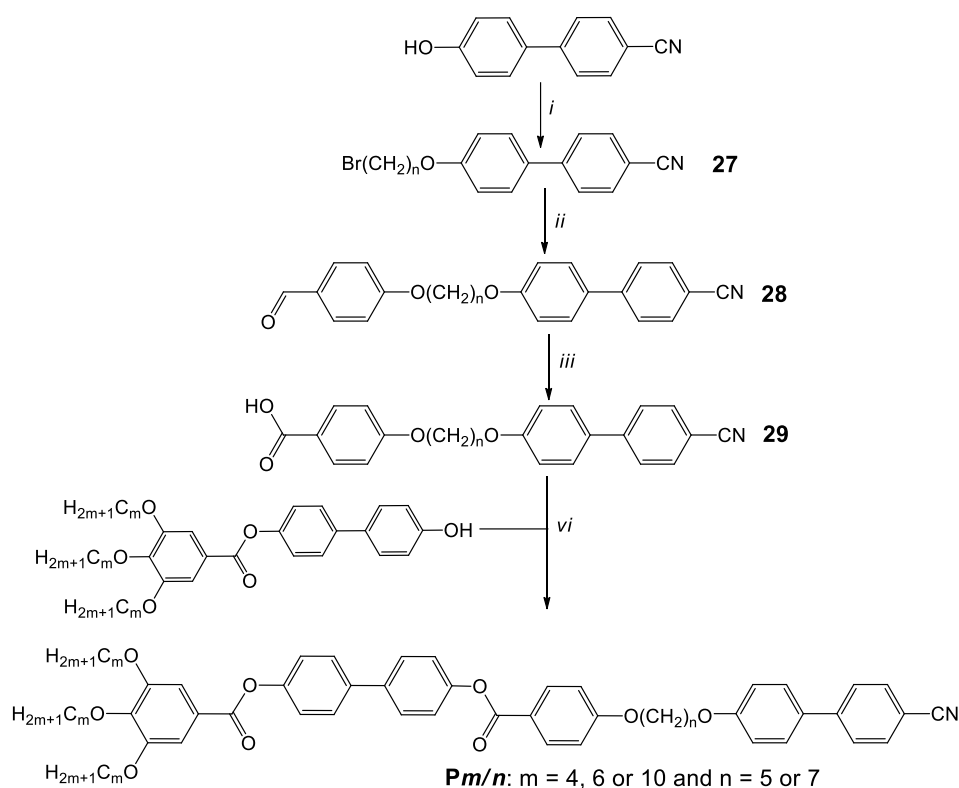
**Figure 32.** Demonstration of an optical storage device using compound **Od** (with X=  $-OC_{10}H_{21}$ ). Prototype observed under the crossed polarisers. The system changes from ordered to disordered state with the illumination of UV light of wavelength 365 nm along with heat filter to avoid any heat effects. One can see the bright regions (masked area) and dark regions (illuminated area) with respect to UV light illumination. Intensity used is  $5mW/cm^2$  and time of illumination is 10 minutes.[A240]

## 5. Combination of structural features of polycatenars with mesogenic dimers and bent-core mesogens

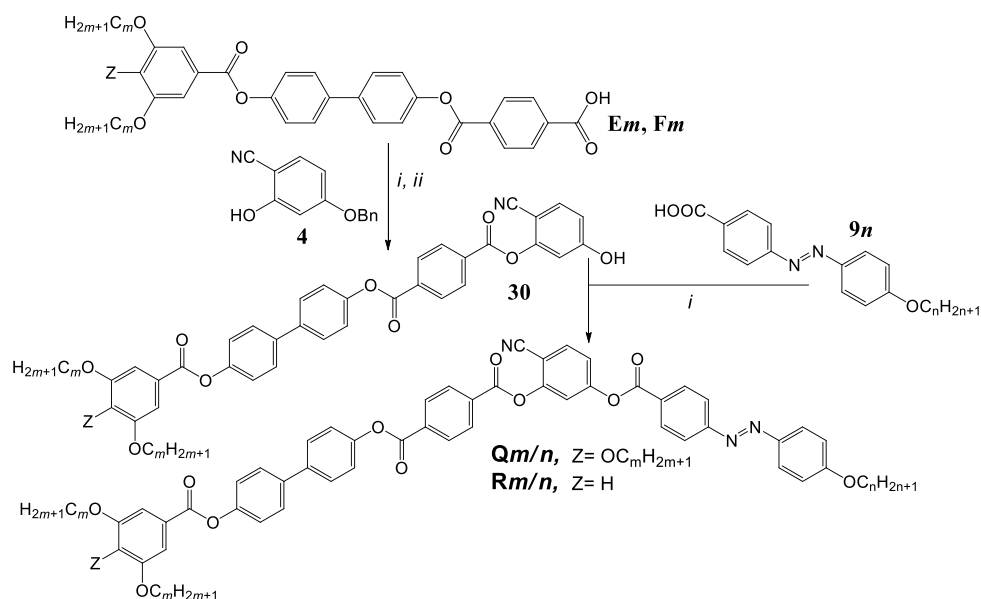
Aiming to combine the liquid crystalline properties of both bent-core and polycatenars in single molecules different classes of new LC molecules were reported [AA25-AA27] synthesized and investigated. Therefore, in Pub AA25 polycatenars in the form of dimers having two different rigid segments connected with aliphatic spacers were synthesized and investigated (compounds **Pm/n**, Scheme 9).

The spacers were selected to have odd number of carbon atoms to induce bending of the whole molecular structure aiming to induce polar LC phases formed by bent-core molecules.[62,66] No cubic or tetragonal phases were observed in these materials as those formed by polycatenars molecules but only nematic phases were detected. It was not possible to further investigate these nematic phases because of their monotropic nature and their short range.

Very recently the first examples of photo responsive hockey-stick (HS) polycatenars (**Qm/n** and **Rm/n**, **Scheme 10**) were also synthesized and investigated as reported in Pub. AA26 and AA27.



**Scheme 9.** Synthesis of the dimeric compounds **Pm/n**. Reagents and conditions: i.  $\text{Br}(\text{CH}_2)_n\text{Br}$ , KI,  $\text{K}_2\text{CO}_3$ , dry acetone, stirring, reflux, 24 h; ii. 4-hydroxybenzaldehyde, KI,  $\text{K}_2\text{CO}_3$ , DMF, stirring, 85 °C, 6 h; iii. resorcinol,  $\text{NaOCl}_2$ ,  $\text{NaH}_2\text{PO}_4$ , then  $\text{H}^+$ ; vi. 1.  $\text{SOCl}_2$ , few drops of DMF, stirring, 80 °C, 1h; 2. Dry DCM, TEA, few drops of pyridine, reflux, 6 h.[AA25]



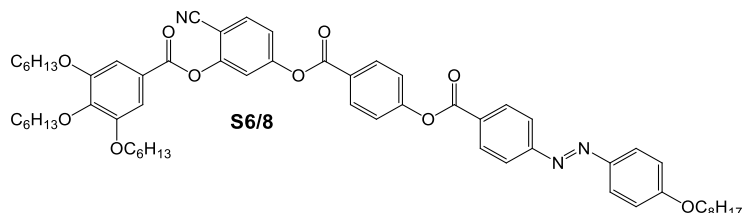
**Scheme 10.** Synthesis of the hockey-stick (HS) polycatenars **Q<sub>m/n</sub>** and **R<sub>m/n</sub>**. Reagents and conditions: i. 1. SOCl<sub>2</sub>, DMF, reflux, 1 h.; 2. Et<sub>3</sub>N, dry pyridine, DCM, reflux 6 hrs.; ii. H<sub>2</sub>/Pd/C, dry THF, stirring 48 hrs., 25 °C.[AA26,AA27]

In these two articles new azobenzene-based HS polycatenars derived from 4-cyanoresorcinol bent-core unit connected to two side arms with different lengths were reported. The long arm is a fork-like double or triple alkoxyated wing, while the short arm is azobenzene-based wing terminated with a single variable alkoxy chain. In both types of materials differing in the chain volume at the crowded end, wide temperature ranges of lamellar smectic A phases (up to 170 K) are observed beside the achiral Iso<sub>1</sub> phase for the shorter derivatives. On chain elongation helical self-assembly of the  $\pi$ -conjugated rods in networks occurs resulting in the formation of nanostructured Cub<sub>bi</sub>/Ia3d phases, in most cases stable even around room temperatures. At the transition from SmA to Cub<sub>bi</sub> phases, additional unknown three-dimensional (3D) phase is observed in some materials. For all investigated compounds no current peak could be observed in the SmC or SmA phases up to a voltage of 200 V<sub>pp</sub> in a 10  $\mu$ m or 6  $\mu$ m ITO cell, indicating the non-polar nature of these smectic phases.

Based on the XRD results and using Materials Studio software, a possible explanation for the loss of polar order in such phases was given. The reason is attributed to the distorted packing of the molecules giving rise to a significant distortion for the directed packing of the bent directions of the cores. A polar order could be expected only if a uniform bend-direction with preferred packing of the bent-core molecules with parallel organization could be achieved, which is not the case in the studied HS polycatenars.

Shifting the position of the bent 4-cyanoresorcinol core in compound **Q6/8** with  $m = 6$  and  $n = 8$  to be more close to the crowded end leads to the hockey-stick molecule **S6/8**. [AA26] This modification results in complete removing of the SmA phase with no formation of 3D Cub

or Tet phases. Instead, a nematic phase with SmC-cybotactic clusters ( $N_{CybC}$ ) in addition to different types of smectic phases are formed. Obviously, the reduced molecular symmetry, which requires a mixed packing of the short and long wings leads to a reduced packing density which is unfavourable for chirality synchronization as required for the formation of helical network phases. More details are given in Pub. AA26.



Overall, this study can be considered as an important step toward the unification of polycatenar self-assembly and bent-core self-assembly which requires further work.[241,242]

## 6. Summary and conclusions

The main goal of the work was to introduce new strategies toward the design and investigations of novel classes of nanostructured self-assembled functional materials, as well as their structure-property relationships. This was planned to understand the fundamental factors leading to the macroscopic chirality in soft matter systems of achiral molecules which is a contemporary research topic with great importance for the general understanding of spontaneous mirror symmetry breaking with a great impact on the discussion around the emergence of uniform chirality in biological systems and for technological applications. Additionally, photoswitchable materials for the manipulation of the physical and chiroptical properties by light irradiation were synthesized and investigated.

Therefore, different classes of photo responsive liquid crystalline materials, namely bent-core LCs and polycatenars were designed and synthesized. Different synthetic strategies were used, and extensive studies were performed to fully characterize the liquid crystalline phases exhibited by these materials. This provided very useful insights about the factors leading to mirror symmetry breaking in soft matter systems and guidelines for molecular design of new functional materials capable of formation of mirror symmetry broken LC phases.

In the first part of the work, the effect of substitution at the apex of azobenzene-based bent-core mesogens with different halogen or pseudohalogen groups were systematically studied. Therefore, several types of central bent-core units have been used to synthesize BCLCs including 4-cyanoresorcinol, 4-bromoresorcinol, 4-iodoresorcinol, 4-chlororesorcinol, 4-fluororesorcinol and 4-methylresorcinol. This leads to the discovery and investigations of



different new LC phases and new phase sequences. Among all of the synthesized compounds mirror symmetry breaking was observed in the fluid synclinic SmC phases assigned as SmC<sub>s</sub><sup>[\*]</sup> and SmC<sub>s</sub>P<sub>R</sub><sup>[\*]</sup> exhibited by BCLCs derived from 4-cyanoresorcinol (section 3.1.5) and in a new type of soft semicrystalline dark conglomerate (DC) phases assigned as HNC phases (section 3.2.2) formed by 4-bromoresorcinol, 4-iodoresorcinol or 4-methylresorcinol derivatives. The HNC phases were successfully proven to represent a third type of DC phases with intermediate properties between the LC sponge phases and the semicrystalline HNF phases. It was proved from the DFT calculations that the larger the halogen group size, the stronger is the twisting of the molecule and the stronger the tendency to form HNC phases (I > Br). Guidelines for the design of materials forming this type of HNC phase were successfully established.

In the second part of the work, the focus has shifted to photo responsive polycatenar LCs, which results in interesting optical properties beside the discovery of new LC phase. Therefore, different types of azobenzene-based polycatenars were designed and synthesized. The target compounds were designed by covalent bonds or by intermolecular interactions using either hydrogen or halogen bonding. Ambidextrous mirror symmetry breaking was observed in different types of LC phases exhibited by these polycatenars including Iso<sub>1</sub><sup>[\*]</sup> and Cub<sub>bi</sub><sup>[\*]</sup>/I23 in addition to helical network formation in the achiral Cub<sub>bi</sub>/Ia3d phase. It was possible to identify the molecular packing in the double gyroid (Cub<sub>bi</sub>/Ia3d) phase as well as solving the exact structure of a new bicontinuous tetragonal (Tet<sub>bi</sub>) phase, which is considered as step forward to understand the factors leading to structure complexity in soft matter systems. Ambidextrous mirror-symmetry breaking in such polycatenars was successfully controlled by alkyl chain engineering and by aromatic core fluorination (section 4.5).

For both BCLCs and polycatenar LCs new modes of photo switching were reported. For BCLCs isothermal photo switching between chiral and achiral LC phases as well as between ferroelectric and antiferroelectric states were demonstrated (section 3.1.8). In the case of polycatenars, it was possible to photo switch between the chiral Iso<sub>1</sub><sup>[\*]</sup> and the achiral SmA phases (section 4.2), between the Cub<sub>bi</sub><sup>[\*]</sup>/I23 and the achiral Cub<sub>bi</sub>/Ia3d phase as well as between chiral Cub<sub>bi</sub><sup>[\*]</sup>/I23 and a chiral crystalline phase (Cr<sup>[\*]</sup>, section 4.5). These findings could lead to interesting perspectives for chirality switching and phase modulation by interaction with nonpolarized light, which in turn could lead to the possibility of application of these materials in optical shutters, electronic or mechanical modulation devices. Also, the possibility of using some selected examples in optical storage devices was demonstrated (section 4.6). Moreover, some of the synthesized materials exhibiting 3D Cub<sub>bi</sub> phases are

currently under investigation for the possibility of their application as semiconductors in cooperation with Prof. Alexey Eremin (Otto-von-Guericke-Universität, Magdeburg) and the results are very promising.

In the last part of the thesis new classes of LC materials were represented (Compounds **Qm/n** and **Rm/n** (section 5) aiming to combine liquid crystalline properties of bent cores and polycatenars in single molecules. Though, no polar LC phases were observed, wide ranges of Cub<sub>bi</sub> phases were exhibited by these materials, making them excellent candidates for technological applications. Therefore, the current focus of the applicant is the design and synthesis of related molecules aiming to obtain a novel class of molecules able to display polar phases as well as 3D mesophases, which is expected to widen the range of possible applications. Moreover, the relation between the formation of helical networks and deformation of the cubic lattice or generation of new modes of helical self-assembly in the tetragonal phases is still open question to be answered in the future which is also in the focus of further research.

## 7. References

Note that references AA1-AA30 can be found in the publications list given on page number 3 and are attached to this thesis.

- 
- AA1. M. Alaasar, M. Prehm, M. Nagaraj, J. K. Vij, C. Tschierske, *Adv. Mater.* **2013**, *25*, 2186.  
AA2. M. Alaasar, M. Prehm, K. May, A. Eremin, C. Tschierske, *Adv. Funct. Mater.* **2014**, *24*, 1703.  
AA3. M. Alaasar, M. Prehm, M.-G. Tamba, N. Sebastián, A. Eremin, C. Tschierske, *Chem. Phys. Chem.* **2016**, *17*, 278.  
AA4. M. Alaasar, M. Prehm, S. Poppe, C. Tschierske, *Chem. Eur. J.* **2017**, *23*, 5541.  
AA5. M. Alaasar, M. Prehm, S. Belau, N. Sebastian, M. Kurachkina, A. Eremin, C. Chen, F. Liu and C. Tschierske, *Chem. Eur. J.* **2019**, *25*, 6362.  
AA6. M. Alaasar, M. Prehm, C. Tschierske, *Liq. Cryst.* **2014**, *41*, 126.  
AA7. M. Alaasar, S. Poppe, C. Tschierske, *Liq. Cryst.* **2017**, *44*, 729.  
AA8. M. Alaasar, A. Eremin, S. Poppe, C. Kerzig, C. Klopp, C. Tschierske, *J. Mater. Chem. C* **2017**, *5*, 8454.  
AA9. M. Alaasar, M. Prehm, C. Tschierske, *Liq. Cryst.* **2013**, *40*, 656.  
AA10. M. Alaasar, M. Prehm, C. Tschierske, *Chem. Comm.* **2013**, *49*, 11062.  
AA11. M. Alaasar, M. Prehm, M. Brautzsch, C. Tschierske, *Soft Matter* **2014**, *10*, 7285.  
AA12. M. Alaasar, M. Prehm, M. Brautzsch, C. Tschierske, *J. Mater. Chem. C* **2014**, *2*, 5487.

- 
- AA13. M. Alaasar, M. Prehm, C. Tschierske, *Chem. Eur. J.* **2016**, *22*, 6583.
- AA14. M. Alaasar, M. Prehm, C. Tschierske, *RSC Advances* **2016**, *6*, 82890.
- AA15. M. Alaasar, M. Prehm, Y. Cao, F. Liu, C. Tschierske, *Angew. Chem. Int. Ed.* **2016**, *55*, 312.
- AA16. M. Alaasar, S. Poppe, Q. Dong, F. Liu, C. Tschierske, *Angew. Chem.* **2017**, *129*, 10941.
- AA17. M. Alaasar, S. Poppe, Y. Cao, C. Chen, F. Liu, C. Zhu, C. Tschierske, *J. Mater. Chem. C* **2020**, *8*, 12902.
- AA18. M. Alaasar, Y. Cao, Y. Liu, F. Liu, C. Tschierske, *Chem. Eur. J.* **2022**, e202201857.
- AA19. M. Alaasar, S. Poppe, Q. Dong, F. Liu, C. Tschierske, *Chem. Comm.* **2016**, *52*, 13869.
- AA20. M. Alaasar, X. Cai, F. Kraus, M. Giese, F. Liu, C. Tschierske, *J. Mol. Liq.* **2022**, *351*, 118597.
- AA21. M. Alaasar, J.-C. Schmidt, X. Cai, F. Liu, C. Tschierske, *J. Mol. Liq.* **2021**, *332*, 115870.
- AA22. M. Alaasar, S. Poppe, C. Tschierske, *J. Mol. Liq.* **2019**, *277*, 233.
- AA23. M. Alaasar, A. F. Darweesh, X. Cai, F. Liu, C. Tschierske, *Chem. Eur. J.* **2021**, *27*, 14921.
- AA24. M. Alaasar, S. Poppe, *Liq. Cryst.* **2020**, *47*, 939.
- AA25. M. Alaasar, C. Tschierske, *Liq. Cryst.* **2017**, *44*, 387.
- AA26. M. Alaasar, X. Cai, Y. Cao, F. Liu, *New J. Chem.* **2022**, *46*, 15871.
- AA27. M. Alaasar, S. Poppe, *J. Mol. Liq.* **2022**, *351*, 118613.
- AA28. M. Alaasar, C. Tschierske, *Liq. Cryst.* **2019**, *46*, 124.
- AA29. M. Alaasar, J.-C. Schmidt, A. F. Darweesh, C. Tschierske, *J. Mol. Liq.* **2020**, *310*, 113252.
- AA30. M. Alaasar, C. Tschierske, M. Prehm, *Liq. Cryst.* **2011**, *38*, 925.
31. F. Reinitzer, *Monatsh. Chem.* **1888**, *9*, 421.
32. D. Demus, *Mol. Cryst. Liq. Cryst.* **2001**, *364*, 25-91
33. D. Demus, J. W. Goodby, G. W. Gray, H. W. Spiess, V. Vill (Hg.); *Handbook of Liquid Crystal*, Wiley-VCH, Weinheim, **1998**.
34. J. P. F Lagerwall, G. Scalia, *Current Applied Physics* **2012**, *12*, 1387.
35. L. Schmidt-Mende, A. Fechtenkotter, K. Mullen, E. Moons, R. Friend, J. MacKenzie, *Science* **2001**, *293*, 1119.
36. R. Jakoby, A. Gaebler, C. Weickhmann, *Crystals* **2020**, *10*, 514.
37. E. Bokusoglu, M. B. Pantoja, P. C. Mushenheim, X. Wang, N. L. Abbott, *Annu. Rev. Chem. Biomol. Eng.* **2016**, *7*, 96.

- 
38. Z.G. Zheng, Y.Q. Lu, Q. Li, *Adv. Mater.* **2020**, 1905318.
39. K. Bisoyi, T. J. Bunning, Q. Li, *Adv. Mater.* **2018**, 1706512.
40. C. Tschierske, *Top. Curr. Chem.* **2012**, 318, 1.
41. S. Chandraskhar, B. K. Sadashiva, K. A. Suresh, *Pramana* **1977**, 5, 471.
42. S. Kumar, *Chem. Soc. Rev.* **2006**, 35, 83.
43. D. Demus, H. Stegemeyer (Ed.), *Topics in Physical Chemistry: Liquid Crystals*. Steinkopff Verlag, Darmstadt, 1994, 6 – 49.
44. S. Kutsumizu, K. Morita, T. Ichikawa, *Liq. Cryst.* **2002**, 29, 1447.
45. S. Chandraskhar, *Liquid Crystals*, Cambridge University Press; 2. Edition, New York **1993**, 6f.
46. M. Cestari, S. Diez-Berart, D. A. Dunmur, A. Ferrarini, M. R. de la Fuente, D. J. B. Jackson, D. O. Lopez, G. R. Luckhurst, M. A. PerezJubindo, R. M. Richardson, J. Salud, B. A. Timimi, H. Zimmermann, *Phys. Rev. E* **2011**, 84, 31704.
47. V. P. Panov, M. Nagaraj, J. K. Vij, Y. P. Panarin, A. Kohlmeier, M. G. Tamba, R. A. Lewis, G. H. Mehl, *Phys. Rev. Lett.* **2010**, 105, 167801.
48. P. A. Henderson, C. T. Imrie, *Liq. Cryst.* **2011**, 38, 1407.
49. R. J. Mandle, E. J. Davis, C. T. Archbold, C. C. A. Voll, J. L. Andrews, S. J. Cowling, J. W. Goodby, *Chem. Eur. J.* **2015**, 21, 8158.
50. R. J. Mandle, C. C. A. Voll, D. J. Lewis, J. W. Goodby, *Liq. Cryst.* **2016**, 4, 13.
51. D. A. Paterson, J. P. Abberley, W. T. A. Harrison, J. M. D. Storey, C. T. Imrie, *Liq. Cryst.* **2017**, 44, 127.
52. A. Knežević, M. Sapunar, A. Buljan, I. Dokli, Z. Hameršak, D. Kontrec, A. Lesac, *Soft Matter* **2018**, 14, 8466.
53. Y. Arakawa, K. Komatsu, H. Tsuji, *New J. Chem.* **2019**, 43, 6786.
54. Y. Arakawa, H. Tsuji, *J. Mol. Liq.* **2019**, 289, 111097.
55. R. Walker, D. Pocięcha, J. M. D. Storey, E. Gorecka, C. T. Imrie, *Chem. Eur. J.* **2019**, 25, 13329.
56. Y. Arakawa, Y. Ishida, H. Tsuji, *Chem. Eur. J.* **2020**, 26, 3767.
57. Y. Arakawa, K. Komatsu, J. Feng, C. Zhu, H. Tsuji, *Mater. Adv.* **2021**, 2, 261.
58. Y. Arakawa, K. Komatsu, Y. Ishida, T. Shiba, H. Tsuji, *Materials* **2022**, 15, 1709.
59. R. J. Mandle, J. W. Goodby, *Angew. Chem. Int. Ed.* **2018**, 57, 7096.
60. S. M. Jansze, A. Martínez-Felipe, J. M. D. Storey, A. T. M. Marcelis, C. T. Imrie, *Angew. Chem. Int. Ed.* **2015**, 127, 653.
61. R. J. Mandle, *Molecules* **2022**, 27, 2689.

- 
62. R. J. Mandle, S. J. Cowling, J. W. Goodby, *Chem. Eur. J.* **2017**, *23*, 14554.
63. H. Nishikawa, K. Shiroshita, H. Higuchi, Y. Okumura, Y. Haseba, S. I. Yamamoto, K. Sago, H. Kikuchi, *Adv. Mater.* **2017**, *29*, 1702354.
64. X. Chen, E. Korblova, D. Dong, X. Wei, R. Shao, L. Radzihovsky, M. A. Glaser, J. E. MacLennan, D. Bedrov, D. M. Walba, N. A. Clark, *Proc. Natl. Acad. Sci. U. S. A.* **2020**, *117*, 14021.
65. R. J. Mandle, S. J. Cowling, J. W. Goodby, *Liq. Cryst.* **2021**, *48*, 1780.
66. C. L. Folcia, J. Ortega, R. Vidal, T. Sierra, J. Etxebarria, *Liq. Cryst.* **2022**, *49*, 889.
67. J. Zhou, R. Xia, M. Huang, S. Aya, *J. Mater. Chem. C* **2022**, *10*, 8762.
68. R. J. Mandle, N. Sebastián, J. Martínez-Perdiguero, A. Mertelj, *Nat. Comm.* **2021**, *12*, 4962.
69. H. Nishikawa, F. Araoka, *Adv. Mater.* **2021**, *33*, 2101305.
70. Y. Song, J. Li, R. Xia, H. Xu, X. Zhang, H. Lei, W. Peng, S. Dai, S. Aya, M. Huang, *Phys. Chem. Chem. Phys.* **2022**, *24*, 11536.
71. D. Vorländer, K. Fuchs, E. E. Katscher, *Ber. Dtsch. Chem. Ges.* **1929**, *62*, 2381.
72. D. Vorländer, A. Apel, *Ber. Dtsch. Chem. Ges.* **1932**, *65*, 1101
73. G. Pelzl, I. Wirth, W. Weissflog, *Liq. Cryst.* **2001**, *28*, 969.
74. T. Niori, T. Sekine, T. Furukawa, H. Takezoe, *J. Mater. Chem.* **1996**, *6*, 1231.
75. H.-S. Kitzerow, C. Bahr, Chirality in Liquid Crystals, ed. H.-S. Kitzerow, C. Bahr, Springer-Verlag, New York, **2001**.
76. S. T. Lagerwall, Ferroelectric and Antiferroelectric Liquid Crystals, Wiley VCH, Weinheim, **1999**.
77. J. F. Scott, *Science* **2007**, *315*, 954.
78. A. S. Tayi, A. Kaeser, M. Matsumoto, T. Aida, S. I. Stupp, *Nat. Chem.* **2015**, *7*, 281.
79. H. Takezoe, E. Gorecka, M. Čepič, *Rev. Mod. Phys.* **2010**, *82*, 897.
80. W. Weissflog, G. Pelzl, K. Merzweiler, R. Stannarius, A. Eremin, *Soft Matter* **2012**, 2671.
81. S. Radhika, B. K. Sadashiva, V. A. Raghunathan, *Ferroelectrics* **2008**, *364*, 20.
82. S. Umadevi, B. K. Sadashiva, *Liq. Cryst.* **2005**, *32*, 287.
83. R. A. Reddy, C. Tschierske, *J. Mater. Chem.* **2006**, *16*, 907.
84. M. B. Ros, J. L. Serrano, M. R. de la Fuente, C. L. Folcia, *J. Mater. Chem.* **2005**, *15*, 5093.
85. H. Takezoe, Y. Takanishi, *Jpn. J. Appl. Phys. Part 1* **2006**, *45*, 597.
86. R. A. Reddy, U. Baumeister, C. Keith, H. Hahn, H. Lang, C. Tschierske, *Soft Matter* **2007**, *3*, 558.
22. C. Keith, G. Dantlgraber, R. A. Reddy, U. Baumeister, C. Tschierske, *Chem. Mater.* **2007**, *19*, 694.

- 
88. C. Keith, A. R. Reddy, A. Hauser, U. Baumeister, C. Tschierske, *J. Am. Chem. Soc.* **2006**, *128*, 3051.
89. C. Tschierske, G. Dantlgraber, *Pramana* **2003**, *61*, 455.
90. B. Glettner, S. Hein, R. A. Reddy, U. Baumeister, C. Tschierske, *Chem. Comm.* **2007**, 2596.
91. T. J. Dingemans, E. T. Samulski, *Liq. Cryst.* **2000**, *27*, 131.
92. W. Weissflog, H. Nádasi, U. Dunemann, G. Pelzl, S. Diele, A. Eremin, H. Kresse, *J. Mater. Chem.* **2001**, *11*, 2748.
93. M. W. Schröder, S. Diele, N. Pancenko, W. Weissflog, G. Pelzl, *J. Mater. Chem.* **2002**, *12*, 1331.
94. H. N. S. Murthy, M. Bodyagin, S. Diele, U. Baumeister, G. Pelzl, W. Weissflog, *J. Mater. Chem.* **2006**, *16*, 1634.
95. L. E. Hough, M. Spannuth, M. Nakata, D. A. Coleman, C. D. Jones, G. Dantlgraber, C. Tschierske, J. Watanabe, E. Korblova, D. M. Walba, J. E. MacLennan, M. A. Glaser, N. A. Clark, *Science* **2009**, *325*, 452.
96. K. J. K. Semmler, T. J. Dingemans, E. T. Samulski, *Liq. Cryst.* **1998**, *24*, 799.
97. N. Chattham, E. Korblova, R. Shao, D. M. Walba, J. E. MacLennan, N. A. Clark, *Liq. Cryst.* **2009**, *36*, 1309.
98. H. N. Shreenivasa Murthy, M. Bodyagin, S. Diele, U. Baumeister, G. Pelzl, W. Weissflog, *J. Mater. Chem.* **2006**, *16*, 1634.
99. R. A. Reddy, C. Zhu, R. Shao, E. Korblova, T. Gong, Y. Shen, E. Garcia, M. A. Glaser, J. E. MacLennan, D. M. Walba, N. A. Clark, *Science* **2011**, *332*, 72.
100. D. Pocięcha, M. Cepić, E. Gorecka, J. Mieczkowski, *Phys. Rev. Lett.* **2003**, *91*, 185501.
101. Y. Shimbo, E. Gorecka, D. Pocięcha, F. Araoka, M. Goto, Y. Takanishi, K. Ishikawa, J. Mieczkowski, K. Gomola, H. Takezoe, *Phys. Rev. Lett.* **2006**, *97*, 113901.
102. C. Keith, M. Prehm, Y. P. Panarin, J. K. Vij, C. Tschierske, *Chem. Comm.* **2010**, *46*, 3702.
103. K. Gomola, L. Guo, S. Dhara, Y. Shimbo, E. Gorecka, D. Pocięcha, J. Mieczkowski, H. Takezoe, *J. Mater. Chem.* **2009**, *19*, 4240.
104. L. Guo, K. Gomola, E. Gorecka, D. Pocięcha, S. Dhara, F. Araoka, K. Ishikawa, H. Takezoe, *Soft Matter* **2011**, *7*, 2895.
105. K. Gomola, L. Guo, D. Pocięcha, F. Araoka, K. Ishikawa, H. Takezoe, *J. Mater. Chem.* **2010**, *20*, 7944.
106. Y. P. Panarin, M. Nagaraj, S. Sreenilayam, J. K. Vij, A. Lehmann, C. Tschierske, *Phys. Rev. Lett.* **2011**, *107*, 247801.

- 
107. M. Nagaraj, Y. P. Panarin, J. K. Vij, C. Keith, C. Tschierske, *Appl. Phys. Lett.* **2010**, *97*, 213505.
108. Y. Shimbo, Y. Takanishi, K. Ishikawa, E. Gorecka, D. Pocięcha, J. Mieczkowski, K. Gomola, H. Takezoe, *Jpn. J. Appl. Phys.* **2006**, *45*, 282
109. A. Ermin, A. Jákl, *Soft Matter* **2013**, *9*, 615.
110. B. Champagne, J. Guthmuller, F. Perreault, A. Soldera, *J. Phys. Chem.* **2012**, *116*, 7552.
111. A. Bogojawlenski, N. Winogradov, *Z. Phys. Chemie.* **1908**, *64*, 229.
112. A. Natansohn, P. Rochon, *Chem. Rev.* **2002**, *102*, 4139.
113. S. Manickasundaram, P. Kannan, Q. M. A. Hassan, P. K. Palanisamy, *J. Mater. Sci. Mater. Electron.* **2008**, *19*, 1045.
114. C. Saravanan, S. Senthil, P. Kannan, *J. Polym. Sci. A.* **2008**, *46*, 7843.
115. P. Rochon, E. Batalla, A. Natansohn, *Appl. Phys. Lett.* **1995**, *66*, 136.
116. S. Wu, S. Yao, W. She, D. Luo, H. Wang, *J. Mater. Sci.* **2003**, *38*, 401.
117. S. Yuquan, Q. Ling, L. Zao, Z. Xinxin, Z. Yuxia, Z. Jianfeng, J. A. Delaire, K. Nakatani, Y. Atassi, *J. Mater. Sci.* **1999**, *34*, 1513.
118. L. Qiu, Y. Shen, J. Hao, J. Zhai, F. Zu, T. Z. Zhao, K. Clays, A. Persoons, *J. Mater. Sci.* **2004**, *39*, 2335.
119. V. Prasad, D. S. S. Rao, K. Prasad, *Liq. Cryst.* **2001**, *28*, 643.
120. V. Prasad, *Liq. Cryst.* **2001**, *28*, 145.
121. V. Prasad, *Mol. Cryst. Liq. Cryst. Sci. Technol, Sect A.* **2001**, *363*, 167.
122. N. G. Nagaveni, A. Roy, V. Prasad, *J. Mater. Chem.* **2012**, *22*, 8948.
- A123. M. Alaasar, *Liq. Cryst.* **2016**, *43*, 2208.
124. W. Weissflog, in *Handbook of Liquid Crystals*, 2nd ed; J. W. Goodby, P. J. Collings, T. Kato, C. Tschierske, H. F. Gleeson, P. Raynes, Eds.; Wiley-VHC: Weinheim, Germany, **2014**; *Volume 5*, pp. 89–174.
125. C. Dressel, T. Reppe, S. Poppe, M. Prehm, H. Lu, X. Zeng, G. Ungar, C. Tschierske, *Adv. Funct. Mater.* **2020**, *30*, 2004353.
126. T. Reppe, C. Dressel, S. Poppe, A. Eremin, C. Tschierske, *Adv. Optical Mater.* **2020**, 2001572.
127. S. Kutsumizu, *Isr. J. Chem.* **2012**, *52*, 844.
128. G. Ungar, F. Liu, X. Zeng, Cubic and 3D Thermotropic Liquid Crystal Phases and Quasicrystals. In *Handbook of Liquid Crystals*, 2nd ed; J. W. Goodby, P. J. Collings, T. Kato, C. Tschierske, H. F. Gleeson, P. Raynes, Eds.; Wiley-VHC: Weinheim, Germany, **2014**; *Volume 5*, pp. 363–436.

- 
129. J. M. Seddon, R. H. Templer, Polymorphism of Lipid-Water Systems. In Handbook of Biological Physics; R. Lipowsky, E. Sackmann, Eds.; Elsevier: Amsterdam, the Netherlands, **1995**; Volume 1, pp. 97–160.
130. C. Chen, R. Kieffer, H. Ebert, M. Prehm, R.-B. Zhang, X. Zeng, F. Liu, G. Ungar, C. Tschierske, *Angew. Chem. Int. Ed.* **2020**, *59*, 2725.
131. X. Zeng, S. Poppe, A. Lehmann, M. Prehm, C. Chen, F. Liu, H. Lu, G. Ungar, C. Tschierske, *Angew. Chem. Int. Ed.* **2019**, *131*, 7453.
132. S. Poppe, X. Cheng, C. Chen, X. Zeng, R.-B. Zhang, F. Liu, G. Ungar, C. Tschierske, *J. Am. Chem. Soc.* **2020**, *142*, 3296.
133. X. B. Zeng, G. Ungar, *J. Mater. Chem. C* **2020**, *8*, 5389.
134. G. W. Gray, B. Jones, F. Marson, *J. Chem. Soc.* **1957**, 393.
135. D. Demus, A. Gloza, H. Hartung, A. Hauser, I. Rapphel, A. Wiegeleben, *Cryst. Res. Technol.* **1981**, *16*, 1445.
- A136. Y. Cao, M. Alaasar, A. Nallapaneni, M. Salamończyk, P. Marinko, E. Gorecka, C. Tschierske, F. Liu, N. Vaupotič, C. Zhu, *Phys. Rev. Lett.* **2020**, *125*, 027801.
137. T. Reppe, S. Poppe, C. Tschierske, *Chem. Eur. J.* **2020**, *26*, 16066.
138. C. Dressel, F. Liu, M. Prehm, X. Zeng, G. Ungar, C. Tschierske, *Angew. Chem. Int. Ed.* **2014**, *53*, 13115.
139. T. Kato, *Angew. Chem. Int. Ed.* **2010**, *49*, 7847.
140. T. Kato, M. Yoshio, T. Ichikawa, B. Soberats, H. Ohno, M. Funahashi, *Nat. Rev. Mater.* **2017**, *2*, 17001.
141. O. Kwon, X. Cai, W. Qu, F. Liu, J. Szydłowska, E. Gorecka, M. J. Han, D. K. Yoon, S. Poppe, C. Tschierske, *Adv. Funct. Mater.* **2021**, 2102271.
142. C. Tschierske, C. Dressel, *Symmetry* **2020**, *12*, 1098.
143. C. Tschierske, G. Ungar, *ChemPhysChem* **2016**, *17*, 9.
144. C. Dressel, W. Weissflog, C. Tschierske, *Chem. Comm.* **2015**, *51*, 15850.
145. W. Weissflog, L. Kovalenko, I. Wirth, S. Diele, G. Pelzl, H. Schmalfuss, H. Kresse, *Liq. Cryst.* **2000**, *27*, 677.
146. U. Dunemann, M. W. Schröder, R. A. Reddy, G. Pelzl, S. Diele, W. Weissflog, *J. Mater. Chem.* **2005**, *15*, 4051.
147. L. Kovalenko, M. W. Schröder, R. A. Reddy, S. Diele, G. Pelzl, W. Weissflog, *Liq. Cryst.* **2005**, *32*, 857.



- 
148. G. Pelzl, W. Weissflog. Mesophase behaviour at the borderline between calamitic and banana-shaped mesogens. In: Ramamoorthy A, editor. *Thermotropic Liquid Crystals: Recent Advances*. The Netherlands: Springer; **2007**. p. 1–58.
149. W. Weissflog, H. N. S. Murthy, S. Diele, G. Pelzl, *Phil. Trans Royal Soc A*. **2006**, *364*, 2657.
150. A. Eremin, S. Diele, G. Pelzl, H. Nadasi, W. Weissflog, H. Kresse, *Phys. Rev. E*. **2001**, *64*, 051707.
151. L. Pan, B. K. McCoy, S. Wang, W. Weissflog, C. C. Huang, *Phys. Rev. Lett.* **2010**, *105*, 117802.
152. D. Pocięcha, E. Goreęka, M. Čepič, N. Vaupotic, W. Weissflog, *Phys. Rev. E*. **2006**, *74*, 021702.
153. I. Wirth, S. Diele, A. Eremin, G. Pelzl, S. Grande, L. Kovalenko, N. Pancenko, W. Weissflog, *J. Mater. Chem.* **2001**, *11*, 1642.
154. C. Keith, A. Lehmann, U. Baumeister, M. Prehm, C. Tschierske, *Soft Matter*. **2010**, *6*, 1704.
155. G. Shanker, M. Prehm, M. Nagaraj, J. K. Vij, C. Tschierske, *J. Mater. Chem.* **2011**, *21*, 18711.
- A156. M. Alaasar, M. Prehm, M. Poppe, M. Nagaraj, J. K. Vij, C. Tschierske. *Soft Matter* **2014**, *10*, 5003.
157. J. Barberá, L. Puig, P. Romero, J. L. Serrano, T. Sierra, *J. Am. Chem. Soc.* **2006**, *128*, 4487.
158. C. Tschierske, H. Zschke, *J. prakt. Chem.* **1989**, *331*, 365.
159. C. Tschierske, D. J. Photinos, *J. Mater. Chem.* **2010**, *20*, 4263.
160. F. Vita, F. C. Adamo, O. Francescangeli, *J. Mol. Liq.* **2018**, *267*, 564.
161. A. Jakli, *Liq. Cryst. Rev.* **2013**, *1*, 65.
162. A. de Vries, *Mol. Cryst. Liq. Cryst.* **1970**, *10*, 219.
163. G. Shanker, M. Prehm, M. Nagaraj, J. K. Vij, M. Weyland, A. Eremin, C. Tschierske, *ChemPhysChem*. **2014**, *15*, 1323.
164. O. Francescangeli, F. Vita, E. T. Samulski, *Soft Matter* **2014**, *10*, 7685.
165. H. F. Gleeson, S. Kaur, V. Görtz, A. Belaissaoui, S. Cowling, J. W. Goodby, *ChemPhysChem*. **2014**, *15*, 1251.
166. N. Vaupotic, J. Szydłowska, M. Salamonczyk, A Kovarova, J Svoboda, M Osipov, D Pocięcha, E. Goreęka, *Phys. Rev. E*. **2009**, *80*, 030701.
167. C. Tschierske, *Top. Curr. Chem.* **2011**, *318*, 1.

- 
168. M. Hird, *Chem. Soc. Rev.* **2007**, *36*, 2070.
169. F. Guittard, E. Taffin de Givenchy, S. Geribaldi, A. Cambon, *J. Fluorine Chem.* **1999**, *100*, 85.
170. J.W. Goodby, I. M. Saez, S. J. Cowling, J. S. Gasowska, R. A. MacDonald, S. Sia, P. Watson, K. J. Toyne, M. Hird, R. A. Lewis, S. E. Lee, V. Vaschenko, *Liq. Cryst.* **2009**, *36*, 567
171. M. Bremer, P. Kirsch, M. Klasen-Memmer, K. Tarumi, *Angew. Chem. Int. Ed.* **2013**, *52*, 8880.
172. J. P. Bedel, J. C. Rouillon, J. P. Marcerou, M. Laguerre, H. T. Nguyen, M. F. Achard, *J. Mater. Chem.* **2002**, *12*, 2214.
173. R. A. Reddy, B. K. Sadashiva, *J. Mater. Chem.* **2002**, *12*, 2627.
174. H. N. Shreenivasa Murthy, B. K. Sadashiva, *Liq. Cryst.* **2004**, *31*, 1337
175. G. Dantlgraber, D. Shen, S. Diele, C. Tschierske, *Chem. Mater.* **2002**, *14*, 1149.
176. C. V. Yelamaggad, I. Swamy Shashikala, U. S. Hiremath, G. Liao, A. Jakli, D. S. Shankar Rao, S. Krishna Prasad, Q. Li, *Soft Matter* **2006**, *2*, 785
177. K. M. Fergusson, M. Hird, *J. Mater. Chem.* **2010**, *20*, 3069.
178. J. W. Goodby, P. J. Collings, T. Kato, et al. Handbook of Liquid Crystals. 2nd ed. Vol. 5 (Weinheim: Wiley-VCH), **2014**, p. 34–36.
179. G. Pelzl, A. Eremin, S. Diele, H. Kresse, W. Weissflog, *J. Mater. Chem.* **2002**, *1*, 2591.
180. Y. Jang, R. Balachandran, C. Keith, A. Lehmann, C. Tschierske, J. K. Vij, *Soft Matter.* **2012**, *8*, 10479.
181. P. S. Salter, C. Tschierske, S. J. Elston, E. P. Raynes, *Phys. Rev. E.* **2011**, *84*, 031708.
182. A. Immirzi, B. Perini, *Acta Crystallogr. Sect. A.* **1977**, *33*, 216.
- A183. N. Sebastián, S. Belau, A. Eremin, M. Alaasar, M. Prehm, C. Tschierske, *Phys. Chem. Chem. Phys.* **2017**, *19*, 5895.
- A184. A. Lehmann, M. Alaasar, M. Poppe, S. Poppe, M. Prehm, M. Nagaraj, S. P. Sreenilayam, Y. P. Panarin, J. K. Vij, C. Tschierske, *Chem. Eur. J.* **2020**, *26*, 4714.
- A185. M. Poppe, M. Alaasar, A. Lehmann, S. Poppe, M.-G. Tamba, M. Kurachkina, A. Eremin, M. Nagaraj, J. K. Vij, X. Cai, F. Liu, C. Tschierske. *J. Mater. Chem. C* **2020**, *8*, 3316.
186. A. Jákli, V. Prasad, D. S. S. Rao, G. Liao, I. Janossy, *Phys. Rev. E* **2005**, *71*, 021709.
187. N. G. Nagaveni, V. Prasad, A. Roy, *Liq. Cryst.* **2013**, *40*, 1405.
188. G. G. Nair, S. K. Prasad, U. S. Hiremath, C. V. Yelamaggad, *J. Appl. Phys.* **2001**, *90*, 48.
- A189. M. Kohout, M. Alaasar, A. Poryvai, V. Novotná, S. Poppe, C. Tschierske, J. Svoboda, *RSC Adv.* **2017**, *7*, 35805.

- 
190. D. A. Paterson, J. Xiang, G. Singh, R. Walker, D. M. Agra-Kooijman, A. Martiez-Felipe, M. Gao, J. M. D. Storey, S. Kumar, O. D. Lavrentovich, C. T. Imrie, *J. Am. Chem. Soc.* **2016**, *138*, 5283
191. G. Pelzl, S. Diele, W. Weissflog, *Adv. Mater.* **1999**, *11*, 707.
192. E. Cruickshank, K. Anderson, J. M. D. Storey, C.T. Imrie, E. Gorecka, D. Pocięcha, A. Makal, M.M. Majewska, *J. Mol. Liq.* **2022**, *346*, 118180.
193. G. Dantlgraber, A. Eremin, S. Diele, A. Hauser, H. Kresse, G. Pelzl, C. Tschierske, *Angew. Chem. Int. Ed.* **2002**, *41*, 2408;
194. G. Heppke, D. D. Parghi, H. Sawade, *Liq. Cryst.* **2000**, *27*, 313.
195. J. Thisayukta, Y. Nakayama, S. Kawachi, H. Takezoe, J. Watanabe, *J. Am. Chem. Soc.* **2000**, *122*, 7441.
196. G. Dantlgraber, S. Diele, C. Tschierske, *Chem. Comm.* **2002**, *23*, 2768.
197. C. Keith, R. A. Reddy, U. Baumeister, H. Hahn, H. Lang, C. Tschierske, *J. Mater. Chem.* **2006**, *16*, 3444.
198. H. Hahn, C. Keith, H. Lang, R. A. Reddy, C. Tschierske, *Adv. Mater.* **2006**, *18*, 2629.
199. C. Keith, G. Dantlgraber, R. A. Reddy, U. Baumeister, M. Prehm, H. Hahn, H. Lag, C. Tschierske, *J. Mater. Chem.* **2007**, *17*, 3796.
200. Y. Zhang, U. Baumeister, C. Tschierske, M. O'Callaghan, C. Walker, *Chem. Mater.* **2010**, *22*, 2869.
201. R. A. Reddy, B. K. Sadashiva, *Liq. Cryst.* **2003**, *30*, 1031.
202. A. Roy, M. Gupta, S. Radhika, B. K. Sadashiva, R. Pratibha, *Soft Matter* **2012**, *8*, 7207.
203. J. Ortega, C. L. Folcia, J. Etxebarria, N. Gimeno, M. B. Ros, *Phys. Rev. E: Stat., Nonlinear, Soft Matter Phys.* **2003**, *68*, 11707-1-4.
204. S. Kang, Y. Saito, N. Watanabe, M. Tokita, Y. Takanishi, H. Takezoe, J. Watanabe, *J. Chem. Phys. B.* **2006**, *110*, 5205.
205. D. M. Walba, L. Eshat, E. Körblova, R. K. Shoemaker, *Cryst. Growth Des.* **2005**, *5*, 2091.
206. D. Chen, J. E. MacLennan, R. Shao, D. K. Yoon, H. Wang, E. Körblova, D. M. Walba, M. A. Glaser, N. A. Clark, *J. Am. Chem. Soc.* **2011**, *133*, 12656.
207. J. M.-Perdiguero, I. Alonso, C. L. Folcia, J. Etxebarria, J. Ortega, *J. Mater. Chem.* **2009**, *19*, 5161.
208. C. Zhang, N. Diorio, O.D. Lavrentovich, A. Jáklı, *Nat. Comm.* **2014**, *5*, 3302.
209. H. Niwano, M. Nakata, J. Thisayukta, D. R. Link, H. Takezoe, J. Watanabe, *J. Phys. Chem. B* **2004**, *108*, 14889.

- 
210. H. Kurosu, M. Kawasaki, M. Hirose, M. Yamada, S. Kang, J. Thisayukta, M. Sone, H. Takezoe, J. Watanabe, *J. Phys. Chem. A* **2004**, *108*, 4674.
211. J. Thisayukta, H. Takezoe, J. Watanabe, *Jpn. J. Appl. Phys.* **2001**, *40*, 3277.
212. H. Kresse, J. Saltetnokova, H. Nadasi, W. Weissflog, A. Hauser, *Liq. Cryst.* **2001**, *28*, 1017.
213. E. Bialecka-Florjanczyk, I. Sledzinska, E. Górecka, J. Przedmojski, *Liq. Cryst.* **2008**, *35*, 401.
214. A. Zep, M. Salamonczyk, N. Vaupotič, D. Pocięcha, E. Gorecka, *Chem. Comm.* **2013**, *49*, 3119.
215. C. Zhu, C. Wang, A. Young, F. Liu, I. Gunkel, D. Chen, D Walba, J. Maclellan, N. Clark, A. Hexemer, *Nano Lett.* **2015**, *15*, 3420.
216. G. B. Deepa, S. Radhika, B. K. Sadashiva, R. Pratibha, *Phy. Rev. E.* **2013**, *87*, 062508.
217. D. G. Bhat, R. Selvaraj, S. B. Kapanipathaiya, P. Ramarao, *ChemPhysChem* **2015**, *16*, 825.
218. S. K. Lee, X. Li, S. Kang, M. Tokita, J. Watanabe, *J. Mater. Chem.* **2009**, *19*, 4517
219. S. Lee, H. Kim, T. J. Shin, E. Tsai, J. M. Richardson, E. Korblova, D. M. Walba, N. A. Clark, S. B. Lee, D. K. Yoon, *Soft Matter* **2015**, *11*, 3653.
220. I. Miyake, Y. Takanishi, N. V. S. Rao, M. K. Paul, K. Ishikawa, H. Takezoe, *J. Mater. Chem.* **2005**, *15*, 4688.
221. A. Belaissaoui, S. J. Kowling, J. W. Goodby, *Liq. Cryst.* **2013**, *40*, 822.
222. H. Ocak, B. Bilgin-Eran, M. Prehm, C. Tschierske, *Soft Matter* **2013**, *9*, 4590.
223. E. Tsai, J. M. Richardson, E. Korblova, M. Nakata, D. Chen, Y. Shen, R. Shao, N. A. Clark, D. M. Walba, *Angew. Chem. Int. Ed.* **2013**, *52*, 5254.
224. D. Chen, Y. Shen, J. Agüero, E. Korblova, D. M. Walba, N. Kapernaum, F. Giesselmann, J. Watanabe, J. E. Maclellan, M. A. Glaser, N. A. Clark, *ChemPhysChem* **2014**, *15*, 1502.
- A225. B. N. Sunil, M. K. Srinatha, G. Shanker, G. Hegde, M. Alaasar, C. Tschierske, *J. Mol. Liq.* **2020**, *304*, 112719.
226. C. Dressel, T. Reppe, M. Prehm, M. Brautzsch, C. Tschierske, *Nat. Chem.* **2014**, *6*, 971.
- A227. Y. Cao, M. Alaasar, L. Zhang, C. Zhu, C. Tschierske, F. Liu, *J. Amer. Chem. Soc.*, **2022**, *144*, 6936.
228. V. Luzzati, A. Tardieu, T. Gulik-Krzywicki, E. Rivas, F. Reiss-Hussn, *Nature* **1968**, *220*, 485.
229. T. Sakaizumi, M. Namikawa, O. Ohashi, *J. Mol. Str.* **1995**, *345*, 189.
230. J. Hine, *Reaktivität und Mechanismus in der Organischen Chemie*, Thieme Stuttgart, **1960**.

- 
231. F. G. Riddell, *The conformational analysis of Heterocyclic compounds*, Academic Press, **1980**.
232. V. F. Petrov, V. A. Vinkurov, V. V. Belyav, *Mol. Cryst. Liq. Cryst.* **2010**, *518*, 40.
233. C. Tschierske, D. Joachimi, H.-M. Vorbrod, H. Zschke, A. Wiegeleben, A. Hauser, D. Demus, *Liq. Cryst.*, **1989**, *5*, 177.
234. E. Kleinpeter, H. Köhler, A. Lunow, C. Tschierske, H. Zschke, *Tetrahedron*, **1988**, *44*, 1609.
235. Y. Arakawa, S. Kang, H. Tsuji, J. Watanabe, G.-i. Konishi. *RSC Adv.*, **2016**, *6*, 16568.
236. S. T. Lagerwall, A. Dahlgren, P. Jägelmalm, P. Rudquist, K. D'have', H. Pauwels, R. Dabrowski, W. Drzewinski, *Adv. Funct. Mater.* **2001**, *11*, 87.
237. A. I. Smirnova, B. Heinrich, B. Donnio, D. W. Bruce, *RSC Adv.* **2015**, *5*, 75149.
238. D.W. Bruce, P. Metrangolo, F. Meyer, T. Pilati, C. Präsang, G. Resnati, G. Terraneo, S. G. Wainwright, A. C. Whitwood, *Chem. Eur. J.* **2010**, *16*, 9511.
239. Y. Chen, H. Yu, L. Zhang, H. Yang, Y. Lu, *Chem. Comm.* **2014**, *50*, 9647.
- A240. J. M. Shivanna, M. Alaasar, G. Hegde, *J. Mol. Liq.* **2021**, *341*, 117341.
241. J. Matraszek, D. Pocięcha, N. Vaupotič, M. Salamończyk, M. Vogrin, E. Gorecka, *Soft Matter* **2020**, *16*, 3882.
242. J. M. Wolska, D. Pocięcha, J. Mieczkowski, E. Gorecka, *Liq. Cryst.* **2016**, *43*, 235.

# A Liquid Crystalline Phase with Uniform Tilt, Local Polar Order and Capability of Symmetry Breaking

Mohamed Alaasar,\* Marko Prehm, Mamatha Nagaraj, Jagdish K. Vij,  
and Carsten Tschierske\*

Spontaneous symmetry breaking, especially the formation of chiral superstructures by molecular self-assembly of achiral molecules or racemic mixtures of chiral molecules is of actual interest in pursuit of generation of chiral nanostructures.<sup>[1]</sup> Recently, work on spontaneous reflection symmetry breaking has moved from crystalline assemblies into the field of fluid liquid crystalline superstructures,<sup>[2,3]</sup> namely LC phases formed by bent-core molecules, for which spontaneous formation of macroscopic chiral superstructures was observed in smectic (lamellar) phases,<sup>[4–8]</sup> B4-type soft crystal phases<sup>[9,10]</sup> and nematic phases.<sup>[11]</sup> In the lamellar phases of bent core mesogens the molecular bend restricts the rotation of the molecules around their long axes. This leads to a directed packing of these molecules, giving rise to polar order with a direction of the polar moment along the bend direction and parallel to the layer planes (Figure 1).<sup>[4,5]</sup> Depending to the degree of polar coupling, which is influenced by the strength of the molecular bend and the packing density of the molecules, the rotation of the molecules around their long axes is more or less restricted, leading to polar ordered domains with coherence lengths ranging from microscopic to macroscopic. If the domains have macroscopic size the polar direction in adjacent layers can be opposite (antipolar), giving rise to antiferroelectric switching smectic phases (SmP<sub>A</sub>) or identical (synpolar), providing ferroelectric switching (SmP<sub>F</sub> phases) under an applied electric AC field.<sup>[5,6]</sup> Ferroelectric and antiferroelectric switching can be distinguished by the appearance of only one and two polarization current peaks during a half period of an applied triangular wave voltage, respectively.<sup>[5]</sup> If the domains are only short range the coupling of the electric field with the polar domains is too weak to create a macroscopic polarization and no polarization current could be measured (paraelectric switching).<sup>[12]</sup> For polar domains with a medium coherence length macroscopic

polar order can be induced under a sufficiently strong applied field and in this case relatively broad polarization peaks can be observed. These smectic phases composed of macroscopically randomized polar domains of appreciable size are assigned as SmP<sub>R</sub>. Only the non-tilted SmAP<sub>R</sub> phase has been reported so far.<sup>[13,14]</sup> However, similar to ordinary smectic LC phases of conventional rod-like molecules, also the polar smectic phase of bent-core mesogens can either be tilted (SmCP phases) or non-tilted (SmAP phases). As a tilt reduces the symmetry of polar layers to C<sub>2</sub>, chirality arises in the layers of the SmCP phases due to the combination of tilt direction and polar direction (Figure 1a) though the molecules themselves are achiral.<sup>[5,6]</sup>

As not only the polar direction, but also the tilt can either be identical in adjacent layers (synclinc tilt) or opposite (anticlinc tilt), in total four different structures can be distinguished, namely SmC<sub>s</sub>P<sub>A</sub> and SmC<sub>a</sub>P<sub>F</sub> which have opposite chirality sense in adjacent layers and hence represent achiral “mesoforms” and SmC<sub>a</sub>P<sub>A</sub>, SmC<sub>s</sub>P<sub>F</sub> which have identical chirality sense in the layers and therefore exist in two enantiomeric forms (Figure 1b).<sup>[5,6]</sup> Besides this suprastructural chirality (layer chirality) formation of helical superstructures due to the bias of helical molecular conformations,<sup>[3,5,8,15,16,10]</sup> negative bent elastic constants<sup>[17]</sup> and surface pinning effects<sup>[8,10]</sup> represents a second possible source of chirality in the LC phases of achiral bent-core molecules. These helical superstructures can, for example, be observed in the above mentioned B4 phases and some nematic phases.

Herein we report a new LC phase (SmC<sub>s</sub>P<sub>R</sub>) with uniform (synclinc) tilt, composed of polar domains with appreciable coherence length and randomized polar direction.<sup>[13,14]</sup> This phase can be considered as the tilted analog of the previously reported SmAP<sub>R</sub> phase. However, in contrast to the non-tilted SmAP<sub>R</sub> phase in this new phase the molecules are tilted and it is composed of SmC<sub>s</sub>P<sub>F</sub> domains which are chiral due to the combination of synclinc tilt and polar order, and therefore, under certain conditions, this phase can become macroscopically chiral.

The bent-core compound **1** (Figure 2a), showing this new phase combines a 4-cyanoresorcinol based bent-core unit with two azobenzene wings. The 4-cyanoresorcinol core is a bent structural unit<sup>[18]</sup> providing a reduced bend (>120° angle between the rod-like wings)<sup>[18b]</sup> compared to other units and therefore new LC phases at the borderline between rod-like and bent-core molecules can be expected. Azobenzene cores have previously been used for photoisomerizable bent-core mesogens<sup>[19,20]</sup> and in attempts to produce biaxial nematic phases.<sup>[21]</sup> The synthesis, purification and analytical data of compound **1** are reported in the Supporting Information.

Dr. M. Alaasar  
Department of Chemistry, Faculty of Science  
Cairo University, Giza, Egypt  
E-mail: m\_alaasar@yahoo.com

Dr. M. Alaasar, Dr. M. Prehm, Prof. Dr. C. Tschierske  
Institute of Chemistry  
Martin Luther University Halle-Wittenberg  
Kurt-Mothes Str.2, D-06120 Halle/Saale, Germany  
E-mail: Carsten.tschierske@chemie.uni-halle.de

Dr. M. Nagaraj, Prof. Dr. J. K. Vij  
Department of Electronic and Electrical Engineering  
Trinity College  
University of Dublin, Dublin 2, Ireland  
E-mail: jvij@tcd.ie



DOI: 10.1002/adma.201205180

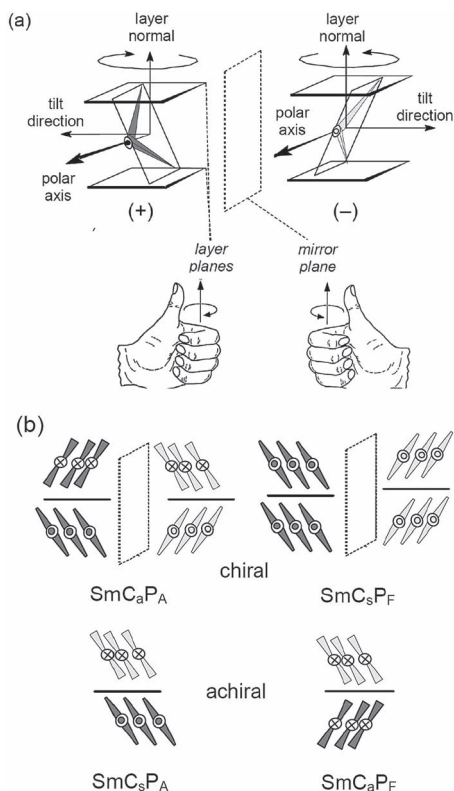


**Figure 1.** a) Superstructural chirality (layer chirality) arising from the combination of tilt and polar order in layers of smectic LC phases of bent-core molecules; reversing either tilt direction or polar direction reverses the chirality sense; b) the four possible structures resulting from the combination of tilt and polar order; combination of layers with the same chirality sense leads to homogeneously chiral smectic phases  $\text{SmC}_a\text{P}_A$  and  $\text{SmC}_s\text{P}_F$ , whereas combination of layers with opposite chirality sense leads to the achiral smectic phases  $\text{SmC}_s\text{P}_A$  and  $\text{SmC}_a\text{P}_F$ ; in b) the view is along the polar axis, dots indicate that the polar axis is pointing out of the projection plane, crosses indicate that the polar axis is pointing into the projection plane; distinct gray levels indicate the chirality sense;<sup>[5,6]</sup> adopted from.<sup>[5c]</sup>

Upon cooling from the isotropic liquid state, compound **1** shows a series of phase transitions with relatively small transition enthalpy values (see Figure 2a,b). Focus of this communication is exclusively on the new  $\text{SmC}_s\text{P}_R$  phase occurring in the temperature range between 95 and 139.5 °C in between a  $\text{SmC}_s\text{P}_A$  phase at lower and a small range of a nematic (N) phase at higher temperature.

Under the polarizing microscope this phase shows a fan-like texture, indicating a smectic phase (Figure 2c) or a birefringent Schlieren texture comprising exclusively 4-brush disclinations (Figure 2d), indicating phase biaxiality. In homeotropic cells with a medium cell gap (7.6  $\mu\text{m}$ ) a low birefringent texture composed of distinct domains is observed between crossed polarizers (Figure 2g). Uncrossing the polarizers by a small angle leads to the appearance of dark and bright domains with a maximum contrast at an angle of ca 15°. Uncrossing the polarizer in the other direction reverses the dark and bright domains (Figure 2e,f), whereas rotation of the sample between crossed polarizers gives no significant change of brightness (Figure 2h,i). This indicates that the distinct regions represent

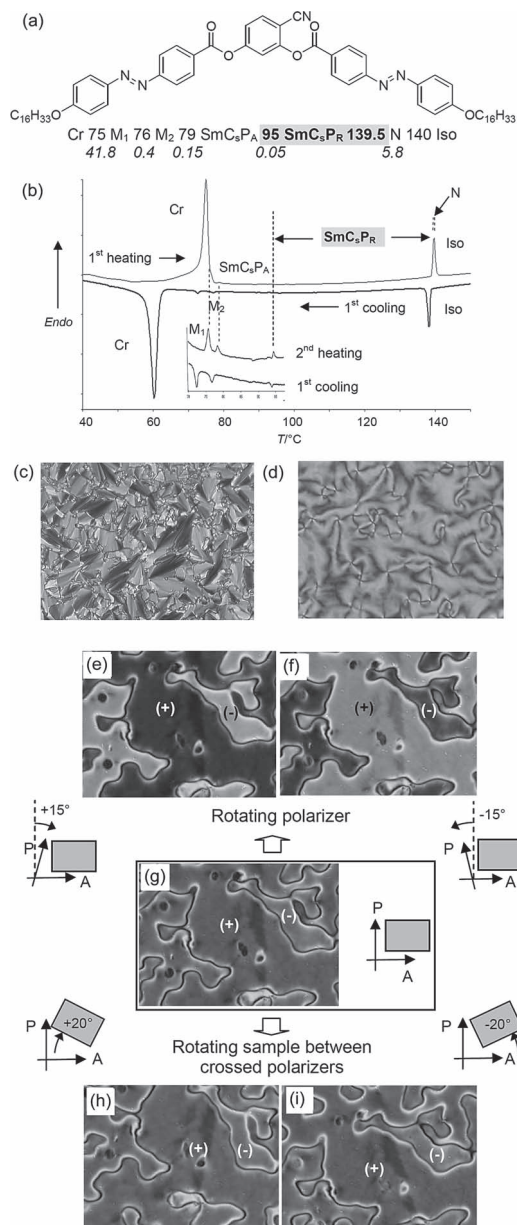


**Figure 2.** Structure, calorimetric and optical properties of compound **1**. a) Structure, transition temperatures ( $T/^\circ\text{C}$ ) and transition enthalpies (lower line,  $\Delta H/\text{kJ mol}^{-1}$ ) of compound **1**;<sup>[a]</sup> b) DSC heating and cooling curves ( $10 \text{ K min}^{-1}$ ) of compound **1** and c,d) textures of the  $\text{SmC}_s\text{P}_R$  phase between crossed polarizers; c) fan-like texture at  $T = 105 \text{ }^\circ\text{C}$  in a planar  $6 \mu\text{m}$  cell and d) Schlieren texture at  $T = 135 \text{ }^\circ\text{C}$  in a  $10 \mu\text{m}$  homeotropic cell. e-i) Textures as seen for the  $\text{SmC}_s\text{P}_R$  phase at  $T = 138 \text{ }^\circ\text{C}$  in a  $7.6 \mu\text{m}$  homeotropic cell: g) between crossed polarizers and e,f) between slightly uncrossed polarizers, showing dark and bright domains, indicating the presence of areas with opposite chirality sense; h,i) show the texture between crossed polarizers, but after rotation of the sample by  $20^\circ$  either clockwise or anticlockwise; the birefringence does not change which confirms chirality as origin of the effects seen in e-g); observations in a thinner  $5.9 \mu\text{m}$  cell are shown in Figure S3; abbreviations: Cr = crystalline solid; Iso = isotropic liquid;  $M_1$ ,  $M_2$  = polar switching mesophases with unknown structure;  $\text{SmC}_s\text{P}_A$  = synclinal tilted antiferroelectric SmC phase;  $\text{SmC}_s\text{P}_R$  = synclinal tilted SmC phase with randomized local ferroelectric order; N = nematic phase formed by SmC-type cybotactic clusters, as the phase range is very small no separate transition enthalpy values for the Iso-N transition and the N- $\text{SmC}_s\text{P}_R$  transitions could be recorded.

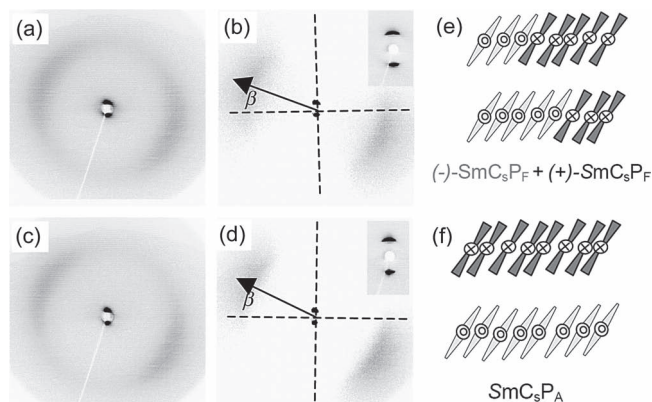


**Figure 3.** 2D-XRD patterns of a surface aligned sample of compound **1**: a,b) in the  $\text{SmC}_5\text{P}_R$  phase at  $T = 135\text{ }^\circ\text{C}$  and c,d) in the  $\text{SmC}_5\text{P}_A$  phase at  $T = 85\text{ }^\circ\text{C}$ ; a,c) original patterns and b,d) patterns after subtraction of the scattering in the isotropic phase at  $T = 145\text{ }^\circ\text{C}$ , showing the tilt more clearly; the insets in b), d) show the small angle scatterings (see also Figs. S1 and S2); e,f) show models of the phase structures; e)  $\text{SmC}_5\text{P}_R$  phase (only one tilt direction is shown, corresponding to the alignment observed in the XRD patterns, also only two polar directions are shown for clarity, in reality, there is almost randomization of the polar director due to the possible collective rotation around the long axes<sup>[23]</sup>), and f)  $\text{SmC}_5\text{P}_A$  phase.

chiral domains with opposite handedness and excludes that distinct tilt orientations are responsible for this effect. This chiral texture is reproducibly observed between glass slides with medium sample thickness ( $>4$  to  $<9\text{ }\mu\text{m}$ ) but it is not detectable in thicker (Figure 2d) or thinner cells (Figure S3). At the transition to the nematic phase the chirality of the domains completely disappears (Figure S4) and it is immediately recovered after cooling to the  $\text{SmC}_5\text{P}_R$  phase. At the transition to the achiral  $\text{SmC}_5\text{P}_A$  phase below  $T = 95\text{ }^\circ\text{C}$  realignment of the molecules takes place and leads to strongly increased birefringence which hides the effects of chirality, and hence, it is not clear if chirality is retained or removed at this transition.

The XRD diffraction pattern of a surface aligned sample of this phase shows a diffuse ring in the wide angle region with a maximum at  $d = 0.47\text{ nm}$ , corresponding to the mean lateral distance between the molecules in the LC phase (Figure 3a,b). The relatively sharp reflection in the small angle region is located on the meridian and has its maximum at  $d = 5.0\text{ nm}$ . As obvious after subtraction of the scattering in the isotropic phase the positions of the wide and small angle scattering maxima are inclined which indicates a synclinc tilted organization of the molecules with a tilt angle of  $\beta = 21^\circ$  at  $T = 135\text{ }^\circ\text{C}$  (Figure 3b). Comparison with the measured molecular length  $L = 6.4\text{ nm}$ <sup>[22]</sup> indicates a monolayer structure. Hence, this phase is a synclinc tilted smectic ( $\text{SmC}_s$ ) phase. However, the ring-like shape observed in the original diffraction pattern (Figure 3a) indicates a significant tilt director distribution. The diffraction pattern does not significantly change in the low temperature phase between  $79$  and  $95\text{ }^\circ\text{C}$  (Figure 3c,d), only the diffuse wide angle scattering becomes a bit more focused, indicating reduced director fluctuations.

Electro-optical investigations were carried out in a  $6\text{ }\mu\text{m}$  indium tin oxide (ITO) coated cell under an applied triangular

wave voltage. After transition from the isotropic liquid via the short nematic range to the  $\text{SmC}$  phase, in this  $\text{SmC}$  phase a relatively broad single peak appears in each half cycle of the applied triangular wave voltage (Figure 4b,c). A small peak already appearing in the isotropic liquid phase (Figure 4a) was assigned to conductivity, most probably due to traces of ionic impurities, and it is labeled as C. The single current peak increases in intensity as the temperature decreases and reaches a polarization value of  $P_S \sim 260\text{ nC cm}^{-2}$  close to the phase transition at  $T = 95\text{ }^\circ\text{C}$ . The shape of the peak and the relatively high threshold voltage are similar to those observed for the Langevin-type switching process in  $\text{SmAP}_R$  phases.<sup>[13,14]</sup> This indicates that in this phase there are local polar ordered domains with randomized polar directions<sup>[23]</sup> (Figure 3e) which are aligned under the electric field and then show ferroelectric-like switching (Figure 3f). Therefore, this phase is assigned as  $\text{SmC}_5\text{P}_R$ . The local structure is  $\text{SmC}_5\text{P}_F$ , which is synclinc and synpolar (ferroelectric), and therefore, intrinsically chiral (see Figure 1b).<sup>[5,6]</sup>

On further cooling, at  $95\text{ }^\circ\text{C}$ , two well developed sharp peaks appear (Figure 4d), indicating the transition to a tristable antiferroelectric switching process.<sup>[5]</sup> The tilt remains synclinc (see XRD patterns in Figure 3c,d), i.e. the phase at lower temperature is  $\text{SmC}_5\text{P}_A$ , which is achiral (see Figure 1b).<sup>[5,6]</sup> Under the field applied across a homogeneously aligned cell a birefringent fan-like texture, with dark extinctions inclined with the directions of polarizer and analyzer, is observed. Neither in the  $\text{SmC}_5\text{P}_R$  phase nor in the  $\text{SmC}_5\text{P}_A$  phase the switching process is associated with a change of the orientation of the extinctions (see Figure 4e-j), which indicates that in both phases the switching takes place by a collective rotation around the molecular long axis.<sup>[5]</sup>

Compound **1** was further investigated in a planar cell of  $10\text{ }\mu\text{m}$  thickness by dielectric spectroscopy in a frequency range of  $100\text{ Hz}$  and  $10\text{ MHz}$  on cooling from the isotropic phase and at temperatures in between  $145\text{ }^\circ\text{C}$  and  $75\text{ }^\circ\text{C}$ . The frequency dependence of the imaginary part of the dielectric permittivity ( $\epsilon''_{\perp}$ ) for selected temperatures is shown in Figure 5a (for original data before fitting, see Figure S5). Three relaxation processes, P1, P2 and P3, in the measured frequency range are being observed. P2 (the medium frequency relaxation process) and P3 (the high frequency relaxation process) can be observed only below  $95\text{ }^\circ\text{C}$  and therefore are not considered here. The low frequency process P1 is observed in the entire temperature region of the  $\text{SmC}_5\text{P}_R$  phase. The dielectric strength ( $\delta\epsilon$ ) and the relaxation frequency ( $f_R$ ) are obtained by fitting the relaxation spectra to the Havriliak-Negami equation.<sup>[24]</sup> Figure 5b,c shows the temperature dependence of  $\delta\epsilon$  and  $f_R$  for the process P1.  $\delta\epsilon$  diverges and  $f_R$  decreases somewhat on approaching the  $\text{SmC}_5\text{P}_R$  to  $\text{SmC}_5\text{P}_A$  phase transition at  $95\text{ }^\circ\text{C}$ . This result is rather similar to that observed for the  $\text{SmAP}_R$  to  $\text{SmAP}_A$  phase transition<sup>[13,14]</sup> and supports the assignment of the phase as  $\text{SmC}_5\text{P}_R$ .

Overall, the  $\text{SmC}_5\text{P}_R$  phase is a new phase occurring besides the polar ( $\text{SmCP}_A$ ,  $\text{SmCP}_F$ ) and the non-polar and paraelectric  $\text{SmC}$  phases of bent-core mesogens.<sup>[12,25]</sup> In the order  $\text{SmC}$ - $\text{SmC}_5\text{P}_R$ - $\text{SmC}_5\text{P}_A$  the coherence length of the polar domains increases, which is the key for the distinct properties, namely polar switching and achiral symmetry breaking with formation



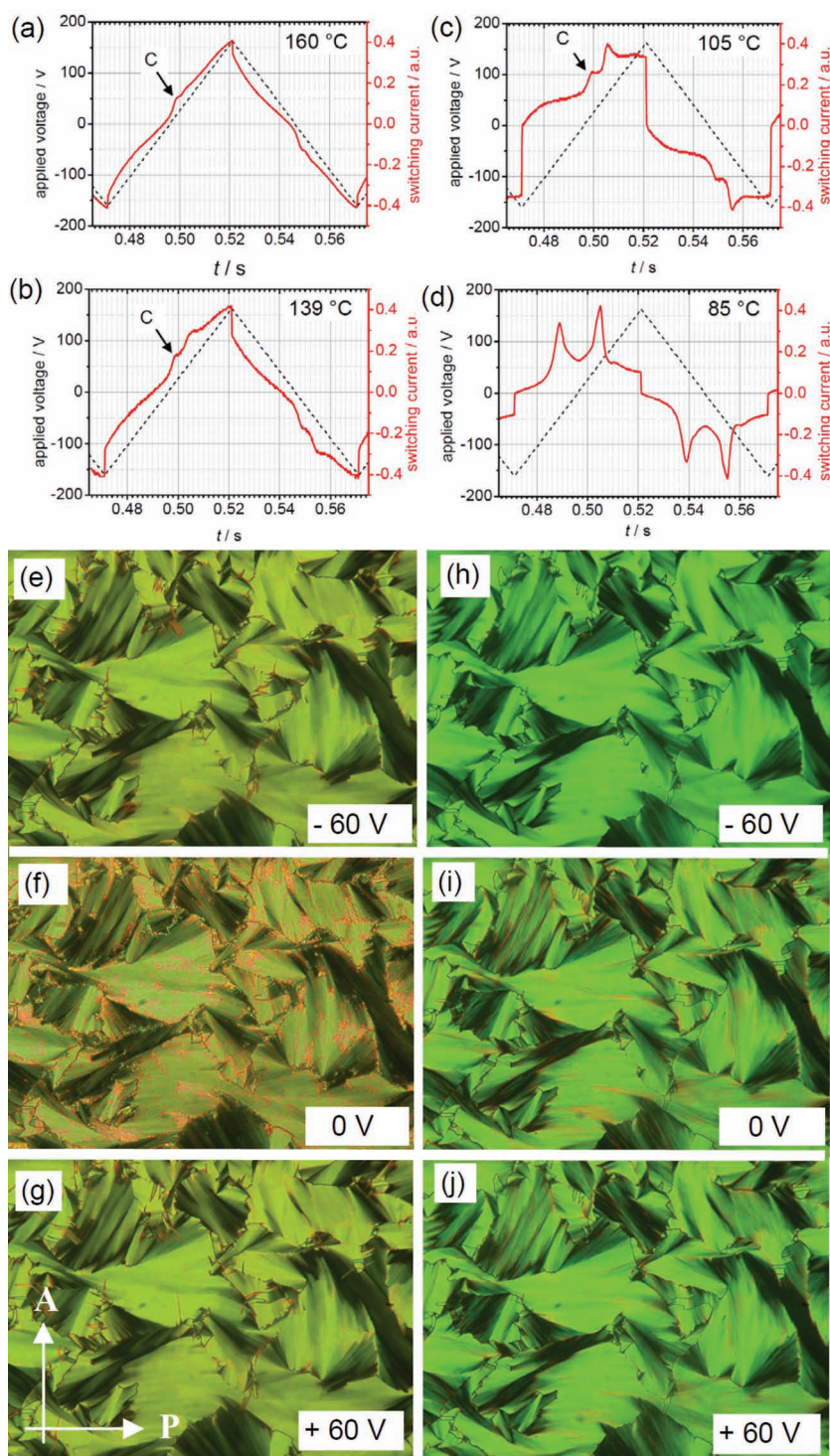


**Figure 4.** a-d) Switching current response curves in 6 μm ITO cells on applying a triangular wave field (10 Hz); a) isotropic liquid at  $T = 160$  °C; peak C is assigned to conductivity which is most probably due to traces of ionic impurities in the compound itself or from the glass surfaces; b) SmC<sub>s</sub>P<sub>R</sub> phase at  $T = 139$  °C and c) at  $T = 105$  °C and d) SmC<sub>s</sub>P<sub>A</sub> phase at  $T = 85$  °C; e-j) textures under an applied DC voltage between crossed polarizers (parallel rubbing, rubbing direction parallel to polarizer, direction of the polarizers is shown in g)); e-g) in the SmC<sub>s</sub>P<sub>R</sub> phase at  $T = 105$  °C and h-j) in the SmC<sub>s</sub>P<sub>A</sub> at  $T = 85$  °C, e,h) at  $-60$  V, f,i) after switching off the field (0 V) and g,j) at  $+60$  V.

of macroscopic chiral domains. This new phase also completes the series of different randomized phases of bent-core molecules, the non-tilted phases with randomized polar direction (SmAP<sub>R</sub>,<sup>[13,14]</sup> SmAP<sub>AR</sub>,<sup>[26]</sup> SmAP<sub>α</sub><sup>[27]</sup>) and the tilted smectic phases SmC<sub>R</sub><sup>[28]</sup> and SmC<sub>R</sub>P<sub>FE</sub>.<sup>[29]</sup> In the non-polar de Vries-like SmC<sub>R</sub> phase the tilt is randomized;<sup>[28]</sup> the biaxial SmC<sub>s</sub>P<sub>R</sub> phase has uniform tilt and randomized polar direction, whereas the previously reported uniaxial SmC<sub>R</sub>P<sub>FE</sub> phase has randomized tilt and stronger polar coupling, leading to field induced and surface stabilized ferroelectric states.<sup>[29]</sup> There is presently no clear indication of chirality in the SmC<sub>R</sub>P<sub>FE</sub> phase with only weak tilt correlation,<sup>[29]</sup> whereas it is found here for the SmC<sub>s</sub>P<sub>R</sub> phase with strong tilt correlation. The loss of chirality at the transition to the N phase (Figure S4) supports the idea that chirality preliminary arises from the coupling of long range synclinic tilt with local ferroelectric order. The fact that macroscopic chirality is observed only in thin cells with distinct thickness ( $>4$  to  $<9$  μm) suggests that surface effects support the formation of macroscopic chiral domains and fix the chirality sense once established. The chiral domains were observed in cells with parallel rubbing direction of the surfaces as well as between ordinary microscopy slides, independent of the orientation of the two glass surfaces with respect to each other. Therefore, it is thought that chirality in this case does not arise from surface pinning with distinct director alignment on the two opposite surfaces.<sup>[8,10]</sup> If chirality would be induced by this kind of surface pinning, then there should be an unequal distribution of the domains with opposite chirality, because the helix would develop with different probability in the two opposite directions if the angle between the alignment directions at the two surfaces is not exactly 90° (or 180°). In this case the helix should also have a different pitch depending on the helix sense, and hence the angle of rotation of the polarized light should be different in the chiral domains with opposite handedness; both effects were not observed.

In bulk samples and in thicker cells helix formation appears to be only local, which is considered to contribute to the nearly ring-like distribution of the diffuse wide angle scattering (Figure 3a). In very thin homeotropic cells the helix pitch appears to be much shorter than the cell gap and therefore the influence of the director orientation becomes

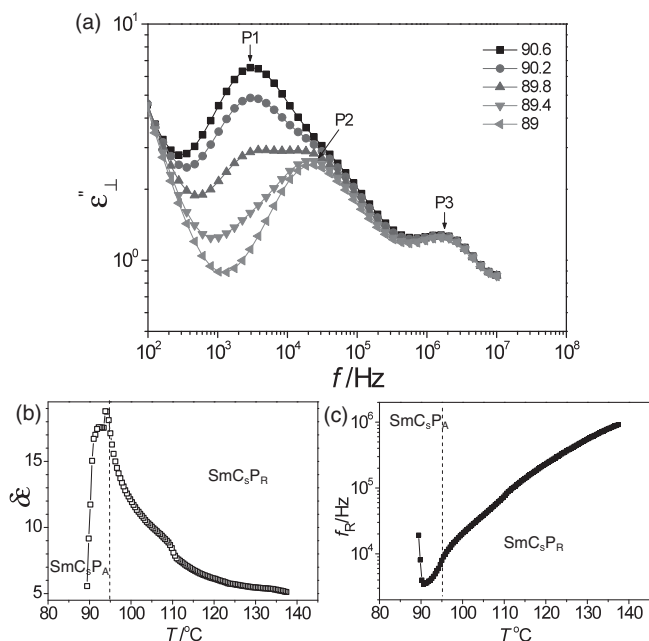


**Figure 5.** a) Frequency dependence of the imaginary part of dielectric permittivity ( $\epsilon''_{\perp}$ ) for selected temperatures measured in a planar cell ( $T/^{\circ}\text{C}$ ); P1, P2, P3 are the three relaxation processes; b, c)  $T$ -dependence of b) dielectric strength ( $\delta\epsilon$ ) and c) relaxation frequency ( $f_R$ ) of the relaxation process P1; a reproducible small step in the  $\delta\epsilon$  and  $f_R$  plots at  $T = 110^{\circ}\text{C}$  may indicate an increase in the size of the polar domains at this temperature. However, there is no indication of a phase transition being observed at such a temperature using POM, DSC and XRD.

dominating (see Figure S3). The unique combination of local polarity and chirality with the capability of forming macroscopic chiral domains under certain conditions could provide a key for the understanding of the development of chirality and optical activity in other fluid phases of bent-core molecules<sup>[5a,11,15]</sup> and more generally for achiral symmetry breaking events in soft matter. Additional options for this class of bent-core mesogens are chirality flipping by rotation around the long molecular axis and circularly polarized light (CPL) induced modulation of superstructural chirality.<sup>[30]</sup> The possibility of photochemical *trans-cis* isomerization of the azobenzene units using specific wavelengths<sup>[31]</sup> (isomerization to the *cis*-isomer using  $\lambda = 365\text{ nm}$  and transformation back to the *trans*-isomer by thermal annealing, see Figure S6 and associated explanations in the SI) could provide additional options for potential application of these azobenzene derived bent-core mesogens.

## Supporting Information

Supporting Information (experimental procedures and characterization data, investigation methods, XRD patterns, electro-optical and dielectric data) is available from the Wiley Online Library or from the author.

## Acknowledgements

M. A. acknowledges the Alexander von Humboldt Foundation for the research fellowship at MLU Halle; M.P. acknowledges the support by the

Cluster of Excellence "Nanostructured materials". JKV thanks SFI (TIDA) award for 2012.

Received: December 17, 2012  
Published online: February 20, 2013

- [1] a) I. Weissbuch, L. Leiserowitz, M. Lahav, *Top. Curr. Chem.* **2005**, 259, 123; b) A. R. A. Palmans, E. W. Meijer, *Angew. Chem. Int. Ed.* **2007**, 46, 8948.
- [2] V. Percec, P. Leowanawat, *Isr. J. Chem.* **2011**, 51, 1107.
- [3] C. Tschierske, in *Chirality at the Nano Scale* (Ed. D. B. Amabilino), Wiley-VCH, Weinheim, Germany **2009**, p. 271.
- [4] T. Niori, T. Sekine, J. Watanabe, T. Furukawa, H. Takezoe, *J. Mater. Chem.* **1996**, 6, 1231.
- [5] a) R. A. Reddy, C. Tschierske, *J. Mater. Chem.* **2006**, 16, 907; b) H. Takezoe, Y. Takanishi, *Jpn. J. Appl. Phys.* **2006**, 45, 597; c) C. Keith, R. A. Reddy, M. Prehm, U. Baumeister, H. Kresse, J. L. Chao, H. Hahn, H. Lang, C. Tschierske, *Chem. Eur. J.* **2007**, 13, 2556.
- [6] D. R. Link, G. Natale, R. Shao, J. E. MacLennan, N. A. Clark, E. Korblova, D. M. Walba, *Science* **1997**, 278, 1924.
- [7] a) G. Dantlgraber, A. Eremin, S. Diele, A. Hauser, H. Kresse, G. Pelzl, C. Tschierske, *Angew. Chem. Int. Ed.* **2002**, 41, 2408; b) L. E. Hough, M. Spannuth, M. Nakata, D. A. Coleman, C. D. Jones, G. Dantlgraber, C. Tschierske, J. Watanabe, E. Korblova, D. M. Walba, J. E. MacLennan, M. A. Glaser, N. A. Clark, *Science* **2009**, 325, 452.
- [8] H. Takezoe, *Top. Curr. Chem.* **2012**, 318, 303.
- [9] a) H. Niwano, M. Nakata, J. Thisayukta, D. R. Link, H. Takezoe, J. Watanabe, *J. Phys. Chem. B* **2004**, 108, 14889; b) L. E. Hough, H. T. Jung, D. Krüerke, M. S. Heberling, M. Nakata, C. D. Jones, D. Chen, D. R. Link, J. Zasadzinski, G. Heppeke, J. P. Rabe, W. Stocker, E. Korblova, D. M. Walba, M. A. Glaser, N. A. Clark, *Science* **2009**, 325, 456.
- [10] D. M. Walba, L. Eshdat, E. Korblova, R. K. Shoemaker, *Cryst. Growth Des.* **2005**, 5, 2091.
- [11] a) G. Pelzl, A. Eremin, S. Diele, H. Kresse, W. Weissflog, *J. Mater. Chem.* **2002**, 12, 2591; b) T. Niori, J. Yamamoto, H. Yokoyama, *Mol. Cryst. Liq. Cryst.* **2004**, 409, 475; c) V. Görtz, J. W. Goodby, *Chem. Commun.* **2005**, 3262; d) V. Görtz, *Liq. Cryst. Today* **2010**, 19, 37; e) C. Präsang, A. C. Whitwood, D. W. Bruce, *Chem. Commun.* **2008**, 2137; f) P. S. Salter, P. W. Benzie, R. A. Reddy, C. Tschierske, S. J. Elston, E. P. Raynes, *Phys. Rev. E* **2009**, 80, 031701.
- [12] A. Eremin, M. Floegel, U. Kornek, S. Stern, R. Stanarius, *Phys. Rev. E* **2012**, 86, 051701.
- [13] a) Y. Shimbo, E. Gorecka, D. Pocięcha, F. Araoka, M. Goto, Y. Takanishi, K. Ishikawa, J. Mieczkowski, K. Gomola, H. Takezoe, *Phys. Rev. Lett.* **2006**, 97, 113901; b) K. Gomola, L. Guo, E. Gorecka, D. Pocięcha, J. Mieczkowski, K. Ishikawa, H. Takezoe, *Chem. Commun.* **2009**, 6592; c) M. Gupta, S. Datta, S. Radhika, B. K. Sadashiva, A. Roy, *Soft Matter* **2011**, 7, 4735.
- [14] a) C. Keith, M. Prehm, Y. P. Panarin, J. K. Vij, C. Tschierske, *Chem. Commun.* **2010**, 46, 3702; b) G. Shanker, M. Prehm, M. Nagaraj, J. K. Vij, C. Tschierske, *J. Mater. Chem.* **2011**, 21, 18711.
- [15] a) D. J. Earl, M. A. Osipov, H. Takezoe, Y. Takanishi, M. R. Wilson, *Phys. Rev. E* **2005**, 71, 021706; b) H. S. Jeong, S. Tanaka, D. K. Yoon, S.-W. Choi, Y. H. Kim, S. Kawachi, F. Araoka, H. Takezoe, H.-T. Jung, *J. Am. Chem. Soc.* **2009**, 131, 15055.
- [16] H. Kurosu, M. Kawasaki, M. Hirose, M. Yamada, S. Kang, J. Thisayukta, M. Sone, H. Takezoe, J. Watanabe, *J. Phys. Chem. A* **2004**, 108, 4674.
- [17] a) I. Dozov, *Europhys. Lett.*, **2001**, 56, 247; b) V. P. Panov, M. Nagaraj, J. K. Vij, A. Kohlmeier, M. G. Tamba, R. A. Lewis, G. H. Mehl, *Phys. Rev. Lett.* **2010**, 105, 167801.

- [18] a) L. Kovalenko, M. W. Schröder, R. A. Reddy, S. Diele, G. Pelzl, W. Weissflog, *Liq. Cryst.* **2005**, *32*, 857; b) I. Wirth, S. Diele, A. Eremin, G. Pelzl, S. Grande, L. Kovalenko, N. Pancenko, W. Weissflog, *J. Mater. Chem.* **2001**, *11*, 1642; c) C. Keith, A. Lehmann, U. Baumeister, M. Prehm, C. Tschierske, *Soft Matter* **2010**, *6*, 1704.
- [19] a) N. G. Nagaveni, A. Roy, V. Prasad, *J. Mater. Chem.* **2012**, *22*, 8948; b) C. L. Folcia, I. Alonso, J. Ortega, J. Etxebarria, I. Pintre, M. B. Ros, *Chem. Mater.* **2006**, *18*, 4617; c) D. D. Sarkar, R. Deb, N. Chakraborty, V. S. Rao Nandiraju, *Liq. Cryst.* **2012**, *39*, 1003.
- [20] M.-G. Tamba, A. Bobrovsky, V. Shibaev, G. Pelzl, U. Baumeister, W. Weissflog, *Liq. Cryst.* **2011**, *38*, 1531.
- [21] a) V. Prasad, S.-W. Kang, K. A. Suresh, L. Joshi, Q. Wang, S. Kumar, *J. Am. Chem. Soc.* **2005**, *127*, 17224; b) K. V. Le, M. Mathews, M. Chambers, J. Harden, Q. Li, H. Takezoe, A. Jakli, *Phys. Rev. E* **2009**, *79*, 030701; c) D. Photinos, C. Tschierske, *J. Mater. Chem.* **2010**, *20*, 4263.
- [22] Measured with CKP models (space-filling models by Corey, Pauling and Koltun, see R. B. Corey, L. Pauling, *Rev. Sci. Instr.* **1953**, *24*, 621) between the ends of the molecule in a 120° bent conformation with all-*trans* alkyl chains.
- [23] Due to the presence of tilt there should be a deviation from a completely isotropic distribution of the polar directors.
- [24] S. Havriliak Jr., S. Negami, *Polymer* **1967**, *8*, 161.
- [25] A. Eremin, H. Nadasi, G. Pelzl, S. Diele, H. Kresse, W. Weissflog, S. Grande, *Phys. Chem. Chem. Phys.* **2004**, *6*, 1290.
- [26] K. Gomola, L. Guo, D. Pocięcha, F. Araoka, K. Ishikawa, H. Takezoe, *J. Mater. Chem.* **2010**, *20*, 7944.
- [27] Y. P. Panarin, M. Nagaraj, S. Sreenilayam, J. K. Vij, A. Lehmann, C. Tschierske, *Phys. Rev. Lett.* **2011**, *107*, 247801.
- [28] a) R. A. Reddy, U. Baumeister, C. Tschierske, *Chem. Commun.*, **2009**, 4236; b) R. A. Reddy, U. Baumeister, J.-L. Chao, H. Kresse, C. Tschierske, *Soft Matter* **2010**, *6*, 3883.
- [29] G. Dantlgraber, U. Baumeister, S. Diele, H. Kresse, B. Lühmann, H. Lang, C. Tschierske, *J. Am. Chem. Soc.* **2002**, *124*, 14852; in this reference the phase assignment SmCP<sub>R</sub> was used for this polar smectic phase with randomized tilt. As in the meanwhile SmAP<sub>R</sub> phases with randomized polar direction were also found; the more precise phase assignment SmC<sub>R</sub>P<sub>FE</sub> is used here; in this notation P<sub>FE</sub> refers to the experimental observed ferroelectric switching process.
- [30] H. Kim, T. K. Lim, S. T. Shin, C. K. Lee, F. Araoka, M. Ofuji, Y. Takanishi, H. Takezoe, *Phys. Rev. E* **2004**, *69*, 061701.
- [31] No influence of thermal annealing on the phase transition temperatures was observed.

# 4-Cyanoresorcinol-Based Bent-Core Mesogens with Azobenzene Wings: Emergence of Sterically Stabilized Polar Order in Liquid Crystalline Phases

Mohammed Alaasar,\* Marko Prehm, Kathrin May, Alexey Eremin,\* and Carsten Tschierske\*

A new series of azobenzene containing bent-core molecules incorporating 4-cyanoresorcinol as the central core unit exhibiting cybotactic nematic, rectangular, columnar, and different types of tilted smectic (SmC) phases are synthesized. The mesophase behavior and phase structures are characterized in bulk and freely suspended films using a variety of experimental techniques. Depending on the chain length and temperature a series of different mesophases is observed in these compounds, ranging from cybotactic nematic via paraelectric SmC phases, polarization randomized SmC<sub>s</sub>P<sub>R</sub> phases to ferroelectric and antiferroelectric SmC phases, associated with increasing size and correlation length of the polar domains. Spontaneous formation of chiral domains is observed in the paraelectric SmC and the SmC<sub>s</sub>P<sub>R</sub> phases and discussed in relation with superstructural chirality, bend elastic constants, and surface effects.

## 1. Introduction

Materials with spontaneous or induced polar order, which can be switched between polar and apolar states, are of potential interest for applications in sensors, memory and display devices. Most ferroelectrics and antiferroelectrics represent inorganic and organic solid state materials.<sup>[1]</sup> Liquid crystalline (LC) ferroelectrics are of special interest as they can be easily processed into devices and their configuration can be switched by external stimuli.<sup>[1]</sup> LC phases of chiral molecules in tilted smectic phases (SmC\* phases) provided the first examples of LC ferroelectric and antiferroelectric materials.<sup>[3]</sup> In the mid 90's a novel type of mesogenic material breathed new life into

this field and brought new expectations: the so-called banana-shaped LCs or bent-core LCs. Since the pioneering results by Niori et al.,<sup>[4]</sup> extensive research has been carried out on these LCs, and the results have allowed to appreciate new kind of truly fascinating materials. The occurrence of novel and intriguing polar mesophases, the induction of supramolecular chirality using achiral molecules and the noticeable optical, ferroelectric and antiferroelectric responses of these materials are, among others, aspects that are now well documented.<sup>[5]</sup>

Recently, the research became focused on materials at the borderline between rod-shaped and bent-core mesogens: such as hockey stick molecules, mesogenic

dimers combining rod-like and bent-core units, molecules with exceptionally short core units with only four or less aromatic rings and molecules with a reduced bend.<sup>[6]</sup> Varying the chemical structure of these compounds made it possible to design materials exhibiting a whole spectrum of phases from paraelectric to ferro- and antiferroelectric phases.<sup>[7,8]</sup> 4-Cyanoresorcinols represent a typical structure of this kind providing a reduced bend due to the effects of the CN group on the conformation of the adjacent ester group.<sup>[9–11]</sup> It was demonstrated in previous studies that this structural unit can be used to generate bent-core mesogens with broad regions of cybotactic nematic phases,<sup>[11]</sup> transitions between different types of orthogonal phases, non-polar SmA phases,<sup>[10]</sup> SmAP<sub>R</sub> phases with randomized polarization<sup>[1,2]</sup> and antiferroelectric SmAP<sub>A</sub> phases<sup>[10,13]</sup> have been observed. A new SmAP phase, in which the polarization rotates uniformly from layer to layer with a fixed angle between adjacent layers, was also suggested recently.<sup>[14]</sup>

In this work new bent-core mesogens combining the bent 4-cyanoresorcinol core with two rod-like azobenzene wings were synthesized and investigated. The azobenzene units could lead to materials with enhanced nonlinear optical (NLO) properties.<sup>[15]</sup> Another important attractive feature of these compounds is the transformation between its *trans* and *cis* configurations by light absorption (photoisomerism) which can be used to modify the mesophase structure.<sup>[16]</sup> Such materials could be used for holographic media, optical storage, reversible optical waveguides, and other applications.<sup>[17–20]</sup> Azobenzene cores have previously been used for photoisomerizable bent-core mesogens<sup>[21,22]</sup> and in attempts to produce biaxial nematic phases.<sup>[23,24]</sup> Combining photoswitchable azobenzenes with

Dr. M. Alaasar, Dr. M. Prehm, Prof. C. Tschierske  
Institute of Chemistry, Organic Chemistry  
Martin-Luther-University Halle-Wittenberg  
Kurt-Mothes-Str. 2, 06120, Halle, Germany  
E-mail: M.Alaasar@yahoo.com;  
Carsten.tschierske@chemie.uni-halle.de

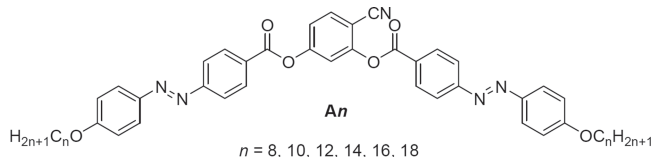
Dr. M. Alaasar  
Department of Chemistry  
Faculty of Science  
Cairo University  
Giza, Egypt

K. May, Dr. A. Eremin  
Institute for Experimental Physics  
Otto-von-Guericke University Magdeburg  
Universitätsplatz 2, 39106, Magdeburg, Germany  
E-mail: alexey.eremin@ovgu.de



DOI: 10.1002/adfm.201302295

liquid crystalline ferroelectrics also provides access to potential new multifunctional materials where polar response can be modulated by light.<sup>[25–29]</sup> Recently we have reported a first example of a 4-cyanoresorcinol with two azobenzene wings (compound **A14**).<sup>[8]</sup> An interesting feature of this compound is the formation of synclinal tilted SmC phases with an enhanced polarizability, which show surface supported achiral symmetry breaking.

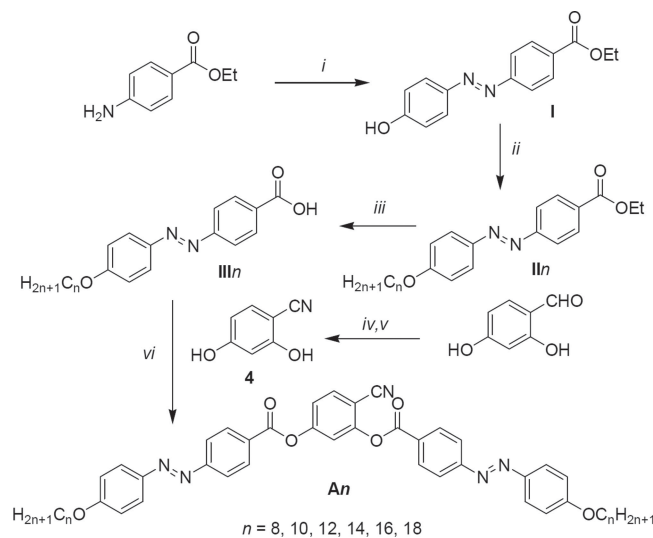


Herein, we report the synthesis and investigation of the complete series of these azobenzene bent-core mesogens **An** having even numbered alkyl chains with  $n$  ranging from 8 to 18. With these compounds additional investigations, especially Second Harmonic Generation (SHG) experiments and investigations of freely suspended thin films were performed and the whole sequence of different phases formed by these compounds was investigated and gained important new insights into the development of polar order in tilted smectic phases. It turned out to be more complex than in the orthogonal case due to the effects of tilt on packing density, layer modulation, elastic constants and superstructural chirality. The sequence observed on decreasing temperature is Iso –  $N_{CybC}$  – SmC –  $SmC_S P_R$  –  $SmC_S P_F$  –  $M_1$  –  $SmC_S P_A$  associated with increasing correlation length of polar domains. Already the isotropic and the nematic phases show field-induced polar order indicated by SHG activity as also found for all other tilted smectic phases of these compounds. This behavior is attributed to polar domains occurring well before the conventional antiferroelectric switchable  $SmC P_A$  phase is reached. In the paraelectric SmC phase the domains are small. The  $SmC_S P_R$  phase indicates a temperature range of the SmC phase where the size of the polar domains reaches an appreciable size and which can be regarded as the tilted analog to the previously reported  $SmA P_R$  phase.<sup>[12,13]</sup> Further growth of the ferroelectric domains leads to a  $SmC_S P_F$  phase which becomes modulated in the temperature range of the phase assigned as  $M_1$ , before the antiferroelectric switching  $SmC_S P_A$  phase with alternating polar direction in adjacent layers is formed. Spontaneous formation of chiral domains was observed for all compounds under certain conditions in the SmC and  $SmC_S P_R$  phases and it is assumed to be the result of the combined effects of superstructural chirality and surface anchoring.

## 2. Results

### 2.1. Synthesis

The synthesis of the bent-core compounds **A8–A18** is shown in **Scheme 1**. As reported previously 2,4-dihydroxybenzotriole (**4**) was prepared from commercially available 2,4-dihydroxybenzaldehyde by the formation of the oxime, followed by



**Scheme 1.** Synthetic route to the bent core molecules **An**; reagents and conditions: *i*) 1.  $NaNO_2$ , HCl,  $H_2O$ , 0–5 °C, 2. phenol, NaOH, 3.  $NaHCO_3$ ; *ii*)  $C_nH_{2n+1}Br$ , KI,  $K_2CO_3$ , 2-butanone, reflux 6 h; *iii*) 1. EtOH, KOH, reflux, 12 h, 2. HCl/ $H_2O$ , 20 °C; *iv,v*)  $H_2NOH \cdot HCl$ ,  $Ac_2O$ , *v*) NaOH,  $H_2O$ ;<sup>[30]</sup> *v*)  $N,N'$ -dicyclohexylcarbodiimide, 4-dimethylaminopyridine, 20 °C, 24 h.

dehydration.<sup>[30]</sup> All the homologues acids **III<sub>n</sub>** were synthesized according to the method described before in four steps.<sup>[22]</sup> First the azobenzene was prepared by diazotization of ethyl 4-aminobenzoate and coupling of the resulting diazonium salt with phenol yielding ethyl 4-(4-hydroxyphenylazo)benzoate (**I**). Compound **I** was alkylated with 1-bromoalkane in the presence of potassium carbonate to give ester compounds **II<sub>n</sub>**. Then the ester compounds **II<sub>n</sub>** were hydrolyzed under basic conditions to yield the benzoic acids **III<sub>n</sub>**. In the final step, the benzoic acids **III<sub>n</sub>** were esterified with 4-cyanoresorcinol (**4**) in the presence of  $N,N'$ -dicyclohexylcarbodiimide (DCC) and 4-dimethylaminopyridine (DMAP) as catalyst using dry dichloromethane as solvent to achieve the target compounds **A8–A18**. The final bent-core compounds were first purified by column chromatography and then by crystallization using ethanol/chloroform mixture. Complete synthetic procedures and analytical data are reported in the electronic supporting information.

### 2.2. Investigation Methods

The synthesized compounds **A8–A18** were investigated by polarized light optical microscopy (Optiphot 2, Nikon) in conjunction with a heating stage (FP82HT, Mettler) and by differential scanning calorimetry (DSC-7 Perkin Elmer). The assignment of the mesophases was made on the basis of combined results of optical textures and X-ray diffraction (XRD). The measurements were done at  $Cu-K\alpha$  line ( $\lambda = 1.54 \text{ \AA}$ ) using standard Coolidge tube source with a Ni-filter. Investigations of oriented samples were performed using a 2D-detector (HI-Star, Siemens AG). Uniform orientation was achieved by alignment in a magnetic field ( $B \approx 1 \text{ T}$ ) using thin capillaries. The orientation once achieved is maintained by slow cooling ( $0.1 \text{ K min}^{-1}$ ) in the presence of the magnetic field. Electro-optical experiments

have been carried out using a home built electro-optical setup in commercially available ITO coated glass cells (E.H.C., Japan, polyimide coated for planar alignment, antiparallel rubbing, thickness 6  $\mu\text{m}$  and measuring area 1  $\text{cm}^2$ ).

Measurements of optical second harmonic generation (SHG) have been performed using a Nd:YAG laser operating at  $\lambda = 1064 \text{ nm}$  (10 ns pulse width and 10 Hz repetition rate). The primary beam was incident at an angle of  $30^\circ$  to the cell normal. The SHG signal was detected in transmission by a photomultiplier tube (Hamamatsu). The acquired signal was calibrated using a 50  $\mu\text{m}$  reference quartz plate.

Freely-suspended films were drawn over a custom-made rectangular glass frame with a 10 mm  $\times$  3 mm slit and two brass electrodes. The frame has been mounted into a Linkam LTS 350 heating stage. The temperature controller provided an accuracy of 0.1 K. Optical observations have been made with a polarizing microscope AxioImager Pol (Carl Zeiss GmbH) equipped with a high-resolution cooled charge-coupled device (CCD) camera AxioCam HR (Carl Zeiss GmbH). We carried out the observations in reflected light between crossed polarizers as well as between slightly uncrossed polarizers.

### 2.3. Mesophases and Transition Temperatures Depending on Alkyl Chain Length and Temperature

Figure 1 shows the mesophases and the transition temperatures for the synthesized homologous compounds with different terminal alkoxy chain lengths (for numerical data, see Table 1, DSC traces are shown in Figure S1). As can be seen from Figure 1, for the shortest homologue A8 a nematic phase ( $N_{\text{Cybc}}$ ) is observed in a relatively wide temperature range, which on cooling to 83  $^\circ\text{C}$  is replaced by a mesophase with spherulitic texture which was identified as a rectangular columnar phase by XRD ( $\text{Col}_{\text{rec}}$ , see Figure 2c–e and Section 2.5) also known as  $B_{1\text{rev}}$  phase. Increasing the alkoxy chain length to  $n = 10$

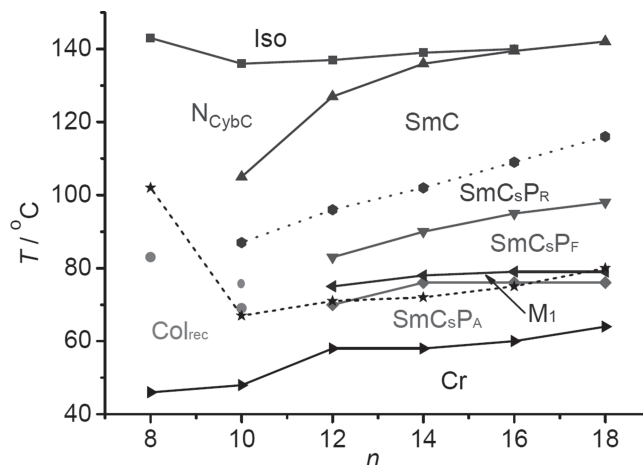


**Figure 1.** Plot of the transition temperatures of compounds A8–A18 as a function of the alkyl chain length. The connections between the data points serve as guides for the eyes and indicate the upper temperature limits for the distinct mesophases; stars (connected by a dashed line) indicate the melting temperatures observed on heating,  $\blacktriangleright$  (bottom solid line) the crystallization temperature on cooling.

(compound A10) induces additional tilted smectic phases ( $\text{SmC}$  and  $\text{SmC}_s\text{P}_R$  phases) between the  $N_{\text{Cybc}}$  and the  $\text{Col}_{\text{rec}}$  phase and modifies the structure of the  $\text{Col}_{\text{rec}}$ -phase. A typical feature of the  $\text{SmC}$  phases is SHG activity under an applied electric field and that under certain conditions a conglomerate of chiral domains is observed (see below).

For the next homologue A12, the  $\text{Col}_{\text{rec}}$  phase completely disappears. The nematic range becomes smaller and the  $\text{SmC}$  phase is stabilized. Additional phase transitions with very small enthalpy values can be observed in the smectic phase region on cooling before crystallization takes place. For all compounds A12–A18 there is a sequence of five distinct smectic phases, assigned as  $\text{SmC}$ ,  $\text{SmC}_s\text{P}_R$ ,  $\text{SmC}_s\text{P}_F$ ,  $M_1$  and  $\text{SmC}_s\text{P}_A$ . For

**Table 1.** Phase transition temperatures ( $T$  in  $^\circ\text{C}$ ) and associated enthalpy values (in square brackets,  $\Delta H$  in  $\text{kJ mol}^{-1}$ ) of compounds A8–A18.<sup>a)</sup>

Compd.	$n$	Phase transitions
A8	8	Cr 102 [60.7] ( $\text{Col}_{\text{rec}}$ 83 [6.6]) $N_{\text{Cybc}}$ 143 [1.0] Iso
A10	10	Cr 68 [22.7] $\text{Col}_{\text{rec}2}$ 69 [3.0] <sup>b)</sup> $\text{Col}_{\text{rec}1}$ 73 [0.5] $\text{SmC}_s\text{P}_R$ 87 [-] $\text{SmC}$ 105 [ $<0.01$ ] $N_{\text{Cybc}}$ 136 [1.1] Iso
A12	12	Cr 71 [17.4] ( $\text{SmC}_s\text{P}_A$ 70 [0.3]) $M_1$ 75 [0.2] $\text{SmC}_s\text{P}_F$ 83 [-] $\text{SmC}_s\text{P}_R$ 96 [-] $\text{SmC}$ 127 [0.15] $N_{\text{Cybc}}$ 137 [2.0] Iso
A14	14	Cr 72 [23.0] $\text{SmC}_s\text{P}_A$ 76 [0.4] $M_1$ 78 [0.1] $\text{SmC}_s\text{P}_F$ 90 [-] $\text{SmC}_s\text{P}_R$ [-] 102 $\text{SmC}$ 136 [0.5] $N_{\text{Cybc}}$ 139 [3.0] Iso
A16 <sup>b)</sup>	16	Cr 75 [41.8] ( $\text{SmC}_s\text{P}_A$ 76 [0.4]) $M_1$ 79 [0.15] $\text{SmC}_s\text{P}_F$ [-] 95 $\text{SmC}_s\text{P}_R$ [-] 109 $\text{SmC}$ 139.5 $N_{\text{Cybc}}$ 140 [5.8] <sup>c)</sup> Iso
A18	18	Cr 80 [40.7] ( $\text{SmC}_s\text{P}_A$ 76 [0.4]) $M_1$ 79 [0.1]) $\text{SmC}_s\text{P}_F$ 98 [-] $\text{SmC}_s\text{P}_R$ [-] 116 $\text{SmC}$ 142 [6.3] Iso

<sup>a)</sup>Transition temperatures and enthalpy values were taken from the second DSC heating scans (10  $\text{K min}^{-1}$ , see also Figure S1); transition without detectable DSC peak were determined by polarizing microscopy; values between brackets are monotropic phase transitions and in this case the enthalpy values are taken from the first DSC cooling scans; abbreviations: Cr = crystalline solid; Iso = isotropic liquid;  $N_{\text{Cybc}}$  = nematic phase composed of  $\text{SmC}$ -type cybotactic clusters;  $\text{SmC}$  = synclitic tilted paraelectric  $\text{SmC}$  phase composed of small  $\text{SmC}_s\text{P}_F$  domains;  $\text{SmC}_s\text{P}_R$  =  $\text{SmC}$  phase with significantly increased domain size;  $\text{SmC}_s\text{P}_F$  = ferroelectric  $\text{SmC}$  phase;  $M_1$  = highly viscous LC phase;  $\text{SmC}_s\text{P}_A$  = synclitic tilted antiferroelectric  $\text{SmC}$  phase ( $B_2$  phase);  $\text{Col}_{\text{rec}}$  and  $\text{Col}_{\text{rec}1}$  = centered rectangular columnar phases with  $c2mm$  lattice ( $B_{1\text{rev}}$  phase);  $\text{Col}_{\text{rec}2}$  = non-centered rectangular columnar phase (undulated smectic phase); <sup>b)</sup>this transition shows significant hysteresis, on cooling the transition takes place at 62  $^\circ\text{C}$ ; <sup>c)</sup>transitions not resolved, enthalpy value is the total of the  $\text{SmC} - N_{\text{Cybc}} - \text{Iso}$  transitions.

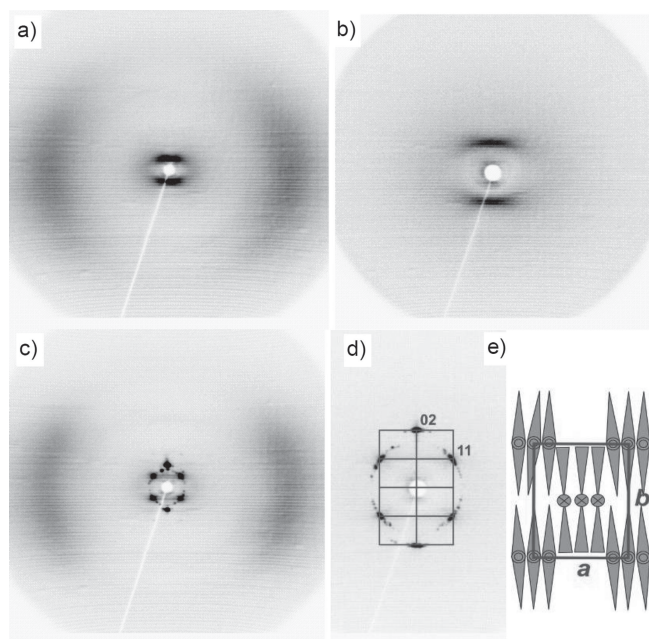


**Figure 2.** XRD investigation of an aligned sample of compound **A8**: a) wide angle and b) small angle scattering of the  $N_{\text{Cybc}}$  phase at  $T = 120$  °C, c) wide angle and d) small angle scattering with reciprocal lattice and indexation as a centered  $\text{Col}_{\text{rec}}$  phase at  $T = 80$  °C; e) model of the  $\text{Col}_{\text{rec}}$  ( $B1_{\text{rev}}$ ) phase.

longer chains, the nematic range becomes smaller and it completely disappears for **A18** with the longest alkoxy chains. In the following, the distinct LC phases will be discussed in more detail.

## 2.4. Nematic Phases

On cooling from the isotropic liquid state, all compounds with the exception of **A18** form a nematic phase. The Iso- $N$  transitions are associated with transition enthalpies between 1.0 (**A8**) and 3.0  $\text{kJ mol}^{-1}$  (**A14**), increasing with growing chain length. For the longer homologue **A16**, the Iso- $N_{\text{Cybc}}$  transition is close to the  $N_{\text{Cybc}}$ -SmC transition and therefore, the contributions of the enthalpies of the Iso- $N_{\text{Cybc}}$  and  $N_{\text{Cybc}}$ -SmC transitions cannot be separated. In the temperature range of the nematic phases the XRD patterns of magnetically aligned samples ( $B \sim 1\text{T}$ ) show a diffuse scattering in the wide angle region centered at the equator (Figure 2a, see also Figure S3 and S4 for the other homologues) with a maximum at  $d = 0.46$  nm ( $T = 140$  °C). The diffuse scattering in the small angle region has a dumbbell-like shape, indicating the existence of cybotactic clusters of the SmC type; hence these nematic phases are assigned as  $N_{\text{Cybc}}$ .<sup>[10,31]</sup> The splitting of the small angle scattering maxima of compound **A8** is  $\Delta\chi/2 = 28^\circ$  ( $T = 140$  °C) and it only slightly decreases to  $\Delta\chi/2 = 25^\circ$  at  $T = 90$  °C (see Figure S2). In case of compound **A10**, the maximum close to the clearing temperature is  $\Delta\chi/2 = 18^\circ$  and a strong temperature dependence is observed, reaching a minimum of  $\Delta\chi/2 = 4\text{--}5^\circ$  close to the transition to the SmC phase (Figure 3a). This obser-

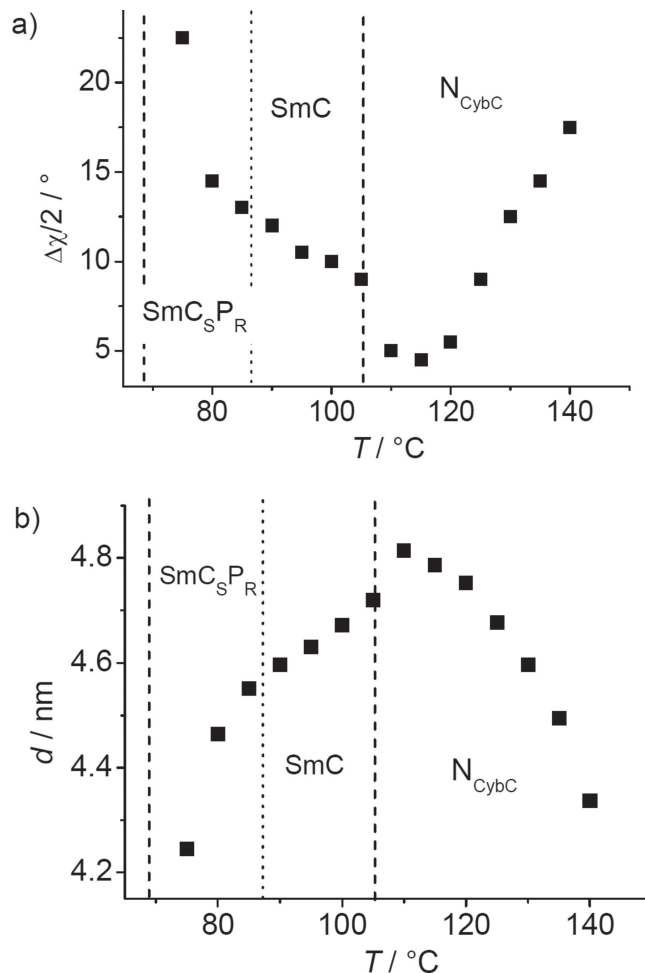


**Figure 3.** Temperature dependence a) of the splitting ( $\Delta\chi/2$ ) of the small angle scattering and b) of the  $d$ -value of the maxima of the small angle scattering in the  $N_{\text{Cybc}}$ , the SmC and the SmC<sub>S</sub>P<sub>R</sub> phases of compound **A10**.

vation is in line with the increase of the  $d$ -value on decreasing temperature (Figure 3b).

For compounds **A12** and **A14** with longer chains and short nematic ranges  $\Delta\chi/2$  is only around  $12^\circ$  (see Figure S5 and Figure 4a). As the  $\Delta\chi/2$  splitting can in a first approximation be related to the tilt of the molecules in the SmC clusters, this indicates a tilted organization of the molecules in all  $N_{\text{Cybc}}$  phases with a tendency of decreasing tilt with increasing chain length. The transition enthalpies  $N_{\text{Cybc}}$  to SmC ( $<0.01\text{--}0.5$   $\text{kJ mol}^{-1}$ ) are much smaller than the Iso- $N_{\text{Cybc}}$  transition enthalpy values (1.0–3.0  $\text{kJ mol}^{-1}$ ), in line with the cybotactic cluster structure of the nematic phases.

## 2.5. Col<sub>rec</sub> Phases of Compounds A8 and A10

Upon cooling the nematic phase of **A8** the XRD pattern changes significantly at  $T = 83$  °C, at the transition to the low temperature phase with spherulitic texture (Figure 5b). This transition is associated with a significant enthalpy change (see

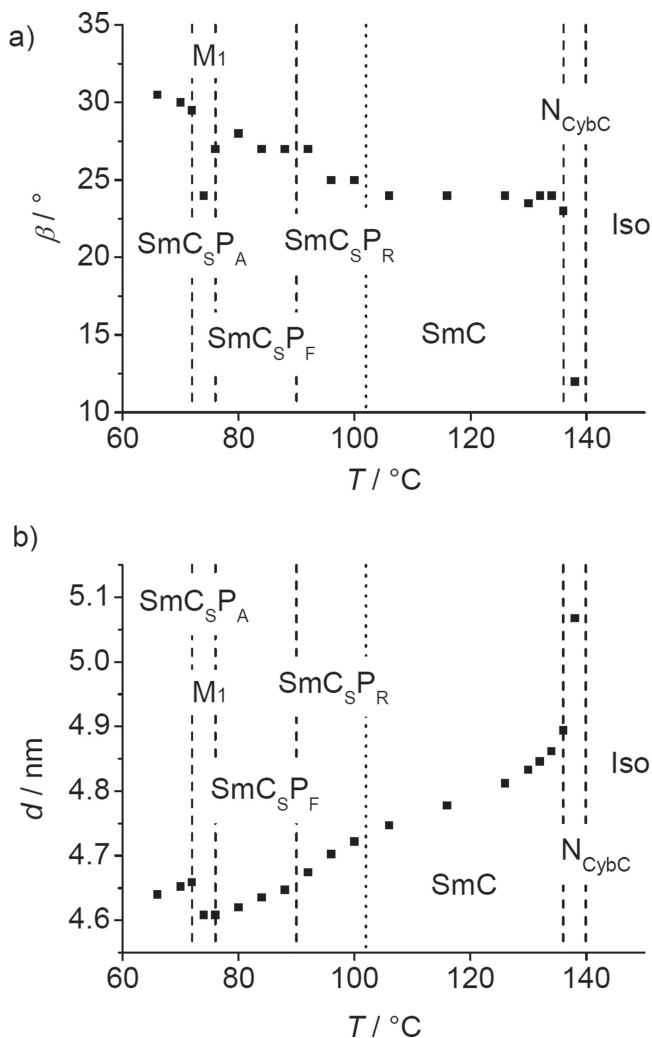


**Figure 4.** Temperature dependence a) of the tilt angle  $\beta$  (calculated from the splitting  $\Delta\chi/2$ ) and b) of the  $d$ -value of the XRD patterns in the LC phases of compound A14.

**Figure 6a).** At this transition the wide angle scattering remains diffuse, indicating a fluid LC phase, and in the small angle region several sharp Bragg peaks appear (Figure 2c,d). These peaks can be indexed on a centered rectangular lattice with the parameters  $a = 3.7$  nm and  $b = 4.6$  nm ( $T = 70$  °C, see Table S1). The position of the wide-angle scattering maxima remain on the equator, indicating the alignment of the molecules with their long axes parallel to  $b$ . The parameter  $b$  is in good agreement with the molecular length ( $L_{mol} = 4.6$  nm for a  $120^\circ$  bent molecule with stretched wing groups and the alkyl chains in *all-trans* conformation as determined using space filling models). Both observations are in line with a nontilted organization of the molecules. The 2D lattice results from the formation of ribbons; the lateral diameter of these ribbons can be calculated from  $a/2$  to be approximately 4–5 molecules organized side-by-side. These XRD data, together with the typical texture indicate a rectangular columnar LC ribbon phase ( $Col_{rec}$ ), typical for short chain bent core mesogens also

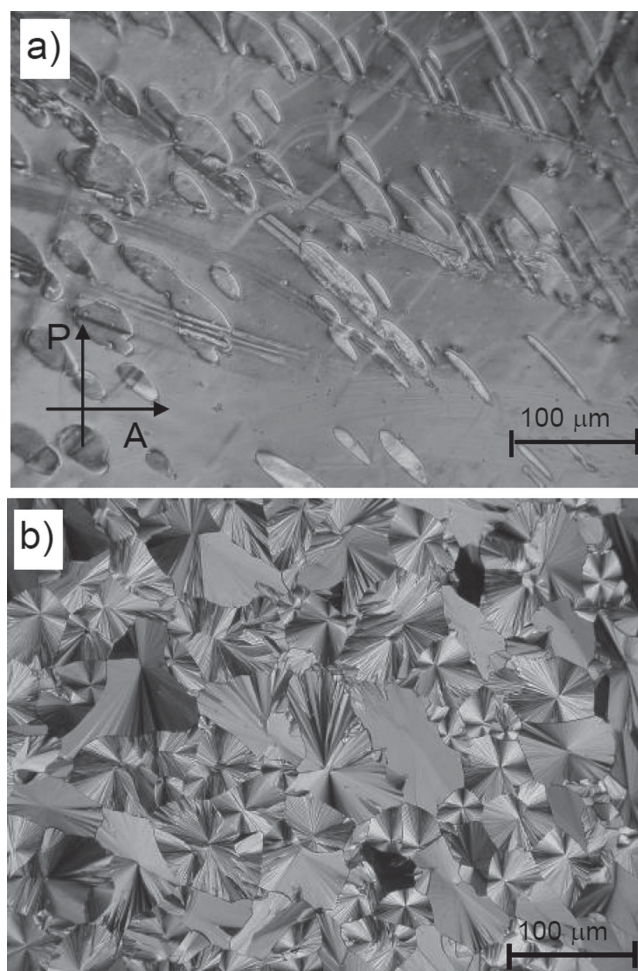


**Figure 5.** Optical micrographs of textures observed between crossed polarizers in a homeotropic cell for compound A8: a) nematic phase at  $T = 130$  °C and b)  $Col_{rec}$  phase ( $B_{1rev}$  phase) at  $T = 80$  °C. For a colour version of the textures, see Figure S8 in the Supporting Information.

assigned as  $B_{1rev}$ .<sup>[32]</sup> In this phase the molecules are polar ordered in the ribbons with antiparallel organization of the polar direction between adjacent ribbons (see Figure 2e).<sup>[33]</sup> At the transition from  $N_{CybC}$  to  $Col_{rec}$  the relatively strong tilt of the molecules in the  $N_{CybC}$  phase is suddenly removed completely.

For compound A10 additional SmC phases appear between the  $N_{CybC}$  phase and the  $Col_{rec}$  phase. The parameters  $a = 5.43$  nm and  $b = 4.95$  nm (at  $T = 70$  °C; see Figure S3e and Table S1) indicate a  $Col_{rec}$  phase composed of broader ribbons, formed by about 6 molecules in the cross section ( $Col_{rec1}$  phase;  $B_{1rev}$  phase). On further cooling a transition to a second mesophase with 2D lattice takes place, associated with a significant enthalpy change. For this non-centered rectangular columnar phase with the parameters  $a = 10.10$  nm and  $b = 4.93$  nm ( $T = 60$  °C, see Figure S3f and Table S1) an undulated smectic structure is assumed ( $Col_{rec2}$  phase, USm phase). In both low temperature phases the parameter  $b$  corresponds well with the molecular length ( $L_{mol} = 5.1$  nm), which is in line with



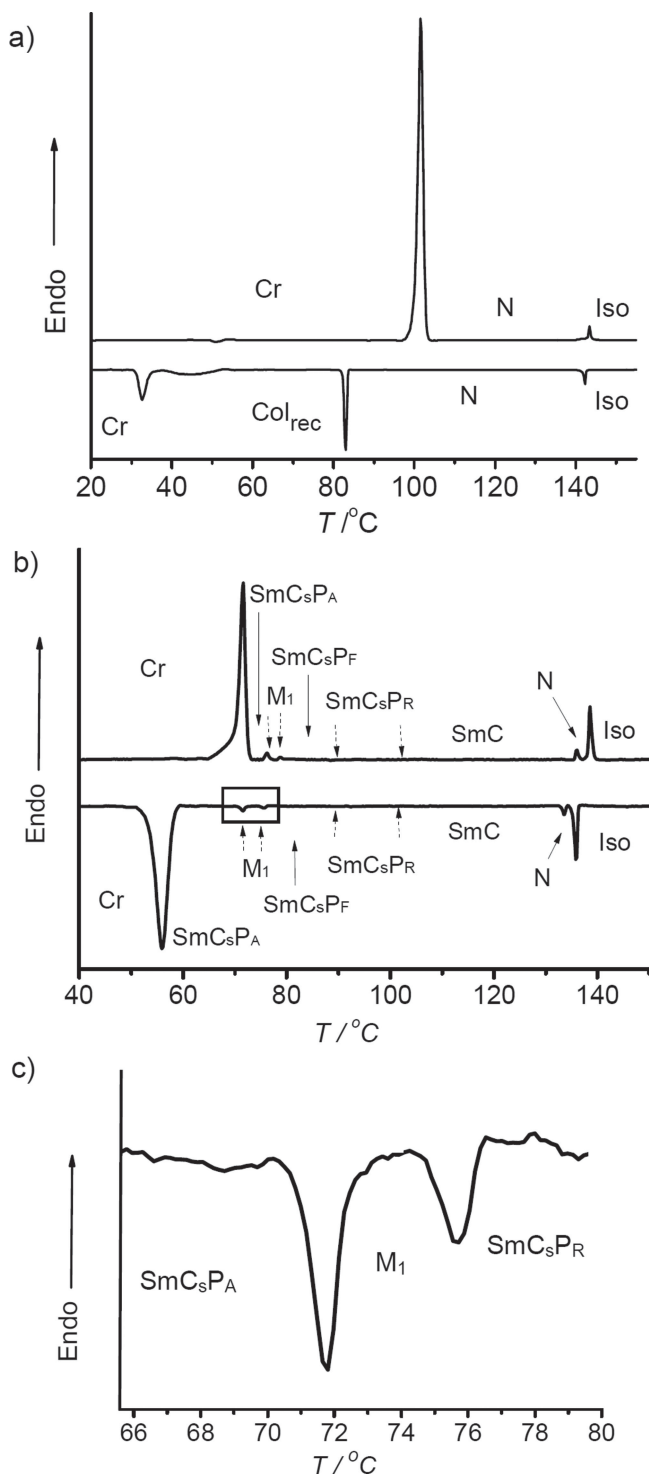


**Figure 6.** a,b) DSC heating (top) and cooling (bottom) traces at a rate of  $10 \text{ K min}^{-1}$ : a) compound **A8** and b) compound **A14**; c) shows the DSC cooling trace of compound **A14** for the temperature range of the  $\text{SmC}_s\text{P}_R$ - $\text{M}_1$ - $\text{SmC}_s\text{P}_F$  transition between  $80^\circ\text{C}$  and  $65^\circ\text{C}$ .

a non-tilted organization of the molecules. These 2D-modulated low temperature LC phases of compounds **A8** and **A10** do not exhibit any response to an applied electric field.<sup>[32]</sup>

## 2.6. Smectic Phases

### 2.6.1. DSC and Optical Investigations

A different kind of behavior is observed for compounds **A12–A18**. All these compounds show essentially the same sequence of five distinct smectic phases occurring below the nematic phase (compounds **A12–A16**), only for **A18** the nematic phase is missing (see Figure 1 and Table 1). The smectic phase sequence for all these compounds is  $\text{SmC} - \text{SmC}_s\text{P}_R - \text{SmC}_s\text{P}_F - \text{M}_1 - \text{SmC}_s\text{P}_A$ , the assignment of the distinct smectic phases is based on the experimental results described below.

All enthalpies of the phase transitions between the smectic phases are very small (only  $0.1\text{--}0.4 \text{ kJ mol}^{-1}$ ) and increase slightly with growing chain length (Table 1, Figure 6b and S1). No enthalpy values could be determined for the transition between the phases assigned as  $\text{SmC}$ ,  $\text{SmC}_s\text{P}_R$  and  $\text{SmC}_s\text{P}_F$  in any case. The enthalpy of the phase transition  $\text{SmC}_s\text{P}_F - \text{M}_1$  is very small ( $0.1\text{--}0.2 \text{ kJ mol}^{-1}$ ). The highest transition enthalpy in the smectic LC range is observed for the  $\text{M}_1 - \text{SmC}_s\text{P}_A$  transition which is for all compounds around  $0.4 \text{ kJ mol}^{-1}$ . Hence, it appears that this is the major transition in the smectic region, associated with the most significant changes of the phase structure.

In planar cells the smectic phases develop with a typical fan texture. With decreasing temperature the smooth fans become sharper and the birefringence significantly increases, indicated by the change of the interference color from red to dark green, due to the increase of the order parameter of the aromatic cores with decreasing temperature (see Figure 7f,g,  $6 \mu\text{m}$  cell, any bluish interference color appears green due to orange color of the compound). A tiny, but distinct jump in interference color is observed at a specific temperature in the  $\text{SmC}$  region of all compounds (see Figure S10). At this temperature also other effects were observed, like a step in the dielectric strength, as previously reported in ref. [8] for compound **A16** (see Figure S15), and stripe pattern formation in free standing films of compound **A14** (see below). Therefore, the region previously assigned as  $\text{SmC}_s\text{P}_R$ <sup>[8]</sup> obviously includes two very similar phases, a high temperature paraelectric  $\text{SmC}$  phase and a low temperature phase assigned as  $\text{SmC}_s\text{P}_R$  (Figure 1, hexagonal dots connected by a dotted line). Additional phase transitions to the following phases are associated with only slight textural changes. The major changes are a further jump of the birefringence color from green to yellowish green at the  $\text{SmC}_s\text{P}_R$ - $\text{SmC}_s\text{P}_F$  transition (Figure 7g,h) and an increased viscosity occurring at the transition to the phase assigned as  $\text{M}_1$  (Figure 7i) which becomes fluid again at the next transition to  $\text{SmC}_s\text{P}_A$  (Figure 7j).

Under homeotropic anchoring conditions some of the textural changes are better pronounced. Especially remarkable are the  $\text{SmC}$  and  $\text{SmC}_s\text{P}_R$  phase regions for which a low birefringent texture composed of distinct chiral domains is reproducibly observed for all compounds **A $n$**  by uncrossing the polarizers by a small angle (Figure 8a–c). This leads to the appearance of dark and bright domains; uncrossing the polarizer in the opposite direction reverses the brightness of the domains (Figure 8a,b). That the domains are due to chirality and not the result of a different tilt-alignment is shown by rotation of the

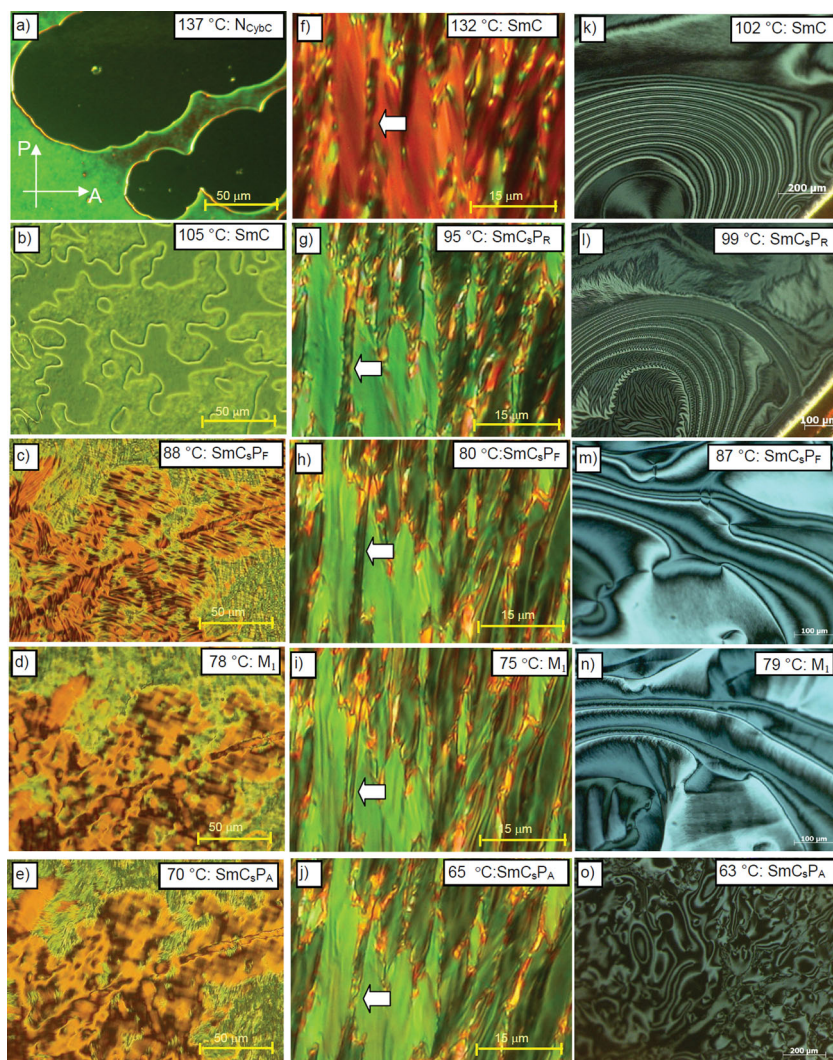


**Figure 7.** Optical micrographs of the textures observed for the different LC phases of compound **A14** in a homeotropic cell (left column), in a planar cell (middle column, arrows indicate a region where textural changes can be identified) and in free standing films (right column) at the indicated temperatures for the indicated LC phase types. In a) the homeotropic alignment (dark areas) is developing from the initially formed homogeneous alignment (green areas).

sample between crossed polarizers, which gives no significant change of brightness, independent on the angle. (Figure 8d,e). This corroborates that the distinct regions indeed represent chiral domains with opposite handedness.<sup>[8]</sup> The chiral domains are clearly visible for the SmC and SmC<sub>s</sub>P<sub>R</sub> phases of all compounds without any change at the SmC – SmC<sub>s</sub>P<sub>R</sub> transition, but they disappear at the transition to the N<sub>Cybc</sub> phases. The transition of the SmC<sub>s</sub>P<sub>R</sub> phase to the SmC<sub>s</sub>P<sub>F</sub> phase is associated with an anchoring transition to a birefringent defect texture (Figure 7b,c). At this transition birefringence strongly increases and it becomes difficult to detect the chiral domains anymore. However, it appears that chirality is conserved in the few remaining low birefringent regions and reheating into the SmC<sub>s</sub>P<sub>R</sub> phase completely restores the chiral domains. Possible reasons for achiral symmetry breaking in the SmC and SmC<sub>s</sub>P<sub>R</sub> phases are discussed in Section 3.3. The next phase transitions

to the phases assigned as M<sub>1</sub> and SmC<sub>s</sub>P<sub>A</sub> are associated with minor textural changes (Figure 7c–e,h–j).

### 2.6.2. Behavior in Freely Suspended Films

The polar character of the smectic phases was studied in freely suspended films in compound **A14**. The films were prepared in the smectic phase near the transition into the nematic. The SmC phase exhibited a typical schlieren texture in thin (<200 nm) and in thick films (>5 μm). Observing the films under inclined incidence, we could confirm that the phase has a synclonic character. No polar response to an in-plane DC electric field was found. On the contrary, dielectric re-orientation was observed in an AC field. The slow (optical) axis is aligned perpendicular to the electric field. Distinct changes occur at the SmC – SmC<sub>s</sub>P<sub>R</sub> transition at about 102 °C, which is accompanied by the formation of a network of strings, similar to that described previously<sup>[34]</sup> (Figure 7k,l). The width of the stripes increases with decreasing temperature over an interval of 3–4 K (Figure 7m). This transition coincides with the inflection points in the SHG signal intensity vs. *T* (see Section 2.6.5) and polarization vs. *T* curves (see Section 2.6.4). There is also a distinct jump in dielectric strength Δε at this transition, as reported previously for **A16** (see Figure S15).<sup>[8]</sup> So the SmC – SmC<sub>s</sub>P<sub>R</sub> transition appears to be associated with a distinct increase of the size of the polar domains.

At about 90 °C, corresponding to the SmC<sub>s</sub>P<sub>R</sub> – SmC<sub>s</sub>P<sub>F</sub> transition, the stripe pattern has disappeared and a smooth schlieren texture is observed (Figure 7m). This phase shows a clear polar response to an electric field exhibiting 2π director inversion walls typical for polar films (see Section 2.6.4).

These findings indicate that the phase has a residual polarization. That is why we designated it as SmC<sub>s</sub>P<sub>F</sub>. The polar director aligns along the electric field and the *c*-director (tilt) is perpendicular to it. We found this behavior in thick and in very thin films as well.

The transition into the M<sub>1</sub> phase is marked by development of a mosaic-like schlieren texture (Figure 7n). No response to an electric field could be found in this phase.

During the next transition, the texture becomes more distorted in thick films. On the other hand, thin films exhibit a typical schlieren texture (Figure 7o). The texture response to an electric field was found only in thin films. The switching character showed an odd-even effect as typical for antiferroelectrics. There is a reorganization of the *c*-director only in films with odd number of layers; for films with an even number of layers either no response is observed or the *c*-director aligns parallel

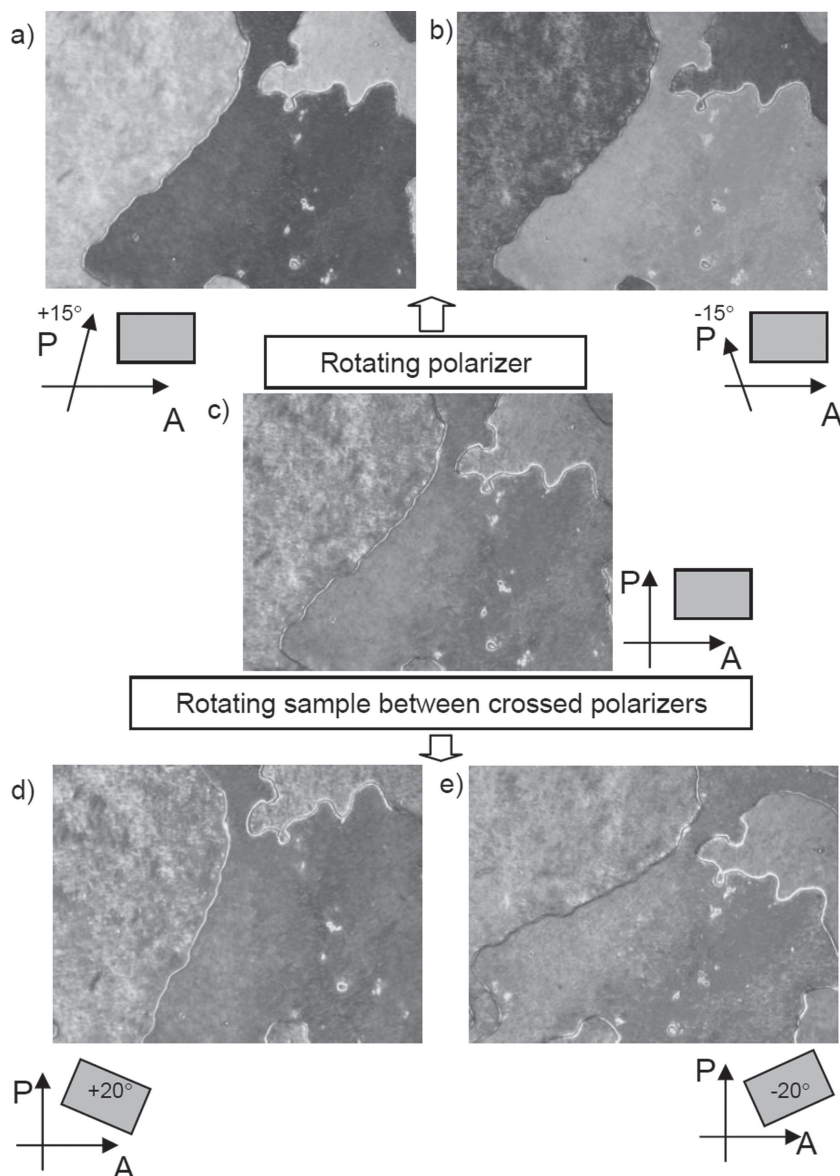


**Figure 8.** Textures of the SmC phase of compound **A14** at  $T = 130\text{ }^{\circ}\text{C}$  between glass slides (homeotropic alignment): c) between crossed polarizers and a,b) between slightly uncrossed polarizers, showing dark and bright domains, indicating the presence of areas with opposite chirality sense; d,e) show the texture between crossed polarizers, but after rotation of the sample by  $20^{\circ}$  either clockwise or anticlockwise; the birefringence does not change which confirms chirality as origin of the effects seen in a–c); there is no change of the textures at the transition to the  $\text{SmC}_s\text{P}_R$  phase. For a colour version, see Figure S9 in the Supporting Information.

to the applied field. This effect is a direct evidence for an antiferroelectric structure of the phase.<sup>[35]</sup> Therefore, we designated this phase as  $\text{SmC}_s\text{P}_A$ .

### 2.6.3. XRD Studies

Samples of **A14** aligned by magnetic field were studied by 2D XRD. At the transition from the  $\text{N}_{\text{CyBC}}$  to the SmC phase the four diffuse spots in the small angle region transform into two peaks located beside the meridian, whereas the maxima

of the diffuse scattering in the wide angle region remains on the equator, indicating a synclinal arrangement of the molecules in the smectic phase (Figure 9c,d). No fundamental changes in the XRD patterns are visible at the following phase transitions until crystallization. A more detailed analysis of the XRD data indicates an increase of the tilt angle with decreasing temperature in all SmC and  $\text{SmC}_s\text{P}_R$  phases. In agreement with this, the  $d$ -values become smaller with decreasing temperature (Figure 4, S5 and S7). These trends continue in the  $\text{SmC}_s\text{P}_F$  phase. As shown in Figure 4a for compound **A14**, in the  $\text{SmC}_s\text{P}_A$  phases at lower temperature the tilt angles ( $\beta = 29\text{--}31^{\circ}$ ) are larger than in the  $\text{SmC}_s\text{P}_R$  and  $\text{SmC}_s\text{P}_F$  phases and the  $d$ -values are also increased (Figure 4b). This is due to a chain stretching induced by the denser packing of the molecules in the  $\text{SmC}_s\text{P}_A$  phases. An increase of the packing density in the  $\text{SmC}_s\text{P}_A$  phases is also found for compounds **A12** (Figure S5) and compound **A16** (Figure S7). The  $\text{M}_1$ -phases represent a discontinuity in the development of the  $d$ -values and tilt-angles. There is a jump to smaller tilt angles at the  $\text{SmC}_s\text{P}_F - \text{M}_1$  transition and an increase of the  $d$ -values in the  $\text{M}_1$ -phase. This confirms that a denser packing of the molecules starts in the  $\text{M}_1$  phase region. Overall the transition  $\text{SmC} - \text{SmC}_s\text{P}_R - \text{SmC}_s\text{P}_F$  is nearly continuous, as also indicated by the absence of any transition enthalpy. Major changes with significant increase of the packing density, associated with distinct jumps in  $d$ -values and tilt angles, take place at the  $\text{SmC}_s\text{P}_F - \text{M}_1$  and  $\text{M}_1 - \text{SmC}_s\text{P}_A$  transitions.

Denser packing in the  $\text{M}_1$  and  $\text{SmC}_s\text{P}_A$  phases is also evident from a slight shift of the position of the wide angle scattering maximum from 0.48 to 0.46 nm (Figure 10b and S7c). Also the layer reflection becomes more intense in the  $\text{M}_1$  and  $\text{SmC}_s\text{P}_A$  phases which is in line with the development of sharper interlayer interfaces resulting from a denser packing of the aromatic cores (Figure 10a and S7d).

### 2.6.4. Electro-Optical Studies in ITO Cells and Free Standing Films

Electro-optical investigations were carried out in  $6\text{ }\mu\text{m}$  indium tin oxide (ITO) coated cells with polyimide alignment layer under an applied triangular wave voltage. Figure 11 shows the current response curves at different temperatures for **A14** and Figure 12 shows the dependence of the polarization on temperature for the same compound. Switching curves obtained in  $2\text{ }\mu\text{m}$  cells are shown in Figure S12. Upon application of a triangular wave voltage of frequency

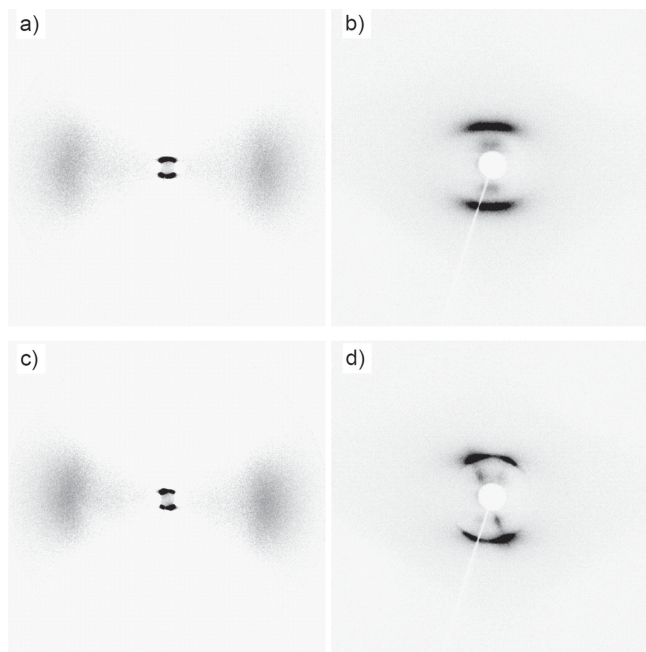


**Figure 9.** XRD investigation of an aligned sample of compound **A14**: a,b)  $N_{CyBC}$  phase at  $T = 138$  °C; c,d) SmC phase at  $T = 132$  °C; a,c) wide angle patterns after subtraction of the pattern of the isotropic phase (150 °C) and b,d) small angle scattering after subtraction of the pattern of the isotropic phase (150 °C).

10 Hz a relatively weak and rather broad single peak per half cycle of the applied voltage was observed in the current curves in the SmC phase range, which increases in intensity as temperature decreases (see Figure 11a,b). In the  $SmC_sP_R$  region the slope of the  $I$  vs.  $T$  curve increases and reaches a polarization value of  $P_S \sim 130$  nC cm<sup>-2</sup> close to the transition to the  $SmC_sP_F$  phase occurring at  $T = 90$  °C (see Figure 12). Below this temperature, the shape of the current response curves changes and two widely separated peaks appear and grow in intensity (Figure 11c,d,  $P_S \sim 360$  nC cm<sup>-2</sup>). Both peaks appear to be positioned at the ends of the conductive part of the curve symmetrically with respect to the field inversion point (Figure 11c and S12c,d). This indicates that the switching occurs hysteresis free. With further decreasing temperature the distance between the peaks decreases and the polarization value rises to  $P_S \sim 440$  nC cm<sup>-2</sup> (Figure 11d) A switching with two polarization peaks and similar polarization values between 540 and 660 nC cm<sup>-2</sup> is also observed in the two LC phases at lower temperature ( $M_1$ ,  $SmC_sP_A$ , Figure 11e,f).

Under the field applied across a homogeneously aligned cell a birefringent fan-like texture, with dark extinctions inclined with the directions of polarizer and analyzer, is observed (Figure S11). This confirms a synclitic tilt in these smectic phases as also deduced from the XRD investigation of aligned samples (Figure 9c,d). Neither in the SmC or  $SmC_sP_R$  phases nor in the  $SmC_sP_F$  phase or in one of the low temperature phases the switching process is associated with a change of the orientation of the extinctions (see Figure S11), which indicates

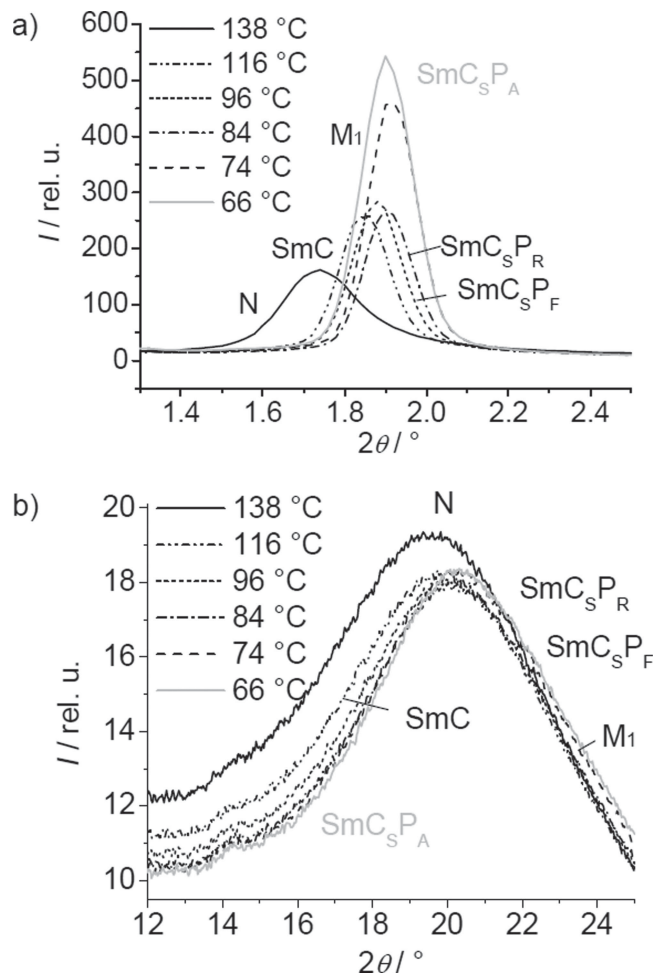


**Figure 10.** a) Small angle and b) wide angle  $\theta$ -scans over the XRD patterns of compound **A14** at different temperatures. For a clearer identification of the distinct curves, see colour version in Figure S6 in the Supporting Information.

that in all phases switching takes place by a collective rotation around the molecular long axis.

Electro-optical investigation of free standing films shows only a dielectric response to a 100 Hz AC electric field in the SmC phase down to 102 °C. Below this temperature, in the  $SmC_sP_R$  and  $SmC_sP_F$  regions, a polar response on an external electric field is observed; the switching is ferroelectric and independent on the film thickness and the number of layers (Figure 13). In the whole temperature range of both phases the molecular long axis is perpendicular to the field direction, in line with the polar moment being along the bend direction and the switching taking place around the molecular long axis. Only regions with a fine stripe pattern, occurring in the  $SmC_sP_R$  phase below the transition at 102 °C do not respond to the electric field. It appears that the modulation resulting in stripe formation is responsible for the absence of a response in these regions of the thin films. As the stripes are dominating in the  $SmC_sP_R$  range and disappear in the  $SmC_sP_F$  phase, the switching becomes uniformly ferroelectric in the temperature

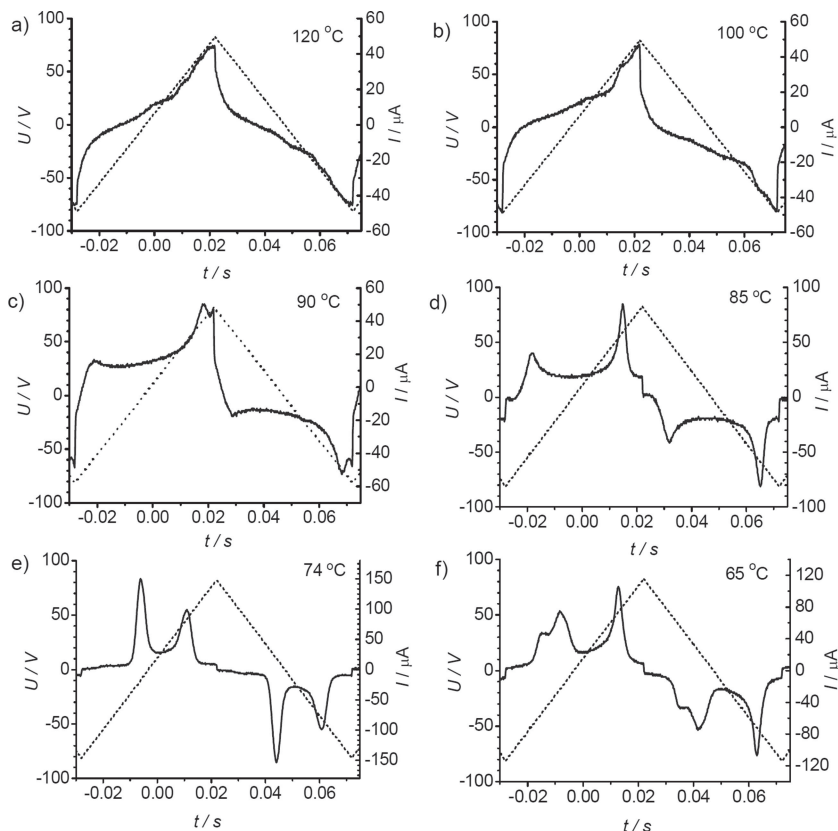


**Figure 11.** a–f) Switching current response curves for compound **A14** in a 6  $\mu\text{m}$  ITO cell on applying a triangular wave field (10 Hz); the dotted line indicates the applied triangular wave voltage; a) SmC phase at  $T = 120\text{ }^\circ\text{C}$ ; b) SmC<sub>s</sub>P<sub>R</sub> phase at  $T = 100\text{ }^\circ\text{C}$ ; c) SmC<sub>s</sub>P<sub>R</sub> – SmC<sub>s</sub>P<sub>F</sub> transition at  $T = 90\text{ }^\circ\text{C}$ ; d) SmC<sub>s</sub>P<sub>F</sub> phase at  $T = 85\text{ }^\circ\text{C}$ ; e) M<sub>1</sub> phase at  $T = 74\text{ }^\circ\text{C}$  and f) SmC<sub>s</sub>P<sub>A</sub> phase at  $T = 65\text{ }^\circ\text{C}$ ; different scales are used for the current response plots; for more switching current curves in the SmC region, see Figure S13 and for investigations in 2  $\mu\text{m}$  cells, see Figure S12.

range of the SmC<sub>s</sub>P<sub>F</sub> phase. This is in line with dielectric results obtained for the SmC/SmC<sub>s</sub>P<sub>R</sub> phase region of compound **A16** (Figure S15), where a high dielectric strength is observed in the SmC<sub>s</sub>P<sub>R</sub> region close to the SmC<sub>s</sub>P<sub>F</sub> phase and it steeply decreases on approaching the M<sub>1</sub> phase.<sup>[8]</sup> This is indicative of a strong increase of the polar domain size in the temperature range of the SmC<sub>s</sub>P<sub>F</sub> phase.

The M<sub>1</sub> phase does not show any response in freely suspended films, neither to DC nor to AC fields, most probably due to the high viscosity. In ITO cells, under higher field strength, antiferroelectric switching is observed in both phases M<sub>1</sub> and SmC<sub>s</sub>P<sub>A</sub> (Figure 11e). In the SmC<sub>s</sub>P<sub>A</sub> phase antiferroelectric switching is observed as well in free standing films. In the films the response depends on the film thickness and occurs with an odd-even effect of the number of layers on the response. This phase at lowest temperature behaves like a typical B2 phase of bent-core molecules.

### 2.6.5. SHG Investigations

Second harmonic generation (SHG) is a powerful tool to detect macroscopic polar order in the ground state and in

field induced states of LC phases.<sup>[36]</sup> A plot of SHG intensity versus temperature for compound **A14** is shown in Figure 14a. Under constant applied electric field ( $E_{pp} = 20\text{ V } \mu\text{m}^{-1}$ ) a very weak SHG signal is already observed in the isotropic phase at  $T = 148\text{ }^\circ\text{C}$ . It is retained in the nematic phase. In the temperature range of the SmC phase it slightly grows on cooling,<sup>[37]</sup> the slope increases in the SmC<sub>s</sub>P<sub>R</sub> region and then it continuously and rapidly increases in the SmC<sub>s</sub>P<sub>F</sub> phase range to reach the saturation in the M<sub>1</sub> phase. The SHG response remains nearly constant in the temperature region of the M<sub>1</sub> phase and also in the upper temperature range of the SmC<sub>s</sub>P<sub>A</sub> phase and then it drops (s. Figure S14b). There is a different field dependence of the SHG signal in the temperature range of the SmC and SmC<sub>s</sub>P<sub>F</sub> phases. In the SmC range the SHG signal continuously grows without reaching a saturation upon increasing the applied voltage (maximum:  $25\text{ V } \mu\text{m}^{-1}$ , Figure 14b), whereas in the SmC<sub>s</sub>P<sub>F</sub> phase, close to the transition to the M<sub>1</sub> phase a distinct plateau is reached at a voltage of  $\sim 17\text{ V } \mu\text{m}^{-1}$  (Figure 14c) the former typical for paraelectric switching, the latter indicating polar switching above a certain threshold voltage.

In concord with the current reversal measurements, no residual SHG signal was found after switching off the applied field in ITO cells in the switchable phases. It appears that the SmC phase behaves as a paraelectric phase<sup>[7,34,37]</sup> with unusually high

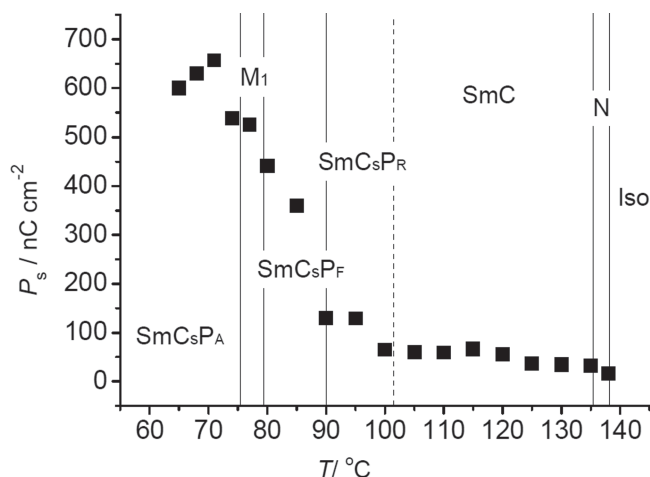


**Figure 12.** Polarization as function of temperature as measured for compound **A14** in a 6  $\mu\text{m}$  ITO cell on applying a triangular wave field (10 Hz) at  $160\text{ V}_{pp}$ .

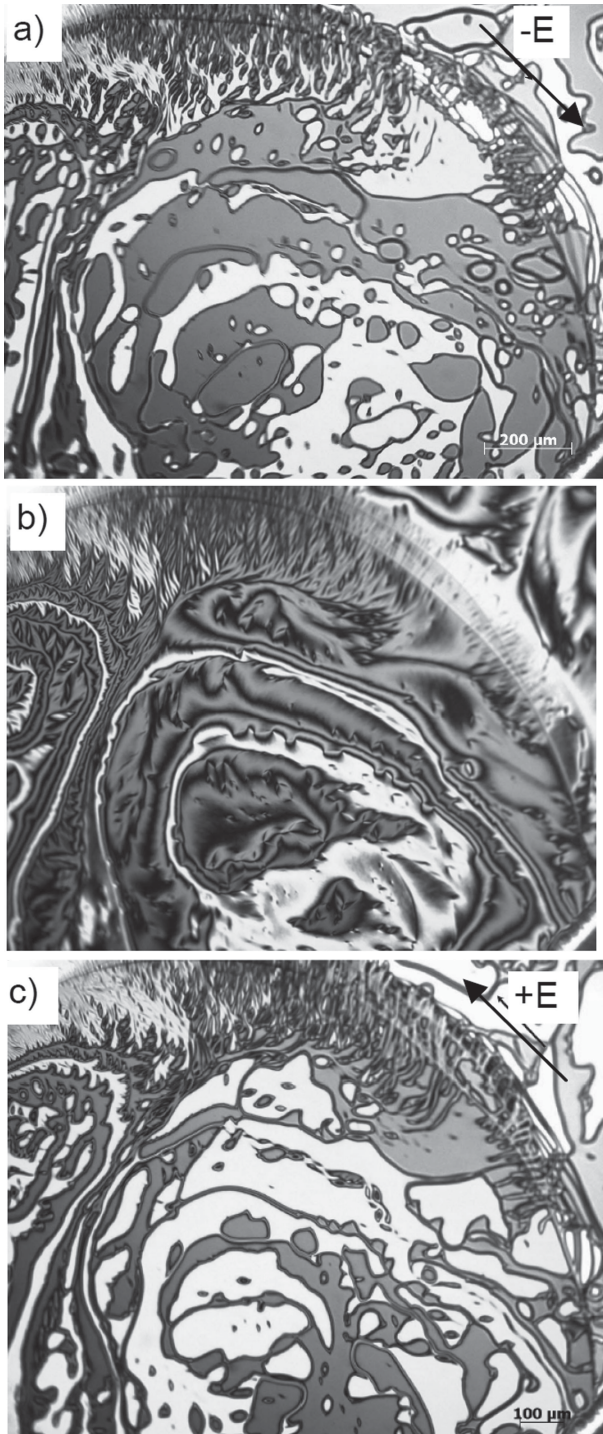


**Figure 13.** Reorientation of the polar director in a freely-suspended film in the  $\text{SmC}_s\text{P}_R$  phase of **A14** at  $T = 97\text{ }^\circ\text{C}$ : a)  $E = -12\text{ V/mm}$ , b)  $E = 0\text{ V/mm}$ , c)  $E = +12\text{ V/mm}$ ; the field direction is indicated by arrows; the film is observed under inclined incidence.

susceptibility to an electric field, in the  $\text{SmC}_s\text{P}_R$  phase range the switching appears to be ferroelectric as in the  $\text{SmC}_s\text{P}_F$  phase. On the contrary, all switchable phases below  $\text{SmC}_s\text{P}_R$

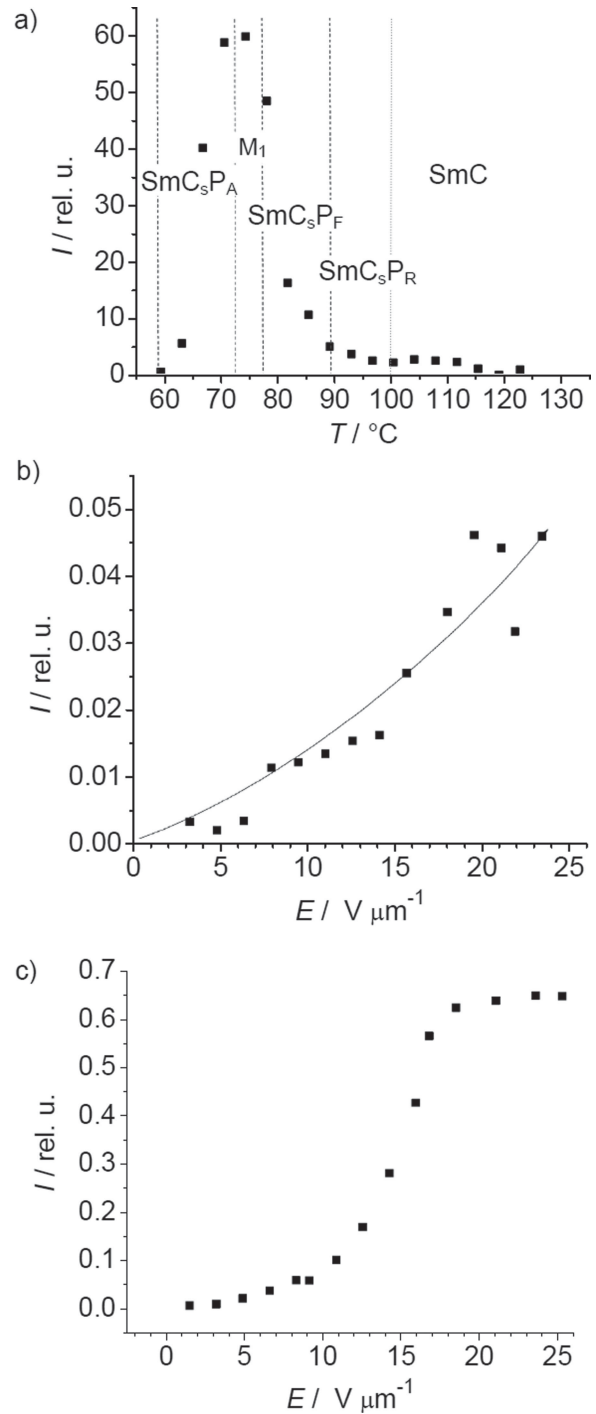


**Figure 14.** a) SHG intensity of compound **A14** vs. temperature ( $6\text{ } \mu\text{m}$  ITO cell, applied voltage:  $20\text{ V}/\mu\text{m}$ ) and dependence of the SHG-Intensity on the applied voltage b) in the  $\text{SmC}$  phase at  $T = 110\text{ }^\circ\text{C}$  and c) in the  $\text{SmC}_s\text{P}_F$  phase at  $T = 78\text{ }^\circ\text{C}$ .

behave as antiferroelectrics in ITO cells; even the phase designated as  $\text{SmC}_s\text{P}_F$  does not exhibit bistable switching. Possible reasons are outlined in the discussion.

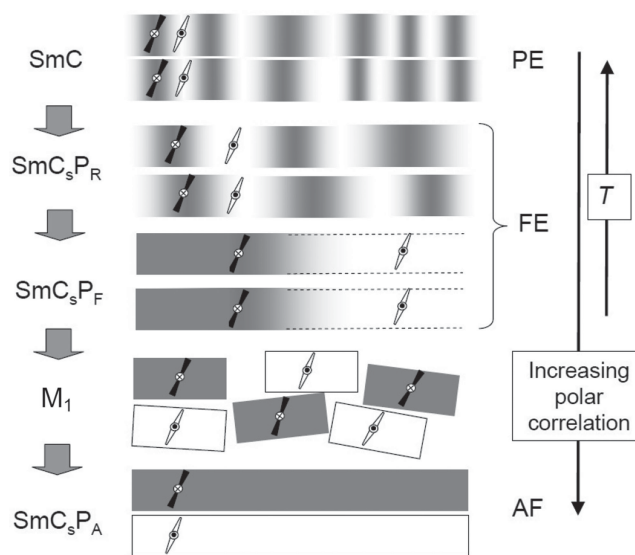
### 3. Discussion

#### 3.1. Phase Sequence Depending on Alkyl Chain Length and Temperature

As expected, nematic phases dominate for the short chain compounds and the nematic range decreases with chain elongation. All nematic phases represent  $N_{\text{Cybc}}$  phases as typical for bent-core mesogens and the size of the cybotactic SmC clusters increases with alkyl chain length and with decreasing temperature.<sup>[10]</sup> The tilt in the SmC clusters decreases with rising chain length, but there is no uniform temperature dependence. For the compounds with short chains ( $n = 8, 10$ ) the core-core interactions dominate, which lead to a transition from the  $N_{\text{Cybc}}$  phases to  $\text{Col}_{\text{rec}}$  phases, occurring directly (A8) or via a SmC phase (A10). In the  $\text{Col}_{\text{rec}}$  phases polar ribbons of non-tilted molecules arranged on a centered rectangular lattice with antiparallel correlation between the ribbons ( $B_{\text{Irev}}$  phases). In this  $\text{Col}_{\text{rec}}$  phase of A8 there are relatively large interfaces between the aromatic ribbons and the columns incorporating the aliphatic chains and this is unfavorable for molecules with longer chains. At first the ribbon diameter is increased for compound A10 in the  $\text{Col}_{\text{rec1}}$  phase and at lower temperature a transition to non-centered rectangular columnar phase ( $\text{Col}_{\text{rec2}}$  phase), presumably representing an undulated smectic phase, takes place. For molecules with  $n > 10$  columnar phases are removed and formation of smectic phases is favored. In the smectic phases there is a tendency to increased tilt with rising alkyl chain length, which is the result of the increased area required by longer conformationally disordered chains. With decreasing temperature the packing density of the aromatic cores increases. This gives rise to local polar domains in the SmC phase, the size and the correlation length of these domains increases with decreasing temperature leading to the  $\text{SmC}_s\text{P}_R$  phase. At the transition to the  $M_1$  phase the combination of a denser packing and enhanced polar order most probably leads to a layer modulation, which is assumed to be the reason for the relatively high viscosity of this phase. In the  $\text{SmC}_s\text{P}_A$  phase with highest packing density the molecules adopt antiferroelectric order (see Figure 15).

#### 3.2. Development of Polar Order

The phase sequence Iso – ( $N_{\text{Cybc}}$ ) – SmC –  $\text{SmC}_s\text{P}_R$  –  $\text{SmC}_s\text{P}_F$  –  $M_1$  –  $\text{SmC}_s\text{P}_A$  – Cr is typically observed for compounds An with sufficient chain length ( $n > 10$ ). Figure 15 shows the observed development of polar order in the series of smectic phases. SmC-type cybotactic clusters were already found in the nematic phase ( $N_{\text{Cybc}}$ ) which persisted also in the isotropic phase. Field-induced SHG in the nematic and isotropic phases may be attributed to the polar order within the clusters.<sup>[38]</sup> The polar domains persist in the SmC phase too, which are probably responsible for the current response observed in the ITO cells and an enhanced field-induced SHG. On the other hand, the response of the phase to an electric field remains paraelectric in the SmC region. In the  $\text{SmC}_s\text{P}_R$  region these domains reach appreciable size and macroscopic ferroelectric domains can be

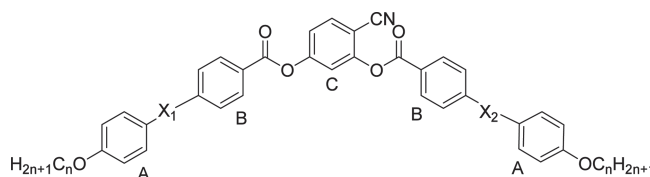


**Figure 15.** Development of polar order in the SmC phases of compounds An depending on temperature; PE, FE and AF denote paraelectric, ferroelectric and antiferroelectric switching, respectively.

observed in freely suspended films. In analogy to the  $\text{SmAP}_R$  phase, we designate this phase as  $\text{SmC}_s\text{P}_R$ , as a SmC phase with uniform tilt, but with randomly distributed polar domains. In the  $\text{SmC}_s\text{P}_F$  phase the size of the polar domains diverges and a polar phase develops. Observation of the polar response and inversion walls in freely-suspended films unambiguously indicates that the phase has a residual polarization. Hence, we designate it as  $\text{SmC}_s\text{P}_F$ . Antiferroelectric-type switching found in ITO cells seems to contradict our finding. This contradiction can be explained by a strong surface anchoring on the glass, which prevents a bistable switching and leads to a hysteresis-free director reorientation. Another possibility is the formation of a modulated structure of the director as observed in freely suspended films, which suppress the uniform ferroelectric state in the absence of a field. As the polarization is still relatively small a relatively high threshold field is required for ferroelectric switching, despite the switching itself appears to be thresholdless.

Further increased polar coupling leads to the highly viscous phase  $M_1$ . The viscosity in this  $M_1$  phase might be due to the layer distorting effect provided by polar order and chirality to the layers, though a layer modulation is not evident from the XRD patterns. As polar order becomes stronger the packing density in the layers is further increased and the layers become sufficiently robust to withstand layer distortion, leading to the transition to the  $\text{SmC}_s\text{P}_A$  phase. The fact that there are two polarization peaks in the whole temperature region from  $\text{SmC}_s\text{P}_F$  via  $M_1$  to  $\text{SmC}_s\text{P}_A$  and that these peaks come closer by reducing the temperature without distinct jump at the phase transitions (Figure 11b–e) supports the suggested stabilization of the  $\text{SmC}_s\text{P}_A$  structure in the ITO cells.

As the largest enthalpy value is associated with the  $M_1$ - $\text{SmC}_s\text{P}_A$  transition it is assumed that major changes take place at this transition and therefore all phases above this temperature are associated with a growing size of the polar  $\text{SmC}_s\text{P}_F$

**Table 2.** Comparison of 4-cyano substituted bent-shad mesogens with different linking groups  $X_1$  and  $X_2$ .

Comp.	$X_1$	$X_2$	Phase transitions $T/^\circ\text{C}$	Ref.
<b>A12</b>	–N=N–	–N=N–	Cr 71 (SmC <sub>5</sub> P <sub>A</sub> 70) M <sub>1</sub> 75 SmC <sub>5</sub> P <sub>F</sub> 83 SmC <sub>5</sub> P <sub>R</sub> 96 SmC 127 N <sub>Cybc</sub> 137 Iso	
<b>B12</b>	–N=CH–	–CH=N–	Cr 65 SmCP <sub>A</sub> 122 SmC 141 SmA 188 Iso	[9]
<b>C12</b>	–OOC–	–COO–	Cr 100 SmAP <sub>A</sub> 112 SmA 185 Iso	[10]
<b>D12</b>	–COO–	–OOC–	Cr 103 (SmCP <sub>A</sub> '' 68 SmCP <sub>A</sub> ' 75 SmCP <sub>A</sub> 94) SmC 109 N <sub>Cybc</sub> 129 Iso	[10]

domains and increasing polar correlation between them. Some of the continuous transitions, especially the SmC–SmC<sub>5</sub>P<sub>R</sub> transitions, manifest only under certain conditions.

### 3.3. Achiral Symmetry Breaking

Another important observation is the chirality in the SmC/SmC<sub>5</sub>P<sub>R</sub> phase region, which is observed by the formation of conglomerates of macroscopic chiral domains for all compounds in sufficiently thin cells. It appears at the N<sub>Cybc</sub>–SmC transition and is retained in the SmC<sub>5</sub>P<sub>R</sub> phase. The origin of this chirality should be the locally chiral SmC<sub>5</sub>P<sub>F</sub> structure in the polar domains. The coupling of this superstructural chirality with the molecular chirality,<sup>[39]</sup> in this case with the conformational molecular chirality<sup>[40,41]</sup> favors molecular conformations with a helical shape and a distinct helix sense. As helical molecules cannot pack exactly parallel<sup>[42]</sup> the emergence of chirality leads to a reduction or even possibly to an inversion of the bend elastic constant  $k_{33}$ .<sup>[43]</sup> Formation of the chiral domains is supported by surface anchoring, as indicated by the thickness dependence of this phenomenon<sup>[8]</sup> and the absence of chiral domains in freely suspended films. However also the above mentioned specific molecular and superstructural factors provided by the compounds and their distinct modes of self-assembly are favorable for the occurrence of chiral segregation for the compounds under discussion. Hence, the combined effects of superstructural chirality and surface interaction should contribute to achiral symmetry breaking.

### 3.4. Comparison with Related 4-Cyanoresorcinol-Based Bent-Core Mesogens

A comparison of compound **A12** with the liquid crystalline properties of previously reported related compounds with the same chain length, where only the azo group is replaced by other linking groups, like –CH=N–, –COO– or –OOC–<sup>[9,10]</sup> (other compounds **B12–D12**), is shown in **Table 2**.

Considering the mesophase stability (clearing temperatures) the azobenzene **A12** is similar to compound **D12** with

phenylbenzoate wings. For both compounds, only tilted smectic phases were observed and a nematic phase (N<sub>Cybc</sub>) is formed at higher temperatures. The Schiff base mesogen **B12** and the terephthalate **C12** behave differently; they have about 50 K higher clearing temperatures; show no nematic phases and have a higher tendency to form non-tilted phases, the terephthalate forming exclusively SmA phases. The absence of N phases and the higher mesophase stability indicate a denser molecular packing, which is most likely due to the reduced electron density in rings B which provides stronger  $\pi$ -stacking interactions between these rings.<sup>[22]</sup> The presence of electron deficit rings seems also to favor the formation of nontilted phases. Compounds **A12** and **B12** with double bonds involved in the  $\pi$ -conjugation pathway between the benzene rings have about 30–40 K lower melting points compared to the ester compounds **C12** and **D12**, being more flexible, but having a significant component of the C = O dipole aligned perpendicular to the molecular long axis. In all cases polar order develops in a stepwise manner via paraelectric SmA or SmC phases on decreasing temperature. The specific feature of the azobenzenes **An** is that this transition takes place via a new SmC<sub>5</sub>P<sub>R</sub> phase, a ferroelectric SmC<sub>5</sub>P<sub>F</sub> phase<sup>[44,45]</sup> and an additional highly viscous phase M<sub>1</sub>. Moreover, among the compounds mentioned in **Table 2** only for **A12** chiral domains were reported in the SmC range. Advantageous is also the low melting point of **A12** which is comparable with the Schiff base compound **B12**. The azobenzenes **An** provide the additional option of modulation of the phase structure and mode of polar order by photoisomerization,<sup>[25–29]</sup> which is presently under investigation.

## 4. Summary and Conclusions

We have reported the synthesis and phase behavior of a series of photosensitive azo functionalized bent-core molecules consisting of 4-cyanoresorcinol as central core. This series allowed the investigation of the development of polar order in tilted smectic phases depending on chain length and temperature. It appears that with increasing polar domain size a ferroelectric phase is formed first which becomes modulated and then changes to the antiferroelectric phase. It turned out that this transition from nonpolar to polar phases is more com-



plex than that observed for the nontilted smectic phases, most probably due to the restrictions provided by tilt and chirality in the  $\text{SmC}_s\text{P}_F$  clusters. All observed LC phases, with exception of the  $\text{SmC}_s\text{P}_A$  phase at lowest temperature are composed of polar  $\text{SmC}_s\text{P}_F$  domains with distinct size. The  $\text{SmC}$  phase is a paraelectric  $\text{SmC}$  phase; especially in the  $\text{SmC}_s\text{P}_R$  region the domains reach an appreciable size and this region is considered as a close relative of the  $\text{SmAP}_R$  phase. Overall, the phase structures are very sensitive to the conditions and the proposed models need further confirmation by additional investigations and comparison with phase sequences of other series of structural related compounds which are in progress. Besides these fundamental studies of the phase structures reported herein, the *trans-cis* photoisomerization of the azobenzene wings (see Figure S16) provides additional possibilities for the modification of the phase structure, polar order and chirality with these new bent-core mesogens, potentially leading to photoswitchable multifunctional ferro- and antiferroelectric LCs.

## Supporting Information

Supporting Information is available from the Wiley Online Library or from the author.

## Acknowledgements

M. Alaasar is grateful to the Alexander von Humboldt Foundation for the research fellowship at the Martin-Luther University Halle-Wittenberg; A. Eremin acknowledges German Research Foundation DFG (project ER 467/2) for the financial support.

Received: July 8, 2013

Revised: August 15, 2013

Published online: November 27, 2013

- [1] a) S. Horiuchi, Y. Tokura, *Nature Mater.* **2008**, *7*, 357; b) A. S. Tayi, A. K. Shveyd, A. C.-H. Sue, J. M. Szarko, B. S. Rolczynski, D. Cao, T. J. Kennedy, A. A. Sarjeant, C. L. Stern, W. F. Paxton, W. Wu, S. K. Dey, A. C. Fahrenbach, J. R. Guest, H. Mohseni, L. X. Chen, K. L. Wang, J. F. Stoddart, S. I. Stupp, *Nature* **2012**, *488*, 485.
- [2] a) *Handbook of Liquid Crystals* (Eds: D. Demus, J. Goodby, G. W. Gray, H.-W. Spiess, V. Vill), Wiley-VCH, Weinheim **1998**; b) *Handbook of Liquid Crystals*, 2nd Ed, (Eds: J. W. Goodby, P. J. Collings, H. Gleeson, P. Raynes, T. Kato, C. Tschierske), Wiley-VCH, Weinheim **2013**.
- [3] a) A. Fukuda, Y. Takanishi, T. Isozaki, K. Lshikawa, H. Takezoe, *J. Mater. Chem.* **1994**, *4*, 997; b) S. T. Lagerwall, *Ferroelectric and Antiferroelectric Liquid Crystals*, Wiley-VCH, Weinheim **1999**.
- [4] T. Niori, T. Sekine, J. Watanabe, T. Furukawa, H. Takezoe, *J. Mater. Chem.* **1996**, *6*, 1231.
- [5] a) G. Pelzl, S. Diele, W. Weissflog, *Adv. Mater.* **1999**, *11*, 707; b) C. Tschierske, G. Dantlgraber, *Pramana* **2003**, *61*, 455; c) D. M. Walba, *Top. Stereochem.* **2003**, *24*, 457; d) M. B. Ros, J. L. Serrano, M. R. De la Fuente, C. L. Folcia, *J. Mater. Chem.* **2005**, *15*, 5093; e) R. A. Reddy, C. Tschierske, *J. Mater. Chem.* **2006**, *16*, 907; f) H. Takezoe, Y. Takanishi, *Jpn. J. Appl. Phys.* **2006**, *45*, 597; g) A. Jáklí, C. Bailey, J. Harden, *Thermotropic Liquid Crystals. Recent Advances* (Ed: A. Ramamoorthy), Springer, The Netherlands **2007**, Ch. 2, p.59; h) A. Eremin, A. Jakli, *Soft Matter* **2013**, *9*, 615.
- [6] a) W. Weissflog, H. N. Sheenivasa Murthy, S. Diele, G. Pelzl, *Philos. Trans. R. Soc., London, Ser. A* **2006**, *364*, 2657; b) G. Pelzl, W. Weissflog, *Thermotropic Liquid Crystals. Recent Advances* (Ed: A. Ramamoorthy), Springer, The Netherlands **2007**, Ch. 1, p.1.
- [7] A. Eremin, M. Floegel, U. Kornek, S. Stern, R. Stanarius, H. Nadasi, W. Weissflog, C. Zhu, Y. Shen, C. S. Park, J. MacLennan, N. Clark, *Phys. Rev. E* **2012**, *86*, 051701.
- [8] M. Alaasar, M. Prehm, M. Nagaraj, J. K. Vij, C. Tschierske, *Adv. Mater.* **2013**, *25*, 2186.
- [9] I. Wirth, S. Diele, A. Eremin, G. Pelzl, S. Grande, L. Kovalenko, N. Pancenko, W. Weissflog, *J. Mater. Chem.* **2001**, *11*, 1642.
- [10] L. Kovalenko, M. W. Schröder, R. A. Reddy, S. Diele, G. Pelzl, W. Weissflog, *Liq. Cryst.* **2005**, *32*, 857.
- [11] C. Keith, A. Lehmann, U. Baumeister, M. Prehm, C. Tschierske, *Soft Matter* **2010**, *6*, 1704.
- [12] a) Y. Shimbo, E. Gorecka, D. Pocięcha, F. Araoka, M. Goto, Y. Takanishi, K. Ishikawa, J. Mieczkowski, K. Gomola, H. Takezoe, *Phys. Rev. Lett.* **2006**, *97*, 113901; b) K. Gomola, L. Guo, E. Gorecka, D. Pocięcha, J. Mieczkowski, K. Ishikawa, H. Takezoe, *Chem. Commun.* **2009**, 6592; c) L. Guo, S. Dhara, B. K. Sadashiva, S. Radhika, R. Pratibha, Y. Shimbo, F. Araoka, H. Takezoe, *Phys. Rev. E* **2010**, *81*, 011703; d) M. Gupta, S. Datta, S. Radhika, B. K. Sadashiva, A. Roy, *Soft Matter* **2011**, *7*, 4735.
- [13] a) C. Keith, M. Prehm, Y. P. Panarin, J. K. Vij, C. Tschierske, *Chem. Commun.* **2010**, 46, 3702; b) G. Shanker, M. Prehm, M. Nagaraj, J. K. Vij, C. Tschierske, *J. Mater. Chem.* **2011**, *21*, 18711.
- [14] Y. P. Panarin, M. Nagaraj, S. Sreenilayam, J. K. Vij, A. Lehmann, C. Tschierske, *Phys. Rev. Lett.* **2011**, *107*, 247801.
- [15] J. Etxebarria, M. B. Ros, *J. Mater. Chem.* **2008**, *18*, 2919.
- [16] a) M. Eich, J. H. Wendorff, B. Beck, H. Ringsdorf, *Makromol. Chem., Rapid Commun.* **1987**, *8*, 59; b) S. Sie, A. Natasohn, P. Rochon, *Chem. Mater.* **1993**, *5*, 403; c) A. Natasohn, P. Rochon, *Chem. Rev.* **2002**, *102*, 4139; d) A. Chanishvili, G. Chilaya, G. Petriashvili, P. Collings, *J. Phys. Rev. E* **2005**, *71*, 051705.
- [17] a) P. Rochon, E. Batalla, A. Natanson, *Appl. Phys. Lett.* **1995**, *66*, 136; b) D.Y. Kim, S.K. Li, L. Tripathy, J. Kumar, *Appl. Phys. Lett.* **1995**, *66*, 1166.
- [18] S. Kawata, Y. Kawata, *J. Opt. Soc. Am.* **2001**, *B18*, 1777.
- [19] a) X. Meng, A. Natanson, C. Barrett, P. Rochon, *Macromolecules* **1996**, *29*, 946; b) M. Ho, A. Natanson, C. Barrett, P. Rochon, *Can. J. Chem.* **1995**, *73*, 1773; c) A. Natanson, P. Rochon, M. Ho, C. Barrett, *Macromolecules* **1995**, *28*, 4179.
- [20] a) K. Ichimura, *Chem. Rev.* **2000**, *100*, 1847; b) R. Hagen, T. Bieringer, *Adv. Mater.* **2001**, *13*, 1805; c) O. Yaroshchuk, Y. Reznikov, *J. Mater. Chem.* **2012**, *22*, 286; d) H. M. D. Bandara, S. C. Burdette, *Chem. Soc. Rev.* **2012**, *41*, 1809.
- [21] a) N. G. Nagaveni, A. Roy, V. Prasad, *J. Mater. Chem.* **2012**, *22*, 8948; b) C. L. Folcia, I. Alonso, J. Ortega, J. Etxebarria, I. Pintre, M. B. Ros, *Chem. Mater.* **2006**, *18*, 4617; c) D. D. Sarkar, R. Deb, N. Chakraborty, V. S. R. Nandiraju, *Liq. Cryst.* **2012**, *39*, 1003; d) M.-G. Tamba, A. Bobrovsky, V. Shibaev, G. Pelzl, U. Baumeister, W. Weissflog, *Liq. Cryst.* **2011**, *38*, 1531; e) M. Vijaysrinivasan, P. Kannan, A. Roy, *Liq. Cryst.* **2012**, *39*, 1465.
- [22] M. Alaasar, M. Prehm, C. Tschierske, *Liq. Cryst.* **2013**, *40*, 656.
- [23] a) V. Prasad, S.-W. Kang, K. A. Suresh, L. Joshi, Q. Wang, S. Kumar, *J. Am. Chem. Soc.* **2005**, *127*, 17224; b) K. V. Le, M. Mathews, M. Chambers, J. Harden, Q. Li, H. Takezoe, A. Jakli, *Phys. Rev. E* **2009**, *79*, 030701.
- [24] D. Photinos, C. Tschierske, *J. Mater. Chem.* **2010**, *20*, 4263.
- [25] L. Dinescu, R. P. Lemieux, *Adv. Mater.* **1999**, *11*, 42.
- [26] A. Langhoff, F. Giesselmann, *ChemPhysChem* **2002**, *3*, 424.
- [27] A. Saipa, M. A. Osipov, K. W. Lanham, C. H. Chang, M. D. Walba, F. Giesselmann, *Mater. Chem.* **2006**, *16*, 4170.
- [28] P. Beyer, M. Krueger, F. Giesselmann, R. Zentel, *Adv. Funct. Mater.* **2007**, *17*, 109.

- [29] M. Knežević, M. Warner, *Appl. Phys. Lett.* **2013**, *102*, 043902.
- [30] a) E. Marcus, *Ber. Dtsch. Chem. Ges.* **1891**, *24*, 3650; b) J. L. Serrano, T. Sierra, Y. Gonzalez, C. Bolm, K. Weickardt, A. Magnus, G. Moll, *J. Am. Chem. Soc.* **1995**, *117*, 8312.
- [31] a) O. Francescangeli, F. Vita, C. Ferrero, T. Dingemans, E. T. Samulski, *Soft Matter* **2011**, *7*, 895; b) D. Wiant, S. Stojadinovic, K. Neupane, S. Sharma, K. Fodor-Csorba, A. Jakli, J. T. Gleeson, S. Sprunt, *Phys. Rev. E* **2006**, *73*, 030703; c) N. Vaupotic J. Szydłowska, M. Salamonczyk, A. Kovarova, J. Svoboda, M. Osipov, D. Pocięcha, E. Gorecka, *Phys. Rev. E* **2009**, *80*, 030701.
- [32] N. Vaupotic, D. Pocięcha, E. Gorecka, *Top. Curr. Chem.* **2012**, *318*, 281.
- [33] a) D. Shen, A. Pegenau, S. Diele, I. Wirth, C. Tschierske, *J. Am. Chem. Soc.* **2000**, *122*, 1593–1601; b) J. Szydłowska, J. Mieczkowski, J. Matraszek, D. W. Bruce, E. Gorecka, D. Pocięcha, D. Guillon, *Phys. Rev. E* **2003**, *67*, 031702; c) Y. Takahashi, H. Takezoe, J. Watanabe, Y. Takahashi, A. Iida, *J. Mater. Chem.* **2006**, *16*, 816.
- [34] a) A. Eremin, A. Nemes, R. Stannarius, G. Pelzl, W. Weissflog, *Soft Matter* **2008**, *4*, 2186; b) A. Eremin, A. Nemes, R. Stannarius, G. Pelzl, W. Weissflog, *Phys. Rev. E* **2008**, *78*, 061705.
- [35] D. Link, J. MacLennan, N. Clark, *Phys. Rev. Lett.* **1996**, *77*, 2237.
- [36] a) S.-W. Choi, Y. Kinoshita, B. Park, H. Takezoe, T. Niori, J. Watanabe, *Jpn. J. Appl. Phys.* **1998**, *37*, 3408; b) R. Macdonald, F. Kentischer, P. Warnick, G. Heppke, *Phys. Rev. Lett.* **1998**, *81*, 4408; c) S. H. Hong, J. C. Williams, R. J. Twieg, A. Jákli, J. Gleeson, S. Sprunt, B. Ellman, *Phys. Rev. E* **2010**, *82*, 041710.
- [37] A weak SHG signal was previously observed in the SmC region of a hockey stick molecule, this could also be regarded as a SmCP<sub>R</sub> phase, though no current peak and no chiral domains were observed in this case: A. Eremin, S. Stern, R. Stannarius, *Phys. Rev. Lett.* **2008**, *101*, 247802.
- [38] This is interesting if one compares these compounds with the 1,2,4-oxadiazoles, for which ferroelectric switching was proposed for a nematic phase (O. Francescangeli, V. Stanic, S. I. Torgova, A. Strigazzi, N. Scaramuzza, C. Ferrero, I. P. Dolbnya, T. M. Weiss, R. Berardi, L. Muccioli, S. Orlandi, C. Zannoni, *Adv. Funct. Mater.* **2009**, *19*, 2592), but which are completely SHG silent, i.e., for which no field induced polar order could be confirmed by SHG, see a) G. Shanker, M. Nagaraj, A. Kokot, J. K. Vij, M. Prehm, C. Tschierske, *Adv. Funct. Mater.* **2012**, *22*, 1671; b) G. Shanker, M. Prehm, M. Nagaraj, J. K. Vij, M. Weyland, A. Eremin, C. Tschierske, unpublished.
- [39] H. Ocak, B. Bilgin-Eran, M. Prehm, S. Schymura, J. P. F. Lagerwall, C. Tschierske, *Soft Matter* **2011**, *7*, 8266.
- [40] a) D. J. Earl, M. A. Osipov, H. Takezoe, Y. Takahashi, M. R. Wilson, *Phys. Rev. E* **2005**, *71*, 021706; b) H. S. Jeong, S. Tanaka, D. K. Yoon, S.-W. Choi, Y. H. Kim, S. Kawauchi, F. Araoka, H. Takezoe, H.-T. Jung, *J. Am. Chem. Soc.* **2009**, *131*, 15055; c) S. Kawauchi, S.-W. Choi, K. Fukuda, K. Kishikawa, J. Watanabe, H. Takezoe, *Chem. Lett.* **2007**, *36*, 750; d) S.-W. Choi, S. Kang, Y. Takahashi, K. Ishikawa, J. Watanabe, H. Takezoe, *Chirality* **2007**, *19*, 250; e) F. Yan, C. A. Hixson, D. J. Earl, *Soft Matter* **2009**, *5*, 4477.
- [41] H. Takezoe, *Top. Curr. Chem.* **2012**, *318*, 303.
- [42] R. Lemineux, *Chem. Soc. Rev.* **2007**, *36*, 2033.
- [43] a) I. Dozov, *Europhys. Lett.* **2001**, *56*, 247; b) V. Görtz, *Liq. Cryst. Today* **2010**, *19*, 37.
- [44] A similar kind of transition involving ferroelectric switching and highly viscous intermediate states in free standing films was recently observed for 4,6-dichlororesorcinol based bent core mesogens;<sup>[7]</sup> this indicates that these states might be general features of the transition from local ferroelectric to long range antiferroelectric polar order.
- [45] Considering the antiferroelectric response found in all smectic phases with macroscopic polar order, some of the SmCP<sub>A</sub> subtypes reported for compound **D12**<sup>[10]</sup> might also be related to those reported herein.

# Development of Polar Order in the Liquid Crystal Phases of a 4-Cyanoresorcinol-Based Bent-Core Mesogen with Fluorinated Azobenzene Wings

Mohamed Alaasar,<sup>\*,[a, b]</sup> Marko Prehm,<sup>[a]</sup> Maria-Gabriela Tamba,<sup>[c]</sup> Nerea Sebastián,<sup>[c]</sup> Alexey Eremin,<sup>\*,[c]</sup> and Carsten Tschierske<sup>\*,[a]</sup>

A bent-core mesogen consisting of a 4-cyanoresorcinol unit as the central core and laterally fluorinated azobenzene wings forms four different smectic LC phase structures in the sequence SmA–SmC<sub>s</sub>–SmC<sub>s</sub>P<sub>AR</sub>–M, all involving polar SmC<sub>s</sub>P<sub>s</sub> domains with growing coherence length of tilt and polar order on decreasing temperature. The SmA phase is a cluster-type de Vries phase with randomized tilt and polar direction; in the paraelectric SmC<sub>s</sub> phase the tilt becomes uniform, although

polar order is still short-range. Increasing polar correlation leads to a new tilted and randomized polar smectic phase with antipolar correlation between the domains (SmC<sub>s</sub>P<sub>AR</sub>) which then transforms into a viscous polar mesophase M. As another interesting feature, spontaneous symmetry breaking by formation of a conglomerate of chiral domains is observed in the non-polar paraelectric SmC<sub>s</sub> phase.

## 1. Introduction

Liquid crystals (LCs) represent a unique state of soft matter combining long-range orientational or positional order with molecular mobility.<sup>[1]</sup> These materials find a wide range of applications in modern technologies,<sup>[2]</sup> but also contribute to the fundamental understanding of soft self-assembly of molecules into complex functional structures.<sup>[3]</sup> Discovery of spontaneous polar order and achiral symmetry breaking in bent-core liquid crystals (BCLCs) opened a new area in the field of LC research.<sup>[4,5]</sup> Since then, many different classes of BCLCs have been synthesized and this area has become a topic of contemporary research.<sup>[6–11]</sup> Usually the BCLCs form tilted smectic phases with macroscopic polar order in the layers (SmCP) and distinct correlation of the polar order (synpolar = P<sub>s</sub> and antipolar = P<sub>A</sub>) and tilt (synclinc = C<sub>s</sub> and anticlinc = C<sub>a</sub>) between the layers (SmC<sub>s</sub>P<sub>s</sub>, SmC<sub>s</sub>P<sub>A</sub>, SmC<sub>a</sub>P<sub>s</sub> and SmC<sub>a</sub>P<sub>A</sub>).<sup>[5]</sup> More recently, also non-tilted smectic phases (SmAP) have been found with transitions from short-range polar order (paraelectric

SmA) via intermediate structures named as randomized phases (SmAP<sub>R</sub>)<sup>[12,13]</sup> to polar smectic phases with long-range polar order (SmAP<sub>A</sub>, SmAP<sub>s</sub>).<sup>[13–15]</sup> However, tilted versions of these randomized polar phases were unknown.<sup>[16]</sup> 4-Cyanoresorcinol derived BCLCs, with a reduced bend due to the influence of the CN group on the conformation of the adjacent ester group, represent typical mesogens with a structure at the borderline between the rod- and bent-shape.<sup>[17–19]</sup> In previous work it has been reported that this structural unit can be used to generate bent-core mesogens with new liquid crystalline phases and new phase sequences.<sup>[20–25]</sup> One of the most important outcomes was that combining 4-cyanoresorcinol with the azobenzene wings results in the formation of a new synclinc tilted SmC phase (SmC<sub>s</sub>) with an enhanced polarizability, designated as SmC<sub>s</sub>P<sub>R</sub>, showing surface supported achiral symmetry breaking.<sup>[24,25]</sup> This phase was considered as the tilted analogue of the non-tilted randomized polar smectic A phase (SmAP<sub>R</sub>).<sup>[12,13]</sup>

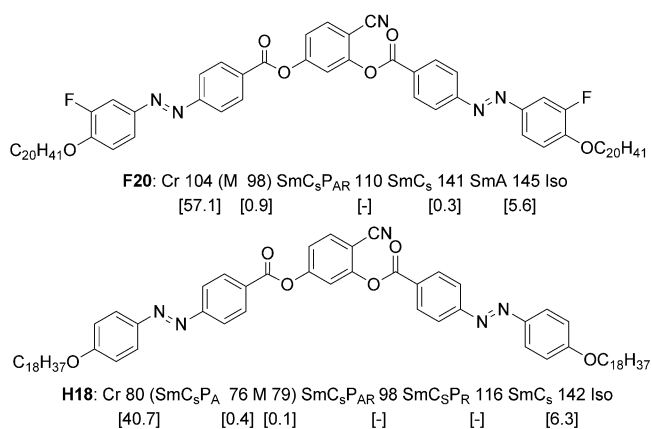
Herein we report the synthesis and investigation of a new 4-cyanoresorcinol-based bent-core mesogen **F20** involving fluorinated azobenzene wings (see Scheme 1). Polarizing microscopic and electro-optical measurements in bulk samples and freely suspended films and second harmonic generation (SHG) experiments, dielectric investigations, and X-ray diffraction (XRD) were performed. With decreasing temperature uniform tilt appears first, leading to a SmA–SmC<sub>s</sub> transition and then coherence of polar order grows continuously throughout the SmC<sub>s</sub> range. In a certain temperature range a new tilted and antiferroelectric phase with limited coherence length of polar order (SmC<sub>s</sub>P<sub>AR</sub>), representing the tilted version of the SmAP<sub>AR</sub> phase, was discovered.

[a] Dr. M. Alaasar, Dr. M. Prehm, Prof. Dr. C. Tschierske  
Institute of Chemistry, Organic Chemistry  
Martin Luther University Halle-Wittenberg  
Kurt-Mothes Str. 2, 06120 Halle/Saale (Germany)  
E-mail: carsten.tschierske@chemie.uni-halle.de

[b] Dr. M. Alaasar  
Department of Chemistry  
Faculty of Science  
Cairo University, Giza (Egypt)  
E-mail: malaasar@sci.cu.edu.eg

[c] Dr. M.-G. Tamba, Dr. N. Sebastián, Dr. A. Eremin  
Institute for Experimental Physics  
Otto-von-Guericke University Magdeburg  
Universitätsplatz 2, 39106 Magdeburg (Germany)  
E-mail: alexey.eremin@ovgu.de

Supporting Information and ORCID(s) from the author(s) for this article are available on the WWW under <http://dx.doi.org/10.1002/cphc.201500891>.

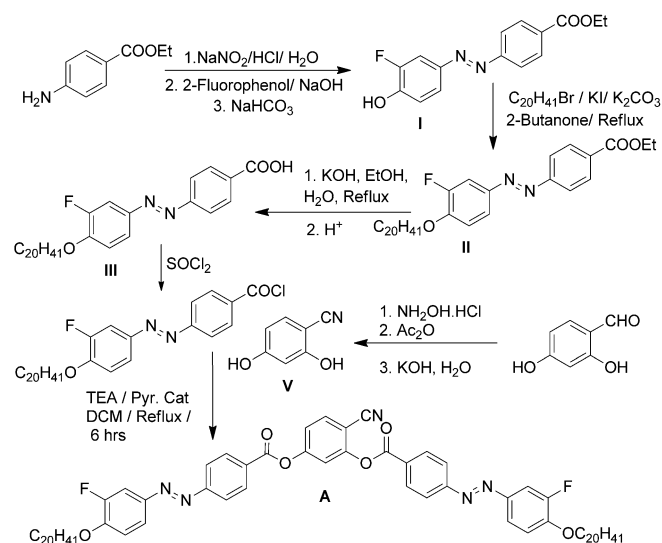


**Scheme 1.** Chemical structures of compound **F20** discussed herein and a related non-fluorinated 4-cyanoresorcinol derivative **H18** with their transitions ( $T/C$ ,  $\Delta H/kJ mol^{-1}$ , values in square brackets)<sup>[25]</sup> values between brackets are monotropic phase transitions; abbreviations: Cr = crystalline solid; Iso = isotropic liquid; SmA = de Vries-type smectic A phase; SmC<sub>s</sub> = synclinc tilted smectic phase capable of mirror symmetry breaking; SmC<sub>s</sub>P<sub>AR</sub> = antiferroelectric switching synclinc tilted SmC phase composed of SmC<sub>s</sub>P<sub>S</sub> domains; SmC<sub>s</sub>P<sub>A</sub> = antiferroelectric switching polar SmC phase with alternating polar direction between the layers (B2 phase), M = unknown mesophase; the phase assignment of **H18** is adjusted to the notation used in this manuscript (the SmC<sub>s</sub>P<sub>AR</sub> phase of **H18** was previously designated as SmC<sub>P</sub>, based on the results of investigation of freely suspended films, see explanations in Section 3).

## Methods

### Synthesis

The synthesis of the bent-core compound **F20** is shown in Scheme 2. 2,4-Dihydroxybenzonitrile (**V**) was prepared from 2,4-dihydroxybenzaldehyde by oxime formation, followed by dehydration.<sup>[17]</sup> The acid **III** was synthesized from ethyl 4-(3'-fluoro-4'-hydroxyphenylazo)benzoate (**I**) by alkylation with 1-bromooctane in the presence of potassium carbonate to give the ester **II**, which was then hydrolyzed under basic conditions to yield the acid **III**.<sup>[26]</sup> The benzoic acid **III** was first converted to the benzoyl chloride



**Scheme 2.** Synthesis of compound **F20**.

with thionyl chloride, which then was used for the acylation of 4-cyanoresorcinol (**V**) in the presence of triethylamine (TEA) and a catalytic amount of dry pyridine in dry dichloromethane (DCM) as solvent. The obtained compound **F20** was purified by column chromatography using DCM followed by recrystallization from an ethanol/chloroform mixture (1:1). The detailed synthetic procedures and analytical data are reported in the Supporting Information.

### Characterization Methods

For determination of the phase transitions the synthesized compound **F20** was investigated by polarized light optical microscopy (POM) using a Nikon (Optiphot 2) microscope in conjunction with a heating stage (FP82HT, Mettler); the material was sandwiched between non-treated microscopy glass plates for homeotropic alignment or investigated in polyimide (PI)-coated 6  $\mu m$  ITO cells (EHC, Japan) in planar alignment. Differential scanning calorimetry was performed in aluminium pans on a DSC-7 calorimeter (Perkin Elmer) with heating and cooling rates of 10 K min<sup>-1</sup>.

XRD investigations were conducted at Cu<sub>K $\alpha$</sub>  line ( $\lambda = 1.54 \text{ \AA}$ ) using a standard Coolidge tube source with a Ni-filter. Investigations of oriented samples were performed using a 2D-detector (Vantec 500, Bruker). Uniform orientation was achieved by slow cooling of a small droplet of this compound on a glass substrate. Alignment was achieved at the air-sample interface on the top of the droplet. The exposure time was 15 min and the sample to detector distance was 8.95 cm and 26.7 cm for wide and small angle measurement, respectively.

Polarization current measurements and electro-optical investigations were carried out with a home-built setup using commercially available ITO-coated glass cells (E.H.C., Japan, polyimide-coated, antiparallel rubbing, thickness 6  $\mu m$ , measuring area 1 cm<sup>2</sup>). Complex dielectric permittivity was measured on cooling runs in the frequency range of 10 Hz–10 MHz with the impedance analyzer Solartron 1260A in an 8  $\mu m$  Instec cell with planar antiparallel rubbing. Capacitance of the cell was carefully calibrated before being filled in the isotropic state.

Optical second harmonic generation (SHG) measurements have been performed using a Nd:YAG laser operating at  $\lambda = 1064 \text{ nm}$  with 10 ns pulse width and 10 Hz repetition rate. The primary beam was incident at an angle of 30° to the cell normal and the SHG signal was detected in transmission by a photomultiplier tube (Hamamatsu). The acquired signal was calibrated using a 50  $\mu m$  reference quartz plate.

Freely suspended films were studied using polarising optical microscopy in transmission and reflection modes. The films were drawn across a 3  $\times$  10 mm glass frame with a pair of electrodes attached to it. The thickness of the films was determined from the reflection spectra obtained by an USB spectrometer. The polar properties of the films were studied by observation of the director inversion walls under an action of AC and DC electric fields. We made observations using a 575 nm narrow band filter to suppress *trans-cis* isomerisation during the experiment.

## 2. Results and Discussion

### 2.1. DSC and Optical Investigations

Phase sequences, transition temperatures and associated enthalpies of compound **F20** are given in Scheme 1; the DSC plots on heating and cooling are shown in Figure 1. Besides the melting and crystallization events there is a major phase transition with an enthalpy of 5.6 kJ mol<sup>-1</sup> for the Iso–SmA

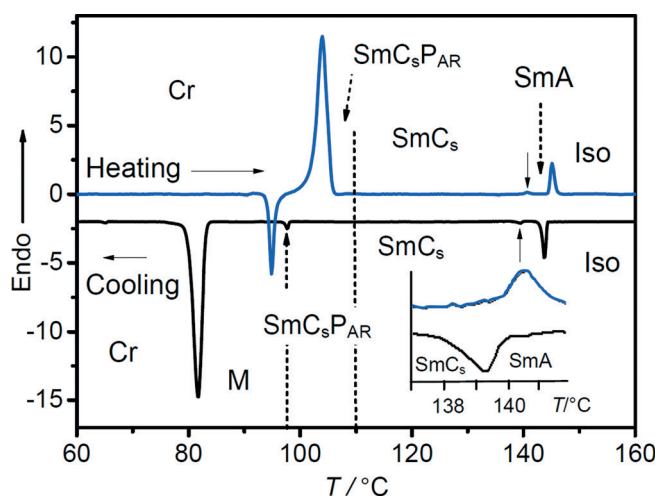


**Figure 1.** DSC heating (blue) and cooling traces (black) of compound **F20** at a rate of  $10 \text{ K min}^{-1}$ , the inset shows the enlarged region of the  $\text{SmC}_5$ – $\text{SmA}$  transition.

transition at  $145^\circ\text{C}$  and two additional transitions with much smaller enthalpy values at  $T=141^\circ\text{C}$  ( $0.3 \text{ kJ mol}^{-1}$ ,  $\text{SmA}$ – $\text{SmC}_5$ ) and at  $T=98^\circ\text{C}$  ( $0.9 \text{ kJ mol}^{-1}$ , on cooling,  $\text{SmC}_5\text{P}_{\text{AR}}$ – $\text{M}$ ). Though the enthalpy change of the  $\text{SmA}$ – $\text{SmC}_5$  transition is relatively small it appears to be weakly first-order. No enthalpy is found for the  $\text{SmC}_5$ – $\text{SmC}_5\text{P}_{\text{AR}}$  transition at  $T=110^\circ\text{C}$ , it clearly being continuous.

Optical investigation between crossed polarizers confirms the DSC data. Upon cooling from the isotropic liquid in planar alignment ( $6 \mu\text{m}$  polyimide coated ITO cell) a uniaxial smectic A phase with a typical fan texture develops (Figure 2a). In this texture, the dark extinction brushes coincide with the directions of polarizer and analyzer. At the phase transition at  $T=141^\circ\text{C}$ , the smooth fans in the planar samples become broken and the extinction crosses become inclined with the directions of the polarizers, indicating the onset of a uniform (synclinal) tilt. The appearing optical tilt is about  $25$ – $30^\circ$  ( $\text{SmC}_5$  phase, Figure 2b). This transition is associated with an increase of birefringence (interference colour of the POM texture changes from green to yellowish green). The increase of birefringence at the  $\text{SmA}$ – $\text{SmC}_5$  transition and on further cooling in the  $\text{SmC}$  range may suggest an increase of the order parameter and higher packing density of the aromatic cores due to an increased bias of the rotation around the long molecular axis with decreasing temperature. A similar increase of birefringence has been observed for the  $\text{SmA}$ – $\text{SmC}$  transitions in rod-like de Vries materials where the simultaneous growth of tilt and birefringence was attributed to an increasing bias of azimuthal fluctuations.<sup>[27]</sup> This is a strong indication that the  $\text{SmA}$  phase of **F20** is a de Vries-type phase.<sup>[28]</sup> On further cooling, the birefringence continuously increases further (greenish yellow to orange/red, see Figure 2c) and the optical tilt grows up to  $35$ – $38^\circ$  in the temperature range of the  $\text{SmC}_5\text{P}_{\text{AR}}$  phase, in line with a further increasing bias of the rotation around the long axis. An additional jump to higher birefringence is indicated by the colour change from orange/red to green at the next phase transition to the M phase at  $98^\circ\text{C}$  (Figure 2d).

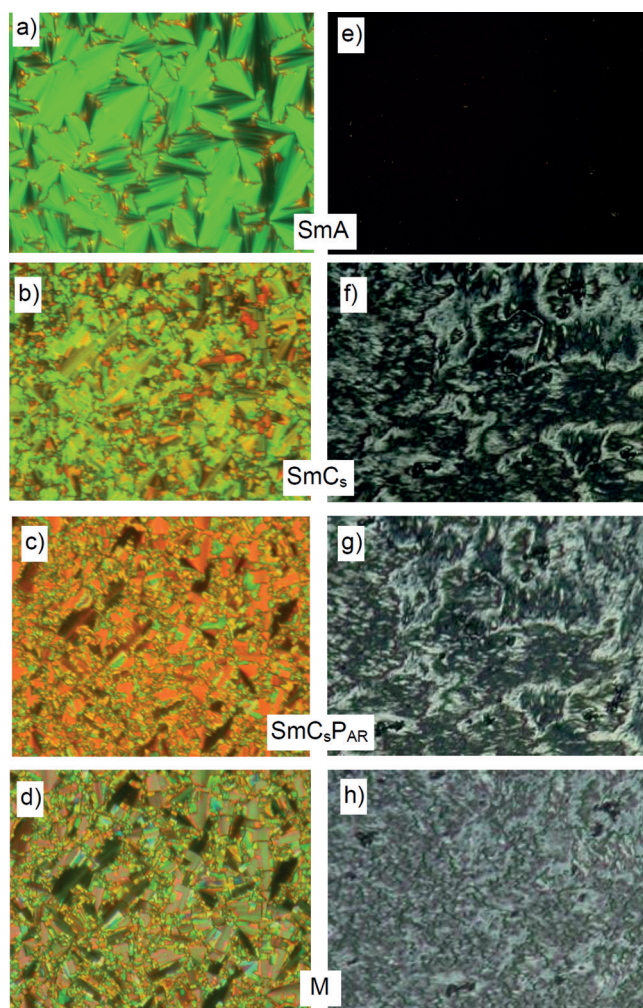


**Figure 2.** Optical micrographs of the textures observed for the different LC phases of compound **F20** in a planar cell (left column) and in a homeotropic cell (right column): a,e)  $\text{SmA}$  phase at  $T=142^\circ\text{C}$ ; b,f)  $\text{SmC}_5$  phase at  $T=137^\circ\text{C}$ ; c,g)  $\text{SmC}_5\text{P}_{\text{AR}}$  phase at  $T=105^\circ\text{C}$  and d,h) M phase at  $T=95^\circ\text{C}$ .

Under homeotropic anchoring conditions (between non-treated glass plates) the  $\text{SmA}$  phase appears pseudo-isotropic, confirming optical uniaxiality (Figure 2e). At  $141^\circ\text{C}$  the homeotropic areas become birefringent, indicating the transition to an optically biaxial LC phase, in line with the above mentioned transition to a  $\text{SmC}_5$  phase (Figure 2f). On further cooling the birefringence continuously increases without significant textural changes (Figure 2g). A change in the schlieren texture is only observed at the  $\text{SmC}_5\text{P}_{\text{AR}}$ – $\text{M}$  transition at  $T=98^\circ\text{C}$  (Figure 2h).

In the temperature range of the  $\text{SmC}_5$  phase between  $110$  and  $141^\circ\text{C}$  a low birefringent texture composed of distinct chiral domains is observed in thin homeotropic samples by uncrossing the polarizers by a small angle of about  $2$ – $5^\circ$  (Figures 3a,c). This leads to the appearance of dark and bright domains; uncrossing the polarizer in the opposite direction reverses the brightness of the domains (Figure 3a–c). That the domains are due to chirality and not only the result of a different tilt alignment is shown by rotation of the sample between crossed polarizers, which gives no significant change in bright-

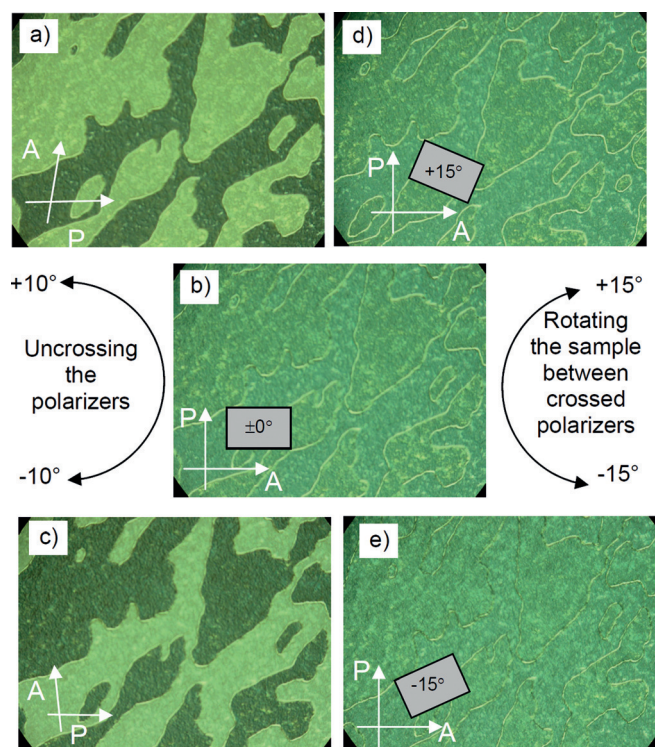


**Figure 3.** Textures of the  $\text{SmC}_S$  phase of compound **F20** at  $T = 130^\circ\text{C}$ : a,c) between slightly uncrossed polarizers, showing dark and bright domains, indicating the presence of areas with opposite chirality sense; b) between crossed polarizers and d,e) texture between crossed polarizers after rotation of the sample by  $15^\circ$  either clockwise or anticlockwise; the birefringence does not change, which confirms chirality as origin of the effects seen in (a–c).

ness, independent of the angle (Figures 3c–e). This corroborates that the distinct regions indeed represent chiral domains with opposite handedness. The chiral domains appear immediately at the  $\text{SmA}$ – $\text{SmC}_S$  transition and slowly fade on cooling (Figure S3). As the birefringence of the homeotropic texture continuously increases on cooling it becomes more and more difficult to detect the chiral domains and these domains become nearly invisible around  $110^\circ\text{C}$ . This means that either these domains become invisible due to the increased birefringence or that chirality is erased on approaching the phase transition to the  $\text{SmC}_S\text{P}_{\text{AR}}$  phase at  $T = 110^\circ\text{C}$ . It should also be noted that no indication of chiral segregation with conglomerate formation can be observed in freely suspended films (see below), which indicates that polar surface interactions are required.

## 2.2. XRD Studies

Compound **F20** was investigated by 2D XRD of surface-aligned samples in the temperature range between 100 and  $150^\circ\text{C}$ . All patterns show a diffuse scattering in the wide-angle region and one sharp Bragg reflection in the small-angle region at  $d = 5.4$ – $5.6$  nm (Figure 4). This  $d$ -value is significantly smaller than the single-molecule length ( $d/L_{\text{mol}} = 0.68$ – $0.70$ ;  $L_{\text{mol}} = 7.95$  nm in an extended conformation with all-*trans* alkyl chains), in line

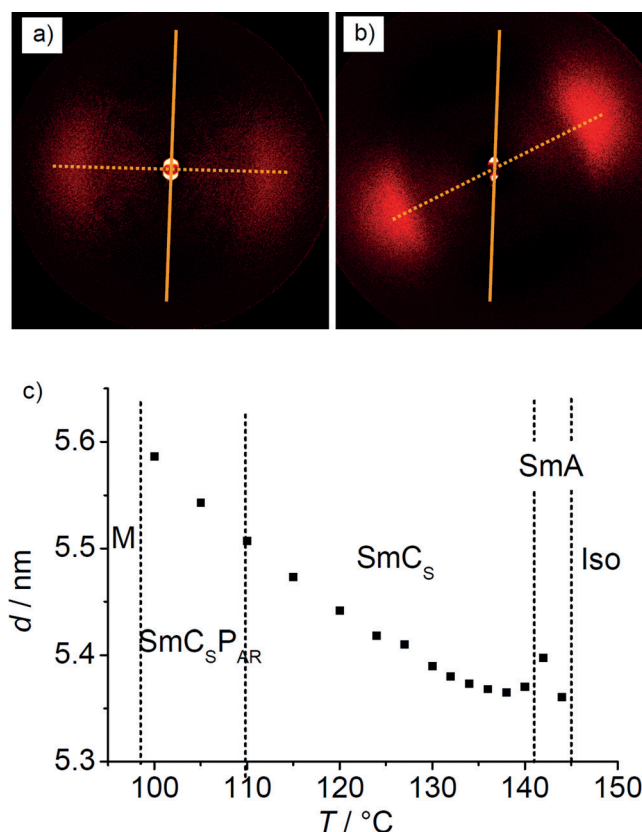


**Figure 4.** XRD investigation of an aligned sample of compound **F20**: a) 2D pattern in the  $\text{SmA}$  phase at  $144^\circ\text{C}$  and b) in the  $\text{SmC}_S$  phase at  $130^\circ\text{C}$ , both after subtraction of the scattering in the isotropic liquid state at  $160^\circ\text{C}$ , the original XRD patterns and the XRD patterns in the  $\text{SmC}_S\text{P}_{\text{AR}}$  range are shown in Figure S2; c) shows the temperature dependence of the  $d$  value (see also Table S1).

with a single-layer structure with significant tilt or intercalation of the alkyl chains. In the  $\text{SmA}$  phase the maxima of the diffuse scattering in the wide-angle region are perpendicular to the position of the layer reflection, indicating an on average non-tilted arrangement of the molecules (Figure 4a), whereas after the transition to the  $\text{SmC}_S$  phase at  $T = 141^\circ\text{C}$  a clear deviation from the orthogonal distribution can be detected (Figure 4b). A tilt angle of about  $20^\circ$  could be calculated from the position of the diffuse wide-angle scattering maxima with respect to the layer reflections on the meridian of the 2D diffraction patterns. The tilt angle does not change in the temperature range between  $141$  and  $100^\circ\text{C}$ . As the optical tilt was found to rise with decreasing temperature (see Section 2.1), it appears that the change in the optical tilt is mainly due to a temperature dependence of the tilt of the aromatic cores, increasing at lower temperature. Furthermore, the unequal intensity distribution of the scattering maxima in the wide-angle region with respect to the meridian (there is nearly no scattering in the north-west and south-east quadrants) is a clear confirmation of a synclinal tilted structure in this temperature range. The temperature dependence of the  $d$ -values is shown in Figure 4c. There is a small drop of the  $d$ -value at the  $\text{SmA}$ – $\text{SmC}_S$  phase transition at  $T = 141^\circ\text{C}$ , as typical for de Vries-type  $\text{SmA}$ – $\text{SmC}_S$  transitions<sup>[28]</sup> (Figure 4c). A slight rise of  $d$  is observed on fur-

ther cooling in the whole  $\text{SmC}_s$  range, down to the crystallization at  $T=100^\circ\text{C}$ , indicating a further increase of the packing density in the  $\text{SmC}_s$  range ( $\text{SmC}_s$  and  $\text{SmC}_s\text{P}_{\text{AR}}$ ). The increase in packing density must be stronger than the effect of growing tilt on the layer spacing. At  $100^\circ\text{C}$  the sample crystallized during the exposure time of the XRD experiments and therefore the M phase occurring below  $98^\circ\text{C}$  cannot be investigated.

### 2.3. SHG, Dielectric Investigations and Electro-Optical Studies

Second harmonic generation (SHG) activity is the most powerful and reliable method to detect polar order in LC phases.<sup>[29]</sup> A plot of field-induced SHG intensity versus temperature for compound **F20** is shown in Figure 5a. Under constant applied electric field ( $E_{\text{pp}}=10.75\text{ V}\mu\text{m}^{-1}$ ) a small SHG signal appears around  $110^\circ\text{C}$ , close to the  $\text{SmC}_s\text{--SmC}_s\text{P}_{\text{AR}}$  transition, and it is growing continuously until crystallization at  $T=94^\circ\text{C}$ . It is

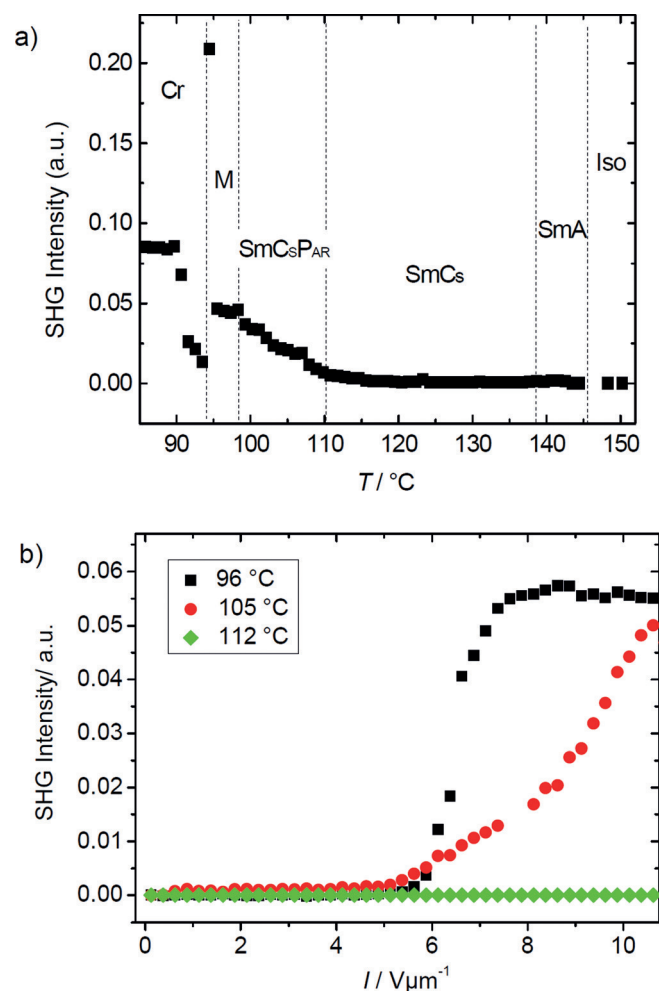


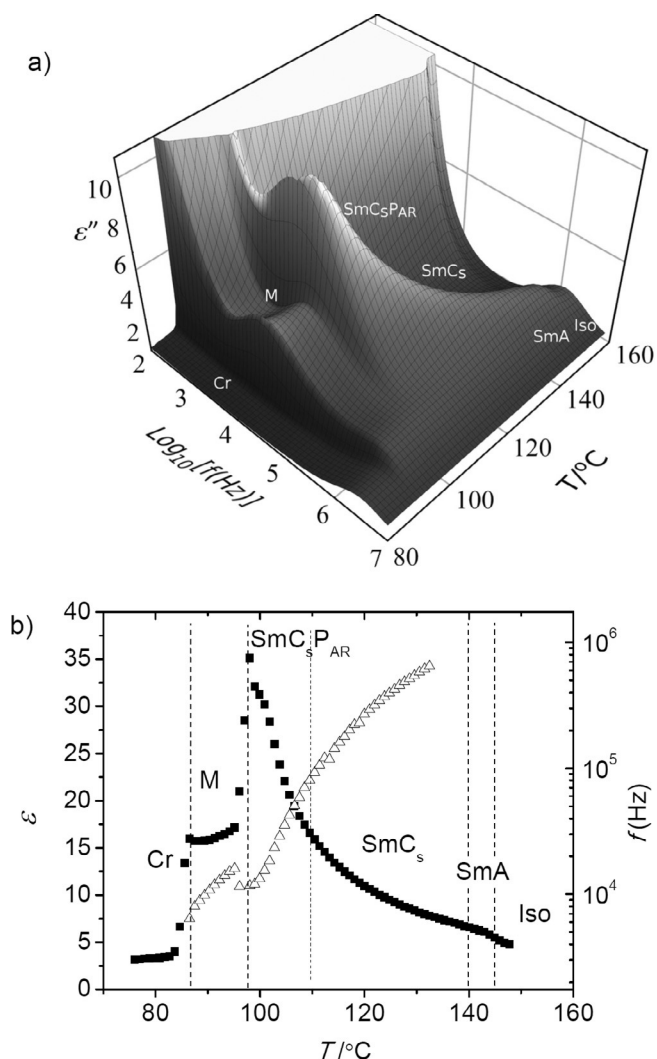
**Figure 5.** a) SHG intensity vs. temperature of compound **F20** at an applied voltage of  $10.4\text{ V}\mu\text{m}^{-1}$  ( $6\text{ }\mu\text{m}$  cell) and b) field dependence of the SHG signal in the  $\text{SmC}_s$  phase at  $T=112^\circ\text{C}$  (green rhomboids), in the  $\text{SmC}_s\text{P}_{\text{AR}}$  phase at  $T=105^\circ\text{C}$  (red dots) and in the M phase at  $T=96^\circ\text{C}$  (black squares) in a  $10\text{ }\mu\text{m}$  cell; for additional data see also Figure S5.

noteworthy that, shortly before crystallization takes place, there is a reproducible jump of the SHG activity to high values (see Figure 5a). An SHG signal is retained in the crystalline state where it is still observed in the field-free state, indicating a non-centrosymmetric polar crystalline phase (Figure S5b). In the LC phases, however, there is no SHG activity in the absence of an applied field (see Figure S5a), indicating no residual polarisation.

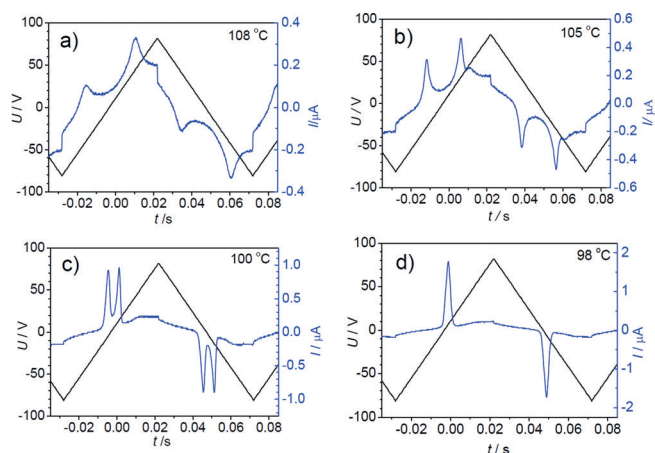
There is a distinct field dependence of the SHG signal in the different phases (see Figure 5b). In the temperature range between  $110$  and  $98^\circ\text{C}$  ( $\text{SmC}_s\text{P}_{\text{AR}}$ ) the SHG signal starts to appear around  $5\text{ V}\mu\text{m}^{-1}$  and grows on further increasing the field strength, reaching a maximum at  $10.5\text{ V}\mu\text{m}^{-1}$ . This kind of field dependence with a smooth increase is typical for LC phases with randomized polar order in the ground state where the polar domains align along the field and their size strongly increasing under the field, thus leading to ferroelectric or antiferroelectric polar switching as previously reported for related non-tilted smectic phases ( $\text{SmAP}_{\text{R}}$ ,  $\text{SmAP}_{\text{AR}}$  phases, respectively).<sup>[12,30,31]</sup> In our compound, the switching appears antiferroelectric. The dipole moments of the developing polar domains appear to be small, which is reflected in the small slope of the SHG curve (Figure 5a). This is in line with the polarization ( $P_s$ ) measurements in Figure 8, where  $P_s$  is continuously increasing with decreasing temperature over the  $\text{SmC}_s\text{P}_{\text{AR}}$  range. In the M-phase below  $98^\circ\text{C}$  a steep rise in the SHG signal intensity is observed between  $5$  and  $7\text{ V}\mu\text{m}^{-1}$  and a plateau is already reached at lower field strength ( $\sim 7\text{--}8\text{ V}\mu\text{m}^{-1}$ ) as is typical for polar  $\text{SmCP}_{\text{A}}$  phases (Figure 5b).

Figure 6a shows the temperature and frequency dependence of the dielectric losses ( $\epsilon''$ ) as measured for **F20** in a  $8\text{ }\mu\text{m}$  planar cell on cooling from the isotropic phase. The high-frequency mode observed at low temperatures arises from the relaxation of the ITO of the cell. A single clear relaxation process associated with the material is obtained for the whole temperature range. Spectra were fitted to the Havriliak–Negami equation<sup>[32]</sup> and the static dielectric permittivity (reflecting the strength of the relaxation process) and the relaxation frequency of the mode are given in Figure 6b. The polar domain structure is supported by dielectric investigations. After a slight jump at the Iso–SmA transition, the permittivity grows continuously over the SmA and  $\text{SmC}_s$  temperature ranges without appreciable leaps, in line with a continuous growth of polar domains in the complete LC temperature range down to  $98^\circ\text{C}$ .<sup>[33]</sup> Critical behavior of the relaxation mode on approaching this temperature, with a rapid decrease of the frequency and fast increase of the dielectric strength (Figure 6b), is indicative of the collective character of the relaxation process. At  $T=98^\circ\text{C}$  the frequency shows a minimum and the permittivity significantly drops, evidencing the softening of the polar fluctuations at the transition to the M phase. In this phase the strength of the mode becomes considerably lower, in agreement with the development of a polar structure with antipolar correlation.

Electro-optical investigations were carried out in  $6\text{ }\mu\text{m}$  PI-coated ITO cells. The polarization current response was measured under an applied triangular wave voltage with a frequen-



**Figure 6.** a) Temperature and frequency dependence of the imaginary part of the dielectric permittivity of **F20** and b) temperature dependence of the static dielectric permittivity (black squares) and relaxation frequency (unfilled triangles) of the dielectric mode. Planar rubbed  $8\ \mu\text{m}$  cell was employed in the dielectric measurements.



**Figure 7.** Switching current response curves for compound **F20** in  $6\ \mu\text{m}$  ITO cell on applying a triangular wave field of  $26.7\ \text{V}_{\text{pp}}\ \mu\text{m}^{-1}$  ( $10\ \text{Hz}$ ) at the indicated temperatures; different scales are used for the current response plots.

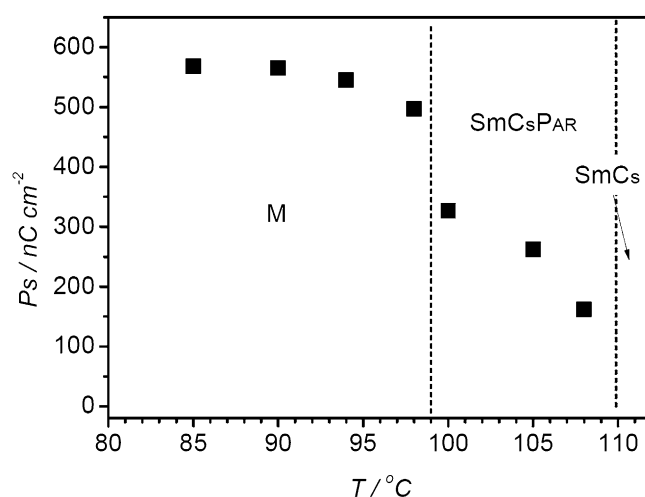


**Figure 8.** a) Polarization as function of temperature as measured for compound **F20** in a  $6\ \mu\text{m}$  ITO cells on applying a triangular wave field ( $10\ \text{Hz}$ ) of  $26.7\ \text{V}_{\text{pp}}\ \mu\text{m}^{-1}$ .

cy of  $10\ \text{Hz}$ . Figure 7 collates the current response curves at different temperatures and Figure 8 shows the dependence of the calculated polarization values on temperature. Even under a relatively high triangular wave field of  $27.6\ \text{V}_{\text{pp}}\ \mu\text{m}^{-1}$  no current peak was observed in the SmA and SmC<sub>5</sub> phase ranges, confirming the non-polar (paraelectric) nature of these phases. At  $T=110\ ^\circ\text{C}$  two broad peaks appear (Figure 7a); with further decreasing temperature the peaks grow ( $P_s \sim 300\ \text{nCcm}^{-2}$ ), become sharper and move closer to each other (Figure 7b,c) and at the next phase transition to the phase M at  $T=98\ ^\circ\text{C}$  the two peaks merge to a single peak, centred at  $0\ \text{V}$  crossing<sup>[34]</sup> with polarization values reaching  $P_s \sim 500\text{--}580\ \text{nCcm}^{-2}$  (Figures 7d, 8). This would mean that the SmC<sub>5</sub>P<sub>s</sub> domains grow under the applied field and below the paraelectric SmC<sub>5</sub> range these domains are switched above a certain threshold voltage between two polar states with relaxation at  $0\ \text{V}$ . At  $0\ \text{V}$  the correlation between the domains becomes predominately antipolar; therefore, this range of the SmC<sub>5</sub> phase is designated as SmC<sub>5</sub>P<sub>AR</sub>. Further reducing the temperature leads to a further growth of the polar domains, giving rise to an almost macroscopic field-induced polar order in the M-phase region. This field-induced SmC<sub>5</sub>P<sub>s</sub> state relaxes into smaller polar SmC<sub>5</sub>P<sub>s</sub> domains with antipolar correlation between them after reducing the field. Though the field dependence of the SHG activity is typical for SmCP<sub>A</sub> phases, there is only a single peak positioned at zero-voltage crossing (Figure 7d), which could be considered as an indication of “superparaelectric” switching.<sup>[36]</sup> However, in the case of the M-phase considered here the merging of the two polarization peaks of an antiferroelectric switching to only one might also be supported by a slow relaxation, caused by the relatively high viscosity of this phase.

In optical investigations, no change in the position of the extinction crosses could be observed in the SmC<sub>5</sub> and SmC<sub>5</sub>P<sub>AR</sub> phases (see Figure S4), only the birefringence is slightly reduced at  $0\ \text{V}$ , thus indicating that in these SmC<sub>5</sub> phases the switching takes place by rotation around the long axis. In the M phase the optical response is more complicated and the ob-



served switching mechanism depends on the frequency and rotation on a cone contributes to the switching process.

## 2.4. Investigation of Freely Suspended Films

The unusual structural features of the mesophases are particularly well seen in freely suspended (FS) films. In FS films, the smectic layers are perfectly aligned by the LC/air interface and the tilt director is not affected by the interface as in case of the glass substrate. We used 3  $\mu\text{m}$  thick films which are comparable in thickness with the glass samples. The SmA phase is completely dark, confirming a uniaxial phase. Schlieren texture appears below the SmA phase, marking the transition into the SmC<sub>s</sub> phase (Figure 9a). The director weakly responds to an

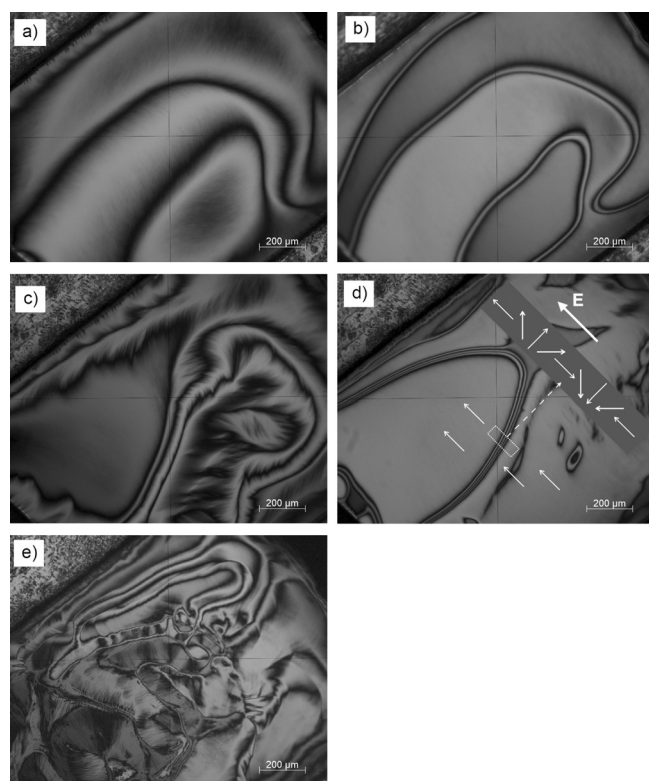


**Figure 9.** Textures in freely-suspended films a) schlieren texture in the SmC<sub>s</sub> phase in the field-free state  $T = 114\text{ }^\circ\text{C}$ , b) inversion  $\pi$  walls occur under the action of an AC in-plane electric field with  $f = 300\text{ Hz}$  and  $E_{pp} = 45\text{ V mm}^{-1}$ ; c) fine structure of the schlieren texture in the SmC<sub>s</sub>P<sub>AR</sub> phase at  $T = 108\text{ }^\circ\text{C}$ ; d)  $2\pi$  inversion walls occurring under an action of the in-plane DC field  $E_{pp} = 3\text{ V mm}^{-1}$  ( $T = 108\text{ }^\circ\text{C}$ ) and e) broken schlieren texture of the M phase ( $T = 98\text{ }^\circ\text{C}$ ). The images were made under illumination with a 575 nm narrow-band filter.

applied electric field forming  $\pi$  inversion (Figure 9b). This indicates purely dielectric behaviour (due to an induced polarisation). There is a textural change at  $T = 112\text{ }^\circ\text{C}$  (approximately corresponding to the SmC<sub>s</sub>–SmC<sub>s</sub>P<sub>AR</sub> transition, see Figure 9c); the smooth schlieren texture becomes disturbed by a pattern of fine stripes and the texture shows polar response to electric fields. This is recognized by occurrence of  $2\pi$  inversion walls under DC fields (Figure 9d). Splitting of the  $2\pi$  walls and

merging of  $\pi$  walls under polarity inversion suggests the presence of a residual polarisation in this SmC-type phase.<sup>[20]</sup> However, the polar response depends on the film thickness similar to the odd–even effect in antiferroelectrics. In this material, however, the response alternation occurs at much larger thicknesses than a single layer. A rough estimation of the thickness difference in two polar domains yield about  $(100 \pm 20)\text{ nm}$ , which corresponds to  $\sim 18$  smectic layers. Large chunks of polar layer stacks can be observed around  $100\text{ }^\circ\text{C}$ , decreasing in size with rising temperature and persisting until the transition to SmA.

The last transition occurs at about  $98\text{ }^\circ\text{C}$ . The schlieren texture becomes broken in pattern of rectangles (Figure 9e). The films become very viscous and no response to an electric field could be found. The character of this phase cannot be determined from these observations. Therefore, this low temperature phase is designated as M, though by electro-optical investigations it is confirmed to be a polar antiferroelectric switching SmC phase (SmCP<sub>AR</sub>, see Section 3.3). It appears that this is an additional intermediate phase with still unknown superstructure associated with the transition from short-range to long-range polar order in tilted smectic phases.

## 3. Conclusions and Summary

Compound F20 forms distinct smectic phases involving a tilted organization of the molecules in domains. Tilt is randomized between the domains in the uniaxial SmA phase, which thus can be considered as a cluster-type de Vries-like smectic phase. Tilt becomes uniformly synclinic in the SmC<sub>s</sub> phase region. With further decreasing temperature, a denser core packing is achieved and this leads to restriction of the rotation around the long axis, giving rise to an increasing coherence length of polar order with decreasing temperature. As the polar domains combine synclinic tilt and polar order the local structure is SmC<sub>s</sub>P<sub>S</sub>. Polar order is short-range in the paraelectric range between  $141$  and  $110\text{ }^\circ\text{C}$  (SmC<sub>s</sub>). In the temperature range between  $\sim 110$  and  $98\text{ }^\circ\text{C}$  (SmC<sub>s</sub>P<sub>AR</sub>) the polar coherence length significantly grows, so that the applied field increases the size of the polar domains to such an extent that relatively broad polarization current peaks can be observed, as typical for locally polar smectic phases with randomized polar order.<sup>[12,13]</sup> Without applied field there is a preferred antipolar packing of the SmC<sub>s</sub>P<sub>S</sub> domains, as indicated by the two polarization peaks observed during one period of a triangular wave voltage. The observation of large chunks of polar layer stacks in the FS films corroborates the proposed SmC<sub>s</sub>P<sub>S</sub> domain structure in the SmC<sub>s</sub> and SmC<sub>s</sub>P<sub>AR</sub> ranges. In addition, the critical behavior of the dielectric relaxation mode below  $110\text{ }^\circ\text{C}$  with a steeper increase of its amplitude is consistent with the picture of a continuous growth of polar local order, showing similar behavior to that reported for the SmA–SmAP<sub>R</sub>–SmAP<sub>A</sub> transition.<sup>[33,35]</sup> Therefore, the temperature range between  $110$  and  $98\text{ }^\circ\text{C}$ , designated as SmC<sub>s</sub>P<sub>AR</sub>, is considered as the tilted analogue of the SmAP<sub>AR</sub> phase.<sup>[32]</sup> The transition between paraelectric SmC<sub>s</sub> and SmC<sub>s</sub>P<sub>AR</sub> at  $\sim 110\text{ }^\circ\text{C}$  is continuous, only indicated by the significant rise of polarization and field-induced

SHG activity. Only at the transition to the low-temperature phase M, the polar  $\text{SmC}_5\text{P}_5$  domains become nearly long-range, but this is associated with additional changes in the phase structure, leading to increased viscosity and mosaic-like textures of the FS films. The M phase could have an increased packing density of the molecules, similar to B5-like phases.<sup>[6,35]</sup> Another possibility could be the formation of an additional superlattice due to an emerging antipolar organization to escape from the developing macroscopic polar order. Unfortunately, due to crystallization during the exposure time there is no XRD pattern available for the M phase. Nevertheless, based on textural features and the observed electro-optical properties, the M phase can be considered as based on a  $\text{SmCP}_A$ -like structure derived from a smectic phase with increased packing density and enhanced coherence length of polar order in the layers. There are indications from dielectric investigations that some polydomain characteristics of the preceding LC phases are retained even in this phase.

Like other 4-cyanoresorcinol-derived BCLCs, **F20** belongs to the weakly bent molecules, being characterized by phase sequences involving a continuous increase in the polar domain size with decreasing temperature. As typical for such compounds, the switching takes place by rotation around the long axis. The easy rotation around the long axis decreases the coherence length of polar order, which also reduces the coupling between the layers, leading to cluster-type de Vries-like  $\text{SmA}$  phases at high temperature and synclinal  $\text{SmC}_5$  phases with  $\text{SmC}_5\text{P}_5$  domain structure below them (Figure 10). Due to the domain structure there are strong effects of the conditions and surface interactions on the actually observed behaviour.

The recently reported compounds **Hn**, related to **F20**, but without the fluoro substituents and chain lengths between  $n = 12$ –18 (see Scheme 1)<sup>[24,25]</sup> behave very similarly. In both cases

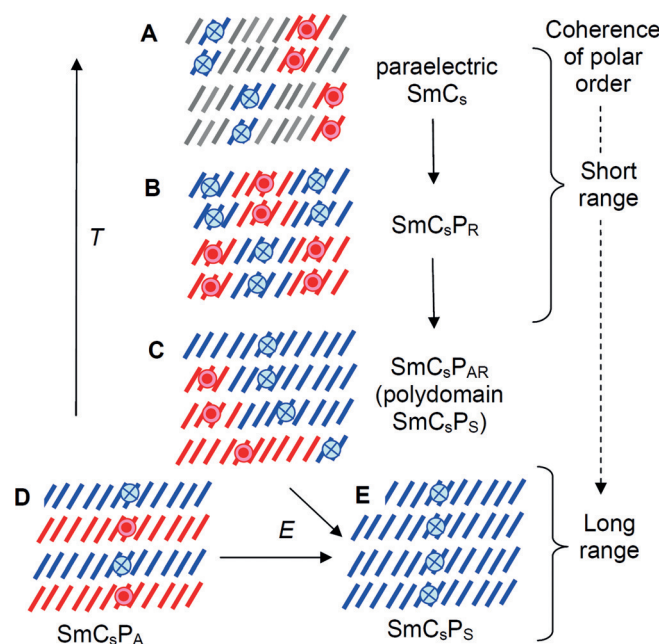


**Figure 10.** Schematic presentation of the proposed development of polar order in the  $\text{SmC}_5$  phases of weakly bent molecules.

$\text{SmC}_5$  phases with increasing polar domain size dominate the phase sequences. One difference is that for the fluorinated compound **F20** an additional  $\text{SmA}$  phase is observed as high-temperature phase above the  $\text{SmC}_5$  phase.<sup>[25]</sup> In both series paraelectric  $\text{SmC}_5$  phases (Figure 10A), capable of formation of chiral conglomerates, were observed, and on further cooling randomized polar phases develop continuously. Also the M phase occurring below the  $\text{SmC}_5\text{P}_{AR}$  phase has essentially the same features as those observed for compounds **Hn** (designated there as M1 phase).<sup>[25]</sup> Only the  $\text{SmC}_5\text{P}_A$  phase with long-range antipolar order (Figure 10D), and occurring below the M phase, is not observed for **F20**, most probably due to a higher crystallization tendency which does not allow sufficient supercooling to reach this phase.

For compound **F20** the observation of a  $\text{SmC}_5\text{P}_5$  domain structure in freely suspended films and two polarization peaks in electro-optical studies is explained by a  $\text{SmC}_5\text{P}_{AR}$  phase structure composed of  $\text{SmC}_5\text{P}_5$  domains with appreciable size and preferred antipolar correlation. This kind of polydomain  $\text{SmC}_5\text{P}_5$  phases (Figure 10C) has previously been designated as  $\text{SmC}_5\text{P}_F$  for the series of compounds **Hn**. The reason is that for **H18** the  $\text{SmC}_5\text{P}_5$  domains are obviously larger than in the case of **F20**, so that in this case uniform polar order without visible domain structure was observed in the FS films.<sup>[25]</sup> These polydomain  $\text{SmC}_5\text{P}_5$  phases appear to be associated with a varying  $\text{SmC}_5\text{P}_5$  domain size intermediate between the randomized  $\text{SmCP}_R$  phases (Figure 10B) and the  $\text{SmCP}_S$  and  $\text{SmCP}_A$  phases with long-range polar order in the individual layers (Figure 10D,E). In the case of **H18** the paraelectric  $\text{SmC}_5$  phase and the  $\text{SmC}_5\text{P}_{AR}$  phase (previously assigned as  $\text{SmC}_5\text{P}_F$ ) are separated by an additional short  $\text{SmC}_5\text{P}_R$  phase region<sup>[25]</sup> which is absent or very small for the fluorinated compound **F20**. Hence, the phase region previously designated as  $\text{SmC}_5\text{P}_F$  can actually be considered as  $\text{SmC}_5\text{P}_{AR}$ , too. Thus, as shown in Figure 10, the common sequence for growing domain size in the  $\text{SmC}_5$  range is paraelectric  $\text{SmC}_5$ – $\text{SmC}_5\text{P}_R$  (randomized  $\text{SmC}_5\text{P}_5$ )– $\text{SmC}_5\text{P}_{AR}$  (polydomain  $\text{SmC}_5\text{P}_5$ ).

Mirror symmetry breaking is observed in the paraelectric  $\text{SmC}_5$  phases of both compounds **F20** and **Hn** by chiral conglomerate formation (Figure 3), indicating that this must be a general phenomenon, typically found for locally polar  $\text{SmC}_5$  phases of weakly bent molecules.<sup>[24,25,36,37]</sup> It is thought to result from a synchronization of chiral conformers<sup>[7,9,38,39]</sup> in the densely packed polar  $\text{SmC}_5\text{P}_5$  domains, stabilized by the diastereomeric relation with the superstructural chirality of the  $\text{SmC}_5\text{P}_5$  structure and the preorganization by surface pinning of tilt and polar director.<sup>[5]</sup> The domain structure is clearly observed in the paraelectric  $\text{SmC}_5$  phase range and persists in the  $\text{SmC}_5\text{P}_R$  range (**Hn**), but fades in the  $\text{SmC}_5\text{P}_{AR}$  range (Figure S3). It appears that with growing coherence length of polar order the antipolar coupling of the  $\text{SmC}_5\text{P}_5$  domains leads to a macroscopic racemic structure that is optically inactive. It could also be possible that with growing size of the  $\text{SmC}_5\text{P}_5$  domains the helical twist, arising due to the homochiral synchronization of the molecules, is suppressed by the layer structure. This local helical distortion could also play a role in the formation of the M phase structure, allowing a compensation of the developing

macroscopic polar order and simultaneously retaining some local twist deformation of the layers. The absence of indications of optical activity in FS films of the  $\text{SmC}_s$ ,  $\text{SmC}_s\text{P}_R$  and  $\text{SmC}_s\text{P}_{AR}$  phases could be due to the absence of polar surface stabilization and straitening and sharpening of the layers in these films, thus suppressing the chirality synchronization.

In summary, formation of polarization randomized smectic phases is not limited to  $\text{SmA}$  phases. Such structures are also involved in the continuous development of polar order in tilted smectic phases, leading to the sequence paraelectric  $\text{SmC}_s$ – $\text{SmC}_s\text{P}_R$ – $\text{SmC}_s\text{P}_{AR}$  with growing coherence length of polar order (Figure 10). In these tilted smectic phases the emerging polar order is associated with the development of superstructural chirality, which can couple with the conformational chirality, leading to a chirality synchronization of the involved molecules,<sup>[39]</sup> and thus has an additional modifying effect on the phase structures. The competition between emerging helical twist and organization in layers, together with electrostatic interactions due to the emerging polar order might be responsible for the limited coherence length of polar order over broad temperature ranges and for the formation of additional intermediate phases (e.g. M) at the phase transition from short and medium range to truly long range polar order, being the only transition in the  $\text{SmC}_s$  range associated with a measurable transition enthalpy.

## Acknowledgements

This work was supported by the DFG (Grant Ts 39/24-1, ER 467/8-1). N.S. thanks the Alexander von Humboldt Foundation for a Postdoctoral Research Fellowship; we thank H. Takezoe (Emeritus Prof. at TIT Tokyo, Japan) and R. Stannarius (Univ. Magdeburg, Germany) for discussions.

**Keywords:** azobenzene · bent-core liquid crystals · de Vries phase · ferroelectricity · mirror symmetry breaking

- J. W. Goodby, P. J. Collings, T. Kato, C. Tschierske, H. F. Gleeson, P. Raynes, *Handbook of Liquid Crystals*, 2nd ed., Wiley-VCH, Weinheim, 2014.
- a) J. P. F. Lagerwall, G. Scalia, *Curr. Appl. Phys.* **2012**, *12*, 1387–1412; b) E.-K. Fleischmann, R. Zentel, *Angew. Chem. Int. Ed.* **2013**, *52*, 8810–8827; *Angew. Chem.* **2013**, *125*, 8972–8991; c) M. Bremer, P. Kirsch, M. Klasen-Memmer, K. Tarumi, *Angew. Chem. Int. Ed.* **2013**, *52*, 8880–8896; *Angew. Chem.* **2013**, *125*, 9048–9065.
- C. Tschierske, *Angew. Chem. Int. Ed.* **2013**, *52*, 8828–8878; *Angew. Chem.* **2013**, *125*, 8992–9047.
- T. Niori, J. Sekine, J. Watanabe, T. Furukava, H. Takezoe, *J. Mater. Chem.* **1996**, *6*, 1231–1233.
- D. R. Link, G. Natale, R. Shao, J. E. Maclennan, N. A. Clark, E. Korblova, D. M. Walba, *Science* **1997**, *278*, 1924–1927; D. M. Walba in *Materials-Chirality: Topics in Stereochemistry*, Vol. 24 (Eds.: M. M. Green, R. J. M. Nolte, E. W. Meijer), Wiley, New York, **2003**, pp. 457–518.
- G. Pelzl, S. Diele, W. Weissflog, *Adv. Mater.* **1999**, *11*, 707–724.
- R. A. Reddy, C. Tschierske, *J. Mater. Chem.* **2006**, *16*, 907–961.
- H. Takezoe, Y. Takahashi, *Jpn. J. Appl. Phys.* **2006**, *45*, 597–624.
- C. Tschierske, G. Dantlgraber, *Pramana* **2003**, *61*, 455–481.
- M. B. Ros, J. L. Serrano, M. R. de La Fuente, C. L. Folcia, *J. Mater. Chem.* **2005**, *15*, 5093–5098.
- a) A. Jakli, C. Bailey, J. Harden in *Thermotropic Liquid Crystals* (Ed.: A. Ramamoorthy), Springer, Dordrecht, **2007**, pp. 59–83; b) A. Eremin, A. Jakli, *Soft Matter* **2013**, *9*, 615–637.
- a) D. Pocięcha, M. Copic, E. Gorecka, J. Mieczkowski, *Phys. Rev. Lett.* **2003**, *91*, 185501; b) Y. Shimbo, E. Gorecka, D. Pocięcha, F. Araoka, M. Goto, Y. Takahashi, K. Ishikawa, J. Mieczkowski, K. Gomola, H. Takezoe, *Phys. Rev. Lett.* **2006**, *97*, 113901; c) K. Gomola, L. Guo, E. Gorecka, D. Pocięcha, J. Mieczkowski, K. Ishikawa, H. Takezoe, *Chem. Commun.* **2009**, 6592–6594; d) K. Gomola, L. Guo, S. Dhara, Y. Shimbo, E. Gorecka, D. Pocięcha, J. Mieczkowski, H. Takezoe, *J. Mater. Chem.* **2009**, *19*, 4240–4247; e) S. Radhika, B. K. Sadashiva, R. Pratibha, *Liq. Cryst.* **2010**, *37*, 417–425; f) M. Gupta, S. Datta, S. Radhika, B. K. Sadashiva, A. Roy, *Soft Matter* **2011**, *7*, 4735–4741.
- a) C. Keith, M. Prehm, Y. P. Panarin, J. K. Vij, C. Tschierske, *Chem. Commun.* **2010**, *46*, 3702–3704; b) G. Shanker, M. Prehm, N. Nagaraj, J. K. Vij, C. Tschierske, *J. Mater. Chem.* **2011**, *21*, 18711–18714; c) M. Nagaraj, Y. P. Panarin, J. K. Vij, C. Keith, C. Tschierske, *Appl. Phys. Lett.* **2010**, *97*, 213505; d) Y. P. Panarin, M. Nagaraj, J. K. Vij, C. Keith, C. Tschierske, *EPL* **2010**, *92*, 26002.
- A. Eremin, S. Diele, G. Pelzl, H. Nadasi, W. Weissflog, J. Salfetnikova, H. Kresse, *Phys. Rev. E* **2001**, *64*, 51707.
- R. A. Reddy, C. Zhu, R. Shao, E. Korblova, T. Gong, Y. Shen, E. Garcia, M. A. Glaser, J. E. Maclennan, D. M. Walba, N. A. Clark, *Science* **2011**, *332*, 72–77.
- E. Gorecka, N. Vaupotic, D. Pocięcha in *Handbook of Liquid Crystals*, Vol. 4, 2nd ed. (Eds.: J. W. Goodby, P. J. Collings, T. Kato, C. Tschierske, H. F. Gleeson, P. Raynes), Wiley-VCH, Weinheim, **2014**, pp. 681–710.
- I. Wirth, S. Diele, A. Eremin, G. Pelzl, S. Grande, L. Kovalenko, N. Pancenko, W. Weissflog, *J. Mater. Chem.* **2001**, *11*, 1642–1650.
- L. Kovalenko, M. W. Schröder, R. A. Reddy, S. Diele, G. Pelzl, W. Weissflog, *Liq. Cryst.* **2005**, *32*, 857–865.
- C. Keith, A. Lehmann, U. Baumeister, M. Prehm, C. Tschierske, *Soft Matter* **2010**, *6*, 1704–1721.
- A. Eremin, M. Floegel, U. Kornek, S. Stern, R. Stanarius, H. Nadasi, W. Weissflog, C. Zhu, Y. Shen, C. S. Park, J. Maclennan, N. Clark, *Phys. Rev. E* **2012**, *86*, 051701.
- W. Weissflog, H. N. S. Murthy, S. Diele, G. Pelzl, *Philos. Trans. R. Soc. London Ser. A* **2006**, *364*, 2657–2679; G. Pelzl, W. Weissflog in *Thermotropic Liquid Crystals. Recent Advances* (Ed.: A. Ramamoorthy), Springer, Dordrecht, **2007**, pp. 1–58.
- Y. P. Panarin, M. Nagaraj, S. Sreenilayam, J. K. Vij, A. Lehmann, C. Tschierske, *Phys. Rev. Lett.* **2011**, *107*, 247801.
- M. Alaasar, M. Prehm, M. Poppe, M. Nagaraj, J. K. Vij, C. Tschierske, *Soft Matter* **2014**, *10*, 5003–5016.
- M. Alaasar, M. Prehm, M. Nagaraj, J. K. Vij, C. Tschierske, *Adv. Mater.* **2013**, *25*, 2186–2191.
- M. Alaasar, M. Prehm, K. May, A. Eremin, C. Tschierske, *Adv. Funct. Mater.* **2014**, *24*, 1703–1717.
- M. Alaasar, M. Prehm, M. Brautzsch, C. Tschierske, *J. Mater. Chem. C* **2014**, *2*, 5487–5501.
- D. Nonnenmacher, S. Jagiella, Q. Song, R. P. Lemieux, F. Giesselmann, *ChemPhysChem* **2013**, *14*, 2990–2995.
- a) A. De Vries, *J. Chem. Phys.* **1979**, *71*, 25–31; b) S. T. Lagerwall, P. Rudquist, F. Giesselmann, *Mol. Cryst. Liq. Cryst.* **2009**, *510*, 148–157; c) J. P. F. Lagerwall, F. Giesselmann, *ChemPhysChem* **2006**, *7*, 20–45.
- a) S.-W. Choi, Y. Kinoshita, B. Park, H. Takezoe, T. Niori, J. Watanabe, *Jpn. J. Appl. Phys.* **1998**, *37*, 3408–3411; b) R. Macdonald, F. Kentischer, P. Warnick, G. Heppke, *Phys. Rev. Lett.* **1998**, *81*, 4408–4411.
- K. Gomola, L. Guo, D. Pocięcha, F. Araoka, K. Ishikawa, H. Takezoe, *J. Mater. Chem.* **2010**, *20*, 7944–7952.
- L. Guo, K. Gomola, E. Gorecka, D. Pocięcha, S. Dhara, F. Araoka, K. Ishikawa, H. Takezoe, *Soft Matter* **2011**, *7*, 2895–2899.
- S. Havriliak, S. Negami, *J. Polym. Sci. Part C* **1966**, *14*, 99–117.
- a) A. Eremin, H. Nadasi, G. Pelzl, S. Diele, H. Kresse, W. Weissflog, S. Grande, *Phys. Chem. Chem. Phys.* **2004**, *6*, 1290–1298; b) D. Pocięcha, E. Gorecka, M. Cepic, N. Vaupotic, K. Gomola, J. Mieczkowski, *Phys. Rev. E* **2005**, *72*, 060701; c) D. Pocięcha, E. Gorecka, M. Cepic, N. Vaupotic, W. Weissflog, *Phys. Rev. E* **2006**, *74*, 021702.
- M. F. Achard, J. P. Bedel, J. P. Marcerou, H. T. Nguyen, J. C. Rouillon, *Eur. Phys. J. E* **2003**, *10*, 129–134.

- [35] H. Nádasi, W. Weissflog, A. Eremin, G. Pelzl, S. Diele, B. Das, S. Grande, *J. Mater. Chem.* **2002**, *12*, 1316–1324.
- [36] E. Westphal, H. Gallardo, G. F. Caramori, N. Sebastián, M.-G. Tamba, A. Eremin, S. Kawauchi, M. Prehm, C. Tschierske, *Chem. Eur. J.* submitted.
- [37] H. Ocak, B. Bilgin-Eran, D. Güzeller, M. Prehm, C. Tschierske, *Chem. Commun.* **2015**, *51*, 7512–7515.
- [38] a) H. Takezoe, *Top. Curr. Chem.* **2011**, *318*, 303–330; b) D. J. Earl, M. A. Osipov, H. Takezoe, Y. Takanishi, M. R. Wilson, *Phys. Rev. E* **2005**, *71*, 021706; c) S.-W. Choi, S. Kang, Y. Takanishi, K. Ishikawa, J. Watanabe, H. Takezoe, *Chirality* **2007**, *19*, 250–254; d) F. Yan, C. A. Hixson, D. J. Earl, *Soft Matter* **2009**, *5*, 4477–4483.
- [39] a) C. Dressel, T. Reppe, M. Prehm, M. Brautzsch, C. Tschierske, *Nat. Chem.* **2014**, *6*, 971–977; b) C. Dressel, F. Liu, M. Prehm, X. Zeng, G. Ungar, C. Tschierske, *Angew. Chem. Int. Ed.* **2014**, *53*, 13115–13120; *Angew. Chem.* **2014**, *126*, 13331–13336; c) C. Tschierske, G. Ungar, *ChemPhysChem.* **2015**, DOI: 10.1002/cphc.201500601.

---

Manuscript received: October 7, 2015

Accepted Article published: November 19, 2015

Final Article published: December 4, 2015

---

## Liquid Crystals | Hot Paper |

## Development of Polar Order by Liquid-Crystal Self-Assembly of Weakly Bent Molecules

Mohamed Alaasar,<sup>\*[a, b]</sup> Marko Prehm,<sup>[a]</sup> Silvio Poppe,<sup>[a]</sup> and Carsten Tschierske<sup>\*[a]</sup>

**Abstract:** Organic ferroelectrics are of growing importance for multifunctional materials. Here we provide an understanding of the distinct stages of the development of sterically induced polar order in liquid-crystalline (LC) soft matter. Three series of weakly bent molecules derived from 4-cyanoresorcinol as the bent core unit with laterally fluorinated azobenzene wings have been synthesized, and the effects of the position of fluorine substitution, alkyl-chain length, and temperature on the LC self-assembly and polar order were studied. In the LC phases a paraelectric–ferroelectric transition took place as the size of the polar domains gradually increased, thereby crossing a permittivity maximum, similar to inorganic solid-state ferroelectrics. An increase in polar co-

herence length simultaneously led to a transition from synpolar to antipolar domain correlation in the high-permittivity paraelectric range. Associated with the emergence of polar order was the development of a tilted organization of the molecules and a growing coherence of tilt. This led to a transition from non-tilted via tilt-randomized uniaxial to long-range-tilted biaxial smectic phases, and to surface-stabilized symmetry breaking with the formation of chiral conglomerates and field-induced tilt. Moreover, there is a remarkably strong effect of the position of fluorination; polar order is favored by peripheral core substitution and is suppressed by inside-directed fluorination.

## Introduction

Organic compounds with extended aromatic building blocks have attracted growing importance as charge carrier and optical materials. The majority of these materials are composed of a functional  $\pi$ -conjugated core unit and flexible chains that provide processibility due to reduced melting points and increased solubility, yet retain the organization of the functional units.<sup>[1]</sup> However, the alkyl chains also have an active function because they can modify the self-assembly and thus can lead to the emergence of new properties and functionalities. In the ideal case, this gives rise to the liquid-crystalline (LC) state, which intrinsically combines long-range order with mobility. In these LC phases the organization of the aromatic cores can be addressed by different types of external stimuli.<sup>[2]</sup> Liquid crystals are now considered as a fourth state of matter that provides a wide range of soft functional materials<sup>[3]</sup> for numerous application in daily life, such as liquid-crystal displays (LCDs),

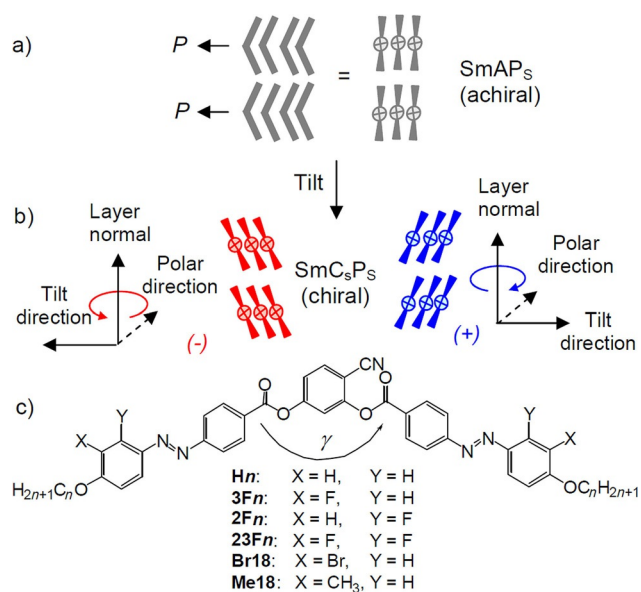
adjustable optical elements, tunable lasers, semiconducting layers in organic field effect transistors,<sup>[4]</sup> light-emitting diodes, photovoltaic cells, and photo-recording devices,<sup>[5,6]</sup> which thus makes them the supramolecular systems with the largest impact on the global economy.<sup>[7]</sup> In the wider field of materials, organic ferroelectrics,<sup>[8]</sup> in particular those with LC properties,<sup>[9,10]</sup> have attracted significant interest and the discovery of ferroelectricity, antiferroelectricity, and spontaneous mirror-symmetry breaking in bent-core liquid crystals (BCLCs) have breathed a new area in the field of liquid crystals.<sup>[11–13]</sup> In these ferroelectric and antiferroelectric materials, polar order is due to the restricted rotation of BCLCs around their long axis (Scheme 1a). Because in these materials the polar order is often combined with a tilt of the molecules with respect to the layer normal, the symmetry is reduced to  $C_2$ , which leads to superstructural layer chirality (Scheme 1b).<sup>[13,14]</sup> Previous research in this field has predominantly focused on high-polarization ferroelectric and antiferroelectric bent-core molecules with a bending angle of  $\gamma \approx 120^\circ$  (Scheme 1c).<sup>[12,13]</sup> However, high-permittivity paraelectrics and related materials with medium-range polar order are also of significant interest for super-capacitors and other applications.<sup>[15]</sup> Therefore, molecules at the cross-over between rodlike ( $\gamma \approx 180^\circ$ ) and bent shapes ( $\gamma \approx 120^\circ$ ),<sup>[16–20]</sup> hockey-stick molecules with the bend shifted to one end,<sup>[21–4]</sup> and molecules with comparatively short bent-core units<sup>[25,26]</sup> are receiving growing interest.

The aim of this article is to provide an understanding of the development of polar order in lamellar LC phases at the cross-over from rodlike to bent molecular shapes, which depends on alkyl-chain length, temperature, and the position of core

[a] Dr. M. Alaasar, Dr. M. Prehm, S. Poppe, Prof. Dr. C. Tschierske  
Institute of Chemistry, Martin Luther University Halle-Wittenberg  
Kurt Mothes Str. 2, 06120 Halle (Saale) (Germany)  
E-mail: carsten.tschierske@chemie.uni-halle.de

[b] Dr. M. Alaasar  
Department of Chemistry, Faculty of Science, Cairo University, Giza (Egypt)  
E-mail: malaasar@sci.cu.edu.eg

Supporting information and the ORCID identification number for the author of this article can be found under <http://dx.doi.org/10.1002/chem.201606035> and contains synthesis and analytical data for the compounds, additional experimental data (DSC traces, textures, XRD data, polarization current curves and electro-optical studies), and a supporting discussion (effects of core structure and photoisomerization in solution).



**Scheme 1.** Development of: a) polar order ( $P_S$  = synpolar,  $P_A$  = antipolar), and b) tilt ( $C_S$  = synclinal,  $C_A$  = anticlinal) and chirality (red/blue color) in the lamellar phases of bent-core LCs. c) Chemical structures of the considered 4-cyanoresorcinol based BCLCs.

fluorination. To this end, we have synthesized and investigated a series of new bent-core molecules based on a central 4-cyanoresorcinol core with fluorinated rodlike azobenzene side groups (Scheme 1c).

The 4-cyanoresorcinol bisbenzoate core unit<sup>[27,28]</sup> was chosen because of its comparatively weak and temperature-dependent molecular bend ( $\gamma \approx 130$ – $145^\circ$ ) that arises from the effects of the CN group on the conformation of the adjacent ester group.<sup>[16,27a,29,32a,b]</sup> Azobenzenes were used as peripheral units because of their light-induced *trans*–*cis* isomerization ability, which is of interest for potential applications of the compounds as multifunctional photochromic and photoisomerizable materials.<sup>[30–32]</sup> Due to the unique combination of high polarity and low polarizability, and also steric and conformational effects,<sup>[33]</sup> fluorination of the aromatic core is a powerful tool for tailoring rodlike LC materials for modern liquid-crystal technologies<sup>[34–35]</sup> and bent-core mesogens for new applications.<sup>[13,16,36,37]</sup> Fluorine substitution of the weakly bent mesogens **Hn**<sup>[32]</sup> in the peripheral 3-positions, adjacent to the terminal alkoxy chains, led to the new series of compounds **3Fn** ( $n=4$ – $20$  with even-numbered chains) reported herein (Scheme 1c). Only compound **3F20**, with the longest chains, has been described previously.<sup>[37]</sup> An investigation of the chain length and temperature-dependent development of distinct LC-phase structures and polar order in the complete **3Fn** series is reported herein. New phases and phase sequences are provided and lead to the universal phase diagram shown in Figure 1a, which reveals a gradual development of polar order through low- and high-permittivity paraelectric phases as the size of the ferroelectric domains increased (Figure 1b). Polar order is removed by shifting the position of fluorine from the peripheral 3-positions to the inner 2-positions (compounds **2Fn** with  $n=8$ – $16$ ) or adding F-substituents to the 2-positions

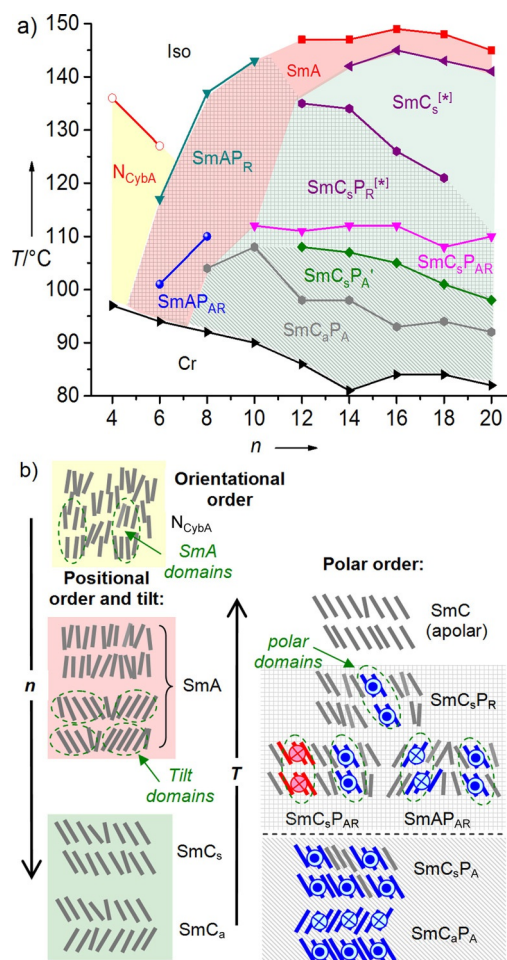


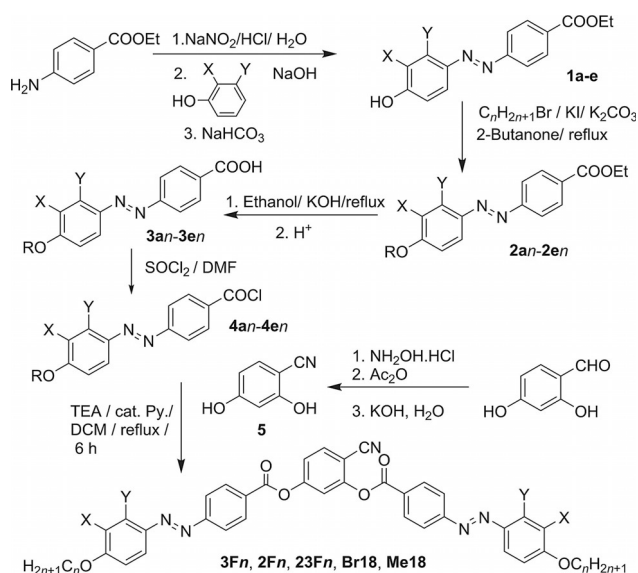
**Figure 1.** a) Plot of the transition temperatures of compounds **3Fn** as a function of the alkyl chain length ( $n$ ). The solid black line indicates the crystallization temperature on cooling; the colored lines indicate the upper temperature limits for the corresponding mesophases; colored areas depict the molecular organization (yellow = nematic, red = SmA, and green = SmC ranges); the square-grid pattern indicates LC phases composed of ferroelectric domains and the parallel-line pattern (bottom) indicates LC phases composed of polar layers. b) Simplified models of the fundamental phase structures under discussion and their development depending on temperature and alkyl-chain length; dots and crosses indicate opposite polar directions, red/blue colors indicate opposite chirality; the abbreviations are explained in Table 1; only one chirality is shown for the tilt-randomized  $SmAP_{AR}$  structure, although on a larger scale the structure is racemic (see also Figure 6b).

(compounds **23Fn** with  $n=8$ – $16$ ). Replacement of the fluorine in **3F18** by the larger bromine (compound **Br18**) reduces polar order, which is completely removed if it is replaced by the nonpolar methyl group (compound **Me18**). These investigations allow a general understanding of the development of polar order in soft matter and the unusual phenomena associated with the formation and growth of polar domains, such as spontaneous mirror-symmetry breaking and electric-field-induced tilt by a non-classical electroclinic effect, and the relationship of these phenomena to the molecular structure.

## Results and Discussion

### Synthesis

The synthesis of new fluorinated compounds **3Fn** ( $n=4-18$ ), **2Fn**, and **23Fn**, and the related brominated and methylated compounds **Br18** and **Me18**, was performed as shown in Scheme 2. The target materials were obtained by acylation of 4-cyanoresorcinol (**5**) with two equivalents of the appropriate



**Scheme 2.** Synthesis of the bent-core mesogens (a: X = F, Y = H; b: X = H, Y = F; c: X = Y = F; d: X = Br, Y = H, e: X = CH<sub>3</sub>, Y = H; Py = pyridine); see also Scheme 1c for the structures of the bent-core mesogens.

azobenzene-based benzoyl chloride (**4an-4en**).<sup>[38]</sup> All acylation reactions were carried out in the presence of triethylamine as the base and pyridine as the acylation catalyst.<sup>[37]</sup> Benzoic acids **3an-3en** were synthesized in a coupling reaction between substituted phenols and the diazonium salt of ethyl 4-aminobenzoate to give the azobenzenes (**1a-e**) in the first step. This was followed by etherification of **1a-e** with different 1-bromoalkanes to give ester compounds **2an-2en**, which were then hydrolyzed under basic conditions to give desired acids **3an-3en**.<sup>[38]</sup>

### Development of tilt and polar order in the LC phases of 3-fluorinated compounds (3Fn)

The phase sequences, transition temperatures, and associated transition enthalpies of the series of even-numbered homologues of compounds **3Fn** ( $n=4-20$ ) are collated in Table 1 and shown graphically in Figure 1a. The phase abbreviations are explained in Table 1 and Figure 1b and will be elaborated on in this section. In brief, SmA and SmC denote lamellar phases with non-tilted or tilted organization of the molecules in the layers, respectively, suffixes P<sub>R</sub> and P<sub>AR</sub> indicate high-permittivity paraelectric phases composed of ferroelectric domains, P<sub>A</sub> indicates antiferroelectric LC phases with macroscopic polar

order and [\*] indicates the formation of chiral conglomerates in the corresponding phases.

As shown schematically in Figure 1, all compounds **3Fn** with  $n=12-20$  exhibited a uniaxial SmA phase range at high temperature, which was followed on cooling by biaxial LC phases that represent tilted paraelectric (SmC<sub>s</sub><sup>[\*]</sup>, SmC<sub>s</sub>P<sub>R</sub><sup>[\*]</sup>, SmC<sub>s</sub>P<sub>AR</sub>) and polar (SmC<sub>s</sub>P<sub>A</sub>, SmC<sub>d</sub>P<sub>A</sub>) smectic phases (Table 1). In the LC temperature range, only the SmA–SmC and the paraelectric–antiferroelectric transitions were associated with enthalpy changes, whereas the other transitions were continuous. Other phase sequences were observed for the short-chain compounds ( $n=4-10$ ). For chain lengths of  $n=6-10$ , uniaxial high-permittivity paraelectric smectic phases (SmAP<sub>R</sub> and SmAP<sub>AR</sub>) developed, whereas compounds with  $n=4$  and 6 formed cybotactic nematic phases (N<sub>CyBA</sub>). In the following, the development of the distinct LC phases is discussed step by step, starting with the nematic phases. In later sections, the **3Fn** series will be compared with related compounds and the effects of changing the position of fluorination will be discussed.

### Compounds 3F4 and 3F6 and the non-skewed cybotactic nematic phases

The shortest homologue of the **3Fn** series, with  $n=4$ , formed a monotropic (metastable) nematic phase at  $T=136^\circ\text{C}$  that rapidly crystallized at  $T=97^\circ\text{C}$ , whereas the nematic phase of the next highest homologue, **3F6**, was enantiotropic. The XRD pattern of an oriented sample of the nematic phase of **3F6** in a magnetic field ( $B \approx 1\text{ T}$ , see Figure 2a, b) showed diffuse scattering with a maximum at  $d=0.45\text{ nm}$  located on the equator and diffuse scattering with a single maximum at  $d=3.88\text{ nm}$  on the meridian, which is slightly shorter than the molecular length  $L_{\text{mol}}=4.4\text{ nm}$  (determined for an assumed  $\Lambda$ -shaped

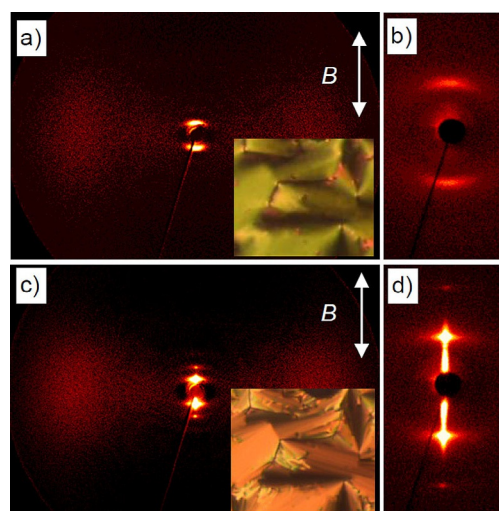


**Figure 2.** XRD patterns of a magnetically aligned sample of compound **3F6**. a, b) N<sub>CyBA</sub> phase at 122 °C, and c, d) SmA phase at 110 °C. a, c) The complete patterns after subtraction of scattering in the isotropic liquid state at 130 °C, and b, d) the small-angle patterns. Insets: the corresponding optical textures (between crossed polarizers, horizontal and vertical) in planar alignment (see also Figure S7).

Table 1. Phase transitions of compounds **3Fn**.<sup>[a]</sup>

<i>n</i>	<i>T</i> [°C] ( $\Delta H$ [kJ mol <sup>-1</sup> ])								
<b>3F4</b>	4	Cr 164 (108.2)						<i>N</i> <sub>cybA</sub> 136 (0.9)	Iso
<b>3F6</b>	6	Cr 112 (49.3)		<i>SmAP</i> <sub>AR</sub> 101 (-)		<i>SmAP</i> <sub>R</sub> 117 (0.2)		<i>N</i> <sub>cybA</sub> 128 (0.9)	Iso
<b>3F8</b>	8	Cr 112 (60.7)	<i>SmC</i> <sub>dP<sub>A</sub></sub> 104 (3.4)		<i>SmAP</i> <sub>AR</sub> 110 (-)	<i>SmAP</i> <sub>R</sub> 137 (3.2)			Iso
<b>3F10</b>	10	Cr 108 (30.2)	<i>SmC</i> <sub>dP<sub>A</sub></sub> 108 (2.4)		<i>SmC</i> <sub>sP<sub>AR</sub></sub> 112 (-)	<i>SmAP</i> <sub>R</sub> 143 (4.6)			Iso
<b>3F12</b>	12	Cr 104 (27.3)	<i>SmC</i> <sub>dP<sub>A</sub></sub> 98 (-)	<i>SmC</i> <sub>sP<sub>A</sub></sub> 108 (1.1)	<i>SmC</i> <sub>sP<sub>AR</sub></sub> ≈ 111 (-)	<i>SmC</i> <sub>sP<sub>R</sub></sub> <sup>[*]</sup> 135 (-)		<i>SmA</i> 147 (5.5)	Iso
<b>3F14</b>	14	Cr 101 (36.0)	<i>SmC</i> <sub>dP<sub>A</sub></sub> 98 (-)	<i>SmC</i> <sub>sP<sub>A</sub></sub> 107 (0.9)	<i>SmC</i> <sub>sP<sub>AR</sub></sub> ≈ 112 (-)	<i>SmC</i> <sub>sP<sub>R</sub></sub> <sup>[*]</sup> 134 (-)	<i>SmC</i> <sub>s</sub> <sup>[*]</sup> 142 (0.2)	<i>SmA</i> 147 (6.2)	Iso
<b>3F16</b>	16	Cr 101 (32.3)	<i>SmC</i> <sub>dP<sub>A</sub></sub> 93 (-)	<i>SmC</i> <sub>sP<sub>A</sub></sub> 105 (0.8)	<i>SmC</i> <sub>sP<sub>AR</sub></sub> ≈ 112 (-)	<i>SmC</i> <sub>sP<sub>R</sub></sub> <sup>[*]</sup> 126 (-)	<i>SmC</i> <sub>s</sub> <sup>[*]</sup> 145 (0.2)	<i>SmA</i> 149 (5.7)	Iso
<b>3F18</b>	18	Cr 102 (57.1)	<i>SmC</i> <sub>dP<sub>A</sub></sub> 94 (-)	<i>SmC</i> <sub>sP<sub>A</sub></sub> 101 (0.9)	<i>SmC</i> <sub>sP<sub>AR</sub></sub> ≈ 108 (-)	<i>SmC</i> <sub>sP<sub>R</sub></sub> <sup>[*]</sup> 121 (-)	<i>SmC</i> <sub>s</sub> <sup>[*]</sup> 143 (0.3)	<i>SmA</i> 148 (6.1)	Iso
<b>3F20</b>	20	Cr 104 (57.1)	<i>SmC</i> <sub>dP<sub>A</sub></sub> 92 (-)	<i>SmC</i> <sub>sP<sub>A</sub></sub> 98 (0.9)	<i>SmC</i> <sub>sP<sub>AR</sub></sub> ≈ 110 (-)		<i>SmC</i> <sub>s</sub> <sup>[*]</sup> 141 (0.3)	<i>SmA</i> 145 (5.6)	Iso

[a] Transition temperatures and enthalpy values (in square brackets) were taken from the second DSC heating scans (10 K min<sup>-1</sup>); transitions without detectable DSC peak were determined by using polarizing microscopy without an applied field, the *SmAP*<sub>R</sub>-*SmAP*<sub>AR</sub> and *SmC*<sub>sP<sub>AR</sub></sub>-*SmC*<sub>s</sub><sup>[\*]</sup>-*SmC*<sub>sP<sub>R</sub></sub><sup>[\*]</sup> transition temperatures were determined by investigations under a triangular wave field of 27 V<sub>pp</sub> μm<sup>-1</sup> in all cases; values in italics are monotropic phase transitions and in this case the enthalpy values were taken on cooling. Abbreviations: Cr = crystalline solid; Iso = isotropic liquid; *N*<sub>cybA</sub> = nematic phase with cybotactic clusters of the *SmA*-type; *SmA* = uniaxial smectic phase; *SmAP*<sub>R</sub> = high-permittivity paraelectric *SmA* phase with one broad polarization current peak per half-period of an applied electric field; *SmAP*<sub>AR</sub> = uniaxial (tilt randomized) high-permittivity paraelectric *SmC* phase with two polarization current peaks per half-period of an applied electric field; *SmC*<sub>s</sub><sup>[\*]</sup> = synclinal tilted (biaxial) smectic C phase (*SmC*<sub>s</sub>) capable of surface-induced mirror-symmetry breaking (<sup>[\*]</sup>); *SmC*<sub>sP<sub>AR</sub></sub><sup>[\*]</sup> = high-permittivity range of the paraelectric *SmC*<sub>s</sub> phase with one broad polarization current peak per half-period of an applied electric field; *SmC*<sub>sP<sub>R</sub></sub><sup>[\*]</sup> = high-permittivity paraelectric range of the *SmC*<sub>s</sub><sup>[\*]</sup> phase with two polarization current peaks per half-period of an applied electric field; *SmC*<sub>sP<sub>A</sub></sub> = antiferroelectric switching polar and synclinal tilted *SmC*<sub>s</sub> phase; *SmC*<sub>sP<sub>A</sub></sub> = antiferroelectric switching polar anticlinal tilted *SmC* phase; see also Figure 1b. For selected DSC scans, see Figure S6; data for **3F20** were taken from reference [37] and the phase notation was adjusted to the rules used herein.

conformation with a bending angle of 120° and stretched all-*trans* alkyl chains; see Figure S9 in the Supporting Information). This diffraction pattern indicates a nematic phase composed of cybotactic clusters with local *SmA* structure (*N*<sub>cybA</sub>);<sup>[39,40]</sup> this non-skewed type of cybotactic nematic phase is rarely observed for bent-core mesogens, which usually prefer tilted arrangements.<sup>[28]</sup>

### Uniaxial *SmA* and *SmAP*<sub>R</sub> phases

At *T* = 110 °C, the diffuse scattering in the small-angle region of the diffraction pattern of **3F6** transformed into a sharp Bragg peak with *d* = 4.0 nm, which is typical for a transition to a smectic phase (Figure 2c,d). The maximum of the diffuse scattering in the wide-angle region remained perpendicular to the small-angle reflection, which indicated a non-tilted organization of the molecules in the layers on average. The *d*-spacing in this *SmA* phase was only slightly smaller than the molecular length (*d*/*L*<sub>mol</sub> = 0.91 nm), in line with a monolayer *SmA* structure. This phase assignment is in agreement with optical investigations between crossed polarizers, which indicated typical fan textures in planar alignment (molecules parallel to the surfaces) with dark extinction crosses parallel to the directions of polar-

izer and analyzer (Figure 2c, inset, and Figure S7b). In homeotropic cells (layers parallel to the surfaces) the textures appeared completely dark between crossed polarizers, that is, this phase is optically uniaxial, as is typical for the *SmA* phase. *SmA* phases were formed by all compounds **3Fn** with *n* ≥ 8, and for these compounds it was the first LC phase observed on cooling from the isotropic liquid state (Table 1, Figure 1a).

As shown in the plots in Figure 3, in the high-temperature range of all *SmA* phases (including those designated as *SmAP*<sub>R</sub>), an increase in the layer spacing (*d*) was observed on cooling, which is due to the increased packing density of the aromatic cores with decreasing temperature. The denser packing led to alkyl-chain stretching and this increased the layer *d*-spacing. However, the slope of the *d* = *f*(*T*) function decreased until a maximum was reached and then *d* decreased on further cooling. The decrease in *d* began in the temperature range of the uniaxial *SmA* phase and, therefore, was attributed to a developing tilt with the formation of randomly aligned tilt domains (de Vries-like smectic phase<sup>[41]</sup>) and partially also to a reduction in the effective molecular length owing to a decrease in the angle  $\gamma$  between the two rodlike azobenzene units (Figure 1c), which thus favors the development of polar domains. On further cooling, the formation of tilted smectic phases



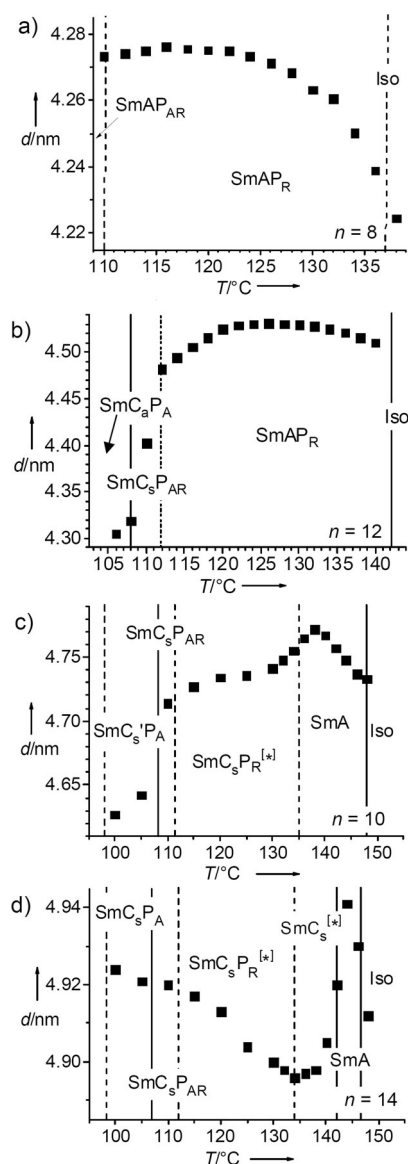


**Figure 3.** Temperature dependence of the  $d$ -value of compounds: a) **3F8** ( $L_{\text{mol}} = 5.1$  nm), b) **3F10** ( $L_{\text{mol}} = 5.6$  nm), c) **3F12** ( $L_{\text{mol}} = 6.1$  nm), and d) **3F14** ( $L_{\text{mol}} = 6.6$  nm) measured by using SAXS on cooling to the crystallization temperature.  $L_{\text{mol}}$  was determined as shown in Figure S9; note that a tilt had already arisen in the SmA range, so the SmA–SmC phase transitions do not correspond to the maxima of the  $d$ -values; data points in the Iso range refer to the maxima of the diffuse small-angle scattering.

(SmC) was observed for all compounds with  $n > 4$ , which is in line with the proposed contribution of tilt to the layer shrinkage. As the alkyl-chain length ( $n$ ) increased, the SmC range broadened and the temperature range of the SmA phase became smaller and shifted to higher temperatures up to  $n = 16$ , but even for the longest homologues ( $n = 18, 20$ ) a small range of the SmA phase was retained (Figure 1a). The response of the SmA phases to an applied electric field changed with chain length, the applied field strength, and temperature. The remarkable feature of short-chain compounds **3F6**, **3F8**, and **3F10** is that a relatively broad single current peak was reproducibly observed over the whole SmA range in each half-

period of an applied triangular wave field (Figure 4a and Figure S13). This peak is thought to be the result of a Langevin-type growth and switching of ferroelectric domains under the applied electric field, as known for SmAP<sub>R</sub> phases.<sup>[42,43,44]</sup> The current peak occurred above a certain threshold field, which increased with the chain length. Similarly, under a fixed field strength ( $E = 27 \text{ V}_{\text{pp}} \mu\text{m}^{-1}$ ) the temperature of the emergence of this peak was continuously shifted to lower temperature as the chain length increased (Table 1 and Figure 1a). For compound **3F12** there was no current peak in the SmA range and the emergence of the current peak coincided with the onset of uniform tilt at the SmA–SmC<sub>s</sub>P<sub>R</sub><sup>[\*]</sup> transition. For the following homologues ( $n > 12$ ), the current peak appeared within the temperature range of the tilted smectic phase, which led to SmC<sub>s</sub><sup>[\*]</sup>–SmC<sub>s</sub>P<sub>R</sub><sup>[\*]</sup> transitions. The single-peak switching in the SmC<sub>s</sub>P<sub>R</sub><sup>[\*]</sup> ranges is associated with an increase in the birefringence of the planar sample under the applied electric field (Figure S16i–k), which confirmed that this peak is indeed due to a polarization. The polarization calculated from the peak area was largest for the SmAP<sub>R</sub> phase of **3F6** ( $P \approx 160 \text{ nC cm}^{-2}$ ) and, as the chain length increased, decreased to only  $\approx 50 \text{ nC cm}^{-2}$  in the SmC<sub>s</sub>P<sub>R</sub><sup>[\*]</sup> ranges of compounds **3F12–3F18**. No polarization peak could be observed in the SmA phases of the long-chain compounds **3F10–3F20**, which are considered to be low-permittivity paraelectric SmA phases, in contrast to the SmAP<sub>R</sub> (and SmAP<sub>AR</sub>) phases, which are considered to be high-permittivity paraelectric phases.

#### The uniaxial SmAP<sub>AR</sub> range of compounds **3F6** and **3F8**

Within the uniaxial smectic phases of compounds **3F6** and **3F8**, with the shortest chains, the mode of switching changed below a certain temperature (Figure 4 and Figure S11). For compound **3F8**, for example, the broad single peak in the SmAP<sub>R</sub> range (Figure 4a) was replaced by two sharp current peaks per half-period of the applied triangular wave voltage at  $T = 108^\circ\text{C}$  and  $20 \text{ V}_{\text{pp}} \mu\text{m}^{-1}$  (Figure 4b). These current peaks were positioned at the maximum voltages and merged closer to each other on further cooling (Figure 4c,d). At the transition to this uniaxial SmA phase, designated as SmAP<sub>AR</sub> (for textures see Figure 4e and inset), the polarization jumped from 150 to approximately  $700 \text{ nC cm}^{-2}$  and then further increased to about  $800 \text{ nC cm}^{-2}$ , which indicated the development of an almost macroscopic polarization under the applied field (Figure 5a). The absence of an enthalpy change at this transition (see Table 1 and Figure S6a) means that, despite the high polarization values, this phase range should still belong to the paraelectric range. Moreover, the temperature at which the two switching peaks occurred shows a strong field dependence, and shifted to a higher temperature as the strength of the applied electric field was increased ( $T = 107, 110, \text{ and } 112^\circ\text{C}$  for 16, 27, and  $33 \text{ V}_{\text{pp}} \mu\text{m}^{-1}$ ; see Figure S12). For compound **3F6**, the same behavior as for **3F8** was found, but the two widely separated current peaks demerged at a slightly lower temperature ( $T = 101^\circ\text{C}$  and  $27 \text{ V}_{\text{pp}} \mu\text{m}^{-1}$ ; see Figure S11).

Optical investigations of the SmAP<sub>AR</sub> range indicated a planar fan texture with dark extinctions parallel to the direc-

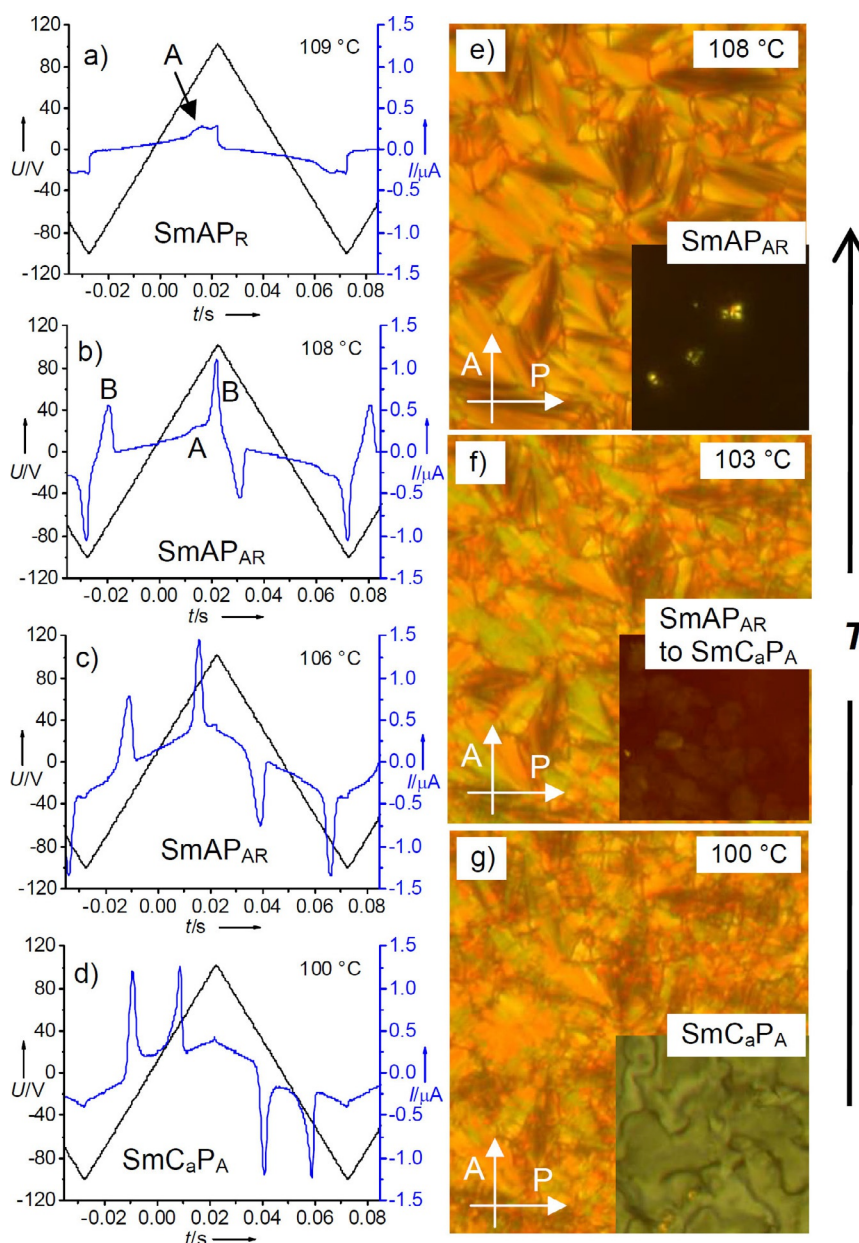


**Figure 4.** Switching-current response curves and textures for compound **3F8** ( $6 \mu\text{m}$  PI-coated ITO cell). a–d) Polarization current response curves on application of a triangular wave field ( $20 \text{ V}_{pp} \mu\text{m}^{-1}$ ,  $10 \text{ Hz}$ ); e–g) textures observed for planar samples (molecules parallel to the substrate surfaces) between crossed polarizers; e) the  $\text{SmAP}_{AR}$  phase, f) the  $\text{SmAP}_{AR}$ – $\text{SmC}_a\text{P}_A$  transition, and g) the  $\text{SmC}_a\text{P}_A$  phase. Insets: the corresponding textures in homeotropic alignment (layers parallel to the substrate surfaces), as observed between nontreated microscopy glass plates. The temperature dependence of the polarization is shown in Figure 5a and DSC plots are shown in Figure S6a.

tions of the polarizers (Figure 6a), which changed under the applied electric field to a texture composed of dark and bright (orange) areas (Figure 6c). In Figure 6a,c, and e, the alignment of the layers is slightly inclined with the orientation of the crossed polarizers and rotation of the sample to the opposite direction of inclination exchanged the brightness of the domains. This indicates a field-induced uniform (synclinc) tilt with opposite tilt direction in the distinct areas (Figure 6c,d).

Upon removal of the field, the direction of tilt was retained (Figure 6e,f), which indicated that the synclinc tilted state was preserved at  $E=0$ ; therefore, we concluded the presence of

a uniaxial smectic phase composed of ferroelectric  $\text{SmC}_s\text{P}_S$  domains that are tilt-randomized in the pristine state (Figure 6a,b). Under an applied field the domains grew and adopted a uniform tilt correlation, which led to a field-induced biaxial and synpolar  $\text{SmC}_s\text{P}_S$  state (Figure 6c,d) that relaxed to an antipolar  $\text{SmC}_s\text{P}_A$  state at  $E=0$  (Figure 6e,f). This field-induced formation of a tilted organization could be considered as a non-classical type of electroclinic effect<sup>[45,22]</sup> or, alternatively, as a transition to a field-induced and surface-stabilized state.<sup>[16b,46]</sup> The tilt direction was retained during relaxation and also after field reversal, which indicated an antiferroelectric

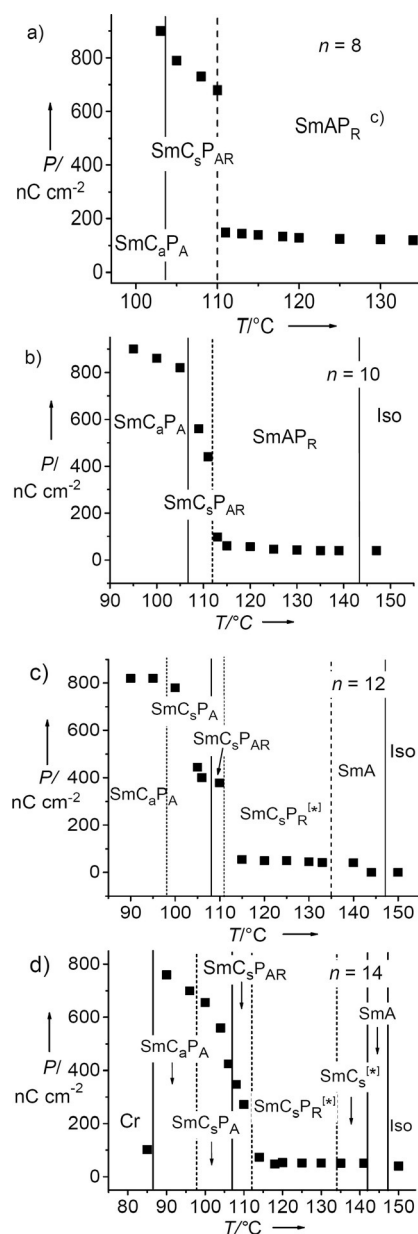


**Figure 5.** a, b) The temperature dependence and development of polarization ( $26.7 \text{ V}_{pp} \mu\text{m}^{-1}$ ,  $10 \text{ Hz}$ ) for: a) **3F8**, b) **3F10**, c) **3F12**, and d) **3F14**, as observed on cooling. Solid lines indicate phase transitions associated with a transition enthalpy, dashed lines indicate continuous transitions.

switching by collective rotation around the molecular long axis (Figure 6 d, f). This range of the uniaxial  $\text{SmA}$  phase, which represents a lamellar phase composed of tilt-randomized  $\text{SmC}_s\text{P}_S$  domains with a dominant antipolar correlation between them in the ground state (Figure 6 b), was designated as  $\text{SmAP}_{AR}$ .<sup>[47–49]</sup> At the  $\text{SmAP}_R$ – $\text{SmAP}_{AR}$  transition, the preferred mode of correlation between the ferroelectric domains changed from synpolar in  $\text{SmAP}_R$  (single current peak) to antipolar in  $\text{SmAP}_{AR}$  (double current peak).

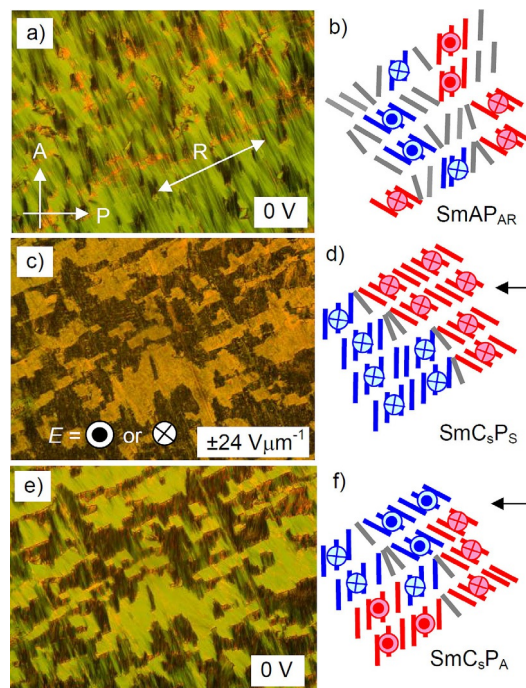


**Figure 6.** Textures observed in DC field experiments in the  $\text{SmAP}_{AR}$  phase range of **3F8** at  $T = 108^{\circ}\text{C}$ : a) before application of an electric field, c) under the electric field and after reversal of the field, and e) after removal of the applied field (planar ITO cell between crossed polarizers, see arrows in a). b, d, f) Models of the molecular organization in the distinct states; R is the rubbing direction.

### The biaxial $\text{SmC}_s\text{P}_{AR}$ phase of compound **3F10**

For the next homologue, **3F10**, a birefringent schlieren texture spontaneously occurred at  $T = 112^{\circ}\text{C}$  on cooling of the homeotropically aligned uniaxial  $\text{SmAP}_R$  phase (Figure S8a). In the XRD patterns, a decrease in the layer spacing from  $d = 4.6$  to  $4.3 \text{ nm}$  started at approximately  $125^{\circ}\text{C}$  in the  $\text{SmAP}_R$  phase and continued in the biaxial phases (Figure 3 b), in line with a growing tilt as the temperature was decreased. Optical investigations of planar samples confirmed a synclinal tilted organization (Figure S15 h). At the transition to this biaxial phase, two widely separated polarization peaks appeared in each half-period of an applied triangular wave field, which rapidly merged closer and increased in size (Figure S14), just as found for the  $\text{SmAP}_{AR}$  phase of **3F8** (Figure 4 a–d). In electro-optical investigations, the removal of the applied field and inversion of the field direction did not change the tilt direction (Figure S15 g–i), which indicated that in this phase the switching process also takes place by rotation around the molecular long axis (Figure S15 j–l). This biaxial smectic phase, designated as  $\text{SmC}_s\text{P}_{ARv}$ , behaves just like the  $\text{SmAP}_{AR}$  phase of **3F8**, except that the tilt correlation between the  $\text{SmC}_s\text{P}_S$  domains was already synclinal before application of an electric field, which indicated that the elongated alkyl chains favor the long-range tilt correlation between the  $\text{SmC}_s\text{P}_S$  domains. Similar to the  $\text{SmAP}_{AR}$  range, the polarization in the  $\text{SmC}_s\text{P}_{AR}$  phase also strongly increased from approximately  $50$  to  $800 \text{ nC cm}^{-2}$  (Figure 5 b).

**Development of polar order in the SmC phases of 3F12–3F20:**  
*SmC<sub>s</sub>P<sub>R</sub><sup>[\*]</sup>, SmC<sub>s</sub>P<sub>R</sub><sup>[\*]</sup>, and SmC<sub>s</sub>P<sub>AR</sub> ranges*

For compound **3F10**, the phase biaxiality appeared to develop simultaneously with the double peak switching at the SmAP<sub>R</sub>–SmC<sub>s</sub>P<sub>AR</sub> transition, whereas for the next homologue, **3F12**, the phase biaxiality emerged along with the appearance of the single current peak (peak A in Figure 7a; see also Figure S13b) at  $T = 135\text{ °C}$  ( $E = 27\text{ V}\mu\text{m}^{-1}$ ), that is, by chain elongation the SmAP<sub>R</sub> phase was replaced by a SmC<sub>s</sub>P<sub>R</sub> phase with long-range tilt.

The texture of the homeotropically aligned sample of the SmC<sub>s</sub>P<sub>R</sub> phase of **3F12** before application of an electric field is shown in Figure 8. On viewing between crossed polarizers, there were areas with uniformly weak birefringence separated by dark domain walls (Figure 8b). After uncrossing the polarizers by a small angle ( $\approx 5\text{--}10^\circ$ ), the distinct areas became dark and bright, and uncrossing the polarizer in the opposite direction reversed the brightness (Figure 8a,c). Rotation of the sample between crossed polarizers did not change the brightness, which means that simple tilt domains could be excluded and the formation of a conglomerate of optical active domains

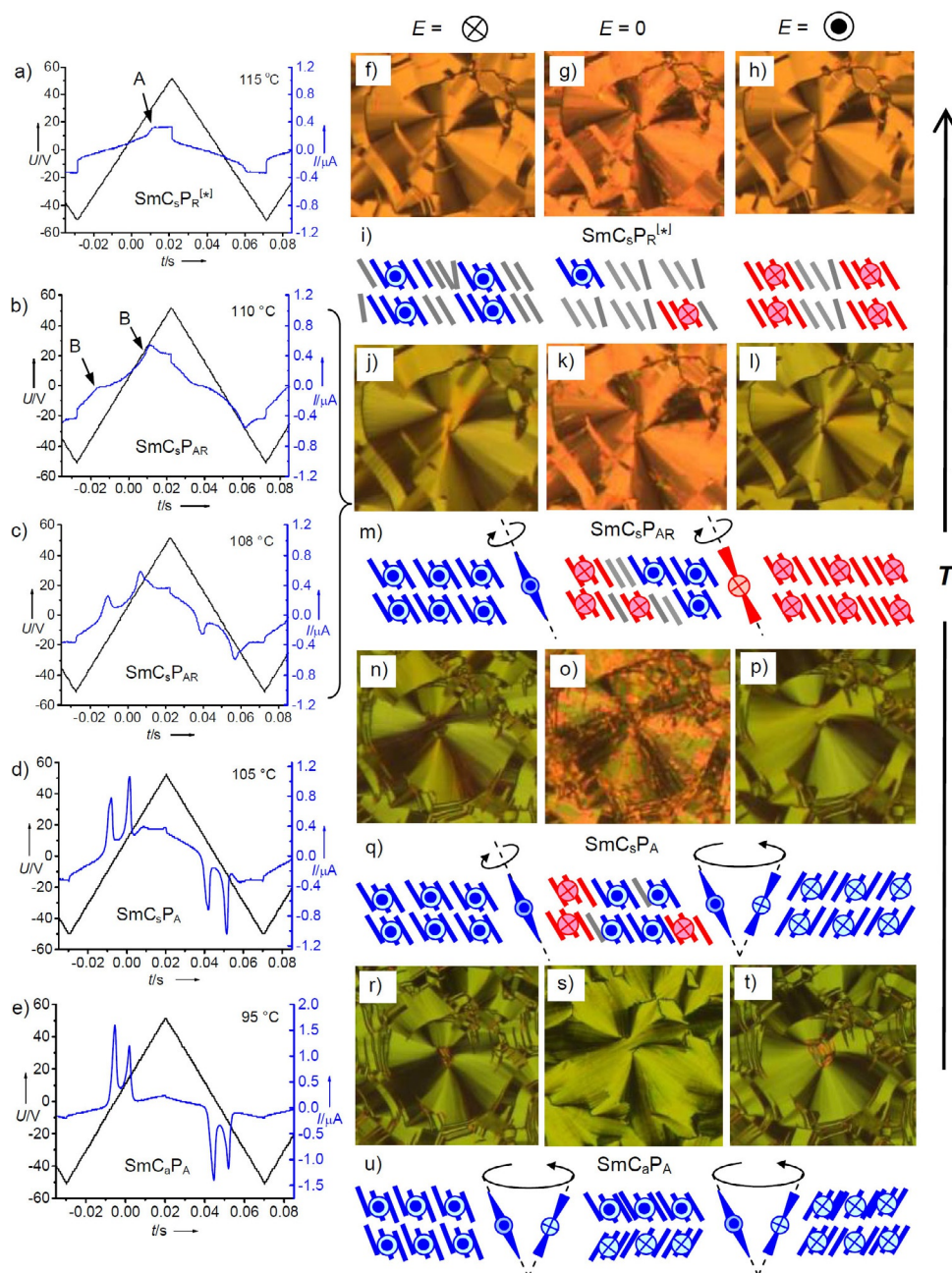


**Figure 7.** a–e) Switching current response curves of compound **3F12** on application of a triangular wave field (10 Hz in  $6\text{ }\mu\text{m}$  ITO cell). f–h, j–l, n–p, r–t) Textures observed between crossed polarizers in DC field experiments at  $+6.7\text{ V}\mu\text{m}^{-1}$  (left column),  $0\text{ V}$  (middle column), and  $-6.7\text{ V}\mu\text{m}^{-1}$  (right column). i, m, q, u) Models of the molecular reorganization in the switching processes. o, s) The green color corresponds to the next lower order of birefringence, due to the intense yellow/orange color of the azo-compound blue and purple birefringence colors appear green. For the DSC plots, see Figure S6c.

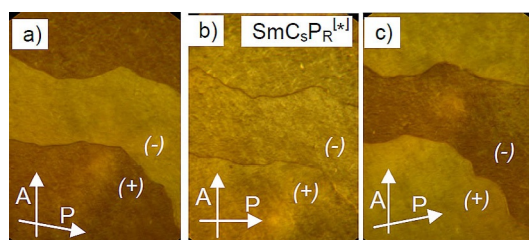


**Figure 8.** Optical textures of the homeotropically aligned (layers parallel to the substrate surfaces)  $\text{SmC}_5\text{P}_R^{[*]}$  phase of **3F12** at  $T = 133^\circ\text{C}$ : b) between crossed polarizers and a, c) between polarizers that were slightly uncrossed in opposite directions, which indicates the optical activity of the distinct domains.

was observed. This indicates chiral conglomerate formation in these  $\text{SmC}_5\text{P}_R$  phases, which led to the designation  $\text{SmC}_5\text{P}_R^{[*]}$ , in which  $^{[*]}$  indicates the conglomerate structure. On cooling, the chiral domains disappeared and simultaneously two broad and widely separated polarization peaks developed at  $T = 111^\circ\text{C}$  (peaks **B** in Figure 7b–d), as also observed for the  $\text{SmC}_5\text{P}_{AR}$  phase of **3F10**. However, the broad shape of the two emerging polarization peaks in the  $\text{SmC}_5\text{P}_{AR}$  range of compound **3F12** is distinct from the sharp peaks in the  $\text{SmAP}_{AR}$  and  $\text{SmC}_5\text{P}_{AR}$  phases of shorter homologues **3F8** and **3F10**. Peak broadening increased as the chain length increased and is associated with a smoother increase in the polarization in the  $\text{SmC}_5\text{P}_{AR}$  range to only around  $400\text{ nC cm}^{-2}$  (see Figure 5c for **3F12** and Figure 5d for **3F14**). It appears that the lateral expansion of the conformationally disordered long alkyl chains reduces the polar packing of the aromatic cores, which thus reduces the overall polarity of the domains and requires a larger domain size to achieve the same polarization as observed for compounds with shorter chains. Apparently, high polarization density leads to small domains with a narrow size distribution and results in sharp polarization peaks, whereas low polarization density requires larger domains that have a broader size distribution, which leads to broader polarization peaks.

For compounds **3Fn** with  $n > 12$ , a chiral domain formation appeared together with the onset of tilt, whereas the emergence of a current peak was delayed and took place significantly after tilt correlation, that is, the paraelectric  $\text{SmC}$  phase is divided into a low-permittivity chiral  $\text{SmC}_5^{[*]}$  range at the highest temperature, followed at lower temperature by chiral and achiral high-permittivity  $\text{SmC}_5\text{P}_R^{[*]}$  and  $\text{SmC}_5\text{P}_{AR}$  ranges, respectively. In the planar textures of the  $\text{SmC}_5\text{P}_R^{[*]}$  and  $\text{SmC}_5\text{P}_{AR}$  ranges of all compounds **3Fn**, the orientation of the extinction crosses is inclined with the directions of polarizer and analyzer under the electric field and at  $E = 0$  (Figure 7f–h and j–l and Figure S16i–k and l–n). This confirmed a synclinal tilt correlation and a switching by reorganization of the molecules through rotation around the molecular long axis (Figure 7i, m). This switching requires a threshold field that decreased as the temperature was decreased due to growing polarization and domain size. For a fixed field strength ( $27\text{ V }\mu\text{m}^{-1}$ ), the temperature of the appearance of the single polarization peak ( $\text{SmC}_5^{[*]}-\text{SmC}_5\text{P}_R^{[*]}$  transition temperature) decreased as the chain length increased, and for compound **3F20** with the lon-

gest chains the  $\text{SmC}_5\text{P}_R^{[*]}$  range appeared to be completely absent and a direct  $\text{SmC}_5^{[*]}-\text{SmC}_5\text{P}_{AR}$  transition, without an intermediate  $\text{SmC}_5\text{P}_R^{[*]}$  phase, was observed (Table 1 and Figure 1a).<sup>[37]</sup> Dielectric studies of this compound<sup>[37]</sup> have confirmed a continuous increase in the dielectric permittivity in the paraelectric  $\text{SmC}$  range, which reached a maximum in the  $\text{SmC}_5\text{P}_{AR}$  range just before the transition to the antiferroelectric  $\text{SmC}_5\text{P}_A$  phase (Figure 9b),<sup>[50]</sup> in line with previously reported paraelectric–ferroelectric transitions.<sup>[51]</sup> Furthermore, chunks of  $\text{SmC}_5\text{P}_5$  domains about 10 to 20 layers thick have been observed by using polarizing microscopy in freely suspended films of the  $\text{SmC}_5\text{P}_{AR}$  range of **3F20**, which thus supports the proposed polar domain structure of the  $\text{SmC}_5\text{P}_{AR}$  phase.<sup>[37]</sup>

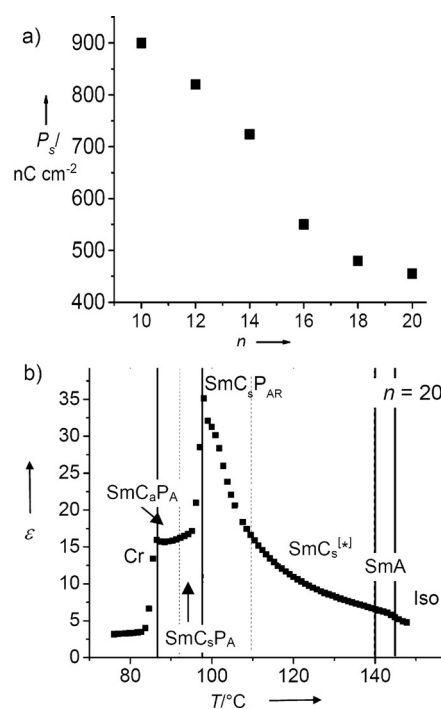


**Figure 9.** a) Spontaneous polarization ( $P_s$ ) in the  $\text{SmC}_5\text{P}_A$  phases depending on alkyl-chain length ( $n$ ), measured at  $T = 95^\circ\text{C}$  ( $T = 90^\circ\text{C}$  for **3F20**) under an applied field of  $26.7\text{ V}_{pp}\mu\text{m}^{-1}$  at 10 Hz. b) Temperature dependence of the static dielectric permittivity ( $\epsilon$ ) of compound **3F20** (reproduced from reference [37] with adjustment to the phase designation used herein; thin dotted lines indicate continuous transitions).

The unique feature of the **3Fn** series is that four different types of polarization-randomized smectic phases, the uniaxial ( $\text{SmAP}_R$ ,  $\text{SmAP}_{AR}$ )<sup>[42,47]</sup> and the biaxial ( $\text{SmC}_5\text{P}_R^{[*]}$  and  $\text{SmC}_5\text{P}_{AR}$ )<sup>[32a,b,37]</sup> have been observed side by side for the first time in a single series of compounds, which provides insights into the actual structure of these high-permittivity paraelectric phases and the relationships between them. The broad single peak in the  $\text{SmAP}_R$  phases was attributed to a Langevin-type switching.<sup>[42]</sup> However, in the synclinal-tilted  $\text{SmC}_5\text{P}_R^{[*]}$  phases of the higher homologues<sup>[32a,b,37]</sup> the tilt and polar order are intrinsically coupled due to the restricted rotation around the molecular long axis and, therefore, the polar direction cannot be completely randomized. Due to the uniform tilt, there is an

Ising-like synpolar coupling between the  $\text{SmC}_5\text{P}_5$  domains that supports the formation of synpolar order under the applied field, even if the local polarization is relatively weak. As the domain size and polarization increased at reduced temperature, a growing preference for an antipolar correlation between the  $\text{SmC}_5\text{P}_5$  domains developed, which led to a transition to tristable switching in the  $\text{SmC}_5\text{P}_{\text{AR}}$  ranges. Even in the uniaxial  $\text{SmAP}_{\text{R}}$  and  $\text{SmAP}_{\text{AR}}$  phases with randomized tilt, the local tilt could provide cooperativity by Ising-like polar coupling and this could contribute to the polar response in these uniaxial phases.

For all compounds **3Fn**, chiral conglomerates appeared (Figure 8) just at the onset of phase biaxiality (tilt) at the  $\text{SmA}-\text{SmC}_5^{[*]}$  or  $\text{SmA}-\text{SmC}_5\text{P}_{\text{R}}^{[*]}$  transition and faded as the achiral  $\text{SmC}_5\text{P}_{\text{AR}}$  region was approached. Mirror-symmetry breaking in the synclinic  $\text{SmC}$  phases of achiral bent-core molecules requires the presence of an intrinsically chiral  $\text{SmC}_5\text{P}_5$  structure with  $C_2$  symmetry.<sup>[14]</sup> In the  $\text{SmC}^{[*]}$  and  $\text{SmC}_5\text{P}_{\text{R}}^{[*]}$  ranges, the Ising-like synpolar coupling between the local  $\text{SmC}_5\text{P}_5$  domains and the further stabilization of this coupling by polar surface interactions in the homeotropic cells are assumed to lead to long-range uniform chirality and the emergence of conglomerates of macroscopically chiral domains (see Figure 8).<sup>[32]</sup> Moreover, the 4-CN group supports twisted minimum-energy conformations, thus compounds **3Fn** are considered to be transiently chiral molecules that favor chirality synchronization in their smectic phases.<sup>[52,27a,53]</sup> The  $\text{SmC}_5\text{P}_{\text{AR}}$  range with synclinic tilt correlation, but antipolar correlation between adjacent  $\text{SmC}_5\text{P}_5$  domains, is on a macroscopic scale racemic and, therefore, achiral. This is in line with the fading of the chiral domains at the transition to  $\text{SmC}_5\text{P}_{\text{AR}}$ .

### Macroscopic polar $\text{SmC}_5\text{P}_{\text{A}}$ and $\text{SmC}_{\text{a}}\text{P}_{\text{A}}$ phases

For all compounds with  $n > 6$ , a further reduction in temperature led to an increase in the size and polarization of the ferroelectric domains, which gave rise to phase transitions to antipolar  $\text{SmC}$  phases composed of polar layers, associated with a transition enthalpy that decreased as the alkyl-chain length increased (Table 1). Short-chain compounds **3F8** and **3F10** formed exclusively anticlinic tilted  $\text{SmC}_{\text{a}}\text{P}_{\text{A}}$  phases on cooling of the paraelectric  $\text{SmAP}_{\text{AR}}$  and  $\text{SmC}_5\text{P}_{\text{AR}}$  phases, respectively. In these  $\text{SmC}_{\text{a}}\text{P}_{\text{A}}$  phases, antiferroelectric switching took place with high polarization values and by rotation around the tilt cone, as is typical for the  $B_2$  phases of bent-core molecules.<sup>[13]</sup> This mode of switching is indicated by flipping of the dark extinction crosses from parallel to inclined with the direction of the polarizers, either clockwise or anticlockwise depending on the field direction (Figure 7r–u and Figure S16r–t). The polarization values were high ( $\approx 900 \text{ nC cm}^{-2}$ ) for the short homologues and decreased to about  $450 \text{ nC cm}^{-2}$  as the alkyl-chain length increased (Figure 9a). For homologues with  $n \geq 12$ , an additional synclinic  $\text{SmC}_5\text{P}_{\text{A}}$  range was introduced between the  $\text{SmC}_5\text{P}_{\text{AR}}$  and the  $\text{SmC}_{\text{a}}\text{P}_{\text{A}}$  phases. The  $\text{SmC}_5\text{P}_{\text{A}}-\text{SmC}_{\text{a}}\text{P}_{\text{A}}$  transition temperature, which was not associated with any transition enthalpy, only slightly decreased with chain elongation from  $T = 98^\circ\text{C}$  for **3F12** to  $T = 92^\circ\text{C}$  for **3F20** (Table 1). The absence of

a transition enthalpy confirmed that both phases belong to the polar smectic phases with long-range polar order in the layers. However, for compounds **3F14–3F20**, the switching in the  $\text{SmC}_5\text{P}_{\text{A}}$  phases takes place by rotation around the long axis, as indicated by the fixed position of the dark extinctions with and without an applied field (Figure S16o–q). Only in the  $\text{SmC}_5\text{P}_{\text{A}}$  phase of **3F12**, the shortest homologue with this phase, is the position of the extinctions retained after switching off the applied field and changes after field reversal (Figure 7n–p). Because there are two polarization peaks (Figure 7d), bistable switching could be excluded and the actual switching process was interpreted as a combination of two switching mechanisms (Figure 7q). A relaxation after switching off the field at 0 V took place by rotation around the long axis, which thus retained the position of the extinctions (Figure 7n, o). After field reversal, a switching occurred by rotation on the tilt cone, which rotated the position of the extinctions to the opposite direction (Figure 7o, p) and indicated an inversion of the tilt direction.<sup>[54]</sup> In general, the high packing density in the highly polarized  $\text{SmC}$  phases of strongly bent molecules suppresses the switching around the long axis, whereas the low packing density and reduced polar order of weakly bent and weakly tilted molecules are favorable for rotation around the molecular long axis.<sup>[55]</sup> Therefore, it can be deduced that in the  $\text{SmC}_5\text{P}_{\text{A}}$  phase the packing density still increases and that a critical limit of packing density and bending angle is achieved at the  $\text{SmC}_5\text{P}_{\text{A}}-\text{SmC}_{\text{a}}\text{P}_{\text{A}}$  transition, where the tilt correlation and the switching mechanism change. The  $\text{SmC}_5\text{P}_{\text{A}}$  phase of **3F12**, which combines both switching mechanisms, represents an intermediate case with intermediate packing density. In the  $\text{SmC}_5\text{P}_{\text{A}}$  ranges of all compounds with  $n \geq 12$  the barrier for rotation around the molecular long axis still increased as the temperature was decreased, which led to the strong growth in the polarization in the  $\text{SmC}_5\text{P}_{\text{A}}$  ranges (Figure 5c, d).

### Overall phase sequence depending on temperature and chain length

Because the shape of bent molecules based on 4-cyanoresorcinol can change from being almost rodlike to increasingly bent as the temperature is decreased,<sup>[27a]</sup> restriction of the rotation around the long axis, increased packing density, and increased coherence length of polar order were observed as the temperature was reduced. For only weakly bent molecules there are entropically favored interlayer fluctuations along the molecular long axes that transfer polar order predominately between the layers, whereas rotation around the long axis reduces polar order in the layers (see Figure 10, left). The weak synpolar coupling in all directions leads to the polarization randomized paraelectric  $\text{SmAP}_{\text{R}}$  and  $\text{SmC}_5\text{P}_{\text{R}}^{[*]}$  phases with a single switching current peak and small polarization values.

The transition from a preferred synpolar correlation in  $\text{SmAP}_{\text{R}}/\text{SmC}_5\text{P}_{\text{R}}^{[*]}$  to the antipolar correlation in the  $\text{SmAP}_{\text{AR}}/\text{SmC}_5\text{P}_{\text{AR}}$  phases is thought to be mainly the result of the stronger molecular bend, which disfavors fluctuations parallel the molecular long axes, but favors fluctuations by intercalations of the two individual rodlike wings (see Figure 10, right). This

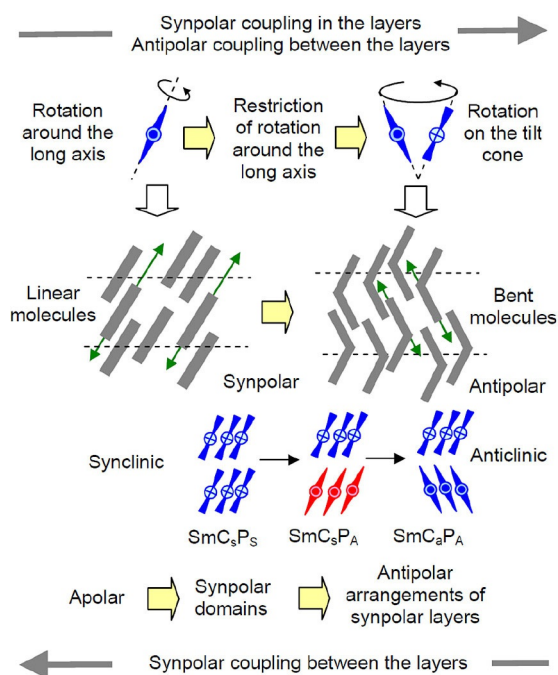


**Figure 10.** Effects of molecular rotations (top line) and out-of-layer fluctuations (green arrows, middle) on the mesophase structure of the tilted smectic phases formed by molecules with shapes at the transition from linear to bent.

leads to a preference of antipolar coupling between the layers, whereas the simultaneous reduction in the ability to rotate around the long axis strengthens the polar coupling in the layers. Thus, two polarization peaks are observed in the paraelectric SmAP<sub>AR</sub> and SmC<sub>s</sub>P<sub>AR</sub> phases and the polarization values increase. Further increase in in-layer polarization finally leads to polar layers in the antipolar SmC<sub>s</sub>P<sub>A</sub> and SmC<sub>a</sub>P<sub>A</sub> phases, which resemble the B<sub>2</sub>-type polar smectic phases of typical (strongly bent) bent-core mesogens. In the **3Fn** series, the increase in the coherence length of polar order unavoidably leads to antipolar correlation even before macroscopic polarization is achieved. However, as previously shown, the inter-layer fluctuations of the rodlike wings can be suppressed by the introduction of nanosegregating silyl groups to the ends of the alkyl chains,<sup>[56,57]</sup> and this shifts the synpolar–antipolar transition into the region of the macroscopic polar smectic phases, which thus leads to the ferroelectric switching SmC<sub>s</sub>P<sub>F</sub><sup>[58,59]</sup> and SmAP<sub>F</sub> phases.<sup>[60]</sup>

There is also a significant effect of chain length; short chains ( $n=4-6$ ) have a small segregation tendency from the aromatic cores<sup>[61]</sup> and this led to cybotactic nematic phases and SmA phases (SmAP<sub>R</sub>, SmAP<sub>AR</sub>). For medium chain lengths ( $n=8-10$ ), core–chain nanosegregation is increased, which favors polar packing in the layers and tilting. Therefore, the medium-length chain compounds have high polarization values and an increased tendency for antipolar packing in adjacent layers, and this leads to a dominance of the high-polarization SmC<sub>s</sub>P<sub>A</sub> phase. For long chains ( $n=12-20$ ), the growing mismatch between the cross-sectional areas of the rigid aromatic cores and the conformationally disordered flexible chains gave rise to fur-

ther increased tilt and reduced the packing density, as indicated by the increased tilt, reduced polarization, and the decreased temperature range of the SmC<sub>s</sub>P<sub>R</sub><sup>[\*]</sup> phase. Simultaneously, as the chain length increased the temperature-dependent development of the coherence length of polar order became more continuous, which led to an increase in the temperature range of the high-permittivity paraelectric SmC<sub>s</sub>P<sub>AR</sub> region above the paraelectric–antiferroelectric transition and the emergence of an additional synclinc SmC<sub>s</sub>P<sub>A</sub> range in the antiferroelectric phase region before the transition to the B<sub>2</sub>-like anticlinc SmC<sub>a</sub>P<sub>A</sub> phase (Figure 1a). In the SmC<sub>s</sub>P<sub>A</sub> range there was still an increasing packing density that led to increased polarization; tilt correlation and the switching process change at a critical coherence length of polarization at the SmC<sub>s</sub>P<sub>A</sub>–SmC<sub>a</sub>P<sub>A</sub> transition.

### Effects of the replacement of F by H or larger groups in the 3-positions

A comparison of compounds **3Fn** (Figure 1a) with the related nonfluorinated analogues **Hn** ( $X, Y=H$ ; see Figure 11)<sup>[32a,b]</sup> showed that core fluorination at the periphery led to increased stability of the smectic phases and shifted the nematic range to much shorter chain lengths. Moreover, there was a reduced tendency for the fluorinated compounds to form uniformly tilted phases. Therefore, the N<sub>Cybc</sub> phase of **Hn** was replaced by the N<sub>Cyba</sub> phase and uniaxial smectic phases (SmA, SmAP<sub>R</sub>, SmAP<sub>AR</sub>) were introduced, which were completely missing in the nonfluorinated **Hn** compounds. The stronger tilt in the **Hn** series might also be responsible for the presence of an additional, possibly modulated, M<sub>1</sub> phase that separates the paraelectric and antiferroelectric smectic phases. In both series there is mirror-symmetry breaking in the SmC<sub>s</sub><sup>[\*]</sup> and SmC<sub>s</sub>P<sub>R</sub><sup>[\*]</sup>

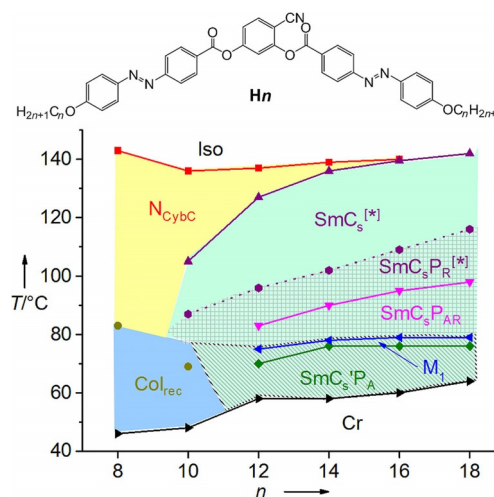


**Figure 11.** Plot of the transition temperatures of compounds **Hn**<sup>[32a,b]</sup> as a function of the alkyl-chain length ( $n$ ); the solid black line indicates the crystallization temperature on cooling, the colored lines indicate the upper temperature limits for the distinct mesophases; modified with adjustment to the phase designations used herein. Abbreviations: N<sub>Cybc</sub>=cybotactic nematic phase composed of SmC clusters; Col<sub>rec</sub>=rectangular columnar ribbon phase (B<sub>1</sub> phase); M<sub>1</sub>=unknown mesophase with high viscosity; for other abbreviations, see Table 1 and Figure 1b.

ranges, as indicated by surface-stabilized conglomerate formation. However, only compounds **3Fn** formed the B<sub>2</sub>-like SmC<sub>a</sub>P<sub>A</sub> phase with long-range polar layers, whereas the paraelectric SmC<sub>s</sub><sup>[\*]</sup>, SmC<sub>s</sub>P<sub>R</sub><sup>[\*]</sup>, and SmC<sub>s</sub>P<sub>AR</sub> phases, and the SmC<sub>s</sub>P<sub>A</sub> phase with a limited coherence length of polar order were found in both series. Thus, increased polar order is achieved in the fluorinated **3Fn** compounds. These effects of core fluorination appear to be the result of increased core–core interactions between the electron-deficient fluorinated aromatic units.<sup>[62]</sup>

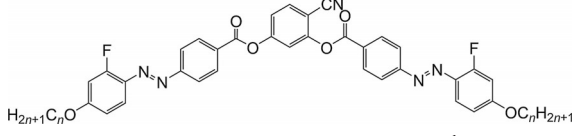
Moreover, in **3Fn** and **Hn** compounds there is an opposite effect on the polar order due to increasing chain length. For compounds **3Fn**, the SmC<sub>s</sub>P<sub>R</sub><sup>[\*]</sup> and SmC<sub>s</sub>P<sub>AR</sub> phases were destabilized as the chain length increased, whereas for compounds **Hn** these phases were stabilized (compare Figures 1a and 11). It appears that for compounds **Hn**, the polar core–core interactions were supported by increased core–chain nanosegregation that increased with growing chain length. For fluorinated compounds **3Fn** with stronger core–core interactions, core–chain segregation is not required. In this case, it even disturbs the development of polar order because longer fluid alkyl chains could reduce the packing density of the aromatic cores due to the increased lateral expansion of the disordered alkyl chains.

Replacement of fluorine (crystal volume  $cv = 12.8 \text{ nm}^3$ )<sup>[63]</sup> in **F18** with the more bulky and less polar bromine ( $cv = 33.0 \text{ nm}^3$ ) reduced the phase-transition temperatures considerably (compound **3Br18**, Table 2), although an Iso–SmA–SmC<sub>s</sub><sup>[\*]</sup>–SmC<sub>s</sub>P<sub>AR</sub> phase sequence was retained. However, the polarization was smaller ( $P \approx 100 \text{ nCcm}^{-2}$ ) and the polarization peaks were much broader in the SmC<sub>s</sub>P<sub>AR</sub> range (Figure S19), which indicated a smaller polarization and a significant size distribution of the polar domains. In this case, no transition to a macroscopically polar SmCP<sub>A</sub> phase could be found before crystallization took place at  $T = 67^\circ\text{C}$ . The replacement of Br by a nonpolar CH<sub>3</sub> group with similar volume ( $cv = 31.7 \text{ nm}^3$ ) further reduced the LC phase stability considerably, removed the nontilted SmA phase, and removed the polar order completely, to leave only a nematic (N<sub>Cybc</sub>) and a nonpolar and nonchiral SmC phase (see Table 2). This was mainly attributed to the unfavorable reduction in core–core interactions by the nonpolar and electron-donating CH<sub>3</sub> group.

### Effects of variation in the F substitution pattern

A change in the position of the lateral fluorine substituents from the *ortho* position (**3Fn**) to the *meta* position with respect to the terminal alkyloxy chains (**2F**) reduced the melting and clearing temperatures (Tables 1 and 3). Moreover, only LC

**Table 3.** Phase transitions of compounds **2Fn** with fluorination at the 2-position.<sup>[a]</sup>

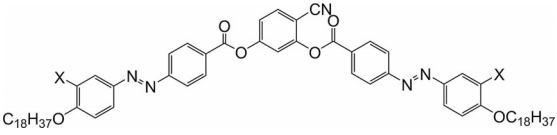


	<i>n</i>	<i>T</i> [°C] ( $\Delta H$ [kJ mol <sup>-1</sup> ])			
<b>2F8</b>	8	Cr 107 (43.0)		N <sub>Cybc</sub> 117 (0.7)	Iso
<b>2F10</b>	10	Cr 86 (40.8)		N <sub>Cybc</sub> 100 (0.9)	Iso
<b>2F12</b>	12	Cr 92 (43.5)	<i>SmC</i> 69 (0.3)	N <sub>Cybc</sub> 112 (0.9)	Iso
<b>2F14</b>	14	Cr 91 (40.1)	<i>SmC</i> 91 (0.9)	N <sub>Cybc</sub> 104 (1.4)	Iso
<b>2F16</b>	16	Cr 92 (50.7)	<i>SmC</i> 102 (0.9)	N <sub>Cybc</sub> 108 (1.7)	Iso

[a] Transition temperatures and enthalpy values (in brackets) were taken from the second DSC heating scans (10 Kmin<sup>-1</sup>); italicized values are monotropic phase transitions and in this case the enthalpy values were taken from the first DSC cooling scans. For abbreviations see Table 1 and Figure 11.

phases with tilted organization (N<sub>Cybc</sub> phases; see Figure S17 and SmC<sub>s</sub> phases) were observed. Neither chiral domain formation nor any polarization current peaks or optical response to the applied fields could be observed up to an electric field of  $33 \text{ V}_{pp} \mu\text{m}^{-1}$ . Therefore, the introduction of F substitution at this position favored tilt, reduced mesophase stability, and removed polar order, which is mainly attributed to the unfavorable steric effect of fluorine in this inside-directed position. This is in line with previous observations made for rodlike molecules.<sup>[34]</sup>

**Table 2.** Effect of different 3-position substituents on the LC phases and polar order.<sup>[a]</sup>



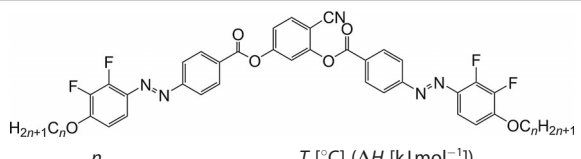
	<i>X</i>	<i>T</i> [°C] ( $\Delta H$ [kJ mol <sup>-1</sup> ])							
<b>H18</b>	H	Cr 80	<i>SmC<sub>s</sub>P<sub>A</sub></i> 76	<i>M<sub>1</sub></i> 79	<i>SmC<sub>s</sub>P<sub>AR</sub></i> ≈ 98	<i>SmC<sub>s</sub>P<sub>R</sub></i> <sup>[*]</sup> ≈ 116	<i>SmC<sub>s</sub></i> <sup>[*]</sup> 142		Iso <sup>[2b]</sup>
<b>3F18</b>	F	Cr 102	<i>SmC<sub>a</sub>P<sub>A</sub></i> 94	<i>SmC<sub>s</sub>P<sub>A</sub></i> 101	<i>SmC<sub>s</sub>P<sub>AR</sub></i> ≈ 108	<i>SmC<sub>s</sub>P<sub>R</sub></i> <sup>[*]</sup> 121	<i>SmC<sub>s</sub></i> <sup>[*]</sup> 143	SmA 148	Iso
<b>Br18</b>	Br	Cr 86 (23.4)			<i>SmC<sub>s</sub>P<sub>AR</sub></i> 82 (-)		<i>SmC<sub>s</sub></i> <sup>[*]</sup> 108 (0.2)	SmA 117 (3.7)	Iso
<b>Me18</b>	CH <sub>3</sub>	Cr 79 (69.9)					<i>SmC</i> 90 (0.8)	N <sub>Cybc</sub> <sup>[b]</sup> 92 (1.8)	Iso

[a] Abbreviations are explained in Table 1; italicized values are monotropic phase transitions. [b] Based on the presence of the low-temperature SmC phase, the nematic phase is designated as N<sub>Cybc</sub>.



The use of two lateral fluorine substituents at the *ortho* and *meta* positions (**23Fn** series, Table 4) led to transition temperatures that were higher compared with the **2Fn** series, but lower than the **3Fn** series. A nematic phase could not be observed, and the SmA phase appeared only as a monotropic

**Table 4.** Phase transitions of series of 2,3-difluorinated compounds **23Fn**.<sup>[a]</sup>



$n$	$T$ [°C] ( $\Delta H$ [kJ mol <sup>-1</sup> ])			
<b>23F8</b>	8	Cr 133 (28.7)		Iso
<b>23F10</b>	10	Cr 131 (39.3)	<i>SmA</i> 129 (3.5)	Iso
<b>23F12</b>	12	Cr 126 (36.9)	<i>SmC<sub>s</sub><sup>[*]</sup></i> 134 (4.9)	Iso
<b>23F14</b>	14	Cr <sub>1</sub> 71 (22.9)	Cr <sub>2</sub> 122 (37.8)	<i>SmC<sub>s</sub><sup>[*]</sup></i> 136 (5.9)
<b>23F16</b>	16	Cr <sub>1</sub> 83 (26.2)	Cr <sub>2</sub> 123 (36.1)	<i>SmC<sub>s</sub><sup>[*]</sup></i> 140 (6.4)

[a] Transition temperatures and enthalpy values (in brackets) were taken from the second DSC heating scans (10 K min<sup>-1</sup>); values in italics are monotropic phase transitions and in this case the enthalpy values were taken from the first DSC cooling scans. For abbreviations, see Table 1.

phase for  $n=10$ . Compounds with  $n \geq 12$  exclusively formed the nonpolar *SmC<sub>s</sub><sup>[\*]</sup>* phase, which showed chiral conglomerates in homeotropic alignment (Figure S18). Although chiral conglomerate formation indicated a paraelectric phase with *SmC<sub>s</sub>P<sub>s</sub>* domain structure, no polarization current peaks could be observed in the triangular wave experiments (up to 33 V<sub>pp</sub> μm<sup>-1</sup>). Due to the relatively high melting points and increased crystallization tendency, the temperature ranges with polar switching could not be accessed for compounds **23Fn**.

A comparison of the effect of the azobenzene wings with respect to other rodlike units is given in the Supporting Information, Section S5.1.

## Conclusions

Three series of bent-core molecules that consisted of a 4-cyanoresorcinol-based central core and laterally fluorinated azobenzene wings have been synthesized and investigated, which provided fundamental insights into the development of polar order and spontaneous symmetry breaking by self-assembly of the achiral bent-core molecules in lamellar LC phases (Figure 1). It shows that locally tilted and polar *SmC<sub>s</sub>P<sub>s</sub>* domains already emerge in the SmA phase. As the size of these ferroelectric domains increased, macroscopic polar order developed continuously from the low-permittivity SmA phases (SmA) through a series of uniaxial (*SmAP<sub>R</sub>*, *SmAP<sub>AR</sub>*) and biaxial (*SmC<sub>s</sub>P<sub>R</sub><sup>[\*]</sup>*, *SmC<sub>s</sub>P<sub>AR</sub>*) high-permittivity paraelectric smectic phases to the antiferroelectric polar smectic phases (*SmC<sub>s</sub>P<sub>A</sub>*

and *SmC<sub>a</sub>P<sub>A</sub>*). As known for inorganic solid-state ferroelectrics (e.g., perovskites),<sup>[15]</sup> the paraelectric–ferroelectric transition takes place through gradual changes in the polar domain size and by crossing a permittivity maximum temperature that corresponds to the *SmAP<sub>AR</sub>*–*SmCP<sub>A</sub>* and *SmC<sub>s</sub>P<sub>AR</sub>*–*SmCP<sub>A</sub>* transitions (see Figure 9b),<sup>[37]</sup> which are the only transitions of this process that are associated with the small transition enthalpy (Table 1). However, increasing polar coherence length led to a strengthening of the antipolar correlation between the ferroelectric domains, which thus gave rise to antiferroelectric switching in the high-permittivity paraelectric *SmAP<sub>AR</sub>* and *SmC<sub>s</sub>P<sub>AR</sub>* ranges. Because the development of polar order is associated with the development of a tilted organization in the polar domains and a growing coherence of tilt between these domains, the paraelectric phases showed unusual effects, such as spontaneous symmetry breaking, nonclassical electroclinic effects, and field-induced phase transitions. In the paraelectric phases and most *SmC<sub>s</sub>P<sub>A</sub>* phases, the switching took place by rotation around the molecular long axis, whereas it occurred by rotation around the tilt cone only in the high-polarization (B<sub>2</sub>-like) *SmC<sub>a</sub>P<sub>A</sub>* phase with enhanced packing density.

Core fluorination at the periphery appeared to give increased electrostatic interactions between the aromatic cores, which thus removed nematic phases and led to enhanced smectic phase stability, increased polar order, and increased stability of chiral conglomerate type *SmC<sup>[\*]</sup>* phases. It also modified the core packing, which led to reduced tilt and the emergence of additional tilt-randomized paraelectric *SmC* phases (*SmAP<sub>R</sub>* and *SmAP<sub>AR</sub>*). These polar effects are dominant for core substitution in the peripheral 3-position, at which steric effects are small. The importance of polar interactions was also evident from the effects of replacing F with Br and CH<sub>3</sub>. With decreased electron-acceptor ability, the polar phases were destabilized and finally removed completely. Fluorination at the inside-directed 2-position strongly reduced smectic phase stability<sup>[34a]</sup> and polar order and removed superstructural chirality due to the dominant steric distortion of the packing of the bent cores by F-substitution in this position.

Overall, this work provides clues to understand the development of polar order in the LC phases of achiral bent-core mesogens that depend on temperature, chain length, and core structure, and it indicates similarities to related transitions in solid-state ferroelectrics. The advantage of fluid materials with polar responses is their ability to be processed easily and addressed by a variety of external stimuli. The azo linkage in all reported compounds can undergo light-induced *trans*–*cis* isomerization (see the Supporting Information, Section S5.2 for preliminary investigations in solution) that could in future be used for optically addressing polar order and chirality.

## Experimental Section

### Synthesis

Benzoic acids **3an–3en** (2.4 mmol), synthesized according to the procedures given in the references,<sup>[38]</sup> were heated at reflux with excess SOCl<sub>2</sub> (3 mL) and a catalytic amount DMF for 1 h to give

corresponding benzoyl chlorides **4an–4en**. Excess thionyl chloride was removed under reduced pressure. The formed benzoyl chloride was then dissolved in dry  $\text{CH}_2\text{Cl}_2$  (20 mL) and 4-cyanoresorcinol **5** (1.2 mmol)<sup>[28]</sup> previously dissolved in  $\text{CH}_2\text{Cl}_2$  (10 mL) was added to the solution, followed by addition of triethylamine (2.8 mmol) and a catalytic amount of pyridine. The reaction mixture was then heated at reflux for 6 h under an argon atmosphere. The reaction mixture was cooled to RT and washed with 10% HCl (2 × 50 mL) and cold water (2 × 50 mL). The aqueous phase was extracted with  $\text{CH}_2\text{Cl}_2$  (3 × 50 mL) and the combined organic phases were dried over anhydrous  $\text{Na}_2\text{SO}_4$ . The crude residue obtained after the removal of solvent was purified by using chromatography on silica gel with chloroform as the eluent to give an orange material that was crystallized from a chloroform/ethanol mixture to give the final bent-core compounds. The analytical data for **3F12**, **2F12**, and **23F12** are given as representative examples below; the analytical data for all other reported compounds are collated in the Supporting Information.

#### 4-Cyano-1,3-phenylene-bis-[4-(3-fluoro-4-dodecyloxyphenyl-azo)benzoate] (**3F12**)

Orange powder (yield 68%);  $^1\text{H}$  NMR (400 MHz,  $\text{CDCl}_3$ ):  $\delta$  = 8.40 (d,  $J$  = 8.5 Hz, 2H; Ar-H), 8.33 (d,  $J$  = 8.5 Hz, 2H; Ar-H), 8.07–7.93 (m, 4H; Ar-H), 7.83 (d,  $J$  = 8.6 Hz, 3H; Ar-H), 7.79–7.70 (m, 2H; Ar-H), 7.59 (d,  $J$  = 2.2 Hz, 1H; Ar-H), 7.36 (dd,  $J$  = 8.5, 2.2 Hz, 1H; Ar-H), 7.10 (t,  $J$  = 8.6 Hz, 2H; Ar-H), 4.14 (t,  $J$  = 6.6 Hz, 4H;  $\text{OCH}_2\text{CH}_2$ ), 1.95–1.81 (m, 4H;  $\text{OCH}_2\text{CH}_2$ ), 1.60–1.16 (m, 36H;  $\text{CH}_2$ ), 0.88 ppm (t,  $J$  = 6.7 Hz, 6H;  $\text{CH}_3$ );  $^{13}\text{C}$  NMR (126 MHz,  $\text{CDCl}_3$ ):  $\delta$  = 163.44 (COOAr), 163.08 (–COOAr), 155.89 (CAr-O- $\text{CH}_2$ ), 155.79 (CAr-O- $\text{CH}_2$ ), 154.77, 153.87, 153.45, 151.89, 150.92, 150.87, 150.83, 150.78, 146.46, 146.43, 146.39, 133.99, 131.65, 131.41, 129.57, 129.19, 123.94, 123.93, 122.89, 122.82, 120.01, 117.34, 114.73 (CN), 113.44, 113.41, 107.96, 107.89, 107.81, 107.74, 104.28 (CAr-CN), 69.56 (CAr-O- $\text{CH}_2$ ), 31.89, 29.63, 29.61, 29.56, 29.51, 29.32, 29.31, 29.04, 25.87, 22.67, 14.09 ppm ( $\text{CH}_3$ );  $^{19}\text{F}$  NMR (470 MHz,  $\text{CDCl}_3$ ):  $\delta$  = –132.27––132.73 ppm (m); elemental analysis calcd (%) for  $\text{C}_{57}\text{H}_{65}\text{F}_2\text{N}_5\text{O}_6$ : C 71.60, H 7.06, N 7.32; found: C 71.63, H 7.00, N 7.31.

#### 4-Cyano-1,3-phenylene-bis-[4-(2-fluoro-4-dodecyloxyphenyl-azo)benzoate] (**2F12**)

Orange powder (yield 66%);  $^1\text{H}$  NMR (400 MHz,  $\text{CDCl}_3$ ):  $\delta$  = 8.39 (d,  $J$  = 8.5 Hz, 2H; Ar-H), 8.32 (d,  $J$  = 8.5 Hz, 2H; Ar-H), 8.07–7.97 (m, 4H; Ar-H), 7.89–7.78 (m, 3H; Ar-H), 7.59 (d,  $J$  = 2.2 Hz, 1H; Ar-H), 7.36 (dd,  $J$  = 8.5, 2.2 Hz, 1H; Ar-H), 6.82–6.73 (m, 4H; Ar-H), 4.04 (t,  $J$  = 6.5 Hz, 4H;  $\text{OCH}_2\text{CH}_2$ ), 1.89–1.76 (m, 4H;  $\text{OCH}_2\text{CH}_2$ ), 1.64–1.17 (m, 36H;  $\text{CH}_2$ ), 0.88 ppm (t,  $J$  = 6.8 Hz, 6H;  $\text{CH}_3$ );  $^{13}\text{C}$  NMR (126 MHz,  $\text{CDCl}_3$ ):  $\delta$  = 164.09 (COOAr), 164.05 (COOAr), 164.01 (CAr-O- $\text{CH}_2$ ), 163.96 (CAr-O- $\text{CH}_2$ ), 163.46, 163.20, 163.11, 161.13, 156.33, 156.22, 154.78, 153.46, 134.93, 134.89, 134.87, 134.84, 133.97, 131.63, 131.39, 129.47, 129.09, 122.96, 122.89, 120.00, 118.59, 118.56, 117.36, 114.74 (CN), 111.56, 111.54, 111.52, 111.49, 104.28 (CAr-CN), 102.42, 102.23, 68.93 (CAr-O- $\text{CH}_2$ ), 68.92 (CAr-O- $\text{CH}_2$ ), 31.87, 29.63, 29.61, 29.55, 29.52, 29.32, 29.30, 28.97, 25.92, 22.66, 14.09 ppm ( $\text{CH}_3$ );  $^{19}\text{F}$  NMR (470 MHz,  $\text{CDCl}_3$ ):  $\delta$  = –119.77––120.14 (m); elemental analysis calcd (%) for  $\text{C}_{57}\text{H}_{67}\text{F}_2\text{N}_5\text{O}_6$ : C 71.60, H 7.06, N 7.32; found: C 71.60, H 7.11, N 7.38.

#### 4-Cyano-1,3-phenylene-bis-[4-(2,3-difluoro-4-dodecyloxy-phenylazo)benzoate] (**23F12**)

Orange powder (yield 68%);  $^1\text{H}$  NMR (400 MHz,  $\text{CDCl}_3$ ):  $\delta$  = 8.40 (d,  $J$  = 8.5 Hz, 2H; Ar-H), 8.32 (d,  $J$  = 8.5 Hz, 2H; Ar-H), 8.09–7.97 (m,

4H; Ar-H), 7.83 (d,  $J$  = 8.6 Hz, 1H; Ar-H), 7.67–7.54 (m, 3H; Ar-H), 7.36 (dd,  $J$  = 8.5, 2.1 Hz, 1H; Ar-H), 6.88–6.76 (m, 2H; Ar-H), 4.15 (t,  $J$  = 6.6 Hz, 4H;  $\text{OCH}_2\text{CH}_2$ ), 1.95–1.80 (m, 4H;  $\text{OCH}_2\text{CH}_2$ ), 1.68–1.14 (m, 36H;  $\text{CH}_2$ ), 0.88 ppm (t,  $J$  = 6.6 Hz, 6H;  $\text{CH}_3$ );  $^{13}\text{C}$  NMR (126 MHz,  $\text{CDCl}_3$ ):  $\delta$  = 163.37 (COOAr), 163.01 (COOAr), 156.02 (CAr-O- $\text{CH}_2$ ), 155.92 (CAr-O- $\text{CH}_2$ ), 154.73, 153.42, 151.95, 151.19, 151.10, 149.11, 149.02, 142.68, 142.58, 140.70, 140.60, 135.55, 135.52, 135.49, 134.00, 131.66, 131.42, 129.93, 129.55, 123.13, 123.06, 120.03, 117.33, 114.70 (CN), 111.98, 111.95, 108.46, 104.31 (CAr-CN), 70.08 (CAr-O- $\text{CH}_2$ ), 31.89, 29.62, 29.60, 29.54, 29.49, 29.32, 29.27, 29.02, 25.80, 22.66, 14.08 ppm ( $-\text{CH}_3$ );  $^{19}\text{F}$  NMR (470 MHz,  $\text{CDCl}_3$ ):  $\delta$  = –145.72––146.13 (m), –157.86––158.19 ppm (m); elemental analysis calcd (%) for  $\text{C}_{57}\text{H}_{65}\text{F}_4\text{N}_5\text{O}_6$ : C 69.00, H 6.60, N 7.06; found: C 68.98, H 6.61, N 6.99.

#### Analytical methods

Thin-layer chromatography (TLC) was performed on aluminum sheet precoated with silica gel. Starting materials were obtained from commercial sources and used without further purification. Solvents were dried by using standard methods as required. The purity and the chemical structures of all synthesized compounds were confirmed by the spectral data. The structural characterization of the as-synthesized bent-core compounds is based on  $^1\text{H}$ ,  $^{13}\text{C}$ , and  $^{19}\text{F}$  NMR spectroscopy in solution in  $\text{CDCl}_3$  with tetramethylsilane as the internal standard (Varian Unity 400 spectrometer). Microanalyses were performed by using a Leco CHNS-932 elemental analyzer.

#### Investigation methods

The phase behavior of the synthesized compounds was investigated by using polarizing optical microscopy (PLM), differential scanning calorimetry (DSC), X-ray diffraction (XRD) studies, and electro-optical measurements. All compounds were thermally stable, as confirmed by the reproducibility of thermograms after several heating and cooling cycles. The assignment of the mesophases was made on the basis of combined results of optical textures, electro-optical studies, and XRD. For optical microscopy, an Optiphot 2 polarizing microscope (Nikon) in conjunction with a heating stage (FP82HT, Mettler) was used. Photoisomerization of the azo-benzene group was negligible under the experimental conditions used, so the formation of *trans-cis* mixtures could be excluded. DSC was performed by using a DSC-7 (PerkinElmer) and a scanning rate of 10  $\text{K min}^{-1}$ . XRD was done with the  $\text{Cu}_{\text{K}\alpha}$  line ( $\lambda$  = 1.54 Å) by using a standard Coolidge tube source with a Ni filter. Investigations of oriented samples were performed by using a 2D detector (H1-Star, Siemens AG). Uniform orientation was achieved by alignment in a magnetic field ( $B \approx 1$  T) by using thin capillaries. Once achieved, the orientation was maintained by slow cooling ( $0.1 \text{ K min}^{-1}$ ) in the presence of the magnetic field. Electro-optical experiments were carried out by using a home-built electro-optical setup under an applied triangular wave voltage in commercially available indium tin oxide (ITO) coated glass cells (E.H.C., Japan; polyimide (PI) coated for planar alignment, antiparallel rubbing, thickness 6 and 10  $\mu\text{m}$ , and 1  $\text{cm}^2$  measuring area).

#### Acknowledgements

The work was supported by the DFG (grant Ts 39/24-1). M.A. acknowledges the support by the Alexander von Humboldt Foundation for the research fellowship at Martin Luther University Halle-Wittenberg, Germany.

## Conflict of interest

The authors declare no conflict of interest.

**Keywords:** azo compounds · ferroelectricity · fluorine · liquid crystals · mirror-symmetry breaking

- [1] A. Zielinska, M. Leonowicz, H. Li, T. Nakanishi, *Curr. Opin. Coll. Interf. Sci.* **2014**, *19*, 131–139.
- [2] C. Tschierske, *Angew. Chem. Int. Ed.* **2013**, *52*, 8828–8878; *Angew. Chem.* **2013**, *125*, 8992–9047.
- [3] *Handbook of Liquid Crystals* (Eds.: J. W. Goodby, P. J. Collings, T. Kato, C. Tschierske, H. F. Gleeson, P. Raynes), 2nd ed., Wiley-VCH, Weinheim **2014**.
- [4] a) S. Yang, Y. Liu, H. Tan, C. Wu, Z. Wu, G. Shena, R. Yua, *Chem. Commun.* **2012**, *48*, 2861–2863; b) T. Kato, N. Mizoshita, K. Kishimoto, *Angew. Chem. Int. Ed.* **2006**, *45*, 38–68; *Angew. Chem.* **2006**, *118*, 44–74; c) S. Kumar, *Chem. Soc. Rev.* **2006**, *35*, 83–109; d) E.-K. Fleischmann, R. Zentel, *Angew. Chem. Int. Ed.* **2013**, *52*, 8810–8827; *Angew. Chem.* **2013**, *125*, 8972–8991.
- [5] a) I. Tahar-Djebbar, F. Nekelson, B. Heinrich, B. Donnio, D. Guillon, D. Kreher, F. Mathevet, A. J. Attias, *Chem. Mater.* **2011**, *23*, 4653–4656; b) T. Donaldson, P. A. Henderson, M. F. Achard, C. T. Imrie, *J. Mater. Chem.* **2011**, *21*, 10935–10941; c) O. Yaroshchuk, Y. Reznikov, *J. Mater. Chem.* **2012**, *22*, 286–300.
- [6] a) G. C. Kuang, X. R. Jia, M. J. Teng, E. Q. Chen, W. S. Li, Y. Ji, *Chem. Mater.* **2012**, *24*, 71–80; b) J. Vergara, N. Gimeno, M. Cano, J. Barber, P. Romero, J. L. Serrano, M. B. Ros, *Chem. Mater.* **2011**, *23*, 4931–4940.
- [7] J. F. Stoddart, *Nat. Chem.* **2009**, *1*, 14–15.
- [8] a) A. S. Tayi, A. K. Shveyd, A. C.-H. Sue, J. M. Szarko, B. S. Rolczynski, D. Cao, T. J. Kennedy, A. A. Sarjeant, C. L. Stern, W. F. Paxton, W. Wu, S. K. Dey, A. C. Fahrenbach, J. R. Guest, H. Mohseni, L. X. Chen, K. L. Wang, J. F. Stoddart, S. I. Stupp, *Nature* **2012**, *488*, 485–489; b) A. S. Tayi, A. Kaeser, M. Matsumoto, T. Aida, S. I. Stupp, *Nat. Chem.* **2015**, *7*, 281–294.
- [9] a) S. T. Lagerwall, *Ferroelectric and Antiferroelectric Liquid Crystals*, Wiley-VCH, Weinheim, **1999**; b) H.-S. Kitzerow, C. Bahr, *Chirality in Liquid Crystals*, Springer, New York, **2001**.
- [10] D. Miyajima, F. Araoka, H. Takezoe, J. Kim, K. Kato, M. Takata, T. Aida, *Science* **2012**, *336*, 209–213.
- [11] T. Niori, J. Sekine, J. Watanabe, T. Furukawa, H. Takezoe, *J. Mater. Chem.* **1996**, *6*, 1231–1233.
- [12] D. Shen, A. Pegenau, S. Diele, I. Wirth, C. Tschierske, *J. Am. Chem. Soc.* **2000**, *122*, 1593–1601.
- [13] a) G. Pelzl, S. Diele, W. Weissflog, *Adv. Mater.* **1999**, *11*, 707–724; b) R. A. Reddy, C. Tschierske, *J. Mater. Chem.* **2006**, *16*, 907–961; c) H. Takezoe, Y. Takanishi, *Jpn. J. Appl. Phys.* **2006**, *45*, 597; d) A. Eremin, A. Jákli, *Soft Matter* **2013**, *9*, 615–637.
- [14] D. R. Link, G. Natale, R. Shao, J. E. MacLennan, N. A. Clark, E. Körblova, D. M. Walba, *Science* **1997**, *278*, 1924–1927.
- [15] a) T. M. Shaw, S. Trolrier-McKinstry, P. C. McIntyre, *Annu. Rev. Mater. Sci.* **2000**, *30*, 263–298; b) R. Waser, O. Lohse, *Integr. Ferroelectr.* **1998**, *21*, 27; c) J.-H. Park, Y. Kim, *J. Korean Phys. Soc.* **1998**, *32*, 967–969.
- [16] a) G. Pelzl, W. Weissflog, in *Thermotropic Liquid Crystals: Recent Advances* (Ed.: A. Ramamoorthy), Springer, The Netherlands, **2007**, pp. 1–58; b) W. Weissflog, H. N. S. Murthy, S. Diele, G. Pelzl, *Phil. Trans. Royal Soc. A* **2006**, *364*, 2657–2679.
- [17] J. P. F. Lagerwall, F. Giesselmann, M. D. Wand, D. M. Walba, *Chem. Mater.* **2004**, *16*, 3606–3615.
- [18] Y. P. Panarin, M. Nagaraj, S. Sreenilayam, J. K. Vij, A. Lehmann, C. Tschierske, *Phys. Rev. Lett.* **2011**, *107*, 247801.
- [19] M. Alaasar, M. Prehm, M. Poppe, M. Nagaraj, J. K. Vij, C. Tschierske, *Soft Matter* **2014**, *10*, 5003–5016.
- [20] S. P. Sreenilayam, Y. P. Panarin, J. K. Vij, V. P. Panov, A. Lehmann, M. Poppe, M. Prehm, C. Tschierske, *Nat. Commun.* **2016**, *7*, 11369, DOI: 10.1038/ncomms11369.
- [21] F. C. Yu, L. J. Yu, *Chem. Mater.* **2006**, *18*, 5410–5420.
- [22] A. Eremin, S. Stern, R. Stannarius, *Phys. Rev. Lett.* **2008**, *101*, 247802.
- [23] a) P. Sathyanarayana, S. Radhika, B. K. Sadashiva, S. Dhara, *Soft Matter* **2012**, *8*, 2322–2327; b) D. Malkar, B. K. Sadashiva, A. Roy, *Soft Matter* **2016**, *12*, 4960–4966.
- [24] M. Horčić, V. Kozmík, J. Svoboda, V. Novotná, D. Pocięcha, *J. Mater. Chem. A* **2013**, *1*, 7560–7567.
- [25] R. K. Nath, R. Deb, N. Chakraborty, G. Mohiuddin, D. S. S. Raob, N. V. S. Rao, *J. Mater. Chem. A* **2013**, *1*, 13439.
- [26] W. Weissflog, U. Baumeister, M. G. Tamba, G. Pelzl, H. Kresse, R. Friedemann, G. Hempel, R. Kurz, M. Roos, K. Merzweiler, A. Jákli, C. Zhang, N. Diorio, R. Stannarius, A. Eremin, U. Korneke, *Soft Matter* **2012**, *8*, 2671–2685.
- [27] a) I. Wirth, S. Diele, A. Eremin, G. Pelzl, S. Grande, L. Kovalenko, N. Panchenko, W. Weissflog, *J. Mater. Chem.* **2001**, *11*, 1642–1650; b) L. Kovalenko, M. W. Schröder, R. A. Reddy, S. Diele, G. Pelzl, W. Weissflog, *Liq. Cryst.* **2005**, *32*, 857–865.
- [28] C. Keith, A. Lehmann, U. Baumeister, M. Prehm, C. Tschierske, *Soft Matter* **2010**, *6*, 1704–1721.
- [29] A. Eremin, M. Floegel, U. Kornek, S. Stern, R. Stannarius, H. Nadasi, W. Weissflog, C. Zhu, Y. Shen, C. S. Park, J. MacLennan, N. Clark, *Phys. Rev. E* **2012**, *86*, 051701.
- [30] H. M. D. Bandara, S. C. Burdette, *Chem. Soc. Rev.* **2012**, *41*, 1809–1825.
- [31] M. Alaasar, *Liq. Cryst.* **2016**, *43*, 2208–2243.
- [32] a) M. Alaasar, M. Prehm, M. Nagaraj, J. K. Vij, C. Tschierske, *Adv. Mater.* **2013**, *25*, 2186–2191; b) M. Alaasar, M. Prehm, K. May, A. Eremin, C. Tschierske, *Adv. Funct. Mater.* **2014**, *24*, 1703–1717; c) M. Alaasar, M. Prehm, C. Tschierske, *Chem. Eur. J.* **2016**, *22*, 6583–6597; d) M. Alaasar, M. Prehm, C. Tschierske, *Chem. Commun.* **2013**, *49*, 11062–11064.
- [33] C. Tschierske, *Top. Curr. Chem.* **2011**, *318*, 1–108.
- [34] a) M. Hird, *Chem. Soc. Rev.* **2007**, *36*, 2070–2095; b) F. Guittard, E. Taffin de Givenchy, S. Geribaldi, A. Cambon, *J. Fluorine Chem.* **1999**, *100*, 85–96; c) J. W. Goodby, I. M. Saez, S. J. Cowling, J. S. Gasowska, R. A. MacDonald, S. Sia, P. Watson, K. J. Toyne, M. Hird, R. A. Lewis, S. E. Lee, V. Vaschenko, *Liq. Cryst.* **2009**, *36*, 567–605.
- [35] M. Bremer, P. Kirsch, M. Klasen-Memmer, K. Tarumi, *Angew. Chem. Int. Ed.* **2013**, *52*, 8880–8896; *Angew. Chem.* **2013**, *125*, 9048–9065.
- [36] a) J. P. Bedel, J. C. Rouillon, J. P. Marcerou, M. Laguerre, H. T. Nguyen, M. F. Achard, *J. Mater. Chem.* **2002**, *12*, 2214–2220; b) R. A. Reddy, B. K. Sadashiva, *J. Mater. Chem.* **2002**, *12*, 2627–2632; c) H. N. Shreenivasa Murthy, B. K. Sadashiva, *Liqu. Cryst.* **2004**, *31*, 1337–1346; d) G. Dantlgraber, D. Shen, S. Diele, C. Tschierske, *Chem. Mater.* **2002**, *14*, 1149–1158; e) C. V. Yelamaggad, I. Swamy Shashikala, U. S. Hiremath, G. Liao, A. Jakli, D. S. Shankar Rao, S. Krishna Prasad, Q. Li, *Soft Matter* **2006**, *2*, 785–792; f) K. M. Fergusson, M. Hird, *J. Mater. Chem.* **2010**, *20*, 3069–3078.
- [37] M. Alaasar, M. Prehm, M.-G. Tamba, N. Sebastian, A. Eremin, C. Tschierske, *ChemPhysChem* **2016**, *17*, 278–287.
- [38] a) M. Alaasar, M. Prehm, Y. Cao, F. Liu, C. Tschierske, *Angew. Chem. Int. Ed.* **2016**, *55*, 312–316; *Angew. Chem.* **2016**, *128*, 320–324; b) M. Alaasar, M. Prehm, M. Brautzsch, C. Tschierske, *J. Mater. Chem. C* **2014**, *2*, 5487–5501; c) M. Alaasar, M. Prehm, C. Tschierske, *RSC Adv.* **2016**, *6*, 82890–82899.
- [39] N. Vaupotic, J. Szydłowska, M. Salamonczyk, A. Kovarova, J. Svoboda, M. Osipov, D. Pocięcha, E. Gorecka, *Phys. Rev. E* **2009**, *80*, 030701(R).
- [40] C. Tschierske, D. J. Photinos, *J. Mater. Chem.* **2010**, *20*, 4263–4294.
- [41] a) A. De Vries, *J. Chem. Phys.* **1979**, *71*, 25–31; b) S. T. Lagerwall, P. Rudquist, F. Giesselmann, *Mol. Cryst. Liq. Cryst.* **2009**, *510*, 148–157; c) for a review see J. P. F. Lagerwall, F. Giesselmann, *ChemPhysChem* **2006**, *7*, 20–45.
- [42] a) D. Pocięcha, M. Cepic, E. Gorecka, J. Mieczkowski, *Phys. Rev. Lett.* **2003**, *91*, 185501; b) Y. Shimbo, E. Gorecka, D. Pocięcha, F. Araoka, M. Goto, Y. Takanishi, K. Ishikawa, J. Mieczkowski, K. Gomola, H. Takezoe, *Phys. Rev. Lett.* **2006**, *97*, 113901; c) K. Gomola, L. Guo, S. Dhara, Y. Shimbo, E. Gorecka, D. Pocięcha, J. Mieczkowski, H. Takezoe, *J. Mater. Chem.* **2009**, *19*, 4240–4247; d) L. Guo, K. Gomola, E. Gorecka, D. Pocięcha, S. Dhara, F. Araoka, K. Ishikawa, H. Takezoe, *Soft Matter* **2011**, *7*, 2895–2899.
- [43] C. Keith, M. Prehm, Y. P. Panarin, J. K. Vij, C. Tschierske, *Chem. Commun.* **2010**, *46*, 3702–3704.
- [44] M. Gupta, S. Datta, S. Radhika, B. K. Sadashiva, A. Roy, *Soft Matter* **2011**, *7*, 4735–4741.

- [45] H. Ocak, M. Poppe, B. Bilgin-Eran, G. Karanlık, M. Prehm, C. Tschierske, *Soft Matter* **2016**, *12*, 7405–7422.
- [46] H. N. Shreenivasa Murthy, M. Bodyagin, S. Diele, U. Baumeister, G. Pelzl, W. Weissflog, *J. Mater. Chem.* **2006**, *16*, 1634–1643.
- [47] K. Gomola, L. Guo, D. Pocięcha, F. Araoka, K. Ishikawa, H. Takezoe, *J. Mater. Chem.* **2010**, *20*, 7944–7952.
- [48] Previously, a SmAP<sub>A</sub> domain structure was proposed for this phase and the temperature-dependent SmAP<sub>R</sub>–SmAP<sub>AR</sub> phase sequence was inverted; see reference [47].
- [49] N. Sebastian, S. Belau, A. Eremin, M. Alaasar, M. Prehm, C. Tschierske, *Phys. Chem. Chem. Phys.* **2017**, *19*, 5895–5905.
- [50] In reference [32b] the SmC<sub>S</sub>P<sub>AR</sub> phase of related nonfluorinated compounds was designated as SmC<sub>S</sub>P<sub>S</sub> based on preliminary investigations in FS films, which indicated the presence of large SmC<sub>S</sub>P<sub>S</sub> domains. In reference [37] the same phase was reported for **3F20** and this phase was renamed SmC<sub>S</sub>P<sub>AR</sub> based on the dielectric investigations and given the presence of two polarization current peaks in each half-cycle of the applied triangular voltage.
- [51] a) A. Eremin, H. Nadasi, G. Pelzl, S. Diele, H. Kresse, W. Weissflog, S. Grande, *Phys. Chem. Chem. Phys.* **2004**, *6*, 1290–1298; b) D. Pocięcha, E. Gorecka, M. Cepic, N. Vaupotic, K. Gomola, J. Mieczkowski, *Phys. Rev. E* **2005**, *72*, 060701(R); c) D. Pocięcha, E. Gorecka, M. Cepic, N. Vaupotic, W. Weissflog, *Phys. Rev. E* **2006**, *74*, 021702.
- [52] a) C. Dressel, T. Reppe, M. Prehm, M. Brautzsch, C. Tschierske, *Nat. Chem.* **2014**, *6*, 971–977; b) C. Tschierske, G. Ungar, *ChemPhysChem* **2016**, *17*, 9–26.
- [53] M. Alaasar, M. Prehm, M. Brautzsch, C. Tschierske, *Soft Matter* **2014**, *10*, 7285–7296.
- [54] An inversion of the dark extinctions was observed because some polar order was retained at 0 V, most probably in the surface layers, which then acted as command layers that determined the tilt direction in the bulk sample (Figure 7 n–q).
- [55] a) J. Szydłowska, J. Mieczkowski, J. Matraszek, D. W. Bruce, E. Gorecka, D. Pocięcha, D. Guillon, *Phys. Rev. E* **2003**, *67*, 031702; b) C. Keith, R. A. Reddy, U. Baumeister, C. Tschierske, *J. Am. Chem. Soc.* **2004**, *126*, 14312–14313; c) M. Nakata, R. F. Shao, J. E. MacLennan, W. Weissflog, N. A. Clark, *Phys. Rev. Lett.* **2006**, *96*, 067802.
- [56] a) C. Keith, R. A. Reddy, A. Hauser, U. Baumeister, C. Tschierske, *J. Am. Chem. Soc.* **2006**, *128*, 3051–3066; b) C. Keith, R. A. Reddy, M. Prehm, U. Baumeister, H. Kresse, J. L. Chao, H. Hahn, H. Lang, C. Tschierske, *Chem. Eur. J.* **2007**, *13*, 2556–2577.
- [57] Y. Zhang, U. Baumeister, C. Tschierske, M. O’Callaghan, C. Walker, *Chem. Mater.* **2010**, *22*, 2869–2884.
- [58] G. Dantlgraber, A. Eremin, S. Diele, A. Hauser, H. Kresse, G. Pelzl, C. Tschierske, *Angew. Chem. Int. Ed.* **2002**, *41*, 2408–2412; *Angew. Chem.* **2002**, *114*, 2514–2518.
- [59] E. Westphal, H. Gallerdo, G. F. Caramori, N. Sebastian, M.-G. Tamba, A. Eremin, S. Kawauchi, M. Prehm, C. Tschierske, *Chem. Eur. J.* **2016**, *22*, 8181–8197.
- [60] R. A. Reddy, C. Zhu, R. Shao, E. Korblova, T. Gong, Y. Shen, E. Garcia, M. A. Glaser, J. E. MacLennan, D. M. Walba, N. A. Clark, *Science* **2011**, *332*, 72–77.
- [61] a) C. Tschierske, *J. Mater. Chem.* **1998**, *8*, 1485–1508; b) C. Tschierske, *Isr. J. Chem.* **2012**, *52*, 935–959.
- [62] a) C. A. Hunter, J. K. M. Sanders, *J. Am. Chem. Soc.* **1990**, *112*, 5525–5534; b) C. R. Martinez, B. L. Iverson, *Chem. Sci.* **2012**, *3*, 2191–2201.
- [63] A. Immirzi, B. Perini, *Acta Crystallogr. Sect. A* **1977**, *33*, 216–218.

---

 Manuscript received: December 27, 2016

Accepted Article published: February 13, 2017

Final Article published: March 28, 2017

## Liquid Crystals

## Polar Order, Mirror Symmetry Breaking, and Photoswitching of Chirality and Polarity in Functional Bent-Core Mesogens

Mohamed Alaasar,<sup>\*,[a, b]</sup> Marko Prehm,<sup>[a]</sup> Sebastian Belau,<sup>[c]</sup> Nerea Sebastián,<sup>[c]</sup> Marharyta Kurachkina,<sup>[c]</sup> Alexey Eremin,<sup>\*,[c]</sup> Changlong Chen,<sup>[d]</sup> Feng Liu,<sup>[d]</sup> and Carsten Tschierske<sup>\*,[a]</sup>

**Abstract:** In recent years, liquid crystals (LCs) responding to light or electrical fields have gained significant importance as multifunctional materials. Herein, two new series of photoswitchable bent-core liquid crystals (BCLCs) derived from 4-cyanoresorcinol as the central core connected to an azobenzene based wing and a phenyl benzoate wing are reported. The self-assembly of these molecules was characterized by differential scanning calorimetry (DSC), polarizing light microscopy (POM), electro-optical, dielectric, second harmonic generation (SHG) studies, and XRD. Depending on the direction of the COO group in the phenyl benzoate wing, core-fluorination, temperature, and the terminal alkyl chain length, cybotactic nematic and lamellar (smectic) LC phases were observed. The coherence length of the ferroelectric fluctuations increases continuously with decreasing

temperature and adopts antipolar correlation upon the condensation into superparaelectric states of the paraelectric smectic phases. Finally, long-range polar order develops at distinct phase transitions; first leading to polarization modulated and then to nonmodulated antiferroelectric smectic phases. Conglomerates of chiral domains were observed in the high permittivity ranges of the synclitic tilted paraelectric smectic phases of these achiral molecules, indicating mirror symmetry breaking. Fine-tuning of the molecular structure leads to photoresponsive bent-core (BC)LCs exhibiting a fast and reversible photoinduced change of the mode of the switching between ferroelectric- and antiferroelectric-like as well as a light-induced switching between an achiral and a spontaneous mirror-symmetry-broken LC phase.

## 1. Introduction

Liquid crystals (LC) represent an important class of functional materials for numerous applications, ranging from materials for displays,<sup>[1,2]</sup> photovoltaics,<sup>[3]</sup> photonics,<sup>[4]</sup> soft nanolithography,<sup>[5]</sup> for ion carriers,<sup>[6]</sup> biosensors,<sup>[7]</sup> and as membrane-forming materials<sup>[8]</sup> to mention only a few.<sup>[9–11]</sup> Therefore, the design of new compounds and especially understanding of the relationship between the molecular structure and the liquid crystallinity as well as application properties are of fundamental inter-


est.<sup>[12]</sup> One of the relevant application related properties is polar order. Polar order in the fluid state requires a reduction of the phase symmetry, which is usually achieved by the permanent chirality of the involved molecules.<sup>[13–15]</sup> The discovery of polar order and mirror-symmetry-broken chiral mesophases formed by bent-core liquid crystals (BCLCs)<sup>[16–22]</sup> opened the door to polar LCs formed by achiral molecules. In lamellar LC phases, the reduction of the phase symmetry results from the combination of tilt and restricted rotation around the molecular long axis.<sup>[16,23]</sup> As a result of polar order and transient molecular chirality, spontaneous mirror symmetry breaking and chiral conglomerate formation<sup>[21,24–26]</sup> was observed in different types of mesophases formed by BCLCs such as helical nano-filament ( $B_4$ ) phases<sup>[27–30]</sup> and related soft crystalline phases,<sup>[31]</sup> sponge-like dark conglomerate phases (DC phases),<sup>[21,32–35]</sup> and more recently the twist bend nematic ( $N_{TB}$ ) phases.<sup>[36]</sup> Chiral conglomerate formation was also observed in paraelectric SmC phases<sup>[37,38]</sup> and nematic phases of bent-core mesogens,<sup>[39,40]</sup> which initiated the search for spontaneous mirror symmetry breaking in other LC systems.<sup>[24,26,41,42]</sup> Overall, BCLCs lead to new types of molecular self-assembly and have significantly contributed to the field of supramolecular stereochemistry. One of the contemporary challenges concerns the switching of their polar order and chirality by light, and for this purpose photoswitchable BCLCs are required.

[a] Dr. M. Alaasar, Dr. M. Prehm, Prof. Dr. C. Tschierske  
Institute of Chemistry, Martin Luther University Halle-Wittenberg  
Kurt Mothes Str. 2, 06120 Halle (Saale) (Germany)  
E-mail: carsten.tschierske@chemie.uni-halle.de

[b] Dr. M. Alaasar  
Department of Chemistry, Faculty of Science, Cairo University, Giza (Egypt)  
E-mail: malaasar@sci.cu.edu.eg

[c] Dr. S. Belau, Dr. N. Sebastián, M. Kurachkina, Prof. Dr. A. Eremin  
Department of Nonlinear Phenomena, Institute of Physics  
Otto von Guericke University Magdeburg, Magdeburg (Germany)  
E-mail: alexey.eremin@ovgu.de

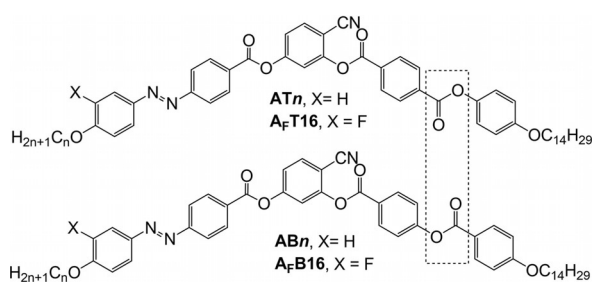
[d] C. Chen, Prof. Dr. F. Liu  
State Key Laboratory for Mechanical Behavior of Materials  
Xi'an Jiaotong University, Xi'an 710049 (P. R. China)

 Supporting information and the ORCID identification number(s) for the author(s) of this article can be found under:  
<https://doi.org/10.1002/chem.201806180>.

Azobenzene-based liquid crystalline materials, exhibiting reversible *trans*–*cis* isomerization upon irradiation with light represent an important class of photoswitchable materials, which can be used for many applications in diverse photodriven devices<sup>[43–49]</sup> and in photonics.<sup>[50]</sup> Therefore, combining the ferroelectric and spontaneously chiral LC phases formed by BCLCs and the photoswitchable nature of the azobenzene units could lead to potential new multifunctional materials in which the polar response can be modified with light.<sup>[51]</sup> For this reason, azobenzene-based BCLCs have attracted the attention of several researchers in recent years.<sup>[52–61]</sup>

Compounds with molecular shapes at the cross-over between linear (rod-like) and bent shapes (BCLCs), such as mesogenic dimers with odd spacers,<sup>[62–69]</sup> hockey stick molecules,<sup>[70–72]</sup> and molecules with reduced length of the bent core<sup>[73]</sup> or with a reduced bending angle<sup>[74]</sup> have received significant attention, because they provide new LC phase structures. 4-Cyanoresorcinol is a very useful bent-core unit with reduced bending angle, which has led to a number of new and unique mesophases,<sup>[37,38,75–82]</sup> for example, the nontilted antiferroelectric SmAP<sub>A</sub> phase<sup>[83]</sup> and a short-pitch heliconical smectic phase designated as SmC<sub>5</sub>P<sub>F</sub><sup>hel</sup>.<sup>[84–86]</sup> In previous work, the 4-cyanoresorcinol core was combined with two identical wings, either azobenzenes or phenyl benzoates,<sup>[37,38,76–86]</sup>

Herein, we report new BCLCs derived from a 4-cyanoresorcinol central core connected to two different rod-like wings, in which one is azobenzene-based (A) and the other is either a benzoylated 4-hydroxybenzoate wing (B) in compounds **ABn** or a phenyl terephthalate wing (T) in compounds **ATn**; these are different in the direction of the COO group between the two outer benzene rings (see Scheme 1). The terminal alkoxy chain at the ester-based wing in both types of compounds was fixed to *m* = 14, whereas that connected to the azobenzene containing side arm has chain lengths *n* = 8, 12, 16, and 20. The effect of a peripheral fluorine substitution at the outer ring of the azobenzene-based wing (A<sub>F</sub>) was investigated for one example from each series (A<sub>F</sub>**B16** and A<sub>F</sub>**T16**). In Section 3.1, we will focus on the series of terephthalate compounds **ATn** and in Sections 3.2 and 3.3 the focus is on the series **ABn** and compound **A<sub>F</sub>B16**, respectively, both involving a 4-hydroxybenzoate core. We will show that on decreasing the temperature for all compounds, a continuous evolution of polar order from apolar or low permittivity paraelectric (N<sub>CyBCr</sub> SmA, SmC) via high permittivity paraelectric (SmC<sup>[\*]</sup>, SmAP<sub>R</sub>



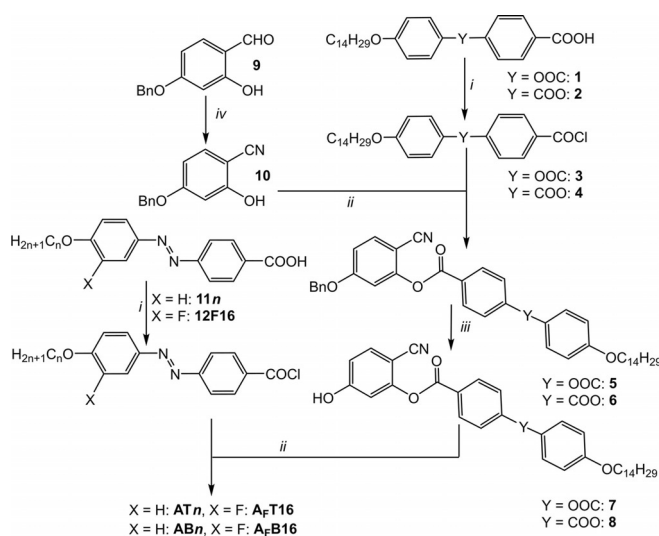
**Scheme 1.** Chemical structures and designation of the bent-core molecules under investigation.

SmC<sub>5</sub>P<sub>R</sub><sup>[\*]</sup>) to superparaelectric (SmC<sub>5</sub>P<sub>AR</sub>, SmC<sub>a</sub>P<sub>AR</sub>) states is followed by distinct phase transitions to polarization modulated (SmC<sub>5</sub>P<sub>A</sub>) and nonmodulated macroscopic polar synclitic smectic phases (SmC<sub>5</sub>P<sub>A</sub>, SmC<sub>5</sub>'P<sub>A</sub>). Although in the SmC range, the structure of the phase, established by X-ray scattering, does not show any significant difference, the electro-optical switching behavior and observation of chiral structures suggest a variety of states distinguished in this temperature region. We designate them tentatively as SmC<sub>5</sub><sup>[\*]</sup>, SmC<sub>5</sub>P<sub>R</sub><sup>[\*]</sup>, and SmC<sub>5</sub>P<sub>AR</sub> ranges and consider them as temperature ranges of one paraelectric SmC<sub>5</sub> phase, which has different polar cluster sizes and hence distinct properties. The ranges of the paraelectric SmC<sub>5</sub> phases are shown in bold in Tables 1 and 2 and indicated in red in the graphics, whereas green is used for all polar phases. Owing to the involved azobenzene unit, all compounds are photoisomerizable, and in Section 3.4 it is shown that they provide new modes of photoinduced switching of BCLCs, namely a fast and reversible photoinduced change of the mode of polar switching, and a photoswitching between spontaneous symmetry-broken chiral and achiral LC states.

## 2. Experimental Section

### 2.1 Synthesis

The target BCLCs **ABn**, **A<sub>F</sub>B16**, **ATn**, and **A<sub>F</sub>T16** were synthesized as shown in Scheme 2. Details of the synthesis of the intermediates and final compounds as well as their analytical data are reported in the Supporting Information (Section S1).



**Scheme 2.** Synthetic route to the bent-core mesogens **ABn**, **A<sub>F</sub>B16**, **ATn**, and **A<sub>F</sub>T16**: i) SOCl<sub>2</sub>, DMF, reflux 1 h;<sup>[77]</sup> ii) Et<sub>3</sub>N, pyridine, CH<sub>2</sub>Cl<sub>2</sub>, reflux, 6 h;<sup>[31a,37,38]</sup> iii) H<sub>2</sub>, 10% Pd/C, THF, stirring, 48 h at 25 °C; iv) 1) H<sub>2</sub>NOH, 2) Ac<sub>2</sub>O, 3) NaOH.

### 2.2 Methods

The thermal behavior of all synthesized materials was studied by polarizing optical microscopy (POM), differential scanning calorimetry (DSC), and by electro-optical investigation under a triangular wave field. All compounds with *n* = 16 were investigated by X-ray diffraction (XRD) by using a synchrotron source; dielectric studies

**Table 1.** Transitions of compounds **AT<sub>n</sub>** and **A<sub>F</sub>T16** on heating (H) and cooling (C).<sup>[a]</sup>

Compd.	X	n	T [°C] [ $\Delta H$ (kJ mol <sup>-1</sup> )]							
<b>AT8</b>	H	8	H: Cr	80 SmC <sub>s</sub> P <sub>A</sub> [42.7]	110 SmC <sub>a</sub> P <sub>AR</sub> [0.2]	115 SmAP <sub>R</sub> [-]	≈ 155 SmA [-]	165 Iso [6.2]		
			C: Iso	164 SmA [7.0]	≈ 154 SmAP <sub>R</sub> [-]	114 SmC <sub>a</sub> P <sub>AR</sub> [-]	109 SmC <sub>s</sub> P <sub>A</sub> [0.2]	82 SmC <sub>s</sub> P <sub>A</sub> [-]	58 Cr [14.7]	
<b>AT12</b>	H	12	H: Cr	82 SmC <sub>s</sub> P <sub>A</sub> [30.0]	111 SmC <sub>s</sub> P <sub>AR</sub> [0.8]	115 SmC <sub>s</sub> <sup>[*]</sup> [-]	145 SmA [-]	164 Iso [7.4]		
			C: Iso	163 SmA [7.6]	144 SmC <sub>s</sub> <sup>[*]</sup> [-]	114 SmC <sub>s</sub> P <sub>AR</sub> [-]	110 SmC <sub>s</sub> P <sub>A</sub> [1.0]	82 SmC <sub>s</sub> P <sub>A</sub> [-]	39 Cr [24.3]	
<b>AT16</b>	H	16	H: Cr	90 SmC <sub>s</sub> P <sub>A</sub> [60.9]	109 SmC <sub>s</sub> P <sub>AR</sub> [0.8]	112 SmC <sub>s</sub> P <sub>R</sub> <sup>[*]</sup> [-]	127 SmC <sub>s</sub> <sup>[*]</sup> [-]	157 SmA [-]	165 Iso [7.4]	
			C: Iso	Iso 163 SmA [7.4]	156 SmC <sub>s</sub> <sup>[*]</sup> [-]	≈ 126 SmC <sub>s</sub> P <sub>R</sub> <sup>[*]</sup> [-]	111 SmC <sub>s</sub> P <sub>AR</sub> [-]	109 SmC <sub>s</sub> P <sub>A</sub> [0.8]	78 SmC <sub>s</sub> P <sub>A</sub> [-]	62 Cr [45.1]
<b>AT20</b>	H	20	H: Cr	93 SmC <sub>s</sub> P <sub>A</sub> [69.2]	103 SmC <sub>s</sub> P <sub>AR</sub> [0.6]	110 SmC <sub>s</sub> P <sub>R</sub> <sup>[*]</sup> [-]	154 SmA [0.2]	162 Iso [7.4]		
			C: Iso	161 SmA [6.3]	154 SmC <sub>s</sub> P <sub>R</sub> <sup>[*]</sup> [0.1]	109 SmC <sub>s</sub> P <sub>AR</sub> [-]	101 SmC <sub>s</sub> P <sub>A</sub> [0.6]	SmC <sub>s</sub> P <sub>A</sub> [-]	63 Cr [32.5]	
<b>A<sub>F</sub>T16</b>	F	16	H: Cr	114 SmC <sub>s</sub> P <sub>A</sub> [27.5]	121 SmC <sub>s</sub> P <sub>AR</sub> [1.3]	127 SmC <sub>s</sub> P <sub>R</sub> <sup>[*]</sup> [-]	152 SmA [-]	166 Iso [7.9]		
			C: Iso	165 SmA [7.4]	152 SmC <sub>s</sub> P <sub>R</sub> <sup>[*]</sup> [-]	127 SmC <sub>s</sub> P <sub>AR</sub> [-]	120 SmC <sub>s</sub> P <sub>A</sub> [1.2]	107 SmC <sub>s</sub> P <sub>A</sub> [-]	100 Cr [26.0]	

[a] Transition temperatures and enthalpy values (in square brackets) were taken from the second DSC scans (10 Kmin<sup>-1</sup>); continuous transitions without detectable DSC peaks were determined by polarizing microscopy or switching experiments under triangular wave fields; abbreviations: Cr = crystalline solid; Iso = isotropic liquid; SmA = uniaxial smectic phase; SmC<sub>s</sub> = synclitic tilted smectic phase (identical tilt direction in adjacent layers); SmC<sub>s</sub><sup>[\*]</sup> modulated SmC<sub>s</sub> phase; SmC<sub>a</sub> = anticlinic tilted smectic phase (tilt direction is opposite in adjacent layers); P<sub>R</sub> = high permittivity paraelectric range showing one broad polarization current peak per half period of an applied E-field; P<sub>AR</sub> = superparaelectric range showing two polarization current peaks per half period of an applied E-field; P<sub>A</sub> = antiferroelectric switching polar phase; phases without extension do not show a measurable polarization current peak; [\*] = LC phase showing a conglomerate of chiral domains in homeotropic alignment; see Figure 9 and Figure S19b (in the Supporting Information) for models of the phase structures. Note that SmC<sub>s</sub><sup>[\*]</sup>, SmC<sub>s</sub>P<sub>R</sub><sup>[\*]</sup>, and SmC<sub>s</sub>P<sub>AR</sub>, shown in bold, do not represent separate phases, but are considered as ranges of one paraelectric SmC<sub>s</sub> phase with continuously growing polar cluster size.

and second harmonic generation (SHG) experiments were performed with compounds **AT16** and **AB16**. The used methods are described in Section S2 in the Supporting Information. The error of the *d*-values in XRD is about 0.02 nm and approximately 3° for the tilt angle; for current response and SHG, the accuracy is about 5%.

### 3. Results and Discussion

#### 3.1. Compounds **AT<sub>n</sub>** with a terephthalate wing

The phase sequences, transition temperatures, and the associated transition enthalpies of compounds **AT<sub>n</sub>** and the fluorinated compound **A<sub>F</sub>T16** (X = F) are collated in Table 1 and shown graphically in Figure 1. The DSC plots for compounds **AT16** and **A<sub>F</sub>T16**, as examples, are shown in Figure 2. Compound **AT16**, as representative example for compounds with *n* ≥ 12, is discussed in the following in more detail.

##### 3.1.1 Investigation of compound **AT16**

#### DSC and optical investigations

As shown in Figure 3a, in planar alignment, a fan texture is observed for **AT16** and at 157 °C the extinction crosses change their orientation from being parallel to slightly inclined with respect to the directions of polarizer and analyzer (Figure 3b). Si-

multaneously, in homeotropic samples, the optical isotropic texture becomes birefringent with development of a Schlieren texture, indicating a transition from SmA to a synclitic tilted SmC<sub>s</sub> phase (see insets in Figure 3a,b), which is not visible in the DSC traces (Figure 2a), and therefore assumed to be second order. On further cooling, the birefringence of the planar samples increases and the Schlieren texture in the homeotropic samples is also changing (see Figure 3b–f and Figure S13 in the Supporting Information). The increase of birefringence in the planar samples at the SmA–SmC transition (Figure 3a,b) suggests a de Vries-type SmA phase composed of tilt direction randomized SmC<sub>s</sub> clusters.<sup>[87]</sup>

#### X-ray scattering

Laboratory XRD results show a diffuse scattering in the wide-angle region and only one sharp Bragg reflection in the small-angle region, corresponding to *d* = 5.1–5.3 nm (Figure 4) in the whole mesomorphic temperature range (Figure S12 in the Supporting Information). This indicates that all phases represent smectic phases without any in-plane positional order. The measured *d*-value is a bit smaller than the single molecule length (*d*/*L*<sub>mol</sub> = 0.76–0.79, with *L*<sub>mol</sub> = 6.7 nm determined for a Λ-shaped conformation with 120° bending angle with all-*trans*

**Table 2.** Transitions of compounds **AB<sub>n</sub>** and **A<sub>F</sub>B16** on heating (H) and cooling (C).<sup>[a]</sup>

Compd.	X	n		T (°C) [ $\Delta H$ (kJ mol <sup>-1</sup> )]						
<b>AB8</b>	H	8	H: Cr	128 Iso						
			C: Iso	127 N <sub>Cybc</sub>	69 SmC <sub>s</sub>	62–40 <sup>[b]</sup> Cr				
<b>AB12</b>	H	12	H: Cr	126 Iso						
			C: Iso	117 N <sub>Cybc</sub>	89 SmC <sub>s</sub>	82 SmC <sub>s</sub> P <sub>AR</sub>	77 SmC <sub>s</sub> P <sub>A</sub>	67 SmC <sub>s</sub> 'P <sub>A</sub> <sup>[c]</sup>		
<b>AB16</b>	H	16	H: Cr	123 Iso						
			C: Iso	123 N <sub>Cybc</sub>	121 SmC <sub>s</sub> P <sub>R</sub> <sup>[*]</sup>	96 SmC <sub>s</sub> P <sub>AR</sub>	80 SmC <sub>s</sub> P <sub>A</sub>	73 SmC <sub>s</sub> 'P <sub>A</sub>	66 SmC <sub>s</sub> P <sub>A</sub>	48 B <sub>5</sub>
<b>AB20</b>	H	20	H: Cr	123 SmC <sub>s</sub> P <sub>R</sub> <sup>[*]</sup>	132 Iso					
			C: Iso	131 SmC <sub>s</sub> P <sub>R</sub> <sup>[*]</sup>	90 SmC <sub>s</sub> P <sub>AR</sub>	75 SmC <sub>s</sub> P <sub>A</sub>	64 M			
<b>A<sub>F</sub>B16</b>	F	16	H: Cr	88 SmC <sub>s</sub> P <sub>AR</sub>	105 SmC <sub>s</sub> P <sub>R</sub> <sup>[*]</sup>	132 Iso				
			C: Iso	131 SmC <sub>s</sub> P <sub>R</sub> <sup>[*]</sup>	104 SmC <sub>s</sub> P <sub>AR</sub>	87 SmC <sub>s</sub> P <sub>A</sub>	84 SmC <sub>s</sub> P <sub>A</sub>	60 Cr		

[a] Transition temperatures and enthalpy values were measured as mentioned in Table 1; abbreviations: N<sub>Cybc</sub> = nematic phase with cybotactic clusters of the SmC-type; SmC<sub>s</sub>P<sub>AR</sub>, SmC<sub>s</sub>P<sub>A</sub> = different types of antiferroelectric switching polar and synclitic tilted SmC<sub>s</sub> phase; B<sub>5</sub> = hexatic SmC<sub>s</sub>P<sub>A</sub> phase, and M = unknown (soft) crystalline phase,<sup>[103]</sup> for other phase assignments, see Table 1. [b] Broad transition, see Figure S30 (in the Supporting Information) for DSC. [c] No crystallization is observed on further cooling, only the viscosity increases. [d] Enthalpy involves the transitions in the M/Cr phase region, for DSC, see Figure S37 (in the Supporting Information).

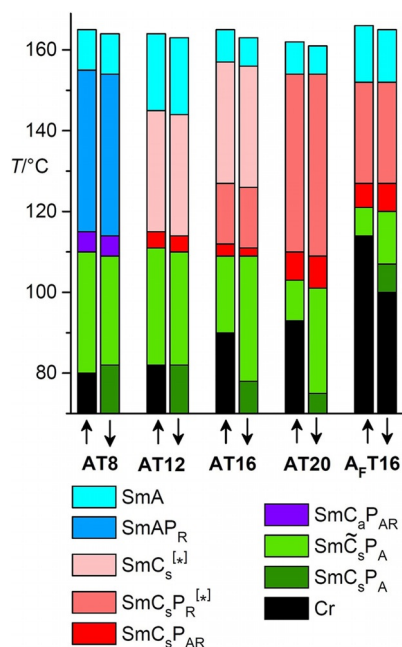


**Figure 1.** Graphical comparison of the phases and transition temperatures of the investigated compounds **AT<sub>n</sub>** and **A<sub>F</sub>T16** on heating (↑) and cooling (↓). For abbreviations of the phase structures, see Table 1. Color code: blue = SmA phases; red = paraelectric SmC ranges, and green = polar SmC phases. See Figure 9 and Figure S19b (in the Supporting Information) for models of the phase structures.

stretched alkyl chains, see Figure S11 in the Supporting Information), in line with a tilted organization of the molecules in all smectic phases (uniform tilt in SmC<sub>s</sub> or randomized tilt in SmA) with single-layer structure and conformationally disordered alkyl chains. The tilted organization of the molecules is confirmed by the 2D diffraction patterns of aligned samples. In the SmA phase range, the maxima of the diffuse scattering in the wide-angle region are perpendicular to the position of the layer reflection (see Figure 4a), whereas after the transition to the synclitic SmC<sub>s</sub> phase at  $T = 157^\circ\text{C}$ , a clear deviation from the orthogonal position of about  $20^\circ$  can be observed (Figure 4b), although the change in the  $d$ -value is small (Figure 4c).

The development of the tilt angle depending on temperature, as estimated from the 2D XRD pattern (position of the diffuse wide-angle scattering (WAXS) maxima with respect to the layer reflections), shows an almost continuous growth of the tilt with decreasing temperature from  $16^\circ$  at  $T = 150^\circ\text{C}$  in the SmC<sub>s</sub> phase to  $24^\circ$  at  $80^\circ\text{C}$ , just before the transition to the SmC<sub>s</sub>P<sub>A</sub> phase (Figure 4d). Remarkably, the  $d$ -values rises with decreasing temperature (Figure 4c), which is the opposite tendency as would be expected for a growing tilt with lowering temperature (Figure 4d). Therefore, we conclude that the effect of growing packing density (growing polar order), leading to stretching of the alkyl chains, is larger than the inverse effect of growing tilt on  $d$ . The growing packing density is in line with the decreasing  $d$ -value of the WAXS from 0.48 nm in



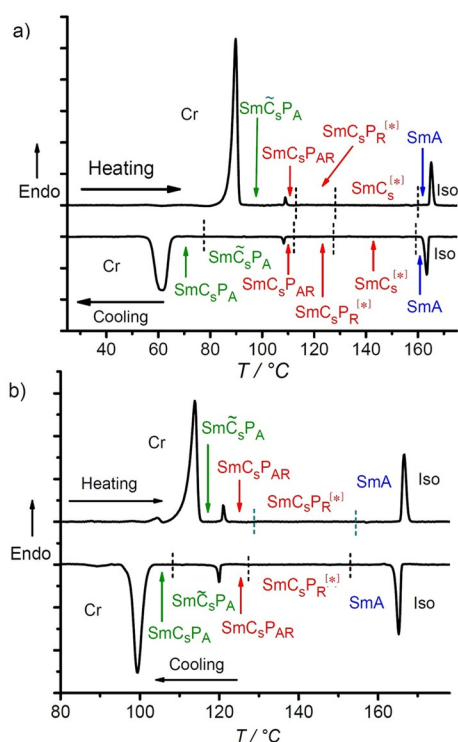


**Figure 2.** DSC heating and cooling traces at a rate of  $10 \text{ K min}^{-1}$  for a) compound **AT16** and b) compound **A<sub>7</sub>T16**. Dotted lines indicate continuous transitions without visible DSC peaks. In this and the following figures, green indicates macroscopic polar phases whereas red stands for paraelectric phase ranges.

the SmA phase to 0.45 nm in the  $\text{Sm}\tilde{\text{C}}_s\text{P}_A$  phase (Figure 5 c). This means that for BCLCs, the  $d$ -values of the layer reflection alone cannot be used as a reliable indication of tilt.

Investigation of **AT16** by high-resolution synchrotron X-ray powder diffraction experiments shows a splitting of the small-angle scattering into two close reflections with different intensities, indicating a layer modulation. Although this is only observed between  $93^\circ\text{C}$  and  $80^\circ\text{C}$  (Figure 5 a and Figure S13 a in the Supporting Information), we assume that there is layer modulation in the whole temperature range between the transitions at  $109^\circ\text{C}$  and  $75^\circ\text{C}$ , albeit with a shorter correlation length. This is in line with textural observations of homeotropic samples on cooling, where the Schlieren texture becomes mosaic-like at  $109^\circ\text{C}$  and turns back to a Schlieren texture around the transition at  $T=78^\circ\text{C}$  (see Figure 3 d  $\rightarrow$  e  $\rightarrow$  f and Figure S14 f  $\rightarrow$  g in the Supporting Information); in planar samples, no clear textural changes can be observed. Although assignment to a specific lattice is not possible with only two reflections,<sup>[88]</sup> XRD patterns with only the (11) and (20) reflections of a rectangular lattice are typical for the  $B_1$ -type columnar phases of BCLCs composed of ribbons shifted out of the layer plane, that is, along direction  $a$  (Figure 5 c).<sup>[89]</sup> Although the textures are quite distinct from the typical textures of the  $B_1$  phases,<sup>[17,21]</sup> a tentative assignment of the diffraction pattern to the (11) and (20) reflections of a  $c2mm$  lattice leads to parameters  $a=10.74 \text{ nm}$  and  $b=6.98 \text{ nm}$ . The parameter  $a$  corresponds well to about twice the layer distance and  $b$  corre-

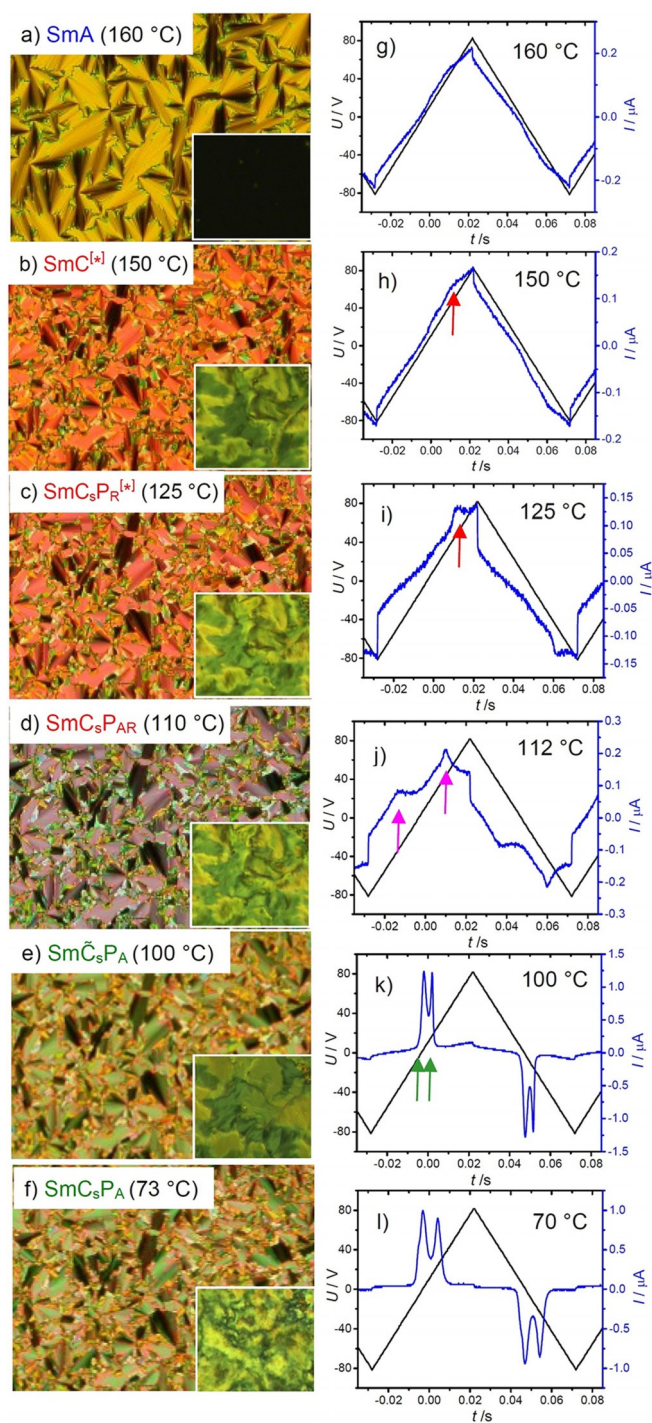


**Figure 3.** Investigation of compound **AT16**: a–f) Optical textures as observed by polarizing microscopy between crossed polarizers (polarizer and analyzer are horizontal and vertical, respectively) in a planar cell ( $6 \mu\text{m}$  PI-coated ITO cell) in the different phases and phase ranges at the given temperatures. The insets show the corresponding textures in a homeotropic cell (for enlarged textures, see Figure S14 in the Supporting Information). g–l) Switching current response curves on applying a triangular wave field ( $27 \text{ V}_{\text{pp}} \mu\text{m}^{-1}$ ,  $10 \text{ Hz}$ ,  $6 \mu\text{m}$  PI-coated ITO cell) in the distinct phases at the given temperatures (for additional switching current curves, see Figure S15 in the Supporting Information).

sponds to about 7–8 molecules organized in the lateral cross section of each ribbon, which is a reasonable number, too. As

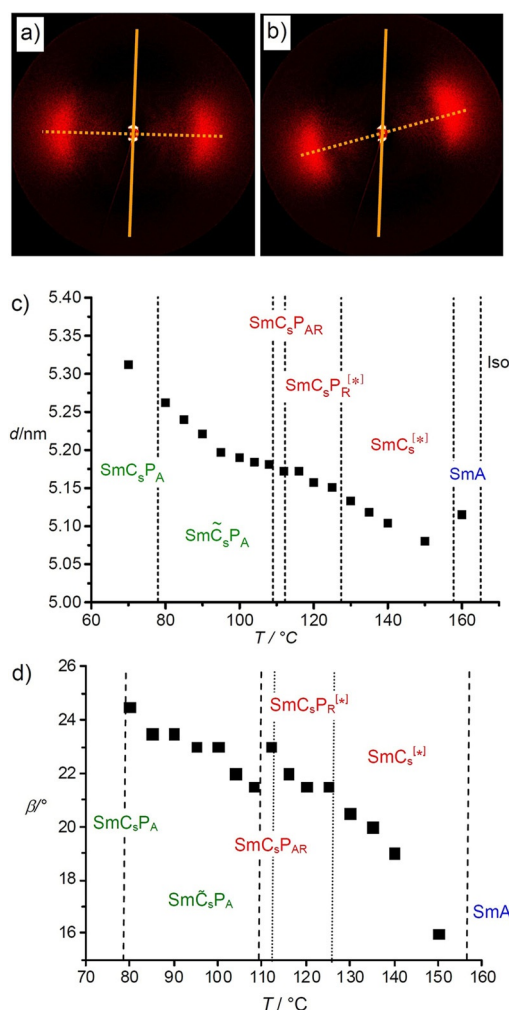


**Figure 4.** XRD of an aligned sample of compound AT16. a) 2D pattern in the SmA phase at 160 °C and b) in the SmC<sub>s</sub> phase at 150 °C, after subtraction of the scattering in the isotropic liquid state at 170 °C (for additional XRD patterns, see Figure S12 in the Supporting Information). c) Temperature dependence of the *d*-spacing (see also Table S1 in the Supporting Information) and d) dependence of tilt on temperature (estimated from the position of the WAXS maxima with respect to the layer reflection).

shown in the electron density (ED) map in Figure 5b, a weakly modulated lamellar phase composed of layers formed by ribbons with high ED (blue/purple) and connected by defects with reduced ED (green), both formed by the aromatic cores having different packing density, is separated by wavy deformed low ED layers of the alkyl chains (red). This structure is distinct from the classical models of B<sub>1</sub>-type columnar phases of BCLCs (Figure 5c),<sup>[17]</sup> because the shift of the ribbons occurs in the layer plane between the layers, that is, along *b* instead of along *a*. In this respect, it is similar to the B<sub>1rev</sub>/B<sub>1rev,tilt</sub> phases having modulated layers (Figure 5d).<sup>[89]</sup> However, a different diffraction pattern with more reflections and different positions would be expected for this structure.<sup>[17,19,21,22,89]</sup> Based on the diffraction pattern and textures and considering the position of these columnar phases at the transition from paraelectric to polar smectic phases, this phase is not designated as B<sub>1</sub>, but more generally as a modulated SmC<sub>s</sub> phase. The modulation is

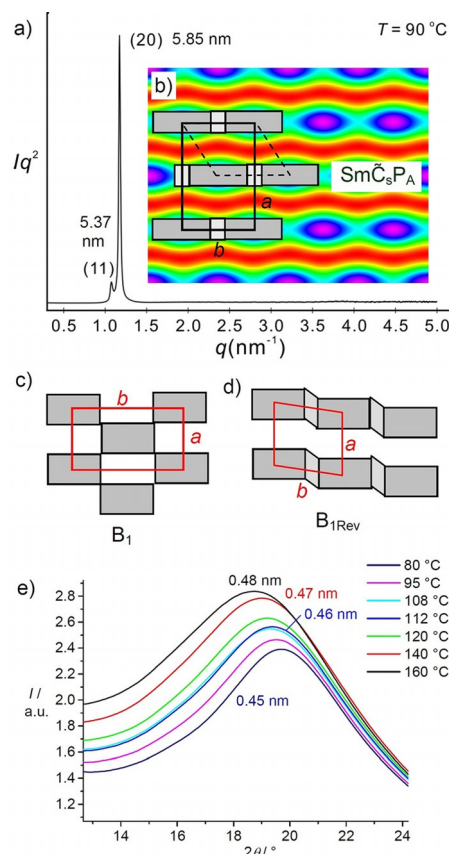


**Figure 5.** a) SAXS diffractogram (synchrotron source) of compound AT16 in the SmC<sub>s</sub>P<sub>A</sub> phase at 90 °C (see Figure S13a in the Supporting Information for a complete temperature scan) with b) reconstructed electron density (ED) map based on the assumed *c2mm* lattice (purple/blue = high ED, aromatics; red = low ED, alkyl chains) showing the proposed organization of the molecules. The gray rectangles indicate the positions of the densely packed aromatic cores (dark gray) and regions with reduced core packing density (light gray), the direction of tilt could be perpendicular to the lattice or in the plane of the lattice. In the latter case, the symmetry would be reduced to *p2* (dashed rhomboid); the alkyl chains are organized in wavy deformed layers (red). c, d) Related models of the B<sub>1</sub>-type phases of BCLCs<sup>[89]</sup> and e) WAXS patterns depending on temperature.

most likely caused by a splay of the developing polarization (see next sections), leading to a periodic polarization-splay state comparable to the B<sub>7</sub> phases.<sup>[88,90–92]</sup>

### Electro-optical studies

Under an applied triangular wave voltage with 27 V<sub>pp</sub> μm<sup>-1</sup> (Figure 3g–l), a broad polarization peak starts to appear at 127 °C (Figure 3i and Figure S15a in the Supporting Information) and continuously increases in intensity with cooling in the SmC<sub>s</sub>P<sub>R</sub><sup>[\*]</sup> range. The current peak asymptotically rises just before the transition to the SmC<sub>s</sub>P<sub>AR</sub> range at 112 °C, indicating polar clusters increasing in size with increasing E-field strength and lowering temperature. No transition enthalpies can be detected for the SmC<sub>s</sub>P<sub>R</sub><sup>[\*]</sup> ↔ SmC<sub>s</sub>P<sub>R</sub><sup>[\*]</sup> and SmC<sub>s</sub>P<sub>R</sub><sup>[\*]</sup> ↔ SmC<sub>s</sub>P<sub>AR</sub> transitions, neither on heating nor on cooling, indicating continuous changes (Figure 2a). The continuous SmC<sub>s</sub>P<sub>R</sub><sup>[\*]</sup> ↔ SmC<sub>s</sub>P<sub>R</sub><sup>[\*]</sup> transition can only be deduced from second harmonic generation

(SHG) investigations (see below) whereas the  $\text{SmC}_5\text{P}_R^{[*]} \rightarrow \text{SmC}_5\text{P}_{AR}$  transition at  $T = 112^\circ\text{C}$  is evident from the change of the shape of the polarization current response curves. At this temperature, two broad polarization peaks start to develop (Figure 3j) and Figure S15b in the Supporting Information), which upon further lowering of the temperature increase in size; these replace the single peak and come closer together (Figure 3i  $\rightarrow$  j, see also Figure S15c in the Supporting Information).<sup>[37,38]</sup>

The phase transition at  $T = 109^\circ\text{C}$  is associated with a small transition enthalpy of approximately  $0.6\text{--}0.8\text{ kJ mol}^{-1}$  (Table 1) and leads to two strong and relatively sharp polarization current peaks in the  $\text{Sm}\check{\text{C}}_5\text{P}_A$  phase range, as is typical for antiferroelectrically switchable smectic phases of bent-core molecules (Figure 3k and Figure S15c–e in the Supporting Information).<sup>[37,38]</sup> On further cooling, a transition to another antiferroelectrically switchable LC phase ( $\text{SmC}_5\text{P}_A$ ) is observed but without any detectable transition enthalpy. At this transition, the shape of the two polarization peaks changes, associated with a broadening and separation of the peaks (Figure 3k  $\rightarrow$  l). The polarization values depending on temperature, plotted in Figure 6 (black triangles), are very small in the  $\text{SmC}_5^{[*]}$  and  $\text{SmC}_5\text{P}_R^{[*]}$  ranges and difficult to separate from contributions of conductivity. This temperature range is considered as paraelectric with almost continuously growing correlation length of the polar fluctuations. A steep increase in the polarization is observed upon approaching the  $\text{SmC}_5\text{P}_{AR}$  range, continuing in the  $\text{SmC}_5\text{P}_{AR}$  range, reaching  $500\text{ nC cm}^{-2}$  at the transition to the  $\text{Sm}\check{\text{C}}_5\text{P}_A$  phase and even  $750\text{ nC cm}^{-2}$  at the next transition to  $\text{SmC}_5\text{P}_A$ . The high polarization is retained in the  $\text{SmC}_5\text{P}_A$  phase (Figure S17 in the Supporting Information); the breakdown observed in Figure 5 is attributed to crystallization under these conditions.

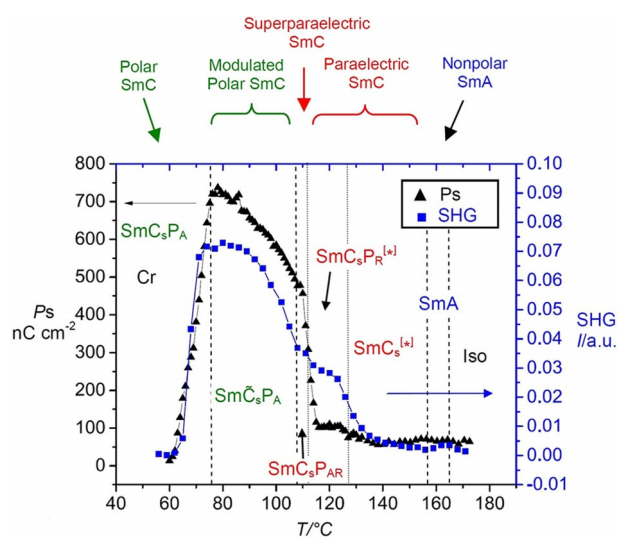


**Figure 6.** Temperature dependence of the second harmonic generation (SHG) signal (blue squares) compared with the switching polarization (black triangles) of compound AT16 as function of temperature as measured in  $6\text{ }\mu\text{m}$  PI-coated ITO cells under a triangular wave field ( $27\text{ V}_{pp}\text{ }\mu\text{m}^{-1}$  at  $10\text{ Hz}$ ). The breakdown of  $P_s$  in the  $\text{SmC}_5\text{P}_A$  range is attributed to crystallization, compare with Figure S17 in the Supporting Information.

## Dielectric spectroscopy

The dielectric spectra in the range from  $10\text{ MHz}$  to  $1\text{ Hz}$  exhibit a dielectric relaxation process at the temperatures below  $140^\circ\text{C}$  (Figure 7a and Figure S18 in the Supporting Information). This process can be attributed to a collective relaxation of the transversal dipole moments of the asymmetric mesogens. The relaxation frequency of the process decreases nearly linearly with temperature in the  $\text{SmC}_5\text{P}_R^{[*]}$  range. In the  $\text{SmC}_5\text{P}_{AR}$  range, the decrease becomes faster and nonlinear. The dielectric strength of this mode exhibits a nearly critical behavior in the vicinity of the  $\text{SmC}_5\text{P}_{AR} \rightarrow \text{Sm}\check{\text{C}}_5\text{P}_A$  phase transition at  $109^\circ\text{C}$ . The relaxation frequency slightly increases below the transition and continues to decrease in a linear fashion with decreasing temperature. At the same time, the dielectric strength of this process reduces significantly in the following  $\text{Sm}\check{\text{C}}_5\text{P}_A$  phase and only slightly increases with decreasing temperature. An electric bias field in the range up to  $12\text{ V}$  in the  $\text{Sm}\check{\text{C}}_5\text{P}_A$  phase enhances the dielectric losses  $\epsilon''$  (Figure 7b). On further cooling, the dielectric strength starts decreasing again below  $78^\circ\text{C}$ , which may be attributed to the phase transition to  $\text{SmC}_5\text{P}_A$  (Figure 7a).

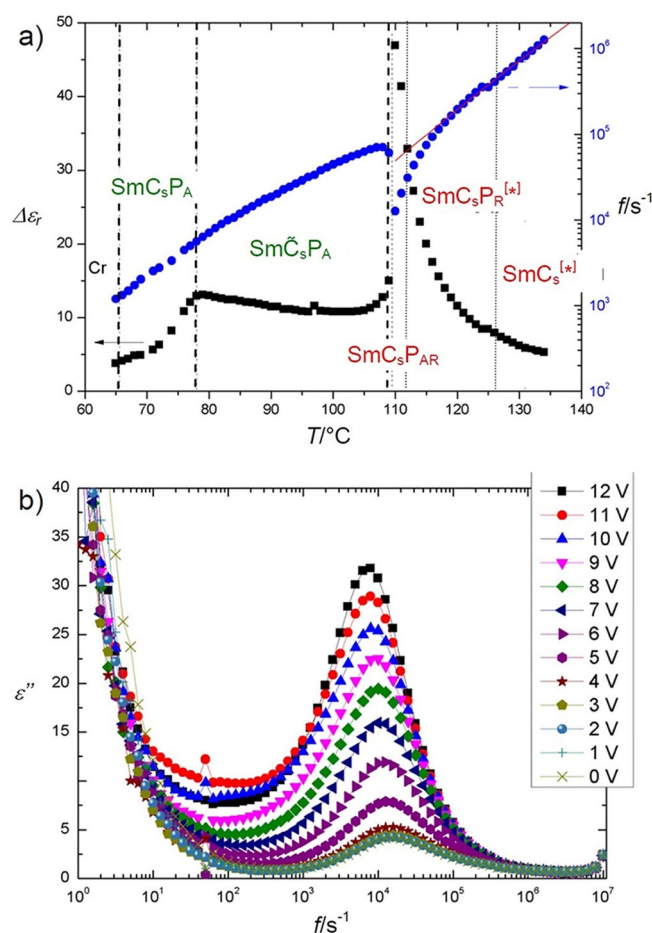


**Figure 7.** Dielectric response of compound AT16. a) Temperature dependence of the frequency and the dielectric strength of a low-frequency mode (for 3D plot of dielectric losses as a function of the frequency and temperature, see Figure S18 in the Supporting Information). b) Enhancement of the dielectric losses of the mode from (a) in a bias field at  $T = 90^\circ\text{C}$ .

## Second harmonic generation studies

SHG studies of **AT16** confirm a continuous increase of the size of the fluctuating polar clusters in the paraelectric  $\text{SmC}$  range ( $\text{SmC}_s^{[*]}, \text{SmC}_s\text{P}_R^{[*]}$ ), reaching a maximum in the  $\text{SmC}_s\text{P}_{AR}$  range just before the transition to the antiferroelectric  $\text{SmC}_s\text{P}_A$  phase (Figure 6, blue squares), similar to the previously reported paraelectric–ferroelectric transitions of 4-cyanoescorcinol BCLCs derived compounds with two terephthalate wings.<sup>[80]</sup>

Neither the isotropic nor the  $\text{SmA}$  phase shows any appreciable SHG activity. Field-induced SHG first develops in the  $\text{SmC}^{[*]}$  phase below 157 °C and grows continuously on cooling (Figure 6). The SHG intensity increases continuously with increasing applied field without any detectable threshold (Langevin-like, see Figure 8a, 145 and 135 °C). Such a behavior can be attributed to the growing polar correlations in the paraelectric  $\text{SmC}_s$  phase and an increase of the amplitude of the fluctuating dipole moment. The SHG response increases drastically upon approaching the  $\text{SmC}_s\text{P}_{AR}$  range at 112 °C (Figure 8a, 119 °C). This occurs concurrently with the softening of the polar mode in the dielectric spectra, nearly critical behavior of the dielectric permittivity  $\epsilon'$  (Figure 7a), and a drastic increase of the switching polarization  $P_s$  (Figure 6). The field-dependence of the SHG response has a rather step-like shape with a plateau at high fields and a steep but smooth slope at a low field (Figure 8a). This is in agreement with the fact that the current response during the switching has broad peaks (Figure 3j). One interpretation could be that the polar clusters with a fluctuating size and antipolar order develop. The thresh-

old behavior is only weakly pronounced and the phase appears superparaelectric.<sup>[93]</sup> The SHG response changes again upon the transition into the antiferroelectric phase. The signal has a sharper threshold behavior and a plateau at high fields (Figure 8b). Sharper current response peaks (Figure 3k,l) accompany the changes of the SHG activity.

## Chiral domains and mirror symmetry breaking

In the  $\text{SmC}_s^{[*]}/\text{SmC}_s\text{P}_R^{[*]}$  range of the paraelectric  $\text{SmC}_s$  phase, the formation of conglomerates of chiral domains was observed in thin cells with homeotropic alignment, as detected by rotating one of the polarizers from the crossed position by a small angle, approximately 5°–10° in the clockwise direction, where dark and bright domains were observed. Rotating the polarizer with the same angle in an anti-clockwise direction reverses the dark and bright domains. Moreover, rotating the sample between crossed polarizers does not lead to any change in the optical textures, thus confirming that the chirality and not a simple director alignment is responsible for the observed effect (see Figure S16 in the Supporting Information and Figure 17a,b in Section 3.4). On the other hand, chirality is not visible in planar alignment and in freely suspended films, meaning that the chiral conglomerate structure is stabilized in the homeotropic cells, similar to the case of conglomerate formation in nematic phases of BCLCs.<sup>[39,94]</sup> We assume that the basis of chirality in the investigated smectic phases is the formation of a helical structure with the helix axis parallel to the layer normal, owing to the escape from a growing polarization in the clusters.<sup>[95,84,96]</sup> This might be combined with a synchronization of helical molecular conformations of the transiently chiral 4-cyanoescorcinol based bent-core mesogens, allowing a denser packing.<sup>[25,26]</sup> A helical modulation of the polar direction, combined with chirality synchronization of the involved molecules was recently indicated in simulations of nematic phases of bent dimesogens for which a polar twist model ( $N_{PT}$ )<sup>[97]</sup> was proposed as an alternative model of the helical low-temperature nematic phases, known as  $N_x$  or  $N_{TB}$  phases. In the smectic phases reported here, the developing chirality can in addition couple through diastereomeric relations with the layer chirality of the  $\text{SmC}_s\text{P}_F$  clusters, defined by tilt direction and polar direction.<sup>[23]</sup> With growing polarization and cluster size, the energy gain of this cooperative coupling between transient molecular and superstructural chirality increasingly compensates for unfavorable entropic effects of segregation and reduced conformational diversity.<sup>[25,26]</sup> If a uniform tilt direction is stabilized by the surface anchoring of the molecules, then the preferred tilt and chirality of the  $\text{SmC}_s\text{P}_F$  clusters can become biased over macroscopic areas.<sup>[25,37,38]</sup> Therefore, the formation of conglomerates of chiral domains is considered as an indication of the appreciable correlation length of the fluctuating polar  $\text{SmC}_s\text{P}_F$  clusters in the paraelectric  $\text{SmC}_s$  range ( $\text{SmC}_s^{[*]}, \text{SmC}_s\text{P}_R^{[*]}$ ). If the polar coherence length falls below a critical value, then only the achiral  $\text{SmC}_s$  phase is observed (see compound **AB12** in Table 2). Because the chirality is not permanent, the spontaneously developing handedness is stochastic and on a macroscopic length scale a

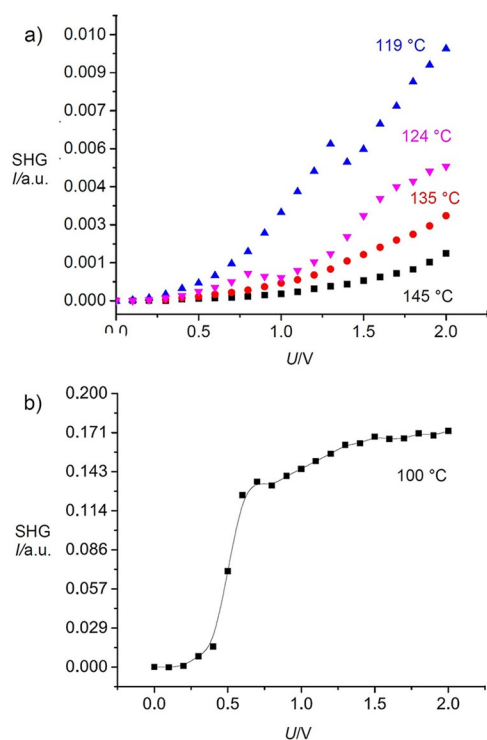


**Figure 8.** a) Field-induced SHG in the paraelectric  $\text{SmC}_s^{[*]}$  (black, red) and the randomized  $\text{SmC}_s\text{P}_R^{[*]}$  phases (magenta, blue) of **AT16**. b) The step-like field dependence of the SHG in the antiferroelectric  $\text{SmC}_s\text{P}_A$  phase at  $T = 100$  °C.

conglomerate of the chiral domains is observed. The optical activity can result from a long pitch helical structure acting as an optical wave guide, or from the layer optical chirality of the local  $\text{SmC}_5\text{P}_F$  structure,<sup>[98]</sup> or a combination of both. On cooling, at the transition from  $\text{SmC}_5\text{P}_R^{[*]}$  to  $\text{SmC}_5\text{P}_{AR}$ , the chiral conglomerate structure disappears owing to the macroscopic racemic structure of this phase. This on–off switching of spontaneous macroscopic chirality depending on the phase symmetry is similar to that observed in cubic phases at the  $Im\bar{3}m$  ( $I432$ )– $la\bar{3}d$  transition.<sup>[99]</sup> Although chirality changes the phase symmetry, we still consider  $\text{SmC}_5\text{P}_R^{[*]}$  and  $\text{SmC}_5\text{P}_{AR}$  as distinct states of the same paraelectric  $\text{SmC}_5$  phase, because chirality is not completely spontaneous and requires surface support.

### 3.1.2 Homologous series of compounds $\text{AT}_n$

All of the synthesized  $\text{AT}_n$  derivatives with  $n=12$ – $20$  exhibit essentially the same sequence of a nonpolar  $\text{SmA}$  high-temperature phase, a paraelectric  $\text{SmC}_5$  phase, involving the  $\text{SmC}_5^{[*]}/\text{SmC}_5\text{P}_R^{[*]}$  and  $\text{SmC}_5\text{P}_{AR}$  ranges, the polar modulated  $\text{Sm}\check{\text{C}}_5\text{P}_A$  phase and the nonmodulated  $\text{SmC}_5\text{P}_A$  phases at lowest temperature (Figures S22–S26 in the Supporting Information). In this sequence, the polar coherence length continuously increases with a distinct jump at the  $\text{SmC}_5\text{P}_{AR}$ – $\text{Sm}\check{\text{C}}_5\text{P}_A$  transition, the only one with  $\Delta H$  (see Figure 2a). Already in the  $\text{SmA}$  range there are  $\text{SmC}_5$  clusters with short-range correlation of tilt (de Vries-type  $\text{SmA}$  phase). At the  $\text{SmA}$ – $\text{SmC}_5^{[*]}$  transition, the tilt alignment becomes long-range synclinal and polar (ferroelectric) fluctuations grow with decreasing temperature. After reaching a critical size, the polar fluctuations condense into  $\text{SmC}_5\text{P}_F$  clusters, which assume an antipolar correlation in the superparaelectric  $\text{SmC}_5\text{P}_{AR}$  range and then the clusters grow further with formation of ribbons in the polarization splay modulated  $\text{Sm}\check{\text{C}}_5\text{P}_A$  phase and finally these ribbons fuse to quasi infinite polar layers with antipolar correlation in the  $\text{SmC}_5\text{P}_A$  phase, which is considered to represent a classical  $\text{B}_2$ -type phase of BCLCs (see Figure 9).<sup>[16,17,23]</sup>

Compound **AT8** with the shortest alkyl chain (for DSC, see Figure S19a and for POM, see Figure S20a–e in the Supporting Information) has a reduced tilt. For this compound, the Langlevin-type switching can already be observed in the  $\text{SmA}$  phase before uniform tilt is established ( $\text{SmAP}_R$  range below  $T \approx 155^\circ\text{C}$ , see Figure S20g in the Supporting Information).<sup>[79,100]</sup> An anticlinic tilt develops together with the double peak switching, as indicated in the planar textures by extinction crosses coinciding with the directions of the polarizers (Figure S20c in the Supporting Information). This provides a new anticlinic  $\text{SmC}_5\text{P}_{AR}$  phase (see Figure S19b in the Supporting Information), completing the presently known series of nontilted  $\text{SmAP}_{AR}$ <sup>[101]</sup> and synclinal tilted  $\text{SmC}_5\text{P}_{AR}$  phase types.<sup>[38,102]</sup> Clearly, the reduced tilt of the mesogens leads to a reduced layer coupling, which favors the anticlinic tilt instead of the synclinal. The anticlinic tilt is replaced by a synclinal on further cooling in the modulated  $\text{Sm}\check{\text{C}}_5\text{P}_A$  phase and the synclinal tilt is retained on further cooling in the polar  $\text{SmC}_5\text{P}_A$  phase (Figure S20d,e,i,j, for more details see Section S3.2 and Figures S19–S21 in the Supporting Information).

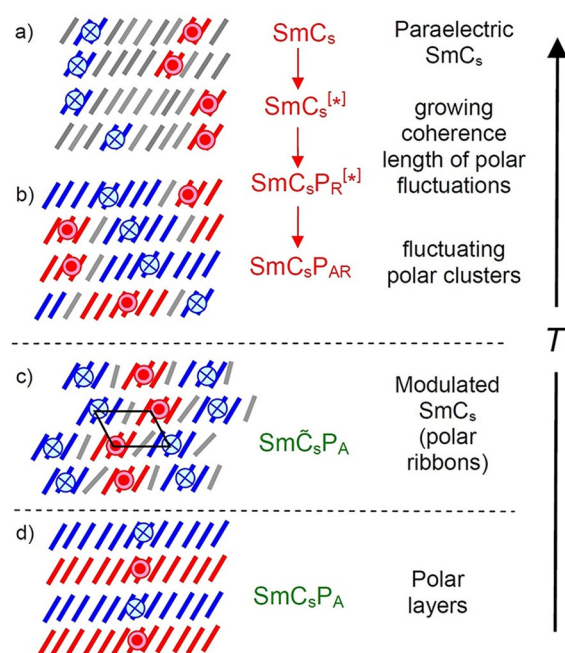


**Figure 9.** Schematic presentation of the proposed development of polar order in the ground state structures of the  $\text{SmC}_5$  phases of compounds  $\text{AT}_n$ . Dotted lines indicate phase transitions, color indicates chirality, and dots and crosses indicate the preferred polar direction in the (fluctuating) clusters or layers. The gray molecules have a randomized polar direction.

### 3.1.3 The core-fluorinated compound $\text{A}_7\text{T16}$

Owing to a higher melting point, the LC range of the fluorinated compound **A<sub>7</sub>T16** is narrower than that of the nonfluorinated compound **AT16**, but with essentially the same phase sequence; that is, the  $\text{SmA}$  phase is followed by a paraelectric  $\text{SmC}_5$  phase with continuous transition from  $\text{SmC}_5\text{P}_R^{[*]}$  to  $\text{SmC}_5\text{P}_{AR}$ , followed by phase transitions to the polar  $\text{Sm}\check{\text{C}}_5\text{P}_A$  and  $\text{SmC}_5\text{P}_A$  phases (Table 1 and Figure 1). Also, the textures and polarization current curves are very similar to **AT16** and indicate the occurrence of layer modulation in the temperature range between approximately  $110$  and  $121^\circ\text{C}$  (see Figures S27 and S28 in the Supporting Information), although it is not evident from the small-angle X-ray scattering (SAXS) pattern in this case, even by using synchrotron radiation (Figure S29 in the Supporting Information). Clearly, the ED modulation along the modulated layers is smaller (reducing the peak intensity) or the correlation length of the layer modulation is shorter (broadening the small scatterings) than for **AT16**. Overall, there seems to be no significant effect of the monofluorination of a single benzene ring on the sequence and structures of the LC phases.

### 3.2. Compounds $\text{B}_n$ with a 4-hydroxybenzoate wing

All  $\text{AB}_n$  compounds ( $n=8, 12, 16,$  and  $20$ , see Table 2 and Figure 10) involving a 4-hydroxybenzoate based wing have approximately  $30$ – $50$  K higher melting points and about  $40$  K lower LC–Iso transition temperatures compared with compounds  $\text{AT}_n$ . Therefore, these compounds exhibit only monotropic LC phases except the longest derivative **AB20**. The  $\text{SmA}$

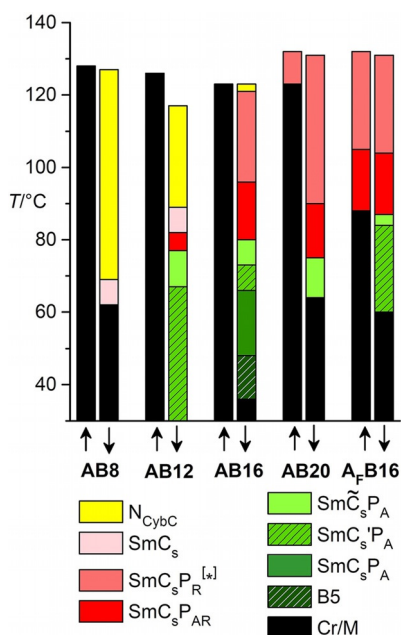


**Figure 10.** Graphical comparison of the phases and transition temperatures of the investigated compounds **AB $n$**  and **A $_n$ B16** on heating ( $\uparrow$ ) and cooling ( $\downarrow$ ). For abbreviations of the phase structures, see Table 2. Color code: yellow = N phase; red = paraelectric SmC ranges, and green = polar SmC phases; see Figure 9 for models of the phase structures.

phase of compounds **AT $n$**  ( $n=8-16$ ) is replaced by a skewed cybotactic nematic phase ( $N_{Cybc}$  for texture, see Figure S32 in the Supporting Information)<sup>[77]</sup> in the series of compounds **AB $n$** . The nematic phase range decreases with growing chain length and is completely removed and replaced by a paraelectric  $SmC_sP_R^{[*]}$  phase for the longest homolog **AB20**. With lowering temperature, the paraelectric  $SmC_sP_R^{[*]}$  and  $SmC_sP_{AR}$  ranges are replaced by a series of polar SmC phases ( $SmC_sP_{AR}$ ,  $SmC_sP_A$ ,  $SmC_sP_A$ ), which have almost identical textures, but all are separated by distinct phase transitions with small transition enthalpy values (0.3–0.5 kJ mol<sup>-1</sup>, see Figure 11 and Table 2 and Figures S30–S38 in Sections S3.6–S3.9 in the Supporting Information for the data of the individual compounds).<sup>[103]</sup>

The X-ray diffraction pattern of a magnetically aligned sample of the nematic phase of **AB16** (Figure 12a) indicates a

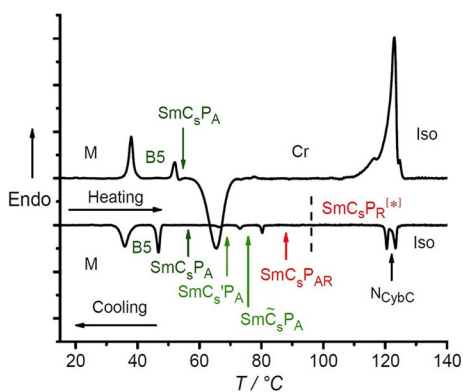


**Figure 11.** DSC heating and cooling traces of compound **AB16** at a rate of 10 K min<sup>-1</sup>. The dashed line indicates continuous transition.

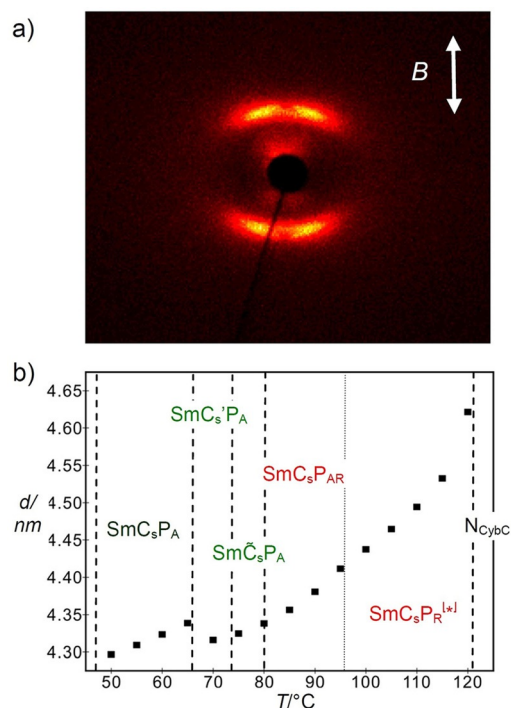


**Figure 12.** XRD investigations of compound **AB16**. a) Diffraction pattern of the  $N_{Cybc}$  phase of a magnetically aligned sample at 123 °C (for a scan over this pattern, see Figure S34 d in the Supporting Information) and b) temperature dependence of the  $d$ -value. For additional XRD data, see Figure S34 (in the Supporting Information).

tilt angle of approximately 25° (Figure S34d in the Supporting Information). This means that already in the nematic phase, the tilt is relatively large, comparable with that found for the  $SmC_sP_A$  phase of **AT16** at lowest temperature. At the transition from the  $N_{Cybc}$  to the  $SmC_sP_R^{[*]}$  phase at  $T=121$  °C, the alignment is lost and therefore no direct determination of the tilt angle was possible. However, the  $d$ -value of the layer reflection in the smectic phases (Figure 12b,  $d=4.3-4.6$  nm) is significantly smaller than the related values recorded for compound **AT16** (Figure 4c,  $d=5.1-5.3$  nm) although they have the same molecular length ( $L_{mol}=6.7$  nm). This is in line with a much larger tilt of compound **AB16** in the smectic phases. The layer distance  $d$  decreases with decreasing temperature, indicating a further growing tilt of the molecules on cooling (Figure 12b).

Synchrotron SAXS confirms a layer modulation in the temperature range between 73–80 °C ( $SmC_sP_A$  phase, Figure S34a–c in the Supporting Information). However, as in the case of compound **AT16**, there is only a limited number of very weak additional reflections besides the layer reflection (Figure S34b in the Supporting Information).<sup>[88]</sup> This indicates the presence of a layer modulation ( $SmC_s$  phase) although the precise molecular organization is still unknown.<sup>[88]</sup> Hence, it appears that layer modulation is a general feature of the transition from (super)paraelectric to macroscopically polar phases of bent-core mesogens.<sup>[37,80,104]</sup>

Electro-optical investigations confirm that only a nonpolar  $SmC_s$  phase is formed below the  $N_{Cybc}$  phases of compound **AB8** with relatively short chains (Table 2, Figure 10). The ab-

sence of a polarization peak indicates a short coherence length of polar order in this SmC phase, which is in line with the absence of mirror symmetry breaking. An achiral SmC phase is also formed by **AB12**, whereas for the compounds **AB16** and **AB20** with longer chains, the achiral SmC<sub>s</sub> phase is completely replaced by a chiral paraelectric SmC<sub>s</sub>P<sub>R</sub><sup>[\*]</sup> phase (see Figure 10 and Figure S35 in the Supporting Information), in line with an increased coherence length of the polar order. Two widely separated and relatively sharp polarization current peaks located at the voltage maxima start to develop in the SmC<sub>s</sub>P<sub>AR</sub> range of **AB16** (Figure 13 b). In the following polar SmC phases (SmC<sub>s</sub>P<sub>A</sub> to SmC<sub>s</sub>P<sub>A</sub>), the polarization values rise further to almost 1000 nCcm<sup>-2</sup> (see Figures 13 and 14, and Figure S33 in the Supporting Information).

Dielectric spectra of compound **AB16** in the range from 10 MHz to 1 Hz are presented in Figure 15 a. A relaxation process, related to a collective relaxation of the transversal dipole moments, in the range 10–100 kHz was observed. The dielectric strength continuously increases in the range of the paraelectric SmC<sub>s</sub>P<sub>R</sub><sup>[\*]</sup> range and in the SmC<sub>s</sub>P<sub>AR</sub> range, exhibiting a subcritical behavior at the transition to the antiferroelectric SmC<sub>s</sub>P<sub>A</sub> phase at 80 °C. The critical character of the behavior of  $\Delta\epsilon_r$  is less pronounced compared with **AT16** (Figure 8 a). In particular, there is no strong discontinuity of the dielectric permittivity across the paraelectric–antiferroelectric transition. Plotting inverse values of  $\Delta\epsilon_r$ , we find nearly a linear dependence with temperature, which can be extrapolated to the Néel temperature  $T_N = 56$  °C (Figure S36 a in the Supporting Information), the temperature of the transition to uniformly polar layers. This temperature is significantly lower than the actually observed SmC<sub>s</sub>P<sub>AR</sub> to SmC<sub>s</sub>P<sub>A</sub> transition, and suggests that only

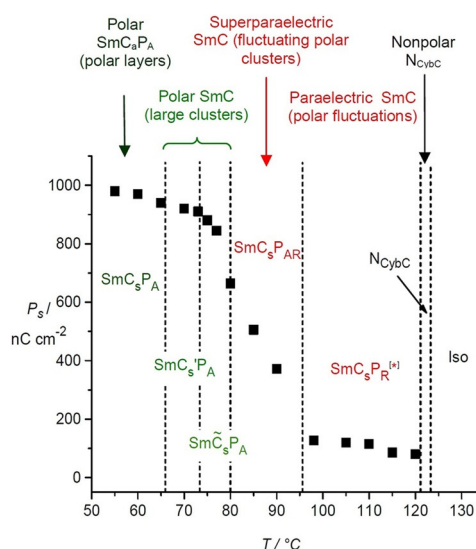


**Figure 14.** Polarization as a function of temperature as measured for compound **AB16** in a 6  $\mu\text{m}$  PI-coated ITO cell on applying a triangular wave field ( $33 \text{ V}_{\text{pp}} \mu\text{m}^{-1}$  at 10 Hz).

between 48 and 66 °C a typical B<sub>2</sub>-type SmC<sub>s</sub>P<sub>A</sub> phase composed of alternating ferroelectric layers is formed. Comparing the dielectric behavior with the dependence  $P_s(T)$  (Figure 14), we find that the subcritical  $\Delta\epsilon_r(T)$  also corresponds to a nearly continuous increase of the switching polarization in the SmC<sub>s</sub>P<sub>R</sub><sup>[\*]</sup>/SmC<sub>s</sub>P<sub>AR</sub> phase range. This suggests that the SmC<sub>s</sub>P<sub>A</sub> and SmC<sub>s</sub>P<sub>A</sub> phases of **AB16** are still of the cluster type and the long-range ferroelectric order in the layers is mostly suppressed at high temperatures. Therefore, only the low-temper-

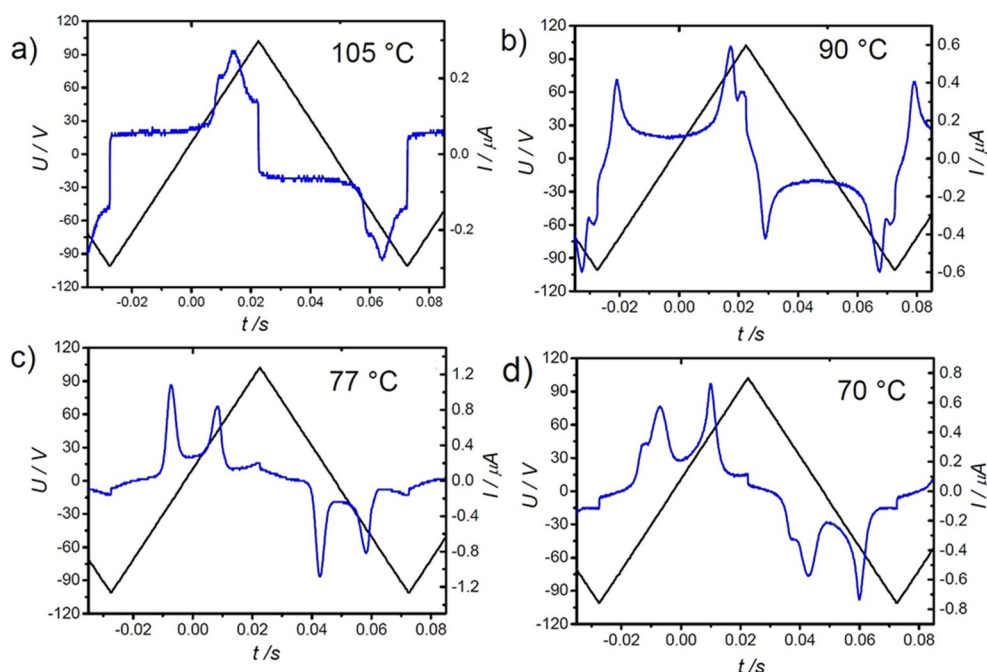


**Figure 13.** a–d) Switching current response curves of compound **AB16** as measured on applying a triangular wave field ( $33 \text{ V}_{\text{pp}} \mu\text{m}^{-1}$ , 10 Hz, 6  $\mu\text{m}$  PI-coated ITO cell) at the indicated temperatures. The third peak in d) is also observed for the related compound with two azobenzene wings<sup>[37b]</sup> and might indicate two different relaxation mechanisms of the ferroelectric to the AF states, which might be due to the anchoring effect of the surfaces (see also Figure S33 in the Supporting Information).

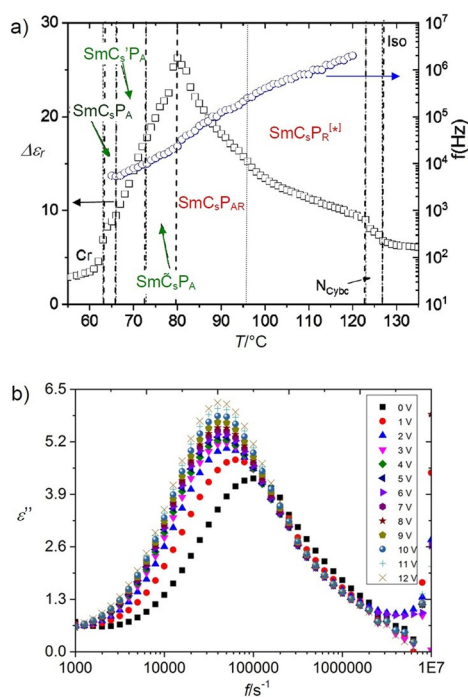


**Figure 15.** Dielectric investigation of **AB16**. a) Temperature dependence of the frequency and the dielectric strength of a low-frequency mode. b) Enhancement of the dielectric losses of the mode from a) in a bias field at  $T=80\text{ }^{\circ}\text{C}$  in  $\text{SmC}_5\text{P}_A$  shortly after transition from  $\text{SmC}_5\text{P}_{AR}$ .

ature polar  $\text{SmC}_5$  phase is designated as  $\text{SmC}_5\text{P}_A$  whereas all polar smectic phases occurring at a higher temperature and having a shorter polar coherence length, assigned as  $\text{SmC}_5'\text{P}_A$  and  $\text{Sm}\tilde{\text{C}}_5\text{P}_{AR}$ , respectively, are considered as superparaelectric. The decrease in temperature from  $120\text{ }^{\circ}\text{C}$  to  $65\text{ }^{\circ}\text{C}$  leads to a nearly linear decrease of the relaxation frequency (Figure S36 b in the Supporting Information). The activation energy of the relaxation process is about  $53\text{ kJ mol}^{-1}$  for the paraelectric  $\text{SmC}_5\text{P}_R^{[*]}$  phase and  $E_a=47\text{ kJ mol}^{-1}$  for the antiferroelectric  $\text{SmC}_5\text{P}_A$  phase. At the same time, applied bias electric fields in the range up to 12 V in the  $\text{Sm}\tilde{\text{C}}_5\text{P}_A$  phase at  $80\text{ }^{\circ}\text{C}$  enhances the dielectric losses  $\epsilon''$  (Figure 15 b) owing to the growing polar cluster size, but this field-induced increase is less pronounced than in the modulated  $\text{Sm}\tilde{\text{C}}_5\text{P}_A$  phase of compound **AT16** (Figure 7 b).

These observations suggest that the critical behavior of the polar order is more strongly suppressed in the paraelectric phase of compound **AB16** compared with **AT16** (compare Figures 7 a and 15 a). This may be attributed to a reduced packing density for compound **ABn** with relatively electron-rich aromatics in the 4-hydroxybenzoate wing and the stronger tilt achieved in their self-assembly. However, the polarization values measured under an applied electric field in the polar smectic phases are high in both series of compounds, being  $750\text{ nC cm}^{-2}$  for **AT16** (Figure 6) and reaching even  $900\text{--}1000\text{ nC cm}^{-2}$  for **AB16** (Figure 14). An increased flexibility of the phenylbenzoate wings of compound **ABn** in the less densely packed paraelectric phases might require lower temperatures to reach a critical coherence length of polar order ( $80\text{ }^{\circ}\text{C}$  vs.  $110\text{ }^{\circ}\text{C}$ ) and also leads to an expansion of the  $\text{SmC}_5\text{P}_{AR}$

phase range. Once polar order is established, the packing density increases further, giving rise to additional  $\text{SmC}_5\text{P}_A$  subtypes ( $\text{Sm}\tilde{\text{C}}_5\text{P}_{AR}$ ,  $\text{SmC}_5'\text{P}_A$ ). The larger collective contribution of the C=O dipoles to the transversal molecular dipole moment along the polar director might contribute to the enhanced polarization of **AB16** after achieving a dense packing in the  $\text{SmC}_5\text{P}_A$  phase. An extended comparison of compounds **ATn** and **ABn** involving related symmetric compounds is given in Section S4 in the Supporting Information (Table S2).

### 3.3 Compounds **A<sub>F</sub>B16** with fluorinated azobenzene side-arm

For the fluorinated compound **A<sub>F</sub>B16**, the melting point ( $88\text{ }^{\circ}\text{C}$ ) is much lower compared with that of **AB16** ( $123\text{ }^{\circ}\text{C}$ ), leading to additional enantiotropic LC phases. Moreover, the nematic phase formed by **AB16** is completely removed (Table 2 and Figure 10). The LC phases and the phase sequence of **A<sub>F</sub>B16** are almost identical with those of **AB20**, suggesting that reducing the electron density of the core by fluorination has the same effect as elongation of the alkyl chain. Hence, core-fluorination in the case of compounds **ABn** is a useful tool for expansion of the LC phase region; more details can be found in Section S3.10 in the Supporting Information (Figures S39–S42).

### 3.4 Isothermal photoswitching between ferroelectric (FE)-like and antiferroelectric (AF)-like, and between chiral and achiral states

The azobenzene unit involved in the molecular structures allows photoinduced isomerization of the azobenzene unit under UV irradiation (for solution spectra, see Figure S43 in the Supporting Information), which in turn can be used to modify the materials properties. Previous attempts of photoinduced switching with azobenzene-based BCLCs were based on a transition of the antiferroelectric  $B_2$  or the  $B_7$  phases into the isotropic liquid state, which reduces  $P_{sv}$ <sup>[52,53]</sup> whereas here we report a photoswitching of the mode of switching under an E-field as well as an on/off switching of superstructural chirality.

In the first case, a sample of compound **AB16**, placed in a  $6\text{ }\mu\text{m}$  indium tin oxide (ITO) cell on a temperature-controlled heating stage, was illuminated at  $T=101\text{ }^{\circ}\text{C}$ , that is, close to the  $\text{SmC}_5\text{P}_{AR}\text{--}\text{SmC}_5\text{P}_R^{[*]}$  transition temperature, by light with 405 nm wavelength for 2 s. The antiferroelectric-like double peak switching changes into a ferroelectric-like single peak switching and relaxes back to the AF-like mode almost immediately after switching off the light source ( $<3\text{ s}$ ; see Figure 16). This allows, for the first time, a photoinduced change of the mode of the switching. That the switching is not due to any thermal effect was checked by control experiments with LC compounds without any azobenzene core as described in Section S5 in the Supporting Information (Figures S46–S48).

Likewise, the symmetry-broken  $\text{SmC}_5^{[*]}$  phase of **AT16** was successfully switched to the achiral  $\text{SmA}$  phase under light irradiation (405 nm,  $5\text{ mW mm}^{-2}$ , see Figure 17 a,b→c). The transition to a  $\text{SmA}$  phase is evident from the optical isotropic ap-



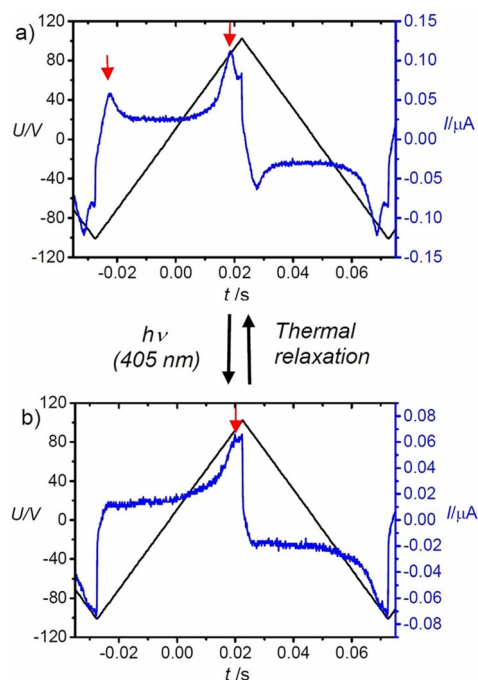


**Figure 16.** Reversible isothermal switching between a) antiferroelectric-like and b) ferroelectric-like switching in the paraelectric SmC phase range as recorded for compound **AB16** at  $T = 101$  °C in a  $6 \mu\text{m}$  ITO cell. A related switching of compound **AT16** is shown in Figure S44 (in the Supporting Information).

pearance in homeotropic alignment, accompanied by the formation of birefringent defects (Maltese crosses, see inset in Figure 17c). Also, this process is fast and reversible ( $< 3$  s). After switching off the light, the chiral domains almost immediately (within  $< 3$  s) reform (Figure 17c  $\rightarrow$  d,e). However, there appears to be no chiral memory, meaning that the positions of the chiral domains change during the switching process (Figure 17a,b  $\rightarrow$  d,e). This is attributed to the fluidity of these smectic phases, leading to flow of the material, but it also shows that the chirality in these phases is not based on a chiral surface effect. The change of molecular shape from a rather well-defined bent shape to a more nonspecific one by *trans* $\rightarrow$ *cis* photoisomerization leads to a decrease in the packing density and a reduction of the coherence length of polar order below a critical value, thus changing the mode of polar switching. The reduced packing density is also responsible for the observed photoinduced on-off switching of chirality.

In contrast to previous reported work on chirality modulation based on photoisomerization in LCs, the chirality is in this case not based on a molecular chirality,<sup>[46,47,105–107]</sup> but the chirality is spontaneously formed by molecular self-assembly of achiral molecules in the LC state. A related on-off switching of this kind of superstructural chirality in a fluid LC phase was only reported for a polycatenar compound<sup>[48]</sup> and for the  $N_{\text{TB}}-N$  transition in mesogenic dimers.<sup>[67]</sup> In all other cases, soft crystalline conglomerate phases, in most cases representing helical nano-filament (HNF) phases, were involved. For example, uniform chirality has been achieved with circular polarized light during the growth of HNF phases of mesogenic azobenzene

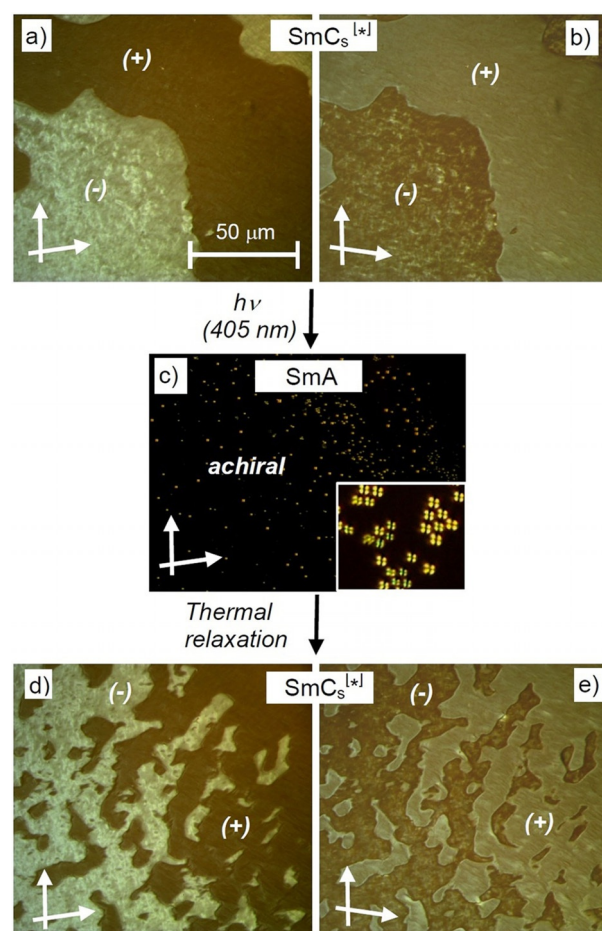


**Figure 17.** a–e) Reversible isothermal photo on-off switching of chirality as observed for **AT16** at  $T = 152$  °C in a homeotropic cell (ca.  $10 \mu\text{m}$ ). The inset in (c) shows an enlarged region, indicating that the small spots in (c) represent Maltese crosses as typical for defects in homeotropic SmA phases (see also Figure S45 in the Supporting Information).

dimers.<sup>[56,108]</sup> In another report, a mesogenic trimer was switched by UV irradiation between an achiral phase and a symmetry-broken soft crystalline phase with chiral conglomerate structure.<sup>[109]</sup> However, there were no reports of photoinduced chirality switching in any fluid conglomerate type smectic phase of achiral BCLCs. The reason might be that in these densely packed polar smectic phases, the molecular shape is strongly fixed in the binding sites provided by the surrounding bent and polar ordered molecules and in this way *trans* $\rightarrow$ *cis* photoisomerization is efficiently inhibited. In the case reported here, only the correlation length of the polar order is modified, which takes place much more easily and therefore photoisomerization can easily change the molecular shape.

## 4. Summary and Conclusions

We have reported the synthesis and investigation of two new series of nonsymmetric photosensitive bent-core molecules consisting of 4-cyanoresorcinol as the central core and two different wing groups, an azobenzene and a phenylbenzoate wing with two distinct directions of one of the COO groups

(**ATn** and **ABn**). Compounds with a terephthalate-based wing **ATn** show broader LC phases, lower melting temperatures and a smaller tilt compared with the phenylbenzoate analogs **ABn**, whereas core fluorination in both series retains the fundamental phase sequence.

In the two series of compounds there is a transition from nonpolar de Vries-like SmA (**ATn**) or from  $N_{C_{2v}BC}$  phases (**ABn**), both formed by small synclincic  $SmC_5$  clusters, via paraelectric  $SmC_5$  and  $SmC_5P_R$  phases to antiferroelectric  $SmC_5P_A$  phases upon lowering the temperature and thus increasing packing density (see Figures 1, 8, and 10). At the transition from the paraelectric phases with short correlation length of polar order (fluctuating clusters in  $SmC_5^{[*]}$  and  $SmC_5P_R^{[*]}$ ) to the polar smectic  $SmC_5P_A$  phase, at first the polar correlation becomes antipolar already in the superparaelectric range of the  $SmC_5$  phase ( $SmC_5P_{AR}$ ). Then, the layers become modulated owing to the developing splay of polarization ( $Sm\tilde{C}_5P_A$ ), before the non-modulated antiferroelectric SmC phase ( $SmC_5P_A$ ) with quasi infinite polar layers, but antipolar correlation between them ( $B_2$ -type polar “banana” phase), is formed (see Figure 9).<sup>[17,19,21]</sup> Only for the short-chain compound **AT8**, is the tilt relatively small, leading to a nontilted and achiral paraelectric  $SmAP_R$  phase followed by a transition to an anticlinic  $SmC_5P_{AR}$  phase, replacing the related synclincic phases of the long chain compounds (Figure 1). For the series **ABn**, with one inverted COO group, a smoother development of polar order takes place, involving an additional polar  $SmC_5P_A$  phase with domain structure (Figure 2).

Mirror symmetry breaking by surface-assisted formation of chiral conglomerates sets in at a distinct coherence length of the fluctuating  $SmC_5P_F$  clusters in the homeotropically aligned paraelectric  $SmC_5$  phases ( $SmC_5^{[*]}$  and  $SmC_5P_R^{[*]}$  ranges) and these are considered as long-pitch heliconical  $SmC_5$  phases.

Moreover, we reported for the first time a photoinduced switching of azobenzene-derived BCLCs between a ferroelectric-like switching and an antiferroelectric-like switching, in addition to reversible photoinduced on–off switching of chirality. This is based on the limited correlation length of the polar order in the paraelectric and superparaelectric SmC ranges, which can easily be affected by the change of the molecular shape owing to the *trans*–*cis* isomerization process and this represents a new concept for developing photoswitchable LC materials towards specific applications.

## Acknowledgments

The work was supported by the DFG (Grants Ts 39/24-2 and ER 467/8-2) and the National Natural Science Foundation of China (No. 21761132033, 21374086). Nerea Sebastián acknowledges the financial support of the Humboldt Foundation. We thank Beamline BL16B1 at SSRF (Shanghai Synchrotron Radiation Facility, China) for providing beam time.

## Conflict of interest

The authors declare no conflict of interest.

**Keywords:** azobenzenes · ferroelectricity · liquid crystals · mirror symmetry breaking · photoswitching

- [1] N. Koide, *The Liquid Crystal Display Story*, Springer, Tokyo, 2014.
- [2] *Handbook of Liquid Crystals* (Eds.: J. W. Goodby, P. J. Collings, T. Kato, C. Tschierske, H. Gleeson, P. Raynes), Wiley-VCH, Weinheim, 2014.
- [3] a) S. Sergeev, W. Pisula, Y. H. Geerts, *Chem. Soc. Rev.* 2007, 36, 1902; b) M. O'Neill, S. M. Kelly, *Adv. Mater.* 2011, 23, 566; c) H. Iino, T. Usui, J. Hanna, *Nat. Commun.* 2015, 6, 6828; d) M. Kumar, S. Kumar, *Polym. J.* 2017, 49, 85.
- [4] I. C. Khoo, *Prog. Quantum Electron.* 2014, 38, 77.
- [5] a) K. Nickmans, A. P. H. J. Schenning, *Adv. Mater.* 2018, 30, 1703713; b) C. Tang, E. M. Lennon, G. H. Fredrickson, E. J. Kramer, C. J. Hawker, *Science* 2008, 322, 429.
- [6] T. Kato, M. Yoshio, T. Ichikawa, B. Soberats, H. Ohno, M. Funahashi, *Nat. Rev. Mater.* 2017, 2, 17001.
- [7] S. Sivakumar, K. L. Wark, J. K. Gupta, N. L. Abbott, F. Caruso, *Adv. Funct. Mater.* 2009, 19, 2260.
- [8] a) C. Li, J. Cho, K. Yamada, D. Hashizume, F. Araoka, H. Takezoe, T. Aida, Y. Ishida, *Nat. Commun.* 2015, 6, 8418; b) N. Marets, D. Kuo, J. R. Torrey, T. Sakamoto, M. Henmi, H. Katayama, T. Kato, *Adv. Healthcare Mater.* 2017, 6, 1700252.
- [9] Q. Li, *Nanoscience with Liquid Crystals*, Springer, Cham, 2014.
- [10] J. P. F. Lagerwall, G. Scalia, *Liquid Crystals with Nano and Microparticles*, World Scientific, Singapore 2017.
- [11] T. Kato, J. Uchida, T. Ichikawa, T. Sakamoto, *Angew. Chem. Int. Ed.* 2018, 57, 4355; *Angew. Chem.* 2018, 130, 4438.
- [12] C. Tschierske, *Angew. Chem. Int. Ed.* 2013, 52, 8828; *Angew. Chem.* 2013, 125, 8992.
- [13] *Chirality in Liquid Crystals* (Eds.: H. S. Kitzerow, C. Bahr), Springer, New York, 2001.
- [14] a) M. E. Lines, A. M. Glass, *Principles and Applications of Ferroelectrics and Related Materials*, Oxford University Press, New York, 2001; b) J. F. Scott, *Science* 2007, 315, 954; c) A. S. Tayi, A. Kaeser, M. Matsumoto, T. Aida, S. I. Stupp, *Nat. Chem.* 2015, 7, 281.
- [15] a) S. T. Lagerwall, *Ferroelectric and Antiferroelectric Liquid Crystals*, Wiley-VCH, Weinheim, 1999; b) H. Takezoe, E. Gorecka, M. Čepič, *Rev. Mod. Phys.* 2010, 82, 897.
- [16] T. Niori, T. Sekine, J. Watanabe, T. Furukawa, H. Takezoe, *J. Mater. Chem.* 1996, 6, 1231.
- [17] G. Pelzl, S. Diele, W. Weissflog, *Adv. Mater.* 1999, 11, 707.
- [18] M. B. Ros, J. L. Serrano, M. R. de la Fuente, C. L. Folcia, *J. Mater. Chem.* 2005, 15, 5093.
- [19] H. Takezoe, Y. Takanishi, *Jpn. J. Appl. Phys. Part 1* 2006, 45, 597.
- [20] A. Eremin, A. Jáklí, *Soft Matter* 2013, 9, 615.
- [21] R. A. Reddy, C. Tschierske, *J. Mater. Chem.* 2006, 16, 907.
- [22] H. Takezoe, A. Eremin, *Bent-Shaped Liquid Crystals*, Taylor and Francis, Boca Raton, 2017.
- [23] D. R. Link, G. Natale, R. Shao, J. E. MacLennan, N. A. Clark, E. Korblova, D. M. Walba, *Science* 1997, 278, 1924.
- [24] “Spontaneous achiral symmetry breaking in liquid crystalline phases”: H. Takezoe in *Liquid Crystals. Topics in Current Chemistry*, Vol. 318 (Ed.: C. Tschierske), Springer, Berlin, 2011, pp. 303–330.
- [25] C. Tschierske, *Liq. Cryst.* 2018, 45, 2221.
- [26] C. Tschierske, G. Ungar, *ChemPhysChem* 2016, 17, 9.
- [27] T. Sekine, T. Niori, J. Watanabe, T. Furukawa, S.-W. Choi, H. Takezoe, *J. Mater. Chem.* 1997, 7, 1307.
- [28] L. E. Hough, H. T. Jung, D. Kruerke, M. S. Heberling, M. Nakata, C. D. Jones, D. Chen, D. R. Link, J. Zasadzinski, G. Heppke, J. P. Rabe, W. Stocker, E. Korblova, D. M. Walba, M. A. Glaser, N. A. Clark, *Science* 2009, 325, 456.
- [29] C. Zhang, N. Diorio, O. D. Lavrentovich, A. Jáklí, *Nat. Commun.* 2014, 5, 3302.
- [30] K. V. Le, H. Takezoe, F. Araoka, *Adv. Mater.* 2017, 29, 1602737.
- [31] a) M. Alaasar, M. Prehm, M. Brautzsch, C. Tschierske, *J. Mater. Chem. C* 2014, 2, 5487; b) M. Alaasar, M. Prehm, M. Brautzsch, C. Tschierske, *Soft Matter* 2014, 10, 7285; c) M. Alaasar, M. Prehm, C. Tschierske, *Chem. Eur. J.* 2016, 22, 6583.

- [32] a) G. Dantlgraber, A. Eremin, S. Diele, A. Hauser, H. Kresse, G. Pelzl, C. Tschierske, *Angew. Chem. Int. Ed.* **2002**, *41*, 2408; *Angew. Chem.* **2002**, *114*, 2514; b) C. Keith, R. A. Reddy, A. Hauser, U. Baumeister, C. Tschierske, *J. Am. Chem. Soc.* **2006**, *128*, 3051.
- [33] "Nanoscale stereochemistry in liquid crystals": C. Tschierske in *Chirality at the Nanoscale* (Ed.: D. B. Amabilino), Wiley-VCH, Weinheim, **2009**, pp. 271–304.
- [34] L. E. Hough, M. Spannuth, M. Nakata, D. A. Coleman, C. D. Jones, G. Dantlgraber, C. Tschierske, J. Watanabe, E. Körblová, D. M. Walba, J. E. Maclennan, M. A. Glaser, N. A. Clark, *Science* **2009**, *325*, 452.
- [35] M. Nagaraj, *Liq. Cryst.* **2016**, *43*, 2244.
- [36] D. Chen, M. Nakata, R. Shao, M. R. Tuchband, M. Shuai, U. Baumeister, W. Weissflog, D. M. Walba, M. A. Glaser, J. E. Maclennan, N. A. Clark, *Phys. Rev. E* **2014**, *89*, 022506.
- [37] a) M. Alaasar, M. Prehm, M. Nagaraj, J. K. Vij, C. Tschierske, *Adv. Mater.* **2013**, *25*, 2186; b) M. Alaasar, M. Prehm, K. May, A. Eremin, C. Tschierske, *Adv. Funct. Mater.* **2014**, *24*, 1703.
- [38] a) M. Alaasar, M. Prehm, S. Poppe, C. Tschierske, *Chem. Eur. J.* **2017**, *23*, 5541; b) M. Alaasar, M. Prehm, M.-G. Tamba, N. Sebastian, A. Eremin, C. Tschierske, *ChemPhysChem* **2016**, *17*, 278.
- [39] a) G. Pelzl, A. Eremin, S. Diele, H. Kresse, W. Weissflog, *J. Mater. Chem.* **2002**, *12*, 2591; b) T. Niori, J. Yamamoto, H. Yokoyama, *Mol. Cryst. Liq. Cryst.* **2004**, *409*, 475; c) V. Görtz, C. Southern, N. W. Roberts, H. F. Gleeson, J. W. Goodby, *Soft Matter* **2009**, *5*, 463.
- [40] V. Görtz, J. W. Goodby, *Chem. Commun.* **2005**, 3262.
- [41] a) C. Dressel, T. Reppe, M. Prehm, M. Brautzsch, C. Tschierske, *Nat. Chem.* **2014**, *6*, 971–977; b) M. Alaasar, S. Poppe, Q. Dong, F. Liu, C. Tschierske, *Chem. Commun.* **2016**, *52*, 13869.
- [42] H. Sasaki, Y. Takahashi, J. Yamamoto, A. Yoshizawa, *Soft Matter* **2017**, *13*, 6521.
- [43] Q. Li, *Liquid Crystals Beyond Displays: Chemistry, Physics, and Applications*, Wiley, New York, **2012**.
- [44] V. P. Shibaev, A. Y. Bobrovsky, *Russ. Chem. Rev.* **2017**, *86*, 1024.
- [45] a) O. S. Bushuyev, A. Tomberg, T. Friščić, C. J. Barrett, *J. Am. Chem. Soc.* **2013**, *135*, 12556; b) H. F. Yu, *Prog. Polym. Sci.* **2014**, *39*, 781.
- [46] H. K. Bisoyi, T. J. Bunning, Q. Li, *Adv. Mater.* **2018**, *30*, 1706512.
- [47] Y.-H. Lee, L. Wang, H. Yang, S.-T. Wu, *Opt. Express* **2015**, *23*, 22658.
- [48] a) M. Alaasar, S. Poppe, Q. Dong, F. Liu, C. Tschierske, *Angew. Chem. Int. Ed.* **2017**, *56*, 10801; *Angew. Chem.* **2017**, *129*, 10941; b) M. Alaasar, S. Poppe, C. Tschierske, *J. Mol. Liq.* **2019**, *277*, 233.
- [49] H. K. Bisoyi, Q. Li, *Chem. Rev.* **2016**, *116*, 15089.
- [50] H. F. Yu, T. Ikeda, *Adv. Mater.* **2011**, *23*, 2149.
- [51] M. Martínez-Abadía, B. Robles-Hernández, M. R. de la Fuente, R. Giménez, M. B. Ros, *Adv. Mater.* **2016**, *28*, 6586.
- [52] a) A. Jákli, V. Prasad, D. S. S. Rao, G. Liao, I. Janossy, *Phys. Rev. E* **2005**, *71*, 021709; b) N. G. Nagaveni, V. Prasad, A. Roy, *Liq. Cryst.* **2013**, *40*, 1405; c) G. G. Nair, S. K. Prasad, U. S. Hiremath, C. V. Yelamaggad, *J. Appl. Phys.* **2001**, *90*, 48; d) M. Alaasar, M. Prehm, C. Tschierske, *Liq. Cryst.* **2013**, *40*, 656; e) M. Alaasar, M. Prehm, C. Tschierske, *Liq. Cryst.* **2014**, *41*, 126; f) M. Kohout, M. Alaasar, A. Poryvai, V. Novotná, S. Poppe, C. Tschierske, *J. Svoboda, RSC Adv.* **2017**, *7*, 35805.
- [53] M. Alaasar, *Liq. Cryst.* **2016**, *43*, 2208.
- [54] M. Jasiński, D. Pocięcha, H. Monobe, J. Szczytko, P. Kaszyński, *J. Am. Chem. Soc.* **2014**, *136*, 14658.
- [55] N. Gimeno, I. Pintre, M. M. Abadía, J. L. Serrano, M. Blanca Ros, *RSC Adv.* **2014**, *4*, 19694.
- [56] A. Zep, K. Sitkowska, D. Pocięcha, E. Gorecka, *J. Mater. Chem. C* **2014**, *2*, 2323.
- [57] T. Ueda, S. Masuko, F. Araoka, K. Ishikawa, H. Takezoe, *Angew. Chem. Int. Ed.* **2013**, *52*, 6863; *Angew. Chem.* **2013**, *125*, 7001.
- [58] N. G. Nagaveni, A. Roy, V. Prasad, *J. Mater. Chem.* **2012**, *22*, 8948.
- [59] M. Horčić, V. Kozmík, J. Svoboda, V. Novotná, D. Pocięcha, *J. Mater. Chem. C* **2013**, *1*, 7560.
- [60] N. Trišovi, J. Antanasijević, T. T. Katona, M. Kohout, M. Salamonczyk, S. Sprunt, A. Jákli, K. F. Csorba, *RSC Adv.* **2015**, *5*, 64886.
- [61] L. Rahman, S. Kumar, C. Tschierske, G. Israel, D. Ster, G. Hegde, *Liq. Cryst.* **2009**, *36*, 397.
- [62] V. P. Panov, R. Balachandran, J. K. Vij, M. G. Tamba, A. Kohlmeier, G. H. Mehl, *Appl. Phys. Lett.* **2012**, *101*, 234106.
- [63] J. W. Emsley, M. Lelli, A. Lesage, G. R. Luckhurst, *J. Phys. Chem. B* **2013**, *117*, 6547.
- [64] V. Borshch, Y.-K. Kim, J. Xiang, M. Gao, A. Jákli, V. P. Panov, J. K. Vij, C. T. Imrie, M. G. Tamba, G. H. Mehl, O. D. Lavrentovich, *Nat. Commun.* **2013**, *4*, 2635.
- [65] D. Chen, J. H. Porada, J. B. Hooper, A. Klitnick, Y. Shen, M. R. Tuchband, E. Körblová, D. Bedrov, D. M. Walba, M. A. Glaser, J. E. Maclennan, N. A. Clark, *Proc. Natl. Acad. Sci. USA* **2013**, *110*, 15931.
- [66] a) R. J. Mandle, C. C. A. Voll, D. J. Lewis, J. W. Goodby, *Liq. Cryst.* **2016**, *43*, 13; b) R. J. Mandle, *Chem. Eur. J.* **2017**, *23*, 8771; c) R. J. Mandle, *Chem. Rec.* **2018**, *18*, 1; d) J. W. Goodby, *Liq. Cryst.* **2017**, *44*, 1755.
- [67] D. A. Paterson, J. Xiang, G. Singh, R. Walker, D. M. Agra-Kooijman, A. Martínez-Felipe, M. Gao, J. M. D. Storey, S. Kumar, O. D. Lavrentovich, C. T. Imrie, *J. Am. Chem. Soc.* **2016**, *138*, 5283.
- [68] A. Lesac, U. Baumeister, I. Dokli, Z. Hameršak, T. Ivšić, D. Kontrec, M. Viskić, A. Knežević, R. J. Mandle, *Liq. Cryst.* **2018**, *45*, 1101.
- [69] J. P. Abberley, R. Killah, R. Walker, J. M. D. Storey, C. T. Imrie, M. Salamonczyk, C. Zhu, E. Gorecka, D. Pocięcha, *Nat. Commun.* **2018**, *9*, 228.
- [70] F. C. Yu, L. J. Yu, *Chem. Mater.* **2006**, *18*, 5410.
- [71] a) M. Monika, V. Prasad, N. G. Nagaveni, *Liq. Cryst.* **2015**, *42*, 1490; b) R. Deb, R. K. Nath, M. K. Paul, N. V. S. Rao, F. Tuluri, Y. Shen, R. Shao, D. Chen, C. Zhu, I. I. Smalyukh, N. A. Clark, *J. Mater. Chem.* **2010**, *20*, 7332; c) R. K. Nath, D. D. Sarkar, D. S. S. Rao, N. V. S. Rao, *Liq. Cryst.* **2012**, *39*, 889; d) M. Horčić, V. Kozmík, J. Svoboda, V. Novotná, D. Pocięcha, *J. Mater. Chem. C* **2013**, *1*, 7560; e) E. Enz, S. Findeisen-Tandel, R. Dabrowski, F. Giesselmann, W. Weissflog, U. Baumeister, J. Lagerwall, *J. Mater. Chem.* **2009**, *19*, 2950.
- [72] M. Alaasar, S. Poppe, C. Kerzig, C. Klopp, A. Eremin, C. Tschierske, *J. Mater. Chem. C* **2017**, *5*, 8454.
- [73] W. Weissflog, U. Baumeister, M.-G. Tamba, G. Pelzl, H. Kresse, R. Friedemann, G. Hempel, R. Kurz, M. Roos, K. Merzweiler, A. Jákli, C. Zhang, N. Diorio, R. Stannarius, A. Eremin, U. Kornek, *Soft Matter* **2012**, *8*, 2671.
- [74] a) G. Pelzl, W. Weissflog in *Thermotropic Liquid Crystals: Recent Advances* (Ed.: A. Ramamoorthy), Springer, Dordrecht, **2007**, pp. 1–58; b) W. Weissflog, H. N. S. Murthy, S. Diele, G. Pelzl, *Phil. Trans. R. Soc. A* **2006**, *364*, 2657.
- [75] I. Wirth, S. Diele, A. Eremin, G. Pelzl, S. Grande, L. Kovalenko, N. Panchenko, W. Weissflog, *J. Mater. Chem.* **2001**, *11*, 1642.
- [76] L. Kovalenko, M. W. Schröder, R. A. Reddy, S. Diele, G. Pelzl, W. Weissflog, *Liq. Cryst.* **2005**, *32*, 857.
- [77] C. Keith, A. Lehmann, U. Baumeister, M. Prehm, C. Tschierske, *Soft Matter* **2010**, *6*, 1704.
- [78] C. Keith, M. Prehm, Y. P. Panarin, J. K. Vij, C. Tschierske, *Chem. Commun.* **2010**, *46*, 3702.
- [79] N. Sebastián, S. Belau, A. Eremin, M. Alaasar, M. Prehm, C. Tschierske, *Phys. Chem. Chem. Phys.* **2017**, *19*, 5895.
- [80] M. Alaasar, M. Prehm, M. Poppe, M. Nagaraj, J. K. Vij, C. Tschierske, *Soft Matter* **2014**, *10*, 5003.
- [81] E. Westphal, H. Gallerdo, G. F. Caramori, N. Sebastian, M.-G. Tamba, A. Eremin, S. Kawachi, M. Prehm, C. Tschierske, *Chem. Eur. J.* **2016**, *22*, 8181.
- [82] a) H. Ocak, B. Bilgin-Eran, M. Prehm, S. Schymura, J. P. F. Lagerwall, C. Tschierske, *Soft Matter* **2011**, *7*, 8266; b) H. Ocak, B. Bilgin-Eran, D. Güzeller, M. Prehm, C. Tschierske, *Chem. Commun.* **2015**, *51*, 7512; c) H. Ocak, M. Poppe, B. Bilgin-Eran, G. Karanlık, M. Prehm, C. Tschierske, *Soft Matter* **2016**, *12*, 7405.
- [83] A. Eremin, S. Diele, G. Pelzl, H. Nádasi, W. Weissflog, J. Salfetnikova, H. Kresse, *Phys. Rev. E* **2001**, *64*, 051707.
- [84] S. P. Sreenilayam, Y. P. Panarin, J. K. Vij, V. P. Panov, A. Lehmann, M. Poppe, M. Prehm, C. Tschierske, *Nat. Commun.* **2016**, *7*, 11369.
- [85] This phase was first designated as SmAP<sub>cr</sub>, ref. [86], and later identified to be a weakly tilted smectic phase with a short-pitch helix perpendicular to the layer planes (SmCP<sub>cr</sub>, ref. [80], SmC<sub>3</sub>P<sub>F</sub><sup>hel</sup>, ref. [84]).
- [86] Y. P. Panarin, M. Nagaraj, S. Sreenilayam, J. K. Vij, A. Lehmann, C. Tschierske, *Phys. Rev. Lett.* **2011**, *107*, 247801.
- [87] a) A. De Vries, *J. Chem. Phys.* **1979**, *71*, 25; b) S. T. Lagerwall, P. Rudquist, F. Giesselmann, *Mol. Cryst. Liq. Cryst.* **2009**, *510*, 148; c) J. P. F. Lagerwall, F. Giesselmann, *ChemPhysChem* **2006**, *7*, 20.
- [88] Attempts to obtain aligned samples for SAXS and grazing-incidence (GI)SAXS experiments failed so far.
- [89] N. Vaupotic, D. Pocięcha, E. Gorecka, in *Topics in Current Chemistry*, Vol. 318, Springer, Berlin, **2012**, p. 281.

- [90] D. A. Coleman, J. Fernsler, N. Chattham, M. Nakata, Y. Takanishi, E. Körblova, D. R. Link, R.-F. Shao, W. G. Jang, J. E. MacLennan, O. Mondainn-Monval, C. Boyer, W. Weissflog, G. Pelzl, L.-C. Chien, J. Zasadzinski, J. Watanabe, D. M. Walba, H. Takezoe, N. A. Clark, *Science* **2003**, *301*, 1204.
- [91] N. Vaupotič, M. Čopič, *Phys. Rev. E* **2005**, *72*, 031701.
- [92] D. A. Coleman, C. D. Jones, M. Nakata, N. A. Clark, D. M. Walba, W. Weissflog, K. Fodor-Csorba, J. Watanabe, V. Novotna, V. Hamplova, *Phys. Rev. E* **2008**, *77*, 021703.
- [93] M. F. Achard, J. P. Bedel, J. P. Marceroua, H. T. Nguyen, J. C. Rouillon, *Eur. Phys. J. E* **2003**, *10*, 129.
- [94] P. S. Salter, P. W. Benzie, R. A. Reddy, C. Tschierske, S. J. Elston, E. P. Raynes, *Phys. Rev. E* **2009**, *80*, 031701.
- [95] According to the simple phenomenological theory of Pikin and Indenbom, ref. [96], the helical pitch in a chiral SmC phase can be described as:  $q = 2\pi/p_0 = (A + \mu P_s/\theta)K^{-1}$ , in which  $\mu$  is the flexoelectric coefficient,  $P_s$  is the spontaneous polarization,  $\theta$  is the molecular tilt angle,  $K$  is the effective elastic constant, and  $A$  is the Lifshitz invariant, which is responsible for the formation of the helix of a certain sense owing to the molecular chirality.
- [96] S. A. Pikin, V. I. Indenbom, *Ferroelectrics* **1978**, *20*, 151.
- [97] A. G. Vanakaras, D. J. Photinos, *Liq. Cryst.* **2018**, *45*, 2184.
- [98] L. E. Hough, N. A. Clark, *Phys. Rev. Lett.* **2005**, *95*, 107802.
- [99] X. Zeng, M. Prehm, G. Ungar, C. Tschierske, F. Liu, *Angew. Chem. Int. Ed.* **2016**, *55*, 8324; *Angew. Chem.* **2016**, *128*, 8464.
- [100] a) L. Guo, K. Gomola, E. Gorecka, D. Pocięcha, S. Dhara, F. Araoka, K. Ishikawa, H. Takezoe, *Soft Matter* **2011**, *7*, 2895; b) D. Pocięcha, E. Gorecka, M. Cepic, N. Vaupotic, W. Weissflog, *Phys. Rev. E* **2006**, *74*, 021702.
- [101] K. Gomola, L. Guo, D. Pocięcha, F. Araoka, K. Ishikawa, H. Takezoe, *J. Mater. Chem.* **2010**, *20*, 7944.
- [102] M. Alaasar, M. Prehm, C. Tschierske, *RSC Adv.* **2016**, *6*, 82890.
- [103] The DSC traces shown in Figure 9 indicate reversible phase transitions in the supercooled LC range of **AB16** below SmC<sub>s</sub>P<sub>A</sub>. The relatively high enthalpy values might indicate transitions to a hexatic (B<sub>5</sub>-like) and a crystalline mesophase (M) on further cooling. As these mesophases rapidly crystallize, a more detailed investigation was not possible.
- [104] E. Westphal, H. Gallardo, N. Sebastian, A. Eremin, M. Prehm, M. Alaasar, C. Tschierske, *J. Mater. Chem. C* **2019**, *7*, 3064.
- [105] a) B. L. Feringa, *Angew. Chem. Int. Ed.* **2017**, *56*, 11060; *Angew. Chem.* **2017**, *129*, 11206; b) D. Pijper, B. L. Feringa, *Soft Matter* **2008**, *4*, 1349.
- [106] H. K. Bisoyi, Q. Li, *Angew. Chem. Int. Ed.* **2016**, *55*, 2994; *Angew. Chem.* **2016**, *128*, 3046.
- [107] Z. Zheng, Y. Li, H. K. Bisoyi, L. Wang, T. J. Bunning, Q. Li, *Nature* **2016**, *531*, 352.
- [108] S.-W. Choi, T. Izumi, Y. Hoshino, Y. Takanishi, K. Ishikawa, J. Watanabe, H. Takezoe, *Angew. Chem. Int. Ed.* **2006**, *45*, 1382; *Angew. Chem.* **2006**, *118*, 1410.
- [109] H. Sasaki, Y. Takanishi, J. Yamamoto, A. Yoshizawa, *ChemistrySelect* **2018**, *3*, 3278.

---

Manuscript received: December 12, 2018

Revised manuscript received: January 21, 2019

Accepted manuscript online: February 14, 2019

Version of record online: April 11, 2019

## New azobenzene containing bent-core liquid crystals based on disubstituted resorcinol

M. Alaasar<sup>a,b\*</sup>, M. Prehm<sup>a</sup> and C. Tschierske<sup>a</sup>

<sup>a</sup>Institute of Chemistry, Martin-Luther-University Halle-Wittenberg, Halle, Germany; <sup>b</sup>Department of Chemistry, Cairo University, Giza, Egypt

(Received 1 August 2013; accepted 29 August 2013)

New bent-core molecules with 4,6-dichlororesorcinol or 4-chloro-2-methylresorcinol as the central unit, and azobenzene with different alkyloxy chain length as side arms were synthesised. The mesophase behaviour of the new compounds was investigated by polarising optical microscopy, differential scanning calorimetry, X-ray diffraction studies and electro-optical measurements. It is found that 4,6-dichlororesorcinol is more conducive towards mesomorphism than 4-chloro-2-methylresorcinol. The liquid crystalline properties of all of the prepared compounds are greatly affected by the lateral substitution on the outer ring. 4,6-Dichlororesorcinol-based compounds without lateral substitution show nematic phases with cybotactic cluster of the SmC-type ( $N_{CyBC}$ ). Moreover, depending on the chain length, the nematic phase appears as enantiotropic phase for the shortest homologue and as monotropic phase for the higher homologues.

**Keywords:** bent-core liquid crystals (BCLCs); azobenzene; 4,6-dichlororesorcinol; 4-chloro-2-methylresorcinol; nematic phase

### 1. Introduction

Liquid crystals (LCs) nowadays are the basis of displays in mobile telecommunication and computing devices. The LC molecules used in these devices have a rod-like shape. However, since the proposal by Niori et al. [1] that new polar and chiral mesophases could be obtained by using molecules with a bent-core structure, this type of bent-core LCs has attracted a great deal of attention. Many different LC phases, generally denoted as B-type mesophases, have already been described and reviewed in literature [2–5]. The interest in using the azobenzene structure as building block for LC molecules is based on two reasons. One is that this system allows delocalised electronic charge distribution between donor and acceptor groups at both sides of the  $\pi$ -system. This possibility is interesting for the design of materials with good nonlinear optical properties. In particular for optical second-harmonic generation (SHG), the azobenzene structure seems to be a good candidate to be incorporated in bent-core molecules. An additional attractive feature of the azo group is the *trans-cis* isomerisation by light absorption. In the field of LCs, this property gives rise to a new added value to the materials, which can be used for many applications, including holographic media [6,7], optical storage [8], reversible optical waveguides [9–11] and photo-alignment of LC systems [12].

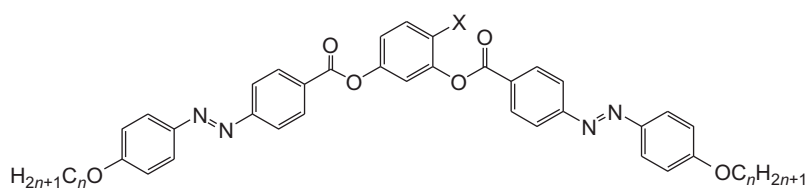
First examples of azo-containing bent-core mesogens have already been reported by Vorländer [13].

More recent examples of azo-functionalised bent-core materials exhibiting interesting physical properties have been reported by Prasad et al. [14–19] and other groups [20–27]. Often nematic phases were observed for these compounds. Nematic phases of bent-core liquid crystals (BCLCs) are quite distinct from those formed by rod- or disc-like mesogens. This is due to a special cluster structure of these nematic phases [28–31] and the distinct shape of the molecules enabling restricted rotation and polar packing, which makes them candidates for biaxial [32] and ferroelectric nematic phases [33,34].

Recently, we have reported that 4-chlororesorcinol bis[4-(4-*n*-alkoxyphenylazo)benzoates] (compounds **D<sub>n</sub>** in Table 1) form two mesophases depending on the chain length [26]. The lower homologues with alkyloxy chain containing 8 or 10 carbon atoms (*n*) show nematic and B<sub>6</sub> phases, while the higher homologues with  $n \geq 12$  show only the nematic phase. The formation of an intercalated smectic phase (B<sub>6</sub>) for molecules with shorter chains and nematic phases for compounds with longer chains is unusual and inverse to usual phase sequences. We have also reported that modification of the lateral substituent in 4-position on the central ring (F, Br or CN) proved to be very useful for obtaining azobenzene based bent-core mesogens with new phase sequences [26,27].

Here, we report new series of azobenzene containing bent-core molecules. Focus is on the effect of an additional substituent at the bent 4-chlororesorcinol

\*Corresponding author. Email: [M\\_Alaasar@yahoo.com](mailto:M_Alaasar@yahoo.com)

Table 1. Phase transition temperatures and mesophase types of compounds **Cn** and **Dn** [14,25,26].


Compound	X	<i>n</i>	Heating ( <i>T</i> /°C)	Cooling ( <i>T</i> /°C)
<b>C10</b>	H	10	Cr 147 Iso	— <sup>a</sup>
<b>C12</b>	H	12	Cr 145 Iso	Iso 136 Cr
<b>C14</b>	H	14	Cr 133 Iso	Iso 128 B <sub>1</sub> 126 Cr
<b>C16</b>	H	16	Cr 132 Iso	Iso 129 B <sub>1</sub> 123 Cr
<b>C18</b>	H	18	Cr 125 B <sub>1</sub> 131 Iso	Iso 130 B <sub>1</sub> 118 Cr
<b>D8</b>	Cl	8	Cr 115 Iso	Iso 105 B <sub>6</sub> 84 Cr
<b>D10</b>	Cl	10	Cr 105 Iso	Iso 96 <i>N</i> 80 B <sub>6</sub> 79 Cr
<b>D12</b>	Cl	12	Cr 102 Iso	Iso 94 <i>N</i> 78 Cr
<b>D14</b>	Cl	14	Cr 101 Iso	Iso 90 <i>N</i> 81 Cr
<b>D16</b>	Cl	16	Cr 105 Iso	Iso 99 <i>N</i> 86 Cr

Notes: <sup>a</sup>The crystallisation temperature is not given in [14] for **C10**. Cr = crystalline solid; B<sub>1</sub> = two-dimensional banana phase; B<sub>6</sub> = intercalated smectic banana phase; *N* = nematic phase; Iso = isotropic liquid.

unit on the LC properties, either a second chlorine group in 6-position (4,6-dichlororesorcinol-based compounds **An**, see Figure 1) or an additional methyl group in 2-position (4-chloro-2-methylresorcinol based compounds **Bn**, see Figure 2). Few examples of BCLCs based on a 4,6-dichlororesorcinol have been reported previously [28,29,35–41], but there is no report combining the 4,6-dichlororesorcinol core with azobenzene units and there is also no report on any BCLCs based on 4-chloro-2-methylresorcinol as a central core unit. In addition, structural variants of the 2,6-dichlororesorcinol compounds **An** were synthesised in order to study the effect of introducing lateral halogens (F or Br) on the outer rings of these BC molecules (compounds **AFn** and **ABrn**, see Figure 2). The phase behaviour of all these new compounds has been investigated by polarising optical microscopy (POM) and differential scanning calorimetry (DSC). The 4,6-dichlororesorcinol derivatives **An**, shown in Figure 1, are liquid crystalline materials while all other synthesised related compounds, shown in Figure 2, are not. Selected examples of the compounds with

LC phases were also investigated by X-ray diffraction (XRD) and electro-optical measurements.

## 2. Results and discussion

### 2.1 Synthesis

The synthesis of the bent-core compounds under investigation is shown in Scheme 1. Ethyl-4-(4-hydroxyphenylazo)benzoate (**1a**) and ethyl-4-(3-fluoro-4-hydroxyphenylazo)benzoate (**1b**) were synthesised according to a previously reported method [22]. 4-(4-*n*-Alkyloxyphenylazo)benzoates (**2a**) and 4-(4-*n*-alkyloxyphenylazo)benzoic acids (**3a**) are synthesised using the method described before [26,27]. The experimental details for each step along with the analytical data for the remaining compounds and for the final bent-core molecules are given in Section 4.

### 2.2 Characterisation

The purity and the chemical structures of all compounds synthesised were confirmed by the spectral data. The structure characterisation of the synthesised

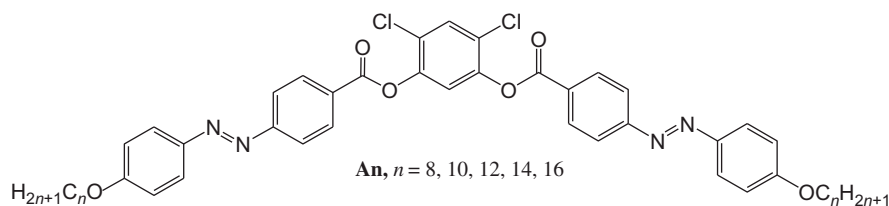


Figure 1. Chemical structure of the synthesised liquid crystalline 4,6-dichlororesorcinol compounds **An** (for phase transitions, see Table 2).

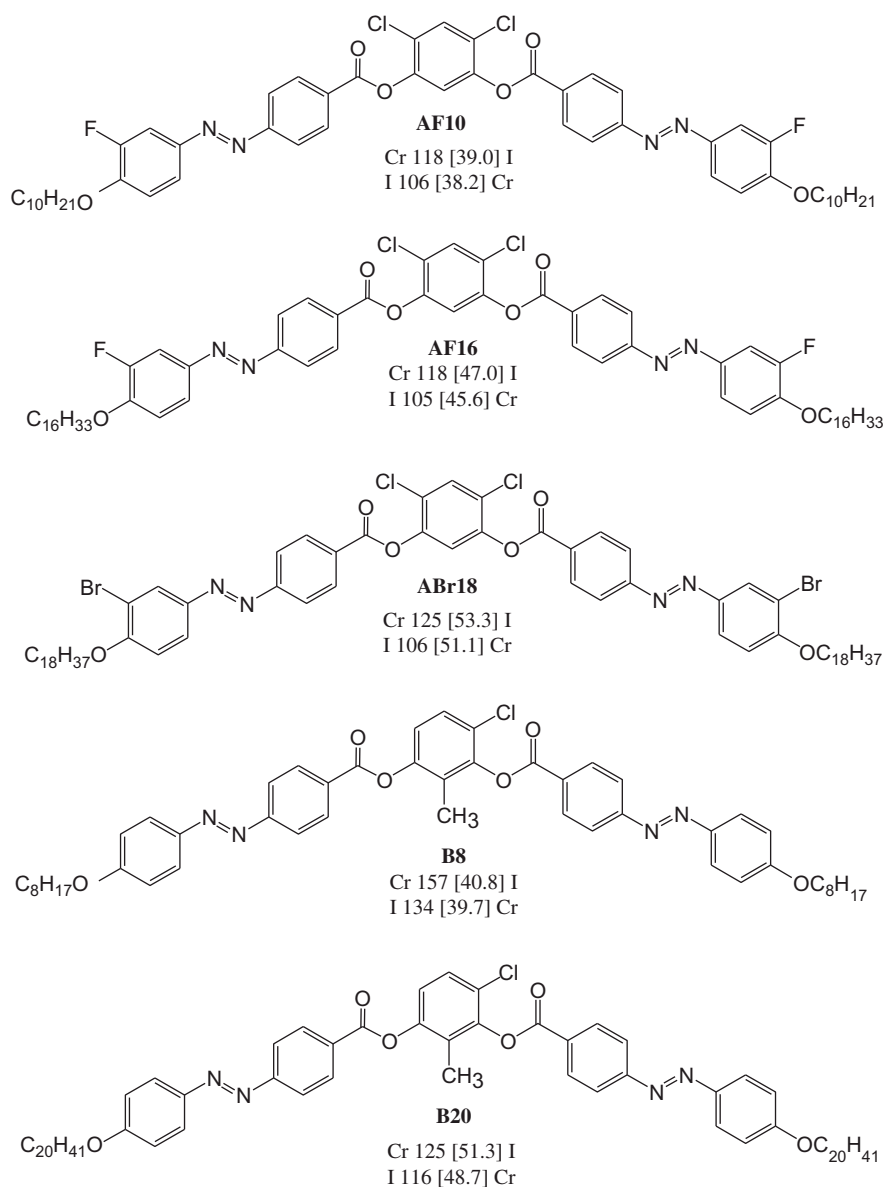


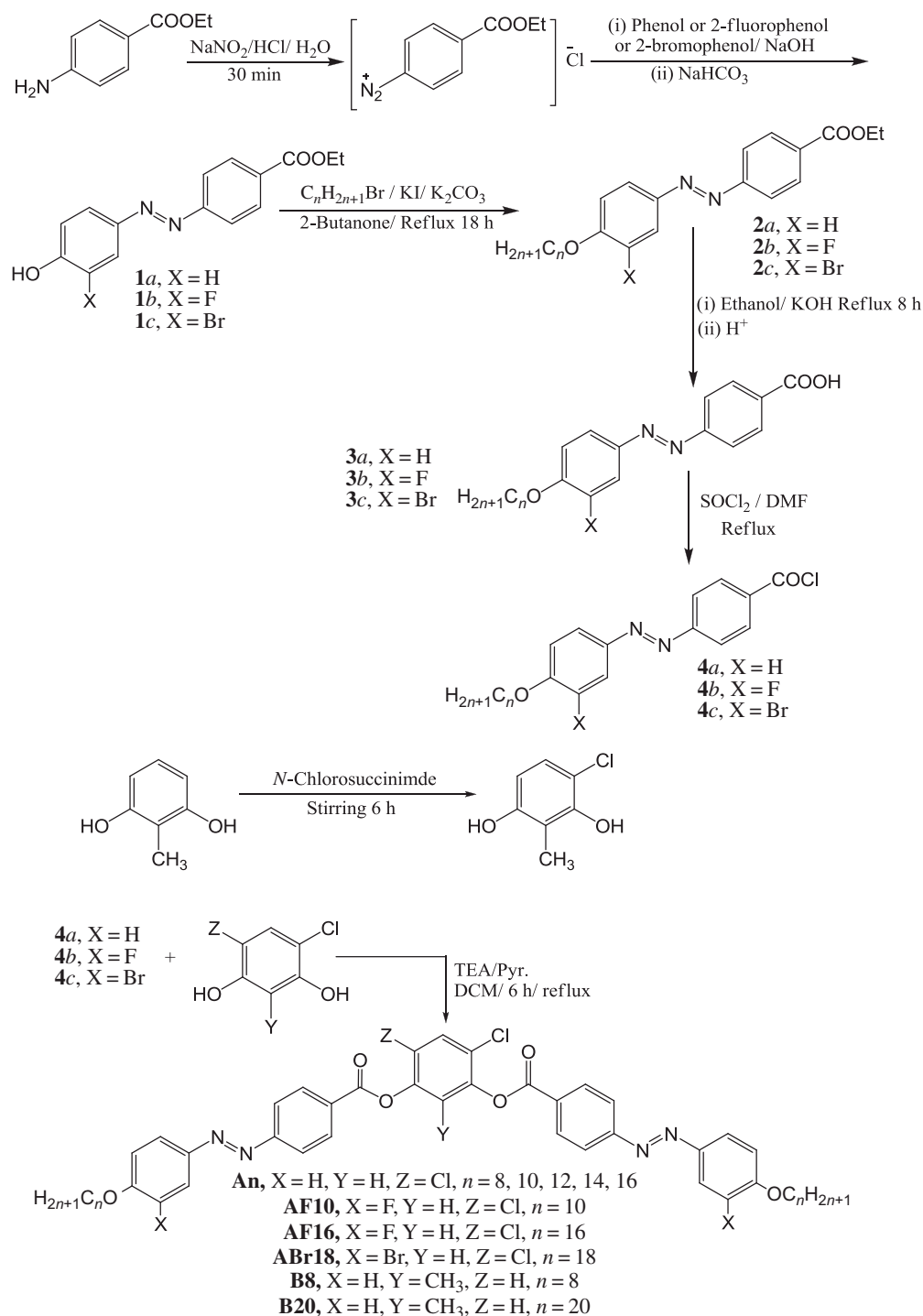
Figure 2. Chemical structures, melting temperatures (top lines) and crystallisation temperatures (bottom lines,  $T/^\circ\text{C}$ ) and corresponding enthalpies ( $\Delta H/\text{kJ mol}^{-1}$ , in brackets, data recorded by DSC at a rate of  $10 \text{ K min}^{-1}$ ) of the synthesised non-liquid crystalline compounds **AFn**, **ABrn** and **Bn**.

bent-core compounds is based on  $^1\text{H-NMR}$  (Varian Unity 500 and Varian Unity 400 spectrometers, in  $\text{CDCl}_3$  solutions, with tetramethylsilane as internal standard). Microanalyses were performed using a Leco CHNS-932 (Ceramic Co., Ltd., Hunan, China (Mainland)) elemental analyser.

The mesophase behaviour and transition temperatures of the prepared bent-core molecules were measured using a Mettler FP-82 HT (Mettler-Toledo GmbH, Gießen, Germany) hot-stage and control unit in conjunction with a Nikon Optiphot-2 polarising microscope (Nikon Instruments, Melville, NY, USA). The associated enthalpies were obtained from DSC thermograms which were recorded on a Perkin-Elmer

DSC-7 (PerkinElmer, Rodgau, Germany), heating and cooling rate:  $10 \text{ K min}^{-1}$ . The electro-optical switching characteristics were examined using a triangular-wave method using  $6\text{-}\mu\text{m}$  polyimide-coated ITO cells (EHC, Japan).

The XRD patterns were recorded with a two-dimensional (2D) detector (Vantec 500, BRUKER AXS, Inc., Madison, WI, USA). Ni-filtered and pinhole-collimated  $\text{CuK}\alpha$  radiation was used. The exposure time was 30 min and the sample to detector distance was 9.0 cm. Uniform orientation was achieved by alignment in a magnetic field ( $B \approx 1 \text{ T}$ ) using thin capillaries. The samples were held on a temperature-controlled heating stage.



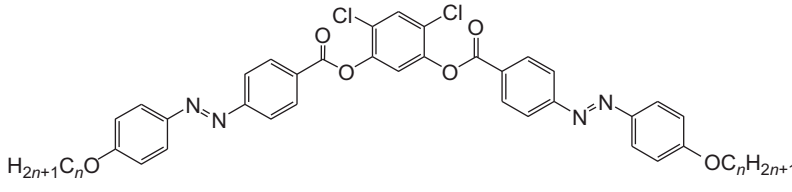
Scheme 1. Synthesis of bent core molecules under investigation.

### 2.3 Mesomorphic properties

The transition temperatures ( $^{\circ}\text{C}$ ) and the associated enthalpies ( $\text{kJ mol}^{-1}$ ) obtained from DSC thermograms of the series of the 4,6-dichlororesorcinol-based bent-core molecules **An** (Figure 1) are given in Table 2. The DSC thermograms obtained for compounds **A8**, **A10** and **A14** as examples are shown in Figure 3. All

compounds are thermally stable as confirmed by the reproducibility of thermograms on several heating and cooling cycles. All compounds form nematic phases, one of the compound **A8** with the shortest chain is enantiotropic, and those of the longer homologues are monotropic. Examples of typical textures are shown in Figure 4.



Table 2. Phase transition temperatures, mesophase types and transition enthalpies of compounds **An**.<sup>a</sup>


Compound	<i>n</i>	Heating <i>T</i> /°C [ $\Delta H$ /kJ mol <sup>-1</sup> ]	Cooling <i>T</i> /°C [ $\Delta H$ /kJ mol <sup>-1</sup> ]
<b>A8</b>	8	Cr <sub>1</sub> 111 [23.2] Cr <sub>2</sub> 116 [38.5] N 141 [2.1] Iso	Iso 139 [2.1] N 98 [44.0] Cr
<b>A10</b>	10	Cr 128 [55.8] Iso	Iso 127 [2.0] N 96 [50.5] Cr
<b>A12</b>	12	Cr 125 [57.0] Iso	Iso 122 [2.1] N 107 [55.1] Cr
<b>A14</b>	14	Cr 124 [62.3] Iso	Iso 117 [2.0] N 99 [61.2] Cr
<b>A16</b>	16	Cr 121 [71.6] Iso	Iso 117 [1.1] N 101 [67.7] Cr

Notes: <sup>a</sup>Transition temperatures and enthalpy values were taken from the second DSC heating scans (10 K min<sup>-1</sup>). Cr = crystalline solid; N = nematic phase; Iso = isotropic liquid.

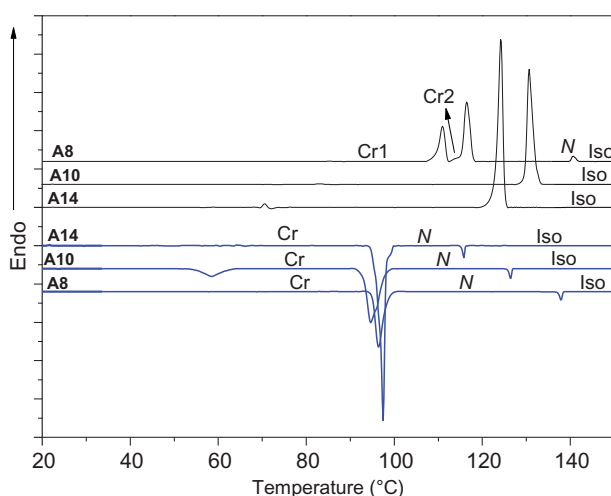


Figure 3. (colour online) DSC thermograms obtained for compounds **A8**, **A10** and **A14** as examples for the **An** series; heating and cooling rates were 10 K min<sup>-1</sup>.

The clearing temperatures of the compounds **An** decrease with chain elongation from *n* = 8–14 and remain almost the same with further chain elongation

(*n* = 16), see Figure 5. The crystallisation temperatures have a tendency to rise with growing chain length, with a distinct maximum for **A12**. Therefore, the nematic phase range observed on cooling has a maximum for **A8** with *n* = 8 (41 K) and then narrows with increasing the number of carbon atoms in the alkoxy chain (see Figure 5).

Comparison of the parent resorcinol derivatives **Cn** and the 6-chlororesorcinols **Dn** (Table 1) with the new 4,6-dichlororesorcinols **An** (Table 2) shows that monochlorination (compounds **Dn**) introduces B<sub>6</sub> phases for the shorter homologues and replaces the B<sub>1</sub> phases of the longer homologues **Cn** by nematic phases (Table 1). When the second chlorine substituent is introduced on the central core unit in 6-position (compounds **An**), the B<sub>6</sub> phases are removed and for all chain lengths exclusively nematic phases were observed (Table 2). The nematic phase stability is slightly enhanced compared to the monochlorinated compounds **Dn**.

On carrying out electro-optical experiments using a triangular wave voltage for the two compounds **A8** and **A16** with the shortest and the longest alkyl chains,

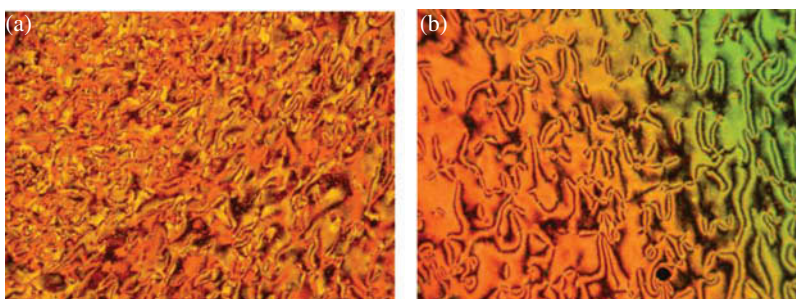


Figure 4. (colour online) Optical micrograph observed in a homeotropic cell for the nematic phase: (a) **A8** at *T* = 117°C and (b) **A10** at *T* = 128°C.

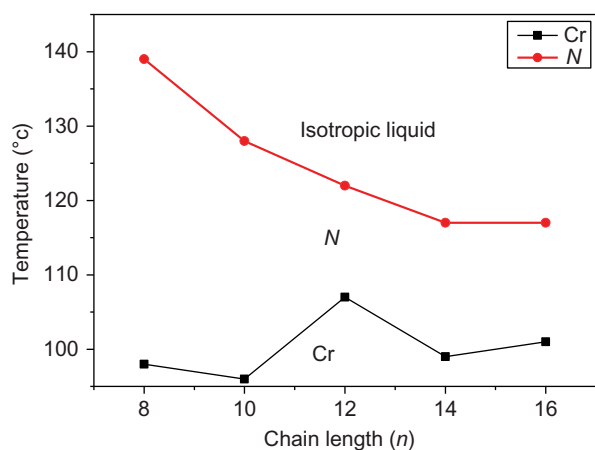


Figure 5. (colour online) Plot of the transition temperatures on cooling of compounds (**A8–A16**) as a function of the number of carbons ( $n$ ) in the alkyloxy chain.

no current peak could be observed in the nematic phases of these compounds up to a voltage of 200 V<sub>pp</sub> in a 6- $\mu$ m ITO cell, indicating the non-switching behaviour of these phases, as one would expect (see [33,34] for reports of polar order in nematic phases of some bent-core mesogens).

It is most likely that the nematic phases in series **An** represent cybotactic nematic phases as typical for bent-core mesogens [29]. XRD measurements were conducted on compound **A8** as an example. The diffraction pattern (Figure 6) shows a diffuse scattering in the wide angle region with a maximum at  $d = 0.45$  nm and a weak diffuse scattering in the small-angle region with a maximum at  $d = 4.24$  nm. The diffuse small-angle scattering has clear maxima besides the meridian (dumbbell shape), which can be attributed to the existence of cybotactic cluster of the SmC-type. From the intensity distribution, a tilt angle of the molecules within the clusters of around

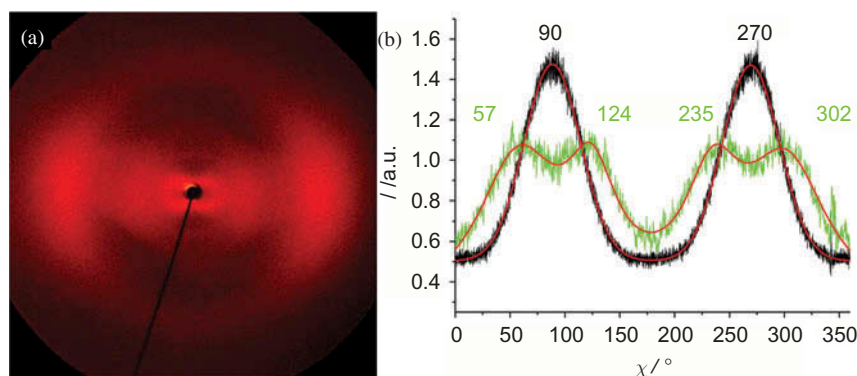


Figure 6. (colour online) XRD investigations of the nematic phase of compound **A8**: (a) diffraction pattern at 120°C; (b) intensity distribution of the diffuse scatterings along  $\chi$ , black curve wide angle scattering (15°–25°,  $2\theta$ ), green curve small-angle scattering (2°–5°,  $2\theta$ ), in red are the resulting lines after fitting to Lorentz functions.

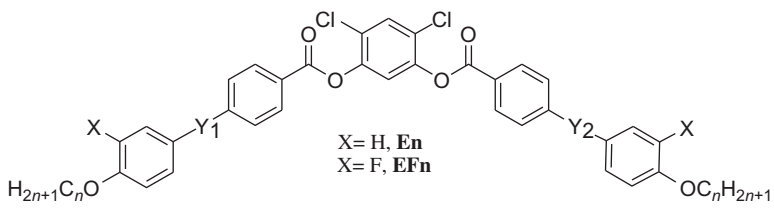
50° can be estimated. It is assumed that also the nematic phases of the higher homologues represent the same type of cybotactic nematic phases composed of SmC-clusters ( $N_{\text{CybC}}$  phases).

Aiming to induce other mesophases in the prepared compounds and to reduce the melting points, we synthesised three additional compounds (**AF10**, **AF16** and **ABr18**) by introducing a lateral halogen group at the outer ring of the bent-core molecules in the *ortho* positions with respect to the alkyloxy chain (see Figure 2). Unfortunately, all three compounds are non-mesomorphic irrespective of the type of the halogen (fluorine or bromine). The melting points and the crystallisation temperatures are not significantly influenced by the additional substituents, but LC phases are absent. For compound **AF10**, the nematic phase is depressed compared to the non-substituted compounds **A10** by at least 23 K.

In order to study the effect of introducing a methyl group at the central benzene in compounds **Dn**, we synthesised two compounds with 4-chloro-2-methylresorcinol cores (**B8** and **B20**, see Figure 2) but again these are non-mesomorphic compounds having relatively high melting points and also higher crystallisation temperatures compared to the related 4,6-dichlororesorcinol compounds (**An** series).

#### 2.4 Comparison with related compounds

In Table 3, compounds **A8–A12** and **AF10** are compared with related bent-core mesogens with the same chain length and having imine linking groups [35,36] instead of azo linking groups. If the  $-\text{N}=\text{N}-$  linkages in compounds **A8** and **A10** ( $n = 8, 10$ ) were replaced by imine groups (**E8** and **E10**), then the same phase type, i.e. nematic phases, was observed, but for the azobenzenes **An**, the stability of the N phase strongly decreases with chain elongation, whereas the

Table 3. Comparison of azobenzene based bent-core mesogens (**An** and **AF10**) with related Schiff base compounds (**En** and **EF10**).<sup>a</sup>


Compound	<i>n</i>	Y <sub>1</sub>	Y <sub>2</sub>	X	<i>T</i> /°C	Reference
<b>A8</b>	8	–N=N–	–N=N–	H	Cr 116 <i>N</i> 141 Iso	
<b>E8</b>	8	–N=CH–	–CH=N–	H	Cr 126 <i>N</i> 148 Iso	[36]
<b>A10</b>	10	–N=N–	–N=N–	H	Cr 127 ( <i>N</i> 96) Iso	
<b>E10</b>	10	–N=CH–	–CH=N–	H	Cr 114 <i>N</i> 147 Iso	[35]
<b>A12</b>	12	–N=N–	–N=N–	H	Cr 125 ( <i>N</i> 107) Iso	
<b>E12</b>	12	–N=CH–	–CH=N–	H	Cr 111 USmC 113 SmC 121 <i>N</i> 137 Iso	[36]
<b>AF10</b>	10	–N=N–	–N=N–	F	Cr 126 Iso	
<b>EF10</b>	10	–N=CH–	–CH=N–	F	Cr 79 (SmCP <sub>A</sub> 54) SmA 137 Iso	[35]

Note: <sup>a</sup>Cr = crystalline solid; *N* = nematic phase; Iso = isotropic liquid; USmC = smectic C phase with undulated structure; SmCP<sub>A</sub> = anti-ferroelectric polar smectic C phase.

effect of chain elongation is smaller for the Schiff base compounds **En**. Further increasing the chain length leads to the formation of SmC and undulated SmC phases in the case of Schiff base compound **E12**, whereas the *N* phase is retained for the azobenzenes **An** ( $n = 8–16$ ); even compound **A16** has only a nematic phase. It appears that the more polar imine groups in compounds **En** favour the segregation of the aromatics and aliphatic chains more strongly than it is the case for the azobenzenes **An**. Also, the core–core interactions could be stronger for compounds having the polar Schiff base units, which is also favourable for the formation of smectic phases.

Comparing the effect of increasing number of Cl-substituents at the core unit indicates that replacing one H atom of the resorcinol unit by Cl in compounds **Cn** removes the B<sub>1</sub> phases which are replaced by B<sub>6</sub> phases (short chains) or *N* phases (long chains) in the related 4-chloro substituted compounds **Dn** (see Table 1). Upon introduction of the second Cl-substituent in 6-position (compounds **An**, see Table 2) also the B<sub>6</sub> phase is removed and the nematic phases are stabilised. This indicates that the tendency of formation of (modulated) smectic phases is reduced and nematic phases are stabilised by increasing the number of Cl substituents at the resorcinol core. This can be mainly attributed to the effect of these substituents on the bending angle. With increasing number of substituent in *ortho* position to the ester groups, the average shape of the molecules becomes less bent, as previously confirmed by NMR investigations with related Schiff base derived bent-core molecules [36].

Introducing a lateral fluorine group at the outer ring in compounds **An** destabilises the nematic phase and results in crystalline compounds **AFn**. Replacing the –N=N– linkage in compound **AF10** by an imine group [35] in compound **EF10** leads to a monotropic SmCP<sub>A</sub> phase and an enantiotropic SmA phase. In this case, introduction of F reduces the LC phase stability by only 10 K and replaces the nematic phase by smectic phases (compare compounds **E10** and **EF10** in Table 3). This indicates that the effect of peripheral F-substitution strongly depends on the core structure, probably due to a distinct effect of these F-atoms on the electron density distribution along the distinct  $\pi$ -conjugated units. Overall, compared to the Schiff bases, the azobenzenes **An**, especially those with long alkoxy chains, have lower mesophase stabilities and form predominantly skewed (SmC-cluster type) cybotactic nematic phases.

### 3. Conclusion

In summary, we reported a new series of halogen-substituted photosensitive bent-core molecules exhibiting nematic phases (series **An**). An enantiotropic nematic phase is observed for the shortest homologue (**A8**) and monotropic nematic phases are observed for all higher homologues (**A10–A16**). The nematic phases represent cybotactic nematic phases composed of SmC clusters (N<sub>Cybc</sub>) and these nematic phases are strongly dominating, even long-chain compounds form only nematic phases. The mesogens with additional halogen (X = F or Br) at the periphery are only crystalline and show no LC phases. Moreover,

we used 4-chloro-2-methylresorcinol as the central core unit for the first time in bent-core molecules; however, the results show that this bent unit leads to non-mesomorphic compounds (**B8** and **B20**). Finally, comparing the prepared materials with related Schiff base compounds indicates that the  $\text{-N=N-}$  linkage is less conducive to mesomorphism than the  $\text{-CH=N-}$  linkage, especially smectic phases are suppressed.

## 4. Experimental details

### 4.1 General

The synthesis was carried out according to Scheme 1. Thin layer chromatography (TLC) was performed on aluminium sheet pre-coated with silica gel. Analytical quality chemicals were obtained from commercial sources and used as obtained. The solvents were dried using the standard methods when required.

### 4.2 Synthetic procedures and analytical data

#### 4.2.1 Ethyl-4-(3-bromo-4-hydroxyphenylazo) benzoate (**1c**)

A stirred mixture of ethyl *p*-aminobenzoate (8.25 g, 0.05 mol) and 16% HCl (30 ml) was cooled below 5°C and a solution of NaNO<sub>2</sub> (3.52 g, 0.051 mol) in water (10 ml) was added drop wise in such a way that the temperature of the reaction mixture was 0–5°C. This cold solution was added drop wise to a cold mixture of 2-bromophenol (8.99 g, 0.052 mol), NaOH (10 g, 0.25 mol) and water (15 ml). The temperature of this mixture was maintained below 5°C throughout the addition. The solution was made basic with 100 mL of a saturated solution of NaHCO<sub>3</sub>. A brown solid precipitated, which was filtered off and washed with distilled water and recrystallised from aq. ethanol to give an orange solid.

Yield 66%; m.p. 156°C; <sup>1</sup>H-NMR (400 MHz, acetone)  $\delta$ : 8.35–8.09 (m, 3H, Ar-H), 8.03–7.83 (m, 3H, Ar-H), 7.23 (d,  $J = 8.6$  Hz, 1H, Ar-H), 6.1 (s, 1H, OH), 4.50–4.25 (q,  $J = 7.1$  Hz, 2H,  $\text{-CH}_2\text{CH}_3$ ), 1.40 (t,  $J = 7.1$  Hz, 3H, CH<sub>3</sub>).

#### 4.2.2 Ethyl-4-(3-fluoro-4-alkyloxyphenylazo) benzoate (**2b**)

Compound **1b** (0.01 mol), *n*-alkylbromide (0.012 mol), K<sub>2</sub>CO<sub>3</sub> (2.76 g, 0.02 mol) and a catalytic amount of KI were mixed in 100 ml of 2-butanone. The mixture was heated under reflux for 18 hours under argon atmosphere, cooled to room temperature and poured into ice (100 g). The product was extracted into CH<sub>2</sub>Cl<sub>2</sub> (50 ml  $\times$  3) and the extract washed with distilled water (100 ml  $\times$  3) and dried

over Na<sub>2</sub>SO<sub>4</sub>. The crude product obtained after removal of the solvent was recrystallised twice using ethanol. As an example, the analytical data obtained for ethyl-4-(3-fluoro-4-decyloxyphenylazo)benzoate are as follows: yield 74.5%, m.p. 91°C; <sup>1</sup>H-NMR (400 MHz, CDCl<sub>3</sub>)  $\delta$ : 8.18 (d,  $J = 8.6$  Hz, 2H, Ar-H), 7.90 (d,  $J = 8.6$  Hz, 2H, Ar-H), 7.83–7.75 (m, 1H, Ar-H), 7.72 (dd,  $J = 12.0, 2.3$  Hz, 1H, Ar-H), 7.08 (t,  $J = 8.6$  Hz, 1H, Ar-H), 4.42 (q,  $J = 7.1$  Hz, 2H,  $\text{-CH}_2\text{CH}_3$ ), 4.13 (t,  $J = 6.6$  Hz, 2H,  $\text{-OCH}_2\text{CH}_2$ ), 2.00–1.78 (m, 2H,  $\text{-OCH}_2\text{CH}_2$ ), 1.61–1.18 (m, 17H, CH<sub>2</sub> and CH<sub>3</sub>), 0.89 (t,  $J = 6.8$  Hz, 3H, CH<sub>3</sub>).

#### 4.2.3 Ethyl-4-(3-bromo-4-octadecyloxyphenylazo) benzoate (**2c**)

This was prepared using the same method used for **2b**; yield 92%; m.p. 77°C, <sup>1</sup>H-NMR (400 MHz, CDCl<sub>3</sub>)  $\delta$ : 8.26–8.12 (m, 3H, Ar-H), 7.99–7.85 (m, 3H, Ar-H), 7.01 (d,  $J = 8.8$  Hz, 1H, Ar-H), 4.42 (q,  $J = 7.1$  Hz, 2H,  $\text{-CH}_2\text{CH}_3$ ), 4.13 (t,  $J = 6.5$  Hz, 2H,  $\text{-OCH}_2\text{CH}_2$ ), 1.97–1.78 (m, 2H,  $\text{-OCH}_2\text{CH}_2$ ), 1.62–1.15 (m, 33H, CH<sub>2</sub> and CH<sub>3</sub>), 0.88 (t,  $J = 6.8$  Hz, 3H, CH<sub>3</sub>).

#### 4.2.4 4-(3-Fluoro-4-alkyloxyphenylazo)benzoic acids (**3b**)

Compound **2b** (1.0 g) was dissolved in 95% ethanol (50 ml) and 10% aq. NaOH (2 ml) was added. The mixture was heated under reflux for 6 hours, cooled to room temperature, poured into ice cold water (100 ml), and acidified with dil. HCl. The crude product obtained by filtration was recrystallised twice using glacial acetic acid. As an example, the analytical data obtained for ethyl-4-(3-fluoro-4-decyloxyphenylazo)benzoic acid are as follows: yield 95%; phase transitions: crystalline 140°C smectic C 212°C nematic 252°C isotropic; <sup>1</sup>H-NMR (400 MHz, DMSO-d<sub>6</sub>)  $\delta$ : 8.11 (d,  $J = 8.6$  Hz, 2H, Ar-H), 7.90 (d,  $J = 8.6$  Hz, 2H, Ar-H), 7.87–7.78 (m,  $J = 8.7$  Hz, 1H, Ar-H), 7.71 (dd,  $J = 12.1, 2.3$  Hz, 1H, Ar-H), 7.39 (t,  $J = 8.8$  Hz, 1H, Ar-H), 4.17 (t,  $J = 6.5$  Hz, 2H,  $\text{-OCH}_2\text{CH}_2$ ), 1.83–1.69 (m, 2H,  $\text{-OCH}_2\text{CH}_2$ ), 1.51–1.16 (m, 14H, CH<sub>2</sub>), 0.85 (t,  $J = 6.8$  Hz, 3H, CH<sub>3</sub>).

#### 4.2.5 4-(3-Bromo-4-octadecyloxyphenylazo)benzoic acid (**3c**)

This was prepared using the same method used for **3b**; yield 97%; phase transitions: crystalline 147°C smectic C 209°C nematic 212°C isotropic; <sup>1</sup>H-NMR (400 MHz, DMSO-d<sub>6</sub>)  $\delta$ : 8.17–8.06 (m, 3H, Ar-H), 7.99 (dd,  $J = 8.8, 2.3$  Hz, 1H, Ar-H), 7.92

(d,  $J = 8.4$  Hz, 2H, Ar-H), 7.33 (d,  $J = 8.9$  Hz, 1H, Ar-H), 4.18 (t,  $J = 6.2$  Hz, 2H,  $-\text{OCH}_2\text{CH}_2$ ), 1.84–1.70 (m,  $J = 14.1, 6.8$  Hz, 2H,  $-\text{OCH}_2\text{CH}_2$ ), 1.53–1.11 (m, 30H,  $\text{CH}_2$ ), 0.83 (t,  $J = 6.7$  Hz, 3H,  $\text{CH}_3$ ).

#### 4.2.6 4-Chloro-2-methylresorcinol

This was prepared according to the method described in [42] as follows: To a solution of 2-methylresorcinol (40 g, 322 mmol) in 750 ml of methanol was added (45.17 g, 0.338 mol) of *N*-chlorosuccinimide. The mixture was stirred for 6 hours. The solvent was evaporated and the resulting solid was triturated in 500 ml of a 2:1 mixture of hexane/ethyl acetate. The brown crystalline precipitate (succinimide) was filtered off and rinsed with a little extra solvent. The filtrate was concentrated to give the crude product, which was further purified on silica eluting with 4:1 hexanes/ethylacetate. Appropriate fractions were combined, and evaporated. The product was crystallised from about 1:8 ether/hexane.

Yield 64.8%; m.p. 61°C;  $^1\text{H-NMR}$  (400 MHz,  $\text{DMSO-d}_6$ )  $\delta$ : 9.33 (s, 1H, OH), 8.77 (s, 1H, OH), 6.91 (d,  $J = 8.7$  Hz, 1H, Ar-H), 6.32 (d,  $J = 8.7$  Hz, 1H, Ar-H), 1.98 (s, 3H,  $\text{CH}_3$ ).

#### 4.2.7 Final bent-core molecules

These were prepared as follows: 2.4 mmol of the acid **3a-c** was heated under reflux with thionyl chloride (3 ml) and a catalytic amount of *N,N*-dimethylformamide (DMF) for 1 hour. The excess of thionyl chloride was removed by distillation under reduced pressure. The acid chloride (**4a-c**) was then dissolved in dry dichloromethane (DCM, 20 ml). To this solution, 4,6-dichlororesorcinol or 2-methyl-4-chlororesorcinol (1.2 mmol) previously dissolved in DCM (10 ml) was added, followed by the addition of triethylamine (TEA, 2.8 mmol) and a catalytic amount of pyridine (pyr.). The solution was then refluxed for 6 hours under an argon atmosphere. After cooling the reaction mixture to the room temperature, it was washed with 10% HCl ( $2 \times 50$  mL) and several times with cold water then extracted with dichloromethane ( $3 \times 50$  mL) and finally dried over anhydrous sodium sulphate. The crude residue obtained after removal of solvent was chromatographed on silica gel using chloroform as eluent. Removal of solvent from the eluate afforded an orange material which was recrystallised twice from chloroform/ethanol mixture to give the final bent-core compounds.

**A8**: Yield 80%;  $^1\text{H-NMR}$  (500 MHz,  $\text{CDCl}_3$ )  $\delta$ : 8.33 (d,  $J = 8.6$  Hz, 4H, Ar-H), 8.00–7.90 (m, 8H, Ar-H), 7.65 (s, 1H), 7.42 (s, 1H), 7.03 (d,  $J = 8.6$  Hz,

4H, Ar-H), 4.05 (t,  $J = 6.6$  Hz, 4H,  $-\text{OCH}_2\text{CH}_2$ ), 1.86–1.76 (m, 4H,  $-\text{OCH}_2\text{CH}_2$ ), 1.53–1.22 (m, 20H,  $\text{CH}_2$ ), 0.88 (t,  $J = 7.0$  Hz, 6H,  $\text{CH}_3$ ).

Elemental analysis: Calc. for  $\text{C}_{48}\text{H}_{52}\text{Cl}_2\text{N}_4\text{O}_6$  C, 67.68; H, 6.15; N, 6.58. Found C, 67.70; H, 6.15; N, 6.59%.

**A10**: Yield 81%;  $^1\text{H-NMR}$  (400 MHz,  $\text{CDCl}_3$ )  $\delta$ : 8.35 (d,  $J = 8.6$  Hz, 4H, Ar-H), 8.03–7.91 (m, 8H, Ar-H), 7.67 (s, 1H), 7.44 (s, 1H), 7.02 (d,  $J = 8.6$  Hz, 4H, Ar-H), 4.06 (t,  $J = 6.6$  Hz, 4H,  $-\text{OCH}_2\text{CH}_2$ ), 1.89–1.77 (m, 4H,  $-\text{OCH}_2\text{CH}_2$ ), 1.56–1.20 (m, 28H,  $\text{CH}_2$ ), 0.89 (t,  $J = 6.8$  Hz, 6H,  $\text{CH}_3$ ).

Elemental analysis: Calc. for  $\text{C}_{52}\text{H}_{60}\text{Cl}_2\text{N}_4\text{O}_6$  C, 68.79; H, 6.66; N, 6.17. Found C, 68.77; H, 6.66; N, 6.18%.

**A12**: Yield 78%;  $^1\text{H-NMR}$  (400 MHz,  $\text{CDCl}_3$ )  $\delta$ : 8.35 (d,  $J = 8.6$  Hz, 4H, Ar-H), 7.97–8.02 (m, 8H, Ar-H), 7.67 (s, 1H), 7.44 (s, 1H), 7.02 (d,  $J = 8.6$  Hz, 4H, Ar-H), 4.06 (t,  $J = 6.5$  Hz, 4H,  $-\text{OCH}_2\text{CH}_2$ ), 1.89–1.78 (m, 4H,  $-\text{OCH}_2\text{CH}_2$ ), 1.56–1.20 (m, 36H,  $\text{CH}_2$ ), 0.88 (t,  $J = 6.8$  Hz, 6H,  $\text{CH}_3$ ).

Elemental analysis: Calc. for  $\text{C}_{56}\text{H}_{68}\text{Cl}_2\text{N}_4\text{O}_6$  C, 69.77; H, 7.11; N, 5.81. Found C, 69.74; H, 7.12; N, 5.78%.

**A14**: Yield 77%;  $^1\text{H-NMR}$  (400 MHz,  $\text{CDCl}_3$ )  $\delta$ : 8.35 (d,  $J = 8.6$  Hz, 4H, Ar-H), 7.97–8.03 (m, 8H, Ar-H), 7.67 (s, 1H), 7.44 (s, 1H), 7.03 (d,  $J = 9.0$  Hz, 4H, Ar-H), 4.06 (t,  $J = 6.6$  Hz, 4H,  $-\text{OCH}_2\text{CH}_2$ ), 1.90–1.75 (m, 4H,  $-\text{OCH}_2\text{CH}_2$ ), 1.56–1.19 (m, 44H,  $\text{CH}_2$ ), 0.88 (t,  $J = 6.9$  Hz, 6H,  $\text{CH}_3$ ).

Elemental analysis: Calc. for  $\text{C}_{60}\text{H}_{76}\text{Cl}_2\text{N}_4\text{O}_6$  C, 70.64; H, 7.51; N, 5.49. Found C, 70.70; H, 7.47; N, 5.48%.

**A16**: Yield 65%;  $^1\text{H-NMR}$  (400 MHz,  $\text{CDCl}_3$ )  $\delta$ : 8.35 (d,  $J = 8.6$  Hz, 4H, Ar-H), 7.98–8.02 (m, 8H, Ar-H), 7.67 (s, 1H), 7.44 (s, 1H), 7.02 (d,  $J = 8.5$  Hz, 4H, Ar-H), 4.06 (t,  $J = 6.6$  Hz, 4H,  $-\text{OCH}_2\text{CH}_2$ ), 1.88–1.78 (m, 4H,  $-\text{OCH}_2\text{CH}_2$ ), 1.56–1.21 (m, 52H,  $\text{CH}_2$ ), 0.88 (t,  $J = 6.8$  Hz, 6H,  $\text{CH}_3$ ).

Elemental analysis: Calc. for  $\text{C}_{64}\text{H}_{84}\text{Cl}_2\text{N}_4\text{O}_6$  C, 71.42; H, 7.87; N, 5.21. Found C, 71.42; H, 7.88; N, 5.20%.

**AF10**: Yield 75%;  $^1\text{H-NMR}$  (400 MHz,  $\text{CDCl}_3$ )  $\delta$ : 8.36 (d,  $J = 8.6$  Hz, 4H, Ar-H), 7.99 (d,  $J = 8.6$  Hz, 4H, Ar-H), 7.82 (d,  $J = 8.6$  Hz, 2H, Ar-H), 7.74 (dd,  $J = 11.9, 2.3$  Hz, 2H, Ar-H), 7.67 (s, 1H, Ar-H), 7.44 (s, 1H, Ar-H), 7.10 (t,  $J = 8.6$  Hz, 2H, Ar-H), 4.14 (t,  $J = 6.6$  Hz, 4H,  $-\text{OCH}_2\text{CH}_2$ ), 1.94–1.81 (m, 4H,  $-\text{OCH}_2\text{CH}_2$ ), 1.58–1.17 (m, 28H,  $\text{CH}_2$ ), 0.88 (t,  $J = 6.8$  Hz, 6H,  $\text{CH}_3$ ).

Elemental analysis: Calc. for  $\text{C}_{52}\text{H}_{58}\text{Cl}_2\text{F}_2\text{N}_4\text{O}_6$  C, 66.16; H, 6.19; N, 5.49. Found C, 66.18; H, 6.19; N, 5.50%.

**AF16:** Yield 66%;  $^1\text{H-NMR}$  (500 MHz,  $\text{CDCl}_3$ )  $\delta$ : 8.35 (d,  $J = 8.6$  Hz, 4H, Ar-H), 7.98 (d,  $J = 8.6$  Hz, 4H, Ar-H), 7.82 (d,  $J = 8.6$  Hz, 2H, Ar-H), 7.74 (dd,  $J = 11.9, 2.3$  Hz, 2H, Ar-H), 7.67 (s, 1H, Ar-H), 7.45 (s, 1H, Ar-H), 7.09 (t,  $J = 8.6$  Hz, 2H, Ar-H), 4.14 (t,  $J = 6.6$  Hz, 4H,  $-\text{OCH}_2\text{CH}_2$ ), 1.96–1.74 (m, 4H,  $-\text{OCH}_2\text{CH}_2$ ), 1.58–1.17 (m, 52H,  $\text{CH}_2$ ), 0.87 (t,  $J = 6.8$  Hz, 6H,  $\text{CH}_3$ ). Elemental analysis: Calc. for  $\text{C}_{64}\text{H}_{82}\text{Cl}_2\text{F}_2\text{N}_4\text{O}_6$  C, 69.11; H, 7.43; N, 5.04. Found C, 69.10; H, 7.44; N, 5.03%.

**ABr18:** Yield 60%;  $^1\text{H-NMR}$  (400 MHz,  $\text{CDCl}_3$ )  $\delta$ : 8.36 (d,  $J = 8.5$  Hz, 4H, Ar-H), 8.23 (d,  $J = 2.3$  Hz, 2H, Ar-H), 8.06–7.86 (m, 6H, Ar-H), 7.67 (s, 1H, Ar-H), 7.44 (s, 1H, Ar-H), 7.03 (d,  $J = 8.9$  Hz, 2H, Ar-H), 4.14 (t,  $J = 6.5$  Hz, 4H,  $-\text{OCH}_2\text{CH}_2$ ), 1.97–1.79 (m, 4H,  $-\text{OCH}_2\text{CH}_2$ ), 1.64–1.14 (m, 60H,  $\text{CH}_2$ ), 0.88 (t,  $J = 6.8$  Hz, 6H,  $\text{CH}_3$ ). Elemental analysis: Calc. for  $\text{C}_{68}\text{H}_{90}\text{Br}_2\text{Cl}_2\text{N}_4\text{O}_6$  C, 63.30; H, 7.03; N, 4.34. Found C, 63.26; H, 7.10; N, 4.33%.

**B8:** Yield 78%;  $^1\text{H-NMR}$  (400 MHz,  $\text{CDCl}_3$ )  $\delta$ : 8.44–8.30 (m, 4H, Ar-H), 8.04–7.90 (m, 8H, Ar-H), 7.42 (d,  $J = 8.7$  Hz, 1H, Ar-H), 7.15 (d,  $J = 8.7$  Hz, 1H, Ar-H), 7.02 (d,  $J = 8.8$  Hz, 4H, Ar-H), 4.06 (t,  $J = 6.6$  Hz, 4H,  $-\text{OCH}_2\text{CH}_2$ ), 2.18 (s, 3H,  $\text{CH}_3$ ), 1.90–1.76 (m, 4H,  $-\text{OCH}_2\text{CH}_2$ ), 1.63–1.20 (m, 20H,  $\text{CH}_2$ ), 0.90 (t,  $J = 6.8$  Hz, 6H,  $\text{CH}_3$ ). Elemental analysis: Calc. for  $\text{C}_{49}\text{H}_{55}\text{ClN}_4\text{O}_6$  C, 70.78; H, 6.67; N, 6.74. Found C, 70.77; H, 6.71; N, 6.71%.

**B20:** Yield 59%;  $^1\text{H-NMR}$  (500 MHz,  $\text{CDCl}_3$ )  $\delta$ : 8.43–8.28 (m, 4H, Ar-H), 8.04–7.89 (m, 8H, Ar-H), 7.42 (d,  $J = 8.7$  Hz, 1H, Ar-H), 7.15 (d,  $J = 8.7$  Hz, 1H, Ar-H), 7.03 (d,  $J = 7.1$  Hz, 4H, Ar-H), 4.06 (t,  $J = 6.5$  Hz, 4H,  $-\text{OCH}_2\text{CH}_2$ ), 2.18 (s, 3H,  $\text{CH}_3$ ), 1.90–1.75 (m, 4H,  $-\text{OCH}_2\text{CH}_2$ ), 1.58–1.15 (m, 68H,  $\text{CH}_2$ ), 0.88 (t,  $J = 6.9$  Hz, 6H,  $\text{CH}_3$ ). Elemental analysis: Calc. for  $\text{C}_{73}\text{H}_{103}\text{ClN}_4\text{O}_6$  C, 75.06; H, 8.89; N, 4.80. Found C, 75.10; H, 8.86; N, 4.84%.

### Acknowledgements

M. Alaasar is grateful to the Alexander von Humboldt Foundation for the research fellowship at Martin-Luther University, Halle, Germany.

### References

- [1] Niori T, Sekine T, Watanabe J, Furukawa T, Takezoe H. Distinct ferroelectric smectic liquid crystals consisting of banana shaped achiral molecules. *J Mater Chem.* 1996;6:1231–1233.
- [2] Pelzl G, Diele S, Weissflog W. Banana-shaped compounds – a new field of liquid crystals. *Adv Mater.* 1999;11:707–724.
- [3] Ros MB, Serrano JL, Fuente MR, de la, Folcia CL. Banana-shaped liquid crystals: a new field to explore. *J Mater Chem.* 2005;15:5093–5098.
- [4] Reddy RA, Tschierske C. Bent-core liquid crystals: polar order, superstructural chirality and spontaneous desymmetrisation in soft matter systems. *J Mater Chem.* 2006;16:907–961.
- [5] Takezoe H, Takanishi Y. Bent-core liquid crystals: their mysterious and attractive world. *Jpn J Appl Phys.* 2006;45:597–625.
- [6] Rochon P, Batalla E, Natanson A. Optically induced surface gratings on azoaromatic polymer films. *Appl Phys Lett.* 1995;66:136–138.
- [7] Kim DY, Li SK, Tripathy L, Kumar J. Laser-induced holographic surface relief gratings on nonlinear optical polymer films. *Appl Phys Lett.* 1995;66:1166–1168.
- [8] Haus HA. Linearity of optical amplifiers and the Tomonaga approximation. *J Opt Soc Am.* 2001;B18:1777–1779.
- [9] Meng X, Natansohn A, Barrett C, Rochon P. Azo polymers for reversible optical storage. 10. Cooperative motion of polar side groups in amorphous polymers. *Macromolecules.* 1996;29:946–952.
- [10] Ho M, Natansohn A, Barrett C, Rochon P. Azo polymers for reversible optical storage. 8. The effect of polarity of the azobenzene groups. *Can J Chem.* 1995;73:1773–1778.
- [11] Natansohn A, Rochon P, Ho M, Barrett C. Azo polymers for reversible optical storage. 6. Poly[4-[2-(methacryloyloxy)ethyl]azobenzene]. *Macromolecules.* 1995;28:4179–4183.
- [12] Ichimura K. Photoalignment of liquid-crystal systems. *Chem Rev.* 2000;100:1847–1873.
- [13] Vorländer D. Die Richtung der Kohlenstoff-Valenzen in Benzol-Abkömmlingen. *Ber Dtsch Chem Ges.* 1929;62:2831–2835.
- [14] Prasad V. Liquid crystalline compounds with V-shaped molecular structures: synthesis and characterization of new azo compounds. *Liq Cryst.* 2001;28:145–150.
- [15] Prasad V, Rao DSS, Prasad SK. A novel class of banana-shaped azo compounds exhibiting antiferroelectric switching behaviour. *Liq Cryst.* 2001;28:643–646.
- [16] Prasad V. Bent-shaped achiral azo compounds exhibiting banana mesophases. *Mol Cryst Liq Cryst.* 2001;363:167–179.
- [17] Prasad V, Jákli A. Achiral bent-core azo compounds: observation of photoinduced effects in an antiferroelectric tilted smectic mesophase. *Liq Cryst.* 2004;31:473–479.
- [18] Prasad V, Kang SW, Qi X, Kumar SJ. Photoresponsive and electrically switchable mesophases in a novel class of achiral bent-core azo compounds. *J Mater Chem.* 2004;14:1495–1502.
- [19] Prasad V, Kang SW, Suresh KA, Joshi L, Wang Q, Kumar S. Thermotropic uniaxial and biaxial nematic and smectic phases in bent-core mesogens. *J Am Chem Soc.* 2005;127:17224–17227.
- [20] Folcia CL, Alonso I, Ortega J, Etxebarria J, Pintre I, Ros MB. Achiral bent-core liquid crystals with azo and azoxy linkages: structural and nonlinear optical properties and photoisomerization. *Chem Mater.* 2006;18:4617–4626.
- [21] Pintre IC, Gimeno N, Serrano JL, Ros MB, Alonso I, Folcia CL, Ortega J, Etxebarria J. Liquid crystalline and nonlinear optical properties of bent-shaped compounds derived from 3,4'-biphenylene. *J Mater Chem.* 2007;17:2219–2227.

- [22] Lutfor MR, Hegde G, Kumar S, Tschierske C, Chigrinov VG. Synthesis and characterization of bent-shaped azobenzene monomers: Guest–host effects in liquid crystals with azo dyes for optical image storage devices. *Opt Mater.* 2009;32:176–183.
- [23] Rahman L, Kumar S, Tschierske C, Israel G, Ster D, Hegde G. Synthesis and photoswitching properties of bent shaped liquid crystals containing azobenzene monomers. *Liq Cryst.* 2009;36:397–407.
- [24] Vijaysrinivasan M, Kannan P, Roy A. Dual switchable six-ring bent-core liquid crystals with azo linkages exhibiting  $B_1$  and  $B_2$  mesophases. *Liq Cryst.* 2012;39:1465–1475.
- [25] Nagaveni NG, Roy A, Prasad V. Achiral bent-core azo compounds: effect of different types of linkage groups and their direction of linking on liquid crystalline properties. *J Mater Chem.* 2012;22:8948–8959.
- [26] Alaasar M, Prehm M, Tschierske C. Influence of halogen substituent on the mesomorphic properties of five-ring banana-shaped molecules with azobenzene wings. *Liq Cryst.* 2013;40:656–668.
- [27] Alaasar M, Prehm M, Nagaraj M, Vij JK, Tschierske C. A liquid crystalline phase with uniform tilt, local polar order and capability of symmetry breaking. *Adv Mater.* 2013;25:2186–2191.
- [28] Ocak H, Bilgin-Eran B, Prehm M, Schymura S, Lagerwallbd JPF, Tschierske C. Effects of chain branching and chirality on liquid crystalline phases of bent-core molecules: blue phases, de Vries transitions and switching of diastereomeric states. *Soft Matter.* 2011;7:8266–8280.
- [29] Keith C, Lehmann A, Baumeister U, Prehm M, Tschierske C. Nematic phases of bent-core mesogens. *Soft Matter.* 2010;6:1704–1721.
- [30] Francescangeli O, Vita F, Ferrero C, Dingemans T, Samulski ET. Cybotaxis dominates the nematic phase of bent-core mesogens: a small-angle diffuse X-ray diffraction study. *Soft Matter.* 2011;7:895–901.
- [31] Francescangeli O, Samulski ET. Insights into the cybotactic nematic phase of bent-core molecules. *Soft Matter.* 2010;6:2413–2420.
- [32] Tschierske C, Photinos DJ. Biaxial nematic phases. *J Mater Chem.* 2010;20:4263–4294.
- [33] Francescangeli O, Stanic V, Torgova SI, Strigazzi A, Scaramuzza N, Ferrero C, Dolbnya IP, Weiss TM, Berardi R, Muccioli L, Orlandi S, Zannoni C. Ferroelectric response and induced biaxiality in the nematic phase of a bent-core mesogen. *Adv Funct Mater.* 2009;19:2592–2600.
- [34] Shanker G, Nagaraj M, Kocot A, Vij JK, Prehm M, Tschierske C. Nematic phases in 1,2,4-oxadiazole-based bent-core liquid crystals: is there a ferroelectric switching? *Adv Funct Mater.* 2012;22:1671–1683.
- [35] Kwon S-S, Kim T-S, Lee C-K, Choi H, Shin S-T, Park J-K, Zin W-C, Chien L-C, Choi S-S, Choi E-J. Banana-shaped molecules with 4,6-dichlorinated central core: effect of lateral substituents and terminal chains on the formation of antiferroelectric smectic mesophases. *Liq Cryst.* 2006;33:1005–1014.
- [36] Weissflog W, Lischka C, Diele S, Pelzl G, Wirth I, Grande S, Kresse H, Schmalfluss H, Hartung H, Stettler A. Banana-shaped or rod-like mesogens? Molecular structure, crystal structure and mesophase behaviour of 4,6-dichloro-1,3-phenylene bis[4-(4-n-subst.-phenyliminomethyl) benzoates]. *Mol Cryst Liq Cryst.* 1999;333:203–235.
- [37] Lee C-K, Kwon S-S, Zin W-C, Kim D-C, Shin S-T, Song J-H, Choi E-J, Chien L-C. Mesomorphic properties of achiral halogen-substituted banana-shaped Compounds. *Liq Cryst.* 2003;30:415–421.
- [38] Yelamaggad CV, Mathews M, Nagamani SA, Rao DSS, Prasad SK, Findeisen S, Weissflog W. A novel family of salicylaldehyde-based five-ring symmetric and nonsymmetric banana-shaped mesogens derived from laterally substituted resorcinol: synthesis and characterization. *J Mater Chem.* 2007;17:284–298.
- [39] Weissflog W, Dunemann U, Schröder MW, Diele S, Pelzl G, Kresse H, Grande S. Field-induced inversion of chirality in SmCPA phases of new achiral bent-core mesogens. *J Mater Chem.* 2005;15:939–946.
- [40] Fodor-Csorba K, Vajda A, Jákli A, Trimmel CSG, Demus D, Gács-Baitz E, Hollye S, Gallif G. Ester type banana-shaped liquid crystalline monomers: synthesis and physical properties. *J Mater Chem.* 2004;14:2499–2506.
- [41] Weissflog W, Nádasi H, Dunemann U, Pelzl G, Diele S, Eremin A, Kresse H. Influence of lateral substituents on the mesophase behaviour of banana-shaped mesogens. *J Mater Chem.* 2001;11:2748–2758.
- [42] Lukhtanov EA, Vorobiev AV. Mild synthesis of asymmetric 2'-carboxyethyl-substituted fluoresceins. *J Org Chem.* 2008;73:2424–2427.



## Cybotactic nematic phases of photoisomerisable hockey-stick liquid crystals

Mohamed Alaasar<sup>a,b</sup>, Silvio Poppe<sup>a</sup> and Carsten Tschierske<sup>a</sup>

<sup>a</sup>Institute of Chemistry, Martin-Luther-University Halle-Wittenberg, Halle, Germany; <sup>b</sup>Department of Chemistry, Faculty of Science, Cairo University, Giza, Egypt

### ABSTRACT

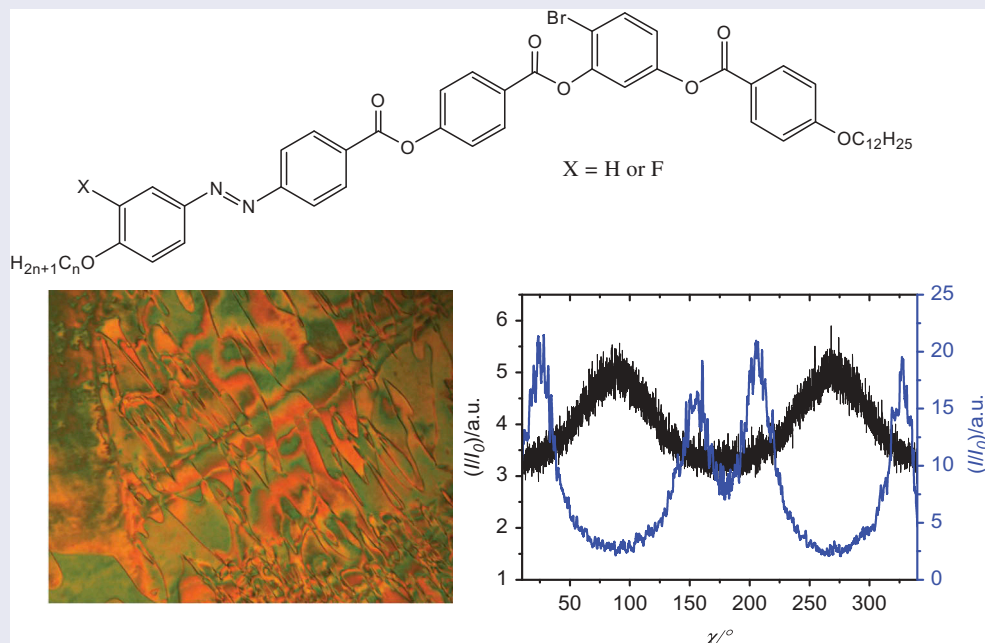
New five-ring hockey-stick liquid crystalline materials with 4-bromoresorcinol as the central core unit and an azobenzene-based side arm were synthesised and their mesophase behaviour was investigated by polarising optical microscopy, differential scanning calorimetry, X-ray diffraction and under a triangular wave electric field. Additional structural modification was done by introducing a lateral fluorine atom in the terminal ring of one of the side arms. It is found that regardless of the alkyl chain length or the lateral fluorine substitution, all of the prepared materials are liquid crystalline exhibiting nematic phases composed of cybotactic clusters of the SmC-type ( $N_{CybC}$ ) in addition to a monotropic SmC phase for the longest homologue.

### ARTICLE HISTORY

Received 24 August 2016  
Accepted 11 September 2016

### KEYWORDS

Hockey-stick liquid crystals; azobenzene; nematic phases; SmC phases



## 1. Introduction

The discovery of polar and chiral mesophases formed by achiral bent-core liquid crystals (BCLCs) opened the door to novel types of ferroelectric materials and to spontaneous mirror symmetry breaking in soft matter [1–5], for example, in helical nanofilament type B4-phases [6,7], dark conglomerate (DC) phases [4,5,8] and, as the most recent branch, the twist-bend nematic phases ( $N_{TB}$ ) [9–11]. Azobenzene is one of the most studied photo-isomerisable and photochromic units,

exhibiting reversible *trans/cis* isomerisation upon irradiation with light [12–16]. In the field of LCs, this property gives rise to added value to the materials, which can be used for applications in diverse fields, such as photonics [14], and photo-driven devices [15,16]. First examples of azo-containing BCLCs were reported already in 1929 by Vorländer [17]. Other recent examples of azo functionalised bent-core materials exhibiting interesting physical properties have been reported by several research groups [18–23] and was recently reviewed [24]. We have reported



azobenzene-based BCLCs with bromine, iodine and methyl groups in the 4-position of the central resorcinol core forming mirror-symmetry broken mesophases, designated as helical nano-crystallite (HNC) phases [25–30]. Beside the BCLCs, there is a growing interest in liquid crystalline materials with chemical structures at the borderline between BCLCs and rod-like (calamitic) LCs which are known as hockey-stick LCs (HSLCs). Though most of the HSLCs form non-polar nematic and smectic phases [31–37], some of them are capable to retain features of BCLCs, as for example the response to electric field [38–40]. The question arose if the LC phases of HSLCs could show mirror symmetry breaking if building blocks, known to support the development of symmetry breaking in BCLCs, are involved in HSLCs.

Therefore, we report herein a new series of azobenzene-containing HSLCs involving the 4-bromoresorcinol core as the bent unit (compounds **An**) with  $n = 8, 12, 20$ . In addition, the core fluorinated compound **AF12** was synthesised in order to study the effect of introducing lateral fluorine on the outer ring of these hockey-stick molecules (see Scheme 1). The LC phase behaviour of all these new materials has been investigated by polarising optical microscopy and differential scanning calorimetry (DSC). The longest homologue **A20** was also investigated by X-ray diffraction (XRD) and with respect to switching under an applied electric field.

## 2. Results and discussion

### 2.1. Synthesis

The synthesis of compounds **An** and **AF12** is outlined in Scheme 1. These compounds were obtained by esterification of the azobenzene-derived benzoic acids **3/n** and **3F12** with 4-bromoresorcinol monobenzoate **6**. The 4-(4'-*n*-alkyloxyphenylazo)benzoic acids **1/n** and 4-(4'-*n*-alkyloxy-3'-fluorophenylazo)benzoic acid **1F12** synthesised according to the methods described previously [41] were esterified with 4-hydroxybenzaldehyde to give the corresponding aldehydes **2/n** and **2F12**. The desired acids (**3/n** and **3F12**) were obtained by oxidising the aldehydes **2/n** and **2F12** using similar oxidation procedure to that reported elsewhere [42]. Purification of the final compounds was performed by column chromatography with dichloromethane as an eluent followed by recrystallisation from chloroform/ethanol mixture. The synthesis of the compounds, together with the experimental details for each step with the analytical

data for the final hockey-stick compounds, are given in the Supplemental data.

### 2.2. Characterisation

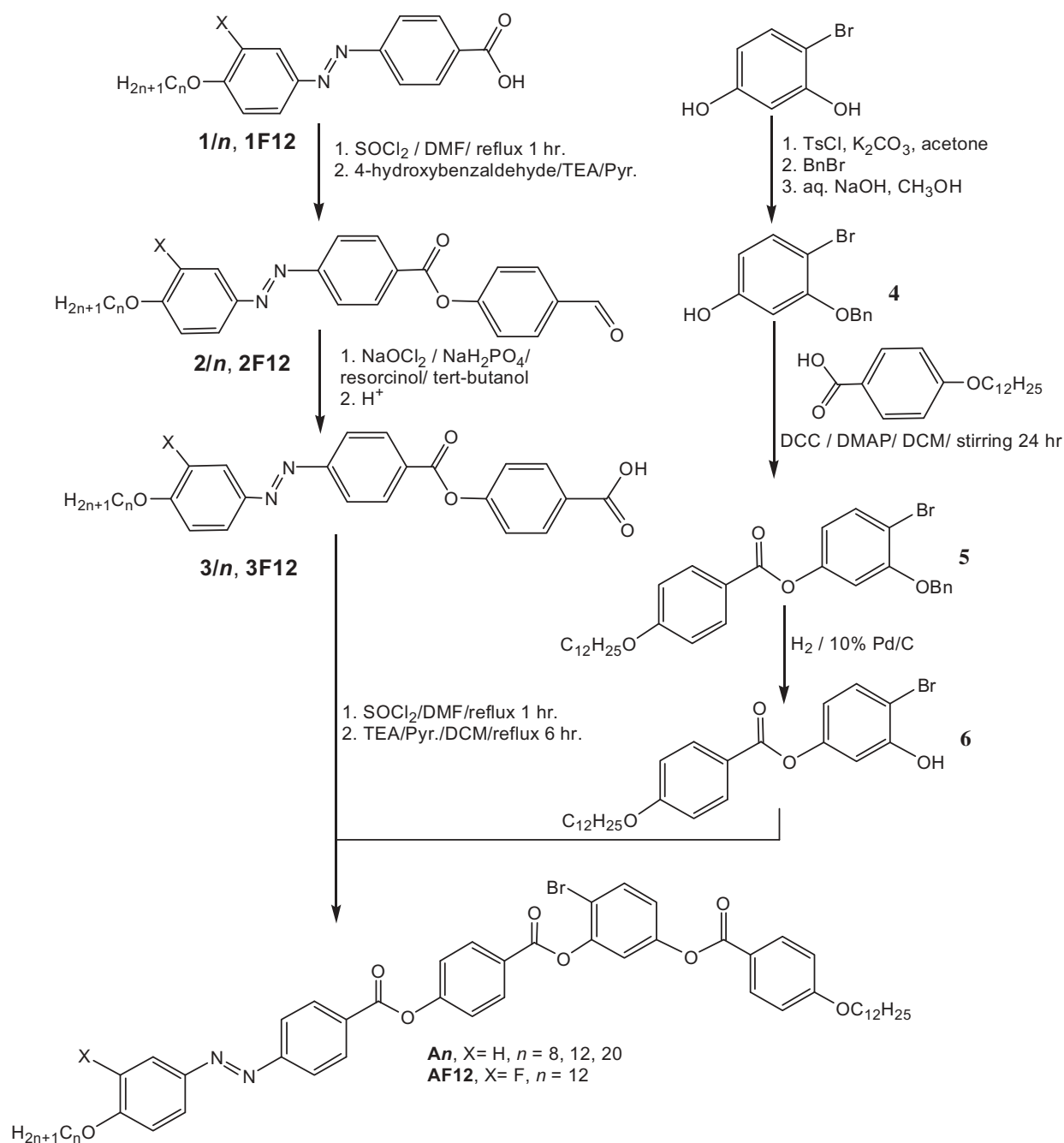
The mesophase behaviour and transition temperatures of the prepared HSLCs were measured using a Mettler FP-82 HT hot stage and control unit in conjunction with a Nikon Optiphot-2 polarising microscope. The associated enthalpies were obtained from DSC-thermograms which were recorded on a Perkin-Elmer DSC-7, with heating and cooling rate  $10 \text{ K min}^{-1}$ . The electro-optical switching characteristics were examined using the triangular-wave method [43] using  $6 \mu\text{m}$  polyimide-coated indium tin oxide (ITO) cells, EHC, Japan.

The X-ray diffraction patterns were recorded with a 2D detector (Vantec 500, Bruker). Ni filtered and pin hole collimated  $\text{CuK}\alpha$  radiation was used. For the wide-angle X-ray diffraction measurements, the exposure time was 15 min and the sample to detector distance was 9.0 cm. Uniform orientation was achieved by alignment in a magnetic field ( $B \approx 1 \text{ T}$ ) using thin capillaries. The samples were held on a temperature-controlled heating stage.

### 2.3. Mesomorphic properties

The transition temperatures ( $^{\circ}\text{C}$ ) and the associated enthalpies ( $\text{kJ mol}^{-1}$ ) obtained from DSC thermograms of compounds **An** and **AF12** are given in Table 1 and represented graphically in Figure 1. The DSC thermograms obtained for compounds **A8** and **A20** as examples are shown in Figure 2. All compounds are thermally stable as confirmed by the reproducibility of thermograms on several heating and cooling cycles.

On heating the shortest derivative **A8** with  $n = 8$ , a direct transition from the crystalline state to the isotropic liquid takes place at  $T = 114^{\circ}\text{C}$ . On cooling the isotropic liquid state of **A8**, a monotropic nematic phase is observed below  $\sim 114^{\circ}\text{C}$  (see Figure 3(a)) which crystallises at  $87^{\circ}\text{C}$ . On chain elongation, the melting temperatures decrease and the monotropic nematic phase is converted to enantiotropic liquid crystalline phase. For example, compound **A12** with  $n = 12$  exhibits an enantiotropic nematic phase that exists over a wider temperature range (32 K on cooling) compared to that of **A8** (27 K). Further chain elongation (compound **A20**) induces an additional LC phase below the nematic phase. Based on textural observations between crossed polarisers, it is a biaxial smectic phase, most probably being a SmC phase (see



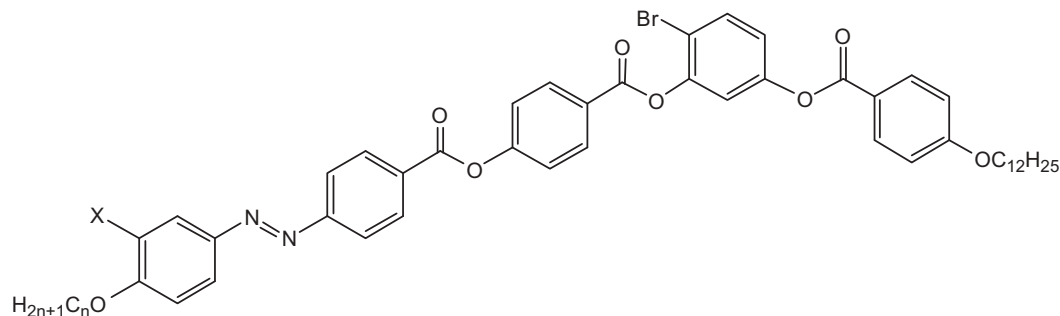
**Scheme 1.** Synthesis of the hockey-stick molecules under discussion.

DMF = N,N-dimethylformamide; TEA = triethylamine; Pyr. = pyridine; DCM = dichloromethane; DCC = N,N'-dicyclohexylcarbodiimide; DMAP = 4-(dimethylamino)pyridine; TsCl = p-toluenesulfonyl chloride; BnBr = benzylbromide.

Figure 3(b)). The absence of in-plane order (SmI, SmF) is confirmed by the small enthalpy of the N–SmC transition ( $\Delta H = 0.5 \text{ kJ}\cdot\text{mol}^{-1}$ ) [44,45]. This monotropic SmC phase between the nematic and the crystalline phases narrows the nematic phase range compared to the shorter homologues.

None of the compound with very distinct chain lengths shows an indication of symmetry breaking or HNC phase formation in their LC phases, not even in the SmC phase

[46,47]. As core fluorination is known to affect the formation of DC and HNC phases considerably [25–28], compound AF12 with a lateral fluorine atom at the outer ring of the bent core molecule in the ortho position with respect to the alkyl chain (see Scheme 1) was synthesised. The melting point and the crystallisation temperature are not significantly influenced by the additional fluorine substituent (compare A12 and AF12 in Figure 1). Also the type of the mesophase is not affected by the peripheral

**Table 1.** Phase transition temperatures, mesophase types and transition enthalpies of compounds **An** and **AF12**.<sup>a</sup>

Comp.	<i>n</i>	X	Phase behaviour and transition temperatures <i>T</i> /°C [ $\Delta H$ /kJ·mol <sup>-1</sup> ]
A8	8	H	Cr 114 [76.2] Iso
A12	12	H	Cr 87 [70.9] N <sub>Cybc</sub> 114 [0.4] Iso Cr 100 [51.2] N <sub>Cybc</sub> 112 [0.37] Iso
A20	20	H	Cr 79 [45.7] N <sub>Cybc</sub> 111 [0.4] Iso Cr 99 [49.5] N <sub>Cybc</sub> 108 [0.65] Iso
AF12	12	F	Cr 86 [53.2] SmC 94 [0.5] N <sub>Cybc</sub> 107 [0.7] Iso Cr 101 [37.9] N <sub>Cybc</sub> 106 [0.4] Iso Cr 80 [37.8] N <sub>Cybc</sub> 104 [0.5] Iso

<sup>a</sup>Transition temperatures and enthalpy values were taken from the second DSC heating scans (upper lines) and cooling scans (lower lines) with 10 K min<sup>-1</sup>; Cr = crystalline solid; SmC = smectic C phase; N<sub>Cybc</sub> = nematic phase composed of cybotactic clusters of the SmC-type; Iso = isotropic liquid.

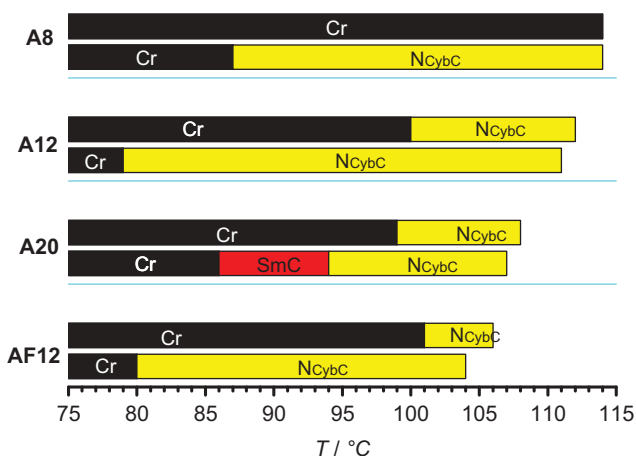


**Figure 1.** (colour online) Plot of the transition temperatures of compounds (**A8**–**A20** and **AF12**) as a function of the number of carbons (*n*) in the alkyl chain.

fluorination of the aromatic core as **AF12** shows only a nematic phase similar to its related analogue **A12**. However, the clearing temperature as well as the range of the nematic phase of **AF12** is reduced compared to **A12**.

In switching experiments using a triangular wave voltage, no current peak could be observed in the nematic phases of all compounds **An** and **AF12** up to a voltage of 200 V<sub>pp</sub> in a 6 μm ITO cell, indicating the nonpolar nature of these nematic phases [48,49]. Also the SmC phase of compound **A20** was found to be nonpolar as no current

peak could be detected. There is also no optical response on the applied fields, except some electro-convections occurring in the nematic phases at high voltage [48].

X-ray diffraction measurements were performed with compound **A20** as an example. The X-ray diffraction pattern of a magnetically aligned sample (Figure 4 (a)) shows a diffuse scattering in the wide angle region with a maximum at  $d = 0.45$  nm positioned on the equator, and a weak diffuse scattering in the small angle region with a maximum at  $d = 5.02$  nm. The diffuse small angle scattering has clear maxima beside the meridian (dumbbell shape) with relatively high intensity compared to the wide angle scattering, indicating the presence of cybotactic clusters of the SmC type and thus confirming a skewed cybotactic nematic phase (N<sub>Cybc</sub> phase) [50–52]. The tilt  $\beta$  in the cluster is about 34° which is in line with the maximum possible value  $\beta = 44^\circ$  as calculated with  $\cos\beta = d/L_{\text{mol}}$  ( $L_{\text{mol}} = 7.0$  nm determined between the ends of the alkyl chains in a conformation with 120° bend of the aromatic core and stretched alkyl chains (see Figure 5)). Formation of a cybotactic nematic phase is in agreement with the low transition enthalpy value observed for the N–SmC transition ( $\Delta H = 0.5$  kJ·mol<sup>-1</sup>) being smaller than the N–Iso transition enthalpy ( $\Delta H = 0.7$  kJ·mol<sup>-1</sup>). This kind of cybotactic nematic phases is a typical feature of BCLCs [50,52] and other compounds with extended rigid cores [53].

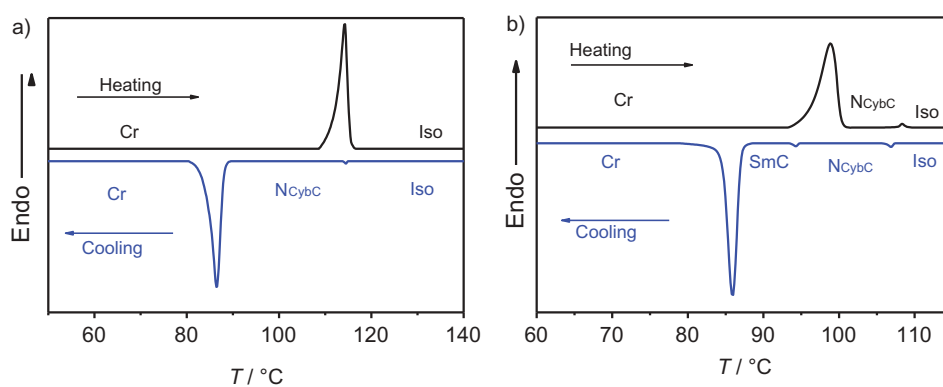


**Figure 2.** (colour online) DSC thermograms obtained for (a) compound **A8** and (b) **A20**, with  $10 \text{ K min}^{-1}$  heating and cooling rates.

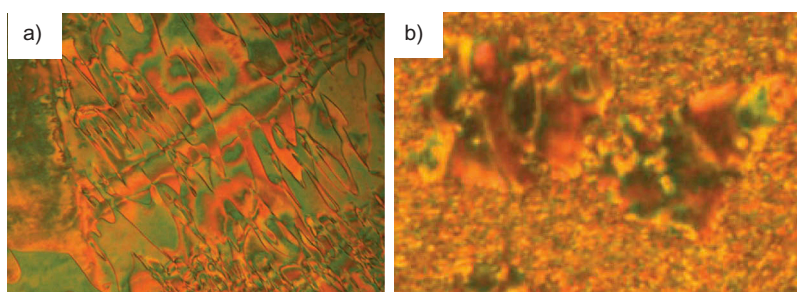


**Figure 3.** (colour online) Optical micrographs observed in a homeotropic cell for compound **A20**: (a) in the nematic phase at  $T = 105^\circ\text{C}$  and (b) in the SmC phase at  $T = 90^\circ\text{C}$ .

Unfortunately, the investigation of the monotropic SmC phase exhibited by **A20** was not possible due to rapid crystallisation during the time of exposure.

### 3. Comparison with related compounds

Compounds **B $n$**  (see Scheme 2), reported by Monika et al. [37], have the same aromatic core structure as well as the same sequence and types of linkage units as in compounds **A $n$** , only without the bromine at the bent resorcinol core. Comparing **A12** with **B12** with the same alkyl chain length at the end of the azobenzene-containing side arm indicates that the bromine atom at the apex of the bent core molecule suppresses the smectic phases (SmC<sub>a</sub> and SmX) of **B12** and induces a nematic phase. Moreover, the melting, clearing and crystallisation temperatures are reduced by the lateral bromine substituent. These differences in the mesophase types and in the transitions temperatures between both compounds may be attributed to the weaker core–core interactions present in compound **A12** compared to **B12** as a result of the bromine substitution. There are two major effects of bromine: one is the effect on the molecular conformation by favouring twisted conformations [26] and the other is the

direct distortion of the packing of the aromatic cores due to the bulkiness of this lateral substituent.

Comparison with the series of related bent-core molecules **C $n$**  (see Scheme 2) with the same orientation of the COO linking groups and the same number of benzene rings, only differing in the position of the bent 4-bromoresorcinol core, indicates that the HNC phases of compounds **C $n$**  are completely removed, though the LC–Iso transition temperatures of both series are in the same range. Obviously the reduced molecular symmetry, which requires a mixed packing of the short and long wings, leads to a reduced packing density which is unfavourable for chirality synchronisation [54] as required for the formation of HNC and DC phases.

### 4. Photosensitivity

To study the *trans-cis* photoisomerisation of the prepared hockey-stick molecules, UV-vis absorption spectroscopy was performed on compound **A20**. Figure 6 shows the effects of UV irradiation on the UV-vis spectra of **A20** in chloroform solution at three different conditions: (a) freshly prepared, (b) exposed to 365 nm light and (c) after storing the sample in dark overnight. A maximum absorption at 367 nm is observed for the freshly prepared sample as a result of the  $\pi$ – $\pi^*$

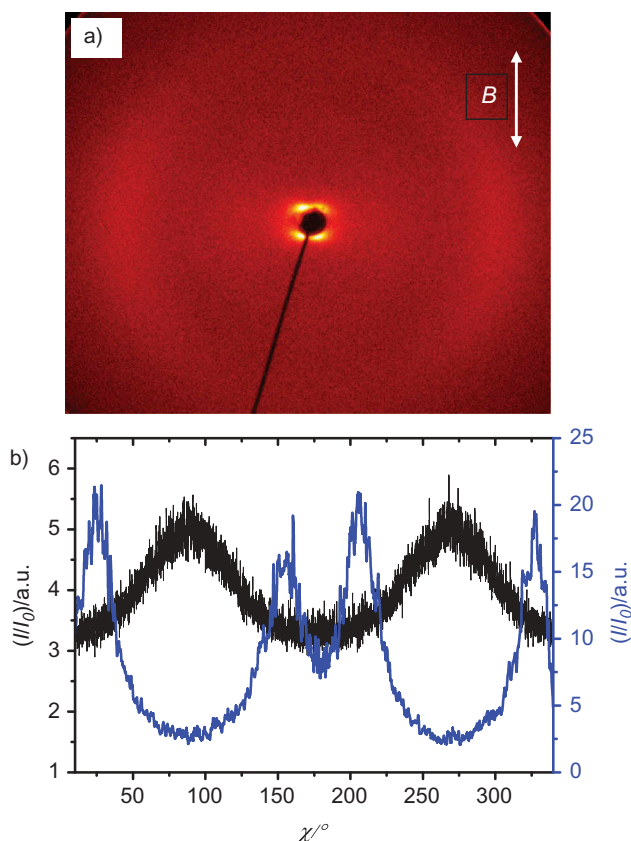


**Figure 4.** (colour online) XRD investigations of the nematic phase of compound **A20**: (a) diffraction pattern at 95°C; (b) intensity distribution of the diffuse scatterings along  $\chi$ , black curve wide angle scattering (15–25°  $2\theta$ ) and blue curve small angle scattering (2–5°  $2\theta$ ).

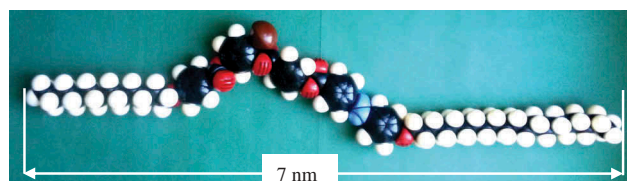
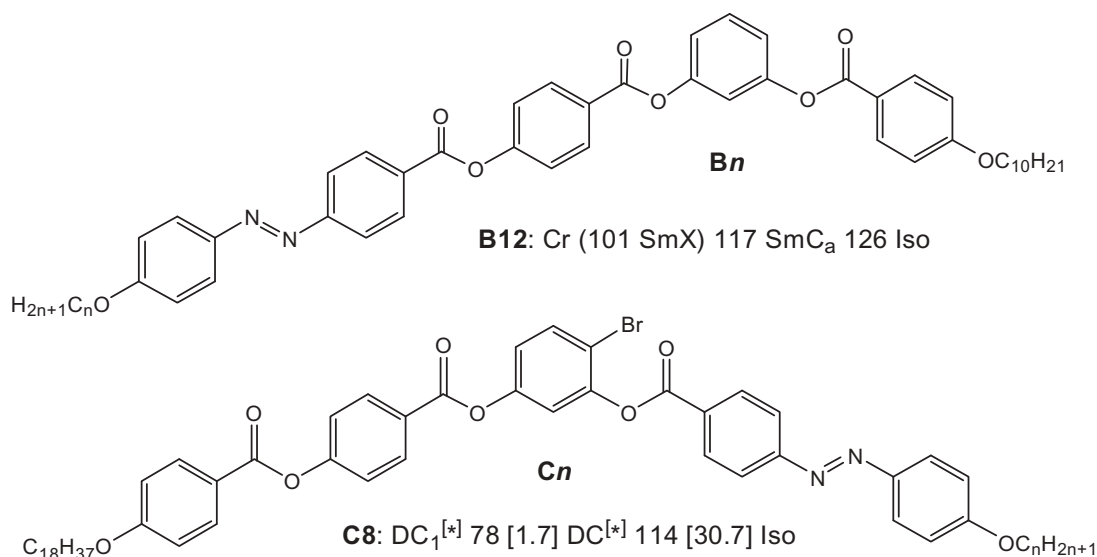


**Figure 5.** (colour online) CPK molecular model of compound **A20**.

transition of the chromophore in the molecule indicating the presence of the more stable *trans*-isomer. After irradiation with 365 nm light for 20 mins, the absorption at 367 nm decreases greatly and another absorption band at 465 nm starts to appear confirming the transformation from the *trans*-isomer to the less stable *cis*-isomer. Measuring the same solution after storing in dark overnight gives nearly an identical spectrum to that observed for the freshly prepared solution indicating the relaxing back of the *cis*-isomer to the *trans*-isomer. These results are very similar to that reported for the hockey-stick molecules **Bn** [37] as well as for other azobenzene-containing BCLCs [29,46,47,55].

## 5. Summary and conclusions

In summary, we reported new halogen-substituted azobenzene-containing hockey-stick molecules exhibiting mainly nematic phases (compounds **An** and



**Scheme 2.** Chemical structures of (a) HSLCs **Bn** with the transition temperatures  $T/^\circ\text{C}$  for compound **B12** [37] and (b) 4-bromoresorcinol derived BCLCs **Cn** forming the HNC phases (DC<sub>1</sub><sup>[\*]</sup> and DC<sup>[\*]</sup>) with the transition temperatures  $T/^\circ\text{C}$  of **C8** [28].

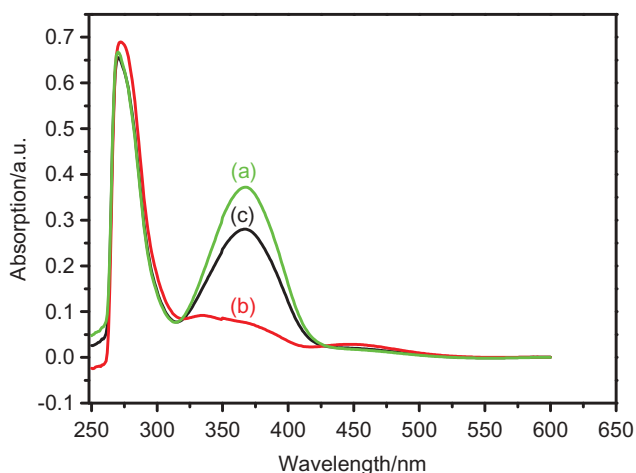


**Figure 6.** (colour online) UV-vis spectra (absorbance vs. wavelength) of **A20** dissolved in chloroform (0.02 mM solution) at 25° C. (a) Freshly prepared sample, *trans*-isomer before irradiation, green line; (b) *cis*-isomer as obtained after 20 mins irradiation with light of 366 nm wavelength, red line; (c) *trans*-isomer after keeping the sample in dark overnight, black line.

**AF12).** A monotropic nematic phase is observed for the shortest homologue (**A8**) which converts to an enantiotropic phase on chain elongation (**A12** and **A20**) in addition to the formation of a monotropic SmC phase for the longest homologue (**A20**). The mesogen with additional peripheral fluorine substitution (**AF12**) exhibits also a nematic phase similar to its non-fluorinated analogue **A12**. X-ray diffraction carried out for the longest homologue (**A20**) proved that the nematic phases are composed of cybotactic clusters of the SmC type ( $N_{Cybc}$ ) similar to that formed by BCLCs. Comparing the prepared materials with related hockey-stick compounds without bromine substitution indicates that halogen substitution at the apex of the bent-core structure reduces the formation of smectic phases and favours nematic phases as a result of the reduced core–core interactions. Finally, the *trans-cis* photoisomerisation in solution was studied by performing UV-vis absorption spectroscopy for one selected example.

## Acknowledgment

The work was funded by the Deutsche Forschungsgemeinschaft [Grant Ts 39/24-1].

## Disclosure statement

No potential conflict of interest was reported by the authors.

## Funding

The work was funded by the Deutsche Forschungsgemeinschaft [Grant Ts 39/24-1].

## ORCID

Mohamed Alaasar  <http://orcid.org/0000-0003-4155-8644>

## References

- [1] Niori T, Sekine T, Watanabe J, et al. Distinct ferroelectric smectic liquid crystals consisting of banana shaped achiral molecules. *J Mater Chem.* 1996;6:1231–1233. DOI:10.1039/jm9960601231
- [2] Pelzl G, Diele S, Weissflog W. Banana-shaped compounds - a new field of liquid crystals. *Adv Mater.* 1999;11:707–724. DOI:10.1002/(ISSN)1521-4095
- [3] Ros B, Serrano J, Fuente R, et al. Banana-shaped liquid crystals: a new field to explore. *J Mater Chem.* 2005;15:5093–5098. DOI:10.1039/b504384k
- [4] Reddy R, Tschierske C. Bent-core liquid crystals: polar order, superstructural chirality and spontaneous desymmetrisation in soft matter systems. *J Mater Chem.* 2006;16:907–961. DOI:10.1039/B504400F
- [5] Eremin A, Jáklí A. Polar bent-shape liquid crystals – from molecular bend to layer splay and chirality. *Soft Matter.* 2013;9:615–637. DOI:10.1039/C2SM26780B
- [6] Sekine T, Niori T, Watanabe J, et al. Spontaneous helix formation in smectic liquid crystals comprising achiral molecules. *J Mater Chem.* 1997;7:1307–1309. DOI:10.1039/a702026k
- [7] Hough LE, Spannuth M, Nakata M, et al. Helical nanofilament phases. *Science.* 2009;325:452–456. DOI:10.1126/science.1170028
- [8] Link DR, Natale G, Shao R, et al. Spontaneous formation of macroscopic chiral domains in a fluid smectic phase of achiral molecules. *Science.* 1997;278:1924–1927. DOI:10.1126/science.278.5345.1924.
- [9] Emsley JW, Lelli M, Lesage A, et al. A comparison of the conformational distributions of the achiral symmetric liquid crystal dimer CB7CB in the achiral nematic and chiral twist-bend nematic phases. *J Phys Chem B.* 2013;117:6547–6557. DOI:10.1021/jp4001219
- [10] Borshch V, Kim Y-K, Xiang J, et al. Nematic twist-bend phase with nanoscale modulation of molecular orientation. *Nature Commun.* 2013;4:2635. DOI:10.1038/ncomms3635
- [11] Chen D, Porada JH, Hooper JB, et al. Chiral heliconical ground state of nanoscale pitch in a nematic liquid crystal of achiral molecular dimers. *Proc Natl Acad Sci.* 2013;110:15931–15936. DOI:10.1073/pnas.1314654110
- [12] Chen Y, Yu H, Zhang L, et al. Photoresponsive liquid crystals based on halogen bonding of azopyridines. *Chem Commun.* 2014;50:9647–9649. DOI:10.1039/C4CC02344G
- [13] Demus D, Goodby J, Gray GW, et al. *Handbook of liquid crystals.* Weinheim, Germany: Wiley-VCH; 1998.
- [14] Li Q. *Liquid crystals beyond displays: chemistry, physics, and applications.* Hoboken, NJ: John Wiley & Sons; 2012.

- [15] Yu HF, Ikeda T. Photocontrollable liquid-crystalline actuators. *Adv Mater.* 2011;23:2149–2180. DOI:10.1002/adma.v23.19
- [16] Bushuyev OS, Tomberg A, Friščić T, et al. Shaping crystals with light: crystal-to-crystal isomerization and photomechanical effect in fluorinated Azobenzenes. *J Am Chem Soc.* 2013;135:12556–12559. DOI:10.1021/ja4063019
- [17] Vorländer D. Die Richtung der Kohlenstoff-Valenzen in Benzol-Abkömmlingen. *Ber Dtsch Chem Ges.* 1929;62:2831–2835. DOI:10.1002/cber.19290621026.
- [18] Gimeno N, Pintre I, Martínez-Abadía M, et al. Bent-core liquid crystal phases promoted by azo-containing molecules: from monomers to side chain polymers. *RSC Adv.* 2014;4:19694–19702. DOI:10.1039/c4ra02079k
- [19] Srinivasan MV, Kannan P, Roy P. Photo and electrically switchable B7 mesophase exhibiting asymmetric bent-core liquid crystals. *New J Chem.* 2013;37:1584–1590. DOI:10.1039/c3nj41030g
- [20] Nagaveni NG, Roy A, Prasad V. Achiral bent-core azo compounds: effect of different types of linkage groups and their direction of linking on liquid crystalline properties. *J Mater Chem.* 2012;22:8948–8959. DOI:10.1039/c2jm30709j
- [21] Trišović N, Salamonczyk M, Antanasijević J, et al. Azo-containing asymmetric bent-core liquid crystals with modulated smectic phases. *RSC Adv.* 2015;5:64886–64891. DOI:10.1039/C5RA09764A
- [22] Rahman L, Kumar S, Tschierske C, et al. Synthesis and photoswitching properties of bent-shaped liquid crystals containing azobenzene monomers. *Liq Cryst.* 2009;36:397–407. DOI:10.1080/02678290902923428
- [23] Horčić M, Kozmík V, Svoboda J, et al. Transformation from a rod-like to a hockey-stick-like and bent-shaped molecule in 3,4'-disubstituted azobenzene-based mesogens. *J Mater Chem C.* 2013;1:7560–7567. DOI:10.1039/c3tc31593b
- [24] Alaasar M. Azobenzene containing bent-core liquid crystals: an overview. *Liq Cryst.* 2016;1–36. DOI:10.1080/02678292.2016.1175676
- [25] Alaasar M, Prehm M, Tschierske C. A new room temperature dark conglomerate mesophase formed by bent-core molecules combining 4-iodoresorcinol with azobenzene units. *Chem Commun.* 2013;49:11062–11064. DOI:10.1039/c3cc45938a
- [26] Alaasar M, Prehm M, Brautzsch M, et al. Dark conglomerate phases of azobenzene derived bent-core mesogens—relationships between the molecular structure and mirror symmetry breaking in soft matter. *Soft Matter.* 2014;10:7285–7296. DOI:10.1039/C4SM01255K
- [27] Alaasar M, Prehm M, Brautzsch M, et al. 4-Methylresorcinol based bent-core liquid crystals with azobenzene wings – a new class of compounds with dark conglomerate phases. *J Mater Chem C.* 2014;2:5487–5501. DOI:10.1039/C4TC00533C
- [28] Alaasar M, Prehm M, Tschierske C. Helical Nano-crystallite (HNC) phases – chirality synchronization of achiral bent-core mesogens in a new type of dark conglomerates. *Chem Eur J.* 2016;22:6583–6597. DOI:10.1002/chem.201505016
- [29] Alaasar M, Prehm M, Tschierske C. Influence of halogen substituent on the mesomorphic properties of five-ring banana shaped molecules with azobenzene wings. *Liq Cryst.* 2013;40:656–668. DOI:10.1080/02678292.2013.767949
- [30] Alaasar M, Prehm M, Tschierske C. mirror symmetry breaking in fluorinated bent-core mesogens. *RSC Adv.* 2016;6:82890–82899. DOI:10.1039/C6RA18482K
- [31] Gude V, Upadhyaya K, Mohiuddin G, et al. New family of four-ring bent-core nematic liquid crystals with a highly polar end-group. *Liq Cryst.* 2013;40:120–129. DOI:10.1080/02678292.2012.744476
- [32] Yu FC, Yu LJ. Mesophases of achiral bent molecules. *Chem Mater.* 2006;18:5410–5420. DOI:10.1021/cm060459d
- [33] Kang S, Saito Y, Watanabe N, et al. Low-birefringent, chiral banana phase below calamitic nematic and/or smectic C phases in oxadiazole derivatives. *J Phys Chem B.* 2006;110:5205–5214. DOI:10.1021/jp057307a
- [34] Fergusson KM, Hird M. The dramatic influence of the location of bend and of lateral fluoro substitution on the mesomorphic properties of angular chiral esters based on a 1,3-disubstituted benzene ring. *J Mater Chem.* 2010;20:3069–3078. DOI:10.1039/b923267b
- [35] Matharu AS, Grover C, Komitov L, et al. Ferro-, ferri- and antiferro-electric behaviour in a bent shaped mesogen. *J Mater Chem.* 2000;10:1303–1310. DOI:10.1039/b000128g
- [36] Weissflog W, Dunemann U, Tandel SF, et al. At the boundary to banana shaped liquid crystals: polar properties of phases formed by new asymmetric achiral four-ring bent-core mesogens. *Soft Matter.* 2009;5:1840–1847. DOI:10.1039/b819758j
- [37] Monika M, Prasad V, Nagaveni NG. Hockey stick-shaped azo compounds: effect of linkage groups and their direction of linking on mesomorphic properties. *Liq Cryst.* 2015;42:1490–1505. DOI:10.1080/02678292.2015.1066889
- [38] Deb R, Nath RK, Paul MK, et al. Four-ring achiral unsymmetrical bent core molecules forming strongly fluorescent smectic liquid crystals with spontaneous polar and chiral ordered B7 and B1 phases. *J Mater Chem.* 2010;20:7332–7336. DOI:10.1039/c0jm01539c
- [39] Yoon DK, Deb R, Chen D, et al. Organization of the polarization splay modulated smectic liquid crystal phase by topographic confinement. *Proc Nat Acad Sci.* 2010;107:21311–21315. DOI:10.1073/pnas.1014593107
- [40] Nath RK, Sarkar DD, Rao DSS, et al. Influence of polar substituents on the mesomorphism of non-symmetrical achiral four-ring bent-core compounds: synthesis and characterization. *Liq Cryst.* 2012;39:889–902. DOI:10.1080/02678292.2012.689375
- [41] Alaasar M, Prehm M, Cao Y, et al. Spontaneous mirror-symmetry breaking in isotropic liquid phases of photo-isomerizable achiral molecules. *Angew Chem Int Ed.* 2016;55:312–316. DOI:10.1002/anie.201508097
- [42] Alaasar M, Prehm M, Poppe M, et al. Development of polar order and tilt in lamellar liquid crystalline phases of a bent-core mesogen. *Soft Matter.* 2014;10:5003–5016. DOI:10.1039/C4SM00593G
- [43] Miyasato K, Abe S, Takezoe H, et al. Direct method with triangular waves for measuring spontaneous

- polarization in ferroelectric liquid crystals. *Jpn J Appl Phys.* **1983**;22:L661–L663. DOI:10.1143/JJAP.22.L661
- [44] Gray GW, Goodby JW. *Smectic liquid crystals: textures and structures.* New York (NY): Leonard Hill; **1984.**
- [45] Goodby JW, Mandle RJ, Davis EJ, et al. What makes a liquid crystal? The effect of free volume on soft matter. *Liq Cryst.* **2015**;42:593–622.
- [46] Alaasar M, Prehm M, Nagaraj M, et al. A liquid crystalline phase with uniform tilt, local polar order and capability of symmetry breaking. *Adv Mater.* **2013**;25:2186–2191. DOI:10.1002/adma.201205180
- [47] Alaasar M, Prehm M, May K, et al. 4-Cyanoresorcinol based bent-core mesogens with azobenzene wings – emergence of sterically stabilised polar order in liquid crystalline phases. *Adv Funct Mater.* **2014**;24:1703–1717. DOI:10.1002/adfm.201302295
- [48] Francescangeli O, Stanic V, Torgova SI, et al. Ferroelectric response and induced biaxiality in the nematic phase of a bent-core mesogen. *Adv Funct Mater.* **2009**;19:2592–2600. DOI:10.1002/adfm.200801865
- [49] Shanker G, Nagaraj M, Kocot A, et al. Nematic phases in 1,2,4-oxadiazole-based bent-core liquid crystals: is there a ferroelectric switching? *Adv Funct Mater.* **2012**;22:1671–1683. DOI:10.1002/adfm.v22.8
- [50] Keith C, Lehmann A, Baumeister U, et al. Nematic phases of bent-core mesogens. *Soft Matter.* **2010**;6:1704–1721. DOI:10.1039/b923262a
- [51] Francescangeli O, Vita F, Ferrero C, et al. Cybotaxis dominates the nematic phase of bent-core mesogens: a small-angle diffuse X-ray diffraction study. *Soft Matter.* **2011**;7:895–901. DOI:10.1039/C0SM00745E
- [52] Alaasar M, Prehm M, Tschierske C. New azobenzene containing bent-core liquid crystals based on disubstituted resorcinol. *Liq Cryst.* **2014**;41:126–136. DOI:10.1080/02678292.2013.840393
- [53] Breckon R, Chakraborty S, Zhang C, et al. Nanostructures of nematic materials of laterally branched molecules. *ChemPhysChem.* **2014**;15:1457–1462. DOI:10.1002/cphc.201300578
- [54] Tschierske C, Ungar G. Mirror symmetry breaking by chirality synchronisation in liquids and liquid crystals of achiral molecules. *ChemPhysChem.* **2016**;17:9–26. DOI:10.1002/cphc.v17.1
- [55] Alaasar M, Prehm M, Tamba M-G, et al. Development of polar order in the liquid crystal phases of a 4-cyanoresorcinol-based bent-core mesogen with fluorinated azobenzene wings. *ChemPhysChem.* **2016**;17:278–287. DOI:10.1002/cphc.201500891



Cite this: *J. Mater. Chem. C*, 2017,  
5, 8454

## Cluster phases of 4-cyanoresorcinol derived hockey-stick liquid crystals†

Mohamed Alaasar,<sup>ib</sup>\*<sup>ab</sup> Silvio Poppe,<sup>a</sup> Christoph Kerzig,<sup>a</sup> Christoph Klopp,<sup>c</sup>  
Alexey Eremin<sup>ib</sup>\*<sup>c</sup> and Carsten Tschierske<sup>ib</sup>\*<sup>a</sup>

Here, we report the synthesis and investigations of hockey-stick liquid crystalline materials derived from 4-cyanoresorcinol as the central core unit. The effect of distinct linking groups (N=N, COO, OOC) and the effect of inverting the direction of the cyano group on the resorcinol core with respect to the different side arms on the liquid crystalline properties were investigated. The self-assembly was characterized by polarising optical microscopy (POM), differential scanning calorimetry (DSC), X-ray diffraction (XRD), electro-optical and second harmonic generation (SHG) experiments and dielectric spectroscopy. It is found that depending on the alkyl chain length, nematic and smectic liquid crystalline phases were observed. All nematic phases exhibited by the compounds with the CN group adjacent to the shorter rod-like arm of the mesogen are  $N_{CybA}$  phases composed of large non-tilted (SmA-type) cybotactic clusters, while inverting the direction of the cyano group leads to nematic phases composed of smaller cybotactic clusters ( $N_{CybC}$ ) with tilted-smectic correlations. The former compounds form additional non-tilted (SmA) and tilted smectic (SmC) composed of polar domains with a strong polar response. There is a transition from synclitic to anticlinic molecular arrangement (SmC<sub>s</sub> and SmC<sub>a</sub> phases) with decreasing temperature and mirror symmetry breaking in the SmC<sub>s</sub> phases. The synclitic-anticlinic transition is associated with a reduction of the polar domain size, being opposite to observations made for related bent-core compounds and is attributed to the combined effects of nano-segregation and entropy.

Received 26th April 2017,  
Accepted 11th July 2017

DOI: 10.1039/c7tc01816a

rsc.li/materials-c

### 1. Introduction

Liquid crystals (LCs) are widely used in various technological applications such as displays,<sup>1</sup> optoelectronics,<sup>2</sup> biosensors,<sup>3</sup> and in charge carrier materials.<sup>4</sup> The discovery of bent-core liquid crystals (BCLCs) opened doors to a new interesting field of research due to the unique and rich variety of mesomorphic structures exhibited by these materials. In addition to conventional smectic and nematics, these structures include different kinds of polar, chiral and nano-segregated phases.<sup>5</sup> For example, achiral BCLCs can form ferroelectric and anti-ferroelectric LC phases and mesophases that show spontaneous mirror symmetry breaking such as helical nanofilament phases<sup>6,7</sup> and dark

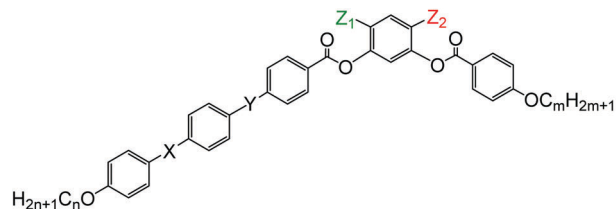
conglomerate phases (DC phases).<sup>8</sup> BCLCs are known for their potential to form biaxial and polar nematic phases with cybotactic cluster structures which makes them very different from conventional nematic phases of most rod-like molecules.<sup>9–15</sup> In most cases, bent-core nematics are  $N_{CybC}$ <sup>16</sup> phases, formed by tilted SmC clusters, and only few of them are  $N_{CybA}$  phases, formed by non-tilted SmA clusters.<sup>9,17</sup> Cluster phases are important for several reasons. Smectic clusters in nematic phases (cybotactic nematic phases) were reported to be responsible for significant enhancement of the bend elastic constant,<sup>18</sup> the flexoelectric effect in bent-core nematics,<sup>19</sup> extraordinary magnetic field effects<sup>20</sup> and an unusual electro-optic response in amorphous blue phases.<sup>21</sup> Enhanced response and fast switching are important features for technological applications. Cluster formation is also associated with N–N<sub>TB</sub> transitions observed for mesogenic dimers with odd-numbered spacers.<sup>22</sup> Although cluster phases have been intensively studied in colloidal systems,<sup>23</sup> the physics of cluster phases in liquid crystals remains much less explored.<sup>24</sup> These cybotactic clusters persist over large temperature ranges and cannot be described as pre-transitional fluctuations. Moreover, polar clusters in smectic phases lead to a wide range of different low and high permittivity paraelectric and polarization randomized smectic phases occurring between the non-polar

<sup>a</sup> Institute of Chemistry, Martin-Luther-University Halle-Wittenberg,  
Kurt-Mothes Str. 2, 06120 Halle, Germany.  
E-mail: carsten.tschierske@chemie.uni-halle.de

<sup>b</sup> Department of Chemistry, Faculty of Science, Cairo University, P.O. 12613, Giza,  
Egypt. E-mail: malaasar@sci.cu.edu.eg

<sup>c</sup> Department of Nonlinear Phenomena, Institute for Experimental Physics,  
Otto von Guericke University Magdeburg, Magdeburg, Germany.  
E-mail: alexey.ereimin@ovgu.de

† Electronic supplementary information (ESI) available. See DOI: 10.1039/c7tc01816a



**An/m**, X = -N=N-, Y = -COO-, Z<sub>1</sub> = H, Z<sub>2</sub> = CN, n = 2,6,20 and m = 6, 12  
**Bn/m**, X = -COO-, Y = -COO-, Z<sub>1</sub> = H, Z<sub>2</sub> = CN, n = 6 and m = 6, 12  
**Cn/m**, X = -OOC-, Y = -COO-, Z<sub>1</sub> = H, Z<sub>2</sub> = CN, n = 6 and m = 6, 12  
**Dn/m**, X = -COO-, Y = -OOC-, Z<sub>1</sub> = H, Z<sub>2</sub> = CN, n = 6, 12 and m = 6, 12

**E6/12**, X = -N=N-, Y = -COO-, Z<sub>1</sub> = CN, Z<sub>2</sub> = H, n = 6 and m = 12

**F6/6**, X = -COO-, Y = -OOC-, Z<sub>1</sub> = CN, Z<sub>2</sub> = H, n = 6 and m = 6

Scheme 1 Chemical structures of the HSLCs under investigations.

smectic phases of rod-like molecules and the macroscopically polar smectic phases of the BCLCs.<sup>25</sup>

The incorporation of azobenzene units into the molecular structures of bent-core liquid crystalline systems widens the range of their application because azobenzenes undergo reversible *trans-cis* isomerization upon irradiation with light.<sup>5f,26</sup> Recently, we have reported several examples of azobenzene containing BCLCs with lateral cyano (CN) substitution in the 4-position of the central resorcinol core that show mirror-symmetry breaking in the fluid smectic C phases (SmC<sub>s</sub><sup>[\*]</sup> and SmC<sub>s</sub>P<sub>R</sub><sup>[\*]</sup>)<sup>27</sup> and form a series of distinct paraelectric, polarization randomized and polar smectic phases.<sup>28</sup> These tilted and related non-tilted high permittivity paraelectric phases were typically found in bent-core mesogens with a reduced bent.<sup>27–30</sup> Molecular structures at the crossover between BCLCs and linear rod-like (calamitic) molecules have received growing interest in recent years, to understand how spatial correlations of shape-anisometric molecules result in the development of novel phase structures.<sup>27–33</sup> Hockey-stick liquid crystals (HSLCs) represent a class of asymmetric molecular forms where one side arm of the bent mesogen is significantly longer than the other (Scheme 1).<sup>34–49</sup>

The motivation of this study is to examine if the LC phases of HSLCs could still exhibit cluster formation in the nematic phases and a significant degree of polar order and mirror symmetry breaking in their smectic phases if 4-cyanoresorcinol, known to support reduced bending of the BCLCs<sup>16a,27,50</sup> is used as a core unit. To achieve that, a new class of HSLCs containing the 4-cyanoresorcinol core as the central unit and two arms of different lengths have been designed and synthesized (see Scheme 1). One arm is a simple 4-alkoxybenzoate unit, whereas the longer arm has three benzene rings. Series **An/m** contains an azobenzene unit, whereas compounds **Bn/m**, **Cn/m** and **Dn/m** involve different types of phenyl benzoate based wings. Moreover, the direction of the cyano group at the apex was inverted in compounds **E6/12** and **F6/6**, (see Scheme 1). The mesophase behaviour of all these new materials was investigated by polarizing optical microscopy (POM), differential scanning calorimetry (DSC) and electro-optical measurements. X-ray diffraction (XRD), dielectric spectroscopy and second harmonic generation (SHG) measurements were performed

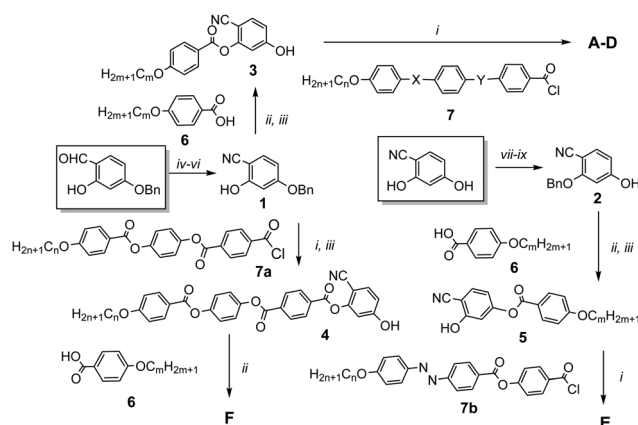
for selected examples and quantum mechanical calculations were performed to understand the observed differences (see the Experimental section).

Besides low permittivity skewed cybotactic nematic phases, high permittivity non-skewed cybotactic nematic phases were also observed, followed by high permittivity SmA and synclinic tilted SmC<sub>s</sub> phases capable of forming surface stabilized chiral domains and low permittivity anticlinic SmC<sub>a</sub> phases. Remarkably, no ferroelectric or anti-ferroelectric smectic phases with fully developed polar layers could be obtained for the BCLCs at reduced temperatures. The temperature-dependence of nano-segregation between the aromatic and aliphatic segments, competing with entropic effects and packing constraints, is considered to be responsible for the observed phase sequences. Overall, this work provides an understanding of the self-assembly of HSLCs and its dependence on the molecular structure, as well as contributes to the knowledge about the relations between the molecular structure and different modes of cluster formation in nematic and smectic phases. These clusters are of significant importance for the materials properties and thus for their use in numerous applications.

## 2. Results and discussion

### 2.1 Synthesis

The synthesis of the new HSLCs **A–F**, discussed herein, was carried out as shown in Scheme 2. Compounds **A–D** and **F** were synthesised starting from 4-benzyloxy-2-hydroxybenzaldehyde which was converted to 4-benzyloxy-2-hydroxybenzonitrile (**1**) as described in the literature.<sup>16a</sup> On the other hand, compound **E** was synthesised starting from 4-cyanoresorcinol.<sup>16a,27</sup> A sequence of tosylation, benzylation and detosylation gave 2-benzyloxy-4-hydroxybenzonitrile **2**. Acylation of the free phenolic OH groups of **1** and **2**, followed by hydrogenolytic deprotection led to



Scheme 2 Synthetic route to compounds **A–F** (X = N=N, COO, OOC, Y = COO, OOC, see Scheme 1 and Schemes S1–S4 in the ESI†); reagents and conditions: (i) Et<sub>3</sub>N, pyridine, CH<sub>2</sub>Cl<sub>2</sub>, reflux 6 h; (ii) DCC, DMAP, CH<sub>2</sub>Cl<sub>2</sub>, stirring 24 h; (iii) H<sub>2</sub>, 10% Pd–C, stirring 24 h at 45 °C; (iv) NH<sub>3</sub>OH<sup>+</sup> Cl<sup>–</sup>, Na<sub>2</sub>CO<sub>3</sub>, stirring 30 min; (v) Ac<sub>2</sub>O, reflux 3 h; (vi) aq. KOH, stirring 72 h, 25 °C; (vii) TsCl, K<sub>2</sub>CO<sub>3</sub>, acetone, reflux 18 h; (viii) BnBr, reflux 18 h; (ix) aq. NaOH, CH<sub>3</sub>OH, stirring 20 h, 25 °C.

phenols 3–5, which after second acylation with the benzoic acid forming the other arm led to compound A–F. The rod-like benzoic acids involving the azobenzene unit were prepared as described elsewhere,<sup>45</sup> while the synthetic procedures for the benzoic acids without an azo unit as well as other intermediates are described in the ESI† in detail. Acylations with simple 4-alkoxy benzoic acids (6) were performed using the DCC method, whereas all acylations with rod-like benzoic acids were conducted with acid chlorides 7 in the presence of triethylamine as a base and pyridine as a catalyst. The crude compounds A–F were purified by column chromatography using dichloromethane followed by recrystallization from an ethanol/chloroform (1:1) mixture to yield the desired materials. Detailed procedures and the analytical data of the newly synthesised compounds are reported in the ESI.†

## 2.2 Azobenzene containing hockey-stick compounds An/m

Compounds An/m containing an azobenzene side arm opposite to the direction of the CN group form four different types of enantiotropic mesophases with phase sequences depending on the alkyl chain length (see Table 1). Compound A2/12 with one very short ethoxy chain has a non-tilted smectic (SmA) phase and a nematic phase (N) above it, while compounds A6/6 and A6/12 additionally form two different types of tilted SmC phases. In planar cells, the nematic phase appears with a *Schlieren* texture, apparently involving exclusively 4-brush disclinations (Fig. 1e) which rapidly undergo homeotropic alignment with the formation of a completely dark pseudoisotropic texture. At the transition to the SmA phase, the *Schlieren* texture changes into a typical fan pattern with dark extinction brushes oriented parallel to the polarizers (Fig. 1f). In homeotropically aligned cells, the completely dark isotropic appearance is retained and the N–SmA transition is only recognized by spinodal decomposition between

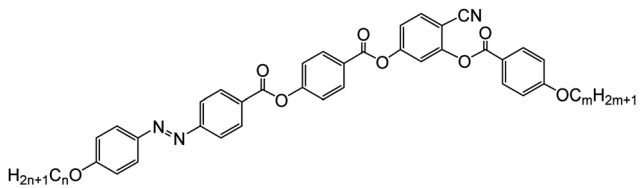
two slightly different dark states, indicating a first-order phase transition (Fig. 1a).

At the transition from the SmA phase to the SmC phase of A6/12, the *Schlieren* texture suddenly develops in the homeotropically aligned sample (Fig. 1c). This transition can also be detected in the planar alignment, where the fan-shaped texture observed in the SmA phase becomes broken (compare Fig. 1f and g). For compounds A6/6 and A6/12, a transition between two different types of SmC phases is observed, that is from the synclinc SmC phase at high temperature (SmC<sub>s</sub>) to the anticlinic SmC<sub>a</sub> phase at lower temperature. This transition can be observed in both homeotropic and planar alignments. In homeotropic samples, the four-brush *Schlieren* texture of the SmC<sub>s</sub> phase becomes distorted (Fig. 1c and d).

In cells with planar alignment, the broken fan texture of the SmC<sub>s</sub> phase (Fig. 1g) converts to a uniform fan texture again but with irregular stripes across the fans and the orientation of the extinction brushes being parallel to the polarizers (Fig. 1h). In both textures, the transition is accompanied by a reduction of the birefringence in the anticlinic SmC<sub>a</sub> range (also see Fig. S16 and S17, ESI†). In freely suspended films, the SmC<sub>s</sub>–SmC<sub>a</sub> transition is particularly well observed. This transition is accompanied by nucleation of domain walls with opposite tilt of the director in the SmC<sub>s</sub> phase and disappearance of the Meyer domains at the transition to the anticlinic SmC<sub>a</sub> phase (Fig. 2).<sup>51</sup>

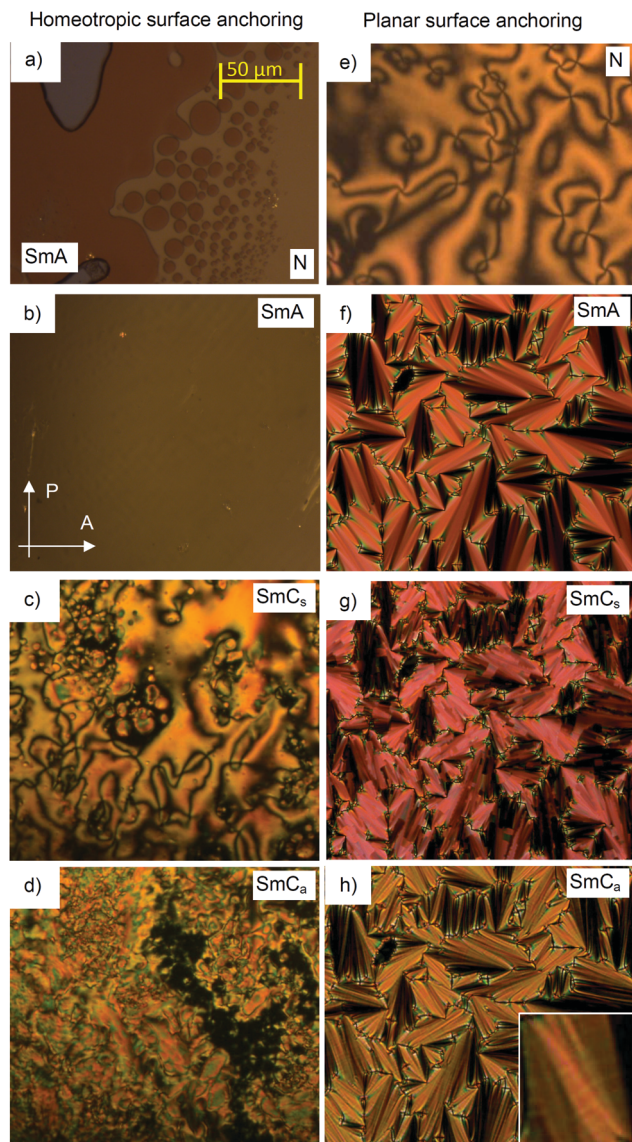
The anticlinic SmC<sub>a</sub> phase is relatively rare and the SmC<sub>s</sub>–SmC<sub>a</sub> transition is seldom observed for achiral rod-like LC compounds. It was, for example, reported for dimesogens with siloxane spacers<sup>52</sup> and molecules with branched terminal chains.<sup>53</sup> In contrast, for BCLC SmC<sub>a</sub> phases are quite common (SmC<sub>a</sub>P<sub>A</sub>/SmC<sub>a</sub>P<sub>F</sub>)<sup>8</sup> and the SmC<sub>s</sub>–SmC<sub>a</sub> transition is a typical feature of HSLCs.<sup>35,39,46,47</sup> The temperature range of the SmC<sub>s</sub> phase of the synthesized HSLCs is widened (A6/6 → A6/12),

Table 1 Phase transition temperatures, mesophase types, and transition enthalpies [ $\Delta H$ /kJ mol<sup>-1</sup>] of compounds An/m<sup>a</sup>



Comp.	<i>n</i>	<i>m</i>	Phase transitions <i>T</i> /°C [ $\Delta H$ /kJ mol <sup>-1</sup> ]
A6/6	6	6	<i>H</i> : → Cr 127 [89.8] SmC <sub>a</sub> 164 [–] SmC <sub>s</sub> 170 [–] SmA 206 [–] N <sub>CyBA</sub> 219 [6.2] Iso → <i>C</i> : ← Cr < 20 M <sub>x</sub> ~ 115 [–] SmC <sub>a</sub> 162 [–] SmC <sub>s</sub> 167 [–] SmA 205 [–] N <sub>CyBA</sub> 217 [6.2] Iso ←
A2/12	2	12	<i>H</i> : → Cr 146 [55.6] SmA 194 [–] N <sub>CyBA</sub> 227 [8.0] Iso → <i>C</i> : ← Cr 105 [66.9] SmA 193 [–] N <sub>CyBA</sub> 224 [8.3] Iso ←
A6/12	6	12	<i>H</i> : → Cr 117 [79.7] SmC <sub>a</sub> 174 [–] SmC <sub>s</sub> 183 [–] SmA 206 [–] N <sub>CyBA</sub> 214 [6.8] Iso → <i>C</i> : ← Cr 16 [12.5] SmC <sub>a</sub> 168 [–] SmC <sub>s</sub> 182 [–] SmA 204 [–] N <sub>CyBA</sub> 210 [6.8] Iso ←
A20/12	20	12	<i>H</i> : → Cr 94 [39.3] SmC <sub>s</sub> 188 [–] SmA 190 [1.1] Iso → <i>C</i> : ← Cr 62 [42.1] SmC <sub>s</sub> 184 [–] SmA 188 [1.3] Iso ←

<sup>a</sup> Transition temperatures and enthalpy values were taken from the second DSC heating (*H*) scans and cooling (*C*) scans at 10 K min<sup>-1</sup>; SmC<sub>s</sub>–SmC<sub>a</sub> transitions were determined in homeotropic samples; abbreviations: Cr = crystalline solid; SmA = non-tilted smectic phase; N<sub>CyBA</sub> = nematic phase composed of cybotactic clusters of the SmA-type; SmC<sub>s</sub> = synclinc tilted high permittivity smectic phase (SmC<sub>s</sub>P<sub>R</sub><sup>[\*]</sup>); SmC<sub>a</sub> = anticlinic smectic C phase; M<sub>x</sub> = unidentified mesophase; Iso = isotropic liquid.



**Fig. 1** Optical micrographs observed for compound **A6/6** in a planar cell (6  $\mu\text{m}$  PI coated cell, right column) and in a homeotropic cell (between ordinary non-treated microscopy slides, left column); (a) demixing at the  $\text{SmA}-\text{N}_{\text{CyBA}}$  transition at  $T = 206$   $^{\circ}\text{C}$  and (e) the  $\text{N}_{\text{CyBA}}$  phase at  $T = 215$   $^{\circ}\text{C}$ ; (b and f)  $\text{SmA}$  phase at  $T = 190$   $^{\circ}\text{C}$ ; (c and g)  $\text{SmC}_s$  phase at  $T = 160$   $^{\circ}\text{C}$  and (d and h)  $\text{SmC}_a$  phase at  $T = 140$   $^{\circ}\text{C}$ ; the inset shows the stripe pattern across the fans; the orientation of the polarizer and analyzer for all cases is shown in (b).

or the  $\text{SmC}_s$  phase is induced (**A2/12**  $\rightarrow$  **A6/12**) upon chain elongation at the shorter or longer arm.<sup>47</sup> Further chain elongation completely removes the nematic and  $\text{SmC}_a$  phases, and only the  $\text{SmC}_s$  phase is observed below the  $\text{SmA}$  phase of compound **A20/12** (see Fig. S15, ESI<sup>†</sup>). This indicates that not only the length of the alkyl chain at the shorter arm of the rigid core favours synclinal interlayer correlation, as reported previously,<sup>47</sup> but also the elongation of the chain at the longer arm, as shown here. The reason is that these chains contribute to an elongation of the flexible part of the mesogenic wings making the overall configuration more rod-shaped. This, in

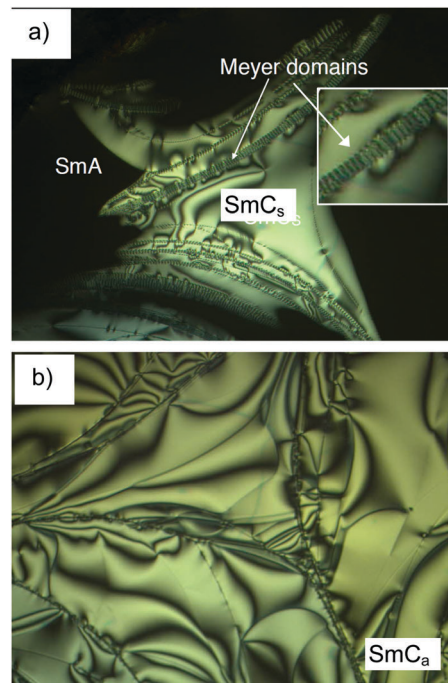


**Fig. 2** Polarising microscopy images of a freely suspended film of compound **A6/6** (a) at the  $\text{SmA}-\text{SmC}_s$  transition at  $T = 170$   $^{\circ}\text{C}$  and showing the Meyer domains growing from the layer steps and (b) in the  $\text{SmC}_a$  phase at  $T = 147$   $^{\circ}\text{C}$ . The width of the images is about 400  $\mu\text{m}$ .

return, favours synclinal tilt correlations in neighbouring layers.<sup>47</sup>

For compounds **A6/6**, **A2/12** and **A6/12**, the  $\text{N}$ -Iso transition enthalpy has an unusually high value ( $\Delta H = 6.2\text{--}8.3$   $\text{kJ mol}^{-1}$ , see Table 1 and Fig. 3), being in the same range as typical for the  $\text{Iso}-\text{SmA}$  transition enthalpies and being almost ten times larger than the typical  $\text{N}$ -Iso transition enthalpies of other rod-like LCs, BCLCs and HSLCs. In contrast, the  $\text{N}-\text{SmA}$  transition as well as the  $\text{SmA}-\text{SmC}_s$  and  $\text{SmC}_s-\text{SmC}_a$  transitions of these compounds is not visible in the DSC thermograms (see Fig. 3a), though at least the  $\text{SmC}_s-\text{SmC}_a$  transition is expected to be of first order.<sup>47</sup> Compound **A20/12** with two long chains behaves differently. The nematic phase is completely replaced by the  $\text{SmA}$  phase and the  $\text{SmA}-\text{Iso}$  transition enthalpy is only 1.2  $\text{kJ mol}^{-1}$  (Table 1), which is in the typical range of  $\text{SmA}-\text{Iso}$  transitions of simple rod-like molecules.

Unfortunately, the investigation of the nematic phases of compounds **An/m** by X-ray diffraction was not possible due to very high temperature ranges ( $> 200$   $^{\circ}\text{C}$ ) of the nematic phases (Table 1). Aligned samples could not be obtained for the same reason and, therefore, the discussion of XRD data is limited to the analysis of powder patterns. Compound **A6/6** as a representative example (see Fig. S21 and Table S1, ESI<sup>†</sup>) shows a single sharp Bragg peak with  $d = 4.41$  nm in the  $\text{SmA}$  phase at 180  $^{\circ}\text{C}$ . The position of the layer reflection does not significantly change upon cooling, being  $d = 4.44$  and 4.46 nm in the  $\text{SmC}_s$  and  $\text{SmC}_a$  phases at  $T = 165$  and 130  $^{\circ}\text{C}$ , respectively (a weak second order reflection occurs in the  $\text{SmC}_a$  phase). The wide-angle region is diffuse with a maximum at  $d = 0.46$  nm in

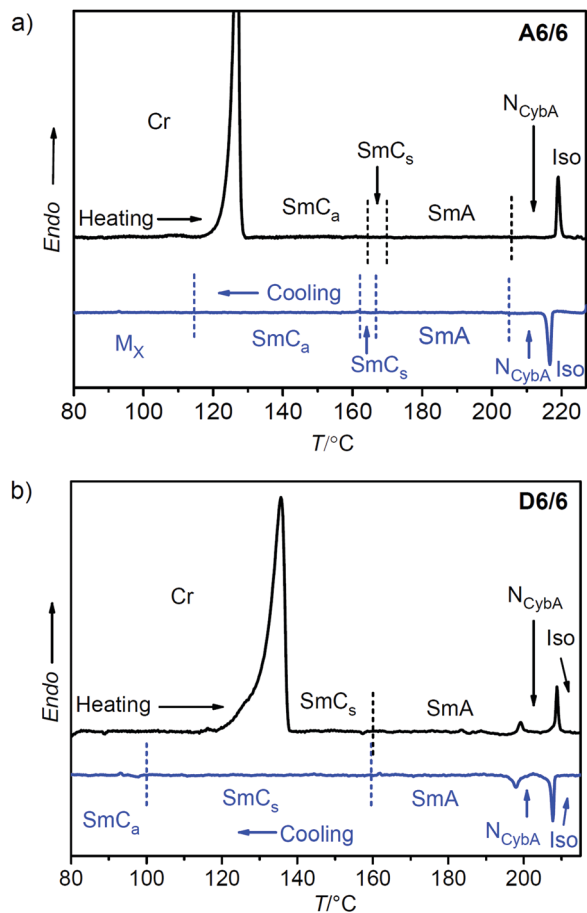


Fig. 3 DSC thermograms obtained for: (a) compound **A6/6** and (b) compound **D6/6**; with  $10 \text{ K min}^{-1}$  heating and cooling rates; for phase abbreviations, see Table 1; for additional DSCs, see Fig. S20 (ESI†).

all three smectic phases (Fig. S21, ESI†), confirming fluid smectic LC phases without in-plane order. The  $d$ -spacing corresponds approximately to the molecular length ( $L_{\text{mol}} = 4.5 \text{ nm}$ , as determined for a hockey-stick-shaped conformation with an assumed  $120^\circ$  bending angle and stretched alkyl chains, see Fig. 4a–c). This close similarity of calculated molecular lengths and measured  $d$ -values, even in the tilted smectic phases, indicates that the smectic phases do not represent simple single layer structures, but must be considered as strongly interdigitated double layer structures resulting from the breaking of the up-down asymmetry of the bent-position by antiparallel molecular organization (Fig. 4a and b). The slight increase of the  $d$ -value despite the onset of tilt at the SmA–SmC transition, and the increasing bend of the molecules (leading to a shorter effective molecular length)<sup>39</sup> upon cooling could mean that either the orientational order parameter is small in the SmA phase and there is already randomized tilt (de Vries phases<sup>54</sup>) or that the degree of interdigitation decreases upon decreasing the temperature.

Because the nematic phases of compounds **An/m** were found at temperatures above SmA phases, they are assumed to be composed of cybotactic clusters of the SmA type, thus representing  $N_{\text{CyBA}}$  phases. As mentioned above, there is no detectable

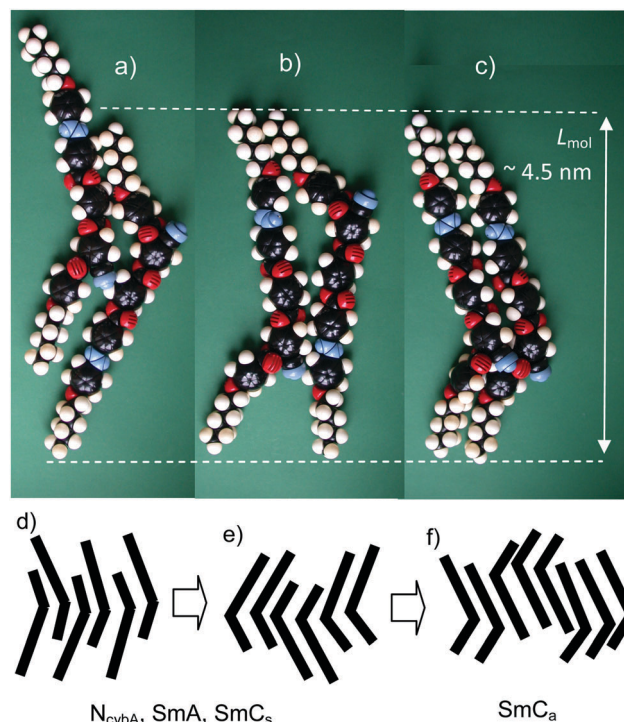
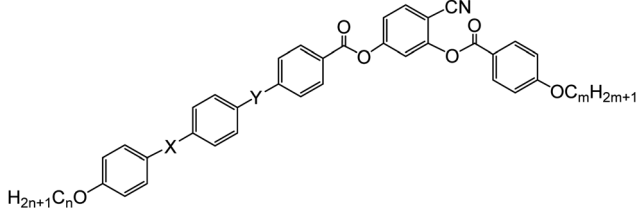


Fig. 4 (a–c) CPK models of **A6/6** showing the distinct modes of self assembly in the cybotactic clusters and layers (a) intercalated bilayer structure with antiparallel (up-down symmetric) arrangement of the molecules and polar order developing parallel to the layers, (b) antiparallel arrangement of the molecules with complete segregation of aromatic cores and aliphatic chains and (c) parallel organization of the molecules with broken up-down symmetry and complete segregation of chains and cores. (d–f) Schematic models showing the organization of the aromatic cores (d) in the clusters forming the high permittivity smectic and cybotactic nematic phases with aromatic–aliphatic intercalation and polar packing of the molecules; (e) increasing core–chain segregation leads to polar bundles, (f) assuming anti-polar and up-down randomized packing in the low permittivity SmC<sub>a</sub> phases.

transition enthalpy for the  $N_{\text{CyBA}}$ –SmA transitions of these compounds, while the  $N_{\text{CyBA}}$ –Iso transition enthalpy has an unusually high value for compounds **An/m** with short alkyl chains ( $n \leq 6$ ). This would mean that there is only a small structural change occurring at the  $N_{\text{CyBA}}$ –SmA transition and, therefore, we assume strong clustering in the  $N_{\text{CyBA}}$  phase and an unusually large size of these clusters. Based on these observations, such  $N_{\text{CyBA}}$  phases can be considered as strongly distorted SmA phases with short-range layer periodicity. Such “giant cluster” nematic phases, being intermediate between typical nematic and smectic phases have occasionally been suggested for previously reported BCLCs<sup>16a,55</sup> and HSLCs.<sup>49</sup>

### 2.3 Hockey-stick compounds **Bn/m–Dn/m** without an azobenzene unit

To study the effect of replacing the N=N unit on the meso-phase behaviour, three different types of isomeric HSLCs involving COO groups instead of the N=N linkage and differing in the orientation of the COO groups (COO vs. OOC) were synthesized and investigated (see Scheme 1 and Table 2).

Table 2 Phase transition temperatures, mesophase types, and transition enthalpies [ $\Delta H/\text{kJ mol}^{-1}$ ] of compounds **Bn/m–Dn/m**<sup>a</sup>


Comp.	X	Y	n	m	Phase transitions $T/^\circ\text{C}$ [ $\Delta H/\text{kJ mol}^{-1}$ ]
<b>B6/6</b>	COO	COO	6	6	$H: \rightarrow \text{Cr } 126 [51.8] \text{ SmC}_a \text{ } 144 [-] \text{ SmA } 200 [-] \text{ N}_{\text{CyBA}} \text{ Iso } 201 [6.7] \text{ Iso } \rightarrow$ $C: \leftarrow \text{Cr } < 20 \text{ SmC}_a \text{ } 140 [-] \text{ SmA } 199 [-] \text{ N}_{\text{CyBA}} \text{ } 200 [5.3] \text{ Iso } \leftarrow$
<b>B6/12</b>	COO	COO	6	12	$H: \rightarrow \text{Cr } 117 [44.7] \text{ SmC}_a \text{ } 161 [-] \text{ SmA } 205 [7.5] \text{ Iso } \rightarrow$ $C: \leftarrow < 20 \text{ SmC}_a \text{ } 155 [-] \text{ SmA } 204 [7.1] \text{ Iso } \leftarrow$
<b>C6/6</b>	OOC	COO	6	6	$H: \rightarrow \text{Cr } 170 [76.1] \text{ SmA } [-] 216 [7.5] \text{ Iso } \rightarrow$ $C: \leftarrow \text{Cr } 120 [41.4] \text{ SmC}_s \text{ } 147 [-] \text{ SmA } 214 [8.1] \text{ Iso } \leftarrow$
<b>C6/12</b>	OOC	COO	6	12	$H: \rightarrow \text{Cr } 153 [48.5] \text{ SmC}_a \text{ } 163 [-] \text{ SmC}_s \text{ } 168 [-] \text{ SmA } 217 [8.5] \text{ Iso } \rightarrow$ $C: \leftarrow \text{Cr } 128 [43.6] \text{ SmC}_a \text{ } 162 [-] \text{ SmC}_s \text{ } 166 [-] \text{ SmA } 216 [8.8] \text{ Iso } \leftarrow$
<b>C12/6</b>	OOC	COO	12	6	$H: \rightarrow \text{Cr } 162 [49.9] \text{ SmC}_a \text{ } 165 [-] \text{ SmC}_s \text{ } 172 [-] \text{ SmA } 214 [7.8] \text{ Iso } \rightarrow$ $C: \leftarrow \text{Cr } 134 [47.7] \text{ SmC}_a \text{ } 154 [-] \text{ SmC}_s \text{ } 168 [-] \text{ SmA } 212 [8.3] \text{ Iso } \leftarrow$
<b>C12/12</b>	OOC	COO	12	12	$H: \rightarrow \text{Cr } 156 [40.2] \text{ SmC}_s \text{ } 180 [-] \text{ SmA } 209 [6.9] \text{ Iso } \rightarrow$ $C: \leftarrow \text{Cr } 130 [38.5] \text{ SmC}_s \text{ } 178 [-] \text{ SmA } 208 [7.9] \text{ Iso } \leftarrow$
<b>D6/6</b>	COO	OOC	6	6	$H: \rightarrow \text{Cr } 138 [47.6] \text{ SmC}_s \text{ } 160 [-] \text{ SmA } 198 [0.5] \text{ N}_{\text{CyBA}} \text{ } 209 [1.3] \text{ Iso } \rightarrow$ $C: \leftarrow \text{Cr } 45 [9.0] \text{ SmC}_a \text{ } 100 [-] \text{ SmC}_s \text{ } 160 [-] \text{ SmA } 198 [0.5] \text{ N}_{\text{CyBA}} \text{ } 208 [1.3] \text{ Iso } \leftarrow$
<b>D6/12</b>	COO	OOC	6	12	$H: \rightarrow \text{Cr } 80 [19.0] \text{ SmC}_a \text{ } 96 [-] \text{ SmC}_s \text{ } 178 [-] \text{ SmA } 211 [5.5] \text{ Iso } \rightarrow$ $C: \leftarrow \text{Cr } 53 [14.2] \text{ SmC}_a \text{ } 72 [-] \text{ SmC}_s \text{ } 176 [-] \text{ SmA } 210 [6.3] \text{ Iso } \leftarrow$

<sup>a</sup> Transition temperatures and enthalpy values were taken from the second DSC heating scans and cooling scans at  $10 \text{ K min}^{-1}$ ; while the transitions without detectable enthalpy were determined by optical investigations in homeotropic cells; for abbreviations see Table 1.

**Phenyl benzoates Bn/m.** Unlike compound **A6/6** with  $X = \text{N}=\text{N}$ , compound **B6/6** with  $X = \text{COO}$  shows only the  $\text{N}_{\text{CyBA}}$ ,  $\text{SmA}$  and  $\text{SmC}_a$  phases, *i.e.* no synclitic  $\text{SmC}_s$  phase is formed, and the mesophase stability (clearing temperature) is slightly reduced by *ca.* 10–20 K. This means, that the series **Bn/m**, having all COO groups directed in the same direction, and parallel to the direction of the CN groups (thus having the highest dipole vector along the long arm), has an increased tendency to form anticlinic tilted  $\text{SmC}_a$  phases, leading to a direct  $\text{SmA}$ – $\text{SmC}_a$  transition (see Fig. S18, ESI†). Similar to **A6/6**, compound **B6/6** has an unusually high transition enthalpy for the  $\text{Iso}$ – $\text{N}_{\text{CyBA}}$  transition and no measurable enthalpy for the  $\text{N}_{\text{CyBA}}$ – $\text{SmA}$  transition, being in line with the proposed giant cluster structure of these  $\text{N}_{\text{CyBA}}$  phases.

**Terephthalates Cn/m.** Inverting the direction of the terminal ester group in the longer arm of compounds **Bn/m** results in isomeric terephthalates **Cn/m** ( $X = \text{OOC}$ , see Table 2). All these terephthalates **Cn/m** have mesophase stabilities and phase sequences comparable with those of azobenzenes **An/m**, though the melting points are strongly increased. This is because the terephthalate unit is known to increase the intermolecular interactions by improved  $\pi$ -stacking interactions of the involved electron deficit terephthalate unit.<sup>28a,31,50,56</sup> For this reason, the nematic phase is completely removed and only an  $\text{Iso}$ – $\text{SmA}$  transition is observed already for the short chain

compound **C6/6**.  $\text{SmA}$ – $\text{SmC}_s$ – $\text{SmC}_a$  transitions were found for compounds **C6/12** and **C12/6** with medium chain length and upon further chain elongation (**C12/12**) the  $\text{SmC}_a$  phase is suppressed (see Table 1), similar to the series **An/m**.

**Hydroquinone bisbenzoates Dn/m.** For hydroquinone bisbenzoates **Dn/m** ( $X = \text{COO}$ ,  $Y = \text{OOC}$ ) having the direction of carboxyl group  $Y$  inverted with respect to **Bn/m**, the same phase sequence as observed for **A6/6**, *i.e.*  $\text{SmC}_a$ – $\text{SmC}_s$ – $\text{SmA}$ – $\text{N}_{\text{CyBA}}$  is found for the shortest homologue **D6/6** (see Table 2) and upon chain elongation the nematic phase is removed (see Table 2). However, for compound **D6/6** the  $\text{N}_{\text{CyBA}}$ – $\text{Iso}$  transition enthalpy is much smaller ( $\sim 1.2 \text{ kJ mol}^{-1}$ ), compared to those of **A6/6** and **B6/6** and there is also an observable enthalpy for the  $\text{N}_{\text{CyBA}}$ – $\text{SmA}$  transition (Fig. 3b). Probably, the enhanced electron density of the hydroquinone esters reduces the packing density and the  $\text{N}_{\text{CyBA}}$  phase is in this case an ordinary cybotactic nematic phase involving relatively small clusters.<sup>16</sup>

**Synclitic–anticlinic transitions.** For all compounds **An/m**, **Cn/m** and **Dn/m** with relatively short chains and showing  $\text{SmC}_s$ – $\text{SmC}_a$  transitions, there is no clear change of the orientation of the dark extinction crosses in planar aligned samples at the  $\text{SmA}$ – $\text{SmC}_s$  transition (Fig. 1f and g). Especially after alignment by application of an electric field, the extinctions remain strictly parallel to the polarizer in the  $\text{SmC}_s$  phase range (Fig. 5b and e). This means that in the planar alignment, the tilt develops at the

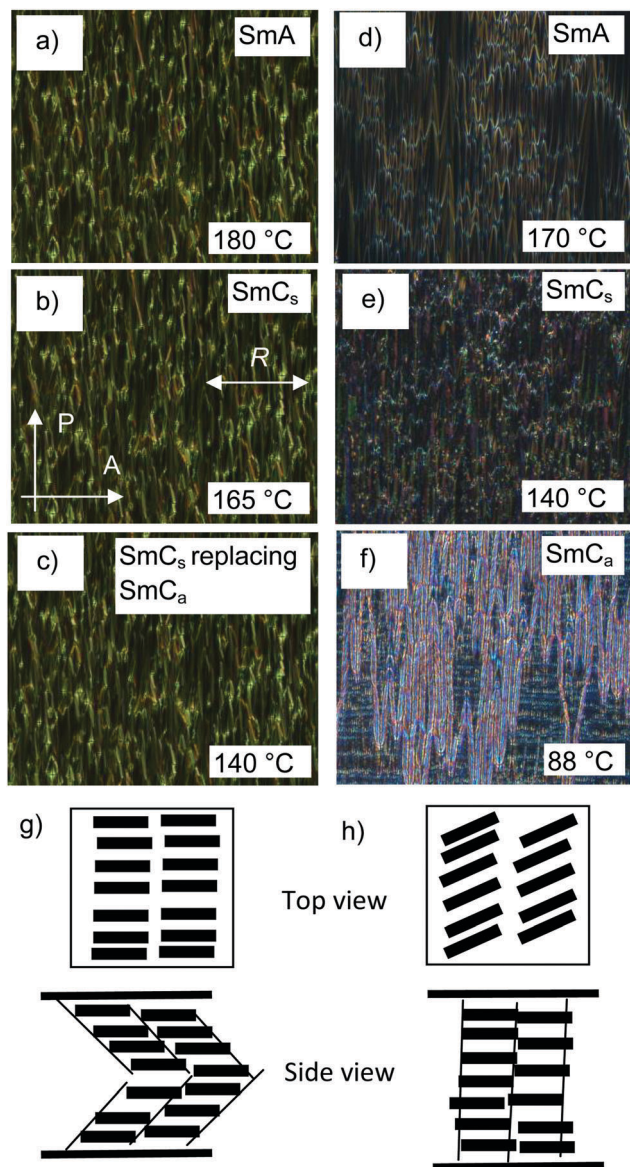


**Fig. 5** (a–f) Textures as observed in the distinct LC phases in a 6 μm ITO cell after application a DC field of +10 V μm<sup>-1</sup> between crossed polarizers: (a–c) compound **A6/12**, (a) in the SmA phase at  $T = 180$  °C, (b) in the SmC<sub>s</sub> phase range at  $T = 165$  °C and (c) in the temperature range of the SmC<sub>a</sub> phase at  $T = 140$  °C (the textures do not change, because at the SmA–SmC<sub>s</sub> transition the layers tilt with retention of the in-plane alignment of the mesogens), see (g). (d–f) Compound **D6/6**, (d) in the SmA phase at  $T = 170$  °C, (e) in the SmC<sub>s</sub> phase range at  $T = 140$  °C and (f) in the SmC<sub>a</sub> phase at  $T = 88$  °C; (g and h) models of molecular organization in the SmC<sub>s</sub> phases in planar cells; (g) tilted layers in chevron geometry and (h) bookshelf geometry with in-plane tilt of the molecules (see Fig. S19b and d, ESI† for the corresponding textures); the directions of the polarizer and analyzer and the rubbing direction ( $R$ ) in (a–f) are indicated in (b).

SmA–SmC<sub>s</sub> transition through tilting of the layers and the formation of a bookshelf geometry (Fig. 5g) and not by an in-plane tilting of the molecules in the non-tilted layers (Fig. 5h). In this configuration, the SmC<sub>s</sub>–SmC<sub>a</sub> transition is not possible without re-arranging the layers and the formation of the topological defects. Therefore, either the textures become

strongly distorted upon transition into the SmC<sub>a</sub> phase (Fig. 5e and f), or the SmC<sub>s</sub>–SmC<sub>a</sub> transition is delayed or even suppressed (Fig. 5b and c). This can also lead to an anchoring transition at the SmC<sub>s</sub>–SmC<sub>a</sub> transition, explaining the strong textural change often observed at this transition in the planar textures of the investigated compounds (see for example Fig. 5f and Fig. S17b–d, ESI†).<sup>35,39,40,46</sup> The specific mode of alignment depends on the surface properties and the molecular structure. The SmC<sub>s</sub> phases of compounds involving an azo group (**An/m**) show the strongest tendency to tilt the layers (Fig. 5a–c and g). There is also a strong effect of the chain length. For compounds with short chains, tilting of the layers is preferred, whereas for compounds with long chains ( $n, m > 10$ ), forming exclusively the SmC<sub>s</sub> phase (compounds **A20/12** and **C12/12**) in-plane tilting takes place by retention of the layer orientation perpendicular to the surface (Fig. 5h) leading to extinctions inclined with respect to the polarizers (Fig. S19b and d, ESI†).

#### 2.4 Electro-optical investigations, non-linear optic and dielectric studies of compounds A6/6 and D6/6

Electro-optical investigations, non-linear optics and dielectric spectroscopy studies were performed with compounds **A6/6** and **D6/6** as representative examples of compounds with high and low  $N_{\text{CyBA}}$ –Iso transition enthalpies (see Tables 1 and 2), *i.e.* larger and smaller clusters, respectively.

**Hydroquinone bisbenzoate D6/6.** The focus is first on **D6/6** showing a low Iso– $N_{\text{CyBA}}$  transition enthalpy. Under an applied triangular wave voltage, a very weak and broad current peak is observed in each half cycle of the applied  $E$ -field ( $E = 26.7$  V μm<sup>-1</sup>, Fig. 6a) in the nematic phase region, which continuously increases in intensity and becomes a broad single peak in the temperature range of the SmA phase (Fig. 6b). Around the SmA–SmC<sub>s</sub> transition, it splits into two broad peaks (Fig. 6c) and upon further decreasing the temperature one of these peaks disappears again, leaving only one broad peak at the transition to the SmC<sub>a</sub> phase (Fig. 6d) which disappears on further cooling. The possibility of polar switching of HSLCs was widely discussed by several authors,<sup>35,40,46</sup> but no clear indications of polar switching could be observed so far, except for free standing films.<sup>31,50,57</sup> The often observed single peak in the current response curves under triangular wave fields were therefore mainly attributed to ionic conductivity.<sup>46</sup>

To examine if there is polar order and if the current peaks could be assigned to the electric polarization, second harmonic generation (SHG) was investigated. No spontaneous SHG was found in compound **D6/6**, but in an electric field, a very weak signal could be detected already in the nematic and the SmA phase. In the SmC<sub>s</sub> range around 130 °C,  $I^{2\omega}(T)$  starts rapidly increasing upon decreasing the temperature, reaching a maximum at the transition into the SmC<sub>a</sub> phase at 100 °C (Fig. 7a). This growth and the maximum of the non-linear optical response  $I^{2\omega}(T)$  are accompanied by an increase of the real part of the dielectric constant  $\epsilon'(T)$ , which exhibits a maximum at the SmC<sub>s</sub>–SmC<sub>a</sub> transition temperature (Fig. 7b). This behaviour is indicative of the development of the polar order at the transition into the SmC<sub>a</sub> phase and softening of the polar

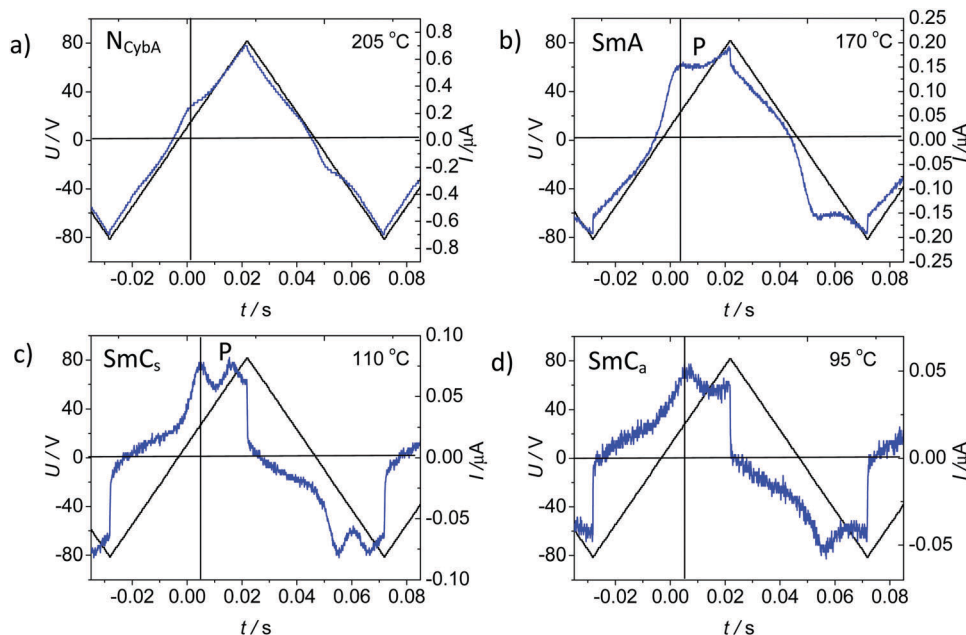


Fig. 6 Polarization current response curves as observed in the distinct LC phases of compound **D6/6** under a triangular wave field ( $26.7 \text{ V}_{\text{pp}} \mu\text{m}^{-1}$ , 10 Hz); the peak (the shoulder in (b)) designated as P is considered as a polarization peak; see Fig. S23 (ESI<sup>†</sup>) for a tighter temperature scan of the range between 110 and 95 °C.

response in the  $\text{SmC}_a$  phase range at lower temperature. Yet, the maxima are very broad and the behaviour of  $\varepsilon'(T)$  (as well as  $I^{\omega}(T)$ ) differs significantly from the paraelectric-ferroelectric transition.<sup>28</sup> We suppose, that in the  $\text{SmA}$  and  $\text{SmC}_s$  phases, the polar fluctuations are restricted to the clusters, whose size, remaining bound, significantly increases upon approaching the transition into the  $\text{SmC}_a$  phase. In the  $\text{SmC}_a$  range, SHG as well as  $\varepsilon$  decreases, perhaps as the polar domain size decreases and relatively strong anti-polar correlation cancels the polarization.

Based on these results, the current peaks in Fig. 6 could be interpreted as follows. There is one peak due to the ionic conductivity which is found at all temperatures and is almost temperature independent (vertical lines in Fig. 6a–d). The second peak (designates as P), evolving in the  $\text{SmC}_s$  range, is considered as a polarization current peak. It is relatively broad as typically found for the Langevin-type paraelectric switching of polar domains.<sup>26</sup> This peak grows and is shifted to higher field strength in the  $\text{SmC}_s$  range close to the  $\text{SmC}_s$ – $\text{SmC}_a$  transition temperature. After reaching the  $\text{SmC}_a$  range, the applied maximum voltage is no more sufficient for switching and therefore this peak cannot be recorded.

This increase of the threshold field with the lowering of temperature is opposite to the observations made for the related 4-cyanoresorcinol based BCLCs, where decreasing the temperature reduces the threshold field.<sup>27–30</sup> These effects might be due to two competing effects: the growth of polar order in the domains and a decreasing polar coherence length. Overall, it appears that the  $\text{N}_{\text{CyBA}}$  and  $\text{SmA}$  phases of **D6/6** represent low permittivity paraelectric phases which become high permittivity paraelectric after the onset of tilt in the  $\text{SmC}_s$  range. However, there is no transition to a ferroelectric phase,

again because at the transition to anticlinic tilt, the polar domain size obviously decreases again. The small transition enthalpy  $\text{Iso}$ – $\text{N}_{\text{CyBA}}$  is in line with the low coherence length of polar order in the relatively small cybotactic domains of the  $\text{N}_{\text{CyBA}}$  phase of **D6/6**.

**Azobenzene compound A6/6.** Compound **A6/6**, showing a high  $\text{N}_{\text{CyBA}}$ – $\text{Iso}$  transition enthalpy behaves quite differently. In this case, two small current peaks can be observed in each half period of the triangular wave voltage already in the isotropic liquid as well as in the  $\text{SmA}$  and  $\text{SmC}_s$  phases (Fig. S24a–f, ESI<sup>†</sup>). The small peak at lower voltage, nearly independent of the temperature is assumed to be due to the ionic conductivity. The second, larger peak, was already found in the  $\text{N}_{\text{CyBA}}$  and  $\text{SmA}$  phases. Similarly to **D6/6**, it shifts to higher voltage with decreasing temperature in the  $\text{SmC}_s$  range and it cannot be observed in the  $\text{SmC}_a$  phase, because the threshold field becomes higher than the applied field (Fig. S24g and h, ESI<sup>†</sup>).

In line with this observation, an appreciable SHG signal can be induced by an electric field already in the nematic and  $\text{SmA}$  phases (Fig. 8a), which suggests increasing susceptibility of polar order to an external electric field. The dependence of the SHG on an applied electric field exhibits a step-like form (Fig. 8b). This can indicate that the polar clusters require a critical field strength to nucleate and grow. The signal also persists in the isotropic phase up to  $5^\circ$ – $8^\circ$  above the clearing point which is correlated with the rather strong current response peak observed under the triangular-wave electric field (Fig. S24 and S25, ESI<sup>†</sup>). The field-induced formation of the polar clusters could also be observed in the dielectric spectra. The real part of the static dielectric permittivity  $\varepsilon'$  is rather small but exhibits a local maximum at the  $\text{N}$ – $\text{SmA}$  transition (Fig. 8c).



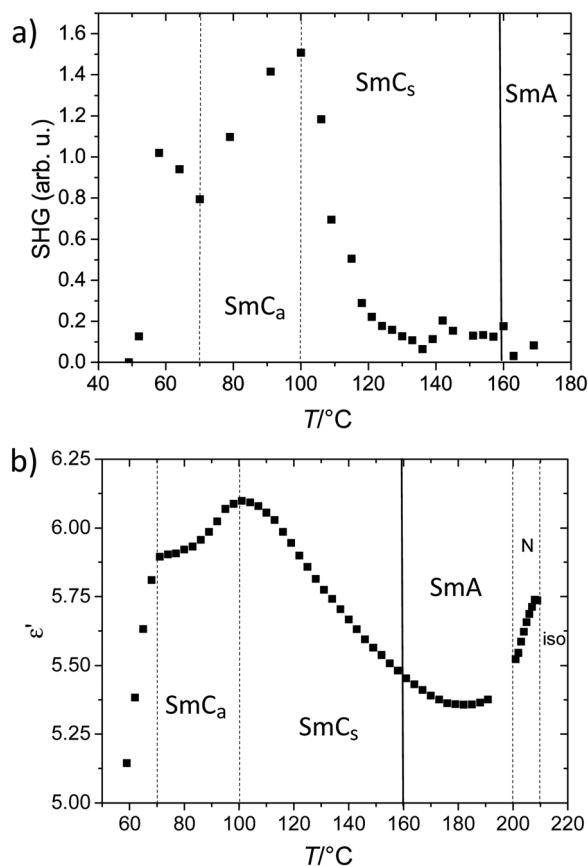


Fig. 7 (a) Field-induced SHG in compound **D6/6** measured in a 10  $\mu\text{m}$  cell exposed to a 10 Hz square-wave field  $E_{\text{pp}} = 30 \text{ V } \mu\text{m}^{-1}$ . (b) The real part of the static dielectric permittivity measured at 5 kHz.

The dielectric relaxation appears only at high frequency  $> 1 \text{ MHz}$ . A distinctive feature of this compound is the behaviour of  $\epsilon'$  under bias voltage. Application of a bias results in the development of a low-frequency mode, which can be attributed to the formation of the polar domains (Fig. 8d).

It appears that in the  $N_{\text{CyBA}}$ , SmA and SmC<sub>s</sub> phases of **A6/6**, there is an appreciable local polar correlation which grows under the applied electric field. This is in agreement with the rather high transition enthalpy of the Iso- $N_{\text{CyBA}}$  transition. However,  $\epsilon'$  decreases after the N-SmA transition (Fig. 8c) and, as also observed for **A6/6**, the switching threshold voltage increases in the SmC<sub>a</sub> range (Fig. S24, ESI<sup>†</sup>). This is in line with the previous report on free standing films of HSLCs where the high temperature SmC<sub>s</sub> phase shows ferroelectric switching and the SmC<sub>a</sub> phase at low temperature does not exhibit a measurable polarization.<sup>57</sup> Hence, it appears that the loss of polar order in the SmC<sub>a</sub> range is a specific feature of HSLCs, being very distinct from the BCLCs having two similar side-arms. For such compounds, a reduction of temperature usually leads to an increase of polar coherence in the layers and transition to ferroelectric or anti-ferroelectric switching.<sup>27–29</sup>

**Mirror symmetry breaking.** As shown in Fig. 9 for **D6/6**, as an example, in homeotropic alignment a conglomerate of chiral domains can be observed in the temperature range of the

synclinal SmC<sub>s</sub> phases of all compounds reported herein. These domains are indicated by observation under a polarizing microscope where the analyzer is slightly uncrossed by anticlockwise rotation from the 90° crossed position (Fig. 9a). The domains invert their brightness when the polarisers are uncrossed in opposite directions (Fig. 9c) thus indicating optical activity of the domains. The chiral domains disappear at the transition to SmA on heating and also at the transition to the anticlinal SmC<sub>a</sub> phase on cooling.

The formation of chiral domains indicates that the polarization cannot be fully randomized in these SmC<sub>s</sub> phases under these conditions. It is proposed that there is an Ising-like distribution leading to a small polarization of the (SmC<sub>s</sub>P<sub>R</sub>-like) domains. In the pristine state, these domains are small and fully randomized on a macroscopic length scale, so that the bulk phase is apolar and achiral. However, these domains can grow under an electric field to such a size that polar switching becomes possible (Langevin-type switching,<sup>25</sup> see the above discussions). Also, the alignment by polar surfaces can obviously lead to a transition from small domains to macroscopic domains with uniform tilt and deviation of the polar direction from a completely polarization randomized structure. This is assumed to lead to the surface stabilized chiral domains observed in thin homeotropic cells. Such chiral domains have previously been observed for SmC<sub>s</sub> phases of weakly bent 4-cyanoresorcinol based BCLCs (paraelectric SmC<sub>s</sub><sup>[\*]</sup> and SmC<sub>s</sub>P<sub>R</sub><sup>[\*]</sup> phases).<sup>27</sup> It is shown here, that this kind of polarization randomized SmC<sub>s</sub> phase (SmC<sub>s</sub>P<sub>R</sub><sup>[\*]</sup>) can also be found for HSLCs.

## 2.5 Discussion of phase structures and the development of polar order in the series An/m-Dn/m

In order to explain the special behaviour of the HSLCs, the reduced symmetry of the HSLCs compared to typical BCLCs must be considered. In contrast to the BCLCs, having a bent in the middle of the molecule, for these non-symmetric HSLCs polar order due to the directed packing of the bent molecules can only be accomplished if the rigid aromatic cores and the flexible lipophilic chains are partly mixed (Fig. 4a and d). In this way, the molecular bows can register and the alkyl chains can contribute to the overall bent molecular shape.<sup>58</sup> Thus, polar order is easily achieved. Due to the high flexibility of the molecular structure and the relatively weak bend, the molecular shape is close to that of a cylinder and out-of-layer fluctuations can support the synclinal tilt and allow an easy coupling of the layer polarisations between the layers. However, the mixing of the incompatible aromatics and aliphatic chains becomes increasingly unfavorable with decreasing temperature (and growing chain length). Moreover, strengthening the core-chain segregation reduces the out-of-layer fluctuations, which together with the growing bend of the molecules favours anticlinal tilt. Even more importantly, segregation of aromatics and alkyl chains would break the up-down symmetry of the layers as soon as the polar order develops (Fig. 4c). As this mode of polar order would be entropically unfavourable, the size of the polar domains is limited and the overall packing tends to become up-down randomized (Fig. 4e) and polarization randomized, as

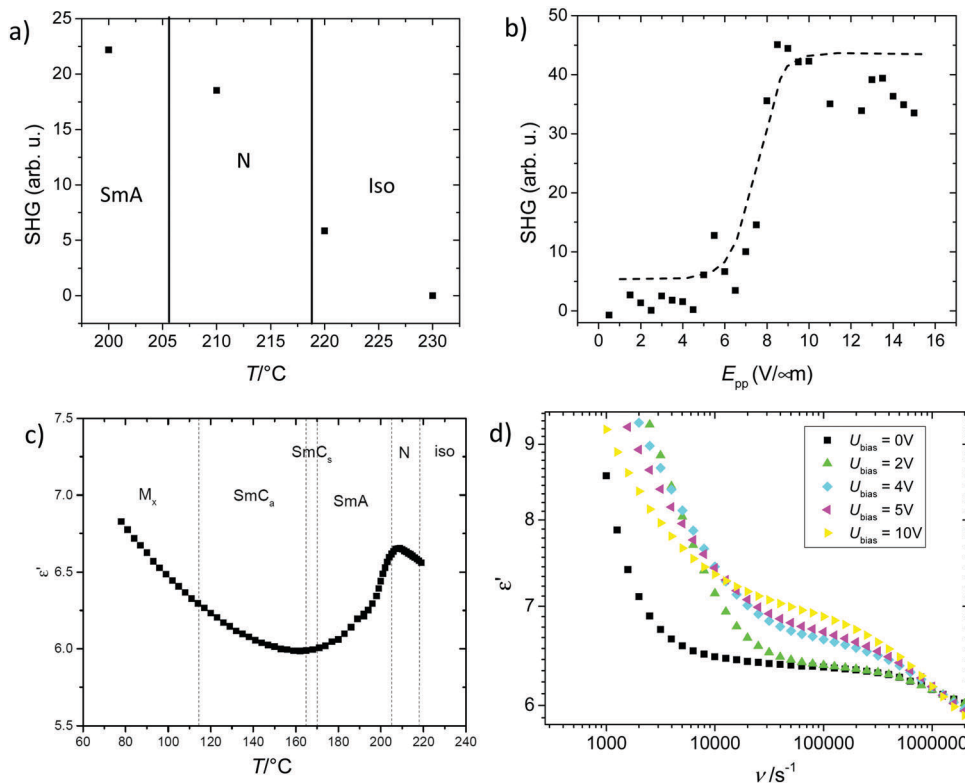


**Fig. 8** Dielectric and SHG data of compound **A6/6**. (a) Temperature dependence of the field-induced SHG signal measured at  $E_{pp} = 30 \text{ V } \mu\text{m}^{-1}$  and  $f = 10 \text{ Hz}$ ; (b) field-dependence of the SHG signal in the SmA phase at  $T = 200 \text{ }^\circ\text{C}$ ; (c) temperature dependence of the static dielectric permittivity and (d) dielectric spectra in the SmA phase under different biases measured at  $T = 200 \text{ }^\circ\text{C}$ .

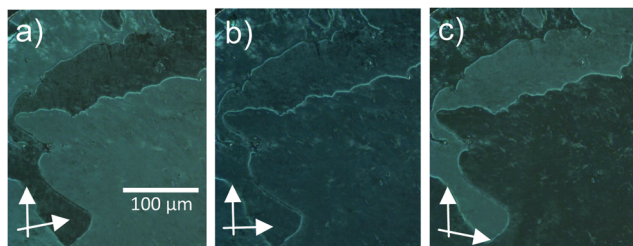


**Fig. 9** Chiral domains observed in the SmC<sub>s</sub> phase of **D6/6**. Note that rotation of the sample between the polarizer does not change the brightness of the domains, confirming that not the tilt alignment is responsible for the observed effect.

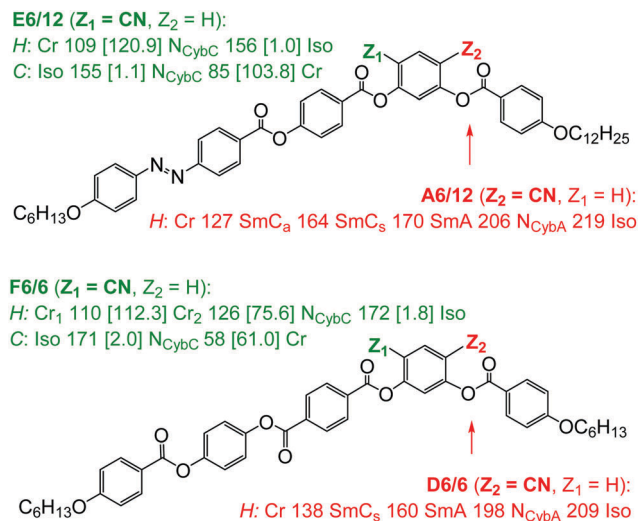
shown in Fig. 4f. In this way, long-range polar order cannot develop and the coherence length of polar correlations is diminished from SmC<sub>s</sub> (Fig. 4d and e) to SmC<sub>a</sub> (Fig. 4f), in line with the experimental observations. Only in the solid crystalline state, when the impact of entropy is small, the polar order can be retained and indeed, for **A6/6** a spontaneous SHG signal is observed. The randomized up-down organization retains the monolayer structure which is analogous to the self-assembly of rod-like molecules having one perfluorinated and one non-fluorinated alkyl chain at opposite ends.<sup>59</sup> Also, in this case there is local segregation, though only single layer structures were found.<sup>59</sup>

Although the effect of chain length has not been investigated systematically, it is obvious that longer chains support the

formation of smectic phases with respect to nematic phases and disfavours the formation of the anticlinic SmC<sub>a</sub> phase, as previously known. It is shown that not only the elongation of the alkyl chain at the shorter arm extends the SmC<sub>s</sub> range of HSLCs, but also the chain attached to the longer rod-like arms, apparently being even more efficient in this respect (compare **C6/6**, **C6/12** and **C12/6** in Table 2). It appears that the hysteresis of the SmC<sub>s</sub>–SmC<sub>a</sub> transition on cooling, previously reported to be up to  $5 \text{ K}$ <sup>47</sup> is especially strong for compounds with long alkyl chains, reaching  $11 \text{ K}$  for **C12/6** and  $24 \text{ K}$  for **D6/12**. There appears to be an additional effect of the position of the longer chain (compare **C12/6** with **C6/12**) which needs further examples to be generalized. The introduction of very long chains ( $> \text{C}_{12}\text{H}_{25}$ , see compound **A20/12**) appears to reduce the SmA–Iso transition enthalpy which indicates reduced polar order, probably by reduced core packing density due to the significant lateral expansion of the long chains and combined with increased aromatic–aliphatic segregation, disfavoring the polar intercalated bilayer organization in Fig. 4d.

## 2.6 Effect of inverting the direction of the CN group at the apex

Inversion of the direction of the CN group at the apex has a dramatic effect on the transition temperatures, phase ranges and phase structures, as shown in Scheme 3. Comparing the isomeric compounds **A6/12** and **E6/12**, both involving the azo linking unit and differing only in the orientation of the CN



**Scheme 3** Effect of the direction of the cyano group. Chemical structures, transition temperatures ( $T/^\circ\text{C}$ ) and mesophase types observed on heating (*H*) and cooling (*C*) of compounds **E6/12** and **F6/6** (green), having the CN group besides the longer rod (with transition enthalpies,  $\Delta H/\text{kJ mol}^{-1}$ , between square brackets) compared to compounds **A6/6** and **D6/6** (red) having the CN group besides the shorter benzoate unit.

group, indicates that the melting and clearing temperatures are reduced for **E6/12**, the  $\text{SmA}$  and  $\text{SmC}$  phases are completely removed and the nematic phase is the only mesophase observed for this compound.<sup>60</sup> A similar behavior was observed by comparing the isomeric hydroquinone bisbenzoates **D6/6** and **F6/6** with the opposite direction of the CN group.

As shown in Fig. 10a the X-ray diffraction pattern of a magnetically aligned sample of the nematic phase of **F6/6**, as an example, shows a diffuse scattering in the wide-angle region with a maximum at  $d = 0.46$  nm positioned on the equator, and a weak diffuse scattering in the small angle region with a maximum at  $d = 3.3$  nm, being considerably shorter than the molecular length. The diffuse small-angle scattering has a dumbbell-like shape with intensity comparable to the wide-angle scattering. This shape is a typical feature of cybotactic clusters of the  $\text{SmC}$ -type, thus confirming a skewed cybotactic nematic phase ( $N_{\text{Cybc}}$  phase);<sup>16</sup> the tilt  $\tau$  in the cybotactic clusters is relatively high, about  $35^\circ$ – $36^\circ$  (Fig. 10b). Similar XRD results were also obtained for compound **E6/12** (see Fig. S22, ESI<sup>†</sup>). In contrast to the majority of the  $N_{\text{CybA}}$ -Iso transition enthalpies in compounds **An/m** and **Bn/m**, the  $N_{\text{Cybc}}$ -Iso transition enthalpies of **E6/12** and **F6/6** are much smaller and are in the typical range as expected for this kind of phase transition. In line with this, the size of the clusters should be relatively small and no polarization peak can be detected in these nematic phases, confirming the absence of polar domains.

## 2.7 Quantum mechanical calculations

In quantum mechanical calculations using the model compounds **A1/1** and **E1/1** with the methyl groups replacing the alkyl chains, we observed minimum structures with a helical twist (Fig. S26, ESI<sup>†</sup>),

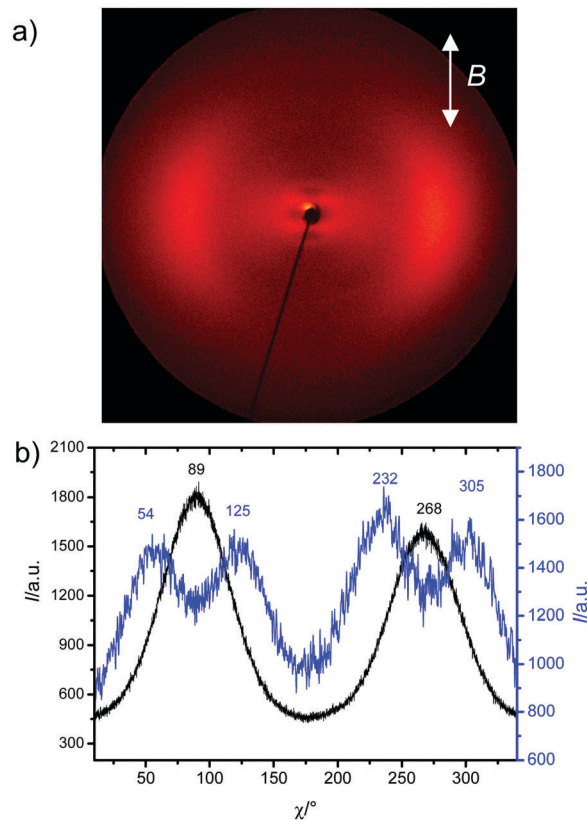


**Fig. 10** XRD investigations of the nematic phase of compound **F6/6**: (a) diffraction pattern of a magnetically aligned sample of the nematic phase (field direction is indicated by the arrow) at  $95^\circ\text{C}$ ; (b) intensity distribution of the diffuse scatterings along  $\chi$ , the black curve denotes wide-angle scattering ( $15^\circ$ – $25^\circ$   $2\theta$ ) and the blue curve small-angle scattering ( $2^\circ$ – $5^\circ$   $2\theta$ ).

as previously reported for related bent-core compounds.<sup>27b,c</sup> However, a comparison of the energies of all optimized structures revealed that in the global minimum structure of both **A1/1** and **E1/1** all benzene rings as well as the connecting groups are perfectly in one plane (see, Fig. 11a and b). The respective planar conformer is more stable by approximately  $1.5$   $\text{kJ mol}^{-1}$  compared to the twisted one (LANL2DZ basis set). Further refinement by DFT computations using the 6-31G basis set gives a preference for the planar conformations by 4 to 5  $\text{kJ mol}^{-1}$ . Despite the similar planarity in the global minimum structures, the position of the cyano group has a significant influence on the bending angle (calculated as the angle between the lines connecting the terminal ether oxygens with the carbon atoms 1 and 3 of the resorcinol core); in **A1/1** and **E1/1**, the bending angle  $\gamma$  is  $107^\circ$  and  $135^\circ$ , respectively. Though the actual bending angle might be affected by the molecular self-assembly in the LC phases, the calculations indicate a general trend of a more pronounced molecular bend for compounds **An/m**–**Dn/m** compared to **En/m** and **Fn/m**, being in line with the distinct phase behaviour. Only the strongly bent compound **An/m**–**Dn/m** having the CN group co-linear with the longer wing are capable of forming smectic phases and developing polar order, whereas the isomeric compounds **En/m** and **Fn/m** having the CN group inclined with the longer arm have a much smaller bend and consequently

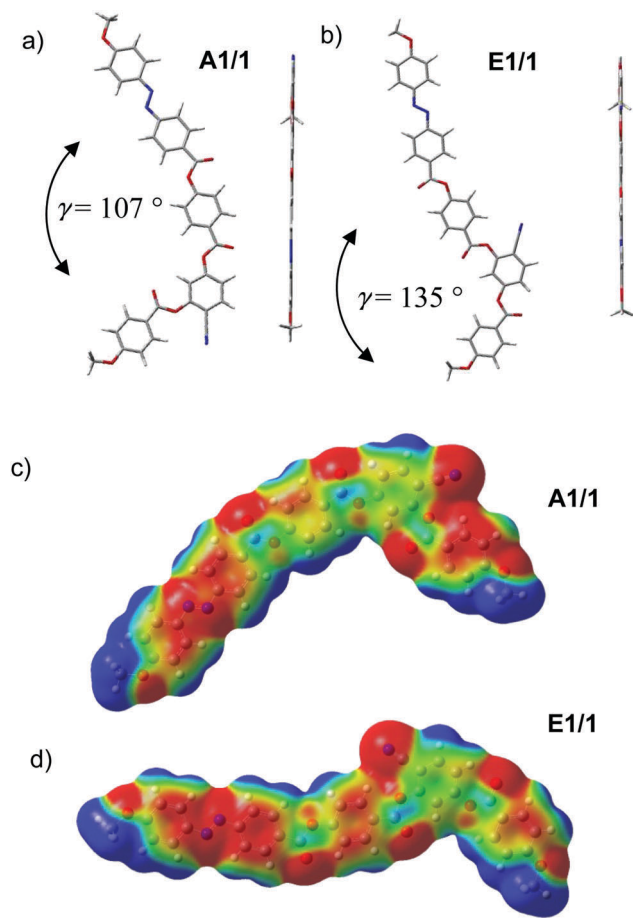


**Fig. 11** (a and b) Energy minimized molecular conformers (global minima, for local minima, see Fig. S26, ESI†) at the B3LYP/LANL2DZ level of theory of the model compounds (a) **A1/1** and (b) **E1/1** perpendicular to the plane of the resorcinol core (left) indicating changes in the bending angle and along the shorter wing and parallel to the plane of the resorcinol core (right), indicating the absence of twist. (b and c) Electrostatic potential maps of (b) **A1/1** and (c) **E1/1** with the same scaling; red colors indicate electron-rich areas, whereas bluish colors indicate electron-poor areas.

behave like laterally substituted rod-like molecules forming non-polar nematic phases.

The non-twisted molecular conformation of the molecules in the ground state is surprising and in conflict with the observation of chiral domains in all  $\text{SmC}_s$  phases. This could, in principle, have two explanations. Either the chirality is exclusively based on the layer chirality (supported by polar surface interaction, see above)<sup>8</sup> and not affected by the transient molecular chirality<sup>61</sup> or the helical conformations of the molecules in the LC bulk state are stabilized in the lamellar bulk assemblies compared to the solvated single molecules in the simulations, and thus become the global low energy conformers during the process of self-assembly.

For the planar energy minimum structures, the electrostatic potential maps were calculated. Depending on the position of the CN group, there is a substantial change in the surface potential in the benzene rings adjacent to the resorcinol core (see, Fig. 11c and d). In compound **E1/1**, the surface potentials

of the two adjacent benzene rings are comparable, whereas they significantly differ in compound **A1/1**. Thus, for compounds **An/m**, electrostatic donor–acceptor interactions could favor an antiparallel packing as shown in Fig. 4a and d, being favorable for the development of polar order in the nematic and high temperature smectic phases and for a non-staggered packing of the aromatics, reducing the tendency to form tilted phases.

### 3. Summary and conclusions

In summary, non-symmetric five-ring HSLCs involving the 4-cyanoresorcinol central core have been synthesized. LC phase structures and the polarity of the mesophases were investigated for determining the effect of the chemical structure of the mesogenic arms, CN substitution of the core and the lengths of the terminal chains. Cybotactic nematic  $N_{\text{CybA}}$  and  $N_{\text{CybC}}$  phases as well as paraelectric  $\text{SmA}$ , synclincic  $\text{SmC}_s$  and anticlinic  $\text{SmC}_a$  phases were found. If the CN group is adjacent to the long side arm of the hockey-stick molecule, non-polar  $N_{\text{CybC}}$  phases with comparatively low transition temperatures and forming small  $\text{SmC}$  clusters are dominating. Compounds with the CN group adjacent to the shorter wing have higher LC phase stability and form additional non-tilted phases. Moreover, these compounds have larger cybotactic clusters in the nematic phases ( $N_{\text{CybA}}$ ) and polar clusters in the smectic phases, thus leading to the phase sequence  $N_{\text{CybA}}\text{-SmA-SmC}_s\text{-SmC}_a$  in some cases. The coherence length of polar order increases on cooling, but significantly drops when anticlinic order develops, which is attributed to the dissymmetry of the hockey-stick molecules. A model is proposed where polar order easily develops as long as segregation between aromatic cores and alkyl chains is weak, *i.e.* at high temperature and for short chains, allowing an up-down symmetry in the polar layers (Fig. 4d). On approaching the  $\text{SmC}_s\text{-SmC}_a$  transition, core-chain segregation locally breaks the up-down symmetry. However, polar layers or larger polar domains cannot be formed, because they experience an entropic penalty, thus leading to the loss of long range polar order with the formation of an antiparallel and anti-polar organization of small bundles of molecules, giving rise to low permittivity of the paraelectric  $\text{SmC}_a$  phases (Fig. 4f). This reduction of the coherence length of polar order at the  $\text{SmC}_s\text{-SmC}_a$  transition is distinct from the related symmetric BCLCs where up-down symmetry is permanent and transitions to antiferroelectric  $\text{SmC}_a\text{P}_A$  phases composed of polar layers are typically observed.<sup>28,29</sup> Remarkable is also the strong dependence of the  $\text{SmC}_s\text{-SmC}_a$  transition on the conditions, leading to delay or depression of the  $\text{SmC}_s\text{-SmC}_a$  transition in some cases. Overall, this work provides clues for the understanding of the unusual properties of HSLCs and poses new challenges in understanding cluster phases in soft condensed systems.

### 4. Experimental section

#### 4.1 Materials

Detailed procedures for synthesis and the analytical data of the newly synthesised compounds are described in the ESI.†

Thin layer chromatography (TLC) was performed on an aluminium sheet pre-coated with silica gel. Analytical quality chemicals were obtained from commercial sources and used as obtained. The solvents were dried using the standard methods when required.<sup>62</sup> The purity and the chemical structures of all compounds synthesized were confirmed by the spectral data and elemental analysis. The structural characterization is based on <sup>1</sup>H-NMR (Varian Unity 500 and Varian Unity 400 spectrometers, in CDCl<sub>3</sub> solutions, with tetramethylsilane as internal standard). Microanalyses were performed using a Leco CHNS-932 elemental analyzer.

#### 4.2 Investigation methods

The thermal behaviour of all synthesized compounds was studied by polarizing optical microscopy (POM) and differential scanning calorimetry (DSC). For polarizing microscopy, a Mettler FP-82 HT hot stage and a control unit in conjunction with a Nikon Optiphot-2 polarizing microscope were used. DSC-thermograms were recorded using a Perkin-Elmer DSC-7 with heating and cooling rates of 10 K min<sup>-1</sup>. Electro-optical switching characteristics were examined in 6 μm polyimide coated ITO cells (EHC Japan) using the triangular-wave method.<sup>63</sup> Freely suspended films were prepared by drawing over a 5 mm opening in a glass plate placed on the FS1 heating stage (INSTEC, USA). The optical observations were made in transmission mode using an AxioImager polarising microscope (Zeiss GmbH).

XRD patterns were recorded using a 2D detector (Vantec-500, Bruker). Ni filtered and pin hole collimated CuK<sub>α</sub> radiation was used (Kristalloflex 560H, Siemens). Samples were measured in thin glass capillaries (nematic phases) or as small droplets on a glass substrate (smectic phases, beam parallel to the surface). The exposure time was 15 min and the sample-to-detector distances were 9.5 and 27.4 cm for the capillaries and 8.95 and 26.7 cm for the droplets, for small angle and wide angle scattering experiments, respectively. Capillaries were investigated in a magnetic oven after cooling from Iso (1 K min<sup>-1</sup>) under a magnetic field of 1 T, applied perpendicular to the capillary and the direction of the X-ray beam. The temperature was kept constant during exposure.

Second harmonic generation (SHG) measurements were performed using a Nd:YAG laser operating at λ = 1064 nm (10 ns pulse width and 10 Hz repetition rate). The primary beam was incident at an angle of 30° to the cell normal. The SHG signal was detected in transmission using a photomultiplier tube H10721-210 (Hamamatsu). The acquired signal was calibrated using a 50 μm reference quartz plate. Dielectric measurements were performed in cooling runs in the frequency range of 100 Hz–10 MHz using a Solartron 1260A impedance analyzer in a 12 μm gold cell. The capacitance of the cell was carefully calibrated before being filled in the isotropic state and the measuring field was 0.5 V<sub>rms</sub>.

#### 4.3 Quantum-mechanical computations

These were carried out using the Gaussian 09 package<sup>64</sup> using DFT methods. To find the minimum energy conformation of the model compounds **A1/1** and **E1/1** (*n*, *m* = 1), 17 and 13

different starting geometries, respectively, were optimized using the functional B3LYP, basis set LANL2DZ and the solvation model (IEFPCM, solvent chlorobenzene). For that, starting structures with different angles between the planes of the benzene rings and varying orientations of functional groups, e.g., azo, carboxyl as well as methoxy, were used. All geometry optimizations were accompanied by frequency analyses. The absence of negative vibrational frequencies indicated convergence on (local) minimum energy structures.

## Acknowledgements

The work was supported by the DFG (Grant TS 39/24-1, ER 467/8-1). We thank Dr Nerea Sebastián for discussion of the dielectric results.

## References

- 1 C. Hilsum, *Philos. Trans. R. Soc. London, Ser. A*, 2010, **368**, 1027.
- 2 B. R. Kaafarani, *Chem. Mater.*, 2011, **23**, 378.
- 3 (a) S. Sivakumar, K. L. Wark, J. K. Gupta, N. L. Abbott and F. Caruso, *Adv. Funct. Mater.*, 2009, **19**, 2260; (b) A. Agarwal, E. Huang, S. Palecek and N. L. Abbott, *Adv. Mater.*, 2008, **20**, 4804; (c) H. Tan, S. Yang, G. Shen, R. Yu and Z. Wu, *Angew. Chem., Int. Ed.*, 2010, **49**, 8608; (d) A. D. Rey, *Soft Matter*, 2010, **6**, 3402.
- 4 M. O'Neill and S. M. Kelly, *Adv. Mater.*, 2011, **23**, 566.
- 5 (a) T. Niori, T. Sekine, J. Watanabe, T. Furukawa and H. Takezoe, *J. Mater. Chem.*, 1996, **6**, 1231; (b) R. A. Reddy and C. Tschierske, *J. Mater. Chem.*, 2006, **16**, 907; (c) H. Takezoe and Y. Takanishi, *Jpn. J. Appl. Phys.*, 2006, **45**, 597; (d) A. Eremin and A. Jáklí, *Soft Matter*, 2013, **9**, 615; (e) J. Etxebarria and M. B. Ros, *J. Mater. Chem.*, 2008, **18**, 2919; (f) M. Alaasar, *Liq. Cryst.*, 2016, **43**, 2208.
- 6 T. Sekine, T. Niori, J. Watanabe, T. Furukawa, S. W. Choi and H. Takezoe, *J. Mater. Chem.*, 1997, **8**, 1307.
- 7 L. E. Hough, M. Spannuth, M. Nakata, D. A. Coleman, C. D. Jones, G. Dantlgraber, C. Tschierske, J. Watanabe, E. Körblova, D. M. Walba, J. E. MacLennan, M. A. Glaser and N. A. Clark, *Science*, 2009, **325**, 452.
- 8 D. R. Link, G. Natale, R. Shao, J. E. MacLennan, N. A. Clark, E. Körblova and D. M. Walba, *Science*, 1997, **278**, 1924.
- 9 C. Tschierske and D. J. Photinos, *J. Mater. Chem.*, 2010, **20**, 4263.
- 10 (a) L. A. Madsen, T. J. Dingemans, M. Nakata and E. T. Samulski, *Phys. Rev. Lett.*, 2006, **96**, 219804; (b) Y. Galerne, *Phys. Rev. Lett.*, 2006, **96**, 219803.
- 11 (a) J.-H. Lee, T.-K. Lim, W.-T. Kim and J.-I. Jin, *J. Appl. Phys.*, 2007, **101**, 034105; (b) R. Stannarius, *J. Appl. Phys.*, 2008, **104**, 036104; (c) G. S. Lee, J. S. Cho, J. C. Kim, T.-H. Yoon and S. T. Shin, *J. Appl. Phys.*, 2009, **105**, 094509.
- 12 R. Stannarius, A. Eremin, M.-G. Tamba, G. Pelzl and W. Weissflog, *Phys. Rev. E: Stat., Nonlinear, Soft Matter Phys.*, 2007, **76**, 061704.

- 13 V. Prasad, S.-W. Kang, K. A. Suresh, L. Joshi, Q. Wang and S. Kumar, *J. Am. Chem. Soc.*, 2005, **127**, 17224.
- 14 (a) G. Shanker, M. Nagaraj, A. Kocot, J. K. Vij, M. Prehm and C. Tschierske, *Adv. Funct. Mater.*, 2012, **22**, 1671; (b) O. Francescangeli, V. Stanic, S. I. Torgova, A. Strigazzi, N. Scaramuzza, C. Ferrero, I. P. Dolbnya, T. M. Weiss, R. Berardi, L. Muccioli, S. Orlandi and C. Zannoni, *Adv. Funct. Mater.*, 2009, **19**, 2592.
- 15 M. Alaasar and C. Tschierske, *Liq. Cryst.*, 2017, **44**, 387.
- 16 (a) C. Keith, A. Lehmann, U. Baumeister, M. Prehm and C. Tschierske, *Soft Matter*, 2010, **6**, 1704; (b) O. Francescangeli, F. Vita, C. Ferrero, T. Dingemans and E. T. Samulski, *Soft Matter*, 2011, **7**, 895; (c) S. Kumar and A. N. Gowda, *Liq. Cryst. Rev.*, 2015, **3**, 99; (d) M. Alaasar, M. Prehm and C. Tschierske, *Liq. Cryst.*, 2014, **41**, 126.
- 17 N. Vaupotic, J. Szydłowska, M. Salamonczyk, A. Kovarova, J. Svoboda, M. Osipov, D. Pocięcha and E. Gorecka, *Phys. Rev. E: Stat., Nonlinear, Soft Matter Phys.*, 2009, **80**, 030701.
- 18 (a) S. Aya, H. Obara, D. Pocięcha, F. Araoka, K. Okano, K. Ishikawa, E. Gorecka, T. Yamashita and H. Takezoe, *Adv. Mater.*, 2014, **26**, 1918; (b) S. Aya, S. Ogino, Y. Hayashi, K. Okano, D. Pocięcha, K. V. Le, F. Araoka, S. Kawachi, E. Gorecka, N. Vaupotic, H. Takezoe and K. Ishikawa, *Phys. Rev. E: Stat., Nonlinear, Soft Matter Phys.*, 2014, **90**, 042506.
- 19 J. Harden, B. Mbanga, N. Eber, K. Fodor-Csorba, S. Sprunt, J. T. Gleeson and A. Jákli, *Phys. Rev. Lett.*, 2006, **97**, 157802.
- 20 (a) T. Ostapenko, D. B. Wiant, S. N. Sprunt, A. Jákli and J. T. Gleeson, *Phys. Rev. Lett.*, 2008, **101**, 247801; (b) O. Francescangeli, F. Vita, F. Fauth and E. T. Samulski, *Phys. Rev. Lett.*, 2011, **107**, 207801.
- 21 K. V. Le, M. Hafuri, H. Ocak, B. Bilgin-Eran, C. Tschierske, T. Sasaki and F. Araoka, *ChemPhysChem*, 2016, **17**, 1425.
- 22 W. D. Stevenson, Z. Ahmed, X. B. Zeng, C. Welch, G. Ungar and G. H. Mehl, *Phys. Chem. Chem. Phys.*, 2017, **19**, 13449.
- 23 (a) T. H. Zhang, J. Klok, R. Hans Tromp, J. Groenewold and W. K. Kegel, *Soft Matter*, 2012, **8**, 667; (b) J. Groenewold and W. K. Kegel, *J. Phys.: Condens. Matter*, 2004, **16**, S4877.
- 24 (a) G. W. Stewart and R. M. Morrow, *Phys. Rev.*, 1927, **30**, 232; (b) A. De Vries, *Mol. Cryst. Liq. Cryst.*, 1970, **10**, 31; (c) R. Breckon, S. Chakraborty, C. Zhang, N. Diorio, J. T. Gleeson, S. Sprunt, R. J. Twieg and A. Jákli, *ChemPhysChem*, 2014, **15**, 1457; (d) M. Gao, Y.-K. Kim, C. Zhang, V. Borshch, S. Zhou, H.-S. Park, A. Jakli, O. D. Lavrentovich, M.-G. Tamba, A. Kohlmeier, G. H. Mehl, W. Weissflog, D. Studer, B. Zuber, H. Gnägi and F. Lin, *Microsc. Res. Tech.*, 2014, **77**, 754; (e) W. Nishiya, Y. Takanishi, J. Yamamoto and A. Yoshizawa, *J. Mater. Chem.*, 2014, **2**, 3677.
- 25 (a) D. Pocięcha, M. Cepic, E. Gorecka and J. Mieczkowski, *Phys. Rev. Lett.*, 2003, **91**, 185501; (b) Y. Shimbo, E. Gorecka, D. Pocięcha, F. Araoka, M. Goto, Y. Takanishi, K. Ishikawa, J. Mieczkowski, K. Gomola and H. Takezoe, *Phys. Rev. Lett.*, 2006, **97**, 113901; (c) K. Gomola, L. Guo, S. Dhara, Y. Shimbo, E. Gorecka, D. Pocięcha, J. Mieczkowski and H. Takezoe, *J. Mater. Chem.*, 2009, **19**, 4240; (d) L. Guo, K. Gomola, E. Gorecka, D. Pocięcha, S. Dhara, F. Araoka, K. Ishikawa and H. Takezoe, *Soft Matter*, 2011, **7**, 2895.
- 26 (a) N. Gimeno, I. Pintre, M. Martínez-Abadía, J. L. Serrano and M. B. Ros, *RSC Adv.*, 2014, **4**, 19694; (b) M. V. Srinivasan, P. Kannan and P. Roy, *New J. Chem.*, 2013, **37**, 1584; (c) N. G. Nagaveni, A. Roy and V. Prasad, *J. Mater. Chem.*, 2012, **22**, 8948; (d) N. Trišović, M. Salamonczyk, J. Antanasijević, S. Sprunt, T. Tóth-Katona, A. Jákli, M. Kohout and K. Fodor-Csorba, *RSC Adv.*, 2015, **5**, 64886.
- 27 (a) M. Alaasar, M. Prehm, M. Nagaraj, J. K. Vij and C. Tschierske, *Adv. Mater.*, 2013, **25**, 2186; (b) M. Alaasar, M. Prehm, K. May, A. Eremin and C. Tschierske, *Adv. Funct. Mater.*, 2014, **24**, 1703; (c) M. Alaasar, M. Prehm, M.-G. Tamba, N. Sebastian, A. Eremin and C. Tschierske, *ChemPhysChem*, 2016, **17**, 278.
- 28 (a) N. Sebastian, S. Belau, A. Eremin, M. Alaasar, M. Prehm and C. Tschierske, *Phys. Chem. Chem. Phys.*, 2017, **19**, 5895; (b) M. Alaasar, M. Prehm, S. Poppe and C. Tschierske, *Chem. – Eur. J.*, 2017, **23**, 5541.
- 29 E. Westphal, H. Gallardo, G. F. Caramori, N. Sebastian, M.-G. Tamba, A. Eremin, S. Kawachi, M. Prehm and C. Tschierske, *Chem. – Eur. J.*, 2016, **22**, 8181.
- 30 H. Ocak, M. Poppe, B. Bilgin-Eran, G. Karanlık, M. Prehm and C. Tschierske, *Soft Matter*, 2016, **12**, 7405.
- 31 (a) G. Pelzl and W. Weissflog, in *Thermotropic Liquid Crystals: Recent Advances*, ed. A. Ramamoorthy, Springer, Amsterdam, 2007, pp. 1–58; (b) W. Weissflog, H. N. Shreenivasa Murthy, S. Diele and G. Pelzl, *Philos. Trans. R. Soc., A*, 2006, **364**, 2657.
- 32 (a) D. Pocięcha, E. Gorecka, M. Cepic, N. Vaupotic, K. Gomola and J. Mieczkowski, *Phys. Rev. E: Stat., Nonlinear, Soft Matter Phys.*, 2005, **72**, 060701; (b) D. Pocięcha, E. Gorecka, M. Cepic, N. Vaupotic and W. Weissflog, *Phys. Rev. E: Stat., Nonlinear, Soft Matter Phys.*, 2006, **74**, 021702.
- 33 (a) A. Eremin, H. Nadasi, G. Pelzl, S. Diele, H. Kresse, W. Weissflog and S. Grande, *Phys. Chem. Chem. Phys.*, 2004, **6**, 1290; (b) A. Eremin, M. Floegel, U. Kornek, S. Stern, R. Stannarius, H. Nadasi, W. Weissflog, C. Zhu, Y. Shen, C. S. Park, J. MacLennan and N. Clark, *Phys. Rev. E: Stat., Nonlinear, Soft Matter Phys.*, 2012, **86**, 051701.
- 34 V. Gude, K. Upadhyaya, G. Mohiuddin and V. S. R. Nandiraju, *Liq. Cryst.*, 2013, **40**, 120.
- 35 (a) F. C. Yu and L. J. Yu, *Chem. Mater.*, 2006, **18**, 5410; (b) F. C. Yu and L. J. Yu, *Liq. Cryst.*, 2008, **35**, 799.
- 36 S. Kang, Y. Saito, N. Watanabe, M. Tokita, Y. Takanishi, H. Takezoe and J. Watanabe, *J. Phys. Chem. B*, 2006, **110**, 5205.
- 37 K. M. Fergusson and M. Hird, *J. Mater. Chem.*, 2010, **20**, 3069.
- 38 A. S. Matharu, C. Grover, L. Komitov and G. Anderson, *J. Mater. Chem.*, 2000, **10**, 1303.
- 39 (a) B. Das, S. Grande, W. Weissflog, A. Eremin, M. W. Schröder, G. Pelzl, S. Diele and H. Kresse, *Liq. Cryst.*, 2003, **30**, 529; (b) W. Weissflog, U. Dunemann, S. F. Tandel, M. G. Tamba, H. Kresse, G. Pelzl, S. Diele, U. Baumeister, A. Eremin, S. Stern and R. Stannarius, *Soft Matter*, 2009, **5**, 1840.
- 40 A. Chakraborty, B. Das, M. K. Das, S. Findeisen-Tandel, M.-G. Tamba, U. Baumeister, H. Kresse and W. Weissflog, *Liq. Cryst.*, 2011, **38**, 1085.
- 41 M. Monika, V. Prasad and N. G. Nagaveni, *Liq. Cryst.*, 2015, **42**, 1490.

- 42 (a) R. Deb, R. K. Nath, M. K. Paul, N. V. S. Rao, F. Tului, Y. Shen, R. Shao, D. Chen, C. Zhu, I. I. Smalyukh and N. A. Clark, *J. Mater. Chem.*, 2010, **20**, 7332; (b) C. D. Jones, R.-F. Shao, A. G. Rappaport, J. E. MacLennan, N. A. Clark, E. Körblová and D. M. Walba, *Liq. Cryst.*, 2006, **33**, 25.
- 43 D. K. Yoon, R. Deb, D. Chen, E. Körblová, R. Shao, K. Ishikawa, N. V. S. Rao, D. M. Walba, I. I. Smalyukh and N. A. Clark, *Proc. Natl. Acad. Sci. U. S. A.*, 2010, **107**, 21311.
- 44 R. K. Nath, D. D. Sarkar, D. S. S. Rao and N. V. S. Rao, *Liq. Cryst.*, 2012, **39**, 889.
- 45 M. Alaasar, S. Poppe and C. Tschierske, *Liq. Cryst.*, 2016, **44**, 729.
- 46 (a) V. Novotná, J. Žurek, V. Kozmík, J. Svoboda, M. Glogarová, J. Kroupa and D. Pocięcha, *Liq. Cryst.*, 2008, **35**, 1023; (b) M. Horčí, V. Kozmík, J. Svoboda, V. Novotná and D. Pocięcha, *J. Mater. Chem. C*, 2013, **1**, 7560.
- 47 E. Enz, S. Findeisen-Tandel, R. Dabrowski, F. Giesselmann, W. Weissflog, U. Baumeister and J. Lagerwall, *J. Mater. Chem.*, 2009, **19**, 2950.
- 48 (a) S. Radhika, H. T. Srinivasa and B. K. Sadashiva, *Liq. Cryst.*, 2011, **38**, 785; (b) D. Malkar, B. K. Sadashiva and A. Ray, *Soft Matter*, 2016, **12**, 4960; (c) P. Sathyanarayana, S. Radhika, B. K. Sadashiva and S. Dhara, *Soft Matter*, 2012, **8**, 2322.
- 49 L. Chakraborty, N. Chakraborty, D. D. Sarkar, N. V. S. Rao, S. Aya, K. V. Le, F. Araoka, K. Ishikawa, D. Pocięcha, E. Gorecka and H. Takezoe, *J. Mater. Chem. C*, 2013, **1**, 1562.
- 50 (a) I. Wirth, S. Diele, A. Eremin, G. Pelzl, S. Grande, L. Kovalenko, N. Pancenko and W. Weissflog, *J. Mater. Chem.*, 2001, **11**, 1642; (b) L. Kovalenko, M. W. Schröder, R. A. Reddy, S. Diele, G. Pelzl and W. Weissflog, *Liq. Cryst.*, 2005, **32**, 857.
- 51 R. Stannarius, A. Eremin and K. Harth, *Liq. Cryst.*, 2017, 1290290, DOI: 10.1080/02678292.2017.
- 52 (a) G. Dantlgraber, S. Diele and C. Tschierske, *Chem. Commun.*, 2002, 2768; (b) H. J. Coles, S. Meyer, P. Lehmann, R. Deschenaux and I. Jauslin, *J. Mater. Chem.*, 1999, **9**, 1085; (c) D. Guillon, M. A. Osipov, S. Mery, M. Siffert, J.-F. Nicoud, C. Bourgoigne and P. Sebastiao, *J. Mater. Chem.*, 2001, **11**, 2700.
- 53 (a) Y. Ouchi, Y. Yoshioka, H. Ishii, K. Seki, M. Kitamura, R. Noyori, Y. Takanishib and I. Nishiyama, *J. Mater. Chem.*, 1995, **5**, 2297; (b) J. Thisayukta and E. T. Samulski, *J. Mater. Chem.*, 2004, **14**, 1554.
- 54 J. P. F. Lagerwall and F. Giesselmann, *ChemPhysChem*, 2006, **7**, 20–45.
- 55 M. Nagaraj, A. Lehmann, M. Prehm, C. Tschierske and J. K. Vij, *J. Mater. Chem.*, 2011, **21**, 17098.
- 56 C. Keith, M. Prehm, Y. P. Panarin, J. K. Vij and C. Tschierske, *Chem. Commun.*, 2010, **46**, 3702.
- 57 R. Stannarius, J. Li and W. Weissflog, *Phys. Rev. Lett.*, 2003, **90**, 025502.
- 58 The diameter of alkyl chains and aromatic cores is comparable, so that this interdigitation has a relatively small destabilizing effect on the layers.
- 59 (a) C. Tschierske, *Top. Curr. Chem.*, 2012, **318**, 1; (b) T. P. Rieker and E. P. Janulis, *Phys. Rev. E: Stat. Phys., Plasmas, Fluids, Relat. Interdiscip. Top.*, 1995, **52**, 2688.
- 60 Photoisomerization of E6/12 was investigated in solution, see Section 2.4 and Fig. S27 in the ESI†.
- 61 C. Tschierske and G. Ungar, *ChemPhysChem*, 2016, **17**, 9.
- 62 H. G. O. Becker, W. Berger, G. Domschke, E. Fanghänel, J. Faust, M. Fischer, F. Gentz, K. Gewalt, R. Gluch, R. Mayer, K. Müller, D. Pavel, H. Schmidt, K. Schollberg, K. Schwetlick, E. Seiler, G. Zeppenfeld, R. Beckert, W. D. Habicher and H. Knölker, *Organikum*, Wiley-VCH, Weinheim, 23rd edn, 2009.
- 63 K. Miyasato, S. Abe, H. Takezoe, A. Fukuda and E. Kuze, *Jpn. J. Appl. Phys.*, 1983, **22**, L661–L663.
- 64 M. J. Frisch, G. W. Trucks, H. B. Schlegel, G. E. Scuseria, M. A. Robb, J. R. Cheeseman, G. Scalmani, V. Barone, B. Mennucci, G. A. Petersson, H. Nakatsuji, M. Caricato, X. Li, H. P. Hratchian, A. F. Izmaylov, J. Bloino, G. Zheng, J. L. Sonnenberg, M. Hada, M. Ehara, K. Toyota, R. Fukuda, J. Hasegawa, M. Ishida, T. Nakajima, Y. Honda, O. Kitao, H. Nakai, T. Vreven, J. A. Montgomery, Jr., J. E. Peralta, F. Ogliaro, M. Bearpark, J. J. Heyd, E. Brothers, K. N. Kudin, V. N. Staroverov, R. Kobayashi, J. Normand, K. Raghavachari, A. Rendell, J. C. Burant, S. S. Iyengar, J. Tomasi, M. Cossi, N. Rega, J. M. Millam, M. Klene, J. E. Knox, J. B. Cross, V. Bakken, C. Adamo, J. Jaramillo, R. Gomperts, R. E. Stratmann, O. Yazyev, A. J. Austin, R. Cammi, C. Pomelli, J. W. Ochterski, R. L. Martin, K. Morokuma, V. G. Zakrzewski, G. A. Voth, P. Salvador, J. J. Dannenberg, S. Dapprich, A. D. Daniels, Ö. Farkas, J. B. Foresman, J. V. Ortiz, J. Cioslowski and D. J. Fox, *Gaussian 09 Revision B.01*, Gaussian Inc., Wallingford, CT, 2009.

## Influence of halogen substituent on the mesomorphic properties of five-ring banana-shaped molecules with azobenzene wings

M. Alaasar<sup>a,b\*</sup>, M. Prehm<sup>a</sup> and C. Tschierske<sup>a</sup>

<sup>a</sup>Department of Organic Chemistry, Institute of Chemistry, Martin-Luther-University Halle-Wittenberg, Halle, Germany;

<sup>b</sup>Department of Chemistry, Faculty of Science, Cairo University, Giza, Egypt

(Received 4 December 2012; final version received 15 January 2013)

Three new series of bent-shaped molecules with 4-chlororesorcinol, 4-bromoresorcinol or 4-fluororesorcinol as the central unit, and azobenzene with different alkoxy chain length as side arms were synthesised. The mesophase behaviour was investigated by polarising optical microscopy, and differential scanning calorimetry. A representative example has also been characterised by X-ray diffraction (XRD) studies. It is found that almost all of the materials prepared are monotropic liquid crystalline. Depending on the substituent at the central unit and on the chain length nematic phases, B<sub>6</sub> phases, a B<sub>4</sub>-like dark conglomerate phase and a modulated/undulated anticlinic SmC phase were found. As a unique feature, upon reducing the chain length a transition from nematic to B<sub>6</sub>-type smectic phases was observed, which is reverse to usually observed phase sequences. The UV–vis absorption spectroscopy was also performed to study the effect of light-induced *trans*–*cis*-isomerisation on the prepared compounds.

**Keywords:** bent-core liquid crystals; azobenzene; nematic phase; anticlinic SmC phase; B<sub>6</sub> phases; B<sub>4</sub>-like dark conglomerate phase

### 1. Introduction

Liquid crystal research on bent-core compounds has been given much attention over the past decade due to the discovery of outstanding properties of the new mesophases which differ significantly from mesophases of calamitic and disc-like compounds.[1–6] The remarkable behaviour of liquid crystalline (LC) materials possessing a bent molecular shape is the spontaneous formation of polar order even without molecular chirality. This leads to anti-ferroelectric and ferroelectric switching smectic and columnar phases, and to spontaneous achiral symmetry breaking on a mesoscopic scale in tilted polar smectic phases.[7]

Azobenzene compounds are materials of interest for different reasons. Due to their rod-like shape, terminally substituted azobenzenes represent one of the oldest classes of liquid crystals forming nematic and smectic phases. Azobenzene moieties can be inserted into discotic, dimeric, oligomeric and polymeric structures. Azobenzene molecular fragments have two stable isomers under different wavelength stimulation making these molecules attractive for possible molecular switches and nonlinear optics uses.[8–10] The unique *trans*–*cis*-photoisomerisation of the azobenzene molecular fragments is promising for a diverse array of applications, including holographic media,[11,12] optical storage,[13] reversible optical waveguides,[14–16] photoalignment of LC

systems [17] and drug delivery [18]. Pioneering work has been done in the field of azo-containing bent-core mesogens by Prasad et al.[19–23] More examples of azo-functionalised bent-core materials exhibiting interesting physical properties such as nonlinear optics, guest–host effects in liquid crystals with azo-dyes have been reported.[24–27]

Resorcinol is the most widely used central unit for bent-shaped compounds which exhibit B-type phases as well as smectic or nematic phases.[28,29] There are several studies on five-ring bent-core mesogens in which the central phenyl ring was substituted at different positions by polar groups [30–32]; especially substituents in the 4-position of the bent unit play an important role. Thus, in the present study to investigate the effect of a halogen substituent in the 4-position on five-ring bent-core LC consisting of azobenzene groups in the side arms and terminal alkoxy chains, we have synthesised three novel series of bent-shaped molecules (see Figure 1) derived from 4-chlororesorcinol (*An*), 4-bromoresorcinol (*Bn*) or 4-fluororesorcinol (*Cn*) as the central unit.

### 2. Experimental

#### 2.1 General

Thin layer chromatography (TLC) was performed on aluminium sheet precoated with silica gel. Analytical quality chemicals were obtained from commercial

\*Corresponding author. Email: M\_Alaasar@yahoo.com



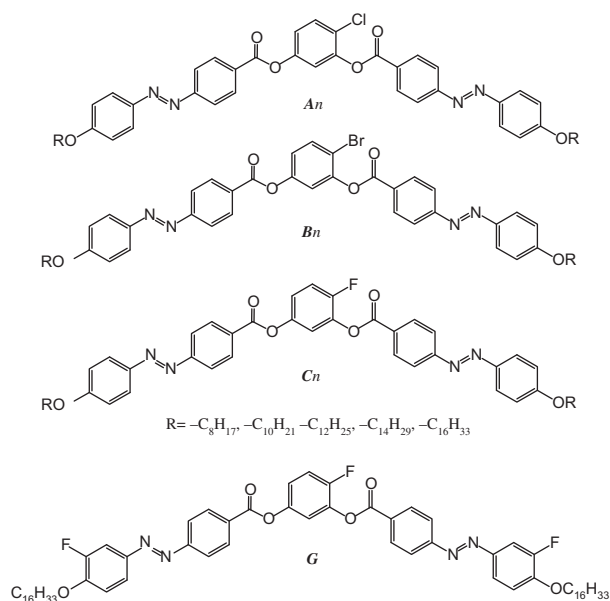


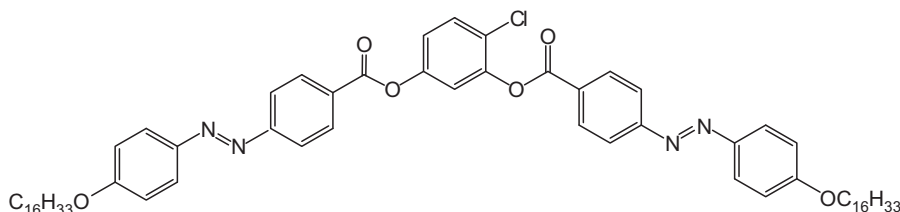
Figure 1. Structures of the synthesised bent-core compounds.

sources and used as obtained. The solvents were dried using the standard methods when required. The purity and the chemical structures of all compounds synthesised were confirmed by the spectral data. The structure characterisation of the synthesised bent-core compounds is based on <sup>1</sup>H-NMR (Varian Unity 500 and Varian Unity 400 spectrometers, in CDCl<sub>3</sub> solutions, with tetramethylsilane as internal standard). Microanalyses were performed using a Leco CHNS-932 elemental analyser.

The mesophase behaviour and transition temperatures of the prepared bent-core molecules were measured using a Mettler FP-82 HT hot stage and control unit in conjunction with a Nikon Optiphot-2 polarising microscope. The associated enthalpies were obtained from differential scanning calorimetry (DSC)-thermograms which were recorded on a Perkin-Elmer DSC-7, heating and cooling rate: 10 K min<sup>-1</sup>.

The UV spectra were recorded using a HP/Agilent, 8453 UV-vis spectrophotometer.

#### 4-Chloro-1,3-phenylene bis-[4-(4-hexadecyloxyphenylazo)benzoate], *A16*:



The X-ray diffraction (XRD) were recorded with a 2D detector (HI-STAR, Siemens). Ni filtered and pin hole collimated CuK $\alpha$  radiation was used. The exposure time was 60 min and the sample to detector distance was 8.8 cm. Alignment was achieved upon slow cooling (rate: 1 K min<sup>-1</sup>–0.1 K min<sup>-1</sup>) of a small droplet of the sample on a glass plate and takes place at the sample–glass or at the sample–air interface, with domains fibre-like disordered around an axis perpendicular to the interface. The aligned samples were held on a temperature-controlled heating stage.

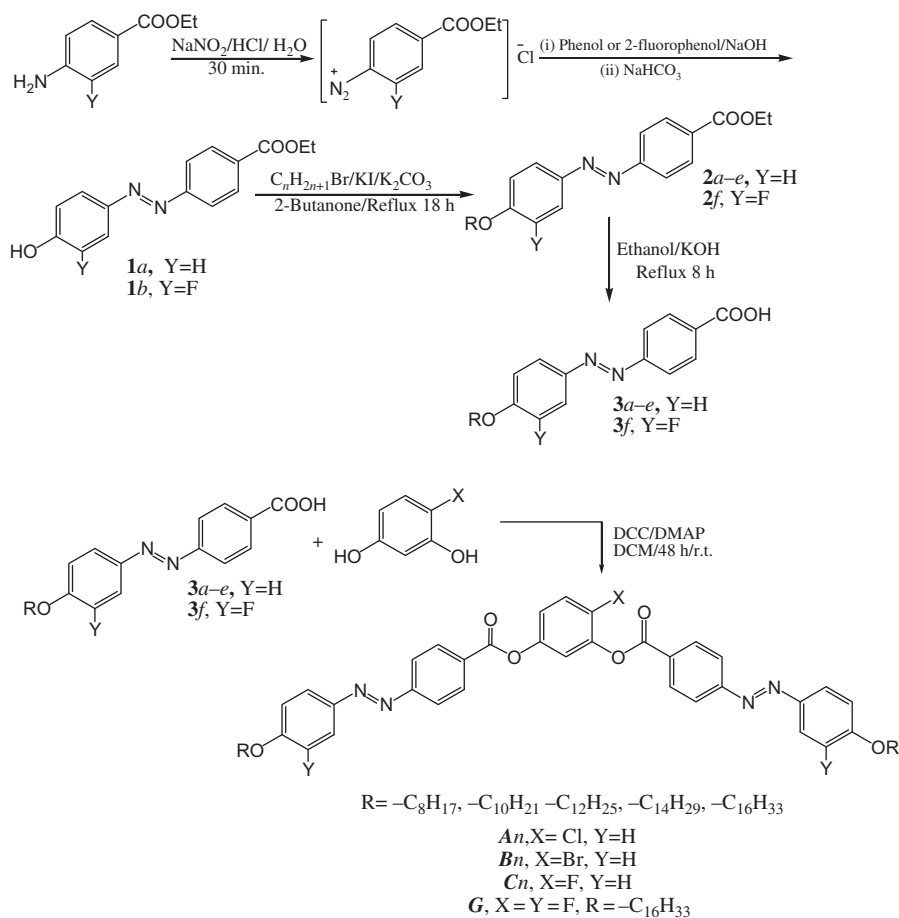
## 2.2 Synthesis details

The synthesis of the bent-core compounds under investigation is shown in Scheme 1. 4-(*n*-Alkyloxyphenylazo)benzoic acids homologues **3a–e** are synthesised according to the method described before [33] in three steps as shown in Scheme 1. Initially, the diazonium salt was prepared with sodium nitrite in the presence of three equivalents of aqueous hydrochloric acid, which was coupled with phenol or 2-fluorophenol to yield ethyl 4-(4-hydroxyphenylazo)benzoate (**1a**) or ethyl 4-(3-fluoro-4-hydroxyphenylazo)benzoate (**1b**), respectively. Compound **1a** or **1b** was then alkylated with 1-bromoalkane in 2-butanone as solvent in the presence of potassium carbonate to give ester compounds **2a–e** and **2f**, respectively. Finally, the ester compounds were hydrolysed under basic conditions to yield the acids **3a–e** and **3f**, respectively.

The final bent-core compounds were prepared as follows:

The mixture of 1.2 mmol of 4-substituted resorcinol, 2.4 mmol of the acid **3a–e** or **3f**, 2.4 mmol of dicyclohexylcarbodiimide and dimethylaminopyridine as catalyst in 40 ml of dry dichloromethane was stirred at room temperature under an argon atmosphere for 48 h. The precipitate was filtered, the solvent was evaporated. The crude products were purified by column chromatography on silica gel using dichloromethane and recrystallised from ethanol/CHCl<sub>3</sub> mixture.

The analytical data obtained for one compound from each series as a representative example and for compound **G** are as follows:



Scheme 1.

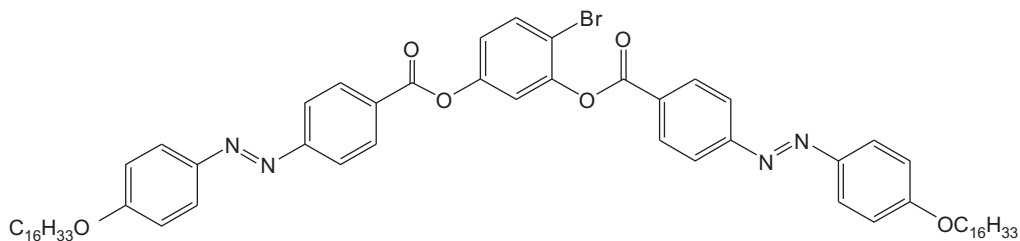
$^1\text{H-NMR}$  (400 MHz,  $\text{CDCl}_3$ )  $\delta$  8.36 (d,  $J = 8.7$  Hz, 2H, Ar-H), 8.29 (d,  $J = 8.7$  Hz, 2H, Ar-H), 8.00–7.91 (m, 8H, Ar-H), 7.55 (d,  $J = 8.8$  Hz, 1H, Ar-H), 7.33 (d,  $J = 2.6$  Hz, 1H, Ar-H), 7.19 (dd,  $J = 8.7, 2.6$  Hz, 1H, Ar-H), 7.00 (d,  $J = 8.2$  Hz, 4H, Ar-H), 4.04 (t,  $J = 6.6$  Hz, 4H,  $-\text{OCH}_2\text{CH}_2$ ), 1.86–1.75 (m, 4H,  $-\text{OCH}_2\text{CH}_2$ ), 1.52–1.13 (m, 52H,  $\text{CH}_2$ ), 0.86 (t,  $J = 6.8$  Hz, 6H,  $\text{CH}_3$ ).

Elemental Analysis: Calc. for  $\text{C}_{64}\text{H}_{85}\text{ClN}_4\text{O}_6$  C, 73.78; H, 8.22; Cl, 3.40; N, 5.38. Found C, 73.77; H, 8.25; Cl, 3.39; N, 5.40%.

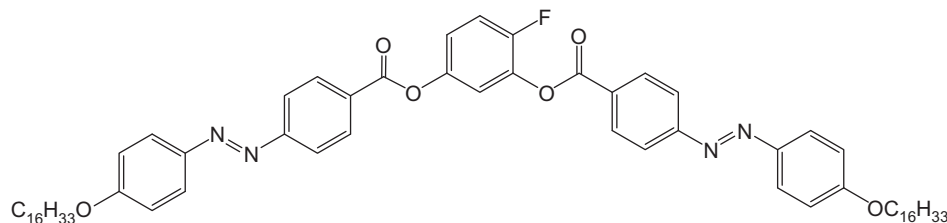
$^1\text{H-NMR}$  (400 MHz,  $\text{CDCl}_3$ )  $\delta$  8.38 (d,  $J = 8.7$  Hz, 2H, Ar-H), 8.32 (d,  $J = 8.7$  Hz, 2H, Ar-H), 8.02–7.92 (m, 8H, Ar-H), 7.73 (d,  $J = 8.7$  Hz, 1H, Ar-H), 7.35 (d,  $J = 2.6$  Hz, 1H, Ar-H), 7.15 (dd,  $J = 8.7, 2.7$  Hz, 1H, Ar-H), 7.01 (d,  $J = 8.2$  Hz, 4H, Ar-H), 4.06 (t,  $J = 6.5$  Hz, 4H,  $-\text{OCH}_2\text{CH}_2$ ), 1.88–1.78 (m, 4H,  $-\text{OCH}_2\text{CH}_2$ ), 1.56–1.20 (m, 52H,  $\text{CH}_2$ ), 0.88 (t,  $J = 6.8$  Hz, 6H,  $\text{CH}_3$ ).

Elemental Analysis: Calc. for  $\text{C}_{64}\text{H}_{85}\text{BrN}_4\text{O}_6$  C, 70.76; H, 7.36; N, 5.16. Found C, 70.59; H, 7.72; N, 5.08%.

**4-Bromo-1,3-phenylene bis-[4-(4-hexadecyloxyphenylazo)benzoate], B16:**



**4-Fluoro-1,3-phenylene bis-[4-(4-hexadecyloxyphenylazo)benzoate], *C16*:**

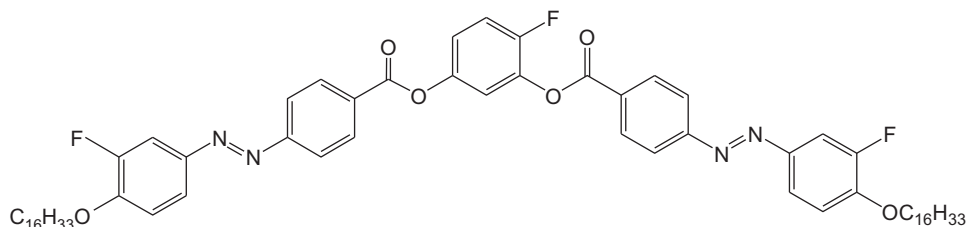


$^1\text{H-NMR}$  (400 MHz,  $\text{CDCl}_3$ )  $\delta$  8.38–8.28 (m, 4H, Ar-H), 8.02–7.93 (m, 8H, Ar-H), 7.34–7.29 (m, 2H, Ar-H), 7.22–7.15 (m, 1H, Ar-H), 7.02 (d,  $J = 8.4$  Hz, 4H, Ar-H), 4.06 (t,  $J = 6.5$  Hz, 4H,  $-\text{OCH}_2\text{CH}_2$ ), 1.89–1.77 (m, 4H,  $-\text{OCH}_2\text{CH}_2$ ), 1.56–1.20 (m, 52H,  $\text{CH}_2$ ), 0.88 (t,  $J = 6.8$  Hz, 6H,  $\text{CH}_3$ ).

Elemental Analysis: Calc. for  $\text{C}_{64}\text{H}_{85}\text{FN}_4\text{O}_6$  C, 74.97; H, 8.36; N, 5.46. Found C, 74.46; H, 8.27; N, 5.45%.

that it has been found from the literature [19] that 1,3-phenylene bis-[4-(4-decyloxyphenylazo)benzoate], compound *D10*, see Figure 2 is nonmesomorphic. On a very recent work,[34] it was reported by the same author that compounds *D* with chain length above  $-\text{C}_{12}\text{H}_{25}$  (*D14*, *D16*) exhibit monotropic and compound *D18* a small range (10 K) of an enantiotropic  $\text{B}_1$  phase. In the same work,[34] compounds *E* and *F* were also prepared to test the effect of introducing

**4-Fluoro-1,3-phenylene bis-[4-(3-fluoro-4-hexadecyloxyphenylazo)benzoate], *G*:**



$^1\text{H-NMR}$  (400 MHz,  $\text{CDCl}_3$ )  $\delta$  8.38–8.26 (m, 4H, Ar-H), 8.05–7.95 (m, 4H, Ar-H), 7.80 (d,  $J = 8.7$  Hz, 2H, Ar-H), 7.72 (d,  $J = 11.9$  Hz, 2H, Ar-H), 7.36–7.29 (m, 2H, Ar-H), 7.20–7.14 (m, 1H, Ar-H), 7.11–7.08 (m, 2H, Ar-H), 4.12 (t,  $J = 6.6$  Hz, 4H,  $-\text{OCH}_2\text{CH}_2$ ), 1.93–1.78 (m, 4H,  $-\text{OCH}_2\text{CH}_2$ ), 1.54–1.15 (m, 52H,  $\text{CH}_2$ ), 0.86 (t,  $J = 6.8$  Hz, 6H,  $\text{CH}_3$ ).

Elemental Analysis: Calc. for  $\text{C}_{64}\text{H}_{83}\text{F}_3\text{N}_4\text{O}_6$  C, 72.42; H, 7.88; N, 5.28. Found C, 72.51; H, 8.84; N, 5.32%.

different substituent on the central ring in compound *Dn*. It was found that introducing  $\text{CH}_3$  or  $\text{NO}_2$  groups in position-2 on the central ring leads to crystalline compounds and no liquid crystals phases were observed.

Thus, we wanted to investigate the effect of introducing a halogen substituent in the central core ring in the structure of that azo-bent-core compound in the 4-position. So, we designed and synthesised the molecules of series (*An-Cn*), anticipating them to be liquid crystalline.

We have synthesised three new series of bent-core azo-compounds shown in Figure 1 belonging to three different homologous series *An*, *Bn* and *Cn*. The substitution at the central core of the molecule was kept fixed in each series and the chain length was varied systematically. Most of the materials prepared

### 3. Results and discussion

#### 3.1 Mesomorphic properties

Before discussing the mesomorphic properties of the prepared compounds we would like to mention

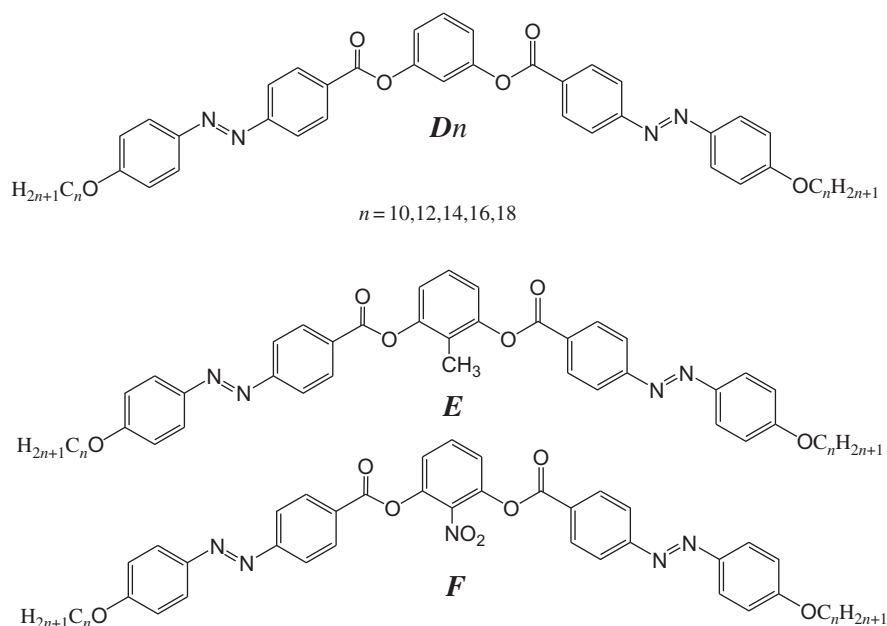


Figure 2. Structures of previously investigated compounds.

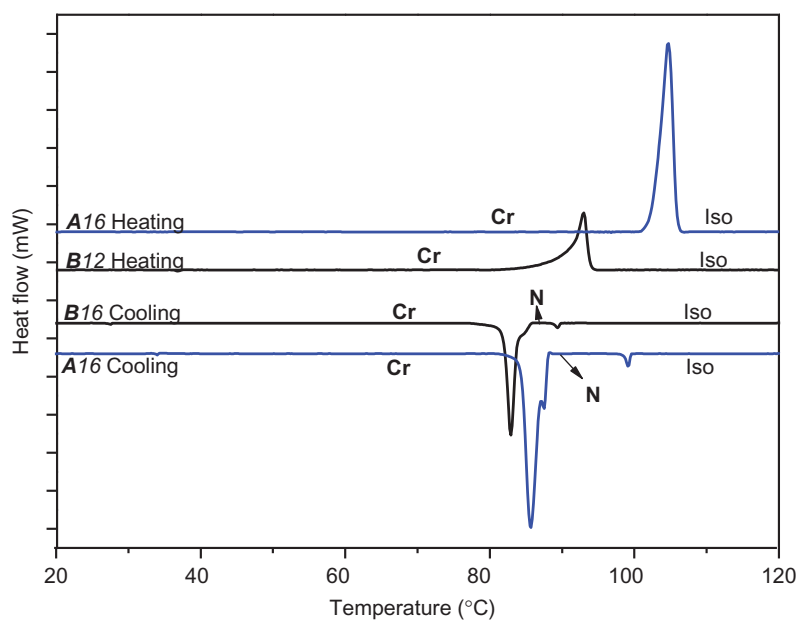
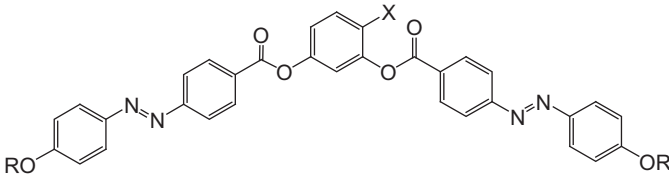
Figure 3. (colour online) DSC thermograms obtained for compounds *A16* and *B12* as examples for the *An* and *Bn* series, respectively; heating and cooling rates were  $10 \text{ K min}^{-1}$ .

exhibit monotropic liquid crystalline phases. The thermal behaviour of all these compounds was studied by polarising optical microscopy (POM) and DSC. The DSC thermograms obtained for compounds *A16* and *B12* as examples for *An* and *Bn* series, respectively, are shown in Figure 3. The transition temperatures ( $^{\circ}\text{C}$ ) and the associated enthalpies ( $\text{kJ mol}^{-1}$ ) obtained from DSC thermograms are given in Table 1. All compounds are thermally stable as confirmed by the

reproducibility of thermograms on several heating and cooling cycles. The results that we obtained for each series will be discussed below, in detail.

### 3.1.1 Series An

The compounds of series *An*, which have chloro group at the central ring of the bent-core structure, exhibit two types of monotropic mesophases. On cooling of

Table 1. Phase transition temperatures, mesophase types, and transition enthalpies of compounds *An-Cn*.<sup>a</sup>


Compound	X	R	Heating $T/^\circ\text{C}$ [ $\Delta H/\text{kJ mol}^{-1}$ ]	Cooling $T/^\circ\text{C}$ [ $\Delta H/\text{kJ mol}^{-1}$ ]
<i>A8</i>	Cl	$-\text{C}_8\text{H}_{17}$	<b>Cr</b> 115 [61.4] <b>Iso</b>	<b>Iso</b> 105 [10.4] <b>B<sub>6</sub></b> 84 [17.3] <b>Cr</b>
<i>A10</i>	Cl	$-\text{C}_{10}\text{H}_{21}$	<b>Cr</b> 105 [60.7] <b>Iso</b>	<b>Iso</b> 96 [0.8] <b>N</b> 80 <sup>b</sup> <b>B<sub>6</sub></b> 79 [36.5] <b>Cr</b>
<i>A12</i>	Cl	$-\text{C}_{12}\text{H}_{25}$	<b>Cr</b> 102 [49.8] <b>Iso</b>	<b>Iso</b> 94 [0.8] <b>N</b> 78 [38.2] <b>Cr</b>
<i>A14</i>	Cl	$-\text{C}_{14}\text{H}_{29}$	<b>Cr</b> 101 [37.3] <b>Iso</b>	<b>Iso</b> 90 [0.3] <b>N</b> 81 [30.8] <b>Cr</b>
<i>A16</i>	Cl	$-\text{C}_{16}\text{H}_{33}$	<b>Cr</b> 105 [48.2] <b>Iso</b>	<b>Iso</b> 99 [1.1] <b>N</b> 86 [45.4] <b>Cr</b>
<i>B8</i>	Br	$-\text{C}_8\text{H}_{17}$	<b>Cr</b> 113 [55.2] <b>Iso</b>	<b>Iso</b> 97 [9.7] <b>B<sub>6</sub></b> 73 [26.4] <b>Cr</b>
<i>B10</i>	Br	$-\text{C}_{10}\text{H}_{21}$	<b>Cr</b> 95 [31.6] <b>Iso</b>	<b>Iso</b> 88 [0.2] <b>N</b> 79 [26.5] <b>DC</b> 78 <sup>c</sup> <b>Cr</b>
			<b>DC</b> 89 <sup>d</sup> <b>Iso</b>	
<i>B12</i>	Br	$-\text{C}_{12}\text{H}_{25}$	<b>Cr</b> 93 [35.7] <b>Iso</b>	<b>Iso</b> 89 [0.7] <b>N</b> 83 [35.6] <b>Cr</b>
<i>B14</i>	Br	$-\text{C}_{14}\text{H}_{29}$	<b>Cr</b> 95 [30.3] <b>Iso</b>	<b>Iso</b> 94 [0.4] <b>N</b> 86 [34.2] <b>Cr</b>
<i>B16</i>	Br	$-\text{C}_{16}\text{H}_{33}$	<b>Cr</b> 98 [40.1] <b>Iso</b>	<b>Iso</b> 95 <sup>b</sup> <b>N</b> 90 [40.4] <b>Cr</b>
<i>C8</i>	F	$-\text{C}_8\text{H}_{17}$	<b>Cr</b> 139 [50.2] <b>Iso</b>	<b>Iso</b> 128 [47.8] <b>Cr</b>
<i>C10</i>	F	$-\text{C}_{10}\text{H}_{21}$	<b>Cr</b> 126 [58.0] <b>Iso</b>	<b>Iso</b> 116 [45.9] <b>Cr</b>
<i>C12</i>	F	$-\text{C}_{12}\text{H}_{25}$	<b>Cr</b> 120 [62.9] <b>Iso</b>	<b>Iso</b> 105 [39.7] <b>Cr</b>
<i>C14</i>	F	$-\text{C}_{14}\text{H}_{29}$	<b>Cr</b> 121 [68.9] <b>Iso</b>	<b>Iso</b> 101 [45.3] <b>Cr</b>
<i>C16</i>	F	$-\text{C}_{16}\text{H}_{33}$	<b>Cr</b> 122 [54.3] <b>Iso</b>	<b>Iso</b> 109 [13.7] <b>USmC<sub>a</sub></b> 99 [40.4] <b>Cr</b>

Notes: Abbreviations: Cr, crystalline solid; N, nematic phase; USmC<sub>a</sub>, nonswitching undulated smectic C phase with anticlinic tilt correlation; Iso, isotropic liquid.

<sup>a</sup>Transition temperatures and enthalpy values were taken from the second DSC heating scans (10 K min<sup>-1</sup>); <sup>b</sup>Enthalpy could not be measured due to the onset of crystallisation; <sup>c</sup>Enthalpy could not be measured due to slow crystallisation; <sup>d</sup>Observed during second heating.

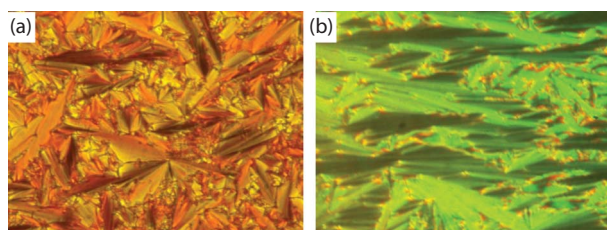


Figure 4. (colour online) Optical micrograph observed in a homeotropic cell for the **B<sub>6</sub>** Phase: (a) *A8* at  $T = 100^\circ\text{C}$  and (b) *A10* at  $T = 80^\circ\text{C}$ .

the lowest homologue *A8* from the isotropic phase formation a focal-conic fan-shaped texture is observed (Figure 4a). The extinction crosses are parallel to polariser and analyser, indicating an orthogonal or anticlinic tilted smectic phase. No homeotropic alignment with pseudoisotropic texture or schlieren texture could be achieved by shearing the sample, a typical behaviour for **B<sub>6</sub>** phases. In electrooptical experiments using a triangular wave voltage no current peak could be observed in this mesophase up to a voltage of 200 V<sub>pp</sub> in a 6 μm ITO cell. These observations, together with the relatively high transition enthalpy value of  $\Delta H = 10.4 \text{ kJ mol}^{-1}$  for the Iso–LC

transition indicate the presence of a **B<sub>6</sub>** phase.[20,35] However, it was not possible to further confirm the phase structure by XRD measurements due to the crystallisation occurring during X-ray exposure time.

With increasing chain length formation of a monotropic nematic phase is observed. On cooling *A10* from the isotropic liquid a nematic phase is formed first which changes to the fan texture of the **B<sub>6</sub>** phase at  $T = 80^\circ\text{C}$  (Figure 4b) then crystallisation occurs rapidly at  $T = 79^\circ\text{C}$ . In the DSC traces this phase transition cannot be separated from the crystallisation peak and therefore no transition enthalpy could be measured for this transition. With further chain elongation the **B<sub>6</sub>** completely disappears for  $n = 12$  to  $n = 16$  and only nematic phases were observed. The clearing temperatures in this series (*An*) decrease with chain elongation from  $n = 8$  to  $n = 14$  then increase again with further elongation ( $n = 16$ ).

### 3.1.2 Series **Bn**

In series **Bn**, the chloro group of series *An* was replaced by a bromo-group. Similar to the *An* series the clearing temperature at first decreases and then increases with growing chain length. Like *A8* the lowest homologue

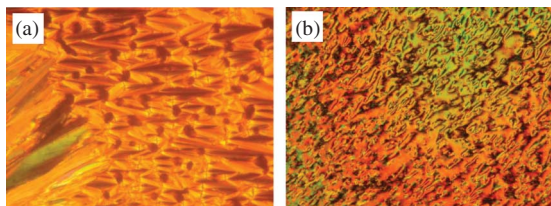


Figure 5. Optical micrographs observed: (a) for **B8** in the  $B_6$  phase at  $T = 85^\circ\text{C}$  and (b) for **B12** in the nematic phase at  $T = 85^\circ\text{C}$ .

in this series, **B8**, shows only the  $B_6$  phase on cooling from the isotropic liquid (Figure 5a). Nematic phases appear by chain elongation for the next synthesised homologues **Bn** with  $n = 10$ – $16$  (see Figure 5b).

It is most likely that the nematic phases in both series **An** and **Bn** represent cybotactic nematic phases as typical for bent-core mesogens.[36] However, in no case it was possible to carry out XRD measurements to investigate the type of the nematic phase ( $N_{\text{cybA}}$  or  $N_{\text{cybC}}$ ) due to the crystallisation occurring during X-ray exposure time for all of the homologues.

Another remarkable observation is the formation of another mesophase on cooling the nematic phase of compound **B10** (see Figure 6a,b) below  $T = 78^\circ\text{C}$ . This phase is optically isotropic and chiral domains with opposite handedness, as indicated by slightly decrossing the polarisers in either one or the other direction can be observed, see Figure 6c,d. This dark conglomerate (DC) phase has high viscosity and the formation of this phase is associated with a high transition enthalpy ( $26.5 \text{ kJ mol}^{-1}$ ). Therefore, a  $B_4$ -like structure with crystallised aromatic cores is likely for this DC phase.[37] However, in contrast to typical

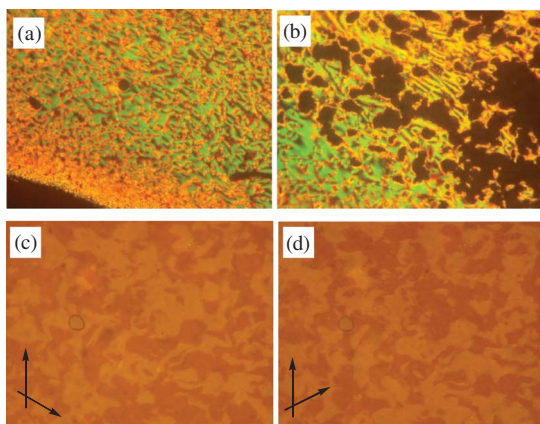


Figure 6. Optical micrograph observed in a homeotropic cell for **B10**: (a) the nematic phase at  $T = 87^\circ\text{C}$ ; (b) the texture of  $B_4$  under crossed polarisers; (c)  $B_4$  phase after rotating one polariser by  $10^\circ$  from the crossed position in clock-wise direction; and (d) in anticlockwise direction.

$B_4$  phases no bluish colour could be observed and the sample crystallises slowly with formation of a highly birefringent crystalline phase; XRD investigations were not possible for this reason. On heating, the nematic phase is not formed again and only the direct transition to the isotropic liquid is observed at  $T = 89^\circ\text{C}$ , approximately the same temperature at which the nematic phase is formed on cooling ( $T = 88^\circ\text{C}$ ). The nematic phase of compound **B10** is only observed on cooling, and hence, represents a monotropic phase with respect to the DC phase. For the following compounds **Bn** with longer alkyl chains ( $n = 12$ – $16$ ) the formation of a DC phase was not observed.

### 3.1.3 Series Cn

In the third series **Cn**, a fluorine atom is introduced in the position 4 of the central ring of the bent-core structure (Table 1). All compounds of this series are nonliquid crystalline except the highest homologue, **C16**, (with chain length  $-\text{OC}_{16}\text{H}_{33}$ ) which shows a monotropic LC phase on cooling from the isotropic liquid. Figure 7 shows the polarising optical micrographs for **C16**. On cooling from the isotropic liquid a transition to a spherulitic texture occurs at  $T = 109^\circ\text{C}$  (Figure 7a, b) and on further cooling at  $T = 99^\circ\text{C}$  a highly birefringent crystalline phase occurs (Figure 7c), which is replaced by a low birefringent second crystalline phase at  $97^\circ\text{C}$  (Figure 7d).

To investigate the nature of the mesophase, we conducted preliminary XRD measurements on compound **C16**. The XRD pattern of a partially aligned sample of **C16** (Figure 8) in the temperature range

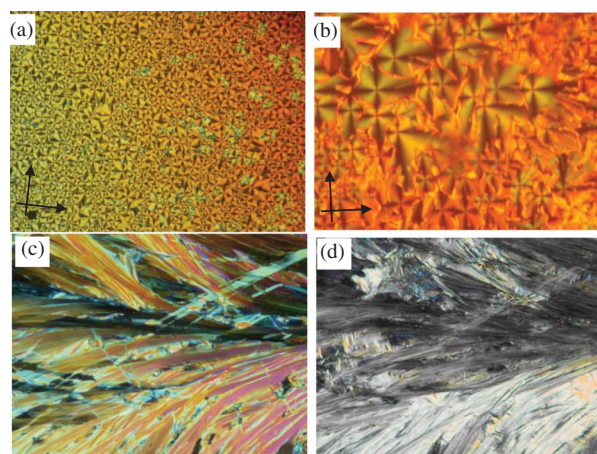


Figure 7. Optical micrographs observed between crossed polarisers for **C16**, (a, b)  $\text{USmC}_a$  phase at  $T = 105^\circ\text{C}$ , (c)  $\text{Cr}_1$  at  $T = 100^\circ\text{C}$ , and (d)  $\text{Cr}_2$  at  $T = 95^\circ\text{C}$  (arrows indicate orientation of polariser and analyser which is identical in (a–d)).

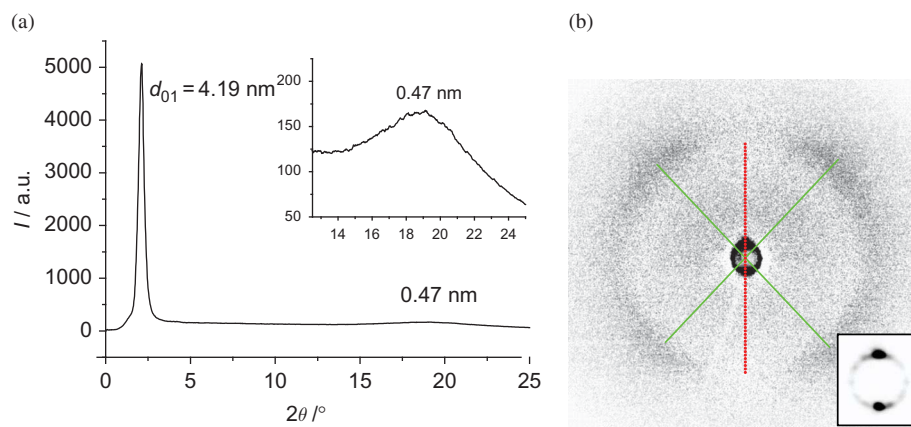


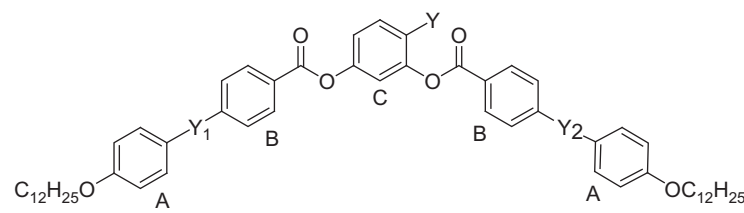
Figure 8. (colour online) XRD data of *C16* ( $R = C_{16}H_{33}$ ) at  $108^\circ\text{C}$ : (a)  $2\theta$  scan, the inset shows the diffuse scattering in the wide angle region; (b) diffraction pattern of the SmC phase after subtraction of the scattering in the isotropic phase at  $T = 130^\circ\text{C}$ , the lines pointing to the positions of the maxima, the inset shows the magnified scattering distribution in the small angle region.

of the LC phase at  $T = 108^\circ\text{C}$  shows four diffuse scatterings in the wide angle region with maxima at  $0.47\text{ nm}$ , confirming the liquid crystalline state of the phase. A sharp reflection in the small angle region with a maximum at  $d = 4.2\text{ nm}$  corresponds to  $0.68 L_{\text{mol}}$  ( $L_{\text{mol}} = 6.2\text{ nm}$  as determined for a V-shaped conformation with  $120^\circ$  bending angle and *all-trans* conformation of the alkyl chains). The maxima of the small angle reflections and the wide angle scattering are not perpendicular to each other, indicating a tilted arrangement of the molecules in that phase. Based on the positions of the maxima of the diffuse scattering in the wide angle region the tilt angle can be calculated to  $\tau = 44^\circ$ . This value is in good agreement with the value  $\tau = 47^\circ$  determined according to  $\cos \tau = d/L_{\text{mol}}$ . The texture of this mesophase is characterised by spherulitic domains which exclude a simple SmC phase and are more indicative of a columnar (a modulated smectic) or an undulated (wavy deformed) smectic phase. Remarkably, the dark extinction crosses are parallel to polariser and analyser (Figure 7a, b) indicating an anticlinic tilt, which is unusual for modulated smectic phases formed by bent-core mesogens.[38] This anticlinic tilt is in line with the equal intensity distribution between the diffuse wide angle scatterings at the right and the left of the 2D pattern. However, the relatively high birefringence is unusual for a smectic LC phase with anticlinic tilt, especially if the high tilt angle around  $45^\circ$  is considered. There are only two spot-like reflections in the small angle region of the XRD pattern of an aligned sample and the position of these small angle scatterings is on the meridian (Figure 8b) which only excludes a hexagonal lattice, but any other mesophase with 2D lattice cannot be excluded. However, as only one reflection is observed

in the small angle region no further assignment of the mesophase structure is possible by XRD. Based on the texture and the available XRD data this mesophase could represent either a modulated smectic phase with layers broken into ribbons or an undulated smectic, i.e. a wavy deformed SmC phase. Probably the modulation/undulation wave length is relatively long and/or its correlation length is relatively short so that the expected additional reflections cannot be observed. The presence of anticlinic tilt is easier explained by assuming an undulated smectic phase. The undulation can probably be supported by splay of polarisation (similar to the  $B_7$  phases).[39] In electrooptical experiments using a triangular wave voltage no current peak could be observed in this mesophase up to a voltage of  $200\text{ V}_{\text{pp}}$  in a  $6\text{ }\mu\text{m}$  ITO cell. Based on these experimental data this phase is tentatively assigned as  $\text{USmC}_a$ . Aiming to stabilise the mesophase observed in *C16* and to carry out more detailed investigations we synthesised compound **G** with an additional fluorosubstituent at each outer rings of the bent-core unit. However, **G** was found to be nonmesomorphic having a relatively high melting point =  $128^\circ\text{C}$  which cannot be significantly supercooled (only about  $4\text{ K}$ ).

### 3.2 Discussion and comparison with related compounds

It is interesting to note that a soft crystalline undulated smectic phase ( $X_1$ ) was observed for related long chain imines with 4-bromoresorcinol core phase of compounds  $\mathbf{Kn}$  ( $n > 8$ ).[35,40] It appears possible that there might be some structural similarity between the liquid crystalline  $\text{USmC}_a$  phase reported herein for the fluorinated compound *C16* and the soft crystalline  $X_1$  phase of the bromine substituted compounds  $\mathbf{Kn}$ .

Table 2. Comparison of 4-halogen substituted bent-shaped mesogens with different linking groups  $Y_1$  and  $Y_2$ .


Comp.	$Y_1$	$Y_2$	Y	$T/^\circ\text{C}$	References
<i>A12</i>	-N=N-	-N=N-	Cl	Cr 102 (N 94) Iso	
<i>H12</i>	-N=N-	-CH=N-	Cl	Cr 75 SmCP <sub>A</sub> 127 Iso	[5]
<i>I12</i>	-OOC-	-COO-	Cl	Cr 110 SmCP <sub>A</sub> 147 Iso	[5]
<i>J12</i>	-COO-	-OOC-	Cl	Cr 98 (DC 80) N 95 Iso	[5,41]
<i>B12</i>	-N=N-	-N=N-	Br	Cr 93 (N 89) Iso	
<i>K12</i>	-N=N-	-CH=N-	Br	X <sub>1</sub> 113 SmCP <sub>A</sub> 134 Iso	[35,40]
<i>L12</i>	-COO-	-OOC-	Br	Cr 92 (DC 78 N 86.5) Iso	[41]

Note: Abbreviations: DC, dark conglomerate phase (optically isotropic mesophase composed of a conglomerate of chiral domains with opposite handedness); X<sub>1</sub>, soft solid undulated smectic phase.[40]

In Table 2 compounds *A12* and *B12* are compared with related bent-core mesogens with the same chain length and having distinct types of linking groups  $Y_1$  and  $Y_2$ .

If the -N=N- linkages in the 4-chlorosubstituted compounds *An* ( $n = 8-16$ ) were replaced by imine groups (*Hn*) then SmCP<sub>A</sub> phases were observed. Compounds like *I12* with carboxyl groups (terephthalates) also show enantiotropic SmCP<sub>A</sub> phases, whereas reversal of the direction of the ester groups (*J12*) leads to monotropic nematic phases with much lower transition temperatures. There are only few 4-bromosubstituted compounds and to the best of our knowledge no 4-fluorosubstituted compounds with this structural motif have been reported. For the bromo-substituted imines *Kn* with  $n > 8$  SmCP<sub>A</sub> phases were reported beside an undulated soft crystalline phase assigned as X<sub>1</sub>. [35,40] Replacing the -N=N- linkage in the bromo-substituted compounds of series *Bn* by an ester group [41] results in compounds *Ln* exhibiting monotropic nematic phases and in some cases an additional optically isotropic DC phase. The clearing temperatures of the esters *Jn* and *Ln* are in the same range as those of the azo-compounds *An* and *Bn*. This shows that, in this structural context the -N=N- linkage behaves similar to the -COO- group if ring B is derived from 4-hydroxybenzoic acid ( $Y_1 = -\text{COO}-$ ,  $Y_2 = -\text{OOC}-$ ), whereas the isomeric compounds with  $Y_1 = -\text{OOC}-$  and  $Y_2 = -\text{COO}-$ , for which rings B represent a terephthalate unit, show much higher mesophase stabilities and preferably form smectic phases instead of nematic. Schiff base compounds (e.g. *H12*, *K12*) behave similar to the terephthalates (e.g.

*I12*), though having slightly lower transition temperatures. Compared to the Schiff bases, the azobenzenes *An* and *Bn* have lower mesophase stabilities and form predominantly nematic phases. Therefore, it appears that the dipole moment of the double bond incorporated in the linking groups  $Y_1$  and  $Y_2$  has a major effect. For the terephthalates (*In*) and the imines (*Hn*, *Kn*) the C=Y bonds are polar and reduce the electron density of ring B, whereas the symmetric -N=N- group in compounds *An* and *Bn* has no internal dipole moment. Similar to the hydroxybenzoates *Jn* and *Ln*, in which ring B is separated from the polar C=O bond by a divalent oxygen atom, the azo-group leads to a relatively high electron density in ring B. As it is known that  $\pi$ -stacking is stronger for electron deficient aromatics [42] this could explain the observed difference in mesophase stability and tendency to form smectic phases.

For the phenylbenzoates *Jn* with  $n = 9-12$  and also for the related bromo-compound *Ln* with  $n = 12, 14$  the phase sequence DC-N-Iso, was reported, the same as reported here for *B10*. However, for compounds *Jn* and *Ln* the DC phases seem to be of the fluid type without crystalline aromatics, as indicated by lower transition enthalpies, only around  $\Delta H = 5-14 \text{ kJ mol}^{-1}$ , and the diffuse wide angle scattering in XRD.[41] A DC phase was also observed for the bromo-substituted Schiff base compounds *Kn* with  $n = 6-8$ . Similar to the DC phase observed for the azobenzene *B10* the transition enthalpy is high ( $\Delta H_{\text{DC-Iso}} = 23-27 \text{ kJ mol}^{-1}$ ). [35] Hence, we conclude that the structure of the DC phase of *B10* should be the same or very similar to the B<sub>4</sub> phase proposed for



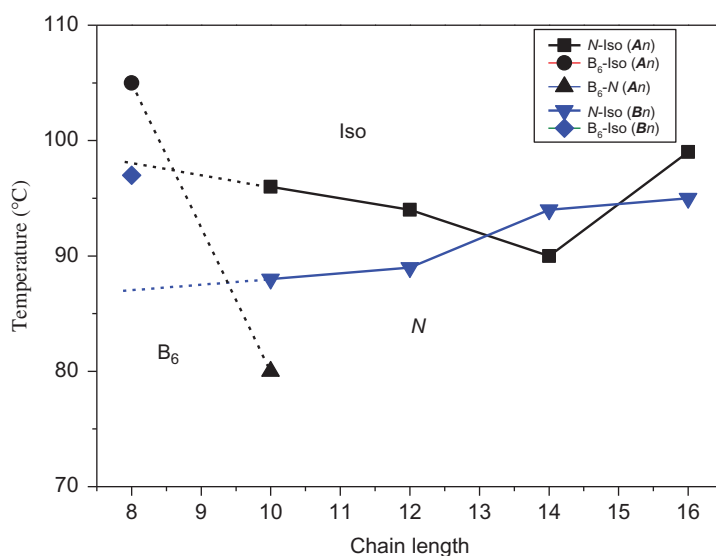


Figure 9. (colour online) Plot of the phase transition temperatures of series *An* (black colour) and *Bn* (blue colour) as a function of the number of carbons in the alkoxy chain.

compounds *Kn* ( $n = 6-8$ ). It appears that the presence of the 4-bromine group at the resorcinol unit is important for the appearance of this phase, as it is not observed for any of the chloro-substituted compounds *Bn*. However, compared with the Schiff base compounds *Kn* the azobenzenes *An* and *Bn* have a higher tendency to form nematic phases, as actually no nematic phases was reported for the whole series of compounds *Kn*.

An interesting point is also the fact that exclusively nematic phases were observed in both series *An* and *Bn* for all long chain homologues, whereas the shorter compounds ( $n = 8$ ) do not form a nematic phase, but a smectic phase ( $B_6$  phase) instead. Moreover, the clearing temperature of this  $B_6$  phase is higher than it can be expected from the extrapolation of the curve of the N-Iso transition temperatures depending on chain length (see Figure 9). This kind of behaviour is unknown for rod-like molecules and contrary to the well established general rules and, to the best of our

knowledge, has also not yet been observed in this way for a homologous series of bent-core mesogens.[43]<sup>1</sup> It must be considered that the  $B_6$  phase can be considered as a modulated smectic phase (ribbon phase of the  $B_1$  type) with only short range correlation of the antipolar arranged polar ribbons along the layers, so that this phase appears like an intercalated smectic phase ( $d = \frac{1}{2} L_{\text{mol}}$ ).[44] Hence, it could be assumed that the transition from the nematic phase, composed of cybotactic clusters, to the  $B_6$  phase, is caused by the fact that shorter alkyl chains allow a denser packing of the bent cores. This leads to a polar packing of these cores, but as the chains are only short, the resulting polar layers are unstable (the segregation between aromatic cores and alkyl chains is not strong enough to form a layer structure). The polar order is cancelled by the transition to the  $B_6$  structure as this allows the antiparallel packing of the polar directions in adjacent ribbons (see Figure 10).

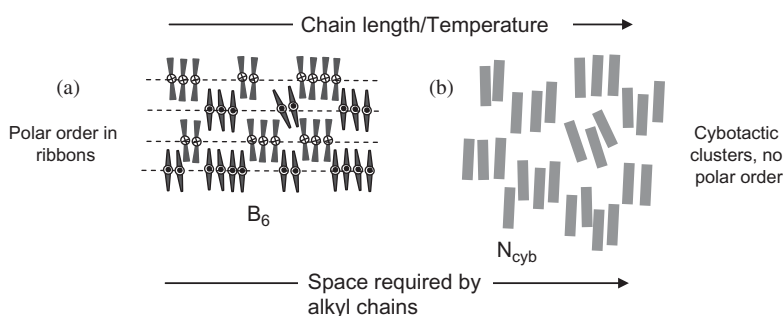


Figure 10. Transition from the  $B_6$  phase to the nematic phase driven by increasing distortion of core packing by the alkyl chain expansion which competes with the increasing segregation tendency.

It is well established that  $B_1$  phases (nonswitching  $B_{1rev}$  phases of the  $Col_r$  type with small lattice parameters) and  $B_6$  phases are preferably found in short chain compounds and compete with the formation of nematic phases. In previously reported cases, the  $B_1/B_6$  phases occurred as low temperature phases below nematic phases of short chain homologues,[2,3,5] but for the compounds reported here the nematic phase is completely removed. So the general rule that in homologous series the nematic phases generally occur by reducing the alkyl chain length is not generally applicable for bent-core mesogens. Due to effect of the chain length on the degree of restriction of the rotation of the bent cores, the phase sequences are more complex and smectic  $B_6$  phases or columnar  $B_1$  phases can partly or completely replace the nematic phases upon reducing the chain length. If this could also be possible for polar smectic phases with monolayer structure (' $B_2$ -type' phases,  $d \sim L_{mol}$ ) remains to be investigated.

### 3.3 Photo-chemical properties

UV-vis absorption spectroscopy was performed on compound *C16*. Figure 11 shows the effects of UV irradiation on the UV-vis spectra of *C16* in chloroform solution as (a) freshly prepared, (b) exposed to 365 nm light and (c) after keeping the sample in dark overnight. Light radiation in the wavelength range 290–380 nm is found to be strongly absorbed with the maximum at 370 nm. This can be attributed to the  $\pi-\pi^*$  transition of the chromophore in the molecule.[45] After exposure to 365 nm light for 1 h

which falls within this absorption band, the absorption at 460 nm appears to increase while dropping in the band at 370 nm. This suggests that the freshly prepared sample in the dark is composed predominantly of the *trans*-isomer in which the molecules absorb at  $\lambda = 370$  nm and transform to the *cis*-isomer. The molecules in the *cis*-form absorb light in the 400–480 nm range centred at  $\lambda = 460$  nm corresponding to the  $n-\pi^*$  transition,[46,47] and consequently transform to the *trans*-isomer. All of the prepared compounds show similar behaviour of *trans-cis* isomerisation upon UV-vis illumination.

To study the effect of light on the prepared compounds we selected compound *C16* with  $R = C_{16}H_{33}$  as a representative example for further investigation. In addition, TLC tests were performed on a freshly prepared solution of *C16* in chloroform and after exposure to ambient light. The fresh sample TLC results in one spot while the exposed sample yields two spots ( $R_f = 0.88$  (*trans*-isomer) and 0.72 (*cis*-isomer) on TLC-aluminium sheets coated with silica gel). The exposed solution was then allowed to evaporate and crystallise at ambient light. When this dried sample is re-dissolved in  $CHCl_3$  and TLC conducted in darkness, only one spot is obtained. These observations show that the molecules are rapidly transforming to the *cis*-isomers in solution under ambient illumination and back to the *trans*-isomer when the solvent is removed. Also the LC-Iso transition temperatures of compounds *An-Cn* decrease when the brightness of the microscope lamp was increased, indicating sensitivity to light also in the liquid and LC state.

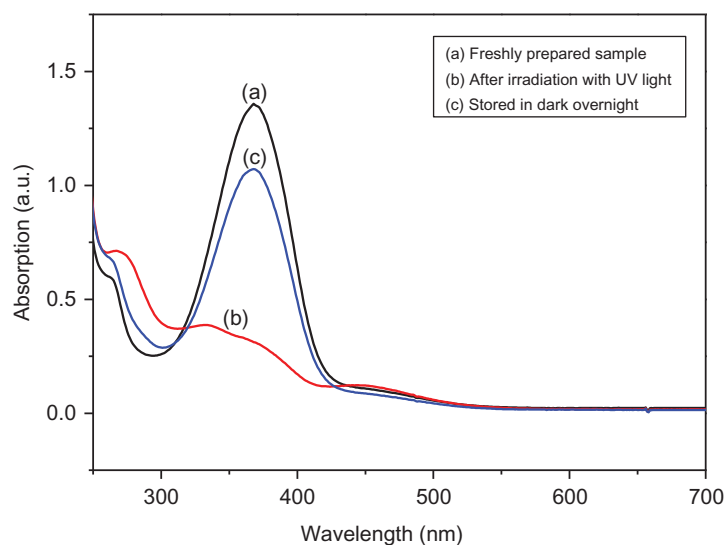


Figure 11. (colour online) UV-vis spectra (absorbance vs. wavelength) of *C16* dissolved in chloroform (0.02 mM solution) at 25°C. (a) Freshly prepared sample, *trans*-isomer before irradiation, black line; (b) *cis*-isomer as obtained after 1 hour irradiation with light of 366 nm wavelength, red line; (c) *trans*-isomer after keeping the sample in dark overnight, blue line.

#### 4. Conclusion

In summary we have reported the synthesis and phase behaviour of three new series of photosensitive bent-core mesogens with azobenzene units containing five aromatic rings with 4-chlororesorcinol, 4-bromoresorcinol or 4-fluororesorcinol as the central bent unit. The nature of the mesophases has been established using POM and DSC studies. We also performed studies of the effect of light irradiation on a selected compound. The measurements reveal that the nature and structure of their liquid crystalline phases are greatly affected by the nature and the polarity of the substituent on the central benzene ring. It was reported in the literature that similar compounds to those prepared here with chain length  $R = C_{10}H_{21}$  or  $R = C_{12}H_{25}$  but without any substitution at the central unit are non liquid crystalline.[19,34] Here, it was found that introducing a chloro or bromo atoms into position-4 on the central benzene ring can give a monotropic  $B_4$ -like dark conglomerate phase,  $B_6$  phases and nematic phases. To the best of our knowledge compound **B10** is the first azobenzene based bent-core LC showing  $B_4$ -like dark conglomerate phase. On the other hand introducing fluorine (series  $C_n$ ) instead of Cl, Br at the same position of the central benzene ring leads to different behaviour, where all homologues of this series are crystalline except the highest homologue, **C16** which shows a monotropic  $USmC_a$  phase with large lattice parameters as concluded from the texture and XRD investigations. As a unique feature, upon reducing the chain length a transition from nematic to  $B_6$ -type smectic phases was observed for homologues  $A_n$  and  $B_n$ , which is reverse to usually observed chain length dependence of smectic–nematic phase sequences.

#### Acknowledgement

M. Alaasar is grateful to the Alexander von Humboldt Foundation for the research fellowship.

#### Notes

- As an exception, it was reported that increasing the spacer length in dimeric rod-like LC decreases the smectic tendencies of the mesogen and increases the nematic tendencies for a given homologues series.

#### References

[1] Niori T, Sekine T, Watanabe J, Furukawa T, Takezoe H. Distinct ferroelectric smectic liquid crystals consisting of banana shaped achiral molecules. *J Mater Chem.* 1996;6:1231–1233.  
 [2] Reddy RA, Tschierske C. Bent-core liquid crystals: polar order, superstructural chirality and spontaneous

desymmetrisation in soft matter systems. *J Mater Chem.* 2006;16:907–961.  
 [3] Takezoe H, Takanishi Y. Bent-core liquid crystals: their mysterious and attractive World. *Jpn J Appl Phys* 2006;45:597–625.  
 [4] Etxebarria J, Blanca M. Bent-core liquid crystals in the route to functional materials. *J Mater Chem.* 2008;18:2919–2926.  
 [5] Pelzl G, Weissflog W. Mesophase behaviour at the borderline between calamitic and banana-shaped mesogens. In: Ramamoorthy A, editor. *Thermotropic liquid crystals: recent advances.* Berlin: Springer; 2007. p. 1–58.  
 [6] Kozmík V, Horčic M, Svoboda J, Novotná V, Pocięcha D. 3-Aminophenol based bent-shaped liquid crystals with an amide linking group. *Liq Cryst.* 2012;39:943–955.  
 [7] Link DR, Natale G, Shao R, MacLennan JE, Clark NA, Körblová E, Walba DM. Spontaneous formation of polar chiral layers from achiral molecules in a novel antiferroelectric liquid crystal phase. *Science* 1997;278:1924–1927.  
 [8] Yesodha SK, Pillai SKS, Tsutsumi N. Stable polymeric materials for nonlinear optics: a review based on azobenzene systems. *Prog Polym Sci.* 2004;29:45–74.  
 [9] Tsukruk VV, Bliznyuk VN. Side chain liquid crystalline polymers at interfaces. *Prog Polym Sci.* 1997;22:1089–1132.  
 [10] Tamba M-G, Alexey B, Valery S, Pelzl G, Baumeister U, Weissflog W. Photochromic azobenzene functionalised banana–calamitic dimers and trimers: mesophase behaviour and photo-orientational phenomena. *Liq Cryst.* 2011;38:1531–1550.  
 [11] Rochon P, Batalla E, Natanson A. Optically induced surface gratings on azoaromatic polymer films. *Appl Phys Lett.* 1995;66:136–138.  
 [12] Kim DY, Li SK, Tripathy L, Kumar J. Laser-induced holographic surface relief gratings on nonlinear optical polymer films. *Appl Phys Lett.* 1995;66:1166–1168.  
 [13] Haus HA. Linearity of optical amplifiers and the Tomonaga approximation. *J Opt Soc Am.* 2001;B18:1777–1779.  
 [14] Meng X, Natansohn A, Barrett C, Rochon P. Azo polymers for reversible optical storage. 10. Cooperative motion of polar side groups in amorphous polymers. *Macromolecules.* 1996;29:946–952.  
 [15] Ho M, Natansohn A, Barrett C, Rochon P. Azo polymers for reversible optical storage. 8. The effect of polarity of the azobenzene groups. *Can J Chem.* 1995;73:1773–1778.  
 [16] Natansohn A, Rochon P, Ho M, Barrett C. Azo polymers for reversible optical storage. 6. Poly[4-[2-(methacryloyloxy)ethyl]azobenzene]. *Macromolecules.* 1995;28:4179–4183.  
 [17] Ichimura K. Photoalignment of liquid-crystal systems. *Chem Rev.* 2000;100:1847–1873.  
 [18] Yamaoka T, Makita Y, Sasatani H, Kim SI, Kimura Y. Linear type azo-containing polyurethane as drug-coating material for colon-specific delivery: its properties, degradation behavior, and utilization for drug formulation. *J Control Release.* 2000;66:187–197.  
 [19] Prasad V. Liquid crystalline compounds with V shaped molecular structures: synthesis and characterization of new azo compounds. *Liq Cryst.* 2001;28:145–150.

- [20] Prasad V, Rao DSS, Prasad SK. A novel class of banana-shaped azo compounds exhibiting antiferroelectric switching behaviour. *Liq Cryst.* 2001;28:643–646.
- [21] Prasad V. Bent-shaped achiral azo compounds exhibiting banana mesophases. *Mol Cryst Liq Cryst.* 2001;363:167–179.
- [22] Prasad V, Jáklí A. Achiral bent-core azo compounds: observation of photoinduced effects in an antiferroelectric tilted smectic mesophase. *Liq Cryst.* 2004;31:473–479.
- [23] Prasad V, Kang SW, Qi X, Kumar SJ. Photo-responsive and electrically switchable mesophases in a novel class of achiral bent-core azo compounds. *J Mater Chem.* 2004;14:1495–1502.
- [24] Prasad V, Kang SW, Suresh KA, Joshi L, Wang Q, Kumar S. Thermotropic uniaxial and biaxial nematic and smectic phases in bent-core mesogens. *J Am Chem Soc.* 2005;127:17224–17227.
- [25] Folcia CL, Alonso I, Ortega J, Etxebarria J, Pintre I, Ros MB. Achiral bent-core liquid crystals with azo and azoxy linkages: structural and nonlinear optical properties and photoisomerization. *Chem Mater.* 2006;18:4617–4626.
- [26] Pintre IC, Gimeno N, Serrano JL, Ros MB, Alonso I, Folcia CL, Ortega J, Etxebarria J. Liquid crystalline and nonlinear optical properties of bent-shaped compounds derived from 3,4'-biphenylene. *J Mater Chem.* 2007;17:2219–2227.
- [27] Lutfor MR, Hegde G, Kumar S, Tschierske C, Chigrinov VG. Synthesis and characterization of bent-shaped azobenzene monomers: guest–host effects in liquid crystals with azo dyes for optical image storage devices. *Opt Mater.* 2009;32:176–183.
- [28] Rahman L, Kumar S, Tschierske C, Israel G, Ster D, Hegde G. Synthesis and photoswitching properties of bent shaped liquid crystals containing azobenzene monomers. *Liq Cryst.* 2009;36:397–407.
- [29] Vijaysrinivasan M, Kannan P, Roy A. Dual switchable six-ring bent-core liquid crystals with azo linkages exhibiting  $B_1$  and  $B_2$  mesophases. *Liq Cryst.* 2012;39:1465–1475.
- [30] Pelzl G, Diele S, Weissflog W. Banana-shaped compounds – a new field of liquid crystals. *Adv Mater.* 1999;11:707–724.
- [31] Weissflog W, Nadasi H, Dunemann U, Pelzl G, Diele S, Eremin A, Kresse H. Influence of lateral substituents on the mesophase behaviour of banana-shaped mesogens. *J Mater Chem.* 2001;11:2748–2758.
- [32] Weissflog W, Murthy HNS, Diele S, Pelzl G. Relationships between molecular structure and physical properties in bent-core mesogens. *Philos Trans R Soc London, Ser. A.* 2006;364:2657–2679.
- [33] Lutfor R, Asik J, Kumar S, Tschierske C. Liquid crystalline banana-shaped monomers derived from 2,7-naphthalene: synthesis and properties. *Liq Cryst.* 2008;35:1263–1270.
- [34] Nagaveni NG, Roy A, Prasad V. Achiral bent-core azo compounds: effect of different types of linkage groups and their direction of linking on liquid crystalline properties. *J Mater Chem.* 2012;22:8948–8959.
- [35] Kang S, Thisayukta J, Takezoe H, Watanabe J, Ogino K, Doi T, Takahashi T. High speed parallel synthesis of banana-shaped molecules and phase transition behaviour of 4-bromo-substituted derivatives. *Liq Cryst.* 2004;31:1323–1336.
- [36] Keith C, Lehmann A, Baumeister U, Prehm M, Tschierske C. Nematic phases of bent-core mesogens. *Soft Matter.* 2010;6:1704–1721.
- [37] Hough LE, Chen D, Jung HT, Link DR, Walba DM, Krüerke D, Zasadzinski J, Glaser MA, Clark NA, Heberling MS, Heppke G, Nakata M, Rabe JP, Jones CD, Stocker W, Körblova E. Helical nanofilament phases. *Science.* 2009;325:456–460.
- [38] Vaupotič N, Pocięcha D, Gorecka E. Polar and apolar columnar phases made of bent-core mesogens. *Top Curr Chem.* 2012;318:281–302.
- [39] Coleman DA, Fernsler J, Chattham N, Nakata M, Takanishi Y, Körblova E, Link DR, Shao R-F, Jang WG, MacLennan JE, Mondainn-Monval O, Boyer C, Weissflog W, Pelzl G, Chien L-C, Zasadzinski J, Watanabe J, Walba DM, Takezoe H, Clark NA. Polarization-modulated smectic liquid crystal phases. *Science.* 2003;29:1204–1211.
- [40] Kang S, Tokita M, Ogino K, Doi T, Takahashi T, Takezoe H, Watanabe J. Distinct layered structure with density modulation in solid phase formed from B2 phase of banana molecules. *Phys Rev E.* 2006;73:11701–11706.
- [41] Weissflog W, Sokolowski S, Dehne H, Das B, Grande S, Schröder MW, Eremin A, Diele S, Pelzl G, Kresse H. Chiral ordering in the nematic and an optically isotropic mesophase of bent-core mesogens with a halogen substituent at the central core. *Liq Cryst.* 2004;31:923–933.
- [42] Steed JW, Atwood JL. *Supramolecular chemistry.* Chichester: Wiley; 2009.
- [43] Date RW, Imrie CT, Luckhurst GR, Seddon JM. Smectogenic dimeric liquid crystals. The preparation and properties of the  $\alpha,\omega$ -bis(4-n-alkylaniline-benzylidene-4'-oxy)alkanes. *Liq Cryst.* 1992;12:203–238.
- [44] Kang S, Tokita M, Takanishi Y, Takezoe H, Watanabe J. Structure of a  $B_6$ -like phase formed from bent-core liquid crystals determined by microbeam X-ray diffraction. *Phys Rev E.* 2007;76:42701–42704.
- [45] Legge CH, Mitchell GR. Photo-induced phase transitions in azobenzene-doped liquid crystals. *J Phys D: Appl Phys.* 1992;25:492–499.
- [46] Lansac Y, Glaser MA, Clark NA, Lavrentovich OD. Photocontrolled nanophase segregation in a liquid-crystal solvent. *Nature* 1999;398:54–57.
- [47] Krentsel TA, Lavrentovich OD, Kumar S. In-situ X-ray measurements of light-controlled layer spacing in a smectic-A liquid crystal. *Mol Cryst Liq Cryst.* 1997;304:463–469.

# A new room temperature dark conglomerate mesophase formed by bent-core molecules combining 4-iodoresorcinol with azobenzene units†

Mohamed Alaasar,<sup>\*ab</sup> Marko Prehm<sup>a</sup> and Carsten Tschierske<sup>\*a</sup>

Cite this: *Chem. Commun.*, 2013, **49**, 11062

Received 3rd August 2013,  
Accepted 4th October 2013

DOI: 10.1039/c3cc45938a

www.rsc.org/chemcomm

**The first bent-core molecules comprising 4-iodoresorcinol as the central core unit and incorporating azobenzene units have been synthesized. A new type of dark conglomerate phase (DC phase) is observed, which remains over a wide temperature range down to room temperature without crystallization.**

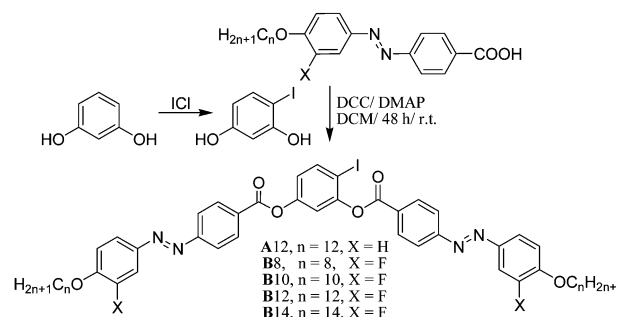
Chirality has been one of the most attractive themes in chemistry since Pasteur's famous resolution experiment showing the handedness of tartaric acid.<sup>1</sup> Since that time spontaneous formation of chiral phases by the self-assembly of achiral molecules or self-resolution of racemic conglomerates has been a well known phenomenon, often observed in the crystalline solid state.<sup>2</sup> However, with bent-core molecules this phenomenon was also found in soft crystals and even in liquid crystals.<sup>3</sup> Spontaneous macroscopic optical activity has been observed for these achiral molecules in the soft crystalline helical nano-filament phases (assigned as HNF phases or B<sub>4</sub> phases)<sup>4</sup> and in fluid polar smectic phases (B<sub>2</sub> phases).<sup>5</sup> These optically nearly isotropic mesophases are composed of conglomerates of macroscopic chiral domains, which can easily be distinguished under a polarizing microscope (dark conglomerate phases, DC phases). Conglomerates of chiral domains were also found in the recently reported birefringent SmC<sub>s</sub>P<sub>R</sub> phase<sup>6</sup> and in nematic phases formed by some bent-core mesogens,<sup>7</sup> however in these cases their formation is dependent on surface interactions which are required to stabilize the chiral domains. The B<sub>4</sub> phase is the best investigated of the DC phases. In these mesophases the chirality arises from a crystalline packing of the aromatic cores in left- or right-handed helical nano-filaments. The packing of the terminal alkyl chains is frustrated and therefore these chains remain in a disordered liquid state.<sup>4</sup> Another characteristic feature of these soft crystalline phases is that the chirality is retained upon

dilution with a large excess of an achiral nematic phase.<sup>8</sup> In contrast to the soft crystalline B<sub>4</sub> phase the formation of the completely fluid DC phases without crystalline nano-filaments is more difficult to understand.<sup>5</sup> A common way to distinguish both types of DC phases is by XRD where the soft crystalline B<sub>4</sub> phases are characterized by the presence of sharp wide angle reflections, whereas only one diffuse halo around  $d = 0.45$  nm is found for the fluid DC phases.

Herein we report a new subtype of DC phases which appears to be intermediate between these two types. Moreover, the reported compounds forming this phase are the first examples of bent-core liquid crystals (BCLCs) containing a 4-iodoresorcinol unit as the central core structure. These materials also contain photoisomerizable azobenzene groups which can be exploited for optical and optoelectronic devices.<sup>9</sup> To the best of our knowledge, the compounds reported herein are the first examples of azo functionalized BCLCs showing DC phases.†

The synthetic pathway leading to the bent core compounds **A12** and **Bn** is given in Scheme 1. The detailed synthetic procedures, purification and analytical data are reported in the ESI.†

Compound **A12** without any lateral substituent on the outer benzene rings (X = H) was found to be non-mesomorphic, having a melting point at  $T = 112$  °C and crystallizing at  $T = 77$  °C. Replacing the hydrogen atoms next to the alkoxy chain by fluorine led to compounds **Bn**, (X = F,  $n = 8$ –14), which all give optically isotropic mesophases composed of a conglomerate of chiral domains (DC phases, see Fig. 2).



**Scheme 1** Synthetic route to the bent core molecules **A<sub>n</sub>** and **B<sub>n</sub>**.<sup>10,11</sup>

<sup>a</sup> Institute of Chemistry, Martin-Luther University Halle-Wittenberg, Kurt-Mothes Str.2, D-06120 Halle/Saale, Germany.

E-mail: carsten.tschierske@chemie.uni-halle; Fax: +49 (0)3455527346;

Tel: +49 (0)34555256664

<sup>b</sup> Department of Chemistry, Faculty of Science, Cairo University, Giza, Egypt.

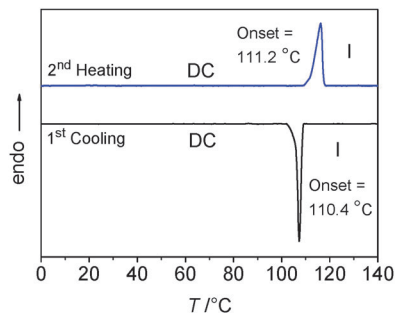
E-mail: M\_Alaasar@yahoo.com; Fax: +20 235727556; Tel: +20 235676595

† Electronic supplementary information (ESI) available: Synthesis, analytical data, and additional data. See DOI: 10.1039/c3cc45938a

**Table 1** Phase transition temperatures ( $T/^\circ\text{C}$ ), mesophase types, and transition enthalpies [ $\Delta H/\text{kJ mol}^{-1}$ ] of compounds **A12** and **Bn**<sup>a</sup>

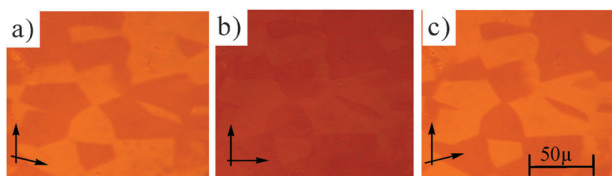
Compd	<i>n</i>	1st heating	1st cooling	2nd heating
<b>A12</b>	12	Cr 112 [35.1] I	I 77 [33.7] Cr	Cr 112 [34.9] I
<b>B8</b>	8	DC 116 [31.5] I	I 107 [27.9] DC	DC 116 [30.6] I
<b>B10</b>	10	DC 116 [25.0] I	I 102 [29.3] DC	DC 115 [23.9] I
<b>B12</b>	12	DC 114 [25.8] I	I 103 [23.7] DC	DC 111 [25.3] I
<b>B14</b>	14	DC 116 [30.2] I	I 109 [32.0] DC	DC 116 [30.1] I

<sup>a</sup> Peak temperatures from DSC at a rate of  $10 \text{ K min}^{-1}$ ; abbreviations: Cr = crystalline solid; DC = dark conglomerate phase; I = isotropic liquid.

**Fig. 1** DSC heating and cooling curves ( $10 \text{ K min}^{-1}$ ) observed for **B14**.

The transition temperatures of the synthesized compounds are summarized in Table 1. All compounds **Bn** exhibit only one mesophase (the DC phase), and the phase transition temperatures are almost the same irrespective of the terminal chain length. Compound **B14**, as a representative example, was investigated in more detail. Upon cooling **B14** under the polarizing microscope the isotropic liquid becomes highly viscous with glass-like appearance at  $109^\circ\text{C}$  but no birefringence is observed between crossed polarizers (Fig. 2b). Fig. 1 shows the heating and the cooling differential scanning calorimetry (DSC) curves obtained for compound **B14**. The formation of this phase is associated with a relatively high transition enthalpy of  $\Delta H \sim 30 \text{ kJ mol}^{-1}$ , which is a value similar to typical transition enthalpies of the  $B_4$  to isotropic liquid transition.<sup>4</sup> The onset temperatures of the transition peaks upon heating and cooling are approximately the same ( $\sim 111^\circ\text{C}$ ) indicating the absence of a hysteresis. Also the transition peaks upon heating and cooling have approximately the same enthalpy values in the first and all following heating-cooling cycles.

Upon further cooling no crystallization occurs down to room temperature (Fig. 1). Even after storage of the sample at room temperature for 6 weeks the same transition temperatures and enthalpies were obtained and there was no indication of any crystallization (see Fig. S1 in the ESI<sup>†</sup>), even the samples obtained

**Fig. 2** Textures of the DC phase of compound **B14** at  $T = 80^\circ\text{C}$ : (b) between crossed polarizers and (a) after rotating one polarizer by  $7^\circ$  from the crossed position in the clock-wise direction and (c) in the anticlockwise direction, showing dark and bright domains, indicating the presence of areas with opposite chirality sense.

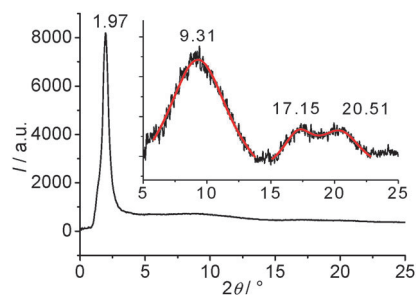
by “crystallization” from solvents appear to be in the mesomorphic state. Uncrossing the polarizers by a small angle leads to the appearance of dark and bright domains with a maximum contrast at an angle of *ca.*  $7^\circ$ . Uncrossing the polarizer in the other direction reverses the dark and bright domains (Fig. 2a and c). Rotating the sample between crossed polarizers does not lead to any change and this indicates that the distinct regions represent chiral domains with opposite handedness.

No current peak could be observed for compound **B14** in electrooptical investigations of the mesophase and no birefringent mesophase is induced under an applied triangular wave voltage of up to  $200 \text{ Vpp}$  in a  $6 \mu\text{m}$  ITO cell. These features are also very similar to those of the soft crystalline  $B_4$  type DC phases (helical nanofilament phases).

However the XRD pattern (see Fig. 3 and Fig. S2, ESI<sup>†</sup>) is different from those of the  $B_4$  phases. For compound **B14** an intense small angle reflection is observed, corresponding to a distance of  $d = 4.63 \text{ nm}$  ( $90^\circ\text{C}$ ). From this  $d$ -value and the molecular length  $L = 6.1 \text{ nm}$  (in a  $120^\circ$  V-shaped conformation and all-*trans* alkyl chains) a  $d/L$  ratio of 0.76 results, which allows a tilt angle of the molecules up to  $\beta = 41^\circ$  ( $\cos \beta = d/L$ ). Whether there is a tilt of the molecules or whether the difference between  $d$  and  $L$  is only due to chain folding and chain interdigitation cannot be decided at present. The reasons are that aligned samples cannot be obtained for DC phases due to their locally distorted structure (see Fig. S2a, ESI<sup>†</sup>) and that optical methods cannot be used for tilt angle determination of these isotropic mesophases.

With the exception of the intense small angle scattering all other scatterings have only very low intensity and are more or less diffuse. The low intensity could, at least partly, be due to the absorption by the heavy atom iodine incorporated in the molecular structure. A broad scattering is found at about  $2\theta = 9.3^\circ$ , corresponding to a mean distance of  $1.0 \text{ nm}$  and in the wide angle region there are two additional even weaker diffuse scattering maxima corresponding to  $d$ -values of  $0.52$  and  $0.43 \text{ nm}$ . So the majority of intensity of the diffuse scattering is found in the medium angle region. This kind of XRD pattern is distinct from the  $B_4$  phases, which show three or more sharp wide angle reflections at larger angles in the  $2\theta$  range of  $18^\circ$ – $28^\circ$ . However, it is also distinct from the fluid DC phases showing only one diffuse halo in the wide angle region at  $2\theta \sim 20^\circ$  besides the small angle layer reflection.<sup>5a</sup>

Though the precise origin of this diffraction pattern is still unclear, in a tentative model it can be assumed that the individual bent-core molecules form densely packed crystalline nano-clusters

**Fig. 3** XRD pattern of the DC phase of compound **B14** at  $T = 90^\circ\text{C}$ ; the inset shows the magnified ( $\sim 40$  fold) wide angle region after baseline correction.

incorporating around 4–6 molecules. The mean distance between these nano-crystallites is assumed to give rise to the weak diffuse scattering with a maximum around 1.0 nm. The further growth of these clusters is obviously inhibited. This might be caused by the packing of helical conformers, which leads to a twist and inhibits the further growth to larger nano-filaments or crystalline layers. Nano-crystallites with identical twist sense arrange in layers with only short range order in the layers. As packing of nano-crystallites with identical chirality is favorable macroscopic chirality develops. The chirality induces twist and bend of the layers which, together with the effects of steric and packing frustrations,<sup>5</sup> gives rise to a strong non-regular deformation or fragmentation of these layers. The correlation length of uniformly oriented domains is in the range of 35 nm (as estimated from the full width at half-maximum of the layer reflection peak) which is below the wavelength of light, thus leading to an optically isotropic appearance of the phase. Some parts of the alkyl chains seem to remain in a disordered state and contribute to the diffuse wide angle scatterings (see Fig. 3).

As it is known that B<sub>4</sub> phases can be diluted by nematic LC hosts to a high degree (>95%) without loss of the chirality<sup>8</sup> we investigated a 1:1 mixture and a 1:9 mixture of B14 with 4'-pentyl-4-cyanobiphenyl (5-CB). In the 1:1 mixture the DC-Iso transition is reduced to 60 °C, but the chiral domains are still clearly visible (see Fig. S3a–c, ESI†). This DC phase rapidly crystallizes at 46 °C (Fig. S3d, ESI†) and upon heating the crystalline material melts at 86 °C to an isotropic liquid. In the 1:9 mixture no DC phase is formed, again compound B14 crystallizes from the nematic phase at *T* = 35 °C and these crystals melt at 52 °C. So, in contrast to B<sub>4</sub> phases there is a clear destabilizing effect of 5-CB on the DC phase. Simultaneously, formation of a crystalline phase is strongly enhanced. It seems that the 5-CB molecules can reduce the frustration of the packing of the molecules and allow the growth of the small nano-crystallites to a macroscopic crystalline phase. It is however not clear if pure B14 crystallizes or if these crystals involve additional 5-CB molecules.

It appears that the presence of the relatively large and highly polarizability of iodine in the 4-position of the resorcinol unit provides bent-core mesogens with new interesting phase structures. The observed kind of DC phase is not reported for related molecules with chlorine at the same position.<sup>11</sup> Bromine seems to be a bit more favorable for the formation of DC phases,<sup>11</sup> § whereas iodine seems to have a much stronger DC-promoting effect. The bulky iodine might lead to strongly twisted helical molecular conformations by twisting the adjacent COO group out of the planes of the adjacent benzene rings,<sup>12</sup> thus favouring layer distortion and formation of chiral superstructures. Iodine–iodine interactions or weak halogen bonding interactions<sup>13</sup> could also contribute to this effect.

In summary, we report herein the first bent-core liquid crystalline materials containing 4-iodine substitution in the central core unit. These compounds exhibit a new type of DC phase¶ occurring in broad temperature ranges including room temperature. Moreover, these are the first examples of azobenzene-based BCLC showing DC phases.‡ The DC phase formed by this kind of molecules is different from the previously reported types and could contribute to an improved understanding of these phases and the occurrence of spontaneous achiral symmetry breaking in soft matter in general. Moreover, the possibilities provided by the

photoisomerizable azobenzene units could lead to interesting perspectives for chirality switching and phase modulation by interaction with circularly polarized light.<sup>9,14</sup>

M.A. acknowledges the support from the Alexander von Humboldt Foundation for the research fellowship at Martin-Luther University Halle-Wittenberg, Germany.

## Notes and references

‡ B<sub>4</sub>-type DC phases have been reported for bent shaped mesogenic dimers combining two rod-like azobenzene units.<sup>15</sup> A B<sub>4</sub>-like DC phase was found recently for one homologue in a series based on a 4-bromoresorcinol core with rod-like azobenzene units upon cooling from a nematic phase, but with a very short range before crystallization.<sup>11</sup>

§ Besides the B<sub>4</sub>-type helical filament phases a soft crystalline dark conglomerate phase with a 2D lattice<sup>17</sup> and for the fluid DC phases, which usually have a single layer structure, an intercalated B<sub>6</sub>-like version was also reported recently,<sup>18</sup> moreover an achiral cubic phase composed of vesicular layer aggregates has been reported.<sup>19</sup>

¶ Dark conglomerate phases were also observed for some 4-bromoresorcinol esters with Schiff base wings.<sup>16</sup>

- 1 L. Pasteur, *C. R. Acad. Sci.*, 1848, **26**, 535.
- 2 *Chirality at the Nanoscale*, ed. D. B. Amabiliino, Wiley-VCH, Weinheim, 2009.
- 3 T. Niori, T. Sekine, J. Watanabe, T. Furukawa and H. Takezoe, *J. Mater. Chem.*, 1996, **6**, 1231; D. R. Link, G. Natale, R. Shao, J. E. MacLennan, N. A. Clark, E. Körblova and D. M. Walba, *Science*, 1997, **278**, 1924; R. A. Reddy and C. Tschierske, *J. Mater. Chem.*, 2006, **16**, 907; H. Takezoe and Y. Takanishi, *Jpn. J. Appl. Phys.*, 2006, **45**, 597.
- 4 T. Sekine, T. Niori, J. Watanabe, S. W. Choi, Y. Takanishi and H. Takezoe, *J. Mater. Chem.*, 1997, **7**, 1307; D. M. Walba, L. Eshdat, E. Körblova and R. K. Shoemaker, *Cryst. Growth Des.*, 2005, **5**, 2091; E. Bialecka-Florjanczyk, I. Sledzinska, E. Gorecka and J. Przedmojski, *Liq. Cryst.*, 2008, **35**, 401; L. E. Hough, H. T. Jung, D. Kruerke, M. S. Heberling, M. Nakata, C. D. Jones, D. Chen, D. R. Link, J. Zasadzinski, G. Heppke, J. P. Rabe, W. Stocker, E. Körblova, D. M. Walba, M. A. Glaser and N. A. Clark, *Science*, 2009, **325**, 456; D. Chen, J. E. MacLennan, R. Shao, D. K. Yoon, H. Wang, E. Körblova, D. M. Walba, M. A. Glaser and N. A. Clark, *J. Am. Chem. Soc.*, 2011, **133**, 12656.
- 5 (a) G. Dantlgraber, A. Eremin, S. Diele, A. Hauser, H. Kresse, G. Pelzl and C. Tschierske, *Angew. Chem., Int. Ed.*, 2002, **41**, 2408; (b) L. E. Hough, M. Spannuth, M. Nakata, D. A. Coleman, C. D. Jones, G. Dantlgraber, C. Tschierske, J. Watanabe, E. Körblova, D. M. Walba, J. E. MacLennan, M. A. Glaser and N. A. Clark, *Science*, 2009, **325**, 452.
- 6 M. Alaasar, M. Prehm, M. Nagaraj, J. K. Vij and C. Tschierske, *Adv. Mater.*, 2013, **25**, 2186.
- 7 G. Pelzl, A. Eremin, S. Diele, H. Kresse and W. Weissflog, *J. Mater. Chem.*, 2002, **12**, 2591; V. Görtz, *Liq. Cryst. Today*, 2010, **19**, 37.
- 8 T. Otani, F. Araoka, K. Ishikawa and H. Takezoe, *J. Am. Chem. Soc.*, 2009, **131**, 12368.
- 9 H. M. Dhammika Bandarab and S. C. Burdette, *Chem. Soc. Rev.*, 2012, **41**, 1809.
- 10 I. Thomsen and K. B. G. Torssell, *Acta Chem. Scand.*, 1991, **45**, 539.
- 11 M. Alaasar, M. Prehm and C. Tschierske, *Liq. Cryst.*, 2013, **40**, 656.
- 12 S. Ananda Rama Krishnan, W. Weissflog and R. Friedemann, *Liq. Cryst.*, 2005, **32**, 847.
- 13 D. W. Bruce, *Struct. Bonding*, 2008, **126**, 161.
- 14 H. Takezoe, *Top. Curr. Chem.*, 2012, **318**, 303.
- 15 S.-W. Choi, T. Izumi, Y. Hoshino, Y. Takanishi, K. Ishikawa, J. Watanabe and H. Takezoe, *Angew. Chem., Int. Ed.*, 2006, **45**, 1382; G. Lee, R. J. Carlton, F. Araoka, N. L. Abbott and H. Takezoe, *Adv. Mater.*, 2013, **25**, 245.
- 16 S. Kang, J. Thisayukta, H. Takezoe, J. Watanabe, K. Ogino, T. Doi and T. Takahashi, *Liq. Cryst.*, 2004, **31**, 1323.
- 17 E. Tsai, J. M. Richardson, E. Körblova, M. Nakata, D. Chen, Y. Shen, R. Shao, N. A. Clark and D. M. Walba, *Angew. Chem., Int. Ed.*, 2013, **52**, 5254.
- 18 H. Ocak, B. Bilgin-Eran, M. Prehm and C. Tschierske, *Soft Matter*, 2013, **9**, 4590.
- 19 S. Kang, M. Harada, X. Li, M. Tokita and J. Watanabe, *Soft Matter*, 2012, **8**, 1916.

CrossMark  
click for updatesCite this: *Soft Matter*, 2014, 10, 7285

# Dark conglomerate phases of azobenzene derived bent-core mesogens – relationships between the molecular structure and mirror symmetry breaking in soft matter†

Mohamed Alaasar,<sup>\*ab</sup> Marko Prehm,<sup>a</sup> Marcel Brautzsch<sup>a</sup> and Carsten Tschierske<sup>\*a</sup>

New 4-bromoresorcinol based bent-core molecules with peripheral fluoro substituted azobenzene wings have been synthesized and the liquid crystalline self-assembly was investigated by differential scanning calorimetry (DSC), optical polarizing microscopy (POM), electro-optic studies and X-ray diffraction (XRD). A new type of optically isotropic mesophase composed of chiral domains with opposite handedness (dark conglomerate phases, DC phases) is observed, which for some homologues with medium alkyl chain length is stable down to ambient temperature. It is proposed that these DC phases are formed by helical twisted nano-domains of limited size and composed of the crystallized aromatic cores which are separated by the disordered alkyl chains. This structure is distinct from the previously known soft helical nano-filament phases (HNF phases, B<sub>4</sub> phases) formed by extended crystalline nano-filaments and also distinct from the fluid sponge phases composed of deformed fluid layers. Comparison with related bent-core molecules having H, F, Cl, I, CH<sub>3</sub> and CN groups in the 4-position at the resorcinol core, either with or without additional peripheral fluorines, provided information about the effects of these substituents on the tendency to form DC phases. Based on these relationships and by comparison with the minimum energy conformations obtained by DFT calculations a hypothesis is provided for the formation of DC phases depending on the molecular structure.

Received 11th June 2014  
Accepted 7th July 2014

DOI: 10.1039/c4sm01255k

www.rsc.org/softmatter

## 1. Introduction

The observation of spontaneous development of macroscopic chirality in soft matter systems of achiral molecules is a contemporary research topic with great importance for the general understanding of spontaneous mirror symmetry breaking, and this might also be useful for numerous practical applications. This phenomenon is in recent years most often found in liquid crystalline phases of some molecules with an extended bent aromatic core (bent-core molecules).<sup>1,2</sup> Helical superstructures in columns<sup>3,4</sup> and self-assembly in helical filaments<sup>5–9</sup> represent other prominent examples of mirror symmetry breaking at the nano-scale.<sup>10</sup> However, in these 1D organizations chiral segregation occurs only locally, along the aggregates, whereas the lateral interaction between them is only weak, so that usually no macroscopic chirality could be achieved in the absence of a chiral dopant.<sup>2</sup> Only for achiral dibenzo[*g,p*]chrysenes with short peripheral chains macroscopic

spontaneous segregation of chiral conformers was observed in a columnar phase.<sup>4</sup> In contrast, in polar smectic LC phases of bent-core liquid crystals (BCLCs) the spontaneous formation of conglomerates of macroscopically chiral domains is more frequently observed. Here chirality emerges in layers (smectic phases) which provides a stronger coupling and therefore can more easily transfer chirality over larger distances.<sup>1</sup> In addition, a geometric layer chirality arising from the combination of tilt and polar order in the polar smectic phases of bent-core molecules is assumed to play an important role in the development of macroscopic chirality in these smectic phases,<sup>11</sup> as it can couple with the molecular conformational chirality *via* diastereomeric interactions. On the other hand, in all cases of lamellar phases the packing of helical entities, ranging from helical conformers of single molecules *via* bent dimesogens to helical nano-filaments, is in competition with the formation of extended flat layers and thus leads to layer distortion.<sup>12</sup> In many cases this distortion is strong enough to remove the macroscopic anisotropic properties of liquid crystals, giving rise to isotropic mesophases which, due to the absence of birefringence, allow an easy identification of chirality by polarizing microscopy. These soft isotropic mesophases composed of a conglomerate of domains with opposite handedness are designated as dark conglomerate phases (DC phases). Depending on the local

<sup>a</sup>Institute of Chemistry, Martin Luther University Halle-Wittenberg, Kurt Mothes Str. 2, D-06120 Halle (Saale), Germany. E-mail: carsten.tschierske@chemie.uni-halle.de

<sup>b</sup>Department of Chemistry, Faculty of Science, Cairo University, Giza, Egypt. E-mail: malaasar@sci.cu.edu.eg

† Electronic supplementary information (ESI) available. See DOI: 10.1039/c4sm01255k

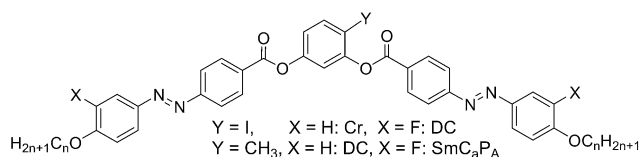




structure of these DC phases they can be classified as liquid crystalline sponge phases,<sup>13–19</sup> formed by strongly deformed fluid layers or as helical nanofilament phases (HNF phases, also assigned as B<sub>4</sub> phases<sup>20</sup>) having crystallized aromatic segments organized in helical nano-scale filaments which are separated by the disordered alkyl chain segments.<sup>21–27</sup> Aside from these two known cases a number of additional DC phases with intermediate or with quite distinct nano-structures can be expected, only a few of them have very recently been observed.<sup>28–30</sup> Moreover, conglomerates of chiral domains were also found in apolar SmC phases with only local polar domains (SmC<sub>s</sub>P<sub>R</sub><sup>[\*]</sup> phases)<sup>31,32</sup> and in nematic phases formed by some bent-core mesogens.<sup>33–35</sup> In these cases of LC phases with reduced order and without long range layer chirality the formation of DC phases is also dependent on surface interactions. However, the relationships between the formation of the distinct types of DC phases and the required molecular structures are still unknown. Therefore, the search for new molecular structures capable of forming DC phases and the investigation of their general structure property relationships is of significant importance. Moreover, DC phases could represent interesting materials for a variety of applications, such as organic semiconductors, thin-film transistors and solar cells,<sup>36</sup> as thin-film polarizers,<sup>37</sup> as nonlinear optical materials<sup>38</sup> as well as for the detection and amplification of chirality,<sup>39</sup> and eventually also for separation of enantiomers and for enantioselective synthesis.<sup>40</sup>

DC phases involving photoisomerizable azobenzene units were previously only reported for dimesogens composed of two azobenzene units connected by odd-numbered aliphatic spacers<sup>41</sup> and for W-shaped molecules.<sup>42</sup> Only recently, we have found that the azobenzene unit is a very useful building block for bent-core mesogens forming new types of HNF-like DC phases.<sup>43,44</sup> Broad regions of these DC phases have been found for 4-iodoresorcinol based<sup>43</sup> as well as 4-methylresorcinol based bent-core mesogens with two azobenzene wings (see Scheme 1).<sup>44</sup> In contrast, related 4-chloro and 4-fluoro substituted compounds do not form any DC phases.

Fluorine substitution at the periphery of the bent aromatic core has a significant effect on the liquid crystalline behaviour of BCLCs,<sup>45</sup> for example it can change the switching from antiferroelectric to ferroelectric.<sup>1,46</sup> In the case of the azobenzene based BCLCs it affects the formation of DC phases. Whereas F-substitution is required for the formation of DC phases of 4-iodoresorcinols with two azobenzene wings,<sup>43</sup> it removes the DC phase in the case of the analogous 4-methyl substituted compounds (Scheme 1).<sup>44</sup>



**Scheme 1** Effect of fluorine substitution (X = F vs. H) on the formation of DC phases in azobenzene-based BCLCs (abbreviations; DC = dark conglomerate phase, SmC<sub>a</sub>P<sub>A</sub> = anticlinic tilted antiferroelectric switching SmC phase, Cr = crystalline solid).<sup>43,44</sup>

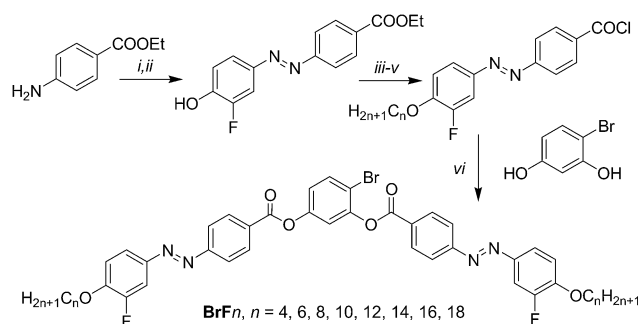
Here we report a new class of DC phase forming BCLCs based on 4-bromoresorcinol and having additional fluorine atoms at the periphery of the attached azobenzene wings, adjacent to the terminal alkyl chains. These compounds are compared with related compounds with F, Cl, I, CH<sub>3</sub> and CN substituents in the 4-position at the resorcinol core, either with or without additional peripheral fluorine substitution.<sup>31,32,43,44,47,48</sup> The designation of the molecules reported herein follows the general notation **YX<sub>n</sub>**, where Y indicates the 4-substituent at the resorcinol core, X = F indicates the presence of peripheral fluorines, the absence of X indicates a non-fluorinated compound where X = H and *n* gives the alkyl chain length (see Scheme 1). Besides the series of 4-bromoresorcinol compounds **BrF<sub>n</sub>** also some additional compounds (**HF12**, **FF12**, **ClF12**, **MF12**, **IF16**) required for proper comparisons were newly synthesized. DFT calculations provide information about the effects of the different substituents Y on the minimum energy conformations, which is related to the experimentally determined tendency to form DC phases of different types. A hypothesis is provided for the prediction of formation of DC phase depending on the molecular structure.

## 2. Experimental

### 2.1 Synthesis

The synthesis of the target BCLCs **BrF<sub>n</sub>** was performed by acylation of 4-bromoresorcinol with two equivalents of the appropriate 4-(4-*n*-alkoxy-3-fluorophenylazo)benzoyl chloride in the presence of triethylamine as base and pyridine as acylation catalyst (Scheme 2).<sup>49</sup> Details of synthesis of the intermediates and final compounds as well as analytical data are reported in the ESI.†

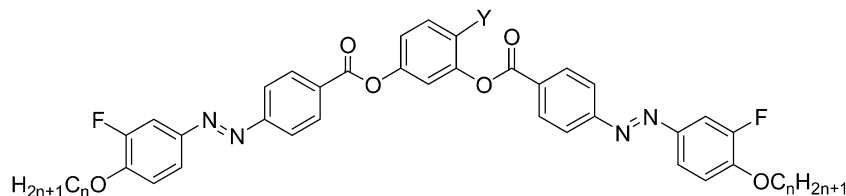
In analogy to the synthesis of compounds **BrF<sub>n</sub>** also the 4-substituted resorcinol based bent-core mesogens **HF12** (X = F, Y = H), **FF12** (X, Y = F), **ClF12** (X = F, Y = Cl), **MF12** (X = F, Y = CH<sub>3</sub>) and **IF16** (X = F, Y = I) have been synthesized. The analytical data and other details of these new compounds (see Table 1) are also reported in the ESI.†



**Scheme 2** Chemical structures and synthesis of compounds **BrF<sub>n</sub>**. *Reagents and conditions:* (i) NaNO<sub>2</sub>, HCl, H<sub>2</sub>O, 0 °C, 30 min; (ii) 1. 2-fluorophenol, NaOH, 0–5 °C, 3 h, 2. NaHCO<sub>3</sub>; (iii) C<sub>n</sub>H<sub>2n+1</sub>Br, K<sub>2</sub>CO<sub>3</sub>, KI, 2-butanone, reflux, 18 h; (iv) 1. KOH, EtOH, reflux, 8 h, (2) H<sup>+</sup>; (v) SOCl<sub>2</sub>, DMF, reflux, 1 h; (vi) TEA, pyridine, CH<sub>2</sub>Cl<sub>2</sub>, reflux, 6 h.



**Table 1** Phase transition temperatures ( $T/^\circ\text{C}$ ), mesophase types, and transition enthalpies [ $\Delta H/\text{kJ mol}^{-1}$ ] of the synthesized compounds **BrFn**, **IF16**, **HF12**, **FF12**, **ClF12** and **MF12**<sup>a</sup>



Compound	Y	n	1 <sup>st</sup> heating	1 <sup>st</sup> cooling
<b>BrF4</b>	Br	4	Cr 157 [57.7] Iso	Iso 117 [50.4] Cr
<b>BrF6</b>	Br	6	Cr 126 [45.9] Iso	Iso 96 [23.8] DC
<b>BrF8</b>	Br	8	Cr 119 [55.0] Iso	Iso 96 [25.9] DC
<b>BrF10</b>	Br	10	Cr 106 [19.0] Iso	Iso 99 [25.6] DC
<b>BrF12</b>	Br	12	Cr 106 [24.6] Iso	Iso 98 [25.7] DC
<b>BrF14</b>	Br	14	Cr 108 [67.2] Iso	Iso 99 [26.1] DC
<b>BrF16</b>	Br	16	Cr 100 [30.2] Iso	Iso 93 [28.5] <sup>b</sup> DC 89 [26.6] Cr
<b>BrF18</b>	Br	18	Cr 102 [30.5] Iso	Iso 89 [39.1] Cr
<b>IF16</b>	I	16	Cr 111 [20.7] Iso	Iso 104 DC 103 [28.5] <sup>c</sup> Cr
<b>HF12</b>	H	12	Cr <sub>1</sub> 81 [21.2] Cr <sub>2</sub> 138 [40.5] Iso	Iso 130 [16.5] Cr <sub>1</sub> 103 [34.2] Cr <sub>2</sub> 75 [21.6] Cr <sub>3</sub>
<b>FF12</b>	F	12	Cr 120 [60.2] Iso	Iso 116 [18.0] SmC <sub>a</sub> P <sub>A</sub> <sup>d</sup> 106 [45.0] Cr
<b>ClF12</b>	Cl	12	Cr 114 [51.3] Iso	Iso 95 [11.1] SmC <sub>a</sub> P <sub>A</sub> <sup>d</sup> 75 [37.1] Cr
<b>MF12</b>	CH <sub>3</sub>	12	Cr 90 [40.4] Iso	Iso 88 [13.9] SmC <sub>a</sub> P <sub>A</sub> <sup>d</sup> 72 [31.9] Cr

<sup>a</sup> Peak temperatures from DSC with rate 10 K min<sup>-1</sup>; for phase transitions in the second heating scan see Table S1; abbreviations: Cr = crystalline solid; DC = dark conglomerate phase; SmC<sub>a</sub>P<sub>A</sub> = antclinic tilted antiferroelectric SmC phase; Iso = isotropic liquid. <sup>b</sup> Obtained on cooling with 2 K min<sup>-1</sup>. <sup>c</sup> Transition enthalpy value could not be determined for the DC–Cr transition due to overlapping. <sup>d</sup> The spontaneous polarization value ( $P_s$ ) calculated in the SmC<sub>a</sub>P<sub>A</sub> phase for **FF12** is 460 nC cm<sup>-2</sup>; for **ClF12** is 480 nC cm<sup>-2</sup> and that for **MF12** is 640 nC cm<sup>-2</sup> (representative current response curves are shown in Fig. S11).

## 2.2 Methods

The mesophase behaviour and transition temperatures were measured using a Mettler FP-82 HT hot stage and a control unit in conjunction with a Nikon Optiphot-2 polarizing microscope. The associated enthalpies were obtained from DSC-thermograms which were recorded on a Perkin-Elmer DSC-7 with heating and cooling rates of 10 K min<sup>-1</sup>. Electro-optical switching characteristics were examined in 6 μm polyimide coated ITO cells (EHC Japan) using the triangular-wave method. XRD patterns were recorded with a 2D detector (Vantec-500, Bruker). Ni filtered and pin hole collimated CuK<sub>α</sub> radiation was used. The exposure time was 15 min and the sample to detector distance was 8.95 and 26.7 cm for wide angle and small angle scattering experiments, respectively. Samples were aligned by slow cooling (rate: 1 K min<sup>-1</sup> to 0.1 K min<sup>-1</sup>) of a small droplet on a glass plate and takes place at the sample–air interface. The samples were held on a temperature-controlled heating stage.

## 3. Results and discussion

### 3.1 Mesomorphic properties of compounds **BrFn** depending on terminal alkyl chain length

The phase sequences, transition temperatures (°C) and associated phase transition enthalpies (kJ mol<sup>-1</sup>) are summarized in Table 1 (see also Table S1† for data from the second heating scans). In the series of the bromosubstituted compounds **BrFn**

only the shortest homologue **BrF4** having a relatively high melting point at  $T = 157^\circ\text{C}$  is non-mesomorphic. Also for the next homologue **BrF6** a direct transition from the crystalline state to the isotropic liquid takes place on heating at 126 °C, but on cooling from the isotropic state a highly viscous optically isotropic mesophase appears at  $T = 96^\circ\text{C}$ , as indicated by microscopy between crossed polarizers. Rotating the analyzer by a small angle out of the precise 90° position leads to the appearance of dark and bright domains. Rotating the analyzer in the opposite direction reverses the dark and bright domains (see Fig. 1 for compound **BrF12**). Rotating the sample between crossed polarizers does not lead to any change and this indicates that the distinct regions represent chiral domains with opposite handedness, as typical for dark conglomerate phases (DC phases). No crystallization of this DC phase is observed upon cooling to room temperature. In the following heating cycles crystallization takes place either in the DC phase region or after transition of the DC phase to the isotropic liquid (see Fig. S1†). No crystallization is observed for any of the next homologues with  $n = 8$ –14 (see Table 1 and Fig. 2b), even after storage for one year at room temperature.

All compounds **BrF8**–**BrF14** have very similar transition temperatures. The melting of the DC phases (second heating scans) takes place around 106 °C and the formation of the DC phase on cooling occurs between 96 and 99 °C (see Table 1 and Fig. 2a). Hence, there is a supercooling of this phase transition by about 8 K (peak temperatures), which is found nearly



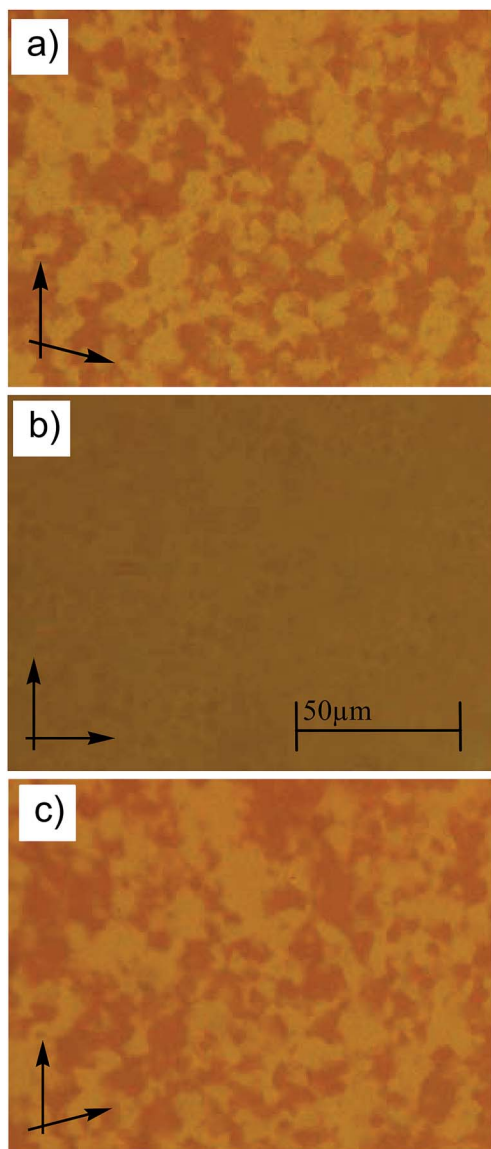


Fig. 1 Textures of the DC phase of compound **BrF12** at  $T = 80\text{ }^{\circ}\text{C}$ : (b) between crossed polarizers and (a) after rotating one polarizer by  $7^{\circ}$  from the crossed position in clock-wise direction and (c) in the anti-clockwise direction, showing dark and bright domains, indicating the presence of areas with opposite chirality sense.

independent of the scanning rate (2 or  $10\text{ K min}^{-1}$ ). The formation of the DC phases is associated with relatively high transition enthalpies, ranging between  $\Delta H \sim 23.8$  and  $28.5\text{ kJ mol}^{-1}$ , only slightly rising with growing chain length. Upon further chain elongation for **BrF16** with  $n = 16$ , the DC phase becomes unstable and immediately after its formation crystallization takes place. For the longest homologue **BrF18** ( $n = 18$ ) the DC phase is completely removed and only a birefringent crystalline phase is observed.

In electro-optical experiments no current peak could be observed in the DC phases of any of the prepared materials **BrF6–BrF14** and also no birefringence is induced under an applied triangular wave voltage up to  $200\text{ Vpp}$  in a  $6\text{ }\mu\text{m}$  ITO cell. This behaviour is similar to those known for soft crystalline

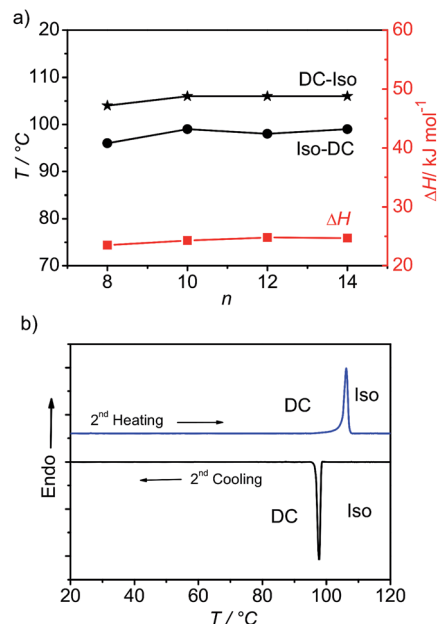


Fig. 2 (a) Dependence of DC–Iso transition temperatures (on heating and cooling scans with  $10\text{ K min}^{-1}$ ) and transition enthalpy values (on cooling from the isotropic liquid) of compounds **BrF8–BrF14** depending on alkyl chain length  $n$  and (b) DSC heating and cooling curves of compound **BrF12** with a rate of  $10\text{ K min}^{-1}$ .

HNF phases ( $B_4$  phases) and the DC phases of other related azobenzene based bent core mesogens,<sup>43,44</sup> but it is clearly distinct from most of the fluid sponge-like smectic phases.

XRD investigation of the DC phases of compounds **BrF6**, **BrF8**, **BrF12** and **BrF14** (see Fig. 3a and b, 4 and S2–5<sup>†</sup>) shows an intense reflection with  $d$ -values in between half of the molecular length  $L_{\text{mol}}/2$  and the full length  $L_{\text{mol}}$  (see Fig. 3c). For the determination of  $L_{\text{mol}}$  a  $120^{\circ}$  V-shaped conformation with all-*trans* alkyl chains was assumed (see Fig. S6<sup>†</sup>). The  $d/L_{\text{mol}}$  ratio was thus calculated to be in the range of 0.78–0.80 for all investigated compounds.

A linear increase of the  $d$ -values is observed with increasing length of the terminal chains from  $d = 3.46\text{ nm}$  for **BrF6** to  $d = 4.76\text{ nm}$  for **BrF14** (Fig. 3c). Thus the intense small angle scattering is assigned to a layer reflection. The  $d/L$  ratio around 0.78–0.80 would, according to  $d/L_{\text{mol}} = \cos \beta$ , allow a tilt angle of the molecules of around  $38^{\circ}$ . This relatively large difference between  $d$  and  $L_{\text{mol}}$  is similarly found for the DC phases of the related 4-iodo and 4-methylresorcinols **Ifn** and **Mn**,<sup>43,44</sup> but distinguishes these DC phases from the previously reported HNF phases where  $d$  is usually close to the molecular length.<sup>24,25</sup> No alignment could be achieved and therefore in the 2D patterns all scatterings form closed rings with uniform intensity distribution (see Fig. 3a). This is due to the disordered meso-scale structure, which is an inherent and very typical feature of all DC phases and leads to their optically isotropic appearance as well as to a broadening of the scattering; the domain size (determined using the Scherrer equation and assuming  $K = 1$ )<sup>50</sup> is in the range of 30–42 nm and grows with increasing alkyl chain length (see Fig. 3c).



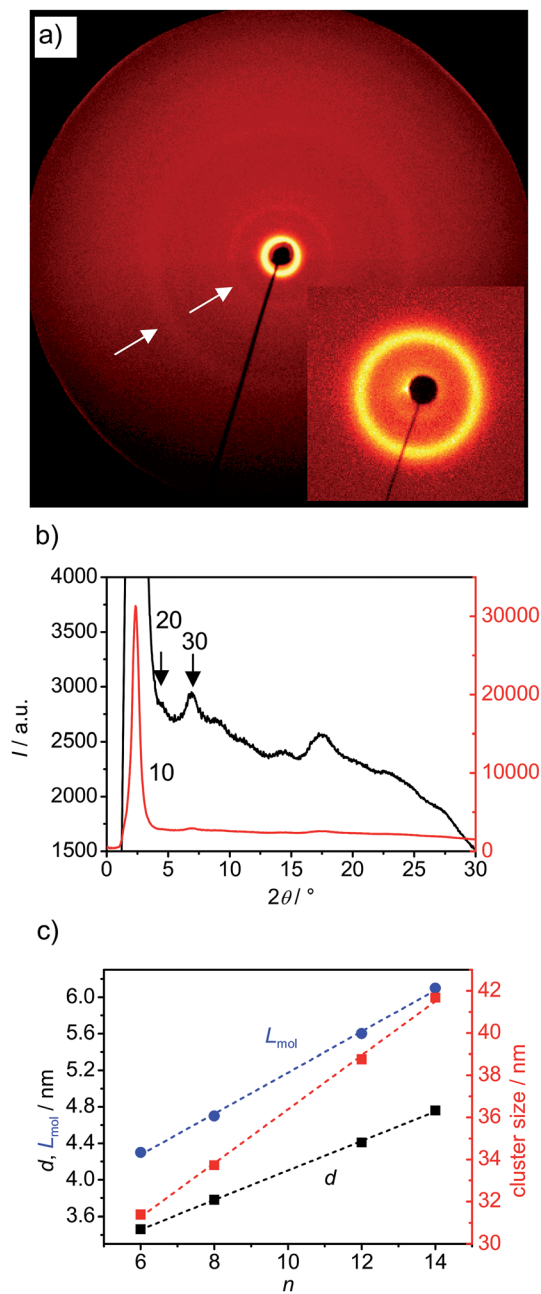


Fig. 3 (a) 2D XRD pattern of the DC phase of **BrF8** at  $T = 90\text{ }^{\circ}\text{C}$ , the inset shows the small angle region; (b)  $2\theta$ -scans over this XRD pattern; (c) dependence of  $d$ -values, molecular lengths ( $L_{\text{mol}}$ ; the used conformation is shown in Fig. S6†) and cluster size (determined using the Scherrer equation and assuming  $K = 1$ ) in the DC phases of compounds **BrF6**–**BrF14** on the chain length.

The  $2\theta$  scan over the diffraction pattern of compound **BrF8** is shown in Fig. 3b, those of compounds **BrF6**, **BrF12** and **BrF14** are collated in Fig. 4. Beside the strong layer reflections very weak and broad scattering maxima are observed in the medium angle region ( $2\theta = 5\text{--}9^{\circ}$ ) and in the wide angle region ( $2\theta = 14\text{--}28^{\circ}$ ). This pattern excludes fluid sponge phases, which would show exclusively one completely diffuse wide angle scattering besides the layer reflection. The wide angle scattering is, similarly to the HNF phases, characterized by several scattering

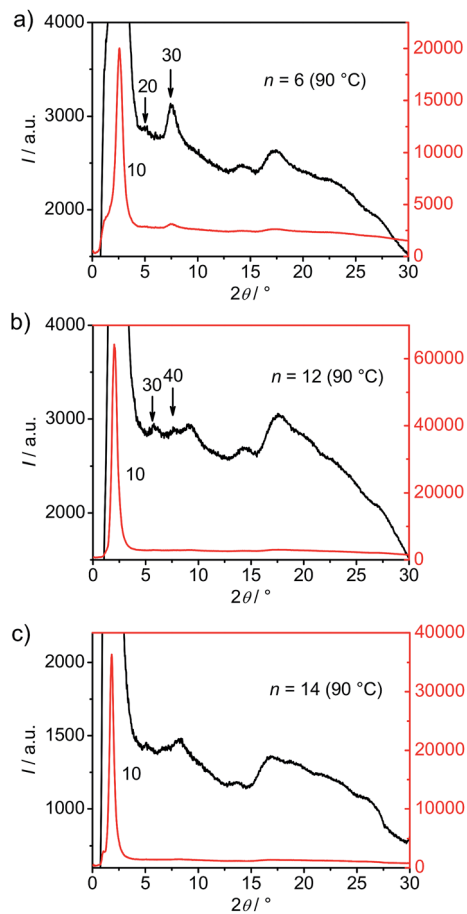


Fig. 4 Comparison of  $2\theta$ -scan over the XRD patterns of the DC phase of (a) **BrF6**, (b) **BrF12** and (c) **BrF14** at  $T = 90\text{ }^{\circ}\text{C}$  (for more details, see Fig. S2–S5†).

maxima up to  $2\theta = 28^{\circ}$ . However, in contrast to typical patterns of HNF phases ( $B_4$  phases, see Fig. 5b), the wide angle reflections are much broader and have significantly reduced intensity (compare red line in Fig. 5a with 5b, both shown in the logarithmic scale). For compounds **BrF8**–**BrF12** most reflections in the medium angle region can be indexed as harmonics (up to 4<sup>th</sup> order) of the layer reflection (see Fig. 4 and S2–S5†), as it is also the case for the previously reported **Mn** compounds<sup>44</sup> and usually found for HNF phases.<sup>18,24–26</sup> Only the XRD pattern of compound **BrF14**, the compound with the longest alkyl chain among the compounds with stable DC phases, appears a bit different from the others, as the medium angle scatterings cannot be assigned as higher order layer reflections and also the shape of the wide angle scattering is a bit different (Fig. 4c).

Fig. 5a shows a comparison of the  $2\theta$ -scans of the DC phases of the related compound **M14** ( $Y = \text{CH}_3$ ), **BrF14** ( $Y = \text{Br}$ ) and **I14** ( $Y = \text{I}$ ) all having the same chain length. It clearly indicates that, though the position of the 10 reflection is nearly identical in all cases, the positions and intensities of the medium and wide angle scattering maxima are very distinct for the halogen substituted compounds **I14** and **BrF14** compared to the methyl substituted compound **M14**. The scattering intensity of the iodo compounds **I14** is the lowest, followed by the bromine



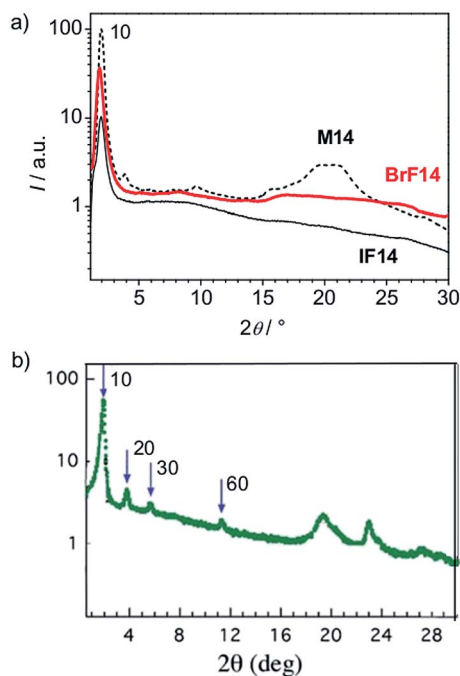


Fig. 5 (a) Comparison of the  $2\theta$ -scans of the DC phases of compounds **BrF14**, **IF14** and **M14** (base line is shifted for better visibility; the scattering intensity of the **IFn** compounds is so low that scattering by air contributes to the diffuse scattering in the medium angle range ( $5\text{--}10^\circ$ ) of the XRD pattern of these *l*-substituted compounds) and (b) typical  $2\theta$ -scans of a HNF phase (B<sub>4</sub> phase) of a benzylideneaniline based bent-core mesogen (P-8-OPIMB) reproduced with modifications and permission from ref. 21, copyright RSC 2009.

substituted compounds **BrFn** and compounds **Mn**. Though having a higher intensity the wide angle scattering profile of the bromo compound **BrF14** is similar to **IF14**, indicating similarities in the molecular organizations in their DC phases.

### 3.2 Investigation of mixtures of compounds **BrFn** with 5-CB

It is known that HNF phases of benzylideneanilines can be diluted by nematic LC hosts to a high degree (>95%) without loss of the chirality.<sup>51</sup> This is a direct consequence of the helical nano-filament structure of these phases, allowing a swelling of the filaments by the nematic LC and transfer of chirality from the nano-filaments to the nematic LC. This effect is not observed for the sponge type liquid crystalline DC phases involving distorted fluid smectic layers. Therefore, investigation of mixtures with 4'-*n*-pentyl-4-cyanobiphenyl (5-CB) could be used as a tool providing additional information about the microstructure of the DC phases of compounds **BrFn**.

The 1 : 1 mixtures of **BrF8** or **BrF10** with 5CB do not show any DC phase. On heating these mixtures only a direct transition from the crystalline material to the isotropic liquid state occurs at  $57^\circ\text{C}$  and  $54^\circ\text{C}$ , respectively (Table 2). On cooling both of these mixtures form a nematic phase which crystallizes with formation of highly birefringent crystalline phases at  $T \sim 36^\circ\text{C}$  and  $33^\circ\text{C}$ , respectively (see Table 2), but no DC phase is formed. The next homologue **BrF12** behaves differently; on heating this

Table 2 Phase transition temperatures and mesophase types of 1 : 1 mixtures of 5-CB and compounds **BrF8**–**BrF18** and comparison with related 4-methylresorcinol derivatives **M14**–**M18**<sup>a</sup> (ref. 44)

Mixture	Heating $T$ / °C	Cooling $T$ / °C
<b>BrF8</b> + 5-CB	Cr 57 Iso	Iso 43 N 36 Cr
<b>BrF10</b> + 5-CB	Cr 54 Iso	Iso 42 N 33 Cr
<b>BrF12</b> + 5-CB	Cr <sup>[*]</sup> 40 DC 55 Iso	Iso 53 DC 38 Cr <sup>[*]</sup>
<b>BrF14</b> + 5-CB	Cr 38 DC 64 Iso	Iso 46 DC 35 Cr
<b>BrF16</b> + 5-CB	Cr <sub>1</sub> 33 Cr <sub>2</sub> 69 Iso	Iso 63 Cr
<b>BrF18</b> + 5-CB	Cr <sub>1</sub> 42 Cr <sub>2</sub> 75 Iso	Iso 65 Cr
<b>M14</b> + 5-CB	Cr 85 Iso	Iso 54 N 53 Cr
<b>M16</b> + 5-CB	Cr 64 DC 73 Iso	Iso 66 DC
<b>M18</b> + 5-CB	DC 77 Iso	Iso 77 DC

<sup>a</sup> Transition temperatures were taken from the observed textures using the polarized optical microscopy; abbreviations: N = nematic phase; Cr<sup>[\*]</sup> = crystalline phase composed of a conglomerate of chiral domains; for other abbreviations please see Table 1.

mixture a transition from the crystalline phase to the DC phase occurs at  $40^\circ\text{C}$  (see Fig. S7d–f†). On further heating a transition from the DC phase to the isotropic liquid takes place at  $55^\circ\text{C}$ . On cooling this mixture from the isotropic liquid the transition to the DC phase takes place at  $T \sim 53^\circ\text{C}$  followed by crystallization at  $38^\circ\text{C}$ . Interestingly, this crystalline phase is nearly isotropic and composed of domains with opposite handedness (see Fig. S7a–c†). The mixture of the next homologue **BrF14** shows similar behaviour to that of **BrF12**, except that this weakly birefringent crystalline phase is achiral or the chiral domains are too small to be detected. Mixing the longer crystalline compounds **BrF16** and **BrF18** with 5-CB does not give any DC phases (see Table 2).

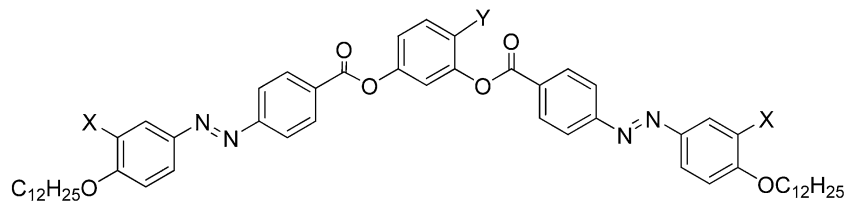
The significant destabilization of the DC phases by 5-CB confirms that the DC phases of compounds **BrFn** should be different from the classical HNF phases.<sup>21,24–26</sup> It appears that these phases are formed by smaller nano-domains instead of long helical nano-filaments, in line with the results of the XRD studies showing relatively broad wide angle scatterings. Because no extended filaments are formed, no gel-like networks of these fibers are possible and therefore these compounds can take up only a limited amount of 5-CB, which is directly incorporated between the bent-core molecules and thus reduces the stability of the DC phases. The highest tendency for DC phase formation appears to be provided by the medium chain compounds **BrF12** and **BrF14**. Comparison with results obtained with related compounds indicate that the 5-CB mixtures of compounds **BrFn** behave very similar to the 5-CB mixtures of the iodo compounds **IFn**,<sup>43</sup> whereas for the 4-methylresorcinols **Mn** the DC phases in the mixtures have higher stability and their regions are shifted to longer alkyl chain lengths (Table 2), indicating slightly more stable aggregates.

### 3.3 Comparison of different types of 4-substituted resorcinol based BCLCs with azobenzene units

In Table 3 compound **BrF12** is compared with the non-substituted compound **H12** (ref. 52) and related BCLCs with



**Table 3** Phase transition temperatures ( $T/^\circ\text{C}$ ) and mesophase types as observed for different types of 4-substituted resorcinols (Y) with azobenzene wings and the effect of peripheral F-atoms (X = H, F)<sup>a</sup>



Compound	Y	$cv^b/\text{nm}^3$	$\mu^c/\text{D}$	X	$T/^\circ\text{C}$	Ref.
<b>H12</b>	H	7		H	Cr 145 Iso	52
<b>HF12</b>	H			F	Cr 138 Iso	
<b>F12</b>	F	13	1.60	H	Cr 120 Iso	47
<b>FF12</b>	F			F	Cr 120 (SmCP <sub>A</sub> 119) Iso	
<b>Cl12</b>	Cl	27	1.69	H	Cr <sub>1</sub> 90 Cr <sub>2</sub> 103 (N 97) Iso	47
<b>ClF12</b>	Cl			F	Cr 115 (SmCP <sub>A</sub> 97) Iso	
<b>Br12</b>	Br	33	1.70	H	Cr (N 83) 93 Iso	47
<b>BrF12</b>	Br			F	<b>DC 106 Iso</b>	
<b>I12</b>	I	45	1.70	H	Cr 112 Iso	43
<b>IF12</b>	I			F	<b>DC 111 Iso</b>	43
<b>M12</b>	CH <sub>3</sub>	32	0.37	H	<b>DC 102 Iso</b>	44
<b>MF12</b>	CH <sub>3</sub>			F	Cr 90 SmCP <sub>A</sub> 92 Iso	
<b>CN12</b>	CN	23	4.18	H	Cr 71 (SmC <sub>s</sub> P <sub>A</sub> 70) M <sub>1</sub> 75 SmC <sub>s</sub> P <sub>F</sub> 83 SmC <sub>s</sub> P <sub>R</sub> <sup>[*]</sup> 96 SmC 127 N 137 Iso	32
<b>CNF12</b>	CN			F	Cr 104 SmC <sub>s</sub> P <sub>A</sub> 108 SmC <sub>s</sub> P <sub>R</sub> <sup>[*]</sup> 135 SmA 147 Iso	<sup>d</sup>

<sup>a</sup> Abbreviations: N = nematic phase; SmA = nonpolar smectic A phase; SmC = paraelectric smectic C phase; SmC<sub>s</sub>P<sub>R</sub><sup>[\*]</sup> = synclitic tilted SmC phase composed of SmC<sub>s</sub>P<sub>F</sub> domains with randomized polar directions, homeotropically aligned samples of this phase are composed of a conglomerate of chiral domains; SmC<sub>s</sub>P<sub>F</sub> = polar SmC phase composed of enlarged ferroelectric domains; M<sub>1</sub> = highly viscous antiferroelectric switching SmC phase; SmCP<sub>A</sub> = antiferroelectric switching SmC phase (B2 phase); SmC<sub>s</sub>P<sub>A</sub> = synclitic tilted antiferroelectric SmC phase (B2 phase); for other abbreviations see Table 1. <sup>b</sup> Crystal volumes of Immirzi.<sup>53</sup> <sup>c</sup> Dipole moments of the corresponding phenyl derivatives.<sup>54</sup> <sup>d</sup> Unpublished data.

other substituents in the 4-position of the resorcinol core, like halogens (Y = F, Cl, I), methyl and cyano. Comparison of the different azobenzene based BCLCs (all with  $n = 12$ ) indicates that there is a tendency for reduction of the melting points by the substituents Y which becomes the more important the larger these substituents are. Thus LC phases can be observed for most of the 4-substituted compounds, whereas the non-substituted compounds **H12** and **HF12** represent relatively high melting solids. There appears to be a dependence of the phase type on the volume of Y (crystal volumes  $cv$  of Immirzi<sup>53</sup>) and the polarity of the C–Y bond (dipole moments  $\mu$  of the Ph–Y compounds<sup>54</sup>). For molecules with X = H and having polar substituents Y at the resorcinol core no LC phase is observed (Y = F, I) or nematic phases are dominating (Y = Cl, Br, CN), whereas the nonpolar methyl group is obviously favourable for the formation of DC phases (compound **M12**). Introducing peripheral F-substituents increases the tendency for formation of polar SmC phases (SmCP<sub>A</sub>) if the 4-substituent is small (Y = F, Cl, CN). Formation of DC phases is only supported by peripheral fluorination of BCLCs with large and polar substituents Y (Y = Br, I).

So, overall, large substituents in the 4-position at the resorcinol core appear to be favourable for DC phase formation, although there is an additional effect of peripheral F-substitution. Obviously the effect of peripheral fluorine substitution is the reverse for BCLCs with polar and non-polar substituents

Y. While for the methyl-substituted compounds the introduction of F removes the DC phase and a SmCP<sub>A</sub> phase is formed, for compounds with large polar halogens (Br, I) introduction of peripheral F-substitution induces DC phases. The reason for this behaviour is not yet clear.

As can be deduced from the comparison in Fig. 2a and 6a, the transition enthalpy values of the DC–Iso transitions and the corresponding transition enthalpy values of the iodine substituted compounds **IF8–IF14** and for the bromine substituted analogues **BrF8–BrF14** are in the same range, once again confirming the similarity between the DC phases of the two series, already concluded from the similarity of the XRD patterns. Nevertheless, the DC–Iso transition temperatures and the related transition enthalpy values of compounds **IFn** are slightly higher (by  $\sim 3$  to 10 K and  $\sim 2$  to 6 kJ mol<sup>-1</sup>, respectively) than those of their bromine substituted analogues **BrFn**. This might be due to the increased polarizability provided by iodine, increasing the attractive dispersion forces between the molecules. In line with increased intermolecular interactions a denser packing of compounds **IFn** could provide a stronger effect of molecular conformational chirality (helicity) on the aggregate stability and aggregate size. Also the observation that compounds **IF8–IF14** exhibit exclusively the DC phases and do not show any crystallization, while compounds **BrF8–BrF14** show crystalline phases in the first heating and thus form monotropic DC phases (though, the DC phases once formed



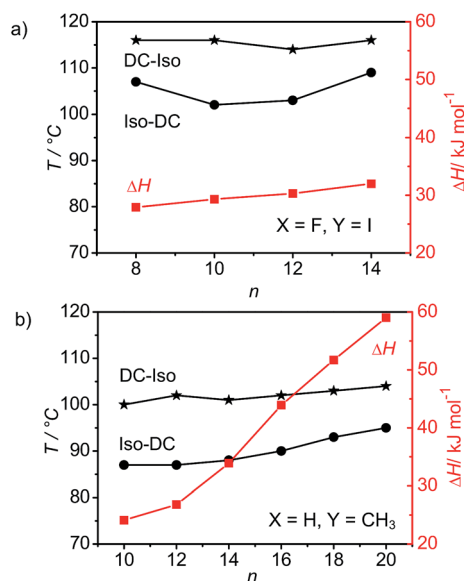


Fig. 6 Dependence of DC–Iso transition temperatures (on heating and cooling scans with  $10 \text{ K min}^{-1}$ ) and transition enthalpy values (on cooling from the isotropic liquid) of two series of compounds related to **BrFn** (a) the 4-iodine-substituted compounds **IF8–IF14** (ref. 43) and (b) the 4-methyl-substituted compounds **M10–M20** (ref. 44) depending on the alkyl chain length  $n$ .

also do not crystallize) is in line with a stronger distortion of the long range molecular packing in the case of the iodo compounds. This could be attributed to the larger size of iodine compared to Br, which could provide a stronger helical twist of the molecular conformations.

Comparison of the series **BrFn** (Fig. 2a) with the methyl-substituted compounds **Mn** (Fig. 6b) with chain length  $n = 10$ – $14$  indicates about  $10 \text{ K}$  higher DC–Iso transition temperatures for the compound having the more polar bromine substituent (and an additional peripheral F-substituent). The DC–Iso transition enthalpy values are comparable in both series, but for compound **Mn** there is a much stronger enthalpy increase upon chain elongation and in this case alkyl chain crystallization significantly contributes to the transition enthalpies.<sup>44</sup> There are clear difference also in the XRD patterns of the methyl substituted and the halogen substituted BCLCs (see Fig. 5a), indicating that the DC phases of compounds **Mn** are different from those of **BrFn** and **IFn**. The presence of only lower harmonics (up to the 4<sup>th</sup>) of the layer reflections (5<sup>th</sup> and 6<sup>th</sup> order harmonics of the layer reflections has been reported for typical  $B_4$  phases, see for example Fig. 5b (ref. 21)) and the significantly increased broadness of the wide angle scatterings indicates a stronger distortion of layer structures and filament formation in the case of the halogen substituted compounds. This is also in line with the reduced resistance of the DC phases of compounds **BrFn** and **IFn** against dilution with the nematic phase of 5-CB (see Table 2).

DFT calculations of the model compounds **F1**, **Br1**, **I1**, **M1** and **CN1** with  $n = 1$  were performed with the Gaussian 09 package,<sup>55</sup> using the B3LYP functional and LANL2DZ basis set using the solvation model IEFPCM in solvent chlorobenzene to

investigate the effects of the 4-substituents on the bending angle ( $\gamma$ ) and on the twist of the wing groups in the lowest energy conformation. The results are summarized in Fig. 7 where two different projections are shown and in Table 4, providing numerical values of bending angles  $\gamma$  and twist angles  $\alpha$  and  $\beta$ . In Fig. 7a the view is perpendicular to the resorcinol ring and in Fig. 7b the view is parallel to this ring along the wing in the 3-position. For all compounds, except **CN1**, the bending angle  $\gamma$  is not significantly affected by the 4-substituent and is around  $120$ – $123^\circ$  in all cases (see Fig. 7a and Table 4). Only for **CN1** it is increased to about  $130^\circ$  due to the dipole interactions between the CN group and the adjacent C=O group, in line with previous investigations.<sup>56</sup> This contributes to the very different behaviour of the cyanoresorcinols **CNn** (ref. 31 and 32) compared to the other considered compounds (see Table 3).

The azobenzene units themselves are linear and the benzene rings in these wings as well as the C=O groups of the carboxylate groups are nearly coplanar in all cases. Different minimum energy conformations result from the twist of the planes of the azobenzene wings with respect to the resorcinol core and thus to each other, leading to chiral conformers for all investigated compounds. The angle  $\alpha_1$ , which describes the twist between the plane of the azobenzene wing in the 1-position with respect to the plane of the resorcinol core, is around  $50^\circ$  for all halogen substituted compounds. Larger differences can be found for the twist  $\alpha_2$  of the azobenzenes in the 3-position which changes between  $\alpha_2 = 49$  and  $109^\circ$  (see Fig. 7b and Table 4). Overall, the effective twist between the planes of the two azobenzene wings  $\beta$  increases in the order  $F < Br < CH_3 < I$  roughly in line with the growing size of the 4-substituent (see cv in Table 3; only the effect of the  $CH_3$  group is larger than that of Br though their volumes are nearly equal). This is in line with the observed tendency of these molecules to form DC phases. Accordingly, no DC phase was found for any of the resorcinol and 4-fluororesorcinol derivatives, whereas DC phases were found for compounds with  $Y = Br, CH_3$  and  $I$ . Although for  $Y = CN$  the twist angle  $\beta$  is the largest, these molecules behave differently, due to the increased bending angle ( $\gamma \sim 130^\circ$ ) and the possibility of antiparallel compensation of the very large dipoles of these groups. Therefore, these CN-substituted compounds do not form DC phases, but preferably form nematic and SmC phases. Nevertheless, the large twist in the low energy conformation might be responsible for the formation of chiral domains in some of the birefringent SmC phases of these compounds ( $SmC_sP_R^{[*]}$ ).<sup>31,32</sup>

Based on the combination of experimentally observed structure property relationships (Table 3) and results of DFT calculations the following relationships between the molecular structure and formation of DC phases can be hypothesized. As the azobenzene wings are completely flat the only source of conformational chirality is in this case the central part of the molecules, *i.e.* the connections between the resorcinol core and azobenzene wings. For this reason the substitution in position 4 at the resorcinol is important and has a significant effect on the molecular conformation and hence the ability to form DC phases. Due to the rigidity of the azobenzenes the



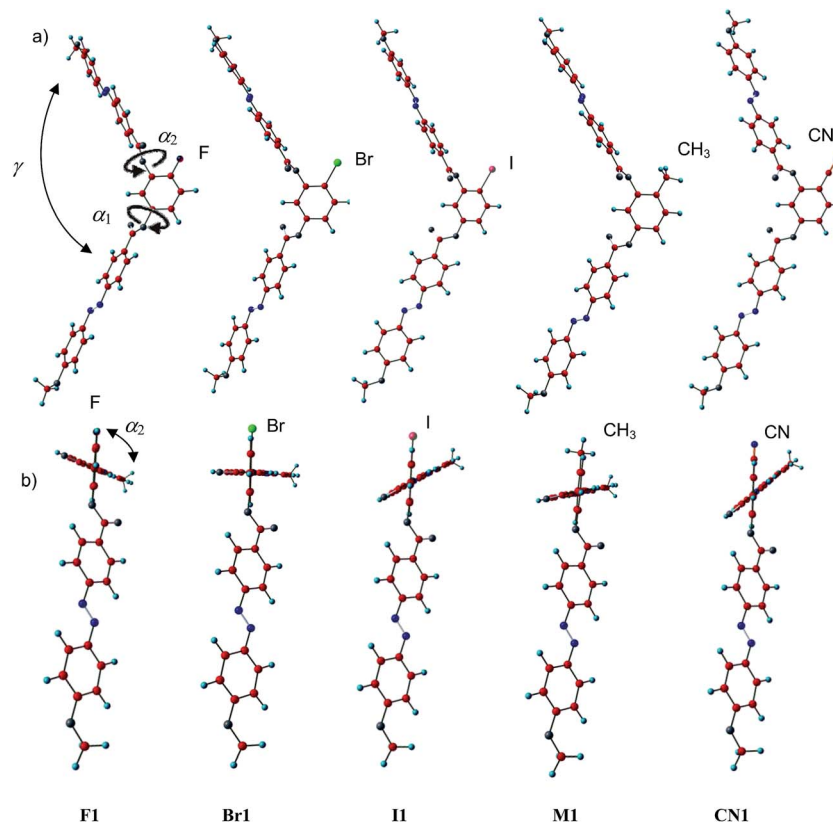


Fig. 7 Energy minimized molecular conformers of the model compounds ( $n = 1$ ) as observed under two distinct perspectives, (a) perpendicular to the plane of the resorcinol core indicating changes of the bending angle  $\gamma$  and (b) along the azobenzene wing in the 3-position and parallel to the plane of the resorcinol core, indicating the distinct degrees of twist between the two planes of the azobenzene wings; the angles  $\alpha_1$ ,  $\alpha_2$  and  $\gamma$  are explained for F1.

Table 4 Selected parameters of the energy minimized conformers obtained by DFT calculations of the distinct model compounds Y1 ( $n = 1$ ) depending on the 4-substituent Y at the resorcinol core<sup>a</sup>

Y	$\alpha_1/^\circ$	$\alpha_2/^\circ$	$\beta/^\circ$	$\gamma/^\circ$
F	50.9	109.1	31.8	121.5
Br	48.8	89.8	41.4	120.1
I	49.8	58.1	72.1	123.4
CH <sub>3</sub>	53.6	72.4	54.0	119.9
CN	44.8	49.0	86.2	129.7

<sup>a</sup>  $\beta$  = twist between the planes of the azobenzenes, calculated according to  $\beta = (90 - \alpha_1) + (90 - \alpha_2)$ , where  $\alpha_1$  and  $\alpha_2$  represent the twist angles of the planes of the azobenzenes with respect to the plane of the resorcinol unit, ( $\alpha_1$  azobenzene in the 1-position,  $\alpha_2$  in the 3 position);  $\gamma$  = bending angle which is calculated as the angle between the lines connecting the terminal ether oxygens at the azobenzenes with the carbon atoms 1 and 3 of the resorcinol core, respectively.

conformational chirality provided by the core has a strong effect on the overall molecular shape, providing a strong distortion to any packing in layers/filaments, thus leading to strongly distorted types of semicrystalline DC phases.<sup>57</sup> In contrast, other typical wing groups such as phenylbenzoates,<sup>2</sup> benzylideneanilines<sup>58</sup> and biphenyls<sup>2</sup> can themselves easily adapt twist conformations and can therefore contribute to the overall conformational chirality. In line with this, for such compounds

a bulky substituent in the central core unit is not required for DC phase formation. Moreover, as the helical twist can arise in the peripheral wing units the molecular shape is less distorted and such compounds can more easily adapt to the organization in twisted layers and extended helical filaments, predominately leading to the previously reported types of DC phases, the LC smectic sponges (phenyl benzoates) and the soft crystalline HNF phases (benzylidene anilines), respectively.

## 4. Conclusions and summary

Bent-core molecules derived from 4-bromoresorcinol with peripherally fluorinated azobenzene wings (**BrFn**) represent new materials forming optically isotropic DC phases composed of conglomerates of uniformly chiral domains, which can be observed for a chain length range  $n = 8$ –14 as the only mesophase, whereas shorter and longer homologues form only birefringent crystalline phases. The DC phases of compounds with  $n = 10$ –14 are stable down to ambient temperature and do not crystallize even after prolonged storage. For related compounds without the peripheral fluoro substitution (**Brn**) a DC phase was observed for only one homologue ( $n = 10$ ) as a monotropic phase, whereas the other homologues form monotropic nematic and B<sub>6</sub> phases.<sup>47</sup> This indicates a strong DC phase stabilizing effect of peripheral F substitution in this case, which is reverse to the





4-methylresorcinols, for which DC phases were found for the non-fluorinated compounds **Mn** whereas the fluorinated compounds **MFn** form antiferroelectric switching SmCP<sub>A</sub> phases (B2 phases).<sup>44</sup> XRD investigations and the relatively high viscosity of these DC phases indicate that they do not belong to the fluid sponge type smectic LC phases, but are more related to the soft crystalline HNF phases. However, in contrast to the classical HNF phases the helical nano-filaments appear to be not well developed, so that the helical twist gives rise to a strongly disordered structure formed by nanoscale twisted domains of crystallized aromatic cores separated by disordered alkyl chains. In this way the DC phases are similar to those formed by the related 4-iodoresorcinol derivatives,<sup>43</sup> but distinct from those formed by the previously reported B<sub>4</sub> type HNF phases of the benzylideneanilines.<sup>24</sup> It is thought that for the compounds **BrFn** the filaments are disrupted into smaller segments, as also proposed for the methyl substituted compounds **Mn**, and it appears that the degree of disruption increases in the order **Mn** < **BrFn** < **IFn**.

DFT calculations allowed the estimation of the effects of the substituents Y on the minimum energy conformers. This indicates that the azobenzenes themselves are flat and that mainly steric effects of the substituent Y lead to an increase of the twist between the planes of the azobenzene wings with increasing size of Y. This appears to be favourable for chiral segregation and layer distortion, due to the difficulty in the parallel packing of these highly twisted molecular species. The strong layer distortion is thought to be responsible for the preferred formation of twisted nano-domains instead of sponge-like deformed layers or extended helical nano-filaments.

The effect of polarity on the molecular conformation is the strongest for the CN substituted compounds, giving rise to a less bent (more rod-like) molecular shape, which appears to be unfavourable for formation of DC phases, but favours the formation of nematic and SmC phases. Nevertheless, the strong twist between the planes of the azobenzenes leads to a high “strength of chirality” of the energy minimum conformers which allows chiral segregation even in some of their polarization randomized SmC phases (SmC<sub>2</sub>P<sub>R</sub><sup>[\*]</sup> phases).

In summary, the development of new types of DC phases depending on the molecular structure was investigated in a systematic way. Relationships between the molecular structure and formation of distinct types of DC phases were found and possible reasons for these relationships were hypothesized. We believe that this study will contribute to the improvement of the general knowledge about DC phases and the mechanisms of achiral symmetry breaking in soft matter as well as to the design of new molecules showing DC phases. BCLCs involving azo linkages are also very versatile materials due to their photochromic effects and high birefringence. Moreover, the *trans-cis* photoisomerization of the azobenzene wings in these BCLCs could lead to interesting perspectives for chirality switching and phase modulation by interaction with nonpolarized, linear or circular polarized light, *i.e.* to unique and potentially useful multifunctional chiral materials for application in high-density data storage systems, sensors, photonic switches and molecular logic gates,<sup>59,60</sup> as well as with potential for discrimination of chiral physical forces and molecular species.

## Acknowledgements

M. Alaasar is grateful to the Alexander von Humboldt Foundation for the research fellowship at the Martin-Luther University Halle-Wittenberg, Germany.

## References

- (a) R. A. Reddy and C. Tschierske, *J. Mater. Chem.*, 2006, **16**, 907; (b) H. Takezoe and Y. Takanishi, *Jpn. J. Appl. Phys.*, 2006, **45**, 597; (c) A. Eremin and A. Jakli, *Soft Matter*, 2013, **9**, 615.
- H. Takezoe, *Top. Curr. Chem.*, 2012, **318**, 303.
- (a) F. Vera, J. L. Serrano and T. Sierra, *Chem. Soc. Rev.*, 2009, **38**, 781; (b) M. Lehmann, M. Jahr, B. Donnio, R. Graf, S. Gemming and I. Popov, *Chem.–Eur. J.*, 2008, **14**, 4414; (c) C. Roche, H.-J. Sun, M. E. Prendergast, P. Leowanawat, B. E. Patridge, P. A. Heiney, F. Araoka, R. Graf, H. W. Spiess, X. Zeng, G. Ungar and V. Percec, *J. Am. Chem. Soc.*, 2014, **136**, 7169–7185; (d) M. H. C. J. V. Houtem, F. Benaskar, C. F. C. Fitié, R. Martín-Rapún, J. A. J. M. Vekemans and E. W. Meijer, *Org. Biomol. Chem.*, 2012, **10**, 5898; (e) R. Q. Albuquerque, A. Timme, R. Kress, J. Senker and H.-W. Schmidt, *Chem.–Eur. J.*, 2013, **19**, 1647.
- H. Nagayama, S. K. Varshney, M. Goto, F. Araoka, K. Ishikawa, V. Prasad and H. Takezoe, *Angew. Chem.*, 2010, **49**, 445.
- (a) D. Pijper and B. L. Feringa, *Soft Matter*, 2008, **4**, 1349; (b) K. Maeda and E. Yashima, *Top. Curr. Chem.*, 2006, **265**, 88; (c) C. C. Lee, C. Grenier, E. W. Meijer and A. P. H. J. Schenning, *Chem. Soc. Rev.*, 2009, **38**, 671; (d) W. Jin, Y. Yamamoto, T. Fukushima, N. Ishii, J. Kim, K. Kato, M. Takata and T. Aida, *J. Am. Chem. Soc.*, 2008, **130**, 9434.
- J. V. Selinger, M. S. Spector and J. M. Schnur, *J. Phys. Chem. B*, 2001, **105**, 1757.
- E. Barry, Z. Hensel, Z. Dogic, M. Shribak and R. Oldenbourg, *Phys. Rev. Lett.*, 2006, **96**, 018305.
- A. Lohr and F. Würthner, *Angew. Chem., Int. Ed.*, 2008, **47**, 1232.
- (a) E. Yashima, K. Maeda, H. Iida, Y. Furusho and K. Nagai, *Chem. Rev.*, 2009, **109**, 6102; (b) H. Jinnai, T. Kaneko, K. Matsunaga, C. Abetz and V. Abetz, *Soft Matter*, 2009, **5**, 2042.
- D. B. Amabilino, *Chirality at the Nanoscale*, VCH-Wiley Weinheim, 2009.
- D. R. Link, G. Natale, R. Shao, J. E. MacLennan, N. A. Clark, E. Körblová and D. M. Walba, *Science*, 1997, **278**, 1924.
- E. A. Matsumoto, G. P. Alexander and R. D. Kamien, *Phys. Rev. Lett.*, 2009, **103**, 257804.
- (a) G. Dantlgraber, A. Eremin, S. Diele, A. Hauser, H. Kresse, G. Pelzl and C. Tschierske, *Angew. Chem., Int. Ed.*, 2002, **41**, 2408; (b) G. Dantlgraber, S. Diele and C. Tschierske, *Chem. Commun.*, 2002, 2768; (c) C. Tschierske and G. Dantlgraber, *Pramana*, 2003, **61**, 455; (d) C. Keith, R. A. Reddy, A. Hauser, U. Baumeister and C. Tschierske, *J. Am. Chem. Soc.*, 2006, **128**, 3051; (e) C. Keith, R. A. Reddy, U. Baumeister, H. Hahn, H. Lang and C. Tschierske, *J. Mater. Chem.*, 2006, **16**, 3444; (f) H. Hahn, C. Keith,



- H. Lang, R. A. Reddy and C. Tschierske, *Adv. Mater.*, 2006, **18**, 2629; (g) C. Keith, G. Dantlgraber, R. A. Reddy, U. Baumeister, M. Prehm, H. Hahn, H. Lag and C. Tschierske, *J. Mater. Chem.*, 2007, **17**, 3796; (h) C. Keith, G. Dantlgraber, R. A. Reddy, U. Baumeister and C. Tschierske, *Chem. Mater.*, 2007, **19**, 694; (i) Y. Zhang, U. Baumeister, C. Tschierske, M. O'Callaghan and C. Walker, *Chem. Mater.*, 2010, **22**, 2869.
- 14 L. E. Hough, M. Spannuth, M. Nakata, D. A. Coleman, C. D. Jones, G. Dantlgraber, C. Tschierske, J. Watanabe, E. Körblova, D. M. Walba, J. E. MacLennan, M. A. Glaser and N. A. Clark, *Science*, 2009, **325**, 452.
- 15 G. Heppke, D. D. Parghi and H. Sawade, *Liq. Cryst.*, 2000, **27**, 313.
- 16 J. Thisayukta, Y. Nakayama, S. Kawauchi, H. Takezoe and J. Watanabe, *J. Am. Chem. Soc.*, 2000, **122**, 7441.
- 17 R. A. Reddy and B. K. Sadashiva, *Liq. Cryst.*, 2003, **30**, 1031.
- 18 A. Roy, M. Gupta, S. Radhika, B. K. Sadashiva and R. Pratibha, *Soft Matter*, 2012, **8**, 7207.
- 19 J. Ortega, C. L. Folcia, J. Etxebarria, N. Gimeno and M. B. Ros, *Phys. Rev. E: Stat., Nonlinear, Soft Matter Phys.*, 2003, **68**, 11707.
- 20 T. Niori, T. Sekine, J. Watanabe, T. Furukawa and H. Takezoe, *J. Mater. Chem.*, 1996, **6**, 1231.
- 21 J. M. Perdiguero, I. Alonso, C. L. Folcia, J. Etxebarria and J. Ortega, *J. Mater. Chem.*, 2009, **19**, 5161.
- 22 C. Zhang, N. Diorio, O. D. Lavrentovich and A. Jáklí, *Nat. Commun.*, 2014, **5**, 3302.
- 23 (a) A. Jáklí, Y.-M. Huang, K. Fodor-Csorba, A. Vajda, G. Galli, S. Diele and G. Pelzl, *Adv. Mater.*, 2003, **15**, 1606; (b) W. Weissflog, M. W. Schröder, S. Diele and G. Pelzl, *Adv. Mater.*, 2003, **15**, 630.
- 24 (a) L. E. Hough, H. T. Jung, D. Kröuerke, M. S. Heberling, M. Nakata, C. D. Jones, D. Chen, D. R. Link, J. Zasadzinski, G. Heppke, J. P. Rabe, W. Stocker, E. Körblova, D. M. Walba, M. A. Glaser and N. A. Clark, *Science*, 2009, **325**, 456; (b) D. M. Walba, L. Eshat, E. Körblova and R. K. Shoemaker, *Cryst. Growth Des.*, 2005, **5**, 2091; (c) D. Chen, J. E. MacLennan, R. Shao, D. K. Yoon, H. Wang, E. Körblova, D. M. Walba, M. A. Glaser and N. A. Clark, *J. Am. Chem. Soc.*, 2011, **133**, 12656.
- 25 (a) J. Thisayukta, H. Takezoe and J. Watanabe, *Jpn. J. Appl. Phys.*, 2001, **40**, 3277; (b) H. Niwano, M. Nakata, J. Thisayukta, D. R. Link, H. Takezoe and J. Watanabe, *J. Phys. Chem. B*, 2004, **108**, 14889; (c) H. Kurosu, M. Kawasaki, M. Hirose, M. Yamada, S. Kang, J. Thisayukta, M. Sone, H. Takezoe and J. Watanabe, *J. Phys. Chem. A*, 2004, **108**, 4674.
- 26 H. Kresse, J. Saltetnokova, H. Nadasi, W. Weissflog and A. Hauser, *Liq. Cryst.*, 2001, **28**, 1017.
- 27 Biphenyl based dimesogens: (a) E. Bialecka-Florjanczyk, I. Sledzinska, E. Górecka and J. Przedmojski, *Liq. Cryst.*, 2008, **35**, 401; (b) A. Zep, M. Salamonczyk, N. Vaupotič, D. Pocięcha and E. Gorecka, *Chem. Commun.*, 2013, **49**, 3119.
- 28 (a) H. Ocak, B. Bilgin-Eran, M. Prehm and C. Tschierske, *Soft Matter*, 2012, **8**, 7773; (b) H. Ocak, B. Bilgin-Eran, M. Prehm and C. Tschierske, *Soft Matter*, 2013, **9**, 4590.
- 29 E. Tsai, J. M. Richardson, E. Körblova, M. Nakata, D. Chen, Y. Shen, R. Shao, N. A. Clark and D. M. Walba, *Angew. Chem., Int. Ed.*, 2013, **52**, 5254.
- 30 G. B. Deepa, S. Radhika, B. K. Sadashiva and R. Pratibha, *Phys. Rev. E: Stat., Nonlinear, Soft Matter Phys.*, 2013, **87**, 062508.
- 31 M. Alaasar, M. Prehm, M. Nagaraj, J. K. Vij and C. Tschierske, *Adv. Mater.*, 2013, **25**, 2186.
- 32 M. Alaasar, M. Prehm, K. May, A. Eremin and C. Tschierske, *Adv. Funct. Mater.*, 2014, **24**, 1703.
- 33 (a) G. Pelzl, A. Eremin, S. Diele, H. Kresse and W. Weissflog, *J. Mater. Chem.*, 2002, **12**, 2591; (b) T. Niori, J. Yamamoto and H. Yokoyama, *Mol. Cryst. Liq. Cryst.*, 2004, **409**, 475.
- 34 (a) V. Görtz and J. W. Goodby, *Chem. Commun.*, 2005, 3262; (b) V. Görtz, *Liq. Cryst. Today*, 2010, **19**, 37.
- 35 More recently helical superstructures, the so-called twist bent nematic phases, were reported for mesogenic dimers with odd-numbered spacers: (a) J. W. Emsley, M. Lelli, A. Lesage and G. R. Luckhurst, *J. Phys. Chem. B*, 2013, **117**, 6547; (b) V. Borshch, Y.-K. Kim, J. Xiang, M. Gao, A. J. ákli, V. P. Panov, J. K. Vij, C. T. Imrie, M. G. Tamba, G. H. Mehl and O. D. Lavrentovich, *Nat. Commun.*, 2013, **4**, 2635; (c) D. Chen, J. H. Porada, J. B. Hooper, A. Klittnick, Y. Shen, M. R. Tuchband, E. Körblova, D. Bedrov, D. M. Walba, M. A. Glaser, J. E. MacLennan and N. A. Clark, *Proc. Natl. Acad. Sci. U. S. A.*, 2013, **110**, 15931.
- 36 (a) D. K. Yoon, Y. Yi, Y. Shen, E. D. Körblova, D. M. Walba, I. I. Smalyukh and N. A. Clark, *Adv. Mater.*, 2011, **23**, 1962; (b) D. Chen, C. Zhu, H. Wang, J. E. MacLennan, M. A. Glaser, E. Körblova, D. M. Walba, J. A. Rego, E. A. S. -Bustamante and N. A. Clark, *Soft Matter*, 2013, **9**, 462.
- 37 E. Peeters, J. Lub, J. A. M. Steebakkers and D. J. Broer, *Adv. Mater.*, 2006, **18**, 2412.
- 38 (a) I. C. Pintre, J. L. Serrano, M. B. Ros, J. M. Perdiguero, I. Alonso, J. Ortega, C. L. Folcia, J. Etxebarria, R. Alicante and B. Villacampa, *J. Mater. Chem.*, 2010, **20**, 2965; (b) C. L. Folcia, I. Alonso, J. Etxebarria, I. Pintre and M. B. Ros, *Chem. Mater.*, 2006, **18**, 4617.
- 39 G. Lee, R. J. Carlton, F. Araoka, N. L. Abbott and H. Takezoe, *Adv. Mater.*, 2013, **25**, 245.
- 40 T. Ueda, S. Masuko, F. Araoka, K. Ishikawa and H. Takezoe, *Angew. Chem.*, 2013, **125**, 7001.
- 41 Dimesogen azobenzene: (a) S.-W. Choi, T. Izumi, Y. Hoshino, Y. Takanishi, K. Ishikawa, J. Watanabe and H. Takezoe, *Angew. Chem., Int. Ed.*, 2006, **45**, 1382; (b) G. Lee, R. J. Carlton, F. Araoka, N. L. Abbott and H. Takezoe, *Adv. Mater.*, 2013, **25**, 245; (c) A. Zep, K. Sitkowska, D. Pocięcha and E. Gorecka, *J. Mater. Chem. C*, 2014, **2**, 2323.
- 42 I. Miyake, Y. Takanishi, N. V. S. Rao, M. K. Paul, K. Ishikawa and H. Takezoe, *J. Mater. Chem.*, 2005, **15**, 4688.
- 43 M. Alaasar, M. Prehm and C. Tschierske, *Chem. Commun.*, 2013, **49**, 11062.
- 44 M. Alaasar, M. Prehm, M. Brautzsch and C. Tschierske, *J. Mater. Chem. C*, 2014, **2**, 5487.
- 45 There are numerous different effects of the F-substituents at the aromatic core, which influence each other and hence



- specific effects are difficult to distinguish. Firstly, due to their slightly larger size compared to that of hydrogen, fluorine substituents change the steric intermolecular interactions and also have effects on the conformation of the adjacent alkyl chains. Secondly, fluorine has a strong influence on the intermolecular interactions as a result of its electronegative character, which affects the electron density of the aromatic ring leading to changes in the  $\pi$ - $\pi$  stacking and  $\pi$ ···H-C electrostatic interactions between the aromatic rings, (M. O. Sinnokrot and C. D. Sherrill, *J. Am. Chem. Soc.*, 2004, **126**, 7690) as well as the polarization, surface charge distribution and polarizability of the whole conjugated  $\pi$ -system.
- 46 R. A. Reddy, V. A. Raghunathan and B. K. Sadashiva, *Chem. Mater.*, 2005, **17**, 274.
- 47 M. Alaasar, M. Prehm and C. Tschierske, *Liq. Cryst.*, 2013, **40**, 656.
- 48 I. Niezgodna, D. Pocięcha and Z. Galewski, *Thermochim. Acta*, 2014, **587**, 59.
- 49 M. Alaasar, M. Prehm and C. Tschierske, *Liq. Cryst.*, 2014, **41**, 126.
- 50 A. Guinier, *X-ray Diffraction*, Freeman, San Francisco, 1963.
- 51 T. Otani, F. Araoka, K. Ishikawa and H. Takezoe, *J. Am. Chem. Soc.*, 2009, **131**, 12368; F. Araoka, G. Sugiyama, K. Ishikawa and H. Takezoe, *Opt. Mater. Express*, 2011, **1**, 27.
- 52 N. G. Nagaveni, A. Roy and V. Prasad, *J. Mater. Chem.*, 2012, **22**, 8948.
- 53 A. Immirzi and B. Perini, *Acta Crystallogr., Sect. A: Cryst. Phys., Diffr., Theor. Gen. Crystallogr.*, 1977, **33**, 216.
- 54 D. R. Lide, *CRC Handbook of Chemistry and Physics, Internet Version*, 2005, <http://www.hbcpnetbase.com>.
- 55 M. J. Frisch *et al.*, Gaussian 09, Revision A.1, Gaussian Inc., Wallingford CT, 2009.
- 56 (a) I. Wirth, S. Diele, A. Eremin, G. Pelzl, S. Grande, L. Kovalenko, N. Pancenko and W. Weissflog, *J. Mater. Chem.*, 2001, **11**, 1642; (b) L. Kövalenko, M. W. Schröder, R. A. Reddy, S. Diele, G. Pelzl and W. Weissflog, *Liq. Cryst.*, 2005, **32**, 857.
- 57 In contrast to the rigid resorcinol based bent-core mesogens, reported here, the azobenzene based dimesogens form HNF type DC phases,<sup>27</sup> presumably because in this case the inherent bent of the odd-numbered alkylene space provides helical conformational chirality, and because this kind of spacer is “softer” these molecules can still adopt helical nanofilaments even in the presence of the rigid azobenzene units.
- 58 Z. Fang and C. Cao, *J. Mol. Struct.*, 2013, **1036**, 447.
- 59 H. G. Heller and J. R. Langan, *J. Chem. Soc., Perkin Trans. 2*, 1981, 341.
- 60 P. Schmitz, H. Gruler and M. Eberhardt, *Mol. Cryst. Liq. Cryst.*, 1995, **262**, 129.



# 4-Methylresorcinol based bent-core liquid crystals with azobenzene wings – a new class of compounds with dark conglomerate phases†

Cite this: *J. Mater. Chem. C*, 2014, 2, 5487

Mohamed Alaasar,<sup>\*ab</sup> Marko Prehm,<sup>a</sup> Marcel Brautzsch<sup>a</sup> and Carsten Tschierske<sup>\*a</sup>

Stochastic achiral symmetry breaking in soft matter systems, leading to conglomerates of macroscopically chiral domains (so-called dark conglomerate = DC phases) is of contemporary interest from a fundamental scientific point of view as well as for numerous potential applications in chirality sensing and non-centrosymmetric materials. Herein we report the synthesis and investigation of first azobenzene containing bent-core mesogens derived from 4-methylresorcinol forming DC phases with a new structure, distinct from the known fluid sponge-like distorted smectic phases as well as from the helical nano-filament phases (HNF phases, B<sub>4</sub> phases). The effects of chain length and other structural modifications on achiral symmetry breaking were investigated. Homologues with relatively short alkyl chains form achiral intercalated lamellar LC phases (B<sub>6</sub> phases), but on increasing the chains, these are replaced by the chiral and optically isotropic DC phases. Compounds with the longest alkyl chains form low birefringent crystalline conglomerates which represent less distorted versions of the optically isotropic DC-phases. Introducing additional peripheral substituents at both outer rings removes the DC phases. The DC phases were also removed and replaced by modulated smectic phases if the azo groups were replaced by ester units, showing that azo groups favour DC phase formation with new nanostructures, distinct from the previously known types.

Received 17th March 2014  
Accepted 22nd April 2014

DOI: 10.1039/c4tc00533c

[www.rsc.org/MaterialsC](http://www.rsc.org/MaterialsC)

## 1. Introduction

Since the discovery of polar order and chirality in the liquid crystalline (LC) phases of compounds with a bent aromatic core (bent-core liquid crystals = BCLCs)<sup>1</sup> this field has become a thrust area of liquid crystal research by providing a significant impact on the general understanding of molecular self-assembly in soft condensed matter.<sup>2,3</sup> Moreover, these materials are also of significant interest for numerous practical applications, as ferroelectric, flexoelectric and pyroelectric,<sup>4</sup> for command surfaces and sensors,<sup>5</sup> non linear optical applications<sup>6</sup> and in fast switching electrooptical devices.<sup>7</sup> A great fraction of contemporary interest is focussed on the so-called dark conglomerate phases (DC phases).<sup>8–18</sup> The common feature of these DC phases is the absence of birefringence due to a local distortion of long range periodicity and the inherent phase chirality indicated by stochastic achiral symmetry breaking, leading to conglomerates of macroscopically chiral domains. These DC phases can be subdivided

into the liquid crystalline smectic phases (sponge phases)<sup>8–15</sup> and the soft crystalline helical nanofilament phases (HNF phases, also assigned as B<sub>4</sub> phases).<sup>16–19</sup> In the sponge type DC phases, layers without in-plane order are strongly deformed in a nonregular way, so that uniformly oriented regions become smaller than the wavelength of light. In contrast, the HNF phases are composed of helical filaments with a crystalline packing of the aromatic cores in twisted ribbons, here only the chains are in a disordered state. As there is no preferred direction for these filaments these phases appear optically isotropic. The major tool for distinguishing these two structures is XRD, where the wide angle scattering around  $d = 0.45$  nm is completely diffuse for the LC sponge phases whereas for the soft crystalline HNF phases a series of relatively sharp scattering could be found in this region.<sup>16a,20,21</sup> The reduced symmetry as a result of the tilted organization of molecules in polar layers (layer chirality),<sup>3,16</sup> the collective segregation of chiral molecular conformations and a combination of both are considered as possible origins of the remarkable chirality and mirror symmetry breaking in these soft matter structures.<sup>2a,b,8,17a,22</sup> HNF phases might become interesting materials for a number of applications, such as organic semiconductors for thin-film transistors and solar cells,<sup>23</sup> as thin-film polarizers,<sup>22</sup> as nonlinear optical materials<sup>24</sup> as well as for the detection and amplification of chirality.<sup>25</sup>

<sup>a</sup>Institute of Chemistry, Martin Luther University Halle-Wittenberg, Kurt Mothes Str. 2, D-06120 Halle (Saale), Germany. E-mail: [carsten.tschierske@chemie.uni-halle.de](mailto:carsten.tschierske@chemie.uni-halle.de)

<sup>b</sup>Department of Chemistry, Faculty of Science, Cairo University, Giza, Egypt. E-mail: [malaasar@sci.cu.edu.eg](mailto:malaasar@sci.cu.edu.eg)

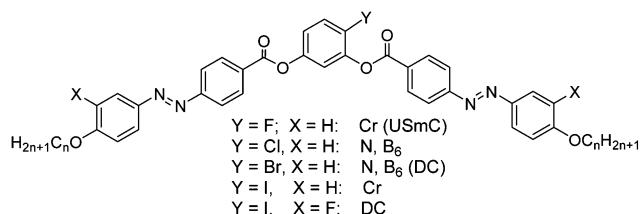
† Electronic supplementary information (ESI) available. See DOI: 10.1039/c4tc00533c



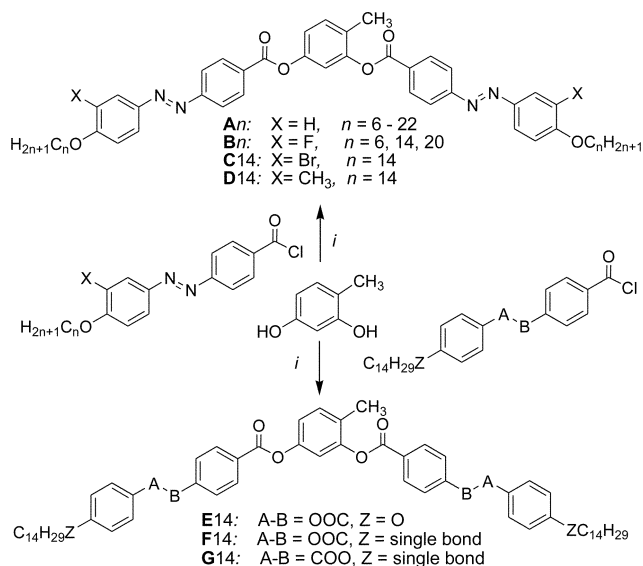
Interestingly, almost all of the known BCLCs with HNF phases incorporate the hydrolytically unstable benzylideneaniline (Schiff base) moiety with the exception of only very few recent examples.<sup>26–28</sup> This calls for new materials with DC phases, showing enhanced chemical stability and providing new phase sequences involving the HNF phases. A broader variety of different molecular structures could also lead to an improved understanding of the molecular structural factors governing the formation of distinct subtypes of DC phases, thus providing rules for the directed design of such materials.

BCLCs incorporating azo ( $-\text{N}=\text{N}-$ ) linkages represent versatile materials due to their photochromic effects in addition to high birefringence and high polarizability, leading to significant nonlinear optical activity.<sup>6,29,30</sup> The *cis-trans* isomerisation of the azo linkage in the presence of UV light could be used, for example, in high-density data storage systems, for sensors, photonic switches and molecular logic gates.<sup>31</sup> Though a variety of azobenzene based BCLCs with interesting properties have been reported,<sup>29,32–34</sup> until recently no such BCLCs with DC phases have been available; only bent dimesogens combining two rod-like azobenzene units *via* an odd-numbered alkylene spacer were reported.<sup>27</sup> We have found that iodine<sup>28</sup> or bromine<sup>34a</sup> substitution in 4-position at the bent central resorcinol unit of azobenzene based BCLCs leads to a new type of DC-phases (Scheme 1).<sup>28</sup> Hence, it appears that the size of the halogens is of importance. Bulky halogen atoms like bromine ( $cv = 0.33 \text{ nm}^3$ )<sup>35</sup> or iodine ( $cv = 0.45 \text{ nm}^3$ ),<sup>35</sup> seem to be favourable for formation of DC phases, whereas no DC phases were found for BCLC with hydrogen<sup>32e</sup> or smaller halogens in the same position (see Scheme 1; F:  $cv = 0.13 \text{ nm}^3$ ; Cl:  $cv = 0.27 \text{ nm}^3$ ).<sup>34,35</sup> Hence, the question arose if azobenzene BCLCs with other bulky groups at the bent core, having a size comparable to iodine/bromine, could also lead to azobenzene based BCLCs showing DC phases. The methyl group has a size ( $cv = 0.32 \text{ nm}^3$ )<sup>35</sup> comparable to bromine but it is almost non-polar in contrast to the C-halogen bonds which introduce a significant dipole moment.

Here we report a series of new BCLCs derived from 4-methylresorcinol<sup>36,37</sup> possessing two azobenzene side arms (**An**, see Scheme 2). These compounds show  $B_6$  phases if the terminal chains are short and a new type of dark conglomerate phases if the chains are sufficiently long. Besides these isotropic DC



**Scheme 1** LC phases found for 4-halogenoresorcinol based bent-core mesogens with azobenzene wings (abbreviations: Cr = crystalline solid, USmC = undulated smectic phase; N = nematic phase, B<sub>6</sub> = intercalated smectic phase formed by ribbons with only short range register; DC = dark conglomerate phase; phases in brackets were observed only for one homologue in a small temperature range).<sup>28,34a</sup>



**Scheme 2** Structures of the 4-methylresorcinol derived bent-core liquid crystalline compounds **An–Gn** (for **An**:  $n$  is an even number except **A9**) and their synthesis; reagents and conditions: (i)  $\text{Et}_3\text{N}$ , pyridine,  $\text{CH}_2\text{Cl}_2$ , reflux, 6 h.

phases also a birefringent crystalline conglomerate was observed for a long chain compound. The formation of this phase depends on the applied cooling rates and the transition between the isotropic and birefringent types of conglomerate phases was studied. In addition, the effect of lateral groups X (see Scheme 2, X = F, Br, CH<sub>3</sub>) at the outer rings of these BCLCs (compounds **Bn**, **C14** and **D14**, respectively) has been investigated. The phase behaviour of these new compounds is compared with related compounds incorporating terephthalate or benzoate based wing groups instead of the azobenzenes, either reported in the literature<sup>36</sup> or synthesized herein (**E14**, **F14** and **G14** see Section 3.6).

## 2. Experimental

### Synthesis

The synthesis of the target BCLCs **A/n–D/n** with azobenzene wings was performed as shown in Scheme 2 by acylation of 4-methylresorcinol with 4-(4- $n$ -alkoxyphenylazo)benzoyl chlorides (X = H) or their 3-substituted derivatives with X = F, CH<sub>3</sub>, Br (see Scheme S1†). For the synthesis of compounds **E14–G14** appropriately substituted benzoyl chlorides (see Scheme S2†) were used for the acylation reactions.<sup>37</sup> Details of the synthesis of the intermediates and final compounds as well as analytical data are reported in the ESI.†

### Methods

The mesophase behaviour and transition temperatures were measured using a Mettler FP-82 HT hot stage and a control unit in conjunction with a Nikon Optiphot-2 polarizing microscope. The associated enthalpies were obtained from DSC-thermograms which were recorded on a Perkin-Elmer DSC-7, the



heating and cooling rate was  $10 \text{ K min}^{-1}$ . Electro-optical switching characteristics were examined in  $6 \mu\text{m}$  polyimide coated ITO cells (EHC Japan) using the triangular-wave method. XRD patterns were recorded with a 2D detector (Vantec-500, Bruker). Ni filtered and pin hole collimated  $\text{CuK}\alpha$  radiation was used. The exposure time was 15 min and the sample to detector distance was 8.95 and 26.7 cm for small angle and wide angle scattering experiments, respectively. Samples were aligned by slow cooling (rate:  $1\text{--}0.1 \text{ K min}^{-1}$ ) of a small droplet of the compound on a glass plate and takes place at the sample–air interface. The samples were held on a temperature-controlled heating stage.

DFT computation was carried out with the Gaussian 09 package.<sup>38</sup> Geometry optimization was performed with the B3LYP functional and the LAN L2 DZ basis set. The solvation model was IEFPCM with solvent chlorobenzene.

### 3. Results and discussion

#### 3.1 Overview over the LC phases formed by compounds *An–Dn*

The thermal behaviour of all synthesized compounds was studied by polarizing optical microscopy (POM) and differential scanning calorimetry (DSC). The transition temperatures ( $^{\circ}\text{C}$ ), the associated phase transition enthalpies ( $\text{kJ mol}^{-1}$ ) and the phase sequences of compounds *An*, *Bn*, **C14** and **D14** are given in Table 1. All compounds are thermally stable as confirmed by the reproducibility of thermograms in several heating and cooling cycles. Related compounds **E/14–G/14** with phenylbenzoate wing groups instead of the azobenzenes, synthesized for comparison purposes, are described and discussed in Section 3.6.

#### 3.2 $B_6$ -type intercalated smectic phases of the short chain compounds **A6** and **A8**

Compounds *An* without lateral substituents at the outer rings of the bent-core structure exhibit two different types of mesophases. On heating the shortest homologue (**A6**, with  $n = 6$ ) a transition from the crystalline state to a focal-conic fan-shaped texture is observed at  $T = 124 \text{ }^{\circ}\text{C}$  (Fig. 1a). The dark extinctions are parallel to a polarizer and an analyzer, indicating an average orthogonal or anticlinic tilted smectic phase. No homeotropic alignment with pseudoisotropic areas or with birefringent Schlieren texture, as typical for SmA or SmC phases, respectively, could be achieved by shearing the sample. Instead, a fine fan-texture is immediately reformed after releasing shear stress (see Fig. S2†), as typical for intercalated smectic phases of bent-core mesogens, assigned as  $B_6$  phases.

The XRD pattern (Fig. 1b and c) shows only one sharp peak in the small angle region corresponding to a  $d$ -value of 2.0 nm ( $T = 80 \text{ }^{\circ}\text{C}$ ), which is smaller than half of the molecular length ( $L_{\text{mol}}$ ) in a conformation with a  $120^{\circ}$  bent aromatic unit and the alkyl chains in the most stretched all-trans conformation. For compound **A6**  $L_{\text{mol}}$  is between 4.3 and 4.5 nm, depending on the assumed conformation shown in Fig. S1.† This confirms the intercalated  $B_6$ -type smectic phase deduced from optical

investigations. According to the present understanding, this is a frustrated smectic phase with layers broken into ribbons and adopting a staggered organization with only short range periodicity between the ribbons (see Fig. 1d); the layer frustration takes place in the direction perpendicular to the molecular bending plane (Fig. 1d).<sup>39,40</sup>

The wide angle scattering is diffuse and has a maximum at 0.43 nm, in line with the LC state of this phase. For an aligned sample this scattering is split into four maxima indicating the presence of a tilt of about  $26^{\circ}$  (Fig. 1b and S12†). This tilt could arise either from a tilt of the molecular bending planes, or alternatively, from the inherently tilted orientation of the individual rod-like wings of the bent-core mesogens, similar to anticlinic SmC phases.<sup>41</sup> The latter would be in line with recent microbeam XRD results obtained for  $B_6$  phases of Schiff base compounds.<sup>39a</sup> In this case the orientation of the molecules would be on average orthogonal and the splitting is related to the angle of the molecular bent of  $128^{\circ}$  which is in good agreement with the geometry provided by the molecular structure. This would also be in line with the optical textures which have the extinction brushes strictly parallel to the polarizers (see Fig. 1a). However, the measured  $d$  value is a bit shorter than half the molecular length ( $2d/L_{\text{mol}} \sim 0.9$ ) which in this case must be attributed to partial intercalation and conformational disorder of the alkyl chains. On cooling **A6** from the isotropic state the  $B_6$  phase appears at  $T = 129 \text{ }^{\circ}\text{C}$  and remains on cooling down to room temperature without visible crystallization of the sample (for DSC traces, see Fig. 2a), but the sample becomes glass-like solid without any change of the texture at  $\sim 40 \text{ }^{\circ}\text{C}$ . This might indicate a transition to a glassy state of the  $B_6$  phase or an isomorphous crystallization. As no clear DSC peak (only a small hump between 40 and  $50 \text{ }^{\circ}\text{C}$ , see Fig. 2a) was observed in the cooling traces and crystallization is observed  $>35 \text{ }^{\circ}\text{C}$  on heating, a glassy  $B_6$  phase ( $gB_6$ ) appears more likely.

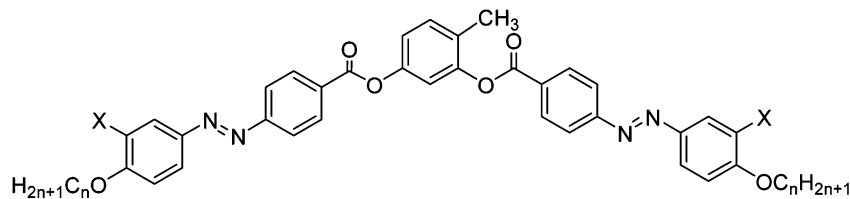
In electrooptical investigations using a triangular wave voltage no current peak could be observed in the whole temperature range of this mesophase up to a voltage of  $200 \text{ V}_{\text{pp}}$  in a  $6 \mu\text{m}$  ITO cell. These observations, together with the relatively high transition enthalpy value of  $\Delta H = 12.3 \text{ kJ mol}^{-1}$  for the Iso–LC transition at  $T = 129 \text{ }^{\circ}\text{C}$  are in line with the suggested  $B_6$  phase. With increasing chain length ( $n = 8$  and  $9$ ) the  $B_6$  phase is retained but the Iso– $B_6$  transition temperature decreases to  $96 \text{ }^{\circ}\text{C}$  for **A8** and to  $87 \text{ }^{\circ}\text{C}$  for **A9**, and the  $B_6$  phase becomes monotropic (metastable) for these two compounds.

#### 3.3 Competition between $B_6$ and DC phases in **A9**

On cooling the  $B_6$  phase of **A9** a highly viscous, almost solid-like optically isotropic mesophase starts to grow at  $T = 85 \text{ }^{\circ}\text{C}$  (Fig. 3a and b). Uncrossing the polarizers by a small angle leads to the appearance of dark and bright domains. Uncrossing the polarizer in the opposite direction reverses the dark and bright domains (Fig. 3c and d). Rotating the sample between crossed polarizers does not lead to any change and this indicates that the distinct regions represent chiral domains with opposite handedness, as typical for dark conglomerate phases (DC phases). The distribution of the areas of domains with opposite chirality is on average 1 : 1.



**Table 1** Phase transition temperatures ( $T/^\circ\text{C}$ ), mesophase types, and transition enthalpies ( $\Delta H/\text{kJ mol}^{-1}$ , values in square brackets) of compounds **A $n$** , **B $n$** , **C14** and **D14**<sup>a</sup>



Comp.	$n$	X	Heating	Cooling
<b>A6</b>	6	H	Cr 124 [41.0] B <sub>6</sub> 131 [11.9] Iso	Iso 129 [12.3] B <sub>6</sub>
<b>A8</b>	8	H	Cr 111 [35.9] Iso	Iso 96 [11.1] B <sub>6</sub> 62 [9.1] Cr
<b>A9</b>	9	H	Cr 110 [37.4] Iso	Iso 87 [9.4] B <sub>6</sub> 67 [16.5] Cr <sup>f</sup>
<b>A10</b>	10	H	DC 100 [22.7] Iso <sup>b</sup> Cr 107 [37.4] Iso	Iso 87 [9.4] B <sub>6</sub> ~ 85 DC [ $\geq 9.1$ ] 67 Cr <sup>f</sup> Iso 87 [24.1] DC
<b>A12</b>	12	H	DC 100 [25.5] Iso <sup>c</sup> Cr 109 [38.1] Iso	DC 102 [27.3] Iso <sup>b</sup> Iso 87 [26.8] DC
<b>A14</b>	14	H	DC 101 [31.4] Iso	Iso 88 [33.9] DC
<b>A16</b>	16	H	DC 102 [40.8] Iso	Iso 90 [43.9] DC
<b>A18</b>	18	H	DC 103 [49.6] Iso	Iso 93 [51.7] DC
<b>A20</b>	20	H	Cr <sup>[*]</sup> 99 DC 104 [68.0] <sup>d</sup> Iso DC 104 [56.7] Iso <sup>e</sup>	Iso 92 [70.8] Cr <sup>[*]</sup> Iso 95 [59.0] DC <sup>g</sup> Iso 96 [76.5] Cr <sup>[*]</sup>
<b>A22</b>	22	H	Cr <sup>[*]</sup> 105 [73.2] Iso	Iso 88 [8.6] SmC <sub>a</sub> P <sub>A</sub> 67 [10.5] Cr <sup>h</sup>
<b>B6</b>	6	F	Cr 112 [41.3] Iso	Iso 90 [15.2] SmC <sub>a</sub> P <sub>A</sub> 74 [39.8] Cr
<b>B14</b>	14	F	Cr 90 [32.9] SmC <sub>a</sub> P <sub>A</sub> 95 [12.8] Iso	Iso 92 [16.0] SmC <sub>a</sub> P <sub>A</sub> 82 [77.7] Cr
<b>B20</b>	20	F	Cr 95 [93.0] Iso	Iso 30 [53.2] Cr
<b>C14</b>	14	Br	Cr 78 [77.2] Iso	Iso 33 [0.9] SmC < 20 Cr
<b>D14</b>	14	CH <sub>3</sub>	Cr 79 [47.9] Iso	

<sup>a</sup> Before measurement the compounds were melted and heated to 150 °C to remove traces of enclosed solvent, afterwards they were cooled with 10 K min<sup>-1</sup> to room temperature; the phase transition temperatures (peak temperatures) were taken from the following heating and cooling scans at 10 K min<sup>-1</sup>, if not otherwise specified; abbreviations: SmC = synclitic tilted birefringent smectic phase; SmC<sub>a</sub>P<sub>A</sub> = anticlinic tilted antiferroelectric SmC phase; Iso = isotropic liquid; Cr<sup>[\*]</sup> = crystalline phase composed of a conglomerate of chiral domains, for other explanations, see Scheme 1.

<sup>b</sup> Obtained on heating after previous cooling to 75 °C with 10 K min<sup>-1</sup>. <sup>c</sup> Obtained on heating after previous cooling to 80 °C with 20 K min<sup>-1</sup>.

<sup>d</sup> Total enthalpy for both transitions. <sup>e</sup> Obtained on heating after previous cooling to 80 °C with 2 K min<sup>-1</sup>. <sup>f</sup> The actual phase sequence strongly depending on conditions, see DSC traces in Fig. 2b; transition enthalpy value could not be determined for the B<sub>6</sub>-DC transition (see Section 3.3). <sup>g</sup> Cooling with 2 K min<sup>-1</sup>. <sup>h</sup> Partial crystallization.

The formation of the DC phase is slow and on further cooling the remaining B<sub>6</sub> phase rapidly crystallizes with formation of a birefringent crystalline phase (see Fig. 3b) at  $T = 67^\circ\text{C}$ , while the DC phase only very slowly crystallizes. On heating the areas of the DC phase go to the isotropic liquid state at  $T = 100^\circ\text{C}$ , while the birefringent crystalline regions of the sample melt to a clear liquid at  $T = 110^\circ\text{C}$ . This indicates that the B<sub>6</sub>-phase, formed first, is thermodynamically unstable and upon annealing is replaced by the isotropic DC phase and a birefringent crystalline phase. Formation of the DC phase is in competition with fast crystallization, but the DC phase once formed crystallizes only slowly (see Fig. S3†). However, after slow cooling (2 K min<sup>-1</sup>) to  $\sim 70^\circ\text{C}$ , followed by immediate heating, a uniform DC phase can be obtained (see 3<sup>rd</sup> heating curve in Fig. 2b).<sup>42</sup>

### 3.4 DC phases of the long chain compounds A10–A22

**3.4.1 Optical and calorimetric investigations.** For the next homologues with  $n = 10$ –18 the DC phase is the only observed

mesophase and it is directly formed upon cooling the isotropic liquid (see Fig. S4† for textures observed for compound **A14**). The growth process from the isotropic liquid, as observed between slightly uncrossed polarizers, is shown for compound **A10** in Fig. 4. The distinct chiral domains grow with a circular shape (Fig. 4a–c) and finally coalesce to a mosaic-like pattern with sharp linear boundaries, representing the Voronoi cells separating the germs of circular domain growth (Fig. 4d). In this respect the formation of the DC phases reported herein is distinct from previously reported cases, showing fractal growth.<sup>43</sup>

The melting of the DC phases (DC–Iso-transition) takes place around 100–104 °C and the crystallization of the DC phase (Iso–DC transition) is found between 87 and 95 °C for all compounds **A10**–**A20** and both transition temperatures increase slightly with rising alkyl chain length (see Table 1 and Fig. 5a). Hence, there is a supercooling of this phase transition by about 10 K (peak temperatures at scanning rates of 10 K min<sup>-1</sup>). The formation of the DC phases is associated with relatively high



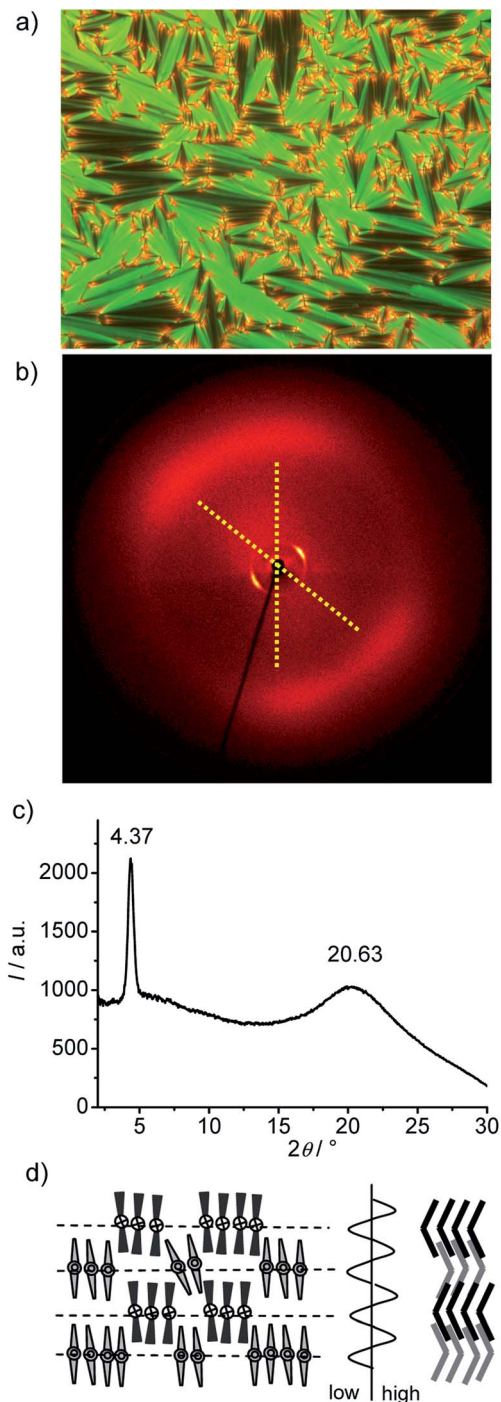


**Fig. 1** Compound **A6**. (a) Texture (crossed polarizers) as observed for the  $B_6$  phase at  $T = 120$  °C (on cooling, textures observed after applying shear stress are shown in Fig. S2†); (b) XRD pattern of an aligned sample of the  $B_6$ -phase at 80 °C; (c)  $2\theta$ -scan over this pattern and (d) the proposed model of the molecular organization in the  $B_6$  phase, left: view along the bending direction, right: side view perpendicular to the molecular bending plane (in this direction the ribbons are quasi infinite) and the assumed electron density modulation profile in the middle.<sup>41</sup>

transition enthalpies, ranging between  $\Delta H \sim 24$  and  $59$   $\text{kJ mol}^{-1}$  (measured in cooling scans), strongly rising with growing alkyl chain length from **A10** to **A20** (see Table 1 and Fig. 5a).

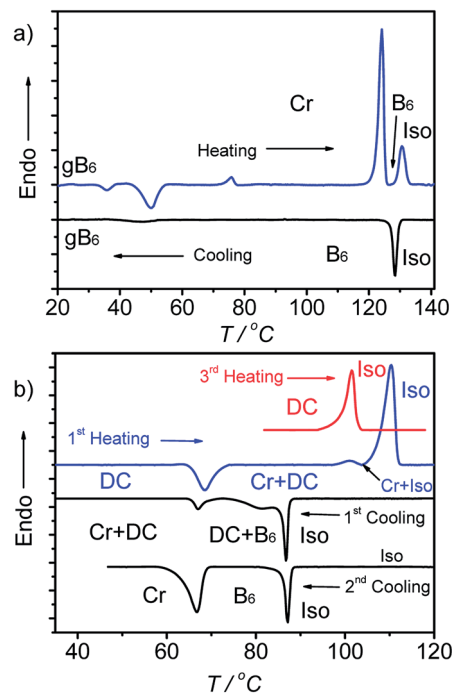


**Fig. 2** DSC heating and cooling traces of compounds (a) **A6** and (b) **A9** in heating and cooling runs with a rate of  $10$   $\text{K min}^{-1}$  (the 3rd heating was recorded after slow cooling with  $2$   $\text{K min}^{-1}$  to  $80$  °C followed by immediate heating with a rate of  $10$   $\text{K min}^{-1}$ ).

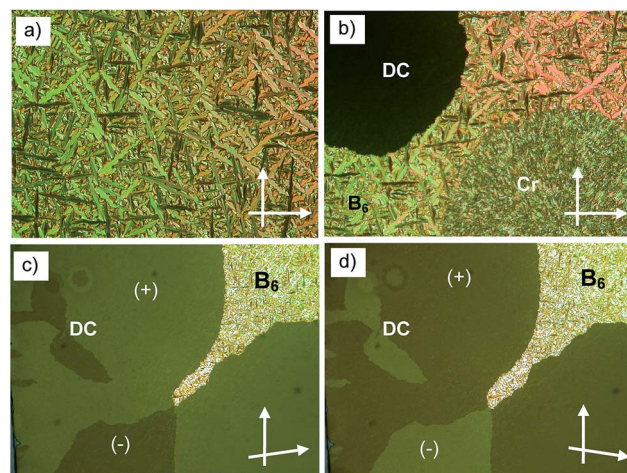


**Fig. 3** Optical micrographs observed for **A9** between crossed polarizers: (a)  $B_6$  phase at  $T = 86$  °C; (b) growth of the DC phase and the birefringent crystalline phase from the  $B_6$  phase; (c) DC phase as grown from  $B_6$  ( $T = 83$  °C, different region) after rotating one polarizer by  $10^\circ$  from the crossed position in the anticlockwise direction and (d) in the clockwise direction, showing the chiral domains (on a larger field of view the stochastically distributed chiral domains occupy equal areas); the texture related to (c), (d), but between  $90^\circ$  crossed polarizers is shown in Fig. S3b†; additional textures are shown in Fig. S3a, c and d.†

Compounds **A10** and **A12** easily crystallize on cooling or on reheating, but the DC phases of compounds with longer chains ( $n = 14$ – $20$ ) do not crystallize, once the DC phase is formed, as





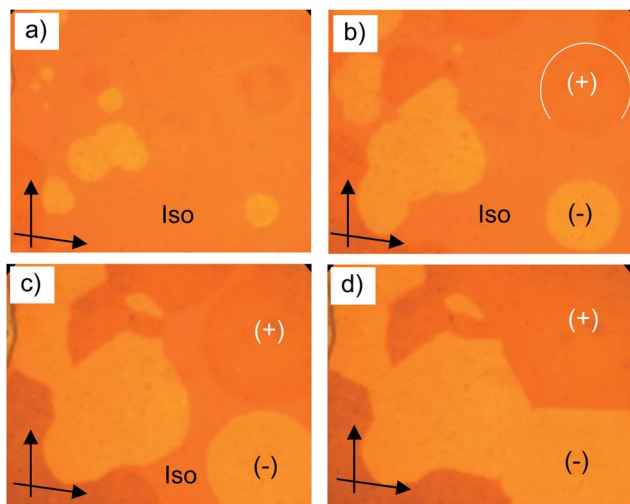


Fig. 4 a–d) Growth of the circular chiral domains of the DC phase of **A10** upon cooling from the isotropic liquid state at  $T = 87\text{ }^{\circ}\text{C}$  as observed between slightly uncrossed polarizers (see arrows); the textures of the DC phase of **A14** are shown in Fig. S4.†

shown in Fig. 5b for compound **A18** as an example (for additional DSC curves, see Fig. S7 and S8). In the case of the long chain compound **A20** a different behaviour is observed which is discussed here in some more detail. For this compound there is a strong effect of the cooling rate on the phase sequence and the phase structure (see Fig. 5c and d). On cooling from the isotropic liquid phase with a low rate of  $\leq 2\text{ K min}^{-1}$  (Fig. 5c, curve b) the DC phase is formed at  $T = 95\text{ }^{\circ}\text{C}$  and it does not crystallize on further cooling, and on heating only a single peak is observed at  $T = 104\text{ }^{\circ}\text{C}$  (Fig. 5c, curve a), similar to compounds **A14**–**A18** (Fig. 5b). The transition enthalpy is  $\sim 57\text{ kJ}$

$\text{mol}^{-1}$  on heating and  $\sim 59\text{ kJ mol}^{-1}$  on cooling. However, on cooling with a faster rate of  $\geq 5\text{ K min}^{-1}$  (Fig. 5d, curve d) a crystalline phase with a weakly birefringent spherulitic texture (see Fig. 6b) is formed at  $T = 92\text{ }^{\circ}\text{C}$  and the transition enthalpy is now significantly larger, around  $\sim 71\text{ kJ mol}^{-1}$  on cooling.<sup>44</sup> The spherulitic texture (Fig. 6b) is similar to those found for columnar or (modulated) smectic LC phases, however, this phase is solid-like and does not flow on applying shear forces, and therefore, this is a crystalline phase.

Interestingly, also this crystalline phase is chiral and composed of domains with opposite handedness, *i.e.* dark and bright domains become visible if the polarizers are slightly uncrossed (see Fig. 6a and c), hence, this birefringent conglomerate phase is assigned as  $\text{Cr}^{[*]}$ . Each of the spherulites appears to have uniform chirality, so it seems that the chirality is determined by each nucleus and is preserved through the growth process.<sup>45</sup> On further cooling the  $\text{Cr}^{[*]}$  phase is retained and does not change down to room temperature, but on heating to  $T = 99\text{ }^{\circ}\text{C}$  it transforms into the DC phase. At this transition the spherulitic texture becomes uniformly isotropic and the chirality as well as the sign of chirality in the distinct domains is retained (see Fig. 6e–g). This temperature corresponds to the position of the exotherm II in the heating curve c in Fig. 5d. The unusual shape of the DSC heating curve c is characterized by a significant tailing which rises up to a local maximum I, before it abruptly goes through an exotherm II, and finally the peak maximum III is reached. This kind of DCS curve is always found for the heating curves after cooling the sample with rates  $\geq 5\text{ K min}^{-1}$ , independent of the used heating rates (see Fig. S9†). The endothermic tailing I, starting at  $T \sim 85\text{ }^{\circ}\text{C}$ , is interpreted as a result of a chain melting process which leads to a softening of the  $\text{Cr}^{[*]}$  phase. This obviously allows a denser packing (crystallization) of other molecular parts, giving rise to the exotherm II in the heating curve. At this temperature the  $\text{Cr}^{[*]}$  phase transforms into the DC phase, *i.e.* this transition is accompanied by a layer deformation which leads to the formation of the optically isotropic DC phase at  $T = 99\text{ }^{\circ}\text{C}$ . On further heating this DC phase melts into the isotropic liquid at the endothermic peak III at  $T = 104\text{ }^{\circ}\text{C}$ . Once formed (either on cooling the preformed DC phase or on slow cooling from the isotropic liquid state), the DC phase is stable and it is retained down to room temperature; only a single peak at  $T = 104\text{ }^{\circ}\text{C}$  is observed on heating (curve e in Fig. 5d). Even after storage at room temperature for more than 8 weeks the same transition temperatures and enthalpies were obtained. The persistence of the DC phases might be the result of the freezing of disordered alkyl chain segments into an immobilized, probably a glassy state, which, once formed, inhibits the transformation into the chiral  $\text{Cr}^{[*]}$  phase or any other crystalline phase.

Compound **A22** with the longest chains is a crystalline solid with a melting point at  $T = 105\text{ }^{\circ}\text{C}$ . No formation of a DC phase could be detected at any cooling rate. Also in this case the crystalline phase formed on cooling consists of a conglomerate of chiral crystals (see Fig. S5†), though the chiral domains cannot be observed with the same clarity as for **A20**, because the birefringence is higher and no uniform texture is obtained. In the following focus is on the DC phases of compounds **A10**–**A20**.

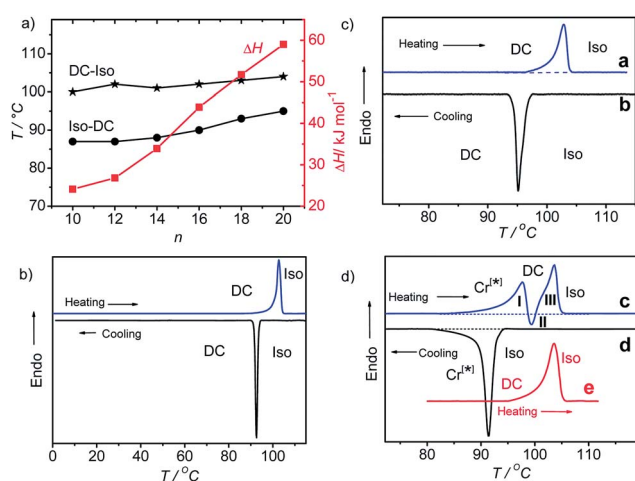
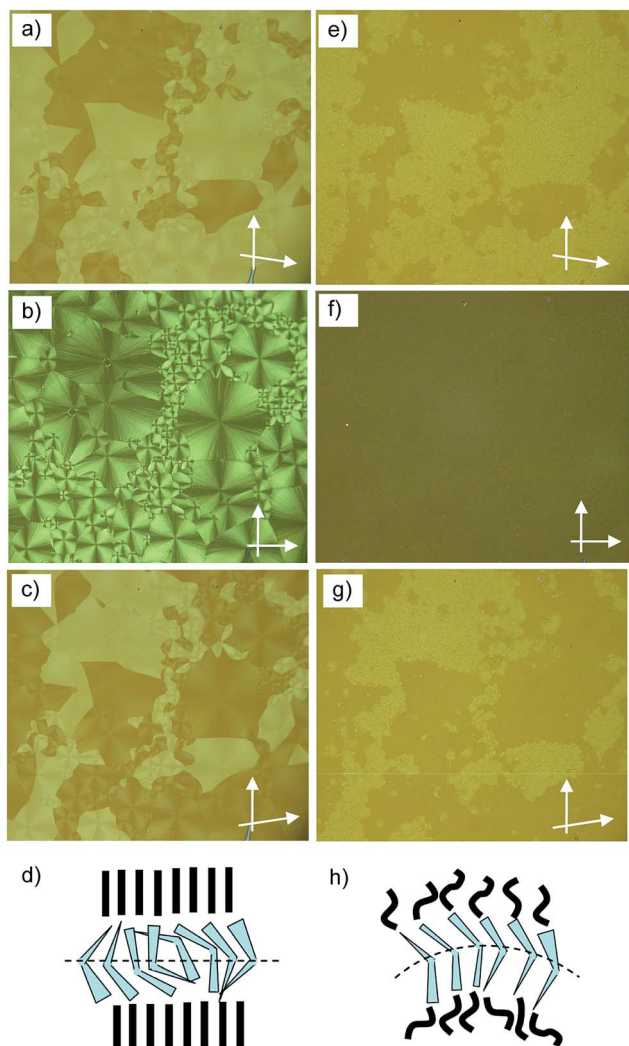


Fig. 5 a) Dependence of DC–Iso transition temperatures (on heating and cooling scans with  $10\text{ K min}^{-1}$ ) and transition enthalpy values (on cooling from the isotropic liquid) of compounds **A10**–**A20** on alkyl chain length  $n$ ; (b–d) DSC heating and cooling curves of (b) compound **A18** at  $10\text{ K min}^{-1}$ , (c) compound **A20** at  $2\text{ K min}^{-1}$  and (d) compound **A20** with a rate of  $10\text{ K min}^{-1}$  (curves c and d); curve e was recorded after cooling with  $2\text{ K min}^{-1}$ .





**Fig. 6** Textures of compound **A20** as observed between crossed and slightly uncrossed polarizers. (a–c)  $\text{Cr}^{\text{I}^*||}$  phase at  $T = 93^\circ\text{C}$  as obtained upon cooling with a rate of  $5\text{ K min}^{-1}$  and (e–g) DC phase as obtained on heating to  $100^\circ\text{C}$ ; (b and f) between crossed polarizers and (a and e) between slightly uncrossed polarizers with the analyzer rotated  $8^\circ$  clockwise and (c and g) rotated  $8^\circ$  anticlockwise; (d and h) show models of the molecular organization; (d) in the  $\text{Cr}^{\text{I}^*||}$  phase the alkyl chains are fully crystallized, the aromatics are more disordered and have a stronger helical twist than in the DC phase; (h) in the DC phase where the chains are disordered, allowing a denser and more ordered packing of the aromatic cores (“core crystallization”); this leads to a reduced molecular twist (reduced optical activity) and a stronger layer deformation, giving rise to optical uniaxiality.

**3.4.2 Electrooptical investigations of the DC phases.** In electrooptical experiments no current peak could be observed in the DC phases and also no birefringence is induced under an applied triangular wave voltage up to  $200\text{ V}_{\text{pp}}$  in a  $6\ \mu\text{m}$  ITO cell. These features are similar to those known for soft crystalline HNF phases ( $\text{B}_4$  phases) and distinct from most fluid sponge phases.

**3.4.3 Investigation of the DC phases by XRD.** XRD investigations of **A14** in the DC phase (see Fig. 7) indicate an intense layer reflection with its weak second to fifth order harmonic in the small and medium angle region ( $d = 4.47\text{ nm}$ ,  $T = 70^\circ\text{C}$ ). No

alignment could be achieved and therefore in the 2D patterns, all scattering form closed rings with uniform intensity distribution (see Fig. 7 and S13–S17<sup>†</sup>). This is due to the disordered meso-scale structure, which is an inherent feature of all DC phases and leads to their optically isotropic appearance as well as to a broadening of all XRD reflections. The  $2\theta$  scans of the other compounds **An** are collated in Fig. 8.

In all cases the  $d$ -value is significantly larger than  $L_{\text{mol}}/2$ , but also smaller than the single molecular length, indicating a tilted monolayer-like organization of the molecules in the DC phases. The  $d$ -value of the layer reflection grows, as expected, with rising molecular length (Fig. 9a). The ratio  $d/L_{\text{mol}}$  is  $\sim 0.73$ – $0.75$  for all investigated compounds which would, according to  $d/L_{\text{mol}} = \cos \beta$ , lead to a tilt angle around  $40^\circ$ .<sup>46</sup> This relatively large difference between  $d$  and  $L_{\text{mol}}$  distinguishes these DC phases from the previously reported HNF phases where  $d$  is usually close to the molecular length.<sup>16,17</sup>

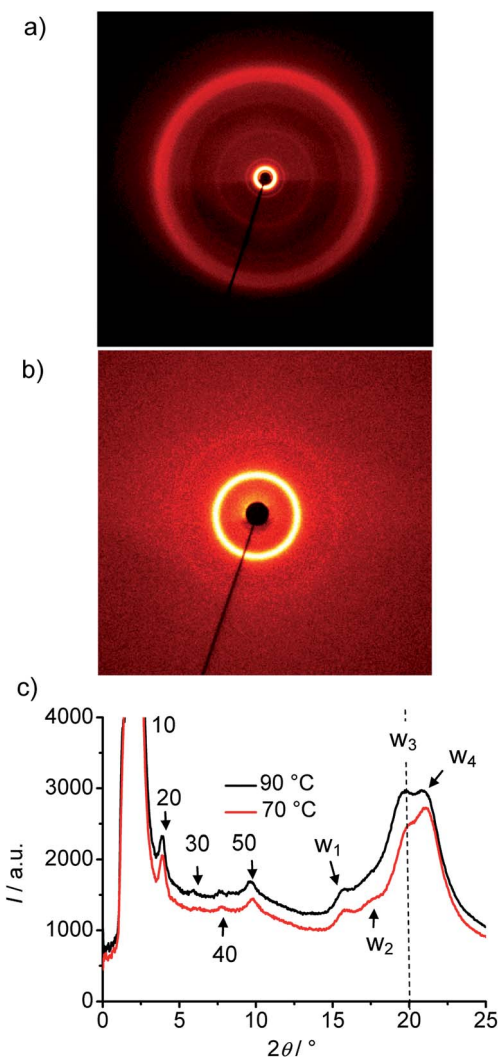


**Fig. 7** XRD pattern of the DC phase of compound **A14** at  $T = 70^\circ\text{C}$ , (a) complete diffraction pattern, (b) small angle region and (c)  $2\theta$ -scans at  $T = 70^\circ\text{C}$  and  $T = 90^\circ\text{C}$ .



In the medium angle region of the diffraction patterns of compounds **A14**–**A20** there are additional distinct scattering maxima on top of a broad diffuse scattering covering the range between  $2\theta = 5^\circ$  and  $2\theta = 15^\circ$  (see Fig. 8), only for **A10** exclusively the diffuse scattering could be observed. These reflections can be indexed as higher harmonics of the layer reflection (see Fig. 7c), as also found for the HNF phases. In the wide angle range there is a broad feature which could be fitted to 4 maxima ( $w_1$ – $w_4$ ) in the  $2\theta$  range between  $19$  and  $21^\circ$  (see Fig. 7c). This pattern excludes fluid sponge phases, showing exclusively a very diffuse wide angle scattering besides the layer reflection. However, it is also distinct from the typical patterns of HNF phases ( $B_4$  phases), where the wide angle reflections have other positions and appear as significantly sharper separate peaks.<sup>9,20,21</sup>

With growing chain length the intensity of the second harmonics of the small angle scattering decreases and it has completely disappeared for compound **A18** (Fig. 8), whereas the (50) and (40) reflections increase in intensity, most probably due to the changing electron density modulation resulting from the changing thickness of the aliphatic layers and other structural modifications. There is also a nearly continuous change of the positions of the wide angle scattering (Fig. 8 and 9), indicating continuous structural transformations depending on the

chain lengths. An indexing of the wide angle diffraction patterns was not attempted, because of the limited number and the diffuse character of the reflections. Due to the overlapping of several scattering maxima the precise assignment of the positions of the maxima is difficult and the presence of additional scattering in this region cannot be excluded. In any case, the scattering in this region should result from the packing of the crystallized (mainly aromatic) segments on a 2D in-plane lattice. The significant line broadening is thought to be due to the limited correlation length of the crystalline micro-domains.

Major changes can be observed for the scattering  $w_3$  occurring around  $2\theta \sim 19$ – $20^\circ$  which decreases in intensity (compare Fig. 8a–e) and is shifted to smaller  $d$ -values (see Fig. 9b) from **A14** to **A20**. Based on its  $d$ -value in the range between 0.46 and 0.43 nm and its strong intensity dependence on temperature (see discussions below) it is thought that this scattering is most likely due to the mean distance between less ordered (not crystallized) segments of the alkyl chains. The observation that with increasing chain length the position of  $w_3$  is shifted to smaller  $d$ -values would be in line with a denser chain packing for longer chains.

The temperature effect on the XRD pattern of compound **A14** in the DC phase is shown in Fig. 7c. There is no significant influence on the intensities and positions of the scattering

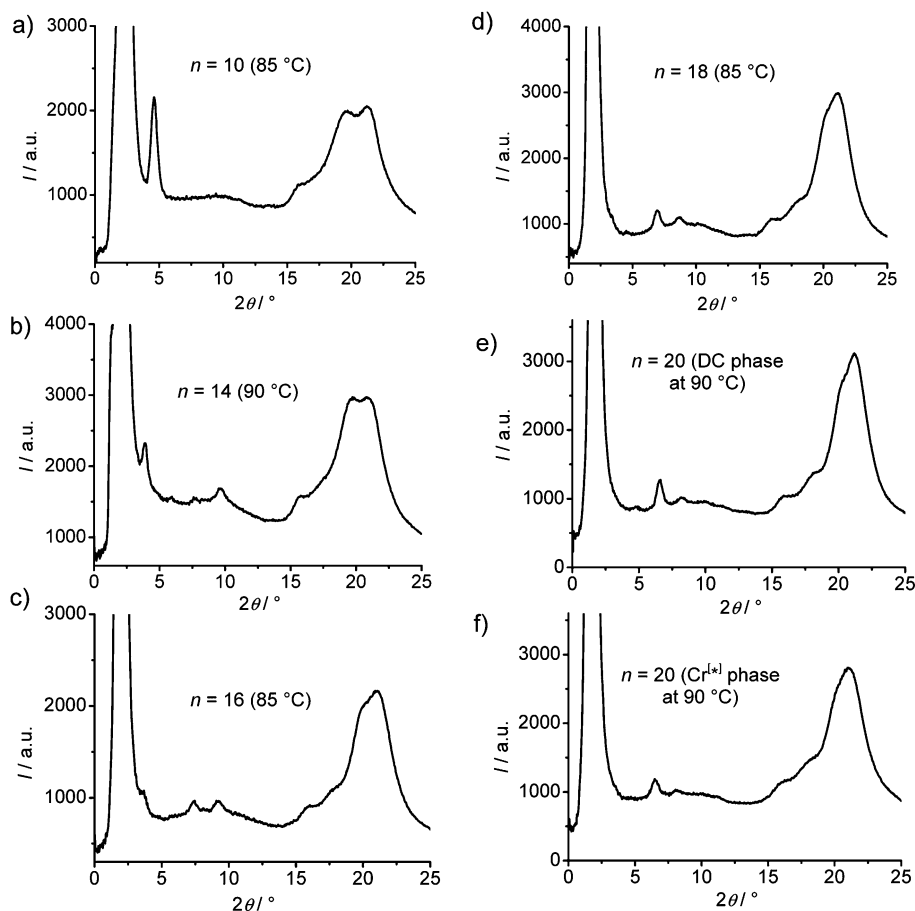


Fig. 8 Comparison of  $2\theta$ -scans of the XRD patterns at the indicated temperatures for (a) **A10**, (b) **A14**, (c) **A16**, (d) **A18** and (e) **A20** in the DC phase (cooling rate  $0.5 \text{ K min}^{-1}$  in all cases) and (f) **A20** in the  $\text{Cr}^{[is]}$  phase (after cooling with rate  $10 \text{ K min}^{-1}$ ).



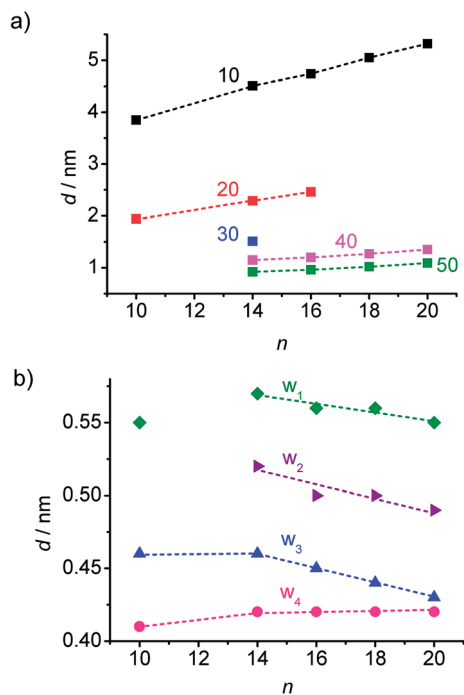


Fig. 9 Dependence of the XRD reflex position in the DC phases of compounds A10–A20 on chain length, (a)  $d$ -values of the layer reflections with the observed higher harmonics and (b) wide angle scattering maxima, the assignment of the reflections is shown in Fig. 7c, see also Fig. S13–S17.†

maxima with exception of  $w_3$  which is strongly reduced at decreased temperature, though its position is retained. Reducing the temperature has obviously a similar effect on the intensity of this scattering like increasing the alkyl chain length. This supports the assumption that this scattering maximum does not belong to the 2D in-plane lattice and could be attributed to the mean distance between the disordered alkyl chain segments. The fraction of the more disordered alkyl chain segments becomes smaller as temperature is reduced and as the alkyl chain length is increased, because longer chains provide a higher tendency for chain crystallization, as mentioned above. This corresponds with the observed strong rise of the DC-Iso transition enthalpy from 24.1 kJ mol<sup>-1</sup> for A/10 to 59 kJ mol<sup>-1</sup> for A/20 (see Table 1 and Fig. 5a; values on heating). In line with increasing chain crystallization by chain elongation, the optically isotropic DC phase of compound A20 is in competition with a low birefringent crystalline conglomerate phase Cr<sup>[\*]</sup> and exclusively a Cr<sup>[\*]</sup> phase is formed by A22 with the longest chains.

For compound A20 the XRD patterns were recorded at the same temperature ( $T = 90^\circ\text{C}$ ) after slow cooling (0.5 K min<sup>-1</sup> Fig. 8e) in the DC phase as well as after fast cooling (10 K min<sup>-1</sup> Fig. 8f) in the Cr<sup>[\*]</sup> phase. Surprisingly, the two XRD patterns look very similar, only all scattering appear to be a bit broader and have slightly lower intensity in the birefringent Cr<sup>[\*]</sup> phase, though the sample and exposure time were identical. This is reproducibly observed and would suggest a reduced local order in the Cr<sup>[\*]</sup> phase compared to the DC phase. This is in line with

the suggested core crystallization as origin of the exotherm (II) occurring on heating at the transition from the birefringent Cr<sup>[\*]</sup> phase to the optically isotropic DC phase (see curve c in Fig. 5d). Because chirality is observed in the birefringent Cr<sup>[\*]</sup> phase as well as in the isotropic DC phase, the aromatic cores should in both phases adopt chiral helical conformations with uniform helix sense, which is opposite in the distinct chiral domains. At the Cr<sup>[\*]</sup>–DC transition the contrast between the dark and bright domains decreases (compare Fig. 6a, e and c, g). This reduced optical activity indicates a reduction of the helical twist of the molecular conformations at the transition from the crystalline to the DC phase. Molecular entities with uniform helix sense cannot be densely packed in nondistorted layers and thus induce twist and curvature. This distortion increases with growing packing density of the helical entities, and therefore the denser core packing leads to a stronger layer deformation force, giving rise to the formation of the optically isotropic DC phase. The birefringent Cr<sup>[\*]</sup> phase, formed on rapid cooling appears to be dominated by optimized alkyl chain packing (chain crystallization), which allows a non-twisted lamellar or modulated lamellar organization of the molecules, but without optimized core-packing. The aromatic cores remain in a strongly twisted helical conformation, leading to a high optical activity, but the strong molecular twist also leads to a disruption of the aromatic layers into smaller domains (see Fig. 6d). Upon heating the Cr<sup>[\*]</sup> phase, the alkyl chain order decreases and a growing fraction of these chains becomes disordered. This allows a denser core packing, simultaneously leading to a reduced helicity of the molecular conformations (reduced optical activity) and, giving rise to a strong layer distortion and formation of the DC phase with an increased alkyl chain disorder. This means that the isotropic DC phases are the result of the optimization of core packing and represent disordered versions of the birefringent crystalline conglomerates (Cr<sup>[\*]</sup> phases), providing improved alkyl chain packing. With rising alkyl chain length the chain crystallization becomes increasingly more important. For compound A20 formation of the optical isotropic DC phase can still be achieved by using sufficiently slow cooling rates, so that the slow core crystallization can take place and determine the structure, leading to the DC phase. On fast cooling, however, densest core packing obviously cannot be achieved and the fast chain crystallization leads to a non-twisted lamellar organization, giving rise to the birefringent conglomerate phase Cr<sup>[\*]</sup> with reduced core order and enhanced optical activity. For compound A22 chain crystallization dominates at all cooling rates, and hence, exclusively a crystalline phase is formed.

Low birefringent crystalline conglomerate phases were also observed for compounds A14–A18, but for these compounds very high cooling rates ( $\gg 20\text{ K min}^{-1}$ ) are required for their formation and there is apparently always a coexistence of these birefringent Cr<sup>[\*]</sup> phases with the isotropic DC phases, which makes the investigations difficult. Fig. 10 shows representative textures and DSC curves as obtained for compound A16 after rapid cooling (30 K min<sup>-1</sup> for the texture and 50 K min<sup>-1</sup> before recording the DSC trace a). For these compounds core crystallization is sufficiently fast compared to alkyl chain



crystallization and therefore DC phases can be observed for moderate cooling rates. The  $Cr^{[*]}$  phases are absent for all shorter homologues starting with **A12**, which have the smallest contribution of alkyl chain crystallization to the total transition enthalpy value (Fig. 5a); here self-assembly is dominated by optimized core packing, which leads to DC phase formation.

**3.4.4 Molecular conformation and structure property relations.** DFT calculations of the model compound **A1** with  $n = 1$  (Gaussian 09 package, B3LYP functional and the LAN L2 DZ basis set) indicate a bent and helically twisted chiral molecular conformation as the minimum energy conformation shown in Fig. 11. The 4-methyl group at the resorcinol core unit does not induce a significant deviation from the  $120^\circ$  bending angle between the two azobenzene wings. Also, the azobenzene units themselves are linear and the benzene rings in these wings as well as the C=O groups are nearly coplanar. However, the methyl group at the 4-position at the resorcinol core induces a significant twist of the adjacent carboxyl group together with the coplanar azobenzene wing out of the plane of the resorcinol unit by  $72.4^\circ$ , which is much larger than that of the azobenzene wings adjacent to H-6 ( $53.6^\circ$ ). This strong twist leads to an overall helical molecular conformation and this is assumed to be responsible for a high tendency for chiral segregation and distorted packing in layers. Though the understanding of the general structure property relations with respect to formation of DC phases is still at the infancy it appears that the presence of relatively flat and rigid aromatic  $\pi$ -systems, as provided by azobenzenes and to some extent also by Schiff base units is favorable for formation of soft crystalline DC phases. So, it

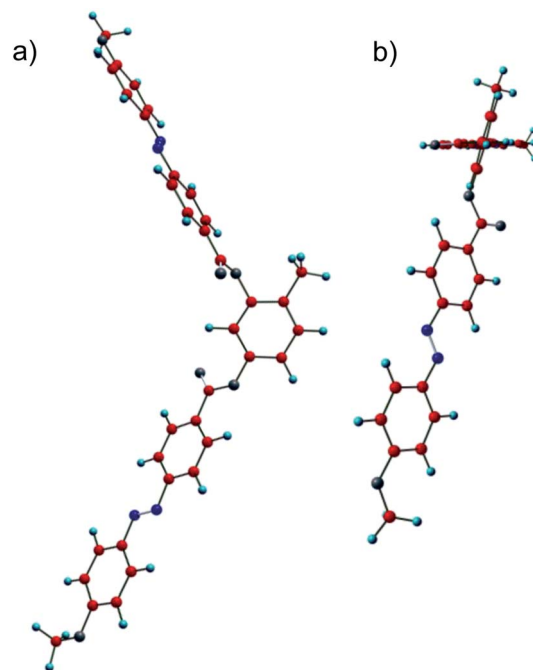


Fig. 11 Energy minimized molecular conformer of the model compound **A1** ( $n = 1$ ) as observed under two distinct perspectives (a) perpendicular to the bending plane and (b) along the azobenzene wing adjacent to the methyl group.

appears that  $\pi$ -stacking favours DC phase formation. In the case of the azobenzenes the presence of an additional relatively bulky substituent, such as I, Br or  $CH_3$  seems to be required, probably by providing a stronger molecular twist. In contrast, formation of LC sponge type DC phases is favoured for bent-core compounds with more flexible phenylbenzoate wings and having long and flexible or bulky end groups at the termini.<sup>8</sup> However, final conclusions cannot be drawn here and require further investigations.

**3.4.5 Investigation of mixtures with 5-CB.** It is known that HNF phases can be diluted by nematic LC hosts to a high degree (>95%) without the loss of the chirality.<sup>47</sup> This is a direct consequence of the helical nanofilament structure of these phases, allowing a swelling of the filaments by the nematic LC and transfer of chirality from the nanofilaments to the nematic LC. This effect is not observed for the sponge type DC phases formed by distorted fluid smectic phases. Therefore, investigation of mixtures with 5-CB could provide additional information concerning the microstructure of the DC phases of compounds **An**. The 1 : 1 mixture of **A14** with 4'-*n*-pentyl-4-cyanobiphenyl (5-CB) does not show any DC phase. On heating this mixture only a direct transition from the crystalline material to the isotropic liquid state occurs at  $85^\circ\text{C}$  which is below the DC-Iso transition temperature of pure **A14** ( $T = 101^\circ\text{C}$ ). On cooling this mixture a transition from the isotropic liquid to the nematic phase takes place at  $T \sim 54^\circ\text{C}$ , but no chiral domains can be observed. The nematic phase rapidly crystallizes with formation of a highly birefringent crystalline phase at  $T \sim 53^\circ\text{C}$  (see Table 2 and Fig. S19†).

The longer compounds **A16–A20** behave differently; for the 1 : 1 mixtures the DC phases were retained and their

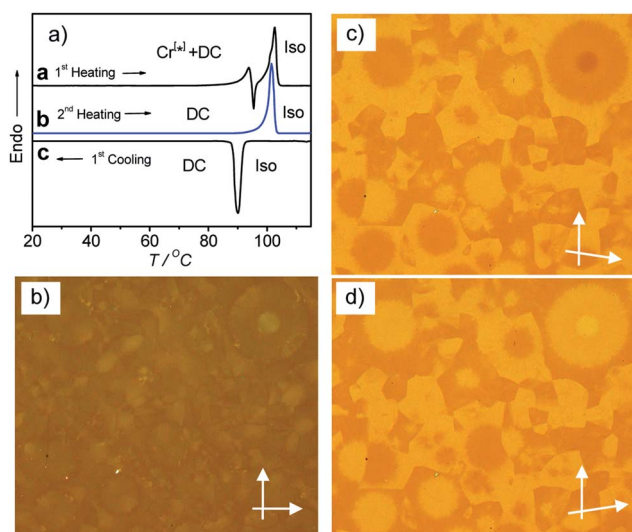


Fig. 10 Compound **A16**: (a) DSC traces ( $10\text{ K min}^{-1}$ ): curve a, heating after previous cooling with  $50\text{ K min}^{-1}$ ; curves b and c, heating/cooling with  $10\text{ K min}^{-1}$ ; (b) low birefringent texture of the  $Cr^{[*]}$  phase as obtained after fast cooling ( $30\text{ K min}^{-1}$ ); (c) same texture between slightly uncrossed polarizers and (d) after reversal of the direction of one polarizer, indicating the presence of a chiral conglomerate; remarkable is the presence of a domain with higher contrast in the center of the circular domain at the top right; probably, the birefringent textures develop as surface layers and in these regions goes through the complete sample.



temperature ranges increase with growing chain length (Table 2 and Fig. S20†). However, at only slightly higher 5-CB concentration, as for example, in the 4 : 6 mixtures of compounds **A16**–**A20** with 5-CB the chiral DC phase is lost and instead a heterogenous mixture is obtained indicating that the amount of 5-CB which can be mixed into the DC phases of compounds **An** is strongly limited. So, compared with the HNF phases, the DC phases of compounds **An** can only be retained if the alkyl chains are sufficiently long, but also in this case much less 5-CB is tolerated. These observations, in conjunction with the XRD studies, confirm that the DC phases of compounds **An** should be different from the classical HNF phases. It appears that these phases are formed by smaller nano-domains instead of long helical filaments, in line with the results discussed in the previous sections. Because no extended filaments are formed, no gel-like networks of these fibers are possible and therefore these compounds can take up only a limited amount of 5-CB, which is directly incorporated between the bent-core molecules thus reducing the stability of the DC phases.

Mixing the longest homologue **A22**, which does not show any DC phase, with 5-CB in 1 : 1 ratio induces a DC phase as an enantiotropic phase between  $T = 59\text{ }^{\circ}\text{C}$  and  $87\text{ }^{\circ}\text{C}$  (see Fig. S21†). This shows that 5-CB can reduce the chain crystallization and thus allow the formation of the DC phase even if the pure compound itself does not show any DC phase. However, no DC phase can be induced in the fluorinated compounds **Bn** ( $X = \text{F}$ , 1 : 1 mixtures with 5-CB) that show polar smectic phases and are discussed in Section 3.5.

### 3.5 Polar and non-polar smectic phases formed by compounds **Bn**–**Dn** with additional peripheral substituents

In order to investigate the effect of introducing a lateral substitution on the outer two benzene rings in the periphery of the aromatic core of the bent-core liquid crystals **An**, related molecules **Bn**, **C14** and **D14** were synthesized (Scheme 2). In the series of compounds **Bn** with  $X = \text{F}$  all compounds show the same type of mesophase, irrespective of the chain length (see Table 1). As an example, on heating **B14** in a homeotropic cell a schlieren texture is observed at  $T = 90\text{ }^{\circ}\text{C}$  (see Fig. S6a†) indicating the presence of a SmC phase. The relatively high transition enthalpy ( $\Delta H \sim 12.8\text{ kJ mol}^{-1}$ ) is in the range as usually found for polar SmC phases (for representative DSC traces, see

Table 2 Phase transition temperatures and mesophase types of 1 : 1 mixtures of 5-CB and compounds **A14**–**A22** and **B14**<sup>a</sup>

Mixture	Heating $T/^{\circ}\text{C}$	Cooling $T/^{\circ}\text{C}$
<b>A14</b> –5-CB	Cr <sub>1</sub> 39 Cr <sub>2</sub> 85 Iso	Iso 54 N 53 Cr
<b>A16</b> –5-CB	Cr 64 DC 73 Iso	Iso 66 DC
<b>A18</b> –5-CB	DC 77 Iso	Iso 72 DC
<b>A20</b> –5-CB	DC 80 Iso	Iso 78 DC
<b>A22</b> –5-CB	Cr <sup>[*]</sup> 59 DC 87 Iso	Iso 80 DC 37 Cr <sup>[*]</sup>
<b>B14</b> –5-CB	Cr 63 Iso	Iso 61 Cr

<sup>a</sup> Transition temperatures were taken from the observed textures using polarized optical microscopy; abbreviations: N = nematic phase, for other abbreviations please see Table 1.

Fig. S10†). The presence of two polarization reversal peaks in each half period of an applied triangular wave voltage ( $160\text{ V}_{\text{pp}}$ , see Fig. 12a) indicate an antiferroelectric switching process. The spontaneous polarization value was calculated to be  $P_s = 650\text{ nC cm}^{-2}$  at  $85\text{ }^{\circ}\text{C}$ . On cooling the compound in a  $6\text{ }\mu\text{m}$  ITO coated cell under an external applied field circular domains are formed (Fig. 12c). At 0 V the position of the extinction crosses is parallel to the polarizers, indicating an anticlinic tilted  $\text{SmC}_a\text{P}_A$  phase. Under an applied electric field the extinction crosses in the circular domains become inclined to the directions of the polarizers, indicating a field induced synclinc  $\text{SmC}_s\text{P}_F$  phase. By changing the direction of the applied electric field three distinct states (see Fig. 12b–d) can be clearly observed confirming a tristable switching process by rotation on a cone. Based on these results it is concluded that this is a  $\text{B}_2$ -type polar SmC phase with an anticlinic antiferroelectric  $\text{SmC}_a\text{P}_A$  ground state structure.

Replacing the fluorine substituents in **Bn** by methyl groups (**D14**) leads to a monotropic SmC phase (for texture see Fig. S6b†) without polar order, also indicated by the much smaller SmC–Iso transition enthalpy values ( $0.9\text{ kJ mol}^{-1}$ ) and the observation that no current peak could be observed up to a voltage of  $200\text{ V}_{\text{pp}}$  in a  $6\text{ }\mu\text{m}$  ITO cell. It appears that increasing the size of the peripheral substituents X reduces the packing density significantly, thus leading to strong reduction of mesophase stability in the order  $\text{H} \sim \text{F} > \text{CH}_3 > \text{Br}$ , at first leading to a loss of polar order for  $X = \text{CH}_3$  and finally to a complete

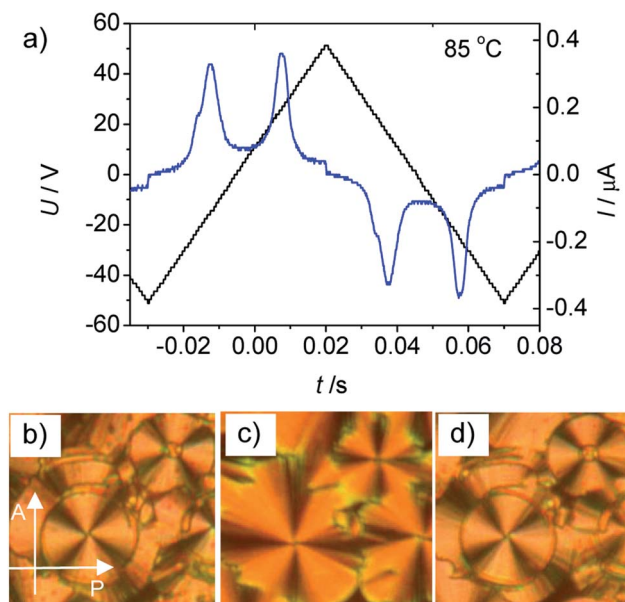


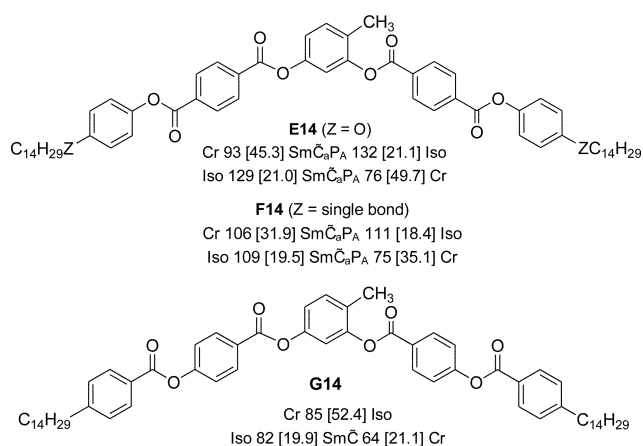
Fig. 12 Electrooptical investigation of compound **B14**. (a) Switching current response curve recorded by applying a triangular wave voltage ( $160\text{ V}_{\text{pp}}$ ,  $10\text{ Hz}$ ,  $5\text{ k}\Omega$ ) to a  $6\text{ }\mu\text{m}$  coated ITO cell with a homogeneous PI alignment layer at  $85\text{ }^{\circ}\text{C}$  in the  $\text{SmC}_a\text{P}_A$  phase; (b–d) optical textures as obtained at  $T = 79\text{ }^{\circ}\text{C}$  under an applied DC voltage between crossed polarizers (parallel rubbing), rubbing direction parallel to the polarizer, direction of the polarizers is shown in (b); (b) field induced  $\text{SmC}_s\text{P}_F$  state at  $+10\text{ V}$ ; (c),  $\text{SmC}_a\text{P}_A$  ground state after switching off the field ( $0\text{ V}$ ) and (d) the field induced  $\text{SmC}_s\text{P}_F$  state at  $-10\text{ V}$ .



suppression of all mesophases for  $X = \text{Br}$ . As the electronegative F atoms increase the polarity of the core region, and hence increase the segregation of the core from the lipophilic alkyl chains, there is no significant mesophase destabilization or a slight stabilization if H is replaced by F (compare **A14** and **B14** in Table 1). But nevertheless, chiral segregation is removed. The dominance of steric effects of Br and  $\text{CH}_3$  leads to the loss of polar order and to the lowest LC phase stability for these compounds.

### 3.6 Effects of replacing the azo groups by ester groups

Aiming to investigate the effects of replacing the azo linking groups in compounds **A14** by ester groups, compounds **E14**, **F14** and **G14** were synthesized. As shown in Scheme 3, the mesophase exhibited by **E14** is enantiotropic with a relatively wide LC range and much higher transition temperatures than found for **A14**. The texture of the LC phase (Fig. S6c†) is similar to those observed for modulated smectic phases of bent-core mesogens.<sup>48</sup> On applying a triangular wave electric field of 160  $V_{\text{pp}}$  to **E14** in a 6  $\mu\text{m}$  ITO cell, two polarization reversal peaks can be clearly observed in the switching current response curve (see Fig. S22†) indicating antiferroelectric switching. The spontaneous polarization value,  $P_s = 310 \text{ nC cm}^{-2}$  at 120  $^\circ\text{C}$  is only about one half of that usually observed for  $\text{SmCP}_A$  phases ( $\sim 600\text{--}800$  in the  $B_2$  phases) and is in the typical range as observed for modulated  $\text{SmCP}_A$  phases. By changing the direction of the applied electric field (Fig. S23†), no change in the texture could be observed, confirming that the switching process in this mesophase takes place by collective rotation around the long axis of the molecules. This mode of switching is also in line with a modulated structure of this  $\text{SmCP}_A$  phase ( $\text{Sm}\tilde{C}_a\text{P}_A$ ); for a nondistorted flat  $\text{SmC}_a\text{P}_A$  phase a switching on a cone would be more likely.



**Scheme 3** Chemical structures of the synthesized 4-methylresorcinol based terephthalates **E14**, **F14** and benzoate **G14** with transition temperatures ( $T/^\circ\text{C}$ ) and corresponding enthalpies ( $\Delta H/\text{kJ mol}^{-1}$ , given in square brackets) on heating (top lines) and cooling (bottom lines, both recorded at a rate of 10  $\text{K min}^{-1}$ ); abbreviations:  $\text{Sm}\tilde{C}_a\text{P}_A$  = modulated antiferroelectric switching anticlinic  $\text{SmC}$  phase;  $\text{Sm}\tilde{C}$  = non-switchable modulated  $\text{SmC}$  phase with synclinc tilt correlation, for other abbreviations, see Scheme 1 and Table 1; for DSC traces, see Fig. S11.†

In XRD measurements of compound **E14** (Fig. S18†) several equally spaced sharp reflections can be found in the small angle region, indicating a lamellar structure with a  $d$ -value of 4.83 nm. The diffuse scattering in the wide angle region shows four intensity maxima beside the equator, from which a tilt angle of the molecules of  $\sim 28^\circ$  could be calculated. As the extinction crosses are approximately parallel to the polarizers (Fig. S6c†) and an equal intensity of the wide angle scattering is found (Fig. S18a and b†) the tilt correlation should be anticlinic. Though there are indications of layer modulations or undulations from other experimental data, these are not visible in the XRD patterns. Either the modulation wavelength is very long, so that the layer reflections are not resolved into separate reflections, or the reflections with  $h$  and  $k \neq 0$  are too weak to be detected with the used XRD setup.

Replacing the terminal alkoxy chains in **E14** by alkyl chains in compound **F14** (see Scheme 3, for DSC traces see Fig. S11a†) leads to a compound with about 20 K lower clearing temperature which can also be assigned as  $\text{Sm}\tilde{C}_a\text{P}_A$  based on the observed textures and measured  $P_s$  values ( $P_s = 300 \text{ nC cm}^{-2}$  at 95  $^\circ\text{C}$ , see Fig. S24†). The major difference between the two compounds is the inclination of the dark extinctions upon applying an electric field (Fig. S25†), indicating that the switching process in this case takes place on a cone; so probably the modulation wavelength of **F14** is larger than for **E14**.

Inverting the direction of the terminal ester group in compound **G14** (see Scheme 3) further reduces the transition temperatures, which are now similar to those of the azobenzene derivative **A14** (for DSC traces see Fig. S11b†). Also in this case the texture is similar to those of some modulated smectic phases (Fig. S6d†). The position of the extinction crosses is inclined with the orientation of the polarizers and thus indicates a synclinc tilted organization of the molecules. In electrooptic studies (160  $V_{\text{pp}}$  in a 6  $\mu\text{m}$  ITO cell) no current response can be detected. This might be due to a shorter modulation wavelength than in the case of **E14**, which is known to suppress polar switching or would require very high voltages. Also the observation of a uniform synclinc tilt would be in line with a  $B_{1\text{rev}}$ -like modulated  $\text{SmC}$  phase with an oblique lattice. However, it was not possible to further confirm the proposed phase structure by XRD due to the rapid crystallization. Overall, replacing the azobenzene wings by terephthalates (**E14**, **F14**) or benzoates (**G14**) removes the DC phases and leads to polar and apolar smectic phases with a significant tendency for layer modulation or undulation.

## 4. Conclusions and summary

New bent-core liquid crystalline materials combining 4-methylresorcinol with azobenzene wings were synthesized and investigated. The short homologues ( $n = 6\text{--}8$ ) exhibit intercalated smectic phases ( $B_6$  phases) which upon increasing the chain length ( $n = 9\text{--}20$ ) convert to DC phases and for the longest homologue ( $n = 22$ ) only a crystalline phase was observed. For compound **A20** formation of the optically isotropic DC phase is in competition with formation of a low birefringent crystalline conglomerate ( $\text{Cr}^{[*]}$ ) and the observed phase type is strongly



dependent on the cooling rate. It appears that formation of the Cr<sup>[\*]</sup> phase is favored by chain crystallization, whereas in the isotropic DC phases core crystallization is dominating. Based on the XRD patterns and high viscosity the DC phases of compounds **An** belong to the soft crystalline DC phases, but they are distinct from the previously reported B<sub>4</sub>-type HNF phases by the absence of extended filaments as indicated by the results of their mixtures with 5-CB.

Introduction of additional substituents at the outer rings of the bent-core molecules **An** removes the DC phases and replaces them first by polar smectic phases (X = F, SmC<sub>a</sub>P<sub>A</sub>). Upon further enlargement of these substituents (X = CH<sub>3</sub>) also polar order is removed, yielding a non-polar SmC phase which is then removed for the compound with the largest substituent X = Br. Replacing the azo groups by ester groups in the related terephthalates or benzoates also removes the DC phases and leads to different types of modulated SmC phases which in most cases show polar switching.

Overall, new modifications of isotropic as well as birefringent conglomerate phases were observed and the relationship between molecular structure and formation of these phases was identified. It appears that the azobenzene unit is a specially powerful tool for introducing new types of chiral conglomerate phases, distinct from the typical B<sub>4</sub> type phases found for benzylidene imines. There seems to be a whole zoo of different types of these DC phases, ranging from the fluid B<sub>2</sub>-like sponge phases to several distinct types of soft crystalline phases, including modulated subtypes;<sup>49–51</sup> obviously only a small fraction of the potential structures has been explored yet. Moreover, the possibilities provided by introduction of the photo-isomerizable azobenzene units into BCLC forming DC phases could lead to interesting perspectives for chirality switching and phase modulation, leading to unique and potentially useful multifunctional chiral materials for application in chiral discrimination of chiral physical forces and molecular species<sup>22</sup> and as non-centrosymmetric materials.

## Acknowledgements

M. Alaasar is grateful to the Alexander von Humboldt Foundation for the research fellowship at the Martin-Luther University Halle-Wittenberg, Germany.

## References

- 1 T. Sekine, T. Niori, J. Watanabe, T. Furukawa, S. W. Choi and H. Takezoe, *J. Mater. Chem.*, 1997, **7**, 1307.
- 2 (a) R. A. Reddy and C. Tschierske, *J. Mater. Chem.*, 2006, **16**, 907; (b) H. Takezoe and Y. Takanishi, *Jpn. J. Appl. Phys., Part 1*, 2006, **45**, 597; (c) G. Pelzl, S. Diele and W. Weissflog, *Adv. Mater.*, 1999, **11**, 707; (d) C. Tschierske, *Angew. Chem., Int. Ed.*, 2013, **52**, 8828; (e) V. Görtz and J. W. Goodby, *Chem. Commun.*, 2005, 3262; (f) G. Pelzl and W. Weissflog, in *Thermotropic Liquid Crystals*, ed. A. Ramamoorthy, Springer, The Netherlands, 2007, pp. 58–83; (g) I. Dierking, *Angew. Chem., Int. Ed.*, 2010, **49**, 29; (h) A. Eremin and A. Jákli, *Soft Matter*, 2013, **9**, 615.
- 3 D. R. Link, G. Natale, R. Shao, J. E. MacLennan, N. A. Clark, E. Körblova and D. M. Walba, *Science*, 1997, **278**, 1924.
- 4 (a) J. Harden, B. Mbanga, N. Eber, K. Fodor-Csorba, S. Sprunt, J. T. Gleeson and A. Jákli, *Phys. Rev. Lett.*, 2006, **97**, 157802; (b) A. C. Charif, N. Diorio, K. Fodor-Csorba, J. E. Puskásad and A. Jákli, *RSC Adv.*, 2013, **3**, 17446.
- 5 (a) W. Iglesias, T. J. Smith, P. B. Basnet, S. R. Stefanovic, C. Tschierske, D. J. Lacks, A. Jákli and E. K. Mann, *Soft Matter*, 2011, **7**, 9043; (b) W. Iglesias, N. L. Abbott, E. K. Mann and A. Jákli, *ACS Appl. Mater. Interfaces*, 2012, **4**, 6884.
- 6 J. Etxebarria and M. B. Ros, *J. Mater. Chem.*, 2008, **28**, 2919.
- 7 M. Nagaraj, Y. P. Panarin, J. K. Vij, C. Keith and C. Tschierske, *Appl. Phys. Lett.*, 2010, **97**, 213505.
- 8 (a) G. Dantlgraber, A. Eremin, S. Diele, A. Hauser, H. Kresse, G. Pelzl and C. Tschierske, *Angew. Chem., Int. Ed.*, 2002, **41**, 2408; (b) G. Dantlgraber, S. Diele and C. Tschierske, *Chem. Commun.*, 2002, 2768; (c) C. Tschierske and G. Dantlgraber, *Pramana*, 2003, **61**, 455; (d) C. Keith, R. A. Reddy, A. Hauser, U. Baumeister and C. Tschierske, *J. Am. Chem. Soc.*, 2006, **128**, 3051; (e) C. Keith, R. A. Reddy, U. Baumeister, H. Hahn, H. Lang and C. Tschierske, *J. Mater. Chem.*, 2006, **16**, 3444; (f) H. Hahn, C. Keith, H. Lang, R. A. Reddy and C. Tschierske, *Adv. Mater.*, 2006, **18**, 2629; (g) C. Keith, G. Dantlgraber, R. A. Reddy, U. Baumeister, M. Prehm, H. Hahn, H. Lag and C. Tschierske, *J. Mater. Chem.*, 2007, **17**, 3796; (h) C. Keith, G. Dantlgraber, R. A. Reddy, U. Baumeister and C. Tschierske, *Chem. Mater.*, 2007, **19**, 694; (i) Y. Zhang, U. Baumeister, C. Tschierske, M. O'Callaghan and C. Walker, *Chem. Mater.*, 2010, 2869; (j) H. Ocak, B. Bilgin-Eran, M. Prehm and C. Tschierske, *Soft Matter*, 2012, **8**, 7773.
- 9 L. E. Hough, M. Spannuth, M. Nakata, D. A. Coleman, C. D. Jones, G. Dantlgraber, C. Tschierske, J. Watanabe, E. Körblova, D. M. Walba, J. E. MacLennan, M. A. Glaser and N. A. Clark, *Science*, 2009, **325**, 452.
- 10 G. Heppke, D. D. Parghi and H. Sawade, *Liq. Cryst.*, 2000, **27**, 313.
- 11 J. Thisayukta, Y. Nakayama, S. Kawauchi, H. Takezoe and J. Watanabe, *J. Am. Chem. Soc.*, 2000, **122**, 7441.
- 12 (a) R. A. Reddy and B. K. Sadashiva, *Liq. Cryst.*, 2003, **30**, 1031; (b) A. Roy, M. Gupta, S. Radhika, B. K. Sadashiva and R. Pratibha, *Soft Matter*, 2012, **8**, 7207.
- 13 (a) J. Ortega, C. L. Folcia, J. Etxebarria, N. Gimeno and M. B. Ros, *Phys. Rev. E: Stat., Nonlinear, Soft Matter Phys.*, 2003, **68**, 11707; (b) N. Gimeno, A. Sanchez-Ferrer, N. Sebastian, R. Mezzenga and M. B. Ros, *Macromolecules*, 2011, **44**, 9586.
- 14 M. Nagaraj, K. Usami, Z. Zhang, V. Görtz, J. W. Goodby and H. F. Gleeson, *Liq. Cryst.*, 2014, **41**, 800.
- 15 (a) A. Jákli, Y.-M. Huang, K. Fodor-Csorba, A. Vajda, G. Galli, S. Diele and G. Pelzl, *Adv. Mater.*, 2003, **15**, 1606; (b) W. Weissflog, M. W. Schröder, S. Diele and G. Pelzl, *Adv. Mater.*, 2003, **15**, 630.
- 16 (a) L. E. Hough, H. T. Jung, D. Krüerke, M. S. Heberling, M. Nakata, C. D. Jones, D. Chen, D. R. Link, J. Zasadzinski, G. Heppke, J. P. Rabe, W. Stocker, E. Körblova,





- D. M. Walba, M. A. Glaser and N. A. Clark, *Science*, 2009, **325**, 456; (b) D. M. Walba, L. Eshat, E. Körblová and R. K. Shoemaker, *Cryst. Growth Des.*, 2005, **5**, 2091; (c) D. Chen, J. E. MacLennan, R. Shao, D. K. Yoon, H. Wang, E. Körblová, D. M. Walba, M. A. Glaser and N. A. Clark, *J. Am. Chem. Soc.*, 2011, **133**, 12656.
- 17 (a) J. Thisayukta, H. Takezoe and J. Watanabe, *Jpn. J. Appl. Phys., Part 1*, 2001, **40**, 3277; (b) H. Niwano, M. Nakata, J. Thisayukta, D. R. Link, H. Takezoe and J. Watanabe, *J. Phys. Chem. B*, 2004, **108**, 14889; (c) H. Kurosu, M. Kawasaki, M. Hirose, M. Yamada, S. Kang, J. Thisayukta, M. Sone, H. Takezoe and J. Watanabe, *J. Phys. Chem. A*, 2004, **108**, 4674.
- 18 H. Kresse, J. Saltetnokova, H. Nadasi, W. Weissflog and A. Hauser, *Liq. Cryst.*, 2001, **28**, 1017.
- 19 V. Prasad, *Liq. Cryst.*, 2001, **28**, 1115.
- 20 H. Nadasi, C. Lischka, W. Weissflog, I. Wirth, S. Diele, G. Pelzl and H. Kresse, *Mol. Cryst. Liq. Cryst.*, 2003, **399**, 69.
- 21 J. Martínez-Perdiguero, I. Alonso, C. L. Folcia, J. Etxebarria and J. Ortega, *J. Mater. Chem.*, 2009, **15**, 5161.
- 22 H. Takezoe, *Top. Curr. Chem.*, 2012, **318**, 303.
- 23 D. K. Yoon, Y. Yi, Y. Shen, E. D. Körblová, D. M. Walba, I. I. Smalyukh and N. A. Clark, *Adv. Mater.*, 2011, **23**, 1962.
- 24 J. Ortega, N. Pereda, C. L. Folcia, J. Etxebarria and M. B. Ros, *Phys. Rev. E: Stat. Phys., Plasmas, Fluids, Relat. Interdiscip. Top.*, 2000, **63**, 011702.
- 25 G. Lee, R. J. Carlton, F. Araoka, N. L. Abbott and H. Takezoe, *Adv. Mater.*, 2013, **25**, 245.
- 26 E. Bialecka-Florjanczyk, I. Sledzinska, E. Górecka and J. Przedmojski, *Liq. Cryst.*, 2008, **35**, 401.
- 27 (a) S.-W. Choi, T. Izumi, Y. Hoshino, Y. Takanishi, K. Ishikawa, J. Watanabe and H. Takezoe, *Angew. Chem., Int. Ed.*, 2006, **45**, 1382; (b) G. Lee, R. J. Carlton, F. Araoka, N. L. Abbott and H. Takezoe, *Adv. Mater.*, 2013, **25**, 245.
- 28 M. Alaasar, M. Prehm and C. Tschierske, *Chem. Commun.*, 2013, **49**, 11062.
- 29 I. C. Pintre, J. L. Serrano, M. B. Ros, J. M. Perdiguero, I. Alonso, J. Ortega, C. Folcia, J. Etxebarria, R. Alicante and B. Villacampa, *J. Mater. Chem.*, 2010, **20**, 2965.
- 30 Y. Zang, J. Martínez-Perdiguero, U. Baumeister, C. Walker, J. Etxebarria, M. Prehm, J. Ortega, C. Tschierske, M. O'Callaghan, A. Harant and M. Handschy, *J. Am. Chem. Soc.*, 2009, **131**, 18366.
- 31 (a) H. G. Heller and J. R. Langan, *J. Chem. Soc., Perkin Trans. 1*, 1981, **2**, 341; (b) P. Schmitz, H. Gruler and M. Eberhardt, *Mol. Cryst. Liq. Cryst.*, 1995, **262**, 129.
- 32 (a) V. Prasad, S.-W. Kang and S. Kumar, *J. Mater. Chem.*, 2003, **13**, 1259; (b) V. Prasad and A. Jáklí, *Liq. Cryst.*, 2004, **31**, 473; (c) V. Prasad, S.-W. Kang, X. Qi and S. Kumar, *J. Mater. Chem.*, 2004, **14**, 1495; (d) A. Jáklí, V. Prasad, D. S. S. Rao, G. Liao and I. Janossy, *Phys. Rev. E: Stat., Nonlinear, Soft Matter Phys.*, 2005, **71**, 02170911; (e) N. G. Nagaveni, A. Roy and V. Prasad, *J. Mater. Chem.*, 2012, **22**, 8948; (f) C. L. Folcia, I. Alonso, J. Ortega, J. Etxebarria, I. Pintre and M. B. Ros, *Chem. Mater.*, 2006, **18**, 4617; (g) I. C. Pintre, N. Gimeno, J. L. Serrano, M. B. Ros, I. Alonso, C. L. Folcia, J. Ortega and J. Etxebarria, *J. Mater. Chem.*, 2007, **17**, 2219; (h) J. Etxebarria and M. B. Ros, *J. Mater. Chem.*, 2008, **18**, 2919; (i) I. C. Pintre, J. L. Serrano, M. B. Ros, J. M. Perdiguero, I. Alonso, J. Ortega, C. L. Folcia, J. Etxebarria, R. Alicante and B. Villacampa, *J. Mater. Chem.*, 2010, **20**, 2965; (j) M. Vijaysrinivasan, P. Kannan and A. Roy, *Liq. Cryst.*, 2012, **39**, 1465.
- 33 (a) M. Alaasar, M. Prehm, M. Nagaraj, J. K. Vij and C. Tschierske, *Adv. Mater.*, 2013, **25**, 2186; (b) M. Alaasar, M. Prehm, K. May, A. Eremin and C. Tschierske, *Adv. Funct. Mater.*, 2013, **24**, 1703.
- 34 (a) M. Alaasar, M. Prehm and C. Tschierske, *Liq. Cryst.*, 2013, **40**, 656; (b) M. Alaasar, M. Prehm and C. Tschierske, *Liq. Cryst.*, 2014, **41**, 126.
- 35 cv = crystal volumes, calculated using the increments of A. Immirzi: A. Immirzi and B. Perini, *Acta Crystallogr., Sect. A: Cryst. Phys., Diffr., Theor. Gen. Crystallogr.*, 1977, **33**, 216.
- 36 Very few examples of BCLCs based on 4-methylresorcinol have been reported previously: (a) U. Dunemann, M. W. Schröder, R. A. Reddy, G. Pelzl, S. Diele and W. Weissflog, *J. Mater. Chem.*, 2005, **15**, 4051; (b) W. Weissflog, G. Pelzl, H. Kresse, U. Baumeister, K. Brand, M. W. Schröder, M. G. Tamba, S. Findeisen-Tandel, U. Kornek, S. Stern, A. Eremin, R. Stannarius and J. Svoboda, *J. Mater. Chem.*, 2010, **20**, 6057.
- 37 C. Keith, A. Lehmann, U. Baumeister, M. Prehm and C. Tschierske, *Soft Matter*, 2010, **6**, 1704.
- 38 M. J. Frisch, *et al.*, *Gaussian 09, Revision A.1*, Gaussian Inc., Wallingford CT, 2009.
- 39 (a) S. Kang, M. Tokita, Y. Takanishi, H. Takezoe and J. Watanabe, *Phys. Rev. E: Stat., Nonlinear, Soft Matter Phys.*, 2007, **76**, 042701; (b) S. Kang, S. K. Lee, M. Tokita and J. Watanabe, *Phys. Rev. E: Stat., Nonlinear, Soft Matter Phys.*, 2009, **80**, 042703.
- 40 Also dielectric studies confirm the similarity of the B<sub>6</sub> phases having short-range ordered ribbons with the B<sub>1</sub> phases formed by a long range 2D lattice of ribbons: H. Kresse, H. Schmalfuss and W. Weissflog, *Liq. Cryst.*, 2001, **28**, 799.
- 41 The electron density modulation occurs between the regions where alkyl chains are mixed with the central units of the bent cores (low electron density) and the regions with overlapping parts of the rod-like wings (high electron density).
- 42 Due to this overlapping of phase transition and crystallization the transition enthalpy values could not be determined for the B<sub>6</sub>-DC transition.
- 43 I. Dierking, *Liq. Cryst. Today*, 2003, **12**, 1.
- 44 The difference of the transition temperatures in the cooling curves b and d in Fig. 5c and d is mainly due to the very different cooling rate used.
- 45 A similar texture was recently described for mixtures of B<sub>4</sub> phases with nematic LC and was interpreted as an alignment of the helical nanofilaments by the nematic director, we think that in our case this texture has different origin and indicates a crystalline conglomerate phase: F. Araoka, G. Sugiyamam, K. Ishikawa and H. Takezoe, *Adv. Funct. Mater.*, 2013, **23**, 2701.



- 46 The molecular length in the Chevron shaped conformation (see Fig. S1†) was used for calculations; a partial intercalation of the alkyl chains, leading to a reduced tilt angle, cannot be excluded.
- 47 T. Otani, F. Araoka, K. Ishikawa and H. Takezoe, *J. Am. Chem. Soc.*, 2009, **131**, 12368.
- 48 R. A. Reddy, U. Baumeister, C. Keith and C. Tschierske, *J. Mater. Chem.*, 2007, **17**, 62.
- 49 H. Ocak, B. Bilgin-Eran, M. Prehm and C. Tschierske, *Soft Matter*, 2013, **9**, 4590.
- 50 I. Miyake, Y. Takanishi, N. V. S. Rao, M. K. Paul, K. Ishikawa and H. Takezoe, *J. Mater. Chem.*, 2005, **15**, 4688.
- 51 E. Tsai, J. M. Richardson, E. Körblova, M. Nakata, D. Chen, Y. Shen, R. Shao, N. A. Clark and D. M. Walba, *Angew. Chem., Int. Ed.*, 2013, **52**, 5254.



## Chirality

## Helical Nano-crystallite (HNC) Phases: Chirality Synchronization of Achiral Bent-Core Mesogens in a New Type of Dark Conglomerates

Mohamed Alaasar,<sup>\*[a, b]</sup> Marko Prehm,<sup>[a]</sup> and Carsten Tschierske<sup>\*[a]</sup>

**Abstract:** Spontaneous generation of macroscopic homochirality in soft matter systems by self-assembly of exclusively achiral molecules under achiral conditions is a challenging task with relevance for fundamental scientific research and technological applications. Dark conglomerate phases (DC phases), being optically isotropic mesophases composed of conglomerates of macroscopic chiral domains and formed by some non-chiral bent-core mesogens, represent such a case. Here we report two new series of non-symmetric bent-core molecules capable of forming a new type of mirror symmetry broken DC phases. In the synthesized molecules, a bent 4-bromoresorcinol core is connected to a phenyl benzoate wing and an azobenzene wing with or without additional peripheral fluorine substitution. The self-assembly was investigated by DSC, polarizing microscopy, electro-optical studies and XRD. Chiral and apparently achiral

DC phases were observed besides distinct types of lamellar liquid crystalline phases with different degree of polar order, allowing the investigation of the transition from smectic to DC phases. This indicates a process in which increased packing density at first gives rise to restricted rotation and thus to growing polar order, which then leads to chirality synchronization, layer frustration and nano-scale crystallization. Topological constraints arising from the twisted packing of helical conformers in lamellar crystals is proposed to lead to amorphous solids composed of helical nano-crystallites with short coherence length (HNC phases). This is considered as a third major type of DC phases, distinct from the previously known liquid crystalline sponge phases and the helical nano-filament phases (HNF phases). Guidelines for the molecular design of new materials capable of self-assembly into these three types of DC phases are proposed.

## 1. Introduction

Chirality is a basic feature of living matter observed at various hierarchical levels from the subatomic level through molecules, self-assembled supramolecular structures and phases to macroscopic objects.<sup>[1]</sup> The investigation of the development of chirality from achiral molecules became a major research topic in the recent decade.<sup>[2]</sup> Significant progress has been made in the construction of chiral aggregates, such as fibres and dye aggregates.<sup>[3]</sup> However, examples of spontaneous generation of macroscopic homochirality only with achiral molecules and under achiral conditions, are extremely rare outside crystalline solid-state materials<sup>[4,5]</sup> and mainly found in liquid crystals

(LCs).<sup>[6-16]</sup> Molecules with a non-linear bent shape, the so-called bent-core liquid crystals (BCLCs) represent an exciting class of such compounds that have received significant attention due to their remarkable and unique properties, such as macroscopic polar order and spontaneous mirror symmetry breaking, being of general interest for fundamental soft matter science as well as for potential applications.<sup>[6,17-23]</sup> An actual challenge is the understanding of the so-called dark conglomerate phases (DC phases), representing complex mirror symmetry broken mesophases, occurring as intermediate states between the disordered liquids and the long-range ordered crystalline state (Figure 1a).<sup>[6,7,24-27]</sup> The common feature of these DC phases is the absence of birefringence due to a distortion of long-range periodic order, that is, they are optically isotropic and therefore appear "dark" between crossed polarizers. Moreover, in most cases spontaneous chirality, leading to conglomerates of macroscopically chiral domains with significant optical activity was observed, though the involved molecules are achiral.<sup>[28]</sup> More recently, spontaneous chirality was also found in some nematic phases of achiral bent-core molecules (chiral domain phases<sup>[29]</sup> and  $N_{TB}$  phases<sup>[13-15]</sup>) and conglomerate structures were observed in some bicontinuous cubic phases<sup>[30]</sup> and even in isotropic liquids of polycatenar (multi-chain) rod-like mesogens, having no molecular bend.<sup>[10,31,32]</sup> This shows that spontaneous mirror symmetry breaking is a rather general phenomenon, not limited to the BCLCs.<sup>[10]</sup>

[a] Dr. M. Alaasar, Dr. M. Prehm, Prof. Dr. C. Tschierske  
Institute of Chemistry  
Martin Luther University Halle-Wittenberg  
Kurt Mothes Str. 2, 06120 Halle (Saale) (Germany)  
Fax: (+49) 345-5527643  
E-mail: carsten.tschierske@chemie.uni-halle.de

[b] Dr. M. Alaasar  
Department of Chemistry, Faculty of Science  
Cairo University, Giza (Egypt)  
Fax: (+49) 345-5527643  
E-mail: malaasar@sci.cu.edu.eg

Supporting information and ORCID number from the author for this article are available on the WWW under <http://dx.doi.org/10.1002/chem.201505016>.

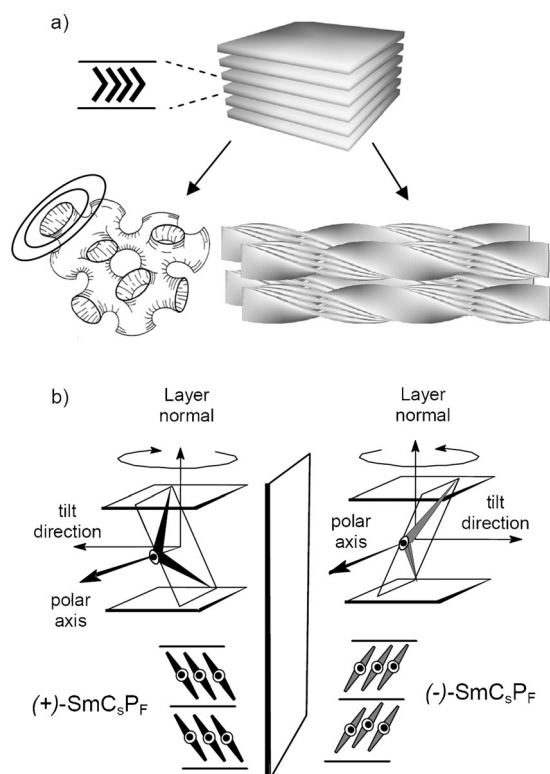
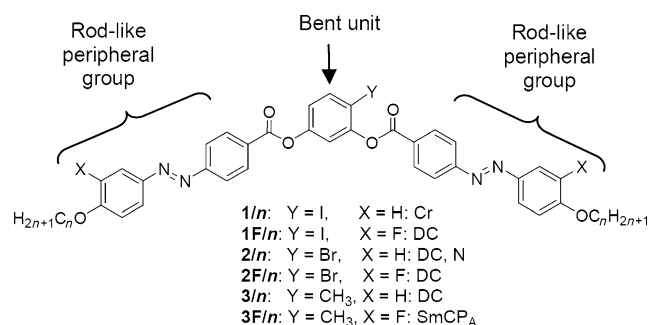


**Figure 1.** a) The two major types of dark conglomerate (DC) phases of BCLCs (bottom) are considered as derived from the lamellar organization of bent-core mesogens (top) by layer deformation arising from packing constraints due to the bent molecular shape and chirality synchronization; the picture of the sponge phase is taken from Ref. [38]; b) Chirality arising from the polar and tilted organization of the molecules in layers, ribbons or domains combining uniform tilt direction and uniform polar direction ( $\text{SmC}_s\text{P}_F$ ). The orthogonal combination of tilt and polar order leads to superstructural chirality (layer chirality) being inverted either by inverting tilt or polar direction.<sup>[17,37]</sup>

Chirality evolves in a cooperative process between a twist emerging by LC self-assembly and the chirality synchronization<sup>[10,32]</sup> of helical conformers<sup>[7,33]</sup> of the involved transiently chiral, but statistically achiral molecules.<sup>[34]</sup> In the case of the bent-core mesogens, the molecular structure favours director orientations with local twist, bend and splay, due to the effect of the molecular shape on the respective elastic constants<sup>[35]</sup> and developing packing constraints.<sup>[24,36]</sup> For LC phases of BCLCs involving a tilted organization in a lamellar assembly, there is an additional source of chirality, emerging as soon as an organization of the molecules with preferred uniform bend-direction develops, which then leads to emergence of polar order being directed perpendicular to layer normal and tilt direction. This orthogonal combination of tilt, polar director and layer normal results in a chiral organization in space, designated as layer chirality (see Figure 1 b).<sup>[17]</sup> Reversing either tilt direction or polar direction reverses the handedness of this layer chirality. Therefore,  $\text{SmC}$  phases, ribbons or domains (clusters) composed of layers or layer fragments with identical tilt and polar direction ( $\text{SmC}_s\text{P}_F$ ) are intrinsically chiral.<sup>[37]</sup> For BCLCs this superstructural chirality additionally couples with the above mentioned chiralities, being based on helical conformations

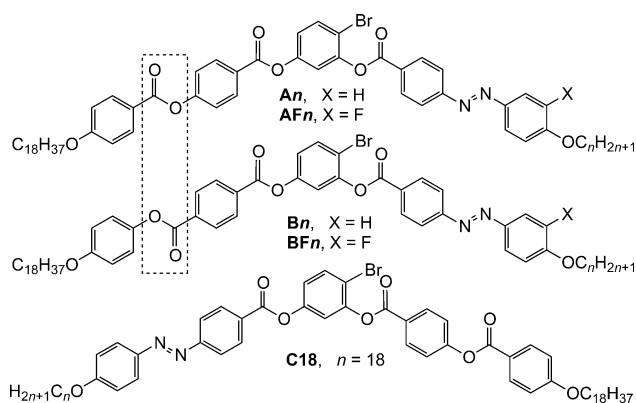
and superstructures, thus leading to energetically favourable and unfavourable diastereomeric pairs.

For BCLCs, there are two distinct major types of DC phases, the sponge phases representing deformed smectic LC phases with sponge like structure<sup>[24,38–49]</sup> and the helical nano-filament phases (HNF phases or B4 phases),<sup>[50]</sup> in which the molecules are organized in stacks of twisted ribbons forming arrays of helical nano-scale filaments (see Figure 1 a).<sup>[25,51–58]</sup> A major difference between these two types is provided by the local molecular order. In the sponge phases there is a lamellar organization in layers, in which the individual molecules have no fixed positions; hence, these are considered as truly liquid crystalline phases. In contrast, there is crystal-like packing in the individual nano-scale filaments forming the HNF phases, representing robust glassy solids. In recent years, further modifications and intermediate structures between these two types have been reported.<sup>[59–63]</sup> For example, there are liquid crystalline DC phases composed of ribbons (modulated DC phases)<sup>[64,65]</sup> and also sponge-like structures involving hexatic and possibly crystal-like order.<sup>[66]</sup> Twist grain boundary (TGB)-like DC phases were also reported<sup>[67]</sup> and chiral molecules can form homogeneously chiral versions of the DC phases.<sup>[68]</sup> In addition, DC phases with crystalline local structure, but being distinct from the HNF phases have recently been observed for several azobenzene based bent-core molecules shown in Scheme 1.<sup>[69–73]</sup>



**Scheme 1.** Chemical structures of previously reported BCLCs with two azobenzene peripheral groups (“wings”) and their mesophases (Cr = birefringent crystal, DC = dark conglomerate phase, N = nematic phase and  $\text{SmCP}_A$  = antiferroelectric switching tilted smectic phase).<sup>[69–73]</sup>

Herein we report a new class of DC phase forming non-symmetric BCLCs derived from the 4-bromoresorcinol core and combining an azobenzene peripheral group with a phenyl benzoate-based wing.<sup>[74]</sup> Within the phenyl benzoate wing the direction of the COO unit is inverse in the series **An** and **Bn** (see Scheme 2). The effect of a peripheral fluorine substitution at the outer ring of the azobenzene unit (compounds **AFn** and **BFn**; X = F), the effect of changing the position of the bromine substituent (**C18**) and replacing the bromine by chlorine (**D18** and **E18**, see Section 2.5) have also been studied for selected examples. Only those compounds having the azobenzene wing located adjacent to the bromine-substituted side of the bent-core are capable of forming DC phases, in some cases occurring below  $\text{SmC}$  phases. These DC phases, composed of hel-



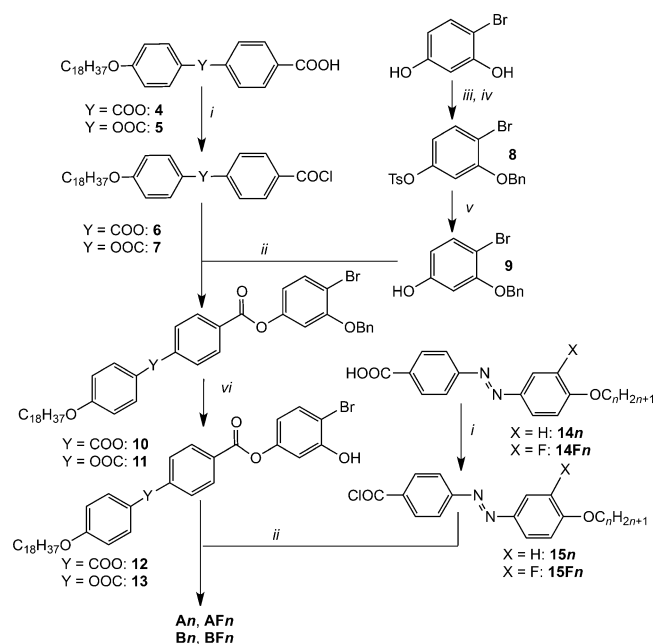
**Scheme 2.** Chemical structures of the 4-bromoresorcinol-based bent-core molecules under investigation.

ical nano-crystallites (helical nano-crystallite phases = HNC phases), are considered as a third type of DC phases besides the previously known LC sponge phases and the HNF phases. The transition from the SmC phases to the DC phases was investigated, indicating a process in which a continuous growth of packing density leads to restricted rotation and development of polar order that is followed by chirality synchronization and dense crystal-like packing. Because the evolving crystalline order is incompatible with the simultaneously developing curvature, the coherence length of crystalline order is limited to the formation of nano-size crystallites.

## 2. Results and Discussion

### 2.1. Synthesis

The synthesis of the target BCLCs **An**, **AFn**, **Bn** and **BFn** was performed as shown in Scheme 3. In the first step the 3-benzyl protected 4-bromoresorcinol **9** was acylated with the benzoyl chlorides **6** and **7**, respectively. After hydrogenolytic deprotection the 4-bromoresorcinol monoesters **12** and **13** involving the phenyl benzoate-based wings were obtained. The final bent-core compounds **An**, **AFn**, **Bn** and **BFn** were obtained by acylation of the 3-OH groups of compounds **12** and **13** with one equivalent of the appropriate benzoyl chloride **15n** or **15Fn** involving the azobenzene units. All acylations were carried out in the presence of triethylamine as base and pyridine as acylation catalyst.<sup>[71]</sup> Details of synthesis of the intermediates and final compounds as well as analytical data are reported in the Supporting Information. The syntheses of the compounds with inverted orientation of the azobenzene wing (**C18**) and having chlorine instead of bromine as 4-substituent at the resorcinol core (**D18** and **E18**) are described in the Supporting Information (see Table 4 in Section 2.5 for structures). The reference compound **2/18**, having two azobenzene wings combined with the 4-bromoresorcinol core (see Scheme 1 and Section 2.5) has been synthesized according to the procedures given in Ref. [72].



**Scheme 3.** Synthetic route to the bent-core mesogens **An**, **AFn**, **Bn** and **BFn**. Reagents and conditions: *i*)  $\text{SOCl}_2$ , DMF, reflux, 1 h; *ii*)  $\text{Et}_3\text{N}$ , pyridine,  $\text{CH}_2\text{Cl}_2$ , reflux, 6 h; *iii*)  $\text{TsCl}$ ,  $\text{K}_2\text{CO}_3$ , acetone, reflux 16 h; *iv*) Benzylbromide, reflux, 16 h; *v*) aq.  $\text{NaOH}$ ,  $\text{CH}_3\text{OH}$ , reflux, 12 h; *vi*)  $\text{H}_2$ , 10% Pd/C, THF, 48 h,  $25^\circ\text{C}$ .

### 2.2. Compounds **An** and **AFn** with a 4-hydroxybenzoate wing

Compounds **A2** and **AF2** with  $n=2$  form crystalline solids with relatively high melting points, whereas the compounds **An** and **AFn** with longer chains ( $n=8, 18$ ) exhibit highly viscous optically isotropic phases which, once formed, do not crystallize (see Table 1).<sup>[75]</sup> There is no birefringence between crossed polarizers, but rotating the analyser by a small angle out of the precise  $90^\circ$  position leads to the appearance of dark and bright domains. Rotating the analyser in the opposite direction reverses the dark and bright domains (see Figure 2) whereas rotating the sample between crossed polarizers does not lead to any change, indicating that the distinct regions rotate the plane of polarized light into opposite directions and hence represent chiral domains with opposite handedness, as typical for DC phases ( $\text{DC}^{[*]}$  phases).

The  $\text{DC}^{[*]}$ -Iso transitions are associated with relatively high transition enthalpies, being around  $\Delta H \approx 30 \text{ kJ mol}^{-1}$  (see Figure 3, Figure S11 (the Supporting Information) and Table 1). In the  $\text{DC}^{[*]}$  ranges of all compounds there is an additional transition ( $\text{DC}_1^{[*]}-\text{DC}^{[*]}$ ) that is associated with a relatively small transition enthalpy ( $\Delta H \approx 1.3-4.4 \text{ kJ mol}^{-1}$ , see Figure 2 and Table 1). This transition can be supercooled by 20–30 K (see Figure 3), but no change in the optical texture is observed at this transition either on heating or on cooling.<sup>[76]</sup>

The XRD pattern of **A18** in the  $\text{DC}^{[*]}$  phase at  $100^\circ\text{C}$  (Figure 4) shows a single strong reflection in the small angle region, in line with a lamellar structure. The  $d$ -value of 5.2 nm is between half of the molecular length and the full molecular length ( $L=7.3 \text{ nm}$  in the most extended conformation with all-*trans* alkyl chains) and could be explained by a tilted organiza-

**Table 1.** Phase transition temperatures  $T$  [°C], mesophase types, and transition enthalpies ( $\Delta H$  [kJ mol<sup>-1</sup>]) of compounds **An** and **AFn**.<sup>[a]</sup>

Compd.	X	n	Phase transitions $T$ [°C] ( $\Delta H$ [kJ mol <sup>-1</sup> ])
<b>A2</b>	H	2	H→Cr 154 (56.3) Iso Cr 135 (56.8) Iso←C
<b>A8</b>	H	8	H→DC <sub>1</sub> <sup>[*]</sup> 78 [1.7] DC <sup>[*]</sup> 114 [30.7] Iso DC <sub>1</sub> <sup>[*]</sup> 54 (1.3) DC <sup>[*]</sup> 108 (30.0) Iso←C
<b>A18</b>	H	18	H→DC <sub>1</sub> <sup>[*]</sup> 78 (4.4) DC <sup>[*]</sup> 116 (27.2) Iso DC <sub>1</sub> <sup>[*]</sup> 54 (4.1) DC <sup>[*]</sup> 109 (29.4) Iso←C
<b>AF2</b>	F	2	H→Cr 140 (50.9) Iso Cr 124 (50.8) Iso←C
<b>AF8</b>	F	8	H→DC <sub>1</sub> <sup>[*]</sup> 78 (4.2) DC <sup>[*]</sup> 126 (31.8) Iso DC <sub>1</sub> <sup>[*]</sup> 54 (3.9) DC <sup>[*]</sup> 120 (33.2) Iso←C
<b>AF18</b>	F	18	H→DC <sub>1</sub> <sup>[*]</sup> 78 (3.4) DC <sup>[*]</sup> 119 (24.0) Iso DC <sub>1</sub> <sup>[*]</sup> 54 (3.1) DC <sup>[*]</sup> 112 (25.8) Iso←C

[a] The compounds were melted and heated to 150 °C to remove traces of enclosed solvent, afterwards they were cooled with 10 Kmin<sup>-1</sup> to room temperature; the phase transition temperatures (peak temperatures) were taken from the following heating (H→) and cooling scans (←C) at 10 Kmin<sup>-1</sup>; abbreviations: Cr=crystalline solid; DC<sup>[\*]</sup>, DC<sub>1</sub><sup>[\*]</sup>=optically isotropic mesophases composed of chiral domains with opposite handedness (dark conglomerate phases, HNC phases); Iso=isotropic liquid.

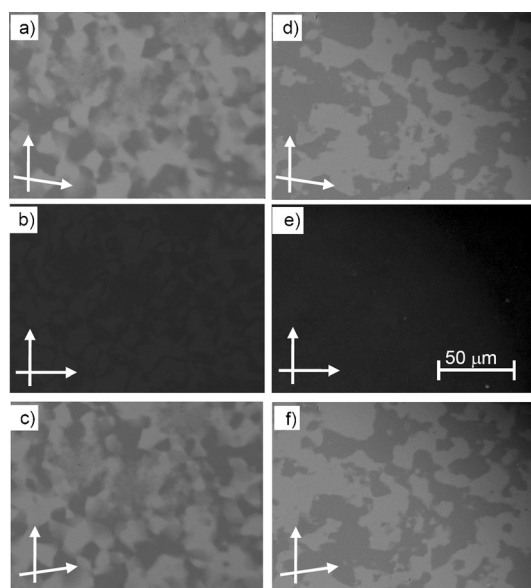


**Figure 2.** Textures of the DC<sup>[\*]</sup> phases of compound **A8** (left column) and **AF8** (right column) at  $T=90$  °C and  $120$  °C, respectively: b) and e) between crossed polarizers; a) and d) after rotating one polarizer by  $12^\circ$  from the crossed position in clockwise direction and c) and f) in anticlockwise direction, showing dark and bright domains, indicating the presence of areas with opposite chirality sense (the same textures are observed in the DC<sub>1</sub><sup>[\*]</sup> phases of both compounds at room temperature); contrast was enhanced to improve visibility.

tion of the molecules or a structure with intercalated alkyl chains. The observation of strongly tilted smectic phases in the series of the related compounds **Bn** and **BFn** (see Section 2.3) supports the interpretation of the reduced  $d$ -value as being the result of a tilted organization of the molecules.<sup>[77]</sup> The

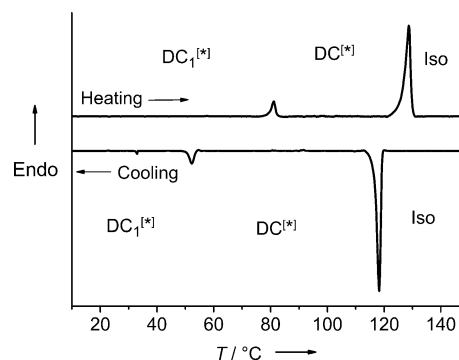


**Figure 3.** DSC heating and cooling scans of **AF8** with a rate of  $10$  Kmin<sup>-1</sup>.

small angle scattering is not resolution limited; from the full width at half maximum (FWHM) a correlation length of the lamellar domains in the range of 20 nm can be estimated, which corresponds to about four layers. In the middle and wide angle region of the XRD pattern numerous very weak scattering maxima are visible (Figure 4a). The combination of a broadened small angle scattering and a series of very weak and relatively broad wide angle scatterings is typical for amorphous solids composed of nano-crystallites, similar to XRD patterns recorded for amorphous nano-crystallized polymers.<sup>[78]</sup> Based on these XRD data and the high viscosity, a fluid sponge like structure can be excluded. The shape of the wide angle diffraction patterns is also distinct from the soft crystalline HNF phases, but similar to the XRD patterns recorded for the DC<sup>[\*]</sup> phases of compounds **2F/n** with two azobenzene wings (see Scheme 1).<sup>[71]</sup> As typical for DC phases no aligned samples could be obtained by attempted surface alignment (see the Experimental Section), and therefore the 2D diffraction pat-

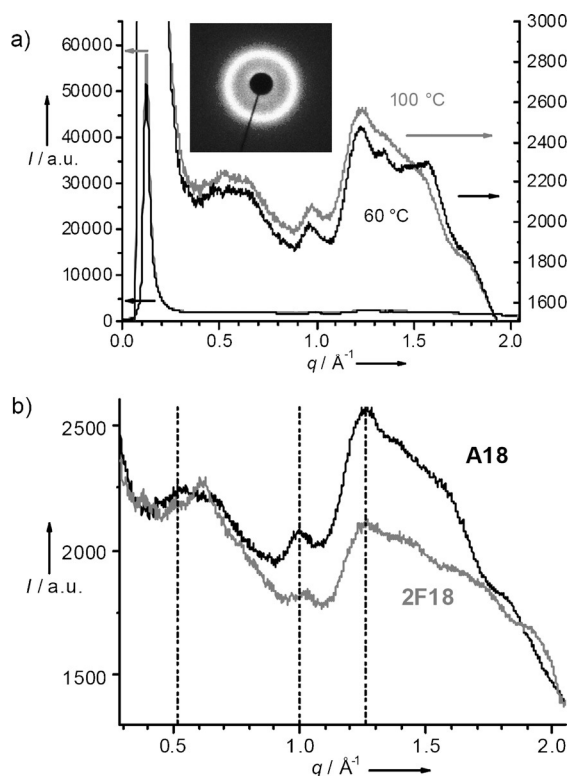


**Figure 4.** XRD intensity profiles of **A18**: a) DC<sup>[\*]</sup> phase at 100 °C and DC<sub>1</sub><sup>[\*]</sup> phase at 60 °C; the inset shows the scattering in the small angle region at  $T=60$  °C; b) comparison of the intensity profiles of the DC<sup>[\*]</sup> phases of compounds **A18** (100 °C) and **2F18**<sup>[71]</sup> (60 °C) normalized to the intensity of the layer reflection.

terns show the typical closed rings without any direction dependent intensity modulation (see inset in Figure 4a). Similar diffraction patterns were observed for the other investigated compounds of the series **An** and **AFn** (the Supporting Information, Figures S12–S16). A structure composed of disordered and helically twisted nano-crystallites, representing short segments of the helical nano-filaments, separated by less ordered molecules filling the defects, is suggested for the DC<sup>[\*]</sup> phases of compounds **An** and **AFn**. This type of DC<sup>[\*]</sup> phases is designated as helical nano-crystallite phase (HNC phase). At the transition to the DC<sub>1</sub><sup>[\*]</sup> phase the XRD pattern does not change significantly, for example, the  $d$ -value of the layer reflection rises slightly to 5.3 nm at 60 °C and in the wide angle region the scattering at higher angles become more pronounced (Figure 4a). This indicates that the fundamental structure is retained, though a closer packing is achieved in the DC<sub>1</sub><sup>[\*]</sup> phase.

### 2.3. Compounds **Bn** and **BFn** with a terephthalate wing

The short and medium chain length terephthalates **Bn** with  $n < 14$  and **BFn** with  $n < 12$  form either crystalline solids (**BF8**) or DC<sup>[\*]</sup> phases (**B8–B12** and **BF10**), very similar to the 4-hydroxybenzoates **An** and **AFn** (Table 2). The major difference is the absence of the additional sharp DC<sub>1</sub><sup>[\*]</sup>–DC<sup>[\*]</sup> transition, though there are broad features in the DC<sup>[\*]</sup> phases over tem-

perature ranges of about 25–30 K in the heating and cooling scans (see, for example, Figure 5a). This indicates slow continuous transformations within the DC ranges, though the phase remains optically isotropic and there is no other visible change in this temperature range.<sup>[79]</sup>

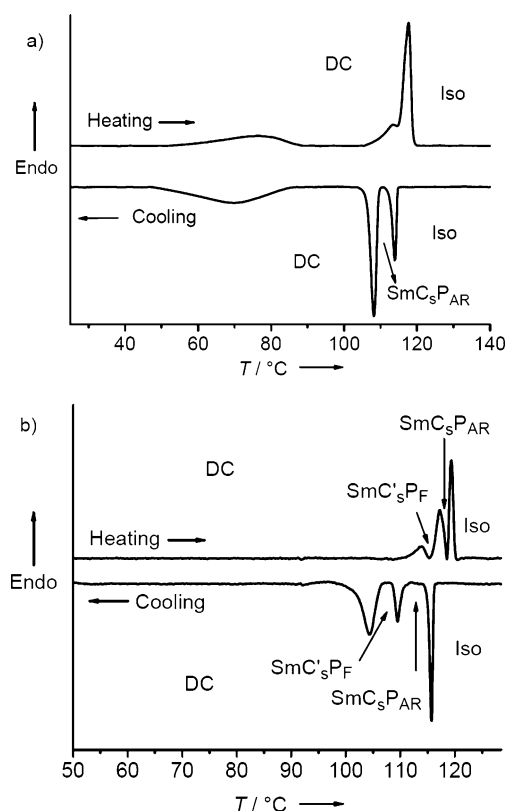
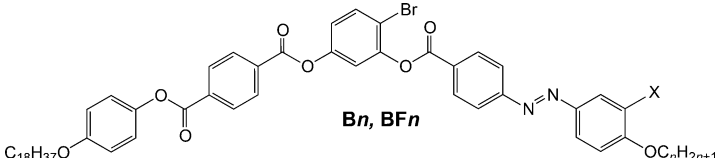


**Figure 5.** DSC heating and cooling scans of a) **BF14** with a rate of 10 Kmin<sup>-1</sup> and b) of **BF18** with a rate of 5 Kmin<sup>-1</sup>.

More complicated phase sequences, involving DC phases and birefringent smectic phases, were observed for compounds **Bn** ( $n=14, 18$ ) and **BFn** ( $n=12–18$ ) with longer alkyl chains. In the isotropic mesophases of these compounds no chiral domains can be detected by microscopy between slightly uncrossed polarizers. As conglomerates of chiral domains were observed for the shorter homologues of the series **Bn** and **BFn** and also after addition of 5-CB to the medium and long chain compounds of these series (see Section 2.4). It is assumed that these optically isotropic phases also represent DC phases, but with a much smaller size of the chiral domains, so that they cannot be resolved by polarizing microscopy; therefore the phase designation is “DC” without superscript [\*]. For compounds **B18**, **BF14** and **BF16** there is only one additional smectic phase above the DC phase (Figure 5a), whereas for compounds **B14** and **BF18** even two smectic phases can be observed (Figure 5b). For most compounds the smectic phases are monotropic, that is, they can only be observed upon cooling from the isotropic liquid, whereas on heating only DC phases were found. However, the longest homologues **B18** and **BF18** form the smectic LC phases on heating as well as on

**Table 2.** Phase transition temperatures  $T$  [°C], mesophase types, and transition enthalpies ( $\Delta H$  [kJ mol<sup>-1</sup>]) of compounds **Bn** and **BFn**.<sup>[a]</sup>



Compd.	X	n	Phase transitions $T$ [°C] ( $\Delta H$ [kJ mol <sup>-1</sup> ])
<b>B8</b>	H	8	H → DC <sup>[*]</sup> 106 (22.7) Iso DC <sup>[*]</sup> 98 (22.0) Iso ← C
<b>B10</b>	H	10	H → DC <sup>[*]</sup> 110 (21.3) Iso DC <sup>[*]</sup> 101 (20.8) Iso ← C
<b>B12</b>	H	12	H → DC <sup>[*]</sup> 107 (20.1) Iso DC <sup>[*]</sup> 101 (19.8) Iso ← C
<b>B14</b>	H	14	H → DC 108 (22.7) Iso DC 98 (11.6) SmC <sub>s</sub> P <sub>F</sub> 101 (3.7) SmC <sub>s</sub> P <sub>AR</sub> 105 (5.1) Iso ← C
<b>B18</b>	H	18	H → DC 105 (11.2) SmC <sub>s</sub> P <sub>AR</sub> 108 (4.6) Iso DC 96 (20.6) SmC <sub>s</sub> P <sub>AR</sub> 106 (5.2) Iso ← C
<b>BF8</b>	F	8	H → Cr 113 (29.0) Iso Cr 100 (28.8) Iso ← C
<b>BF10</b>	F	10	H → DC <sup>[*]</sup> 116 (20.9) Iso DC <sup>[*]</sup> 109 (17.8) Iso ← C
<b>BF12</b>	F	12	H → DC 111 (23.7) DC 87 (3.3) SmC <sub>s</sub> P <sub>A</sub> 101 (6.7) SmC <sub>s</sub> P <sub>A</sub> 109 (12.8) Iso ← C
<b>BF14</b>	F	14	H → DC 117 (23.3) Iso DC 108 (14.9) SmC <sub>s</sub> P <sub>AR</sub> 114 (5.5) Iso ← C
<b>BF16</b>	F	16	H → DC 116 (23.6) Iso DC 105 (12.9) SmC <sub>s</sub> P <sub>AR</sub> 114 (8.2) Iso ← C
<b>BF18</b>	F	18	H → DC 112 (3.0) SmC <sub>s</sub> P <sub>F</sub> 115 (6.8) SmC <sub>s</sub> P <sub>AR</sub> 117 (7.7) Iso DC 102 (14.3) SmC <sub>s</sub> P <sub>F</sub> 109 (3.4) SmC <sub>s</sub> P <sub>AR</sub> 115 (6.0) Iso ← C

[a] Transitions were determined as described in Table 1; abbreviations: DC = optically isotropic phase (HNC phase) without visible conglomerate structure; SmC<sub>s</sub>P<sub>AR</sub> = polarization randomized smectic phase composed of SmC<sub>s</sub>P<sub>F</sub> domains and showing two polarization current peaks; SmC<sub>s</sub>P<sub>F</sub> = antiferroelectric switching polar SmC phase with increased packing density (B5-like); for other abbreviations, see Table 1.

cooling, thus representing enantiotropic phases. Again, the observed phase sequences are very similar for the series of fluorinated and non-fluorinated compounds **BFn** and **Bn**, respectively. Only the compounds with  $n=12$  behave differently; the non-fluorinated compound **B12** forms a DC<sup>[\*]</sup> phase, whereas the fluorinated compound **BF12** has two smectic phases besides the DC phase, being slightly different from those of the long chain homologues (see Section 9 in the Supporting Information and Figure S26 for a more detailed discussion of these smectic phases). The formation of additional smectic LC phases before the transition to the DC phase allows some additional insight into the mode of development of layer distortion and chirality in the DC phases under discussion. In the following the transition from the isotropic liquids through the smectic phases to the DC phases is described in more detail.<sup>[80–82]</sup>

#### Investigation of the smectic phases and smectic-DC transitions

On cooling **BF18** from the isotropic liquid state a birefringent schlieren texture is observed in homeotropic cells (Figure 6a), whereas a broken fan texture is observed in planar cells (Figure 6b). In the fan texture the dark extinctions are inclined by an angle of  $\approx 25^\circ$ , confirming a synclinal tilted smectic phase (SmC<sub>s</sub> phase) with uniform tilt in adjacent layers (Figure 7a,b). On further cooling there is an increase of the birefringence, in-

dicated by a colour change of the fans at  $T=109^\circ\text{C}$  (green to greenish orange, Figure 6c) associated with a transition enthalpy of  $\Delta H \approx 3.4 \text{ kJ mol}^{-1}$ . The extinctions remain unchanged, indicating a transition to a second synclinal tilted SmC<sub>s</sub> phase. The next phase transition at  $T=102^\circ\text{C}$  ( $\Delta H \approx 14.3 \text{ kJ mol}^{-1}$ ) leads to the DC phase (Figure 6d).

The phase transitions are associated with clear changes of polar order as indicated by electro-optical investigations. At the Iso-SmC<sub>s</sub> transition of compound **BF18** two relatively weak and widely separated peaks appear within one period of an applied triangular wave voltage (Figure 6e). The peaks grow in intensity and rapidly merge closer on further cooling (see Figure 6f), indicating a strongly decreasing threshold voltage of the switching on decreasing temperature. The spontaneous polarization values ( $P_s$ ) increase with decreasing temperature and reach a maximum of  $P_s = 500\text{--}650 \text{ nC cm}^{-2}$  at the transition to the low-temperature smectic phase (Figure S23b, the Supporting Information). This development of the shape of the polarization curves is typical for SmC<sub>s</sub>P<sub>AR</sub> phases, which are composed of polar SmC<sub>s</sub>P<sub>F</sub> domains with preferentially antipolar correlation between adjacent domains (see Figure 7c).<sup>[83]</sup> Under an applied electric field the SmC<sub>s</sub>P<sub>F</sub> domains are aligned and the resulting long-range polar SmC<sub>s</sub>P<sub>F</sub> state (Figure 7d or 7e, depending on the direction of the applied field) is switched by the applied triangular wave field between the two polar states with relaxation to the macroscopically apolar polydo-



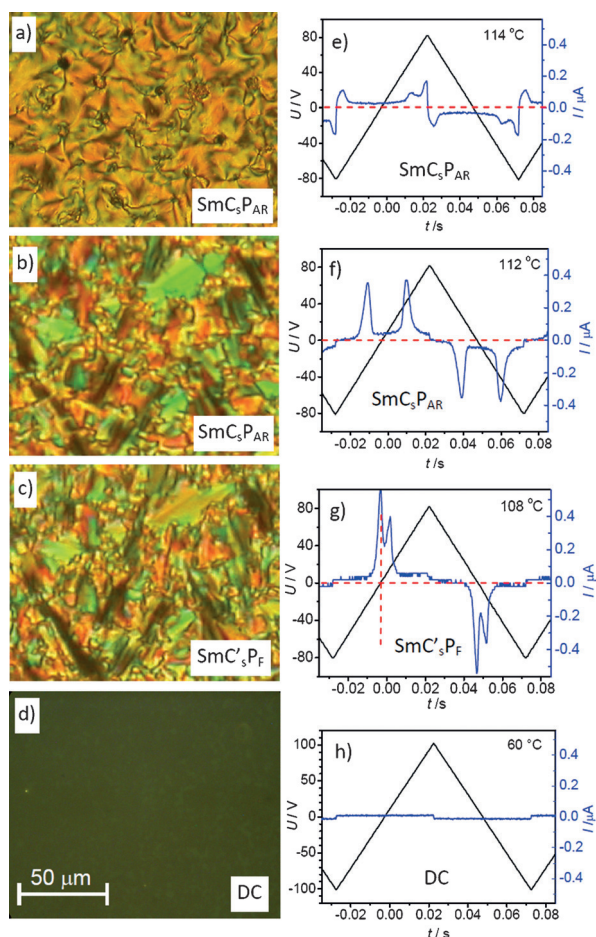


**Figure 6.** Textures (crossed polarizers) and polarization current response curves of compound **BF18** as observed on cooling from the isotropic liquid, a) in a homeotropic cell at  $T = 114^\circ\text{C}$  in the  $\text{SmC}_5\text{P}_{\text{AR}}$  phase; b–d) textures observed in a  $6\ \mu\text{m}$  coated ITO cell with planar alignment at b)  $T = 112^\circ\text{C}$  in the  $\text{SmC}_5\text{P}_{\text{AR}}$  phase, c)  $T = 108^\circ\text{C}$  in the  $\text{SmC}'_5\text{P}_{\text{F}}$  phase and d) at  $T = 60^\circ\text{C}$  in the DC phase; e–h) switching current response curves in the same ITO cell, recorded under a triangular wave voltage (10 Hz, 5 k $\Omega$ ); e) at  $T = 114^\circ\text{C}$  (the small additional peak might be due to a switching process in the proximity of the glass surface or a conductivity) and f) at  $T = 112^\circ\text{C}$  in the  $\text{SmC}_5\text{P}_{\text{AR}}$  phase, g) at  $T = 108^\circ\text{C}$  in the  $\text{SmC}'_5\text{P}_{\text{F}}$  phase and h) at  $T = 60^\circ\text{C}$  in the DC phase; for optical investigations under DC field, see Figure S24 (the Supporting Information).

main state (Figure 7c) at 0 V (superparaelectric switching).<sup>[84]</sup> With decreasing temperature the  $\text{SmC}_5\text{P}_{\text{F}}$  domain size obviously grows, and therefore, less voltage is required for this switching process at lower temperature, leading to a reduced distance between the peaks.<sup>[85]</sup>

At the transition to the second smectic phase at  $T = 109^\circ\text{C}$  the two polarization current peaks come even closer and become non-symmetric ( $P_s \approx 700\ \text{nC cm}^{-2}$ ). The strongly non-symmetric shape of the double peak (see Figure 6g) might be due to the coexistence of two different modes of polar switching in the cell, each one associated with a single peak. It is assumed that a  $\text{SmC}_5\text{P}_{\text{F}}$  domain structure (Figure 7c) is retained in this low temperature phase, but due to the significantly increased size of the  $\text{SmC}_5\text{P}_{\text{F}}$  domains and the enhanced viscosity, the relaxation of the field-induced macroscopic  $\text{SmC}_5\text{P}_{\text{F}}$  state to the polydomain state (Figure 7c) becomes slow. There-

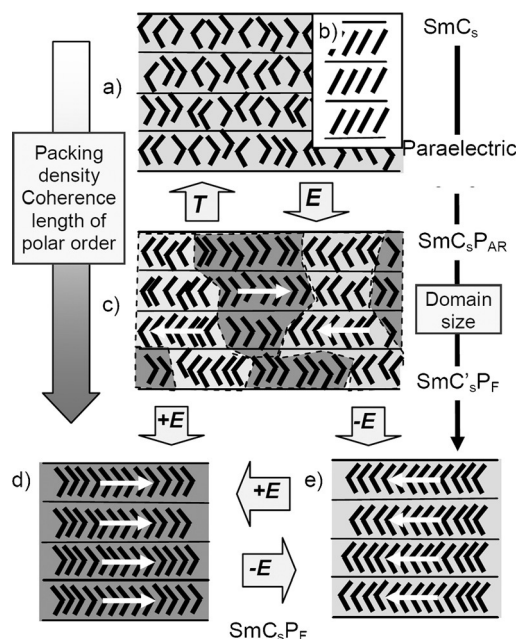


**Figure 7.** Organization of bent-core molecules in the smectic LC phases ( $\text{SmC}$  phases) under discussion and the effects of temperature ( $T$ ) and applied electric fields ( $E$ ) on the mode of LC self-assembly; a) and c–e) show views parallel to the layer planes and perpendicular to the polar axis (white arrows); b) shows the synclinal tilt ( $C_s$ ) if viewed along the polar axis. With growing polar coherence length the following  $\text{SmC}$  subtypes can be found: a) apolar and paraelectric  $\text{SmC}_5$  phases; c)  $\text{SmC}_5\text{P}_{\text{AR}}$  phase and  $\text{SmC}_5\text{P}_{\text{F}}$  domain phase ( $\text{SmC}'_5\text{P}_{\text{F}}$  phase);<sup>[83]</sup> d,e)  $\text{SmC}_5\text{P}_{\text{F}}$  phase and field induced  $\text{SmC}_5\text{P}_{\text{F}}$  states with opposite polar directions (white arrows).

fore, a direct switching between the two field-induced  $\text{SmC}_5\text{P}_{\text{F}}$  states with opposite polar direction (Figure 7d,e) takes place without relaxation to the nonpolar polydomain state, leading to just a single peak. At the surfaces the  $\text{SmC}_5\text{P}_{\text{F}}$  states are additionally stabilized by polar surface interactions, so that a certain threshold voltage is required for this switching (Figure 6g, smaller peak at  $\neq 0\ \text{V}$ ). In the interior of the cell there is no stabilizing surface effect and hence switching takes place at 0 V crossing (larger peak at 0 V). Based on these electro-optical investigations and the XRD data (see below), the low temperature smectic phase is considered to be a modified  $\text{SmC}_5\text{P}_{\text{AR}}$  phase with increased  $\text{SmC}_5\text{P}_{\text{F}}$  domain size and enhanced packing density in the layers (similar to the B5 phases);<sup>[86]</sup> this polydomain  $\text{SmC}_5\text{P}_{\text{F}}$  phase is designated as  $\text{SmC}'_5\text{P}_{\text{F}}$ . Another important point with relation to the discussion of the DC phases is, that in the  $\text{SmC}'_5\text{P}_{\text{F}}$  phase range  $P_s$  decreases with further decreasing temperature (see the Supporting Information, Figure S23b) and at the transition to the DC phase at  $T = 102^\circ\text{C}$  the polarization peaks have completely disappeared (Figure 6h).<sup>[87]</sup> This decrease in  $P_s$  is assumed to be caused by layer deformation, developing already in the  $\text{SmC}'_5\text{P}_{\text{F}}$  phase range. By this layer deformation some polar order is cancelled and thus not all molecules can be addressed by the applied field.

The  $\text{SmC}_5\text{P}_{\text{AR}}$  phases were observed for all long chain compounds **Bn** and **BFn** with  $n > 12$  (see Table 2), as indicated by the typical temperature-dependent development of the polari-

zation current curves (the Supporting Information, Figure S22), but not all compounds form a clearly visible  $\text{SmC}'_s\text{P}_F$  range before the transition to the DC phase. Only compound **BF12**, being at the borderline between the short and long chain compounds behaves a bit different. Though the organization is still predominately synclinic, anticlinic defects modify the observed textures<sup>[88,89]</sup> and switching current curves ( $\text{SmC}_a\text{P}_A$  and  $\text{SmC}'_a\text{P}_A$  phases) as described in the Supporting Information in more detail (see Section 9 in the Supporting Information and Figure S26).

### XRD investigations

The XRD investigation of the mesophases is described here for compound **BF18**; for more details and data of other compounds, see the Supporting Information, Figures S17–S21. Figure 8a shows the development of the scattering profile in the middle and wide angle range depending on temperature and in Figure 9a,b the development of the full width at half maximum (FWHM) and  $d$ -value of the layer scattering, respectively, are shown graphically. The smectic high temperature phase of **BF18** ( $\text{SmC}_s\text{P}_{AR}$ ) appears like a typical fluid smectic phase in the XRD experiments, that is, there is a sharp layer reflection in the small angle region at  $d=5.1$  nm ( $114^\circ\text{C}$ ) and in the wide angle region a diffuse scattering with a maximum at  $d=0.45$  nm (Figure 8a).

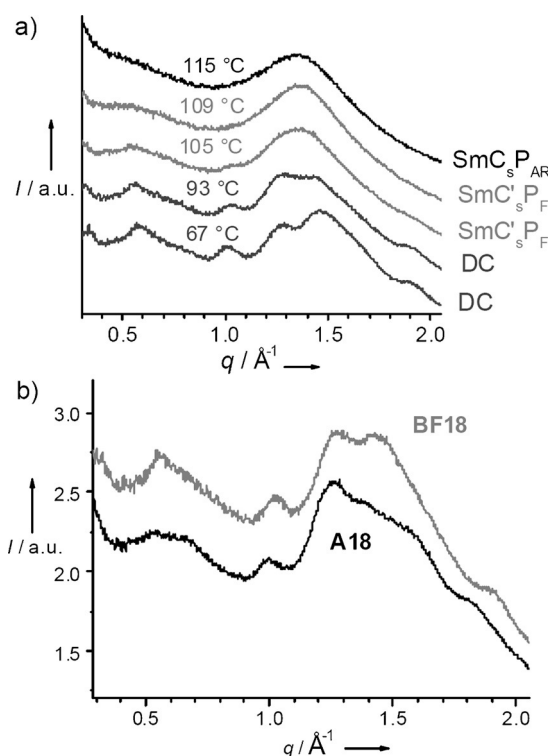


**Figure 8.** a) XRD intensity profile of the mesophases of compound **BF18** depending on temperature (the individual curves are vertically shifted for better visibility) and b) comparison of intensity profile of the DC phase of **BF18** ( $90^\circ\text{C}$ ) with that of the DC<sup>(\*)</sup> phase of compounds **A18** ( $100^\circ\text{C}$ ), normalized to the intensity of the layer reflection.

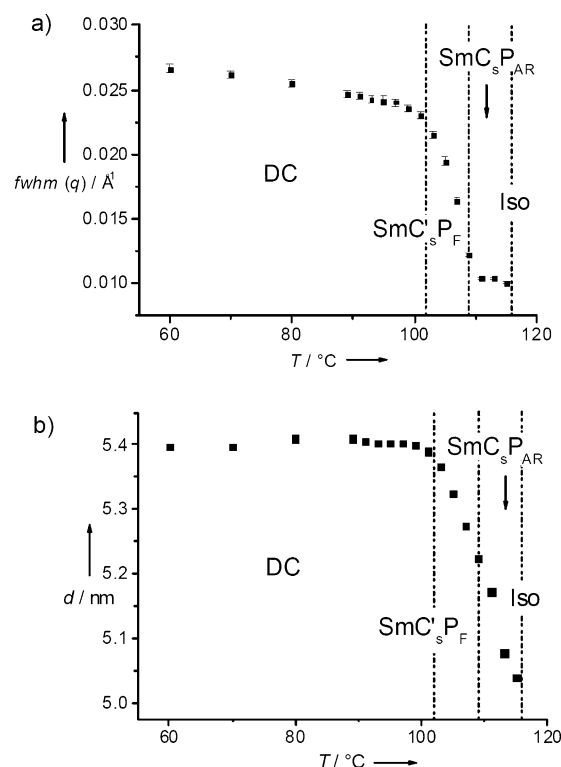


**Figure 9.** Temperature dependence of a) full width at half maximum (FWHM) and b)  $d$ -value of the small angle reflection of **BF18** as measured on cooling (fitted using Gaussian line shapes; the error bars in a) represent the standard deviation of the measurements).

On decreasing the temperature, at the transition to the  $\text{SmC}'_s\text{P}_F$  phase at  $109^\circ\text{C}$  the diffuse wide angle scattering becomes a bit narrower and slightly increases in intensity, which indicates a more ordered packing of the molecules in the layers, similar to observations made for B2–B5 transitions.<sup>[86]</sup> Simultaneously, the FWHM of the layer reflection rises rapidly from  $T=109^\circ\text{C}$  until the transition to the DC phase at  $102^\circ\text{C}$  (Figure 9a). The rise even continues in the DC phase with declining slope. This indicates that there is a continuous development of layer distortion in the  $\text{SmC}'_s\text{P}_F$  range, being in line with the results of electro-optical investigations. It also shows that even after the  $\text{SmC}'_s\text{P}_F$ -to-DC phase transition there are still continuing structural changes in the DC range, in accordance with the observed tailing of the DSC traces (see Figure 5b). As expected, the broadening of the layer reflection at the  $\text{SmC}_s$ -DC transition is associated with a complete loss of any alignment (see the Supporting Information, Figures S19–S21). For the  $d$ -value of the small angle reflection an increase to  $d=5.4$  nm ( $90^\circ\text{C}$ ) can be observed throughout the smectic phases on decreasing temperature, which remains nearly constant below  $T=95^\circ\text{C}$  (Figure 9b). Overall, the increase of FWHM indicates a reduction of the correlation length of the uniformly aligned layer segments due to growing layer deformation and the rising  $d$ -values are in agreement with a stretching of the molecules due to the growing packing density.

In the  $\text{SmC}'_s\text{P}_F$  range some additional broad peaks appear in the middle angle region of the diffraction patterns and the

wide angle scattering becomes broader again (105 °C, Figure 8a). At the transition to the DC phase at  $T=102$  °C the medium angle scatterings become more pronounced and the wide angle scattering splits into two maxima at  $d=0.50$  nm and  $d=0.43$  nm with an additional shoulder around  $d=0.33$  nm, indicating the emergence of local crystalline packing (bottom lines in Figure 8a). The apparent broadening of the wide angle scattering in the  $SmC'_5P_f$  range is assumed to be due to the onset of this splitting. In the DC phase range the wide angle pattern appears similar to the scattering pattern of the  $DC^{[*]}$  phase of compound **A18**, (see Figure 8b) and also to the XRD patterns of the 4-bromoresorcinols **2F/n** with two azobenzene wings (Figure 4b).<sup>[71]</sup> It is however distinct from the typical wide angle scattering patterns of sponge phases and HNF phases.<sup>[25,52,81]</sup> The relatively weak and broad middle- and wide angle scatterings indicate a strongly limited coherence length of crystalline order, as discussed above for the  $DC^{[*]}$  phase (HNC phases) of compound **A18** and further confirmed in the next Section.

## 2.4. Investigation of mixtures with 5-CB

An additional possibility for distinguishing the subtypes of DC phases is provided by investigation of mixed systems with the nematic phase of 4'-*n*-pentyl-4-cyanobiphenyl (5-CB).<sup>[66,69,70,71]</sup> It is known that HNF phases can be diluted by nematic LC hosts to a high degree (>95%) without loss of the chirality.<sup>[90,56b]</sup> This is due to the presence of long helical nano-filaments, allowing a swelling of the filaments by the nematic LC with gel formation and transfer of chirality from the nano-filaments to the nematic LC. This phenomenon is not observed for the sponge-type liquid crystalline DC phases, which are removed upon addition of 5-CB. Here we investigated the 1:1 (w/w) mixtures of 5-CB with a series of selected compounds (see Table 3).

Table 3. Phase transition temperatures and mesophase types of 1:1 mixtures (w/w) of the investigated compounds with 5-CB. <sup>[a]</sup>		
Compd.	Heating $T$ [°C]	Cooling $T$ [°C]
<b>A8</b>	Cr <sub>1</sub> 42 Cr <sub>2</sub> 85 Iso	Iso 70 Cr
<b>A18</b>	Cr 40 $DC^{[*]}$ 91 Iso	Iso 82 $DC^{[*]}$
<b>AF8</b>	Cr <sub>1</sub> 40 Cr <sub>2</sub> 77 Iso	Iso 70 $DC^{[*]}$ 47 Cr
<b>AF18</b>	Cr <sub>1</sub> 38 Cr <sub>2</sub> 97 Iso	Iso 92 $DC^{[*]}$
<b>B8</b>	Cr 79 Iso	Iso 63 N 57 $DC^{[*]}$ 38 Cr
<b>B14</b>	$Cr^{[b]}$ 55 $DC^{[*]}$ 77 Iso	Iso 70 $DC^{[*]}$
<b>B18</b>	$Cr^{[b]}$ 53 $DC^{[*]}$ 83 Iso	Iso 71 $DC^{[*]}$
<b>BF8</b>	Cr 98 Iso	Iso 93 Cr
<b>BF10</b>	Cr 42 $DC^{[*]}$ 70 Iso	Iso 68 $DC^{[*]}$
<b>BF12</b>	Cr 78 Iso	Iso 68 $DC^{[*]}$ 59 Cr
<b>BF16</b>	$Cr^{[*]}$ 68 $DC^{[*]}$ 77 Iso	Iso 73 $DC^{[*]}$ 50 $Cr^{[*]}$
<b>BF18</b>	$Cr^{[*]}$ 70 $DC^{[*]}$ 80 Iso	Iso 74 $DC^{[*]}$ 58 $Cr^{[*]}$

[a] Transition temperatures were taken from the observed textures using polarized optical microscopy; abbreviations: N=nematic phase;  $DC^{[*]}$ =dark conglomerate phase;  $Cr^{[*]}$ =crystalline phase composed of a conglomerate of chiral domains; Cr=birefringent crystalline phase; Iso=isotropic liquid. [b] In the temperature range of this crystalline phase the sample is biphasic.

With exception of the short chain compounds, namely **A8** and **BF8**, which only show a crystalline phase under these conditions, and **B8**, forming a monotropic nematic and a DC phase, in all mixtures  $DC^{[*]}$  phases were observed. The DC-Iso transition temperatures were significantly reduced in comparison with the pure compounds (20–50 K) and all smectic phases were completely suppressed. Remarkably in all cases conglomerates of chiral domains can be clearly identified for the mixed systems (see for example Figure 10). If only slightly higher 5-CB concentration is used, as, for example, in 4:6 (w/w) mixtures of compound **B18** with 5-CB, the chiral  $DC^{[*]}$  phase is lost, indicating that the amount of 5-CB that can be mixed into the DC phases of these compounds is strongly limited. These observations, in conjunction with the XRD studies, confirm that the  $DC^{[*]}$  and DC phases of compounds **An**, **AFn**, **Bn** and **BFn** behave very similar to the  $DC^{[*]}$  phases of 4-bromoresorcinol based BCLCs with two azobenzene-based wings reported previously (**2F/n**, see Scheme 1).<sup>[71]</sup> The induction of macroscopic chiral conglomerates by 5-CB supports the proposed assignment of the apparently achiral isotropic mesophases of the long chain compounds **Bn** and **BFn** as DC phases. The loss of the  $DC^{[*]}$  phases with enhanced 5-CB concentration excludes the presence of extended helical nano-filaments (as present in the HNF phases) and is in line with the proposed HNC structure of the DC phases.

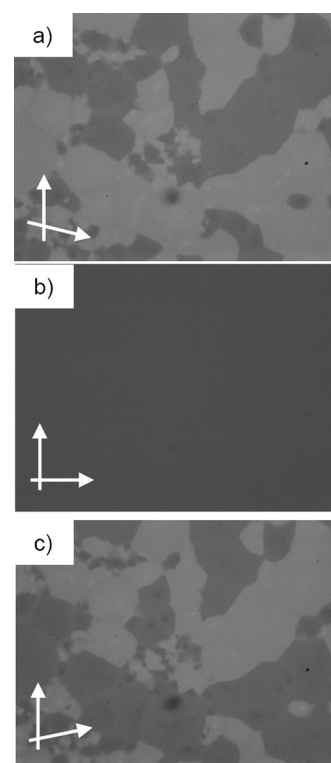


**Figure 10.** Textures of 1:1 (w/w) mixture of compound **BF16** and 5-CB obtained on cooling at  $T=60$  °C: b) between crossed polarizers; a) after rotating one polarizer by 7° from the crossed position in clockwise direction and c) in anticlockwise direction, showing dark and bright domains, indicating the presence of areas with opposite chirality sense; contrast was enhanced to improve visibility.

## 2.5. Discussion of structure–property relations

In the following the effects of structural variations at the bent unit and exchange of the wing groups on HNC phase formation will be described.

### Effects of peripheral fluorine substitution

Fluorine substitution at the periphery appears to have no substantial effect on DC phase formation of compounds **An** and **Bn** (see Tables 1 and 2). Phase types and transition temperatures are very similar for the fluorinated and the non-fluorinated compounds. Only **B12** and **BF12** behave differently, here exclusively the fluorinated compound **BF12** forms a SmC phase besides the DC phase (see Section 9 in the Supporting Information). This weak effect of fluorination is distinct from the effect of peripheral F in the series of the 4-iodoresorcinol (**1/n**) and 4-methylresorcinol-derived BCLCs (**3/n**) with two azobenzene wings (Scheme 1),<sup>[69,71]</sup> in which F-substitution either induces or suppresses DC<sup>[\*]</sup> phase formation for the complete homologous series. The influence of fluorination is less pronounced in the series of the 4-bromoresorcinols **2/n** with two azobenzene wings. Here fluorination retains the DC phases, but suppresses the additional nematic phases of the non-fluorinated compounds. There is presently no clear understanding of the fluorine effect.

### Position of the azobenzene wing with respect to the substituent at the apex

Compound **C18** is the isomer of **A18** with the azobenzene wing shifted to the non-brominated side of the resorcinol core (see Table 4). According to textural investigations the high temperature phase of **C18** is a nematic phase (N), followed by a non-polar and synclinic tilted SmC<sub>s</sub> phase (see the Supporting Information, Figure S25c) and an additional low tempera-

ture phase M (see Figure S25d), which is most probably a modulated version of this SmC<sub>s</sub> phase.<sup>[91]</sup> However, in contrast to **A18**, for **C18** no DC phase was found. This confirms that the orientation of the azobenzene unit with respect to the bulky Br substituent is of significant importance for DC phase formation. It is known that bulky 4-substituents at the resorcinol core lead to a helical distortion of the adjacent COO group.<sup>[8,71,33]</sup> Therefore, it appears that a strong helical twist of the COO group connecting the azobenzene unit with the resorcinol core is important. In line with this, compound **2/18**, having azobenzene wings at both sides also forms a HNC-type DC<sup>[\*]</sup> phase, very similar to **A18**, but in this case accompanied by a small range of an additional nematic phase (see Table 4).<sup>[71–73,92]</sup>

### Bromine versus chlorine at the apex

Replacement of bromine in **A18** by the smaller chlorine in **D18** removes the DC phases (Table 4); compound **D18** forms only a solid (and birefringent) crystalline phase. Exchange of the position of azobenzene and 4-hydroxybenzoate units in **D18** leads to **E18**, which is similar to the analogous bromine-substituted compound **C18** that forms only nematic and SmC<sub>s</sub> phases (Table 4). However, the smaller size of Cl allows easier development of polar order in the SmC<sub>s</sub> phase of this compound. Thus, **E18** has a short range of a paraelectric SmC<sub>s</sub><sup>[\*]</sup> phase (Figure 7a) before the formation of the SmC<sub>s</sub>P<sub>AR</sub> phase takes place at 74 °C (see the Supporting Information, Figure S10). Also for **E18** the SmC<sub>s</sub>P<sub>AR</sub> phase is indicated by the occurrence of two widely separated current peaks (see discussion in Section 2.3 and the Supporting Information, Figure S22d), but this is immediately followed by crystallization. The observation of chiral domains in homeotropic alignment of the paraelectric SmC<sub>s</sub><sup>[\*]</sup> phase indicates surface-stabilized chirality synchronization (see the Supporting Information, Figure S10).<sup>[83,93–95]</sup> In this phase the improved packing of the

**Table 4.** Comparison of compounds with different position of the azobenzene core and showing the effect of replacing X = Br by X = Cl.<sup>[a]</sup>

Compd.	X	Y	Z	Phase transitions <i>T</i> [°C] ( $\Delta H$ [kJ mol <sup>-1</sup> ])
<b>A18</b>	Br	COO	N=N	H → DC <sub>1</sub> <sup>[*]</sup> 78 (4.4) DC <sup>[*]</sup> 116 (27.2) Iso DC <sub>1</sub> <sup>[*]</sup> 54 (4.1) DC <sup>[*]</sup> 109 (29.4) Iso ← C
<b>C18</b>	Br	N=N	OOC	H → Cr 97 (52.1) Iso Cr 70 (32.0) M 78 (1.3) SmC <sub>s</sub> 91 N 92 (4.3) <sup>[b]</sup> Iso ← C
<b>2/18</b>	Br	N=N	N=N	H → Cr 100 (37.9) Iso DC <sup>[*]</sup> 95 (34.7) N 96 (0.6) Iso ← C
<b>D18</b>	Cl	COO	N=N	H → Cr 103 (44.1) Iso Cr 98 (46.7) Iso ← C
<b>E18</b>	Cl	N=N	OOC	H → Cr 100 (59.7) Iso Cr 68 (40.4) SmC <sub>s</sub> P <sub>AR</sub> 74 (0.7) SmC <sub>s</sub> <sup>[*]</sup> 94 (2.7) N 96 (1.1) Iso ← C

[a] SmC<sub>s</sub> = nonpolar SmC<sub>s</sub> phase; M = nonpolar birefringent LC phase, most likely representing a modulated SmC<sub>s</sub> phase; SmC<sub>s</sub><sup>[\*]</sup> paraelectric SmC<sub>s</sub> phase forming chiral domains in thin homeotropic cells. [b] The enthalpy value for the Iso-N transition cannot be separated from that of the N-SmC<sub>s</sub> transition.

bent-cores with the smaller chlorine at the apex allows the formation of surface-stabilized chiral  $\text{SmC}_5\text{P}_F$  surface layers in the homeotropic samples.

### Effects of the direction of the COO group in the phenyl benzoate wings

There is an interesting influence of the direction of the COO group in the phenyl benzoate wing, mainly reducing the conglomerate phase stability and inducing smectic phases if the benzoylated 4-hydroxybenzoate unit (compounds **An** and **AFn**) is replaced by a phenyl terephthalate structure (compounds **Bn** and **BFn**). Usually, terephthalates are known to provide increased stability of crystalline phase (enhanced melting points) and LC phases (enhanced LC-Iso transition temperature) due to improved  $\pi$ -stacking interactions of the involved electron-deficient aromatics.<sup>[96,97]</sup> Indeed, in the series of compounds **Bn** and **BFn** the formation of polar smectic phases indicates an enhanced stability of smectic phases compared to compounds **An** and **AFn** in which these smectic phases are missing. Probably, the increased  $\pi$ -stacking interaction between the electron-deficient terephthalate-based aromatic cores not only supports smectic phase formation, but to some extent also reduces the capability of the layers to assume curvature.

### General molecular design principles towards DC phases

Concerning the relation between DC phase formation and molecular structure, it appears that rigid  $\pi$ -conjugated wings such as Schiff bases,<sup>[17,57,98]</sup> azobenzenes,<sup>[69–71,99,100]</sup> and in some cases also biphenyls,<sup>[56,65]</sup> favour formation of DC phases with crystal-like packing (HNC and HNF phases),<sup>[101,102]</sup> whereas semiflexible wings, such as phenyl benzoates, preferably form fluid sponge-like DC phases if the alkyl chains are sufficiently long<sup>[26,64,103,104]</sup> or terminated by additional oligosiloxane or carbosilane units.<sup>[38,68]</sup> Bulky substituents (halogens,  $\text{CH}_3$ ) increase the molecular helicity if located adjacent to the COO linkages of the resorcinol core. This supports DC phase formation in general,<sup>[94,96–106]</sup> but most efficiently if the wing attached to this COO group is one of the more rigid groups (as for example azobenzene).<sup>[71,107]</sup> Thus, HNC phase formation was found for compounds **A18** and **2/18** having the azobenzene wing adjacent to the bromine, but not for the isomeric compound **C18**, having the azobenzene wing at the non-substituted side of the 4-bromoresorcinol unit. The bulkiness of the 4-substituent at the apex also contributes to a distortion of the dense molecular packing in layers or ribbons, thus suppressing filament formation (HNF phase) and replacing them by nano-crystallites in the HNC phases.

### Chiral domain formation in relation to phase sequence

It appears that the HNC phases show well-developed conglomerate structures (DC<sup>[\*]</sup> phases) if formed directly from the isotropic liquid state (compounds **An**, **AFn** and short chain compounds **Bn** and **BFn**, see Tables 1 and 2), or from a nematic phase (compounds **2/n**). Chirality synchronization and helical

twist within the developing nano-crystals is obviously transferred to the molecules in the coexisting liquid phase which then determines the chirality sense of the next generations of nano-crystal nuclei. However, no chiral domains can be identified for the DC phases formed on cooling the locally polar  $\text{SmC}$  phases of the long chain terephthalates **Bn** and **BFn**. It is thought that in the polar  $\text{SmC}_5\text{P}_F$  domains of these smectic phases chirality fluctuations are already fixed by the diastereomeric relations with the layer chirality (see Figure 1b).<sup>[17]</sup> Thus, in the polar domains of the smectic phases the developing helix sense of the nano-crystals is predominately determined by the local layer chirality in these domains. As these domains are still small in the multidomain  $\text{SmC}$  phases (Figure 7c), also the size of the developing chiral domains is too small to be detected optically. In line with this explanation, DC phases occurring below a nonpolar smectic phase without  $\text{SmC}_5\text{P}_F$  domain structure, such as the B6 phase, have been shown to form well-developed macroscopic conglomerates.<sup>[70,108]</sup> For all investigated long chain terephthalates **Bn** and **BFn**, addition of 5-CB induces chiral conglomerates in the apparently achiral DC phases. The reason could be that the formation of smectic phases is suppressed by 5-CB and the DC phases can directly be formed from the isotropic liquid state, which is known to lead to the formation of macroscopic conglomerates.

## 3. Conclusion

This study contributes to the understanding of DC phase formation by achiral bent-core systems. An amorphous type of DC phases composed of helical nano-crystallites, the HNC phases, is reported and considered as a third major type of DC phases besides the LC sponge phases and the HNF phases (Figure 11). Guidelines for the molecular design of new materi-

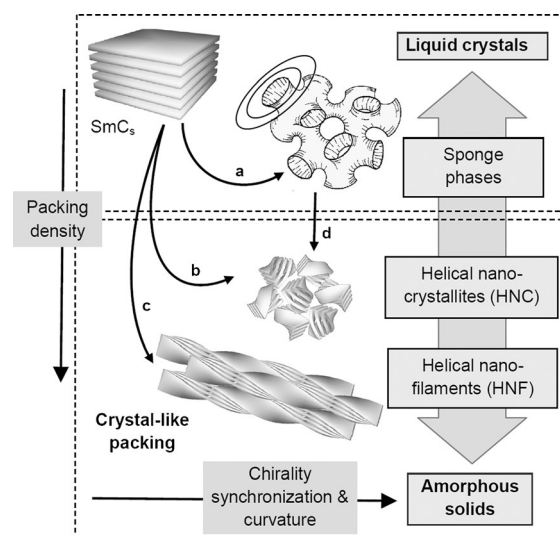


**Figure 11.** The distinct types of dark conglomerate phases (DC phases) of BCLCs ranging from isotropic LCs to amorphous solids and their development with increasing average packing density of the involved molecules; the picture of the sponge phase is taken from Ref. [38].

als forming this kind of DC phase were established. Accordingly, formation of these HNC phases is supported for BCLCs with a bulky substituent (Br) at the apex and a rigid azobenzene wing being located adjacent to this substituent. Either using a smaller Cl substituent or shifting the azobenzene to the opposite side removes the HNC phases.

Long chain compounds **Bn** and **BFn**, forming the HNC phases beside SmC phases provide the opportunity to study the transition from the SmC phases to the HNC phases. In a first step, polar order develops in the SmC<sub>5</sub>P<sub>AR</sub> phase region and the coherence length of polar order increases further at the transition to the SmC<sub>5</sub>P<sub>F</sub> phase. Development of polar order means that the rotation around the molecular long axis is restricted (see Figure 7a–c), favouring the chirality synchronization of the helical conformations of the involved molecules.<sup>[10,32]</sup> Chirality synchronization is supported by the helically deformed local director field, being the result of the combination of twist and bend or splay and bend, spontaneously evolving in the LC phases of bent molecules.<sup>[35]</sup> The denser packing of conformers with uniform chirality allows further increased packing density, thus favouring crystallization.<sup>[109]</sup> However, as the evolving crystalline order is incompatible with the simultaneously developing curvature, the coherence length of crystalline order is limited to nano-sized crystallites.<sup>[110,111]</sup> A structure composed of helical nano-crystallites, separated by less ordered molecules filling the defects between these nano-crystallites, is the preferred structural model for this type of DC phases. Thus, HNC phase formation appears to be analogous to the restricted crystallization observed in numerous semicrystalline polymers,<sup>[112]</sup> but with the constraints provided by the developing curvature replacing the constraints due to the polymer chain connectivity.

As shown in Figure 11, with growing packing density there are at least three distinct major types of DC phases: 1) the fluid sponge phases; 2) the HNC phases; and 3) the HNF phases. In the sponge phases chirality synchronization takes place before crystalline packing is achieved and thus is based on a dynamic route of mirror symmetry breaking (Figure 11, route a).<sup>[10]</sup> In the HNC and HNF phases macroscopic chirality develops together with the evolving crystal-like packing of the molecules (routes b and c). In the HNC phases considered here, layer deformation develops simultaneously with the emergence of crystal-like packing, but alternatively, this process could also take place in two separate steps by crystallization of previously formed sponge phases (Figure 11, route a + d).<sup>[66]</sup> As the local structure in the nano-crystallites is obviously SmC<sub>5</sub>P<sub>F</sub> the inherent superstructural layer chirality also plays a role. It is proposed that all three sources of chirality, conformational molecular chirality, supramolecular helical twist and superstructural layer chirality contribute cooperatively to the mirror symmetry breaking in soft matter systems formed by BCLCs.<sup>[10]</sup>

Helical twist of the bent-core chromophores and the layer chirality of the local SmC<sub>5</sub>P<sub>F</sub> structure (layer optical rotation)<sup>[113]</sup> could in principle lead to the optical activity of the DC phases, but the large optical rotation in most DC phases is assumed to be mainly due to the exciton coupling between the chromo-

phores of adjacent molecules in the helically twisted local structures.<sup>[114]</sup>

The HNC phases reported here could be of interest for potential applications as amorphous  $\pi$ -conjugated materials<sup>[20]</sup> for circular polarized light emission or detection,<sup>[115]</sup> and as chiral templates.<sup>[22]</sup> In addition, the incorporation of the photoisomerizable azobenzene wing provides the possibility of *trans-cis* photoisomerization (for preliminary investigation in solution, see the Supporting Information, Section 3 and Figure S9) to address the mode of self-assembly, chirality and other properties that could lead to additional possibilities for their technological applications.<sup>[100,116]</sup> Finally it is noted that chirality reduces symmetry, in this way providing a route to ferroelectricity, whereas on the other hand, the developing helicity can suppress long-range polar order. Therefore, the understanding of the relations between ferroelectricity, mirror symmetry breaking and molecular structure is of importance for the design of soft organic ferroelectrics, too.<sup>[117]</sup>

## 4. Experimental Section

### Materials

The detailed synthesis and analytical data are reported in the Supporting Information. All compounds were purified by column chromatography using chloroform as eluent followed by recrystallization from ethanol/chloroform (1:1) mixture and characterized by <sup>1</sup>H NMR spectroscopy and elemental analysis.

### Methods

DSC-thermograms were recorded on a Perkin–Elmer DSC-7 with heating and cooling rates of 10 K min<sup>-1</sup>. All compounds are thermally stable in the investigated temperature ranges as confirmed by the reproducibility of thermograms in several heating and cooling cycles. For polarizing microscopy a Mettler FP-82 HT hot stage and control unit in conjunction with a Nikon Optiphot-2 polarizing microscope was used. Electro-optical switching characteristics were examined in 6  $\mu$ m polyimide coated ITO cells (EHC Japan) using the triangular-wave method.<sup>[118]</sup> XRD patterns were recorded with a 2D detector (Vantec-500, Bruker). Ni filtered and pin hole collimated Cu<sub>K $\alpha$</sub>  radiation was used. The exposure time was 15 min and the sample to detector distance was 8.95 and 26.7 cm for small angle and wide angle scattering experiments, respectively. Alignment was attempted by slow cooling (rate: 1 K min<sup>-1</sup> to 0.1 K min<sup>-1</sup>) of a small droplet on a glass plate. Usually, alignment is achieved at the air-sample interface, but for the smectic phases of the compounds investigated herein only partial alignment is obtained (see the Supporting Information, Figure S19a and S20a), which is completely lost as soon as a DC phase forms (Figure S21a). No alignment is possible for compounds with direct Iso-DC transitions. Magnetic alignment was not attempted as this is known to work only if a nematic phase is involved in the phase sequence of BCLCs. For the precise determination of *d*-values powder samples were used which were held in thin glass capillaries and measured on cooling (rate: 1 K min<sup>-1</sup>). The samples were held on a temperature-controlled heating stage.

## Acknowledgements

The work was supported by the DFG (Grant Ts 39/24-1). M.A. acknowledges the support by the Alexander von Humboldt Foundation for the research fellowship at Martin-Luther University Halle-Wittenberg, Germany.

**Keywords:** amorphous materials · azo compounds · chirality · mesophases · self-assembly

- [1] a) A. Guijarro, M. Yus, *The origin of chirality in the molecules of life*, RSC Publishing, Cambridge, **2009**; L. D. Barron, *Space Sci. Rev.* **2008**, *135*, 187–201; b) M. Ávalos, R. Babiano, P. Cintas, J. L. Jimenez, J. C. Palacios, *Tetrahedron: Asymmetry* **2010**, *21*, 1030–1040.
- [2] a) M. Liu, L. Zhang, T. Wang, *Chem. Rev.* **2015**, *115*, 7304–7397; b) Y. Wang, J. Xu, Y. Wang, H. Chen, *Chem. Soc. Rev.* **2013**, *42*, 2930–2962.
- [3] a) I. Weissbuch, L. Leiserowitz, M. Lahav, *Top. Curr. Chem.* **2005**, *259*, 123–163; b) A. R. A. Palmans, E. W. Meijer, *Angew. Chem. Int. Ed.* **2007**, *46*, 8948–8968; *Angew. Chem.* **2007**, *119*, 9106–9126; c) D. B. Amabilino, *Chirality at the Nanoscale*, Wiley-VCH, Weinheim, **2009**; d) M. Safont-Sempere, G. Fernandez, F. Würthner, *Chem. Rev.* **2011**, *111*, 5784–5814.
- [4] K. Soai, T. Kawasaki, A. Matsumoto, *Chem. Rec.* **2014**, *14*, 70–83.
- [5] S. Zhang, S. Yang, J. Lan, S. Yang, J. You, *Chem. Commun.* **2008**, *46*, 6170–6172.
- [6] R. A. Reddy, C. Tschierske, *J. Mater. Chem.* **2006**, *16*, 907–961.
- [7] C. Tschierske, *Nanoscale stereochemistry in liquid crystals*. in D. B. Amabilino, *Chirality at the nanoscale*, Wiley-VCH, Weinheim, **2009**, pp. 271–304.
- [8] H. Takezoe, *Top. Curr. Chem.* **2011**, *318*, 303–330.
- [9] C. Tschierske, *Angew. Chem. Int. Ed.* **2013**, *52*, 8828–8878; *Angew. Chem.* **2013**, *125*, 8992–9047.
- [10] C. Tschierske, G. Ungar, *ChemPhysChem* **2016**, *17*, 9–26.
- [11] K.-U. Jeong, B. S. Knapp, J. J. Ge, S. Jin, M. J. Graham, F. W. Harris, S. Z. D. Cheng, *Chem. Mater.* **2006**, *18*, 680–690.
- [12] C. Roche, H.-J. Sun, M. E. Prendergast, P. Leowanawat, B. E. Partridge, P. A. Heiney, F. Araoka, R. Graf, H. W. Spiess, X. B. Zeng, G. Ungar, V. Percec, *J. Am. Chem. Soc.* **2014**, *136*, 7169–7185.
- [13] a) V. P. Panov, M. Nagaraj, J. K. Vij, Y. P. Panarin, A. Kohlmeier, M. G. Tamba, R. A. Lewis, G. H. Mehl, *Phys. Rev. Lett.* **2010**, *105*, 167801; b) V. Borshch, Y.-K. Kim, J. Xiang, M. Gao, A. Jakli, V. P. Panov, J. K. Vij, C. T. Imrie, M. G. Tamba, G. H. Mehl, O. D. Lavrentovich, *Nat. Commun.* **2013**, *4*, 2635.
- [14] M. Cestari, S. Diez-Berart, D. A. Dunmur, A. Ferrarini, M. R. de La Fuente, D. J. B. Jackson, D. O. Lopez, G. R. Luckhurst, M. A. Perez-Jubindo, R. M. Richardson, J. Salud, B. A. Timimi, H. Zimmermann, *Phys. Rev. E* **2011**, *84*, 031704.
- [15] D. Chen, J. H. Porada, J. B. Hooper, A. Klitnick, Y. Shen, M. R. Tuchband, E. Korblova, D. Bedrov, D. M. Walba, M. A. Glaser, J. E. MacLennan, N. A. Clark, *Proc. Natl. Acad. Sci. USA* **2013**, *110*, 15931–15936.
- [16] H.-S. Kitzerow, C. Bahr, *Chirality in Liquid Crystals*, Springer, New York, **2001**.
- [17] D. R. Link, G. Natale, R. Shao, J. E. MacLennan, N. A. Clark, E. Korblova, D. M. Walba, *Science* **1997**, *278*, 1924–1927.
- [18] H. Takezoe, Y. Takanishi, *Jpn. J. Appl. Phys.* **2006**, *45*, 597–625.
- [19] a) J. Etxebarria, M. B. Ros, *J. Mater. Chem.* **2008**, *18*, 2919–2926; b) A. Eremin, A. Jákli, *Soft Matter* **2013**, *9*, 615–637.
- [20] a) D. K. Yoon, Y. Yi, Y. Shen, E. D. Korblova, D. M. Walba, I. I. Smalyukh, N. A. Clark, *Adv. Mater.* **2011**, *23*, 1962–1967; b) D. Chen, C. Zhu, H. Wang, J. E. MacLennan, M. A. Glaser, E. Korblova, D. M. Walba, J. A. Rego, E. A. S. -Bustamante, N. A. Clark, *Soft Matter* **2013**, *9*, 462–471; c) R. A. Callahan, D. C. Coffey, D. Chen, N. A. Clark, G. Rumbles, D. M. Walba, *ACS Appl. Mater. Interfaces* **2014**, *6*, 4823–4830.
- [21] a) I. C. Pintre, J. L. Serrano, M. B. Ros, J. M. Perdiguero, I. Alonso, J. Ortega, C. L. Folcia, J. Etxebarria, R. Alicante, B. Villacampa, *J. Mater. Chem.* **2010**, *20*, 2965–2971; b) C. L. Folcia, I. Alonso, J. Ortega, J. Etxebarria, I. Pintre, M. B. Ros, *Chem. Mater.* **2006**, *18*, 4617–4626.
- [22] a) G. Lee, R. J. Carlton, F. Araoka, N. L. Abbott, H. Takezoe, *Adv. Mater.* **2013**, *25*, 245–249; b) T. Ueda, S. Masuko, F. Araoka, K. Ishikawa, H. Takezoe, *Angew. Chem. Int. Ed.* **2013**, *52*, 6863–6866; *Angew. Chem.* **2013**, *125*, 7001–7004.
- [23] W. Iglesias and A. Jákli, in *Handbook of Liquid Crystals*, Vol. 8 (Eds.: J. W. Goodby, P. J. Collings, T. Kato, C. Tschierske, H. F. Gleeson, P. Raynes), 2nd Ed., Wiley-VCH, Weinheim, **2014**, pp. 799–817.
- [24] L. E. Hough, M. Spannuth, M. Nakata, D. A. Coleman, C. D. Jones, G. Dantlgraber, C. Tschierske, J. Watanabe, E. Korblova, D. M. Walba, J. E. MacLennan, M. A. Glaser, N. A. Clark, *Science* **2009**, *325*, 452–456.
- [25] L. E. Hough, H. T. Jung, D. Krüerke, M. S. Heberling, M. Nakata, C. D. Jones, D. Chen, D. R. Link, J. Zasadzinski, G. Heppke, J. P. Rabe, W. Stocker, E. Korblova, D. M. Walba, M. A. Glaser, N. A. Clark, *Science* **2009**, *325*, 456–460.
- [26] D. Chen, R. Shao, J. E. MacLennan, M. A. Glaser, E. Korblova, D. M. Walba, N. Gimeno, M. B. Ros, N. A. Clark, *Liq. Cryst.* **2013**, *40*, 1730–1735.
- [27] a) I. Dierking, *Angew. Chem. Int. Ed.* **2010**, *49*, 29–30; *Angew. Chem.* **2010**, *122*, 30–32; b) J. P. F. Lagerwall, F. Giesselmann, *ChemPhysChem* **2010**, *11*, 975–977.
- [28] Z. H. Stachurski, *Materials* **2011**, *4*, 1564–1598.
- [29] V. Görtz, *Liq. Cryst. Today* **2010**, *19*, 37–48.
- [30] a) T. Kajitani, S. Kohmoto, M. Yamamoto, K. Kishikawa, *Chem. Mater.* **2005**, *17*, 3812–3819; b) C. Dressel, F. Liu, M. Prehm, X.-B. Zeng, G. Ungar, C. Tschierske, *Angew. Chem. Int. Ed.* **2014**, *53*, 13115–13120; *Angew. Chem.* **2013**, *125*, 13331–13336.
- [31] M. Alaasar, M. Prehm, Y. Cao, F. Liu, C. Tschierske, *Angew. Chem. Int. Ed.* **2016**, *55*, 312–316; *Angew. Chem.* **2016**, *128*, 320–324.
- [32] C. Dressel, T. Reppe, M. Prehm, M. Brautzsch, C. Tschierske, *Nat. Chem.* **2014**, *6*, 971–977.
- [33] D. J. Earl, M. A. Hixson, H. Takezoe, Y. Takanishi, M. R. Wilson, *Phys. Rev. E* **2005**, *71*, 021796.
- [34] A similar chirality synchronization process was proposed for transiently chiral polymers: a) J. L. Baumgarten, *Macromol. Rapid Commun.* **1994**, *15*, 175–182; b) J. L. Baumgarten, *Macromol. Theory Simul.* **1995**, *4*, 1–43.
- [35] a) R. B. Meyer, Les Nouches Summer School on Theoretical Physics, 1973, *Molecular Fluids* (Eds.: R. Balian, G. Weil), Gordon and Breach, New York **1976**, 272–373; b) I. Dozov, *Europhys. Lett.* **2001**, *56*, 247–253; c) R. Memmer, *Liq. Cryst.* **2002**, *29*, 483–496.
- [36] F. Yan, C. A. Hixson, D. J. Earl, *Phys. Rev. Lett.* **2008**, *101*, 157801.
- [37] Also SmC phases with strictly alternating tilt and polar direction (SmC<sub>a</sub>P<sub>a</sub>) are homogeneously chiral, whereas SmC phases with alternating polar direction and uniform tilt (SmC<sub>s</sub>P<sub>a</sub>) or alternating tilt and uniform polar direction (SmC<sub>s</sub>P<sub>s</sub>) are achiral (“racemic”).<sup>[17]</sup>
- [38] Lyotropic sponge phases of amphiphilic molecules: R. Strey, W. Jahn, G. Porte, P. Bassereau, *Langmuir* **1990**, *6*, 1635–1639.
- [39] a) G. Dantlgraber, A. Eremin, S. Diele, A. Hauser, H. Kresse, G. Pelzl, C. Tschierske, *Angew. Chem. Int. Ed.* **2002**, *41*, 2408–2412; *Angew. Chem.* **2002**, *114*, 2514–2518; b) G. Dantlgraber, S. Diele, C. Tschierske, *Chem. Commun.* **2002**, *23*, 2768–2769; c) C. Tschierske, G. Dantlgraber, *Pramana* **2003**, *61*, 455–481; d) C. Keith, R. A. Reddy, A. Hauser, U. Baumeister, C. Tschierske, *J. Am. Chem. Soc.* **2006**, *128*, 3051–3066; e) C. Keith, R. A. Reddy, U. Baumeister, H. Hahn, H. Lang, C. Tschierske, *J. Mater. Chem.* **2006**, *16*, 3444–3447; f) H. Hahn, C. Keith, H. Lang, R. A. Reddy, C. Tschierske, *Adv. Mater.* **2006**, *18*, 2629–2633; g) C. Keith, G. Dantlgraber, R. A. Reddy, U. Baumeister, M. Prehm, H. Hahn, H. Lag, C. Tschierske, *J. Mater. Chem.* **2007**, *17*, 3796–3805; h) C. Keith, G. Dantlgraber, R. A. Reddy, U. Baumeister, C. Tschierske, *Chem. Mater.* **2007**, *19*, 694–710; i) Y. Zhang, U. Baumeister, C. Tschierske, M. O’Callaghan, C. Walker, *Chem. Mater.* **2010**, *22*, 2869–2884.
- [40] G. Heppke, D. D. Parghi, H. Sawade, *Liq. Cryst.* **2000**, *27*, 313–320.
- [41] J. Thisayukta, Y. Nakayama, S. Kawachi, H. Takezoe, J. Watanabe, *J. Am. Chem. Soc.* **2000**, *122*, 7441–7448.
- [42] R. Amarantatha Reddy, B. K. Sadashiva, *Liq. Cryst.* **2003**, *30*, 1031–1050.
- [43] A. Roy, M. Gupta, S. Radhika, B. K. Sadashiva, R. Pratibha, *Soft Matter* **2012**, *8*, 7207–7214.
- [44] J. Ortega, C. L. Folcia, J. Etxebarria, N. Gimeno, M. B. Ros, *Phys. Rev. E* **2003**, *68*, 11707-1-4.
- [45] S. Kang, Y. Saito, N. Watanabe, M. Tokita, Y. Takanishi, H. Takezoe, J. Watanabe, *J. Chem. Phys. B.* **2006**, *110*, 5205–5214.

- [46] a) M. Nagaraj, K. Usami, Z. Zhang, V. Görtz, J. W. Goodby, H. F. Gleeson, *Liq. Cryst.* **2014**, *41*, 800–811; b) M. Nagaraj, J. C. Jones, V. P. Panov, H. Liu, G. Portale, W. Bras, H. F. Gleeson, *Phys. Rev. E* **2015**, *91*, 042504.
- [47] DC phases were reported to occur below nontilted SmAP<sub>A</sub> phases and hexagonal columnar phases in a series of 1,7-substituted naphthalens with Schiff base wings and 60° bent angles, these DC phases have been designated as B4 phases: a) S. K. Lee, X. Li, S. Kang, M. Tokita, J. Watanabe, *J. Mater. Chem.* **2009**, *19*, 4517–4522; b) X. Li, S. Kang, S. K. Lee, M. Tokita, J. Watanabe, *Jpn. J. Appl. Phys.* **2010**, *49*, 121701; c) X. Li, M. Zhan, K. Wang, H. Zhou, *Chem. Lett.* **2011**, *40*, 820–821; d) T. Bao, K. Wang, M.-S. Zhan, *Liq. Cryst.* **2014**, *41*, 1687–1695.
- [48] a) A. Jáklí, Y.-M. Huang, K. Fodor-Csorba, A. Vajda, G. Galli, S. Diele, G. Pelzl, *Adv. Mater.* **2003**, *15*, 1606–1610; b) W. Weissflog, M. W. Schröder, S. Diele, G. Pelzl, *Adv. Mater.* **2003**, *15*, 630–633.
- [49] a) S. K. Lee, L. Shi, M. Tokita, H. Takezoe, J. Watanabe, *J. Phys. Chem. B* **2007**, *111*, 8698–8701; b) S. K. Lee, L. Shi, M. Tokita, J. Watanabe, *J. Phys. Chem. B* **2008**, *112*, 6762–6766.
- [50] G. Pelzl, S. Diele, W. Weissflog, *Adv. Mater.* **1999**, *11*, 707–724.
- [51] a) D. M. Walba, L. Eshat, E. Körblova, R. K. Shoemaker, *Cryst. Growth Des.* **2005**, *5*, 2091–2099; b) D. Chen, J. E. MacLennan, R. Shao, D. K. Yoon, H. Wang, E. Körblova, D. M. Walba, M. A. Glaser, N. A. Clark, *J. Am. Chem. Soc.* **2011**, *133*, 12656–12663.
- [52] J. Martínez-Perdiguerro, I. Alonso, C. L. Folcia, J. Etxebarria, J. Ortega, *J. Mater. Chem.* **2009**, *19*, 5161–5166.
- [53] C. Zhang, N. Diorio, O. D. Lavrentovich, A. Jáklí, *Nat. Commun.* **2014**, *5*, 3302.
- [54] a) J. Thisayukta, H. Takezoe, J. Watanabe, *Jpn. J. Appl. Phys.* **2001**, *40*, 3277; b) H. Niwano, M. Nakata, J. Thisayukta, D. R. Link, H. Takezoe, J. Watanabe, *J. Phys. Chem. B* **2004**, *108*, 14889–14896; c) H. Kurosu, M. Kawasaki, M. Hirose, M. Yamada, S. Kang, J. Thisayukta, M. Sone, H. Takezoe, J. Watanabe, *J. Phys. Chem. A* **2004**, *108*, 4674–4678.
- [55] H. Kresse, J. Saltetnokova, H. Nadasi, W. Weissflog, A. Hauser, *Liq. Cryst.* **2001**, *28*, 1017–1023.
- [56] a) E. Bialecka-Florjanczyk, I. Sledzinska, E. Górecka, J. Przedmojski, *Liq. Cryst.* **2008**, *35*, 401–406; b) A. Zep, M. Salamonczyk, N. Vaupotič, D. Pocięcha, E. Gorecka, *Chem. Commun.* **2013**, *49*, 3119–3121.
- [57] T. Niori, T. Sekine, J. Watanabe, T. Furukawa, H. Takezoe, *J. Mater. Chem.* **1996**, *6*, 1231–1233.
- [58] C. Zhu, C. Wang, A. Young, F. Liu, I. Gunkel, D. Chen, D. Walba, J. MacLennan, N. Clark, A. Hexemer, *Nano Lett.* **2015**, *15*, 3420–3424.
- [59] G. B. Deepa, S. Radhika, B. K. Sadashiva, R. Pratibha, *Phys. Rev. E* **2013**, *87*, 062508.
- [60] D. G. Bhat, R. Selvaraj, S. B. Kapanipathaiya, P. Ramarao, *ChemPhysChem* **2015**, *16*, 825–832.
- [61] S. Lee, H. Kim, T. J. Shin, E. Tsai, J. M. Richardson, E. Körblova, D. M. Walba, N. A. Clark, S. B. Lee, D. K. Yoon, *Soft Matter* **2015**, *11*, 3653–3659.
- [62] I. Miyake, Y. Takamishi, N. V. S. Rao, M. K. Paul, K. Ishikawa, H. Takezoe, *J. Mater. Chem.* **2005**, *15*, 4688–4694.
- [63] A. Belaissaoui, S. J. Kowling, J. W. Goodby, *Liq. Cryst.* **2013**, *40*, 822–830.
- [64] H. Ocak, B. Bilgin-Eran, M. Prehm, C. Tschierske, *Soft Matter* **2013**, *9*, 4590–4597.
- [65] E. Tsai, J. M. Richardson, E. Körblova, M. Nakata, D. Chen, Y. Shen, R. Shao, N. A. Clark, D. M. Walba, *Angew. Chem. Int. Ed.* **2013**, *52*, 5254–5257; *Angew. Chem.* **2013**, *125*, 5362–5365.
- [66] D. Chen, Y. Shen, J. Agüero, E. Körblova, D. M. Walba, N. Kapernaum, F. Giesselmann, J. Watanabe, J. E. MacLennan, M. A. Glaser, N. A. Clark, *ChemPhysChem* **2014**, *15*, 1502–1507.
- [67] D. Chen, H. Wang, M. Li, M. A. Glaser, J. E. MacLennan, N. A. Clark, *Soft Matter* **2014**, *10*, 9105–9109.
- [68] H. Ocak, B. Bilgin-Eran, M. Prehm, C. Tschierske, *Soft Matter* **2012**, *8*, 7773–7783.
- [69] M. Alaasar, M. Prehm, C. Tschierske, *Chem. Commun.* **2013**, *49*, 11062–11064.
- [70] M. Alaasar, M. Prehm, M. Brautzsch, C. Tschierske, *J. Mater. Chem. C* **2014**, *2*, 5487–5501.
- [71] M. Alaasar, M. Prehm, M. Brautzsch, C. Tschierske, *Soft Matter* **2014**, *10*, 7285–7296.
- [72] M. Alaasar, M. Prehm, C. Tschierske, *Liq. Cryst.* **2013**, *40*, 656–668.
- [73] In ref. [72] it was reported that compounds **2/n** with  $n=6$  forms a B6 phase, a DC-N dimorphism was observed for  $n=8$ , whereas all compounds with  $n=12–16$  form only solid crystalline phases. However, re-investigation of these compound indicated that all compounds with  $n=8–18$  form soft crystalline DC phases accompanied by a small (ca. 1 K) range of a nematic phase, the same sequence as found for the newly synthesized compound **2/18** (see Section 2.5). For **2/8** the DC phase crystallizes on cooling, whereas for **2/10–2/18** no crystallization could be observed.
- [74] Previous examples of asymmetric bent-core compounds combining azobenzene- and ester-based wings: a) N. Trisovic, J. Antanasijevic, T. Toth-Katona, M. Kohout, M. Salamonczyk, S. Sprunt, A. Jáklí, K. Fodor-Csorba, *RSC Adv.* **2015**, *5*, 64886–64891; b) V. Prasad, S.-W. Kang, X. Qi, S. Kumar, *J. Mater. Chem. C* **2004**, *14*, 1495–1502; c) N. G. Nagaveni, V. Prasad, A. Roy, *Liq. Cryst.* **2013**, *40*, 1405–1416; d) N. G. Nagaveni, P. Raghuvanshi, A. Roy, V. Prasad, *Liq. Cryst.* **2013**, *40*, 1238–1254; e) N. Gimeno, I. Pintre, M. Martínez-Abadía, J. L. Serrano, M. B. Ros, *RSC Adv.* **2014**, *4*, 19694–19702; f) M. Vijaysrinivasan, P. Kannan, A. Roy, *Liq. Cryst.* **2012**, *39*, 1465–1475; g) N. G. Nagaveni, A. Roy, V. Prasad, *J. Mater. Chem. C* **2012**, *22*, 8948; h) V. Prasad, S.-W. Kang, K. A. Suresh, L. Joshi, Q. Wang, S. Kumar, *J. Am. Chem. Soc.* **2005**, *127*, 17224–17227; i) M. V. Srinivasan, P. Kannan, A. Roy, *New J. Chem.* **2013**, *37*, 1584–1590.
- [75] No crystallization of the DC<sup>[\*]</sup> phases can be detected, even after storage for one year at room temperature.
- [76] In electro-optical experiments no birefringence is induced under an applied triangular wave voltage up to 200 Vpp in a 6 μm ITO cell and also no current peak could be observed in the DC<sup>[\*]</sup>/DC<sup>[\*]</sup> phases of any of the prepared materials. This behaviour is similar to the DC<sup>[\*]</sup> phases of the related bent-core mesogens involving two azobenzene units (**1F/n**, **2F/n** and **3/n**, see Scheme 1).<sup>[69,70,71]</sup>
- [77] It is known that bent-core molecules involving 4-hydroxybenzoate wings have a higher tendency to form tilted smectic phases compared to those with terephthalate units<sup>[96]</sup>. Therefore, observation of tilted smectic phases above the DC phases of the terephthalates **Bn** would mean that the reduced  $d$ -value in the DC phases of the 4-hydroxybenzoates **An** should be mainly caused by tilting of the molecules. In polar smectic phases tilt can occur in two directions with respect to the polar direction. Usually tilt direction is perpendicular to the polar axis. However, in exceptional cases a “leaning” was observed, in which the tilt of the polar axis takes place (leaning phases)<sup>[95]</sup> or both, tilt and leaning occur simultaneously (SmG phases: N. Chattham, E. Körblova, R. Shao, D. M. Walba, J. E. MacLennan, N. A. Clark, *Phys. Rev. Lett.* **2010**, *104*, 067801). However, these phases are rarely observed and are unlikely for the compounds investigated here, where the 4-substituent at the resorcinol unit provides a significant steric distortion for a leaning-type organization.
- [78] R. Androsch, A. M. Rhoades, I. Stolte, C. Schick, *Eur. Polym. J.* **2015**, *66*, 180–189.
- [79] Similar broad transitions were reported for HNF type DC phases and interpreted as crystallization.<sup>[82]</sup>
- [80] Transitions between polar SmC phases (B2 phases) and sponge phases are well documented,<sup>[6,7,17,19,48,49]</sup> whereas for the HNF phases (B4 phases) B2-B3-B4 transitions were typically found for the original Schiff base materials.<sup>[98]</sup> Also B2-B4 transitions<sup>[54,81]</sup> and B7-B4 transitions<sup>[82]</sup> have been found occasionally. A B6-HNC transition was reported for compound **3/9**.<sup>[70]</sup> B4 phases occurring below nontilted SmAP<sub>A</sub> phases and Col<sub>hex</sub> phases were found for V-shaped molecules with 60° bent angles.<sup>[47]</sup>
- [81] N. Nádasi, C. Lischka, W. Weissflog, I. Wirth, S. Diele, G. Pelzl, H. Kresse, *Mol. Cryst. Liq. Cryst.* **2003**, *399*, 69–84.
- [82] V. Prasad, *Liq. Cryst.* **2001**, *28*, 1115–1120.
- [83] M. Alaasar, M. Prehm, M.-G. Tamba, N. Sebastian, A. Eremin, C. Tschierske, *ChemPhysChem* **2016**, *17*, 278–287.
- [84] M. F. Achard, J. P. Bedel, J. P. Marcerou, H. T. Nguyen, J. C. Rouillon, *Eur. Phys. J. E* **2003**, *10*, 129–134.
- [85] These SmC<sub>s</sub>P<sub>AR</sub> phases with randomized polar order in the ground state have recently been investigated and described in more detail for other BCLCs.<sup>[83]</sup>
- [86] a) H. Nádasi, W. Weissflog, A. Eremin, G. Pelzl, S. Diele, B. Das, S. Grande, *J. Mater. Chem.* **2002**, *12*, 1316–1324; b) A. Eremin, I. Wirth, S.



- Diele, G. Pelzl, H. Schmalfluss, H. Kresse, H. Nadasi, K. Fodor-Csorba, E. Gacs-Baitz, W. Weissflog, *Liq. Cryst.* **2002**, *29*, 775–782.
- [87] A very weak birefringence is retained, visible even after switching off the field, which is most probably due to the presence of surface-stabilised smectic layers persisting even in the DC phase region (see the Supporting Information, Figure S24 g–i).
- [88] C. Keith, R. A. Reddy, M. Prehm, U. Baumeister, H. Kresse, J. Lorenzo Chao, H. Hahn, H. Lang, C. Tschierske, *Chem. Eur. J.* **2007**, *13*, 2556–2577.
- [89] M. Alaasar, M. Prehm, M. Poppe, M. Nagaraj, J. K. Vij, C. Tschierske, *Soft Matter* **2014**, *10*, 5003–5016.
- [90] a) T. Otani, F. Araoka, K. Ishikawa, H. Takezoe, *J. Am. Chem. Soc.* **2009**, *131*, 12368–12372; b) F. Araoka, G. Sugiyama, K. Ishikawa, H. Takezoe, *Adv. Funct. Mater.* **2013**, *23*, 2701–2707; c) Y. Takanishi, H. Yao, T. Fukasawa, K. Ema, Y. Ohtsuka, Y. Takanishi, J. Yamamoto, H. Takezoe, A. Iida, *J. Phys. Chem. A* **2014**, *118*, 3998–4004.
- [91] Confirmation of the phase assignment by XRD was not possible in this case, due to crystallization during exposure time.
- [92] There is no indication of symmetry breaking in this nematic phase.
- [93] a) M. Alaasar, M. Prehm, M. Nagaraj, J. K. Vij, C. Tschierske, *Adv. Mater.* **2013**, *25*, 2186–2191; b) M. Alaasar, M. Prehm, K. May, A. Eremin, C. Tschierske, *Adv. Funct. Mater.* **2014**, *24*, 1703–1717; c) H. Ocak, B. Bilgin-Eran, D. Güzeller, M. Prehm, C. Tschierske, *Chem. Commun.* **2015**, *51*, 7512–7515.
- [94] G. Pelzl, M. W. Schröder, A. Eremin, S. Diele, B. Das, S. Grande, H. Kresse, W. Weissflog, *Eur. Phys. J. E* **2006**, *21*, 293–303.
- [95] E. Westphal, H. Gallardo, G. F. Caramori, N. Sebastin, M.-G. Tamba, A. Eremin, S. Kawachi, M. Prehm, C. Tschierske, *Chem. Eur. J.*; (submitted).
- [96] a) G. Pelzl, W. Weissflog in *Thermotropic Liquid Crystals Recent Advances*, (Ed.: A. Ramamoorthy), Springer, Dordrecht, **2007**, pp. 1–58; b) W. Weissflog, H. N. Shreenivasa Murthy, S. Diele, G. Pelzl, *Philos. Trans. R. Soc. London Ser. A* **2006**, *364*, 2657–2679.
- [97] C. Keith, M. Prehm, Y. P. Panarin, J. K. Vij, C. Tschierske, *Chem. Commun.* **2010**, *46*, 3702–3704.
- [98] T. Sekine, T. Niori, J. Watanabe, T. Furukawa, S. W. Choi, H. Takezoe, *J. Mater. Chem.* **1997**, *7*, 1307–1309.
- [99] S.-W. Choi, T. Izumi, Y. Hoshino, Y. Takanishi, K. Ishikawa, J. Watanabe, H. Takezoe, *Angew. Chem. Int. Ed.* **2006**, *45*, 1382–1385; *Angew. Chem.* **2006**, *118*, 1410–1413.
- [100] A. Zep, K. Sitkowska, D. Pocięcha, E. Gorecka, *J. Mater. Chem. C* **2014**, *2*, 2323–2327.
- [101] Recently also for trimesogens involving flat 2-phenypyrimidine mesogenic units and odd numbered spacers, B4 phase (HNF phase) formation was observed: H. Sasaki, Y. Takanishi, J. Yamamoto, A. Yoshizawa, *J. Phys. Chem. B* **2015**, *119*, 4531–4538.
- [102] There is a number of DC phase forming molecules with oxadiazole-based bent-cores, mainly forming sponge-type DC phases.<sup>[45,46]</sup>
- [103] D. Shen, A. Pegenau, S. Diele, I. Wirth, C. Tschierske, *J. Am. Chem. Soc.* **2000**, *122*, 1593–1601.
- [104] J. Etxebarria, C. L. Folcia, J. Ortega, M. B. Ros, *Phys. Rev. E* **2003**, *67*, 042702.
- [105] a) S. Kang, J. Thisayukta, H. Takezoe, J. Watanabe, K. Ogino, T. Doi, T. Takanishi, *Liq. Cryst.* **2004**, *31*, 1323–1336; b) S. Kang, R. Ishige, E.-W. Lee, M. Tokita, J. Watanabe, *J. Mater. Chem.* **2012**, *22*, 21448–21452.
- [106] W. Weissflog, S. Sokolowski, H. Dehne, B. Das, S. Grande, M. W. Schröder, A. Eremin, S. Diele, G. Pelzl, H. Kresse, *Liq. Cryst.* **2004**, *31*, 923–933.
- [107] I. Wirth, S. Diele, A. Eremin, G. Pelzl, S. Grande, L. Kovalenko, N. Panchenko, W. Weissflog, *J. Mater. Chem.* **2001**, *11*, 1642–1650.
- [108] See textures in Figure 3c,d in ref. [70].
- [109] A. Sicilia, J. J. Arenzon, I. Dierking, A. J. Bray, L. F. Cugliandolo, J. Martinez-Perdiguero, I. Alonso, I. C. Pintre, *Phys. Rev. Lett.* **2008**, *101*, 197801.
- [110] a) J. V. Selinger, M. S. Spector, J. M. Schnur, *J. Phys. Chem. B* **2001**, *105*, 7157–7169; b) D. R. Nelson, L. Peliti, *J. Phys. (Paris)* **1987**, *48*, 1085–1092.
- [111] a) J. Charvolin, J.-F. Sadoc, *Interface Focus* **2012**, *2*, 567–574; b) G. M. Grason, *Rev. Mod. Phys.* **2015**, *87*, 401–419.
- [112] S. T. Milner, *Soft Matter* **2011**, *7*, 2909–2917.
- [113] a) L. Hough, N. A. Clark, *Phys. Rev. Lett.* **2005**, *95*, 107802; b) L. Hough, C. Zhu, M. Nakata, N. Chattham, G. Dantlgraber, C. Tschierske, N. A. Clark, *Phys. Rev. Lett.* **2008**, *101*, 079802.
- [114] G. Pescitelli, L. Di Bari, N. Berova, *Chem. Soc. Rev.* **2014**, *43*, 5211–5233.
- [115] a) Y. Yang, R. Correa da Costa, D.-M. Smilgies, A. J. Campbell, M. J. Fuchter, *Adv. Mater.* **2013**, *25*, 2624–2628; b) Y. Yang, R. Correa da Costa, M. J. Fuchter, A. J. Campbell, *Nature Photon.* **2013**, *7*, 634–638.
- [116] K. Kim, H. Kim, S.-Y. Jo, F. Araoka, D. K. Yoon, S.-W. Choi, *ACS Appl. Mater. Interfaces* **2015**, *7*, 22686–22691.
- [117] A. S. Tayi, A. Kaeser, M. Matsumoto, T. Aida, S. I. Stupp, *Nat. Chem.* **2015**, *7*, 281–293.
- [118] K. Miyasato, S. Abe, H. Takezoe, A. Fukuda, E. Kuze, *Jpn. J. Appl. Phys.* **1983**, *22*, L661–L663.

Received: December 13, 2015

Published online on March 23, 2016


 CrossMark  
 click for updates
Cite this: *RSC Adv.*, 2016, 6, 82890

# Mirror symmetry breaking in fluorinated bent-core mesogens†

Mohamed Alaasar,<sup>\*ab</sup> Marko Prehm<sup>a</sup> and Carsten Tschierske<sup>\*a</sup>

Spontaneous chirality synchronization in the LC phases of achiral bent-core molecules, the so called dark conglomerate mesophases (DC<sup>[\*]</sup> phases), is a challenging task with significant importance for fundamental scientific research and potential applications. Here we report the synthesis and investigation of two new series of achiral bent-core mesogens derived from 4-bromoresorcinol and 4-chlororesorcinol with 2,3-difluorinated azobenzene-based side arms. The self-assembly of these materials was characterized by DSC, polarizing microscopy, X-ray diffraction investigations (XRD) and electro-optical studies. Depending on the type of halogen substituent at the central resorcinol core and on the terminal alkyl chain length different types of mesophases were observed, where 4-bromoresorcinol derived compounds predominately show helical nanocrystallite phases, (HNC phases), representing conglomerates of chiral domains (DC<sup>[\*]</sup>), whereas the related 4-chlororesorcinol based compounds form smectic C phases with a polar domain structure (SmC<sub>s</sub>P<sub>AR</sub>). Comparison with related compounds provides information about the influence of core fluorination on the mesophase behaviour and DC<sup>[\*]</sup> phase formation, thus providing a step forward in uncovering the molecular design principles of LC materials capable of mirror symmetry breaking.

Received 20th July 2016  
Accepted 19th August 2016

DOI: 10.1039/c6ra18482k

www.rsc.org/advances

## 1. Introduction

Since the first report by Niori *et al.*,<sup>1</sup> about polar order in liquid crystalline (LC) phases formed by molecules with a non-linear bent shape, the so-called bent-core liquid crystals (BCLCs), extensive research has been done by several research groups on these fascinating materials.<sup>2</sup> In recent years BCLCs have received great attention due to their remarkable and unique mesophases, especially the development of macroscopic polar order (ferroelectricity) and spontaneous mirror symmetry breaking, though the molecules themselves are achiral. This phenomenon is of general interest for fundamental soft matter science as well as for potential applications. Mirror symmetry breaking is a basic feature of living matter which was in the recent two decades also observed in some cases of LC phases.<sup>2–15</sup> Dark conglomerate phases (DC<sup>[\*]</sup> phases) represent one class of such spontaneously mirror symmetry broken mesophases exhibited by BCLCs.<sup>3,16–19</sup> They are optically isotropic and therefore characterized by completely dark appearance between crossed polarizers, whereas under slightly uncrossed polarizers chiral domains of opposite handedness can be observed. Related chiral domains were recently also observed in some nematic phases of dimesogens with odd-numbered spacers

(twist bend nematic phases (N<sub>TB</sub>)),<sup>9–11,20</sup> in SmC phases formed by some azobenzene-based BCLCs,<sup>21</sup> in bicontinuous cubic phases<sup>22</sup> and even in isotropic liquids formed by some polycatenar molecules.<sup>6,23,24</sup> Also trimesogen can show N<sub>TB</sub> phases and soft crystalline DC<sup>[\*]</sup> phases.<sup>25</sup> The DC<sup>[\*]</sup> phases of BCLCs are classified into three major types (Fig. 1), including the deformed smectic LC phases with sponge like structure,<sup>16,26–36</sup> the helical nano-filament phases (HNF phases or B4 phases) where the molecules are arranged in arrays of helical nano-scale filaments,<sup>17,37–44</sup> and the third type of DC<sup>[\*]</sup> phases being the helical nano-crystallites phases (HNC phases) which were recently observed for some azobenzene based BCLCs (see Scheme 1).<sup>45–49</sup>

Herein we report two new series of BCLCs derived from 4-bromoresorcinol and 4-chlororesorcinol central cores, respectively,<sup>50</sup> with laterally 2,3-difluorinated azobenzene side arms (compounds **BrF<sub>2</sub>n** and **ClF<sub>2</sub>n**, see Scheme 2). The 4-bromoresorcinol based compounds with medium alkyl chain lengths form helical nanocrystallite phases (HNC phase), representing

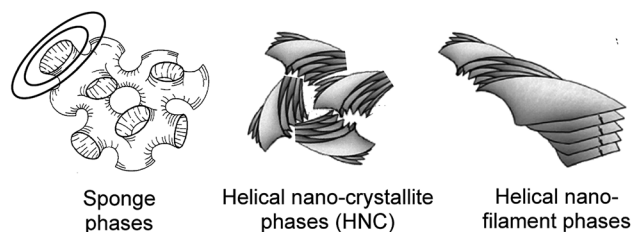
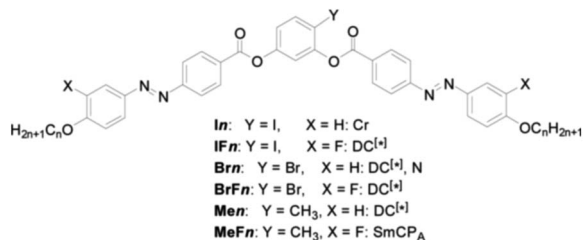


Fig. 1 The three major types of dark conglomerate (DC<sup>[\*]</sup>) phases.<sup>48</sup>

<sup>a</sup>Institute of Chemistry, Martin Luther University Halle-Wittenberg, Kurt Mothes Str. 2, D-06120 Halle (Saale), Germany. E-mail: carsten.tschierske@chemie.uni-halle.de

<sup>b</sup>Department of Chemistry, Faculty of Science, Cairo University, Giza, Egypt. E-mail: malaasar@sci.cu.edu.eg

† Electronic supplementary information (ESI) available. See DOI: 10.1039/c6ra18482k



**Scheme 1** Chemical structures of previously reported BCLCs with azobenzene-based wings with and without peripheral fluorine substitution.<sup>45–47,49</sup> Abbreviations: Cr = crystalline solid; DC<sup>[†]</sup> = dark conglomerate phases (HNC phases) composed of chiral domains with opposite handedness; N = nematic phase; SmCP<sub>A</sub> = antiferroelectric switching smectic phase.

optically isotropic soft crystalline phases forming conglomerates of chiral domains (DC<sup>[†]</sup> phases) which for the longest homologue are replaced by a smectic C phase composed of ferroelectric domains with antipolar correlation (SmC<sub>s</sub>P<sub>AR</sub>).<sup>51</sup> The other series of compounds, which is derived from 4-chlororesorcinol, shows no HNC phases, but exclusively monotropic SmC phases which represent SmC<sub>s</sub>P<sub>AR</sub> phases of a slightly different type. These compounds are compared with previously reported compounds without fluorine substitution or with a reduced number of fluorines in the side arms.<sup>47,49</sup>

## 2. Experimental

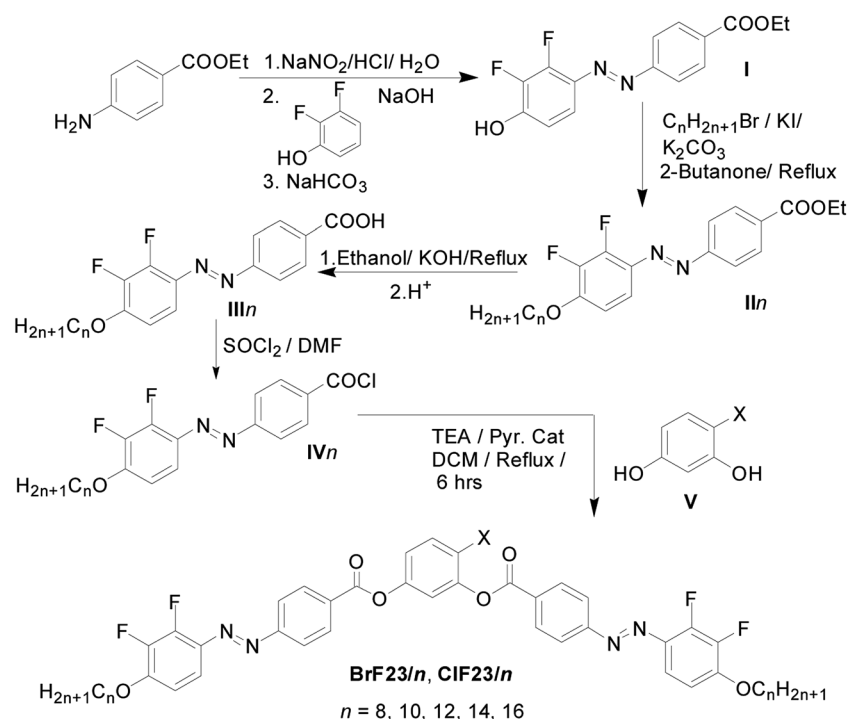
### 2.1. Synthesis

The synthesis of the target BCLCs **BrF<sub>2</sub>n** and **ClF<sub>2</sub>n** was carried out as shown in Scheme 2 by acylation reaction of the 4-

halogenated resorcinol **V** with two equivalents of the benzoyl chlorides **IVn**<sup>24</sup> in the presence of triethylamine as base and pyridine as a catalyst. The final crude bent-core compounds **BrF<sub>2</sub>n** and **ClF<sub>2</sub>n** were purified by column chromatography using dichloromethane followed by recrystallization from ethanol/chloroform (1 : 1) mixture to yield the desired materials. Detailed procedures and the analytical data of the newly synthesised compounds **BrF<sub>2</sub>n** and **ClF<sub>2</sub>n** are reported in the ESI.<sup>†</sup> All compounds are thermally stable as confirmed by the reproducibility of thermograms in several heating and cooling cycles.

### 2.2. Methods

The thermal behaviour of all synthesized compounds was studied by polarizing optical microscopy (POM) and differential scanning calorimetry (DSC). For polarizing microscopy a Mettler FP-82 HT hot stage and control unit in conjunction with a Nikon Optiphot-2 polarizing microscope was used. DSC-thermograms were recorded on a Perkin-Elmer DSC-7 with heating and cooling rates of 10 K min<sup>-1</sup>. Electro-optical switching characteristics were examined in 6 μm polyimide coated ITO cells (EHC Japan) using the triangular-wave method.<sup>52</sup> XRD patterns were recorded with a 2D detector (Vantec-500, Bruker). Ni filtered and pin hole collimated CuK<sub>α</sub> radiation was used. The exposure time was 15 min and the sample to detector distance was 8.95 and 26.7 cm for small angle and wide angle scattering experiments, respectively. Alignment was attempted by slow cooling (rate: 1 K min<sup>-1</sup> to 0.1 K min<sup>-1</sup>) of a small droplet on a glass plate.



**Scheme 2** Synthetic route to the bent-core mesogens under investigations.

### 3. Results and discussion

#### 3.1. Dark conglomerate phases of compounds $\text{BrF}_2n$ with $n \leq 14$

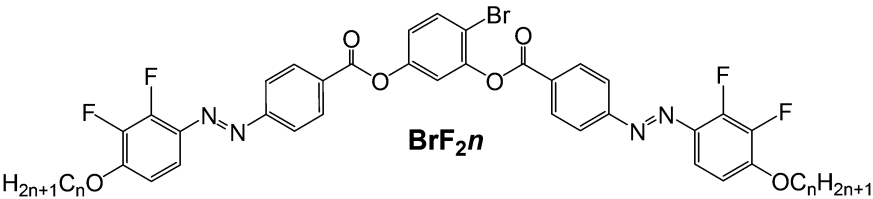
Depending on the terminal chain length, compounds  $\text{BrF}_2n$  with a 4-bromoresorcinol central core form different types of mesophases. The shortest derivative  $\text{BrF}_2\mathbf{8}$  with  $n = 8$  forms a birefringent crystalline solid with melting point  $T = 104^\circ\text{C}$ , whereas compounds  $\text{BrF}_2\mathbf{10}$ – $\text{BrF}_2\mathbf{14}$  with medium chain length exhibit monotropic highly viscous optically isotropic phases which, once formed, do not crystallize even after storage for one year at room temperature (see Table 1). Under crossed polarizers, these isotropic phases appear completely dark between crossed polarizers and on rotating the analyzer by a small angle ( $\sim 10^\circ$ ) out of the crossed position *i.e.* from the  $90^\circ$  position with respect to the polarizer, uniform dark and bright domains appear, indicating the presence of chiral domains ( $\text{DC}^{[*]}$  phases, see Fig. 2). That the distinct regions represent chiral domains with opposite handedness was confirmed by rotating the sample itself between crossed polarizers in different directions, where no change in the dark texture was observed.

The  $\text{DC}^{[*]}$ -Iso transitions are associated with transition enthalpies values around  $\Delta H \sim 21 \text{ kJ mol}^{-1}$  in the cooling cycles (see Fig. 3 and Table 1), similar to their related analogues with only one fluorine substituent in each of the outer rings of the bent-core structure (compounds  $\text{BrFn}$  in Scheme 1).<sup>47</sup> On heating the  $\text{DC}^{[*]}$  phases become unstable and crystallize with formation of a birefringent crystalline phase. This crystallization is immediately followed by the melting of this crystalline phase, leading to the typical “double peak” in the heating scans (see Fig. 3). Similar to the  $\text{DC}^{[*]}$  phases exhibited by related BCLCs with two azobenzene wings ( $\text{IFn}$ ,  $\text{Brn}$ ,  $\text{BrFn}$  and  $\text{Men}$ , see Scheme 1),<sup>45–47,49</sup> no current peak could be observed in these  $\text{DC}^{[*]}$  phases in electro-optical experiments. Moreover, no birefringence is induced in any of the  $\text{DC}^{[*]}$  phases under an applied

triangular wave voltage up to  $200 \text{ V}_{\text{pp}}$  in a  $6 \mu\text{m}$  ITO cell; this is typical for soft crystalline  $\text{DC}^{[*]}$  phases.

The XRD pattern of the  $\text{DC}^{[*]}$  phase exhibited by compound  $\text{BrF}_2\mathbf{10}$  at  $50^\circ\text{C}$  as a representative example is shown in Fig. 4a and b. A single strong scattering in the small angle region is observed. The  $d$ -value of  $4.33 \text{ nm}$  is between half of the molecular length and the full molecular length ( $L_{\text{mol}} = 5.2 \text{ nm}$  in the most extended conformation with all-*trans* alkyl chains). This diffraction pattern is in line with a lamellar organization with  $d = 4.33 \text{ nm}$  where the molecules are organized in a single layer structure with the involved molecules tilted by a certain angle (the maximum tilt estimated from  $d/L_{\text{mol}} = 0.83$  is  $\sim 33^\circ$ ) with respect to the layer normal. The relatively large difference between  $d$  and  $L_{\text{mol}}$  is different from HNF phases having very small difference between the  $d$ -value and  $L_{\text{mol}}$ .<sup>17,38</sup> In the 2D patterns all scatterings form closed rings with uniform intensity distribution as a very typical feature of all  $\text{DC}^{[*]}$  phases. This is due to the randomized orientation of the nanocrystallites, leading to the optical isotropic properties, giving rise to the dark appearance between crossed polarizers (see Fig. 4a). Fig. 4b shows the  $2\theta$  scan over the diffraction pattern of  $\text{BrF}_2\mathbf{10}$ . Beside the strong layer reflections very weak and relatively broad scattering maxima are observed in the medium and wide angle region. This pattern distinguishes this  $\text{DC}^{[*]}$  phase from the fluid sponge-type  $\text{DC}^{[*]}$  phases, which exhibit only one completely diffuse wide angle scattering besides the layer reflection,<sup>26</sup> as well as from the HNF phases (B4 phases) characterized by sharper and more intense wide angle scatterings.<sup>17,38</sup> The results obtained for  $\text{BrF}_2\mathbf{10}$  prove that the  $\text{DC}^{[*]}$  phases formed by compounds  $\text{BrF}_2n$  belong to the helical nanocrystallite phases (HNC phases). Only the number, intensities and positions of the medium- and wide-angle scatterings are distinct, indicating that the fine structure of the local crystal lattice should be a bit different from the previously reported HNC phases of the related azobenzene derived apex-halogenated bent-core compounds.<sup>45,47,48</sup> For example, Fig. 4c

Table 1 Phase transition temperatures ( $T/^\circ\text{C}$ ), mesophase types, and transition enthalpies [ $\Delta H/\text{kJ mol}^{-1}$ ] of compounds  $\text{BrF}_2n^a$



The chemical structure of  $\text{BrF}_2n$  is shown as a bent-core molecule. It consists of a central 4-bromoresorcinol core (a benzene ring with a bromine atom at the 4-position and two hydroxyl groups at the 1 and 3 positions). Each hydroxyl group is esterified with a 4-(2,6-difluorophenyl)azobenzene group. The terminal phenyl rings of these azobenzene groups are substituted with a long alkyl chain of length  $n$ , represented as  $\text{H}_{2n+1}\text{C}_n\text{O}$  and  $\text{OC}_n\text{H}_{2n+1}$ .

Compound	$n$	Heating $T/^\circ\text{C}$ [ $\Delta H/\text{kJ mol}^{-1}$ ]	Cooling $T/^\circ\text{C}$ [ $\Delta H/\text{kJ mol}^{-1}$ ]
$\text{BrF}_2\mathbf{8}$	8	Cr <sub>1</sub> 96 [6.6] Cr <sub>2</sub> 104 [27.5] Iso	Iso 86 [28.5] Cr
$\text{BrF}_2\mathbf{10}$	10	Cr 101 [37.6] Iso	Iso 85 [20.4] $\text{DC}^{[*]}$
$\text{BrF}_2\mathbf{12}$	12	$\text{DC}^{[*]}$ 97 [10.1] Cr 103 [10.9] Iso	Iso 90 [21.0] $\text{DC}^{[*]}$
$\text{BrF}_2\mathbf{14}$	14	$\text{DC}^{[*]}$ 98 [11.9] Cr 103 [7.8] Iso	Iso 92 [21.6] $\text{DC}^{[*]}$
$\text{BrF}_2\mathbf{16}$	16	Cr 97 [26.5] Iso	Iso 96 [6.2] $\text{SmC}_s\text{P}_{\text{AR}}$ 85 [20.2] Cr

<sup>a</sup> The phase transition temperatures (peak temperatures) were taken from the second heating and second cooling scans at  $10 \text{ K min}^{-1}$ ; abbreviations: Cr = crystalline solid;  $\text{DC}^{[*]}$  = dark conglomerate phases (HNC phases) composed of chiral domains with opposite handedness;  $\text{SmC}_s\text{P}_{\text{AR}}$  = polarization randomized smectic phase composed of  $\text{SmC}_s\text{P}_{\text{F}}$  domains and showing two polarization current peaks; Iso = isotropic liquid.

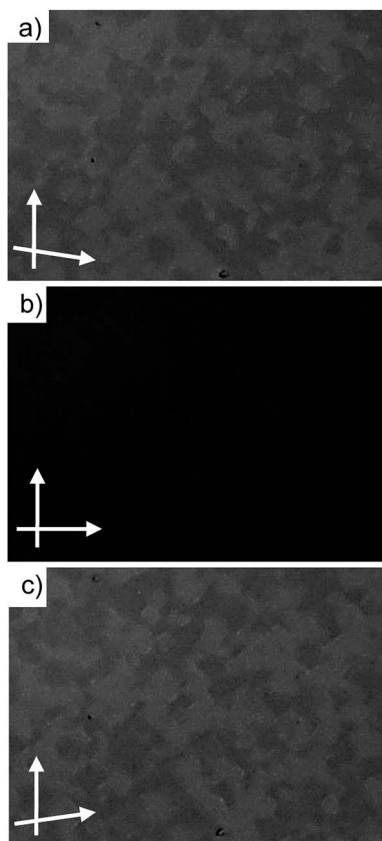


Fig. 2 Textures of the DC<sup>[\*]</sup> phase of compound BrF<sub>2</sub>12 at  $T = 60\text{ }^{\circ}\text{C}$ : (b) under crossed polarizers; (a) after rotating the analyzer by  $10^{\circ}$  from the crossed position with respect to the polarizer in clock-wise direction and (c) in anticlockwise direction, showing dark and bright domains, indicating the presence of areas with opposite chirality sense.

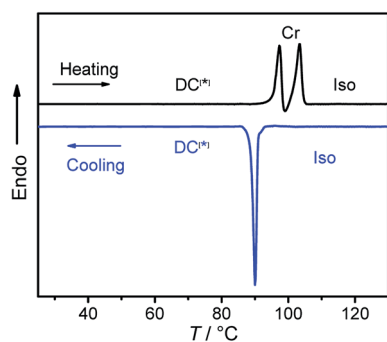


Fig. 3 DSC heating and cooling scans of BrF<sub>2</sub>12 with a rate of  $10\text{ K min}^{-1}$ .

shows the  $2\theta$ -scans of the DC<sup>[\*]</sup> phase of the related compound BrF<sub>2</sub>12 with only one lateral fluorine substituent in each azo-benzene wing and having the chain length  $n = 12$  (Scheme 1).

### 3.2. SmC phase of the long chain compound BrF<sub>2</sub>16

The optically isotropic DC<sup>[\*]</sup> phase is completely removed for the longest derivative in the series BrF<sub>2</sub> $n$  with  $n = 16$ . On cooling BrF<sub>2</sub>16 from the isotropic liquid state a birefringent schlieren

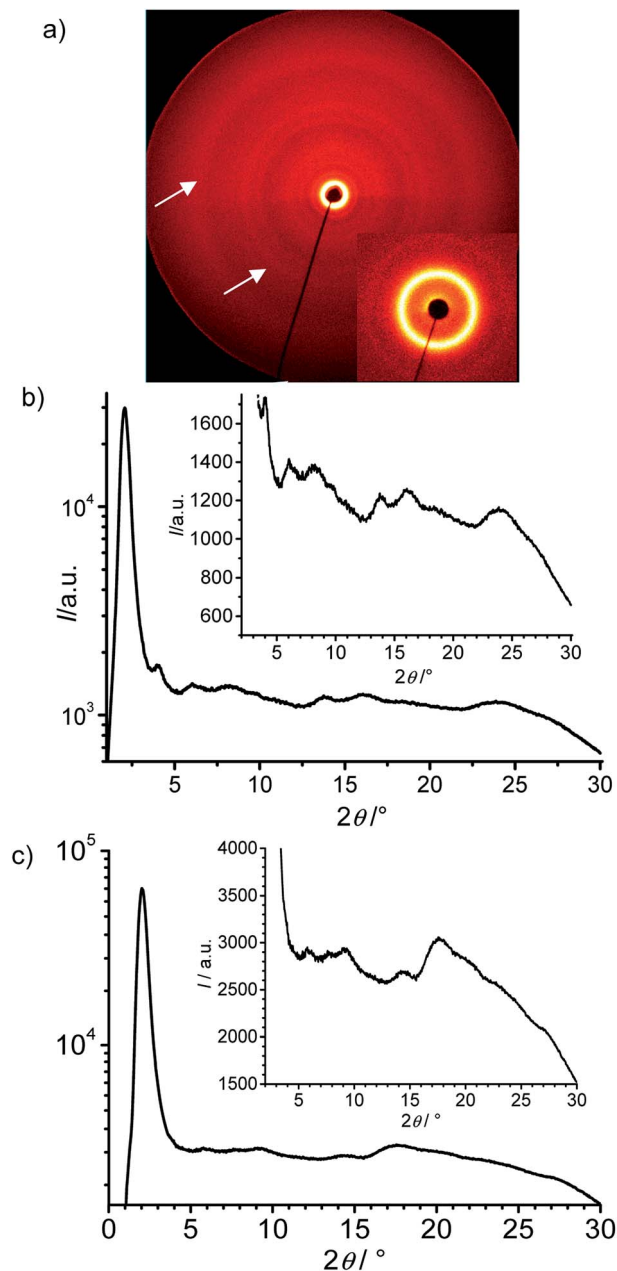


Fig. 4 (a) 2D XRD pattern of the DC<sup>[\*]</sup> phase of BrF<sub>2</sub>10 at  $T = 50\text{ }^{\circ}\text{C}$ , the inset shows the small angle region;  $2\theta$ -scans over this XRD pattern of the DC<sup>[\*]</sup> phase for (b) compound BrF<sub>2</sub>10 at  $T = 50\text{ }^{\circ}\text{C}$  and (c) compound BrF<sub>2</sub>12 at  $T = 90\text{ }^{\circ}\text{C}$ .<sup>47</sup>

texture is observed below  $T = 96\text{ }^{\circ}\text{C}$  in a homeotropic cell (Fig. 5a) and a fan texture is observed in a planar cell where the dark extinctions are inclined by an angle of about  $28^{\circ}$ , indicating a synclinc tilted smectic phase (SmC<sub>s</sub> phase, see Fig. 5b). XRD investigation of this phase was not possible due to the rapid crystallization of the monotropic phase. In electro-optical investigations two polarization current peaks in each half period of an applied triangular wave voltage were observed (Fig. 5c and d). The two polarization peaks are weak and widely separated at the Iso–SmC<sub>s</sub> transition, growing in intensity and coming a bit closer to each other on further cooling, reaching

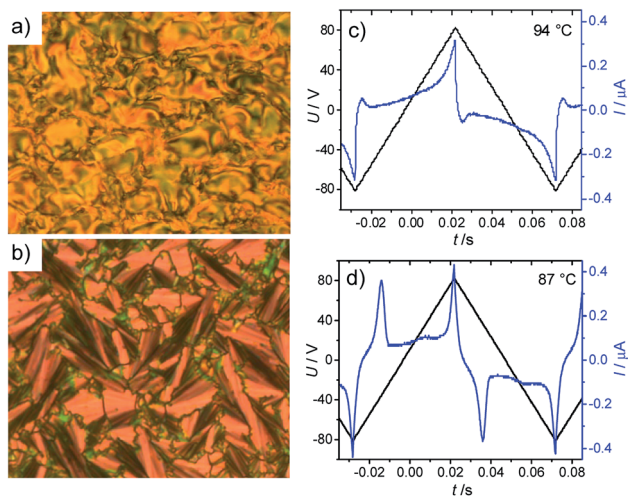


Fig. 5 Textures and polarization current response curve of the  $\text{SmC}_s\text{P}_{\text{AR}}$  phase of compound **BrF<sub>216</sub>**: textures as observed at  $T = 93\text{ }^\circ\text{C}$  (a) in a homeotropic cell; (b) in a  $6\text{ }\mu\text{m}$  coated ITO cell with planar alignment; (c) and (d) switching current response curves in the same ITO cell as recorded under a triangular wave voltage  $160\text{ V}_{\text{pp}}$  (10 Hz, 5 k $\Omega$ ) at the indicated temperatures.

a polarization values  $P = 290\text{ nC cm}^{-2}$ . The mode of appearance of the polarization peaks, their shape and the relatively small polarization values are typical for  $\text{SmC}_s\text{P}_{\text{AR}}$  phases with randomized polar order, described in detail for 4-cyanoresorciol based BLCs.<sup>51</sup> Therefore, the LC phase of compound **BrF<sub>216</sub>** is assigned as  $\text{SmC}_s\text{P}_{\text{AR}}$  phase. In this smectic phase ferroelectric domains with synclinic and antipolar correlation form a field induced  $\text{SmC}_s\text{P}_{\text{F}}$  state which relaxes at reduced voltage back to a macroscopically antipolar structure. The position of the dark extinctions does not change, indicating the relaxation and switching take place by rotation around the molecular long axis (see Fig. S11†).

### 3.3. Investigation of mixtures of compounds **BrF<sub>2n</sub>** with 5-CB

It is well known that the two different types of soft crystalline  $\text{DC}^{[*]}$  phases (HNF and HNC) behave differently upon mixing with 4'-*n*-pentyl-4-cyanobiphenyl (5-CB). The chirality of HNF phases can be retained even at high dilution with a nematic LC host (>95%),<sup>53</sup> while the HNC phases can be diluted only by a small amount (to ~50%) of a nematic LC (5-CB) without loss of the  $\text{DC}^{[*]}$  phase and chirality.<sup>45–47</sup> The mixtures of selected compounds **BrF<sub>2n</sub>** with 5-CB were investigated and compared with the results obtained for their related monofluorinated analogues **BrFn** (see Table 2).

The  $\text{DC}^{[*]}$  phase of the pure compound **BrF<sub>210</sub>** is removed in its 1 : 1 mixture with 5CB and a direct transition from the crystalline state to the isotropic liquid takes place at  $68\text{ }^\circ\text{C}$  on heating (Table 2). On cooling the same mixture from the isotropic liquid state a monotropic nematic phase is formed which crystallizes at  $T \sim 39\text{ }^\circ\text{C}$  without the formation of  $\text{DC}^{[*]}$  phase. The next two homologues **BrF<sub>212</sub>** and **BrF<sub>214</sub>** behave differently;  $\text{DC}^{[*]}$  phases are formed in their 1 : 1 mixtures with

Table 2 Phase transition temperatures and mesophase types of 1 : 1 mixtures of 5-CB and compounds **BrF<sub>10</sub>–BrF<sub>14</sub>** and comparison with related 4-bromoresorcinol derivatives **BrF<sub>10</sub>–BrF<sub>14</sub>**<sup>a46</sup>

Mixture	Heating $T/^\circ\text{C}$	Cooling $T/^\circ\text{C}$
<b>BrF<sub>210</sub></b> + 5-CB	Cr 68 Iso	Iso 47 N 39 Cr
<b>BrF<sub>212</sub></b> + 5-CB	$\text{DC}^{[*]}$ 60 Iso	Iso 56 $\text{DC}^{[*]}$
<b>BrF<sub>214</sub></b> + 5-CB	$\text{DC}^{[*]}$ 58 Iso	Iso 54 $\text{DC}^{[*]}$
<b>BrF<sub>10</sub></b> + 5-CB	Cr 54 Iso	Iso 42 N 33 Cr
<b>BrF<sub>12</sub></b> + 5-CB	$\text{Cr}^{[*]}$ 40 $\text{DC}^{[*]}$ 55 Iso	Iso 53 $\text{DC}^{[*]}$ 38 $\text{Cr}^{[*]}$
<b>BrF<sub>14</sub></b> + 5-CB	Cr 38 $\text{DC}^{[*]}$ 64 Iso	Iso 46 $\text{DC}^{[*]}$ 35 Cr

<sup>a</sup> Transition temperatures were taken from the observed textures using the polarized optical microscopy; abbreviations: N = nematic phase;  $\text{Cr}^{[*]}$  = crystalline phase composed of a conglomerate of chiral domains; for other abbreviations please see Table 1.

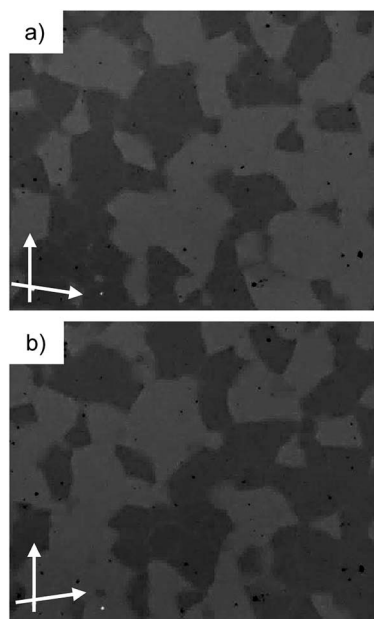


Fig. 6 Textures of the  $\text{DC}^{[*]}$  phase of 1 : 1 mixture of compound **BrF<sub>214</sub>** with 5CB at  $T = 45\text{ }^\circ\text{C}$ : (a) after rotating one polarizer by  $10^\circ$  from the crossed position in clock-wise direction and (b) in anti-clockwise direction, showing dark and bright domains, indicating the presence of areas with opposite chirality sense.

5CB as room temperature mesophases and no crystallization takes place either on heating or cooling (see Fig. 6). Similar to the other HNC phases, only a limited amount of 5-CB can be mixed into the HNC phase of **BrF<sub>2n</sub>** and any further increase of the amount of 5-CB removes the  $\text{DC}^{[*]}$  phases. Comparing the results obtained for **BrF<sub>2n</sub>** compounds with their monofluorinated analogues (compounds **BrFn**, see Table 2)<sup>47</sup> indicate that both types of compounds behave similarly in their mixed systems, which further confirms the similarity of the HNC phases exhibited by the azobenzene based bent-core mesogens.

### 3.4. Compounds **ClF<sub>2n</sub>** with chlorine at the apex

The effect of replacing bromine by a smaller chlorine on the mesophase type has been investigated with the 4-

chlororesorcinol derived compounds  $\text{ClF}_2n$  (see Table 3 for data and Fig. 7 for DSC traces for  $\text{ClF}_214$ ). Unlike series  $\text{BrF}_2n$ , compounds  $\text{ClF}_2n$  do not show any DC<sup>[\*]</sup> phase; instead they form monotropic smectic C phases. On cooling the shorter homologues with  $n = 8$  and 10 from the isotropic liquid state a birefringent SmC phase is observed at the same temperature  $T = 86^\circ\text{C}$  for both derivatives. The investigations of these SmC phases was not possible due to the rapid crystallization starting directly after the appearance of the SmC and for the same reason the value of transition enthalpy for the Iso–SmC transition cannot be separated from that of SmC–Cr transition. For the next homologues with  $n \geq 12$  the SmC phases are formed in a sufficient temperature range enabling electro-optical investigations. The temperature range of the SmC phases in the series  $\text{ClF}_212$ – $\text{ClF}_216$  is increasing with increasing the chain length (see Table 3). Fig. 8a and b shows the textures observed for the SmC phase of compound  $\text{ClF}_216$  upon cooling from the isotropic liquid state, where a birefringent schlieren texture is observed in a homeotropic cell (Fig. 8a). A broken fan texture with the dark extinctions inclined by an angle of  $26^\circ$ , indicating a synclitic tilted smectic phase ( $\text{SmC}_s$  phase) is observed in a planar cell (Fig. 8b).

Under an applied triangular wave voltage of  $160\text{ V}_{\text{pp}}$  in a  $6\ \mu\text{m}$  ITO cell two broad polarization peaks per half period of the applied voltage appears in the SmC phase of all investigated  $\text{ClF}_2n$  compounds with  $n = 12$ – $16$  with a polarization value  $P \sim 100\text{ nC cm}^{-2}$  (see Fig. 8c for  $\text{ClF}_216$ ). Based on the textures and the shape of the polarization curves, the SmC phases exhibited by these materials are assigned as  $\text{SmC}_s\text{P}_{\text{AR}}$  phases, but the shape and the polarization values are very distinct from that of the analogous bromine substituted compound  $\text{BrF}_216$ . The broad diffuse shape of the polarization current peaks is similar to that observed for previously reported  $\text{SmAP}_{\text{AR}}$  phase showing Langevin-type switching.<sup>54</sup> Therefore, we conclude that the switching of the chlorine substituted compounds is also typically Langevin type,<sup>55</sup> meaning that small polar

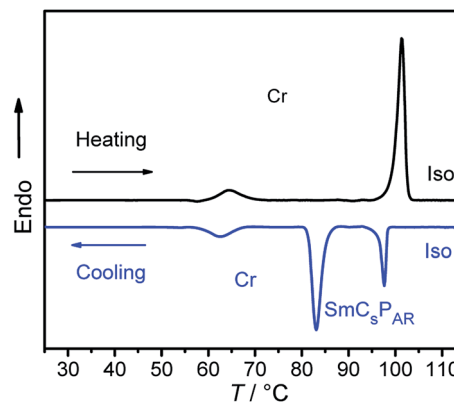


Fig. 7 DSC heating and cooling scans of  $\text{ClF}_214$  with a rate of  $10\text{ K min}^{-1}$ .

domains grow under the electric field and then can be switched between two polar states. This means that the polar domains in the SmC phase of  $\text{ClF}_216$  might have a broader size distribution than those observed in the  $\text{SmC}_s\text{P}_{\text{AR}}$  phase of  $\text{BrF}_216$  and grow to larger domains under the applied field. There is a larger threshold voltage for polar switching of  $\text{BrF}_216$  compared to  $\text{ClF}_216$  though the magnitude of polarization is higher ( $280$  vs.  $100\text{ nC cm}^{-2}$ ). Probably there is larger polarization in the ferroelectric domains of  $\text{BrF}_216$  but also a stronger antipolar correlation between these domains. It appears that bromine substitution favours polar packing compared to the smaller chlorine, though it could be expected that the bend of the bromine substituted compound might be a bit smaller than that of the chlorine substituted,<sup>50a</sup> and additionally, the bulkier bromine is expected to reduce the core packing density for steric reasons. This effect might possibly be attributed to the higher polarizability of bromine and the C–Br bond.

Table 3 Phase transition temperatures ( $T/^\circ\text{C}$ ), mesophase types, and transition enthalpies [ $\Delta H/\text{kJ mol}^{-1}$ ] of compounds  $\text{ClF}_2n^a$

Compound	$n$	Heating $T/^\circ\text{C}$ [ $\Delta H/\text{kJ mol}^{-1}$ ]	Cooling $T/^\circ\text{C}$ [ $\Delta H/\text{kJ mol}^{-1}$ ]
$\text{ClF}_28$	8	Cr 98 [33.1] Iso	Iso 86 [30.7] Cr + $\text{SmC}_x^b$
$\text{ClF}_210$	10	Cr 101 [35.9] Iso	Iso 86 [35.7] Cr + $\text{SmC}_x^b$
$\text{ClF}_212$	12	Cr 101 [25.7] Iso	Iso 94 [6.3] $\text{SmC}_s\text{P}_{\text{AR}}$ 80 [18.5] Cr
$\text{ClF}_214$	14	Cr 101 [37.9] Iso	Iso 98 [8.6] $\text{SmC}_s\text{P}_{\text{AR}}$ 83 [27.5] Cr
$\text{ClF}_216$	16	Cr 105 [35.7] Iso	Iso 100 [7.5] $\text{SmC}_s\text{P}_{\text{AR}}$ 75 [37.2] Cr

<sup>a</sup> The phase transition temperatures were measured as mentioned in Table 1. <sup>b</sup> The value of Iso–SmC transition enthalpy cannot be separated from SmC–Cr transition value. Abbreviations:  $\text{SmC}_x$  = smectic C phase with unknown polar structure, most likely also representing  $\text{SmC}_s\text{P}_{\text{AR}}$  phases; for other abbreviations see Table 1.

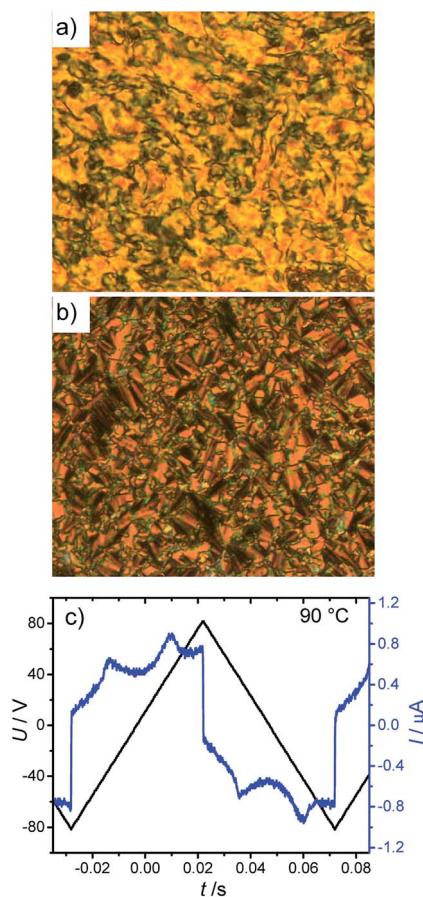


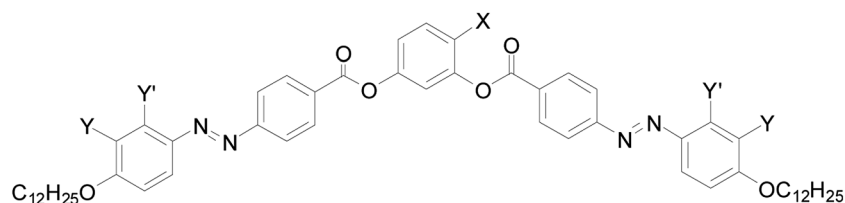
Fig. 8 Textures and polarization current response curve of the  $\text{SmC}_5\text{P}_{\text{AR}}$  phase of compound  $\text{ClF}_216$  at  $T = 90^\circ\text{C}$ : (a) texture as observed in a homeotropic cell; (b) texture observed in a  $6\ \mu\text{m}$  coated ITO cell with planar alignment and (c) switching current response curve in the same ITO cell as recorded under a triangular wave voltage  $160\ \text{V}_{\text{pp}}$  (10 Hz, 5 k $\Omega$ ).

### 3.5. Comparison with related compounds

Table 4 shows a comparison between azobenzene derived BCLCs with 4-bromoresorcinol and 4-chlororesorcinol cores and  $n = 12$  chain length, but with different number of peripheral fluorine substituents. Before discussing the effect of fluorine substitution, it is mentioned here that the larger bromine atom ( $cv \sim 33\ \text{nm}^3$ , crystal volumes  $cv$  of Immirzi)<sup>56</sup> in the 4-position at the resorcinol core favours the formation of HNC phase in all cases compared to the smaller chlorine ( $cv \sim 27\ \text{nm}^3$ ),<sup>56</sup> indicating that the size of the substituent at the apex and the degree of molecular twist induced by this substituent are important for layer distortion and chirality synchronization required for  $\text{DC}^{[*]}$  phase formation.<sup>47</sup> For the BCLCs with 4-bromoresorcinol central core, peripheral fluorination removes the nematic phase and stabilizes the HNC phase, most probably by increasing the attractive  $\pi$ - $\pi$  interactions by reduction of the electron density of the aromatics. However, inserting an additional fluorine atom in the *meta* position with respect to the terminal alkyl chain (compound  $\text{BrF}_212$ ) reduces the HNC phase stability (reduced transition temperature Iso-DC) and favours crystallization. Reduction of HNC phase stability is probably due to the steric effect of the additional fluorine, reducing the packing density. The increased melting points are attributed to the improved  $\pi$ - $\pi$ -stacking ability caused by the further reduction of the electron density by the additional electron withdrawing fluorine.

In the case of the compounds derived from 4-chlororesorcinol the core fluorination removes the nematic phase, too, but in this case it leads first to a macroscopically polar ( $\text{SmC}_a\text{P}_A$ ) and then, after addition of the next fluorine, to a locally polar tilted smectic phase ( $\text{SmC}_5\text{P}_{\text{AR}}$ , see Table 4). The mesophase stability of the LC phases is apparently not affected by fluorination, but the introduction of the second fluorine in *m*-position removes the long range polar order achieved for the monofluorinated compound (two sharp polarization peaks,  $P_s$

Table 4 Phase transition temperatures ( $T/^\circ\text{C}$ ) and mesophase types for different types of 4-bromoresorcinol and 4-chlororesorcinol derived BCLCs with azobenzene wings and the effect of peripheral F-atoms ( $Y, Y' = \text{H}, \text{F}$ )<sup>a</sup>



Comp.	X	Y	Y'	$T/^\circ\text{C}$	Ref.
<b>Br12</b>	Br	H	H	$\text{DC}^{[*]}$ 93 (N 83) Iso	49
<b>BrF12</b>	Br	F	H	$\text{DC}^{[*]}$ 106 Iso	47
<b>BrF<sub>2</sub>12</b>	Br	F	F	$\text{Cr}_1$ 97 $\text{Cr}_2$ 103 ( $\text{DC}^{[*]}$ 90) Iso	
<b>Cl12</b>	Cl	H	H	$\text{Cr}_1$ 90 $\text{Cr}_2$ 103 (N 97) Iso	49
<b>ClF12</b>	Cl	F	H	Cr 115 ( $\text{SmC}_a\text{P}_A$ 97) Iso	47
<b>ClF<sub>2</sub>12</b>	Cl	F	F	Cr 101 ( $\text{SmC}_5\text{P}_{\text{AR}}$ 97) Iso	

<sup>a</sup> Abbreviations: N = nematic phase;  $\text{SmC}_a\text{P}_A$  = anticlinic antiferroelectric switching SmC phase (B2 phase); for other abbreviations see Table 1.



$\sim 500 \text{ nC cm}^{-2}$ , see Fig. S11† in ref. 47) and replaces this by a local polar domain structure (two diffuse polarization peaks,  $P_s \sim 100 \text{ nC cm}^{-2}$ , Fig. 8c). Simultaneously the additional F substituents change the tilt correlation in the smectic phase from anticlinic in ClF12 to synclinic in ClF<sub>2</sub>12 and the switching process from rotation on the tilt-cone for ClF12 (Fig. S10† in ref. 47) to a reorganization around the long axis in the case of ClF<sub>2</sub>*n* (Fig. S11†). This is most probably an effect of the reduced packing density, favoured by the increased bulkiness of the rod-like wings with two adjacent fluorines in each azobenzene wing. Overall, there seems to be a delicate balance of the influence of the two competing effects. It appears that the packing density is increased most efficiently by the electron accepting 3-fluorination adjacent to the 4-alkoxy chain, whereas 2-fluorination in *meta* position to the alkoxy chain contributes more to the unfavourable steric effect of fluorine, thus reducing the packing density. Besides the steric and electronic effects of fluorination, fluorine substitution can also have an effect on the conformation of the Ar–O–CH<sub>2</sub> linkage by influencing orbital interactions<sup>57</sup> and by strengthening weak intra- and intermolecular hydrogen bonding involving C–H bonds,<sup>58</sup> thus supporting the twisting of the molecules and the formation of DC<sup>[\*]</sup> phases.

## 4. Summary and conclusions

Two series of new bent-core liquid crystalline materials combining 4-bromoresorcinol or 4-chlororesorcinol cores with two 2,3-difluorinated and 4-alkoxy substituted azobenzene side arms have been synthesized and investigated. Depending on the size of the halogen atom in 4-position of the central bent core unit (Cl vs. Br) and on the length of the terminal alkyl chains different types of mesophases were observed. It was found that the majority of 4-bromoresorcinol derived compounds ( $n = 10\text{--}14$ ) form HNC-type DC<sup>[\*]</sup> phases which are replaced by a SmC<sub>s</sub>P<sub>AR</sub> phase upon chain elongation ( $n = 16$ ). For the 4-chlororesorcinol derivatives only SmC phases, but no DC<sup>[\*]</sup> phases were observed. The investigated SmC phases represent SmC<sub>s</sub>P<sub>AR</sub> type polar domain phases. The SmC<sub>s</sub>P<sub>AR</sub> phase of the chlorine substituted compound is distinct from that of the related bromine derivative by the significantly broader polarization peaks and the smaller polarization values, indicating a Langevin-type switching (field-induced growth of the polar domains) for the chlorinated compound and a more superparaelectric type of switching<sup>59</sup> (fusion of already existing polar domains) for the brominated compound. The DC<sup>[\*]</sup> phases exhibited by these materials represent helical nano-crystallites phases (HNC) but with a different local structure if compared with the HNC phases of the related azobenzene compound without peripheral fluorine or with only one fluorine.<sup>47,49</sup> Though, core fluorination can favour HNC phase formation and modifies the precise phase structure, it cannot induce DC phases if the core unit would not also support its formation. It also cannot fundamentally change the structure of the DC<sup>[\*]</sup> phase to HNF or fluid DC phases. Introduction of the first fluorine adjacent to the alkoxy chains obviously favors layer formation and DC<sup>[\*]</sup> phase formation (removal of N phases) and development of

polar order, most probably by increasing the attractive  $\pi\text{--}\pi$  interactions by reduction of the electron density of the aromatics. The second fluorine appears to reduce the DC<sup>[\*]</sup> phase stability a bit and appears to reduce the coherence length of local polarization, probably due to its steric effect, reducing the packing density a bit. Thus fluorination is a tool for tailoring HNC phase ranges and the fine structure of the HNC phases. Future work will be devoted to a more detailed analysis of the HNC phases by imaging methods and the investigation of the effects of photoisomerization of the azobenzene units incorporated in the molecular structure of these BCLCs by polarized and nonpolarized light. This could lead to additional possibilities for phase modulation and chirality modulation, which could result in potentially useful applications.

## Acknowledgements

The work was supported by the DFG (Grant Ts 39/24-1). M. Alaasar is grateful to the Alexander von Humboldt Foundation for the research fellowship at the Martin-Luther University Halle-Wittenberg, Germany.

## References

- 1 T. Niori, T. Sekine, J. Watanabe, T. Furukawa and H. Takezoe, *J. Mater. Chem.*, 1996, **6**, 1231–1233.
- 2 (a) R. A. Reddy and C. Tschierske, *J. Mater. Chem.*, 2006, **16**, 907–961; (b) H. Takezoe and Y. Takanishi, *Jpn. J. Appl. Phys., Part 1*, 2006, **45**, 597–625; (c) A. Eremin and A. Jakli, *Soft Matter*, 2013, **9**, 615–637; (d) J. Etxebarria and M. B. Ros, *J. Mater. Chem.*, 2008, **18**, 2919–2926; (e) M. Alaasar, *Liq. Cryst.*, 2016, DOI: 10.1080/02678292.2016.1175676.
- 3 C. Tschierske, Nanoscale stereochemistry in liquid crystals, in *Chirality at the nanoscale*, ed. D. B. Amabilino, Wiley-VCH, Weinheim, 2009, pp. 271–304.
- 4 H. Takezoe, *Top. Curr. Chem.*, 2012, **318**, 303–330.
- 5 C. Tschierske, *Angew. Chem., Int. Ed.*, 2013, **52**, 8828–8878.
- 6 C. Tschierske and G. Ungar, *ChemPhysChem*, 2016, **17**, 9–26.
- 7 K.-U. Jeong, B. S. Knapp, J. J. Ge, S. Jin, M. J. Graham, F. W. Harris and S. Z. D. Cheng, *Chem. Mater.*, 2006, **18**, 680–690.
- 8 C. Roche, H.-J. Sun, M. E. Prendergast, P. Leowanawat, B. E. Partridge, P. A. Heiney, F. Araoka, R. Graf, H. W. Spiess, X. B. Zeng, G. Ungar and V. Percec, *J. Am. Chem. Soc.*, 2014, **136**, 7169–7185.
- 9 (a) V. P. Panov, M. Nagaraj, J. K. Vij, Y. P. Panarin, A. Kohlmeier, M. G. Tamba, R. A. Lewis and G. H. Mehl, *Phys. Rev. Lett.*, 2010, **105**, 167801; (b) V. Borshch, Y.-K. Kim, J. Xiang, M. Gao, A. Jakli, V. P. Panov, J. K. Vij, C. T. Imrie, M. G. Tamba, G. H. Mehl and O. D. Lavrentovich, *Nat. Commun.*, 2013, **4**, 2635.
- 10 M. Cestari, S. Diez-Berart, D. A. Dunmur, A. Ferrarini, M. R. de la Fuente, D. J. B. Jackson, D. O. Lopez, G. R. Luckhurst, M. A. Perez-Jubindo, R. M. Richardson, J. Salud, B. A. Timimi and H. Zimmermann, *Phys. Rev. E*, 2011, **84**, 031704.

- 11 D. Chen, J. H. Porada, J. B. Hooper, A. Klitnick, Y. Shen, M. R. Tuchband, E. Korblova, D. Bedrov, D. M. Walba, M. A. Glaser, J. E. Maclennan and N. A. Clark, *Proc. Natl. Acad. Sci. U. S. A.*, 2013, **110**, 15931–15936.
- 12 S.-W. Choi, T. Izumi, Y. Hoshino, Y. Takanishi, K. Ishikawa, J. Watanabe and H. Takezoe, *Angew. Chem., Int. Ed.*, 2006, **45**, 1382–1385.
- 13 H. -S. Kitzerow and C. Bahr, *Chirality in Liquid Crystals*, Springer-Verlag, New York, 2001.
- 14 A. Belaissaoui, S. J. Kowling and J. W. Goodby, *Liq. Cryst.*, 2013, **40**, 822–830.
- 15 D. Chen, H. Wang, M. Li, M. A. Glaser, J. E. Maclennan and N. A. Clark, *Soft Matter*, 2014, **10**, 9105–9109.
- 16 L. E. Hough, M. Spannuth, M. Nakata, D. A. Coleman, C. D. Jones, G. Dantlgraber, C. Tschierske, J. Watanabe, E. Korblova, D. M. Walba, J. E. Maclennan, M. A. Glaser and N. A. Clark, *Science*, 2009, **325**, 452–456.
- 17 L. E. Hough, H. T. Jung, D. Krüerke, M. S. Heberling, M. Nakata, C. D. Jones, D. Chen, D. R. Link, J. Zasadzinski, G. Heppke, J. P. Rabe, W. Stocker, E. Korblova, D. M. Walba, M. A. Glaser and N. A. Clark, *Science*, 2009, **325**, 456–460.
- 18 D. Chen, R. Shao, J. E. Maclennan, M. A. Glaser, E. Korblova, D. M. Walba, N. Gimeno, M. B. Ros and N. A. Clark, *Liq. Cryst.*, 2013, **40**, 1730–1735.
- 19 (a) I. Dierking, *Angew. Chem., Int. Ed.*, 2010, **49**, 29–30; (b) J. P. F. Lagerwall and F. Giesselmann, *ChemPhysChem*, 2010, **11**, 975–977.
- 20 V. Görtz, *Liq. Cryst. Today*, 2010, **19**, 37–48.
- 21 (a) M. Alaasar, M. Prehm, M. Nagaraj, J. K. Vij and C. Tschierske, *Adv. Mater.*, 2013, **25**, 2186–2191; (b) M. Alaasar, M. Prehm, K. May, A. Eremin and C. Tschierske, *Adv. Funct. Mater.*, 2014, **24**, 1703–1717.
- 22 C. Dressel, F. Liu, M. Prehm, X.-B. Zeng, G. Ungar and C. Tschierske, *Angew. Chem., Int. Ed.*, 2014, **53**, 13115–13120.
- 23 C. Dressel, T. Reppe, M. Prehm, M. Brautzsch and C. Tschierske, *Nat. Chem.*, 2014, **6**, 971–977.
- 24 M. Alaasar, M. Prehm, Y. Cao, F. Liu and C. Tschierske, *Angew. Chem., Int. Ed.*, 2016, **55**, 312–316.
- 25 A. Yoshizawa, Y. Kato, H. Sasaki, Y. Takanishi and J. Yamamoto, *J. Phys. Chem. B*, 2016, **120**, 4843–4851.
- 26 (a) G. Dantlgraber, A. Eremin, S. Diele, A. Hauser, H. Kresse, G. Pelzl and C. Tschierske, *Angew. Chem., Int. Ed.*, 2002, **41**, 2408–2414; (b) C. Keith, R. A. Reddy, A. Hauser, U. Baumeister and C. Tschierske, *J. Am. Chem. Soc.*, 2006, **128**, 3051–3066.
- 27 G. Heppke, D. D. Parghi and H. Sawade, *Liq. Cryst.*, 2000, **27**, 313–320.
- 28 J. Thisayukta, Y. Nakayama, S. Kawauchi, H. Takezoe and J. Watanabe, *J. Am. Chem. Soc.*, 2000, **122**, 7441–7448.
- 29 R. A. Reddy and B. K. Sadashiva, *Liq. Cryst.*, 2003, **30**, 1031–1050.
- 30 A. Roy, M. Gupta, S. Radhika, B. K. Sadashiva and R. Pratibha, *Soft Matter*, 2012, **8**, 7207–7214.
- 31 J. Ortega, C. L. Folcia, J. Etxebarria, N. Gimeno and M. B. Ros, *Phys. Rev. E: Stat., Nonlinear, Soft Matter Phys.*, 2003, **68**, 11707.
- 32 S. Kang, Y. Saito, N. Watanabe, M. Tokita, Y. Takanishi, H. Takezoe and J. Watanabe, *J. Chem. Phys. B*, 2006, **110**, 5205–5214.
- 33 (a) M. Nagaraj, K. Usami, Z. Zhang, V. Görtz, J. W. Goodby and H. F. Gleeson, *Liq. Cryst.*, 2014, **41**, 800–811; (b) M. Nagaraj, J. C. Jones, V. P. Panov, H. Liu, G. Portale, W. Bras and H. F. Gleeson, *Phys. Rev. E*, 2015, **91**, 042504.
- 34 (a) S. K. Lee, X. Li, S. Kang, M. Tokita and J. Watanabe, *J. Mater. Chem.*, 2009, **19**, 4517–4522; (b) T. Bao, K. Wang and M.-S. Zhan, *Liq. Cryst.*, 2014, **41**, 1687–1695.
- 35 (a) A. Jáklí, Y.-M. Huang, K. Fodor-Csorba, A. Vajda, G. Galli, S. Diele and G. Pelzl, *Adv. Mater.*, 2003, **15**, 1606–1610; (b) W. Weissflog, M. W. Schröder, S. Diele and G. Pelzl, *Adv. Mater.*, 2003, **15**, 630–633.
- 36 (a) S. K. Lee, L. Shi, M. Tokita, H. Takezoe and J. Watanabe, *J. Phys. Chem. B*, 2007, **111**, 8698–8701; (b) S. K. Lee, L. Shi, M. Tokita and J. Watanabe, *J. Phys. Chem. B*, 2008, **112**, 6762–6766.
- 37 (a) D. M. Walba, L. Eshat, E. Korblova and R. K. Shoemaker, *Cryst. Growth Des.*, 2005, **5**, 2091–2099; (b) D. Chen, J. E. Maclennan, R. Shao, D. K. Yoon, H. Wang, E. Korblova, D. M. Walba, M. A. Glaser and N. A. Clark, *J. Am. Chem. Soc.*, 2011, **133**, 12656–12663.
- 38 J. M. -Perdiguero, I. Alonso, C. L. Folcia, J. Etxebarria and J. Ortega, *J. Mater. Chem.*, 2009, **19**, 5161–5166.
- 39 C. Zhang, N. Diorio, O. D. Lavrentovich and A. Jáklí, *Nat. Commun.*, 2014, **5**, 3302.
- 40 (a) J. Thisayukta, H. Takezoe and J. Watanabe, *Jpn. J. Appl. Phys., Part 1*, 2001, **40**, 3277; (b) H. Niwano, M. Nakata, J. Thisayukta, D. R. Link, H. Takezoe and J. Watanabe, *J. Phys. Chem. B*, 2004, **108**, 14889–14896; (c) H. Kurosu, M. Kawasaki, M. Hirose, M. Yamada, S. Kang, J. Thisayukta, M. Sone, H. Takezoe and J. Watanabe, *J. Phys. Chem. A*, 2004, **108**, 4674–4678.
- 41 H. Kresse, J. Saltetnokova, H. Nadasi, W. Weissflog and A. Hauser, *Liq. Cryst.*, 2001, **28**, 1017–1023.
- 42 (a) E. Bialecka-Florjanczyk, I. Sledzinska, E. Górecka and J. Przedmojski, *Liq. Cryst.*, 2008, **35**, 401–406; (b) A. Zep, M. Salamonczyk, N. Vaupotič, D. Pocięcha and E. Gorecka, *Chem. Commun.*, 2013, **49**, 3119–3121.
- 43 T. Niori, T. Sekine, J. Watanabe, T. Furukawa and H. Takezoe, *J. Mater. Chem.*, 1996, **6**, 1231–1233.
- 44 C. Zhu, C. Wang, A. Young, F. Liu, I. Gunkel, D. Chen, D. Walba, J. Maclennan, N. Clark and A. Hexemer, *Nano Lett.*, 2015, **15**, 3420–3424.
- 45 M. Alaasar, M. Prehm and C. Tschierske, *Chem. Commun.*, 2013, **49**, 11062–11064.
- 46 M. Alaasar, M. Prehm, M. Brautzsch and C. Tschierske, *J. Mater. Chem. C*, 2014, **2**, 5487–5501.
- 47 M. Alaasar, M. Prehm, M. Brautzsch and C. Tschierske, *Soft Matter*, 2014, **10**, 7285–7296.
- 48 M. Alaasar, M. Prehm and C. Tschierske, *Chem.–Eur. J.*, 2016, **22**, 6583–6597.
- 49 M. Alaasar, M. Prehm and C. Tschierske, *Liq. Cryst.*, 2013, **40**, 656–668.
- 50 For a comparison of chlorine and bromine substituted BCLCs with phenylbenzoate wings, see: (a) W. Weissflog,

- S. Sokolowski, H. Dehne, B. Das, S. Grande, M. W. Schröder, A. Eremin, S. Diele, G. Pelzl and H. Kresse, *Liq. Cryst.*, 2004, **31**, 923–933; (b) S. Kang, J. Thisayukta, H. Takezoe, J. Watanabe, K. Ogino, T. Doi and T. Takahashi, *Liq. Cryst.*, 2004, **31**, 1323–1336.
- 51 M. Alaasar, M. Prehm, M.-G. Tamba, N. Sebastian, A. Eremin and C. Tschierske, *ChemPhysChem*, 2016, **17**, 278–287.
- 52 K. Miyasato, S. Abe, H. Takezoe, A. Fukuda and E. Kuze, *Jpn. J. Appl. Phys., Part 1*, 1983, **22**, L661–L663.
- 53 (a) T. Otani, F. Araoka, K. Ishikawa and H. Takezoe, *J. Am. Chem. Soc.*, 2009, **131**, 12368; (b) F. Araoka, G. Sugiyama, K. Ishikawa and H. Takezoe, *Opt. Mater. Express*, 2011, **1**, 27.
- 54 K. Gomola, L. Guo, D. Pocięcha, F. Araoka, K. Ishikawa and H. Takezoe, *J. Mater. Chem.*, 2010, **20**, 7944–7952.
- 55 Y. Shimbo, E. Gorecka, D. Pocięcha, F. Araoka, M. Goto, Y. Takamishi, K. Ishikawa, J. Mieczkowski, K. Gomola and H. Takezoe, *Phys. Rev. Lett.*, 2006, **97**, 113901.
- 56 A. Immirzi and B. Perini, *Acta Crystallogr., Sect. A: Cryst. Phys., Diffr., Theor. Gen. Crystallogr.*, 1977, **33**, 216–218.
- 57 A. J. Kirby, *The anomeric effect and related stereoelectronic effects at oxygen*, Springer, Berlin, Heidelberg, 1983.
- 58 (a) T. Steiner and G. R. Desiraju, *Chem. Commun.*, 1998, **8**, 891–892; (b) O. Takahashi, Y. Kohno and M. Nishio, *Chem. Rev.*, 2010, **110**, 6049–6076.
- 59 M. F. Achard, J. P. Bedel, J. P. Marcerou, H. T. Nguyen and J. C. Rouillon, *Eur. Phys. J. E*, 2003, **10**, 129–134.

# Spontaneous Mirror-Symmetry Breaking in Isotropic Liquid Phases of Photoisomerizable Achiral Molecules

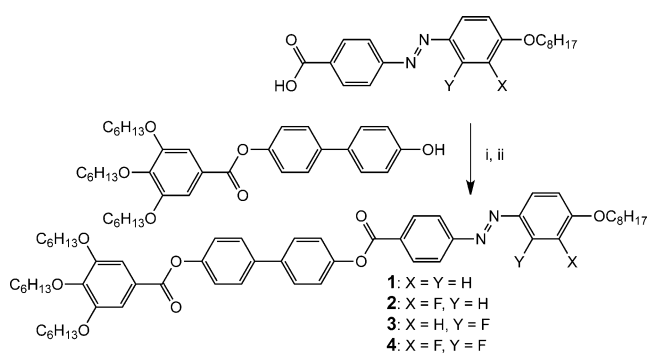
Mohamed Alaasar,\* Marko Prehm, Yu Cao, Feng Liu,\* and Carsten Tschierske\*

**Abstract:** Spontaneous mirror-symmetry breaking is of fundamental importance in science as it contributes to the development of chiral superstructures and new materials and has a major impact on the discussion around the emergence of uniform chirality in biological systems. Herein we report chirality synchronization, leading to spontaneous chiral conglomerate formation in isotropic liquids of achiral and photoisomerizable azobenzene-based rod-like molecules. The position of fluorine substituents at the aromatic core is found to have a significant effect on the stability and the temperature range of these chiral liquids. Moreover, these liquid conglomerates occur in a new phase sequence adjacent to a 3D tetragonal mesophase.

The observation by Pasteur of chiral conglomerate formation during the crystallization of tartrates marked the birth of stereochemistry.<sup>[1]</sup> Since then, symmetry breaking in racemic mixtures of chiral molecules and the synchronization of chiral conformers of achiral molecules during crystallization in chiral space groups have been found in numerous cases.<sup>[2]</sup> Additionally, enantiophobic chirality discrimination between permanently chiral molecules and chirality synchronization of transiently chiral conformers<sup>[3]</sup> on surfaces<sup>[4]</sup> and in fibrous aggregates have been well documented.<sup>[5]</sup> The spontaneous development of chiral conglomerates has also been observed in soft-matter systems, especially in liquid-crystalline (LC) phases of achiral bent-core molecules,<sup>[6–9]</sup> and this has considerable impact on the problem of the development of uniform chirality in biotic systems.<sup>[10]</sup> Surprisingly, spontaneous mirror-symmetry breaking was recently found even in isotropic liquids of achiral molecules, which form conglomerates of two immiscible chiral liquids with opposite handed-

ness (labelled here as Iso<sub>1</sub><sup>[\*]</sup> phases).<sup>[11,12]</sup> Formation of these liquid conglomerates obviously requires a locally twisted cluster structure of the liquids, providing cooperativity and acting as a template for chirality synchronization of the conformers.<sup>[11]</sup> However, the few known Iso<sub>1</sub><sup>[\*]</sup> phases are metastable, with only few exceptions, meaning that they could only be detected on cooling if the formation of the competing crystalline phases is suppressed. Moreover, they were found at high temperatures around 210 °C, where decomposition becomes an issue, thus making their investigation and application difficult.

Herein we report the first chiral liquids formed by photoisomerizable achiral azobenzene-derived compounds **1–4** (Scheme 1). These chiral liquids have Iso<sub>1</sub><sup>[\*]</sup> phases in



**Scheme 1.** Synthetic route to polycatenar molecules **1–4**. Reagents and conditions: i) SOCl<sub>2</sub>, DMF, reflux; ii) Et<sub>3</sub>N, pyridine, CH<sub>2</sub>Cl<sub>2</sub>, reflux. DMF = dimethylformamide.

convenient temperature ranges. These azo-functionalized materials are of special interest because of their photo-sensitive nature, leading to photoisomerizable chiral liquids which could be addressed by linearly or circularly polarized light and thus used for optical, optoelectronic, and sensing devices.<sup>[13–15]</sup>

The synthetic pathway to compounds **1–4** is shown in Scheme 1. Detailed synthetic procedures and analytical data are reported in the Supporting Information and the transition temperatures are summarized in Table 1.

Figure 1, taken as a representative example, shows the differential scanning calorimetry (DSC) curves obtained on heating and cooling of compound **1** (X = Y = H). This compound transforms into a low birefringent tetragonal mesophase (Tet) at  $T = 121$  °C, which melts into an isotropic liquid at  $T = 175$  °C. There are two isotropic liquid phases (Iso<sub>1</sub><sup>[\*]</sup> and Iso) with a phase transition between them at  $T = 189$  °C on heating (see Table 1; Figure 1). The achiral liquid

[\*] Dr. M. Alaasar, Dr. M. Prehm, Prof. Dr. C. Tschierske  
Institute of Chemistry  
Martin Luther University Halle-Wittenberg  
Kurt-Mothes Str. 2, 06120 Halle/Saale (Germany)  
E-mail: carsten.tschierske@chemie.uni-halle.de

Dr. M. Alaasar  
Department of Chemistry, Faculty of Science  
Cairo University  
P.O. 12613 Giza (Egypt)  
E-mail: malaasar@sci.cu.edu.eg

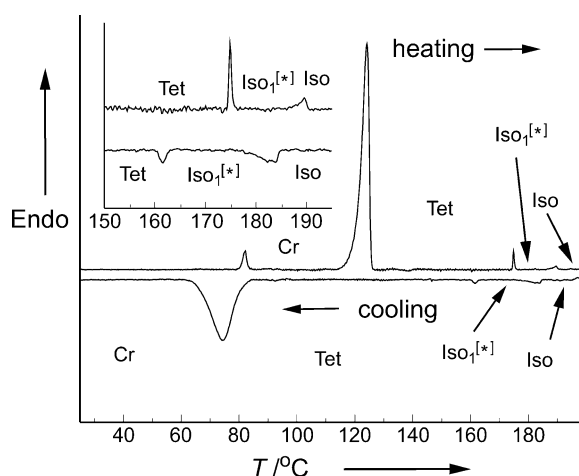
Y. Cao, Prof. Dr. F. Liu  
State Key Laboratory for Mechanical Behavior of Materials  
Xi'an Jiaotong University  
Xi'an 710049 (P. R. China)  
E-mail: feng.liu@mail.xjtu.edu.cn

Supporting information and ORCID(s) from the author(s) for this article are available on the WWW under <http://dx.doi.org/10.1002/anie.201508097>.

**Table 1:** Mesophase types, phase-transition temperatures ( $T/^\circ\text{C}$ ), and transition enthalpies [ $\Delta H/k$ ]  $\text{mol}^{-1}$ ] of compounds 1–4.<sup>[a]</sup>

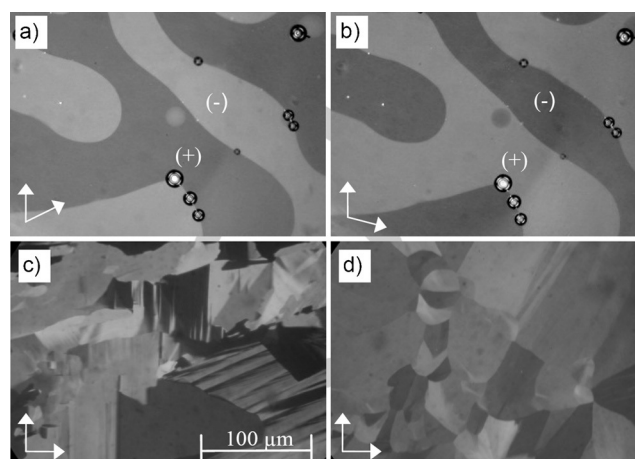
Compd.	Phase sequence
1	Heating: Cr 121 [35.1] Tet 175 [0.7] Iso <sub>1</sub> <sup>[*]</sup> 189 [0.2] Iso Cooling: Iso 185 [0.1] Iso <sub>1</sub> <sup>[*]</sup> 163 [0.3] Tet 76 [33.7] Cr
2	Heating: Cr 137 [45.7] Tet 158 [0.5] Iso <sub>1</sub> <sup>[*]</sup> 169 [ $<0.05$ ] Iso Cooling: Iso 162 [ $<0.05$ ] Iso <sub>1</sub> <sup>[*]</sup> 150 [0.4] Tet 112 [45.9] Cr
3	Heating: Cr 121 [36.9] SmA 155 [0.3] N 170 [0.2] Iso Cooling: Iso 168 [0.4] N 154 [0.1] SmA 80 [31.3] Cr
4	Heating: Cr 128 [47.6] Iso <sub>1</sub> <sup>[*]</sup> 144 [ $<0.05$ ] Iso Cooling: Iso 139 [ $<0.05$ ] Iso <sub>1</sub> <sup>[*]</sup> 114 [2.4] Tet 100 [36.4] Cr

[a] Peak temperatures as determined from first heating and first cooling DSC scans with rate  $10\text{ K min}^{-1}$ . Abbreviations: Cr = crystalline solid; Tet = tetragonal 3D mesophase; SmA = smectic A phase; N = nematic phase; Iso<sub>1</sub><sup>[\*]</sup> = chiral isotropic conglomerate liquid; Iso = achiral isotropic liquid.

**Figure 1.** DSC heating and cooling curves ( $10\text{ K min}^{-1}$ ) measured for 1. Inset: Expanded temperature ranges (150–195 °C) on heating and cooling.

(Iso) as well as the chiral conglomerate liquid (Iso<sub>1</sub><sup>[\*]</sup>) appears dark (optically isotropic) between crossed polarizers and both have low viscosity and easily flow under gravity. However, in the temperature range of the Iso<sub>1</sub><sup>[\*]</sup> phase, occurring below  $189^\circ\text{C}$ , uncrossing the polarizers by a small angle (circa  $2\text{--}5^\circ$ ) in the clockwise or anticlockwise direction leads to the appearance of dark and bright domains. After rotating the analyzer by the same angle in the opposite direction, the dark and bright domains are reversed (Figure 2 a, b). Rotating the sample between crossed polarizers does not lead to any change, indicating that the distinct regions represent optically active domains rotating the plane of polarized light into opposite directions. The Iso<sub>1</sub><sup>[\*]</sup>–Iso phase transition is associated with a small enthalpy change of  $0.2\text{--}0.3\text{ kJ mol}^{-1}$ . The shape of the peak, being relatively sharp at the high-temperature end and having a significant tailing towards the low-temperature side is typically detected for this Iso–Iso<sub>1</sub><sup>[\*]</sup> transition<sup>[11,12]</sup> (Figure 1, inset).<sup>[16]</sup>

On cooling, the liquid–liquid transition between the achiral Iso phase and the chiral conglomerate liquid (Iso<sub>1</sub><sup>[\*]</sup>) takes place at  $T = 185^\circ\text{C}$ , and upon further cooling a meso-

**Figure 2.** Textures of compounds 1 and 4 between nontreated glass substrates (thickness  $\approx 25\ \mu\text{m}$ ). a) Compound 1 in the Iso<sub>1</sub><sup>[\*]</sup> phase at  $T = 180^\circ\text{C}$  after rotating one polarizer by circa  $5^\circ$  from the crossed position in the anticlockwise and b) in the clockwise direction. Dark and bright domains are evident, indicating the presence of a conglomerate of domains with opposite chirality. The conglomerate textures observed for these isotropic liquids were found to be independent of the used substrates, also in homeotropic and planar cells, as long as any contamination with traces of chirality is strictly excluded; in this case unequal areas or only one sign of handedness would be formed. c) Tet phase of compound 1 at  $T = 160^\circ\text{C}$ . d) Tet phase of compound 4 at  $T = 113^\circ\text{C}$ .<sup>[21]</sup> The direction of the polarizers is indicated by arrows. See Figure S12 for a color version of this figure.

phase is formed at  $T = 163^\circ\text{C}$ , indicated by the rapid growth of a low birefringent mosaic-like texture (see Figure 2c). This mesophase is highly viscous and does not flow even under medium mechanical stress, which is indicative of a mesophase with a 3D lattice. The formation of this phase from the adjacent Iso<sub>1</sub><sup>[\*]</sup> phase is associated with a small transition enthalpy of only  $\Delta H \approx 0.3\text{ kJ mol}^{-1}$  (Table 1). Despite the solid-like crystalline optical appearance, XRD investigations show a completely diffuse wide-angle scattering with a maximum at  $d = 0.45\text{ nm}$ , not very distinct from that in the Iso phases, thus confirming that the individual molecules have no fixed positions (Figure 3 a, inset).

There are numerous sharp reflections in the small-angle range (Figure 3 b; Table S1 in the Supporting Information) which can be indexed to a tetragonal 3D lattice (Tet). In previous work tetragonal mesophases were observed as birefringent LC phases, often accompanying bicontinuous cubic phases of rod-like molecules.<sup>[17–19]</sup> A tetragonal phase was also reported for bent-shaped molecules.<sup>[20]</sup> There are different subtypes of tetragonal phases with distinct lattice types, but the structures and the reasons for their formation have not been well understood. Unfortunately, the exact symmetry of the lattice could not be determined from powder XRD patterns and the oriented diffractions could not be achieved at the current stage. The highest symmetry that fits the diffraction pattern is  $P4/mmm$ , though a  $P4_22$  lattice could also be possible. The lattice parameters ( $a = 13.9$  and  $c = 18.9\text{ nm}$ ) are much larger than the molecular length ( $L_{\text{mol}} = 4.9\text{ nm}$  in the most stretched conformation with all-*trans* alkyl chains) and indicate a complex structure of this

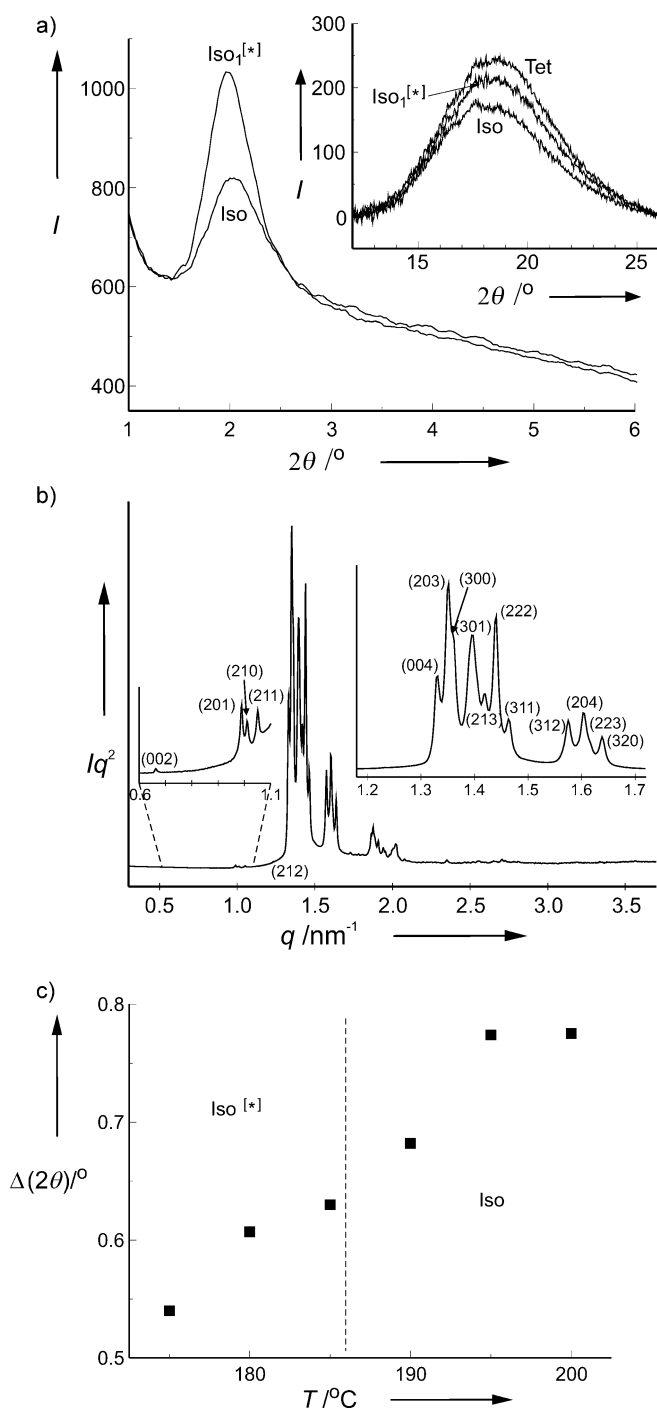


**Figure 3.** XRD data of compound 1: a) small-angle and wide-angle (inset) XRD diffractograms at different temperatures for the Iso phase at  $T=195^\circ\text{C}$ ,  $\text{Iso}_1^{[*]}$  phase at  $T=180^\circ\text{C}$ , and Tet phase at  $T=170^\circ\text{C}$ ; b) SAXS diffractogram of the Tet phase at  $T=160^\circ\text{C}$  with indexation; and c) full width at half maximum (FWHM) of the small-angle scatterings ( $\Delta(2\theta)$ ); fitted using Lorentzian line shapes) depending on temperature as observed in the isotropic liquid phases.

mesophase with about 2500 molecules per unit cell (see the Supporting Information). There is no indication of chirality in the Tet phases of compounds **1**, **2**, and **4** but this could probably be hidden under the birefringence and thus might not be detectable by optical methods.<sup>[21]</sup>

Modification of the parent structure **1** by introducing one lateral fluorine substituent ( $X=\text{F}$ , compound **2**) on the terminal benzene ring next to the alkoxy chain does not change the phase sequence, but reduces the range of the Tet phase and narrows the  $\text{Iso}_1^{[*]}$  range (see Table 1). A further reduction of the transition temperatures was achieved by introducing two fluorine atoms ( $X=Y=\text{F}$ , compound **4**; see Table 1 and Figure 2d). Changing the position of the single fluorine atom from X to Y ( $X=\text{H}$ ,  $Y=\text{F}$ , compound **3**) results in a completely different behavior, where the Tet and  $\text{Iso}_1^{[*]}$  phases are removed and replaced by lamellar (SmA) and nematic (N) LC phases (Figure S11). In compound **3** the larger F atom (compared to H) in the 2-position ( $Y=\text{F}$ ) is pointing to the center of the molecule. This slightly reduces the imbalance of interfacial area between rigid cores and alkyl-chain periphery, thus leading to decreased interface curvature and the formation of SmA and N phases.

In contrast, the F substituent at the peripheral 3-position (that is,  $X=\text{F}$ ) contributes to an increase in the interface curvature<sup>[22]</sup> and thus favors the Tet and  $\text{Iso}_1^{[*]}$  phases for compound **2** and for the disubstituted compound **4**, which has F substituents in both the 2- and 3-positions ( $X=Y=\text{F}$ ; Table 1). Compound **4** behaves similar to the nonsubstituted compound **1**, but forms the  $\text{Iso}_1^{[*]}$  phase at much lower temperature and in a wider temperature region. Thus, fluorination provides a tool for tailoring mirror-symmetry breaking in liquids.

XRD investigation of the Iso phases was performed for compound **1**. As shown in Figure 3a, in both Iso phases there is a diffuse small-angle scattering. The position of the maximum of the small-angle scattering is at  $d=4.3\text{--}4.4\text{ nm}$ , corresponding approximately to the molecular length ( $d/L_{\text{mol}}=0.87\text{--}0.90$ ). This indicates that the  $\text{Iso}_1^{[*]}$  phase has a cybotactic structure. The cybotactic clusters appear to have a helical or a twisted lamellar local structure acting as a template for helical molecular packing with synchronization of chiral conformations. The full width at half maximum of the small-angle scattering changes continuously without a visible step at the Iso– $\text{Iso}_1^{[*]}$  transition, indicating a continuous growth of the size of the cybotactic clusters with decreasing temperature, being in the range of 28 nm at the transition (see Figure 3c). With growing cluster size on decreasing temperature, chiral fluctuations in the achiral Iso phase increase and become long-range at the phase transition. By chirality synchronization of molecular conformations, a denser packing is achieved, giving rise to the detected enthalpic gain. Helical conformations result from the twist of the COO groups in the phenylbenzoate units<sup>[6c]</sup> and probably also from the twist of the biphenyl core. As the liquid state is retained, conformational disorder and molecular motions are partly retained at the transition and thus the overall entropic penalty of this process is decreased. Therefore, the enthalpic gain of chirality synchronization can exceed the entropic penalty of demixing of the enantiomeric conformers of these relatively large molecules.<sup>[11,23,24]</sup> At the  $\text{Iso}_1^{[*]}$ –Tet transition the local clusters fuse to a long-range 3D structure forming the tetragonal lattice.

Figure 4 shows the UV/Vis spectra of compound **1** in chloroform solution. For the freshly prepared sample an

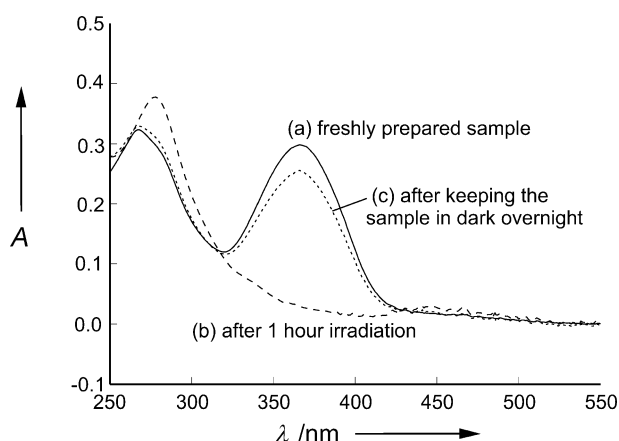


**Figure 4.** UV/Vis spectra of compound **1** dissolved in chloroform at 25 °C.

absorption band maximum was detected at  $\lambda = 367$  nm as a result of a  $\pi\text{-}\pi^*$  transition (solid line).<sup>[25]</sup> After irradiation for one hour with UV light ( $\lambda = 365$  nm), the absorption band at 367 nm disappeared (dashed line),<sup>[26]</sup> indicating that the *trans* isomer has completely transformed to the less stable *cis* isomer. After keeping the solution in the dark overnight, thermal relaxation to the *trans* isomer was nearly complete (dotted line).

In summary, we report the first azobenzene-based polycatenar compounds showing spontaneous breaking of mirror symmetry by chirality synchronization in the isotropic liquid state. Structural modifications by fluorination of the molecular core lead to compounds with lower transition temperatures and broaden the temperature ranges of the corresponding symmetry broken fluids. The photosensitive azobenzene unit may render this class of compounds suitable for potential applications in chirality switching and phase modulation by interaction with light.<sup>[27]</sup>

## Acknowledgements

The work was supported by the DFG (Grant Ts 39/24-1) and the National Natural Science Foundation of China (21374086). We thank beamline BL16B1 at SSRF (Shanghai Synchrotron Radiation Facility, China) for providing the beam times.

**Keywords:** azo compounds · chirality · liquids · self-assembly · symmetry breaking

**How to cite:** *Angew. Chem. Int. Ed.* **2016**, *55*, 312–316  
*Angew. Chem.* **2016**, *128*, 320–324

- [1] L. Pasteur, *Compt. Rend. Acad. Sci.* **1848**, *26*, 535–538.  
[2] a) J. Jacques, A. Collet, S. H. Wilen, *Enantiomers, Racemates and Resolutions*, Krieger, Malabar, **1994**; b) D. B. Amabilino, R. M. Kellogg, *Isr. J. Chem.* **2011**, *51*, 1034–1040; c) C. Viedma, *Phys. Rev. Lett.* **2005**, *94*, 065504; d) R. Raval, *Chem. Soc. Rev.* **2009**, *38*, 707–721.  
[3] A. Zehnacker, M. A. Suhm, *Angew. Chem. Int. Ed.* **2008**, *47*, 6970–6992; *Angew. Chem.* **2008**, *120*, 7076–7100.

- [4] a) I. Weissbuch, L. Leiserowitz, M. Lahav, *Top. Curr. Chem.* **2005**, *259*, 123–156; b) K.-H. Ernst, *Phys. Status Solidi B* **2012**, *249*, 2057–2088.  
[5] a) D. B. Amabilino, *Chirality at the Nanoscale*, Wiley-VCH, Weinheim, **2009**; b) A. R. A. Palmans, E. W. Meijer, *Angew. Chem. Int. Ed.* **2007**, *46*, 8948–8968; *Angew. Chem.* **2007**, *119*, 9106–9126; c) D. Pijper, B. L. Feringa, *Soft Matter* **2008**, *4*, 1349–1372; d) J. Kang, D. Miyajima, T. Mori, Y. Inoue, Y. Itoh, T. Aida, *Science* **2015**, *347*, 646–651.  
[6] a) G. Dantlgraber, A. Eremin, S. Diele, A. Hauser, H. Kresse, G. Pelzl, C. Tschierske, *Angew. Chem. Int. Ed.* **2002**, *41*, 2408–2412; *Angew. Chem.* **2002**, *114*, 2514–2518; b) R. A. Reddy, C. Tschierske, *J. Mater. Chem.* **2006**, *16*, 907–961; c) H. Takezoe, *Top. Curr. Chem.* **2011**, *318*, 303–330; d) L. E. Hough, M. Spannuth, M. Nakata, D. A. Coleman, C. D. Jones, G. Dantlgraber, C. Tschierske, J. Watanabe, E. Körblová, D. M. Walba, J. E. MacLennan, M. A. Glaser, N. A. Clark, *Science* **2012**, *325*, 452–456.  
[7] a) E. H. Kim, O. N. Kadkin, S. Y. Kim, M. G. Choi, *Eur. J. Inorg. Chem.* **2011**, 2933–2941; b) M. Alaasar, M. Prehm, M. Nagaraj, J. K. Vij, C. Tschierske, *Adv. Mater.* **2013**, *25*, 2186–2191; c) M. Alaasar, M. Prehm, K. May, A. Eremin, C. Tschierske, *Adv. Funct. Mater.* **2014**, *24*, 1703–1717.  
[8] a) G. Pelzl, A. Eremin, S. Diele, H. Kresse, W. Weissflog, *J. Mater. Chem.* **2002**, *12*, 2591–2593; b) V. Görtz, J. Goodby, *Chem. Commun.* **2005**, 3262–3264.  
[9] a) V. Borshch, Y.-K. Kim, J. Xiang, M. Gao, A. Jákli, V. P. Panov, J. K. Vij, C. T. Imrie, M. G. Tamba, G. H. Mehl, O. D. Lavrentovich, *Nat. Commun.* **2013**, *4*, 3635; b) D. Chen, J. H. Porada, J. B. Hooper, A. Klitnick, Y. Shen, M. R. Tuchband, E. Körblová, D. Bedrov, D. M. Walba, M. A. Glaser, J. E. MacLennan, N. A. Clark, *Proc. Natl. Acad. Sci. USA* **2013**, *110*, 15931–15936; c) L. Beguin, J. W. Emsley, M. Lelli, A. Lesage, G. R. Luckhurst, B. A. Timimi, H. Zimmermann, *J. Phys. Chem. B* **2012**, *116*, 7940–7951; d) P. A. Henderson, C. T. Imrie, *Liq. Cryst.* **2011**, *38*, 1407–1414; e) T. Ivšić, M. Vinković, U. Baumeister, A. Mikleušević, A. Lesac, *Soft Matter* **2014**, *10*, 9334–9342; f) R. J. Mandle, E. J. Davis, C. T. Archbold, C. C. A. Voll, J. L. Andrews, S. J. Cowling, J. W. Goodby, *Chem. Eur. J.* **2015**, *21*, 8158–8167.  
[10] a) A. Guijarro, M. Yus, *The Origin of Chirality in the Molecules of Life*, RSC Publishing, Cambridge, **2009**; b) J. S. Siegel, *Chirality* **1998**, *10*, 24–27.  
[11] a) C. Dressel, T. Reppe, M. Prehm, M. Brautzsch, C. Tschierske, *Nat. Chem.* **2014**, *6*, 971–977; b) C. Tschierske, G. Ungar, *ChemPhysChem* **2015**, DOI: 10.1002/cphc.201500601.  
[12] C. Dressel, F. Liu, M. Prehm, X. Zeng, G. Ungar, C. Tschierske, *Angew. Chem. Int. Ed.* **2014**, *53*, 13115–13120; *Angew. Chem.* **2014**, *126*, 13331–13336.  
[13] H. M. D. Bandarab, S. C. Burdette, *Chem. Soc. Rev.* **2012**, *41*, 1809–1825.  
[14] H. K. Bisoyi, Q. Li, *Acc. Chem. Res.* **2014**, *47*, 3184–3195.  
[15] a) J.-I. Mamiya, K. Kanie, T. Hiyama, T. Ikeda, T. Kato, *Chem. Commun.* **2002**, 1870–1871; b) O. Tsutsumi, T. Ikeda, *Curr. Opin. Solid State Mater. Sci.* **2002**, *6*, 563–568.  
[16] As well as the Iso–Iso<sub>1</sub><sup>[8]</sup> transitions associated with mirror-symmetry breaking, Iso–Iso<sub>1</sub> transitions between two achiral liquid phases have also been reported: J. W. Goodby, D. A. Dunmur, J. P. Collings, *Liq. Cryst.* **1995**, *19*, 703–709 and Ref. [20].  
[17] M. Vogrin, N. Vaupotič, M. M. Wojcik, J. Mieczkowski, K. Madrak, D. Pocięcha, E. Gorecka, *Phys. Chem. Chem. Phys.* **2014**, *16*, 16067–16074.  
[18] a) A. Levelut, C. Germain, P. Keller, L. Liebert, J. Billard, *J. Phys.* **1983**, *44*, 623–629; b) A.-M. Levelut, E. Hallouin, D. Bennemann, G. Heppke, D. Löttsch, *J. Phys. II* **1997**, *7*, 981–1000; c) A.-M. Levelut, M. Clerc, *Liq. Cryst.* **1998**, *24*, 105–115.

- [19] T. Yamamoto, I. Nishiyama, M. Yoneya, H. Yokoyama, *J. Phys. Chem. B* **2009**, *113*, 11564–11567.
- [20] M. Jasiński, D. Pocięcha, H. Monobe, J. Szczytko, P. Kaszyński, *J. Am. Chem. Soc.* **2014**, *136*, 14658–14661.
- [21] The dark and bright areas in the Tet phases in Figure 2c,d change their brightness on rotating the sample between crossed polarizers and therefore are due to birefringence.
- [22] D. W. Bruce, *Acc. Chem. Res.* **2000**, *33*, 831–840.
- [23] For a discussion on molecular conformational synchronization in nematic liquids by macroscopic torsional strain, see: R. Basu, J. S. Pendery, R. G. Petschek, R. P. Lemieux, C. Rosenblatt, *Phys. Rev. Lett.* **2011**, *107*, 237804.
- [24] These large molecules provide numerous intermolecular interactions, thus providing sufficiently large  $\Delta H$  values, and have a low number of molecules per volume unit, leading to a small contribution of the mixing entropy.
- [25] C. H. Legge, G. R. Mitchell, *J. Phys. D* **1992**, *25*, 492–499.
- [26] Y. Lansac, M. A. Glaser, N. A. Clark, O. D. Lavrentovich, *Nature* **1999**, *398*, 54–57.
- [27] a) S.-W. Choi, T. Izumi, Y. Hoshio, Y. Takanishi, J. Watanabe, H. Takezoe, *Angew. Chem. Int. Ed.* **2006**, *45*, 1382–1385; *Angew. Chem.* **2006**, *118*, 1410–1413; b) A. Zep, K. Sitkowska, D. Pocięcha, E. Gorecka, *J. Mater. Chem. C* **2014**, *2*, 2323–2327.

Received: August 29, 2015

Published online: October 22, 2015





# Isothermal Chirality Switching in Liquid-Crystalline Azobenzene Compounds with Non-Polarized Light

Mohamed Alaasar,\* Silvio Poppe, Qingshu Dong, Feng Liu,\* and Carsten Tschierske\*

**Abstract:** Spontaneous mirror-symmetry breaking is a fundamental process for development of chirality in natural and in artificial self-assembled systems. A series of triple chain azobenzene based rod-like compounds is investigated that show mirror-symmetry breaking in an isotropic liquid occurring adjacent to a lamellar LC phase. The transition between the lamellar phase and the symmetry-broken liquid is affected by *trans*–*cis* photoisomerization, which allows a fast and reversible photoinduced switching between chiral and achiral states with non-polarized light.

Chirality of molecular systems has developed into a major topic in chemistry since its discovery by L. Pasteur.<sup>[1]</sup> It is considered as a prerequisite for emergence of life<sup>[2]</sup> and has numerous technological implications in pharmaceutical and agricultural chemistry<sup>[3]</sup> as well as for applications in nanotechnology and advanced materials.<sup>[4]</sup> In condensed matter phases, chirality can be based on permanent (configurational) or transient (conformational) molecular chirality and on chiral superstructures, arising from the (in most cases helical) organization of molecules (superstructural chirality).<sup>[5]</sup> Circular polarized light represents a chiral environment<sup>[6]</sup> and therefore has often been used, either to induce chirality, or to modify chirality by diastereomeric interaction with existing molecular and superstructural chirality.<sup>[7,8]</sup> In contrast, non-polarized light is achiral (racemic) and therefore cannot induce chirality in the absence of a properly oriented magnetic field or another source of chirality.<sup>[2b,6]</sup> Accordingly, chirality switching by non-polarized light requires chiral molecules, preferably organized in liquid-crystalline (LC) phases combining the molecular order required for helix formation with the mobility required for switching. Photoisomerization changes the molecular shape and this modifies the self-assembly. Examples are light induced SmC\*–SmA

and SmA–N\* transitions (Supporting Information, Scheme S2). In the first case, photoisomerization removes the molecular tilt in the SmC\* structure which is the basis of helix formation perpendicular to the layers.<sup>[9]</sup> In the latter case photoisomerization removes the layer structure (SmA), being incompatible with a helical twist between the molecules. Only in the photoinduced nematic phase without these layers the molecular chirality can couple with the nematic director field and a helical superstructure evolves (N\* phase).<sup>[10]</sup> Recently, it was shown that for achiral bent mesogenic dimers with azobenzene units a helical superstructure is spontaneously formed in the twist-bend nematic phase (N<sub>TB</sub>, Supporting Information, Scheme S2). This spontaneously chiral superstructure is removed by *trans*–*cis* photoinomerization with non-polarized light, leading to a transition to a nematic phase which, due to the absence of molecular chirality, is achiral (N).<sup>[11]</sup>

Herein we report the first example for the opposite process of induction of superstructural chirality by photoisomerization of achiral compounds with non-polarized light. In this case mirror-symmetry breaking takes place at the transition from a higher to a lower order phase which is contrary to common knowledge, where symmetry breaking occurs at the transition from lower to higher order (for example, crystallization from solutions or melts). This discovery is based on our previous work on spontaneous mirror-symmetry breaking in isotropic liquids (Iso<sub>1</sub><sup>[\*]</sup> phases) formed by achiral multi-chained rod-like (polycatenar<sup>[12]</sup>) molecules.<sup>[13–17]</sup> The spontaneous mirror-symmetry breaking in these liquids was proposed to result from the combination of a locally twisted cybotactic cluster structure with the chirality synchronization of the involved transiently chiral molecules.<sup>[15]</sup> The local twist is thought to be due to the local aggregation and parallel organization of the  $\pi$ -conjugated rods and the simultaneous clashing of the bulky terminal alkyl chains. These Iso<sub>1</sub><sup>[\*]</sup> phases<sup>[17]</sup> typically occur besides cubic or non-cubic mesophases with a long-range 3D lattice.<sup>[16]</sup> It was also shown that polycatenar compounds involving azobenzene units photoisomerize in solution, though it was not possible to observe a measurable effect on the bulk state.<sup>[18]</sup> We attributed this to a kinetic hindrance of photoisomerization by the long-range 3D lattice. To replace these 3D phases by fluid lamellar LC phases, we have designed a new class of polycatenar compounds involving a photoisomerizable azobenzene group<sup>[19]</sup> and having only three instead of the previously used four terminal alkyl chains (tricateenar compounds **An**, see Figure 1). These compounds were synthesized, purified, and analyzed as described in the Supporting Information, Scheme S1.

[\*] Dr. M. Alaasar, S. Poppe, Prof. Dr. C. Tschierske  
Institute of Chemistry, Martin-Luther University Halle-Wittenberg  
Kurt-Mothes Str. 2, 06120 Halle/Saale (Germany)  
E-mail: carsten.tschierske@chemie.uni-halle.de

Dr. M. Alaasar  
Department of Chemistry, Faculty of Science, Cairo University  
P.O. 12613 Giza (Egypt)  
E-mail: malaasar@sci.cu.edu.eg

Q. Dong, Prof. Dr. F. Liu  
State Key Laboratory for Mechanical Behavior of Materials  
Xi'an Jiaotong University, Xi'an 710049 (P.R. China)  
E-mail: feng.liu@xjtu.edu.cn

Supporting information (including synthesis of compounds and experimental methods) and the ORCID identification number(s) for the author(s) of this article can be found under:  
<https://doi.org/10.1002/anie.201705559>

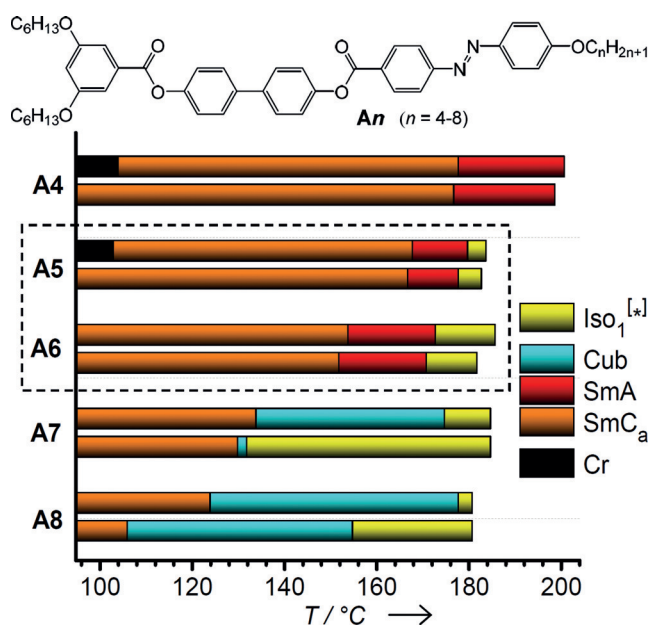


**Figure 1.** Phase transitions of compounds **An** as determined from the second heating (upper columns) and cooling DSC scans (lower columns) with rate  $10\text{ K min}^{-1}$ ; abbreviations: SmA = non-tilted lamellar phase; SmCa = anticlinic tilted lamellar phase; Cub = bicontinuous cubic phase with  $1a\bar{3}d$  lattice; Cr = solid crystal; Iso<sub>1</sub><sup>[\*]</sup> = chiral isotropic conglomerate liquid mesophase;<sup>[17]</sup> the superscript [\*] indicates the presence of a chiral superstructure though the involved molecules are achiral; for numerical data and transition enthalpies, see the Supporting Information, Table S1.

The transition temperatures of compounds **An** are shown graphically in Figure 1 (for numerical data, see the Supporting Information, Table S1). All **An** compounds with  $n = 5-8$  show spontaneous chiral conglomerate formation in a certain temperature range of their isotropic liquid phases (Iso<sub>1</sub><sup>[\*]</sup>). The formation of these Iso<sub>1</sub><sup>[\*]</sup> phases from the achiral isotropic liquid state (Iso) is indicated under the polarizing microscope by the occurrence of chiral domains, identified upon slight rotation of the analyzer by a small angle out of the  $90^\circ$  position, leading to dark and bright domains that invert their brightness after rotating the analyzer by the same angle into the opposite direction (Figure 2c,d; Supporting Information, Figure S12). The domains have circular shapes and flow under gravity as typical for isotropic liquids.<sup>[20]</sup> The Iso<sub>1</sub><sup>[\*]</sup> phases are accompanied by different types of LC phases, depending on the chain length  $n$ . As shown in Figure 1, a cubic phase with  $1a\bar{3}d$  lattice is found for compounds with chain length  $n = 7$  and 8 (**A7**:  $a_{\text{cub}} = 10.0\text{ nm}$ , see Figure 2g,h and the Supporting Information, Table S2; **A8**:  $10.2\text{ nm}$ , see Table S3; for more details of structure elucidation, see Section 3.4.1 of the Supporting Information). The cubic phases are achiral, in line with the racemic  $1a\bar{3}d$  structure being composed of two enantiomeric networks of branched helical columns (Figure 2h; Supporting Information, Figure S16).<sup>[16]</sup> With decreasing chain length, the optical isotropic cubic phase is replaced by less viscous and birefringent LC phases. Polarizing optical microscopy of the LC phases of compounds **A4-A6** indicates uniaxial SmA phases characterized by typical fan textures in planar alignment (layers

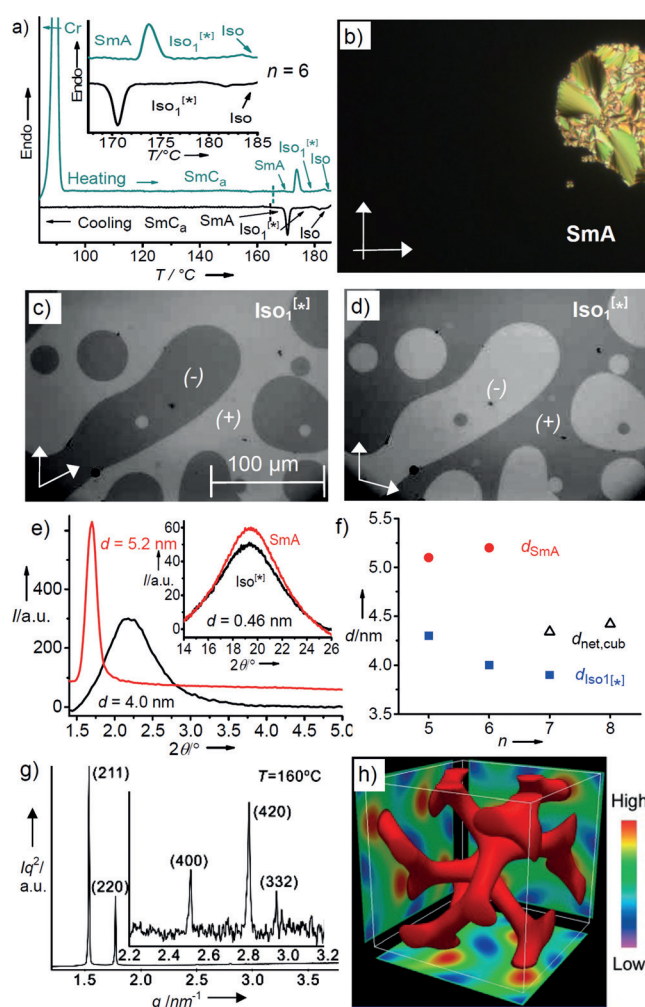


**Figure 2.** Characterization of the mesophases of compounds **An**: a) heating and cooling DSC curves ( $10\text{ K min}^{-1}$ ) recorded for **A6**. b) Texture of the SmA phase ( $T = 170^\circ\text{C}$ ) of **A5** between crossed polarizers with coexisting homeotropic (dark area) and planar alignment (birefringent area). c, d) Chiral domains observed for the Iso<sub>1</sub><sup>[\*]</sup> phase of compound **A6** in a thin film between two glass plates (ca.  $20\ \mu\text{m}$ ) at  $T = 181^\circ\text{C}$ , c) after rotating one polarizer by  $12^\circ$  from the crossed position in anticlockwise and d) in clockwise direction (see also Figure S12). e) SAXS pattern of the SmA phase (red lines) and Iso<sub>1</sub><sup>[\*]</sup> phase (black lines) of **A6** at  $T = 160$  and  $180^\circ\text{C}$ , respectively; the inset shows the corresponding WAXS patterns. f) Development of the  $d$ -spacings  $d_{\text{Iso}_1^{[*]}}$  ( $2\text{ K}$  below Iso-Iso<sub>1</sub><sup>[\*]</sup> transition) and  $d_{\text{SmA}}$  depending on chain length ( $n$ );  $d_{\text{net,cub}} = (3^{1/2}a_{\text{cub}})/4$  is the distance between the two networks in the Cub/ $1a\bar{3}d$  phases. g) SAXS pattern of the Cub/ $1a\bar{3}d$  phase of **A7** ( $T = 160^\circ\text{C}$ ) and h) reconstructed electron density map of the Cub/ $1a\bar{3}d$  phase obtained from (g); see Section 3.4.1 in the Supporting Information for more details.

perpendicular to the substrate) and dark isotropic textures in homeotropic alignment (layers parallel to the substrate, see Figure 2b). Small-angle X-ray scattering (SAXS) confirms the lamellar organization and provides a layer thickness of  $d_{\text{SmA}} = 5.2\text{ nm}$  for the SmA phase of **A6**, as an example (Figure 2e; see also the Supporting Information, Tables S4-S6). This value is slightly larger than the molecular length ( $L_{\text{mol}} = 4.4\text{ nm}$ ), indicating an antiparallel organization of the molecules with intercalation of the single alkyl chains between the biphenyl units of adjacent molecules (Fig-

ure 4a,c). In all cases, on cooling the SmA phase an anticlinic tilted lamellar phase (SmC<sub>a</sub> phase) is observed (Figure 1). This is for some compounds followed by additional tilted and non-tilted smectic, hexatic, and crystalline low-temperature mesophases, which will be discussed in a forthcoming report.

Though the Iso-Iso<sub>1</sub><sup>[\*]</sup> transition is easily detected by POM, the associated enthalpies are very small and the corresponding DSC peaks are broad, very typical for a C<sub>p</sub>-anomaly (see inset in Figure 2a).<sup>[14,17,21]</sup> Also the XRD patterns in the Iso<sub>1</sub><sup>[\*]</sup> and Iso ranges are very similar. As shown in Figure 2e for the Iso<sub>1</sub><sup>[\*]</sup> phase of **A6**, there are only two diffuse scatterings, one in the small- and the other in the wide-angle region of the XRD pattern (at  $d = 0.46$  nm), in line with the presence of only short range order (black line, Figure 2e with inset). The intensity of the small-angle scattering is significantly larger than the wide angle scattering, but it is also significantly broader compared to the smectic phases (red line, Figure 2e), as typical for liquids with a locally ordered structure (cybotaxis).<sup>[14,17,22]</sup> As previously shown, the change of the position and line width of the XRD small-angle scattering at the Iso-Iso<sub>1</sub><sup>[\*]</sup> transitions is continuous without any distinct jump.<sup>[14]</sup> This indicates that the Iso and Iso<sub>1</sub><sup>[\*]</sup> phases are formed by small clusters that grow continuously on cooling and reach the critical size for chirality synchronization at the Iso-Iso<sub>1</sub><sup>[\*]</sup> transition temperature.

Compound **A6** was selected for photoisomerization experiments in solution and in the distinct LC phases. Investigation in solution indicated almost complete *trans*-*cis* isomerization under UV light and back relaxation to the *trans* isomer by thermal relaxation as shown in Figure 3a. Irradiation of the bulk sample with non-polarized 405 nm laser light (5 mW) lowered the SmA-Iso<sub>1</sub><sup>[\*]</sup> transition temperature of **A6** by 10 K. An equilibrium state is reached after a couple of seconds (< 2 s) and relaxes back to the initial transition temperatures (*cis*-to-*trans*) immediately after switching off the light source (< 2 s). This allows an isothermal induction of chirality and a relatively fast and reversible on-off switching of chirality by non-polarized light, as shown in Figure 3b-d (see also the Supporting Information, Video 1). The effect of irradiation on the Iso-Iso<sub>1</sub><sup>[\*]</sup> transition temperature is much smaller, leading to a reduction by only 2 K, thus overall expanding the enantiotropic Iso<sub>1</sub><sup>[\*]</sup> range of **A6** from 11 to about 20 K.<sup>[23]</sup>

The sign of chirality in the chiral domains of the Iso<sub>1</sub><sup>[\*]</sup> phase is retained during repeated switching cycles Iso<sub>1</sub><sup>[\*]</sup>-SmA-Iso<sub>1</sub><sup>[\*]</sup> or Iso<sub>1</sub><sup>[\*]</sup>-Iso-Iso<sub>1</sub><sup>[\*]</sup> (see the Supporting Information, Video 2), though the SmA and Iso phases, as well as the involved molecules, are achiral. It is therefore likely that the chiral information is stored at the surfaces of the glass substrates via surface stabilization of residual helical clusters or chiral surface defects, which then trigger the chirality sense in the developing bulk Iso<sub>1</sub><sup>[\*]</sup> phase. In contrast, the Cub-Iso<sub>1</sub><sup>[\*]</sup> transitions of compounds **A7** and **A8** are not affected by irradiation, as previously also observed for the tetracatenars.<sup>[18]</sup> Probably the long range 3D connected networks of columns in the Cub phase act as templates that kinetically hinder the isomerization.<sup>[24]</sup>

To understand the development of the Iso<sub>1</sub><sup>[\*]</sup> phase in relation to the molecular structure and the self-assembly in

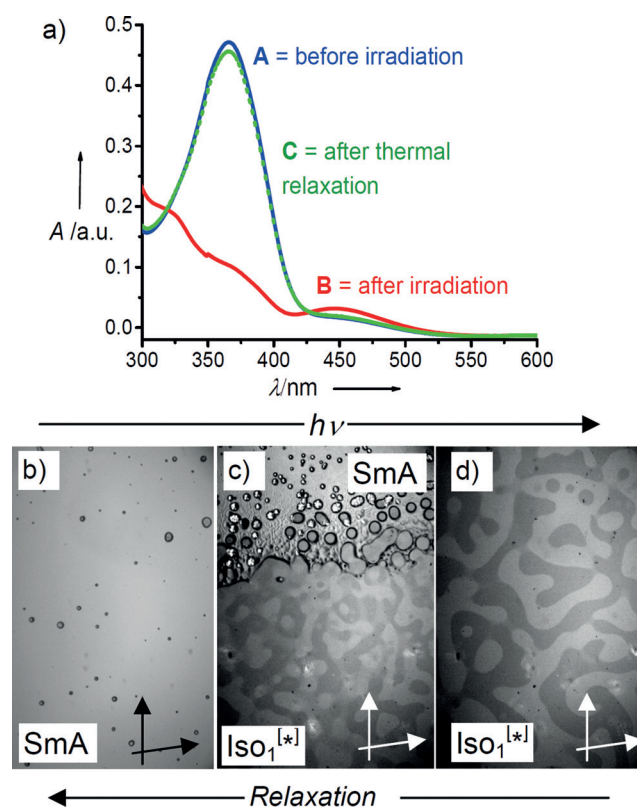


**Figure 3.** a) UV/Vis spectra of **A6** dissolved in chloroform at 25 °C ( $c = 20$  mmol L<sup>-1</sup>). A: freshly prepared solution before irradiation; B: *cis*-isomer as obtained after 1 h irradiation with  $\lambda = 365$  nm; C: after keeping the sample in dark overnight. b-d) Isothermal photoinduced SmA-to-Iso<sub>1</sub><sup>[\*]</sup> transition observed for compound **A6** in a thin film between two glass plates under slightly uncrossed polarizers (arrows) at  $T = 168$  °C: b) SmA phase before illumination with non-polarized 405 nm laser light (5 mW); c) during SmA-to-Iso<sub>1</sub><sup>[\*]</sup> transition upon starting of illumination and d) Iso<sub>1</sub><sup>[\*]</sup> phase as observed during illumination. The reverse sequence is obtained immediately after switching off the light source (see also the Videos in the Supporting Information).

the adjacent LC phases, the phase structures depending on chain length and temperature have been investigated in more detail. The maximum of the small angle X-ray scattering in the Iso<sub>1</sub><sup>[\*]</sup> phases is  $d_{\text{Iso}_1^{[*]}} = 3.9\text{--}4.3$  nm, being significantly smaller than the layer spacing  $d_{\text{SmA}}$  in the adjacent SmA phase ( $d_{\text{SmA}} = 5.1\text{--}5.2$  nm, Figure 2f) and only slightly smaller than the molecular length ( $L_{\text{mol}} = 4.4$  nm for **A6**, Figure 4a,b). This suggests a non-intercalated antiparallel packing of the molecules with completely segregated alkyl chains and aromatic cores in the Iso<sub>1</sub><sup>[\*]</sup> phase (Figure 4b). This non-intercalated packing is distinct from the intercalated organization in the adjacent SmA phase (Figure 4a) and provides an unbalanced ratio of two aromatic cores vs. three alkyl chains, leading to layer frustration, which is released by development of curvature and twist. With growing alkyl chain length the twist of the aggregates increases, thus favoring the chirality synchronization of helical conformers. However, on cooling, the connectivity of the clusters increases, too, until a highly connected network is formed at the Iso<sub>1</sub><sup>[\*]</sup>-Cub/*Ia* $\bar{3}$ *d* phase transition ( $n = 7, 8$ ) leading to the achiral cubic phase (Figure 2h). Accordingly, the distance between the nets

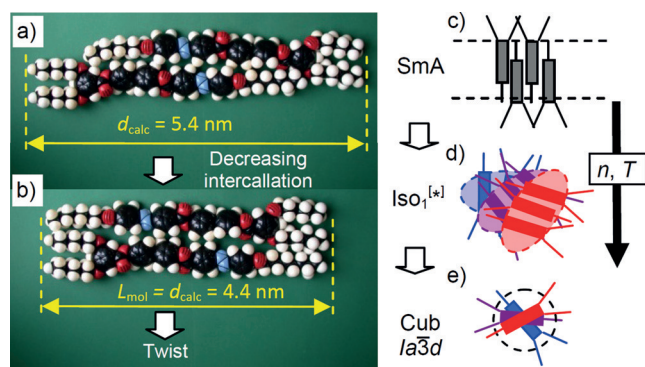


**Figure 4.** Molecular organization in the LC phases and in the cybotactic clusters of the Iso/Iso<sub>1</sub><sup>[\*]</sup> phases: a), b) Molecular models of **A6** showing the molecular dimensions and the changing intercalation at the transition from a) the intercalated packing in the lamellar to b) the segregated packing in the Iso<sub>1</sub><sup>[\*]</sup> and Cub/*la* $\bar{3}$ *d* phases (twist not shown). c)–e) Models showing the cross-sections of c) the layers (SmA); d) the local organization in the twisted ribbons of the Iso<sub>1</sub><sup>[\*]</sup> phases (from front to back the molecules are shown red, purple, blue) and e) the helical columns forming the networks of the Cub/*la* $\bar{3}$ *d* phase.

forming the Cub/*la* $\bar{3}$ *d* phase (Figure 2h),  $d_{\text{net,cub}} = 4.4\text{--}4.5$  nm is close to  $d_{\text{Iso}_1^{[*]}}$  (Figure 2f), confirming that the segregated organization (Figure 4b) is retained in the Cub/*la* $\bar{3}$ *d* phase. Figure 2f also shows that  $d_{\text{Iso}}$  decreases with growing  $n$ , from  $n = 5$  to 7, whereas  $d_{\text{SmA}}$  grows, indicating that the local organization in the Iso<sub>1</sub><sup>[\*]</sup> phases becomes more intercalated, and hence less sterically frustrated with decreasing chain length (Figure 4b→a), in this way favoring the lamellar organization. Deeper chain-core intercalation at decreased temperature (larger contribution of linear *trans*-conformers makes the chains more compatible with the rod-like cores) reduces the curvature further, and the local clusters can fuse to infinite layers with intercalated structure (SmA,  $n = 5, 6$ ; Figure 4a,c). However, in the chiral isotropic liquids of compounds **A5** and **A6** a twisted organization is still retained in the aggregates and the local twist is obviously still sufficient for chirality synchronization to take place, thus leading to the chiral Iso<sub>1</sub><sup>[\*]</sup> phase. Only for the shortest homologue **A4** sufficient twist cannot develop and the SmA phase is directly formed from the achiral Iso phase. This provides an understanding of the formation of symmetry-broken Iso<sub>1</sub><sup>[\*]</sup> phases for compounds **A5** and **A6** occurring besides an SmA phase, just before the cross-over from lamellar to bicontinuous cubic organization in the adjacent LC phases.

In summary, isothermal switching from an achiral LC phase to a mirror-symmetry broken isotropic liquid with non-polarized light was reported for achiral compounds, providing significant potential for technological and nanotechnological applications.

### Acknowledgements

The work was supported by the DFG (Grand Ts 39/24) and the National Natural Science Foundation of China (No. 21374086). We thank Beamline BL16B1 at SSRF (Shanghai

Synchrotron Radiation Facility, China) for providing the beamtimes.

### Conflict of interest

The authors declare no conflict of interest.

**Keywords:** azobenzene · chirality · liquid crystals · mirror-symmetry breaking · photoisomerization

**How to cite:** *Angew. Chem. Int. Ed.* **2017**, *56*, 10801–10805  
*Angew. Chem.* **2017**, *129*, 10941–10945

- [1] L. Pasteur, *C. R. Hebd. Seances Acad. Sci.* **1848**, *26*, 535.
- [2] a) W. A. Bonner, *Origins Life Evol. Biospheres* **1991**, *21*, 59; b) L. D. Barron, *Space Sci. Rev.* **2008**, *135*, 187; c) I. Budin, J. W. Szostak, *Annu. Rev. Biophys.* **2010**, *39*, 245.
- [3] L. Ai Nguyen, H. He, C. Phan-Huy, *Int. J. Biomed. Sci.* **2006**, *2*, 85.
- [4] a) “Materials Chirality”: *Topics in Stereochemistry, Vol. 24* (Eds.: S. E. Denmark, J. Siegel, M. M. Green, R. J. M. Nolte, E. W. Meijer), Wiley, Hoboken, **2003**; b) *Chirality at the nanoscale* (Ed.: D. B. Aamabilino), Wiley-VCH, Weinheim, **2009**; c) H. K. Bisoyi, Q. Li, *Chem. Rev.* **2016**, *116*, 15089.
- [5] E. Yashima, N. Ousaka, D. Taura, K. Shimomura, T. Ikai, K. Maeda, *Chem. Rev.* **2016**, *116*, 13752.
- [6] a) M. Avalos, R. Babiano, P. Cintas, J. L. Jimenez, J. C. Palacios, *Chem. Rev.* **1998**, *98*, 2391; b) G. L. J. A. Rikken, E. Raupach, *Nature* **2000**, *405*, 932; c) A. G. Griesbeck, U. J. Meierhenrich, *Angew. Chem. Int. Ed.* **2002**, *41*, 3147; *Angew. Chem.* **2002**, *114*, 3279; d) B. L. Feringa, R. A. van Delden, *Angew. Chem. Int. Ed.* **1999**, *38*, 3418; *Angew. Chem.* **1999**, *111*, 3624.
- [7] a) G. Balavoine, A. Moradpour, H. B. Kagan, *J. Am. Chem. Soc.* **1974**, *96*, 5152; b) D. Pijper, B. L. Feringa, *Soft Matter* **2008**, *4*, 1349; c) Y. Inoue, *Chem. Rev.* **1992**, *92*, 741.
- [8] a) G. Iftime, F. Lagugne, L. A. Natansohn, P. Rochon, *J. Am. Chem. Soc.* **2000**, *122*, 12646; b) S.-W. Choi, S. Kawachi, N. Y. Ha, H. Takezoe, *Phys. Chem. Chem. Phys.* **2007**, *9*, 3671; c) F. Vera, R. M. Tejedor, P. Romero, J. Barbera, M. B. Ros, J. L. Serrano, T. Sierra, *Angew. Chem. Int. Ed.* **2007**, *46*, 1873; *Angew. Chem.* **2007**, *119*, 1905.
- [9] a) T. Ikeda, T. Sasaki, K. Ichimura, *Nature* **1993**, *361*, 428; b) H. G. Walton, H. J. Coles, D. Guillon, G. Poeti, *Liq. Cryst.* **1994**, *17*, 333; c) A. Langhoff, F. Giesselmann, *ChemPhysChem* **2002**, *3*, 424.
- [10] S. Abraham, V. A. Mallia, K. V. Ratheesh, N. Tamaoki, S. Das, *J. Am. Chem. Soc.* **2006**, *128*, 7692.
- [11] D. A. Paterson, J. Xiang, G. Singh, R. Walker, D. M. Agra-Kooijman, A. Martinez-Felipe, M. Gao, J. M. D. Storey, S. Kumar, O. D. Lavrentovich, C. T. Imrie, *J. Am. Chem. Soc.* **2016**, *138*, 5283.
- [12] a) J. Malthête, H. T. Nguyen, C. Destrade, *Liq. Cryst.* **1993**, *13*, 171; b) H. T. Nguyen, C. Destrade, J. Malthete, *Adv. Mater.* **1997**, *9*, 375.
- [13] C. Dressel, W. Weissflog, C. Tschierske, *Chem. Commun.* **2015**, *51*, 15850.
- [14] C. Dressel, T. Reppe, M. Prehm, M. Brautzsch, C. Tschierske, *Nat. Chem.* **2014**, *6*, 971.
- [15] C. Tschierske, G. Ungar, *ChemPhysChem* **2016**, *17*, 9.
- [16] C. Dressel, F. Liu, M. Prehm, X. Zeng, G. Ungar, C. Tschierske, *Angew. Chem. Int. Ed.* **2014**, *53*, 13115; *Angew. Chem.* **2014**, *126*, 13331.
- [17] The Iso<sub>1</sub><sup>[\*]</sup> phases are distinct from the so-called dark conglomerate phases (DC phases) formed by a completely different class of compounds, the bent-core molecules. DC phases represent

sponge-like deformed lamellar phases, where chirality and conglomerate formation is due to the combination of tilt and polar order (see Ref. [25a]). The Iso<sub>1</sub><sup>[\*]</sup>-Iso transition between two isotropic liquids is (almost) continuous,<sup>[14,15]</sup> whereas the DC-Iso transition, representing a SmCP-Iso transition, is discontinuous and associated with relatively high transition enthalpies ( $\Delta H \approx 10\text{--}25 \text{ kJ mol}^{-1}$ ; see Ref. [25b]).

- [18] a) M. Alaasar, M. Prehm, Y. Cao, F. Liu, C. Tschierske, *Angew. Chem. Int. Ed.* **2016**, *55*, 312; *Angew. Chem.* **2016**, *128*, 320; b) M. Alaasar, S. Poppe, Q. Dong, F. Liu, C. Tschierske, *Chem. Commun.* **2016**, *52*, 13869.
- [19] H. M. Dhammika, S. C. Burdette, *Chem. Soc. Rev.* **2012**, *41*, 1809.
- [20] See the Video in the Supporting Information of Ref. [14].
- [21] M. Jasiński, D. Pocięcha, H. Monobe, J. Szczytko, P. Kaszyński, *J. Am. Chem. Soc.* **2014**, *136*, 14658.
- [22] a) G. W. Stewart, R. M. Morrow, *Phys. Rev.* **1927**, *30*, 232; b) O. Franciscangeli, M. Laus, M. Galli, *Phys. Rev. E* **1997**, *55*, 481.
- [23] The SmA-Iso transition of **A4** is reduced by  $-4 \text{ K}$  during irradiation, but no Iso<sub>1</sub><sup>[\*]</sup> phase is induced; the SmC<sub>a</sub>-SmA transition of **A5** is shifted by  $-3 \text{ K}$ .
- [24] Irradiation of **A7** and **A8** in the tilted SmC<sub>a</sub> range can induce the cubic phase, that is, isomerization to the bent *cis* isomer increases the interfacial curvature and the SmC<sub>a</sub>-Cub transition temperature is shifted by  $7 \text{ K}$  to lower temperature, expanding the cubic phase range by photoisomerization, similar as reported for azobenzene doped SmC<sub>s</sub> phases (see Ref. [26]).
- [25] a) L. E. Hough, M. Spannuth, M. Nakata, D. A. Coleman, C. D. Jones, G. Dantlgraber, C. Tschierske, J. Watanabe, E. Körblova, D. M. Walba, J. E. Maclennan, M. A. Glaser, N. A. Clark, *Science* **2009**, *325*, 452; b) G. Dantlgraber, A. Eremin, S. Diele, A. Hauser, H. Kresse, G. Pelzl, C. Tschierske, *Angew. Chem. Int. Ed.* **2002**, *41*, 2408; *Angew. Chem.* **2002**, *114*, 2514.
- [26] R. Hori, Y. Miwa, K. Yamamoto, S. Kutsumizu, *J. Phys. Chem. B* **2014**, *118*, 3743.

Manuscript received: May 31, 2017

Revised manuscript received: July 10, 2017

Accepted manuscript online: July 18, 2017

Version of record online: August 7, 2017

Cite this: *J. Mater. Chem. C*, 2020, **8**, 12902

# Y-shaped tricatener azobenzenes – functional liquid crystals with synclinic–anticlinic transitions and spontaneous helix formation†

Mohamed Alaasar,<sup>ab</sup> Silvio Poppe,<sup>a</sup> Yu Cao,<sup>cd</sup> Changlong Chen,<sup>c</sup> Feng Liu,<sup>c</sup> Chenhui Zhu<sup>bd</sup> and Carsten Tschierske<sup>ab</sup>

A series of achiral tricatener rod-like molecules with a 3,5-disubstitution pattern at one end and a single alkyl chain at the other end of a rod-like azobenzene derived core is reported. Depending on temperature and alkyl chain length, these Y-shaped compounds self-assemble into different types of liquid crystalline (LC) phases, ranging from non-tilted and synclinic tilted hexatic, *via* non-tilted and anticlinic tilted smectic and bicontinuous cubic LC phases, to a spontaneous mirror symmetry broken isotropic liquid (Iso<sub>1</sub><sup>(\*)</sup>) or a related achiral liquid network phase (Iso<sub>1</sub>). An additional tilted, but uniaxial smectic phase was observed at the transition between anticlinic and synclinic tilt correlation and was investigated by soft resonant X-ray scattering with respect to possible helix formation. This work provides a new concept for the design of technological interesting azobenzene based LC materials with anticlinic tilted smectic C phases (SmC<sub>a</sub>) and with azobenzene units organized in the long range or short range helical network structures of bicontinuous cubic and chiral isotropic liquid phases, respectively. Core fluorination removes all lamellar phases, leaving only the cubic phase over wide temperature ranges, even at ambient temperature.

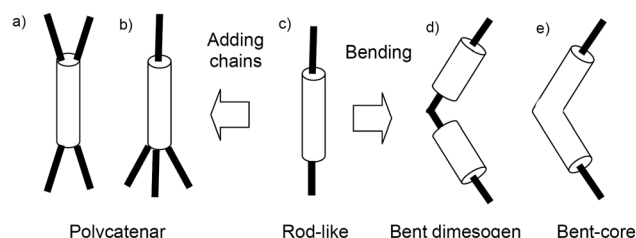
Received 14th July 2020,  
Accepted 24th August 2020

DOI: 10.1039/d0tc03321a

rsc.li/materials-c

## 1. Introduction

There are numerous well established and presently in development applications of liquid crystals (LC) in optical displays,<sup>1</sup> organic electronics and photovoltaics,<sup>2–4</sup> in selective membranes,<sup>5</sup> for ion conducting arrays<sup>2,5</sup> and in nanoscale patterning on the sub-10 nm length scale for use in nanolithography,<sup>6–8</sup> all being essential for the development of present and future technologies. For LC materials there are three fundamental design concepts, molecular shape, amphiphilicity/polyphilicity<sup>9</sup> and chirality.<sup>10–12</sup> With respect to the molecular shape rod-like and disc-like molecules, leading to lamellar and columnar LCs, respectively, represent the majority.<sup>13</sup> More recently, bent molecules<sup>14,15</sup> and polycatenar molecules, having more than only one flexible



**Scheme 1** Different molecular shapes derived from rod-like mesogens by alkyl chain design and by bending the core structure, both providing mirror symmetry broken mesophases.

chain attached to one or both ends of a rod-like polyaromatic core, have received growing attention (Scheme 1). The latter can show transitions from lamellar (smectic = Sm) *via* bicontinuous cubic (Cub<sub>bi</sub>) to columnar (Col) LC phases.<sup>16–20</sup>

In recent years a new feature of the self-assembly of polycatenar mesogens was recognized when spontaneous mirror symmetry breaking was observed<sup>9,21–27</sup> due to supramolecular helix formation which cooperatively couples with chirality synchronization of the involved molecules.<sup>12,22,23</sup> Helical self-assembly has a strong impact on the mesophase structures and leads to complex cubic and non-cubic mesophases with 3D lattices in the case of polycatenars,<sup>28–30</sup> as for example the cubic *I23* (previously “*Im3m*”)<sup>23,31,32</sup> and the tetragonal SmQ phase.<sup>33–37</sup>

<sup>a</sup> Institute of Chemistry, Martin Luther University Halle-Wittenberg, Kurt Mothes Str. 2, D-06120 Halle (Saale), Germany.  
E-mail: carsten.tschierske@chemie.uni-halle.de

<sup>b</sup> Department of Chemistry, Faculty of Science, Cairo University, P.O. 12613 Giza, Egypt. E-mail: malaasar@sci.cu.edu.eg

<sup>c</sup> State Key Laboratory for Mechanical Behaviour of Materials, Shaanxi International Research Center for Soft Matter, School of Materials Science & Engineering, Xi'an Jiaotong University, Xi'an 710049, P. R. China.  
E-mail: feng.liu@xjtu.edu.cn

<sup>d</sup> Advanced Light Source, Lawrence Berkeley National Laboratory, Berkeley, CA 94720, USA. E-mail: chenhuizhu@lbl.gov

† Electronic supplementary information (ESI) available. See DOI: 10.1039/d0tc03321a

Soft helical superstructures<sup>12,38</sup> can also be found in the soft crystalline<sup>38–42</sup> and liquid crystalline<sup>43,44</sup> conglomerate phases (DC, HNF, HNC), helical lamellar ( $\text{SmCP}_F^{\text{hel}}$  and  $\text{SmC}_{\text{TB}}$ )<sup>45,46</sup> and nematic ( $\text{N}_{\text{TB}}$ )<sup>47–50</sup> phases of bent mesogenic dimers, oligomers,<sup>42,45,47–50</sup> and bent-core mesogens (Scheme 1d and e).<sup>14,39–41,43–45</sup>

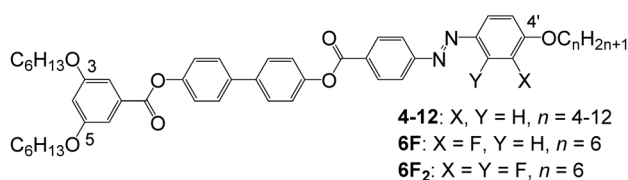
A local helical organization can even be retained in the isotropic liquid phases of some polycatenars, occurring adjacent to  $\text{Cub}_{\text{bi}}$  phases.<sup>21</sup> These isotropic liquids spontaneously segregate into a conglomerate of two immiscible chiral fluids with opposite chirality sense ( $\text{Iso}_1^{[*]}$  phases).<sup>21</sup> This new dynamic mode of chirality synchronization was experimentally observed for different types of achiral, but transiently chiral tetracatenar molecules (Scheme 1a and b).<sup>21,51,52</sup> Photoisomerizable polycatenars with azobenzene units are rare,<sup>53–57</sup> but we succeeded in designing such molecular and supra-molecular polycatenars forming the symmetry broken isotropic liquid ( $\text{Iso}_1^{[*]}$ ).<sup>58,59</sup> In a previous communication we reported that the tricatener compounds **4–8** with a 3,5-substitution pattern at one end (Scheme 2) can be switched between chiral and achiral states by photo-induced *trans-cis* isomerization.<sup>60</sup>

Herein we expand this work to the full series of compounds **4–12** (Scheme 2) including two core fluorinated derivatives (**6F** and **6F<sub>2</sub>**) and mainly focus on the series of unusual smectic and hexatic phases formed by these compounds. Special attention is paid to the formation of the anticlinic  $\text{SmC}_a$  phase<sup>61</sup> instead of the synclinic  $\text{SmC}_s$  phase usually observed for polycatenar compounds<sup>17</sup> and the unexpected transition to synclinic tilted ( $\text{HexF}_s$ ,  $\text{HexI}_s$ ) and non-tilted ( $\text{HexB}$ ) hexatic phases occurring below it. Not only the inverted temperature dependence of the anticlinic to synclinic transitions is remarkable, even more surprising is, that for one homologue the tilted smectic phase becomes optically uniaxial in a certain temperature range. The possibility of helix formation as origin of optical uniaxiality was investigated by resonant soft X-ray scattering (RSOXS) at the carbon K-edge. In addition, it is shown that formation of mirror-symmetry broken liquids can be tailored by alkyl chain design and that bicontinuous networks with cubic symmetry become dominating after core fluorination.

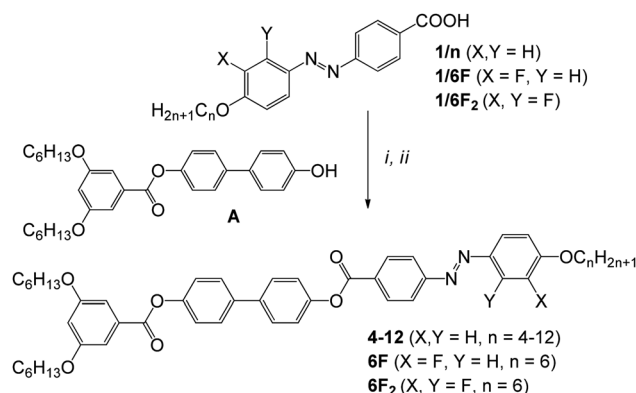
## 2. Experimental

### Synthesis

The synthesis of the azobenzene-based materials **4–8** has been described in detail previously.<sup>60</sup> The synthesis of the longer



**Scheme 2** Tricatener compounds under investigation; the compound name indicates the number of carbon atoms in the 4'-positioned terminal alkoxy chain.



**Scheme 3** Synthesis of compounds **4–12**,<sup>60</sup> **6F** and **6F<sub>2</sub>**. Reagents and conditions: (i) DMF,  $\text{SOCl}_2$ , reflux, 1 h; (ii) dry  $\text{CH}_2\text{Cl}_2$ , dry TEA, dry pyridine, reflux for 6 h.

homologues **9–12** and the two fluorinated compounds **6F** and **6F<sub>2</sub>** was carried out in an analogous way (Scheme 3) as reported in the ESI.†

### Investigations

The compounds were investigated by polarizing optical microscopy (POM), differential scanning calorimetry (DSC) and X-ray diffraction (XRD) including small angle X-ray scattering (SAXS) and wide angle X-ray scattering (WAXS) as outlined in the ESI.† Resonant RSoXS was performed on BL 11.0.1.2 at the Advanced Light Source in Lawrence Berkeley National Laboratory as described in the ESI.†

## 3. Results and discussion

### 3.1. Non-fluorinated compounds 4–12

The observed phase sequences and transition temperatures of all investigated compounds are collated in Table 1 and the development of the distinct modes of LC self-assembly in the homologous series of the non-fluorinated compounds **4–12** is shown graphically in Fig. 1. For compounds **5–8** with intermediate chain length a symmetry broken percolated isotropic liquid phase ( $\text{Iso}_1^{[*]}$ , the asterisk in square brackets indicates a conglomerate of coexisting enantiomeric liquids) is formed, either above a non-tilted lamellar ( $\text{SmA}$ ) phase (compounds **5**, **6**) or a bicontinuous cubic phase with  $Ia\bar{3}d$  lattice (compounds **7**, **8**) before the transition to the ordinary achiral liquid ( $\text{Iso}$ ) takes place.<sup>57</sup> For the longer homologues with  $n = 9–12$  the cubic phase becomes dominating and the  $\text{Iso}_1^{[*]}$  phase is replaced by an achiral percolated liquid phase ( $\text{Iso}_1$ ). Fig. 1 also shows that the  $\text{SmA}$  phase is replaced by an anticlinic tilted  $\text{SmC}_a$  phase at lower temperature and that with increasing chain length hexatic LC phases become dominating as low temperature phases below the cubic phase.

#### 3.1.1 Non-tilted $\text{SmA}$ and anticlinic tilted $\text{SmC}_s$ phases.

The smectic high temperature phases of compounds **4–6** show typical highly birefringent fan-like textures with dark extinctions coinciding with the orientations of polarizer and analyzer in planar alignment (the view is parallel to the layer planes).

Table 1 Phase transition temperatures ( $T/^\circ\text{C}$ ), mesophase types, and transition enthalpies [ $\Delta H/\text{kJ mol}^{-1}$ ] of compounds **4–12**, **6F** and **6F<sub>2</sub>**<sup>a</sup>

**4–12:**  $n = 4\text{--}12$ ,  $X, Y = \text{H}$   
**6F:**  $n = 6$ ,  $X = \text{F}$ ,  $Y = \text{H}$   
**6F<sub>2</sub>:**  $n = 6$ ,  $X = Y = \text{F}$

Comp.	$n$	Phase transitions <sup>a</sup>
<b>4</b>	4	H: Cr 104 [42.1] SmC <sub>a</sub> 178 [–] SmA 201 [2.3] Iso C: Iso 199 [–3.4] SmA 177 [–] SmC <sub>a</sub> 75 [–34.2] Cr
<b>5</b>	5	H: Cr 103 [45.6] SmC <sub>a</sub> 168 [–] SmA 180 [1.6] Iso <sub>1</sub> <sup>[*]</sup> 184 [–] Iso C: Iso 183 [–] Iso <sub>1</sub> <sup>[*]</sup> 178 [–1.8] SmA 167 [–] SmC <sub>a</sub> 65 [–0.2] HexF <sub>s</sub> 63 [–0.5] HexI <sub>s</sub> 55 [–15.9] Cr
<b>6</b>	6	H: Cr 89 [36.5] SmC <sub>a</sub> 151 [–] SmA 173 [1.5] Iso <sub>1</sub> <sup>[*]</sup> 184 [–] Iso C: Iso 182 [–0.05] Iso <sub>1</sub> <sup>[*]</sup> 171 [–1.6] SmA 150 [–] SmC <sub>a</sub> 79 [–] HexF <sub>s</sub> 68 [–1.2] HexI <sub>s</sub>
<b>7</b>	7	H: Cr 85 [31.6] SmC <sub>a</sub> 134 [1.1] Cub 175 [1.8] Iso <sub>1</sub> <sup>[*]</sup> 185 [–] Iso C: Iso 183 [–] Iso <sub>1</sub> <sup>[*]</sup> 132 [–] Cub <sub>bi</sub> + M 130 [–1.4] <sup>b</sup> SmC <sub>a</sub> 82 [–] HexF <sub>s</sub> 75 [–2.2] HexB 38 [–13.8] Cr
<b>8</b>	8	H: Cr 71 [27.6] HexB 87 [2.8] SmC <sub>a</sub> 91 [–] SmC <sub>x</sub> 94 [–] SmC 124 [1.7] Cub <sub>bi</sub> 178 [2.7] Iso <sub>1</sub> <sup>[*]</sup> 181 [–] Iso C: Iso 181 [–] Iso <sub>1</sub> <sup>[*]</sup> 139 [–0.44] Cub <sub>bi</sub> + M 106 [–1.6] SmC 94 [–] SmC <sub>x</sub> 91 [–] SmC <sub>a</sub> 86 [–3.5] HexB
<b>9</b>	9	H: Cr 107 [51.2] Cub <sub>bi</sub> 176 [2.9] Iso C: Iso 171 [–0.3] Iso <sub>1</sub> 157 [–1.2] Cub <sub>bi</sub> 75 [–] HexI <sub>s</sub> 62 [–7.3] Cr H2: HexI <sub>s</sub> 91 [–] SmC <sub>a</sub> 95 [3.3] Cub <sub>bi</sub> 176 [2.9] Iso <sup>c</sup>
<b>10</b>	10	H: Cr <sub>1</sub> 70 [26.9] Cr <sub>2</sub> 84 [6.2] Cub <sub>bi</sub> 171 [2.9] Iso C: Iso 167 [–0.5] Iso <sub>1</sub> 155 [–1.3] Cub <sub>bi</sub> 77 [–] HexI <sub>s</sub> 47 [–7.3] Cr
<b>12</b>	12	H: Cr 100 [35.8] Cub <sub>bi</sub> 176 [2.9] Iso C: Iso 172 [–0.9] Iso <sub>1</sub> 158 [–1.3] Cub <sub>bi</sub> 80 [–] HexI <sub>s</sub> 58 [–8.4] Cr
<b>6F</b>	6	H: Cr 102 [39.8] Cub <sub>bi</sub> 168 [2.7] Iso C: Iso 138 [–1.1] Cub <sub>bi</sub> < 20 Cr
<b>6F<sub>2</sub></b>	6	H: Cr 92 [41.7] Cub <sub>bi</sub> 152 [1.9] Iso C: Iso 127 [–1.3] Cub <sub>bi</sub> < 20 Cr

<sup>a</sup> Peak temperatures as determined from 2nd heating (upper lines; H) and 2nd cooling DSC scans (lower lines; C) with rate 10 K min<sup>–1</sup>; abbreviations: Cr = crystalline solid; Iso = isotropic liquid; Iso<sub>1</sub> = achiral isotropic percolated network liquid; Iso<sub>1</sub><sup>[\*]</sup> spontaneous symmetry broken Iso<sub>1</sub> phase; SmA = nontilted smectic phase; SmC = smectic C phase, with (predominating) synclinic tilt correlation; SmC<sub>a</sub> = anticlinic tilted SmC phase; SmC<sub>x</sub> = optical uniaxial SmC phase; HexF<sub>s</sub> = synclinic tilted hexatic F phases; HexI<sub>s</sub> = synclinic tilted hexatic I phases (see Fig. 6g and h); HexB is a non-tilted hexatic B phase (see Fig. 9b); Cub<sub>bi</sub> = bicontinuous cubic phase with achiral *Ia3d* lattice Cub<sub>bi</sub>/*Ia3d* (see Fig. 13h); M = birefringent mesophase with non-cubic 3D lattice and unknown structure (see Section 3.1.5). <sup>b</sup> Enthalpy involves both transitions Iso<sub>1</sub><sup>[\*]</sup>–Cub<sub>bi</sub> and Cub<sub>bi</sub>–SmC<sub>a</sub>. <sup>c</sup> Second heating after cooling to 70 °C; for DSCs, see Fig. S1 (ESI).

In homeotropic alignment (the view is along the layer normal) they appear optically isotropic in all cases (see Fig. 2a for an example), indicating an SmA phase, where the molecules are organized in layers with the molecular long axes aligned on average parallel to the layer normal. Upon cooling a weakly birefringent Schlieren texture forms in the homeotropic areas whereas the orientation of the dark extinctions in the highly birefringent planar aligned regions does not change at this phase transition (Fig. 2b). Moreover, in thin homeotropic samples a stripe pattern is observed (Fig. 2d).<sup>62</sup> This could indicate either a transition to a non-tilted biaxial SmA<sub>b</sub> phase by freezing the rotation around the long axis<sup>63–67</sup> or to an anticlinic tilted SmC<sub>a</sub> phase by the onset of a tilt of the molecules, with the tilt direction alternating between adjacent layers.<sup>61,68</sup> The slight decrease of the birefringence in the planar texture at the phase transition (colour of the fans changes from yellowish green to green, Fig. 2a and b), indicates the onset of tilt, being in line with the decrease of the XRD layer spacing at this transition (Fig. 3a). Because the direction of the extinctions in the planar aligned areas remains parallel to the polarizers (Fig. 2a–c) it is confirmed that the emerging tilt is opposite in adjacent layers, *i.e.*, this is an anticlinic SmC<sub>a</sub> phase.<sup>61</sup> This SmA–SmC<sub>a</sub> transition takes place without measurable enthalpy change (see DSCs in Fig. S1a and b, ESI†).

On further cooling the birefringence in the planar aligned areas decreases, whereas it increases in the homeotropic (gray) areas, indicating a growing tilt angle in the SmC<sub>a</sub> phase range (Fig. 2b and c). For compound **4** with the shortest alkyl chain at the monosubstituted end, this SmC<sub>a</sub> phase crystallizes on further cooling, whereas for the following homologues additional phase transitions to more ordered lamellar phases can be observed, which will be discussed further below.

Fig. 3 shows the results of XRD studies of compound **6**. The initial increase of the  $d$ -spacing in the SmA range is in line with a growing packing density with decreasing temperature. The decrease of the  $d$ -value of the XRD layer reflection starting at 150 °C (Fig. 3a) confirms the developing tilt at the SmA–SmC<sub>a</sub> transition. At this transition the  $d$ -value ( $d = 5.22$  nm) has a local maximum and is larger than the molecular length in the most extended conformation ( $L_{\text{mol,max}} = 4.5$  nm, Fig. 4a). This can be explained by the formation of an intercalated structure with antiparallel molecular packing. Depending on the degree of intercalation the layer spacing can change from  $d_{\text{min}} = 4.5$  nm for the fully intercalated and completely chain-core segregated structure (Fig. 4a) to  $d_{\text{max}} = 5.6$  nm for the structure with an overlapping of the alkyl chain at the monosubstituted end with the aromatics (Fig. 4c), where the two hexyl chains at the 3,5-disubstituted end are excluded from intercalation



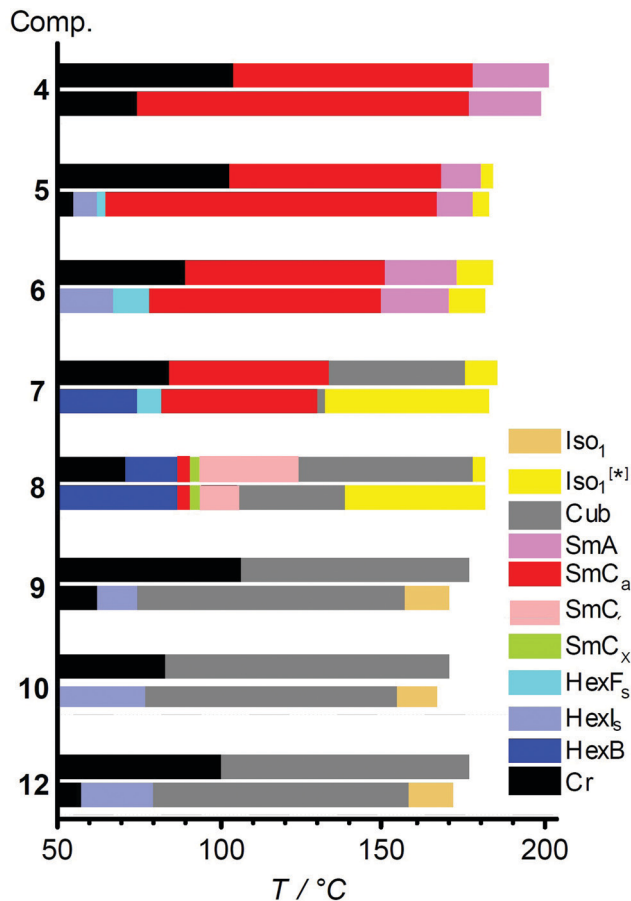


Fig. 1 Bar diagram showing the mesophases and phase transitions of compounds 4–12 on heating (upper columns) and on cooling (lower columns); Cub =  $Cub_{b1}/Ia\bar{3}d$ ; for numerical data and explanations of the phase types, see Table 1.

and assume a tuning fork like conformation. This arrangement provides the densest molecular packing and provides a similar cross sectional area for the two intercalated segments and the two 3,5-hexyl chains, allowing a non-distorted packing in layers. If this structure is assumed, a maximum tilt  $\beta$  of  $\sim 23^\circ$  is calculated according to  $\cos \beta = d/d_{\max}$  for the  $SmC_a$  phase.

However, it was not possible to determine the actual tilt in the  $SmC_a$  phases directly, as the tilt is anticlinic and therefore cannot be observed optically, and in addition, no aligned samples were obtained for XRD investigations. However, an optical tilt of  $15^\circ$  was measured in the synclinc  $HexF_s$  phase and  $10\text{--}11^\circ$  in the  $HexI_s$  phase of this compound (Section 3.1.2). Comparing the development of the  $d$ -values of the layer reflection (Fig. 3a) with these tilt angles leads to an estimated tilt in the range of  $15\text{--}20^\circ$  for the  $SmC_a$  phase.

For achiral rod-like molecules, the synclinc layer correlation is usually favoured by the molecular fluctuations between the layers (out-of-plane fluctuations);<sup>43,69</sup> therefore, the formation of an anticlinic  $SmC_a$  phase is unusual and surprising for the series of tricatens 4–9. Anticlinic  $SmC_a$  phases were first observed for enantiomerically enriched (scalemic) or uniformly chiral rod-like molecules, often with branched (methyl or

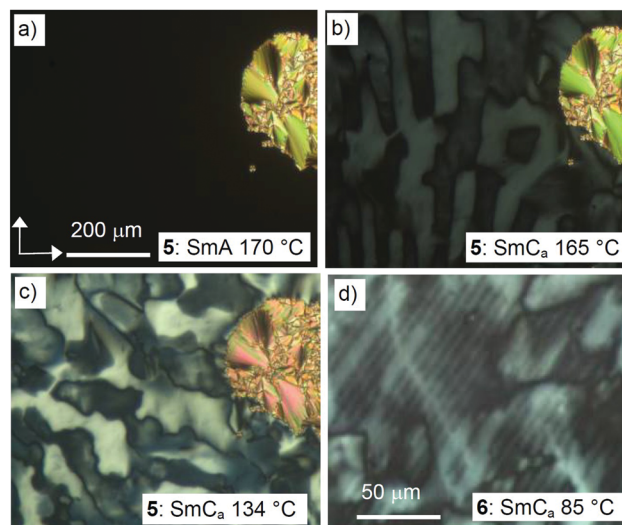


Fig. 2 Textures observed between crossed polarizers (white arrows in (a) for the  $SmA$ – $SmC_a$  transition of (a)–(c) compound 5, between ordinary microscopy glass plates, showing coexisting homeotropic (dark area) and planar alignment (birefringent area) and (d) equidistant stripe patterns observed for compound 6 in the  $SmC_a$  phase; for the textures of the  $HexI$  phase of 5, see Fig. S2 (ESI†).

trifluoromethyl substituted) alkyl end chains.<sup>70</sup> For achiral and racemic molecules it can be promoted by bent spacer units in di- or oligomesogens,<sup>71</sup> especially those with siloxane spacers,<sup>72–75</sup> by mixing rod-like with bent core molecules,<sup>76</sup> by alkyl chain branching (swallow tailed compounds)<sup>77–82</sup> and end group modification,<sup>83,84</sup> including fluorination.<sup>75,82,85–87</sup> However, it was not reported previously for polycatenar (multi-chain rod-like) compounds, which form exclusively synclinc  $SmC_s$  phases.<sup>17,19,88</sup> However, for the so-called hockey-stick molecules with only two terminal chains, one in the 4-position, and the other one at the opposite end in the 3-position, leading to an overall bent molecular shape (Fig. 5), the  $N$ - $SmC_s$ – $SmC_a$  polymorphism is typically observed on cooling.<sup>89–94</sup> It appears that such non-linear molecules with 3-substitution at one end provide an increased chain disorder which decouples the layers more efficiently than in the case of more linear compounds with both chains in 4-positions. This suppresses the out of plane fluctuations and therefore favours  $SmC_a$  over  $SmC_s$ . For the 3,5-disubstitution pattern of the tricatens this effect on chain order and fluctuations is doubled by the two chains in the 3- and in 5-positions, so that only a direct  $SmA$ – $SmC_a$  transition without intermediate  $SmC_s$  phase is observed for compounds 4–6. Thus, the 3,5-disubstitution pattern represents a new powerful design concept for anticlinic, antiferroelectric and eventually orthoconic<sup>95</sup> LC materials. The Y-shaped molecules with 3,5-substitution pattern can anyhow be considered as Siamese twins of two parallel fused hockey stick molecules (Fig. 5). Simultaneously, they resemble a special kind of swallow tailed molecules with the swallow-tail being fused with the rod-like core. Thus, these molecules provide a link between different classes of compounds favoring the anticlinic tilt correlation, the swallow-tailed and the bent molecules (Scheme 1).

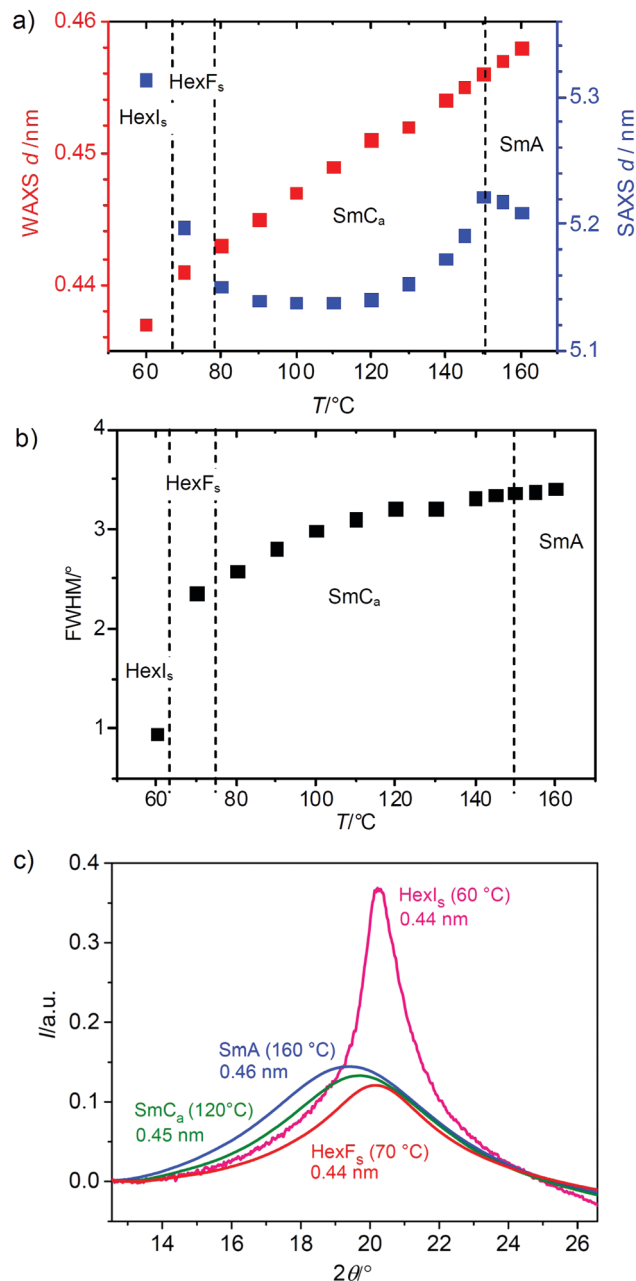


Fig. 3 XRD of compound **6** in the different mesophases: (a) temperature dependence of the  $d$ -spacing of the WAXS scattering (red) and the SAXS (10)-reflection (blue); (b) FWHM and (c) shapes of the WAXS as a function of temperature (with  $d$ -values of the scattering maxima).

The wide angle scattering (see Fig. 3c) is diffuse in the SmA and SmC<sub>a</sub> ranges, being in line with smectic phases with only short-range in-plane order. However, the position of the scattering maximum is continuously shifted from 0.46 nm in the SmA phase to 0.44 nm at the low temperature end of the SmC<sub>a</sub> phase (80 °C) (see red dots in Fig. 3a) and the peak width also decreases, in line with a growing packing density (see Fig. 3b and c).

**3.1.2 Transition to hexatic phases with synclinal tilt.** For compound **4** exclusively the SmA and SmC<sub>a</sub> phases were observed, whereas for compounds **5–9** additional lamellar

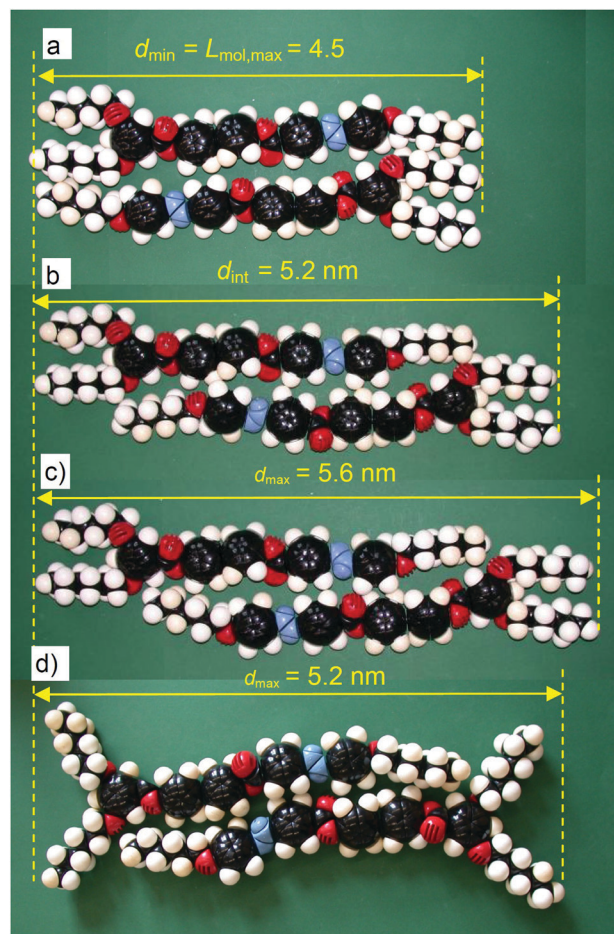


Fig. 4 Molecular dimensions of various molecular pairs of compound **6** depending on the degree of intercalation and the  $d$ -spacing of these possible arrangements within the layers.

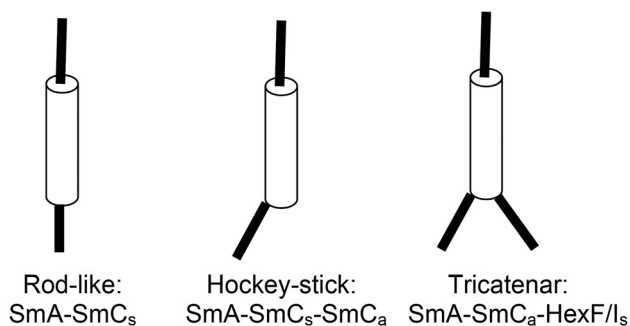
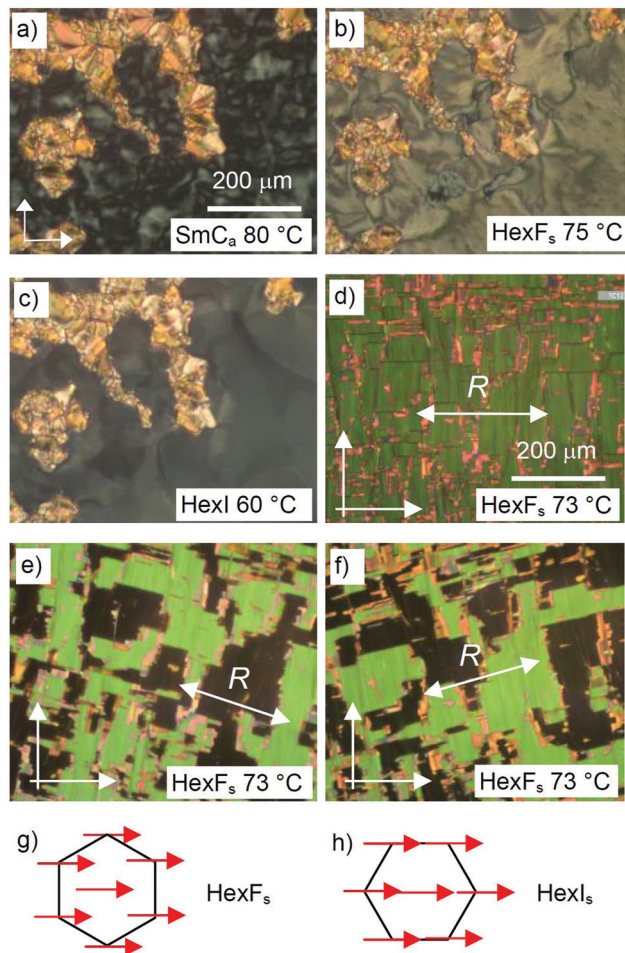


Fig. 5 Effect of the chain topology on the phase sequence on cooling.

phases with enhanced packing density were found below the SmC<sub>a</sub> phase (Table 1), as indicated by the changes in the optical textures and XRD patterns.

Compounds **5** and **6** behave very similar (see Fig. 1 and Table 1; for DSCs, see Fig. S1a and b, ESI<sup>†</sup>) and Fig. 6 shows the change of the textures for compound **6** as a representative example (see also Fig. S3, ESI<sup>†</sup>). Upon cooling the SmC<sub>a</sub> phase of compound **6** to  $T = 79$  °C the birefringence in the homeotropic areas suddenly increases, accompanied by textural



**Fig. 6** (a–c) Phase transitions as observed by polarizing microscopy in the distinct lamellar phases of compound **6** between plain microscopy glass plates; for additional textures, see Fig. S3 (ESI<sup>†</sup>). (d–f) Rotating the sample (in planar cell, 6  $\mu\text{m}$ ,  $R$  indicates the rubbing direction) between crossed polarizers indicates a tilt of  $15^\circ$  at  $T = 73^\circ\text{C}$ ; there is no change of the texture at the transition to  $\text{HexI}_s$ , only the tilt decreases to  $10^\circ$  at  $T = 60^\circ\text{C}$ ; (g) and (h) show the tilt orientation in the layers of the hexatic F and I phases, respectively.

changes in the planar aligned regions; the dark extinctions become birefringent and the fan texture becomes broken, indicating a change of the tilt from anticlinic to synclinc (Fig. 6a and b). A synclinc tilt of  $15^\circ$  can be determined from the tilt-domain texture by rotation of the sample between the crossed polarizers, as shown in Fig. 6d–f. In the XRD pattern the small angle scattering is shifted at the transition at  $79^\circ\text{C}$  to a bit larger  $d$ -values and there is a slight reduction of the width (full width at half maximum = FWHM) of the WAXS (Fig. 3). These are typical features for a  $\text{SmC}_a$ – $\text{HexF}_s$  transition.<sup>96</sup>

At the next transition at  $68^\circ\text{C}$  the homeotropic Schlieren textures become mosaic-like which indicates a transition to another synclinc tilted lamellar phase with stiffened layers. The birefringence of the homeotropic aligned areas decreases (Fig. 6c), in line with a decreasing tilt to  $10^\circ$ , observed in the corresponding planar tilt-domain texture. The shape of the wide angle scattering becomes much narrower with a slightly

non-symmetric lambda-shape as typical for a  $\text{HexI}_s$  phase (Fig. 3c, magenta curve).<sup>97–101</sup> Thus, the phase sequence  $\text{SmC}_a$ – $\text{HexF}_s$ – $\text{HexI}_s$  is proposed for compounds **5** and **6**. In the hexatic phases a pseudo-hexagonal packing of the molecules takes place. However, the 2d lattices in adjacent layers are not long range and the layers are positionally uncorrelated, leading to only bond orientational order instead of long range periodicity.<sup>98–107</sup> The direction of the tilt with respect to the pseudo-hexagonal lattice distinguishes the hexatic F and I phases (Fig. 6g and h). The increase of the  $d$ -spacing by  $\sim 0.15$  nm at the transition from  $\text{SmC}_a$  via  $\text{HexF}_s$  to  $\text{HexI}_s$  (Fig. 3a) can partly be attributed to the growing packing density, causing an alkyl chain stretching and partly to a decreasing tilt with lowering temperature as typical feature of  $\text{SmC}$ – $\text{HexF}$ – $\text{HexI}$  transitions.<sup>102</sup> Remarkably, the smectic-to-hexatic transition is associated with the transition from anticlinic to synclinc tilt which is attributed to the alkyl chain stiffening, supporting interlayer fluctuations and thus favoring the synclinc tilt over the anticlinic.<sup>70,104</sup>

**3.1.3 Transition from synclinc tilted to non-tilted hexatic phases of compounds 7 and 8.** For compounds **7** and **8** the  $\text{SmA}$  phase is replaced by a cubic phase, whereas the tilted lamellar phases occurring at lower temperature are retained.<sup>108</sup> Upon cooling, the  $\text{SmC}_a$  phase of compound **7** converts at  $82$ – $83^\circ\text{C}$  into the synclinc  $\text{HexF}_s$  phase (see Fig. 7b and d). On further cooling to  $75^\circ\text{C}$  the dark extinctions parallel to the polarizers reappear again in the planar samples (Fig. 7d and f) and the homeotropic areas become optically isotropic (Fig. 7c and e) indicating the transition to an optically uniaxial lamellar phase. At this temperature the profile of the XRD wide angle scattering becomes narrower (magenta curve in Fig. 8c) as typical for a transition to a  $\text{HexB}$  phase. This means that in this case the tilt is not only reduced, but apparently completely removed at the transition to the low temperature hexatic ( $\text{HexB}$ ) phase.

The  $\text{HexB}$  low temperature phase is also found for the next homologue **8** below  $86^\circ\text{C}$ . However, in this case, the phase sequence is a bit more complicated (Fig. 9a and 10). On cooling the homeotropic aligned  $\text{SmC}_s$  phase the birefringence at first decreases (Fig. 10d) and it becomes isotropic between  $94$  and  $91^\circ\text{C}$  (Fig. 10c), then the texture becomes birefringent (Fig. 10b) and at the phase transition to the  $\text{HexB}$  phase at  $86^\circ\text{C}$  ( $\Delta H \sim 3$  kJ mol<sup>−1</sup>) it becomes isotropic again (Fig. 10a).

In order to understand the structures of the two uniaxial smectic phases of compound **8**, and to check if for this compound the synclinc–anticlinic transition might be associated with formation of heliconical phases as origin of uniaxiality, as known for  $\text{SmC}^*$  and  $\text{SmC}\alpha^*$  phases of chiral rod-like molecules<sup>61,70,109</sup> and  $\text{SmC}^{hel}$  phases of achiral bent molecules,<sup>45,46</sup> this compound was investigated by RSoXS at the carbon K-edge.<sup>110,111</sup> No resonant peak is observed in the uniaxial hexatic phase range below  $87^\circ\text{C}$ , excluding a heliconical structure as origin of the optical uniaxiality and confirming the proposed non-tilted  $\text{HexB}$  structure. Upon heating, a resonant peak corresponding to twice the  $d$ -value of the non-resonant (01) layer scattering occurs in the temperature range between  $87$  and  $91^\circ\text{C}$  (see Fig. 11c and Table S6, Fig. S15, ESI<sup>†</sup>), indicating a two-layer unit cell and thus an anticlinic  $\text{SmC}_a$  structure in the biaxial

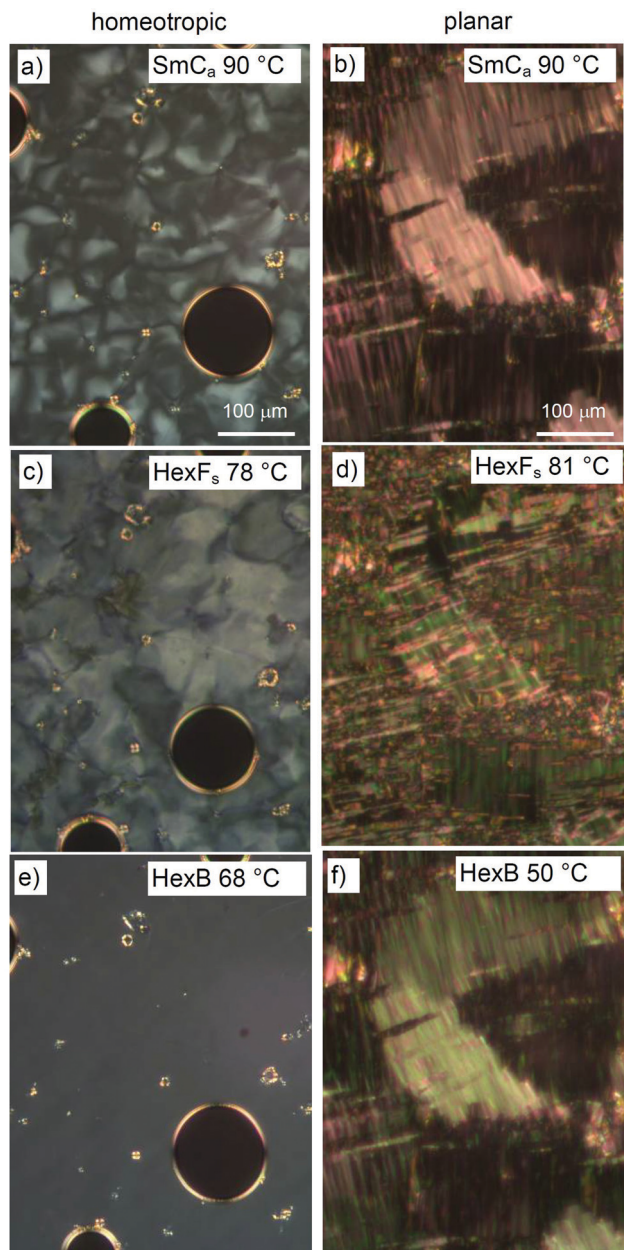


**Fig. 7** Textures observed for the distinct smectic phases of compound **7** in homeotropic (left) and a planar alignment (right) at the indicated temperatures; the textures at the left were observed between plain microscopy glass plates, whereas those right were recorded in a 6 μm PI-coated ITO cell; in homeotropic alignment the birefringence decreases, whereas in planar alignment the birefringence grows with lowering temperature.

phase immediately following the HexB phase on heating (Table 1). Therefore, we attribute this temperature range to an anticlinic SmC<sub>a</sub> phase. Above 91 °C the resonant peak is lost and only the non-resonant layer reflection can be observed, meaning that this smectic phase cannot be anticlinic. It also excludes a short pitch helical phase structure<sup>45,46</sup> as the origin of optical uniaxiality of this tilted smectic phase in the temperature range between 91 and 94 °C. Even the birefringent SmC phase, observed above 94 °C

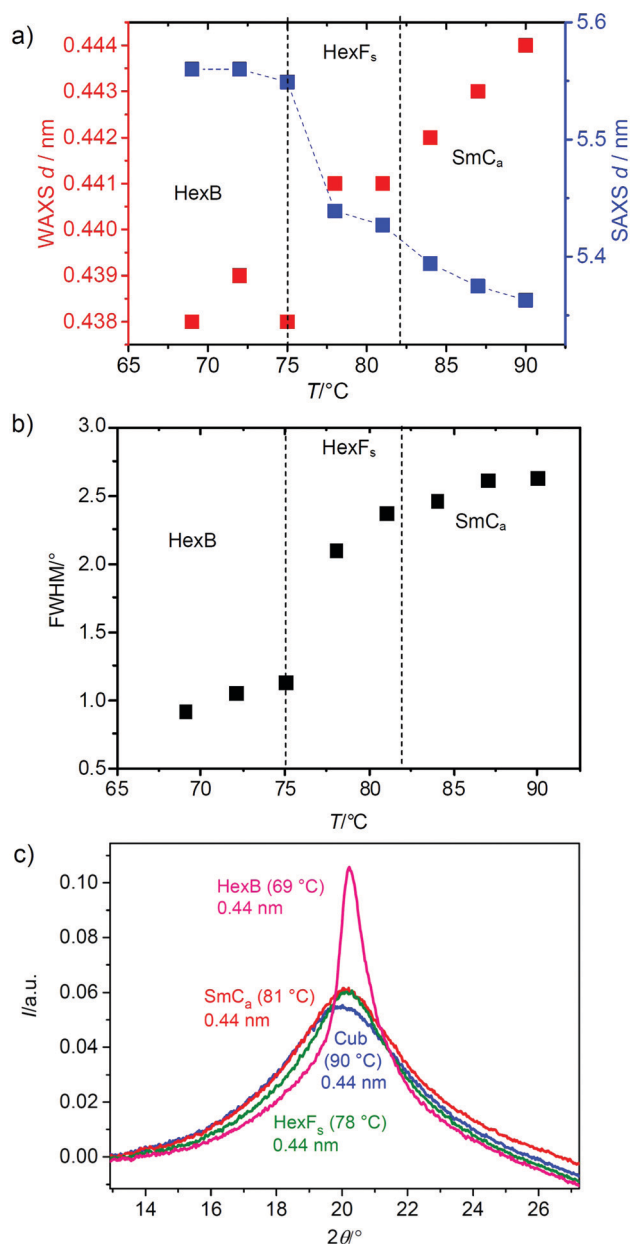


**Fig. 8** XRD of compound **7** in the different mesophases: (a) temperature dependence of the  $d$ -spacing of the SAXS reflections and the WAXS maximum; (b) FWHM and (c) line-shape of the WAXS as a function of temperature with  $d$ -values of the scattering maxima (see also Fig. S8 and Table S1, ESI†).

and up to the transition to the cubic phase, does not show a resonant scattering and therefore cannot be a SmC<sub>a</sub> phase. This is in line with textural observations showing that in the planar fan textures the dark extinctions become slightly birefringent above 94 °C (Fig. S5, ESI†). This could be due to a developing synclinal tilt in the temperature range designated as SmC. This anticlinic to synclinal transition could in principle take place *via* a helical intermediate phase.<sup>45,46</sup> However, there is no RSoXS indication for any helical pitch in the length range covered by the used experimental setup (< 40 nm).<sup>112–114</sup> Therefore, this uniaxial phase range

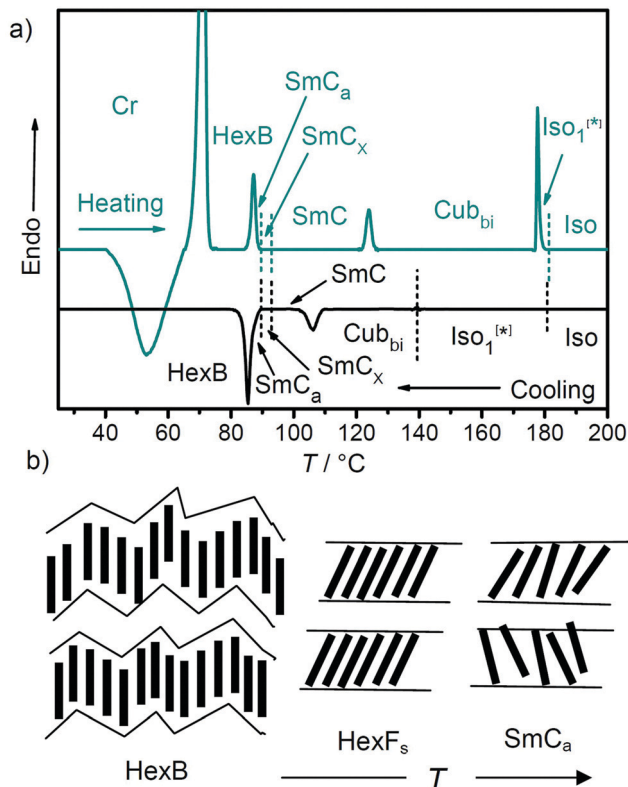


Fig. 9 (a) DSC heating and cooling traces ( $10 \text{ K min}^{-1}$ ) of compound **8** with the phase sequence HexB–SmC<sub>a</sub>–SmC<sub>x</sub>–SmC–Iso<sub>1</sub><sup>[\*]</sup>–Iso and (b) sketch showing the HexB–HexF<sub>s</sub>–SmC<sub>a</sub> transition of compound **7**.

between 91 and 94 °C is tentatively designated as SmC<sub>x</sub>. The optical uniaxiality of the tilted smectic phase could be explained by a longer helix outside the range covered by the RSoXS experiments or by a randomization of the tilt correlation between the layers. Interestingly, in the SmC<sub>x</sub> range there is the coexistence of the non-resonant layer reflections of the SmC and SmC<sub>a</sub> phases (red and blue dots in Fig. 11a), so that uniaxiality could alternatively result from macroscopic tilt randomization due to the development of a synclinc + anticlinic microdomain structure in this temperature range.

Overall, in the smectic phase range there is an increasing tendency towards development of synclinc tilt with growing chain length, but only for compound **8** it obviously becomes more dominating in the high temperature range of the SmC phase. However, even for this compound, at lower temperature there is still a tendency of the swallow-tailed molecules to assume an anticlinic tilt, which we attribute to the contribution of the Y-shaped conformation (Fig. 4d). In this conformation, the out-of-plane interlayer fluctuations are suppressed and hence the anticlinic tilt is favoured. Because for compound **8** the tilt is relatively small, there appears to be no discrete synclinc–anticlinic transition, but instead this transition takes place either in a disordered way by an intermediate loss of tilt correlation or *via* a long pitch helical structure.

After transformation to the SmC<sub>a</sub> phase, further cooling of compound **8** leads to the non-tilted HexB phase. However, for

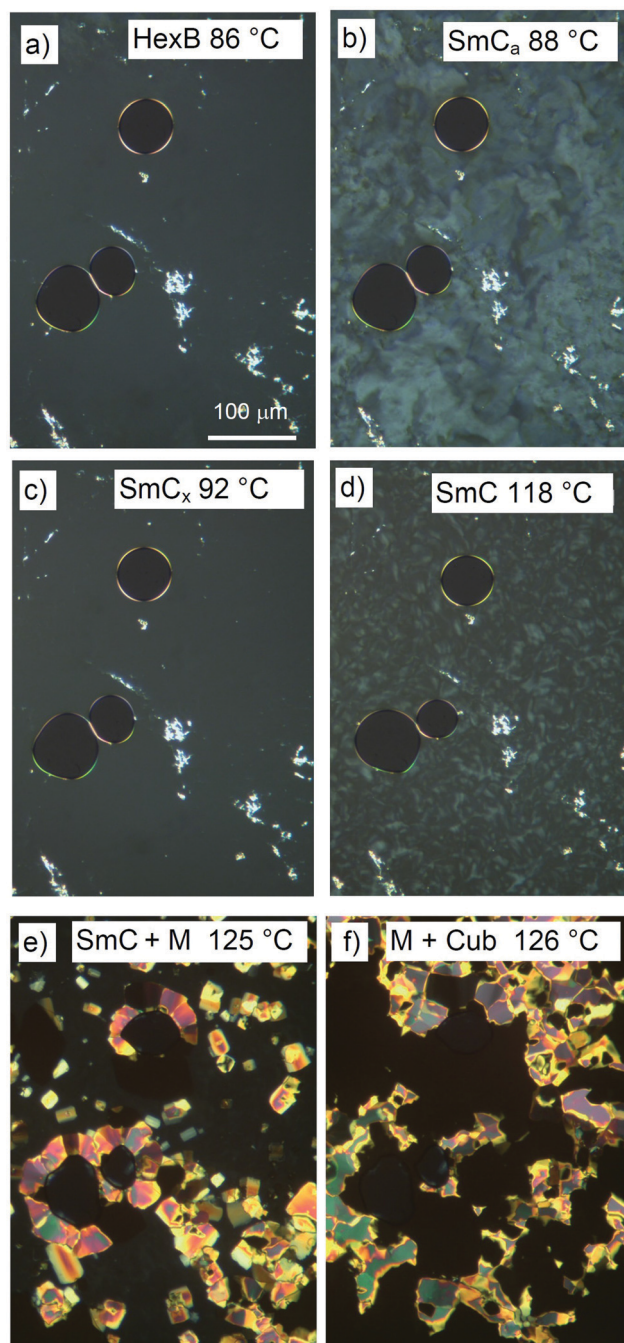


Fig. 10 Textures of compound **8** as observed on heating (after cooling from the isotropic liquid state) in homeotropic alignment (between plain microscopy glass plates) in the designated phases at the given temperatures. (a–d) show the transition between the different lamellar phases and (e and f) show the transition to the Cub<sub>bi</sub> phase. In (e) the majority of the dark area is the homeotropic SmC<sub>a</sub> phase (the low birefringent Schlieren texture is invisible due to the shorter exposure time compared to (d)) whereas in (f) the dark areas represent the growing cubic phase.

the next longer homologues **9–12** the hexatic phase becomes biaxial again and according to XRD form HexI<sub>s</sub> phases (Fig. S6, S7, S10 and S11, ESI<sup>†</sup>). This indicates a HexF<sub>s</sub>–HexB–HexI<sub>s</sub> sequence with a re-entrance of synclinc tilt in the hexatic phases upon chain elongation. A possible model for the HexB

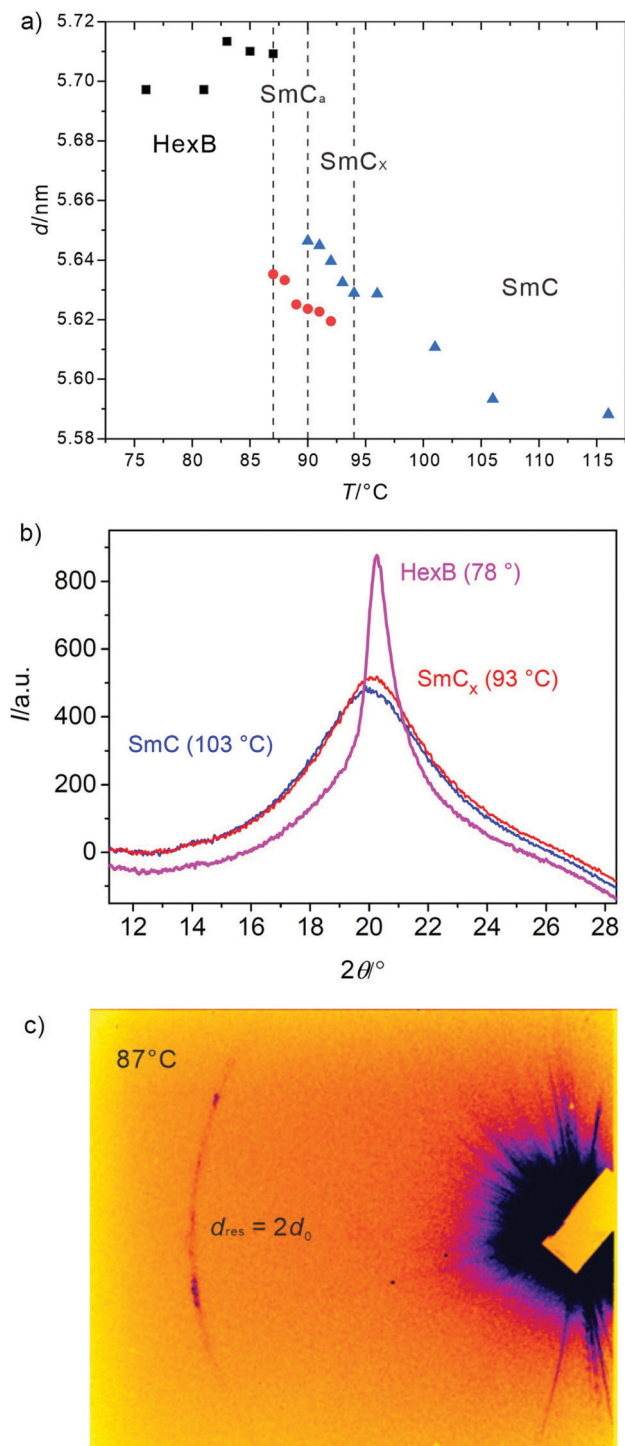


Fig. 11 (a)  $d$ -Spacings of the non-resonant (10) reflection observed on second heating in the lamellar phases of compound **8** (see Fig. S9 and Tables S2, S3 for higher order reflections and WAXS data, ESI†) and (b) profiles of the wide angle scatterings; (c) shows the resonant scattering (CCD image) at 87 °C on heating (for more details see Fig. S15 and Table S6, ESI†).

phase, which explains this unexpected sequence, could be based on a modulated HexI<sub>s</sub> structure with a layer modulation by anticlinic defects in the form of closed contour loops, as

proposed by Korlacki *et al.* (Fig. 9b).<sup>115</sup> Thus, the fundamental layer correlation in the hexatic phases is synclinic for all compounds **8–12**, despite optical investigations indicate a HexF<sub>s</sub>–HexB–HexI<sub>s</sub> sequence with a re-entrance of synclinic tilt upon chain elongation. For the long chain homologues **10** and **12** the non-modulated synclinic HexI<sub>s</sub> phase remains the only lamellar phase occurring below the Cub<sub>bi</sub> phase (Fig. S11 and Table S5, ESI†). Moreover, it appears that with growing chain length the HexF<sub>s</sub> phase range tightens and for compound **8** it is removed and completely replaced by the HexB phase. Therefore, it is likely that the HexB phase represents an intermediate structure between HexF<sub>s</sub> and HexI<sub>s</sub> if the tilt is small and the synclinic correlation weak. For longer chains the synclinic tilt becomes larger and stronger, and this leads to the dominance of HexI<sub>s</sub>.

### 3.1.4 Cubic and non-cubic 3D phases of compounds 7–12.

An optically isotropic Cub<sub>bi</sub> phase was observed for all compounds with chain length  $n = 7–12$  as high temperature phase. The  $1/d$  values appear in a ratio  $\sqrt{6}:\sqrt{8}:\sqrt{14}:\sqrt{16}...$ , which can be indexed to a cubic lattice with  $Ia\bar{3}d$  symmetry and cubic lattice parameters  $a_{\text{cub}} = 10.0 \pm 0.4$  nm (see Table S5, ESI†). As shown in Fig. 1, the Cub<sub>bi</sub> phase occurs at a chain length of  $n \geq 7$  and replaces the SmA phase. For compounds **7** and **8** the tilted smectic phases are retained below this Cub<sub>bi</sub> phase, whereas for longer chain lengths ( $n = 9–12$ ) only the HexI<sub>s</sub> phase is observed besides the dominating Cub<sub>bi</sub> phase (see data of compound **9** in Fig. S6 and S9, ESI†). Due to the hysteresis of the lamellar–Cub<sub>bi</sub> transition some of the lamellar phases of the longer homologues can only be observed on heating.

The formation of these Cub<sub>bi</sub> phase is the result of increasing interface curvature between the aromatic cores and the aliphatic chains, growing with the chain length  $n$  and temperature (Fig. 1). In addition, increasing chain length  $n$  leads to a growing incompatibility of these chains with the aromatic cores. Thus, these chains become more likely to be expelled out of the aromatic layers into the layers of the 3,5-chains (transition  $c \rightarrow b \rightarrow a$  in Fig. 4), where they further increase the steric distortion of flat layers and support the development of saddle-splay curvature. As also shown in Fig. 12, the lateral distance between the two enantiomorphic nets in the  $Ia\bar{3}d$  phase (Fig. 13h), calculated according to  $d_{\text{net,cub}} = \sqrt{3}(a_{\text{cub}}/4)$  is significantly shorter than the molecular length and this difference increases with the alkyl chain length  $n$ . This indicates a completely segregated organization of polyaromatic cores and alkyl chains (Fig. 4a) in the Cub<sub>bi</sub> phases; the remaining difference between  $d_{\text{net}}$  and  $L_{\text{mol}}$  is due to additional chain folding, required to fill the space around the networks completely.

Simultaneously with the transition from the SmC<sub>a</sub> or SmC<sub>s</sub> phase to the cubic phase on heating, highly birefringent areas with rectangular shape develop in the homeotropic samples of compounds **7** and **8**, respectively (M-phase, see Fig. 10e, f and Fig. S4, ESI†). These birefringent domains have a high viscosity and rapidly disappear and transform into the cubic phase, indicating that this birefringent mesophase is metastable with respect to the cubic phase and presumably represents a distorted cubic lattice, probably with tetragonal or orthorhombic symmetry. This metastable M phase is absent for the higher homologues and

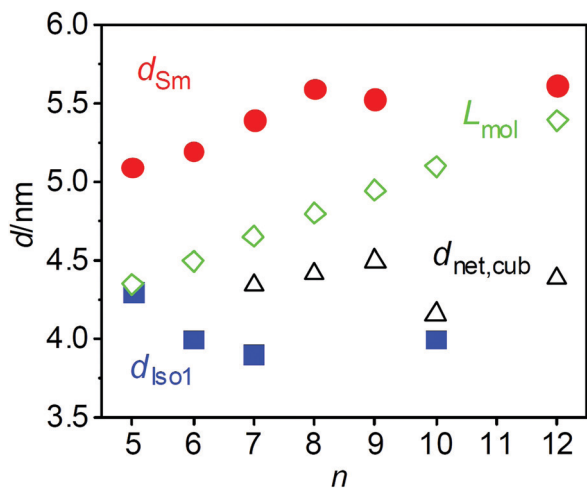


Fig. 12 Development of the  $d$ -values of the layer reflection in the lamellar phase ( $d_{Sm}$ ; **5**: SmA, **6–8**: SmC<sub>a</sub>, **9,12**: HexI<sub>s</sub>), position of the diffuse small angle scattering maximum in the Iso<sub>1</sub>/Iso<sub>1</sub><sup>[\*]</sup> phases ( $d_{Iso1}$ , 2 K below the Iso–Iso<sub>1</sub>/Iso<sub>1</sub><sup>[\*]</sup> transition), network distance in the Cub<sub>bi</sub>/*Ia*3*d* phase ( $d_{net,cub}$ ) and molecular length ( $L_{mol}$ ) depending on chain length ( $n$ ); for lattice parameters of the cubic phases, see Table S5 (ESI<sup>†</sup>).

thus is considered as another competing intermediate structure at the lamellar–Cub<sub>bi</sub> transition. Details of the structure of the Cub<sub>bi</sub>/*Ia*3*d* phases, representing two helical networks with opposite handedness (Fig. 13h) have been discussed previously.<sup>23,60,110</sup>

**3.1.5 Percolated Iso<sub>1</sub> and Iso<sub>1</sub><sup>[\*]</sup> phases of compounds 5–12.** The Iso–Cub transition on cooling is significantly delayed by 19–53 K and is decreasing with growing  $n$ . The Cub<sub>bi</sub> phases of compounds 7–12 are not directly formed from the ordinary isotropic liquid (Iso), but there is a small region of a chiral (Iso<sub>1</sub><sup>[\*]</sup>) or achiral (Iso<sub>1</sub>) liquid mesophase before the transition to the Cub<sub>bi</sub> phase (Table 1, Fig. 13c, d and Fig. S1, ESI<sup>†</sup>). For compounds 5–8 the mirror symmetry broken Iso<sub>1</sub><sup>[\*]</sup> phase, characterized by fluid conglomerates of chiral domains with opposite handedness (see Fig. 13a–c),<sup>12,21,22,52,60</sup> occurs either between the achiral Iso phase and SmA ( $n = 5, 6$ ) or between Iso and Cub<sub>bi</sub> ( $n = 7, 8$ , see Table 1 and Fig. 1). The DSC traces of the long chain homologues 9–12 indicate a broad transition to an achiral Iso<sub>1</sub> phase occurring between the achiral Iso and Cub<sub>bi</sub>/*Ia*3*d* phases on cooling (Fig. 13d), whereas on heating a direct Cub<sub>bi</sub>/*Ia*3*d*–Iso transition takes place. Hence, the achiral Iso<sub>1</sub> phase of compounds 9–12 is only monotropic. In the Iso<sub>1</sub> and Iso<sub>1</sub><sup>[\*]</sup> ranges there are two diffuse XRD scatterings, one in the small and the other in the wide angle region of the XRD patterns. This is in line with the presence of only short range order, as typical for isotropic liquids with a locally ordered cluster structure (cybotaxis)<sup>116,117</sup> and for percolated liquids<sup>118</sup> often occurring besides frustrated LC phases (blue phases, twist grain boundary phases, SmQ phases, *etc.*).<sup>119–124</sup>

As shown in Fig. 14 for compound **10**, as example, the change of the line width of the XRD small angle scattering at the Iso–Iso<sub>1</sub> transition is continuous without any distinct jump, as also found for the Iso–Iso<sub>1</sub><sup>[\*]</sup> transitions.<sup>21,25</sup> The correlation length calculated with the Scherrer equation (assuming  $K = 1$ ) is ~10 nm in the Iso phase at 180 °C and continuously grows to

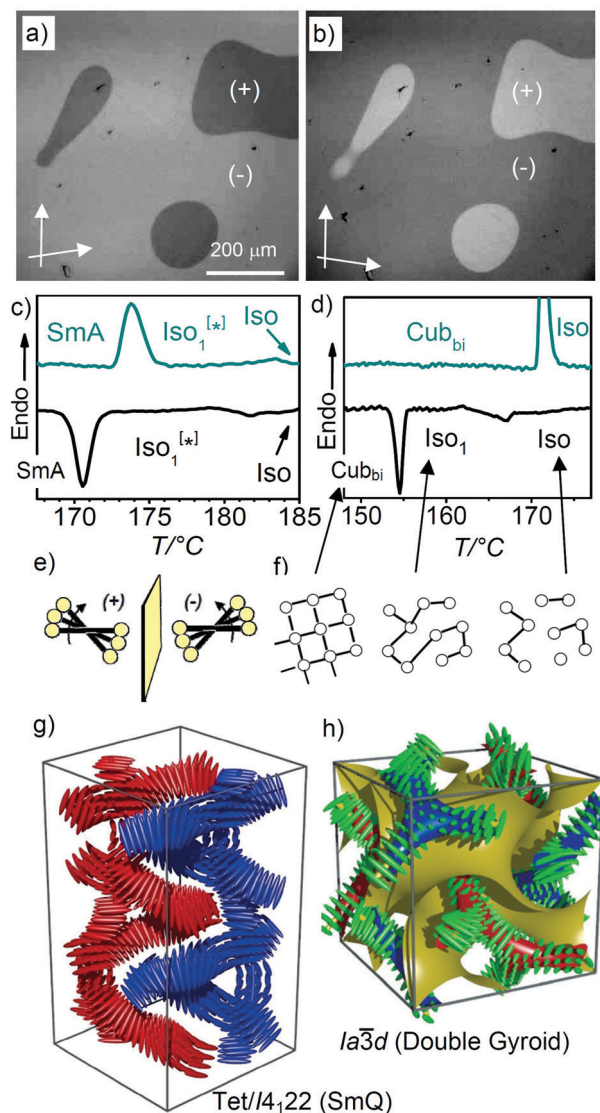


Fig. 13 (a and b) Chiral domains in the Iso<sub>1</sub><sup>[\*]</sup> phase of compound **6** at  $T = 104$  °C as observed by polarizing microscopy between slightly uncrossed polarizers; changing the twist between the polarizer from  $<90^\circ$  to  $>90^\circ$  leads to an inversion of the brightness of the domains, indicating the optical rotation in opposite directions (contrast enhanced); (c) and (d) expanded sections of the DSC traces showing (c) the Iso–Iso<sub>1</sub><sup>[\*]</sup> transition of **6** on heating (top) and cooling (bottom, for complete curves, see Fig. S1, ESI<sup>†</sup>) and (d) the Iso–Iso<sub>1</sub> transition of compound **10**; (e) shows the origin of the helical superstructure due to the clashing of the bulky end chains of the rod-like molecules (yellow dots) arranged with the molecular long axis perpendicular to the local network direction; (f) illustrates the development of the networks (from right to left) by fusing short helical segments to clusters in the Iso range, followed by dynamic network formation in Iso<sub>1</sub>, and long range transmission of helicity in Iso<sub>1</sub><sup>[\*]</sup>, and finally leading to the establishment of the long range cubic lattice after further increase of the network connectivity; (g) and (h) show the helical structures in the (g) SmQ phase (with uniform helix sense in blue and red networks and four-way junctions) and (h) *Ia*3*d* phase (with opposite helix sense in blue and red networks and three way junctions; the minimal surface separating the networks is shown in yellow), assumed to represent the local structures in the chiral Iso<sub>1</sub><sup>[\*]</sup> and the achiral Iso<sub>1</sub> phase, respectively; (g) and (h) were reproduced with permission from ref. 37 and 23, respectively, by permission from Wiley–VCH.

~14 nm in the Iso<sub>1</sub> phase at 165 °C, corresponding to a bit more than just one cubic unit cell. The transition from the chiral Iso<sub>1</sub><sup>[\*]</sup> phase to the achiral Iso<sub>1</sub> phase upon chain elongation occurs from  $n = 8$  to 9 and could either be due to a decreasing network connectivity, falling below the critical length for long range chirality transmission, or due to a change of the local structure. It is chiral, presumably SmQ-like (Fig. 13g),<sup>37</sup> for the chiral Iso<sub>1</sub><sup>[\*]</sup> phase of compounds 5–8 and likely to be achiral (racemic) *Ia* $\bar{3}d$ -like (Fig. 13h) for the achiral Iso<sub>1</sub> phase of the longer homologues 9–12.<sup>25,27</sup> Remarkably, the Iso<sub>1</sub><sup>[\*]</sup>–Iso<sub>1</sub> transition coincides with the disappearance of the M phase, which therefore might represent a mesophases related to the local network structure in the accompanying Iso<sub>1</sub><sup>[\*]</sup> phase. A long-range or local (cybotactic) helical structure being related to the SmQ phase (Fig. 13g) is therefore likely for the M and the Iso<sub>1</sub><sup>[\*]</sup> phase, respectively. With growing chain length the interfacial curvature increases, which leads to a transition from four-way to three-way junctions and formation of a long range or local achiral *Ia* $\bar{3}d$  structure in the Cub<sub>bi</sub> and Iso<sub>1</sub> phases.

### 3.2. Fluorinated compounds 6F and 6F<sub>2</sub>

For compound 6 the influence of introduction of one or two fluorine atoms into the polyaromatic core at the monosubstituted peripheral benzene ring was investigated. Both compounds 6F and 6F<sub>2</sub> (Scheme 1 and Table 1) show exclusively the Cub<sub>bi</sub>/*Ia* $\bar{3}d$  phase (6F:  $a_{\text{Cub}} = 9.48$  nm; 6F<sub>2</sub>:  $a_{\text{Cub}} = 9.35$  nm) which is achiral and does not transform into a smectic phase nor crystallizes on cooling; crystallization is only observed on re-heating (see DSCs in Fig. S1g and h, ESI<sup>†</sup>). Fig. 15 shows the diffraction pattern and the reconstructed electron density map of the Cub<sub>bi</sub> phase of 6F, as an example, confirming the *Ia* $\bar{3}d$  lattice and the bicontinuous network structure (see Fig. S13, ESI<sup>†</sup> for XRD of 6F<sub>2</sub>). Compared with the non-fluorinated compound 6, which only forms smectic LC phases and the Iso<sub>1</sub><sup>[\*]</sup> phase, for both fluorinated compounds 6F and 6F<sub>2</sub> the Iso<sub>1</sub><sup>[\*]</sup> phases as well as the lamellar phases are completely removed. Core fluorination reduces the electron density of the  $\pi$ -system and thus increases the attractive core–core interactions,

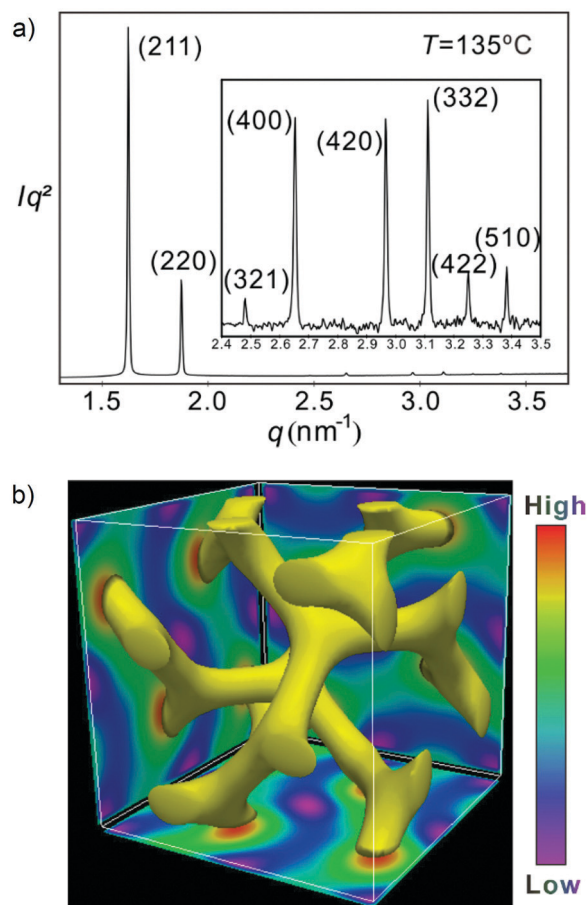


Fig. 15 (a) SAXS diffractogram of compound 6F at 135 °C, the experimental and calculated  $d$ -spacing of the observed SAXS reflection are given in Table S4 (ESI<sup>†</sup>); for WAXS data, see Fig. S14 (ESI<sup>†</sup>); (b) reconstructed 3D electron density map obtained from this powder pattern, showing the network structure of the *Ia* $\bar{3}d$  phase; for electron density histogram, see Fig. S12 (ESI<sup>†</sup>); for XRD data of 6F<sub>2</sub>, see Fig. S13 and Table S5 (ESI<sup>†</sup>).

which obviously excludes the terminal alkyl chains from intercalation (Fig. 4a and b).<sup>125–128</sup> This is confirmed by the lateral distances between the networks, which are 4.10 nm (6F) and 4.05 nm (6F<sub>2</sub>), respectively, being significantly smaller than the fully stretched molecular length ( $L_{\text{mol}} = 4.5$  nm, Fig. 4a). This organization provides increased interface curvature despite of the larger diameter of the fluorinated aromatic cores (Fig. 4a and c). The thus increased interface curvature between aromatic and aliphatic domains favours the Cub<sub>bi</sub>/*Ia* $\bar{3}d$  phase with an achiral (racemic) long range network structure.

## 4. Summary and conclusions

A series of achiral azobenzene-based tricatena molecules with a 3,5-disubstitution pattern at one end is reported. This series of compounds provides a rich variety of distinct modes of LC self-assembly. It includes hexatic phases (HexF<sub>s</sub>, HexI<sub>s</sub>, HexB), a non-tilted SmA phase, synclitic and anticlitic tilted smectic C phases (SmC, SmC<sub>x</sub>, SmC<sub>a</sub>), a bicontinuous cubic phase with *Ia* $\bar{3}d$  lattice, a non-cubic birefringent phase with 3D lattice and

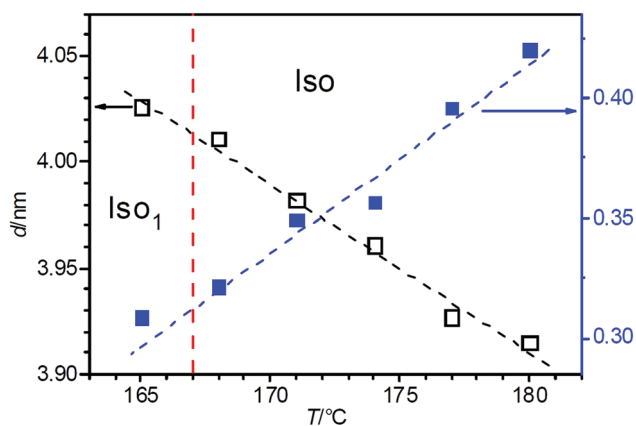


Fig. 14 Development of  $d$ -values and line width (FWHM) of the small angle scattering maximum of compound 10 across the Iso–Iso<sub>1</sub> transition as recorded on cooling.



chiral ( $\text{Iso}_1^{[*]}$ ) as well as achiral ( $\text{Iso}_1$ ) isotropic liquid mesophases. Especially notable are the broad regions of the rare  $\text{SmC}_a$  phases achieved with these achiral compounds, providing a new design concept for anticlinic smectics, eventually leading to practically important orthoconic LCs.<sup>95</sup> Moreover, the phase transition from smectic to hexatic phases is associated with a change of the layer correlation from anticlinic to synclinic on cooling, which is opposite to the usually observed  $\text{SmC}_s$  to  $\text{SmC}_a$  transitions. Obviously the alkyl chains in the 3,5-positions lead to a Y-shaped molecular conformation (Fig. 4d) which supports the anticlinic tilt. An increasing contribution of *trans*-conformers in the alkyl chains at lower temperature reduces the effects of chain disorder and supports the parallel alignment of the alkyl chain, thus leading to the development of a tuning fork like conformation (Fig. 4c), allowing improved out-of-plane inter-layer fluctuations and thus leading to the emergence of synclinic tilt correlation. Simultaneously, this conformation enables a denser packing, thus favouring the development of hexatic phases. This means that the anticlinic–synclinic and the smectic–hexatic transition are coupled.

Another remarkable feature of these compounds is the development of a helical twist in the chiral  $\text{Iso}_1^{[*]}$  phase. These chirality synchronized isotropic liquid phases ( $\text{Iso}_1^{[*]}$ ) occur for compounds with medium alkyl chain length ( $n = 5\text{--}8$ ). Upon further chain elongation ( $n \geq 9$ ) only achiral percolated  $\text{Iso}_1$  phases can be observed (Fig. 1). Development of these  $\text{Iso}_1/\text{Iso}_1^{[*]}$  phases is explained by dynamic network formation after crossing a critical connectivity of the helical aggregates (Fig. 13f), and if, in addition, a homogeneously chiral (e.g.,  $\text{SmQ}$ -like, Fig. 13g) local network structure can develop in the  $\text{Iso}_1^{[*]}$  phase. If the critical network density is not achieved or an achiral network structure (e.g.,  $Ia\bar{3}d$ , Fig. 13f) is preferred, then the percolated network liquid is achiral ( $\text{Iso}_1$ ).

Finally the peripheral fluorination of the aromatic core unit was found to be a powerful tool for stabilization of bicontinuous cubic phases of polycatenar compounds. Though cubic phases are usually found only in relatively small temperature ranges, for the fluorinated compounds **6F** and **6F<sub>2</sub>** wide ranges, even extended below ambient temperature, were observed. This effect of core fluorination is opposite to central core fluorination of other (symmetric) polycatenars which is known to give only smectic phases.<sup>129</sup> Functionality of the reported compounds is provided by the organization of the azobenzene units either in an anticlinic or helical fashion and the possibility of light-induced switching the molecular shape and phase type by *trans*–*cis* isomerization. This was recently demonstrated for chirality switching<sup>58</sup> and could lead to numerous potential applications as photo-tuneable optical and photonic materials.<sup>130</sup>

## Conflicts of interest

There are no conflicts to declare.

## Acknowledgements

This work was supported by the Deutsche Forschungsgemeinschaft (Ts 39/24-2, AL 2378/1-1), the National Natural Science

Foundation of China (No. 21761132033, 21374086). The authors are grateful to Beamline BL16B1 at SSRF (Shanghai Synchrotron Radiation Facility, China) for providing the beamtime. This research used beamline 11.0.1.2 of the Advanced Light Source, which is a DOE Office of Science User Facility under contract no. DE-AC02-05CH11231. Y. C. thanks China Scholarship Council (CSC) for providing financial support (Program No. 201706280170) and ALS Doctoral Fellowship in Residence Program.

## References

- 1 N. Koide, *The Liquid Crystal Display Story*, Springer, Tokyo, 2014.
- 2 T. Kato, J. Uchida, T. Ichikawa and T. Sakamoto, *Angew. Chem., Int. Ed.*, 2018, **57**, 4355.
- 3 S. Sergeev, W. Pisula and Y. H. Geerts, *Chem. Soc. Rev.*, 2007, **36**, 1902.
- 4 W. Pisula, M. Zorn, J. Y. Chang, K. Müllen and R. Zentel, *Macromol. Rapid Commun.*, 2009, **30**, 1179.
- 5 T. Kato, M. Yoshio, T. Ichikawa, B. Soberats, H. Ohno and M. Funahashi, *Nat. Rev. Mater.*, 2017, **2**, 17001.
- 6 C. Sinturel, F. S. Bates and M. A. Hillmyer, *ACS Macro Lett.*, 2015, **4**, 1044.
- 7 K. Nickmans and A. P. Schenning, *Adv. Mater.*, 2018, **30**, 1703713.
- 8 A. Lehmann, A. Scholte, M. Prehm, F. Liu, X. B. Zeng, G. Ungar and C. Tschierske, *Adv. Funct. Mater.*, 2018, **28**, 1804162.
- 9 C. Tschierske, *Angew. Chem., Int. Ed.*, 2013, **52**, 8828.
- 10 *Chirality in Liquid Crystals*, ed. H. S. Kitzerow and C. Bahr, Springer, New York, 2001.
- 11 I. Nishiyama, *Chem. Rec.*, 2009, **9**, 340.
- 12 C. Tschierske, *Liq. Cryst.*, 2018, **45**, 2221.
- 13 *Handbook of Liquid Crystals*, ed. J. W. Goodby, P. J. Collings, T. Kato, C. Tschierske, H. F. Gleeson and P. Raynes, Wiley-VCH, Weinheim, 2nd edn, 2014.
- 14 R. A. Reddy and C. Tschierske, *J. Mater. Chem.*, 2006, **16**, 907.
- 15 A. Eremin and H. Takezoe, *Bent-shaped Liquid Crystals. Structures and Physical Properties*, CRC Press, Taylor & Francis Group, Boca Raton, FL, 2017.
- 16 J. Malthete, H. T. Nguyen and C. Destrade, *Liq. Cryst.*, 1993, **13**, 171.
- 17 (a) H.-T. Nguyen, C. Destrade and J. Malthete, *Adv. Mater.*, 1997, **9**, 375; (b) M. Gharbia, A. Gharbi, H. T. Nguyen and J. Malthete, *Curr. Opin. Colloid Interface Sci.*, 2002, **7**, 312.
- 18 (a) D. Fazio, C. Mongin, B. Donnio, Y. Galerne, D. Guillon and D. W. Bruce, *J. Mater. Chem.*, 2001, **11**, 2852; (b) D. W. Bruce, *Acc. Chem. Res.*, 2000, **33**, 831.
- 19 W. Weissflog, in *Handbook of Liquid Crystals*, ed. J. W. Goodby, P. J. Collings, T. Kato, C. Tschierske, H. F. Gleeson and P. Raynes, Wiley-VCH, Weinheim, 2nd edn, 2014, vol. 5, pp. 89–174.

- 20 T. Yasuda, H. Ooi, J. Morita, Y. Akama, K. Minoura, M. Funahashi, T. Shimomura and T. Kato, *Adv. Funct. Mater.*, 2009, **19**, 411.
- 21 C. Dressel, T. Reppe, M. Prehm, M. Brautzsch and C. Tschierske, *Nat. Chem.*, 2014, **6**, 971.
- 22 C. Tschierske and G. Ungar, *ChemPhysChem*, 2016, **19**, 9.
- 23 C. Dressel, F. Liu, M. Prehm, X.-B. Zeng, G. Ungar and C. Tschierske, *Angew. Chem., Int. Ed.*, 2014, **53**, 13115.
- 24 T. Reppe, C. Dressel, S. Poppe and C. Tschierske, *Chem. Commun.*, 2020, **56**, 711.
- 25 T. Reppe, S. Poppe, X. Cai, Y. Cao, F. Liu and C. Tschierske, *Chem. Sci.*, 2020, **11**, 5902.
- 26 C. Dressel, T. Reppe, S. Poppe, M. Prehm, H. Lu, X. Zeng, G. Ungar and C. Tschierske, *Adv. Funct. Mater.*, 2020, 2004353.
- 27 T. Reppe, S. Poppe and C. Tschierske, *Chem. – Eur. J.*, 2020, **26**, DOI: 10.1002/chem.20200286.
- 28 J. Kain, S. Diele, G. Pelzl, C. Lischka and W. Weissflog, *Liq. Cryst.*, 2000, **27**, 11.
- 29 A.-M. Levelut, B. Donnio and D. W. Bruce, *Liq. Cryst.*, 1997, **22**, 753.
- 30 (a) T. Yamamoto, I. Nishiyama, M. Yoneya and H. Yokoyama, *J. Phys. Chem. B*, 2009, **113**, 11564; (b) M. Yoneya, *Chem. Rec.*, 2011, **11**, 66.
- 31 X. Zeng, G. Ungar and M. Imp  rator-Clerc, *Nat. Mater.*, 2005, **4**, 562.
- 32 X. B. Zeng and G. Ungar, *J. Mater. Chem. C*, 2020, **8**, 5389.
- 33 A. M. Levelut, C. Germain, P. Keller, L. Liebert and J. Billard, *J. Phys.*, 1983, **44**, 623.
- 34 A. M. Levelut, E. Hallouin, D. Bennemann, G. Heppke and D. Loetzsch, *J. Phys. II*, 1997, **7**, 981.
- 35 B. Pansu, Y. Nastishin, M. Imperor-Clerc, M. Veber and H. T. Nguyen, *Eur. Phys. J. E: Soft Matter Biol. Phys.*, 2004, **15**, 225.
- 36 M. Vogrin, N. Vaupot  c, M. M. Wojcik, J. Mieczkowski, K. Madrak, D. Pocięcha and E. Gorecka, *Phys. Chem. Chem. Phys.*, 2014, **16**, 16067.
- 37 H. Lu, X. Zeng, G. Ungar, C. Dressel and C. Tschierske, *Angew. Chem., Int. Ed.*, 2018, **57**, 2835.
- 38 H. Takezoe, *Top. Curr. Chem.*, 2011, **318**, 303.
- 39 M. Alaasar, M. Prehm and C. Tschierske, *Chem. – Eur. J.*, 2016, **22**, 6583.
- 40 K. V. Le, H. Takezoe and F. Araoka, *Adv. Mater.*, 2017, **29**, 1602737.
- 41 S. Shadpour, A. Nemati, N. J. Boyd, L. Li, M. E. Pr  v  t, S. L. Wakerlin, J. P. Vanegas, M. Salamo  czyk, E. de Hegmann, C. Zhu, M. R. Wilson, A. I. J  kli and T. Hegmann, *Mater. Horiz.*, 2019, **6**, 959.
- 42 M. Kurata and A. Yoshizawa, *Chem. Commun.*, 2020, **56**, 8289.
- 43 G. Dantlgraber, A. Eremin, S. Diele, A. Hauser, H. Kresse, G. Pelzl and C. Tschierske, *Angew. Chem., Int. Ed.*, 2002, **41**, 2408.
- 44 L. E. Hough, M. Spannuth, M. Nakata, D. A. Coleman, C. D. Jones, G. Dantlgraber, C. Tschierske, J. Watanabe, E. K  rblova, D. M. Walba, J. E. Maclennan, M. A. Glaser and N. A. Clark, *Science*, 2009, **325**, 452.
- 45 (a) S. P. Sreenilayam, Y. P. Panarin, J. K. Vij, V. P. Panov, A. Lehmann, M. Poppe, M. Prehm and C. Tschierske, *Nat. Commun.*, 2016, **7**, 11369; (b) A. A. S. Green, M. R. Tuchband, R. Shao, Y. Shen, R. Visvanathan, A. E. Duncan, A. Lehmann, C. Tschierske, E. D. Carlson, E. Guzman, M. Kolber, D. M. Walba, C. S. Park, M. A. Glaser, J. E. Maclennan and N. A. Clark, *Phys. Rev. Lett.*, 2019, **122**, 107801; (c) A. Lehmann, M. Alaasar, M. Poppe, S. Poppe, M. Prehm, M. Nagaraj, S. P. Sreenilayam, Y. P. Panarin, J. K. Vij and C. Tschierske, *Chem. – Eur. J.*, 2020, **26**, 4714.
- 46 M. Salamo  czyk, N. Vaupot  c, D. Pocięcha, R. Walker, J. M. D. Storey, C. T. Imrie, C. Wang, C. Zhu and E. Gorecka, *Nat. Commun.*, 2019, **10**, 1922.
- 47 D. A. Paterson, J. Xiang, G. Singh, R. Walker, D. M. Agra-Kooijman, A. Martinez-Felipe, M. Gao, J. M. D. Storey, S. Kumar, O. D. Lavrentovich and C. T. Imrie, *J. Am. Chem. Soc.*, 2016, **138**, 5283.
- 48 R. J. Mandle and J. W. Goodby, *Chem. – Eur. J.*, 2019, **25**, 14454.
- 49 W. D. Stevenson, X. B. Zeng, C. Welch, A. K. Thakur, G. Ungar and G. H. Mehl, *J. Mater. Chem. C*, 2020, **8**, 1041.
- 50 V. Borshch, Y.-K. Kim, J. Xiang, M. Gao, A. Jakli, V. P. Panov, J. K. Vij, C. T. Imrie, M. G. Tamba, G. H. Mehl and O. D. Lavrentovich, *Nat. Commun.*, 2013, **4**, 2635.
- 51 C. Dressel, W. Weissflog and C. Tschierske, *Chem. Commun.*, 2015, **51**, 15850.
- 52 C. Tschierske and C. Dressel, *Symmetry*, 2020, **12**, 1098, DOI: 10.3390/sym12071098.
- 53 H. M. D. Bandara and S. C. Burdette, *Chem. Soc. Rev.*, 2012, **41**, 1809.
- 54 (a) H. K. Bisoyi and Q. Li, *Chem. Rev.*, 2016, **116**, 15089; (b) M. Alaasar, *Liq. Cryst.*, 2016, **43**, 2208.
- 55 (a) X. Peng, H. Gao, Y. Xiao, H. Cheng, F. Huang and X. Cheng, *New J. Chem.*, 2017, **41**, 2004; (b) M. Alaasar, S. Poppe and C. Tschierske, *J. Mol. Liq.*, 2019, **277**, 233.
- 56 H. Chen, R. Zhang, H. Gao, H. Cheng, H. Fang and X. Cheng, *Dyes Pigm.*, 2018, **149**, 512.
- 57 N. G. Nagaveni, M. Gupta, A. Roy and V. Prasad, *J. Mater. Chem.*, 2010, **20**, 9089.
- 58 M. Alaasar, M. Prehm, Y. Cao, F. Liu and C. Tschierske, *Angew. Chem., Int. Ed.*, 2016, **55**, 320.
- 59 M. Alaasar, S. Poppe, Q. Dong, F. Liu and C. Tschierske, *Chem. Commun.*, 2016, **52**, 13869.
- 60 M. Alaasar, S. Poppe, Q. Dong, F. Liu and C. Tschierske, *Angew. Chem., Int. Ed.*, 2017, **56**, 10801.
- 61 H. Takezoe, E. Gorecka and M.   epi  c, *Rev. Mod. Phys.*, 2010, **82**, 897.
- 62 R. Pratibha, N. V. Madhusudana and B. K. Sadashiva, *EPL*, 2007, **80**, 46001.
- 63 R. Pratibha, N. V. Madhusudana and B. K. Sadashiva, *Science*, 2000, **288**, 2184.
- 64 T. Hegmann, J. Kain, S. Diele, G. Pelzl and C. Tschierske, *Angew. Chem., Int. Ed.*, 2001, **40**, 887.
- 65 V. Yelamaggad, I. S. Shashikala, V. P. Tamilenth, D. S. S. Rao, G. G. Nair and S. K. Prasad, *J. Mater. Chem.*, 2008, **18**, 2096.

- 66 B. K. Sadashiva, R. A. Reddy, R. Pratibha and N. V. Madhusudana, *Chem. Commun.*, 2001, 2140.
- 67 K. Kishikawa, T. Inoue, Y. Sasaki, S. Aikyo, M. Takahashi and S. Kohmoto, *Soft Matter*, 2011, 7, 7532.
- 68 J. Lagerwall and F. Giesselmann, *ChemPhysChem*, 2006, 7, 20.
- 69 M. A. Glaser and N. A. Clark, *Phys. Rev. E: Stat., Nonlinear, Soft Matter Phys.*, 2002, **66**, 021711.
- 70 T. Matsumoto, A. Fukuda, M. Johno, Y. Motoyama, T. Yui, S.-S. Seomun and M. Yamashita, *J. Mater. Chem.*, 1999, 9, 2051.
- 71 A. Yamaguchi, A. Yoshizawa, I. Nishiyama, J. Yamamoto and H. Yokoyama, *Mol. Cryst. Liq. Cryst.*, 2005, **439**, 85.
- 72 H. J. Coles, S. Meyer, P. Lehmann, R. Deschenaux and I. Jauslin, *J. Mater. Chem.*, 1999, 9, 1085.
- 73 D. Guillon, M. A. Osipov, S. Mery, M. Siffert, J.-F. Nicoud, C. Bourgogne and P. Sebastiao, *J. Mater. Chem.*, 2001, **11**, 2700.
- 74 G. Dantlgraber, S. Diele and C. Tschierske, *Chem. Commun.*, 2002, 2768.
- 75 N. Olsson, I. Dahl, B. Helgee and L. Komitov, *Liq. Cryst.*, 2004, **31**, 1555.
- 76 K. Kishikawa, N. Muramatsu, S. Kohmoto, K. Yamaguchi and M. Yamamoto, *Chem. Mater.*, 2003, **15**, 3443.
- 77 I. Nishiyama and J. W. Goodby, *J. Mater. Chem.*, 1992, 2, 1015.
- 78 Y. Ouchi, Y. Yoshioka, H. Ishii, K. Seki, M. Kitamura, R. Noyori, Y. Takanishib and I. Nishiyama, *J. Mater. Chem.*, 1995, 5, 2297.
- 79 J. Thisayukta and E. T. Samulski, *J. Mater. Chem.*, 2004, **14**, 1554.
- 80 (a) S.-L. Wu and F.-D. Chen, *Liq. Cryst.*, 2003, **30**, 991–995; (b) S.-L. Wu and F.-D. Chen, *Liq. Cryst.*, 2004, **31**, 607.
- 81 W. Drzewiński, R. Dabrowski, K. Czupryński, J. Przedmojski and M. Neubert, *Ferroelectrics*, 1998, **212**, 281.
- 82 K.-T. Kang, S. K. Lee, C. W. Park, S. H. Cho, J. G. Lee, S.-K. Choi and Y. B. Kim, *Bull. Korean Chem. Soc.*, 2006, 27, 1364.
- 83 I. Nishiyama, T. Yamamoto, J. Yamamoto, J. W. Goodby and H. Yokoyama, *J. Mater. Chem.*, 2003, **13**, 1868.
- 84 S. J. Cowling, A. W. Hall and J. W. Goodby, *Liq. Cryst.*, 2005, **32**, 1483.
- 85 H. T. Nguyen, J. C. Rouillon, A. Babeau, J. P. Marcerou, G. Sigaud, M. Cotrait and H. Allouchi, *Liq. Cryst.*, 1999, **26**, 1007.
- 86 R. Dabrowski, *Ferroelectrics*, 2000, **243**, 1.
- 87 S.-L. Wu and C.-Y. Lin, *Liq. Cryst.*, 2005, **32**, 663.
- 88 The reason for the dominance of synclitic SmC<sub>s</sub> phases in the polycatenar case might be that usually the 3,4-disubstitution or 3,4,5-trisubstitution pattern with a side-by-side organization of the alkyl chains were used and this appears to support synclitic SmC<sub>s</sub> phase formation by parallel chain alignment.
- 89 F. C. Yu and L. J. Yu, *Chem. Mater.*, 2006, **18**, 5410.
- 90 F. C. Yu and L. J. Yu, *Liq. Cryst.*, 2008, **35**, 799.
- 91 E. Enz, S. Findeisen-Tandel, R. Dabrowski, F. Giesselmann, W. Weissflog, U. Baumeister and J. Lagerwall, *J. Mater. Chem.*, 2009, **19**, 2950.
- 92 A. Chakraborty, B. Das, M. K. Das, S. Findeisen-Tandel, M.-G. Tamba, U. Baumeister, H. Kresse and W. Weissflog, *Liq. Cryst.*, 2011, **38**, 1085.
- 93 P. Sathyanarayana, S. Radhika, B. K. Sadashivab and S. Dhara, *Soft Matter*, 2012, **8**, 2322.
- 94 M. Alaasar, S. Poppe, C. Kerzig, C. Klopp, A. Eremin and C. Tschierske, *J. Mater. Chem. C*, 2017, 5, 8454.
- 95 S. T. Lagerwall, A. Dahlgren, P. Jägemalm, P. Rudquist, K. D'havé, H. Pauwels, R. Dabrowski and W. Drzewinski, *Adv. Funct. Mater.*, 2001, **11**, 87.
- 96 M. Neundorf, PhD thesis, Martin-Luther University, Halle-Wittenberg, 1993, pp. 56–59.
- 97 G. Albertini, S. Melone, G. Poeti, F. Rustichelli and G. Torquati, *Mol. Cryst. Liq. Cryst.*, 1984, **104**, 121.
- 98 G. W. Gray and J. W. Goodby, *Smectic Liquid Crystals*, Leonard Hill, Glasgow, 1984.
- 99 J. M. Seddon, Structural Studies of Liquid Crystals by X-ray Diffraction, in *Handbook of Liquid Crystals*, ed. D. Demus, J. Goodby, G. W. Gray, H.-W. Spiess and V. Vill, Wiley-VCH, Weinheim, 1998, pp. 635–679.
- 100 J. J. Benattar, F. Moussa, M. Lambert and C. Germain, *J. Phys., Lett.*, 1981, **42**, 67.
- 101 P. A. C. Gane, A. J. Leadbetter, J. J. Benattar, F. Moussa and M. Lambert, *Phys. Rev. A: At., Mol., Opt. Phys.*, 1981, **24**, 2694.
- 102 S. Shibahara, J. Yamamoto, Y. Takanishi, K. Ishikawa, H. Yokoyama and H. Takezoe, *Phys. Rev. E: Stat., Nonlinear, Soft Matter Phys.*, 2002, **65**, 030702(R).
- 103 Y. Takanishi, K. Miyachi, S. Yoshida, B. Jin, H. Yin, K. Ishikawa, H. Takezoe and A. Fukuda, *J. Mater. Chem.*, 1998, **8**, 1133.
- 104 M. Neundorf, Y. Takanishi, A. Fukuda, S. Saito, K. Murashiro, T. Inukai and D. Demus, *J. Mater. Chem.*, 1995, 5, 2221.
- 105 I. Nishiyama, J. Yamamoto, J. W. Goodby and H. Yokoyama, *J. Mater. Chem.*, 2003, **13**, 2429.
- 106 S. Kundu, T. Ray, S. K. Roy and R. Dabrowski, *Liq. Cryst.*, 2004, **31**, 119.
- 107 F. Beaubois, V. Faye, J. P. Marcerou, H. T. Nguyen and J. C. Rouillon, *Liq. Cryst.*, 1999, **26**, 1351.
- 108 Because the SmC<sub>a</sub> phase is formed from a cubic phase no specific textures can be observed.
- 109 M. Cepic, *ChemPhysChem*, 2014, **15**, 1297.
- 110 Y. Cao, M. Alaasar, A. Nallapaneni, M. Salamończyk, P. Marinko, E. Gorecka, C. Tschierske, F. Liu, N. Vaupotic and C. Zhu, *Phys. Rev. Lett.*, 2020, **125**, 027801.
- 111 V. Lewandowski, N. Vaupotic, D. Pocięcha, E. Gorecka and L. M. Liz-Marzan, *Adv. Mater.*, 2020, 1905591; Y. Cao, C. Feng, A. Jakli, C. Zhu and F. Liu, *Giant*, 2020, 100018, DOI: 10.1016/j.giant.2020.100018.
- 112 A.-M. Levelut and B. Pansu, *Phys. Rev. E: Stat. Phys., Plasmas, Fluids, Relat. Interdiscip. Top.*, 1999, **60**, 6803.
- 113 P. Mach, R. Pindak, A.-M. Levelut, P. Barois, H. T. Nguyen, C. C. Huang and L. Furenlid, *Phys. Rev. Lett.*, 1998, **81**, 1015.

- 114 C. C. Huang, S. Wang, L. Pan, Z. Q. Liu, B. K. McCoy, Y. Sasaki, K. Ema, P. Barois and R. Pindak, *Liq. Cryst. Rev.*, 2015, **3**, 58.
- 115 A. R. Korlacki, A. Fukuda and J. K. Vij, *Europhys. Lett.*, 2007, **77**, 36004.
- 116 (a) C. Keith, A. Lehmann, U. Baumeister, M. Prehm and C. Tschierske, *Soft Matter*, 2010, **6**, 1704; (b) M. Alaasar, M. Prehm and C. Tschierske, *Liq. Cryst.*, 2014, **41**, 126; (c) M. Alaasar, S. Poppe and C. Tschierske, *Liq. Cryst.*, 2017, **44**, 729.
- 117 O. Francescangeli, F. Vita and E. T. Samulski, *Soft Matter*, 2014, **10**, 7685.
- 118 Y. Zhuang and P. Charbonneau, *J. Phys. Chem. B*, 2016, **120**, 7775.
- 119 S. Kutsumizu, *Isr. J. Chem.*, 2012, **52**, 844.
- 120 J. P. Marcerou, R. Farhi, J. C. Rouillon and H. T. Nguyen, *Eur. Phys. J. E: Soft Matter Biol. Phys.*, 2000, **3**, 29.
- 121 H. T. Nguyen, N. Ismaili, N. Isaert and M. F. Achard, *J. Mater. Chem.*, 2004, **14**, 2060.
- 122 J. W. Goodby, D. A. Dunmur and J. P. Collings, *Liq. Cryst.*, 1995, **19**, 703.
- 123 M. Jasinski, D. Pocięcha, H. Monobe, J. Szczytko and P. Kaszynski, *J. Am. Chem. Soc.*, 2014, **136**, 14658.
- 124 M. Manai, A. Gharbi, J. P. Marcerou, H. T. Nguyen and J. C. Rouillon, *Physica B*, 2005, **368**, 168.
- 125 C. A. Hunter and J. K. M. Sanders, *J. Am. Chem. Soc.*, 1990, **112**, 5525.
- 126 C. A. Hunter, K. R. Lawson, J. Perkins and C. J. Urch, *J. Chem. Soc., Perkin Trans. 2*, 2001, 651.
- 127 S. E. Wheeler and J. W. G. Bloom, *J. Phys. Chem. A*, 2014, **118**, 6133.
- 128 K. Kishikawa, *Isr. J. Chem.*, 2012, **52**, 800.
- 129 A. I. Smirnova, B. Heinrich, B. Donnio and D. W. Bruce, *RSC Adv.*, 2015, **5**, 75149.
- 130 (a) *Photoactive Functional Soft Materials: Preparation, Properties, and Applications*, ed. Q. Li, Wiley-VCH, Weinheim, Germany, 2019; (b) H. K. Bisoyi, T. J. Bunning and Q. Li, *Adv. Mater.*, 2018, 1706512.

# Switching Chirophilic Self-assembly: From *meso*-structures to Conglomerates in Liquid and Liquid Crystalline Network Phases of Achiral Polycatenar Compounds

Mohamed Alaasar,<sup>\*[a, b]</sup> Yu Cao,<sup>\*[c]</sup> Yan Liu,<sup>[c, d]</sup> Feng Liu,<sup>[c]</sup> and Carsten Tschierske<sup>\*[a]</sup>

**Abstract:** Spontaneous generation of chirality from achiral molecules is a contemporary research topic with numerous implications for technological applications and for the understanding of the development of homogeneous chirality in biosystems. Herein, a series of azobenzene based rod-like molecules with an 3,4,5-trialkylated end and a single *n*-alkyl chain involving 5 to 20 aliphatic carbons at the opposite end is reported. Depending on the chain length and temperature these achiral molecules self-assemble into a series of liquid and liquid crystalline (LC) helical network phases. A chiral isotropic liquid (Iso<sub>1</sub><sup>[\*]</sup>) and a cubic triple network phase with chiral *I*23 lattice were found for the short chain compounds, whereas non-cubic and achiral cubic phases dominate for the long chain compounds. Among them a mesoscale conglomerate

with *I*23 lattice, a tetragonal phase (Tet<sub>b</sub>) containing one chirality synchronized and one non-synchronized achiral network, an achiral double network *meso*-structure with *la* $\bar{3}$ *d* space group and an achiral percolated isotropic liquid mesophase (Iso<sub>1</sub>) were found. This sequence is attributed to an increasing strength of chirality synchronization between the networks, combined with a change of the preferred mode of chirophilic self-assembly between the networks, switching from enantiophilic to enantiophobic with decreasing chain length and lowering temperature. These nanostructured and mirror symmetry broken LC phases exist over wide temperature ranges which is of interest for potential applications in chiral and photosensitive functional materials derived from achiral compounds.

## Introduction

Functional materials based on helical assemblies are required for photonic band-gap materials, for materials with chiroptical properties, capability of chiral recognition and chiral emission.<sup>[1,2]</sup> These applications require chiral compound, which

are expensive to synthesize and often only available in one of the enantiomeric forms. However, in the process of mirror symmetry breaking, chirality develops spontaneously from achiral or racemic sources, and the sense of chirality can be tuned and fixed by application of chiral dopants or chiral physical forces by means of asymmetry amplification. This was first recognized in crystalline solid-state assemblies<sup>[3,4]</sup> and more recently expanded to aggregation of crystalline fibres in dilute solution<sup>[4,5]</sup> and gels in solvent-swollen systems.<sup>[6]</sup> Liquid crystals, (LCs)<sup>[7,8]</sup> on the other hand, are soft functional materials that combine molecular order and mobility, making them relevant for numerous applications in functional devices, among them, displays, light modulating and sensor devices.<sup>[9]</sup> The reduced order and increased mobility of the molecules in the LC state would be expected to reduce their chiral recognition capability in these systems. Nevertheless, spontaneous generation of macroscopic homochirality was in the recent decade discovered in LCs<sup>[10]</sup> of bent-core molecules,<sup>[11–14]</sup> dimesogens<sup>[15,16]</sup> and specifically designed polycatenar molecules.<sup>[17]</sup> For the latter mirror symmetry breaking was even found in the isotropic liquids state,<sup>[18–20]</sup> which is of relevance for the understanding of the emergence of biochirality.<sup>[20,21]</sup>

In these polycatenar compounds, a rod-like  $\pi$ -conjugated polyaromatic core-structure is decorated with a number of 3 to 6 alkyl chains distributed to both ends.<sup>[22]</sup> The rod-like moieties of these molecules can align side by side, thus forming columnar aggregates,<sup>[10,17]</sup> in which the rod-like cores are arranged predominately perpendicular to the column long axis. The clashing of the bulky aliphatic end-chains leads to a twist between adjacent rafts of molecules, giving rise to a helical

[a] Prof. Dr. M. Alaasar, Prof. Dr. C. Tschierske  
Institute of Chemistry  
Martin-Luther University Halle-Wittenberg  
Kurt-Mothes Str. 2, D-06120 Halle/Saale (Germany)  
E-mail: carsten.tschierske@chemie.uni.halle.de

[b] Prof. Dr. M. Alaasar  
Department of Chemistry  
Faculty of Science  
Cairo University  
P.O. 12613 Giza (Egypt)  
E-mail: malaasar@sci.cu.edu.eg

[c] Dr. Y. Cao, Y. Liu, Prof. Dr. F. Liu  
Shaanxi International Research Center for Soft Matter  
State Key Laboratory for Mechanical Behavior of Materials  
Xi'an Jiaotong University  
Xi An Shi, Xi'an 710049 (P. R. China)  
E-mail: yu.cao@xjtu.edu.cn

[d] Y. Liu  
Wanhua Chemical Group Co  
Ltd., Yantai 265505 (P. R. China)

Supporting information for this article is available on the WWW under <https://doi.org/10.1002/chem.202201857>

© 2022 The Authors. Chemistry - A European Journal published by Wiley-VCH GmbH. This is an open access article under the terms of the Creative Commons Attribution Non-Commercial License, which permits use, distribution and reproduction in any medium, provided the original work is properly cited and is not used for commercial purposes.

superstructure along the columns, which is supported by the chirality synchronization of the helical conformers of the involved molecules.<sup>[10,23,24]</sup> However, in columnar phases there are numerous helix sign inversions which cancel long-range helicity, and hence the columnar LC phases are usually achiral on a macroscopic scale.<sup>[10,25]</sup> Only in few cases at low temperature through-space coupling between the columns can lead to long range helicity,<sup>[26,27]</sup> in most cases after transition to a soft crystalline mesophase.<sup>[28,29]</sup>

In contrast, the bicontinuous cubic ( $Cub_{bi}$ ) LC phases represent networks of branched columns (Figure 1).<sup>[30-35]</sup> In the  $Cub_{bi}$  phases of polycatenar molecules the junctions of the networks transmit chirality by removing helix-reversal defects and thus lead to long range helicity and uniform chirality along the networks.<sup>[10,17,36]</sup> Presently there are two known  $Cub_{bi}$  phases of polycatenar molecules. The  $Ia\bar{3}d$  phase (double gyroid) is composed of two enantiomorphous helical networks and there-

fore represents an achiral *meso*-structure (Figure 1a), i.e. there is enantiophilic coupling between the networks (heterochiral self-assembly).<sup>[17,36]</sup> In contrast, the  $I23$  phase<sup>[37-42]</sup> being composed of three networks (Figure 1b) is chiral and typically forms a conglomerate of chiral domains ( $Cub_{bi}/I23^{(ch)}$ ), meaning that the network coupling becomes enantiophobic (homochiral self-assembly) and mirror symmetry is broken by the formation of a conglomerate of chiral domains.<sup>[10,17,19,43-49]</sup> Most compounds forming these mirror symmetry broken LC phases represent derivatives of 5,5'-diphenyl-2,2'-bithiophene<sup>[17,18,38,39,50]</sup> or 1,2-diphenylethane-1,2-dione (benzil).<sup>[51,52]</sup> More recently hydrogen bonded supramolecules<sup>[53]</sup> and compounds involving functional units, such as charge carriers (BTBT)<sup>[54]</sup> or photosensitive and photoisomerizable azobenzene units were also introduced.<sup>[55-57]</sup> For one of these polycatenar azobenzenes **A10/18** (see Scheme 1,  $n=18$ ) a new tetragonal LC phase was discovered.<sup>[58]</sup> Its structure was proven to represent a non-cubic bicontinuous double network structure ( $Tet_{bi}$ ) composed of a pair of chiral  $P4_12_1$  and  $P4_32_1$  space groups. In this case one network is chiral whereas the other one is racemized and this structure is considered as an intermediate step of the transition between enantiophilic and enantiophobic self-assembly.

Herein we provide an understanding of the effects of the molecular structure on the spontaneous emergence of chirality and the transition between the two different modes of chirophilic interhelical self-assembly, being either enantiophilic or enantiophobic, which is of importance for the design of spontaneously mirror symmetry broken functional materials. To this end the series of taper shaped azobenzene-based polycatenars **A10/ $n$**  (Scheme 1) with a length of the terminal single chain  $n$  ranging from  $n=5$  to  $n=20$  was synthesized and investigated.

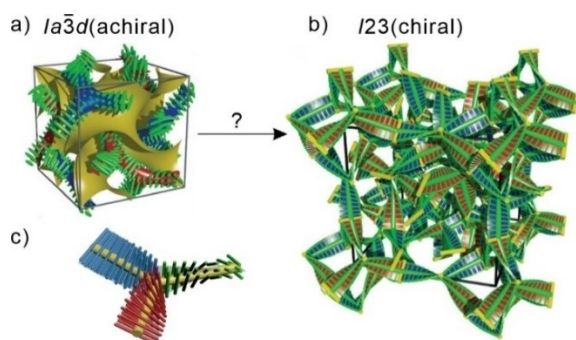
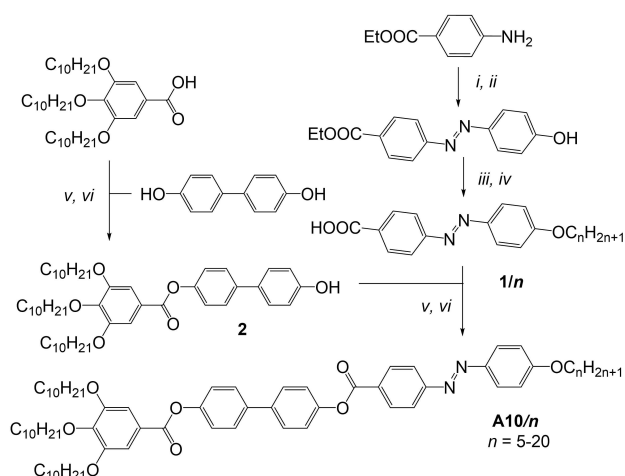


**Figure 1.** Helical network structures of the  $Cub_{bi}$  phases under discussion a) *meso*-structure with  $Ia\bar{3}d$  space group (double gyroid) and b) chiral  $I23^{(ch)}$  phase<sup>[37]</sup> forming a conglomerate.<sup>[17]</sup> Both network structures are composed of three-way junctions; c) a schematic representation of a three-way junction interconnecting three network segments formed by the helical stacking of rafts of three molecules.



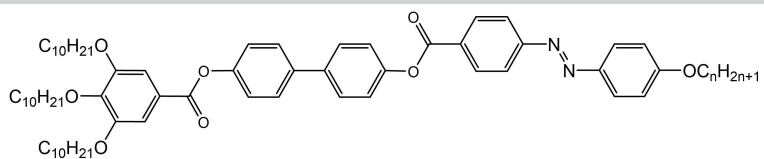
**Scheme 1.** Synthesis of compounds **A10/ $n$** . Reagents and conditions: i:  $NaNO_2$ ,  $HCl$ ,  $H_2O$ ,  $0 \rightarrow 5^\circ C$ , 30 min; ii: 1. phenol,  $NaOH$ ,  $5 \rightarrow 20^\circ C$ , 1 h, 2.  $NaHCO_3$ ; iii:  $C_nH_{2n+1}Br$ ,  $KI$ ,  $K_2CO_3$ , 2-butanone, reflux, 18 h; iv:  $EtOH$ ,  $KOH$ , reflux, 8 h; v:  $SOCl_2$ ,  $DMF$ , reflux 1 h.; vi. dry  $CH_2Cl_2$ , dry TEA, dry pyridine, reflux, 6 h.

## Results

### Synthesis and materials

The synthesis of the azobenzene-based polycatenars **A10/ $n$**  (Scheme 1) was performed in an analogous way to that reported previously<sup>[36,56]</sup> from 4'-hydroxybiphenyl-4-yl 3,4,5-tri-*n*-decyloxybenzoate (**2**)<sup>[59]</sup> and the 4-(4-alkoxyphenyldiazenyl)benzoic acids **1/ $n$**  ( $n=5-12$ , 18,<sup>[60]</sup>  $n=14,16$ <sup>[61,62]</sup>). Compounds **1/ $n$**  were synthesized by Williamson etherification of ethyl 4-(4-hydroxyphenyldiazenyl)benzoate<sup>[63]</sup> with 1-bromo-*n*-alkanes, followed by hydrolysis.<sup>[61,62]</sup> Due to low solubility of these benzoic acids **1/ $n$**  in most organic solvents, neat  $SOCl_2$  was used as activating agent for the acylation reaction with the phenol **2** as described in the Experimental Section.

The compounds **A10/ $n$**  were investigated by polarizing optical microscopy (POM), differential scanning calorimetry (DSC) and X-ray diffraction (XRD) as described in the Experimental Section. The phase sequences and transition temperatures of compounds **A10/ $n$**  are collected in Table 1 and shown graphically in Figure 2. The compounds can be divided into two groups, the short-chain compounds with  $n=5-12$  and the long

**Table 1.** Phase transition temperatures ( $T/^\circ\text{C}$ ), mesophase types, and transition enthalpies [ $\Delta H/\text{kJ mol}^{-1}$ ] of compounds **A10/n**.


Compd.	$n$	Phase sequence
<b>A10/5</b>	5	Cr 78 [45.0] $\text{Cub}_{\text{bi}}/I23^{[*]}$ 168 [1.2] $\text{Iso}_1^{[*]}$ 171 [0.4] Iso Iso 169 [−0.7] $\text{Iso}_1^{[*]}$ 156 [−0.7] $\text{Cub}_{\text{bi}}/I23^{[*]}$ < 20 Cr
<b>A10/6</b>	6	Cr 88 [94.1] $\text{Cub}_{\text{bi}}/I23^{[*]}$ 167 [1.7] Iso Iso 167 [−0.5] $\text{Iso}_1^{[*]}$ 156 [−1.0] $\text{Cub}_{\text{bi}}/I23^{[*]}$ < 20 Cr
<b>A10/7</b>	7	Cr 87 [22.2] $\text{Cub}_{\text{bi}}/I23^{[*]}$ 166 [2.0] Iso Iso 164 [−0.5] $\text{Iso}_1^{[*]}$ 156 [−0.9] $\text{Cub}_{\text{bi}}/I23^{[*]}$ 23 [−22.7] Cr
<b>A10/8</b>	8	Cr 99 [39.8] $\text{Cub}_{\text{bi}}/I23^{[*]}$ 165 [1.4] Iso Iso 163 [−0.5] $\text{Iso}_1^{[*]}$ 156 [−0.7] $\text{Cub}_{\text{bi}}/I23^{[*]}$ 16 [−11.2] Cr
<b>A10/9</b>	9	Cr 86 [37.8] $\text{Cub}_{\text{bi}}/I23^{[*]}$ 163 [1.8] Iso Iso 159 [−0.5] $\text{Iso}_1^{[*]}$ 153 [−1.0] $\text{Cub}_{\text{bi}}/I23^{[*]}$ 21 [−8.1] Cr
<b>A10/10</b>	10	Cr 76 [49.3] $\text{Cub}_{\text{bi}}/I23^{[*]}$ 163 [2.0] Iso Iso 160 [−0.5] $\text{Iso}_1^{[*]}$ 156 [−1.2] $\text{Cub}_{\text{bi}}/I23^{[*]}$ 20 [−3.8] Cr
<b>A10/12</b>	12	Cr 72 [50.7] $\text{Cub}_{\text{bi}}/I23^{[*]}$ 165 [2.2] $\text{Iso}_1 \sim 175$ [1.9] Iso Iso 170 [−2.2] $\text{Iso}_1$ 162 [−0.7] $\text{Iso}_1^{[*]}$ 156 [−1.1] $\text{Cub}_{\text{bi}}/I23^{[*]}$ 22 [−6.7] Cr
<b>A10/14</b>	14	Cr 51 [29.6] X 77 [−] $\text{Cub}_{\text{bi}}/I23 \sim 127$ [−] $\text{Tet}_{\text{bi}} \sim 147$ [−] $\text{Cub}/Ia\bar{3}d$ 157 [2.5] $\text{Iso}_1 \sim 170$ [2.5] Iso Iso $\sim 165$ [−2.4] $\text{Iso}_1$ 149 [−0.5] $\text{Iso}_1^{[*]}$ 144 [−1.0] $\text{Cub}/Ia\bar{3}d \sim 140$ [−] $\text{Tet}_{\text{bi}}$ 30 [−8.6] Cr
<b>A10/16</b>	16	Cr 67 [49.0] X $\sim 75$ [−] $\text{Cub}_{\text{bi}}/I23 \sim 107$ [−] $\text{Tet}_{\text{bi}} \sim 112$ [−] $\text{Cub}_{\text{bi}}/Ia\bar{3}d$ 157 [2.9] $\text{Iso}_1 \sim 170$ [2.9] Iso Iso $\sim 167$ [−3.6] $\text{Iso}_1$ 147 Col 144 [−1.8] <sup>b</sup> $\text{Cub}_{\text{bi}}/Ia\bar{3}d$ 105 [−] $\text{Tet}_{\text{bi}}$ 28 [−19.9] Cr
<b>A10/18</b> <sup>[36,58]</sup>	18	Cr 64 [51.2] X78 [−] $\text{Cub}_{\text{bi}}/I23 \sim 95$ [−] $\text{Tet}_{\text{bi}} \sim 135$ [−] $\text{Cub}_{\text{bi}}/Ia\bar{3}d \sim 157$ [2.8] $\text{Iso}_1 \sim 169$ [3.2] Iso Iso $\sim 165$ [−3.5] $\text{Iso}_1$ 150 [−1.6] $\text{Col}_{\text{hex}}$ 145 [−0.4] $\text{Cub}_{\text{bi}}/Ia\bar{3}d \sim 135$ [−] $\text{Tet}_{\text{bi}}$ 36 [−25.5] Cr
<b>A10/20</b>	20	Cr 71 [55.0] $\text{Cub}_{\text{bi}}/Ia\bar{3}d$ 156 [2.8] $\text{Iso}_1 \sim 167$ [2.3] Iso Iso $\sim 165$ [−4.2] $\text{Iso}_1$ 152 [−1.9] $\text{Col}_{\text{hex}}$ 144 [−0.3] $\text{Cub}_{\text{bi}}/Ia\bar{3}d \sim 135$ [−] $\text{Tet}_{\text{bi}}$ 43 [−28.8] Cr

<sup>a</sup> Peak temperatures as determined from 2<sup>nd</sup> heating (upper lines) and 2<sup>nd</sup> cooling (lower lines) DSC scans with rate 10 K min<sup>−1</sup>; all transitions without visible  $\Delta H$  were taken from continuous XRD scans in combination with optical investigations, these are approximate values, because there is a strong dependence on conditions and sample history; for the broad Iso–Iso<sub>1</sub> transitions the middle of the broad DSC feature is given. Abbreviations: Cr=crystalline solid (most compounds show only partial crystallization on cooling); X=unknown phase; Iso=achiral isotropic liquid; Iso<sub>1</sub>=achiral percolated isotropic liquid phase; Iso<sub>1</sub><sup>[\*]</sup>=ambidextrous chiral isotropic liquid phase;  $\text{Cub}_{\text{bi}}/Ia\bar{3}d$ =achiral bicontinuous cubic phase with  $Ia\bar{3}d$  space group (double gyroid);  $\text{Cub}_{\text{bi}}/I23^{[*]}$ =ambidextrous chiral bicontinuous cubic phase with  $I23$  space group;  $\text{Cub}_{\text{bi}}/I23$ =macroscopically achiral  $\text{Cub}_{\text{bi}}/I23$  phase;  $\text{Tet}_{\text{bi}}$ =tetragonal phase representing a pair of chiral space groups  $P4_12_1/P4_32_1$ ;  $\text{Col}_{\text{hex}}$ =hexagonal columnar phase. Enthalpy value involves both transitions, Iso<sub>1</sub>– $\text{Col}_{\text{hex}}$  and  $\text{Col}_{\text{hex}}$ – $\text{Cub}_{\text{bi}}$ .

chain compounds with  $n=14$ –20, which are described separately in the two following sections.

### Short chain compounds A10/5–A10/12

**Chiral liquid crystalline cubic phase.** – In the DSC heating traces of compounds **A10/5**–**A10/12** (see Figure 3a,b for examples) only one sharp transition around 162–168 °C with an enthalpy of 1.4–2.2 kJ mol<sup>−1</sup> is observed besides the melting event. The transition enthalpy increases with growing  $n$ , while the transition temperatures are almost constant and only slightly decrease without any noticeable odd-even effect (Table 1). At this transition the viscosity of the optically isotropic sample suddenly decreases as typical for a transition of a cubic mesophase at lower temperature to the isotropic liquid at higher.

The small angle X-ray scattering pattern (SAXS) of this cubic phase is indexed in all cases with  $n=5$ –12 to the  $I23$  space group<sup>[37]</sup> with a lattice parameter  $a_{\text{cub}}$  between 17.8 and 18.4 nm (Table 2). Figure 4a shows the indexed SAXS pattern of compound **A10/6** as an example. The SAXS data of the other homologues with  $n=8$ –12 are collated in Figures S8–S10 and

Tables S2–S4 in the Supporting Information. Electron density (ED) reconstruction of the SAXS pattern indicates a bicontinuous cubic phase ( $\text{Cub}_{\text{bi}}$ ) with triple network structure and three-way junctions (Figure 4b,c). In the wide-angle range (WAXS) there is only one diffuse scattering with a maximum around  $d=0.45$  nm for all compounds (Figure S11), confirming the absence of fixed positions for individual molecules and thus the liquid crystalline state of this cubic phase. For all  $\text{Cub}_{\text{bi}}/I23^{[*]}$  phases of compounds **A10/5**–**A10/12** a conglomerate of chiral domains can be observed by polarizing optical microscopy (Figure 5c,d). Accordingly, after rotating the analyser by a small angle (1–5°) out of the 90° crossed orientation the formation of dark and bright domains is observed, which invert their brightness upon rotating the polarizer with the same angle into the opposite direction. This confirms the ambidextrous mirror symmetry breaking in this cubic phase ( $\text{Cub}_{\text{bi}}/I23^{[*]}$ ).

This mirror symmetry broken  $\text{Cub}_{\text{bi}}$  phase is stable over a broad temperature range and no other LC phase is observed. For compounds **A10/10** and **A10/12** the crystallization is very slow and their  $\text{Cub}_{\text{bi}}$  phases can be observed down to ambient temperature (25 °C), even after storing the samples for several months at this temperature no crystallization is observed

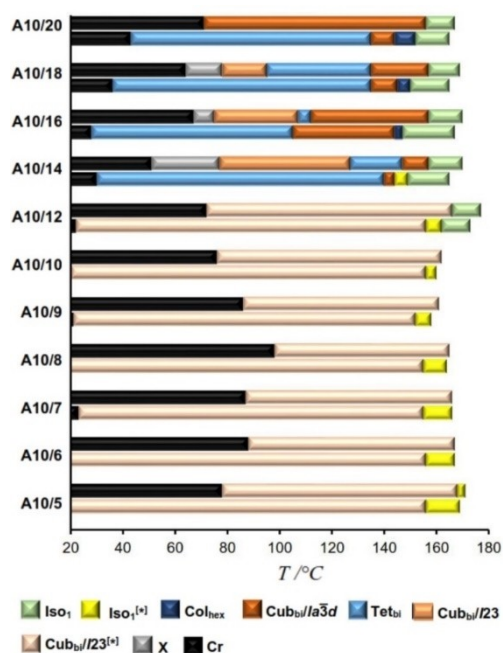


**Figure 2.** Bar diagram showing the mesophases and phase transition temperatures of series A10/*n* on heating (upper bars) and on cooling (lower bars); for abbreviations see Table 1; the ordinary isotropic liquid (Iso) is in all cases at the right side of the bars.

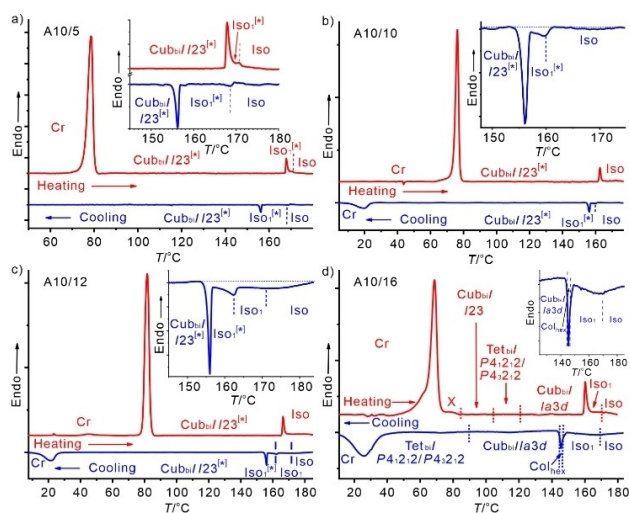


**Figure 3.** DSC second heating and cooling traces at a rate of 10 K min<sup>-1</sup> for selected compounds showing different types of Iso-Cub<sub>bi</sub> transitions: a) A10/5 and b) A10/10 short chain compounds with Iso-Iso<sub>1</sub><sup>[\*]</sup> liquid state diamorphism, c) A10/12 with liquid state triamorphism and d) long chain compound A10/16 with Iso-Iso<sub>1</sub>-(Col<sub>hex</sub>)-Cub<sub>bi</sub> transition. In the cooling scan of A10/16 the Cub<sub>bi</sub>-Col<sub>hex</sub> and Col<sub>hex</sub>-Iso<sub>1</sub> transitions cannot be separated.

(Figure 2 and Table 1). This makes these materials excellent candidates for potential technological applications

**Polyamorphism and mirror symmetry breaking in the liquid state.** – Compounds A10/6–A10/10 show a direct transition from the Cub<sub>bi</sub>/I23<sup>[\*]</sup> phase to the isotropic liquid state (Iso) on heating, whereas on cooling a small range of a

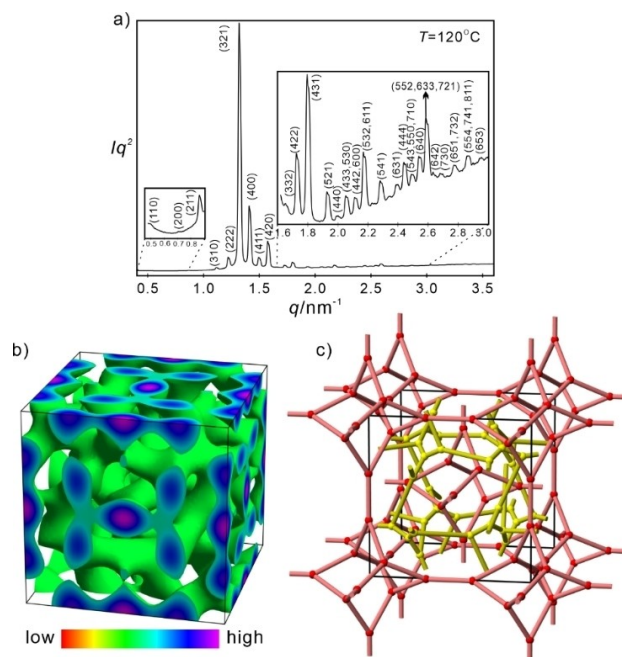


**Figure 4.** a) SAXS diffractogram of A10/6 on heating at  $T = 120\text{ }^{\circ}\text{C}$  in the Cub<sub>bi</sub>/I23<sup>[\*]</sup> phase, b) the reconstructed 3D electron density map and c) schematic presentation of the triple network structure. The inner and outer networks in red are same with each other and the middle network in yellow lies on the Schwarz P minimal surface; thus, the interpenetrated networks in red provide a structure related to the Plumber's Nightmare cubic lattice<sup>[30]</sup> with complex polyhedral frameworks – involving exclusively three way junctions – forming the nodes.

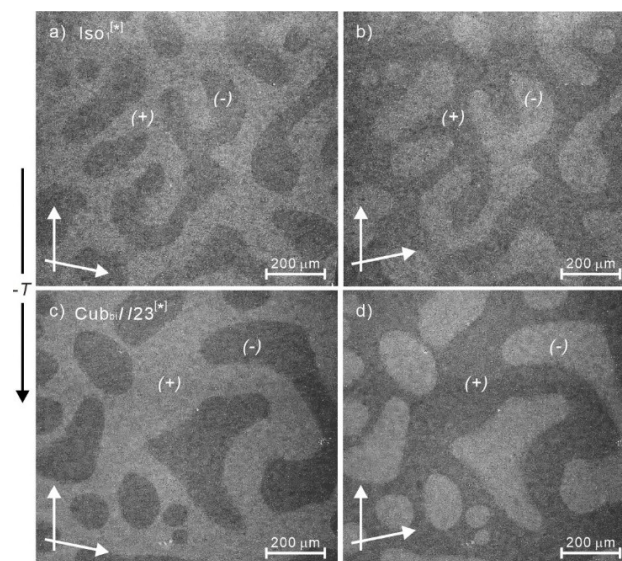


**Figure 5.** Textures of A10/12 as observed by polarizing microscopy between two microscopy glass slides (sample thickness about 50 μm) upon cooling from Iso, a, b) in the Iso<sub>1</sub><sup>[\*]</sup> phase at 162 °C and c, d) in the Cub<sub>bi</sub>/I23<sup>[\*]</sup> phase as formed from Iso<sub>1</sub><sup>[\*]</sup> at 145 °C; a, c) after rotating one of the analysers by 5° in clockwise direction and b, d) after rotating one of the analysers by 5° in anticlockwise direction out of the 90° crossed positions; the arrows indicate the directions of polarizer and analyzer; a, b) and c, d) show the same area, but due to the mobility of the domain boundaries in the Iso<sub>1</sub><sup>[\*]</sup> temperature range they move and change their shape, and therefore a, b) and c, d) appear different; all photos were transformed to grey scale and the contrast was enhanced.

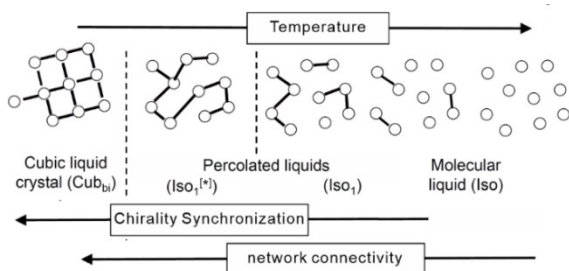


**Table 2.** Selected structural data of the mesophases of the investigated compounds, for a complete list and detailed calculations, see Table S11).<sup>a</sup>

Comp.	Temp. [°C]	Phase	a/nm	$n_{\text{raft}}$	$\Phi/^\circ$
A10/6	120	$I23$	17.78	3.6	7.85
A10/8	140	$I23$	17.68	3.5	7.89
A10/10	100	$I23$	18.26	3.6	7.65
A10/12	100	$I23$	18.44	3.6	7.57
A10/14	157	$la\bar{3}d$	11.14	3.2	8.06
	140	$\text{Tet}_{\text{bi}}$	$a = 11.18$ $c = 12.07$	3.4	7.75
A10/16	110	$I23$	18.19	3.5	7.68
	125 (cooling)	$la\bar{3}d$	11.14	3.2	8.06
	95 (heating)	$I23$	17.96	3.4	7.78
	90 (cooling)	$\text{Tet}_{\text{bi}}$	$a = 11.19$ $c = 12.08$	3.4	7.74
A10/18	150	$la\bar{3}d$	11.23	3.3	7.99
	130	$\text{Tet}_{\text{bi}}$	$a = 11.21$ $c = 11.72$	3.4	7.85
A10/20	85	$I23$	18.66	3.7	7.48
	125	$la\bar{3}d$	11.45	3.3	7.83

<sup>a</sup> For XRD data, see Tables S1–S10 and Figures S7–S13.

mirror symmetry broken isotropic liquid ( $\text{Iso}_1^{[*]}$ ) is observed (Figures 2 and 5a, b and Table 1). Similar to the  $\text{Cub}_{\text{bi}}/I23^{[*]}$  phase it is indicated by a conglomerate of chiral domains with the difference that these domains easily flow, while they do not in the cubic phase. The  $\text{Cub}_{\text{bi}}/I23^{[*]}$  phase develops from this liquid conglomerate phase with smoothly curved boundaries (Figure 5c, d). In contrast, if the  $\text{Cub}_{\text{bi}}/I23^{[*]}$  phase would be directly formed from the achiral isotropic liquid, then straight phase boundaries between the chiral domains would evolve (see ref. [17] for examples). As shown in the DSC traces of compounds A10/5 and A10/10 (Figure 3a, b), the typical feature of the  $\text{Iso}$ – $\text{Iso}_1^{[*]}$  transition, associated with the onset of mirror symmetry breaking, is a relatively small peak (the “bump”) followed by a long tailing over almost 10 K (total  $\Delta H$  is around  $0.5 \text{ kJ mol}^{-1}$ ). The bump at the beginning of the broad DSC feature is associated with the onset of chirality synchronization, leading to mirror symmetry breaking and conglomerate formation at this transition. The tailing is attributed to the further growing network connectivity until at a certain critical network density the cubic 3D lattice is formed at the next sharp transition ( $\Delta H = 0.7$ – $1.2 \text{ kJ mol}^{-1}$ ) on further cooling (Figure 6). This means that ambidextrous mirror symmetry breaking sets in already in the temperature range of the isotropic liquid state

**Figure 6.** Development of network connectivity during the transition from Iso via  $\text{Iso}_1$  and  $\text{Iso}_1^{[*]}$  to  $\text{Cub}_{\text{bi}}$ .<sup>[51]</sup>

before the long-range cubic lattice with  $I23$  space group is formed. Only for compound A10/5 a small range of the  $\text{Iso}_1^{[*]}$  phase of about 2 K can also be observed on heating (see inset in Figure 3a) as an enantiotropic  $\text{Iso}_1^{[*]}$  phase range. For all other compounds it is a monotropic phase, only found on cooling, i.e. it is metastable with respect to the  $\text{Cub}_{\text{bi}}/I23^{[*]}$  phase. The monotropic  $\text{Iso}_1^{[*]}$  range becomes smaller with growing chain length  $n$  (from 13 to 5 K, see Figure 2). It is accompanied by an achiral  $\text{Iso}_1$  phase for  $n = 12$  and 14, and it vanishes for  $n = 16$  and the following homologues.

### Long chain compounds A10/14–A10/20

#### Liquid crystalline polymorphism (mesophases with 3D lattice).

– For compound A10/14 and the following homologues with  $n = 16$ – $20$  different phase sequences were observed which are much more complicated than those of the short chain compounds (Table 1 and Figure 2). For these compounds there are several transitions between different mesophases with 3D lattice which are slow and therefore not visible in the DSC traces. Moreover, many of these transitions are strongly dependent on the conditions (sample history, sample thickness, heating and cooling rates, etc.), some phases are metastable and different coexisting structures are involved. Therefore, for these transitions without visible enthalpy change in the DSC traces only approximate transition temperatures can be provided. For A10/16 as an example (Figure 3d), after melting of the crystals at  $67^\circ\text{C}$  the birefringence decreases in the temperature range indicated as “X range” and the sample becomes optically isotropic at the transition to the  $\text{Cub}_{\text{bi}}/I23$  phase at  $75^\circ\text{C}$ . A weak birefringence re-appears at the next transition at  $107^\circ\text{C}$  to  $\text{Tet}_{\text{bi}}$  and at  $112^\circ\text{C}$  the compound becomes optically isotropic again at the transition to the  $\text{Cub}_{\text{bi}}/la\bar{3}d$  phase. Only the transition to the isotropic liquid state is associated with a sharp DSC peak at  $157^\circ\text{C}$  and  $\Delta H = 2.9 \text{ kJ mol}^{-1}$ . There is an additional broad feature in the isotropic

liquid range around 170 °C which is attributed to a liquid state polymorphism due to the continuous disintegration of the network structure into ever smaller domains (Figure 6). On cooling this broad feature is also observed and followed by a sharp peak at 144–147 °C ( $\Delta H = 1.8 \text{ kJ mol}^{-1}$ ), involving the transition to a birefringent  $\text{Col}_{\text{hex}}$  phase (Figure 7a) which is immediately replaced by the quickly growing  $\text{Cub}_{\text{bi}}/Ia\bar{3}d$  phase (Figures 7b and S6d). Upon further cooling, birefringence sets in at 105 °C corresponding to the  $\text{Cub}_{\text{bi}}/Ia\bar{3}d$  to  $\text{Tet}_{\text{bi}}$  phase transition (Figure 7c) and partial crystallization starts around 30 °C. For all compounds **A10/14–A10/18** the  $\text{Cub}_{\text{bi}}/I23$  phase is only formed upon heating the birefringent crystalline solid and passing an unknown “X range” (see Figure 2). In this X-range there is a broad SAXS scattering, combined with sharp reflections (Figures S12a–S13a). In line with optical investigations it is interpreted as a temperature range where the birefringent crystalline phase coexists with an optically isotropic disordered structure. Upon increasing temperature, the diffuse SAXS as well as the sharp peaks in the X range are slowly replaced by the typical sharp scattering peaks of the *I23* phase. The temperature at which all scatterings associated with the X-range have disappeared and the sample has become completely isotropic is denoted as the X to *I23* transition temperature.

The lattice parameter of the *I23* phase of **A10/14–A10/18** is  $a_{\text{cub}} = 18.0\text{--}18.7 \text{ nm}$  which is in the same range as observed for the shorter homologues (Table 2). The SAXS patterns of the *I23* phase of these long chain compounds (Figures S12b–S13b) are identical with each other and with those recorded for the related compounds with shorter chains. However, no chiral domain can be observed for any of the *I23* phases of compounds **A10/14–A10/18**, even if very thick samples ( $\sim 100 \mu\text{m}$ ) were investigated. This is the first case where no macroscopic conglomerate formation can be found in the *I23* phase of a polycatenar compound ( $\text{Cub}_{\text{bi}}/I23$  phase). Therefore, absence/presence of visible chiral domains cannot be considered as sufficient to classify a  $\text{Cub}_{\text{bi}}$  phase of polycatenar compounds unambiguously to either the  $Ia\bar{3}d$  or *I23* space group; in addition, it needs to be confirmed by SAXS investigation. It is assumed that this cubic phase with chiral *I23* space group still represents a conglomerate, but the size of the chiral domains (according to SAXS the correlation length is 500–1000 nm) is in this case too small to be recognizable by optical investigations in the visible light range. Therefore, this

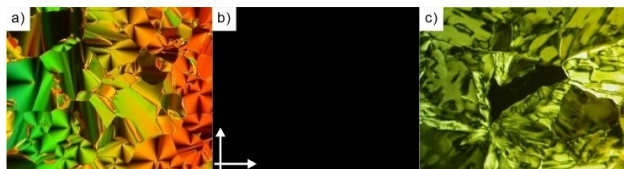


**Figure 7.** Textures observed under POM as recorded between two microscopy glass plates (distance ca. 10  $\mu\text{m}$ ) on cooling for **A10/16** in: a)  $\text{Col}_{\text{hex}}$  phase at 147 °C; b)  $\text{Cub}_{\text{bi}}/Ia\bar{3}d$  phase at 145 °C; c)  $\text{Tet}_{\text{bi}}$  phase at 45 °C; in the dark area the *c*-axis is perpendicular to the substrate. The arrows indicate the directions of polarizer and analyser, which is identical in all three photos; for additional textures of other compounds, see Figures S5 and S6.

mesoscale conglomerate appears optically inactive on a macroscopic length scale.

Upon heating the isotropic  $\text{Cub}_{\text{bi}}/I23$  phase of compounds **A10/14–A10/18** it is replaced by the birefringent tetragonal phase ( $\text{Tet}_{\text{bi}}$ ), followed by a cubic  $\text{Cub}_{\text{bi}}/Ia\bar{3}d$  phase. The diffraction pattern of the  $\text{Tet}_{\text{bi}}$  phase is identical for all compounds (see Figure 8a for an example) and this phase has been analysed in detail in our previous report for the case of compound **A10/18**.<sup>[58]</sup> Accordingly, this tetragonal phase is derived from the  $Ia\bar{3}d$  double gyroid phase by continuous stretching the lattice along the *c*-direction as shown for **A10/16** in Figure 8b,c. The space group is  $P4_12_1/P4_32_12$ , which represents a pair of enantiomorphic chiral space groups as confirmed by high resolution SAXS, simulated diffraction patterns and by resonant soft X-ray scattering (RSoXS) at the Carbon K-edge.<sup>[58]</sup> In all three investigated  $\text{Tet}_{\text{bi}}$  phases the parameter  $a_{\text{tet}}$  is 11.1–12.5 nm, thus corresponding to  $a_{\text{cub}}$  of the adjacent  $Ia\bar{3}d$  phase ( $a_{\text{cub}} = 11.1\text{--}11.5 \text{ nm}$ , Table 2) and the parameter  $c_{\text{tet}}$  rises with lowering temperature until it reaches 14.3–14.6 nm close to the  $\text{Tet}_{\text{bi}}\text{--Cub}_{\text{bi}}/I23$  transition temperature. At the continuous transition to the high temperature cubic phase with  $Ia\bar{3}d$  lattice, the *c*-parameter of the  $\text{Tet}_{\text{bi}}$  phase decreases and becomes identical with  $a_{\text{tet}}$  (Figures 9a,b, S14). At this temperature the compound becomes optically isotropic, remains highly viscous and no chiral domains can be observed. This indicates the transition to an achiral cubic  $Ia\bar{3}d$  phase, which remains till the final transition to the isotropic liquid takes place at  $\sim 157 \text{ °C}$  for all three compounds **A10/14–A10/18**. The SAXS pattern of this high temperature cubic mesophase (Figure 8d) confirms an  $Ia\bar{3}d$  space group with  $a_{\text{cub}} = 11.1\text{--}11.5 \text{ nm}$ , slightly growing with chain length (Table 2). In the *I23* phase the parameter  $a_{\text{cub}}$  is 17.7–18.7 nm, corresponding to an increase by 50% compared to  $a_{\text{cub}}$  in the  $\text{Cub}_{\text{bi}}/Ia\bar{3}d$  phase, in line with the elongation of the networks from a double to a

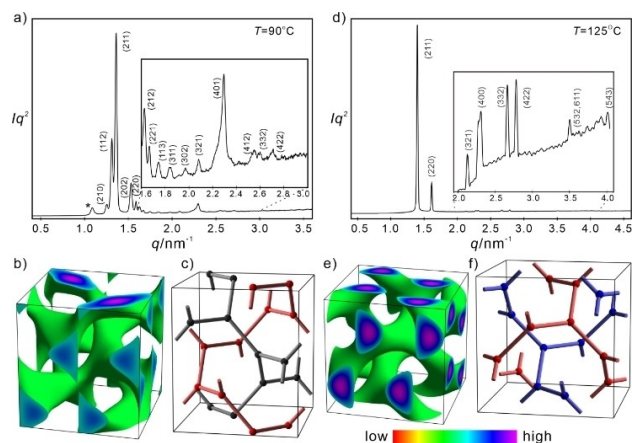


**Figure 8.** SAXS diffractogram of **A10/16** on cooling: a) in the  $\text{Tet}_{\text{bi}}$  phase at  $T = 90 \text{ °C}$  and d) in the  $\text{Cub}_{\text{bi}}/Ia\bar{3}d$  phase at  $T = 125 \text{ °C}$  and the corresponding ED maps of the double network phases b) the  $\text{Tet}_{\text{bi}}$  phase and e) the  $\text{Cub}_{\text{bi}}/Ia\bar{3}d$  phase (the asterisk signal in a) is from Cr). Corresponding schematic presentation of their double network structures are provided in c) and f); in f) there are two enantiomorphic networks with opposite helicity (blue/red), whereas in e) one of the networks (grey) has a reduced coherence length of helix sense.

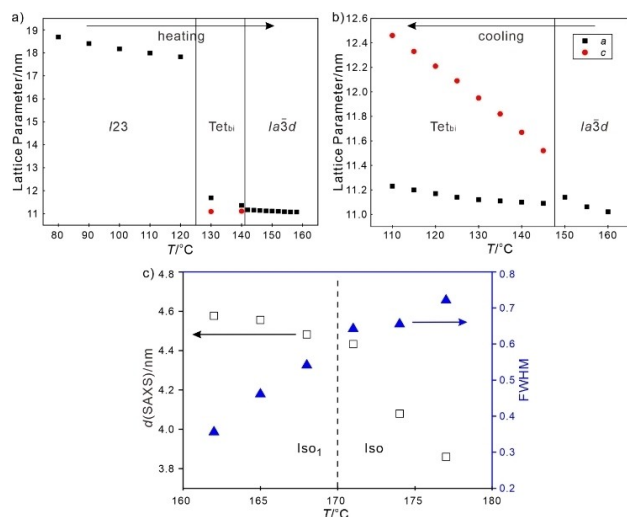


**Figure 9.** Temperature scans of the SAXS of **A10/14**. a) Lattice parameter variation of **A10/14** and during the phase transition on heating and b) between  $Tet_{bi}$  phase and  $Cub_{bi}/Ia\bar{3}d$  phase upon cooling; c) shows  $d$ -spacing and line width at half maximum (FWHM) for the main SAXS reflection as observed on continuous heating in the isotropic liquid state around the  $Iso_1$ -Iso transition, see Figure S14 for additional temperature scans.

triple network structure (Figure 1, Table 2). For **A10/14** the temperature range of the  $Ia\bar{3}d$  cubic phase is only short, but it expands with growing chain length  $n$ . In contrast, the  $Cub_{bi}/I23$  phase range narrows with growing  $n$  and has disappeared for  $n=20$ . This apparently “achiral”  $I23$  phase is metastable with respect to the  $Tet_{bi}$  phase and is replaced in its whole temperature range by the birefringent  $Tet_{bi}$  phase after about 20–60 minutes storage. The actual time required for this transition decreases with rising temperature. For this reason, the  $Cub_{bi}/I23$  phase is only observed on heating from the crystalline solid in a limited temperature range, while on cooling from the isotropic liquid the  $Cub_{bi}/Ia\bar{3}d$  and  $Tet_{bi}$  phases were found exclusively (Figure 2). Moreover, the transition  $Cub_{bi}/I23 \rightarrow Tet_{bi}$  becomes faster with growing chain length from  $n=14$  to  $n=18$  and it totally disappears for the longest compound **A10/20**. For this compound, exclusively a broad region of the  $Cub_{bi}/Ia\bar{3}d$  phase is observed on heating. Upon cooling, the  $Cub_{bi}/Ia\bar{3}d$  phase, developing from the metastable  $Col_{hex}$  phase (see Figure S6c,d), is replaced at 135°C by the birefringent  $Tet_{bi}$  phase (Figure S6e) in a similar way as observed for **A10/18**.

Overall there is a sequence  $Cub_{bi}/I23^{[*]} \rightarrow Cub_{bi}/Ia\bar{3}d + Tet_{bi}$  upon alkyl chain elongation. The phase sequence  $Ia\bar{3}d \rightarrow I23^{[*]} \rightarrow Ia\bar{3}d$  was previously found with growing alkyl chain volume in some other homologous series of rod-like molecules with  $Cub_{bi}$  phases.<sup>[32,38–40,44,50,51,64,65]</sup> This sequence is usually associated with a continuous increase of the twist angle  $\Phi$  between the molecules in the rafts forming the helical networks, leading to a phase sequence involving a long pitch (small twist)  $Ia\bar{3}d_{(L)}$  phase followed by  $I23^{[*]}$  and a short pitch (large twist)  $Ia\bar{3}d_{(S)}$  phase.<sup>[50,51]</sup> The same is found in the present case where the twist angle  $\Phi$  increases from 7.5–7.9° in the  $I23^{[*]}/I23$  phases to 7.8–8.1° in the  $Ia\bar{3}d$  phase (see Table 2),<sup>[66]</sup> in line with a short

pitch  $Ia\bar{3}d_{(S)}$  type of this phase. This is supported by the observation of an induced  $I23^{[*]}$  phase in the contact region with a long pitch  $Ia\bar{3}d_{(L)}$  phase material and its absence in contact with a short pitch  $Ia\bar{3}d_{(S)}$  compound (see Figure S15). Thus, increasing chain volume increases the intermolecular twist  $\Phi$  along the aggregates and this leads to the transition  $Cub_{bi}/I23^{[*]} \rightarrow Cub_{bi}/Ia\bar{3}d_{(S)}$  upon chain elongation. An increase of  $\Phi$  is also observed with rising temperature, indicated by a decreasing lattice parameter within the distinct phase ranges as well as jumps at the transitions between the different network phases (see compounds **A10/14** and **A10/18** in Table 2 and Figure 9a). Thus, the twist  $\Phi$  increases from  $I23$  via  $Tet_{bi}$  to  $Ia\bar{3}d_{(S)}$ , in line with thermal chain expansion.

**$Col_{hex}$  phase.** – In addition, for the three longest homologues **A10/16**–**A10/20** a short range of a  $Col_{hex}$  phase of ~5–6 K is observed on cooling from the isotropic liquid as a metastable phase before the transition to  $Cub_{bi}/Ia\bar{3}d$  phase (Figure 7a). This indicates an increasing intermaterials (aromatics vs. aliphatics) interface curvature with growing chain length  $n$ . Due to the metastability only in one case ( $n=18$ ) the hexagonal lattice could be confirmed by XRD and the lattice parameter was found to be  $a_{hex} = 5.07$  nm.<sup>[58]</sup> About 5 molecules are arranged side by side in the rafts forming the columnar aggregates. In the  $Cub_{bi}$  and  $Tet_{bi}$  phases this number is a bit smaller, between 3.2–3.7 molecules (Table 2). We attribute this, at least in part, to the uniformly helical organization of the  $\pi$ -conjugated rods in the network phases, allowing a denser core packing, while the alkyl chain packing is not changed at the  $Col_{hex}$ - $Cub_{bi}$  transition. This provides an increased aliphatic-aromatic intermaterials interface curvature leading to the reduction of the diameter of the network cores. Remarkably, for compound **A10/14**, being at the borderline to the short-chain compounds, the metastable  $Col_{hex}$  phase is replaced by  $Iso_1^{[*]}$ .

**Polyamorphism in the liquid state.** – In the case of the long chain compounds **A10/16** to **A10/20** there is an extremely broad (30–40 K) and almost symmetric feature in the isotropic liquid range with a maximum around 170°C on heating and around 165°C on cooling, associated with an enthalpy change  $\Delta H = 2.5$ – $4.0$  kJ mol<sup>-1</sup> (Table 1 and Figure 3d). The sample remains optically isotropic and fluid in this temperature range and this transition is not associated with conglomerate formation, and therefore this achiral isotropic mesophase range between the  $Cub_{bi}$  phase and the maximum of the broad DSC feature is named  $Iso_1$ .<sup>[67,68]</sup> The reversible and continuous transition between  $Iso$  and  $Iso_1$  takes place about 10–20 K above the next phase transition to a  $(Cub_{bi}/Col_{hex})$  LC phase. It is attributed to the continuous transition between the ordinary isotropic liquid phase ( $Iso$ ) and a percolated  $Iso_1$  phase by the continuous growth of cybotactic clusters of the networks (Figure 6).<sup>[51,68]</sup> Upon further cooling this broad feature is followed by a sharp peak at 147–152°C, leading to  $Col_{hex}$  followed by the transition to the  $Cub_{bi}/Ia\bar{3}d$  phase at around 144°C (Table 1). The total enthalpy of these two transitions is about 2 kJ mol<sup>-1</sup> which is a bit smaller than the broad feature in the isotropic range, indicating that major molecular aggregation takes already place in the range of the  $Iso$ - $Iso_1$  transition. Figure 9c shows the dependence of the  $d$ -spacing and line

width at half maximum (FWHM) of the diffuse SAXS of **A10/14** on continuous heating in the isotropic liquid range. A continuous decrease of the coherence length across the Iso<sub>1</sub>–Iso transition is observed in the investigated temperature range of the liquid state. This supports the proposed disruption of the networks at the Cub<sub>bi</sub>–Iso<sub>1</sub> transition and the almost continuous reduction of the correlation length of network order with further rising temperature (Figure 6).

For compound **A10/12**, representing a short chain compound located at the borderline to the long chain compounds, there are two DSC features in the isotropic liquid range on cooling (Figure 3c), an almost symmetric and very broad one at higher temperature between 155–185 °C and the typical bump with tailing occurring at 162 °C. The latter is again associated with the onset of chirality synchronization by conglomerate formation, whereas no change can be observed in the temperature range of the broad feature. This indicates a liquid state triamorphism due to the continuous emergence and growth of a local network structure in the Iso<sub>1</sub> range, which reaches the critical connectivity for chirality synchronization at the transition to Iso<sub>1</sub><sup>[\*]</sup> and on further cooling fuses to a long range cubic *I23* network at the next phase transition at 156 °C (Figure 6). In this case a significant molecular aggregation and network formation takes place before chirality synchronization sets in. This kind of triamorphism was previously observed for benzil derived polycatenars.<sup>[51]</sup>

For compound **A10/14**, representing a long chain compound at the border line to the short chain compounds the same liquid state triamorphism Iso–Iso<sub>1</sub>–Iso<sub>1</sub><sup>[\*]</sup> is observed, though in this case the achiral Cub<sub>bi</sub>/*Ia3d* phase is formed instead of the chiral *I23*<sup>[\*]</sup> phase on further cooling (Table 1, Figure 3). This means that chirality synchronization in the liquid state is supported by decreasing chain length and lowering temperature and that upon chain length reduction the internetwork correlation in the adjacent LC phase changes from enantiophilic for  $n = 14$  to enantiophobic for  $n = 12$ .

Overall, there are two groups of compounds. The short chain compounds with  $n = 5–12$  show ambidextrous mirror symmetry breaking in the Cub<sub>bi</sub>/*I23*<sup>[\*]</sup> as well as in the Iso<sub>1</sub><sup>[\*]</sup> phases, whereas for the long chain compounds with  $n = 14–20$  the mirror symmetry broken Cub<sub>bi</sub>/*I23*<sup>[\*]</sup> and Iso<sub>1</sub><sup>[\*]</sup> phases are replaced by mesoscale conglomerates (Tet<sub>bi</sub>/*I23*), and achiral cubic (*Ia3d*), columnar (Col<sub>hex</sub>) and isotropic liquid (Iso<sub>1</sub>) mesophases. Compounds at the transition between these two groups ( $n = 12, 14$ ) show liquid state polyamorphism with a chiral liquid mesophase at low (Iso<sub>1</sub><sup>[\*]</sup>) and an achiral liquid mesophase (Iso<sub>1</sub>) at higher temperature. This indicates that macroscopic mirror symmetry breaking is gradually lost with growing alkyl chain length  $n$  with the major change taking place from  $n = 12 \rightarrow 14$ .

## Discussion

### LC phase transitions in relation to chirality synchronization

As noted in the Introduction, the Cub<sub>bi</sub> phases of polycatenar compounds involve a helical organization of the rod-like molecules along the individual networks and the network junctions ensure a uniform helicity along the networks.<sup>[10,17,18,20,37]</sup> We hypothesize that the capability of a denser chirality synchronized helical organization of the molecules in the networks of the Cub<sub>bi</sub> phases is a main reason for the wide ranges of Cub<sub>bi</sub> phases observed for polycatenar and related rod-like molecules,<sup>[32]</sup> while for other classes of compounds, which do not evolve a helical organization,<sup>[36]</sup> the Cub<sub>bi</sub> phases are rare and restricted to narrow chain volume and temperature ranges.<sup>[30–35,69]</sup> It appears that this stabilization of the networks by chirality synchronization can even be retained after loss of the long-range cubic lattice in the adjacent mirror symmetry broken isotropic liquid mesophases (Iso<sub>1</sub><sup>[\*]</sup>), as observed for the short chain compounds **A10/7–A10/12**.

Both, the kind of network structure (topology, number of interwoven networks, valency and geometry of the junctions), as well as the mode of interhelix interactions between adjacent network, being either enantiophobic or enantiophilic, decide if the overall structure becomes a chiral conglomerate or an achiral *meso*-structure.<sup>[58]</sup> The Cub<sub>bi</sub>/*Ia3d* phase is such a *meso*-structure formed by two enantiomorphic networks with opposite helicity, as proven in previous RSoXS investigations of the *Ia3d* phase of compound **A10/18**.<sup>[36]</sup> This *meso*-structure is stable as long as the interactions between the two helical networks are more or less enantiophilic, too, i.e. if heterochiral self-assembly between the networks is favored. As the networks are stretched along the *c* direction at the continuous transition to the Tet<sub>bi</sub> phase the interhelical interaction appears to change from enantiophilic to enantiophobic, i.e. the homochiral self-assembly of adjacent networks becomes favored. This requires that either the network structure changes, or alternatively, uniform helicity is removed in at least one of the networks. It is proposed that the first case leads to the Cub<sub>bi</sub> phase with chiral *I23* space group, whereas the second case causes a transition to the Tet<sub>bi</sub> phase. As previously shown for **A10/18**, the Tet<sub>bi</sub> phase can be considered as an intermediate phase at the transition between the chiral *I23* phase and the achiral *Ia3d* phase.<sup>[58]</sup> At the transition to this mirror symmetry broken Tet<sub>bi</sub> phase the achiral *meso*-structure of the *Ia3d* phase is broken by retaining uniform helicity only along one network, while losing it along the other one. One network is racemized in the *P4*<sub>1</sub>*2*<sub>1</sub>*2* phase and the other one in the enantiomorphic *P4*<sub>3</sub>*2*<sub>1</sub>*2* phase. This leads to a pair of chiral space groups *P4*<sub>1</sub>*2*<sub>1</sub>*2* and *P4*<sub>3</sub>*2*<sub>1</sub>*2* forming a mesoscale conglomerate, thus providing a new way of mirror symmetry breaking in soft matter by partial *meso*-structure racemization at the transition from enantiophilic to enantiophobic interhelical self-assembly between networks.<sup>[58]</sup>

For the compounds **A10/14–A10/18** reported here, there is a competition between the Tet<sub>bi</sub> and the Cub<sub>bi</sub>/*I23* phases, the former representing the thermodynamically more stable structure. The notable feature of the *I23* phase of all long chain

compounds is the absence of visible conglomerate formation. This could be explained by relatively weak enantiophobic interhelix interactions, tolerating relatively large contact areas between small domains with opposite chirality (racemic interfaces). Therefore, the chiral domains of the conglomerate retain a small size and cannot be detected by optical microscopy. Overall there appears to be a decreasing strength of the enantiophobic character of the interhelical network interaction and a transition to an enantiophilic interaggregate chirality synchronization with rising chain length  $n$ . This leads to a LC phase sequence  $\text{Cub}_{\text{bi}}//I23^{[*]}-\text{Cub}_{\text{bi}}/I23-\text{Tet}_{\text{bi}}/P4_12_2/P4_32_12-\text{Cub}_{\text{bi}}/Ia\bar{3}d$  with growing chain length, i.e. it appears that the changing mode of chirophilic self-assembly modulates the phase structure.

### Liquid state polyamorphism and mirror symmetry breaking

In line with this change of interaggregate chirality synchronization the polyamorphism in the liquid phase changes, too. While for compounds **A10/5–A10/10** a mirror symmetry broken  $\text{Iso}_1^{[*]}$ -phase (presumably with local  $I23$  structure) is observed, it is replaced for the long chain compounds **A10/16–A10/20** by an achiral  $\text{Iso}_1$  phase. Compounds **A10/12** and **A10/14**, located at the transition between the short and long chain compounds show both, the chiral  $\text{Iso}_1^{[*]}$ -phase as well as the achiral  $\text{Iso}_1$  phase in the sequence  $\text{Iso}-\text{Iso}_1-\text{Iso}_1^{[*]}-\text{Cub}_{\text{bi}}$  on cooling, while the  $\text{Cub}_{\text{bi}}$  type switches from the chiral  $I23^{[*]}$  to the achiral  $Ia\bar{3}d$ -type at the transition from **A10/12** to **A10/14** (Figure 2).

For the compounds with short chains ( $n=5-10$ ) the absence of any  $\text{Iso}-\text{Iso}_1$  transition in the liquid range indicates the absence of notable network formation in the liquid state. This is attributed to the relatively weak segregation between rigid aromatic units and the relatively short flexible alkyl chains. Therefore, chirality synchronization is required for the onset of network formation in the liquid state of the short chain compounds. In a feed-back the evolving networks support macroscopic chirality synchronization. Thus, an  $\text{Iso}-\text{Iso}_1^{[*]}$  transition with ambidextrous mirror symmetry breaking is observed, though the driving force of aggregate formation by the self-assembly due to the aromatic-aliphatic segregation is still weak in the liquid state.

In contrast, for the compounds with long chains ( $n=16-20$ ) aromatic-aliphatic segregation becomes stronger, allowing self-assembly by network formation already in the liquid state even in the absence of chirality synchronization. However, on the other hand, there appears to be a weaker driving force for chirality synchronization for these compounds with long chains, leading to the  $\text{Iso}-\text{Iso}_1$  transition without mirror symmetry breaking. Only at the transition between these two different modes of liquid state diamorphism, when segregation and chirality synchronization forces are both sufficiently strong, the  $\text{Iso}-\text{Iso}_1-\text{Iso}_1^{[*]}$  triamorphism is observed ( $n=12, 14$ ).

Considering the network formation as a dynamic mode of supramolecular polymerization the growth is considered as isodesmic around the  $\text{Iso}-\text{Iso}_1$  transition of the long chain compounds and becomes cooperative for the  $\text{Iso}-\text{Iso}_1^{[*]}$  tran-

sition of the short chain compounds.<sup>[70]</sup> It is noted that supramolecular polymerization is in this case only driven by the nano-scale segregation of the polyaromatic units from the aliphatic molecular segments<sup>[71]</sup> and does not involve any specific strong interaction like H-bonding. Therefore, it is sensitive to slight molecular structural modifications like chain length variation.

For the  $\text{Iso}_1^{[*]}$  phase occurring besides the  $\text{Cub}_{\text{bi}}//I23^{[*]}$  phase a  $I23$ -like local triple network structure can be assumed as the most likely structure,<sup>[10]</sup> whereas the local structure in the achiral  $\text{Iso}_1$  phase is less obvious. It could either be a local helical network with  $Ia\bar{3}d$ -like *meso*-structure, as previously proposed for benzil based molecules.<sup>[51]</sup> Alternatively, a random network structure without or with only short-range chirality synchronization along the networks can be envisaged. The latter is supported by the very distinct shapes of the  $\text{Iso}-\text{Iso}_1$  and  $\text{Iso}-\text{Iso}_1^{[*]}$  transitions in the DSC traces, associated with distinct growth mechanisms. The cooperative nature of the  $\text{Iso}-\text{Iso}_1^{[*]}$  transitions (distinct DSC peak) suggests that chirality synchronization might be responsible for the cooperativity. A cooperative growth would also be expected if the  $Ia\bar{3}d$ -like phase structure would be formed, which is also chirality synchronized, though with opposite sign in the two networks. The isodesmic growth in the case of the achiral  $\text{Iso}_1$  phase (broad feature in DSC) is a hint that chirality synchronization is obviously not involved in this transition and therefore a randomized, only short-range helical network structure is proposed for this achiral  $\text{Iso}_1$  phase. This is additionally supported by the observation that for all long chain compounds **A10/16–A10/20** an achiral  $\text{Col}_{\text{hex}}$  phase is formed below  $\text{Iso}_1$  before the transition to the chirality synchronized  $\text{Cub}_{\text{bi}}/Ia\bar{3}d$  phase takes place. For compounds **A10/12** and **A10/14** at the cross-over between short- and long chain compounds the non-helical  $\text{Iso}_1$  phase is formed first and chirality synchronization leads to the  $I23^{[*]}$ -like local structure at the transition to the  $\text{Iso}_1^{[*]}$  range. For compound **A10/12** enantiophobic network coupling is retained at the transition to the chiral  $\text{Cub}_{\text{bi}}//I23^{[*]}$  phase, whereas for **A10/14** the transition to the long-range cubic lattice is associated with development of enantiophilic network correlation in the achiral  $\text{Cub}_{\text{bi}}/Ia\bar{3}d$ -phase.

### Effects of chain length

Though the transition between the  $Ia\bar{3}d$  and  $I23^{[*]}$  type  $\text{Cub}_{\text{bi}}$  phases with a  $\text{Tet}_{\text{bi}}$  phase as intermediate structure at this transition can be understood by a change of the mode of internetwork chirality synchronization from enantiophilic to enantiophobic, there is still the question how this is related to the molecular structure. The effects of chain elongation can be divided into the *general effects* on mesophase-type and -stability, and the *specific chirality related effects*.

Among the *general effects*, a growing chain length  $n$  provides a stronger segregation of the flexible chains from the rod-like units which then supports the self-assembly in the liquid and LC phases. It leads to long-range network formation in the LC phases, and dynamic mesoscale networks in the liquid

state if  $n \geq 12$  (Iso–Iso<sub>1</sub> transition). In addition, the chain volume affects the curvature of the intermaterials dividing interfaces and leads to the metastable Col<sub>hex</sub> phase for long chain compounds with  $n = 16–20$ . However, due to the chain disorder around the columns and networks there is no significant odd–even effect for any of the phase transitions (see Figure 2).

The *specific effects* induce helicity and influence the mode and strength of interhelical network coupling. The imbalance between the cross-sectional areas of cores and chains in polycatenar mesogens leads to the helical twist  $\Phi$  between the rafts of molecules along the networks. Growing chain volume increases  $\Phi$  and reduces the helical pitch length. Thus, alkyl chain elongation supports the chirality synchronization within the individual networks. However, it is also known that a change of the helical twist can modify the mode of interhelical coupling (enantiophilic vs. enantiophobic) though the precise relations are still largely unknown.<sup>[72–74]</sup> The helical pitch length also affects the distances between the network junctions, because the twist between them is a fixed value. If this distance is in conflict with the distances required by amphiphilic self-assembly (e.g. the 70.5° twist between the trigonal junctions in the  $la\bar{3}d$  phase), then the phase structure is changed and the spatial orientation between the helical network segments also changes. This leads to a modified helix orientation which can also affect the preferred mode of coupling between the networks. The interplay between both effects gives rise to the complex phase sequences with a transition between enantiophilic and enantiophobic internetwork correlation (Cub<sub>bi</sub>/ $la\bar{3}d$ –Tet<sub>bi</sub>–(Cub<sub>bi</sub>/ $I23^{[*]}$ )–Cub<sub>bi</sub>/ $I23^{[*]}$ ). There is also an effect of chain length on the strength of chirality synchronization between the networks, because growing chain length decreases the interaggregate interactions (due to growing distances and chain disorder), it reduces the strength of coupling between the networks. As a result, chiral Iso<sub>1</sub><sup>[\*]</sup> and Cub<sub>bi</sub>/ $I23^{[*]}$  phases of the short chain compounds are replaced by the achiral Iso<sub>1</sub> phase and the mesoscale conglomerate type Cub<sub>bi</sub>/ $I23$  phase upon chain elongation.

The sequence  $la\bar{3}d_{(L)} \rightarrow I23^{[*]} \rightarrow la\bar{3}d_{(S)}$  was previously found for polycatenar<sup>[32,38,39,50,51]</sup> and other rod-like molecules and supramolecules, like bis(4-alkoxybenzoyl)hydrazines (BABH-*n*)<sup>[65,75]</sup> and 4'-alkoxy-3'-nitrophenyl-4-carboxylic acid dimers (ANBC-*n*)<sup>[64,76]</sup> Also for these compounds birefringent 3D phases as well as Col<sub>hex</sub> and Iso<sub>1</sub> phases<sup>[32,68]</sup> were reported to accompany their cubic phases, especially around the  $I23^{[*]}$ – $la\bar{3}d$  transitions.<sup>[22,32,41]</sup> The present work provides a preliminary understanding of these phases and their transitions on the basis of the helical self-assembly of the rod-like cores and the effect of the alkyl chains on molecular aggregation, chirophilicity and strength of interhelical coupling.

## Summary and Conclusions

In summary, we reported the soft self-assembly of a series of azobenzene-based polycatenars terminated with a 3,4,5-tridecyloxybenzoate moiety at one end and a single alkoxy chain with varying chain length  $n = 5–20$  at the opposite end. For short

and medium chain homologues an ambidextrous chiral Cub<sub>bi</sub> phase with  $I23$  lattice (Cub<sub>bi</sub>/ $I23^{[*]}$ ) is observed as stable structure. Some Cub<sub>bi</sub> phases do not crystallize once formed, making them candidates for technological applications of the chirality synchronized network structures after asymmetry amplification and formation of uniform chirality. For compounds with a longer chain the achiral Cub<sub>bi</sub> phase with  $la\bar{3}d$  lattice (Cub<sub>bi</sub>/ $la\bar{3}d$ ) and a tetragonal phase with  $P4_12_1/P4_32_2$  lattice were observed as stable LC phases. Overall there appears to be a transition from enantiophobic self-assembly in the chiral  $I23^{[*]}$  phase of the short chain compounds to enantiophilic internetwork interactions in the achiral  $la\bar{3}d$  phase of the long chain compounds. An apparently achiral  $I23$  phase and a tetragonal phase, both representing mesoscale conglomerates, appear as intermediate states at this transition. All compounds show an additional polyamorphism in the isotropic liquid state involving a mirror symmetry broken Iso<sub>1</sub><sup>[\*]</sup> phase for the short chain compound and an achiral Iso<sub>1</sub> phase for the long chain compounds, both occurring below the ordinary Iso phase. It is concluded that there is a growing general driving force for self-assembly with growing chain length. On the other hand, the strength of interhelical chirality synchronization decreases and the mode of chirophilic internetwork interactions changes from being enantiophobic to enantiophilic by growing alkyl chain length. Thus, in the reported case short chains are favourable for mirror symmetry breaking.

Overall, this work contributes to the understanding of supramolecular polymerization of achiral molecules with properly functionalized  $\pi$ -conjugated units into dynamic helical networks, thus leading to the spontaneous emergence of homochirality in LC network phases and isotropic melts of achiral molecules.<sup>[10,18–20]</sup> It is noted that recently a similar mirror symmetry breaking was also observed during solution polymerizations of achiral monomers to covalent helical polymers,<sup>[77]</sup> demonstrating the generality of this concept. Owing to the azobenzene units incorporated in the molecular structures photo switching upon light irradiation (see Figure S16) provides additional possibility for these materials to be used in chiroptical and other technological applications.<sup>[1,2]</sup>

## Experimental Section

**Synthesis:** The appropriate 4-(4-alkoxyphenyldiazenyl)benzoic acid  $1/n$  (1.0 mmol) was converted to the corresponding acid chloride by refluxing under stirring for one hour with excess SOCl<sub>2</sub> (10 mL) and few drops of DMF as a catalyst. The excess SOCl<sub>2</sub> was removed under reduced pressure and 4'-hydroxybiphenyl-4-yl 3,4,5-tridecyloxybenzoate (**2**) (1.0 mmol) dissolved in 25 mL of dry CH<sub>2</sub>Cl<sub>2</sub> was added together with Et<sub>3</sub>N (1.2 mmol) and a catalytic amount of pyridine. The reaction mixture was refluxed for 6 h. At the end of the reaction as confirmed from the TLC, the mixture was cooled, poured into ice-water (100 mL) and the crude product was extracted with CH<sub>2</sub>Cl<sub>2</sub> (3 × 50 mL). The organic layer was washed twice with water and dried over anhydrous MgSO<sub>4</sub> and the solvent was removed under reduced pressure. The resulting orange solid material was purified by column chromatography over silica gel using CH<sub>2</sub>Cl<sub>2</sub> as eluent, followed by recrystallization from EtOH/CHCl<sub>3</sub> mixture (3/1, v/v) to give the final compounds as orange crystals (yields: 55–68% purified compounds). The analytical data of

**A10/5** are given as representative example; those of all other homologous compounds **A10/n** with  $n=6-16$  and 20 are collated in the Supporting Information; compound **A10/18** was reported previously.<sup>[36]</sup>

**A10/5:** <sup>1</sup>H NMR (500 MHz, CDCl<sub>3</sub>) δ 8.37 (d,  $J=7.9$  Hz, 2H, Ar–H), 8.05–7.90 (m, 4H, Ar–H), 7.77–7.59 (m, 4H, Ar–H), 7.44 (s, 2H, Ar–H), 7.38–7.26 (m, 4H, Ar–H, overlapped with CDCl<sub>3</sub>), 7.04 (d,  $J=8.3$  Hz, 2H, Ar–H), 4.15–3.99 (m, 8H, Ar–OCH<sub>2</sub>CH<sub>2</sub>), 1.97–1.68 (m, 8H, Ar–OCH<sub>2</sub>CH<sub>2</sub>), 1.67–1.17 (m, 46H, 23 × CH<sub>2</sub>), 0.97 (t,  $J=7.2$  Hz, 3H, CH<sub>3</sub>), 0.90 (t,  $J=6.9, 3.3$  Hz, 9H, 3 × CH<sub>3</sub>). <sup>13</sup>C NMR (126 MHz, CDCl<sub>3</sub>) δ 165.04, 164.75 (C=O), 162.50, 155.87, 152.99, 150.58, 150.45, 146.88, 143.13, 138.30, 138.11 (C<sub>ar</sub>–O, C<sub>ar</sub>–N), 131.25, 130.38 (C<sub>ar</sub>–H), 128.25 (C<sub>ar</sub>–quart), 128.21, 125.34 (C<sub>ar</sub>–H), 123.84 (C<sub>ar</sub>–quart), 122.56, 122.13, 122.04, 114.86, 108.66 (C<sub>ar</sub>–H), 73.60, 69.31, 68.47 (CH<sub>2</sub>O), 31.94, 31.91, 30.35, 29.73, 29.67, 29.63, 29.60, 29.58, 29.57, 29.39, 29.34, 29.32, 28.86, 28.16, 26.09, 26.06, 22.70, 22.68, 22.44 (CH<sub>2</sub>), 14.10, 14.00 (CH<sub>3</sub>). Elemental analysis, calc. for C<sub>67</sub>H<sub>92</sub>N<sub>2</sub>O<sub>8</sub>: C 76.39%, H 8.80%, N 2.66%, found: C 76.32%, H 8.75%, N 2.59%.

**Investigations:** POM was conducted with an Optiphot 2 Nikon microscope on a Mettler FP82HT heating stage between non-treated microscopy glass plates with a distance of 10–20 μm. Larger distances were achieved by using a wedge-sell configuration. DSC scans were performed with a DSC-7 and DSC-8000 from Perkin Elmer, with heating and cooling rates of 10 Kmin<sup>-1</sup> in aluminium pans (30 μL). In-house XRD was carried out in glass capillaries (1 mm cross section, Hilgenberg) or with open droplets on a glass surface using CuKα radiation ( $\lambda=0.154$  nm) and a Vantec 500 area detector. The detector sample distances were 26.80 cm for SAXS and 9.00 cm for WAXS. The samples were held on a self-made temperature-controlled heating stage. High-resolution SAXS patterns were recorded at beamline BL16B1 of Shanghai Synchrotron Radiation Facility (SSRF) with a MarCCD 165 detector. Powder samples were held in capillaries and temperature controlled with a Linkam hot stage. For each temperature, the samples were irradiated 10–120 s to acquire data with enough resolution and signal intensity for electron density map reconstruction.

## Acknowledgements

M. Alaasar acknowledges the German Research Foundation (DFG) for the financial support (AL2378/1-1, 424355983 and 43494874 – GRK 2670) and F. Liu acknowledges financial supporting from National Natural Science Foundation of China (21761132033). The authors are grateful to Beamline BL16B1 at SSRF (Shanghai Synchrotron Radiation Facility, China) for providing the beamtime. Open Access funding enabled and organized by Projekt DEAL.

## Conflict of Interest

The authors declare no conflict of interest.

## Data Availability Statement

The data that support the findings of this study are available in the supplementary material of this article.

**Keywords:** alkyl chain engineering · azobenzene · chirality · liquid crystals · mirror symmetry breaking

- [1] a) H. K. Bisoyi, Q. Li, *Chem. Rev.* **2022**, *122*, 4887; b) Z. J. Zheng, Y. Q. Lu, Q. Li, *Adv. Mater.* **2020**, *32*, 1905318.
- [2] a) M.-M. Zhang, K. Li, S.-Q. Zang, *Adv. Opt. Mater.* **2020**, *8*, 1902152; b) Y. Zhang, S. Yu, B. Han, Y. Zhou, X. Zhang, X. Gao, Z. Tang, *Matter* **2022**, *5*, 837.
- [3] a) J. L. Pasteur, *Ann. Chim. Phys.* **1848**, *24*, 442; b) E. Yashima, N. Ousaka, D. Taura, K. Shimomura, T. Ikai, K. Maeda, *Chem. Rev.* **2016**, *116*, 13752; c) Y. Wang, J. Xu, Y. Wang, H. Chen, *Chem. Soc. Rev.* **2013**, *42*, 2930; d) T. Matsuura, H. Koshima, *J. Photochem. Photobiol. C* **2005**, *6*, 7; e) D. B. Amabilino, R. M. Kellogg, *Isr. J. Chem.* **2011**, *51*, 1034; f) L. C. Sögütoglu, R. R. Steendam, H. Meeks, E. Vlieg, F. P. Rutjes, *Chem. Soc. Rev.* **2015**, *44*, 6723.
- [4] a) T. Buhse, J. M. Cruz, M. E. Noble-Teran, D. Hochberg, J. M. Ribó, J. Crusats, J. C. Micheau, *Chem. Rev.* **2021**, *121*, 2147; b) B. Chang, X. Li, T. Sun, *Eur. Polym. J.* **2019**, *118*, 365.
- [5] P. J. M. Stals, P. A. Korevaar, M. A. J. Gillissen, T. F. A. de Greef, C. F. C. Fittie, R. P. Sijbesma, A. R. A. Palmans, E. W. Meijer, *Angew. Chem. Int. Ed.* **2012**, *51*, 11297.
- [6] a) M. Liu, L. Zhang, T. Wang, *Chem. Rev.* **2015**, *115*, 7304; b) Y. Sang, M. Liu, *Chem. Sci.* **2022**, *13*, 633.
- [7] C. Tschierske, *Angew. Chem. Int. Ed.* **2013**, *52*, 8828.
- [8] *Handbook of Liquid Crystals*, 2nd ed. (Eds.: J. W. Goodby, P. J. Collings, T. Kato, C. Tschierske, H. Gleeson, P. Raynes) Wiley-VCH, Weinheim, Germany, **2014**.
- [9] a) T. Kato, J. Uchida, T. Ichikawa, T. Sakamoto, *Angew. Chem. Int. Ed.* **2018**, *57*, 4355; b) D. L. Gin, X. Lu, P. R. Nemade, C. S. Pecinovsky, Y. Xu, M. Zhou, *Adv. Funct. Mater.* **2006**, *16*, 865; c) J. Voskuhl, M. Giese, *Aggregate* **2022**, *3*, e124; d) J. Uchida, B. Soberats, M. Gupta, T. Kato, *Adv. Mater.* **2022**, 2109063; e) Y.-K. Kim, J. H. Noh, K. Nayani, N. L. Abbott, *Soft Matter* **2019**, *15*, 6913.
- [10] a) C. Tschierske, G. Ungar, *ChemPhysChem* **2016**, *17*, 9; b) C. Tschierske, *Liq. Cryst.* **2018**, *45*, 2221.
- [11] a) H. Takezoe, *Top. Curr. Chem.* **2012**, *318*, 303; b) K. V. Le, H. Takezoe, F. Araoka, *Adv. Mater.* **2017**, *29*, 1602737.
- [12] a) Y. Takanishi, G. J. Shin, J. C. Jung, S.-W. Choi, K. Ishikawa, J. Watanabe, H. Takezoe, P. Toledano, *J. Mater. Chem.* **2005**, *15*, 4020; b) J. Thisayukta, Y. Nakayama, S. Kawauchi, H. Takezoe, J. Watanabe, *J. Am. Chem. Soc.* **2000**, *122*, 7441.
- [13] a) G. Dantlgraber, A. Eremin, S. Diele, A. Hauser, H. Kresse, G. Pelzl, C. Tschierske, *Angew. Chem. Int. Ed.* **2002**, *41*, 2408; b) L. E. Hough, M. Spannuth, M. Nakata, D. A. Coleman, C. D. Jones, G. Dantlgraber, C. Tschierske, J. Watanabe, E. Körblova, D. M. Walba, J. E. Maclennan, M. A. Glaser, N. A. Clark, *Science* **2009**, *325*, 452.
- [14] a) S. P. Sreenilayam, Y. P. Panarin, J. K. Vij, V. P. Panov, A. Lehmann, M. Poppe, M. Prehm, C. Tschierske, *Nat. Commun.* **2016**, *7*, 11369; b) A. Lehmann, M. Alaasar, M. Poppe, S. Poppe, M. Prehm, M. Nagaraj, S. P. Sreenilayam, Y. P. Panarin, J. K. Vij, C. Tschierske, *Chem. Eur. J.* **2020**, *26*, 4714.
- [15] R. Oikawa, H. Sasaki, Y. Takanishi, M. Sagisaka, J. Yamamoto, A. Yoshizawa, *Soft Matter* **2019**, *15*, 3179.
- [16] a) V. Borshch, Y.-K. Kim, J. Xiang, M. Gao, A. Jákli, V. P. Panov, J. K. Vij, C. T. Imrie, M. G. Tamba, G. H. Mehl, O. D. Lavrentovich, *Nat. Commun.* **2013**, *4*, 2635; b) M. R. Tuchband, D. A. Paterson, M. Salamonczyk, V. A. Normand, A. N. Scarbrough, E. Forsyth, E. Garcia, C. Wang, J. M. D. Storey, D. M. Walba, S. Sprunt, A. Jákli, C. Zhu, C. T. Imrie, N. A. Clark, *Proc. Natl. Acad. Sci. USA* **2019**, *116*, 10698; c) R. J. Mandle, J. W. Goodby, *Chem. Eur. J.* **2019**, *25*, 14454; d) Y. Cao, J. Feng, A. Nallapaneni, Y. Arakawa, K. Zhao, H. Zhang, G. H. Mehl, C. Zhu, F. Liu, *J. Mater. Chem. C* **2021**, *9*, 10020; e) M. M. Majewska, E. Forsyth, D. Pocięcha, C. Wang, J. M. D. Storey, C. T. Imrie, E. Gorecka, *Chem. Commun.* **2022**, *58*, 5285.
- [17] C. Dressel, F. Liu, M. Prehm, X. Zeng, G. Ungar, C. Tschierske, *Angew. Chem. Int. Ed.* **2014**, *53*, 13115.
- [18] C. Dressel, T. Reppe, M. Prehm, M. Brautzsch, C. Tschierske, *Nat. Chem.* **2014**, *6*, 971.
- [19] C. Dressel, W. Weissflog, C. Tschierske, *Chem. Commun.* **2015**, *51*, 15850.
- [20] C. Tschierske, C. Dressel, *Symmetry* **2020**, *12*, 1098.
- [21] a) A. Guijarro, M. Yus, *The origin of chirality in the molecules of life*, RSC Publishing, Cambridge, UK, **2009**; b) Q. Sallembien, L. Bouteiller, J. Crassous, M. Raynal, *Chem. Soc. Rev.* **2022**, *51*, 3436.
- [22] a) H. T. Nguyen, C. Destrade, J. Malthete, *Adv. Mater.* **1997**, *9*, 375; b) D. W. Bruce, *Acc. Chem. Res.* **2000**, *33*, 831; c) W. Weissflog, in

- Handbook of Liquid Crystals*, 2nd Ed., (Eds. J. W. Goodby, J. P. Collings, T. Kato, C. Tschierske, H. F. Gleeson, P. Raynes), Vol. 5, Wiley-VCH, Weinheim, Germany, 2014, pp. 89–174.
- [23] A. Zehnacker, M. A. Suhm, *Angew. Chem. Int. Ed.* **2008**, *47*, 6970.
- [24] R. P. Lemieux, *Chem. Soc. Rev.* **2007**, *36*, 2033.
- [25] M. Lehmann, M. Hügel, *Angew. Chem. Int. Ed.* **2015**, *54*, 4110.
- [26] H. Nagayama, S. K. Varshney, M. Goto, F. Araoka, K. Ishikawa, V. Prasad, H. Takezoe, *Angew. Chem. Int. Ed.* **2010**, *49*, 445.
- [27] a) Y.-X. Li, H.-F. Gao, R.-B. Zhang, K. Gabana, Q. Chang, G. A. Gehring, X.-H. Cheng, X.-B. Zeng, G. Ungar, *Nat. Commun.* **2022**, *13*, 384; b) P. Rybak, A. Krowczynski, J. Szydłowska, D. Pocięcha, E. Gorecka, *Soft Matter* **2006**, *18*.
- [28] a) V. Percec, M. Peterca, T. Tadjiev, X. Zeng, G. Ungar, P. Leowanawat, E. Aqad, M. R. Imam, B. M. Rosen, U. Akbey, R. Graf, S. Sekharan, D. Sebastiani, H. W. Spiess, P. A. Heiney, S. D. Hudson, *J. Am. Chem. Soc.* **2011**, *133*, 12197; b) C. Roche, H. J. Sun, M. E. Prendergast, P. Leowanawat, B. E. Partridge, P. A. Heiney, F. Araoka, R. Graf, H. W. Spiess, X. Zeng, G. Ungar, V. Percec, *J. Am. Chem. Soc.* **2014**, *136*, 7169; c) V. Percec, Q. Xiao, *Isr. J. Chem.* **2021**, *61*, 530.
- [29] A mesophase is considered as LC as long as there is only diffuse scattering in the WAXS range.<sup>[31]</sup>
- [30] J. M. Seddon, R. H. Templer, *Polymorphism in Lipid-Water Systems. In Handbook of Biological Physics* (Eds.: R. Lipowsky, E. Sackman), Elsevier: Amsterdam, The Netherlands, 1995, Volume 1, pp. 97–160.
- [31] G. Ungar, F. Liu, X. Zeng, *Cubic and 3D Thermotropic Liquid Crystal Phases and Quasicrystals. In Handbook of Liquid Crystals 2<sup>nd</sup> Ed.* (Eds.: J. W. Goodby, P. J. Collings, T. Kato, C. Tschierske, H. Gleeson, P. Raynes), Wiley-VCH, Weinheim, Germany, 2014; Volume 5, pp. 363–436.
- [32] S. Kutsumizu, *Isr. J. Chem.* **2012**, *52*, 844.
- [33] A. J. Meuler, M. A. Hillmyer, F. S. Bates, *Macromolecules* **2009**, *42*, 7221.
- [34] S. Hyde, S. Andersson, K. Larsson, Z. Blum, T. Landh, S. Lidin, B. W. Ninham, *The Language of Shape, The Role of Curvature in Condensed Matter: Physics, Chemistry and Biology*; Elsevier, Amsterdam, The Netherlands, 1997.
- [35] L. Han, S. Che, *Adv. Mater.* **2018**, *30*, 1705708.
- [36] Y. Cao, M. Alaasar, A. Nallapaneni, M. Salamończyk, P. Marinko, E. Gorecka, C. Tschierske, F. Liu, N. Vaupotič, C. Zhu, *Phys. Rev. Lett.* **2020**, *125*, 027801.
- [37] X. Zeng, G. Ungar, *J. Mater. Chem. C.* **2020**, *8*, 5389.
- [38] C. Dressel, T. Reppe, S. Poppe, M. Prehm, H. Lu, X. Zeng, G. Ungar, C. Tschierske, *Adv. Funct. Mater.* **2020**, 2004353.
- [39] M. Alaasar, A. F. Darweesh, X. Cai, F. Liu, C. Tschierske, *Chem. Eur. J.* **2021**, *27*, 14921.
- [40] Before discovery of its intrinsic chirality, the cubic I23 phase (being one of the “smectic D” phases<sup>[75,76]</sup>) was considered to have an  $Im\bar{3}m$  lattice with an exceptional large lattice parameter.<sup>[41,42]</sup> After discovery of chirality<sup>[17]</sup> it was first attributed to the chiral space group  $I432^{[53]}$  before the present I23 model was proposed.<sup>[37]</sup> Besides the triple network I23 lattice other alternative models are presently under discussion, see refs. [43,44,47,48] In contrast to these other models, the I23 model in ref. [37] is a triple network structure with junctions having all the same valence of three, the same as in the adjacent  $la\bar{3}d$  phases with only two networks.
- [41] A. M. Levelut, M. Clerc, *Liq. Cryst.* **1998**, *24*, 105.
- [42] X. B. Zeng, G. Ungar, M. Imperor-Clerc, *Nat. Mater.* **2005**, *4*, 562.
- [43] K. Saito, Y. Yamamura, Y. Miwa, S. Kutsumizu, *Phys. Chem. Chem. Phys.* **2016**, *18*, 3280.
- [44] S. Kutsumizu, S. Miisako, Y. Miwa, M. Kitagawa, Y. Xamamura, K. Saito, *Phys. Chem. Chem. Phys.* **2016**, *18*, 17341.
- [45] N. Vaupotic, M. Salamonczyk, J. Matraszek, M. Vogrin, D. Pocięcha, E. Gorecka, *Phys. Chem. Chem. Phys.* **2020**, *22*, 12814.
- [46] J. M. Wolska, J. Wilk, D. Pocięcha, J. Mieczkowski, E. Gorecka, *Chem. Eur. J.* **2017**, *23*, 6853.
- [47] W. Lewandowski, N. Vaupotič, D. Pocięcha, E. Gorecka, L. M. Liz-Marzán, *Adv. Mater.* **2020**, 1905591.
- [48] T. Grabovac, E. Gorecka, D. Pocięcha, N. Vaupotic, *Crystals* **2021**, *11*, 214.
- [49] T. Kajitani, S. Kohmoto, M. Yamamoto, K. Kishikawa, *Chem. Mater.* **2005**, *17*, 3812.
- [50] T. Reppe, C. Dressel, S. Poppe, C. Tschierske, *Chem. Commun.* **2020**, 56, 711.
- [51] a) T. Reppe, S. Poppe, X. Cai, F. Liu, C. Tschierske, *Chem. Sci.* **2020**, *11*, 5902; b) T. Reppe, S. Poppe, C. Tschierske, *Chem. Eur. J.* **2020**, *26*, 16066.
- [52] Few other molecular structures forming chirality synchronized cubic phases were reported in refs. [19,43–46,49].
- [53] M. Alaasar, S. Poppe, Q. Dong, F. Liu, C. Tschierske, *Chem. Commun.* **2016**, 52, 13869.
- [54] a) O. Kwon, X. Cai, W. Qu, F. Liu, J. Szydłowska, E. Gorecka, M. J. Han, D. K. Yoon, S. Poppe, C. Tschierske, *Adv. Funct. Mater.* **2021**, *31*, 2102271; b) O. Kwon, X. Cai, A. Saeed, F. Liu, S. Poppe, C. Tschierske, *Chem. Commun.* **2021**, 57, 6491.
- [55] a) M. Alaasar, J. C. Schmidt, X. Cai, F. Liu, C. Tschierske, *J. Mol. Liq.* **2021**, *332*, 115870; b) M. Alaasar, S. Poppe, Y. Cao, C. Chen, F. Liu, C. Zhu, C. Tschierske, *J. Mater. Chem. C* **2020**, *8*, 12902; c) M. Alaasar, S. Poppe, Q. Dong, F. Liu, C. Tschierske, *Angew. Chem. Int. Ed.* **2017**, *56*, 10801; d) M. Alaasar, S. Poppe, C. Tschierske, *J. Mol. Liq.* **2019**, *277*, 233; e) M. Alaasar, X. Cai, Y. Cao, F. Liu, *New J. Chem.* **2022**, *46*, 15871.
- [56] M. Alaasar, M. Prehm, Y. Cao, F. Liu, C. Tschierske, *Angew. Chem. Int. Ed.* **2016**, *55*, 320.
- [57] a) H. Chen, R. Zhang, H. Gao, H. Cheng, H. Fang, X. Cheng, *Dyes Pigm.* **2018**, *149*, 512; b) N. G. Nagaveni, M. Gupta, A. Roy, V. Prasad, Veena, *J. Mater. Chem.* **2010**, *20*, 9089.
- [58] Y. Cao, M. Alaasar, L. Zhang, C. Zhu, C. Tschierske, F. Liu, *J. Am. Chem. Soc.* **2022**, *144*, 6936.
- [59] J.-S. Seo, Y.-S. Yoo, M.-G. Choi, *J. Mater. Chem.* **2001**, *11*, 1332.
- [60] a) M. Sano, T. Kunitake, *Langmuir* **1992**, *8*, 320; b) M. Sano, D. Y. Sasaki, M. Isayama, T. Kunitake, *Langmuir* **1992**, *8*, 1893.
- [61] a) C. L. Folcia, I. Alonso, J. Ortega, J. Etxebarria, I. Pintre, M. B. Ros, *Chem. Mater.* **2006**, *18*, 4617; b) F. Vera, R. M. Tejedor, P. Romero, J. Barberrá, M. B. Ros, J. L. Serrano, T. Sierra, *Angew. Chem. Int. Ed.* **2007**, *46*, 1873.
- [62] a) M. Alaasar, M. Prehm, M. Nagaraj, J. K. Vij, C. Tschierske, *Adv. Mater.* **2013**, *25*, 2186; b) M. Alaasar, M. Prehm, K. May, A. Eremin, C. Tschierske, *Adv. Funct. Mater.* **2014**, *24*, 1703.
- [63] L.-L. Lai, F.-Y. Su, Y.-J. Lin, C.-H. Ho, E. Wang, C.-H. Hung, Y.-H. Liu, Y. Wan, *Helv. Chim. Acta.* **2002**, *85*, 1517.
- [64] S. Kutsumizu, K. Morita, T. Ichikawa, S. Yano, S. Nojima, T. Yamaguchi, *Liq. Cryst.* **2002**, *29*, 1447.
- [65] a) S. Kutsumizu, H. Mori, M. Fukatami, S. Naito, K. Sakajiri, K. Saito, *Chem. Mater.* **2008**, *20*, 3675; b) Y. Yamamura, Y. Nakazawa, S. Kutsumizu, K. Saito, *Phys. Chem. Chem. Phys.* **2019**, *21*, 23705.
- [66] That the  $\Phi$ -ranges overlap a bit can be attributed to the simultaneous elongation of the molecule by alkyl chain expansion which tends to reduce  $\Phi$  and to the different temperatures of the measurements.
- [67] Iso–Iso<sub>1</sub> transitions were previously reported to occur besides chirality frustrated LC phases of chiral compounds (BP, TGB) and besides cubic LC phases, see<sup>[32,68]</sup>.
- [68] J. W. Goodby, D. A. Dunmur, P. J. Collings, *Liq. Cryst.* **1995**, *19*, 703.
- [69] K. Borisch, S. Diele, P. Göring, H. Kresse, C. Tschierske, *J. Mater. Chem.* **1998**, *8*, 529.
- [70] a) T. F. A. De Greef, M. M. J. Smulders, M. Wolffs, A. P. H. J. Schenning, R. P. Sijbesma, E. W. Meijer, *Chem. Rev.* **2009**, *109*, 5687; b) M. Hartlieb, E. D. H. Mansfield, S. Perrier, *Polym. Chem.* **2020**, *11*, 1083; c) T. Aida, E. W. Meijer, *Isr. J. Chem.* **2020**, *60*, 33.
- [71] C. Tschierske, *Isr. J. Chem.* **2012**, *52*, 935.
- [72] a) A. B. Harris, R. D. Kamien, T. C. Lubensky, *Rev. Mod. Phys.* **1999**, *71*, 1745; b) E. Efrati, W. T. M. Irvine, *Phys. Rev. X* **2014**, *4*, 011003; c) G. M. Grason, *Rev. Mod. Phys.* **2015**, *87*, 401.
- [73] a) J. Lin, Z. Guo, J. Plas, D. B. Amabilino, S. De Feyter, A. P. Schenning, *Chem. Commun.* **2013**, 49, 9320; b) F. Xu, I. J. Khan, K. McGuinness, A. S. Parmar, T. Silva, N. S. Murthy, V. Nanda, *J. Am. Chem. Soc.* **2013**, *135*, 18762; c) S. Díaz-Cabrera, Y. Dorca, J. Calbo, J. Aragó, R. Gómez, E. Ortí, L. Sánchez, *Chem. Eur. J.* **2018**, *24*, 2826.
- [74] E. Frezza, A. Ferrarini, H. B. Kolli, A. Giacometti, G. Cinacchi, *Phys. Chem. Chem. Phys.* **2014**, *16*, 16225.
- [75] D. Demus, G. Kunicke, J. Neelsen, H. Sackmann, *Z. Naturforsch. A* **1968**, *23*, 84.
- [76] G. W. Gray, B. Jones, F. Marson, *J. Chem. Soc.* **1957**, 393.
- [77] G. Yin, T. Namikoshi, M. Teraguchi, T. Kaneko, T. Aoki, *Polymer* **2022**, *245*, 124673.

Manuscript received: June 15, 2022

Accepted manuscript online: July 22, 2022

Version of record online: ■■■, ■■■■





Cite this: *Chem. Commun.*, 2016,  
52, 13869

Received 12th October 2016,  
Accepted 7th November 2016

DOI: 10.1039/c6cc08226b

www.rsc.org/chemcomm

**Achiral supramolecular hydrogen bonded complexes between rod-like 4-(4-alkoxyphenylazo)pyridines and a taper shaped 4-substituted benzoic acid form achiral (*Ia3d*) and chiral "*Im3m*-type" bicontinuous cubic (*I432*) phases and a chiral isotropic liquid mesophase (*Iso*<sub>1</sub><sup>[\*]</sup>). The chiral phases, resulting from spontaneous mirror symmetry breaking, represent conglomerates of macroscopic chiral domains eventually leading to uniform chirality.**

Mirror symmetry breaking in liquid crystalline (LC) and liquid phases of achiral molecules is of significant interest as it provides an efficient way to spontaneous chirogenesis in fluids, thus being of potential importance for the emergence of biochirality as well as providing a new way to produce chiral materials.<sup>1</sup> For example conglomerates of chiral domains were formed by achiral bent-core molecules in the optically isotropic dark-conglomerate (DC) phases<sup>2,3</sup> as well as in birefringent SmC phases<sup>4</sup> and nematic phases.<sup>5</sup> Twist bend nematic phases (*N<sub>TB</sub>*) represent another type of mirror symmetry broken fluids formed by bent-core mesogens,<sup>6</sup> rod-like dimesogens,<sup>7</sup> trimesogens<sup>8</sup> and main chain polymers.<sup>9</sup> Recently, mirror symmetry breaking with formation of chiral conglomerates was even observed in *Im3m*-type bicontinuous cubic phases<sup>10</sup> and in isotropic liquids (*Iso*<sub>1</sub><sup>[\*]</sup>)<sup>11</sup> of achiral rod-like multi-chain (polycatenar) molecules.<sup>1,12</sup> A twisted organization of the molecules in the column segments of the branched networks forming these cubic phases and in the local cybotactic domains of the isotropic liquids is assumed to couple cooperatively with helical conformers of the transiently chiral molecules, leading to the development of macroscopic chirality.<sup>1,10,11</sup> This dynamic mode of mirror symmetry breaking in the liquid state retains high entropy and allows fast reversible chiral segregation in

the presence of relatively weak intermolecular interactions. In order to minimize the unfavourable entropy of mixing, relatively large molecules are required for this process. An efficient way to achieve larger supramolecular units is provided by self assembly of smaller molecules by noncovalent interactions, such as hydrogen bonding, halogen bonding and  $\pi$ -stacking.

Hydrogen-bonding, especially between pyridines and benzoic acids was previously used to design nematic, smectic and columnar mesomorphic materials<sup>13–16</sup> whereas cubic LC phases formed by discrete self assembly between two or three components are rare.‡ The first examples of bicontinuous cubic phases formed through discrete intermolecular hydrogen bonding interaction is provided by the 4'-*n*-alkoxy-3'-nitrobiphenyl-4-carboxylic acids.<sup>17</sup> Cubic phases were also reported for supramolecular systems constructed by self-assembly through intermolecular hydrogen-bond formation between 4,4'-bipyridines and 4-substituted benzoic acids with bulky siloxane moieties<sup>18a</sup> or branched perfluorinated chains.<sup>18b</sup> To the best of our knowledge there are no examples reported up to date for bicontinuous cubic phases formed by supramolecular hydrogen bonded polycatenar LCs<sup>12</sup> and spontaneous symmetry breaking has not yet been reported for any supramolecular polycatenar mesogen.§

Herein we report for the first time how hydrogen bonding can be used to drive mirror-symmetry breaking in an isotropic liquid as well as in cubic phases of supramolecular tetracatenar complexes (**AB8-AB14**) between rod-like 4-phenylazopyridines **Bn**<sup>19,20</sup> with one terminal alkoxy chain and the benzoic acid **A**, having three identical terminal alkoxy chains (Scheme 1).¶ The azopyridines **Bn**<sup>20b</sup> and the benzoic acid derivative **A** were synthesized through the synthetic pathway shown in Scheme 1. The detailed synthetic procedures and analytical data are reported in the ESI.†

The 4-(4-alkoxyphenylazo)pyridines **Bn** represent non-mesomorphic solids which directly melt to isotropic liquids between 66 and 74 °C (Table S1, ESI†).<sup>20b</sup> The benzoic acid **A** exhibits a hexagonal columnar LC phase (Col<sub>hex</sub>) between 162 and 246 °C as indicated by X-ray diffraction (XRD,  $a_{\text{hex}} = 5.4$  nm see Fig. S9 and Table S2, ESI†), in line with the birefringent

<sup>a</sup> Institute of Chemistry, Martin Luther University Halle-Wittenberg, Kurt-Mothes Str.2, D-06120 Halle, Germany. E-mail: carsten.tschierske@chemie.uni-halle.de

<sup>b</sup> Department of Chemistry, Faculty of Science, Cairo University, Giza, Egypt. E-mail: malaasar@sci.cu.edu.eg

<sup>c</sup> State Key Laboratory for Mechanical Behavior of Materials, Xi'an Jiaotong University, Xi'an 710049, P. R. China. E-mail: feng.liu@xjtu.edu.cn

† Electronic supplementary information (ESI) available: Synthesis, analytical data, additional data. See DOI: 10.1039/c6cc08226b





**Scheme 1** Synthetic route to the pyridines **Br**<sup>20b</sup> and the benzoic acid **A** and formation of the polycatenar hydrogen-bonded complexes **ABn**. Reagents and conditions: (i) DCC, DMAP, DCM, stirring, rt, 48 h; (ii) 10%-Pd/C, H<sub>2</sub>, stirring, 45 °C, 48 h; (iii) BrC<sub>n</sub>H<sub>2n+1</sub>, KI, K<sub>2</sub>CO<sub>3</sub>, DMF, stirring, 50 °C, 48 h; (iv) melting with stirring.

fan-like texture observed under the polarizing microscope (PM, Fig. S6a, ESI<sup>†</sup>). The observation of a Col<sub>hex</sub> phase for **A** is attributed to dimer formation by intermolecular H-bonding between the COOH groups, leading to hexacatenar rod-like complexes which arrange side by side and on top of each other thus forming columns being rotationally disordered and arranged on a hexagonal lattice. In the columns the rod-like cores are aligned almost perpendicular to the column long axis, resulting in an optically negative Col<sub>hex</sub> phase (Fig. S6b and c, ESI<sup>†</sup>), as typical for hexacatenars.<sup>12</sup> The supramolecular aggregates **AB8–AB14** were prepared by mixing equimolar amounts of **Br** and **A** and then melting them together in DSC pans (30 μl) with stirring. After crystallization the material was grinded, and this process was repeated to obtain a homogeneous mixture.

Homogenous melting and reproducible transition temperatures were observed for all supramolecular complexes **ABn**. The formation of the supramolecular 1:1 complexes between the benzoic acid **A** and the 4-phenylazopyridines **Br** (for <sup>1</sup>H-NMR, see Fig. S4, ESI<sup>†</sup>) leads to the suppression of the columnar phase and induction of broad cubic LC phase ranges for all hydrogen bonded complexes as determined by differential scanning calorimetry (DSC, see Fig. 1; the intense peaks of the



**Fig. 1** DSC heating and cooling traces (10 K min<sup>-1</sup>) observed for the complex **AB8**. The inset shows the heating and cooling traces for the temperature range of the Iso–Iso<sub>1</sub><sup>[\*]</sup>–Cub<sup>[\*]</sup>/I432 transitions between 175 °C and 205 °C.

**Table 1** Phase transition temperatures (*T*/°C), mesophase types, and transition enthalpies [ $\Delta H$ /J g<sup>-1</sup>] of the supramolecular complexes **ABn**<sup>a</sup>

No.	<i>n</i>	Phase sequence
<b>AB8</b>	8	H: Cr 124 [28] <i>Ia</i> 3 <i>d</i> ~187 [0.1] I432 196 [0.1] Iso <sub>1</sub> <sup>[*]</sup> 200 [0.1] Iso
<b>AB10</b>	10	H: Cr <sub>1</sub> 115 [11] Cr <sub>2</sub> 128 [41] I432 201 [0.8] Iso C: Iso 195 [0.7] I432 75 [35] Cr
<b>AB12</b>	12	H: Cr 123 [48] I432 191 [1.2] Iso C: Iso 182 [1.7] I432 87 [40] Cr
<b>AB14</b>	14	H: Cr 92 [27] I432 184 [1.7] Iso C: Iso 177 [1.8] I432

<sup>a</sup> Peak temperatures as determined from 1st heating (H) and 1st cooling (C) DSC scans with rate 10 K min<sup>-1</sup>; abbreviations: Cr = crystalline solid; I432 = chiral “*Im*3*m*-type” cubic LC phase with I432 symmetry; *Ia*3*d* = achiral cubic LC phase with *Ia*3*d* symmetry; Cr<sup>[\*]</sup> = chiral crystalline solid; Iso<sub>1</sub><sup>[\*]</sup> = chiral isotropic conglomerate liquid; Iso = achiral isotropic liquid.

individual components, see Fig. S5, are absent, ESI<sup>†</sup>), PM and XRD investigations (see Table 1).

Exclusively cubic phases were found for the complexes **AB10–AB14**, whereas for the 1:1 complex **AB8** an additional liquid–liquid transition is indicated in the DSC traces by a broad feature in the isotropic liquid range (Iso–Iso<sub>1</sub> transition, Fig. 1). Between crossed polarizers the liquid phases Iso as well as Iso<sub>1</sub> appear uniformly dark. However, in the Iso<sub>1</sub> phase range slightly rotating the analyzer by a few degrees (*ca.* –7°) out of the 90° orientation with respect to the polarizer leads to the appearance of dark and bright domains, which exchange their brightness after rotation of the analyzer by the same angle into the opposite direction (*ca.* +7°, see Fig. 2a and b). Rotating the sample between crossed polarizers does not lead to any change and these observations confirm that the distinct regions represent chiral domains. This is a clear indication for chirality synchronization in the Iso<sub>1</sub> phase (Iso<sub>1</sub><sup>[\*]</sup>). No such domains can be observed in the Iso phase of **AB8** at higher temperature or in the Iso phases of complexes **AB10–AB14**, which are achiral.

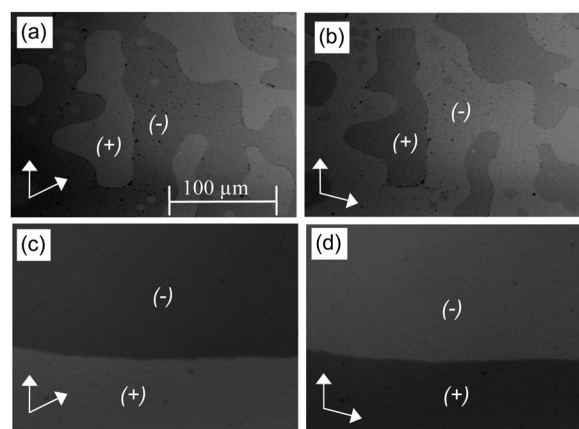


**Fig. 2** Textures of the complex **AB8** on cooling from the isotropic liquid (Iso): (a and b) in Iso<sub>1</sub><sup>[\*]</sup> liquid at *T* = 188 °C and (c and d) in the Cub<sup>[\*]</sup>/I432 LC phase at *T* = 150 °C on further cooling, (a and c) after rotating one polarizer from the crossed position by 7° in anticlockwise direction and (b and d) in clockwise direction, showing dark and bright domains, indicating the presence of areas with opposite chirality sense; the dark spots are aluminium particles resulting from the vigorous stirring in the DSC pans.





Fig. 3 SAXS diffractograms of (a) the Cub/ $Ia\bar{3}d$  phase ( $a_{\text{cub}} = 13.10$  nm) of **AB8**, recorded at  $T = 150$  °C on heating (for wide angle scattering see Fig. S10b, ESI†); (b) the Cub/ $I432$  phase ( $a_{\text{cub}} = 19.46$  nm) of **AB14** at  $T = 140$  °C, the curve on top is enhanced by a factor of 7 and only some diffractions at lower angles are labelled; see also Tables S3–S6 (ESI†).

The transition to the cubic phase is indicated by a small, but relatively sharp peak in the DSC traces (Fig. 1). The transition enthalpy of this transition rises with growing chain length from 0.1 to 1.8 J g<sup>-1</sup> (Table 1). As typical for mesophases with long range 3D lattice there is a hysteresis of this transition to the cubic phase on cooling by ca. 6–9 K. At the Iso<sub>1</sub><sup>[\*]</sup>-Cub<sup>[\*]</sup> transition of **AB8** and the Iso-Cub<sup>[\*]</sup> transitions of the complexes **AB10–AB14** the samples remain optically isotropic, but these transitions are associated with a significant reduction of the fluidity leading to soft viscoelastic solids. The diffuse scattering in the wide angle range of the XRD patterns is retained (Fig. S10b, ESI†) indicating the absence of a long range positional order of the individual molecule as typical for LC phases. In the case of **AB8** the chiral domains in the Iso<sub>1</sub><sup>[\*]</sup> phase grow to huge homogeneously chiral domains of either handedness, even across the original chiral domain boundaries (see Fig. 2c and d). The complexes **AB10–AB14** form the chiral domains directly at the transition from the achiral Iso phase to the Cub<sup>[\*]</sup> phases. Also for these complexes large chiral domains are formed (Fig. S8, ESI†) and on very slow cooling (< 1 K min<sup>-1</sup>) it is even possible to achieve uniform chirality, indicating slow formation of the seeds of the cubic phase combined with a fast growth; the distribution of either chirality sense is stochastic.

The powder XRD patterns of the cubic conglomerate phases of the supramolecules **AB*n*** (Fig. 3b and Fig. S10, ESI†) can be indexed to  $Im\bar{3}m$  lattices with nearly chain length independent lattice



Fig. 4 Reconstructed EDMs: (a) of a unit cell of the Cub/ $Ia\bar{3}d$  phase of **AB8** only showing the high density regions and (b) of the  $Im\bar{3}m$  approximate of the Cub<sup>[\*]</sup>/ $I432$  phase of **AB14** showing the three distinct iso-surfaces with different colour.

parameters ( $a_{\text{cub}} = 19.4$ – $19.5$  nm, see Tables S4–S6, ESI†). Based on this phase assignment the electron density map (EDM) of **AB14** was reconstructed from the powder diffraction pattern, showing a tricontinuous structure of this cubic phase (Fig. 4b). It should be noted here that due to the chirality the actual space group is a chiral one, that with the highest symmetry being  $I432$ . However as the phase angle can represent any value between 0 and  $\pm\pi$  in this non-centrosymmetric lattice we assume the centrosymmetric  $Im\bar{3}m$  structure as a close approximate for electron density reconstruction, limiting the phase choices to 0 and  $\pm\pi$ . The three interwoven but not connected high electron density networks (yellow, purple and blue in Fig. 4b, respectively) involve the hydrogen bonded aromatic cores arranged with their long axes perpendicular to the directions of the column segments forming the labyrinths. Due to the steric crowding of the alkyl chains at the ends the organization of the rods is not exactly parallel, but with a slight angle leading to a helical twist along the networks.<sup>10,21</sup> The network structure leads to a long range transmission of the helix sense once formed and exciton coupling between the twisted  $\pi$ -systems is assumed to mainly contribute to optical rotation.<sup>22</sup> As there are three networks, chirality cannot be cancelled even if the helix sense would be opposite in adjacent networks. The space between the networks is filled by the disordered alkyl chains.

Only the supramolecular complex **AB8** exhibits an additional cubic phase which is achiral based on optical investigations (uncrossing the polarizers by a small angle in clockwise or anti-clockwise direction does not lead to any change). The diffraction pattern in the achiral cubic phase (Fig. 3a) can be indexed to a cubic lattice with  $Ia\bar{3}d$  symmetry ( $a_{\text{cub}} = 13.10$  nm, Table S3, ESI†) and represents a gyroid-type bicontinuous double-network phase as shown in the reconstructed EDM in Fig. 4a. The two interwoven high electron density networks (yellow) are filled with the hydrogen bonded cores, being arranged perpendicular to the column segments of the networks and slightly twisted with respect to each other, thus forming only two helically twisted networks with opposite helix sense, cancelling each other to give an achiral structure.<sup>10</sup> This achiral  $Ia\bar{3}d$  phase is formed on melting the crystalline phase (Cr) at  $T = 124$  °C and on heating transforms into the chiral  $I432$  phase at  $T = 180$ – $187$  °C ( $a_{\text{cub}} = 19.53$  nm) as indicated by optical investigations (appearance of chiral domains), DSC (small enthalpy of 0.1 J g<sup>-1</sup>) and from temperature dependent XRD studies by a change of the diffraction pattern (Table S4, ESI†). This chiral cubic



phase melts at  $T = 196\text{ }^{\circ}\text{C}$  with the formation of the chiral  $\text{Iso}_1^{[*]}$  phase which transforms into the achiral Iso phase at  $T = 200\text{ }^{\circ}\text{C}$ . On cooling **AB8** from the Iso state  $\text{Iso}_1^{[*]}$  is formed at  $T = 190\text{ }^{\circ}\text{C}$ , followed by the transition to the chiral  $\text{Cub}^{[*]}$  phase (*I432*) at  $T = 183\text{ }^{\circ}\text{C}$  (Fig. 1 and Table 1). The chiral domains and the typical diffraction pattern of the *I432* phase are retained till the crystallization at  $T = 75\text{ }^{\circ}\text{C}$ . Interestingly, the crystalline state of **AB8** exhibits also chiral domains as indicated by the textural observations under PM (see Fig. S7, ESI†), thus indicating crystallization in a chiral space group ( $\text{Cr}^{[*]}$ ). Heating this  $\text{Cr}^{[*]}$  phase (which melts at  $T = 114\text{ }^{\circ}\text{C}$ ) leads directly to the chiral *I432* phase without intermediate formation of the achiral *Ia3d* phase. Thus, the chirality once achieved is retained on crystallization and the formation of the *Ia3d* phase is suppressed. The *Ia3d* phase is only obtained after heating the crystalline sample after prolonged storage. It appears that the (metastable)  $\text{Cr}^{[*]}$  phase slowly transforms into an achiral crystalline phase (Cr, m.p. =  $124\text{ }^{\circ}\text{C}$ ) from which the achiral *Ia3d* phase is formed on heating. This means that the cubic *I432* phase is metastable below  $187\text{ }^{\circ}\text{C}$ , but once formed seems to be persistent. The transition *Ia3d*–*I432* observed in the series **AB*n*** on chain elongation and with rising temperature (**AB8**) is in line with the recently proposed helical model, as the effective chain volume increases with rising temperature and growing alkyl chain length and this reduces the helical pitch becoming incompatible with the *Ia3d* structure and leading to formation of the *I432* cubic phase.<sup>10</sup>

In summary, we report herein the design and synthesis of the first examples of hydrogen bonded supramolecular complexes with polycatenar structure showing dynamic mirror-symmetry breaking by chirality synchronization in a liquid conglomerate ( $\text{Iso}_1^{[*]}$ ) at the liquid–liquid transition as well as in chiral “*Im3m*-type” cubic phases ( $\text{Cub}^{[*]}$ /*I432*). The liquid conglomerate is obviously only formed if the alkyl chains are short and nano-segregation between alkyl chain and core unit is sufficiently weak to prevent formation of a long range cubic lattice. Overall, this work could initiate further work on using hydrogen bonding for symmetry breaking in fluids. Moreover, the possibilities provided by the photosensitive azobenzene units<sup>23</sup> could lead to interesting perspectives for chirality switching and phase modulation by interaction with non-polarized and (linear or circular) polarized light.<sup>24</sup>

The work was funded by the DFG (Grant Ts 39/24-1) and the National Natural Science Foundation of China (No. 21374086). We thank Beamline BL16B1 at SSRF (Shanghai Synchrotron Radiation Facility, China) for providing the beamtimes.

## Notes and references

‡ Multiple cooperative hydrogen bonding between amphiphilic glycerol-based or carbohydrate based molecules forming polymeric hydrogen bonding networks are more common.<sup>25</sup>

§ Mirror symmetry breaking by hydrogen bonding in soft matter was previously reported for the  $\text{N}_{\text{TB}}$  phases of hydrogen bonded mesogenic trimers<sup>24</sup> and the cubic phase of a bent molecule.<sup>26</sup>

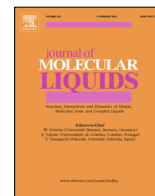
¶ The azopyridine derivatives **B*n*** have previously been used for the formation of supramolecular self-assembled hydrogen bonded<sup>19</sup> and halogen-bonded LCs<sup>20</sup> with light induced phase transitions.

1 C. Tschierske and G. Ungar, *ChemPhysChem*, 2016, **17**, 9.

2 (a) J. Thisayukta, Y. Nakayama, S. Kawachi, H. Takezoe and J. Watanabe, *J. Am. Chem. Soc.*, 2000, **122**, 7441; (b) G. Dantlgraber,

- A. Eremin, S. Diele, A. Hauser, H. Kresse, G. Pelzl and C. Tschierske, *Angew. Chem., Int. Ed.*, 2002, **41**, 2408; (c) L. E. Hough, M. Spannum, M. Nakata, D. A. Coleman, C. D. Jones, G. Dantlgraber, C. Tschierske, J. Watanabe, E. Körblová, D. M. Walba, J. E. MacLennan, M. A. Glaser and N. A. Clark, *Science*, 2009, **325**, 452; (d) H. Sasaki, Y. Takanishi, J. Yamamoto and A. Yoshizawa, *J. Phys. Chem. B*, 2015, **119**, 4531.
- 3 H. Takezoe, *Top. Curr. Chem.*, 2012, **318**, 303.
- 4 (a) M. Alaasar, M. Prehm, M. Nagaraj, J. K. Vij and C. Tschierske, *Adv. Mater.*, 2013, **25**, 2186; (b) M. Alaasar, M. Prehm, K. May, A. Eremin and C. Tschierske, *Adv. Funct. Mater.*, 2014, **24**, 1703.
- 5 V. Görtz, *Liq. Cryst. Today*, 2010, **19**, 37.
- 6 D. Chen, J. H. Porada, J. B. Hooper, A. Klitnick, Y. Shen, M. R. Tuchband, E. Körblová, D. Bedrov, D. M. Walba, M. A. Glaser, J. E. MacLennan and N. A. Clark, *Proc. Natl. Acad. Sci. U. S. A.*, 2013, **110**, 15931.
- 7 (a) V. Borshch, Y.-K. Kim, J. Xiang, M. Gao, A. Jakli, V. P. Panov, J. K. Vij, C. T. Imrie, M. G. Tamba, G. H. Mehl and O. D. Lavrentovich, *Nat. Commun.*, 2013, **4**, 2635; (b) M. Cestari, S. Diez-Berart, D. A. Dunmur, A. Ferrarini, M. R. de la Fuente, D. J. B. Jackson, D. O. Lopez, G. R. Luckhurst, M. A. Perez-Jubindo, R. M. Richardson, J. Salud, B. A. Timimi and H. Zimmermann, *Phys. Rev. E: Stat., Nonlinear, Soft Matter Phys.*, 2011, **84**, 031704; (c) R. J. Mandle, *Soft Matter*, 2016, **12**, 7883.
- 8 (a) R. J. Mandle and J. W. Goodby, *ChemPhysChem*, 2016, **17**, 967; (b) Y. Wang, Z. Zheng, H. K. Bisoyi, K. G. Gutierrez-Cuevas, L. Wang, R. S. Zolab and Q. Li, *Mater. Horiz.*, 2016, **3**, 442.
- 9 G. Ungar, V. Percec and M. Zuber, *Macromolecules*, 1992, **25**, 75.
- 10 C. Dressel, F. Liu, M. Prehm, X. Zeng, G. Ungar and C. Tschierske, *Angew. Chem., Int. Ed.*, 2014, **53**, 13115.
- 11 (a) C. Dressel, T. Reppe, M. Prehm, M. Brautzsch and C. Tschierske, *Nat. Chem.*, 2014, **6**, 971; (b) M. Alaasar, M. Prehm, Y. Cao, F. Liu and C. Tschierske, *Angew. Chem., Int. Ed.*, 2016, **55**, 312; (c) C. Dressel, W. Weissflog and C. Tschierske, *Chem. Commun.*, 2015, **51**, 15850.
- 12 W. Weissflog, in *Handbook of Liquid Crystals*, ed. J. W. Goodby, P. J. Collings, T. Kato, C. Tschierske, H. Gleeson and P. Raynes, Wiley-VCH, Weinheim, 2014, vol. 5, p. 89.
- 13 T. Kato and J. M. J. Frechet, *J. Am. Chem. Soc.*, 1989, **111**, 8533.
- 14 B. Friot, D. Boyd, K. Willis, B. Donnio, G. Ungar and D. W. Bruce, *Liq. Cryst.*, 2000, **27**, 605.
- 15 (a) C. M. Paleos and D. Tsiourvas, *Liq. Cryst.*, 2001, **28**, 1127; (b) T. Kato and Y. Kamikawa, in *Handbook of Liquid Crystals*, ed. J. W. Goodby, P. J. Collings, T. Kato, C. Tschierske, H. Gleeson and P. Raynes, Wiley-VCH, Weinheim, 2014, vol. 5, 513.
- 16 S. M. Jansze, A. Martinez-Felipe, J. M. D. Storey, A. T. M. Marcelis and C. T. Imrie, *Angew. Chem., Int. Ed.*, 2015, **54**, 643.
- 17 (a) G. W. Gray, B. Jones and F. Marson, *J. Chem. Soc.*, 1957, 393; (b) D. Demus, G. Kunicke, J. Neelsen and H. Sackmann, *Z. Naturforsch., A: Phys. Sci.*, 1968, **23**, 84; (c) S. Kutsumizu, *Isr. J. Chem.*, 2012, **52**, 844.
- 18 (a) E. Nishikawa and E. T. Samulski, *Liq. Cryst.*, 2000, **27**, 1463; (b) E. Nishikawa, J. Yamamoto and H. Yokoyama, *Liq. Cryst.*, 2003, **30**, 785.
- 19 (a) J. Mamiya, A. Yoshitake, M. Kondo, Y. Yu and T. Ikeda, *J. Mater. Chem.*, 2008, **18**, 63; (b) K. Aoki, M. Nakagawa and K. Ichimura, *J. Am. Chem. Soc.*, 2000, **122**, 10997; (c) M. Pfletscher, C. Wölper, J. S. Gutmann, M. Mezger and M. Giese, *Chem. Commun.*, 2016, **52**, 8549.
- 20 (a) W. Zhou, T. Kobayashi, H. Zhu and H. F. Yu, *Chem. Commun.*, 2011, **47**, 12768; (b) Y. J. Chen, H. F. Yu, L. Y. Zhang, H. Yang and Y. F. Lu, *Chem. Commun.*, 2014, **50**, 9647.
- 21 K. Saito, Y. Yamamura, Y. Miwa and S. Kutsumizu, *Phys. Chem. Chem. Phys.*, 2016, **18**, 3280.
- 22 G. Pescitelli, L. Di Bari and N. Berova, *Chem. Soc. Rev.*, 2014, **43**, 5211.
- 23 H. M. D. Bandara and S. C. Burdette, *Chem. Soc. Rev.*, 2012, **41**, 1809.
- 24 D. A. Paterson, J. Xiang, G. Singh, R. Walker, D. M. Agra-Kooijman, A. Martinez-Felipe, M. Gao, J. M. D. Storey, S. Kumar, O. D. Lavrentovich and C. T. Imrie, *J. Am. Chem. Soc.*, 2016, **138**, 5283.
- 25 K. Borisch, S. Diele, P. Göring, H. Kresse and C. Tschierske, *Angew. Chem., Int. Ed.*, 1997, **36**, 2087.
- 26 T. Kajitani, S. Kohmoto, M. Yamamoto and K. Kishikawa, *Chem. Mater.*, 2005, **17**, 3812.





# Controlling ambidextrous mirror symmetry breaking in photosensitive supramolecular polycatenars by alkyl-chain engineering



Mohamed Alaasar<sup>a,b,\*</sup>, Xiaoqian Cai<sup>c</sup>, Felix Kraus<sup>d</sup>, Michael Giese<sup>d</sup>, Feng Liu<sup>c</sup>, Carsten Tschierske<sup>a,\*</sup>

<sup>a</sup> Institute of Chemistry, Martin Luther University Halle-Wittenberg, Kurt Mothes Str. 2, D-06120 Halle (Saale), Germany

<sup>b</sup> Department of Chemistry, Faculty of Science, Cairo University, Giza, Egypt

<sup>c</sup> State Key Laboratory for Mechanical Behavior of Materials, Shaanxi International Research Center for Soft Matter, Xi'an Jiaotong University, Xi'an 710049, PR China

<sup>d</sup> Institute of Organic Chemistry, University Duisburg-Essen, Universitätsstraße 7, 45141 Essen, Germany

## ARTICLE INFO

### Article history:

Received 2 December 2021

Revised 17 January 2022

Accepted 19 January 2022

Available online 1 February 2022

### Keywords:

Polycatenar liquid crystals

Hydrogen bonding

Azobenzenes

Helical self-assembly

Cubic phases

Mirror symmetry breaking

Photo switching

## ABSTRACT

Liquid crystalline (LC) photo sensitive materials capable of forming mirror-symmetry broken mesophases are of great interest to produce nano-structured materials for optical and photonic applications. Herein we report how mirror-symmetry breaking could be controlled in photo sensitive supramolecular polycatenars by alkyl chain engineering. For this purpose, three new series of supramolecular photo-switchable multi-chain complexes (polycatenars) formed by intermolecular hydrogen bonding interaction between azopyridines with one variable terminal chain as the proton-acceptors and Y-shaped or taper shaped benzoic acids having either two or three terminal chains as the hydrogen bond-donors were synthesized. The LC self-assembly of these supramolecules was characterized by differential scanning calorimetry (DSC), polarized optical microscopy (POM) and X-ray diffraction (XRD). Depending on the number and length of terminal chains spontaneously chiral isotropic liquid (Iso<sup>l\*</sup>) as well as two different types of three dimensional (3D) bicontinuous cubic phases are observed, which are either chiral (Cub<sub>bi</sub><sup>l\*</sup>/I23) or achiral (Cub<sub>bi</sub>/Ia3d). Moreover, UV light irradiation leads to the first fast and reversible photoinduced transformation between chiral and achiral 3D cubic phases as well as between a chiral crystalline and a chiral cubic liquid crystalline phase.

© 2022 The Authors. Published by Elsevier B.V. This is an open access article under the CC BY license (<http://creativecommons.org/licenses/by/4.0/>).

## 1. Introduction

Spontaneous mirror symmetry breaking in achiral liquid crystalline (LC) compounds is of special interest as it opens the door for providing an efficient way to produce chiral materials, thus being important from a scientific point of view, as well as for applications in functional materials [1–3]. Spontaneous ambidextrous chirality in LCs could be indicated by the observation of chiral conglomerates, which were found in mesophases formed by different classes of LCs. For example, bent-core LCs can form chiral domains in the optically isotropic dark-conglomerate (DC) phases, as well as in the fluid birefringent nematic (N) and SmC phases [4–14]. Another example is the chiral fluid twist bend nematic phases (N<sub>TB</sub>) formed by bent dimesogens [15,16]. Non-covalent interactions, such as hydrogen bonding, has been applied as a very successful way to produce nanostructured functional LCs [17–19].

Intermolecular interactions either hydrogen or halogen-bonding between complementary components, which are in most cases non-mesomorphic, produce LCs with lamellar or columnar phases [20–24]. Inducing LC phases by hydrogen bond formation is known for dimers formed by 4-alkyl(oxy)benzoic acids, cyclohexane carboxylic acids or between benzoic acids and pyridine moieties [25–27]. More examples of LC materials with complex superstructures were also constructed by hydrogen-bond formation [28–33]. One of the interesting LC phases designed by H-bonding is the bicontinuous cubic phase (Cub<sub>bi</sub>) phase. The dimers formed by intermolecular H-bond formation between 4'-n-alkoxy-3'-nitrobi phenyl-4-carboxylic acid molecules (ANBCs) represent the first examples of LCs exhibiting Cub<sub>bi</sub> phases [34,35]. Later, hetero mixtures of ANBCs with 3,5-dialkoxybenzoic acids [36–38], and 2,4-diaminotriazines [39] were also found to form Cub<sub>bi</sub> phases. Cub<sub>bi</sub> phases are three dimensional (3D) LCs phases, representing interwoven networks of branched columns (Fig. 1b,c) characterized by their isotropic appearance under crossed polarizers and are very interesting from applications point of view by providing fast charge transport due to their 3D network structures [40–44].

\* Corresponding author at: Institute of Chemistry, Martin Luther University Halle-Wittenberg, Kurt Mothes Str. 2, D-06120 Halle (Saale), Germany.

E-mail addresses: [mohamed.alaasar@chemie.uni-halle.de](mailto:mohamed.alaasar@chemie.uni-halle.de) (M. Alaasar), [carsten.tschierske@chemie.uni-halle.de](mailto:carsten.tschierske@chemie.uni-halle.de) (C. Tschierske).

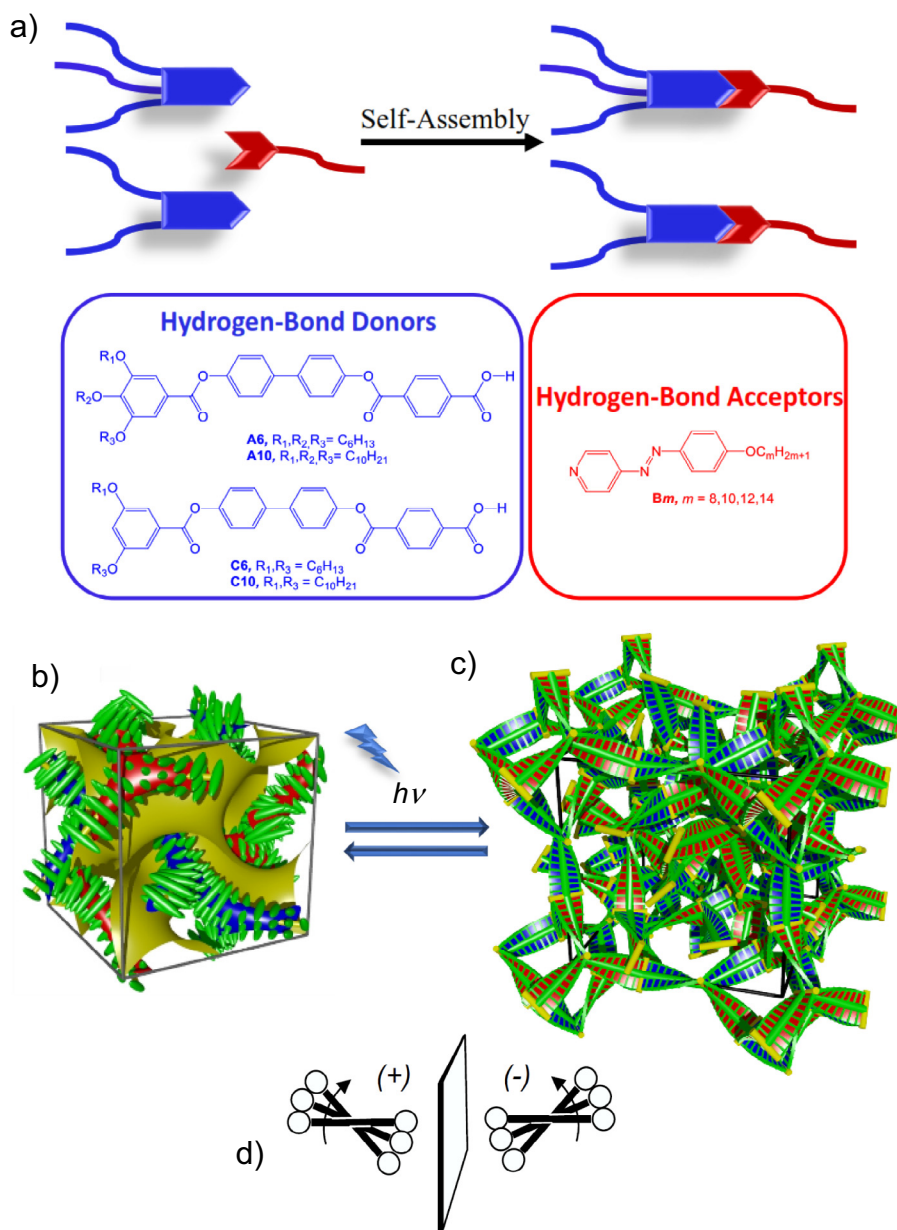


**Fig. 1.** (a) Schematic representation for the hydrogen-bond donors and acceptors yielding photoswitchable aggregates. (b) The double-gyroid achiral bicontinuous  $Ia\bar{3}d$  phase having two networks with opposite chirality (red and blue) [47]. (c) The model proposed for the ambidextrous chiral  $I23$  phase with three continuous networks [54]. (d) The development of the helical twist by the clashing of end groups attached to rod-like cores in the networks. (b) and (c) were reproduced from Refs. [46,49], by permission from Wiley-VCH and RSC, respectively. (For interpretation of the references to colour in this figure legend, the reader is referred to the web version of this article.)

Alkyl chain engineering has been used in the recent decades for the induction of  $Cub_{bi}$  phases by connecting more than only one alkyl chain to the ends of extended rod-like aromatic-core units i.e. polycatenar molecules and supramolecular aggregates [45,46]. By adjusting the volume, length and mode of distribution of the alkyl chains along the hydrogen bonded polyaromatic rods their self-assembly is modified by softening their hard-core interactions and by modification of the interfacial curvature between the nano-segregated aggregates of the rods and the surrounding chains. As the formation of mirror-symmetry broken liquid and LC phases is associated with network formation, a fine tuning of the lipophilic chains is often used to achieve the required degree of intermaterials interface curvature. Wide ranges of  $Cub_{bi}$  phases were found to be formed by taper shaped polycatenars in which the terminal alkyl chains are distributed non-symmetrically at

both ends of the aromatic core [47–53]. Moreover, mirror symmetry breaking was observed in the triple network  $Cub_{bi}$  phases with space group  $I23$  ( $Cub_{bi}^{*1}/I23$ , Fig. 1c)[47,49–51,54] as well as in some cases in isotropic liquids assigned as  $Iso_1^{*1}$  phases [48]. In addition to the chiral  $Cub_{bi}^{*1}/I23$  phase, the achiral gyroid double network  $Cub_{bi}$  phase ( $Ia\bar{3}d$ , Fig. 1b) was also formed by polycatenars [40]. As shown in Fig. 1d, chirality arises from the helical packing of the crowded rod-like molecules with their long axes perpendicular to the local network direction. In addition, by alkyl chain engineering the twist angle between the rods is modified, which can be used to switch the space group of the cubic lattice between  $Iad$  and  $I23$  [49,50]. The  $Cub_{bi}/Ia\bar{3}d$  phase is achiral because of the opposite helix sense in the two enantiomeric networks forming this phase cancel each other (thus forming a *meso*-

structure). In the  $I23$  phase there are three networks and the overall chirality cannot be canceled leading to ambidextrous mirror symmetry breaking with chiral conglomerate formation [40,54].

The introduction of a photo switchable chromophore such as an azobenzene unit in the chemical structure yields light-responsive functional LCs because of the fast and reversible *trans-cis* photoisomerization upon light irradiation [55–65]. Photo switchable LCs phases are of special interest as their optical properties could be manipulated with light and therefore could be exploited for optoelectronic, tuneable photonics, and sensing devices [66–71]. Optical switching between lamellar and cubic phases was successively achieved and reported by Kutsumizu et al. [72,73]. The first examples of supramolecular photosensitive polycatenar LCs designed by either hydrogen-bonding [74] or halogen-bonding supramolecular [75] were reported by our research group. The hydrogen-bonded polycatenars **A6/Bm** (Fig. 1a) exhibit chirality synchronization in the  $Cub_{bi}^{*1}/I23$  phases as well as in the  $Iso_1^{*1}$  phase formed by the shortest homologue [74]. Very recently, the effect of aromatic core fluorination on the chiral network formation of **A6/Bm** systems was investigated in detail [76]. As noted above the size and shape of the core as well as the length of the terminal chains are important factors which control the physical properties of LCs [77–80].

Herein, we use alkyl chain engineering in designing new LCs aiming to control the type of  $Cub_{bi}$  phases as well as network formation in the isotropic liquids exhibited by hydrogen-bonded supramolecular LCs systems (Fig. 1a). For this purpose, three new series of supramolecular polycatenars were designed and synthesized (**A10/Bm**, **C6/Bm** and **C10/Bm**, see Scheme 1). The first type of these supramolecular polycatenars (**A10/Bm**) is formed by intermolecular H-bond formation between a taper-shaped triple chain benzoic acid derivative (**A10**) and azopyridine derivatives (**Bm**) terminated with one alkoxy chain, while the other two types (**C6/Bm** and **C10/Bm**) are formed between the same azopyridine derivatives **Bm** and double chain Y-shaped benzoic acid derivatives (**C6** and **C10**). Depending on the number and length of the terminal alkyl chains of the benzoic acid derivatives, these supramolecular dimers show a series of chiral and achiral  $Cub_{bi}$  phases, mirror-symmetry broken isotropic liquids ( $Iso_1^{*1}$ ) and columnar (Col) mesophases. Moreover, the first fast and reversible photoinduced transformation between chiral and achiral cubic phases was successfully achieved with these new supramolecules.

## 2. Experimental

### 2.1. Synthesis

The synthesis of the new H-bonded supramolecules (**A10/Bm**, **C6/Bm** and **C10/Bm**) is shown in Scheme 1. The proton acceptors 4-(4-alkoxyphenylazo)pyridine **Bm** were synthesized as described before [60,81], while the synthesis details of the benzoic acid derivatives **A10**, **C6** and **C10**, as well as for the final supramolecules are given in the supporting information (SI). Homogenous melting and stable LC mesophases were observed for all supramolecules (Table 1 and Table 2).

### 2.2. Characterization

The formation of hydrogen-bonded 1:1 complexes between the 4-phenylazopyridines **Bm** and the benzoic acid **A6** was discussed and proven in previous work by IR spectroscopy and by the absence of DSC peaks corresponding to the transitions of the individual components [76]. Likewise, the formation of the supramolecules between the complementary components **An** and **Bm** was confirmed by the transition temperatures of the 1:1 complexes

**An:Bm** = **An/Bm** (Table 1), which are distinct from the values of individual components as confirmed by differential scanning calorimetry (DSC) and polarized optical microscopy (POM). In the DSC curves all supramolecules do not show any transition of the pure azopyridine derivatives nor of the pure acids (see Figs. S8–S12), and only transition peaks of the newly formed hydrogen-bonded supramolecules could be observed (see Fig. 3).

POM was performed using a Mettler FP-82 HT hot stage and control unit in conjunction with a Nikon Optiphot-2 polarizing microscope. The associated enthalpies were obtained from DSC thermograms which were recorded on a Perkin-Elmer DSC-7, heating and cooling rate: 10 K min<sup>-1</sup>.

X-ray diffraction (XRD) was performed for selected complexes (**A10/B8**, **B10** and **B14**, **C10/B8**, **B14**, and **C6/B14**, see Tables S3–S18 and Figs. S11–S20). High-resolution small angle powder diffraction experiments were recorded on Beamlines BL16B1 at Shanghai Synchrotron Radiation Facility (SSRF). Samples were held in evacuated 1 mm capillaries. A modified Linkam hot stage with thermal stability within 0.2 °C was used, with a hole for the capillary drilled through the silver heating block and mica windows attached to it on each side.  $\theta$ -calibration and linearization were verified using several orders of layer reflections from silver behenate and a series of *n*-alkanes. A Pilatus detector was used for SAXS. The phase transitions of all complexes are collated in Table 1 and Table 2.

Photo switching experiments were performed using Hönle bluepoint LED eco with 365 nm head with maximum output of 14 W/cm<sup>2</sup>.

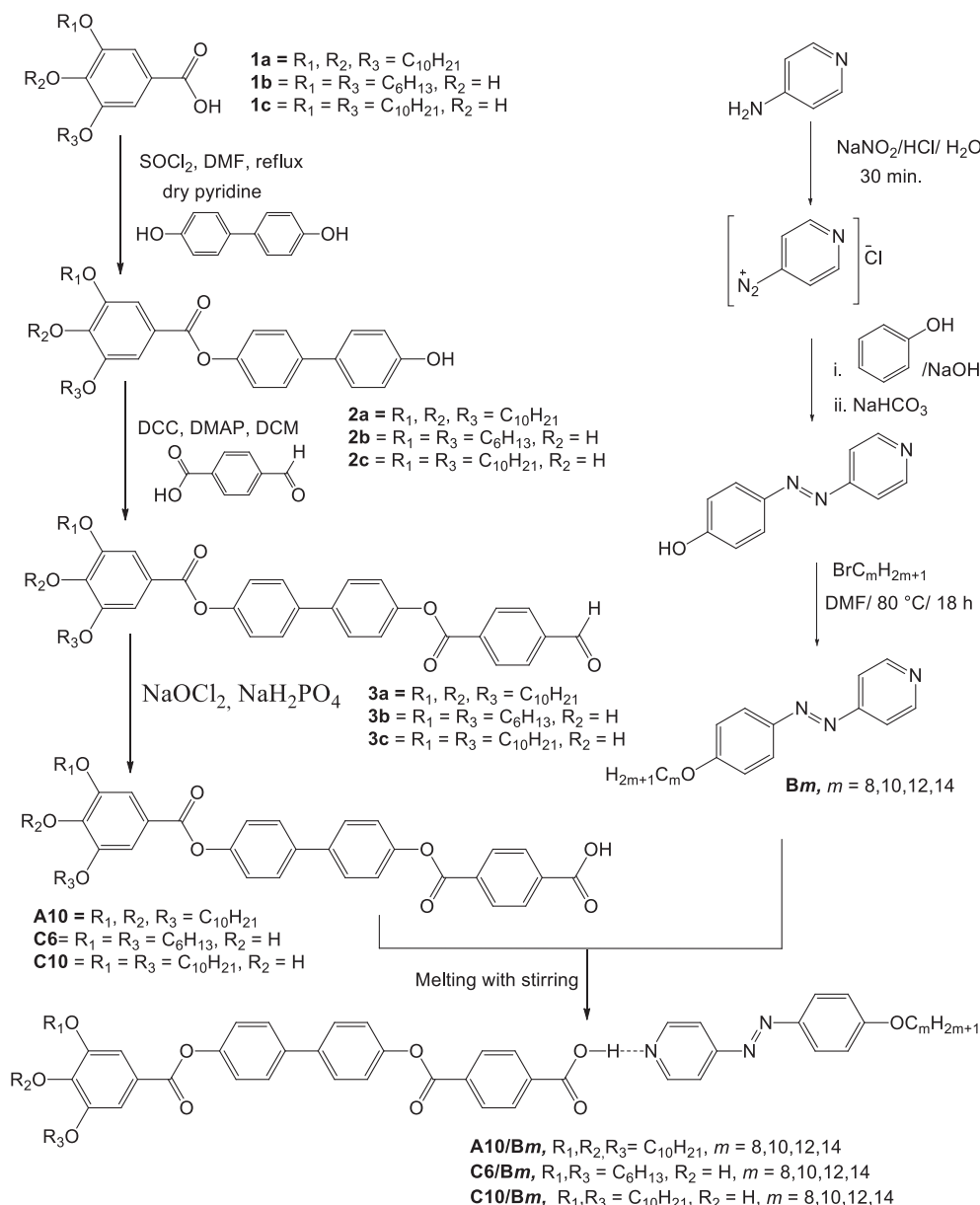
## 3. Results and discussion

### 3.1. Self-assembly of the four-chain supramolecules **An/Bm**

Before discussing the LC behaviour of the hydrogen-bonded complexes, it should be noted that all of the pyridine-based compounds **Bm** are non-mesomorphic i.e. crystalline solids with relatively low melting temperatures (see Table S1, Fig. S11,12), while the hydrogen-bond donor i.e. the benzoic acid derivative **A6** with three hexyloxy chains is a hexagonal columnar LC ( $Col_{hex}$ ,  $a_{hex} = 5.4$  nm) with a high clearing temperature at ~246 °C [74]. Because of the very similar structure of the acid **A6** compared to **A10** with the three hexyloxy chains replaced by three longer decyloxy chains and based on the observed optical textures (see Fig. S7a), the acid **A10** is also considered to exhibit a  $Col_{hex}$  phase between 128 and 230 °C (see Table S2 and Fig. S8). The formation of this phase is a result of dimer formation between the free carboxylic groups leading to hexacatenar supramolecules with six symmetrically distributed terminal chains [74]. Upon H-bond formation with the azopyridine derivatives having only one alkoxy chain different phase sequences of cubic network phases, in some cases accompanied by columnar mesophases, are observed for all resulting 1:1 complexes **An/Bm** (see Table 1 and Fig. 2).

The phase behaviour of the supramolecules **A6/Bm** was discussed in detail in our previous communication [74]. However for comparison reason the transition temperatures of **A6/Bm** as well as for the newly reported aggregates **A10/Bm** are collected in Table 1 and represented graphically in Fig. 2.

The complex formation between **An** and **Bm** leads to the suppression or reduction of the  $Col_{hex}$  phase range exhibited by the pure acids **An** and the induction of new LCs phases. This means that the hexacatenars formed by hydrogen bonding between the benzoic acids **An** are replaced by non-symmetric tetracatenars **An/Bm** involving benzoic acid pyridine H-bonding and having only four terminal chains distributed in 3 + 1 fashion at both ends of the extended aromatic core. This alkyl chain substitution pattern is



**Scheme 1.** Synthesis of the azopyridines **Bm**, the benzoic acids **A10**, **C6**, **C10** and the hydrogen-bonded 1:1 complexes (**A10/Bm**, **C6/Bm** and **C10/Bm**).

known to support the formation of Cub<sub>bi</sub> phases as well as Iso<sup>[\*]</sup> phases due to the smaller average number of alkyl chains which reduces the interface curvature and leads to a transition from non-branched columns in the Col<sub>hex</sub> phase to three-way branched networks in the Cub<sub>bi</sub> phases [60,62].

For all supramolecules **A10/Bm**, only the phase transitions between LC phases as well as the melting and crystallization are visible in the DSC curves. This is not affected by the used heating/cooling rates (5, 10 and 20 K min<sup>-1</sup>). However, all phase transitions could be optically observed under POM (Fig. 2 and Table 1). In all LC phases exhibited by these supramolecules, the WAXS scattering is completely diffuse with a maximum around 0.45 nm confirming the existence of LC phases without fixed positions of the individual molecules (Figures S19-S21).

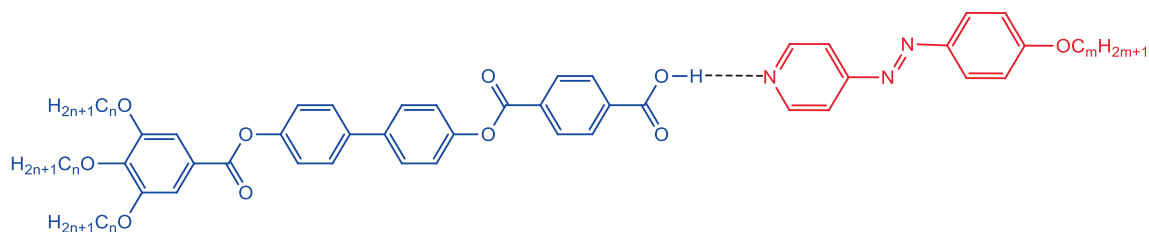
As can be seen from Table 1 and Fig. 2 the shortest supramolecule **A10/B8** of the series **A10/Bm** exhibits two different types of LC phases. Upon heating **A10/B8** from the birefringent crystalline solid a highly viscous and optically isotropic mesophase is observed, which remains over ~20 K. Under slightly uncrossed

polarizers this isotropic phase does not show chiral domains, indicating the presence of an achiral cubic phase (Fig. 4a,b). On further heating the viscosity of the sample does not change but chiral domains, (assigned with <sup>[\*]</sup>) could be observed between not fully crossed polarizers in the temperature range of this second cubic phase till the transition to the highly fluid isotropic liquid state which is achiral again (Fig. 4c,d).

The chiral conglomerate indicates a chiral Cub<sub>bi</sub><sup>[\*]</sup> phase [47]. On cooling **A10/B8** from the isotropic liquid the achiral Cub<sub>bi</sub> phase is observed for a short range ~5 K, while the range of the chiral Cub<sub>bi</sub><sup>[\*]</sup> phase is increased to ~96 K compared to ~67 K on heating. It is also interesting that the formed weakly birefringent crystalline phase on cooling the Cub<sub>bi</sub><sup>[\*]</sup> phase is also chiral, having the chiral domains at the same positions as observed for the Cub<sub>bi</sub><sup>[\*]</sup> phase. This indicates that the chirality information of the Cub<sub>bi</sub><sup>[\*]</sup> mesophase is transferred to the crystalline state resulting in the formation of a mirror-symmetry broken crystalline phase (Cr<sup>[\*]</sup>, Fig. 4e,f). No such Cr<sup>[\*]</sup> phase is observed for the homologous complexes **A10/m** with larger *m*.



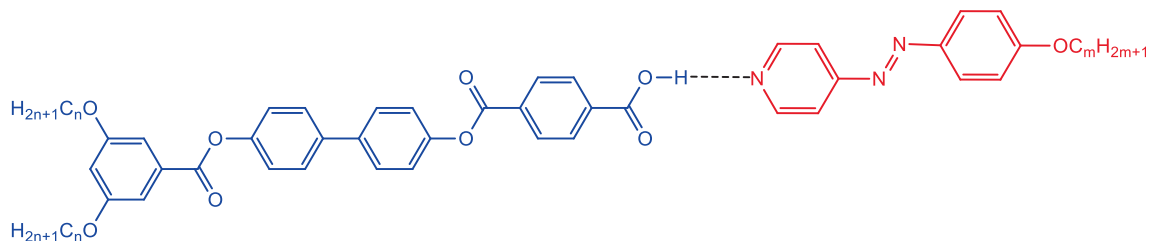
**Table 1**  
Phase transition temperatures ( $T/^\circ\text{C}$ ), mesophase types, and transition enthalpies [ $\Delta H/\text{kJ mol}^{-1}$ ] of the supramolecular complexes **An/Bm**.<sup>a</sup>



Complex	$n$	$m$	Phase transition
<b>A6/B8</b> <sup>74</sup>	6	8	<b>H:</b> Cr 124 [30.3] ~ 187 [0.1] Cub <sub>bi</sub> <sup>l</sup> /I23 196 [0.1] Iso <sup>l</sup> * 200 [0.1] Iso <b>C:</b> Iso 190 [-0.1] Iso <sup>l</sup> * 183 [-0.1] Cub <sub>bi</sub> <sup>l</sup> /I23 75 [-24.8] Cr <sup>l</sup> * 1
<b>A6/B10</b> <sup>74</sup>	6	10	<b>H:</b> Cr <sub>1</sub> 115 [12.2] Cr <sub>2</sub> 128 [45.4] Cub <sub>bi</sub> <sup>l</sup> /I23 201 [0.9] Iso <b>C:</b> Iso 195 [-0.8] Cub <sub>bi</sub> <sup>l</sup> /I23 75 [-38.8] Cr
<b>A6/B12</b> <sup>74</sup>	6	12	<b>H:</b> Cr 123 [54.5] Cub <sub>bi</sub> <sup>l</sup> /I23 191 [1.4] Iso <b>C:</b> Iso 182 [-1.9] Cub <sub>bi</sub> <sup>l</sup> /I23 87 [-45.4] Cr
<b>A6/B14</b> <sup>74</sup>	6	14	<b>H:</b> Cr 92 [31.4] Cub <sub>bi</sub> <sup>l</sup> /I23 184 [1.9] Iso <b>C:</b> Iso 177 [-2.1] Cub <sub>bi</sub> <sup>l</sup> /I23 < 20 Cr
<b>A10/B8</b>	10	8	<b>H:</b> Cr 80 [31.5] Cub <sub>bi</sub> /Ia $\bar{3} d$ 100 [-] Cub <sub>bi</sub> <sup>l</sup> /I23 167 [-] Iso <b>C:</b> Iso 159 [-0.4] Cub <sub>bi</sub> /Ia $\bar{3} d$ 155 [-] Cub <sub>bi</sub> <sup>l</sup> /I23 59 [-37.7] Cr <sup>l</sup> * 1
<b>A10/B10</b>	10	10	<b>H:</b> Cr 100 [40.4] Cub <sub>bi</sub> <sup>l</sup> /I23 160 [-] Cub <sub>bi</sub> /Ia $\bar{3} d$ 167 [-] Iso <b>C:</b> Iso 160 [-] Col <sub>hex</sub> 147 [-0.5] Cub <sub>bi</sub> <sup>l</sup> /I23 60 [-38.4] Cr
<b>A10/B12</b>	10	12	<b>H:</b> Cr 98 [37.9] Cub <sub>bi</sub> <sup>l</sup> /I23 147 [0.5] Cub <sub>bi</sub> /Ia $\bar{3} d$ 154 [-] Col <sub>hex</sub> 172 [-] Iso <b>C:</b> Iso 171 [-] Col <sub>hex</sub> 133 [-] Cub <sub>bi</sub> <sup>l</sup> /I23 47 [-34.4] Cr
<b>A10/B14</b>	10	14	<b>H:</b> Cr 69 [45.2] Cub <sub>bi</sub> <sup>l</sup> /I23 141 [0.5] Cub <sub>bi</sub> /Ia $\bar{3} d$ 159 [-] Col <sub>hex</sub> 175 [-] Iso <b>C:</b> Iso 173 [-] Col <sub>hex</sub> 114 [-0.4] Cub <sub>bi</sub> <sup>l</sup> /I23 32 [-24.2] Cr

<sup>a</sup>Peak temperatures as determined from 2nd heating and 2nd cooling DSC scans with rate 10 K min<sup>-1</sup>; abbreviations: Cr = crystalline solid; Cub<sub>bi</sub>/Ia  $\bar{3} d$  = achiral cubic phase with Ia  $\bar{3} d$  lattice; Cub<sub>bi</sub><sup>l</sup>/I23 = chiral cubic phase with I23 lattice, forming a chiral conglomerate; Col<sub>hex</sub> = hexagonal columnar phase with  $p6mm$  lattice; Iso<sup>l</sup>\* = chiral isotropic conglomerate liquid; Iso = achiral isotropic liquid; for complete structural data, see Tables S6 and S19.

**Table 2**  
Phase transition temperatures ( $T/^\circ\text{C}$ ), mesophase types, and transition enthalpies [ $\Delta H/\text{kJ mol}^{-1}$ ] of the supramolecular complexes **Cn/Bm**.<sup>a</sup>



Complex	$n$	$m$	Phase transition
<b>C6/B8</b>	6	8	<b>H:</b> Cr 119 [35.5] Cub <sub>bi</sub> /Ia $\bar{3} d$ 173 [0.2] Iso <b>C:</b> Iso 166 [-0.5] Cub <sub>bi</sub> /Ia $\bar{3} d$ 90 [-33.0] Cr
<b>C6/B10</b>	6	10	<b>H:</b> Cr 127 [30.3] Cub <sub>bi</sub> /Ia $\bar{3} d$ 157 [0.2] Iso <b>C:</b> Iso 139 [-0.2] Cub <sub>bi</sub> /Ia $\bar{3} d$ 76 [-26.9] Cr
<b>C6/B12</b>	6	12	<b>H:</b> Cr 117 [44.7] Cub <sub>bi</sub> /Ia $\bar{3} d$ 157 [0.3] Iso <b>C:</b> Iso 151 [-0.4] Cub <sub>bi</sub> /Ia $\bar{3} d$ 71 [-41.0] Cr
<b>C6/B14</b>	6	14	<b>H:</b> Cr 99 [28.7] Cub <sub>bi</sub> /Ia $\bar{3} d$ 157 [0.7] Iso <b>C:</b> Iso 151 [-0.9] Cub <sub>bi</sub> /Ia $\bar{3} d$ 58 [-31.7] Cr
<b>C10/B8</b>	10	8	<b>H:</b> Cr 118 [42.3] Cub <sub>bi</sub> /Ia $\bar{3} d$ 183 [2.0] Iso <b>C:</b> Iso 178 [-1.7] Cub <sub>bi</sub> /Ia $\bar{3} d$ 111 [-14.5] Cr <sub>1</sub> 94 [-21.4] Cr <sub>2</sub>
<b>C10/B10</b>	10	10	<b>H:</b> Cr <sup>l</sup> * 103 [37.4] Cub <sub>bi</sub> <sup>l</sup> /I23 178 [1.6] Iso <b>C:</b> Iso 176 [-0.1] Iso <sup>l</sup> * 167 [-0.7] Cub <sub>bi</sub> <sup>l</sup> /I23 94 [-35.6] Cr <sup>l</sup> * 1
<b>C10/B12</b>	10	12	<b>H:</b> Cr <sup>l</sup> * 108 [29.1] Cub <sub>bi</sub> <sup>l</sup> /I23 183 [0.7] Iso <sup>l</sup> * 200 [0.3] Iso <b>C:</b> Iso 188 [-0.3] Iso <sup>l</sup> * 174 [-0.4] Cub <sub>bi</sub> <sup>l</sup> /I23 90 [-27.5] Cr <sup>l</sup> * 1
<b>C10/B14</b>	10	14	<b>H:</b> Cr 103 [33.9] Cub <sub>bi</sub> /Ia $\bar{3} d$ 150 [-] Cub <sub>bi</sub> <sup>l</sup> /I23 185 [2.1] Iso <b>C:</b> Iso 179 [-1.0] Col <sub>hex</sub> 173 [-0.4] Cub <sub>bi</sub> <sup>l</sup> /I23 89 [-23.2] Cr

<sup>a</sup>Peak temperatures as determined from 2nd heating and 2nd cooling DSC scans with rate 10 K min<sup>-1</sup>; for abbreviations see Table 1; for complete structural data, see Table S19.

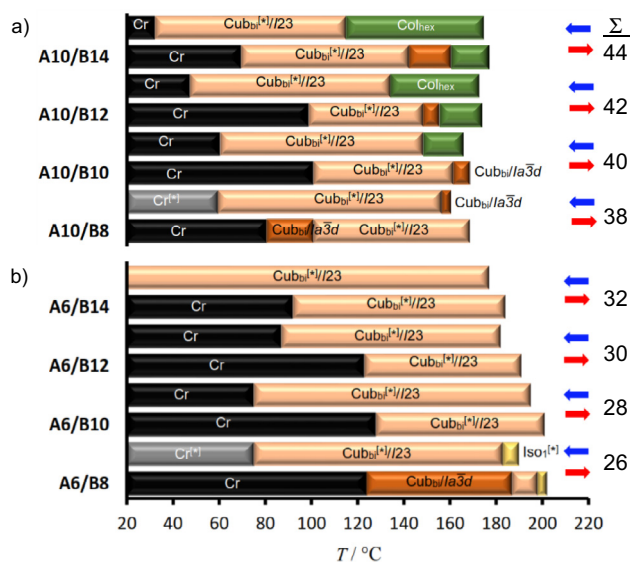


**Fig. 2.** Phase transitions of: (a) the new H-bonded supramolecules **A10/Bm** and (b) the previously reported **A6/Bm** supramolecules as observed by DSC and POM on heating (lower bars, red arrows) and on cooling (upper bars, blue arrows) with  $10 \text{ K min}^{-1}$ ;  $\Sigma n$  is the total number of C-atoms in the lipophilic chains ( $3n + m$ ). (For interpretation of the references to colour in this figure legend, the reader is referred to the web version of this article.)

To study both cubic phases in more detail, the supramolecule **A10/B8** was further investigated by X-ray diffraction with a synchrotron source (Fig. 5 and Tables S3-S5). Upon heating two intense diffraction peaks are observed at  $\sim 90^\circ \text{C}$  in the lower temperature achiral  $\text{Cub}_{\text{bi}}$  phase which are indexed to (211) and (220) reflections known for a  $1a\bar{3}d$  lattice with a cubic lattice parameter of  $a_{\text{cub}} = 13.15 \text{ nm}$  (Fig. 5a) confirming a double network gyroid cubic phase [40]. Moreover, the additional much smaller scatterings at higher  $\theta$ -values fit also with the  $1a\bar{3}d$  space group. In the higher temperature chiral  $\text{Cub}_{\text{bi}}$  phase the most intense peaks can be indexed as (321) and (400) reflections of a  $I23$  lattice (Fig. 5b and Table S4) [76]. The lattice parameter of this chiral cubic phase is  $a_{\text{cub}} = 21.58 \text{ nm}$  and thus 65 % larger than that in the  $1a\bar{3}d$  lattice ( $a_{\text{cub}} = 13.15 \text{ nm}$ ). The increased lattice parameter is in agreement with a transition from a double network to a triple network  $\text{Cub}_{\text{bi}}$  phase [54]. The structures of the two different  $\text{Cub}_{\text{bi}}$  phases was further confirmed by the reconstruction of electron

density maps based on the obtained diffraction patterns, which show the double network structure of the  $1a\bar{3}d$  phase and the triple-network structure of the  $I23$  phase (Fig. 5c,d).

Upon cooling **A10/B8** from the isotropic liquid, a small range of an achiral  $1a\bar{3}d$  phase appears before the chiral  $I23$  phase, as indicated by the absence of any chiral conglomerate texture in the highly viscous and optically isotropic cubic phase. Additional support comes from SAXS investigation, showing the typical diffraction pattern of a cubic phase with  $1a\bar{3}d$  space group (Table S5). However, in this  $1a\bar{3}d$  phase the lattice parameter  $a_{\text{cub}} = 12.32 \text{ nm}$  at  $160^\circ \text{C}$  is significantly smaller than in the low temperature  $1a\bar{3}d$  phase observed at  $90^\circ \text{C}$  on heating ( $a_{\text{cub}} = 13.15 \text{ nm}$ , see Tables 1 and S6).

The next longer hydrogen-bonded supramolecule with  $m = 10$ , i.e. **A10/B10**, shows an inverse phase sequence  $\text{Cub}_{\text{bi}}^*/I23 \rightarrow \text{Cub}_{\text{bi}}/1a\bar{3}d$  on heating (for XRD data, see Tables S7-S9 and Figs. S14). Moreover, on cooling from the isotropic liquid the achiral double network  $\text{Cub}_{\text{bi}}/1a\bar{3}d$  phase is completely replaced by a hexagonal columnar phase ( $\text{Col}_{\text{hex}}$  with  $a_{\text{hex}} = 6.17 \text{ nm}$ , see Fig. 6b and Table S9) followed by the chiral  $\text{Cub}_{\text{bi}}^*/I23$  phase, which is retained till crystallization (see Table 1, Fig. 6a). For the longest supramolecules **A10/B12** and **A10/B14** phase sequences involving three different LC phases are observed on heating ( $\text{Cub}_{\text{bi}}^*/I23 \rightarrow \text{Cub}_{\text{bi}}/1a\bar{3}d \rightarrow \text{Col}_{\text{hex}}/p6mm$ ) and in the cooling cycle the  $\text{Cub}_{\text{bi}}/1a\bar{3}d$  phase is completely removed while only the  $\text{Col}_{\text{hex}}/p6mm$  and  $\text{Cub}_{\text{bi}}^*/I23$  phases are observed (see Fig. 2 and Table 1). The formation of the  $\text{Col}_{\text{hex}}/p6mm$  phase was not observed for any of the supramolecular complexes **A6/Bm** with three shorter hexyloxy chains at the benzoic acid side, indicating that the formation of this columnar phase requires long alkyl chains. The reason for  $\text{Col}_{\text{hex}}$  phase formation is that thermal alkyl chain expansion increases the aromatic-aliphatic interface curvature which then leads to the transition from branched columns in the  $\text{Cub}_{\text{bi}}$  phases to non-branched columns in the  $\text{Col}_{\text{hex}}$  phase.

Overall, in the series of H-bonded complexes **An/Bm** reported here, there are two distinct ranges for the  $1a\bar{3}d$  phase. Those of the compounds with a total number of C-atoms in the aliphatic chains  $\Sigma < 28$  (Fig. 2b) and those with  $\Sigma > 32$  (Fig. 2a). For **A10/B8** there are two  $1a\bar{3}d$  phases, one formed at low temperature on heating before the transition to  $I23$  ( $1a\bar{3}d^{\text{LT}}$  phase), the other one at higher temperature and formed on cooling from the isotropic liquid state ( $1a\bar{3}d^{\text{HT}}$ ). For the higher homologs of the series **A10/**

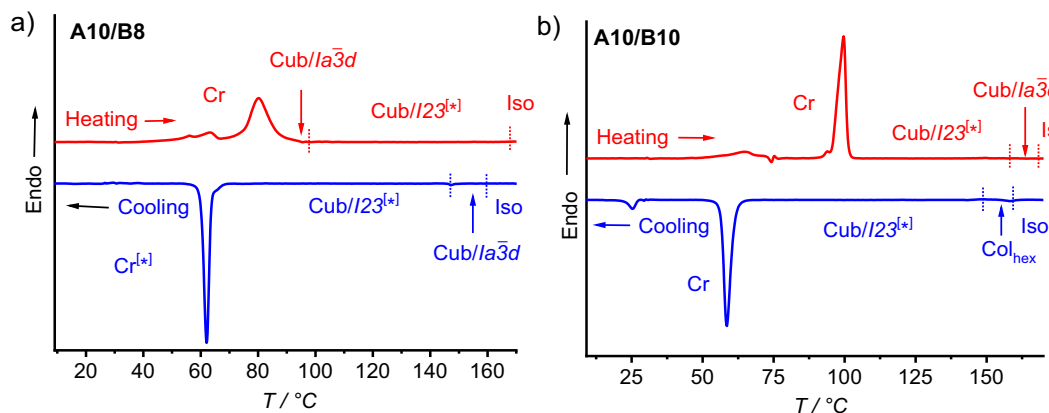


**Fig. 3.** DSC traces for the supramolecular complexes: (a) **A10/B8** and (b) **A10/B10** with heating and cooling rates of  $10 \text{ K.min}^{-1}$ ; the DSCs of the individual components are shown in Figs. S19-S21.

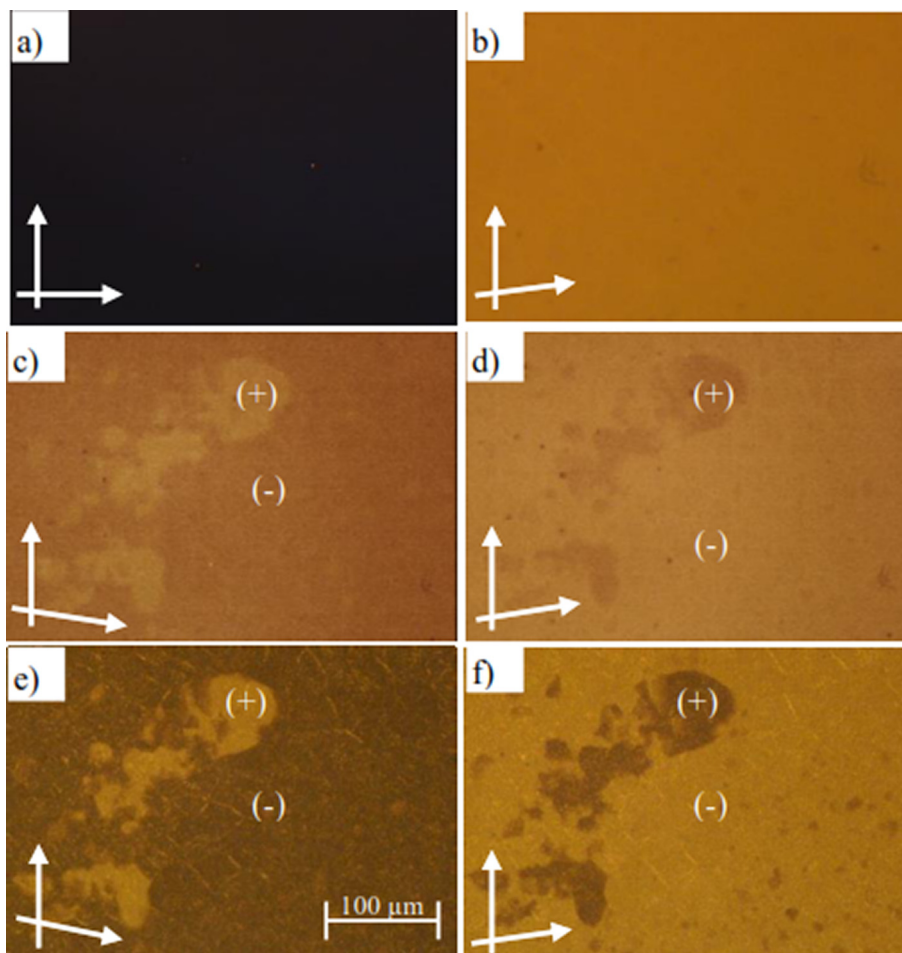


**Fig. 4.** Textures of the supramolecule **A10/B8** as observed on cooling in: (a) the achiral  $\text{Cub}_{\text{bi}}/\bar{Ia}3d$  at  $T = 157$  °C under crossed polarizers; (b) after rotating one polarizer from the crossed position by  $15^\circ$  in clockwise direction; (c,d) in  $\text{Cub}_{\text{bi}}^{*1}/I23$  at  $T = 120$  °C after rotating one polarizer from the crossed position in clockwise or anticlockwise directions with the same angle showing dark and bright domains and in (e,f) in the chiral crystalline phase  $\text{Cr}^{*1}$ .

**Bn** with  $m \geq 8$  there is no  $\bar{Ia}3d^L$  phase, only  $\bar{Ia}3d^{\text{HT}}$ . Moreover, it appears that there are even two distinct types of this  $\bar{Ia}3d^{\text{HT}}$  phase, that of **A10/B8** occurring on cooling from the Iso phase has the smallest  $a_{\text{cub}}$  value (12.3 nm), whereas for compounds with  $m = 10, 14$  it occurs on heating above the  $I23$  phase and has a significantly larger value  $a_{\text{cub}}$  of 13.5–13.6 nm (Fig. 2a). Moreover, all compounds with longer chains than **A10/B8** form a  $\text{Col}_{\text{hex}}$  phase and no  $\bar{Ia}3d^{\text{HT}}$  phase on cooling, though  $\bar{Ia}3d^{\text{HT}}$  is observed on heating above the chiral  $I23$  phase, followed by  $\text{Col}_{\text{hex}}$  on further heating. This could be understood if the  $\bar{Ia}3d^{\text{HT}}$  phase of **A10/B8**, formed on cooling from the achiral isotropic liquid would be achiral due to the absence of any long-range helical twist along the networks. In this case the lattice parameter is exclusively determined by the molecular parameters and volume effects (see Table S6 in SI) and not by any helix pitch length, and therefore can be very different from those of the  $Iad$  phases with helical structure [40,47]. In contrast, the  $\bar{Ia}3d^{\text{HT}}$  phases of compounds **A10/B10** - **A10/B14** developing from the chiral  $I23$  phase on heating and showing larger and very similar lattice parameters are likely to represent helical network phases, i.e. the helical organization present in the networks of the  $I23$  phase is retained at the transition to  $\bar{Ia}3d^{\text{HT}}$ . Only at the transition to  $\text{Col}_{\text{hex}}$  the long-range helical pitch is lost after removal of the network junctions. However, in order to certainly distinguish between helical and non-helical subtypes of the  $\text{Cub}_{\text{bi}}/$

$\bar{Ia}3d^{\text{HT}}$  phase, additional resonant soft X-ray scattering (RSoXS) investigations would be required [40,82].

It should be noted that for the complexes **A10/Bm** no mirror-symmetry broken isotropic liquid phase ( $\text{Iso}_1^{*1}$ ), like that one recorded for the shortest supramolecule in the **A6/Bm** series is observed (see Table 1 and Fig. 2). This means that  $\text{Iso}_1^{*1}$  phase formation requires small chain volumes and is anyhow associated with the  $\bar{Ia}3d \rightarrow I23$  transition of the complexes with relatively short chains.

### 3.2. Liquid crystal self-assembly of the Y-shaped three-chain supramolecules **Cn/Bm**

In order to avoid the formation of  $\text{Col}_{\text{hex}}$  phases and to further modify the LC behaviour in these supramolecular aggregates by alkyl chain engineering, Y-shaped benzoic acid derivatives **Cn** with smaller total chain volume were used as the proton donors (see Fig. 1 and Scheme 1). The formed tricaténars **Cn/Bm** have one less alkyl chain; namely the middle chain at 4-position of the benzoic acids **Cn** is removed compared to the related analogues **An** (see Fig. 7 and Table 2). This modification increases the melting temperatures of all **Cn/Bm** complexes compared to the complexes **An/Bm** and retains the 3D cubic phases formed by the **An/Bm** supramolecules. However, for the aggregates **C6/Bm** having shorter alkyl chains at the benzoic acid side exclusively the achiral  $\text{Cub}_{\text{bi}}/\bar{Ia}3d$

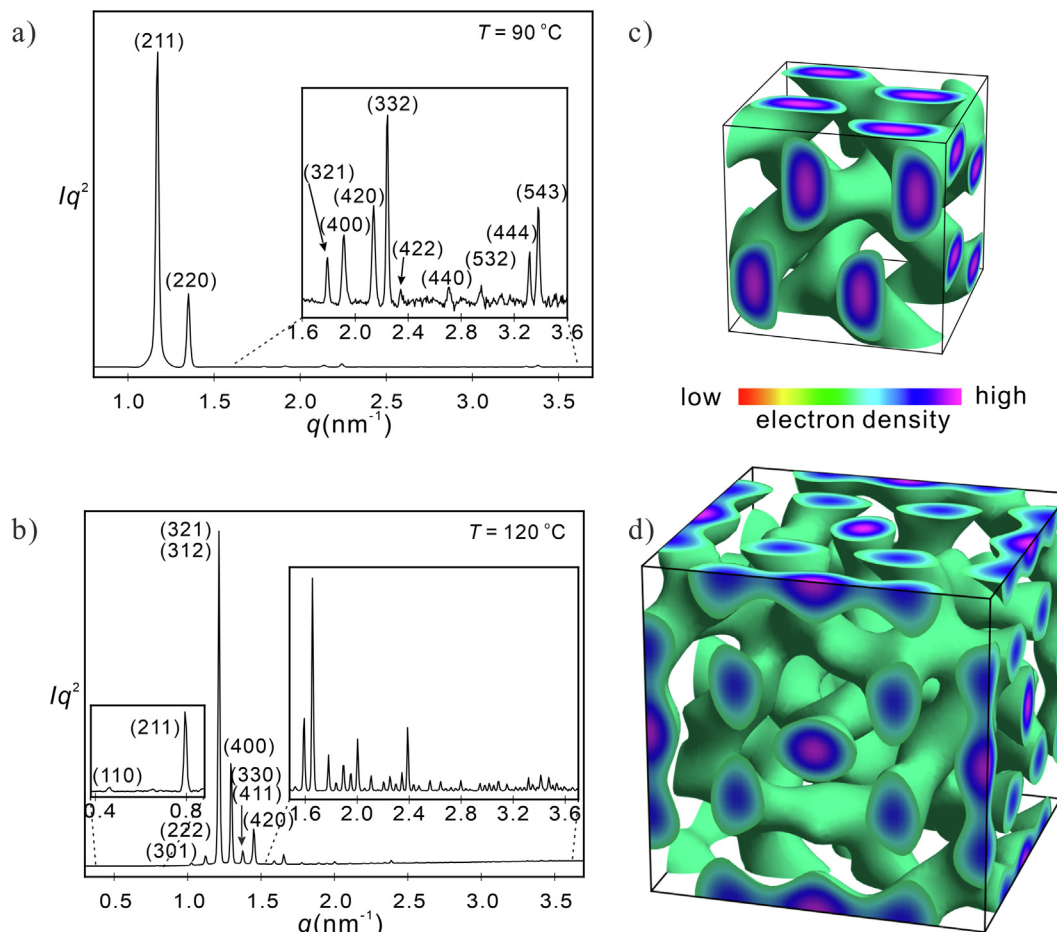


**Fig. 5.** (a,b) SAXS diffractograms of **A10/B8** on heating: a) in the  $\text{Cub}_{\text{bi}}/\text{Ia}\bar{3}d$  phase at 90 °C ( $a_{\text{cub}} = 13.15$  nm) and b) in the  $\text{Cub}_{\text{bi}}^*/\text{I}23$  phase at 120 °C ( $a_{\text{cub}} = 21.58$  nm); (c, d) electron density maps of (c) the  $\text{Ia}\bar{3}d$  phase and (d) the  $\text{I}23$  phase reconstructed from the diffraction data in (a, b); for numerical XRD data, see Tables S3, S4 in SI.

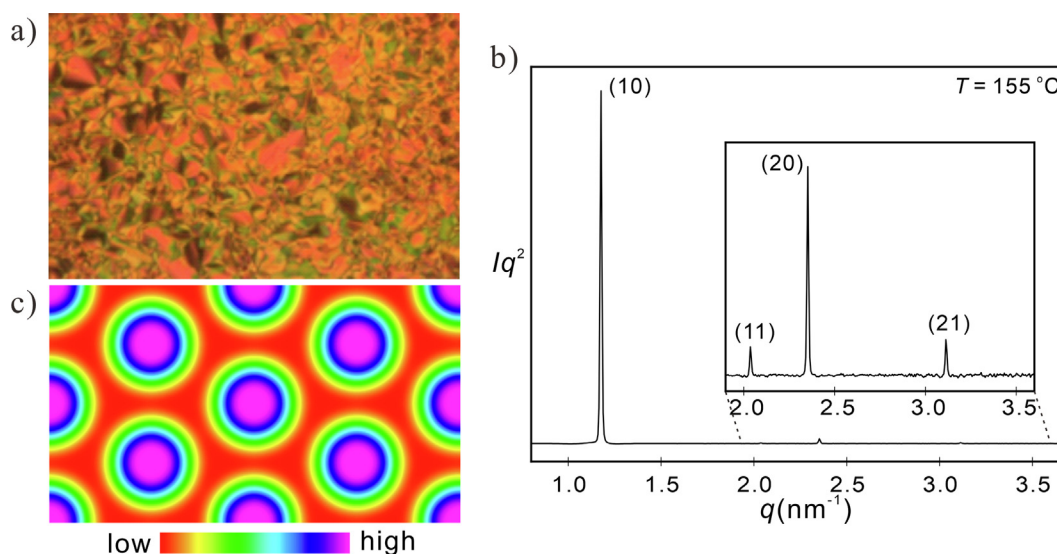


**Fig. 6.** (a) Texture of the supramolecule **A10/B10** as observed on cooling in the  $\text{Col}_{\text{hex}}/p6mm$  phase at  $T = 155$  °C; (b) SAXS diffractogram at 155 °C upon cooling of **A10/B10** ( $a_{\text{hex}} = 6.17$  nm); (c) reconstructed electron density map for  $\text{Col}_{\text{hex}}/p6mm$  phase of **A10/B10**.

phase is observed (see Fig. 7, for XRD data see Fig. S16 and Table S13, S14).

Increasing the number of carbon atoms in the terminal chains of the proton donor **Cn** to  $n = 10$  instead of 6 results in the formation

of **C10/Bm** supramolecules. In this case for the shortest derivative **C10/B8** the achiral  $\text{Cub}_{\text{bi}}/\text{Ia}\bar{3}d$  phase (see Fig. S17) is retained like in **C6/B8**. On chain elongation mirror-symmetry breaking is induced in the crystalline state ( $\text{C}r^{[*]}$ ) as well as in the cubic phase

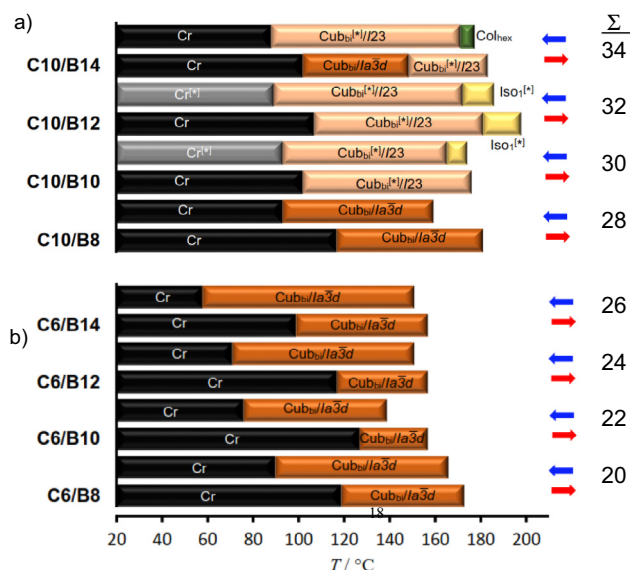


**Fig. 7.** Phase transitions of the new H-bonded supramolecules: (a) **C10/Bm** and (b) **C6/Bm** as observed by DSC and POM on heating (lower bars, red arrows) and on cooling (upper bars, blue arrows) with  $10 \text{ K min}^{-1}$ .  $\Sigma$  is the total number of C-atoms in the lipophilic chains ( $2n + m$ ). (For interpretation of the references to colour in this figure legend, the reader is referred to the web version of this article.)

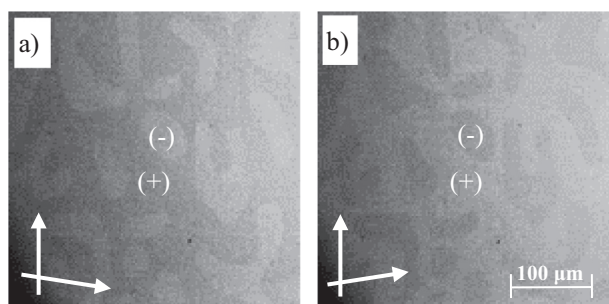


**Fig. 8.** Textures of the supramolecule **C10/B10** as observed on cooling in the chiral  $\text{Iso}_1^{[*]}$  phase at  $T = 170 \text{ °C}$ : (a) after rotating one polarizer from the crossed position in clockwise direction and (b) in anticlockwise direction showing dark and bright domains.

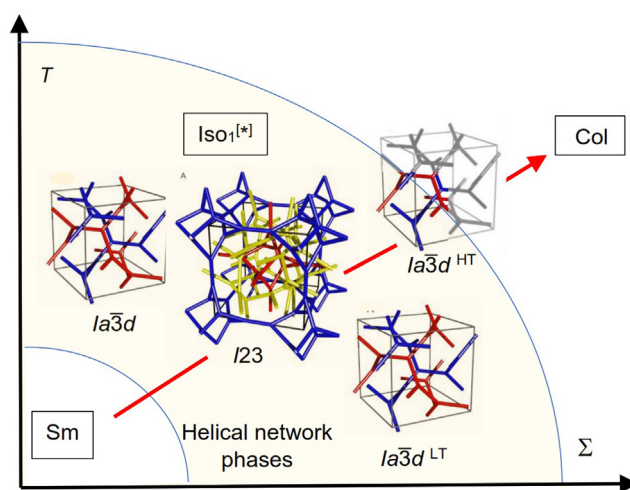


**Fig. 9.** Development of the different network phases depending on chain volume and temperature.

and even after transition to the isotropic liquid as observed for both middle chain homologues **C10/B10** and **C10/B12**. Chirality of these phases was confirmed by the dark and bright domains observed in the cooling cycles in the highly fluid isotropic liquid under slightly uncrossed polarizers (Fig. 8a, b). This indicates a chiral isotropic liquid, composed of a conglomerate of chiral domains ( $\text{Iso}_1^{[*]}$ ), which is not formed by any of the **A10/Bm** aggregates.

The  $\text{Iso}_1^{[*]}$  phase of **C10/B10** appears only on cooling as metastable phase and as enantiotropic one for **C10/B12**, associated with a characteristic broad feature in the DSC traces (see Fig. S27 and S28) and exists over temperature ranges of  $\sim 9 \text{ K}$  and  $\sim 14 \text{ K}$  for **C10/B10** and **C10/B12**, respectively. The  $\text{Iso}_1^{[*]}$  phase of both complexes transforms into the chiral triple network  $\text{Cub}_{bi}^{[*]}/I23$  phase on cooling. Because it appears adjacent to a  $\text{Cub}_{bi}^{[*]}/I23$  phase it seems that this  $\text{Iso}_1^{[*]}$  phase represents a distorted version of the  $I23$  phase, retaining a long-range chirality synchronization due to a local  $I23$ -like network structure in the isotropic liquid state. Similar to **A6/B8** and **A10/B8** chirality could be also retained in the crystalline state ( $\text{Cr}^{[*]}$ ) even after sample storage for several months (Table 2).

For the longest supramolecule **C10/B14** the  $\text{Iso}_1^{[*]}$  phase is removed and replaced by a  $\text{Col}_{hex}$  phase on cooling from the achiral isotropic liquid at  $\sim T = 179 \text{ °C}$ . It is a metastable phase for a short temperature range of  $\sim 6 \text{ K}$  followed by  $\text{Cub}_{bi}^{[*]}/I23$  at  $T = 173 \text{ °C}$  which then transforms to a birefringent crystalline phase (Cr) at  $T = 89 \text{ °C}$  (for XRD see Table S16-S18 and Fig. S18). Upon heating a  $\text{Cub}_{bi}/Ia3d^{LT}$  phase is found (similar to complex **A10/B8**), which transforms at  $150 \text{ °C}$  into the  $\text{Cub}_{bi}^{[*]}/I23$  phase on further heating.

### 3.3. Discussion of the self-assembly and mirror symmetry breaking in the $\text{Cub}_{bi}$ phases

The series **An/Bm** and **Cn/Bm** cover different and partly overlapping chain volume ranges ( $\Sigma = 26\text{--}44$  and  $20\text{--}34$ , respectively) which leads to different sections of a common phase sequence evolving in each of the series (see Figs. 2 and 7). The change of the substitution pattern of the benzoic acid does not modify the mesophase types and leads only to a slight shift of the distinct phase ranges with respect to  $\Sigma$ . Among the  $\text{Cub}_{bi}$  phases there is obviously only one type of  $I23$  phase and possibly three or even four subtypes of the  $Ia3d$  phase. The  $Ia3d$  phase occurring for complexes with  $\Sigma = 28$  is replaced by the  $I23$  phase upon increasing the alkyl chain volume ( $\Sigma = 26\text{--}44$ ; Figs. 2b, 7b). Moreover, there is a re-entrance of the  $Ia3d$  lattice for complexes with largest chain volume ( $\Sigma = 40\text{--}44$ ). This sequence  $Ia3d \rightarrow I23 \rightarrow Ia3d$  was previously observed in several homologous series of polycatenar mesogens [42,49] and was attributed to an increasing helical twist between the molecules, which modifies the cubic space group and leads to two subtypes of  $Ia3d$  phases, the long pitch and the short pitch phases [49–51,54]. However, in the series of H-bonded complexes reported here, there is no such clear trend of the helical pitch length (see Tables S6 and S19). Nevertheless, there are two distinct chain volume ranges of the  $Ia3d$  phase. The  $Ia3d$  phase of the high chain volume complexes occurs below  $I23$  for **A10/B8** and **C10/B14** (Fig. 2a, 7a), but upon further chain elongation it becomes a high temperature phase above  $I23$  which competes with the  $\text{Col}_{hex}$  phase ( $Ia3d^{HT}$ ).

It appears that the type of  $Ia3d$  phase is not only a function of the helical twist, but also influenced by the changing interface curvature at the lamellar-columnar transition. The  $Ia3d^{LT}$  phase seems to be stabilized by reduced chain expansion and therefore is more considered as being derived from a lamellar phase by curvature,

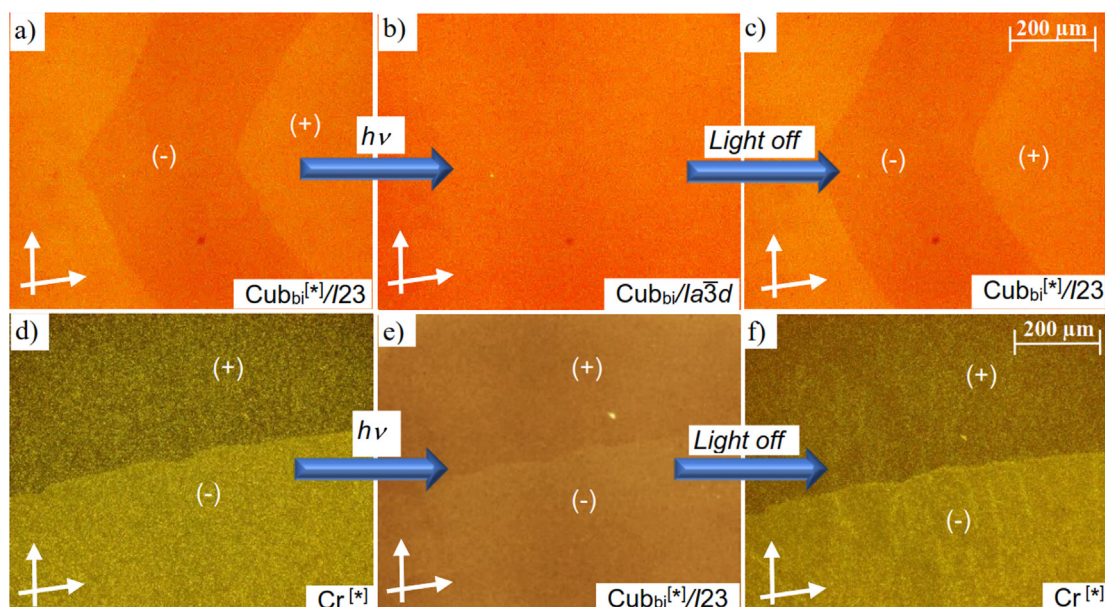


**Fig. 10.** (a–c) Reversible isothermal photo-off-on switching of chirality as observed for **A10/B8** in a homeotropic cell at  $T = 150\text{ }^{\circ}\text{C}$ ; (a) and (c) show chiral conglomerate textures of the chiral  $I23$  phase, whereas the photoinduced achiral  $Ia3d$  phase in b) shows no such domains. (d–f) Switching between the  $\text{Cr}^{[*]}$  and the  $\text{Cub}_{\text{bi}}^{[*]}/I23$  phase by retaining chirality and conglomerate texture at  $T = 70\text{ }^{\circ}\text{C}$ .

whereas the formation of the  $Ia3d^{\text{HT}}$  phase is associated with thermal alkyl chain expansion and thus is considered as more related to columnar self-assembly and fusion of these columns to networks. Moreover, it is hypothesized that the  $Ia3d^{\text{HT}}$  phase formed from the chiral  $I23$  phase on heating (complexes **A10/B10** – **A10/B14**) retains its helical network structure and becomes a meso-structure, but if formed on cooling from the achiral isotropic liquid (**A10/B8**) the  $Ia3d^{\text{HT}}$  phase apparently evolves as a non-helical network phase, like those known for lyotropic systems and polymers and in this case only after transition to  $I23$  a long range network helicity develops [40]. For complexes with longer chains this achiral  $Ia3d^{\text{HT}}$  phase is replaced by  $\text{Col}_{\text{hex}}$  on cooling. On heating the  $Ia3d^{\text{HT}}$  phase develops from the  $I23$  phase and is retained as long as there is sufficient network connectivity and helix synchronization. The proposed overall picture of the development of the distinct cubic phases is sketched in Fig. 9.

### 3.4. Isothermal photo switching in mirror symmetry broken network phases

The incorporation of azo units into the structures of the newly reported supramolecules allows the possibility of studying photoisomerization under UV irradiation. All previously studied azobenzene-based polycatenars elucidated the possibility of photo-switching in solutions as well as between different fluid LC phases, which in most cases represent lamellar or nematic phases [64,65,83–87]. Only recently, successful isothermal light-induced transformation between  $\text{SmC}$  and  $\text{Cub}_{\text{bi}}$  phases was reported for binary mixtures of azobenzene molecules with 4'-*n*-alkoxy-3'-nitro biphenyl-4-carboxylic acid or 4'-*n*-hexadecyloxy-3'-cyanobiphenyl-4-carboxylic acid, but not for polycatenars [72,73,88]. A breakthrough came with the first report about the rapid and reversible photo switching between chiral  $\text{Iso}_1^{[*]}$  and achiral lamellar  $\text{SmA}$  phases exhibited by azobenzene-based polycatenars.<sup>62</sup> The next issue to be addressed was to check the possibility to photo switch between chiral and achiral cubic phases (Fig. 1b,c). To the best of our knowledge, up to date there is no report about such transfor-

mation. The supramolecule **A10/B8** was selected for such investigations as a representative example. **A10/B8** was sandwiched between normal glass slides on a temperature controlled heating stage and irradiated firstly in the chiral  $\text{Cub}_{\text{bi}}^{[*]}/I23$  phase at  $T = 150\text{ }^{\circ}\text{C}$ , i.e. close to  $\text{Cub}_{\text{bi}}^{[*]}/I23$  -  $\text{Cub}_{\text{bi}}/Ia3d$  phase transition temperature, by UV light (365 nm). As obvious from Fig. 10a,b, the conglomerate texture disappears upon irradiation within  $< 3\text{ s}$ . This indicates that a fast isothermal transformation from the chiral to the achiral  $\text{Cub}_{\text{bi}}$  phase was achieved. The achiral  $\text{Cub}_{\text{bi}}/Ia3d$  phase relaxes back to the chiral domain texture of the  $\text{Cub}_{\text{bi}}^{[*]}/I23$  phase almost immediately after switching off the light source ( $< 3\text{ s}$ ; see Fig. 10c). Therefore, this observation elucidates the first example of a fast and reversible photoswitching between a chiral and an achiral cubic LC mesophase.

Likewise, a photoinduced isothermal transition from the crystalline  $\text{Cr}^{[*]}$  phase to the liquid crystalline  $\text{Cub}_{\text{bi}}^{[*]}/I23$  phase at  $T = 70\text{ }^{\circ}\text{C}$  was also achieved, which is also very fast and reversible (see Fig. 10d–f). The completely isotropic texture of  $\text{Cub}_{\text{bi}}^{[*]}/I23$  phase relaxes back to the low birefringent texture of the  $\text{Cr}^{[*]}$  phase after switching the light off. In both cases the chiral domains after switching off the light source are observed in the same regions with the same handedness as before light irradiation. This is attributed to the high viscosity due to the 3D lattice of the cubic phases and the storage of the chiral information at least at the interfaces to the glass substrates. These transitions are mainly due to a shift of the phase transition temperatures by photoisomerization. The bent shape of the photoinduced *cis*-isomer shifts the phase transitions  $\text{Cub}_{\text{bi}}^{[*]}/I23$  -  $\text{Cub}_{\text{bi}}/Ia3d$  and  $\text{Cr}^{[*]}$  -  $\text{Cub}_{\text{bi}}^{[*]}/I23$  to lower temperatures. Therefore, the supramolecules reported herein represent the first examples of materials capable of photo-switching between chiral and achiral 3D networks by light irradiation. Moreover, it was also possible to photo-switch between crystalline and liquid crystalline phases.

## 4. Summary and conclusions

In summary, we reported the design, synthesis, and molecular self-assembly of new photosensitive nanostructured supramolecu-

lar azopyridine-based polycatenars formed by intermolecular hydrogen-bond between Y-shaped or taper shaped benzoic acids and linear azopyridine derivatives (Fig. 1a). The formation of mirror-symmetry broken  $\text{Cub}_{\text{bi}}^{*1}$  and  $\text{Iso}_{\text{ol}}^{*1}$  phases was successfully controlled by alkyl-chain engineering via changing the number and positions as well as the length of terminal alkyl chains at both ends of the supramolecules (Figs. 2 and 7). Chirality synchronization by helical network formation was observed in the triple network cubic phase with  $I23$  symmetry as well as in the isotropic liquid phase ( $\text{Iso}_{\text{ol}}^{*1}$ ). The  $\text{Iso}_{\text{ol}}^{*1}$  phase is observed only adjacent to the  $I23$  cubic phase, which means that it is likely to have a local  $I23$ -like structure. In addition to these chiral phases achiral cubic phases with  $I\bar{a}3d$  symmetry as well as a  $\text{Col}_{\text{hex}}$  phases are observed depending on the length of the terminal alkyl chains (Fig. 9). Moreover, the synthesized supramolecules represent the first examples of fast and reversible photo switching by UV irradiation between  $\text{Cub}_{\text{bi}}^{*1}/I23$  and  $\text{Cub}_{\text{bi}}/I\bar{a}3d$  phases. This could lead to interesting perspectives for chirality switching and phase modulation by interaction with non-polarized light [71], which in turn could be used to improve the materials properties to be applied in optical shutters and other optical, electronic, or mechanical modulation devices.

### CRedit authorship contribution statement

**M. Alaasar:** Conceptualization, Investigation, Data curation, Supervision, Methodology, Writing-original draft, Writing-review and editing. **X. Cai:** Investigation, Methodology, Data curation, Software. **F. Kraus:** Investigation, Methodology. **M. Giese:** Writing-review and editing. **F. Liu:** Data curation, Software, Supervision, Writing-review and editing. **C. Tschierske:** Writing-review and editing, Supervision.

### Declaration of Competing Interest

The authors declare that they have no known competing financial interests or personal relationships that could have appeared to influence the work reported in this paper.

### Acknowledgements

M. Alaasar acknowledges the German Research Foundation (DFG) for the financial support (AL2378/1-1, 424355983). F. Liu thanks Science and Technology Agency of Shaanxi Province (2016KW-050 and 2018KWZ-03) for the financial support. The authors are grateful to Beamline BL16B1 at SSRF (Shanghai Synchrotron Radiation Facility, China) for providing the beamtime.

### Appendix A. Supplementary material

Supplementary data to this article can be found online at <https://doi.org/10.1016/j.molliq.2022.118597>.

### References

- [1] H. Takezoe, Spontaneous achiral symmetry breaking in liquid crystalline phases, in: C. Tschierske (Ed.), *Liquid Crystals, Topics in Current Chemistry*; Springer, Berlin, Vol. 318, 2011, pp 303–330.
- [2] C. Tschierske, *Liq. Cryst.* 45 (2018) 2221.
- [3] C. Tschierske, G. Ungar, *ChemPhysChem.* 17 (2016) 1224.
- [4] T. Sekine, T. Niori, J. Watanabe, T. Furukawa, S.-W. Choi, H. Takezoe, *J. Mater. Chem.* 7 (1997) 1307.
- [5] L.E. Hough, H.T. Jung, D. Kruerke, M.S. Heberling, M. Nakata, C.D. Jones, D. Chen, D.R. Link, J. Zasadzinski, G. Heppke, J.P. Rabe, W. Stocker, E. Koroblova, D.M. Walba, M.A. Glaser, N.A. Clark, *Science* 325 (2009) 456.
- [6] C. Zhang, N. Diorio, O.D. Lavrentovich, A. Jákli, *Nat. Commun.* 5 (2014) 3302.
- [7] K.V. Le, H. Takezoe, F. Araoka, *Adv. Mater.* 29 (2017) 1602737.
- [8] M. Alaasar, M. Prehm, M. Brautzsch, C. Tschierske, *J. Mater. Chem. C* 2 (2014) 5487.

- [9] M. Alaasar, M. Prehm, C. Tschierske, *Chem. Eur. J.* 22 (2016) 6583.
- [10] A. Lehmann, M. Alaasar, M. Poppe, S. Poppe, M. Prehm, M. Nagaraj, S.P. Sreenilayam, Y.P. Panarin, J.K. Vij, C. Tschierske, *Chem. – Eur. J.* 26 (2020) 4714.
- [11] M. Poppe, M. Alaasar, A. Lehmann, S. Poppe, M.G. Tamba, J.K. Vij, M. Kurachkina, X. Cai, F. Liu, A. Eremin, M. Nagaraj, C. Tschierske, *J. Mater. Chem. C* 8 (2020) 3316.
- [12] M. Alaasar, M. Prehm, M. Nagaraj, J.K. Vij, C. Tschierske, *Adv. Mater.* 25 (2013) 2186.
- [13] M. Alaasar, M. Prehm, S. Belau, N. Sebastián, M. Kurachkina, A. Eremin, C. Chen, F. Liu, C. Tschierske, *Chem. Eur. J.* 25 (2019) 6362.
- [14] M. Nagaraj, *Liq. Cryst.* 43 (2016) 2244.
- [15] R.J. Mandle, *Chem. Eur. J.* 23 (2017) 8771.
- [16] J.P. Abberley, R. Killah, R. Walker, J.M.D. Storey, C.T. Imrie, M. Salamończyk, C. Zhu, E. Gorecka, D. Pocięcha, *Nat. Commun.* 9 (2018) 228.
- [17] T. Kato, J. Uchida, T. Ichikawa, T. Sakamoto, *Angew. Chem. Int. Ed.* 57 (2018) 4355.
- [18] Q. Li (Ed.), *Nanoscience with Liquid Crystals*, Springer, Cham, 2014.
- [19] N. Koide (Ed.), *The Liquid Crystal Display Story*, Springer Japan, Tokyo, 2014.
- [20] C.M. Paleos, D. Tsiourvas, *Liq. Cryst.* 28 (2001) 1127.
- [21] X.-H. Cheng, H.-F. Gao, Hydrogen bonding for supramolecular liquid crystals, in: Z.-T. Li, L.-Z. Wu (Eds.), *Hydrogen Bonded Supramolecular Materials*, Lecture Notes in Chemistry, vol. 88, no. 5, 2015, pp. 133–183 (Chapter 5). <https://doi.org/10.1007/978-3-662-45780-1>.
- [22] H.K. Bisoyi, Q. Li, *Angew. Chem. Int. Ed.* 55 (2016) 2994.
- [23] D.W. Bruce, Liquid crystals formed from specific intermolecular interactions, in: P.A. Gale, J.W. Steed (Eds.), *Supramolecular Chemistry: From Molecules to Nanomaterials*, Wiley, vol. 7, 2012, pp. 3493–3514.
- [24] M. Saccone, L. Catalano, *J. Phys. Chem. B.* 123 (2019) 9281.
- [25] T. Kato, J.M.J. Frechet, *Macromolecules* 22 (1989) 3818.
- [26] S.K. Kang, E.T. Samulski, *Liq. Cryst.* 27 (2000) 371.
- [27] S.K. Kang, E.T. Samulski, P. Kang, J. Choo, *Liq. Cryst.* 27 (2000) 377.
- [28] C. Tschierske, *Angew. Chem. Int. Ed.* 52 (2013) 8828.
- [29] T. Kato, in: J.W. Goodby, P.J. Collings, T. Kato, C. Tschierske, H. Gleeson, P. Raynes, (Eds.), *Handbook of Liquid Crystals*, Wiley-VCH, Weinheim, vol. 6, Nanoparticle and Nanostructured Liquid Crystals, 2014.
- [30] R. Zhang, Z. Su, X.-Y. Yan, J. Huang, W. Shan, X.-H. Dong, X. Feng, Z. Lin, S.Z.D. Cheng, *Chem. Eur. J.* 26 (2020) 6741.
- [31] R. Walker, D. Pocięcha, J.P. Abberley, A. Martinez-Felipe, D.A. Paterson, E. Forsyth, G.B. Lawrence, P.A. Henderson, J.M.D. Storey, E. Gorecka, C.T. Imrie, *Chem. Commun.* 54 (2018) 3383.
- [32] R. Walker, D. Pocięcha, A. Martinez-Felipe, J.M.D. Storey, E. Gorecka, C.T. Imrie, *Crystals* 10 (2020) 175.
- [33] S. Bujosa, E.E. Greciano, M.A. Martínez, L. Sánchez, B. Soberats, *Chem. Eur. J.* (2021), <https://doi.org/10.1002/chem.202102446>.
- [34] G.W. Gray, B. Jones, F. Marson, *J. Chem. Soc.* (1957) 393.
- [35] Y. Yamamura, Y. Nakazawa, S. Kutsumizu, K. Saito, *Phys. Chem. Chem. Phys.* 21 (2019) 23705.
- [36] M. Imperor-Clerc, M. Veber, A.M. Levelut, *Chem. Phys. Chem.* 8/9 (2001) 533.
- [37] M. Imperor-Clerc, P. Sotta, M. Veber, *Liq. Cryst.* 27 (2000) 1001.
- [38] X. Zeng, G. Ungar, M. Imperor-Clerc, *Nat. Mater.* 4 (2005) 562.
- [39] A. Kohlmeier, D. Janietz, S. Diele, *Chem. Mater.* 18 (2006) 1483.
- [40] Y. Cao, M. Alaasar, A. Nallapaneni, M. Salamończyk, P. Marinko, E. Gorecka, C. Tschierske, F. Liu, N. Vaupotič, C. Zhu, *Phy. Rev. Lett.* 125 (2020) 027801.
- [41] T. Kato, M. Yoshio, T. Ichikawa, B. Soberats, H. Ohno, M. Funahashi, *Nat. Rev. Mater.* 2 (2017) 17001.
- [42] S. Kutsumizu, *Isr. J. Chem.* 52 (2012) 844.
- [43] O. Kwon, X. Cai, W. Qu, F. Liu, J. Szydlowska, E. Gorecka, M.J. Han, D.K. Yoon, S. Poppe, C. Tschierske, *Adv. Funct. Mater.* 31 (2021) 2102271.
- [44] M. Alaasar, A.F. Darweesh, X. Cai, F. Liu, C. Tschierske, *Chem. Eur. J.* 24 (2021) 14921.
- [45] H.T. Nguyen, C. Destrade, J. Malthe, *Adv. Mater.* 9 (1997) 375.
- [46] W. Weissflog, in: J.W. Goodby, J.P. Collings, T. Kato, C. Tschierske, H.F. Gleeson, P. Raynes (Eds.), *Handbook of Liquid Crystals*, Wiley-VCH, Weinheim, second ed., vol. 5, 2014, pp. 89–174.
- [47] C. Dressel, F. Liu, M. Prehm, X. Zeng, G. Ungar, C. Tschierske, *Angew. Chem. Int. Ed.* 53 (2014) 13115.
- [48] C. Dressel, T. Reppe, M. Prehm, M. Brautzsch, C. Tschierske, *Nat. Chem.* 6 (2014) 971.
- [49] T. Reppe, C. Dressel, S. Poppe, C. Tschierske, *Chem. Commun.* 56 (2020) 711.
- [50] C. Dressel, T. Reppe, S. Poppe, M. Prehm, X. Lu, G. Zeng, C.T. Ungar, *Adv. Funct. Mater.* 2004353 (2020).
- [51] T. Reppe, S. Poppe, X. Cai, Y. Cao, F. Liu, C. Tschierske, *Chem. Sci.* 11 (2020) 5902.
- [52] T. Reppe, S. Poppe, C. Tschierske, *Chem. Eur. J.* 26 (2020) 16066.
- [53] M. Alaasar, S. Poppe, Y. Cao, C. Chen, F. Liu, C. Zhu, C. Tschierske, *J. Mater. Chem. C* 8 (2020) 12902.
- [54] X. Zeng, G. Ungar, *J. Mater. Chem. C* 8 (2020) 5389.
- [55] H. Yu, T. Ikeda, *Adv. Mater.* 23 (2011) 2149.
- [56] Z. Mahimwalla, K.G. Yager, J.-I. Mamiya, A. Shishido, A. Priimagi, C.J. Barrett, *Polym. Bull.* 69 (2012) 967.
- [57] L. De Sio, N. Tabiryan, T. Bunning, B.R. Kimball, C. Umeton, Chapter 1 – Dynamic photonic materials based on liquid crystals, in: E. Wolf (Ed.), *Progress in Optics*, Elsevier, Amsterdam, vol. 58, 2013, pp. 1–64.
- [58] M. Alaasar, *Liq. Cryst.* 43 (2016) 2208.

- [59] M. Saccone, M. Spengler, M. Pfletscher, K. Kuntze, M. Virkki, C. Wölper, R. Gehrke, G. Jansen, P. Metrangolo, A. Priimagi, M. Giese, *Chem. Mater.* 31 (2019) 462.
- [60] M. Pfletscher, C. Wölper, J.S. Gutmann, M. Mezger, M. Giese, *Chem. Commun.* 52 (2016) 8549.
- [61] M. Alaasar, M. Prehm, Y. Cao, F. Liu, C. Tschierske, *Angew. Chem. Int. Ed.* 128 (2016) 320.
- [62] M. Alaasar, S. Poppe, Q. Dong, F. Liu, C. Tschierske, *Angew. Chem., Int. Ed.* 56 (2017) 10801.
- [63] M. Alaasar, M. Prehm, S. Belau, N. Sebastian, M. Kurachkina, A. Eremin, C. Chen, F. Liu, C. Tschierske, *Chem. Eur. J.* 25 (2019) 6362.
- [64] M. Alaasar, S. Poppe, *Liq. Cryst.* 47 (2020) 939.
- [65] J.M. Shivanna, M. Alaasar, G. Hegde, *J. Mol. Liq.* 341 (2021) 117341.
- [66] H.M.D. Bandara, S.C. Burdette, *Chem. Soc. Rev.* 2012 (1809) 41.
- [67] H.K. Bisoyi, Q. Li, *Acc. Chem. Res.* 47 (2014) 3184.
- [68] J.-I. Mamiya, K. Kanie, T. Hiyama, T. Ikeda, T. Kato, *Chem. Commun.* (2002) 1870.
- [69] Z.-G. Zheng, Y.-Q. Lu, Q. Li, *Adv. Mater.* (2020) 1905318.
- [70] H.K. Bisoyi, T.J. Bunning, Q. Li, *Adv. Mater.* 30 (2018) 1706512.
- [71] D.A. Paterson, J. Xiang, G. Singh, R. Walker, D.M. Agra-Kooijman, A. Martinez-Felipe, M. Gao, J.M.D. Storey, S. Kumar, O.D. Lavrentovich, C.T. Imrie, *J. Am. Chem. Soc.* 138 (2016) 5283.
- [72] R. Hori, Y. Miwa, K. Yamamoto, S. Kutsumizu, *J. Phys. Chem. B* 118 (2014) 3743.
- [73] A. Nagai, H. Kondo, Y. Miwa, T. Kondo, S. Kutsumizu, Y. Yamamura, K. Saito, *Bull. Chem. Soc. Jpn.* 91 (2018) 1652.
- [74] M. Alaasar, S. Poppe, Q. Dong, F. Liu, C. Tschierske, *Chem. Commun.* 52 (2016) 13869.
- [75] M. Alaasar, S. Poppe, C. Tschierske, *J. Mol. Liq.* 277 (2019) 233.
- [76] M. Alaasar, J.C. Schmidt, X. Cai, F. Liu, C. Tschierske, *J. Mol. Liq.* 332 (2021) 115870.
- [77] M. Lehmann, M. Dechant, M. Lambov, T. Ghosh, *Acc. Chem. Res.* 52 (2019) 1653.
- [78] E.J. Foster, R.B. Jones, C. Lavigueur, V.E. Williams, *J. Am. Chem. Soc.* 128 (2006) 8569.
- [79] E. Beltrán, J.L. Serrano, T. Sierra, R. Giménez, *J. Mater. Chem.* 22 (2012) 7797.
- [80] P. Staffeld, M. Kaller, S.J. Beardsworth, K. Tremel, S. Ludwigs, S. Laschat, F. Giesselmann, *J. Mater. Chem. C* 1 (2013) 892.
- [81] Y.J. Chen, H.F. Yu, L.Y. Zhang, H. Yang, Y.F. Lu, *Chem. Commun.* 50 (2014) 9647.
- [82] Y. Cao, C. Feng, A. Jakli, C. Zhu, F. Liu, *Giant* 2 (2020) 100018.
- [83] H. Chen, R. Zhang, H. Gao, H. Cheng, H. Fang, X. Cheng, *Dyes Pigments* 149 (2018) 512.
- [84] X. Peng, H. Gao, Y. Xiao, H. Cheng, F. Huang, X. Cheng, *N. J. Chem.* 2017 (2004) 41.
- [85] R. Yamakado, M. Hara, S. Nagano, T. Seki, H. Maeda, *Chem.-Eur. J.* 23 (2017) 9244.
- [86] V. Prasad, S.-W. Kang, S.K. Varshney, N.G. Nagaveni, *Liq. Cryst.* 37 (2010) 121.
- [87] N.G. Nagaveni, M. Gupta, A. Roy, V. Prasad, *J. Mater. Chem.* 20 (2010) 9089.
- [88] R. Hori, D. Furukawa, K. Yamamoto, S. Kutsumizu, *Chem. Eur. J.* 18 (2012) 7346.





# Controlling liquid and liquid crystalline network formation by core-fluorination of hydrogen bonded supramolecular polycatenars

Mohamed Alaasar<sup>a,b,\*</sup>, Jaques-Christopher Schmidt<sup>a</sup>, Xiaoqian Cai<sup>c</sup>, Feng Liu<sup>c,\*</sup>, Carsten Tschierske<sup>a,\*</sup>

<sup>a</sup> Institute of Chemistry, Martin Luther University Halle-Wittenberg, Kurt Mothes Str. 2, D-06120 Halle, Saale, Germany

<sup>b</sup> Department of Chemistry, Faculty of Science, Cairo University, Giza, Egypt

<sup>c</sup> State Key Laboratory for Mechanical Behavior of Materials, Shaanxi International Research Center for Soft Matter, Xi'an Jiaotong University, Xi'an 710049, PR China

## ARTICLE INFO

### Article history:

Received 26 January 2021

Received in revised form 3 March 2021

Accepted 5 March 2021

Available online 09 March 2021

### Keywords:

Polycatenar liquid crystals

Hydrogen bonding

Azobenzenes

Helical self-assembly

Cubic phases

Mirror symmetry breaking

Photo switching

## ABSTRACT

Photo-switchable materials with liquid crystalline (LC) properties and being capable of showing mirror-symmetry breaking are of special interest from a fundamental scientific point of view as well as for the development of  $\pi$ -conjugated materials with tailored superstructures for optical, emissive and photonic materials. Herein we report two new series of supramolecular photosensitive polycatenar (multi-chained) mesogens formed by hydrogen bonding interaction between a taper shaped triple-chain benzoic acid as the hydrogen bond-donor and fluorinated azopyridines with only a single chain as hydrogen bond-acceptors. The self-assembly of these materials was characterized by differential scanning calorimetry (DSC), polarized optical microscopy (POM) and X-ray diffraction (XRD). Depending on the position of the fluorine atom different types of LC phases were observed, including spontaneously chiral isotropic liquid (Iso<sup>h</sup>\*1) and bicontinuous cubic phases (Cub<sub>bi</sub><sup>h</sup>/I23), as well as achiral cubic (Cub<sub>bi</sub>/Ia3d) and non-cubic 3D phases with tetragonal symmetry. This report provides guidelines for the application of core fluorination at different positions as a powerful tool for controlling spontaneous helical self-assembly in supramolecular liquid and liquid crystalline materials.

© 2021 Elsevier B.V. All rights reserved.

## 1. Introduction

Supramolecular chemistry has been applied over the past decades as an effective tool for the design and synthesis of functional materials [1–9], among them the technologically important liquid crystals (LCs) [10–12]. Numerous rod-like and several disc-like supramolecular LCs with lamellar and columnar phases, respectively, have been designed by non-covalent interactions, either hydrogen or halogen-bonding [13–17]. The main advantage of LC systems constructed via intermolecular interaction compared to those designed by conventional chemical synthesis methods is the easily accessible synthetic pathways of the complementary components, which might be in most cases non-mesomorphic and upon mixing them together new LCs are obtained. The role of hydrogen bonding in inducing LCs phases has been early recognized for the dimers of 4-alkyl(oxy)benzoic acids, cyclohexane carboxylic acids and the heterodimeric benzoic acid pyridine complexes [18–20]. More recently it was also used to design LC materials with complex superstructures [21–25], among them different kind of LC network phases, as for example, honeycombs, liquid organic frameworks and bicontinuous cubic phases [26–30].

Bicontinuous cubic (Cub<sub>bi</sub>) phases are known as optically isotropic LC phases with cubic 3D lattice, representing interwoven networks of branched columns (Fig. 1a–c) and occurring at the transition between lamellar and columnar self-assembly [31–34]. The first examples of bicontinuous cubic phases formed through intermolecular hydrogen bonding were reported for the dimers of 4'-*n*-alkoxy-3'-nitrobiphenyl-4-carboxylic acids (ANBCs) [34–36], and later for their mixtures with 3,5-dialkoxybenzoic acids [37–39], for 2,4-diaminotriazines [40] and supramolecular rod-like systems of 4,4'-bipyridine and benzoic acids with silylated or semiperfluorinated segments attached to their alkyl chains [41–43]. Formation of Cub<sub>bi</sub> phases by self-assembly via cooperative hydrogen bonding networks were reported for multi chain diols [44–45], and carbohydrate based amphiphiles [46–48]. Another class of hydrogen-bonded systems, leading to a wide variety of Cub<sub>bi</sub> phases by supramolecular network formation, also including new types of Cub<sub>bi</sub> phases, such as single network phases and diamond lattices, is provided by T-, Π- and X-shaped bolopolyphiles with H-bonding glycerol groups at both ends [27–30]. Cub<sub>bi</sub> phases are very useful for applications requiring fast charge transport due to their 3D network structures [49]. In addition, the Cub<sub>bi</sub> phases are often accompanied by birefringent LC phases with deformed cubic lattice, leading to 3D tetragonal (Tet) and orthorhombic symmetry, often as metastable phases in narrow ranges besides the Cub<sub>bi</sub> phases [50–56]. Their structures and the reasons for their formation are presently not well understood [52,57–60], and

\* Corresponding author at: Institute of Chemistry, Martin Luther University Halle-Wittenberg, Kurt Mothes Str. 2, D-06120 Halle, Saale, Germany.

E-mail address: [mohamed.alaasar@chemie.uni-halle.de](mailto:mohamed.alaasar@chemie.uni-halle.de) (M. Alaasar).

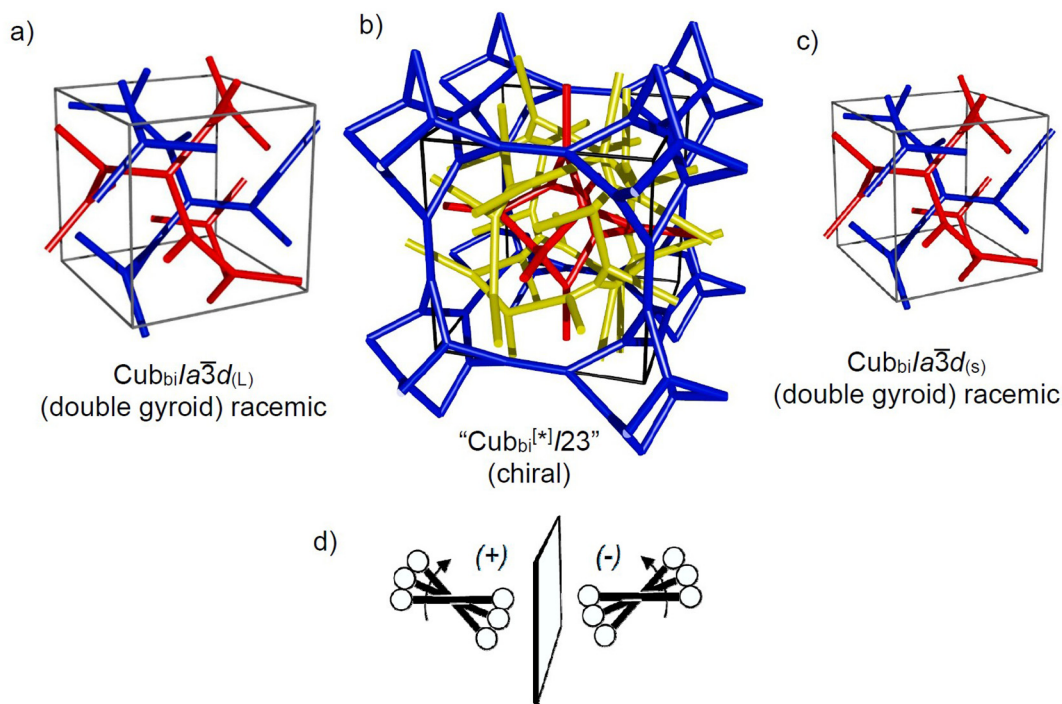


**Fig. 1.** a-c) The three presently known network structures with cubic symmetry formed by rod-like compounds a, c) the double network with  $Ia\bar{3}d$  space group (the double gyroid) and b) the triple network of the mirror symmetry broken  $I23$  phase, the two networks (blue and red) in a) are enantiomorphic, in b) the red and blue networks are identical, but different from the yellow one; in the networks the orientation of the rod-like core is perpendicular to the local network direction; d) shows the development of the helical twist by the clashing of end groups attached to rod-like cores in the networks; from a) to c) the twist between the molecules along the network increases, leading to a transition from the long pitch (Low twist) gyroid ( $Ia\bar{3}d_{(L)}$ ) via the  $I23$  lattice to the short pitch (high twist)  $Ia\bar{3}d_{(S)}$  phase. a-c) Reprinted with permission from ref. [109].

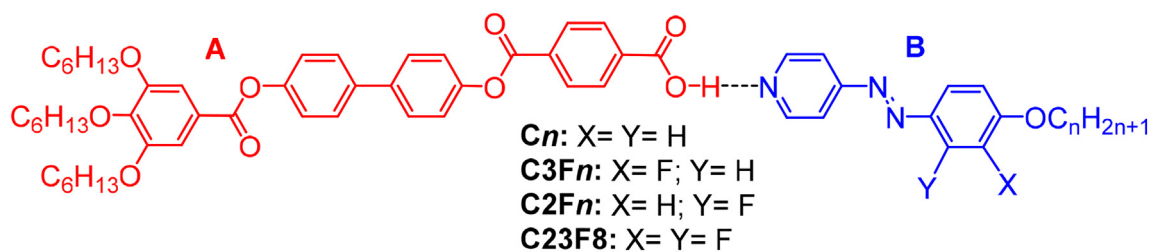
therefore new systems with broader and stable ranges of these more complex 3D phases are required.

Fluorination is a powerful tool for the design of new LCs with unusual and practically important properties [61–65]. The specific effects of F in organic molecules result from a unique combination of high polarity and low polarizability, as well as steric and conformational effects. In previous work chain fluorination was used for the introduction of cubic phases due to nano-segregation and bulkiness [66–69]. It was also shown that aromatic core fluorination removes  $Cub_{bi}$  phases of polycatenar mesogens, (rod-like molecules with more than only two terminal chains) [70,71]. However, our recent work indicated that fluorination at the periphery of such polycatenar molecules can retain  $Cub_{bi}$  phases [72,73]. Herein the effect of aromatic core fluorination on cubic self-assembly in supramolecular H-bonded polycatenar complexes is studied.

Spontaneous mirror symmetry breaking is an interesting topic from both, a general scientific and chemistry point of view, as well as for applications in functional materials [74–76]. Mirror symmetry breaking, often indicated by chiral conglomerate formation, was observed in different mesophases of bent molecules [77–100]. However, the focus herein is on mirror symmetry breaking in  $Cub_{bi}$  phases ( $Cub_{bi}/I23^{l^*}$ ) [101] and isotropic liquids ( $Iso^{l^*}$ ) [102] of non-bent polycatenar systems [70,76,103–105]. A sequence of three  $Cub_{bi}$  phases was often observed with growing alkyl chain length in the sequence  $Ia\bar{3}d-Im\bar{3}m-Ia\bar{3}d$  (Fig. 1a-c). [34,36,72,106–108]. Recent investigations have discovered that  $Cub_{bi}$  phases with  $Im\bar{3}m$  symmetry exhibit spontaneous mirror symmetry breaking and optical activity [101]. Therefore, the actual space group is  $I23$  [109], and new models of their phase structure were postulated [110,111], among them the triple network with exclusively three-way junctions shown in Fig. 1b. In these fluid networks

formed by polycatenar systems the helicity, and hence, the chirality results from the arrangement of the molecules more or less perpendicular to the networks, leading to a mismatch between core diameter and alkyl chain volume, thus providing a helical twist (see Fig. 1d). The fluid network structure allows a synchronization and transmission of chirality within the network over macroscopic distances by removing helix inversion defects. The gyroid ( $Ia\bar{3}d$ ) type double network structure is achiral, because the helix sense is opposite in the two enantiomorphic networks which cancel each other (Fig. 1a, c). In contrast, in the  $I23$  phase composed of three networks (Fig. 1b) this cannot happen and this leads to local mirror symmetry breaking with conglomerate formation [101]. However, occasionally also global mirror symmetry breaking and development of a preferred or even uniform chirality can be observed [105].

Light-responsive LCs, achieved by incorporation of a photo switchable chromophore such as an azobenzene unit in the molecular structure, have great potential for tuneable photonics and photomechanics [112–121]. This is due to the fast and reversible shape changes of the azobenzene units due to the *trans-cis* photoisomerization upon light irradiation. Photoisomerizable helical LC phases are of special interest as a result of the possibility of manipulating chiroptical properties by light, which can be exploited for optical, optoelectronic and sensing devices [122–127]. Switching between lamellar and cubic phases by photoisomerization of mixtures of cubic phase forming materials with an azobenzene based dopant was reported by Kutsumizu et al. [128,129]. Recently we have reported the first examples of photoresponsive hydrogen-bonded [104] as well as halogen-bonded supramolecular polycatenar LCs [130]. The hydrogen-bonded polycatenars **Cn** (see Scheme 1) exhibit dynamic mirror-symmetry breaking by chirality synchronization in isotropic liquid ( $Iso^{l^*}$ ) as well as in  $Cub_{bi}$  phases with  $I23$  symmetry [109].



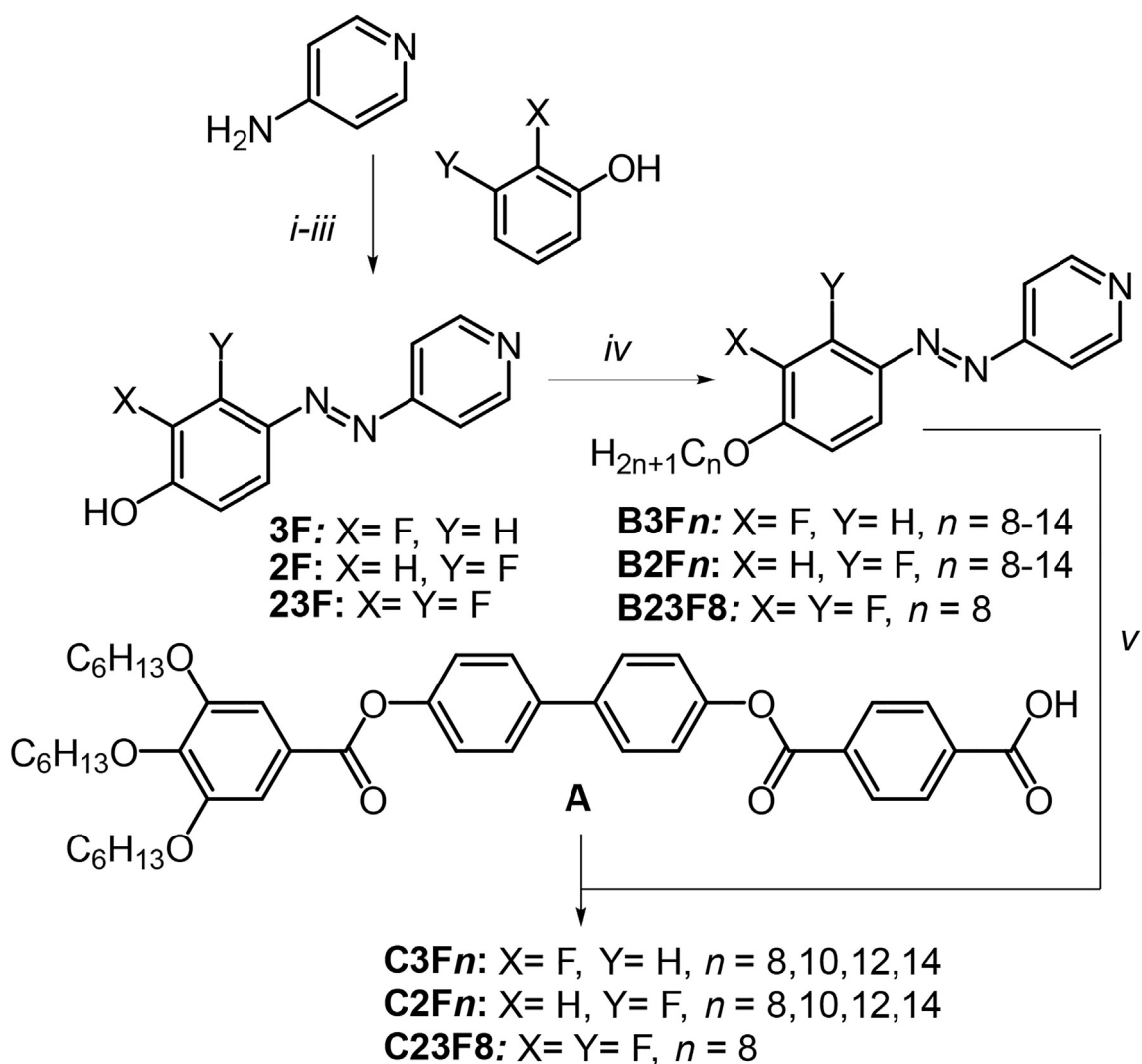
**Scheme 1.** Chemical structures for the previously reported non-fluorinated (**C<sub>n</sub>**) and the fluorinated supramolecular LCs (**C3F<sub>n</sub>**, **C2F<sub>n</sub>** and **C23F8**) reported herein.

Herein, we report the effect of core fluorination on these supramolecular LC polycatenars, constructed by hydrogen-bonding interaction between a taper-shaped triple chain benzoic acid derivative (**A**) and three different types of fluorinated azopyridine derivatives (**B3F<sub>n</sub>**, **B2F<sub>n</sub>** and **B23F8**, see **Scheme 1**). These hydrogen-bonded aggregates show a series of chiral and achiral Cub<sub>b</sub> phases, tetragonal phases and mirror-symmetry broken isotropic liquids, depending on the position of the fluorine atom(s) and the alkyl chain length (*n*).

## 2. Experimental

### 2.1. Synthesis

The synthesis of the azopyridines **B** [104] and the preparation of the H-bonded supramolecules with the benzoic acid derivative **A** [131] is shown in **Scheme 2** and described in detail in the SI. The fluorinated azopyridine derivatives **B3F<sub>n</sub>**, **B2F<sub>n</sub>** were synthesized as previously



**Scheme 2.** Synthesis of the azopyridines (**B3F<sub>n</sub>**, **B2F<sub>n</sub>** and **B23F8**) and the hydrogen-bonded supramolecules (**C3F<sub>n</sub>**, **C2F<sub>n</sub>**, **C23F8**); Reagents and Conditions: i: NaNO<sub>2</sub>, HCl, H<sub>2</sub>O, 0 °C, 30 min.; ii: phenol, NaOH, -5 °C, 1 h; iii: NaHCO<sub>3</sub>, 0 °C, 1 h; iv: BrC<sub>n</sub>H<sub>2n+1</sub>, K<sub>2</sub>CO<sub>3</sub>, KI, DMF, 80 °C, 18 h; v: repeated melting with stirring.

reported [104], while that of **B23F8** was done in a similar manner but starting from 2,3-difluorophenol. The supramolecular polycatenars (**C**) were obtained by mixing equimolar amounts of each of the azopyridine derivatives (**B**) and the benzoic acid derivative **A** and melting them together in a DSC pan with stirring to give an intimate blend (**A** + **B** = **C**). After cooling to room temperature, the formed material was then melted, and the previous process was repeated twice (see SI for more details).

## 2.2. Characterization

The formation of the hydrogen-bonded complexes between the acid **A** and each of the azopyridine derivatives **B** in the LC and crystalline states was investigated by differential scanning calorimetry (DSC), polarized optical microscopy (POM) and small- and wide-angle X-ray scattering (SAXS and WAXS) with the equipment described in the SI and as discussed below. The phase transitions of all complexes **C** are collated in Table 1, whereas Table 2 summarizes the supramolecular volumina [132], lattice parameters and the structural data of the investigated mesophases.

## 3. Results and discussion

### 3.1. IR Studies of complex formation

To confirm the formation of the intermolecular hydrogen bond we performed FTIR investigations [130–136] for the supramolecular complex **C3F10** and its complementary components **A** and **B3F10**. As shown in Fig. 2 the acid **A** has two carbonyl bands one at  $\sim 1692\text{ cm}^{-1}$  and the other at  $\sim 1731\text{ cm}^{-1}$  (Fig. 2; red curve). The first one corresponds to the carbonyl of the carboxylic group involved in an intermolecular hydrogen bond between the free carboxylic acid groups leading to the presence of the acid **A** in a dimeric form. After complexation the intermolecular hydrogen bond between the acid molecules is replaced by another intermolecular hydrogen bond between the acid **A** and the pyridine-based component **B3F10** which results in a blue shift of the carbonyl band from  $1692\text{ cm}^{-1}$  to  $\sim 1695\text{ cm}^{-1}$  (Fig. 2; black curve). The other carbonyl band observed at  $\sim 1731\text{ cm}^{-1}$ , which corresponds to the ester carbonyl in **A** is also blue shifted upon complex formation and appears at  $\sim 1734\text{ cm}^{-1}$ .

The most sensitive band for the azopyridine-derivative **B3F10** is the C–C stretching vibration in the pyridine ring occurring at  $\sim 1585\text{ cm}^{-1}$  (Fig. 2; blue curve), which upon complexation with the acid **A** is also blue shifted to  $\sim 1587\text{ cm}^{-1}$  (Fig. 2; black curve). These results together with the DSC and XRD investigations, as will be discussed below confirm the intermolecular hydrogen bond formation between the acid **A** and each of the pyridine-based derivatives.

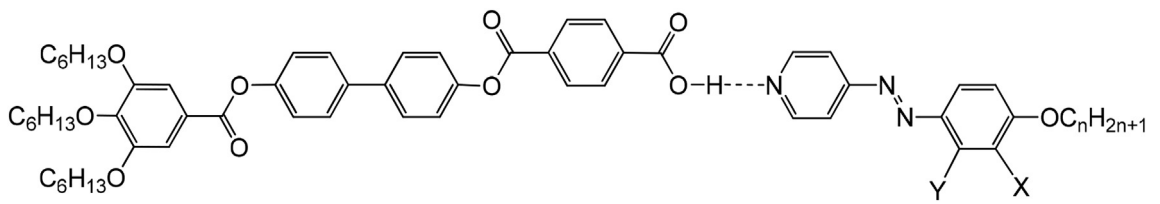
### 3.2. Self-assembly and LC phase behaviour of the systems **A**, **B** and **A** + **B** = **C**

The pyridine-based derivatives **B** melt directly into the isotropic liquid on heating from the crystalline state and on cooling they do not show any mesophase (see Table S1). The benzoic acid **A** i.e. the hydrogen bond donor is a LC exhibiting a hexagonal columnar LC phase ( $\text{Col}_{\text{hex}}$ ,  $a_{\text{hex}} = 5.4\text{ nm}$ ) between 162 and  $246\text{ }^{\circ}\text{C}$  [104]. The formation of a  $\text{Col}_{\text{hex}}$  phase is typical for hexacatenar molecules and supramolecules [70]. The acid **A** forms a hexacatenar dimer with a length of  $L_{2A} = 6.6\text{ nm}$  as a result of the intermolecular hydrogen bond formation between the free carboxylic groups [104]. These dimers form rafts of 5.2 molecules in the cross-section, stacking into columns (Table 2). Upon mixing with the complementary pyridines **B**, having only one chain, the interface curvature is reduced, and different phase sequences of cubic and non-cubic network phases are observed for all resulting complexes **C**, depending on the position of the fluorine substituent (see Table 1).

The transition temperatures of the hydrogen-bonded aggregates **C** are collected in Table 1 and the phase transitions on cooling are represented graphically in Fig. 3. As shown in Table 1, the transition temperatures of the 1:1 complexes **A** + **B** = **C** are very distinct from the individual components and there is no DSC peak at the transition temperatures of the hydrogen-bond donor **A** [104] or the pyridine-based derivatives **B** in the DSC heating and cooling runs measured for the supramolecular complexes (Fig. 4a). This confirms the complete complex formation between the complementary components.

Moreover, the formation of the hydrogen-bonded complexes leads to the suppression of the  $\text{Col}_{\text{hex}}$  phase of the pure benzoic acid **A** and induction of other types of mesophases. This indicates that an intermolecular hydrogen-bonding between the free carboxylic group in **A** and each of the pyridine-based derivatives **B** develops with formation of

**Table 1**  
Phase transition temperatures ( $T/^{\circ}\text{C}$ ), mesophase types, and transition enthalpies [ $\Delta H/k$ ]  $\text{mol}^{-1}$ ] of the supramolecular complexes **C3Fn**, **C2Fn** and **C23F8**.<sup>a</sup>



Complex	n	X	Y	Heating	Cooling
<b>C8</b> <sup>[104]</sup>	8	H	H	Cr 124 [29.4] $\text{Cub}_{\text{bi}}^*/Ia3d$ 187 [0.1] $\text{Cub}_{\text{bi}}^{*1}/I23$ 196 [0.1] $\text{Iso}^{*1}$ 200 [0.1]	Iso 190 [−0.1] $\text{Iso}^{*1}$ 183 [−0.1] $\text{Cub}_{\text{bi}}^*/I23$ 75 [−23.1] $\text{Cr}^{*1}$
<b>C3F8</b>	8	F	H	Cr 92 [31.5] $\text{Cub}_{\text{bi}}^*/I23$ 195 [−] Iso	Iso 180 [−] $\text{Cub}_{\text{bi}}^*/I23$ 57 [−35.3] Cr
<b>C3F10</b>	10	F	H	Cr 99 [44.1] $\text{Cub}_{\text{bi}}^*/I23$ 185 [−] $\text{Cub}_{\text{bi}}^*/Ia3d$ 195 [−] Iso	Iso 185 [−] $\text{Cub}_{\text{bi}}^*/Ia3d$ 180 [−] $\text{Cub}_{\text{bi}}^*/I23$ 51 [−22.5] Cr
<b>C3F12</b>	12	F	H	Cr 101 [40.5] $\text{Cub}_{\text{bi}}^*/I23$ 185 [0.2] $\text{Cub}_{\text{bi}}^*/Ia3d$ 196 [−] Iso	Iso 188 [−] $\text{Cub}_{\text{bi}}^*/Ia3d$ 152 [−0.7] Tet 59 [−30.1] Cr
<b>C3F14</b>	14	F	H	Cr 77 [53.6] $\text{Cub}_{\text{bi}}^*/I23$ 170 [−] $\text{Cub}_{\text{bi}}^*/Ia3d$ 200 [−] Iso	Iso 195 [−] $\text{Col}_{\text{hex}}$ 190 [−] $\text{Cub}_{\text{bi}}^*/Ia3d$ 156 [−0.5] Tet 80 [−] $\text{Cub}_{\text{bi}}^*/I23$ 33 [−32.1] Cr
<b>C2F8</b>	8	H	F	Cr 102 [53.9] $\text{Cub}_{\text{bi}}^*/I23$ 180 [−] $\text{Iso}^{*1}$ 185 [−] Iso	Iso 183 [−] $\text{Iso}^{*1}$ 179 [−] $\text{Cub}_{\text{bi}}^*/I23$ 132 [−] Tet 67 [−29.6] Cr
<b>C2F10</b>	10	H	F	Cr 113 [23.5] $\text{Cub}_{\text{bi}}^*/I23$ 175 [0.5] Iso	Iso 158 [−] $\text{Cub}_{\text{bi}}^*/I23$ 137 [−] Tet 75 [−41.0] Cr
<b>C2F12</b>	12	H	F	Cr 111 [58.5] $\text{Cub}_{\text{bi}}^*/I23$ 172 [0.5] Iso	Iso 159 [−] $\text{Cub}_{\text{bi}}^*/I23$ 71 [−49.4] Cr
<b>C2F14</b>	14	H	F	Cr 84 [38.2] $\text{Cub}_{\text{bi}}^*/I23$ 161 [−] Iso	Iso 159 [−0.9] $\text{Cub}_{\text{bi}}^*/I23$ 60 [−4.5] Cr
<b>C23F8</b>	8	F	F	Cr 81 [40.6] $\text{Cub}_{\text{bi}}^*/I23$ 160 [−] Iso	Iso 158 [−0.3] $\text{Cub}_{\text{bi}}^*/I23$ 43 [−19.0] Cr

<sup>a</sup> Peak temperatures as determined from 2nd heating and 2nd cooling DSC scans with rate  $10\text{ K min}^{-1}$ ; abbreviations: Cr = crystalline solid;  $\text{Cub}_{\text{bi}}^*/Ia3d$  = achiral cubic phase with  $Ia3d$  lattice;  $\text{Cub}_{\text{bi}}^*/I23$  = chiral cubic phase with  $I23$  lattice, forming a chiral conglomerate;  $\text{Col}_{\text{hex}}$  = hexagonal columnar phase;  $\text{Iso}^{*1}$  = chiral isotropic conglomerate liquid; Iso = achiral isotropic liquid.

**Table 2**  
Structural data of the mesophases of the investigated compounds and complexes.<sup>a</sup>

Compd.	Phase	a/nm	V <sub>cell</sub> /nm <sup>3</sup>	V <sub>comp</sub> /nm <sup>3</sup>	n <sub>cell</sub>	d <sub>net</sub> /nm	L <sub>net</sub> /nm	n <sub>raft</sub>	ϕ/°
<b>A</b>	Col <sub>hex</sub>	5.4	11.37	1.973	5.2	–	–	5.2	–
	Ia3d	13.1	2248	1.432	1402	5.67	111	5.68	6.84
	I23	19.53	7449	1.432	4645	8.46	404	5.17	7.15
<b>C3F8</b>	I23	18.93	6783	1.438	4212	8.19	391	4.84	7.37
	Ia3d	12.06	1754	1.487	1053	5.22	102	4.65	7.11
<b>C3F10</b>	I23	18.66	6497	1.487	3902	8.08	386	4.55	7.48
	Ia3d	12.03	1741	1.536	1012	5.21	102	4.46	7.29
<b>C3F12</b>	I23	18.59	6424	1.536	3735	8.05	384	4.37	7.52
	Tet	a = 21.49	8782	1.536	5717	–	–	–	–
		c = 18.66							
<b>C3F14</b>	Col <sub>hex</sub>	5.47	11.66	1.585	6.6	–	–	6.6	–
	Ia3d	12.01	1732	1.585	976	5.20	102	4.31	7.46
	I23	18.58	6414	1.585	3614	8.04	384	4.23	7.51
	Tet	a = 16.36	4692	1.585	2960	–	–	–	–
		c = 17.53							
<b>C2F8</b>	I23	19.62	7553	1.438	4690	8.49	406	5.20	7.12
	Tet	a = 23.0	8533	1.438	5941	–	–	–	–
		c = 16.15							
<b>C2F12</b>	I23	19.53	7449	1.536	4330	8.46	404	4.83	7.15
<b>C2F14</b>	I23	19.61	7541	1.585	4249	8.49	406	4.71	7.12

<sup>a</sup> Abbreviations: n<sub>cell</sub> number of 1:1 complexes **A**<sub>2</sub> or **C** in a unit cell; V<sub>cell</sub> = a<sup>3</sup> = volume of the unit cell; for the tetragonal phases V<sub>cell</sub> = a<sup>2</sup> × c, for columnar phases a height h of 0.45 nm is assumed; V<sub>cell</sub> = h(√3a<sub>hex</sub><sup>2</sup>/2); V<sub>mol</sub> = volume of the 1:1 complex as calculated with the crystal volume increments of Immirzi [132], n<sub>cell</sub> = number of complexes per unit cell, calculated according to 0.893 V<sub>cell</sub>/V<sub>mol</sub>, where the factor 0.893 is a correction for the different packing density in the crystalline and the LC state; d<sub>net</sub> = lateral distance between the nets in the Ia3d phase, calculated according to: d<sub>net</sub> = √3(a<sub>cub</sub>/4); L<sub>net</sub> = total length of the networks per unit cell (L<sub>net</sub> = 8.485d<sub>Ia3d</sub> and L<sub>net</sub> = 20.68d<sub>I23</sub>, respectively [109]); n<sub>raft</sub> = number of 1:1 complexes organized in each 0.45 nm tick raft of the networks or columns, calculated according to n<sub>raft</sub> = n<sub>cell</sub>/(L<sub>net</sub>/0.45); for Col<sub>hex</sub>: n<sub>raft</sub> = n<sub>cell</sub>; ϕ = twist angle between adjacent supramolecules (or rafts of supramolecules) in the networks of the Ia3d-phases; ϕ(Ia3d) = 70.5°/[0.354a<sub>cub</sub>/0.45 nm], ϕ(I23) = 90°/[0.290a<sub>cub</sub>/0.45 nm]; [109] for XRD data, see Tables S2-S15.

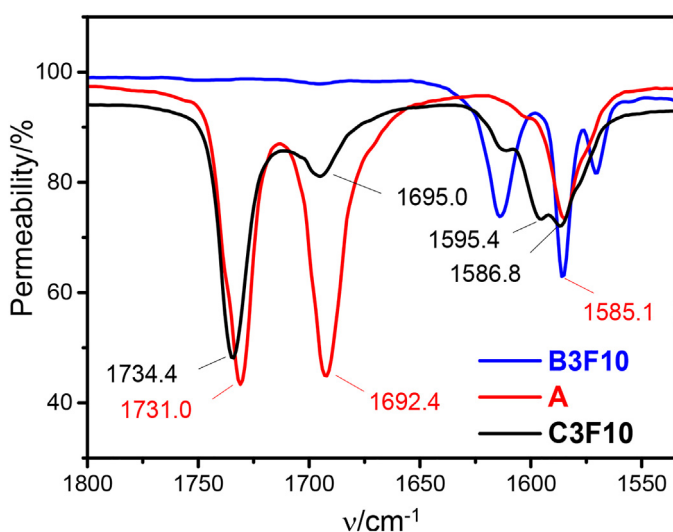


**Fig. 2.** An enlarged area between 1535 cm<sup>-1</sup> and 1800 cm<sup>-1</sup> of FTIR spectra of the supramolecular aggregate **C3F10** (black) and its complementary components **A** (red) and **B3F10** (blue).

the non-symmetric tetracatenar hydrogen bonded complexes **C3Fn**, **C2Fn** and **C23F8**, having three hexyloxy chains at one terminus of the aromatic core and only one alkoxy chain at the other terminus. This mode of the distribution of the terminal chains (3/1) is known to induce Cub<sub>bi</sub> phases as well as mirror symmetry broken isotropic liquids (Iso<sub>bi</sub><sup>\*</sup>) [101,104,117,119].

Though, the phase transitions can be observed optically and monitored by XRD, there are no DSC peaks for most of the phase transitions between the liquid and LC phases. Only the melting and crystallization of the samples are clearly visible in the DSC traces (see Fig. 4). The reasons are that the enthalpy values are small, and all phase transitions involving LC phases with 3D lattice are slow, so that these transitions are

broad. It must also be considered that the complexes **C** are in thermodynamic equilibrium with the two components **A** and **B** and therefore do not represent single component systems composed of only one well defined supramolecular species, but equilibrium mixtures of three components [131]. In the temperature range of the birefringent mesophases, as well as in the cubic ranges, the WAXS is completely diffuse with a maximum around 0.45 nm which confirms LC phases without fixed positions of the individual molecules for all investigated mesophases (Figs. S1 and S2).

### 3.3. Supramolecular polycatenars **C3Fn** with peripheral fluorination

The supramolecular polycatenars **C3Fn**, formed between the acid **A** and the 4-(3-fluoro-4-alkoxyphenylazo)pyridines **B3Fn**, having one fluorine substituent in ortho position with respect to the terminal alkoxy chain, exhibit four different types of LC phases with 3D lattice (Table 1 and Fig. 3, top rows). On heating from the birefringent crystalline solid all complexes **C3Fn** transform into a highly viscous and optically isotropic mesophase which becomes fluid at the phase transition around 195–200 °C (Table 1). For all complexes **C3Fn** a conglomerate of chiral domains is observed between not fully crossed polarizers (see for example Fig. 5). This type of mirror symmetry broken cubic phase, assigned with [1\*], referring to its spontaneous chirality (Cub<sub>bi</sub><sup>\*</sup>) [101]), has the space group I23 [109], as confirmed by XRD (see below).

Only for the shortest homologue **C3F8** the chiral Cub<sub>bi</sub><sup>\*</sup>/I23 phase with a<sub>cub</sub> = 18.93 nm (see Fig. 5, Table S4, Fig. S3a) is observed as the only mesophase, whereas for the longer homologues a wider diversity of different LC phases is observed. For example, on heating the Cub<sub>bi</sub><sup>\*</sup>/I23 phase of complex **C3F10** the mesophase remains highly viscous and optically isotropic, but the conglomerate texture disappears at ~185 °C, meaning that the cubic phase becomes achiral and therefore it is likely that the high temperature Cub<sub>bi</sub> phase has an achiral Ia3d lattice. On cooling the transition from Cub<sub>bi</sub>/Ia3d to Cub<sub>bi</sub><sup>\*</sup>/I23 takes place at 180 °C (Tables 1 and 2). The same phase sequence Cub<sub>bi</sub><sup>\*</sup>/I23-Cub<sub>bi</sub>/Ia3d on heating is observed for all following homologous complexes **C3Fn**.

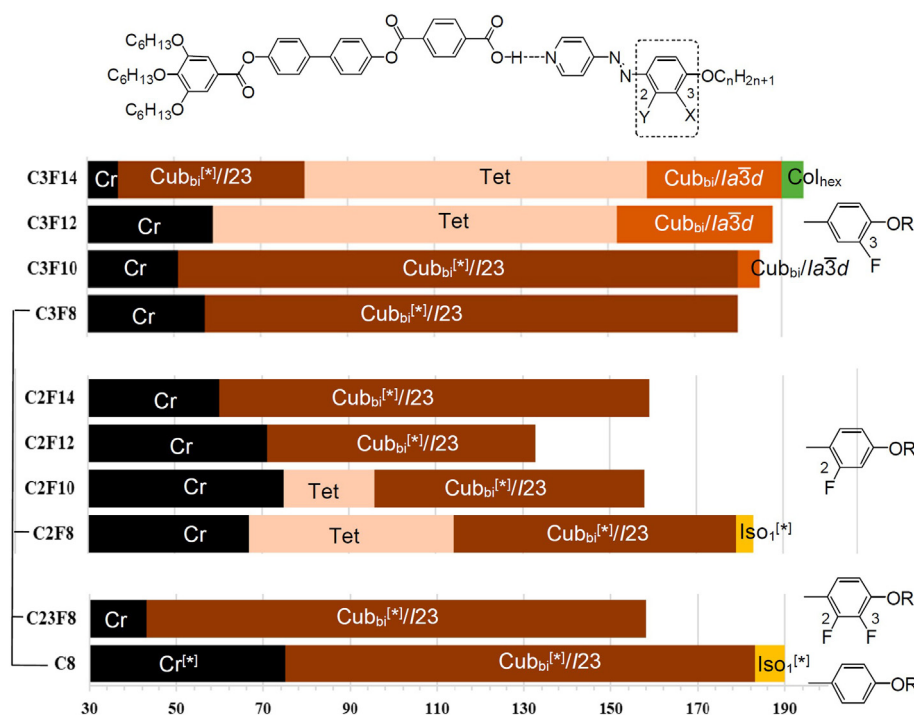


**Fig. 3.** Phase transitions of the fluorinated H-bonded supramolecules (**C2Fn**, **C3Fn**) and a previously reported nonfluorinated supramolecule (**C8**) as observed by DSC on cooling with  $10 \text{ K min}^{-1}$ ; for numerical data, see Table 1.

In order to confirm the cubic phase types, complex **C3F10** was further investigated by X-ray diffraction with a synchrotron source (Fig. 6a, b). For the high temperature achiral  $\text{Cub}_{\text{bi}}$  phase two intense peaks are observed which were indexed to the (211) and (220) reflections of a  $la3d$  lattice with a cubic lattice parameter of  $a_{\text{cub}} = 12.06 \text{ nm}$  (Fig. 6b) corresponding to the double gyroid cubic phase [51,59,104]. Also the additional much smaller scatterings at higher  $\theta$ -angles fit with the  $la3d$  space group (Table S6 and Fig. 6b). In the chiral low temperature cubic phase the highest peaks can be indexed as (321) and (400) reflections of a  $I23$  lattice (Fig. 6a) [59,104]. In this case all additional reflections can be indexed to the  $I23$  lattice (see Table S5) too. In this cubic phase the lattice parameter of  $a_{\text{cub}} = 18.66 \text{ nm}$  is about 55% larger than that in the  $la3d$  lattice, being in line with a transition from a double network to a triple network  $\text{Cub}_{\text{bi}}$  phase upon lowering temperature (Fig. 1c  $\rightarrow$  b) [72,109]. The reconstructed electron density maps obtained from the diffraction patterns confirm the proposed phase structures and show the triple-network structure of the  $I23$  and the double network structure of the  $la3d$  phase (Fig. 6c, d).

The next longer hydrogen bonded complex **C3F12** shows the same phase sequence  $\text{Cub}_{\text{bi}}^{\text{I}^*}/I23$ - $\text{Cub}_{\text{bi}}/la3d$  on heating (for XRD data, see Tables 2, S7, S8 and Figs. S3b, S4a), but the chiral triple network  $\text{Cub}_{\text{bi}}^{\text{I}^*}/I23$  phase is completely removed in the cooling cycle and only the achiral double network  $\text{Cub}_{\text{bi}}/la3d$  at high temperature and a birefringent 3D phase (Tet) at lower temperature (see Table 1, Fig. 3), were observed. Thus, for the longest supramolecule **C3F14** a phase sequence involving even four different LC phases is observed (Figs. 7, 8 and Tables S9-S12). On cooling **C3F14** from the isotropic liquid a direct transition to a birefringent LC phase occurs at  $\sim 195 \text{ }^\circ\text{C}$  (see Fig. 7a), which, based on the XRD investigations, is assigned as a hexagonal columnar phase ( $\text{Col}_{\text{hex}}$  with  $a_{\text{hex}} = 5.47 \text{ nm}$ , see Fig. 8a and Table 2). The formation of a columnar phase for the complexes with longest chains at highest temperature indicates that alkyl chain expansion increases the aromatic-aliphatic interface curvature to such a degree that this complex is at the transition from the bicontinuous network structures to the columnar phases composed of non-branched columns. The distance between the columns in the  $\text{Col}_{\text{hex}}$  phase (5.47 nm) is close

to the lateral distance between the networks in the adjacent  $\text{Cub}_{\text{bi}}/la3d$  phase, calculated according to  $d_{\text{net}} = \sqrt{3}(a_{\text{cub}}/4) = 5.2 \text{ nm}$  (Table 2). The length of the hydrogen bonded dimers **C3F14** is  $L_{\text{mol}} = 6.34 \text{ nm}$  in the stretched conformation with predominately *all-trans*-alkyl chains (Fig. 7e). The length of the individual components **A** and **B3F14** is 3.3 and 3.1 nm, respectively. Thus, the measured lattice parameters confirm the aggregate formation by hydrogen bonding and the reduction of the actual distances compared to the supramolecular length is mainly due to conformational disorder required to fill the curved spaces. Below  $\sim 190 \text{ }^\circ\text{C}$  the  $\text{Col}_{\text{hex}}$  phase is replaced by the optically isotropic and achiral  $\text{Cub}_{\text{bi}}/la3d$  phase (see Fig. 7b for the  $\text{Col}_{\text{hex}}$ - $\text{Cub}_{\text{bi}}$  transition), which is followed by the birefringent Tet phase and then replaced by the optically isotropic and mirror symmetry broken  $\text{Cub}_{\text{bi}}^{\text{I}^*}/I23$  phase (Fig. 7c, d). Thus, for this remarkable system the development from  $\text{Col}_{\text{hex}}$  via the double gyroid network and a birefringent 3D phase to the triple network is observed.

In the birefringent 3D phase range of **C3F14** the small angle XRD pattern shows several sharp reflections (Fig. 8b) which could be indexed to a 3D tetragonal lattice with lattice parameters  $a = 16.36 \text{ nm}$  and  $c = 17.53 \text{ nm}$ . These values are close to  $a_{\text{cub}}$  of the adjacent  $\text{Cub}_{\text{bi}}^{\text{I}^*}/I23$  phase ( $a_{\text{cub}} = 18.58 \text{ nm}$ ). This suggests that the birefringent Tet phases are likely to represent distorted versions of the triple network  $I23$  phase with different modes of deformation of the cubic lattice. In the case of **C3F14** all sides of the cube become shorter and the shrinkage is slightly different in one of the directions. As shown in Table 2 the number of molecules in the rafts of the columns of the  $\text{Col}_{\text{hex}}$  phase of **C3F14** is 6.6 and it decreases to 4.2–4.3 in the networks of the cubic phases. In the  $\text{Cub}_{\text{bi}}$  phases this number increases with decreasing alkyl chain length  $n$  (from  $n_{\text{raft}} = 4.2$  to 5.7, Table 2). The number of molecules per unit cell rises from 976 in the double network  $la3d$  phase via 2960 in the tetragonal phase to 3614 in the triple network  $I23$  phase of **C3F14**. This confirms that in this case the tetragonal phase represents a kind of intermediate structure at the  $la3d$ - $I23$  transition. If at this transition the chirality and conglomerate structure are retained or if the birefringent phase is achiral cannot be decided with certainty, because the linear birefringence is much larger than the effects of optical rotation.

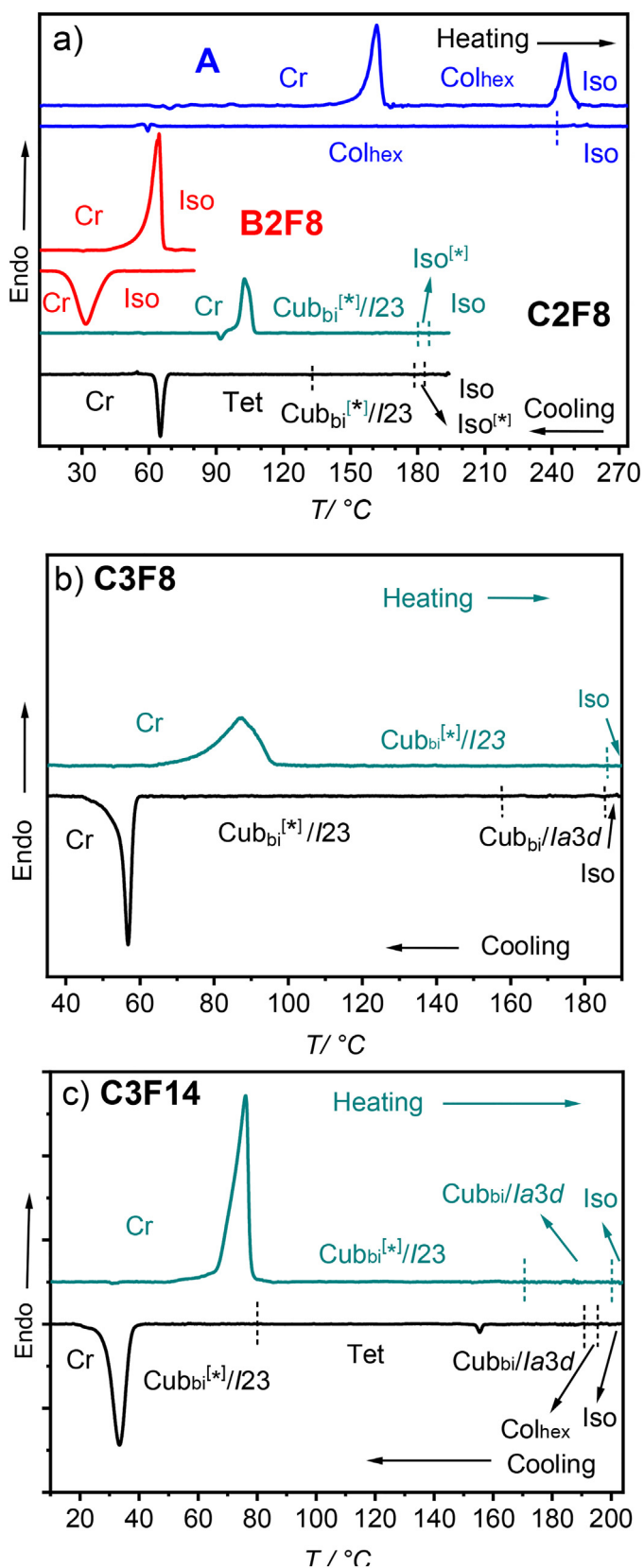


**Fig. 4.** DSC heating and cooling curves ( $10 \text{ K min}^{-1}$ ) for: a) **C2F8** and its individual components the acid **A** (blue curves) and the pyridine based derivative **B2F8** (red curves), b) **C3F8** and c) **C3F14**.

Assuming that the helix structure is maintained in the Tet phase, it can be considered as an additional solution for the problem of retaining a resonance between helical pitch length and junction distance required

by geometrical (space filling) factors, and in addition, to optimize lateral (side-by-side) helix-helix interactions with correct angles and distances between adjacent networks [107,108]. That the lattice parameters  $a$  and  $c$  of the Tet phase of the shorter complex **C3F12** are larger than for the longer complex **C3F14** (Table 2) would indicate a stronger twist (shorter pitch) for **C3F14**, which is in line with the general effects of alkyl chain length and chain volume on the lattice parameters observed in the helical network phases. Interestingly, the tetragonal phases appear to be much more sensitive to this chain length effect than the  $\text{Cub}_{\text{bi}}$  phases, as indicated by the larger change of the lattice parameters with chain length  $n$  (Table 2).

Considering the development of the phase types in the series **C3Fn**, there is a transition from the chiral triple network  $\text{Cub}_{\text{bi}}^{[*]}/I23$  phase ( $n = 8$ ) to the achiral double network  $\text{Cub}_{\text{bi}}/Ia3d$  phase ( $n = 12, 14$ ) with growing chain length and rising temperature. A growing volume of the molecular periphery leads to an increasing twist between the molecules and thus to a shorter helical pitch length (Fig. 1d). Due to the network structure the molecules must arrive parallel to each other at the nodes. Because the angle between the junctions is a fixed value, an increasing twist is connected with decreasing distance between the nodes to retain the helix synchronization at the nodes. Hence, the decreasing helical pitch reduces the lattice parameter (Table 2). This could lead to a steric frustration with the space required by the alkyl chains. The  $\text{Cub}_{\text{bi}}/Ia3d$  phase of the complexes **C3Fn** is proposed to belong to the short pitch type of  $Ia3d$  phase ( $\text{Cub}_{\text{bi}}/Ia3d_{\text{S}}$ ), having a larger twist between adjacent molecules or rafts of molecules along the networks than provided in the  $\text{Cub}_{\text{bi}}^{[*]}/I23$  structure [72,106]. Only the  $Ia3d$  phase of the non-fluorinated complex **A8**, occurring in this case below the  $I23$  phase (in the heating scan, see Table 1), and having the smallest twist angle  $\Phi$  of only  $6.8^\circ$  (the only one below  $7^\circ$ ), is considered as a long pitch  $Ia3d_{\text{L}}$  phase. Interestingly, in this case no Tet phase separates  $Ia3d_{\text{L}}$  and  $I23$ , and upon cooling the  $I23$  lattice is retained. Comparing **C8** and **C3F8** indicates a steric effect of peripheral fluorination, increasing the helical twist and shifting the cubic phase type from  $Ia3d_{\text{L}}$  towards  $I23$ , similar to the effect of alkyl chain elongation.

However, for the complex **C3F14** the twist between the molecules along the networks decreases slightly from  $7.51^\circ$  in  $\text{Cub}_{\text{bi}}^{[*]}/I23$  to  $7.46^\circ$  in  $\text{Cub}_{\text{bi}}/Ia3d$ , meaning that the pitch length in fact slightly increases at the  $I23$ - $Ia3d$  transition. This effect becomes larger with decreasing alkyl chain length; for **C3F10** the helical twist decreases even from  $7.5$  to  $7.1^\circ$  at the  $I23$ - $Ia3d$  transition on heating (Table 2). Though this appears to disagree with the proposed model, comparing the  $\text{Cub}_{\text{bi}}$  phases of the different complexes depending on chain length indicates that in the  $Ia3d$  phase the twist angle in fact rises with growing chain length  $n$  as expected ( $n = 10$ :  $7.1 \text{ nm}$ ;  $n = 14$ :  $7.3 \text{ nm}$ ), whereas for the  $I23$  phase this increase is absent ( $n = 10$ :  $7.5 \text{ nm}$ ;  $n = 14$ :  $7.5 \text{ nm}$ ). This invariance of the lattice parameter is also found for the  $I23$  phase of the complexes of series **C2Fn** ( $n = 8$ :  $7.1 \text{ nm}$ ;  $n = 14$ :  $7.1 \text{ nm}$ ). For **C3F14** the increasing interface curvature leads to the loss of the network structure and non-branched columns can form in the  $\text{Col}_{\text{hex}}$  phase at highest temperature. Overall, it appears that a transition from a long pitch to a short pitch range of the  $Ia3d$  phase takes place with growing chain length by peripheral fluorination and with rising temperature. In a certain pitch length range alternative network phases with  $I23$  and tetragonal lattice become the more stable structures and replace the  $Ia3d$  phase. In the developing alternative network phases the preferred pitch length is independent on that found in the adjacent  $Ia3d$  phase, and therefore it can be different, either larger or smaller. There appears to be a high diversity of helical pitch lengths and lattice parameters in the Tet phases, whereas there is a strong limitation for the cubic  $I23$  lattice. It appears that not only the ratio of pitch length to junction distance is important, but there are additional effects stabilizing either of the helical network structures; one of them could be provided by the lateral helix-helix interaction parameter between the networks, depending on pitch length and helix orientation [107,108,137].

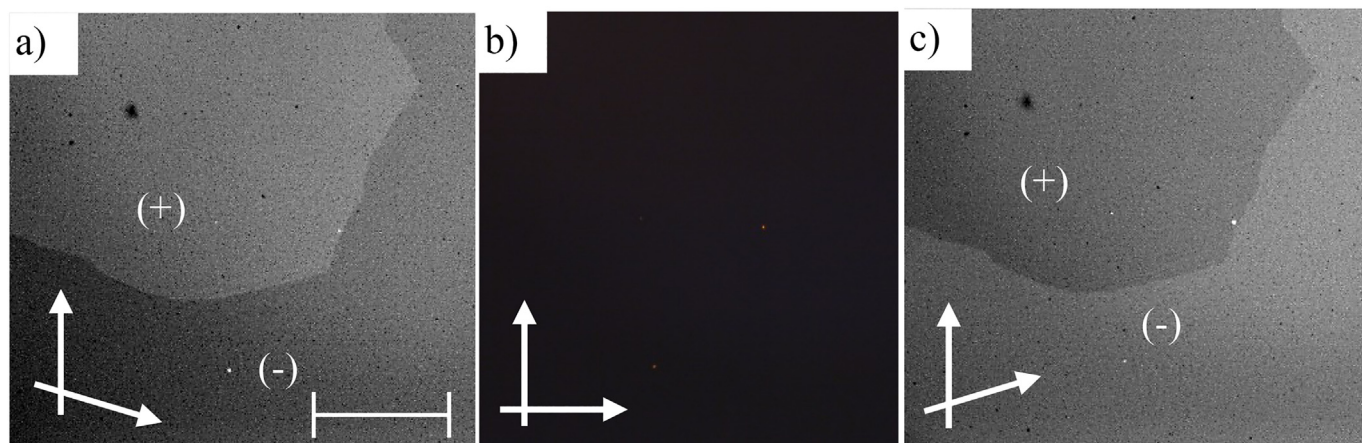


**Fig. 5.** Textures of the supramolecule **C3F8** in the chiral  $\text{Cub}_{\text{bi}}^{*1}/I23$  phase at  $T = 140\text{ }^{\circ}\text{C}$ : a) after rotating one polarizer from the crossed position by  $15^{\circ}$  in clockwise direction showing dark and bright domains, b) under crossed polarizers and c) after rotating one polarizer from the crossed position in anticlockwise direction, indicating a conglomerate of areas with opposite chirality sense; in a, c) the contrast is enhanced for better visibility.

### 3.4. Supramolecular polycatenars **C2Fn** with fluorination directed towards the inside

Shifting the position of the fluorine substituent from the peripheral ortho position with respect to the alkoxy chain at the azopyridine component in the supramolecules **C3Fn** to the inside-directed position results in the isomeric supramolecular polycatenars **C2Fn**. This structural

change reduces the transition temperatures and retains the cubic and non-cubic 3D phases. However, in this series of complexes exclusively the chiral triple network type of  $\text{Cub}_{\text{bi}}$  phases ( $\text{Cub}_{\text{bi}}^{*1}/I23$ ) is observed, meaning that the steric effect on the intermolecular twist and hence, on the phase type is smaller than in the peripheral position (Table 1 and Fig. 3, middle columns). For the shortest derivative **C2F8** the mirror-symmetry breaking is retained even after transition to the isotropic

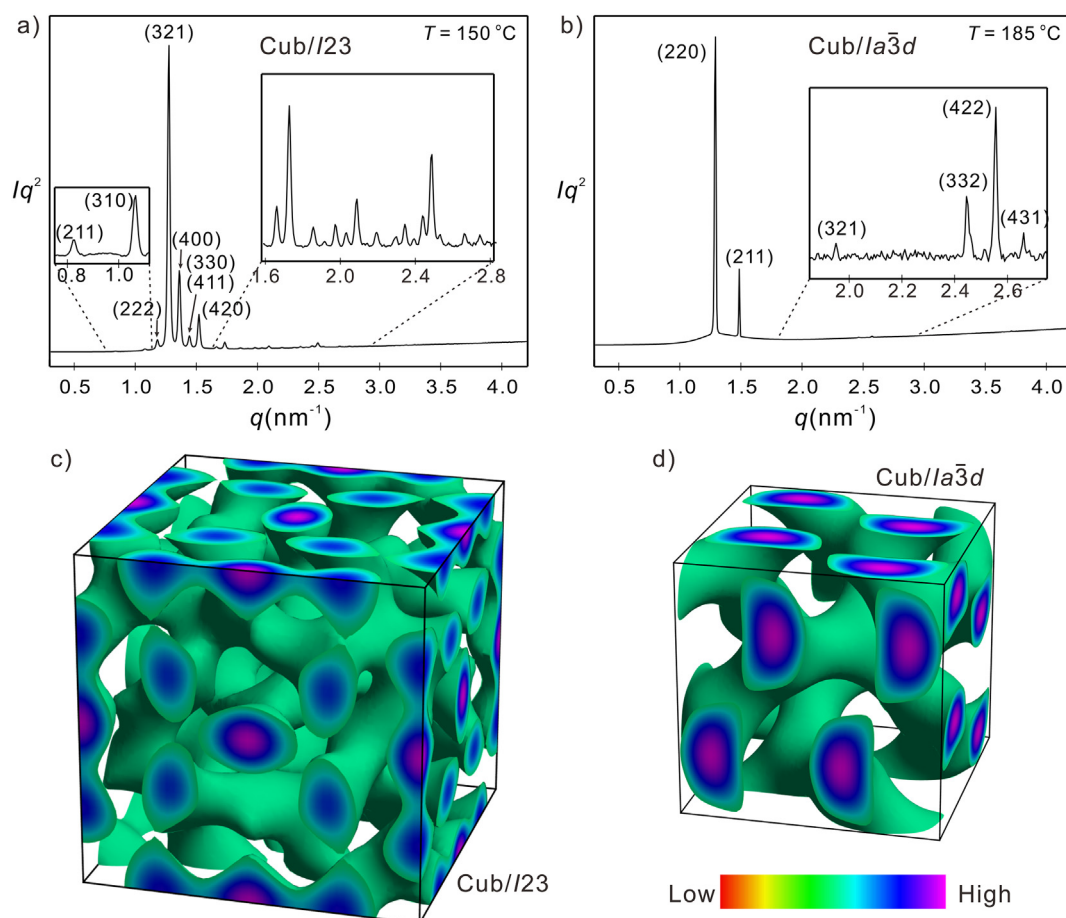


**Fig. 6.** a,b) SAXS diffractogram of **C3F10**: a) in the  $\text{Cub}_{\text{bi}}^{*1}/I23$  phase at  $150\text{ }^{\circ}\text{C}$  ( $a_{\text{cub}} = 18.66\text{ nm}$ ) and b) in the  $\text{Cub}_{\text{bi}}/Ia3d$  phase at  $185\text{ }^{\circ}\text{C}$  ( $a_{\text{cub}} = 12.06\text{ nm}$ ); c, d) electron density maps of c) the  $I23$  phase and d) the  $Ia3d$  phase reconstructed from the diffraction data in a, b); for details, see SI and for numerical XRD data, see Tables S5, S6.



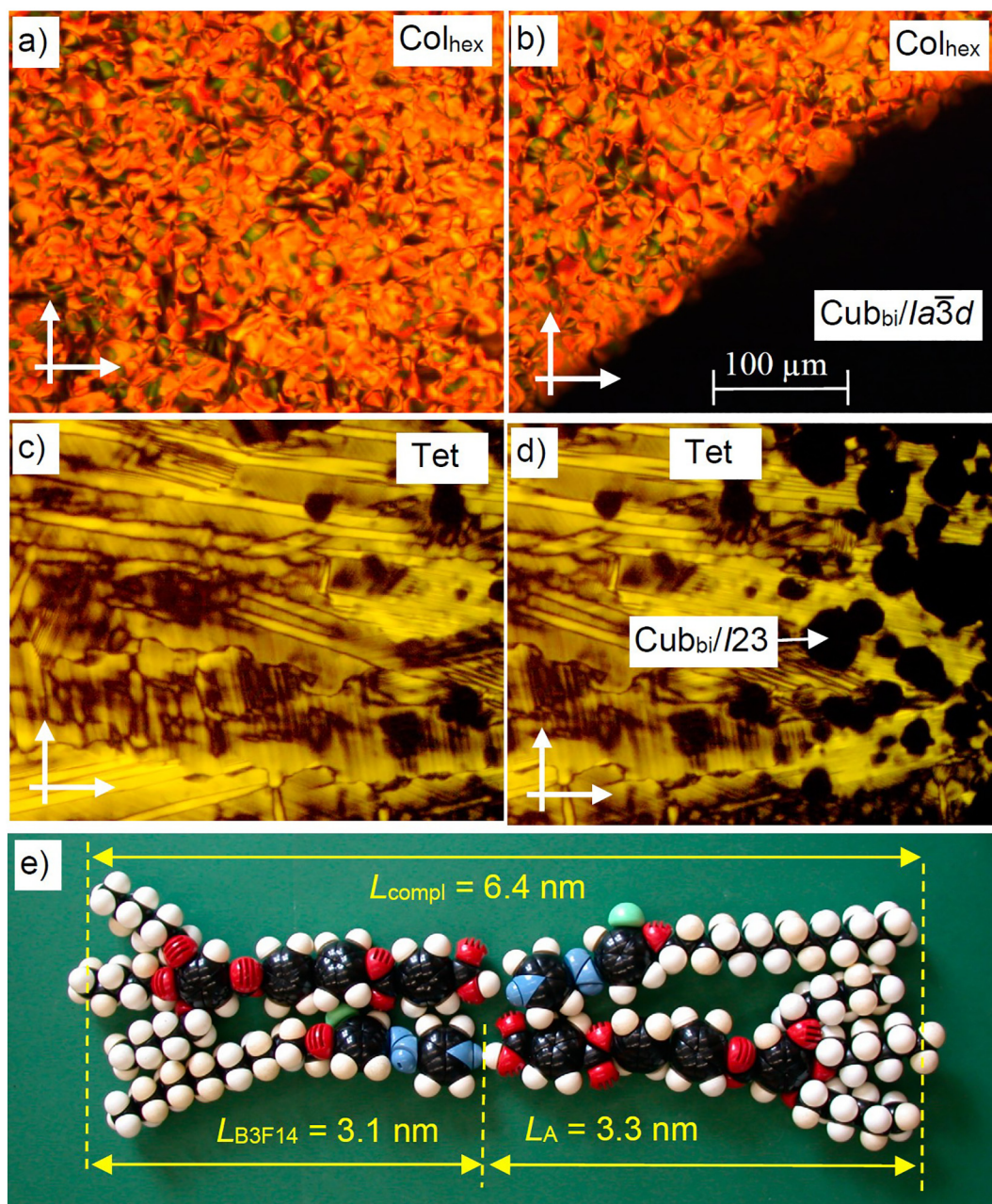


**Fig. 7.** Textures of the supramolecule **C3F14** in the: a)  $Col_{hex}$  phase at  $T = 192\text{ }^{\circ}\text{C}$ ; b) at the  $Col_{hex}$  -  $Cub_{bi}/Ia\bar{3}d$  phase transition at  $T = 190\text{ }^{\circ}\text{C}$ ; c) Tet phase at  $T = 150\text{ }^{\circ}\text{C}$ ; d) at the Tet -  $Cub_{bi}^{[1]}/I23$  phase transition at  $T = 80\text{ }^{\circ}\text{C}$  and e) shows space filling molecular models (CPK model) of a fully intercalated antiparallel pair of H-bonded complexes with full segregation of the hydrogen bonded benzoic acid + pyridine units and partly segregated alkyl chains and aromatic units.

liquid at  $T = 180\text{ }^{\circ}\text{C}$ . Chiral domains can be detected in the highly fluid isotropic liquid between slightly uncrossed polarizers (Fig. 9a, b), indicating a chiral isotropic liquid, composed of a conglomerate of chiral domains ( $Iso_1^{[*]}$ ), as also found for the related nonfluorinated supramolecular polycatenar complex **C8** [104], but not for the 3-fluorinated complexes. The  $Iso_1^{[*]}$  phase of **C2F8** exists over a temperature range of  $\sim 5\text{ K}$  and transforms into the achiral isotropic liquid at  $T = 185\text{ }^{\circ}\text{C}$  (Table 1).

On cooling the complex **C2F8** three different phases are observed, starting with the  $Iso_1^{[*]}$  phase at  $T = 183\text{ }^{\circ}\text{C}$ , followed by  $Cub_{bi}^{[1]}/I23$  at  $T = 179\text{ }^{\circ}\text{C}$  which transforms to a birefringent Tet phase at  $T = 132\text{ }^{\circ}\text{C}$  (Fig. 9c). The lattice parameter of the  $Cub_{bi}^{[1]}/I23$  phase is  $a_{cub} = 19.62\text{ nm}$  (Fig. 10a), which is slightly larger than for the isomeric complex **C3F8** ( $a_{cub} = 18.93\text{ nm}$ ). This means that the twist becomes

smaller, which confirms that in this inside directed position of complex **C2F8** the contribution of fluorine to the crowding of the periphery is reduced. It contributes more to the widening of the aromatic segments and therefore the shift from the high twist  $Ia\bar{3}d_{(S)}$  phase towards the medium twist  $I23$  phase is observed. This steric effect also contributes to the reduction of mesophases stability compared to complexes **C3Fn**. In the series of complexes **C2Fn** the cubic lattice parameter is between 19.53 and 19.62 nm, being almost independent on the alkyl chain length  $n$  (Tables 2, S2). The SAXS pattern of the birefringent mesophases at low temperature can again be indexed to a tetragonal phase, but the positions of the small angle reflections are quite distinct from those observed for the tetragonal phases of **C3F12** and **C3F14** (compare Figs. 10b and 8b). In addition, the lattice parameters  $a = 23.00$  and  $c = 16.15\text{ nm}$  are very different from each

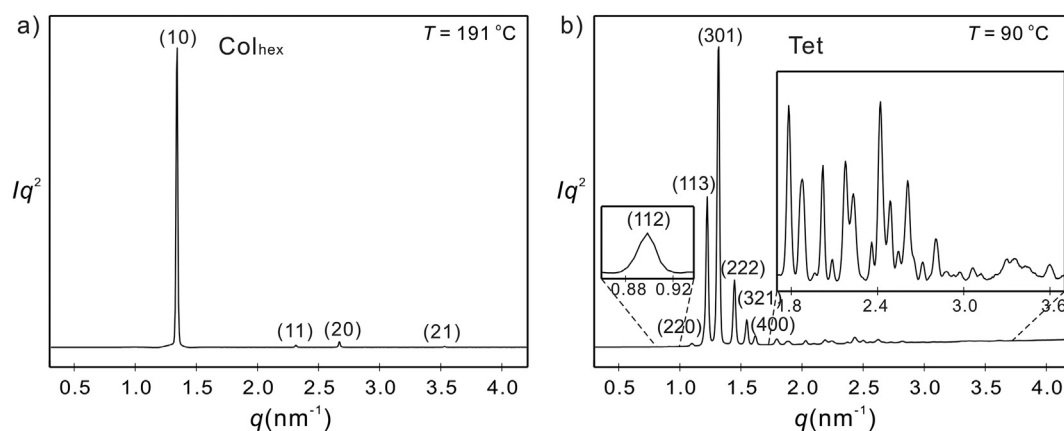


**Fig. 8.** SAXS diffractogram of **C3F14**: a) in the  $Col_{hex}/p6mm$  phase at 191 °C ( $a_{hex} = 5.47$  nm) and b) in the Tet phase at 90 °C ( $a = 16.36$  nm,  $c = 17.53$  nm); for numerical XRD data, see Tables S9–S12.

other, one being much larger and the other smaller than  $a_{cub/I23}$ , whereas for **C3F12** and **C3F14** they are more similar (Table 2). This shows a stronger deformation of the  $I23$  lattice in the series **C2Fn**. Also, the textures observed for the tetragonal phase of **C2F8** (Fig. 9c) have a higher birefringence and are quite different from those observed for the series **C3Fn** (Fig. 7c).

For the next homologue with  $n = 10$  (**C2F10**) the  $Iso_1^{[*]}$  phase is lost in the heating and cooling cycles, but the tetragonal phase still exists as a monotropic phase below  $Cub_{bi}^{[*]}/I23$  (see Table 1). On further chain elongation the tetragonal phase is completely removed (**C2F12** and **C2F14**) and only the mirror symmetry broken  $Cub_{bi}^{[*]}/I23$  phase is observed for these two complexes (see Fig. 3, middle). In this series of complexes, the number of supramolecules in the  $I23$  unit cell is almost the same as found for the non-fluorinated complex **C8**, but it is a bit larger than for the series **C3Fn**, being in line with the smaller twist.

### 3.5. Effects of the degree of fluorination

Comparison of the self-assembly of the monofluorinated supramolecular polycatenars **C2F8** and **C3F8** with the related nonfluorinated complex **C8** [104] and the 2,3-difluorinated **C23F8**, (Fig. 3, see complexes connected with lines) shows that increasing fluorination leads to a lowering of all transition temperatures, which is especially

pronounced for the difluorinated complex **C23F8**, though the dominating cubic phase type is  $I23$  in all four cases with  $n = 8$ . However, the peripheral fluorination in complexes **C3Fn** provides an increased interface curvature and intermolecular twist compared to the nonfluorinated systems **Cn** and the complexes **C2Fn** with inside directed fluorines. This leads to a transition from  $Ia3d_{(L)}$  (**C8**) via a triple network ( $I23$ ) to a short pitch double network  $Ia3d_{(S)}$  phase with growing chain length, rising temperature and by peripheral 3-fluorination. The difluorinated complex **C23F8**, showing exclusively the  $I23$  phase behaves very similar to complex **C3F8**, meaning that the effect of peripheral fluorination, removing alternative 3D phases and suppressing the  $Iso_1^{[*]}$  phase, is dominating.

Comparing the series **C2Fn** and **C3Fn** shows an inverted effect of chain length on the formation of the tetragonal phase(s). In the series **C3Fn** the tetragonal phases are induced and, in the series **C2Fn**, suppressed by chain elongation (Fig. 3). Moreover, there are at least two distinct ranges for the tetragonal phase, either below the triple network  $I23$  phase (**C2F8**, **C2F10**), or below the short pitch  $Ia3d_{(S)}$  phase at the transition to the  $I23$  phase at lower temperature (**C3F14**), see Fig. 3. As also the number of molecules in the unit cell and the  $a:c$  ratios are very different, formation of different types of Tet phases is assumed. It should be noted that tetragonal phases were not observed for the double fluorinated complex **C23F8** or any homologue of the nonfluorinated complexes **Cn**

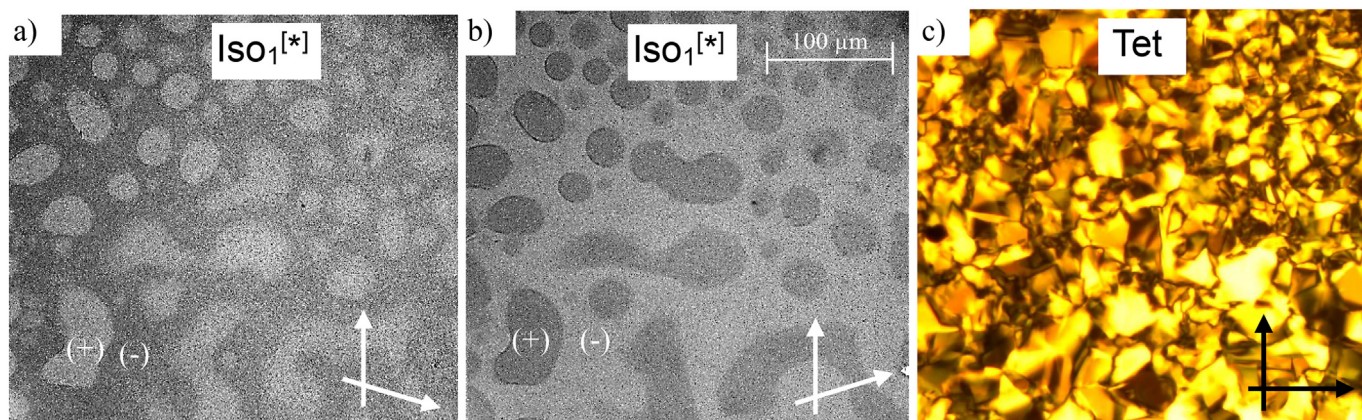


**Fig. 9.** Textures of the supramolecule **C2F8**: a) in the chiral  $Iso_1^{[*]}$  phase at  $T = 180$  °C after rotating one polarizer from the crossed position by 15° in clockwise direction showing dark and bright domains; b) after rotating one of the polarizers in anticlockwise direction with same angle indicating the presence of areas with opposite chirality sense (contrast enhanced) and c) in the tetragonal phase at  $T = 125$  °C.

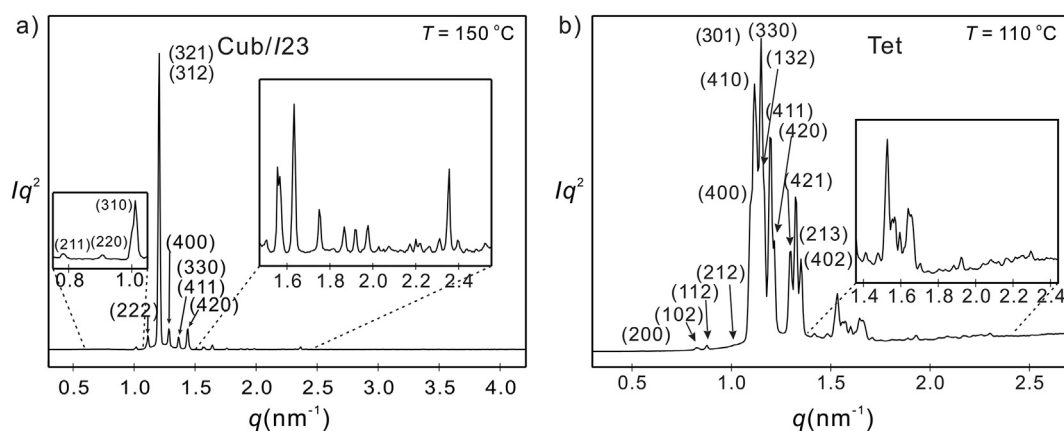


**Fig. 10.** SAXS diffractogram of **C2F8**: a) in the  $\text{Cub}_{\text{bi}}^{*1}/I23$  phase at 150 °C ( $a = 19.62$  nm; for numerical XRD data see Tables S13) and b) in the Tet phase at 110 °C ( $a = 23.00$  nm,  $c = 16.15$  nm).

[118]. This indicates the importance of fluorination as a powerful tool to modify the phase structure of liquid crystalline materials. In contrast, tetragonal phases are dominating for related molecular polycatenars and there is a much smaller effect of core fluorination, as shown in the Supporting Discussion 3.1 in the SI [119].

Though reversible photoisomerization of the complexes **C** takes place in solution (see Fig. S6 in the Supporting Discussion 3.2), no photo-induced transition between the chiral and achiral cubic phases or between the isotropic cubic and the birefringent tetragonal phases was observed in the bulk materials (395 nm laser, 5 mW/mm<sup>2</sup>). This might be a result of the kinetic hindrance of the photoisomerization by the cooperativity [138] provided by the long-range helical network structures fixed in a long range 3D lattice.

### 3.6. $\text{Iso}_1^{*1}$ phase formation

Only for complexes with short chain length ( $n$ ) and without peripheral fluorine the chiral  $\text{Iso}_1^{*1}$  phase is observed as a high temperature phase above the mirror symmetry broken  $\text{Cub}_{\text{bi}}^{*1}/I23$  phase. This means that it is likely that this mirror symmetry broken liquid represents a distorted version of the  $I23$  phase, having no long-range periodicity, but retaining a long-range chirality synchronization due to the remaining local  $I23$ -like network structure, even after transition to the liquid state. This is distinct from those  $\text{Iso}_1^{*1}$  phases occurring besides the achiral  $Ia3d$  cubic phase close to the transition to the lamellar phase, which are assumed to have a local tetragonal  $\text{SmQ}$ -like structure [107,108]. In this tetragonal phase with  $I4_122$  symmetry two interwoven helical networks with uniform chirality are interconnected by 90° four-way junctions [55]. Thus, there appears to be a variety of different  $\text{Iso}_1^{*1}$  phase types [139]. For the complexes **C** the appearance of the chiral isotropic liquid  $\text{Iso}_1^{*1}$  is associated with a short alkyl chain length, the presence of an adjacent  $\text{Cub}_{\text{bi}}^{*1}/I23$  phase (Fig. 1b), and the absence of fluorine in the peripheral 3-position. This obviously allows the  $I23$ -like local structure to be retained with rising temperature and avoids a transition to the achiral  $Ia3d_{(S)}$ -like local structure in the achiral isotropic liquid.

## 4. Summary and conclusions

In summary, we reported the design, synthesis, and investigation of fluorinated supramolecular azobenzene-based polycatenars formed by intermolecular hydrogen-bonding between a taper shaped benzoic acid and a variety of fluorinated azopyridine derivatives. The effect of core fluorination at different positions of the aromatic core on the

development of soft matter network phases was investigated and compared to the parent nonfluorinated supramolecules. Spontaneous mirror symmetry breaking based on chirality synchronization by helical network formation was observed in the isotropic liquid phase ( $\text{Iso}_1^{*1}$ ) and in the triple network cubic phase with  $I23$  symmetry. The mirror symmetry broken isotropic liquid is found for complexes with short chains and without peripheral fluorine and it occurs besides the  $I23$  cubic phase, and therefore, a local  $I23$ -like network structure is proposed. Moreover, the synthesized materials represent the first examples of hydrogen-bonded supramolecular complexes exhibiting 3D tetragonal phases over relatively wide temperature ranges and in different phase sequences, in most cases representing deformed versions of the  $I23$  lattice, appearing as intermediate phases at the  $Ia3d_{(L)}$ - $I23$ -Tet- $Ia3d_{(S)}$ - $\text{Col}_{\text{hex}}$ . These tetragonal phases require further studies to fully solve their structures and to understand the reasons for their formation, which is assumed to be the result of the combined action of minimizing steric frustration and optimizing helix packing in chirality synchronized helical network structures. The network structure not only provides an efficient route to chirality synchronization, leading to new and complex soft matter systems, it appears also to enhance the barrier for *trans-cis* photoisomerizations. Therefore, further materials design and investigations are required to overcome this present limitation.

### Author statement

M. Alaasar: Conceptualization; Investigation; Supervision; Writing - original draft; Writing - review & editing.

J. -C. Schmidt: Investigation; Formal analysis

X. Cai: Investigation, Formal analysis

F. Liu: Investigation; Formal analysis; Writing - review & editing.

C. Tschierske: Conceptualization; Writing - review & editing

### Declaration of competing interest

The authors have no conflict of interest.

### Acknowledgements

M. Alaasar acknowledges the German Research Foundation (DFG) for the financial support (AL2378/1-1). This work is also supported by the National Natural Science Foundation of China (Nos. 21761132033, 21374086). We thank Dr. Chang Huang at Instrument Analysis Center

of Xi'an Jiaotong University for the assistance with WAXS experiments. We thank Beamline BL16B1 at SSRF (Shanghai Synchrotron Radiation Facility, China) for providing the beamtimes.

## Appendix A. Supplementary data

Supplementary data to this article can be found online at <https://doi.org/10.1016/j.molliq.2021.115870>.

## References

- [1] J.-M. Lehn, Beyond chemical synthesis: self-organization?! *Isr. J. Chem.* 58 (2018) 136–141.
- [2] J.F. Stoddart, Mechanically interlocked molecules (MIMs)-molecular shuttles, switches, and machines (nobel lecture), *Angew. Chem. Int. Ed.* 56 (2017) 11094–11125.
- [3] B.-L. Feringa, The art of building small: from molecular switches to motors (Nobel lecture), *Angew. Chem. Int. Ed.* 56 (2017) 11060–11078.
- [4] M.B. Avinash, T. Govindaraju, Architectonics: design of molecular architecture for functional applications, *Acc. Chem. Res.* 51 (2018) 414–426.
- [5] L. Yang, X. Tan, Z. Wang, X. Zhang, Supramolecular polymers: historical development, preparation, characterization, and functions, *Chem. Rev.* 115 (2015) 7196–7239.
- [6] C. Vigier-Carriere, F. Boulmedais, P. Schaaf, L. Jierry, Surface-assisted self-assembly strategies leading to supramolecular hydrogels, *Angew. Chem. Int. Ed.* 57 (2018) 1448–1456.
- [7] X. Yan, F. Wang, B. Zheng, F. Huang, Stimuli-responsive supramolecular polymeric materials, *Chem. Soc. Rev.* 41 (2012) 6042–6065.
- [8] R. Dong, Y. Zhou, X. Huang, X. Zhu, Y. Lu, J. Shen, Functional supramolecular polymers for biomedical applications, *Adv. Mater.* 27 (2015) 498–526.
- [9] D. González-Rodríguez, A.P.H.J. Schenning, Hydrogen-bonded supramolecular  $\pi$ -functional materials, *Chem. Mater.* 23 (2011) 310–325.
- [10] T. Kato, J. Uchida, T. Ichikawa, T. Sakamoto, Functional liquid crystals towards the next generation of materials, *Angew. Chem. Int. Ed.* 57 (2018) 4355–4371.
- [11] Qian Li (Ed.), *Nanoscience With Liquid Crystals*, Springer, Cham, 2014.
- [12] N. Koide, *The Liquid Crystal Display Story*, Springer, Tokyo, 2014.
- [13] C.M. Paleos, D. Tsiourvas, Supramolecular hydrogen-bonded liquid crystals, *Liq. Cryst.* 28 (2001) 1127–1161.
- [14] X.-H. Cheng, H.-F. Gao, Hydrogen bonding for supramolecular liquid crystals, in *hydrogen bonded supramolecular materials*, in: Z.-T. Li, L.-Z. Wu (Eds.), *Lecture Notes in Chemistry*, 88(5), 2015, pp. 133–183, <https://doi.org/10.1007/978-3-662-45780-1>.
- [15] H.K. Bisoyi, Q. Li, Light-directed dynamic chirality inversion in functional self-organized helical superstructures, *Angew. Chem. Int. Ed.* 55 (2016) 2994–3010.
- [16] D.W. Bruce, Liquid crystals formed from specific intermolecular interactions, in: P.A. Gale, J.W. Steed (Eds.), *Supramolecular Chemistry: From Molecules to Nanomaterials*, 7, Wiley 2012, pp. 3493–3514.
- [17] M. Saccone, L. Catalano, Halogen bonding beyond crystals in materials science, *J. Phys. Chem. B* 123 (2019) 9281–9290.
- [18] Kato, J.M.J. Fréchet, Stabilization of a liquid-crystalline phase through noncovalent interaction with a polymer side chain, *Macromolecules* 22 (1989) 3818–3819.
- [19] S.K. Kang, E.T. Samulski, Liquid crystals comprising hydrogen-bonded organic acids I. Mixtures of non-mesogenic acids, *Liq. Cryst.* 27 (2000) 371–376.
- [20] S.K. Kang, E.T. Samulski, P. Kang, J. Choo, Liquid crystals comprising hydrogen-bonded organic acids II. Heterodimers in mixed mesogenic acids, *Liq. Cryst.* 27 (2000) 377–385.
- [21] C. Tschierske, Development of structural complexity by liquid-crystal self-assembly, *Angew. Chem. Int. Ed.* 52 (2013) 8828–8878.
- [22] T. Kato, *Handbook of liquid crystals*, in: J.W. Goodby, P.J. Collings, T. Kato, C. Tschierske, H. Gleeson, P. Raynes (Eds.), *Nanoparticle and Nanostructured Liquid Crystals*, Vol. 6, Wiley-VCH, Weinheim, 2014.
- [23] R. Zhang, Z. Su, X.-Y. Yan, J. Huang, W. Shan, X.-H. Dong, X. Feng, Z. Lin, S.Z.D. Cheng, Frontispiece: discovery of structural complexity through self-assembly of molecules containing rodlike components, *Chem. Eur. J.* 26 (2020) 6741–6756.
- [24] R. Walker, D. Pocięcha, J.P. Abberley, A. Martínez-Felipe, D.A. Paterson, E. Forsyth, G.B. Lawrence, P.A. Henderson, J.M.D. Storey, E. Gorecka, C.T. Imrie, Spontaneous chirality through mixing achiral components: a twist-bend nematic phase driven by hydrogen-bonding between unlike components, *Chem. Commun.* 54 (2018) 3383–3386.
- [25] R. Walker, D. Pocięcha, A. Martínez-Felipe, J.M.D. Storey, E. Gorecka, C.T. Imrie, Twist-bend nematic supramolecular dimers and trimers formed by hydrogen bonding, *Crystals* 10 (2020) 175–191.
- [26] C. Tschierske, C. Nürnberger, H. Ebert, B. Glettner, M. Pehm, F. Liu, X.-B. Zeng, G. Ungar, Complex tiling patterns in liquid crystals, *Interface Focus* 2 (2012) 669–680.
- [27] S. Poppe, X. Cheng, C. Chen, X. Zeng, R.-b. Zhang, F. Liu, G. Ungar, C. Tschierske, Liquid organic frameworks: the single-network “Plumber’s Nightmare” bicontinuous cubic liquid crystal, *J. Am. Chem. Soc.* 142 (2020) 3296–3300.
- [28] C. Chen, R. Kieffer, H. Ebert, M. Pehm, R.-b. Zhang, X. Zeng, F. Liu, G. Ungar, C. Tschierske, Chirality induction through nano-phase separation: alternating network gyroid phase by thermotropic self-assembly of X-shaped bolapolyphiles, *Angew. Chem. Int. Ed.* 59 (2020) 2725–2729.
- [29] X. Zeng, S. Poppe, A. Lehmann, M. Pehm, C. Chen, F. Liu, H. Lu, G. Ungar, C. Tschierske, A self-assembled bicontinuous cubic phase with a single-diamond network, *Angew. Chem. Int. Ed.* 58 (2019) 7375–7379.
- [30] X. Zeng, M. Pehm, G. Ungar, C. Tschierske, F. Liu, Formation of a double diamond cubic phase by thermotropic liquid crystalline self-assembly of bundled bolaamphiphiles, *Angew. Chem. Int. Ed.* 55 (2016) 8324–8327.
- [31] S. Hyde, S. Andersson, K. Larsson, Z. Blum, T. Landh, S. Lidin, B.W. Ninham, *The Language of Shape. The Role of Curvature in Condensed Matter: Physics, Chemistry and Biology*, Elsevier, Amsterdam, 1997 (J. M. Seddon and R. H. Templer, Polymorphism in Lipid-Water Systems. In *Handbook of Biological Physics*; Lipowsky, R. and E., Sackmann, Eds.; Elsevier: Amsterdam, 1995; Vol. 1, pp 97–160; M. L. Lynch and P. T. Spicer, Eds.; *Bicontinuous Liquid Crystals*; Surfactant Science Series 127; CRC Press - Taylor & Francis Group: Boca Raton, USA, 2005).
- [32] A.J. Meuler, M.A. Hillmyer, F.S. Bates, Ordered network mesostructures in block polymer materials, *Macromolecules* 42 (2009) 7221–7250.
- [33] C. Tschierske, Non-conventional liquid crystals-the importance of micro-segregation for self-organisation, *J. Mater. Chem.* 8 (1998) 1485–1508.
- [34] S. Kutsumizu, Recent progress in the synthesis and structural clarification of thermotropic cubic phases, *Isr. J. Chem.* 52 (2012) 844–853.
- [35] G.W. Gray, B. Jones, F. Marson, 71. Mesomorphism and chemical constitution. Part VIII. The effect of 3'-substituents on the mesomorphism of the 4'-n-alkoxydiphenyl-4-carboxylic acids and their alkyl esters, *J. Chem. Soc.* (1957) 393–401.
- [36] Y. Yamamura, Y. Nakazawa, S. Kutsumizu, K. Saito, Molecular packing in two bicontinuous Ia3d gyroid phases of calamitic cubic mesogens BABH(n): roles in structural stability and reentrant behaviour, *Phys. Chem. Chem. Phys.* 21 (2019) 23705–23712.
- [37] M. Imperor-Clerc, M. Veber, A.M. Levelut, Phase transition between single crystals of two thermotropic cubic phases from a mixture of 3,5-didodecyloxybenzoic acid and C18-ANBC, *Chem. Phys. Chem.* 8 (9) (2001) 533–535.
- [38] M. Imperor-Clerc, P. Sotta, M. Veber, Crystal shapes of cubic mesophases in pure and mixed carboxylic acids observed by optical microscopy, *Liq. Cryst.* 27 (2000) 1001–1009.
- [39] X. Zeng, G. Ungar, M. Imperor-Clerc, A triple-network tricontinuous cubic liquid crystal, *Nat. Mater.* 4 (2005) 562–567.
- [40] A. Kohlmeier, D. Janietz, S. Diele, Mesomorphic block molecules: semiperfluorinated 1,3,5-triazine derivatives exhibiting lamellar, columnar, cubic mesophases, *Chem. Mater.* 18 (2006) 1483–1489.
- [41] E. Nishikawa, J. Yamamoto, H. Yokoyama, Synthesis and properties of perfluoroalkoxy substituted benzoic acid derivatives II: forming liquid crystalline cubic phases, *Chem. Letters* 30 (2001) 454–455.
- [42] E. Nishikawa, E.T. Samulski, New mesogens with cubic phases: hydrogen-bonded bipyridines and siloxane-containing benzoic acids I. Preparation and phase behaviour, *Liq. Cryst.* 27 (2000) 1457–1462.
- [43] E. Nishikawa, E.T. Samulski, New mesogens with cubic phases: hydrogen-bonded bipyridines and siloxane-containing benzoic acids II. Structural studies, *Liq. Cryst.* 27 (2000) 1463–1471.
- [44] G. Lattermann, G. Stauffer, Hydroxy group containing liquid crystals: columnar and cubic phases in two chain diols, *Mol. Cryst. Liq. Cryst.* 191 (1) (1990) 199–203.
- [45] K. Borisch, S. Diele, P. Göring, H. Kresse, C. Tschierske, Tailoring thermotropic cubic mesophases: amphiphilic polyhydroxy derivatives, *J. Mater. Chem.* 8 (1998) 529–543.
- [46] K. Borisch, S. Diele, P. Goring, H. Muller, C. Tschierske, Amphiphilic N-benzoyl-1-amino-1-deoxy-d-glucitol derivatives forming thermotropic lamellar, columnar and different types of cubic mesophases, *Liq. Cryst.* 22 (1997) 427–443.
- [47] Y. Cao, M. Alaasar, A. Nallapaneni, M. Salamończyk, P. Marinko, E. Gorecka, C. Tschierske, F. Liu, N. Vaupotič, C. Zhu, Molecular packing in double gyroid cubic phases revealed via resonant soft X-ray scattering, *Phys. Rev. Lett.* 125 (2020), 027801.
- [48] C. Tschierske, Molecular self-organization of amphitropic liquid crystals, *Prog. Polym. Sci.* 21 (1996) 775–852.
- [49] T. Kato, M. Yoshio, T. Ichikawa, B. Soberats, H. Ohno, M. Funahashi, Transport of ions and electrons in nanostructured liquid crystals, *Nat. Rev. Mater.* 2 (2017) 17001.
- [50] G.E. Schröder-Turk, A. Fogden, S.T. Hyde, Bicontinuous geometries and molecular self-assembly: comparison of local curvature and global packing variations in genus-three cubic, tetragonal and rhombohedral surfaces, *Eur. Phys. J. B* 54 (2006) 509–524.
- [51] A. Fogden, S.T. Hyde, Continuous transformations of cubic minimal surfaces, *Eur. Phys. J. B* 7 (1999) 91–104.
- [52] A.-M. Levelut, M. Clerc, Structural investigations on ‘smectic D’ and related mesophases, *Liq. Cryst.* 24 (1998) 105–115.
- [53] D. Demus, D. Marzotko, N.K. Sharma, A. Wiegeleben, The polymorphism of some liquid crystalline 4-n-alkoxy-3'-nitro-biphenylcarboxylic acids, *Kryst. Tech.* 15 (1980) 331.
- [54] C.A. Tyler, D.C. Morse, Orthorhombic Fddd network in triblock and diblock copolymer melts, *Phys. Rev. Lett.* 94 (2005) 208302.
- [55] H. Lu, X. Zeng, G. Ungar, C. Dressel, C. Tschierske, The solution of the puzzle of Smectic-Q: the phase structure and the origin of spontaneous chirality, *Angew. Chem. Int. Ed.* 57 (2018) 2835–2840.
- [56] J. Matraszek, D. Pocięcha, N. Vaupotič, M. Salamończyk, M. Vogrine, E. Gorecka, Bicontinuous orthorhombic soft matter phase made of polycatenar molecules, *Soft Matter* 16 (2020) 3882–3885.
- [57] A.-M. Levelut, E. Hallouin, D. Benemann, G. Heppke, D. Löttsch, The smectic Q phase, a crystal of twist grain boundaries with smectic order, *J. Phys. II* 7 (1997) 981–1000.

- [58] T. Yamamoto, I. Nishiyama, M. Yoneya, H. Yokoyama, Novel chiral effect that produces the anisotropy in 3D structured soft material: chirality-driven cubic—tetragonal liquid crystal phase transition, *J. Phys. Chem. B* 113 (2009) 11564–11567.
- [59] M. Vogrin, N. Vaupotič, M.M. Wojcik, J. Mieczkowski, K. Madrak, D. Pocięcha, E. Gorecka, Thermotropic cubic and tetragonal phases made of rod-like molecules, *Phys. Chem. Chem. Phys.* 16 (2014) 16067–16074.
- [60] M. Jasiński, D. Pocięcha, H. Monobe, J. Szczytko, P. Kaszyński, Tetragonal phase of 6-oxoverdazyl bent-core derivatives with photoinduced ambipolar charge transport and electrooptical effects, *J. Am. Chem. Soc.* 136 (2014) 14658–14661.
- [61] M. Hird, Fluorinated liquid crystals—properties and applications, *Chem. Soc. Rev.* 36 (2007) 2070–2095.
- [62] D. Pauluth, K. Tarumi, Advanced liquid crystals for television, *J. Mater. Chem.* 14 (2004) 1219–1227.
- [63] C. Tschierske, Fluorinated liquid crystals: design of soft nanostructures and increased complexity of self-assembly by perfluorinated segments, *Top. Curr. Chem.* 318 (2011) 1–108.
- [64] K. Kishikawa, Utilization of the perfluoroarene-arene interaction for stabilization of liquid crystal phases, *Isr. J. Chem.* 52 (2012) 800–808.
- [65] M. Spengler, R.Y. Dong, C.A. Michal, M. Pfletscher, M. Giese, Fluorination of supramolecular liquid crystals—tuning tool and analytical probe, *J. Mater. Chem. C* 5 (2017) 2235–2239.
- [66] E. Nishikawa, J. Yamamoto, H. Yokoyama, A polycatenar mesogen with a perfluorinated moiety showing continuous phase transformation between a smectic A phase and a structured, fluid, optically isotropic phase, *Chem. Commun.* (2003) 420–421.
- [67] E. Nishikawa, J. Yamamoto, H. Yokoyama, Polycatenar mesogens with a perfluorinated moiety showing liquid crystalline polymorphism and, microscopically, a continuous smectic A to structured, fluid, optically isotropic phase transition, *J. Mater. Chem.* 13 (2003) 1887–1893.
- [68] Y. Maeda, E. Nishikawa, H. Yokoyama, Morphological phase behaviour under pressure of polycatenar mesogens with a perfluorinated moiety, *Liq. Cryst.* 33 (2006) 865–874.
- [69] X. Zhou, T. Narayanan, Q. Li, New mesogen with thermotropic cubic phase: 3,4,5-tris-(11,11,12,12,13,13,14,14,15,15,16,16,16-tridecafluorohexadecyloxy)benzoic acid, *Liq. Cryst.* 34 (2007) 1243–1248.
- [70] A.I. Smirnova, B. Heinrich, B. Donnio, D.W. Bruce, The influence of lateral fluorination and cyanation on the mesomorphism of polycatenar mesogens and the nature of the SmC phase therein, *RSC Adv.* 5 (2015) 75149–75159.
- [71] H.T. Nguyen, C. Destrade, J. Malthete, Phasmids and polycatenar mesogens, *Adv. Mater.* 9 (1997) 375–388.
- [72] C. Dressel, T. Reppe, S. Poppe, M. Prehm, H. Lu, X. Zeng, G. Ungar, C. Tschierske, Helical networks of  $\pi$ -conjugated rods – a robust design concept for bicontinuous cubic liquid crystalline phases with achiral Ia3d and chiral I23 lattice, *Adv. Funct. Mater.* 2004353 (2020).
- [73] M. Poppe, C. Chen, H. Ebert, S. Poppe, M. Prehm, C. Kerzig, F. Liu, C. Tschierske, Transition from nematic to gyroid-type cubic soft self-assembly by side-chain engineering of  $\Pi$ -conjugated sticky rods, *Soft Matter* 13 (2017) 4381–4392.
- [74] H. Takezoe, Spontaneous achiral symmetry breaking in liquid crystalline phases, in: C. Tschierske (Ed.), *Liquid Crystals, Topics in Current Chemistry*, 318, Springer, Berlin 2011, pp. 303–330.
- [75] C. Tschierske, Mirror symmetry breaking in liquids and liquid crystals, *Liq. Cryst.* 45 (2018) 2221–2252.
- [76] C. Tschierske, G. Ungar, Mirror symmetry breaking by chirality synchronisation in liquids and liquid crystals of achiral molecules, *ChemPhysChem.* 17 (2016) 1224–1251.
- [77] T. Sekine, T. Niori, J. Watanabe, T. Furukawa, S.-W. Choi, H. Takezoe, Spontaneous helix formation in smectic liquid crystals comprising achiral molecules, *J. Mater. Chem.* 7 (1997) 1307–1309.
- [78] L.E. Hough, H.T. Jung, D. Krueker, M.S. Heberling, M. Nakata, C.D. Jones, D. Chen, D.R. Link, J. Zasadzinski, G. Heppke, J.P. Rabe, W. Stocker, E. Korblova, D.M. Walba, M.A. Glaser, N.A. Clark, Helical nanofilament phases, *Science* 325 (2009) 456–460.
- [79] C. Zhang, N. Diorio, O.D. Lavrentovich, A. Jákli, Helical nanofilaments of bent-core liquid crystals with a second twist, *Nat. Commun.* 5 (2014) 3302.
- [80] K.V. Le, H. Takezoe, F. Araoka, Chiral superstructure mesophases of achiral bent-shaped molecules – hierarchical chirality amplification and physical properties, *Adv. Mater.* 29 (2017) 1602737–1602758.
- [81] M. Alaasar, M. Prehm, M. Brautzsch, C. Tschierske, 4-Methylresorcinol based bent-core liquid crystals with azobenzene wings—a new class of compounds with dark conglomerate phases, *J. Mater. Chem. C* 2 (2014) 5487–5501.
- [82] M. Alaasar, M. Prehm, M. Brautzsch, C. Tschierske, Dark conglomerate phases of azobenzene derived bent-core mesogens—relationships between the molecular structure and mirror symmetry breaking in soft matter, *Soft Matter* 10 (2014) 7285–7296.
- [83] M. Alaasar, M. Prehm, C. Tschierske, Helical nano-crystallite (HNC) phases: chirality synchronization of achiral bent-core mesogens in a new type of dark conglomerates, *Chem. Eur. J.* 22 (2016) 6583–6597.
- [84] A. Lehmann, M. Alaasar, M. Poppe, S. Poppe, M. Prehm, M. Nagaraj, S.P. Sreenilayam, Y.P. Panarin, J.K. Vij, C. Tschierske, Stereochemical rules govern the soft self-assembly of achiral compounds: Understanding the heliconical liquid crystalline phases of bent-core mesogens, *Chem. Eur. J.* 26 (2020) 4714–4733.
- [85] M. Poppe, M. Alaasar, A. Lehmann, S. Poppe, M.G. Tamba, J.K. Vij, M. Kurachkina, X. Cai, F. Liu, A. Eremin, M. Nagaraj, C. Tschierske, Controlling the formation of heliconical smectic phases by molecular design of achiral bent-core molecules, *J. Mater. Chem. C* 8 (2020) 3316–3336.
- [86] G. Dantlgraber, A. Eremin, S. Diele, A. Hauser, H. Kresse, G. Pelzl, C. Tschierske, Chirality and macroscopic polar order in a ferroelectric smectic liquid-crystalline phase formed by achiral polyphilic bent-core molecules, *Angew. Chem. Int. Ed.* 41 (2002) 2408–2412.
- [87] C. Keith, R.A. Reddy, A. Hauser, U. Baumeister, C. Tschierske, Silicon-containing polyphilic bent-core molecules: the importance of nanosegregation for the development of chirality and polar order in liquid crystalline phases formed by achiral molecules, *J. Am. Chem. Soc.* 128 (2006) 3051–3066.
- [88] C. Tschierske, Nanoscale stereochemistry in liquid crystals, in: D.B. Amabilino (Ed.), *Chirality at the Nanoscale*, Wiley-VCH Verlag GmbH & Co. KGaA, Weinheim, Germany 2009, pp. 271–304.
- [89] L.E. Hough, M. Spannuth, M. Nakata, D.A. Coleman, C.D. Jones, G. Dantlgraber, C. Tschierske, J. Watanabe, E. Korblova, D.M. Walba, J.E. MacLennan, M.A. Glaser, N.A. Clark, Chiral isotropic liquids from achiral molecules, *Science* 325 (2009) 452–456.
- [90] M. Nagaraj, Dark conglomerate phases of bent-core liquid crystals, *Liq. Cryst.* 43 (2016) 2244–2253.
- [91] M. Alaasar, M. Prehm, K. May, A. Eremin, C. Tschierske, 4-Cyanoresorcinol based bent-core mesogens with azobenzene wings – emergence of sterically stabilised polar order in liquid crystalline phases, *Adv. Funct. Mater.* 24 (2014) 1703–1717.
- [92] M. Alaasar, M. Prehm, S. Belau, N. Sebastián, M. Kurachkina, A. Eremin, C. Chen, F. Liu, C. Tschierske, Polar order, mirror symmetry breaking, and photoswitching of chirality and polarity in functional bent-core mesogens, *Chem. Eur. J.* 25 (2019) 6362–6377.
- [93] M. Alaasar, M. Prehm, S. Poppe, C. Tschierske, Development of polar order by liquid-crystal self-assembly of weakly bent molecules, *Chem. Eur. J.* 23 (2017) 5541–5556.
- [94] R.J. Mandl, The shape of things to come: the formation of modulated nematic mesophases at various length scales, *Chem. Eur. J.* 23 (2017) 8771–8779.
- [95] M. Alaasar, M. Prehm, M. Nagaraj, J.K. Vij, C. Tschierske, A liquid crystalline phase with uniform tilt, local polar order and capability of symmetry breaking, *Adv. Mater.* 25 (2013) 2186–2191.
- [96] S.P. Sreenilayam, Y.P. Panarin, J.K. Vij, V.P. Panov, A. Lehmann, M. Poppe, M. Prehm, C. Tschierske, Spontaneous helix formation in non-chiral bent-core liquid crystals with fast linear electro-optic effect, *Nat. Commun.* 7 (2016) 11369.
- [97] A.A.S. Green, M.R. Tuchband, R. Shao, Y. Shen, R. Visvanathan, A.E. Duncan, A. Lehmann, C. Tschierske, E.D. Carlson, E. Guzman, M. Kolber, D.M. Walba, C.S. Park, M.A. Glaser, J.E. MacLennan, N.A. Clark, Chiral incommensurate helical phase in a smectic of achiral bent-core mesogens, *Phys. Rev. Lett.* 122 (2019) 107801.
- [98] J.P. Abberley, R. Killah, R. Walker, J.M.D. Storey, C.T. Imrie, M. Salamonczyk, C. Zhu, E. Gorecka, D. Pocięcha, Heliconical smectic phase formed by achiral molecules, *Nat. Commun.* 9 (2018) 228.
- [99] M. Salamonczyk, N. Vaupotič, D. Pocięcha, R. Walker, J.M.D. Storey, C.T. Imrie, C. Wang, C. Zhu, E. Gorecka, Multi-level chirality in liquid crystals formed by achiral molecules, *Nat. Commun.* 10 (2019) 1922.
- [100] M. Cestari, S. Diez-Berart, D. A. Dunmur, A. Ferrarini, M. R. de la Fuente, D. J. B. Jackson, D. O. Lopez, G. R. Luckhurst, M. A. Perez-Jubindo, R. M. Richardson, J. Salud, B. A. Timimi, H. Zimmermann, Phase behavior and properties of the liquid-crystal dimer 1,7-bis(4-cyanobiphenyl-4-yl) heptane: a twist-bend nematic liquid crystal, *Phys. Rev. E* 84, 031704.
- [101] C. Dressel, F. Liu, M. Prehm, X. Zeng, G. Ungar, C. Tschierske, Dynamic mirror-symmetry breaking in bicontinuous cubic phases, *Angew. Chem. Int. Ed.* 53 (2014) 13115–13120.
- [102] C. Dressel, T. Reppe, M. Prehm, M. Brautzsch, C. Tschierske, Chiral self-sorting and amplification in isotropic liquids of achiral molecules, *Nat. Chem.* 6 (2014) 971–977.
- [103] D.W. Bruce, Calamitics, cubics, and columnar-liquid-crystalline complexes of silver(I), *Acc. Chem. Res.* 33 (2000) 831–840.
- [104] M. Alaasar, S. Poppe, Q. Dong, F. Liu, C. Tschierske, Mirror symmetry breaking in cubic phases and isotropic liquids driven by hydrogen bonding, *Chem. Commun.* 52 (2016) 13869–13872.
- [105] C. Tschierske, C. Dressel, Mirror symmetry breaking in liquids and their impact on the development of homochirality in abiogenesis: emerging proto-RNA as source of biochirality, *Symmetry* 12 (2020) 1098–1128.
- [106] T. Reppe, C. Dressel, S. Poppe, C. Tschierske, Controlling spontaneous mirror symmetry breaking in cubic liquid crystalline phases by the cycloaliphatic ring size, *Chem. Commun.* 56 (2020) 711–714.
- [107] T. Reppe, S. Poppe, X. Cai, F. Liu, C. Tschierske, Spontaneous mirror symmetry breaking in benzil-based soft crystalline, cubic liquid crystalline and isotropic liquid phases, *Chem. Sci.* 11 (2020) 5902–5908.
- [108] T. Reppe, S. Poppe, C. Tschierske, Controlling mirror symmetry breaking and network formation in liquid crystalline cubic, isotropic liquid and crystalline phases of benzil-based polycatenars, *Chem. Eur. J.* 26 (2020) 16066–16079.
- [109] X. Zeng, G. Ungar, Spontaneously chiral cubic liquid crystal: three interpenetrating networks with a twist, *J. Mater. Chem. C* 8 (2020) 5389–5398.
- [110] K. Saito, Y. Yamamura, Y. Miwa, S. Kutsumizu, A structural model of the chiral “Im3m” cubic phase, *Phys. Chem. Chem. Phys.* 18 (2016) 3280–3284.
- [111] N. Vaupotič, M. Salamonczyk, J. Matraszek, M. Vogrin, D. Pocięcha, E. Gorecka, New structural model of a chiral cubic liquid crystalline phase, *Phys. Chem. Chem. Phys.* 22 (2020) 12814–12820.
- [112] H. Yu, T. Ikeda, Photocontrollable liquid-crystalline actuators, *Adv. Mater.* 23 (2011) 2149–2180.
- [113] Z. Mahimwalla, K.G. Yager, J.-i. Mamiya, A. Shishido, A. Priimagi, C.J. Barrett, Azobenzene photomechanics: prospects and potential applications, *Polym. Bull.* 69 (2012) 967–1006.

- [114] C. Umeton, Chapter 1 - dynamic photonic materials based on liquid crystals, in: L. De Sio, N. Tabiryan, T. Bunning, B.R. Kimball, E. Wolf (Eds.), *Progress in Optics*, 58, Elsevier, Amsterdam 2013, pp. 1–64.
- [115] M. Alaasar, Azobenzene-containing bent-core liquid crystals: an overview, *Liq. Cryst.* 43 (2016) 2208–2243.
- [116] M. Saccone, M. Spengler, M. Pfletscher, K. Kuntze, M. Virkki, C. Wölper, R. Gehrke, G. Jansen, P. Metrangolo, A. Priimagi, M. Giese, Photoresponsive halogen-bonded liquid crystals: the role of aromatic fluorine substitution, *Chem. Mater.* 31 (2019) 462–470.
- [117] M. Pfletscher, C. Wölper, J.S. Gutmann, M. Mezger, M. Giese, A modular approach towards functional supramolecular aggregates—subtle structural differences inducing liquid crystallinity, *Chem. Commun.* 52 (2016) 8549–8552.
- [118] M. Alaasar, M. Prehm, Y. Cao, F. Liu, C. Tschierske, Spontaneous mirror-symmetry breaking in isotropic liquid phases of photoisomerizable achiral molecules, *Angew. Chem. Int. Ed.* 128 (2016) 320–324.
- [119] M. Alaasar, S. Poppe, Q. Dong, F. Liu, C. Tschierske, Isothermal chirality switching in liquid-crystalline azobenzene compounds with non-polarized light, *Angew. Chem. Int. Ed.* 56 (2017) 10801–10805.
- [120] M. Alaasar, M. Prehm, S. Belau, N. Sebastian, M. Kurachkina, A. Eremin, C. Chen, F. Liu, C. Tschierske, Polar order, mirror symmetry breaking, and photoswitching of chirality and polarity in functional bent-core mesogens, *Chem. Eur. J.* 25 (2019) 6362–6377.
- [121] M. Alaasar, S. Poppe, Cybotactic nematic phases with wide ranges in photoresponsive polycatenars, *Liq. Cryst.* 47 (2020) 939–949.
- [122] H.M.D. Bandara, S.C. Burdette, Photoisomerization in different classes of azobenzene, *Chem. Soc. Rev.* 41 (2012) 1809–1825.
- [123] H.K. Bisoyi, Q. Li, Light-directing chiral liquid crystal nanostructures: from 1D to 3D, *Acc. Chem. Res.* 47 (2014) 3184–3195.
- [124] J.-I. Mamiya, K. Kanie, T. Hiyama, T. Ikeda, T. Kato, A rodlike organogelator: fibrous aggregation of azobenzene derivatives with a syn-chiral carbonate moiety, *Chem. Commun.* (2002) 1870–1871.
- [125] Z.-G. Zheng, Y.-Q. Lu, Q. Li, Photoprogrammable mesogenic soft helical architectures: a promising avenue toward future chiro-optics, *Adv. Mater.* 32 (2020) 1905318–1905336.
- [126] H.K. Bisoyi, T.J. Bunning, Q. Li, Stimuli-driven control of the helical axis of self-organized soft helical superstructures, *Adv. Mater.* 30 (2018) 1706512.
- [127] D.A. Paterson, J. Xiang, G. Singh, R. Walker, D.M. Agra-Kooijman, A. Martinez-Felipe, M. Gao, J.M.D. Storey, S. Kumar, O.D. Lavrentovich, C.T. Imrie, Reversible isothermal twist–bend nematic–nematic phase transition driven by the photoisomerization of an azobenzene-based nonsymmetric liquid crystal dimer, *J. Am. Chem. Soc.* 138 (2016) 5283–5286.
- [128] R. Hori, Y. Miwa, K. Yamamoto, S. Kutsumizu, Phase structure and phase transition mechanism for light-induced Ia3d cubic phase in 4'-n-docosyloxy-3'-nitrophenyl-4-carboxylic acid/ethyl 4-(4'-n-docosyloxyphenylazo)benzoate binary mixture, *J. Phys. Chem. B* 118 (2014) 3743–3749.
- [129] A. Nagai, H. Kondo, Y. Miwa, T. Kondo, S. Kutsumizu, Y. Yamamura, K. Saito, Optical switching between liquid-crystalline assemblies with different structural symmetries and molecular orders, *Bull. Chem. Soc. Jpn.* 91 (2018) 1652–1659.
- [130] M. Alaasar, S. Poppe, C. Tschierske, Photoresponsive halogen bonded polycatenar liquid crystals, *J. Mol. Liq.* 277 (2019) 233–240.
- [131] M. Alaasar, J.-C. Schmidt, A.F. Darweesh, C. Tschierske, Azobenzene-based supramolecular liquid crystals: The role of core fluorination, *J. Mol. Liq.* 310 (2020) 113252–113259.
- [132] A. Immirzi, B. Perini, Prediction of density in organic crystals, *Acta Cryst. A33* (1977) 216–218.
- [133] A. Martinez-Felipe, A.G. Cook, J.P. Abberley, R. Walker, J.M.D. Storey, C.T. Imrie, An FT-IR spectroscopic study of the role of hydrogen bonding in the formation of liquid crystallinity for mixtures containing bipyridines and 4-pentoxybenzoic acid, *RSC Adv.* 6 (2016) 108164–108179.
- [134] M. Alaasar, C. Tschierske, M. Prehm, Hydrogen-bonded supramolecular complexes formed between isophthalic acid and pyridine-based derivatives, *Liq. Cryst.* 38 (2011) 925–934.
- [135] D. Bruce, P. Metrangolo, F. Meyer, C. Präsang, G. Resnati, G. Terraneo, A. Whitwood, Mesogenic, trimeric, halogen-bonded complexes from alkoxystilbazoles and 1,4-diodotetrafluorobenzene, *New J. Chem.* 32 (2008) 477–482.
- [136] D.A. Paterson, A. Martínez-Felipe, S.M. Jansze, A.T.M. Marcellis, J.M.D. Storey, C.T. Imrie, New insights into the liquid crystal behaviour of hydrogen-bonded mixtures provided by temperature dependent FTIR spectroscopy, *Liq. Cryst.* 42 (2015) 928–939.
- [137] D.M. Hall, G.M. Grason, How geometric frustration shapes twisted fibres, inside and out: competing morphologies of chiral filament assembly, *Interface Focus* 7 (2017) 20160140.
- [138] L.K.S. von Krbek, C.A. Schalley, P. Thordarson, Assessing cooperativity in supramolecular systems, *Chem. Soc. Rev.* 46 (2017) 2622–2637.
- [139] T. Reppe, C. Dressel, S. Poppe, A. Eremin, C. Tschierske, Swallow-tailed polycatenars: controlling complex liquid crystal self-assembly and mirror symmetry breaking at the lamellae-network cross-over, *Adv. Opt. Mater.* (2020) 2001572–2001589.



# Photoresponsive halogen bonded polycatenar liquid crystals

Mohamed Alaasar<sup>a,b,\*</sup>, Silvio Poppe<sup>b</sup>, Carsten Tschierske<sup>b</sup>

<sup>a</sup> Department of Chemistry, Faculty of Science, Cairo University, Giza, Egypt

<sup>b</sup> Institute of Chemistry, Martin-Luther University Halle-Wittenberg, Kurt-Mothes Str.2, D-06120 Halle/Saale, Germany

## ARTICLE INFO

### Article history:

Received 28 September 2018  
Received in revised form 14 December 2018  
Accepted 15 December 2018  
Available online 18 December 2018

### Keywords:

Polycatenars  
Liquid crystals  
Halogen bond  
Azobenzene  
Photo switching

## ABSTRACT

Photosensitive liquid crystalline materials whose properties could be modified with UV–visible light irradiation are of special interest for photosensitive and photoswitching materials. Herein we represent the first examples of light-responsive halogen bonded supramolecular polycatenars. Photoswitchable liquid-crystalline aggregates were designed and prepared via halogen bond formation between a non-mesogenic taper shaped tetrafluoroiodobenzene based halogen bond-donor and non-mesogenic or mesogenic azopyridine derivatives as halogen bond-acceptors. The liquid crystalline behaviour of the prepared materials was characterized by differential scanning calorimetry (DSC), polarized optical microscope (POM) and X-ray diffraction (XRD). Upon irradiation with UV light, the complexes undergo fast and reversible photoinduced phase transition. Interestingly, some of these halogen-bonded polycatenars exhibit enantiotropic liquid crystalline phases over wide temperature ranges which are the widest among all previously reported photoresponsive perfluoroaryliodide based supramolecular halogen bonded liquid crystals.

© 2018 Elsevier B.V. All rights reserved.

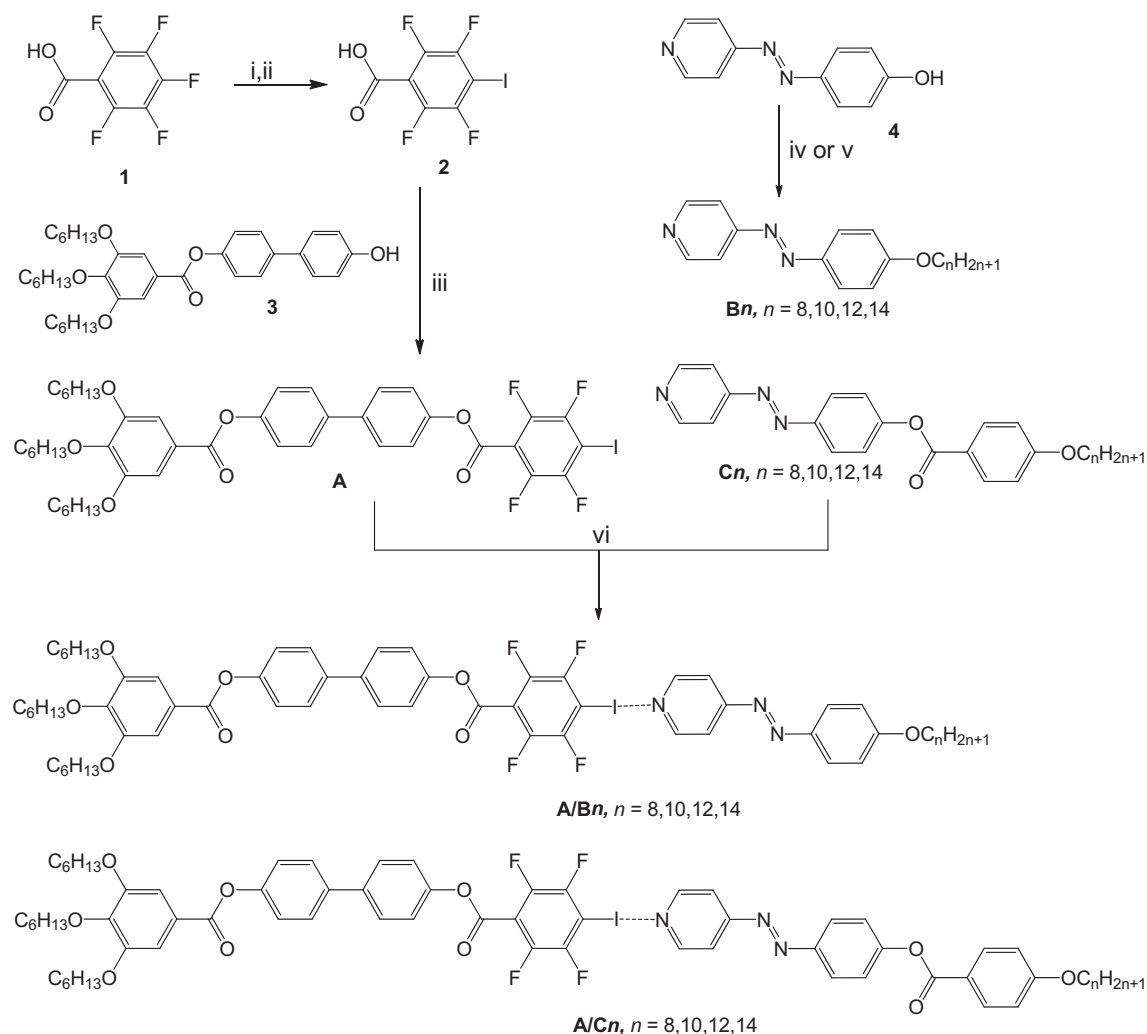
## 1. Introduction

The design of novel photocontrollable and switchable functional materials is an important area of contemporary science [1,2]. Liquid crystals (LCs) have been recognized as one class of functional materials that combine molecular order and mobility with great potential to be used in fields of information technology [3], and flat-panel display technology [4]. In recent years, supramolecular LCs constructed by noncovalent interactions such as hydrogen or halogen bonding became of special interest [5,6]. These types of interaction are extremely fruitful for obtaining LCs with complex superstructures via easily accessible synthetic pathways [7]. Moreover, the mesomorphic properties of supramolecular LCs can be finely tuned by modification of the chemical structures of the starting small molecules. The pioneer work about hydrogen-bonded LCs was reported by Kato and Fréchet using the concept of dimerization between carboxylic groups and pyridine-based compounds [8–10]. On the other hand, halogen-bonding which is less studied represents any noncovalent interaction involving a halogen atom as an electrophile. The main attractive features of halogen bonding are its high directionality, and tunability which make it a powerful tool for designing functional materials [11–13]. The first report about

halogen-bonded LCs was in 2004 by Bruce et al. [14], followed by other reports including photoresponsive halogen-bonded supramolecular LCs with photoinduced phase transitions [15–23]. Due to their unique *trans-cis* isomerization upon photo irradiation, azobenzene based materials represent one of the most attractive photochromes for the manufacture of light-addressable materials [24–28]. The combination of liquid crystalline properties and photosensitivity in the same materials leads to several potential applications such as molecular scissors [29], photo-oscillators [30,31], and optogenetics [32]. Therefore, light responsive supramolecular LCs have been designed by hydrogen or halogen bonding between complementary components with azobenzene unit incorporated in the molecular structure of either the donor or the acceptor [33,34]. One class of halogen or hydrogen acceptors are azopyridine derivatives, with the advantage of possessing light sensitivity related to azobenzene and the capability of self-assembly by hydrogen or halogen bond formation through the pyridyl moiety. In most cases self-assembly by halogen bonding was used to form rod-like supramolecules. However, photoresponsive halogen-bonded supramolecular polycatenar (multi-chain) mesogens have not been reported to date. Therefore, we report herein the first examples of supramolecular polycatenars (**A/Bn** and **A/Cn**, see Scheme 1) formed by intermolecular halogen bond between two different types of azopyridine derivatives with one terminal alkoxy chain (**Bn** or **Cn**) and a taper shaped compound with three terminal alkoxy chains and an iodo-tetrafluoroarene ring (**A**) as the halogen-donor. The fluorination in **A** serves to strengthen the halogen bond with the azopyridine molecules (**Bn** and **Cn**). It is also

\* Corresponding author at: Department of Chemistry, Faculty of Science, Cairo University, Giza, Egypt.

E-mail addresses: [malaasar@sci.cu.edu.eg](mailto:malaasar@sci.cu.edu.eg) (M. Alaasar), [carsten.tschierske@chemie.uni-halle.de](mailto:carsten.tschierske@chemie.uni-halle.de) (C. Tschierske).



**Scheme 1.** Synthetic route to the supramolecular halogen-bonded polycatenars **A/Bn** and **A/Cn**. Reagents and conditions: i. Zn/NH<sub>3</sub> aq.; ii. *n*-BuLi, I<sub>2</sub>; iii. DCC, DMAP, DCM, stirring, rt., 24 h; iv. For **Bn** compounds: BrC<sub>n</sub>H<sub>2n+1</sub>, KI, K<sub>2</sub>CO<sub>3</sub>, DMF, stirring, 50 °C, 48 h; v. For **Cn** compounds: 4-*n*-alkoxybenzoic acids, DCC, DMAP, DCM, stirring, rt., 48 h; vi. Melting with stirring.

known that fluorination is an effective tool to modify the LC properties [35–38].

## 2. Experimental

### 2.1. Synthesis

The complementary components **A**, **Bn** and **Cn** were synthesized through the synthetic pathway shown in Scheme 1. The halogen-bond acceptors **Bn** [19,33,34], and **Cn** [39] were synthesized as described elsewhere, while the detailed synthetic procedure, purification and analytical data for the newly reported halogen-bond donor **A** are reported below.

#### 2.1.1. Synthesis of the halogen-bond donor (**A**)

As shown in Scheme 1; the intermediate 2,3,5,6-tetrafluoro-4-iodobenzoic acid (**2**) was prepared starting from 2,3,4,5,6-pentafluorobenzoic acid as described before [15], while the synthesis of the phenolic compound 4'-hydroxybiphenyl-3,4,5-trihexyloxyphenylbenzoate **3** was carried out using similar method to that reported by Seo et al. [40] To prepare the halogen-bond donor (**A**) 2,3,5,6-tetrafluoro-4-iodobenzoic acid **2** (0.32 g, 1.0 mmol) and 4'-hydroxybiphenyl-3,4,5-trihexyloxyphenylbenzoate **3** (0.59 g, 1.0 mmol) and a catalytic amount of DMAP were dissolved in dichloromethane (DCM) with stirring followed by addition of DCC (0.25 g,

1.2 mmol) previously dissolved in DCM. The reaction mixture was then stirred for 24 h. After the reaction completion, as checked by TLC, the solid byproduct was filtered out and washed three times with DCM. The solvent was then removed under vacuum and the crude white material obtained was purified first with column chromatography using DCM as an eluent followed by recrystallization from ethanol to give 0.60 g,

**Table 1**  
Transition temperatures (*T* °C) and transition enthalpies [KJmol<sup>-1</sup>] of the azopyridine derivatives (**Bn** and **Cn**) [34,39].

Comp.	<i>n</i>	Heating	Cooling	Reference
<b>B8</b>	8	71	70 <sup>a</sup>	[34]
<b>B10</b>	10	67	65 <sup>a</sup>	[34]
<b>B12</b>	12	73	72 <sup>a</sup>	[34]
<b>B14</b>	14	74	72 <sup>a</sup>	[34]
<b>C8</b>	8	Cr 112 [98.8] SmA 128 [2.0] N 141 [1.2] Iso	Iso 139 [−1.3] N 126 [−2.1] SmA 86 [−82.2] Cr	[39]
<b>C10</b>	10	Cr 94 [157.9] SmA 134 [5.0] N 139 [2.3] Iso	Iso 135 [−2.5] N 131 [−5.0] SmA 75 [−137.7] Cr	[39]
<b>C12</b>	12	Cr 96 [188.8] SmA 134 [13.4] Iso	Iso 132 [−13.8] SmA 75 [−185.9] Cr	[39]
<b>C14</b>	14	Cr 97 [190.7] SmA 133 [13.6] Iso	Iso 132 [−14.6] SmA 78 [−192.2] Cr	[39]

Notes: abbreviations: Cr = crystalline solid; N = nematic phase; SmA = smectic A phase; Iso = isotropic liquid.

<sup>a</sup> The crystallization temperatures of **Bn** compounds were measured using POM.



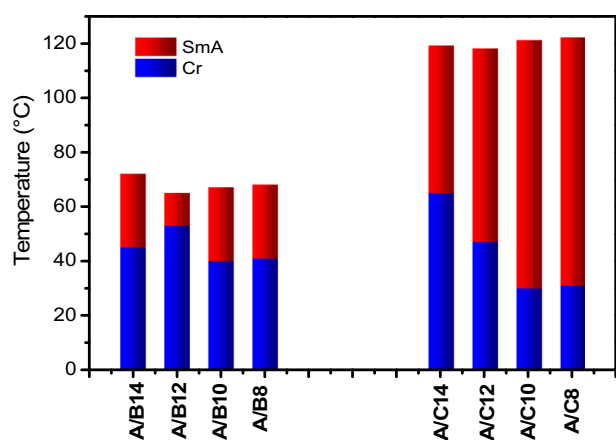


**Fig. 1.** Thermal behaviour of the prepared supramolecular polycatenars as determined upon cooling. Colour legend: red, SmA phase and blue crystal phase (for numerical values see Table 2). (For interpretation of the references to colour in this figure legend, the reader is referred to the web version of this article.)

67.3% yield of compound **A** as colorless crystals. **IR** (KBr pellet,  $\text{cm}^{-1}$ ): 2921, 2850 (Aliphatic CH stretch), 1736 (C=O stretch), 1586, 1470 (Aromatic C=C stretch), 1496, 1473, 1430, 1335, 1297, 1193, 1122;  **$^1\text{H}$  NMR** (400 MHz,  $\text{CDCl}_3$ ):  $\delta$  7.71–7.58 (m, 4H, Ar–H), 7.43 (s, 2H, Ar–H), 7.39–7.21 (m, 4H, Ar–H overlapped with  $\text{CDCl}_3$ ), 4.19–3.95 (m, 6H,  $-\text{OCH}_2\text{CH}_2-$ ), 1.97–1.67 (m, 6H,  $-\text{OCH}_2\text{CH}_2-$ ), 1.64–1.13 (m, 18H,  $\text{CH}_2$ ), 1.02–0.73 (m, 9H,  $\text{CH}_3$ ).  **$^{13}\text{C}$  NMR** (126 MHz,  $\text{CDCl}_3$ ):  $\delta$  (ppm) = 165.00, 152.97, 150.72, 149.46, 143.13, 139.13, 137.76, 128.37, 128.21, 123.75, 122.18, 121.59, 108.64, 73.58, 69.30, 31.92, 31.89, 30.34, 29.71, 29.65, 29.61, 29.56, 29.37, 29.32, 29.29, 26.07, 26.04, 22.68, 22.66, 14.08.  **$^{19}\text{F}$  NMR** (376 MHz,  $\text{CDCl}_3$ ):  $\delta$  (ppm) =  $-117.29$  to  $-118.75$  (m),  $-136.58$  to  $-136.83$  (m).  **$m/z$  HRMS** ( $\text{ES}^-$ ): 915.2400 [ $\text{MNa}$ ] $^+$  calculated for  $\text{C}_{44}\text{H}_{49}\text{F}_4\text{IO}_7$ ; found 915.2351 [ $\text{MNa}$ ] $^+$ .

### 2.1.2. Synthesis of the supramolecular polycatenar complexes (A/B $n$ and A/C $n$ )

The supramolecular polycatenars (A/B $n$  and A/C $n$ ) were prepared by mixing equimolar amounts of each of the azopyridine derivatives (B $n$  or C $n$ ) and the halogen bond donor **A** and melting them together in a DSC pan with stirring to give an intimate blend then cooling to room temperature. The formed crystalline material was then grinded and the previous process was repeated twice. Homogenous melting and stable LC mesophases were observed for all supramolecular complexes. The formation of the halogen-bonded complexes was firstly checked by comparing the  $^1\text{H}$  NMR spectra of the complementary

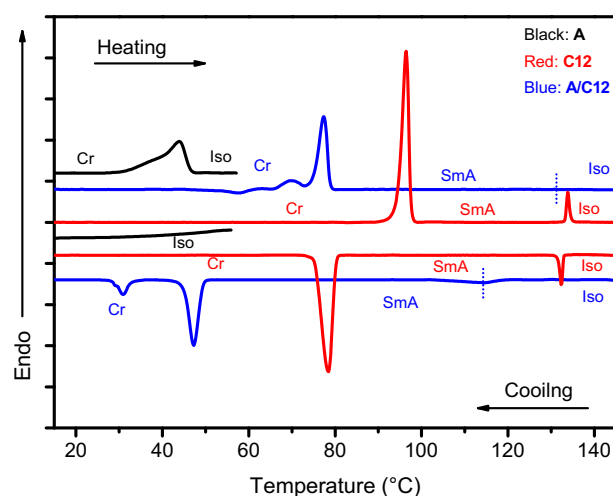


**Fig. 2.** DSC heating and cooling traces ( $10\text{ K min}^{-1}$ ) observed for the complex A/C12 (blue curves) compared to its complementary components **A** (black curves) and **C12** (red curves); the small additional peaks in the DSC traces of the A/C12 complex before melting and after crystallization are due to crystal-crystal transitions between different crystal modifications as often observed for the crystalline phases of LC molecules. (For interpretation of the references to colour in this figure legend, the reader is referred to the web version of this article.)

components with their complexes. For example  $^1\text{H}$  NMR spectra of the individual components **A**, **B8** and their complex A/B8 are given in the supporting information file (Fig. S1). However, there is no difference in the chemical shift of the pure components and their complex. The reason of this behaviour is attributed to the instability of the halogen bond between azopyridine based derivative **B8** and the perfluoroiodo derived compound **A** in chloroform solution [41–43]. The dissociation of the complex in chloroform solution was also proved by  $^{19}\text{F}$  NMR spectra (Fig. S2), where almost identical spectra were observed for compound **A** and its complexes. This was further checked by carrying out TLC in chloroform for the complex A/B8 as an example and comparing it with those of **A** and **B8** as pure components (Fig. S6), where one spot was detected for each of the pure components **A** and **B8** and two spots for the complex A/B8. The two spots observed for A/B8 are at the same positions for **A** and **B8** indicating the dissociation of the complex to its corresponding complementary components. However, the formation of the supramolecular complexes between compound **A** and each of the azopyridines B $n$  or C $n$  in the liquid crystalline and crystalline states was successfully confirmed by differential scanning calorimetry (DSC), polarized optical microscopy (POM), Fourier transform

**Table 2**

Phase transition temperatures ( $T/^\circ\text{C}$ ), mesophase types, and transition enthalpies [ $\Delta H/\text{J}\cdot\text{g}^{-1}$ ] of the complexes A/B $n$  and A/C $n$ .<sup>a</sup>

Complex	$x$	$n$	Heating	Cooling
A/B8	0	8	Cr 69 [44.6] Iso	Iso 68–62 [–1.2] SmA 41 [–24.8] Cr
A/B10	0	10	Cr 71 [42.9] Iso	Iso 67–62 [–1.4] SmA 40 [–22.1] Cr
A/B12	0	12	Cr 72 [56.6] Iso	Iso 65–62 [–1.0] SmA 53 [–30.1] Cr
A/B14	0	14	Cr 76 [48.7] Iso	Iso 72–62 [–3.9] SmA 45 [–36.8] Cr
A/C8	1	8	Cr 76 [37.5] SmA <sup>b</sup> 130–139 [–] Iso	Iso 122–110 [–2.5] SmA 31 [–8.3] Cr
A/C10	1	10	Cr 80 [18.4] SmA <sup>b</sup> 133–139 [–] Iso	Iso 121–108 [–2.5] SmA 30 [–29.8] Cr
A/C12	1	12	Cr 75 [58.2] SmA <sup>b</sup> 133–140 [–] Iso	Iso 118–110 [–2.7] SmA 47 [–38.8] Cr
A/C14	1	14	Cr 88 [10.5] SmA <sup>b</sup> 131–140 [–] Iso	Iso 119–109 [–2.3] SmA 65 [–34.5] Cr

Abbreviations: see Table 1.

<sup>a</sup> Peak temperatures as determined from 2nd heating and 2nd cooling DSC scans with rate  $10\text{ K min}^{-1}$ ;

<sup>b</sup> The SmA-Iso transition in this case was determined using POM.

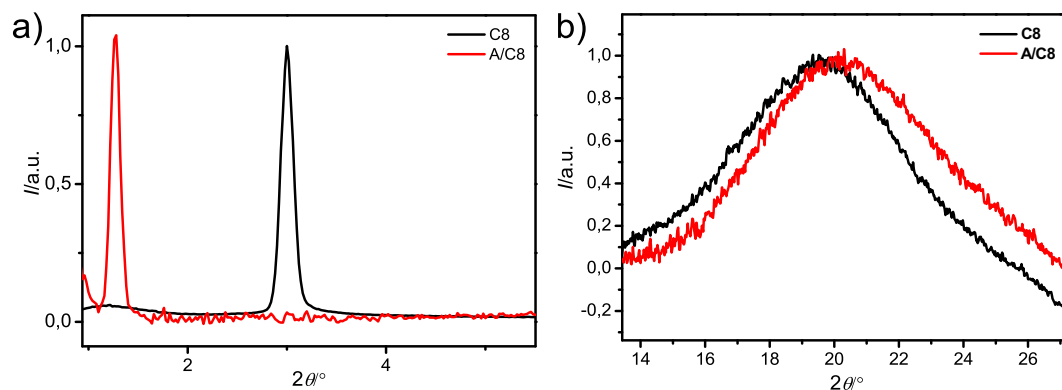


Fig. 3. X-ray powder patterns in the SmA phase of **C8** at  $T = 120$  °C and the halogen-bonded complex **A/C8** at  $T = 100$  °C: a) SAXD and b) WAXD.

infrared (FTIR) spectroscopy and X-ray diffraction measurements (XRD) as discussed below.

### 3. Results and discussion

#### 3.1. Characterization methods

Thin layer chromatography (TLC) was performed on aluminium sheet precoated with silica gel. Analytical quality chemicals were obtained from commercial sources and used as obtained. The solvents were dried using the standard methods when required. The purity and the chemical structures of all compounds synthesized were confirmed by the spectral data. The structure characterization of the synthesized compounds is based on  $^1\text{H}$  NMR,  $^{13}\text{C}$  NMR and  $^{19}\text{F}$  NMR (Varian

Unity 400 spectrometers, in  $\text{CDCl}_3$  solution, with tetramethylsilane as internal standard).

Infrared absorption spectra were measured in dry KBr with a Perkin-Elmer B25 spectrophotometer.

The mesophase behaviour and transition temperatures of the supramolecular complexes were measured using a Mettler FP-82 HT hot stage and control unit in conjunction with a Nikon Optiphot-2 polarizing microscope. The associated enthalpies were obtained from DSC thermograms which were recorded on a Perkin-Elmer DSC-7, heating and cooling rate:  $10\text{ K min}^{-1}$ .

The X-ray diffraction patterns were recorded with a 2D detector (Vantec 500, Bruker). Ni filtered and pin hole collimated  $\text{CuK}\alpha$  radiation was used. For the wide angle X-ray diffraction (WAXD) measurements the exposure time was 15 min and the sample to detector distance was 9.5 cm, small angle X-ray diffraction (SAXD) measurements were

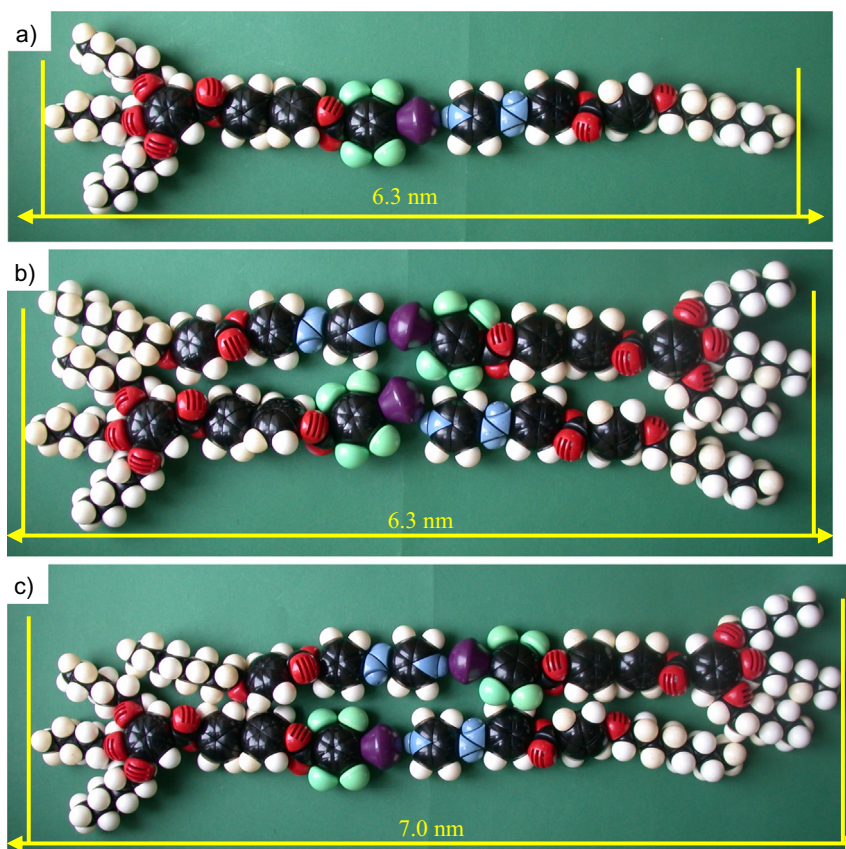


Fig. 4. Space-filling calotte molecular models (CPK models [48]) of a) the halogen-bonded complex **A/C8** and b, c) the distinct arrangements of the complexes in the SmA phase.

carried out with an exposure time of 30 min and a sample to detector distance of 27.40 cm. Uniform orientation was achieved by alignment in a magnetic field ( $B \approx 1$  T) using thin capillaries. The samples were held on a temperature-controlled heating stage.

### 3.2. Liquid crystalline behaviour

Before discussing the phase behaviour of the newly prepared supramolecular polycatenars it should be noted that none of the individual starting azopyridines **Bn** exhibit liquid crystalline properties; all of them are nonmesomorphic compounds having melting points between  $\sim 71$  °C and  $74$  °C [34]. On the other hand compounds **Cn** with an additional benzene ring are mesomorphic exhibiting nematic and SmA phases for the shorter homologues ( $n = 8, 10$ ) and SmA only for the longer homologues ( $n = 12, 14$ ) [39], while the halogen bond donor **A** is nonmesomorphic with relatively low melting point  $\sim 46$ – $48$  °C. For the sake of comparison, the transition temperatures of the pure azopyridine derivatives **Bn** and **Cn** are collected in Table 1.

The transition temperatures of the halogen-bonded aggregates (**A/Bn** and **A/Cn**) are represented graphically in Fig. 1 and numerically in Table 2. The first indication for the formation of the supramolecular complexes was the disappearance of the transition peaks for the individual components in the DSC heating and cooling runs obtained for the newly formed complexes (compare Tables 1 and 2 and see Fig. 2 as an example).

Mixing the non-mesomorphic components **A** and **Bn** together results in complexes **A/Bn** formation which exhibit an induced monotropic SmA phase (Fig. S5) for all complexes with melting temperatures close to those of the pure **Bn** derivatives (Table 2). This implies that the halogen bond formed between the azopyridines **Bn** and compound **A** is responsible for the liquid crystalline behaviour of the supramolecules **A/Bn**. Using compounds **Cn** with an additional benzene ring for complex formation with compound **A** results in removing of the nematic phases exhibited by the pure components **C8** and **C10** with short alkyl chains and SmA phase stabilization.

As can be seen from Fig. 2 the SmA-Iso transition for the complex **A/C12** on cooling is broad and on heating it appears to be even broader, that no enthalpy is measurable on heating and the transition can be only detected by POM. Relatively broad biphasic regions can be observed for all of the prepared complexes and therefore the SmA-Iso transitions are given in Table 2 as temperature ranges instead of single values. This is in agreement with previously reported halogen-bonded LCs. In general broad LC-Iso transition were observed especially for the SmA-Iso transitions [17,44–46]. One reason could be that slight deviation of the molar ratio from being precisely 1:1, leading to a two component system composed of the 1:1 complex and the slight excess (<2%) of one of the components, but why is this not observed for the related hydrogen bonded complexes [34]? That no thermal decomposition takes place during the mixing of the components was checked by TLC (see Fig. S6) and is also obvious from the NMR spectra (Fig. S1). So, it appears that this might be an inherent specific feature of halogen bonded smectic LCs; a possible explanation is given further below.

The mesophase type observed for **A/Cn** complexes is the same as that exhibited by **A/Bn** aggregates, i.e. SmA phase. However, in the case of **A/Cn** complexes, the observed SmA phases are enantiotropic phases with higher stabilities. Moreover, the SmA phase ranges of all **A/Cn** complexes extend over wide temperature ranges compared to those exhibited by **A/Bn** supramolecules or by the halogen bond acceptors **Cn** [39]. The maximum value of the LC phase range as measured on cooling is  $\sim 91$  °C for **A/C8** and lowest value is  $\sim 54$  °C for **A/C14** with longest chain on the azopyridine derivative **C14** (Table 2 and Fig. 1). This indicates that the additional benzene ring in case of **A/Cn** complexes results in increasing mesophase stability. To the best of our knowledge, the SmA phase range of **A/C8** is the widest among all of the previously reported supramolecular perfluoroarylhalide/pyridine based halogen-bonded LCs [15,19]. It should be noted that a similar SmA phase range

of  $\sim 88$  °C was reported for a much smaller rod-like supramolecular complex formed between molecular bromine and the azopyridine **B12** [19], however this is another type of halogen bonding.

### 3.3. X-ray diffraction

To further confirm the complex formation between the halogen donor **A** and the azopyridine derivatives **Bn** or **Cn**, X-ray diffraction (XRD) of a surface aligned sample of **C8** as a pure material and after complexation i.e. **A/C8** was measured as a representative example (Fig. 3). The diffuse wide angle scattering of **C8** at  $d = 0.46$  nm with maxima perpendicular to the direction of the layer reflection (see Fig. S5) indicates the presence of a LC phase with a non-tilted organization of the molecules i.e. SmA phase [47]. In the small angle region, the layer reflection corresponding to  $d = 2.94$  nm which is in the range of the length of **C8**, with  $L = 2.9$  nm in the most extended conformation with all-*trans* conformation of the alkyl chains confirms the presence of a monolayer SmA phase with antiparallel side-by-side packing of the azopyridine units in the rod-layers and almost complete intercalation of the alkyl chains in the aliphatic layers. A similar diffraction pattern was also observed for the complex **A/C8**, but in this case with layer distance,  $d = 6.95$  nm which is slightly larger than the molecular length of the halogen-bonded complex **A/C8** ( $L = 6.3$  nm calculated with CPK model, Fig. 4). The shift of the layer reflection clearly confirms complex formation. There is also a slight shift of the maximum of the

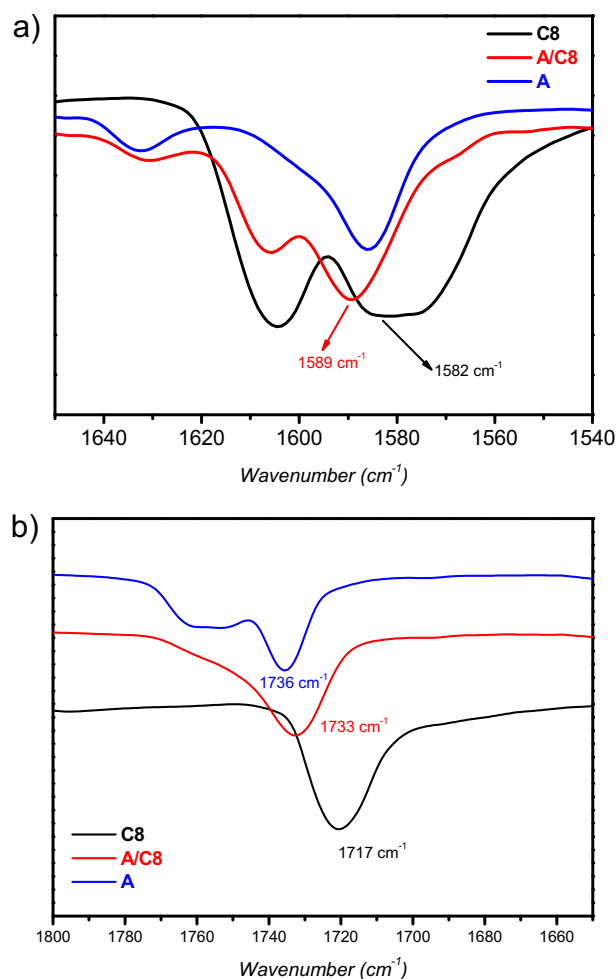


**Fig. 5.** FTIR spectra of the supramolecular complex **A/C8** (red) and its complementary components **A** (blue) and **C8** (black): a) enlarged area between  $1540$   $\text{cm}^{-1}$  and  $1650$   $\text{cm}^{-1}$ ; b) enlarged area between  $1640$   $\text{cm}^{-1}$  and  $1800$   $\text{cm}^{-1}$ . (For interpretation of the references to colour in this figure legend, the reader is referred to the web version of this article.)

wide angle scattering to smaller distances ( $d = 0.45$  nm) due to the reduction of the contribution of the tetrafluorinated benzene to the mean distance between the molecules. The fact that the  $d$  value measured by XRD slightly exceeds the length of that calculated for the complex with space filling molecular models [48] indicates that the molecules adopt an antiparallel packing with a slight shift of the aromatic cores with respect to each other. Probably the bulky and electron deficit tetrafluorinated benzene ring prefers to be organized not between the electron deficient pyridines, but rather between the more electron rich benzene rings of the azopyridine units. If such an organization with interdigitation of the alkyl chain of **C8** between the aromatic cores of the component **A** is assumed a layer distance of 7.0 nm would result, which is close to the experimentally observed value of  $d = 6.95$  nm (see Fig. 4b, c). In addition this organization reduces the interface curvature between the polyaromatic cores and the alkyl chains and this allows the organization in layers.

### 3.4. IR spectra

FTIR spectroscopy is well known as an effective tool for the investigation of intermolecular interactions such as hydrogen [47,49] or halogen bonding [16,50]. Fig. 5a, b show the IR spectra at two different regions for the complex **A/C8** as a representative example (for the complete range of the IR spectra see Fig. S4).

In case of pyridine based derivatives, up to three characteristic stretching bands for the pyridine skeleton could be observed in the IR spectra in the range 1540–1640  $\text{cm}^{-1}$ . The most sensitive band is the one at  $\sim 1586$   $\text{cm}^{-1}$  shifting to higher values of wavenumbers (i.e. blue shift) due to interactions with very small shift due to halogen bonding [16,44]. This behaviour was typically observed with our supramolecular complexes, where the band observed at 1582  $\text{cm}^{-1}$  for the pure azopyridine **C8** (black curve in Fig. 5b) is blue shifted to 1589  $\text{cm}^{-1}$

(red curve in Fig. 5a). Moreover, the ester carbonyl band of the pure halogen bond donor **A** is observed at 1736  $\text{cm}^{-1}$  and that of **C8** is observed at 1717  $\text{cm}^{-1}$ , while a broad carbonyl band is recorded for the complex **A/C8** at wavenumber  $\sim 1733$   $\text{cm}^{-1}$  (Fig. 5b) confirming the formation of the halogen bond between the complementary components.

Whereas IR confirms complex formation in the crystalline state, XRD investigations confirm that also in the LC state halogen bonded complexes should be formed. On the other hand it is shown by NMR that in solution the complexes are completely dissociated into the individual components. It is assumed that this dissociation should also be of relevance for the isotropic liquid state. Therefore, it appears that mesophase formation and formation of halogen bonded complexes are coupled in a cooperative way, i.e. the orientational and positional order in the LC state favours the formation of the halogen bonded complexes and the other way around, the halogen bonded complexes thus formed favour mesophase formation due to the increased aspect ratio of the resulting linear dimeric complexes. However, for the polycatenar aggregates investigated here the aggregate shape with one overcrowded end is in competition with lamellar self-assembly. Therefore, there is only a weak driving force for LC self-assembly. As the halogen bonding is relatively weak the cooperativity is not well developed and the LC phase stability is comparatively low (see comparison with hydrogen bonded aggregates below). It is speculated that the coexistence of different species (components **A**, **B/C** dimeric halogen bonded aggregates, larger aggregates due to  $\pi$ - $\pi$  interactions of the electron deficit perfluorinated aromatics) at the LC-Iso transition could contribute to the relatively broad biphasic SmA-Iso ranges.

### 4. Photosensitivity

The prepared supramolecular complexes are photosensitive and undergo a fast and reversible isothermal phase transition upon illumination

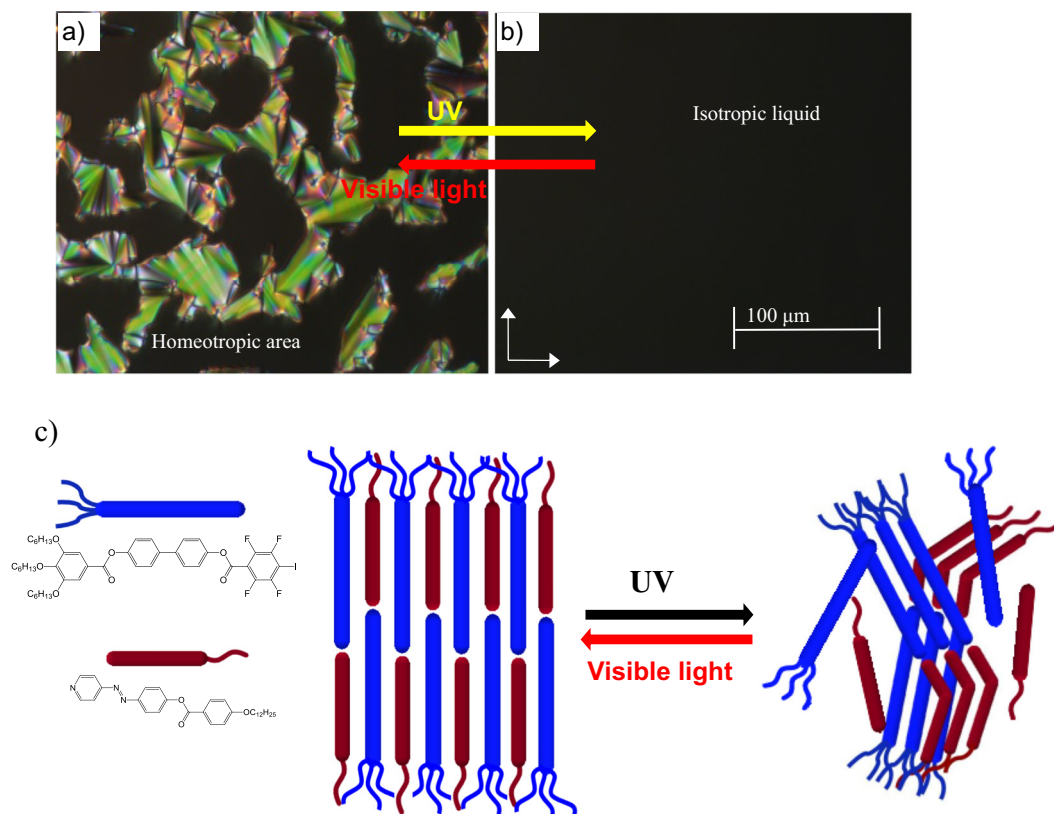
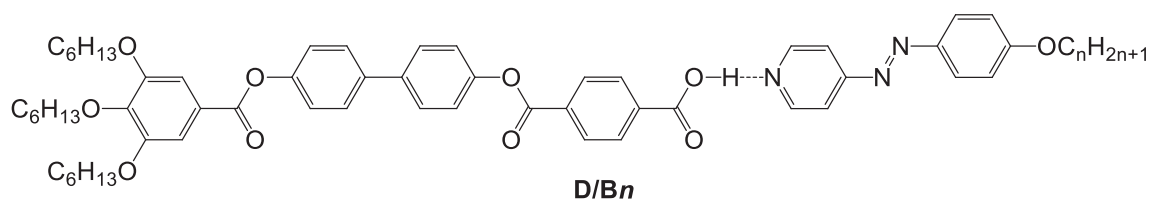


**Fig. 6.** Textures of the complex **A/C12** under crossed polarizers: a) in the SmA phase at  $T = 100$  °C before irradiation with UV light and b) after irradiation with UV light indicating the transformation from the SmA phase to the isotropic liquid phase; the dark areas in a) represent homeotropic areas of SmA phase. c) Schematic illustration of the molecules in the SmA and the isotropic liquid phases.



**n = 8:** Cr 124 Cub ~187 Cub<sup>[\*]</sup> 196 Iso<sup>[\*]</sup> 200 Iso

**n = 10:** Cr<sub>1</sub> 115 Cr<sub>2</sub> 128 Cub<sup>[\*]</sup> 201 Iso

**n = 12:** Cr 123 Cub<sup>[\*]</sup> 191 Iso

**n = 14:** Cr 92 Cub<sup>[\*]</sup> 184 Iso

**Scheme 2.** Supramolecular hydrogen-bonded polycatenars **D/Bn** with the phase sequence and transition temperatures (°C) [34]. Abbreviations: Cub = achiral cubic phase; Cub<sup>[\*]</sup> = chiral cubic phase; Iso<sup>[\*]</sup> = chiral isotropic liquid phase.

with a laser pointer (405 nm, 5 mW/mm<sup>2</sup>) as a result of the presence of the azobenzene units in its molecular structures. We have investigated all of the complexes and they show the same behaviour over the entire SmA phase temperature range, therefore as an example the phase behaviour of **A/C12** is described here in details. Fig. 6a shows the characteristic focal conic fan textures of the SmA phase, coexisting with regions exhibiting homogenous alignment i.e. appearing black between crossed polarizers prior to the UV irradiation. Under UV illumination, the birefringent areas completely disappeared within <3 s (Fig. 6b), indicating a fast and efficient photoinduced phase transition into an isotropic liquid state. On switching off the UV source the dark texture converted back to the original SmA texture in few seconds (<3 s, see also the supported video). As illustrated in Fig. 6c; the SmA-isotropic liquid phase transition achieved upon UV irradiation is a result of *trans-cis* photoisomerization of the azobenzene units, where the molecules are in the more stable *trans* form of the azopyridines and having a rodlike shape, which stabilizes the arrangement of the supramolecules in the SmA phase. Under illumination the azopyridines exist in bent shape form due to the conversion to the less stable *cis* form of the azo units which tends to destabilise the LC phase. This results in vanishing of the SmA phase under UV irradiation and rapid conversion to the isotropic liquid state.

### 5. Comparison with related hydrogen-bonded polycatenars

By comparing the phase behaviour of the halogen-bonded supramolecular polycatenars reported herein **A/Bn** with the recently reported supramolecular polycatenars **D/Bn** (Scheme 2) with the same number of aromatics and driven by hydrogen-bonding between a taper shaped benzoic acid derivative (**D**) and the linear azopyridine derivatives **Bn** [34] we can conclude the following.

In case of the halogen-bonded **A/Bn** complexes the liquid crystalline phases are monotropic SmA phases, while those of the hydrogen-bonded **D/Bn** complexes are enantiotropic cubic phases in addition to mirror symmetry broken chiral isotropic liquid phases [34]. Additionally, the melting and clearing temperatures of the **D/Bn** complexes are much higher compared to those of the **A/Bn** complexes (compare Scheme 2 and Table 2). This is attributed to the large size of the four lateral fluorine atoms replacing the H-atoms at the central benzene ring in case of the halogen-bonded complexes. The thus increased cross sectional area of the fluorinated aromatic cores leads to a reduction of the interface curvature between aromatics and aliphatics and this is responsible of the formation of only lamellar phases rather than bicontinuous cubic phases. In addition, the reduced mesophase stability of the halogen bonded complexes is partly attributed to the steric distortion of the parallel packing of the rod-like cores by the bulky fluorines [51]. Additional contributions might result from the distinct strength of the intermolecular interactions and that hydrogen bonding contributes to core polarity which increases the nano-segregation from the lipophilic alkyl chains, additionally contributing to mesophases stabilization.

Moreover, fast and reversible photoswitching in the bulk state between the lamellar SmA phase and the isotropic liquid was successfully achieved in case of halogen-bonded complexes which was not possible between the cubic phase and the isotropic liquid phase in the case of the tetracatenars **D/Bn** due to a kinetic hindrance of photoisomerization by the more restricted helical packing in the cubic phases [52,53]. Therefore, both halogen and hydrogen bonding interaction represent alternative tools for inducing different types of photosensitive liquid crystalline phases in supramolecular LC systems.

### 6. Summary and conclusion

In summary, we have reported herein the design and synthesis of the first examples of photoswitchable halogen bonded azobenzene-based polycatenar liquid crystals. The formation of the supramolecular complexes was confirmed by DSC, POM, FTIR and XRD. In our materials, fluorination plays an important role as it strengthens the halogen bond formation. The materials showed induced monotropic SmA phases upon mixing nonmesomorphic components (**A/Bn** supramolecules) and enantiotropic SmA phases with high stability on mixing the nonmesomorphic component **A** with the mesomorphic azopyridines **Cn** (**A/Cn** supramolecules). Moreover, all of the prepared complexes show fast and reversible photoinduced SmA-Iso phase transitions due to *trans-cis* photoisomerization of the azopyridine units. In all cases, the crystallization temperatures are suppressed compared to the pure azopyridine derivatives (**Bn** and **Cn**) and the LC phases can be observed close to room temperature ~30 °C (**A/C8** and **A/C10**). To the best of our knowledge, the existence ranges of the enantiotropic SmA phases of **A/Cn** complexes (e.g. 91 K for **A/C8**) are the widest ranges reported up to date for SmA phases exhibited by perfluoroaryliodide based supramolecular halogen bonded LCs [19,54]. Finally, the possibilities provided by phase modulation by interaction with visible and UV light are of great importance for production of functional materials for technological applications [55].

Supplementary data to this article can be found online at <https://doi.org/10.1016/j.molliq.2018.12.088>.

### References

- [1] S. Yagai, A. Kitamura, Recent advances in photoresponsive supramolecular self-assemblies, *Chem. Soc. Rev.* 37 (2008) 1520–1529.
- [2] A. Beharry, G.A. Woolley, Azobenzene photoswitches for biomolecules, *Chem. Soc. Rev.* 40 (2011) 4422–4437.
- [3] T. Kato, J. Uchida, T. Ichikawa, T. Sakamoto, Functional liquid crystals towards the next generation of materials, *Angew. Chem. Int. Ed.* 57 (2018) 4355–4371.
- [4] M. Bremer, P. Kirsch, M. Klasen-Memmer, K. Tarumi, The TV in your pocket: development of liquid-crystal materials for the new millennium, *Angew. Chem. Int. Ed.* 52 (2013) 8880–8896.
- [5] D.W. Bruce, Liquid crystals formed from specific intermolecular interactions, in: P.A. Gale, J.W. Steed (Eds.), *Supramolecular Chemistry: From Molecules to Nanomaterials*, Wiley, Oxford 2012, pp. 3493–3514.

- [6] C.M. Paleos, D. Tsiourvas, Supramolecular hydrogen-bonded liquid crystals, *Liq. Cryst.* 28 (2001) 1127–1161.
- [7] C. Tschierske, Development of structural complexity by liquid-crystal self-assembly, *Angew. Chem. Int. Ed.* 52 (2013) 8828–8878.
- [8] T. Kato, J.M.J. Frechet, A new approach to mesophase stabilization through hydrogen bonding molecular interactions in binary mixtures, *J. Am. Chem. Soc.* 111 (1989) 8533–8534.
- [9] T. Kato, J.M.J. Frechet, Stabilization of a liquid-crystalline phase through noncovalent interaction with a polymer side chain, *Macromolecules* 22 (1989) 3818–3819.
- [10] T. Kato, H. Adachi, A. Fujishima, J.M. Frechet, Self-assembly of liquid crystalline complexes having angular structures through intermolecular hydrogen bonding, *Chem. Lett.* 21 (1992) 265–268.
- [11] L.C. Gilday, S.W. Robinson, T.A. Barendt, M.J. Langton, B.R. Mullaney, P.D. Beer, Halogen bonding in supramolecular chemistry, *Chem. Rev.* 115 (2015) 7118–7195.
- [12] G. Cavallo, P. Metrangolo, R. Milani, T. Pilati, A. Priimagi, G. Resnati, G. Terraneo, The halogen bond, *Chem. Rev.* 116 (2016) 2478–2601.
- [13] H. Wang, H.K. Bisoyi, L. Wang, A.M. Urbas, T.J. Bunning, Q. Li, Photochemically and thermally driven full-color reflection in a self-organized helical superstructure enabled by a halogen-bonded chiral molecular switch, *Angew. Chem. Int. Ed.* 57 (2018) 1627–1631.
- [14] H.L. Nguyen, P.N. Horton, M.B. Hursthouse, A.C. Legon, D.W. Bruce, Halogen bonding: a new interaction for liquid crystal formation, *J. Am. Chem. Soc.* 126 (2004) 16–17.
- [15] D.W. Bruce, P. Metrangolo, F. Meyer, T. Pilati, C. Präsang, G. Resnati, G. Terraneo, S.G. Wainwright, A.C. Whitwood, Structure–function relationships in liquid-crystalline halogen-bonded complexes, *Chem. Eur. J.* 16 (2010) 9511–9524.
- [16] L. González, N. Gimeno, R.M. Tejedor, V. Polo, M.B. Ros, S. Uriel, J.L. Serrano, Halogen-bonding complexes based on bis(iodoethynyl)benzene units: a new versatile route to supramolecular materials, *Chem. Mater.* 25 (2013) 4503–4510.
- [17] G. Cavallo, G. Terraneo, A. Monfredini, M. Saccone, A. Priimagi, T. Pilati, G. Resnati, P. Metrangolo, D.W. Bruce, Superfluorinated ionic liquid crystals based on supramolecular, halogen-bonded anions, *Angew. Chem. Int. Ed.* 55 (2016) 6300–6304.
- [18] A. Priimagi, M. Saccone, G. Cavallo, A. Shishido, T. Pilati, P. Metrangolo, G. Resnati, Photoalignment and surface-relief-grating formation are efficiently combined in low-molecular-weight halogen-bonded complexes, *Adv. Mater.* 24 (2012) OP345–OP352.
- [19] Y. Chen, H. Yu, L. Zhang, H. Yang, Y. Lu, Photoresponsive liquid crystals based on halogen bonding of azopyridines, *Chem. Commun.* 50 (2014) 9647–9649.
- [20] F. Fernandez-Palacio, M. Poutanen, M. Saccone, A. Siiskonen, G. Terraneo, G. Resnati, O. Ikkala, P. Metrangolo, A. Priimagi, Efficient light-induced phase transitions in halogen-bonded liquid crystals, *Chem. Mater.* 28 (2016) 8314–8321.
- [21] M. Pfletscher, S. Hölscher, C. Wölper, M. Mezger, M. Giese, Structure–property relationships in hydrogen-bonded liquid crystals, *Chem. Mater.* 29 (2017) 8462–8471.
- [22] M. Spengler, R.Y. Dong, C.A. Michal, M. Pfletscher, M. Giese, Fluorination of supramolecular liquid crystals – tuning tool and analytical probe, *J. Mater. Chem. C* 5 (2017) 2235–2239.
- [23] M. Giese, T. Krappitz, R.Y. Dong, C.A. Michal, W.Y. Hamad, B.O. Patrick, M.J. MacLachlan, Tuning the photonic properties of chiral nematic mesoporous organosilica with hydrogen-bonded liquid-crystalline assemblies, *J. Mater. Chem. C* 3 (2015) 1537–1545.
- [24] H.M.D. Bandarab, S.C. Burdette, Photoisomerization in different classes of azobenzene, *Chem. Soc. Rev.* 41 (2012) 1809–1825.
- [25] M. Alaasar, Azobenzene-containing bent-core liquid crystals: an overview, *Liq. Cryst.* 43 (2016) 2208–2243.
- [26] H.K. Bisoyi, Q. Li, Light-driven liquid crystalline materials: from photo-induced phase transitions and property modulations to applications, *Chem. Rev.* 116 (2016) 15089–15166.
- [27] M. Alaasar, M. Prehm, Y. Cao, F. Liu, C. Tschierske, Spontaneous mirror-symmetry breaking in isotropic liquid phases of photoisomerizable achiral molecules, *Angew. Chem. Int. Ed.* 128 (2016) 320–324.
- [28] M. Alaasar, S. Poppe, Q. Dong, F. Liu, C. Tschierske, Isothermal chirality switching in liquid-crystalline azobenzene compounds with non-polarized light, *Angew. Chem. Int. Ed.* 56 (2017) 10801–10805.
- [29] M. Zaremba, V. Siksnys, Molecular scissors under light control, *Proc. Natl. Acad. Sci. U. S. A.* 107 (2010) 1259–1260.
- [30] K.M. Lee, T.J. White, Photomechanical response of composite structures built from azobenzene liquid crystal polymer networks, *Polymers* 3 (2011) 1447–1457.
- [31] J. Garcia-Amorós, M. Reig, M.C.R. Castro, A. Cuadrado, M.M.M. Raposo, D. Velasco, Molecular photo-oscillators based on highly accelerated heterocyclic azo dyes in nematic liquid crystals, *Chem. Commun.* 50 (2014) 6704–6706.
- [32] T. Fehrentz, M. Schönberger, D. Trauner, Optochemical genetics, *Angew. Chem. Int. Ed.* 50 (2011) 12156–12182.
- [33] M. Pfletscher, C. Wölper, J.S. Gutmann, M. Mezger, M. Giese, A modular approach towards functional supramolecular aggregates – subtle structural differences inducing liquid crystallinity, *Chem. Commun.* 52 (2016) 8549–8552.
- [34] M. Alaasar, S. Poppe, Q. Dong, F. Liu, C. Tschierske, Mirror symmetry breaking in cubic phases and isotropic liquids driven by hydrogen bonding, *Chem. Commun.* 52 (2016) 13869–13872.
- [35] C. Tschierske, Fluorinated liquid crystals: design of soft nanostructures and increased complexity of self-assembly by perfluorinated segments, *Top. Curr. Chem.* 318 (2011) 1–108.
- [36] M. Hird, Fluorinated liquid crystals – properties and applications, *Chem. Soc. Rev.* 36 (2007) 2070–2095.
- [37] M. Alaasar, M. Prehm, S. Poppe, C. Tschierske, Development of polar order by liquid-crystal self-assembly of weakly bent molecules, *Chem. Eur. J.* 23 (2017) 5541–5556.
- [38] M. Alaasar, M. Prehm, C. Tschierske, Mirror symmetry breaking in fluorinated bent-core mesogens, *RSC Adv.* 6 (2016) 82890–82899.
- [39] M. Alaasar, C. Tschierske, Nematic phases driven by hydrogen-bonding in liquid crystalline nonsymmetric dimers, *Liq. Cryst.* (2018) <https://doi.org/10.1080/02678292.2018.1476740>.
- [40] J.-S. Seo, Y.-S. Yoo, M.-G. Choi, 1,1'-Disubstituted ferrocene containing hexacatenar thermotropic liquid crystals, *J. Mater. Chem.* 11 (2001) 1332–1338.
- [41] A.-C.C. Carlsson, A.X. Veiga, M. Erdélyi, Halogen bonding in solution, in: P. Metrangolo, G. Resnati (Eds.), *Halogen Bonding II. Impact on Materials Chemistry and Life Sciences*, Top. Curr. Chem., 359, Springer, Heidelberg 2015, pp. 49–76, <https://doi.org/10.1007/978-3-319-15732-0>.
- [42] M.G. Sarwar, B. Dragisic, L.J. Salsberg, C. Gouliaras, M.S. Taylor, Thermodynamics of halogen bonding in solution: substituent, structural and solvent effects, *J. Am. Chem. Soc.* 132 (2010) 1646–1653.
- [43] B. Hawthorne, H. Fan-Hagenstein, E. Wood, J. Smith, T. Hanks, Study of the halogen bonding between pyridine and perfluoroalkyl iodide in solution phase using the combination of FTIR and 19F NMR, *Int. J. Spectrosc.* (2013) <https://doi.org/10.1155/2013/216518>.
- [44] J. Xu, X. Liu, J.K.-P. Ng, T. Lin, C. He, Trimeric supramolecular liquid crystals induced by halogen bonds, *J. Mater. Chem.* 16 (2006) 3540–3545.
- [45] Y. Wang, H. Shang, B. Li, H. Zhang, S. Jiang, Modulating the assembly of N-benzylendeaniline by halogen bonding: crystal, cocrystal and liquid crystals, *CrystEngComm* 19 (19) (2017) 3801–3807.
- [46] M. Saccone, F.F. Palacio, G. Cavallo, V. Dichiarante, M. Virkki, G. Terraneo, A. Priimagi, P. Metrangolo, Photoresponsive ionic liquid crystals assembled via halogen bond: en route towards light-controllable ion transporters, *Faraday Discuss.* 203 (2017) 407–422.
- [47] M. Alaasar, C. Tschierske, M. Prehm, Hydrogen-bonded supramolecular complexes formed between isophthalic acid and pyridine-based derivatives, *Liq. Cryst.* 38 (2011) 925–934.
- [48] R.B. Corey, L. Pauling, W. Koltun, Molecular models of amino acids, peptides, and proteins, *Rev. Sci. Instrum.* 8 (1953) 621–627.
- [49] A.G. Martinez-Felipe, J.P. Cook, R. Abberley, J.M.D. Walker, C.T. Imrie Storey, An FT-IR spectroscopic study of the role of hydrogen bonding in the formation of liquid crystallinity for mixtures containing bipyridines and 4-pentoxybenzoic acid, *RSC Adv.* 6 (2016) 108164–108179.
- [50] D. Bruce, P. Metrangolo, F. Meyer, C. Präsang, G. Resnati, G. Terraneo, A. Whitwood, Mesogenic, trimeric, halogen-bonded complexes from alkoxystilbazoles and 1,4-diiodotetrafluorobenzene, *New J. Chem.* 32 (2008) 477–482.
- [51] A.I. Smirnova, B. Heinrich, B. Donnio, D.W. Bruce, The influence of lateral fluorination and cyanation on the mesomorphism of polycatenar mesogens and the nature of the SmC phase therein, *RSC Adv.* 5 (2015) 75149–75159.
- [52] C. Dressel, F. Liu, M. Prehm, X. Zeng, G. Ungar, C. Tschierske, Dynamic mirror-symmetry breaking in bicontinuous cubic phases, *Angew. Chem. Int. Ed.* 53 (2014) 13115–13120.
- [53] , However a light induced switching from a lamellar phase into a cubic phase appears to be possible, see: A. Nagai, H. Kondo, Y. Miwa, T. Kondo, S. Kutsumizu, Y. Yamamura, K. Saito, Optical switching between liquid-crystalline assemblies with different structural symmetries and molecular orders, *Bull. Chem. Soc. Jpn.* 91 (2018) 1652–1659.
- [54] M. Du, L. Li, J. Zhang, K. Li, M. Cao, L. Mo, G. Hu, Y. Chen, H. Yu, H. Yang, Photoresponsive iodine-bonded liquid crystals based on azopyridine derivatives with a low phase transition temperature, *Liq. Cryst.* (2018) <https://doi.org/10.1080/02678292.2018.1468040>.
- [55] M. Saccone, G. Cavallo, P. Metrangolo, G. Resnati, A. Priimagi, Halogen-bonded photoresponsive materials, in: P. Metrangolo, G. Resnati (Eds.), *Halogen Bonding II. Impact on Materials Chemistry and Life Sciences*, Top. Curr. Chem., 359, Springer, Heidelberg 2015, pp. 147–166, <https://doi.org/10.1007/978-3-319-15732-0>.

# Mirror Symmetry Breaking and Network Formation in Achiral Polycatenars with Thioether Tail

Mohamed Alaasar,<sup>\*[a, b]</sup> Ahmed F. Darweesh,<sup>[b]</sup> Xiaoqian Cai,<sup>[c]</sup> Feng Liu,<sup>[c]</sup> and Carsten Tschierske<sup>\*[a]</sup>

**Abstract:** Mirror symmetry breaking in systems composed of achiral molecules is of importance for the design of functional materials for technological applications as well as for the understanding of the mechanisms of spontaneous emergence of chirality. Herein, we report the design and molecular self-assembly of two series of rod-like achiral polycatenar molecules derived from a  $\pi$ -conjugated 5,5'-diphenyl-2,2'-bithiophene core with a fork-like triple alkoxyated end and a variable single alkylthio chain at the other end. In both series of liquid crystalline materials, differing in the chain length at the trialkoxyated end, helical self-assembly of the  $\pi$ -con-

jugated rods in networks occurs, leading to wide temperature ranges ( $> 200$  K) of bicontinuous cubic network phases, in some cases being stable even around ambient temperatures. The achiral bicontinuous cubic  $la\bar{3}d$  phase (gyroid) is replaced upon alkylthio chain elongation by a spontaneous mirror symmetry broken bicontinuous cubic phase ( $I23$ ) and a chiral isotropic liquid phase ( $Iso_1^{*}$ ). Further chain elongation results in removing the  $I23$  phase and the re-appearance of the  $la\bar{3}d$  phase with different pitch lengths. In the second series an additional tetragonal phase separates the two cubic phase types.

## Introduction

Since their discovery in 1888, liquid crystalline (LC) materials have undergone an astonishing development to the present day. They are of great interest as stimuli-responsive and switchable optical materials in displays,<sup>[1]</sup> photonics,<sup>[2]</sup> in sensor,<sup>[3,4]</sup> and telecommunication applications,<sup>[5]</sup> for ion conducting materials,<sup>[6]</sup> in organic electronics and photovoltaics,<sup>[7–9]</sup> and in biomedicine for targeted drug delivery.<sup>[10–12]</sup> LC are usually composed of an anisometric rigid rod-like or disc-like core, providing orientational order, combined with a distinct number of flexible alkyl chains, providing the mobility. In most cases the alkyl chains are connected by ether linkages to the rigid units. In contrast to these alkyl(oxy) chains the related

alkylthio chains were much less used, but nevertheless replacing alkyl or alkoxy by alkylthio chains can often lead to interesting new properties. For example, hexa(alkylthio) triphenylenes were the first columnar LC for which photoconducting properties were reported.<sup>[13]</sup> Alkylthio tails were also used to induce columnar and cubic phase formation in bent-core mesogens.<sup>[14]</sup> 4-(Alkylthio)benzoic acids lead to enhanced cybotactic nematic phase ranges compared to the related 4-*n*-alkoxy-substituted compounds in hydrogen-bonded supramolecular systems.<sup>[15,16]</sup> More recently, the thioether linkage was shown to be advantageous for the design of mesogenic dimers with wide ranges of the twist-bend nematic phase.<sup>[17,18]</sup> Herein the effect of replacing alkyloxy chains of polycatenar LCs by alkylsulfanyl (alkylthio) chains on LC self-assembly and spontaneous mirror symmetry breaking is reported. Polycatenar LCs are rod-like mesogens with multi terminal chains, providing a transition between lamellar and columnar self-assembly by modification of the chain volume. These polycatenars have received significant interests due to their rich mesomorphism including nematic, smectic, bicontinuous cubic ( $Cub_{bi}$ ) and columnar mesophases.<sup>[19–27]</sup>  $Cub_{bi}$  phases are optically isotropic LC with cubic 3D lattice, in most cases occurring at the transition between lamellar and columnar modes of self-assembly as a result of the increasing interface curvature upon growing alkyl chain volume.<sup>[28–33]</sup> The double gyroid with space group  $la\bar{3}d$  is the most common type of  $Cub_{bi}$  phases composed of two interwoven, but not interconnected networks with three way junctions (Figure 1a,c).<sup>[34–37]</sup> In the case of polycatenars the networks are formed by the  $\pi$ -conjugated rods, whereas the flexible chains fill the space between the networks. Because the rods are organized almost perpendicular to the local network direction, their  $\pi$ -systems can overlap and these networks provide 3D conduction pathways for charge

[a] Dr. M. Alaasar, Prof. C. Tschierske  
Institute of Chemistry  
Martin Luther University Halle-Wittenberg  
Kurt Mothes Str. 2, 06120 Halle (Saale) (Germany)  
E-mail: mohamed.alaasar@chemie.uni-halle.de  
carsten.tschierske@chemie.uni-halle.de

[b] Dr. M. Alaasar, Prof. A. F. Darweesh  
Department of Chemistry  
Faculty of Science  
Cairo University, Giza (Egypt)

[c] X. Cai, Prof. F. Liu  
State Key Laboratory for Mechanical Behavior of Materials  
Shaanxi International Research Center for Soft Matter  
Xi'an Jiaotong University, Xi'an 710049 (P. R. China)

Supporting information for this article is available on the WWW under <https://doi.org/10.1002/chem.202102226>

© 2021 The Authors. Chemistry - A European Journal published by Wiley-VCH GmbH. This is an open access article under the terms of the Creative Commons Attribution Non-Commercial NoDerivs License, which permits use and distribution in any medium, provided the original work is properly cited, the use is non-commercial and no modifications or adaptations are made.

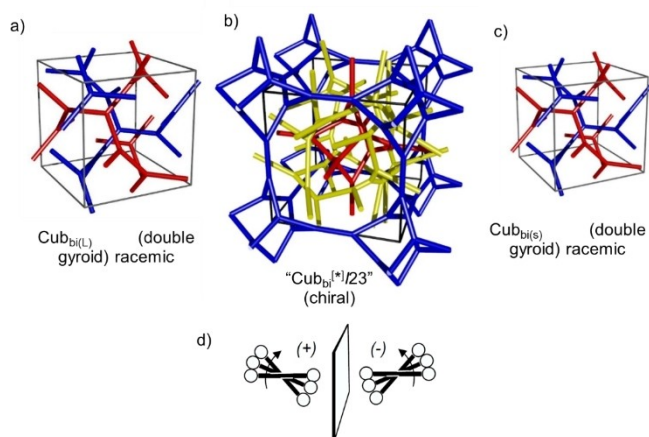


**Figure 1.** a, c) The double network gyroid with  $Ia\bar{3}d$  space group and b) the more complex triple network of the mirror symmetry broken  $I23$  phase, the two networks (blue and red) in a,c) are enantiomorphous, in b) are identical and different from the yellow one; d) the development of the helical twist by the clashing of end groups attached to rod-like cores in the networks; the twist between the molecules along the network increases from a) to c), resulting in a transition from the long pitch ( $Ia\bar{3}d_{(L)}$ ) (Low twist) via the  $I23$  lattice to the short pitch  $Ia\bar{3}d_{(S)}$  (high twist) phase. a–c) Reprinted with permission from Ref. [42, 52].

transportation (see Figure 1), which makes these  $Cub_{bi}$  phases interesting for organic electronics applications.<sup>[7,38]</sup>

In this organization of the  $\pi$ -conjugated rods perpendicular to the networks the rod-like units cannot align perfectly parallel, because the overcrowding of the ends by the multiple alkyl chains induces a twist (Figure 1d). Due to the network structure the twist sense is synchronized along the networks,<sup>[59]</sup> leading to a helical network with uniform chirality along the individual nets. In the gyroid type  $Cub_{bi}$  phase with  $Ia\bar{3}d$  space group the twist is opposite in the two interwoven networks and thus cancels out to an overall achiral structure.<sup>[39,40]</sup> However, recently it was found that there is another type of  $Cub_{bi}$  phase which is chiral and forms conglomerates of chiral domains with opposite handedness.<sup>[39–51]</sup> This is due to the triple network structure of this  $Cub_{bi}$  phase with space group  $I23$  (Figure 1b),<sup>[52]</sup> previously known as  $Im\bar{3}m$ .<sup>[53–57]</sup> In this case the network chirality cannot cancel out and a conglomerate of chiral domains is observed. It is noted that the transition from the achiral to the ambidextrous chiral cubic phase might not only be due to the transition from a racemic double network to a scalemic triple network phase. It is also possible that this transition is accompanied by a transition from an enantiophilic (racemate forming) self-assembly in the double gyroid composed of two intrinsically chiral enantiomorphous networks, to an enantiophobic (conglomerate forming) mode of self-assembly in the  $I23$  phase with three achiral networks. In the latter case the enantiophobic helix-helix interaction becomes dominating, thus leading to identical chirality in all three networks. Importantly, spontaneous mirror symmetry breaking and optical activity can be even retained in the ambidextrous chiral isotropic liquid phases ( $Iso_1^{[k]}$ ) occurring adjacent to the  $Cub_{bi}$  phases with helical network structure.<sup>[58–61]</sup>

The directed design of materials with application relevant nano-scale morphologies and molecular properties for applications requires the fundamental understanding of the structure property relationships. Especially the design of cubic phases and helical network structures showing spontaneous mirror symmetry breaking is still at the infancy and requires systematic studies.<sup>[62]</sup> In order to investigate the effect of alkythio chains on the helical self-assembly of polycatenar compounds new non-symmetric tetracatenar mesogens based on the  $\pi$ -conjugated rod-like 5,5'-diphenyl 2,2'-dithiophene unit (**A10/n** and **A6/n**) were designed, synthesized, investigated and compared with related alkoxy substituted compounds (Scheme 1).

## Experimental

### Synthesis

The synthesis of the tetracatenar phenol **6** (Scheme 1) was conducted in a similar manner to that reported before by Suzuki type boronate cross-coupling reaction,<sup>[58]</sup> while the synthesis of the 4-alkylthiobenzoic acids **8** was performed by Williamson etherification of 4-mercaptobenzoic acid with different alkyl bromides followed by hydrolysis.<sup>[15]</sup> In the final step acylation of **6** with the benzoyl chlorides **8** using triethylamine and a catalytic amount of pyridine led to the target compounds **A10/n** and **A6/n**, as described in the Supporting Information.

### Investigation methods

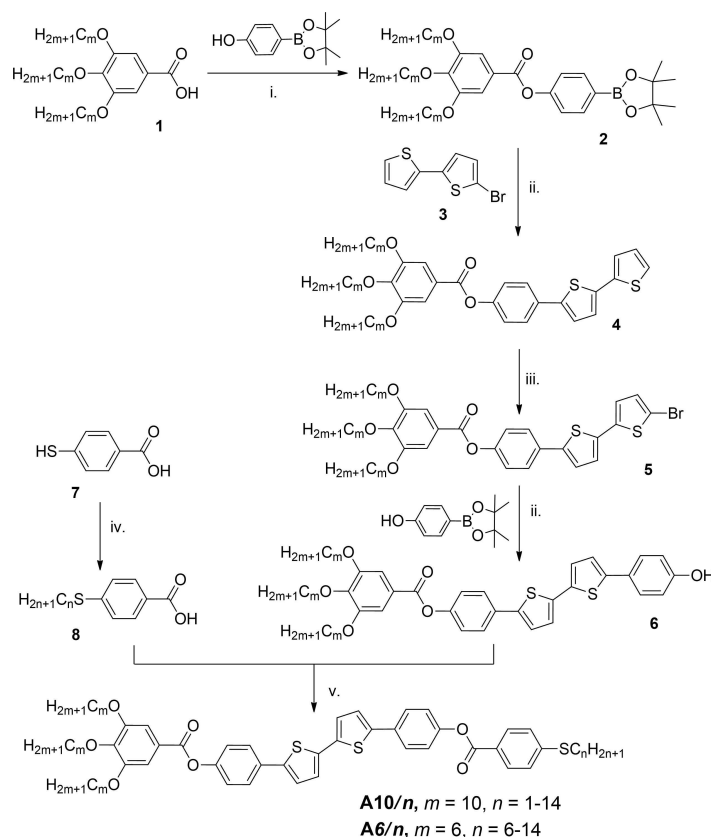
Investigation of the obtained materials was conducted by polarizing optical microscopy (POM) (Optiphot 2, Nikon microscope with a Mettler FP82HT heating stage), differential scanning calorimetry (DSC-7 and DSC-8000 Perkin Elmer, 10 K min<sup>-1</sup> peak temperatures quoted in Table 1), and X-ray diffraction (XRD). In-house XRD was carried out using  $Cu_{K\alpha}$  radiation and a Vantec 500 area detector. High-resolution small/wide-angle X-ray scattering (SAXS/WAXS) experiments were recorded on Beamline BL16B1 at Shanghai Synchrotron Radiation Facility, SSRF. Experiments were carried out on samples in 1 mm glass capillaries under the control of a modified Linkam hot stage with a thermal stability within 0.2 °C. The Pilatus 2M detector was applied in the experiments.  $\theta$  calibration and linearization were testified by using several orders of layer reflections from silver behenate and a series of  $n$ -alkanes.

## Results and Discussion

### Cubic phases

As can be concluded from Figure 2 and Table 1 all the synthesized compounds exhibit wide LC phase ranges with the type of mesophases and their ranges depending on the length of the chains at both ends of the molecules. All of the polycatenars in series **A10/n** with three terminal decyloxy chains at one end of the rod-like molecule and a growing alkythio chain at the other end exhibit  $Cub_{bi}$  phases as indicated from POM and XRD measurements. The cubic phases are characterized by their uniformly dark appearance between crossed polarizers as they are optically isotropic. The transition





**Scheme 1.** Synthesis of polycatenars under investigation. Reagents and conditions: i) DCC, DMAP, DCM, RT, stirring; ii)  $[\text{Pd}(\text{PPh}_3)_4]$ , THF/sat.  $\text{NaHCO}_3$ -solution, reflux; iii) NBS, THF, RT, absence of light; iv) 1) absolute EtOH, KOH,  $\text{H}_{2n+1}\text{C}_n\text{Br}$ , 2) NaOH solution, reflux, 3)  $\text{H}^+$ ; v) 1)  $\text{SOCl}_2$ , 2) Triethylamine, pyridine, DCM, reflux.

from the isotropic liquid to the cubic phase on cooling is identified by a sudden increase of viscosity which is associated with a DSC peak (Table 1 and Figure 3).

For all homologues, there is a 6–12 K supercooling of the Iso–Cub transition compared to the Cub–Iso transition temperature on heating which is a typical feature of cubic LC phases with 3D periodicity (Table 1).<sup>[63]</sup> A series of sharp SAXS peaks appear at the Iso–Cub<sub>bi</sub> transition, replacing the single diffuse scattering observed in the isotropic liquid state. Based on the positions of the scattering maxima two types of Cub<sub>bi</sub> phases can be distinguished. For the short and long chain compounds the two most intense scatters in the SAXS patterns can be indexed to the (211) and (220) reflections of an  $la\bar{3}d$  lattice with lattice parameters  $a_{\text{Cub}}$  around 11 nm (Figure 4a). This assignment to an  $la\bar{3}d$  lattice is in line with the absence of chiral domains in this achiral Cub<sub>bi</sub> phase (see Figure 5g,h, top right/bottom left). In contrast, all compounds with an intermediate chain length form conglomerate of chiral domains (Figure 5d–f). For this Cub<sub>bi</sub> phase the SAXS pattern can be indexed to the (321), (400), (330), (411) and (420) scatterings of an  $I23$  lattice, as shown in Figure 4d for compound **A6/10** as an example. The lattice parameter  $a_{\text{Cub}}$  is between 17.0 and 17.3 nm for compounds **A10/n**, whereas for the compounds **A6/n** with shorter apex chains it is 15.5–16.0 nm. At the  $la\bar{3}d$  to  $I23$  transitions there is a 46–58% increase of the lattice parameter,

in line with the proposed transition from a double to a triple network structure. The electron density (ED) map of this Cub<sub>bi</sub><sup>[36]</sup>/ $I23$  phase, reconstructed based on the diffraction intensities show the complex triple network structure of the  $I23$  phase of **A6/10** as example (Figure 4d).

While in the series **A10/n** the Cub<sub>bi</sub>–Iso transition temperature decreases with growing length of the alkythio chain, the phase range of the Cub<sub>bi</sub> phase at first decreases by chain elongation ( $n = 1 \rightarrow 8$ ) then it remains constant for  $n = 10$  and 12 and starts to increase again for  $n = 14$  (Figure 2). Interestingly, the  $la\bar{3}d$  phase exhibited by the shorter homologues (**A10/1** and **A10/2**) is completely removed and replaced by the  $I23$  phase upon chain elongation (for  $n = 4 \rightarrow 10$ ) and then it re-emerges again for derivatives with  $n \geq 12$ . Therefore, it appears that there are two types of the  $la\bar{3}d$  phase, one is a long pitch (low twist)  $la\bar{3}d_{(L)}$ , favoured by short chains and the other one is a short pitch (high twist)  $la\bar{3}d_{(S)}$ , favoured by long chains and the two types are separated by the  $I23$  phase for medium chains. This sequence  $la\bar{3}d_{(L)}/I23/la\bar{3}d_{(S)}$  is typically observed for homologous series of compounds forming Cub<sub>bi</sub> phases, as for example in the ANBC-ns and BABH-ns,<sup>[34,64–68]</sup> and recently also found for tapered 5,5'-diphenyl-2,2'-dithiophenes upon increasing the volume of the apex substituent or increasing the size of an alicyclic ring at the apex.<sup>[41,44]</sup>

**Table 1.** Phase transitions of compounds **A10/n** and **A6/n**.<sup>[a]</sup>

Comp.	<i>m</i>	<i>n</i>	Phase transitions <i>T</i> /°C [ $\Delta H$ /kJ mol <sup>-1</sup> ]	<i>a</i> <sub>cub</sub> /nm ( <i>T</i> /°C)	$\Phi$ /°	3 <i>m</i> + <i>n</i>
A10/1	10	1	H: Cr < 20 Cub <sub>bi</sub> / <i>la</i> $\bar{3}$ <i>d</i> 212 [1.3] Iso C: Iso 202 [1.0] Cub <sub>bi</sub> / <i>la</i> $\bar{3}$ <i>d</i> Cr < 20	11.5 (150)	7.8	31
A10/2	10	2	H: Cr < 20 Cub <sub>bi</sub> / <i>la</i> $\bar{3}$ <i>d</i> 205 [1.1] Iso C: Iso 200 [< 0.1] Iso <sub>1</sub> <sup>[sk]</sup> 195 [0.8] Cub <sub>bi</sub> / <i>la</i> $\bar{3}$ <i>d</i>	11.6 (150)	7.7	32
A10/4	10	4	H: Cr1 94 [14.3] Cr2 104 [3.1] Cub <sub>bi</sub> <sup>[sk]</sup> / <i>I</i> 23 190 [1.3] Iso C: Iso 189 [0.1] Iso <sub>1</sub> <sup>[sk]</sup> 184 [0.7] Cub <sub>bi</sub> <sup>[sk]</sup> / <i>I</i> 23	17.0 (150)	8.2	34
A10/6	10	6	H: Cr 116 [40.6] Cub <sub>bi</sub> <sup>[sk]</sup> / <i>I</i> 23 190 [2.5] Iso C: Iso 182 [< 0.1] Iso <sub>1</sub> <sup>[sk]</sup> 181 [1.9] Cub <sub>bi</sub> <sup>[sk]</sup> / <i>I</i> 23 57 [22.2] Cr	17.3 (170)	8.1	36
A10/8	10	8	H: Cr 115 [37.9] Cub <sub>bi</sub> <sup>[sk]</sup> / <i>I</i> 23 182 [2.3] Iso C: Iso 176 [< 0.1] Iso <sub>1</sub> <sup>[sk]</sup> 174 [1.9] Cub <sub>bi</sub> <sup>[sk]</sup> / <i>I</i> 23 72 [23.80] Cr	–	–	38
A10/10	10	10	H: Cr 126 [43.7] Cub <sub>bi</sub> <sup>[sk]</sup> / <i>I</i> 23 181 [2.6] Iso C: Iso 172 [1.9] Cub <sub>bi</sub> <sup>[sk]</sup> / <i>I</i> 23 96 [39.6] Cr	17.2 (150)	8.2	40
A10/12	10	12	H: Cr 126 [44.6] Cub <sub>bi</sub> / <i>la</i> $\bar{3}$ <i>d</i> 181 [2.7] Iso C: Iso 172 [1.9] Cub <sub>bi</sub> / <i>la</i> $\bar{3}$ <i>d</i> 96 [41.1] Cr	10.9 (150)	8.2	42
A10/14	10	14	H: Cr 89 [37.0] Cub <sub>bi</sub> / <i>la</i> $\bar{3}$ <i>d</i> 172 [2.8] Iso C: Iso 162 [1.9] Cub <sub>bi</sub> / <i>la</i> $\bar{3}$ <i>d</i> 70 [39.3] Cr	10.9 (150)	8.2	44
A6/6	6	6	H: Cr 129 [34.2] Cub <sub>bi</sub> / <i>la</i> $\bar{3}$ <i>d</i> 207 [2.2] Iso C: Iso 204 [0.3] Iso <sub>1</sub> <sup>[sk]</sup> 190 [0.8] Cub <sub>bi</sub> / <i>la</i> $\bar{3}$ <i>d</i> 78 [28.3] Cr	10.6 (150)	8.5	24
A6/8	6	8	H: Cr 121 [35.2] Cub <sub>bi</sub> / <i>la</i> $\bar{3}$ <i>d</i> 198 [2.1] Iso C: Iso 193 [0.4] Iso <sub>1</sub> <sup>[sk]</sup> 178 [0.5] Cub <sub>bi</sub> / <i>la</i> $\bar{3}$ <i>d</i> 80 [23.2] Cr	10.6 (150)	8.5	26
A6/10	6	10	H: Cr 133 [50.7] Tet 155 [-] Cub <sub>bi</sub> <sup>[sk]</sup> / <i>I</i> 23 192 [2.4] Iso C: Iso 190 [0.4] Iso <sub>1</sub> <sup>[sk]</sup> 181 [0.8] Tet 85 [39.1] Cr	15.5 (150)	9.0	28
A6/12	6	12	H: Cr 85 [46.8] Cub <sub>bi</sub> <sup>[sk]</sup> / <i>I</i> 23 193 [4.5] Iso C: Iso 185 [< 0.1] Iso <sub>1</sub> <sup>[sk]</sup> 183 [1.6] Cub <sub>bi</sub> <sup>[sk]</sup> / <i>I</i> 23 82 [36.2] Cr	15.8 (140)	8.8	30
A6/14	6	14	H: Cr 103 [36.6] Cub <sub>bi</sub> <sup>[sk]</sup> / <i>I</i> 23 191 [3.4] Iso C: Iso 181 [2.4] Cub <sub>bi</sub> <sup>[sk]</sup> / <i>I</i> 23 87 [40.5] Cr	16.0 (140)	8.7	32

[a] Peak temperatures as determined from 2<sup>nd</sup> heating (upper lines) and 2<sup>nd</sup> cooling (lower lines) DSC scans with rate 10 K/min.; Abbreviations: Cr = crystalline solid; Iso = isotropic liquid; Iso<sub>1</sub><sup>[sk]</sup> spontaneous symmetry broken ambidextrous chiral isotropic liquid phase; Cub<sub>bi</sub>/*la* $\bar{3}$ *d* = achiral bicontinuous cubic phase with *la* $\bar{3}$ *d* space group; Cub<sub>bi</sub><sup>[sk]</sup>/*I*23 = ambidextrous chiral bicontinuous cubic phase with *I*23 space group; Tet = non-cubic 3D phase with tetragonal symmetry; *a*<sub>cub</sub> = lattice parameter of the cubic phase;  $\Phi$  = twist angle between adjacent rafts of molecules in the networks of the *la* $\bar{3}$ *d*-phases;  $\Phi$ (*la* $\bar{3}$ *d*) = 70.5°/[0.354*a*<sub>cub</sub>/0.45 nm],  $\Phi$ (*I*23) = 90°/[0.290*a*<sub>cub</sub>/0.45 nm],<sup>[52]</sup> see Table S7 for the full set of structural data and Tables S1–S6 and Figures S3, S4 for XRD data.

As shown in Table 1 all observed Cub<sub>bi</sub> phases represent thermodynamically stable (enantiotropic) phases. For the shortest two homologues **A10/1** and **A10/2** the *la* $\bar{3}$ *d* phase is observed both on heating and cooling over very wide temperature range (>200 K) without any crystallization even after storing the sample for several months. This makes these materials of potential interest for applications which require stable cubic phases around ambient temperature.

While there is a large jump of *a*<sub>cub</sub> at the *la* $\bar{3}$ *d*-*I*23 transitions, the cubic lattice parameter remains almost constant in the *la* $\bar{3}$ *d* ranges of the short and long chain compounds. Within the *I*23 range *a*<sub>cub</sub> first increases and then slightly decreases and between the two *la* $\bar{3}$ *d* ranges in the series of compounds **A10/n** there is a difference of 0.6–0.7 nm with larger values for the compounds with shorter chains (Figure 6a). This inverse dependence of the lattice parameter on the chain length can be interpreted as an effect of the chain volume on the twist between the molecules. Accordingly, for molecules with shorter chains the twist should be smaller, and with growing chain length it should increase. As the distance between the junctions is defined by *a*<sub>cub</sub> as well as the valency of junctions and the twist between them, there are geometric restrictions for the

twist between the molecules along the networks as the molecular rods have to arrive almost parallel to each other at each junction. This is in line with the development of the twist angles in the distinct Cub<sub>bi</sub> phases (see Table 1 and Figure 6a) calculated from the lattice parameters and the molecular dimensions according to the equations developed in Ref. [52] (see Table S7). In the series **A10/n** the twist angle ( $\Phi$ ) increases from 7.8° in the *la* $\bar{3}$ *d* phase of the shortest homologue **A10/1**, approaches a value of 8.2° in the *I*23 phase, and this twist is retained in the *la* $\bar{3}$ *d* phases of the longest homologues. The development of a chiral *I*23 phase in the contact region between the achiral *la* $\bar{3}$ *d* phases of the short compound **A10/2** and the longest compound **A10/14** (Figure 5g–i) confirms that the *la* $\bar{3}$ *d* phases of the two compounds are different from each other, i.e. they represent long pitch *la* $\bar{3}$ *d*<sub>(L)</sub> and short pitch *la* $\bar{3}$ *d*<sub>(S)</sub> phases, respectively.<sup>[41,44,46]</sup>

The effect of temperature on the development of the helical twist was also investigated in the cubic phase ranges of those compounds located around at the Cub<sub>bi</sub>/*la* $\bar{3}$ *d*-*I*23 transitions. As shown in Figure 6b, the helical twist significantly increases from *n* = 2 to *n* = 4 at the transition *la* $\bar{3}$ *d*<sub>(L)</sub>-*I*23, while the *T*-dependence is only small. In contrast, for the compounds with long

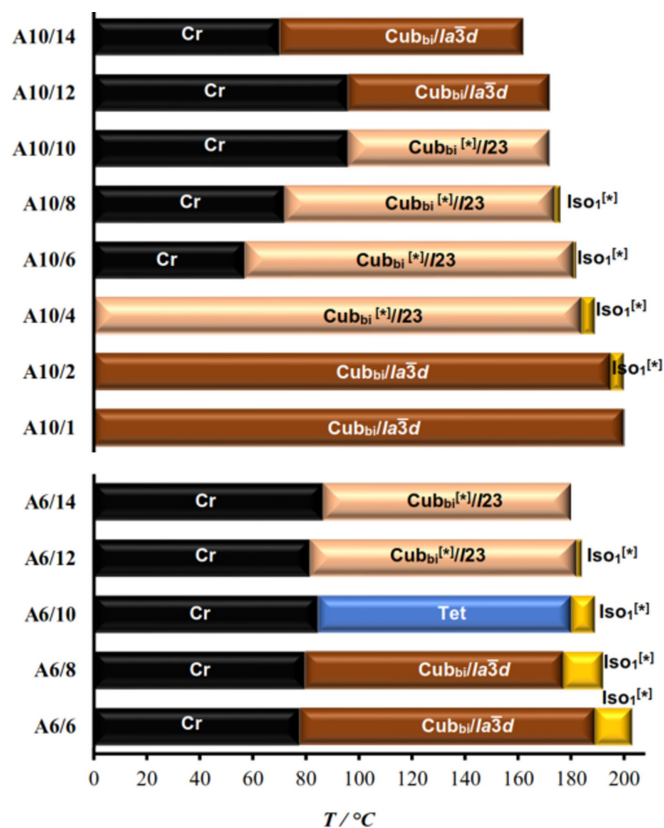


**Figure 2.** Phase transitions of the polycatenar compounds **A10/n** and **A6/n** as observed on cooling with a rate of  $10 \text{ K min}^{-1}$ .

chains ( $n=10,12$ ), located around the  $I23 \rightarrow Ia\bar{3}d_{(s)}$  transition, there is a significant temperature dependence of the twist, growing with rising temperature, as expected for thermal chain expansion. However, there is only a surprisingly small difference between the curves recorded for the  $Ia\bar{3}d_{(s)}$  and  $I23$  phases of these two homologues (magenta and dark blue in Fig.6b). The strong temperature dependence of  $\Phi$  in these two cases (especially if further extrapolated to lower  $T$ ) could be explained by a change of the chain flexibility. At low temperature there is less conformational disorder and the elongation of the  $n$ -alkylthio chain mainly contributes to the elongation of the molecule, thus reducing the twist between the molecules. With growing chain disorder at higher temperature, the contribution to the molecular length decreases, whereas the contribution to the lateral expansion of the  $n$ -alkyl chain grows and  $\Phi$  increases. For shorter RS chains ( $n=2,4$ ) this temperature effect on chain conformation is smaller (red and light blue in Fig.6b).

Decreasing the length of the chains at the trisubstituted end from  $m=10$  (**A10/n**) to  $m=6$  results in the analogue series **A6/n** (Table 1, Figure 2). This structural modification changes slightly the transition temperatures and retains the  $Cub_{bi}$  phases observed in the series **A10/n**. However, in this series the chiral  $Iso_1^{[*]}$  phase is observed for compounds with  $n=6-12$  in relatively wide temperature ranges compared to the **A10/n** series, meaning that the formation of the  $Iso_1^{[*]}$  phase is supported by short chains. As expected, in the series **A6/n** the

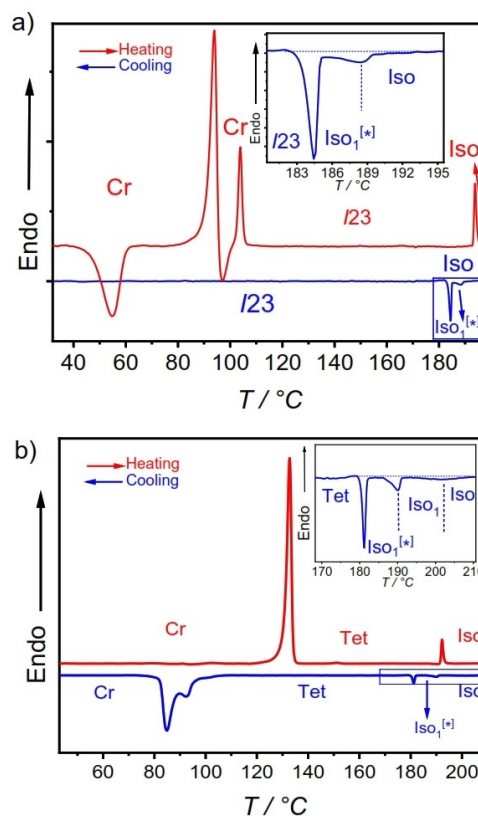


**Figure 3.** DSC heating and cooling traces recorded at  $10 \text{ K min}^{-1}$  of compounds: a) **A10/4** and b) **A6/10**. The insets in a) and b) show enlarged scale for the  $Iso-Iso_1^{[*]}-LC$  transition on cooling.

transition from  $Ia\bar{3}d$  to the triple network  $Cub_{bi}^{[*]}/I23$  phase requires longer apex chains. The short pitch  $Ia\bar{3}d_{(s)}$  region is not reached (Figure 2) in this series because the apex chain length is limited to  $n=14$ .

Interesting is the effect of the total chain volume on the  $Cub_{bi}$  phase type. Whereas in the series **A10/n** a total chain volume corresponding to 32–34  $\text{CH}_2$  units is required for the  $Ia\bar{3}d \rightarrow I23$  transition, this transition requires only 26–28  $\text{CH}_2$  units, i.e. 8  $\text{CH}_2$  units less in the series **A6/n** (Table 1). This means that, though chain elongation of all three chains at the dendritic end provides a much larger increase of chain volume than elongation of the single apex chain by the same number of C-atoms, there is a stronger effect of the chain volume added to the apex compared to the effect of the same chain volume change at the branched end. A possible explanation could be that the RS chains at the apex allow a larger conformational flexibility, thus effectively requiring more space than the conformationally more restricted RO chains at the tapered end. Indeed for related tetracatenar compound with an RO instead of the RS apex chains (**B10/n**) the  $Ia\bar{3}d \rightarrow I23$  transition takes place at 34  $\text{CH}_2$  units and for **B6/n** at 30–32 units.<sup>[69,70]</sup> These values are much closer to each other due to the comparable chain flexibility of the RO chains at both ends.

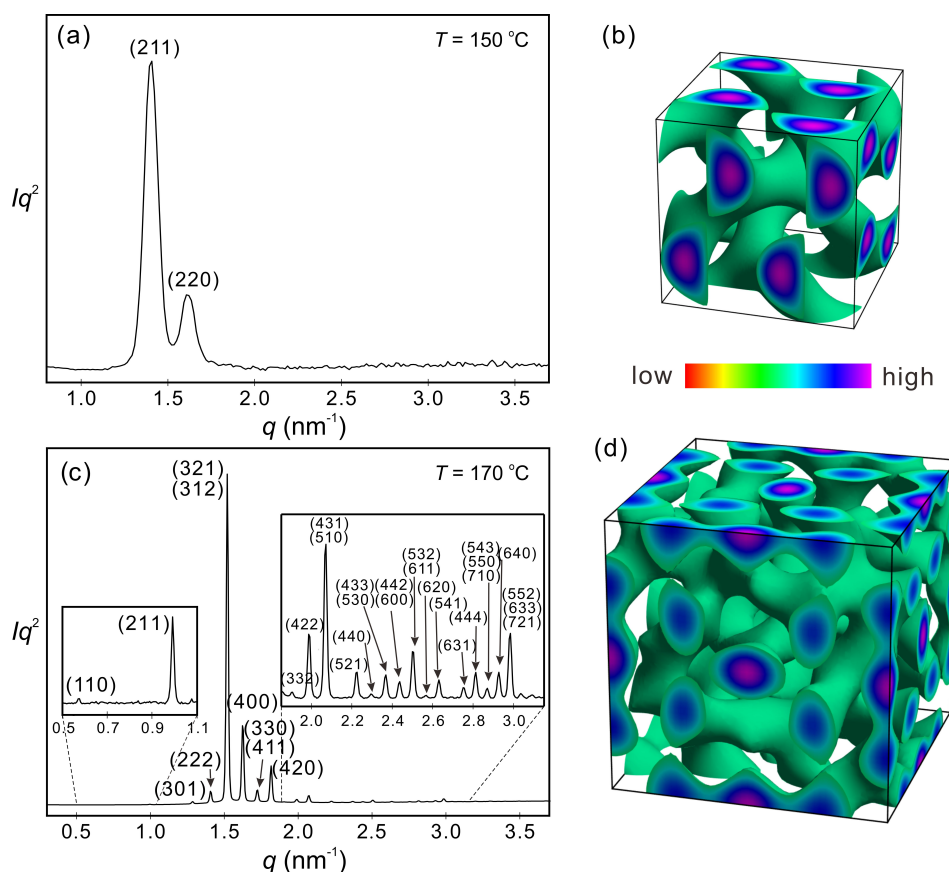


**Figure 4.** SAXS diffractogram as recorded on heating: a) at 150 °C in the  $\text{Cub}_{\text{bi}}/Ia\bar{3}d$  phase of **A10/14**; b) Reconstructed electron density map of **A10/14** in  $\text{Cub}_{\text{bi}}/Ia\bar{3}d$  phase. c) at 170 °C in the  $\text{Cub}_{\text{bi}}^{[*]}/I23$  phase of **A6/10** (for numerical data, see Table S2); d) Reconstructed electron density map of **A6/10** in  $\text{Cub}_{\text{bi}}^{[*]}/I23$  phase; for details of the ED reconstruction, see Section 4 and Figure S5 in the Supporting Information.

### Non-cubic 3D phases

Another difference between series **A10/n** and **A6/n** is that in the latter case an additional birefringent mesophase occurs at the  $Ia\bar{3}d$ - $I23$  transition upon chain elongation, which is missing in the series **A10/n**. On heating **A6/10** under crossed polarizers a transition from the crystalline phase to a highly viscous isotropic mesophase takes place at  $T \sim 133$  °C. Under slightly uncrossed polarizers a conglomerate of dark and bright domains can be easily detected which invert their brightness by inversion of the direction of the polarizers, indicating the chirality of this phase i.e. it is a chiral  $\text{Cub}_{\text{bi}}^{[*]}/I23$  phase. The chirality of  $\text{Cub}_{\text{bi}}^{[*]}/I23$  is lost on further heating at the transition to the fluid isotropic liquid (Iso). On cooling **A6/10** from the achiral Iso phase with a rate of 10 K  $\cdot$  min $^{-1}$  the chirality emerges at  $\sim 181$  °C, while the phase remains highly fluid as in ordinary liquids, indicating the formation of an  $\text{Iso}_1^{[*]}$  phase which exists over  $\sim 7$  K and transforms on further cooling to a birefringent 3D phase (Figure 7). Such birefringent mesophases with non-cubic 3D-lattice were often observed in the vicinity of  $\text{Cub}_{\text{bi}}$  phases formed by polycatenar molecules and could have tetragonal, orthorhombic or rhombohedral lattices,<sup>[42,64,71–74]</sup> the most prominent being the SmQ phase,<sup>[53,75]</sup> and the S4 phase. The 3D phase of **A6/10** could be indexed to a tetragonal lattice

(Tet, see Figure S4). The lattice parameters of the tetragonal phase are  $a = 14.5$  nm and  $c = 18.9$  nm which are close to  $a_{\text{cub}} = 15.5$  nm in the  $I23$  phase. This suggests that the tetragonal phase is likely to result from a stretching of the  $I23$  lattice along one direction. The very similar unit cell volumes ( $3.72$  nm $^3$  for  $I23$  and  $3.95$  nm $^3$  for Tet, see Table S7) and the optical investigations, showing that the birefringence is relatively small, are in line with this explanation. In the temperature range of all  $\text{Cub}_{\text{bi}}$  phases as well as in the Tet phase of **A6/10**, the WAXS is completely diffuse with a maximum around  $0.45$  nm which confirms LCs phases without fixed positions of the individual molecules (see Figure S3).

Upon fast cooling ( $\geq 20$  K  $\cdot$  min $^{-1}$ ) the Tet phase remains over a temperature range of  $\sim 96$  K until the onset of crystallization at  $\sim 85$  °C (Figure 7c). With cooling rates below 10 K  $\cdot$  min $^{-1}$  the  $\text{Cub}_{\text{bi}}$  phase develops together with the Tet phase (Figure 7b) and slowly replaces the Tet phase. This means that the Tet phase is metastable with respect to the non-distorted  $\text{Cub}_{\text{bi}}^{[*]}/I23$  phase. If the Tet phase is chiral or achiral cannot be decided, because the linear birefringence of the Tet phase is much larger than the possible effects of optical rotation. However, it is likely to be a chiral phase as it occurs between two mirror symmetry broken phases,  $\text{Iso}_1^{[*]}$  and  $\text{Cub}_{\text{bi}}^{[*]}/I23$ .

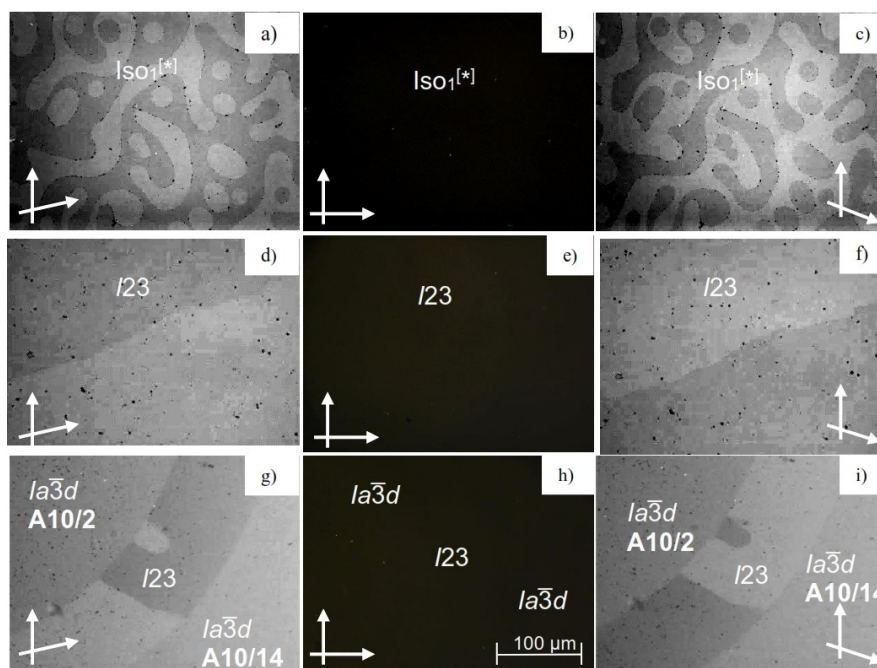


**Figure 5.** Chiral domains observed in: a,c)  $Iso_1^{[*]}$  phase of **A10/2** at 198 °C; d,f)  $I23$  phase of **A10/4** at 150 °C; g,i) the induced  $I23$  phase in the contact regions between the achiral  $Ia\bar{3}d$  phases of **A10/2** and **A10/14** at 170 °C. The textures in left and right columns are between slightly rotated polarizers and in the middle column (b,e,h) are under fully (90°) crossed polarizers and therefore appear completely dark.

### Mirror symmetry broken isotropic liquids

Another interesting feature of series **A10/n** is the observation of an additional transition between two different types of liquid phases on cooling of **A10/2-A10/8** before the transition to the cubic phases (Table 1, Figure 3). On cooling compound **A10/4**, as example, a broad feature occurs in the DSC traces in the temperature range of the isotropic liquid phase, indicating a liquid-liquid transition (Figure 3a). This broad transition is followed by a sharp peak indicating the transition to the cubic phase, associated with a sudden increase of the viscosity. In the temperature range of the broad liquid-liquid transition the emergence of mirror symmetry breaking could be detected by the appearance of chiral domains under slightly uncrossed polarizers (Figure 5a-c). Therefore, this mirror symmetry broken isotropic liquid phase is assigned as  $Iso_1^{[*]}$  phase and considered as a kind of percolated liquid with a dynamic helical network structure.<sup>[45]</sup> Interestingly, the  $Iso_1^{[*]}$  phase appears beside the achiral gyroid  $Ia\bar{3}d$  phase for **A10/2** as well as beside the ambidextrous chiral  $I23$  phase for **A10/4-A10/8**. Its range decreases with chain elongation ( $n=2\rightarrow 8$ ) and is completely removed for compounds **A10/n** with  $n\geq 10$ . This  $Iso_1^{[*]}$  phase is also formed by compounds **A6/6-A6/12**, again associated with the  $Ia\bar{3}d$  to  $I23$  transition. As in the series **A10/n** the  $Iso_1^{[*]}$  phase is metastable, but the monotropic phase region observed on cooling before the transition to the  $Cub_{bi}$  (and Tet) phase is broader (up to 14 K). The development of this phase from the achiral isotropic liquid (Iso) apparently takes place in two steps in this case, at about 202 °C there is the maximum of a very broad and weak DSC feature, which we attribute to the Iso- $Iso_1^{[*]}$

transition, associated with the growth of helical aggregates fusing to local networks (Figure 3b). This Iso-Iso $_1^{[*]}$  transition is most clearly seen for **A6/10**, being directly at the  $Ia\bar{3}d$  to  $I23$  transition and it is not so clear for the other compounds **A6/n**. The peak at 190 °C is associated with the onset of long-range chirality synchronization in the Iso $_1$  range (Iso $_1$ -Iso $_1^{[*]}$  transition) and the much larger peak at 180 °C indicates the transition to the long range periodic Tet phase. That the mirror symmetry broken  $Iso_1^{[*]}$  phase appears in some cases above the achiral double gyroid  $Ia\bar{3}d$  phase can be understood by thermal chain expansion at the transition to the isotropic state. As this is known to induce the transition from  $Ia\bar{3}d_{(L)}$  to  $I23$  (see above) it is postulated that the local structure in the Iso $_1^{[*]}$  phase is  $I23$ -like, leading to chiral conglomerate formation.

### Comparison with related alkoxy substituted polycatenars

In Figure 8 some of the compounds synthesized herein are compared with their analogues having alkoxy instead of the alkylthio chains (**Bm/n**).<sup>[39,58]</sup> As shown in Figure 8 the same phase types and phase sequences are observed in both series. However, replacing S by O increases the Iso $_1^{[*]}$  ranges on the expense of the  $Cub_{bi}$  phases. For the pair **A10/1**, **B10/1** an increased stability of the cubic phase by replacing O by S is observed, whereas for the compounds with longer chains at the apex ( $n=6, 10$ ) this order is reversed. The main effects of replacing ether by thioether linkages are a decreased C-S-C bonding angle (99°) compared to C-O-C (114°),<sup>[76]</sup> a changed molecular shape from almost rod-like to more bent and an

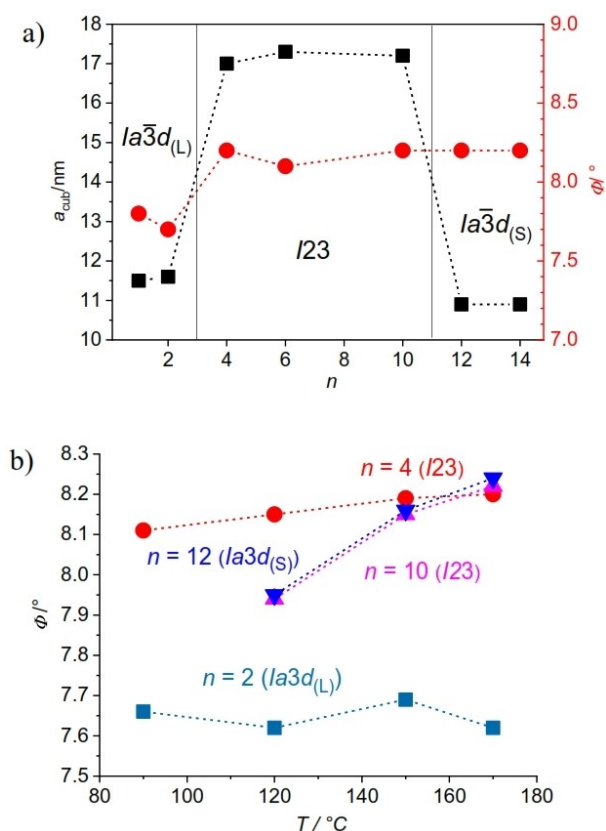


**Figure 6.** Investigation of the cubic phases of compounds **A10/n**. a) Dependence of the twist angle ( $\phi$ ) and lattice parameter ( $a_{\text{cub}}$ ) on RS chain length ( $n$ ); the twist angle ( $\phi$ ) was calculated according to:  $\phi(la\bar{3}d) = 70.5^\circ / [0.354a_{\text{cub}}/0.45 \text{ nm}]$  and  $\phi(I23) = 90^\circ / [0.290a_{\text{cub}}/0.45 \text{ nm}]$ ;<sup>[52]</sup> b) dependence of  $\phi$  on the temperature.

increased C–S bond length (1.82 nm) compared to C–O (1.45 nm).<sup>[76]</sup> The latter decreases the rotational barrier around the C–S bonds compared to the C–O bonds (O–CH<sub>3</sub>: 11.3 kJ mol<sup>-1</sup>; S–CH<sub>3</sub>: 8.4 kJ mol<sup>-1</sup>) and thus increases conformational chain mobility.<sup>[77,78]</sup> Increased conformational chain disorder of arylthioethers is also supported by the decreased conjugation of S with the benzene ring if compared with related arylethers.<sup>[79]</sup> Moreover, the reduced electronegativity of

S compared to O leads to reduced dipolar intermolecular interactions whereas its larger electric polarizability provides stronger dispersion forces between the thioethers. In cases where the conformation is biased, as in heterocycles, a strong mesophase stabilizing effect of S compared to O of about 20 K per S was observed.<sup>[80]</sup> In contrast, the enhanced conformational flexibility around the C–S bonds reduces the stability of LC phases if an alkyl chain is attached to a core unit via a thioether linkage.<sup>[81,82]</sup> The increased stability of the LC phases of the short chain compounds **Am/n** can be attributed to the increased attractive dispersion forces provided by the larger sulphur. For longer chains this stabilizing effect of S is compensated by its mesophase destabilizing effect due to the increased conformational chain mobility and therefore the effect of replacing O by S is reversed for the longer homologues. The increased chain mobility is likely to also contribute to the reduced melting points and reduced crystallization tendency of the thioethers, which besides the suppression of birefringent phases causes a widening of the Cub<sub>bi</sub> ranges in all cases.<sup>[15]</sup> (see Table 2).

## Summary and Conclusions

The design, synthesis, and investigation of two new series of 5,5'-diphenyl-2,2'-bithiophene based polycatenars terminated with thioether chains at the monosubstituted apex is reported. The effect of the RS chain length on the development of helical and mirror symmetry broken soft matter network phases was investigated and compared to the related analogues terminated with alkoxy chains. Depending on the length of the terminal chain, the synthesized materials exhibit different types of LC phase. Very wide ranges of cubic phases, even around room temperature makes these compounds good candidates for technological applications. Spontaneous mirror symmetry breaking based on chirality synchronization in helical networks was observed in the triple network cubic phase with  $I23$  symmetry and in the isotropic liquid phase (Iso<sub>1</sub><sup>[\*]</sup>).<sup>[59]</sup> The mirror symmetry broken isotropic liquid is observed in both series of compounds (**A10/n** and **A6/n**) for medium and short chain compounds. For the series **A10/n** a phase sequence  $la\bar{3}char/Ox00AFnotimplementedd_{(L)}-I23-la\bar{3}d_{(S)}$  with a chiral  $I23$  phase between two achiral  $la\bar{3}d$  phases is observed with chain

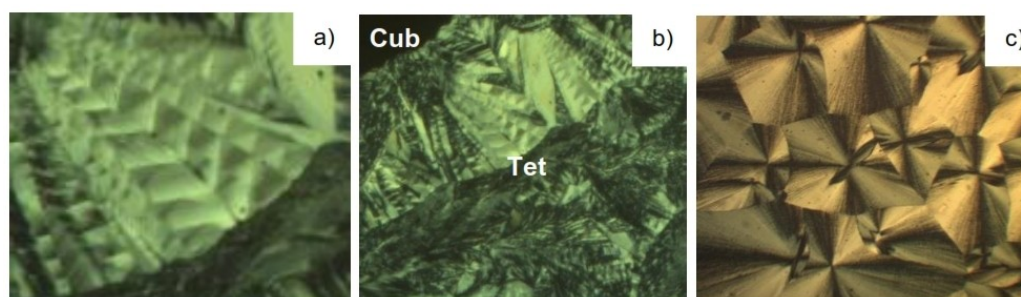


**Figure 7.** Optical textures obtained for compound **A6/10**: a) and b) with a cooling rate of 10 K/min; a) Tet phase at 174 °C; b) Tet + Cub at 125 °C and c) Tet phase at 125 °C using a cooling rate of 20 K/min. Due to the very different appearance it is not clear from these investigations if the 3D phase formed on rapid cooling is the same as on fast cooling only with a different alignment or a slightly different 3D phase.

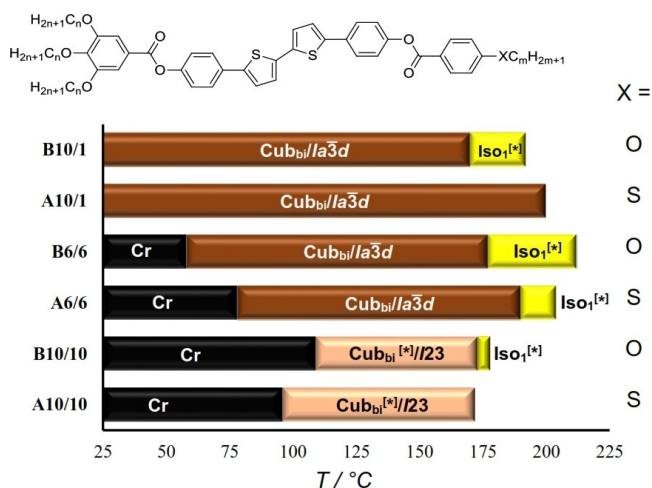


**Figure 8.** Phase transitions of the polycatenar compounds **A10/1**, **A10/10**, **A6/6** and their related analogues **B10/1**,<sup>[39]</sup> **B10/10**,<sup>[39]</sup> and **B6/6**<sup>[58]</sup> as observed on cooling (DSC with rate 10 K min<sup>-1</sup>), for abbreviations see Table 1.

elongation. Mirror symmetry breaking was also induced upon mixing two components forming achiral  $Ia\bar{3}d$  phases.<sup>[50]</sup> At the  $Ia\bar{3}d_{(L)}$ -I23 transition upon chain elongation a tetragonal phase (Tet) is observed in the series **A6/n**, which is suggested to represent a deformed version of the I23 lattice. The precise structure of this Tet phase and related birefringent 3D phases found in other series of polycatenar compounds require further studies.

## Acknowledgements

M. Alaasar acknowledges the German Research Foundation (DFG) for the financial support (AL2378/1-1, 424355983). A. F. Darweesh acknowledges the support by the Alexander von Humboldt Foundation for the research fellowship at Martin Luther University Halle-Wittenberg, Germany. F. Liu thanks the financial support from the National Natural Science Foundation of China (21761132033, 21374086). The authors are grateful to Beamline BL16B1 at SSRF (Shanghai Synchrotron Radiation Facility, China) for providing the beamtime. Open Access funding enabled and organized by Projekt DEAL.

## Conflict of Interest

The authors declare no conflict of interest.

**Keywords:** bithophene · chirality · cubic phases · liquid crystals · mirror symmetry breaking · soft matter

- [1] J. A. Castellano, The Story of Liquid Crystal Displays and the Creation of an Industry, World Scientific, Singapore 2005.  
[2] L. Wang, Q. Li, *Adv. Funct. Mater.* **2016**, *26*, 10–28.

- [3] W. Goodby, P. J. Collings, T. Kato, C. Tschierske, H. Gleeson, P. Raynes, Handbook of Liquid Crystals, 2nd ed., Wiley-VCH, Weinheim, Germany 2014.  
[4] Q. Li, Nanoscience with Liquid Crystals. – From Self-Organized Nanostructures to Applications, Springer, Cham, Switzerland 2014.  
[5] R. Jakoby, A. Gaebler, C. Weickhmann, *Crystals* **2020**, *10*, 514–560.  
[6] H. Iino, J. Hanna, *Polym. J.* **2017**, *49*, 23–30.  
[7] T. Kato, J. Uchida, T. Ichikawa, T. Sakamoto, *Angew. Chem. Int. Ed.* **2018**, *57*, 4355–4371; *Angew. Chem.* **2018**, *130*, 4438–4455.  
[8] M. O'Neill, S. M. Kelly, *Adv. Mater.* **2011**, *23*, 566–584.  
[9] S. Sergeev, W. Pisula, Y. H. Geerts, *Chem. Soc. Rev.* **2007**, *36*, 1902–1929.  
[10] E. Bukusoglu, M. B. Pantoja, P. C. Mushenheim, X. Wang, N. L. Abbott, *Annu. Rev. Chem. Biomol. Eng.* **2016**, *7*, 163–196.  
[11] T. Yasuda, H. Ooi, J. Morita, Y. Akama, K. Minoura, M. Funahashi, T. Shimomura, T. Kato, *Adv. Funct. Mater.* **2009**, *19*, 411–419.  
[12] Y. Chen, P. Ma, S. Gui, *BioMed Res. Int.* **2014**, *2014*, 1–12.  
[13] D. Adam, P. Schuhmachert, J. Sllmerer, L. Hiussllngt, K. Siemensmeyert, K. H. Etbacht, H. Ringsdorf, D. Haarer, *Nature* **1994**, *371*, 141–143.  
[14] S. Kang, M. Harada, X. Li, M. Tokita, J. Watanabe, *Soft Matter* **2012**, *8*, 1916–1922.  
[15] Y. Arakawa, Y. Sasaki, K. Igawa, H. Tsuji, *New J. Chem.* **2017**, *41*, 6514–6522.  
[16] Y. Arakawa, Y. Sasaki, H. Tsuji, *Chem. Lett.* **2017**, *46*, 1657–1659.  
[17] Y. Arakawa, Y. Ishida, H. Tsuji, *Chem. Eur. J.* **2020**, *26*, 3767–3775.  
[18] Y. Arakawa, K. Komatsu, Y. Ishida, H. Tsuji, *Liq. Cryst.* **2021**, *48*, 641–652.  
[19] W. Weissflog, in Handbook of Liquid Crystals, 2nd ed. (Eds: J. W. Goodby, J. P. Collings, T. Kato, C. Tschierske, H. F. Gleeson, P. Raynes), Wiley-VCH, Weinheim, Germany 2014, pp. 89–174.  
[20] D. W. Bruce, *Acc. Chem. Res.* **2000**, *33*, 831–840.  
[21] H. T. Nguyen, C. Destrade, J. Malthete, *Adv. Mater.* **1997**, *9*, 375–388.  
[22] N. T. Nguyen, C. Destrade, J. Malthete, *Liq. Cryst.* **1990**, *8*, 797–811.  
[23] I. Nishiyama, *Chem. Rec.* **2009**, *9*, 340–355.  
[24] M. Yoneya, *Chem. Rec.* **2011**, *11*, 66–76.  
[25] A. Yoshizawa, *Polym. J.* **2012**, *44*, 490–502.  
[26] M. Alaasar, S. Poppe, *Liq. Cryst.* **2019**, *47*, 939–949.  
[27] M. Alaasar, *J. Mol. Liq.* **2021**, *341*, 117341–117347.  
[28] S. Hyde, S. Andersson, K. Larsson, Z. Blum, T. Landh, S. Lidin, B. W. Ninham, The language of shape. The role of curvature in condensed matter: Physics, Chemistry and Biology, Elsevier, Amsterdam 1997.  
[29] A. J. Meuler, M. A. Hillmyer, F. S. Bates, **2009**, *42*, 7221–7250.  
[30] J. M. Seddon, R. H. Templer, Polymorphism in Lipid-Water Systems. In Handbook of Biological Physics; Lipowsky, R. and E. Sackmann, Eds.; Elsevier: Amsterdam, 1995; Vol. 1, pp 97–160.  
[31] G. Ungar, F. Liu, X. B. Zeng, in Handbook of Liquid Crystals (Eds: W. Goodby, P. J. Collings, T. Kato, C. Tschierske, H. Gleeson, P. Raynes), Wiley-VCH, Weinheim, Germany 2014.  
[32] C. Tschierske, *J. Mater. Chem.* **1998**, *8*, 1485–1508.  
[33] L. Hag, S. L. Gras, C. E. Conn, C. J. Drummond, *Chem. Soc. Rev.* **2017**, *46*, 2705–2731.  
[34] A. H. Schoen, *Interface Focus* **2012**, *2*, 658–668.  
[35] S. Kutsumizu, *Isr. J. Chem.* **2012**, *52*, 844–853.  
[36] L. Han, S. Che, *Adv. Mater.* **2018**, *30*, 1705708–1705729.  
[37] M. L. Lynch, P. T. Spicer, Bicontinuous Liquid Crystals, CRC Press, Taylor & Francis Group, Boca Raton, FL 2005.  
[38] O. Kwon, X. Cai, W. Qu, F. Liu, J. Szydłowska, E. Gorecka, M. J. Han, D. K. Yoon, S. Poppe, C. Tschierske, *Adv. Funct. Mater.* **2021**, *31*, 2102271–212280.  
[39] C. Dressel, F. Liu, M. Prehm, X. B. Zeng, G. Ungar, C. Tschierske, *Angew. Chem. Int. Ed.* **2014**, *53*, 13115–13120; *Angew. Chem.* **2014**, *126*, 13331–13336.  
[40] Y. Cao, M. Alaasar, A. Nallapaneni, M. Salamończyk, P. Marinko, E. Gorecka, C. Tschierske, F. Liu, N. Vaupotič, C. Zhu, *Phys. Rev. Lett.* **2020**, *125*, 027801–027806.  
[41] C. Dressel, T. Reppe, S. Poppe, M. Prehm, H. Lu, X. Zeng, G. Ungar, C. Tschierske, *Adv. Funct. Mater.* **2020**, *30*, 2004353–2004368.  
[42] M. Alaasar, J.-C. Schmidt, X. Cai, F. Liu, C. Tschierske, *J. Mol. Liq.* **2021**, *332*, 115870–115884.  
[43] M. Alaasar, S. Poppe, Q. Dong, F. Liu, C. Tschierske, *Chem. Commun.* **2016**, *52*, 13869–13872.  
[44] T. Reppe, C. Dressel, S. Poppe, C. Tschierske, *Chem. Commun.* **2020**, *56*, 711–714.  
[45] T. Reppe, S. Poppe, X. Cai, Y. Cao, F. Liu, C. Tschierske, *Chem. Sci.* **2020**, *11*, 5902–5908.  
[46] T. Reppe, S. Poppe, C. Tschierske, *Chem. Eur. J.* **2020**, *26*, 16066–16079.

- [47] M. Alaasar, S. Poppe, Q. Dong, F. Liu, C. Tschierske, *Angew. Chem. Int. Ed.* **2017**, *56*, 10801–10805; *Angew. Chem.* **2017**, *129*, 10941–10945.
- [48] M. Alaasar, S. Poppe, Y. Cao, C. Chen, F. Liu, C. Zhu, C. Tschierske, *J. Mater. Chem. C* **2020**, *8*, 12902–12916.
- [49] T. Reppe, C. Dressel, S. Poppe, A. Eremin, C. Tschierske, *Adv. Opt. Mater.* **2020**, 2001572–2001589.
- [50] S. Kutsumizu, S. Miisako, Y. Miwa, M. Kitagawa, Y. Yamamurab, K. Saito, *Phys. Chem. Chem. Phys.* **2016**, *18*, 17341–17344.
- [51] J. M. Wolska, J. Wilk, D. Pocięcha, J. Mieczkowski, E. Gorecka, *Chem. Eur. J.* **2017**, *23*, 6853–6857.
- [52] X. Zeng, G. Ungar, *J. Mater. Chem. C* **2020**, *8*, 5389–5398.
- [53] A.-M. Levelut, M. Clerc, *Liq. Cryst.* **1998**, *24*, 105–115.
- [54] X. Zeng, G. Ungar, M. Imperor-Clerc, *Nat. Mater.* **2005**, *4*, 562–567.
- [55] Alternative models of this Cub<sub>bi</sub> phase being composed of only one network and spherical aggregates have also been proposed, see ref. 63, 64.
- [56] K. Saito, Y. Yamamura, Y. Miwa, S. Kutsumizu, *Phys. Chem. Chem. Phys.* **2016**, *18*, 3280–3284.
- [57] N. Vaupotic, M. Salamonczyk, J. Matraszek, M. Vogrin, D. Pocięcha, E. Gorecka, *Phys. Chem. Chem. Phys.* **2020**, *22*, 12814–12820.
- [58] C. Dressel, T. Reppe, M. Prehm, M. Brautzsch, C. Tschierske, *Nat. Chem.* **2014**, *6*, 971–977.
- [59] C. Tschierske, G. Ungar, *ChemPhysChem* **2016**, *17*, 1224–1251.
- [60] C. Tschierske, C. Dressel, *Symmetry* **2020**, *12*, 1098–1128.
- [61] M. Alaasar, M. Prehm, Y. Cao, F. Liu, C. Tschierske, *Angew. Chem. Int. Ed.* **2016**, *128*, 320–324.
- [62] C. Tschierske, *Liq. Cryst.* **2018**, *45*, 2221–2252.
- [63] A. Kummar, V. Molinero, *J. Phys. Chem. B* **2018**, *122*, 4758–4770.
- [64] a) G. W. Gray, B. Jones, F. Marson, *J. Chem. Soc.* **1957**, 393–401; b) H. Schubert, J. Hauschild, D. Demus, S. Hoffmann, *Z. Chem.* **1978**, *18*, 256.
- [65] Y. Yamamura, Y. Nakazawa, S. Kutsumizu, K. Saito, *Phys. Chem. Chem. Phys.* **2019**, *21*, 23705–23712.
- [66] S. Kutsumizu, K. Morita, T. Ichikawa, S. Yano, S. Nojima, T. Yamaguchi, *Liq. Cryst.* **2002**, *29*, 1447–1458.
- [67] D. Demus, D. Marzotko, N. K. Sharma, A. Wiegeleben, *Kryst. Tech.* **1980**, *15*, 331–339.
- [68] S. Kutsumizu, K. Morita, T. Ichikawa, S. Yano, S. Nojima, T. Yamaguchi, *Liq. Cryst.* **2002**, *29*, 1447–1458.
- [69] C. Dressel, PhD Thesis, University Halle, **2015**.
- [70] T. Reppe, Master Thesis, University Hlle, **2015**.
- [71] G. E. Schröder-Turk, A. Fogden, S. T. Hyde, *Eur. Phys. J. B* **2006**, *54*, 509–524.
- [72] A. Fogden, S. T. Hyde, *Eur. Phys. J. B* **1999**, *7*, 91–104.
- [73] C. A. Tyler, D. C. Morse, *Phys. Rev. Lett.* **2005**, *94*, 208302–208305.
- [74] J. Matraszek, D. Pocięcha, N. Vaupotic, M. Salamonczyk, M. Vogrine, E. Gorecka, *Soft Matter* **2020**, *16*, 3882–3885.
- [75] H. Lu, X. Zeng, G. Ungar, C. Dressel, C. Tschierske, *Angew. Chem. Int. Ed.* **2018**, *57*, 2835–2840; *Angew. Chem.* **2018**, *130*, 2885–2890.
- [76] T. Sakaizumi, M. Namikawa, O. Ohashi, *J. Mol. Struct.* **1995**, *345*, 189–195.
- [77] J. Hine, *Reaktivität und Mechanismus in der Organischen Chemie*, Thieme Stuttgart, **1960**.
- [78] F. G. Riddell, *The conformational analysis of Heterocyclic compounds*, Academic Press, **1980**.
- [79] V. F. Petrov, V. A. Vinkurov, V. V. Belyav, *Mol. Cryst. Liq. Cryst.* **2010**, *518*, 40–59.
- [80] C. Tschierske, D. Joachimi, H.-M. Vorbrod, H. Zschke, A. Wiegeleben, A. Hauser, D. Demus, *Liq. Cryst.* **1989**, *5*, 177–190.
- [81] E. Kleinpeter, H. Köhler, A. Lunow, C. Tschierske, H. Zschke, *Tetrahedron* **1988**, *44*, 1609–1612.
- [82] Y. Arakawa, S. Kang, H. Tsuji, J. Watanabe, G.-I. Konishi, *RSC Adv.* **2016**, *6*, 16568–16574.

---

Manuscript received: June 21, 2021

Accepted manuscript online: September 20, 2021

Version of record online: October 7, 2021





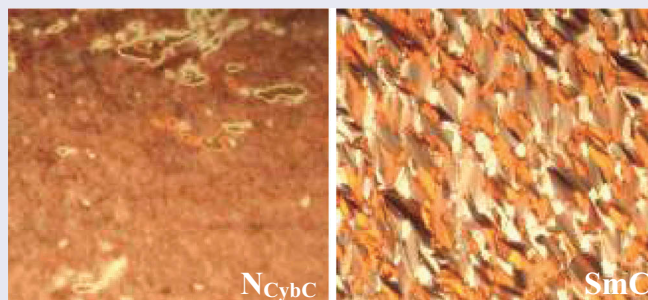
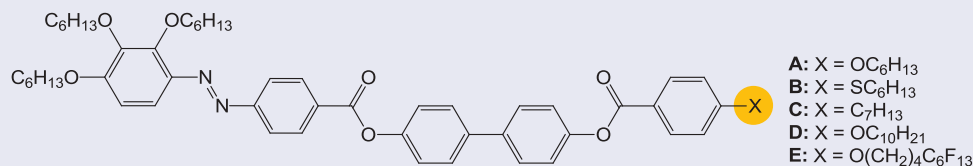
# Cybotactic nematic phases with wide ranges in photoresponsive polycatenars

Mohamed Alaasar<sup>a,b</sup> and Silvio Poppe<sup>b</sup>

<sup>a</sup>Department of Chemistry, Cairo University, Giza, Egypt; <sup>b</sup>Institute of Chemistry, Martin-Luther University Halle-Wittenberg, Halle/Saale, Germany

## ABSTRACT

We report on the synthesis and phase behaviour of new light-responsive polycatenars. The new materials represent tetracatenar molecules with four terminal chains which are substituted at 2,3,4-position in one benzene ring at one terminus and at the other terminus only one chain is present. The liquid-crystalline behaviour of the prepared materials was characterised by differential scanning calorimetry (DSC), polarised optical microscope (POM) and X-ray diffraction (XRD). We investigated the effect of changing the type of one terminal chain, while keeping the remaining three chains fixed on the mesomorphism of these materials. All of the tetracatenars exhibit nematic and smectic C phases. By investigating the nematic phase with XRD it was found that it represents nematic phase with cybotactic clusters of the SmC type ( $N_{CybC}$ ). Moreover, these nematic phases exist over wide temperature ranges for all compounds. Additionally, the photosensitivity of these polycatenars was studied upon light irradiation.



## ARTICLE HISTORY

Received 12 September 2019  
Accepted 4 November 2019

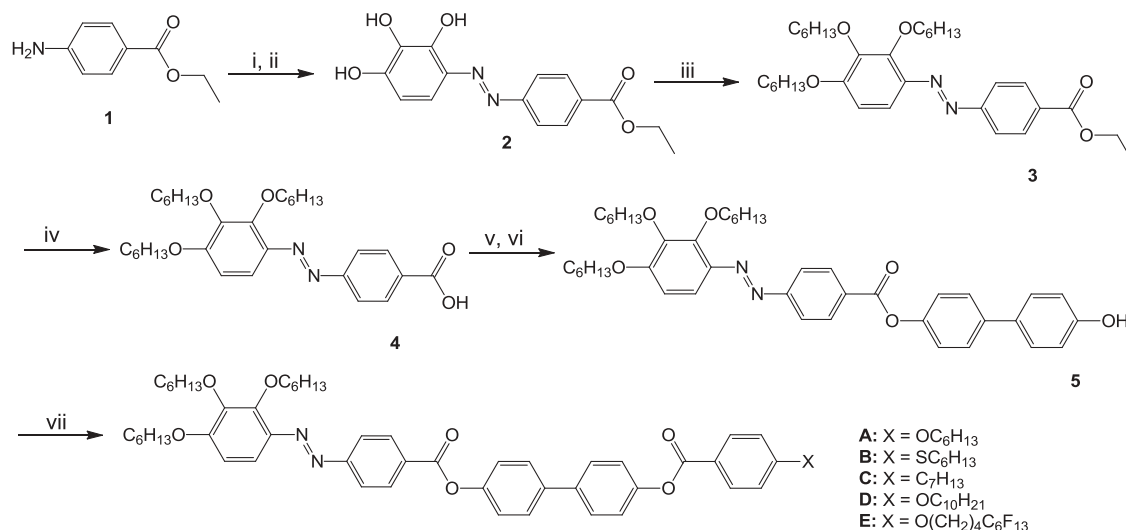
## KEYWORDS

Polycatenars; liquid crystals; azobenzene; photosensitivity; cybotactic nematic

## 1. Introduction

Liquid crystals (LCs) represent one class of functional materials that combine molecular order and mobility, which were applied in electro-optical devices such as flat-panel display [1], in health care and in molecular engineering nanotechnology [2]. Azobenzene functionalised LCs are attractive candidates for the manufacture of photoresponsive materials due to their *trans-cis* isomerisation upon light irradiation [3–14]. Combining the liquid-crystalline properties and photosensitivity in the same materials leads to several potential applications such as molecular scissors [15], photo-oscillators [16,17], optogenetics [18] and organic light-driven

actuators [19–21]. Therefore, azobenzene-based LCs designed by covalent or non-covalent interactions such as hydrogen or halogen bonding between complementary components have attracted the attention of a lot of researchers [22–27]. Huge number of non-conventional LCs that deviate from the well-known rod-like (calamitic), disc-like (discotic) or the bent-core (banana shaped) molecular designs have been reported over the last few decades [28,29]. Polycatenars represent one class of such nonconventional LCs, which have a combination of long rod-like aromatic core and multi-terminal hemi disc shaped segments [30–36]. They are named according to the number of the terminal chains; therefore, tetracatenars consist of four-terminal chains,



**Scheme 1.** Synthesis of the polycatenars **A–E**. Reagents and conditions: i.  $\text{NaNO}_2$ ,  $\text{HCl}$ ; ii.  $\text{NaOH}$ , 1,2,3-trihydroxybenzene; iii.  $\text{BrC}_6\text{H}_{13}$ ,  $\text{KI}$ ,  $\text{K}_2\text{CO}_3$ ,  $\text{DMF}$ , stirring,  $80^\circ\text{C}$ , 48 h; iv.  $\text{NaOH}$ , stirring,  $85^\circ\text{C}$ , for 4 h then  $\text{H}^+$ ; v.  $\text{SOCl}_2$ , few drops of  $\text{DMF}$ , stirring,  $80^\circ\text{C}$ , 1 h; vi. 4,4'-dihydroxybiphenyl, pyridine, stirring,  $100^\circ\text{C}$ , 12 h; vii.  $\text{DCC}$ ,  $\text{DMAP}$ ,  $\text{DCM}$ , stirring, 48 h.

hexacatenars have six terminal chains and so on. Different types of LC phases were observed in polycatenars, e.g. nematic, lamellar, columnar and three-dimensional bicontinuous cubic or tetragonal phases due to the nanosegregation of the flexible chains and the aromatic core. However, there is a few number of azobenzene-based polycatenars reported up to date [37–42]. Recently, we reported new types of photosensitive polycatenars with four or three-terminal alkoxy chains which are distributed in 3 + 1 or 2 + 1 fashion on the terminals of the aromatic core. Both types of these polycatenars exhibit mirror-symmetry breaking in isotropic liquids ( $\text{Iso}_1^{[*]}$  phase) and depending on the number of the terminal alkyl chains, the  $\text{Iso}_1^{[*]}$  phase appeared beside three-dimensional tetragonal phase or beside lamellar  $\text{SmA}$  phase [43,44]. We were also able to achieve fast and reversible photoinduced switching process between the chiral isotropic liquid ( $\text{Iso}_1^{[*]}$  phase) and the achiral  $\text{SmA}$  phase with non-polarised light [44]. Moreover, we reported also photosensitive supramolecular polycatenars designed by intermolecular interaction, i.e. hydrogen and halogen bonds [24,25].

Therefore, in continuation of our interest in studying new photosensitive polycatenars, we report herein the synthesis and liquid-crystalline properties of new azobenzene-based polycatenars (compounds **A–E**, Scheme 1). The new materials are tetracatenars consisting of long aromatic core with five benzene rings and terminated at one side with three hexyloxy chains substituted in the 2, 3 and 4 positions which is known to induce nematic phases [40,41], while at the other end only one terminal chain is present. The latter was varied between hexyloxy-, hexylthio-, heptyl-, decyloxy- or

4-(5,5,6,6,7,7,8,8,9,9,10,10,10-tridecafluorodecyloxy-) chains to study the effect of different chain types on the LC behaviour of these materials.

## 2. Experimental

### 2.1. Synthesis

The target compounds **A–E** were synthesised through the synthetic pathway shown in Scheme 1. The starting 4-[2',3',4'-trihexyloxyphenylazo]benzoic acid (**4**) was synthesised in three steps. The first step is an azo coupling between 1,2,3-trihydroxybenzene and the diazonium salt of ethyl-4-aminobenzoate (**1**) to afford the ester compound **2** [40,45]. The obtained azo dye was then etherified with *n*-hexylbromide to give the ester **3** which was subjected to hydrolysis under basic conditions and finally acidified to yield the acid **4** [40,45]. The obtained acid was converted to the corresponding acid chloride and used in a mono esterification reaction with 4,4'-dihydroxybiphenyl to yield the hydroxy compound **5**. In the final step compound **5**, was esterified with different 4-substituted benzoic acid derivatives via  $\text{DCC}$  in the presence of  $\text{DMAP}$  to give the target polycatenars (**A–E**). The detailed synthetic procedure, purification and analytical data for the intermediates compounds as well as the final polycatenars are given below.

#### 2.1.1. Synthesis of Ethyl-4-[2',3',4'-trihexyloxyphenylazo]benzoate (**3**)

To (1.06 g, 3.5 mmol) of ethyl 4-[2',3',4'-trihydroxyphenylazo]benzoate (**2**) [40,45] dissolved in dry  $\text{DMF}$  (50 mL) under a nitrogen atmosphere was added (2.43 g, 18 mmol)  $\text{K}_2\text{CO}_3$ , (0.2 g, 1.2 mmol)  $\text{KI}$

and (4.0 g, 13.2 mmol) 1-bromohexane. The reaction mixture was heated at 80°C with stirring for 48 h and checked by TLC. The crude product was extracted with CH<sub>2</sub>Cl<sub>2</sub> (3 x 50 mL). The obtained organic layer was washed with water several times and dried over anhydrous MgSO<sub>4</sub> and the solvent was removed under reduced pressure. The resulting oil was chromatographed in a silica column using toluene as an eluent to yield the desired ester (3). Dark red liquid, 0.58 g, 30.0% Yield of 3. <sup>1</sup>H-NMR (500 MHz, CDCl<sub>3</sub>): δ(ppm) 8.17 (d, *J* = 8.7 Hz, 2H, Ar-H), 7.91 (d, *J* = 8.8 Hz, 2H, Ar-H), 7.51 (d, *J* = 9.2 Hz, 1H, Ar-H), 6.70 (d, *J* = 9.2 Hz, 1H, Ar-H), 4.42 (q, *J* = 7.2 Hz, 2H, -OCH<sub>2</sub>CH<sub>3</sub>), 4.25 (t, *J* = 6.5 Hz, 2H, -OCH<sub>2</sub>CH<sub>2</sub>), 4.10–4.02 (m, 4H, -OCH<sub>2</sub>CH<sub>2</sub>), 1.93–1.70 (m, 6H, -OCH<sub>2</sub>CH<sub>2</sub>), 1.60–1.22 (m, 27 H, -CH<sub>2</sub> and CH<sub>3</sub>), 1.00–0.82 (m, 9H, CH<sub>3</sub>).

### 2.1.2. Synthesis of 4-[2',3',4'-trihexyloxyphenylazo]benzoic acid (4)

To (0.58 g, 1.0 mmol) of the ester 3 dissolved in hot ethanol (100 mL) was added (0.35 g, 6.25 mmol) of KOH dissolved in water and the solution was refluxed for 4 h. The reaction mixture was cooled to room temperature and poured into ice (250 g) and acidified with concentrated hydrochloric acid. The obtained orange precipitate was filtered off and washed successively with water and ethanol. No further purification was needed, and the acid was used as it is for the next step. Orange solid, 0.53 g, 91.3% yield of 4. <sup>1</sup>H-NMR (500 MHz, DMSO-*d*<sub>6</sub>): δ(ppm) 8.09 (d, *J* = 8.5 Hz, 2H, Ar-H), 7.86 (d, *J* = 8.5 Hz, 2H, Ar-H), 7.42 (d, *J* = 9.2 Hz, 1H, Ar-H), 6.89 (d, *J* = 9.3 Hz, 1H, Ar-H), 4.15 (t, *J* = 6.2 Hz, 2H, -OCH<sub>2</sub>CH<sub>2</sub>), 4.04 (t, *J* = 6.2 Hz, 2H, -OCH<sub>2</sub>CH<sub>2</sub>), 3.95 (t, *J* = 6.4 Hz, 2H, -OCH<sub>2</sub>CH<sub>2</sub>), 1.87–1.61 (m, 6H, -OCH<sub>2</sub>CH<sub>2</sub>), 1.55–1.15 (m, 24H, CH<sub>2</sub>), 0.98–0.66 (m, 9H, CH<sub>3</sub>).

### 2.1.3. Synthesis of 4'-hydroxy-[1,1'-biphenyl]-4-[2',3',4'-trihexyloxyphenylazo]benzoate (5)

The acid 4 (0.50 g, 0.95 mmol) was heated under reflux with excess thionyl chloride (3 mL) and few drops of DMF for 1 h followed by removal of the excess thionyl chloride by distillation under reduced pressure. To the obtained acid chloride 4,4'-dihydroxybiphenyl (0.93 g, 5.0 mmol) dissolved in dry pyridine (30 mL) was added and the mixture was stirred at 100°C for 12 h. The reaction mixture was cooled to room temperature, poured into ice and acidified with concentrated hydrochloric acid. The obtained orange solid was filtered off, dried and purified by column chromatography using dichloromethane as an eluent to give the hydroxy compound 5 as an orange solid. 0.31 g, 47.0% Yield of 5. <sup>1</sup>H-NMR (500 MHz, CDCl<sub>3</sub>): δ(ppm) 8.35 (d, *J* = 7.3 Hz,

2H, Ar-H), 7.99 (d, *J* = 7.2 Hz, 2H, Ar-H), 7.64–7.51 (m, 3H, Ar-H), 7.46 (d, *J* = 9.2 Hz, 2H, Ar-H), 7.27 (d, 2H, Ar-H overlapped with CDCl<sub>3</sub>), 6.90 (d, *J* = 8.7 Hz, 2H, Ar-H), 6.72 (d, *J* = 9.3 Hz, 1H, Ar-H), 4.98 (s, 1H, Ar-OH), 4.27 (t, *J* = 6.5 Hz, 2H, -OCH<sub>2</sub>CH<sub>2</sub>), 4.12–4.03 (m, 4H, -OCH<sub>2</sub>CH<sub>2</sub>), 1.94–1.73 (m, 6H, -OCH<sub>2</sub>CH<sub>2</sub>), 1.61–1.22 (m, 24H, CH<sub>2</sub>), 1.01–0.80 (m, 9H, CH<sub>3</sub>).

### 2.1.4. Synthesis of the final compounds (A–E)

**2.1.4.1. General procedure.** To the appropriate 4-substituted benzoic acid (1.0 mmol) dissolved in DCM (1.2 mmol) DCC and a catalytic amount of DMAP were added and the solution was kept under stirring for 10 min followed by addition of 4'-hydroxy-[1,1'-biphenyl]-4-[2',3',4'-trihexyloxyphenylazo]benzoate (5, 1.0 mmol) previously dissolved in DCM. The stirring was continued for 48 h and checked by TLC. After the reaction completion; the solid byproduct was filtered out and washed several times with DCM. The crude orange material obtained after solvent removal was purified by column chromatography from DCM followed by recrystallisation from ethanol:chloroform (8:2) to give the desired polycatenars (A–E) in 71–73% yield. The NMR spectra of the final compounds are shown in Figures S1–S10 in the electronic supporting information file (ESI).

#### Compound A

Prepared from 4-hexyloxybenzoic acid. Orange crystals, 72%.

<sup>1</sup>H-NMR (500 MHz, CDCl<sub>3</sub>): δ(ppm) 8.35 (d, *J* = 8.4 Hz, 2H, Ar-H), 8.17 (d, *J* = 8.8 Hz, 2H, Ar-H), 7.99 (d, *J* = 8.4 Hz, 2H, Ar-H), 7.71–7.59 (m, 4H, Ar-H), 7.55 (d, *J* = 9.2 Hz, 1H, Ar-H), 7.38–7.27 (m, 4H, Ar-H), 6.99 (d, *J* = 9.1 Hz, 2H, Ar-H), 6.72 (d, *J* = 9.3 Hz, 1H, Ar-H), 4.27 (t, *J* = 6.5 Hz, 2H, -OCH<sub>2</sub>CH<sub>2</sub>), 4.15–3.97 (m, 6H, -OCH<sub>2</sub>CH<sub>2</sub>), 1.95–1.71 (m, 8H, -OCH<sub>2</sub>CH<sub>2</sub>), 1.63–1.27 (m, 24H, CH<sub>2</sub>), 1.00–0.81 (m, 12H, CH<sub>3</sub>). <sup>13</sup>C-NMR (126 MHz, CDCl<sub>3</sub>): δ (ppm) = 164.95, 164.75, 163.57, 157.17, 156.10, 153.29, 150.61, 150.38, 142.22, 141.03, 138.36, 137.97, 132.29, 131.19, 130.32, 128.22, 128.15, 122.68, 122.14, 121.98, 121.47, 114.30, 111.65, 107.76, 76.29, 73.97, 68.97, 68.33, 31.73, 31.69, 31.54, 31.53, 30.38, 30.29, 29.22, 29.05, 25.84, 25.78, 25.71, 25.64, 22.66, 22.66, 22.58, 22.57, 14.05, 14.04, 13.99. E. A. Calculated for C<sub>56</sub>H<sub>70</sub>N<sub>2</sub>O<sub>8</sub> C, 74.80, H 7.85, N 3.12; found C 74.75, H 7.85, N 3.11%.

#### Compound B

Prepared from 4-hexylthiobenzoic acid [46]. Orange crystals, 73%.

<sup>1</sup>H NMR (500 MHz, CDCl<sub>3</sub>): δ(ppm) 8.35 (d, *J* = 8.5 Hz, 2H, Ar-H), 8.11 (d, *J* = 8.9 Hz, 2H, Ar-H), 7.99 (d, *J* = 8.5 Hz, 2H, Ar-H), 7.72–7.59 (m, 4H, Ar-H), 7.55 (d, *J* = 9.1 Hz, 1H, Ar-H), 7.41–7.27 (m, 6H, Ar-H), 6.72 (d, *J* = 9.3 Hz, 1H, Ar-H), 4.27 (t, *J* = 6.5 Hz, 2H, -OCH<sub>2</sub>CH<sub>2</sub>), 4.07 (t, *J* = 6.6 Hz, 4H, -OCH<sub>2</sub>CH<sub>2</sub>), 3.02 (t, *J* = 6.6

Hz, 2H, -SCH<sub>2</sub>CH<sub>2</sub>), 1.92–1.77 (m, 6H, -OCH<sub>2</sub>CH<sub>2</sub>), 1.73 (q,  $J = 7.5$  Hz, 2H, -SCH<sub>2</sub>CH<sub>2</sub>), 1.61–1.26 (m, 24H, CH<sub>2</sub>), 0.99–0.83 (m, 12H, CH<sub>3</sub>). <sup>13</sup>C-NMR (126 MHz, CDCl<sub>3</sub>):  $\delta$ (ppm) = 164.92, 164.74, 157.17, 156.11, 153.29, 150.48, 150.42, 145.74, 142.22, 141.02, 138.29, 138.12, 131.19, 130.46, 130.31, 128.23, 128.19, 126.25, 125.65, 122.68, 122.05, 122.00, 111.65, 107.76, 76.29, 73.97, 68.97, 31.99, 31.73, 31.69, 31.54, 31.31, 30.38, 30.29, 29.22, 28.68, 28.57, 25.83, 25.78, 25.71, 22.66, 22.66, 22.58, 22.50, 14.05, 14.04, 13.99, 13.97. **E. A.** Calucalted for C<sub>56</sub>H<sub>70</sub>N<sub>2</sub>O<sub>7</sub>S C 73.49, H 7.71, N 3.06; found C 73.40, H 7.67, N 3.05%.

#### Compound C

Prepared from 4-heptylbenzoic acid. Orange crystals, 71%.

<sup>1</sup>H-NMR (500 MHz, CDCl<sub>3</sub>):  $\delta$ (ppm) 8.35 (d,  $J = 8.5$  Hz, 2H, Ar-H), 8.14 (d,  $J = 8.2$  Hz, 2H, Ar-H), 7.99 (d,  $J = 8.5$  Hz, 2H, Ar-H), 7.70–7.60 (m, 4H, Ar-H), 7.55 (d,  $J = 9.1$  Hz, 1H, Ar-H), 7.38–7.28 (m, 6H, Ar-H), 6.72 (d,  $J = 9.3$  Hz, 1H, Ar-H), 4.27 (t,  $J = 6.5$  Hz, 2H, -OCH<sub>2</sub>CH<sub>2</sub>), 4.13–4.00 (m, 4H, -OCH<sub>2</sub>CH<sub>2</sub>), 2.79–2.63 (m, 2H, -CH<sub>2</sub>CH<sub>2</sub>), 1.94–1.74 (m, 6H, -OCH<sub>2</sub>CH<sub>2</sub>), 1.72–1.60 (m, 2H, -CH<sub>2</sub>CH<sub>2</sub>), 1.60–1.18 (m, 26H, CH<sub>2</sub>), 0.99–0.82 (m, 12H, CH<sub>3</sub>). <sup>13</sup>C-NMR (126 MHz, CDCl<sub>3</sub>):  $\delta$ (ppm) = 165.25, 164.75, 157.17, 156.11, 153.29, 150.56, 150.40, 149.45, 142.22, 141.03, 138.33, 138.07, 131.19, 130.32, 130.26, 128.66, 128.23, 128.18, 126.89, 122.68, 122.09, 122.00, 111.65, 107.76, 76.29, 73.98, 68.97, 36.09, 31.76, 31.73, 31.69, 31.54, 31.13, 30.38, 30.29, 29.22, 29.20, 29.11, 25.84, 25.78, 25.72, 25.66, 22.63, 22.58, 14.06, 13.99. Calucalted for C<sub>57</sub>H<sub>72</sub>N<sub>2</sub>O<sub>7</sub> C 76.31, H 8.09, N 3.12; found C 76.25, H 8.00, N 3.09%.

#### Compound D

Prepared from 4-decyloxybenzoic acid. Orange crystals, 73%.

<sup>1</sup>H-NMR (500 MHz, CDCl<sub>3</sub>):  $\delta$ (ppm) 8.35 (d,  $J = 8.5$  Hz, 2H, Ar-H), 8.17 (d,  $J = 8.8$  Hz, 2H, Ar-H), 7.99 (d,  $J = 8.5$  Hz, 2H, Ar-H), 7.65 (t,  $J = 8.2$  Hz, 4H, Ar-H), 7.55 (d,  $J = 9.1$  Hz, 1H, Ar-H), 7.37–7.27 (m, 4H, Ar-H), 6.99 (d,  $J = 8.9$  Hz, 2H, Ar-H), 6.72 (d,  $J = 9.3$  Hz, 1H, Ar-H), 4.27 (t,  $J = 6.5$  Hz, 2H, -OCH<sub>2</sub>CH<sub>2</sub>), 4.14–4.00 (m, 6H, -OCH<sub>2</sub>CH<sub>2</sub>), 1.94–1.73 (m, 8H, -OCH<sub>2</sub>CH<sub>2</sub>), 1.62–1.18 (m, 32H, CH<sub>2</sub>), 0.98–0.79 (m, 12H, CH<sub>3</sub>). <sup>13</sup>C-NMR (126 MHz, CDCl<sub>3</sub>):  $\delta$ (ppm) = 164.95, 164.75, 163.58, 157.17, 156.10, 153.29, 150.61, 150.38, 142.22, 141.03, 138.37, 137.97, 132.29, 131.19, 130.32, 128.23, 128.15, 122.68, 122.14, 121.98, 121.47, 114.31, 111.65, 107.76, 73.98, 68.97, 68.34, 31.87, 31.73, 31.69, 31.54, 30.38, 30.29, 29.54, 29.52, 29.34, 29.29, 29.22, 29.09, 25.97, 25.84, 25.78, 25.72, 22.67, 22.66, 22.58, 14.09, 14.06, 14.05, 13.99. Calucalted for C<sub>60</sub>H<sub>78</sub>N<sub>2</sub>O<sub>8</sub> C 75.44, H 8.23, N 2.93; found C 75.42, H 8.20, N 2.88%.

#### Compound E

Prepared from 4-(5,5,6,6,7,7,8,8,9,9,10,10,10-tridecafluorodecyloxy)benzoic acid [47]. Orange crystals, 71%.

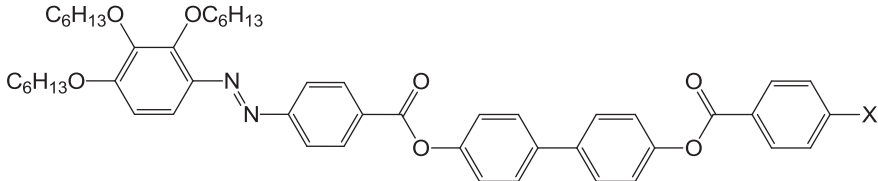
<sup>1</sup>H-NMR (500 MHz, CDCl<sub>3</sub>):  $\delta$ (ppm) 8.35 (d,  $J = 8.6$ , 2H, Ar-H), 8.18 (d,  $J = 8.9$  Hz, 2H, Ar-H), 7.99 (d,  $J = 9.2$  Hz, 2H, Ar-H), 7.70–7.60 (m, 4H, Ar-H), 7.55 (d,  $J = 9.2$  Hz, 1H, Ar-H), 7.38–7.27 (m, 4H, Ar-H), 6.99 (d,  $J = 8.9$  Hz, 2H, Ar-H), 6.72 (d,  $J = 9.3$  Hz, 1H, Ar-H), 4.27 (t,  $J = 6.6$  Hz, 2H, -OCH<sub>2</sub>CH<sub>2</sub>), 4.17–4.00 (m, 6H, -OCH<sub>2</sub>CH<sub>2</sub> and -CH<sub>2</sub>CF<sub>2</sub>-), 2.29–2.10 (m, 2H, CH<sub>2</sub>), 2.03–1.75 (m, 8H, CH<sub>2</sub>), 1.63–1.18 (m, 18H, CH<sub>2</sub>), 0.99–0.82 (m, 9H, CH<sub>3</sub>). <sup>13</sup>C-NMR (126 MHz, CDCl<sub>3</sub>):  $\delta$ (ppm) = 164.75, 163.13, 157.17, 153.29, 142.22, 141.03, 132.35, 131.19, 130.32, 128.25, 128.23, 128.17, 122.68, 122.11, 122.02, 122.00, 114.25, 111.65, 107.76, 76.29, 73.98, 68.97, 67.47, 31.73, 31.69, 31.54, 30.38, 30.29, 29.22, 28.57, 25.84, 25.78, 25.72, 22.67, 22.58, 14.06, 14.05, 13.99. C<sub>56</sub>H<sub>70</sub>N<sub>2</sub>O<sub>7</sub>

## 2.2. Characterisation methods

Thin-layer chromatography (TLC) was performed on aluminium sheet precoated with silica gel. Analytical quality chemicals were obtained from commercial sources and used as obtained. The solvents were dried using the standard methods when required. The purity and the chemical structures of all synthesised materials were confirmed by the spectral data. The structure characterisation of the prepared materials is based on <sup>1</sup>H-NMR and <sup>13</sup>C-NMR (Varian Unity 500 and Varian Unity 400 spectrometers, in CDCl<sub>3</sub> solutions, with tetramethylsilane as internal standard). Microanalyses were performed using a Leco CHNS-932 elemental analyser.

The mesophase behaviour and transition temperatures of the synthesised polycatenars were measured using a Mettler FP-82 HT hot stage and control unit in conjunction with a Nikon Optiphot-2 polarising microscope. The associated enthalpies were obtained from DSC-thermograms which were recorded on a Perkin-Elmer DSC-7, heating and cooling rate: 10 K min<sup>-1</sup>. The optical micrographs were taken with a Leica MDN20 HD camera.

The X-ray diffraction patterns were recorded with a 2D detector (Vantec 500, Bruker). Ni filtered and pinhole collimated CuK $\alpha$  radiation was used. For the wide-angle X-ray diffraction (WAXD) measurements the exposure time was 15 min and the sample to detector distance was 9.5 cm, small-angle X-ray diffraction (SAXD) measurements were carried out with an exposure time of 30 min and a sample to detector distance of 27.40 cm. Uniform orientation was achieved by alignment in a magnetic field ( $B \approx 1$  T) using thin capillaries. The samples were held on a temperature-controlled heating stage.

**Table 1.** Phase transition temperatures ( $T/^\circ\text{C}$ ), mesophase types, and transition enthalpies [ $\Delta H/\text{kJ}\cdot\text{mol}^{-1}$ ] of the polycatenars (**A–E**).<sup>a</sup>


Comp.	X	Heating				Cooling			
<b>A</b>	OC <sub>6</sub> H <sub>13</sub>	Cr 132 [31.2]	SmC 153 [3.9]	N <sub>Cybc</sub> 270 [1.4]	Iso	Iso 263 [1.3]	N <sub>Cybc</sub> 146 [3.3]	SmC 74 [24.1]	Cr
<b>B</b>	SC <sub>6</sub> H <sub>13</sub>	Cr 143 [44.0]	N <sub>Cybc</sub> 243 [1.1]	Iso		Iso 248 [0.4]	N <sub>Cybc</sub> 133 [1.4]	SmC 96 [27.0]	Cr
<b>C</b>	C <sub>7</sub> H <sub>15</sub>	Cr 122 [34.9]	SmC 145 [3.3]	N <sub>Cybc</sub> 256 [1.2]	Iso	Iso 249 [1.2]	N <sub>Cybc</sub> 141 [3.3]	SmC 81 [19.5]	Cr
<b>D</b>	OC <sub>10</sub> H <sub>21</sub>	Cr 121 [22.9]	SmC 162 [4.0]	N <sub>Cybc</sub> 253 [1.5]	Iso	Iso 250 [0.9]	N <sub>Cybc</sub> 159 [3.7]	SmC 92 [20.9]	Cr
<b>E</b>	O(CH <sub>2</sub> ) <sub>4</sub> C <sub>6</sub> F <sub>13</sub>	Cr 126 [22.1]	SmC 198 [1.2]	N <sub>Cybc</sub> 253 [0.8]	Iso	Iso 250 [0.8]	N <sub>Cybc</sub> 196 [1.4]	SmC 104 [20.0]	Cr

Notes: <sup>a</sup>Peak temperatures as determined from second heating and second cooling DSC scans with rate 10 K min<sup>-1</sup>; abbreviations: Cr = crystalline solid; N<sub>Cybc</sub> = nematic phase with cybotactic clusters of the SmC type; SmC = smectic C phase; Iso = isotropic liquid.

### 3. Results and discussion

#### 3.1. Liquid-crystalline behaviour

The LC self-assembly of all synthesised materials was investigated by polarised optical microscope (POM), differential scanning calorimetry (DSC) and X-ray diffraction (XRD). The transition temperatures and the enthalpies associated with different phase transitions are collected in Table 1. As examples, the DSC heating and cooling curves of compounds **A** and **D** are shown in Figure 1 (for the DSC curves of remaining compounds, see Figure S1–S13).

Before discussing the mesomorphic behaviour, we should refer to the LC properties of the starting 4-[2',3',4'-trihexyloxyphenylazo]benzoic acid (**4**). This acid exists in a dimer form as a result of intermolecular hydrogen bonding interaction between the two free carboxylic groups. This dimer possesses a phasid-like structure representing a hexacatenar with six terminal hexyloxy chains. As a result of the distribution of the terminal chains in 2, 3 and 4 positions in the terminal benzene rings, this dimeric acid exhibits nematic and columnar mesophases. The nematic phase is monotropic and exists over a short temperature range ~11 K [40]. In our new materials, we used the same concept of substitution of the terminal hexyloxy chains in position 2, 3 and 4 at one terminus of the molecule aiming to induce nematic phases by the effect of the hexyloxy chain at position 2, which acts as a lateral substituent. The nematic phases with cybotactic clusters (N<sub>Cyb</sub>) are considered as a key to produce the illusive the biaxial nematic phase, which is an important issue from the viewpoint of both scientific concerns and applications [48,49].

We also used only one chain at the other end aiming to check if the synthesised polycatenars could exhibit Iso<sup>1[\*]</sup> phase adjacent to the nematic phase [24,43,44]. Moreover, we have investigated the effect of changing

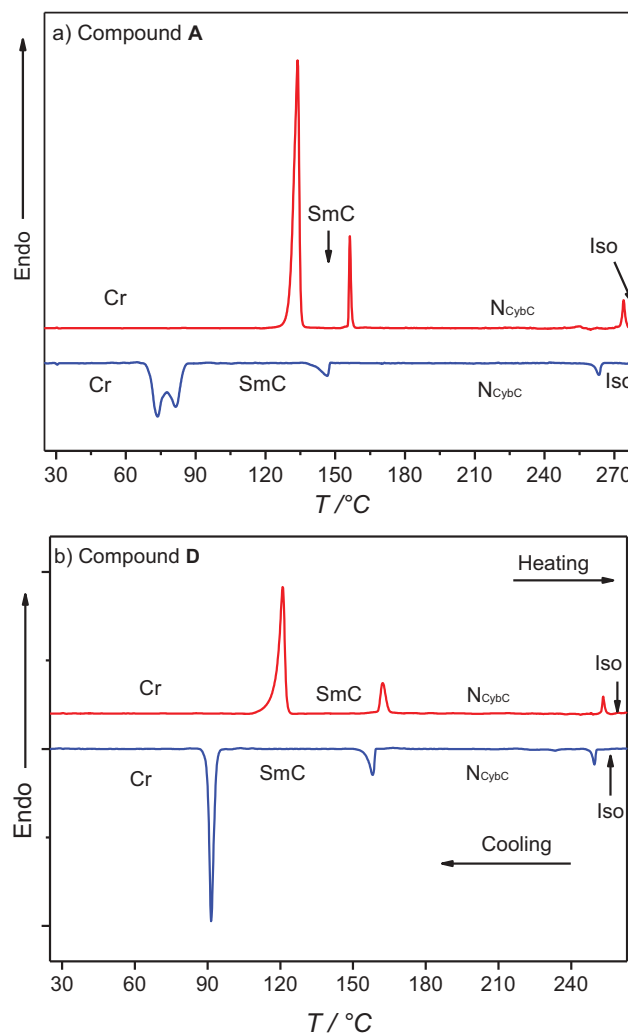


**Figure 1.** (Colour online) DSC heating and cooling curves of compounds **A** and **D** (10 K min<sup>-1</sup> Heating and cooling rates).

the type of one terminal chain on the type and ranges of the mesophases in the new polycatenars (**A–E**).

As can be seen from Table 1 and Figure 2, all the new polycatenars are liquid-crystalline materials. All

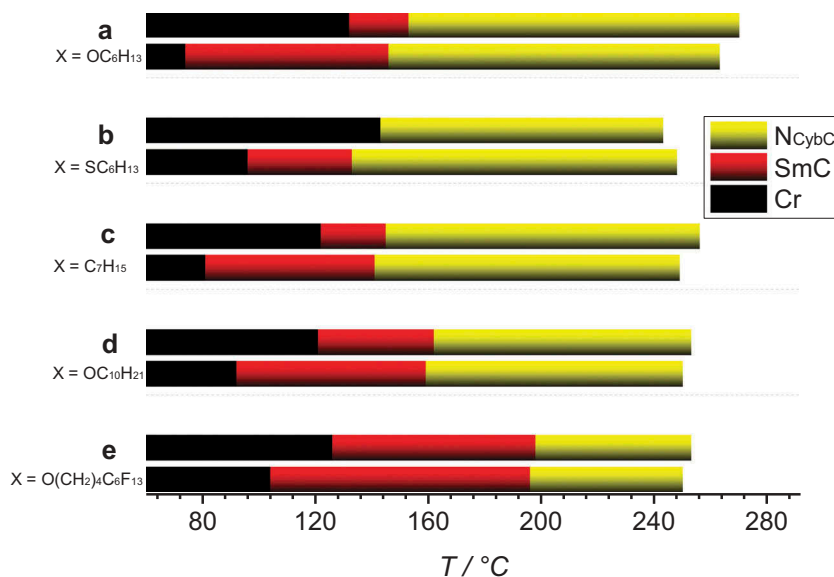


**Figure 2.** (Colour online) Phase transitions of the polycatenars **A–E** as determined from heating (upper columns) and cooling DSC scans (lower columns) with rate  $10 \text{ K min}^{-1}$ . For phase abbreviations and numerical values, see Table 1.

compounds, with the exception of **B** exhibit enantiotropic nematic and smectic C phases. The highest LC phase stabilities are observed for compound **A** with the shortest alkyl chain attached to the aromatic core with oxygen atom, where on heating the SmC phase exists over  $\sim 21 \text{ K}$  and the nematic exists over a wide temperature range  $\sim 117 \text{ K}$  (Figure 3).

The texture of the nematic phases of all compounds was difficult to be distinguished from the SmC texture in homeotropic cells as no schlieren texture could be observed. However, the textural changes were more pronounced in planar  $6 \mu\text{m}$  ITO coated cell, where the nematic phase shows a marble texture and the SmC phase exhibit broken fan-shaped textures with dark extinctions are inclined with the directions of the polarisers (Figure 3(c,d)). The two phases are also accompanied by phase transitions peaks in the DSC heating and cooling scans (Figure 1(a,b) and Table 1) and were investigated by XRD as will be discussed later.

The phase behaviour of **A** is almost the same as that for compound **C**, in which the oxygen atom in the terminal hexyloxy chain (**A**) is replaced by a methylene group (**C**). However, the melting point of **C** ( $122^\circ\text{C}$ ) is lower compared to that of **A** ( $132^\circ\text{C}$ ) as would be expected for alkyl substitution. Replacing the oxygen atom in **A** by a sulphur atom leads to compound **B**. The latter exhibit enantiotropic nematic phase and a monotropic SmC phase with a lower clearing temperature ( $\sim 243^\circ\text{C}$ ) compared to the hexyloxy-substituted analogue **A** ( $\sim 270^\circ\text{C}$ ). This is in consistent with the literature [46,50,51] and is attributed to the steric hindrance caused by the smaller angle of the C–S–C bond with respect to the C–O–C bond

as well as the weaker  $\pi$ -conjugation of the sulphur lone pair with the attached aromatic ring, which in turn results in reduced rotational barriers compared to the alkoxy chain [46].

Elongation of the terminal chain from hexyloxy (compound **A**) to decyloxy chain (compound **D**) does not change the type of the phases but leads to lower melting and clearing temperatures which results in a narrower range of nematic phase and wider range of the SmC phase compared to **A** (Table 1 and Figure 2). Replacing the decyloxy chain in **D** with a perfluorinated terminal chain results in an even wider range of the SmC phase (compound **E**). This agreed with other reports indicating that introducing a fluorinated unit into the terminal chain induces the formation of tilted smectic phases in broad temperature ranges as a result of microsegregation due to the incompatibility, immiscibility and polar contrast of the fluorocarbon and hydrocarbon segments [47,52,53]. However, the nematic phase is always existing for all types of terminal chains, which could be attributed to the lateral hexyloxy chain in position 2 in the outer benzene ring at the other terminus (see section 4). Moreover, in all compounds (**A–E**) no  $\text{Iso}_1^{[*]}$  phases were observed.

### 3.2. XRD investigation

In order to investigate the type of the nematic phases of the new materials (**A–E**), compound **A** was selected for XRD investigation. The X-ray diffraction pattern in the nematic phase at  $T = 160^\circ\text{C}$  (Figure 4) shows a diffuse

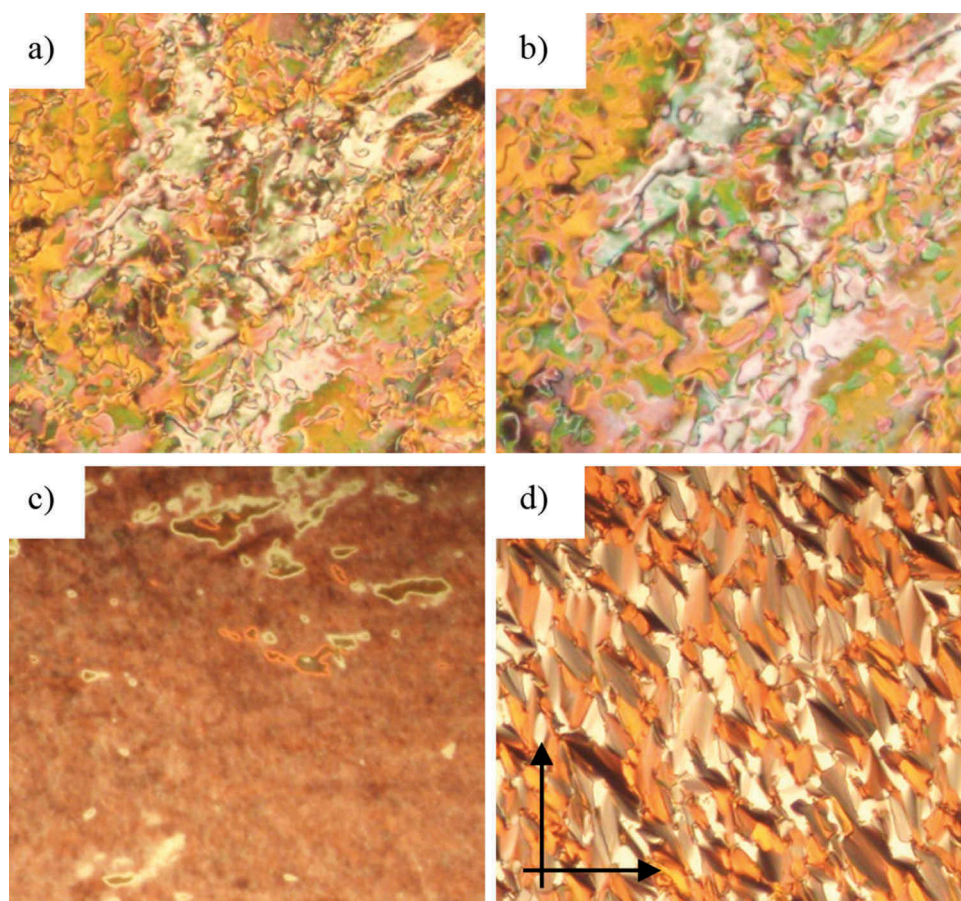


**Figure 3.** (Colour online) Optical textures of compound **A** under crossed polarisers as observed on cooling from the isotropic liquid state; (a) and (b) in homeotropic cell; (c) and (d) in planar 6  $\mu\text{m}$ , ITO coated cell: (a, c) in the  $N_{\text{Cybc}}$  phase at  $T = 170^\circ\text{C}$  and (b, d) in the SmC phase at  $T = 145^\circ\text{C}$ . The directions of the polarisers are shown in d).

scattering in the wide-angle region with a maximum at  $d = 0.45$  nm and an additional diffuse scattering in the small-angle region with a maximum at  $d = 3.08$  nm. The diffuse small-angle scattering has clear maxima beside the meridian (dumbbell shape) with relatively high intensity compared to the wide-angle scattering, which can be attributed to the existence of cybotactic cluster of the SmC-type nematic phase ( $N_{\text{Cybc}}$  phase) [54–59].

From the intensity distribution (Figure 4(b)) a tilt angle of the molecules within the clusters of around  $29.6^\circ$  can be estimated which is in line with the maximum possible value  $\beta = 41.30$  as calculated with  $\cos\beta = d/L_{\text{mol}}$  ( $L_{\text{mol}} = 4.1$  nm determined between the ends of the alkyloxy chains in a stretched conformation). This kind of cybotactic nematic phases is a typical feature of other polycatenars with extended rigid cores [60]. In the smectic phase range of compound **A**, the scattering in the wide-angle region remains diffuse indicating the LC nature of the phase, while the small-angle peak condenses and sharpens with a maximum at  $d = 2.8$  nm. This  $d$ -value is significantly smaller than the single-molecule length, indicating a single layer structure with significant tilt supporting intercalation of the

alkyl chains. A tilt angle of about  $53^\circ$  could be calculated from the position of the diffuse wide-angle scattering maxima with respect to the layer reflections on the meridian of the 2D diffraction patterns.

### 3.3. Photosensitivity

Photosensitivity of the synthesised materials was investigated due to the presence of the azo linkage in their molecular structures. It was found that, they undergo fast and reversible isothermal phase transition upon illumination with light (405 nm, 5  $\text{mW}/\text{mm}^2$ ). Therefore, the N-SmC or N-Iso transitions temperatures in all compounds can be affected by light irradiation. We have investigated compounds **A–E** between normal glass slides under POM in the LC phases, and they show the same behaviour, where both N-SmC and N-Iso transitions temperatures were lowered by around 10 K due to the *cis-trans* photoisomerisation of the azobenzene units. This process is fast and reversible as it takes place in few seconds ( $<3$  s) and if the light source is removed the texture relaxes back to the original state [18,37]. The photosensitivity of the polycatenars **A–**

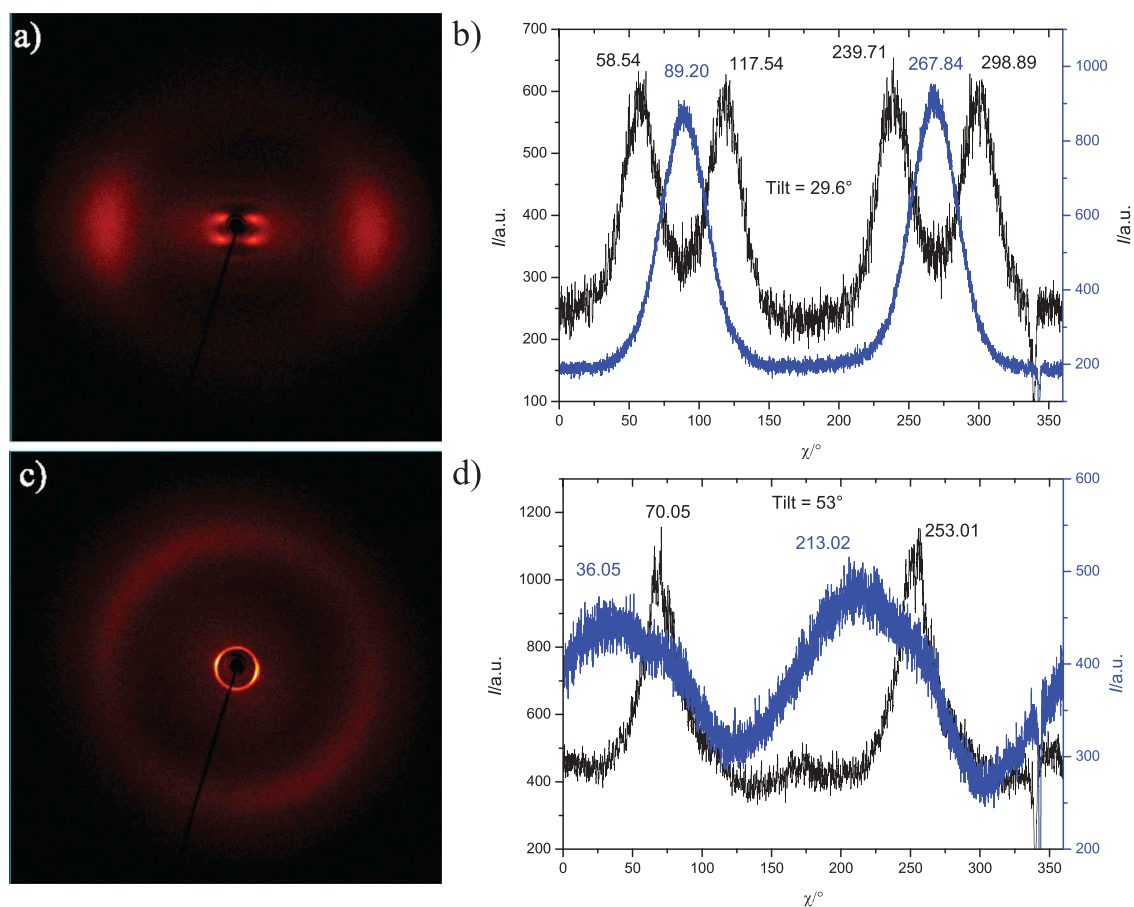


**Figure 4.** (Colour online) XRD investigations of compound **A**: (a, b) in the nematic phase at 160°C; (c, d) in the SmC phase at 145°C; (a) and (c) diffraction patterns; (b) and (d) intensity distribution of the diffuse scatterings along  $\chi$ , blue curve wide-angle scattering (15–25°  $2\theta$ ), black curve small-angle scattering (2–5°  $2\theta$ ).

**E** was further investigated in its chloroform solutions. For example, the UV-vis spectra of **A** in chloroform solution was measured at three different conditions (Figure 5). For the freshly prepared sample, a maximum absorption due to the  $\pi$ - $\pi^*$  transition is located at  $\sim 365$  nm indicating the presence of the molecules in the more stable *trans* isomer (Figure 5; black line). Under light irradiation with 365 nm light for 30 min the absorbance band at 365 nm almost disappear and another weak absorbance band at 465 nm starts to appear indicating the  $n$ - $\pi^*$  transition as a result of *trans-cis* photoisomerisation (Figure 5; red line). Keeping the same solution in dark overnight and measuring it again gives similar spectra for the freshly measured solution (Figure 5; black and blue lines) indicating the relaxing back to the more stable *trans*-isomer.

#### 4. Comparison with related compounds

It is of interest to compare our new materials with hexyloxy chain (compound **A**) or decyloxy chain

(compound **D**) with related compound reported in the literature. Compound **F** (Scheme 2) has the same extended aromatic core with in total five benzene rings and four-terminal alkoxy chains similar to compounds **A** and **D** [43]. The main difference is that, the three hexyloxy chains at one terminus in **F** are substituted at positions 3, 4 and 5 instead of positions 2, 3 and 4 in **A** and **D**. The phase behaviour of **F** is completely different from compounds **A** and **D**, where no nematic phase is observed and instead three-dimensional tetragonal phase is exhibited by **F** beside the chiral isotropic liquid phase ( $\text{Iso}_1^{[*]}$  phase). This indicates that the substitution of the terminal chains at positions 3, 4 and 5 increase the segregation of the aliphatic chains from the aromatic core and support the formation of the three-dimensional (3D) LC phases. The suppression of 3D LC phases (tetragonal, cubic or columnar) and formation of nematic phases in compounds **A**–**E** is attributed to the lateral alkoxy chain in position 2 at the terminus with three alkoxy



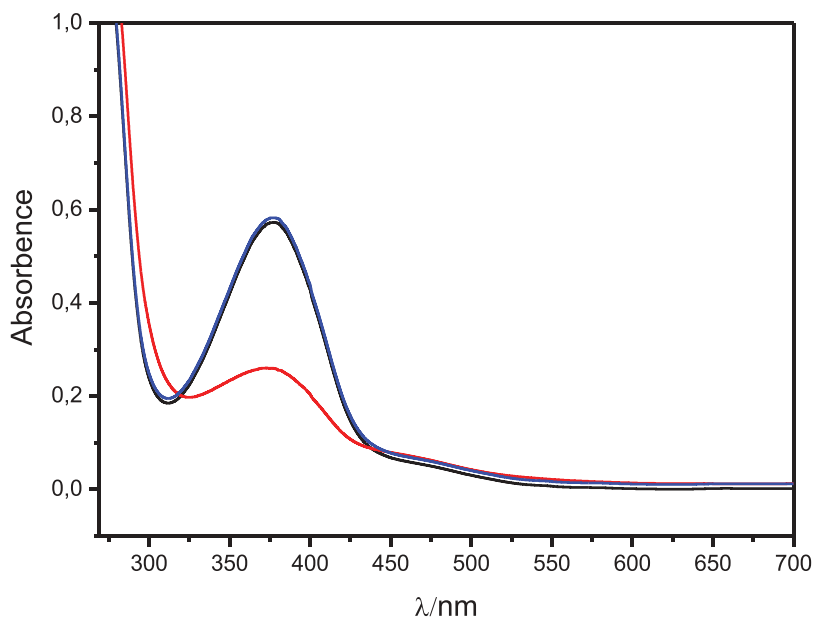
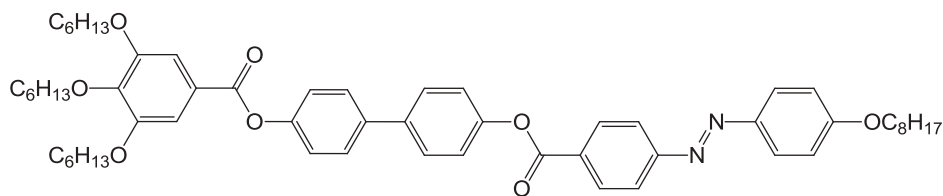


**Figure 5.** (Colour online) UV-vis spectra (absorbance vs. wavelength) of compound **A** dissolved in chloroform (0.02 mM solution) at 25°C: black line: freshly prepared sample, *trans*-isomer before irradiation; red line: *cis*-isomer as obtained after 30-min irradiation with light of 365 nm wavelength and blue line: *trans*-isomer after keeping the sample in dark overnight.



Compound **F**

Heating: Cr 121 Tet 175 Iso<sub>1</sub><sup>[\*]</sup> 189 Iso

Cooling: Iso 185 Iso<sub>1</sub><sup>[\*]</sup> 163 Tet 76 Cr

**Scheme 2.** Chemical structure of compound **F** with phase types and transition temperatures (°C) on heating (upper line) and on cooling (lower line). Abbreviations: Cr = crystalline solid; Tet = tetragonal 3D mesophase; Iso<sub>1</sub><sup>[\*]</sup> = chiral isotropic conglomerate liquid; Iso = achiral isotropic liquid [36].

chains, which removes the positional order and induces nematic phases due to the distortion of rod-like organisation [29].

## 5. Summary and conclusion

In summary, we have reported herein the design and synthesis of photosensitive azobenzene-based polycatenars. The liquid-crystal self-assembly for these materials was investigated DSC, POM and XRD. In our materials, four-terminal chains were connected to the extended aromatic core in 3 + 1 fashion, where three hexyloxy chains are kept fixed and connected at positions 2, 3 and 4 at one terminus, while in the other terminus different types of terminal chains were used. Independent on the type

of the variable terminal chain, all compounds were found to be liquid crystalline exhibiting enantiotropic nematic and smectic C phases, except compound **B** in which the SmC phase is a monotropic one. The nematic phases of all compounds exist over wide temperature ranges with maximum range for compound **A**. Investigating the nematic phase of compound **A** with XRD proved that this nematic phase is composed of cybotactic clusters of the SmC type ( $N_{CybC}$ ). No indication of chiral isotropic liquid (Iso<sup>[\*]</sup>) transitions in any of the materials were observed, indicating that the distribution of the terminal chains in position 2,3 and 4 reduce the segregation of the aromatic core and aliphatic chains, thus reducing the cooperativity of molecular self-assembly. Therefore, chirality synchronisation is

disfavoured in the cybotactic clusters forming the  $N_{CybC}$  phases. Finally, the photosensitivity of the polycatenars was studied both in different LC states and in solution, where all of them show fast and reversible *trans-cis* photoisomerisation of the azobenzene units. The possibilities provided by phase modulation by interaction with UV light are of importance for technological applications.

### Disclosure statement

No potential conflict of interest was reported by the authors.

### ORCID

Mohamed Alaasar  <http://orcid.org/0000-0003-4155-8644>

### References

- [1] Bremer M, Kirsch P, Klasen-Memmer M, et al. The TV in your pocket: development of liquid-crystal materials for the new millennium. *Angew Chem Int Ed.* **2013**;52:8880–8896.
- [2] Kato T, Uchida J, Ichikawa T, et al. Functional liquid crystals towards the next generation of materials. *Angew Chem Int Ed.* **2018**;57:4355–4371.
- [3] Bandarab HMD, Burdette SC. Photoisomerization in different classes of azobenzene. *Chem Soc Rev.* **2012**;41:1809–1825.
- [4] Alaasar M. Azobenzene-containing bent-core liquid crystals: an overview. *Liq Cryst.* **2016**;43:2208–2243.
- [5] Bisoyi HK, Li Q. Light-driven liquid crystalline materials: from photo-induced phase transitions and property modulations to applications. *Chem Rev.* **2016**;116:15089–15166.
- [6] Alaasar M, Prehm M, Tschierske C. Influence of halogen substituent on the mesomorphic properties of five-ring banana shaped molecules with azobenzene wings. *Liq Cryst.* **2013**;40:656–668.
- [7] Alaasar M, Prehm M, Nagaraj M, et al. A liquid crystalline phase with uniform tilt, local polar order and capability of symmetry breaking. *Adv Mater.* **2013**;25:2186–2191.
- [8] Du ML, Li LH, Zhang JT, et al. Photoresponsive iodine-bonded liquid crystals based on azopyridine derivatives with a low phase-transition temperature. *Liq Cryst.* **2019**;46(1):37–44.
- [9] Aya S, Salamon P, Paterson DA, et al. Fast-and-giant photorheological effect in a liquid crystal dimer. *Adv Mater Interf.* **2019**;6:1802032.
- [10] Paterson DA, Xiang J, Singh G, et al. Reversible isothermal twist-bend nematic-nematic phase transition driven by the photoisomerization of an azobenzene-based non-symmetric liquid crystal dimer. *J A Chem Soc.* **2016**;138(16):5283–5289.
- [11] Eremin A, Nadasi H, Hirankittiwong P, et al. Azodendrimers as a photoactive interface for liquid crystals. *Liq Cryst.* **2018**;45(13–15):2121–2131.
- [12] Ube T, Yoda T, Ikeda T. Fabrication of photomobile polymer materials with phase-separated structure of crosslinked azobenzene liquid-crystalline polymer and poly(dimethylsiloxane). *Liq Cryst.* **2018**;45(13–15):2269–2273.
- [13] Paterson DA, Walker R, Abberley JP, et al. Azobenzene-based liquid crystal dimers and the twist-bend nematic phase. *Liq Cryst.* **2017**;44(12–13):2060–2078.
- [14] Arakawa Y, Sasaki Y, Haraguchi N, et al. Synthesis, phase transitions and birefringence of novel liquid crystalline 1,4-phenylene bis(4-alkylthio benzoates) and insights into the cybotactic nematic behaviour. *Liq Cryst.* **2018**;45(6):821–830.
- [15] Zaremba M, Siksnys V. Molecular scissors under light control. *Proc Natl Acad Sci USA.* **2010**;107:1259–1260.
- [16] Lee KM, White TJ. Photomechanical response of composite structures built from azobenzene liquid crystal polymer networks. *Polymers.* **2011**;3:1447–1457.
- [17] Garcia-Amorós J, Reig M, Castro MCR, et al. Molecular photo-oscillators based on highly accelerated heterocyclic azo dyes in nematic liquid crystals. *Chem Commun.* **2014**;50:6704–6706.
- [18] Fehrentz T, Schönberger M, Trauner D. Optochemical genetics. *Angew Chem Int Ed.* **2011**;50:12156–12182.
- [19] Fleischmann EV, Zentel R. Liquid-crystalline ordering as a concept in materials science: from semiconductors to stimuli-responsive devices. *Angew Chem Int Ed.* **2013**;52:8810–8827.
- [20] Nakano M, Ikeda T. Photomechanics: directed bending of a polymer film by light. *Nature.* **2003**;425:145.
- [21] Zhang YY, Xu J, Cheng F, et al. Photoinduced bending behavior of crosslinked liquid-crystalline polymer films with a long spacer. *J Mater Chem.* **2010**;20:7123–7130.
- [22] Saccone M, Palacio FF, Cavallo G, et al. Photoresponsive ionic liquid crystals assembled via halogen bond: en route towards light-controllable ion transporters. *Faraday Discuss.* **2017**;203:407–422.
- [23] Pflötscher M, Wölper C, Gutmann JS, et al. A modular approach towards functional supramolecular aggregates—subtle structural differences inducing liquid crystallinity. *Chem Commun.* **2016**;52:8549–8552.
- [24] Alaasar M, Poppe S, Dong Q, et al. Mirror symmetry breaking in cubic phases and isotropic liquids driven by hydrogen bonding. *Chem Comm.* **2016**;52:13869–13872.
- [25] Alaasar M, Poppe S, Tschierske C. Photoresponsive halogen bonded polycatenar liquid crystals. *J Mol Liq.* **2019**;277:233–240.
- [26] Alaasar M, Tschierske C, Prehm M. Hydrogen-bonded supramolecular complexes formed between isophthalic acid and pyridine-based derivatives. *Liq Cryst.* **2011**;38:925–934.
- [27] Jansze SM, Martínez-Felipe A, Storey J, et al. Phase driven by hydrogen bonding. *Angew Chem Int Ed.* **2015**;54:643–646.
- [28] Tschierske C. Development of structural complexity by liquid-crystal self-assembly. *Angew Chem Int Ed.* **2013**;52:8828–8878.

- [29] Eds, Goodby JW, Collings PJ, Gleeson H, et al. Handbook of liquid crystals. 2nd ed. Vol. 5. Non-conventional liquid crystals. Weinheim: Wiley-VCH; 2014
- [30] Malthete J, Nguyen HT, Destrade C. Phasmids and polycatenar mesogens. *Liq Cryst.* 1993;13:171–187.
- [31] Nguyen HT, Destrade C, Malthete J. Phasmids and polycatenar mesogens. *Adv Mater.* 1997;9:375–388.
- [32] Rowe KE, Bruce DW. The synthesis and mesomorphism of di-, tetra- and hexacatenar liquid crystals based on 2,2'-bipyridine. *J Mater Chem.* 1998;8:331–341.
- [33] Gharbia M, Gharbi A, Nguyen HT, et al. Polycatenar liquid crystals with long rigid aromatic cores: a review of recent works. *Curr Opin Colloid Interface Sci.* 2002;7:312–325.
- [34] Alstermark C, Eriksson M, Nilsson M, et al. Biforked mesogens with ester linkages, derived from 3-(3,4-dialkoxyphenyl)propanoic acid. *Liq Cryst.* 1990;8:75–80.
- [35] Weissflog W, Letko I, Diele S, et al. Mesomorphic behavior of new double swallow-tailed compounds. *Adv Mater.* 1996;8:76–79.
- [36] Shanker G, Prehm M, Yelamaggad CV, et al. Benzylidenehydrazine based room temperature columnar liquid crystals. *J Mater Chem.* 2011;21:5307–5311.
- [37] Chen H, Zhang R, Gao H, et al. Synthesis, self-assembly, metal binding properties of triazole azobenzene based polycatenar dyes through click chemistry. *Dyes Pigments.* 2018;149:512–520.
- [38] Peng X, Gao H, Xiao Y, et al. Synthesis and self-assembly of photoresponsive and luminescent polycatenar liquid crystals incorporating an azobenzene unit interconnecting two 1,3,4-thiadiazoles. *New J Chem.* 2017;41:2004–2012.
- [39] Yamakado R, Hara M, Nagano S, et al. Photoresponsive soft ionic crystals: ion-pairing assemblies of azobenzene carboxylates. *Chem - A Eur J.* 2017;23:9244–9248.
- [40] Prasad V, Kang S-W, Varshney SK, et al. Self-assembly of azo molecules to mesogenic phasmidlike materials through inter-molecular hydrogen bonding. *Liq Cryst.* 2010;37:121–128.
- [41] Nagaveni NG, Gupta M, Roy A, et al. Photosensitive phasmid-like liquid crystalline materials with unusual mesomorphic behaviour. *J Mater Chem.* 2010;20:9089–9099.
- [42] Marini A, Geppi M, Prasad V, et al. NMR study of a phasmid-like liquid crystal. *Chem Phys Lett.* 2011;507:96–99.
- [43] Alaasar M, Prehm M, Cao Y, et al. Spontaneous mirror-symmetry breaking in isotropic liquid phases of photoisomerizable achiral molecules. *Angew Chem Int Ed.* 2016;128:320–324.
- [44] Alaasar M, Poppe S, Dong Q, et al. Isothermal chirality switching in liquid-crystalline azobenzene compounds with non-polarized light. *Angew Chem Int Ed.* 2017;56:10801–10805.
- [45] Baena MJ, Espinet P, Folcia CL, et al. Photoisomerizable metallomesogens and soft crystals based on orthopalladated complexes. *Inorg Chem.* 2010;49:8904–8913.
- [46] Arakawa Y, Sasaki Y, Igawa K, et al. Hydrogen bonding liquid crystalline benzoic acids with alkylthio groups: phase transition behaviour and insights into the cybotactic nematic phase. *New J Chem.* 2017;41(14):6514–6522.
- [47] Kovářová A, Kozmík V, Svoboda J, et al. Naphthalene-based bent-shaped liquid crystals with a semifluorinated terminal chain. *Liq Cryst.* 2012;39:755–767.
- [48] Tschierske C, Photinos DJ. Biaxial nematic phases. *J Mater Chem.* 2010;20:4263–4294.
- [49] Luckhurst GR, Sluckin TJ, ed. Biaxial nematic liquid crystals: theory, simulation and experiment. Chichester (UK): Wiley; 2015.
- [50] Arakawa Y, Kang S, Tsuji H, et al. Development of novel bistolane-based liquid crystalline molecules with an alkylsulfanyl group for highly birefringent materials. *RSC Adv.* 2016;6:16568–16574.
- [51] Arakawa Y, Kang S, Tsuji H, et al. The design of liquid crystalline bistolane-based materials with extremely high birefringence. *RSC Adv.* 2016;6:92845–92851.
- [52] Ziobro D, Dabrowski R, Tykarska M, et al. Synthesis and properties of new ferroelectric and antiferroelectric liquid crystals with a biphenyl benzoate rigid core. *Liq Cryst.* 2012;39:1011–1032.
- [53] Gasowska J, Dabrowski R, Drzewinski W, et al. Comparison of mesomorphic properties in chiral and achiral homologous series of high tilted ferroelectrics and antiferroelectrics. *Ferroelectrics.* 2004;309:83–93.
- [54] Keith C, Lehmann A, Baumeister U, et al. Nematic phases of bent-core mesogens. *Soft Matter.* 2010;6:1704–1721.
- [55] Francescangeli O, Vita F, Ferrero C, et al. Cybotaxis dominates the nematic phase of bent-core mesogens: a small-angle diffuse X-ray diffraction study. *Soft Matter.* 2011;7:895–901.
- [56] Alaasar M, Prehm M, Tschierske C. New azobenzene containing bent-core liquid crystals based on disubstituted resorcinol. *Liq Cryst.* 2014;41:126–136.
- [57] Alaasar M, Poppe S, Tschierske C. Cybotactic nematic phases of photoisomerisable hockey-stick liquid crystals. *Liq Cryst.* 2017;44:729–737.
- [58] Alaasar M, Prehm M, May K, et al. 4-Cyanoresorcinol based bent-core mesogens with azobenzene wings – emergence of sterically stabilised polar order in liquid crystalline phases. *Adv Funct Mater.* 2014;24:1703–1717.
- [59] Alaasar M, Poppe S, Kerzig C, et al. Cluster phases of 4-cyanoresorcinol derived hockey-stick liquid crystals. *J Mater Chem C.* 2017;5:8454–8468.
- [60] Smirnova AI, Heinrich B, Donnio B, et al. The influence of lateral fluorination and cyanation on the mesomorphism of polycatenar mesogens and the nature of the SmC phase therein. *RSC Adv.* 2015;5:75149–75159.



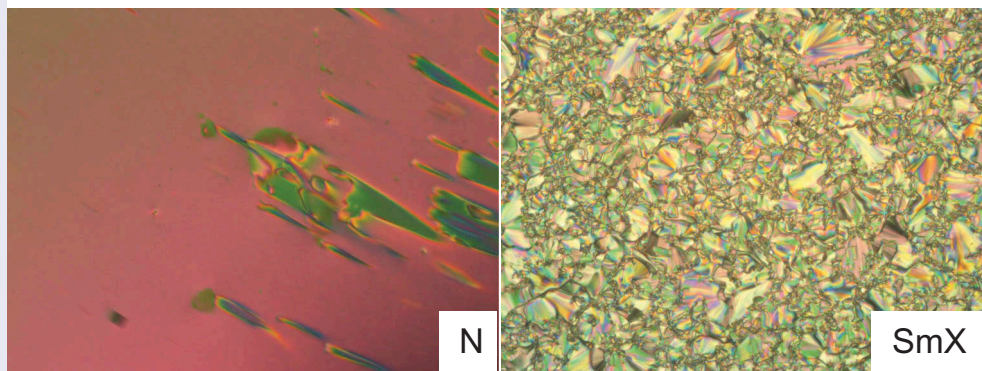
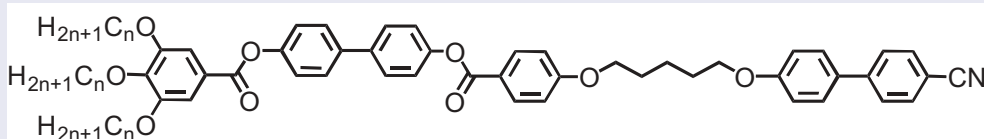
## Non-symmetric ether-linked liquid crystalline dimers with a highly polar end group

Mohamed Alaasar <sup>a,b</sup> and Carsten Tschierske<sup>a</sup>

<sup>a</sup>Institute of Chemistry, Martin Luther University Halle-Wittenberg, Halle, Germany; <sup>b</sup>Department of Chemistry, Faculty of Science, Cairo University, Giza, Egypt

### ABSTRACT

A new class of non-symmetric dimeric compounds derived from 4-cyano-4'-hydroxybiphenyl in which two rigid parts are connected via flexible spacers have been designed and synthesised. These materials possess trialkoxy chains attached at one end of the molecule, while the other end consists of a biphenyl moiety terminated with the highly polar cyano group. The molecular structures of these dimers have been confirmed by elemental analysis and spectroscopic data and their phase behaviour has been characterised by differential scanning calorimetry (DSC) and polarizing optical microscopy (POM). Almost all of the synthesised materials exhibit liquid crystalline properties depending on the number of carbon atoms in the terminal chains, where all short chains derivatives form nematic phases and depending on the length of the internal spacer long terminal chains homologues display crystalline or unidentified smectic phase.



### ARTICLE HISTORY

Received 2 June 2016  
Accepted 11 July 2016

### KEYWORDS

Liquid crystals; polycatenar; cyanobiphenyl; dimers; nematic phase

## 1. Introduction

Since 1980s numerous non-conventional molecular structures were reported to display mesomorphic properties.[1,2] The liquid crystal (LC) dimers containing two mesogenic units connected by a flexible spacer represent one class of these molecular architectures. Dimeric LCs can be classified into two main classes depending on the type of the two mesogenic units: symmetrical and non-symmetrical dimers. In the first class of materials the two mesogenic units are identical, while in the second they are not. In most cases the phase behaviour of dimers are different from their

building blocks and more complex. The subject of LCs dimers is well reviewed in the literature.[3–6] In recent years, there is a growing interest in these materials as they proved to be a rich source for interesting new mesophases. They are able to display wide temperature range blue phases,[7,8] flexoelectric behaviour,[9–11] helical-nanofilament phases (B4 phases) [12,13] and more interestingly some dimeric materials incorporating cyanobiphenyl exhibit a lower temperature nematic mesophase, the so-called twist-bend nematic phase ( $N_{TB}$ ).[14–20] On the other hand, there is a significant progress in the field of mirror

symmetry breaking in liquid crystalline phases formed by bent-core molecules [21–29] and bent-shaped mesogenic dimers.[12,13,20,30,31] Spontaneous formation of chiral domains was also observed in bicontinuous cubic phases [32,33] and in isotropic liquids formed by some achiral polycatenar (multi chain-terminated) molecules.[32,34,35] Up to date, there is only one report about non-symmetric LCs dimers involving polycatenar building blocks, which were found to display three-dimensional (3D) mesophases with cubic symmetry.[36] Therefore, the question arises if the combination of polycatenar and cyanobiphenyl building units in the same molecule could lead to  $N_{TB}$ ,[37] chiral 3D phases [36] or chiral isotropic liquids.[32–35]

In this article, we report about a new class of ether-linked non-symmetric liquid crystalline dimers ( $An/m$ , see Table 1) consisting of cyanobiphenyl group attached to one terminus of a polycatenar molecule which is known to induce the formation of chiral cubic phases and chiral isotropic liquids.[32,33,35] The number of carbon atoms in the terminal alkyl chains ( $n$ ) was varied between 4, 6 and 10, while those in the aliphatic spacer ( $m$ ) were odd numbers and changed between 5 and 7 as it is well known from previous studies that the odd-parity spacers favour the formation of  $N_{TB}$  phases.[15,18,19,37] The phase behaviour of these new dimers has been investigated by polarizing optical microscopy (POM) and differential scanning calorimetry (DSC).

## 2. Characterisation

Thin-layer chromatography (TLC) was performed on aluminium sheet precoated with silica gel. Analytical quality chemicals were obtained from commercial sources and used as obtained. The solvents were dried using the standard methods when required. The purity

and the chemical structures of all synthesised materials were confirmed by the spectral data. The structure characterisation of the prepared materials is based on  $^1\text{H-NMR}$  and  $^{13}\text{C-NMR}$  (Varian Unity 500 and Varian Unity 400 spectrometers, in  $\text{CDCl}_3$  solutions, with tetramethylsilane as internal standard). Microanalyses were performed using a Leco CHNS-932 elemental analyser.

The mesophase behaviour and transition temperatures of the dimeric molecules were measured using a Mettler FP-82 HT hot stage and control unit in conjunction with a Nikon Optiphot-2 polarizing microscope. The associated enthalpies were obtained from DSC-thermograms which were recorded on a Perkin-Elmer DSC-7, heating and cooling rate:  $10\text{ K min}^{-1}$ .

## 3. Results and discussion

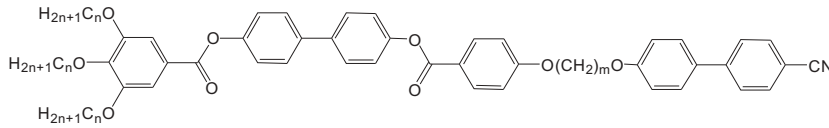
### 3.1. Mesomorphic properties

The transition temperatures ( $^{\circ}\text{C}$ ) and the associated enthalpies ( $\text{kJ mol}^{-1}$ ) obtained from DSC thermograms of the newly synthesised dimers  $An/m$  are given in Table 1 and represented graphically in Figure 1. The DSC thermograms obtained for compounds **A6/5** and **A10/5** as representative examples are shown in Figure 2. All compounds are thermally stable as confirmed by the reproducibility of thermograms on several heating and cooling cycles.

With the exception of **A10/7**, all synthesised compounds exhibit liquid crystalline phases. However, the type of the mesophases depends on the number of the carbon atoms in the aliphatic spacer and/or in the terminal alkyl chains.

Let us first consider compounds incorporating the shorter aliphatic spacer ( $m = 5$ ). On heating the shortest homologue **A4/5** a direct transition from the crystalline state to the isotropic liquid takes place at  $T = 156^{\circ}\text{C}$ . On cooling **A4/5** from the isotropic liquid a nematic phase is

**Table 1.** Phase transition temperatures, mesophase types and transition enthalpies of compounds  $An/m^a$ .



Compound	$n$	$m$	Heating		Cooling	
			$T/^{\circ}\text{C}$	$[\Delta H/\text{kJ.mol}^{-1}]$	$T/^{\circ}\text{C}$	$[\Delta H/\text{kJ.mol}^{-1}]$
<b>A4/5</b>	4	5	Cr 156	[80.4] Iso	Iso 144	[0.5] N 128 [70.3] Cr
<b>A6/5</b>	6	5	Cr 139	[55.6] Iso	Iso 135	[0.6] N 116 [50.5] Cr
<b>A10/5</b>	10	5	Cr <sub>1</sub> 114	[52.9] Cr <sub>2</sub> 125 [27.3] Iso	Iso 111	[1.1] SmX 97 [41.8] Cr
<b>A4/7</b>	4	7	Cr 158	[72.9] Iso	Iso 150	[0.6] N 140 [68.0] Cr
<b>A6/7</b>	6	7	Cr 150	[63.9] Iso	Iso 134	[0.6] N 96 [57.2] Cr
<b>A10/7</b>	10	7	Cr 131	[38.9] Iso	Iso 111	[38.6] Cr

<sup>a</sup>Transition temperatures and enthalpy values were taken from the second DSC heating scans ( $10\text{ K min}^{-1}$ ); abbreviations: Cr = crystalline solid; N = nematic phase; SmX = unidentified smectic phase; Iso = isotropic liquid.

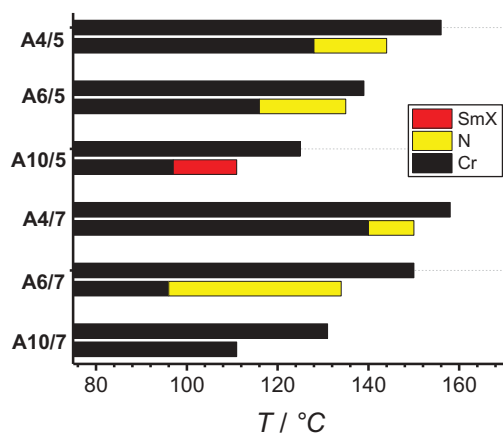


**Figure 1.** (Colour online) Phase behaviour of compounds  $A_n/m$  on heating and cooling scans.

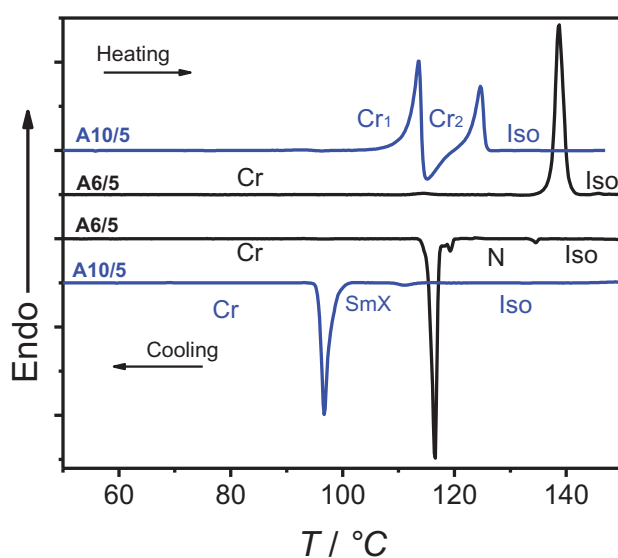


**Figure 2.** (Colour online) DSC thermograms obtained for compounds  $A_6/5$  (black lines) and  $A_{10}/5$  (blue lines); heating and cooling rates are  $10 \text{ K/min}^{-1}$ .

observed at  $T = 144^\circ\text{C}$  with a value of transition enthalpy  $\Delta H = 0.5 \text{ kJ}\cdot\text{mol}^{-1}$  (see Figure 3(a)) which crystallizes on further cooling at  $T = 128^\circ\text{C}$ . Elongation of the terminal alkyl chains from  $n = 4$  to 6 (compound  $A_6/5$ ) leads to a decrease of the melting temperature and also the formation of a monotropic nematic phase (see Figure 3(b)). However, the range of this nematic phase is slightly wider than that observed for  $A_4/5$  (see Figure 1). Further elongation of the terminal chains results in further lowering of the melting temperature as would be expected and completely removes the nematic phase (compound  $A_{10}/5$ ), where a monotropic smectic phase is formed as indicated from the observed optical texture (see Figure 3(c)) and the change of the value of transition enthalpy ( $\Delta H = 1.1 \text{ kJ}\cdot\text{mol}^{-1}$ ). After shearing this unidentified

texture a birefringent schlieren texture could be observed (see Figure 3(d)) in a similar manner to that observed for B2 phase exhibited by bent-core liquid crystals.[38] Moreover, uniform planar or homeotropic alignment was not achieved between glass plates, as typical for B2 phase which usually cannot be aligned.[22] Therefore, the smectic phase of  $A_{10}/5$  it is not an ordinary SmA or SmC phases. Though textural features would support a B2 phase, the Iso-SmX transition enthalpy is unusual small for a B2 phase. Because further investigation/phase confirmation of this phase with X-ray diffraction (XRD) studies or electro optical measurements was not possible due to rapid crystallization during the time of measurement it is assigned as SmX phase.

Increasing the length of the internal spacer from  $m = 5$  to  $m = 7$  results in the formation of the dimeric molecules  $A_4/7$ ,  $A_6/7$  and  $A_{10}/7$ . These materials exhibit similar phase behaviour to that observed in their related analogues with  $m = 5$ , where the melting temperatures for all materials decrease with elongation of the terminal alkyl chains and the nematic phases are observed as monotropic phases for the short terminal chains derivatives  $A_4/7$  and  $A_6/7$ . Moreover, the nematic phase range is also increasing with chain elongation typically as observed for  $A_4/5$  and  $A_6/5$ . However, the nematic phase range of  $A_6/7$  is much wider compared to its analogue  $A_6/5$  (see Figure 1). Another observation is the disappearance of any liquid crystalline phases on further chain elongation, where compound  $A_{10}/7$  is only crystalline with a melting point  $T = 131^\circ\text{C}$ .

### 3.2. Investigation of mixtures with 5-CB

Aiming to stabilise the nematic phases exhibited by the synthesised dimers we investigated the 1:1 mixtures (mole:mole) of the nematic host liquid crystalline material 5-CB ( $4'$ - $n$ -pentyl-4-cyanobiphenyl) with all  $A_n/m$  compounds (see Table 2).

Remarkably in all cases the Cr-Iso transition temperatures were greatly reduced in comparison with the pure compounds (29–58 K), however the formation of the nematic phase in these mixtures depends strongly on the length of the aliphatic spacer.

For the mixtures of the dimeric molecules with  $m = 5$ , the nematic phase was completely removed for the shortest homologue  $A_4/5$  and formed as monotropic phases for the next homologue  $A_6/5$ . Moreover, the nematic phase range for the mixture formed between  $A_6/5$  and 5-CB is 35 K which is much wider compared to the pure compound (19 K). On the other hand, the SmX phase observed in the pure  $A_{10}/5$  is replaced by a monotropic nematic phase which crystallises at  $T = 28^\circ\text{C}$  near to room temperature in the mixed system.

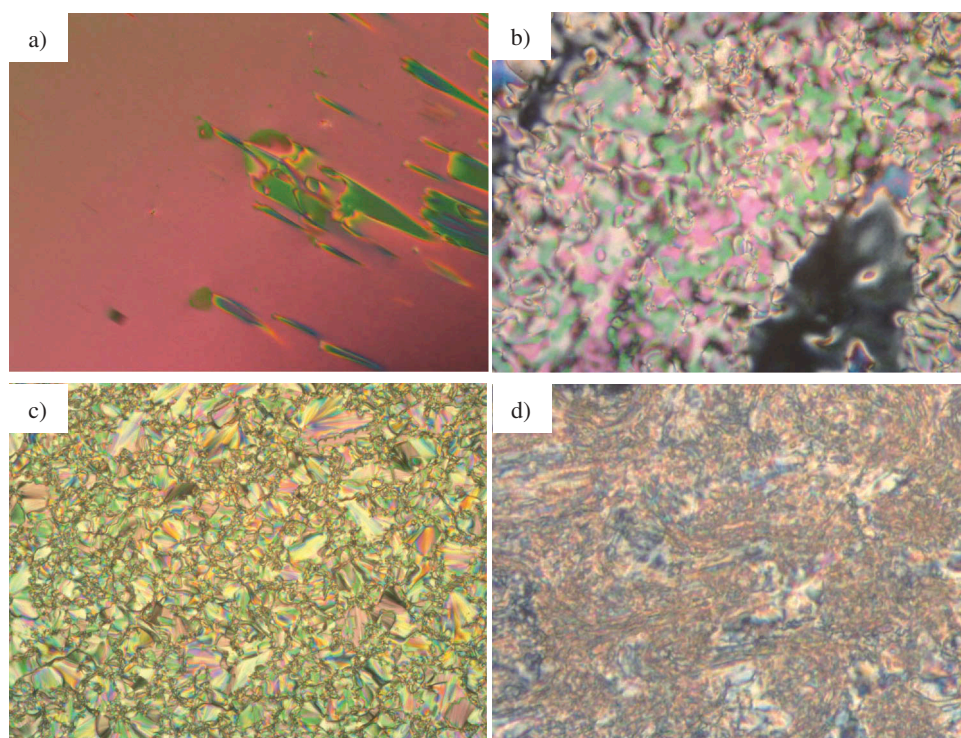


**Figure 3.** (Colour online) Optical micrographs observed in homeotropic cells: the nematic phase of (a) compound **A4/5** at  $T = 140^{\circ}\text{C}$ ; (b) compound **A4/7** at  $T = 147^{\circ}\text{C}$ ; the SmX phase of compound **A10/5** at  $T = 107^{\circ}\text{C}$  (c) before shearing and (d) after shearing.

**Table 2.** Phase transition temperatures and mesophase types of 1:1 mixtures (mole:mole) of the investigated dimers with 5-CBa.

Compd.	Heating $T/^{\circ}\text{C}$	Cooling $T/^{\circ}\text{C}$
<b>A4/5</b>	Cr 102 Iso	Iso 71 Cr
<b>A6/5</b>	Cr 78 Iso	Iso 66 N 31 Cr
<b>A10/5</b>	Cr 64 Iso	Iso 53 N 28 Cr
<b>A4/7</b>	Iso 127 Cr	Iso 114 Cr
<b>A6/7</b>	Cr 93 Iso	Iso 81 Cr
<b>A10/7</b>	Cr 73 Iso	Iso 58 N 33 Cr

<sup>a</sup>Transition temperatures were taken from the observed textures using polarised optical microscopy; for abbreviations see Table 1.

Mixing the other types of dimers with longer spacer ( $m = 7$ ) with 5-CB results in slightly different phase behaviour, where the nematic phases formed by the pure compounds **A4/7** and **A6/7** are completely removed and only crystalline materials are formed in their mixtures. An interesting observation is the formation of a nematic phase for the mixture formed between 5-CB and the longest homologue **A10/7** which is crystalline. Therefore, mixing these dimers with 5-CB removes or induces nematic phases depending on the length of the spacer and/or the terminal alkyl chains.

## 4. Conclusion

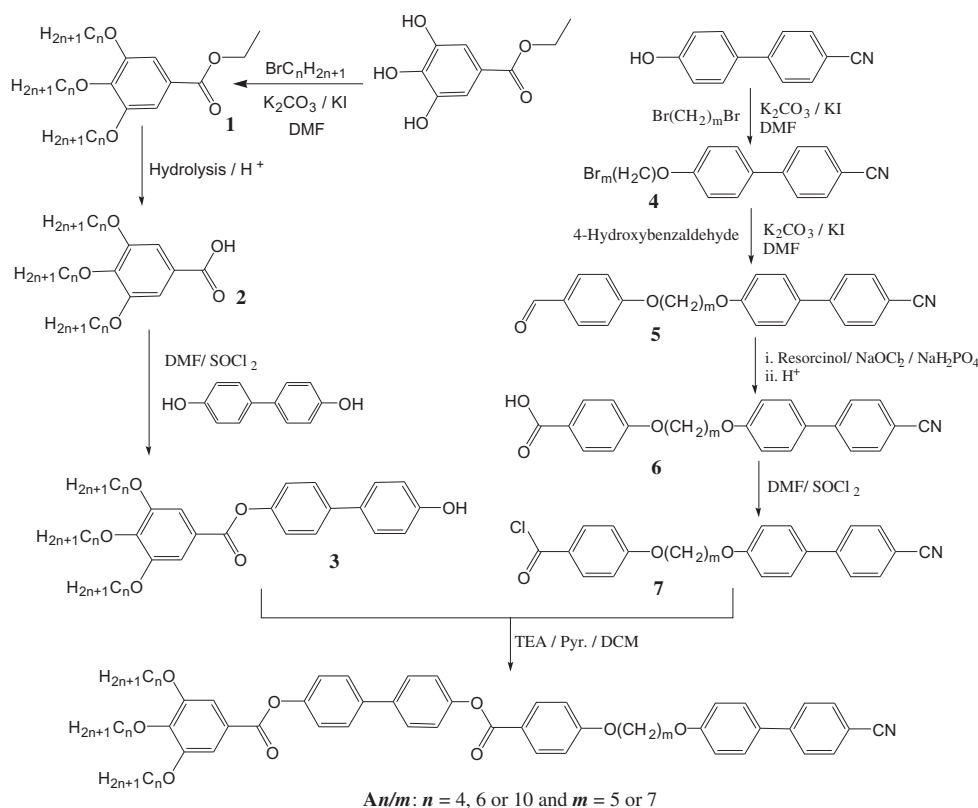
In summary, we reported a new class of dimeric mesogens incorporating the highly polar cyano group at one end of

the molecule and trialkyl chains at the other end (**An/m**), where  $n$  represents the number of carbon atoms in the terminal alkyl chains and  $m$  is the number of carbon atoms in the aliphatic spacer. It was found that these dimeric materials do not form any cubic 3D mesophases or chiral isotropic liquid phases. Moreover, there is no indication of nematic–nematic phase transitions in any of the synthesised dimers but instead the dimeric molecules with  $m = 5$  show monotropic nematic phases for the short chains homologues and SmX phase for the longest homologue with  $n = 10$ . On the other hand, the dimeric molecules with longer internal spacer,  $m = 7$ , form monotropic nematic phases for the homologues with  $n = 4$  or 6 which is totally removed for the longest derivative with  $n = 10$ , where only crystalline material is formed. Additionally, we investigated the 1:1 mixtures formed between these new dimers and 5-CB, where the melting points for all dimers are greatly reduced in their mixed systems and depending on  $m$  or  $n$  nematic phases or crystalline materials are formed by these mixtures.

## 5. Experimental

### 5.1. Synthesis

The synthesis of the non-symmetric dimers under discussion is shown in Scheme 1. As an example the synthesis of the final compound (**A6/5**) is given



**Scheme 1.** Synthesis of the non-symmetric dimers under investigation.

below. The analytical data for  $An/m$  compounds as well as their  $^1\text{H-NMR}$  spectra and the synthesis details for all intermediates are reported in the electronic supporting information file (ESI).

## 5.2. A6/5

The acid **6** (0.40 g, 1.0 mmol) was heated under reflux with excess thionyl chloride (3 mL) and a catalytic amount of DMF for 1 hour. The excess of thionyl chloride was removed by distillation under reduced pressure. The resulting acid chloride was then dissolved in dry dichloromethane (20 mL) followed by addition of the phenolic compound **3** (0.59 g, 1.0 mmol) previously dissolved in DCM, triethylamine (0.17 mL, 1.2 mmol) and a catalytic amount of pyridine and the reaction mixture was then refluxed for 6 hours under argon atmosphere. The reaction progress was checked with TLC and at the end of the reaction the solution was cooled to room temperature, washed with 10% HCl ( $2 \times 50$  mL) and three times with cold water followed by extraction with dichloromethane ( $3 \times 50$  mL) and finally dried over anhydrous sodium sulphate. The crude material was chromatographed on silica gel using DCM followed by recrystallisation from chloroform/ethanol mixture affording 0.65 g (65%) of

**A6/5** as a white powder.  $^1\text{H-NMR}$  (500 MHz,  $\text{CDCl}_3$ )  $\delta$  ppm: 8.22 – 8.11 (d, 2H, Ar–H), 7.74 – 7.58 (m, 8H Ar–H), 7.53 (d, 2H Ar–H), 7.43 (s, 2H Ar–H), 7.33 – 7.22 (m, 4H Ar–H), 7.04 – 6.93 (m, 4H Ar–H), 4.15 – 4.00 (m, 10H, Ar– $\text{OCH}_2\text{CH}_2$ ), 2.00 – 1.65 (m, 12H, Ar– $\text{OCH}_2\text{CH}_2$ ), 1.59 – 1.43 (m, 6H,  $\text{CH}_2$ ), 1.43 – 1.28 (m, 12H,  $\text{CH}_2$ ), 0.98 – 0.84 (m, 9H,  $\text{CH}_3$ ).  $^{13}\text{C-NMR}$  (400 MHz,  $\text{CDCl}_3$ )  $\delta$  ppm: 13.99, 14.06, 22.59, 22.66, 22.72, 25.68, 25.73, 28.85, 28.94, 29.25, 30.28, 31.53, 31.71, 67.84, 68.03, 69.28, 73.57, 108.62, 110.10, 114.29, 115.07, 119.04, 121.64, 122.08, 122.10, 123.83, 127.06, 128.14, 128.15, 128.33, 131.43, 132.31, 132.54, 138.02, 138.16, 143.08, 145.20, 150.52, 150.55, 152.96, 159.64, 163.41, 164.90, 165.03. Elemental Analysis: Calc. for  $\text{C}_{62}\text{H}_{71}\text{NO}_9$ , C, 76.44; H, 7.35; N, 1.44. Found C, 76.42; H, 7.35; N, 1.39 %.

## Acknowledgments

The work was supported by the DFG (Grant Ts 39/24-1).

## Disclosure statement

No potential conflict of interest was reported by the authors.



## Funding

The work was supported by the DFG: [Grant Number Ts 39/24-1].

## ORCID

Mohamed Alaasar  <http://orcid.org/0000-0003-4155-8644>

## References


- [1] Tschierske C. Development of structural complexity by liquid crystal self-assembly. *Angew Chem Int Ed.* **2013**;52:8828–8878.
- [2] Goodby JW, Collings PJ, Gleeson HF, et al., editors. Handbook of liquid crystals. In: Non-conventional liquid crystals. 2nd ed. Vol. 5. Weinheim: Wiley-VCH; **2014**.
- [3] Imrie CT, Henderson PA. Liquid crystal dimers and higher oligomers: between monomers and polymers. *Chem Soc Rev.* **2007**;36:2096–2124.
- [4] Imrie CT, Henderson PA, Yeap G-Y. Liquid crystal oligomers: going beyond dimers. *Liq Cryst.* **2009**;36:755–777.
- [5] Imrie CT, Henderson PA. Liquid crystal dimers and oligomers. *Curr Opin Colloid Interface Sci.* **2002**;7:298–311.
- [6] Yelamaggad CV, Shanker G, Hiremath US, et al. Cholesterol-based nonsymmetric liquid crystal dimers: an overview. *J Mater Chem.* **2008**;18:2927–2949.
- [7] Coles HJ, Pivnenko MN. Liquid crystal ‘blue phases’ with a wide temperature range. *Nature.* **2005**;436:997–1000.
- [8] Yoshizawa A, Sato M, Rokunohe J. A blue phase observed for a novel chiral compound possessing molecular biaxiality. *J Mater Chem.* **2005**;15:3285–3290.
- [9] Blatch AE, Coles MJ, Musgrave B, et al. flexoelectric liquid crystal bimesogens. *Mol Cryst Liq Cryst.* **2003**;401:47–55.
- [10] Coles HJ, Clarke MJ, Morris SM, et al. Strong flexoelectric behavior in bimesogenic liquid crystals. *J Appl Phys.* **2006**;99:034104.
- [11] Atkinson KL, Morris SM, Qasim MM, et al. Increasing the flexoelectric ratio of liquid crystals using highly fluorinated ester-linked bimesogens. *Phys Chem Chem Phys.* **2012**;14:16377–16385.
- [12] Zep A, Sitkowska K, Pocięcha D, et al. Photoresponsive helical nanofilaments of B4 phase. *J Mater Chem C.* **2014**;2:2323–2327. doi:10.1039/c3tc32325k.
- [13] Zep A, Salamonczyk M, Vaupotic N, et al. Physical gels made of liquid crystalline B4 phase. *Chem Commun.* **2013**;49:3119–3121.
- [14] Šepelj M, Lesac A, Baumeister U, et al. Intercalated liquid-crystalline phases formed by symmetric dimers with an  $\alpha,\omega$ -diiminoalkylene spacer. *J Mater Chem.* **2007**;17:1154–1165.
- [15] Mandle RJ, Davis EJ, Archbold CT, et al. Microscopy studies of the nematic NTB phase of 1,11-Di-(1'-cyanobiphenyl-4-yl)undecane. *J Mater Chem C.* **2014**;2:556–566.
- [16] Wang Y, Singh G, Agra-Kooijman DM, et al. Room temperature heliconical twist-bend nematic liquid crystal. *Cryst Eng Comm.* **2015**;17:2778–2782.
- [17] Mandle RJ, Voll CCA, Lewis DJ, et al. Etheric bimesogens and the twist-bend nematic phase. *Liq Cryst.* **2016**;43:13–21.
- [18] Jansze SM, Martínez-Felipe A, Storey JMD, et al. Twist-bend nematic phase driven by hydrogen bonding. *Angew Chem Int Ed.* **2015**;54:643–646.
- [19] Paterson DA, Xiang J, Singh G, et al. A reversible isothermal twist-bend nematic – nematic phase transition driven by the photoisomerisation of an azobenzene-based non-symmetric liquid crystal dimer. *J Am Chem Soc.* **2016**. doi:10.1021/jacs.5b13331.
- [20] Borshch V, Kim Y-K, Xiang J, et al. Nematic twist-bend phase with nanoscale modulation of molecular orientation. *Nature Commun.* **2013**;4:2635.
- [21] Reddy R, Tschierske C. Bent-core liquid crystals: polar order, superstructural chirality and spontaneous desymmetrisation in soft matter systems. *J Mater Chem.* **2006**;16:907–961.
- [22] Alaasar M. Azobenzene containing bent-core liquid crystals: an overview. *Liq Cryst.* **2016**;1–36. doi:10.1080/02678292.2016.1175676.
- [23] Hough LE, Spannuth M, Nakata M, et al. Chiral isotropic liquids from achiral molecules. *Science.* **2009**;325:452–456.
- [24] Alaasar M, Prehm M, Nagaraj M, et al. A liquid crystalline phase with uniform tilt, local polar order and capability of symmetry breaking. *Adv Mater.* **2013**;25:2186–2191.
- [25] Alaasar M, Prehm M, May K, et al. 4-Cyanoresorcinol based bent-core mesogens with azobenzene wings – emergence of sterically stabilised polar order in liquid crystalline phases. *Adv Funct Mater.* **2014**;24:1703–1717.
- [26] Alaasar M, Prehm M, Tschierske C. A new room temperature dark conglomerate mesophase formed by bent-core molecules combining 4-iodoresorcinol with azobenzene units. *Chem Commun.* **2013**;49:11062–11064.
- [27] Alaasar M, Prehm M, Brautzsch M, et al. Dark conglomerate phases of azobenzene derived bent-core mesogens – relationships between the molecular structure and mirror symmetry breaking in soft matter. *Soft Matter.* **2014**;10:7285–7296.
- [28] Alaasar M, Prehm M, Brautzsch M, et al. 4-Methylresorcinol based bent-core liquid crystals with azobenzene wings – a new class of compounds with dark conglomerate phases. *J Mater Chem C.* **2014**;2:5487–5501.
- [29] Alaasar M, Prehm M, Tschierske C. Helical nanocrystallite (HNC) phases – chirality synchronization of achiral bent-core mesogens in a new type of dark conglomerates. *Chem Eur J.* **2016**;22:6583–6597.
- [30] Choi S-W, Izumi T, Hoshino Y, et al. Circular-polarization-induced enantiomeric excess in liquid crystals of an achiral, bent-shaped mesogen. *Angew Chem Int Edit.* **2006**;45:1382–1385.
- [31] Ueda T, Masuko S, Araoka F, et al. A general method for the enantioselective formation of helical nanofilaments. *Angew Chem Int Edit.* **2013**;52:6863–6866.

- [32] Dressel C, Reppe T, Prehm M, et al. Chiral self-sorting and amplification in isotropic liquids of achiral molecules. *Nature Chem.* **2014**;6:971–977.
- [33] Dressel C, Liu F, Prehm M, et al. Dynamic mirror-symmetry breaking in bicontinuous cubic phases. *Angew Chem Int Ed.* **2014**;53:13115–13120.
- [34] Tschierske C, Ungar G. Mirror symmetry breaking by chirality synchronisation in liquids and liquid crystals of achiral molecules. *ChemPhysChem.* **2016**;17:9–26.
- [35] Alaasar M, Prehm M, Cao Y, et al. Spontaneous mirror-symmetry breaking in isotropic liquid phases of photoisomerizable achiral molecules. *Angew Chem Int Ed.* **2016**;55:312–312.
- [36] Wolska JM, Pocięcha D, Mieczkowski J, et al. Double gyroid structures made of asymmetric dimers. *Liq Cryst.* **2016**;43:235–240.
- [37] Mandle RJ, Davis EJ, Voll C-CA, et al. The relationship between molecular structure and the incidence of the NTB phase. *Liq Cryst.* **2014**;42:688–703.
- [38] Shen D, Pegenau A, Diele S, et al. Molecular design of nonchiral bent-core liquid crystals with antiferroelectric properties. *J Am Chem Soc.* **2000**;122:1593–1601.

## PAPER

Cite this: *New J. Chem.*, 2022, 46, 15871

## Transition from lamellar to nanostructure mesophases in azobenzene-based hockey-stick polycatenars†

Mohamed Alaasar, \*<sup>ab</sup> Xiaoqian Cai, <sup>c</sup> Yu Cao <sup>c</sup> and Feng Liu <sup>c</sup>

Photoresponsive nanostructured materials are of great importance for photonic applications. Herein we report the design, synthesis, and liquid crystal (LC) self-assembly of two new series of photoresponsive hockey-stick LCs (HSLCs). The new HSLCs are azobenzene-based polycatenars derived from the 4-cyanoresorcinol bent-core unit. The long arm is a fork-like triple alkoxyated wing, while the short arm is terminated with a single variable alkoxy chain. The molecular self-assembly of these HSLCs is characterized using polarizing optical microscopy (POM), differential scanning calorimetry (DSC), X-ray diffraction (XRD) and electro optical measurements. In both series of LC materials differing in the chain volume at the crowded end, wide temperature ranges of lamellar Smectic A phases (up to 170 K) are observed beside achiral isotropic liquid phases (Iso<sub>1</sub>) for the shorter derivatives. On chain elongation helical self-assembly of the  $\pi$ -conjugated rods in networks occurs resulting in the formation of nanostructured bicontinuous cubic network phases with  $Ia\bar{3}d$  space group (Cub<sub>bi</sub>/ $Ia\bar{3}d$ ), in most cases stable even around room temperatures on cooling. At the transition from SmA to Cub<sub>bi</sub> phases, an additional unknown three-dimensional (3D) phase is formed. A possible explanation for the disappearance of the triple network Cub<sub>bi</sub> phases with  $I23$  symmetry (Cub<sub>bi</sub><sup>[\*]</sup>/ $I23$ ) in these HSLCs is represented based on the phase behaviour of a new material having the central 4-cyanoresorcinol unit shifted to a terminal position of the rod-like core. Finally, the reversible *trans*–*cis* photoisomerization for some selected examples was investigated in chloroform solution.

Received 1st July 2022,  
Accepted 17th July 2022

DOI: 10.1039/d2nj03255d

rsc.li/njc

## 1. Introduction

Since its discovery by V. Luzzati in 1968,<sup>1</sup> cubic liquid crystals (LCs) attracted significant attention due to their complexity and importance in biological structures.<sup>2–6</sup> Such bicontinuous network cubic (Cub<sub>bi</sub>) phases are fascinating for various applications, including ion transportation, catalysis, drug delivery, organic electronic devices and energy conversion.<sup>5,7–9</sup> Therefore, the design and synthesis of new functional cubic LCs are essentials for the development of current and future applications of LCs.

Cub<sub>bi</sub> phases are common for non-symmetric polycatenar LCs<sup>10–15</sup> but rare for bent-core LCs (BCLCs).<sup>16–19</sup> Polycatenars are rod-like molecules terminated with more than two flexible

chains.<sup>20</sup> The nanostructure of the Cub<sub>bi</sub> mesophase is quite complex and characterized by three-dimensional (3D) interconnected networks with cubic symmetry, representing an intermediate state between the lamellar one-dimensional (1D) and the columnar two-dimensional (2D) LC phases.<sup>21,22</sup> Polycatenars are able to display two different types of Cub<sub>bi</sub>, namely the double gyroid achiral Cub<sub>bi</sub> with  $Ia\bar{3}d$  space group (Cub<sub>bi</sub>/ $Ia\bar{3}d$ )<sup>21</sup> and the chiral Cub<sub>bi</sub> with  $I23$  lattice (Cub<sub>bi</sub><sup>[\*]</sup>/ $I23$ ).<sup>22</sup> The achiral (Cub<sub>bi</sub>/ $Ia\bar{3}d$ ) phase is composed of two networks with opposite chirality sense and therefore cancel each other's (Fig. 1a). On the other hand, the chiral (Cub<sub>bi</sub><sup>[\*]</sup>/ $I23$ ) consists of triple networks and therefore the overall chirality of the phase cannot be cancelled (Fig. 1b).

For this reason, under polarizing optical microscope (POM) with slightly uncrossed polarizers dark and bright areas could be only observed in the case of Cub<sub>bi</sub><sup>[\*]</sup>/ $I23$  phase. The dark and bright areas invert their signs on inverting the direction of rotation of the analyzers, indicating the presence of chiral conglomerates with opposite handedness.

The two different cubic phases can be also distinguished by XRD investigations.<sup>21,22</sup> Beside either achiral Cub<sub>bi</sub>/ $Ia\bar{3}d$  or chiral Cub<sub>bi</sub><sup>[\*]</sup>/ $I23$  another bicontinuous phase with tetragonal

<sup>a</sup> Institute of Chemistry, Martin Luther University Halle-Wittenberg, Kurt Mothes Str. 2, D-06120, Halle, Saale, Germany. E-mail: mohamed.alaasar@chemie.uni-halle.de, malaasar@cu.edu.eg

<sup>b</sup> Department of Chemistry, Faculty of Science, Cairo University, Giza, Egypt

<sup>c</sup> Shaanxi International Research Center for Soft Matter, State Key Laboratory for Mechanical Behavior of Materials, Xi'an Jiaotong University, Xi'an, 710049, P. R. China

† Electronic supplementary information (ESI) available. See DOI: <https://doi.org/10.1039/d2nj03255d>

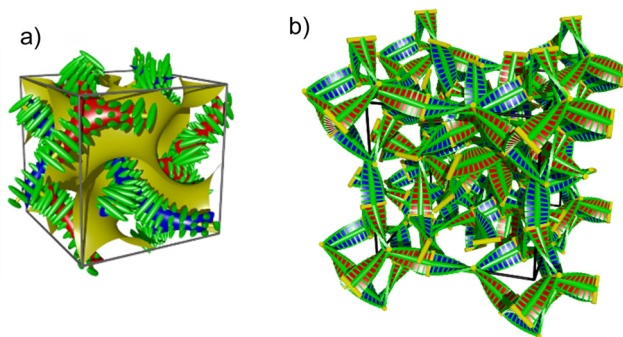


Fig. 1 (a) The double gyroid achiral bicontinuous  $Ia\bar{3}d$  phase with two networks of opposite chirality (red and blue), reproduced from ref. 11 by permission from Wiley-VCH. (b) The chiral  $I23$  phase with triple networks, reproduced from ref. 22 by permission from RSC.

symmetry was recently reported for azobenzene-based polycatenar molecule.<sup>23</sup> Moreover, mirror symmetry breaking was also observed in the isotropic liquid phase assigned as  $Iso_1^{[*]}$  phase in non-symmetric polycatenars.<sup>10–15,24</sup>

Using alkyl chain engineering, we were able to report different types of functional nanostructured azobenzene-based non-symmetric polycatenars exhibiting  $Iso_1^{[*]}$  phase beside a lamellar (Smectic A = SmA) phase in tricatener systems<sup>25,26</sup> or  $Cub_{bi}$  or 3D tetragonal phases in tetracatenar molecules.<sup>12,21,23,24,27,28</sup>

An efficient way to photocontrol the molecular structure and to improve the physical properties toward applications such as optoelectronic sensing devices<sup>29</sup> and organic light-driven actuators<sup>30–32</sup> is the incorporation of the azobenzene unit into the molecular structure.<sup>33</sup> One class of photo switching LCs are azobenzene-based BCLCs, being interesting as a result of their fast photoisomerization.<sup>34–41</sup> One of the most promising bent core units is 4-cyanoescorcinol with low bend angle  $< 120^\circ$ , and therefore induces LC phases at the cross-over between rod-like (calamitic) and bent-core molecules.<sup>42–50</sup>

Recently, we introduced the 4-cyanoescorcinol central core as a bent unit into the molecular structure of linear tricatener to design the first examples of photoresponsive hockey-stick (HS) polycatenars (compounds **Am/n**, Fig. 2).<sup>51</sup> These materials were found to exhibit LC phases that are formed by conventional HS molecules<sup>52–66</sup> as well as by linear polycatenars. Therefore, depending on the terminal chain length orthogonal SmA phases, different types of tilted smectic C (SmC) phases in addition to the achiral  $Cub_{bi}/Ia\bar{3}d$  phase were observed for **Am/n** molecules.<sup>51</sup>

In this report we aim not only to increase the LC phase ranges observed for the related analogues **Am/n**, but also to stabilize the nanostructure  $Cub_{bi}$  mesophase to be room temperature LC phase, which is of great importance from the application point of view. Both targets have been successfully achieved by increasing the volume of the alkyl chains at the crowded end of the aromatic cores (Fig. 2). Therefore, two new series of HS polycatenars were synthesized and investigated (**B6/n** and **B10/n**, Scheme 1). The new polycatenars are derived from 4-cyanoescorcinol as the central bent-core unit connected to a short azobenzene-based side arm terminated with one

variable alkoxy chain and a long biphenyl-based side arm terminated with three alkoxy chains at 3, 4 and 5 positions. The two series differ from each other's in the length of the three alkoxy chains connected to the biphenyl-based wing, where in series **B6/n** three hexyloxy chains were used and in series **B10/n** they are replaced with longer decyloxy chains. The liquid crystalline behaviour of these new HS molecules is characterized by polarizing optical microscopy (POM), differential scanning calorimetry (DSC), X-ray diffraction (XRD) and electro optical measurements.

## 2. Experimental

### 2.1. Synthesis

The synthesis of the new HS polycatenars **B6/n** and **B10/n** was performed as shown in Scheme 1 starting from the benzoic acids **1/n** terminated with three alkoxy chains. The final HS compounds were purified by column chromatography followed by recrystallization from ethanol/chloroform (1:1) mixture. The synthesis details for the intermediates and for the final compounds along with the analytical data are reported in the ESI.† All final materials are thermally stable as proven by the reproducibility of DSC thermograms in repeated heating and cooling cycles.

### 2.2. Methods

The thermal behaviour of all synthesized compounds was studied by polarizing optical microscopy (POM) and differential scanning calorimetry (DSC). For polarizing microscopy, a Mettler FP-82 HT hot stage and control unit in conjunction with a Nikon Optiphot-2 polarizing microscope was used.

DSC-thermograms were recorded on a Perkin-Elmer DSC-7 with heating and cooling rates of  $10 \text{ K min}^{-1}$ . Electro-optical switching characteristics were examined in  $6 \mu\text{m}$  polyimide coated ITO cells (EHC Japan) using the triangular-wave method.<sup>67</sup>

XRD patterns were recorded with a 2D detector (Vantec-500, Bruker). Ni filtered and pin hole collimated  $\text{CuK}_\alpha$  radiation was used. The exposure time was 15 min and the sample to detector distance was 26.7 and 8.95 cm for small angle and wide-angle scattering experiments, respectively. Alignment was attempted by slow cooling (rate:  $1 \text{ K min}^{-1}$  to  $0.1 \text{ K min}^{-1}$ ) of a small droplet on a glass plate. High-resolution small angle powder diffraction (SAXS) experiments were recorded on Beamlines BL16B1 at Shanghai Synchrotron Radiation Facility (SSRF). Samples were held in evacuated 1 mm capillaries. A modified Linkam hot stage with thermal stability within  $0.2 \text{ }^\circ\text{C}$  was used, with a hole for the capillary drilled through the silver heating block and mica windows attached to it on each side.  $q$ -Calibration and linearization were verified using several orders of layer reflections from silver behenate and a series of  $n$ -alkanes. DECTRIS PILATUS 2M detector was used for SAXS.

UV irradiation was performed using Ocean Optics HR-2000 spectrophotometer at a wavelength of 365 nm. UV light

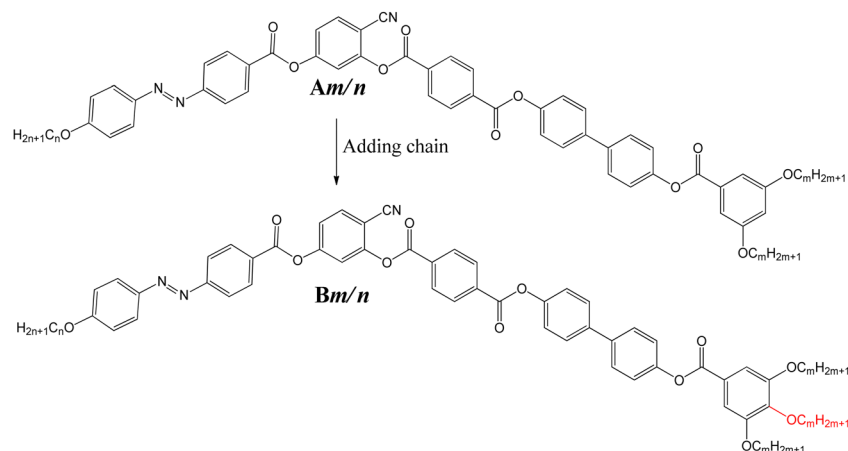
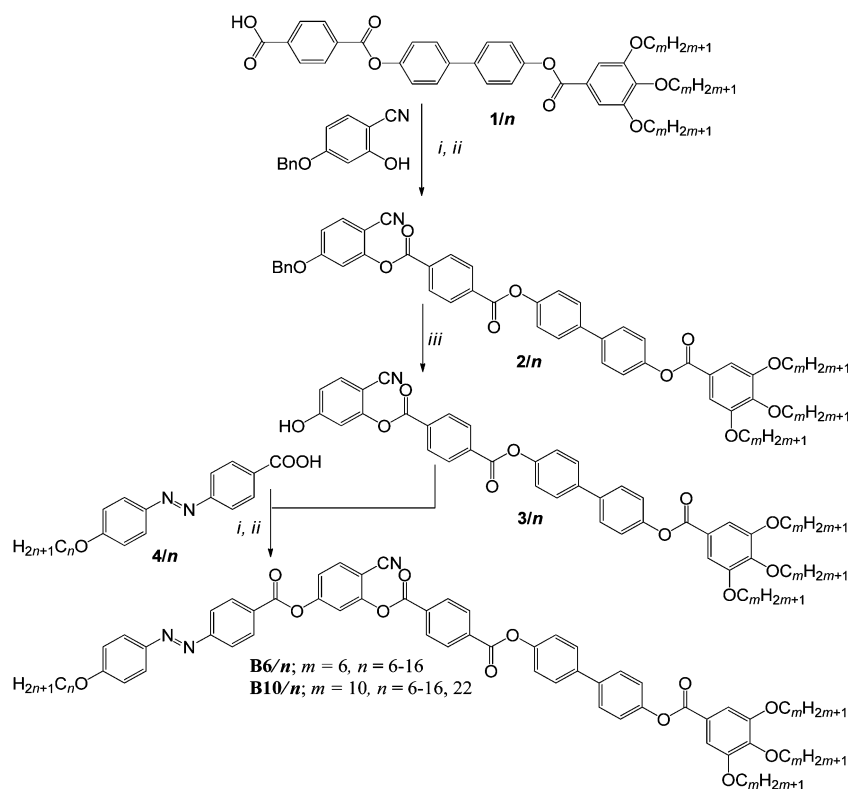


Fig. 2 Chemical structures of the previously reported hockey-stick tricatenars **Am/n**<sup>51</sup> and the new HS tetracatenars **Bm/n**.



Scheme 1 Synthesis of the target HS polycatenars **B6/n** and **B10/n**. Reagents and conditions: (i) DMF,  $\text{SOCl}_2$ , reflux 1 h; (ii) dry  $\text{CH}_2\text{Cl}_2$ , dry TEA, dry pyridine, reflux for 6 h; (iii)  $\text{H}_2$ , Pd/C-10%, dry THF, stirring 24 h.

intensity was measured using UV513AB UV-meter and illumination intensity is fixed at  $1 \text{ mW cm}^{-2}$ .

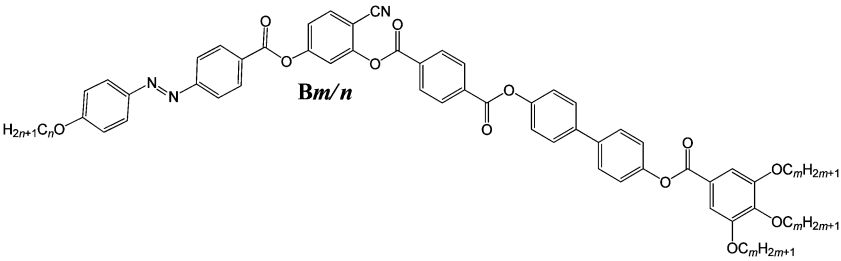
### 3. Results and discussion

#### 3.1. Hockey-stick polycatenars **B6/n**

As can be seen from Table 1 and Fig. 3a the HS materials **B6/n** with three hexyloxy chains connected to the terminal benzene

ring of the long wing of the HS molecules display three different types of LC phases depending on the alkyl chain length at the azobenzene-based side-arm.

On heating the shorter homologues **B6/6** and **B6/8** with  $n = 6$  and  $8$  under POM with crossed polarizers a transition from the highly birefringent crystalline phase to a homeotropically aligned LC phase is observed (Fig. 4a). On applying shearing stress birefringence oily streaks are induced, which relaxes back quickly on removing the shearing stress to an optically

Table 1 Phase transition temperatures ( $T$  (°C)), mesophase types, and transition enthalpies [ $\Delta H$  (kJ mol<sup>-1</sup>)] of compounds **B6/n** and **B10/n**<sup>a</sup>


Cpd.	<i>m</i>	<i>n</i>	Phase Transitions °C [kJ mol <sup>-1</sup> ]
<b>B6/6</b>	6	6	<b>H:</b> Cr 95 [14.8] SmA 175 [3.3] Iso <b>C:</b> Iso 173 [2.9] SmA < 20 Cr
<b>B6/8</b>	6	8	<b>H:</b> Cr 100 [25.8] SmA 175 [3.8] Iso <b>C:</b> Iso 172 [3.9] SmA < 20 Cr
<b>B6/10</b>	6	10	<b>H:</b> Cr 110 [28.8] SmA 168 [3.2] Iso <sub>1</sub> 172 [0.5] Iso <b>C:</b> Iso 169 [0.9] Iso <sub>1</sub> 165 [3.6] SmA < 20 Cr
<b>B6/12</b>	6	12	<b>H:</b> Cr 111 [36.3] SmA 169 [3.1] Iso <sub>1</sub> 172 [0.6] Iso <b>C:</b> Iso 169 [0.7] Iso <sub>1</sub> 166 [3.3] SmA < 20 Cr
<b>B6/14</b>	6	14	<b>H:</b> Cr 120 [59.3] M 127 [0.3] M + Cub <sub>bi</sub> /Ia $\bar{3}d$ 140 [-] Cub <sub>bi</sub> /Ia $\bar{3}d$ 155 [-] SmA 162 [0.9] Iso <sub>1</sub> 168 [2.2] Iso <b>C:</b> Iso 167 [2.8] Iso <sub>1</sub> 159 [3.1] SmA 120 [-] M < 20 Cr
<b>B6/16</b>	6	16	<b>H:</b> Cub <sub>bi</sub> /Ia $\bar{3}d$ 163 [2.1] Iso <b>C:</b> Iso 156 [1.4] Cub <sub>bi</sub> /Ia $\bar{3}d$ < 20 Cr
<b>B10/6</b>	10	6	<b>H:</b> Cr 97 [30.8] SmA 177 [1.9] Iso <sub>1</sub> 180 [0.4] Iso <b>C:</b> Iso 178 [0.9] Iso <sub>1</sub> 175 [1.8] SmA 54 [24.0] Cr
<b>B10/8</b>	10	8	<b>H:</b> Cr 89 [33.0] SmA 170 [1.1] Iso <sub>1</sub> 177 [2.0] Iso <b>C:</b> Iso 177 [2.6] Iso <sub>1</sub> 168 [0.9] SmA 119 [-] M < 20 Cr
<b>B10/10</b>	10	10	<b>H:</b> Cr 97 [46.9] Cub <sub>bi</sub> /Ia $\bar{3}d$ 150 [0.7] SmA 163 [1.1] Iso <sub>1</sub> 177 [2.1] Iso <b>C:</b> Iso 175 [2.7] Iso <sub>1</sub> 157 [0.5] Cub <sub>bi</sub> /Ia $\bar{3}d$ < 20 Cr
<b>B10/12</b>	10	12	<b>H:</b> Cr 98 [49.1] Cub <sub>bi</sub> /Ia $\bar{3}d$ 150 [0.6] SmA 163 [0.9] Iso <b>C:</b> Iso 159 [0.4] Cub <sub>bi</sub> /Ia $\bar{3}d$ < 20 Cr
<b>B10/14</b>	10	14	<b>H:</b> Cr 100 [67.2] Cub <sub>bi</sub> /Ia $\bar{3}d$ 162 [1.7] Iso <b>C:</b> Iso 150 [0.9] Cub <sub>bi</sub> /Ia $\bar{3}d$ < 20 Cr
<b>B10/16</b>	10	16	<b>H:</b> Cr 80 [29.5] Cub <sub>bi</sub> /Ia $\bar{3}d$ 165 [1.4] Iso <b>C:</b> Iso 160 [1.8] Cub <sub>bi</sub> /Ia $\bar{3}d$ < 20 Cr
<b>B10/22</b>	10	22	<b>H:</b> Cr 71 [56.8] Cub <sub>bi</sub> /Ia $\bar{3}d$ 163 [1.4] Iso <b>C:</b> Iso 158 [20.3] Cub <sub>bi</sub> /Ia $\bar{3}d$ 39 Cr [2.0]

<sup>a</sup> Transition temperatures and enthalpy values were taken from the second DSC heating scans (**H**) and cooling scans (**C**) with 10 K min<sup>-1</sup>; abbreviations: Cr = crystalline solid; SmA = orthogonal non-tilted smectic A phase; M = three dimensional mesophase with unknown structure; Cub<sub>bi</sub>/Ia $\bar{3}d$  = achiral cubic phase with Ia $\bar{3}d$  lattice; Iso<sub>1</sub> = achiral isotropic liquid; Iso = isotropic liquid.

isotropic texture (see Fig. S7 in ESI<sup>†</sup>). These observations are typically observed for the non-tilted uniaxial SmA phase. On further heating, the SmA phase remains till transition to the isotropic liquid state without appearance of any additional mesophases. On cooling both compounds from the isotropic liquid clear fan shaped textures could be observed, which confirm again the presence of SmA phase (Fig. 4b). On further cooling the SmA phase remains without any sign of crystallization till ambient temperature which is also confirmed from the DSC investigations (Table 1, Fig. S9 and S10 in the ESI<sup>†</sup>).

On chain elongation and for the next two homologues **B6/10** and **B6/12**, the SmA phase remains the only observed mesophase, down to ambient temperature (Fig. S11 and S12 in the ESI<sup>†</sup>). However, as indicated from the DSC curves there is a broad transition peak in the isotropic liquid range of both compounds which could be recorded on both heating and cooling cycles (e.g. the insets in Fig. 5a and b). This additional isotropic liquid phase is achiral as indicated by POM investigations, where no dark and bright domains could be observed on rotation one of the analyzers from the crossed position with a

small angle either in clockwise or anticlockwise directions. Therefore, this achiral isotropic liquid phase is designated as Iso<sub>1</sub> phase. The Iso<sub>1</sub> phase is known for linear polycatenars<sup>26</sup> and was recently reported for HS tricatensars.<sup>51</sup> The enthalpy values of the SmA–Iso<sub>1</sub> phase transition either on heating or cooling are around 3–4 kJ mol<sup>-1</sup> (Table 1).

On further chain elongation and starting with  $n = 14$  (**B6/14**), a different phase sequence is observed as indicated from POM. On heating **B6/14** a transition takes place from the crystalline state to a highly viscous phase with mosaic-like birefringent texture, which is designated as M phase (see Fig. 4c). The M phase exists over  $\sim 7$  K and the Cr–M phase transition is accompanied with a small peak in the DSC heating curve (Table 1 and Fig. 5a). On further heating some regions of this birefringent texture convert to a completely dark texture which coexists over  $\sim 13$  K. On heating this biphasic texture, a complete isotropic appearance is observed at  $\sim 140$  °C, which is characterized by high viscosity. On slight rotation of one of the analyzers from the crossed position, no dark and bright areas could be detected, indicating the presence of the achiral

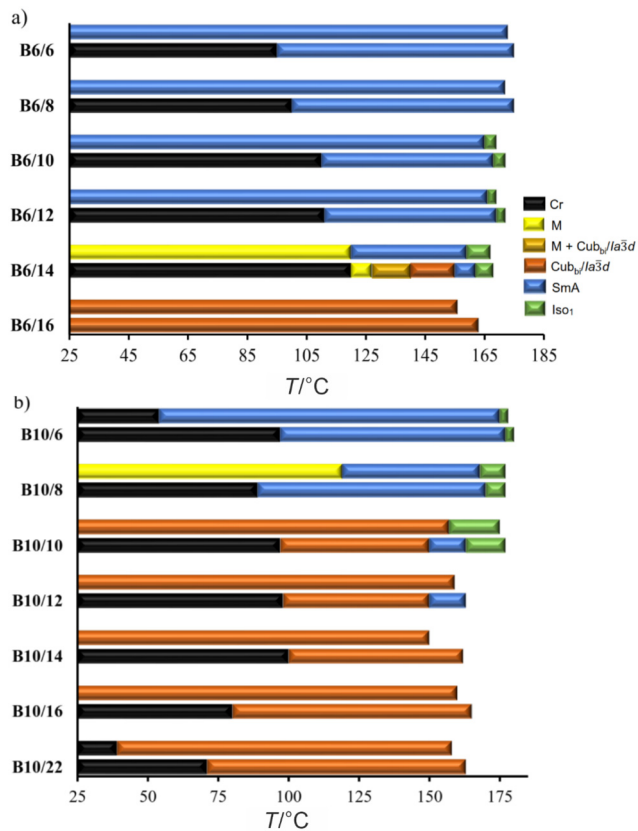


Fig. 3 Phase behaviour of the new polycatenars on heating (lower bars) and on cooling (upper bars) for: (a) series **B6/n** and (b) series **B10/n**. The colour codes are given in (a); for the abbreviations see Table 1.

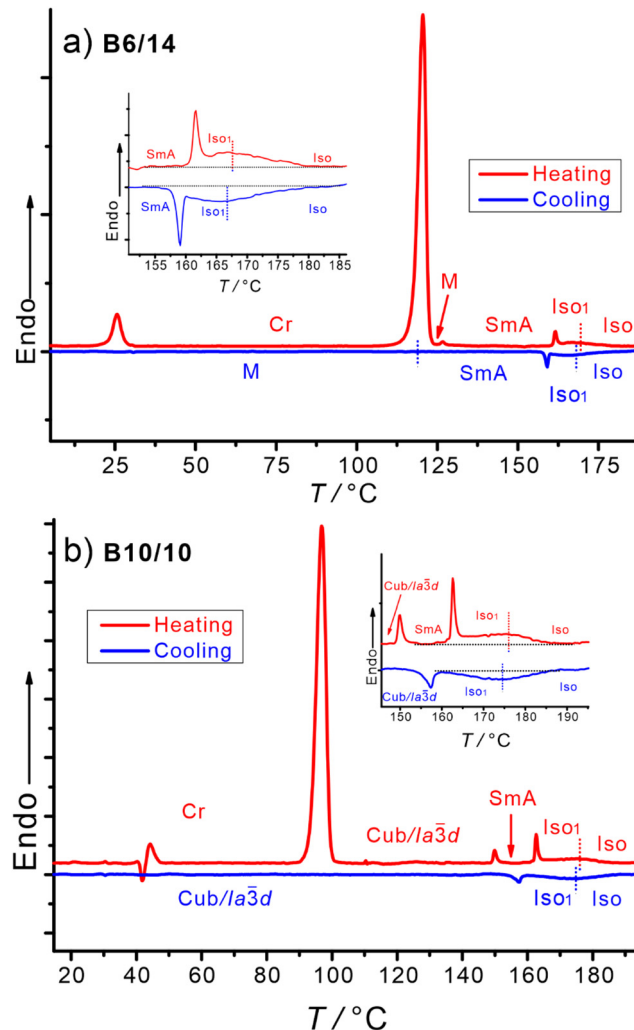


Fig. 5 DSC thermograms obtained for: (a) compound **B6/14** and (b) **B10/10**; with  $10 \text{ K min}^{-1}$  heating and cooling rates. The insets represent an enlarged range showing the Iso<sub>1</sub>–Iso broad transition peaks on heating and cooling; for the remaining DSC curves see ESI† (Fig. S9–S20).

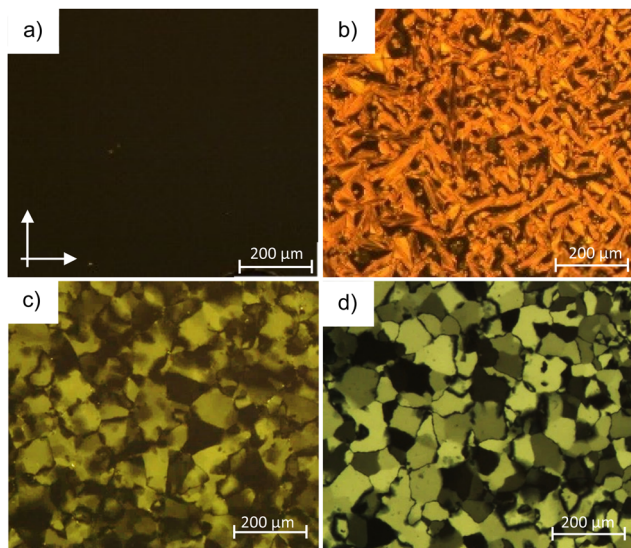


Fig. 4 Optical micrographs observed in a homeotropic cell for: compound **B6/6** in the SmA phase (a) on heating at  $T = 120 \text{ °C}$ ; (b) on cooling at  $T = 150 \text{ °C}$ ; (c) compound **B6/14** in the M phase at  $80 \text{ °C}$  on cooling and (d) compound **B10/8** in the M phase at  $100 \text{ °C}$  on cooling.

three-dimensional cubic phase (Cub). On further heating of this cubic phase, the material becomes less viscous, and the

dark texture is retained, indicating a transition to the homeotropic uniaxial SmA phase. Both transitions of M–Cub + M and Cub + M–SmA are not detected on DSC heating curve but were proven by XRD (will be discussed later).

The Iso<sub>1</sub> phase observed for the medium chain homologues **B6/10** and **B6/12** is also observed for **B6/14** as indicated from the broad transition peaks observed in heating and cooling curves (Fig. 5a). On cooling **B6/14** from the Iso<sub>1</sub> phase, the SmA mesophase is observed for a relatively wide range  $\sim 39 \text{ K}$  followed by the M phase without the appearance of Cub phase again. The M phase remains till room temperature without any sign of crystallization as confirmed from the DSC cooling curve (Fig. 5a) and the optical texture (Fig. 4c).

For the longest homologue **B6/16**, the Iso<sub>1</sub> and SmA phases are totally removed and only the Cub phase is observed over a large temperature range ( $\sim 163 \text{ K}$  on heating and  $\sim 156 \text{ K}$  on cooling). More interesting the Cub phase appears as a room temperature LC mesophase on both heating and cooling cycles (Fig. 3a).

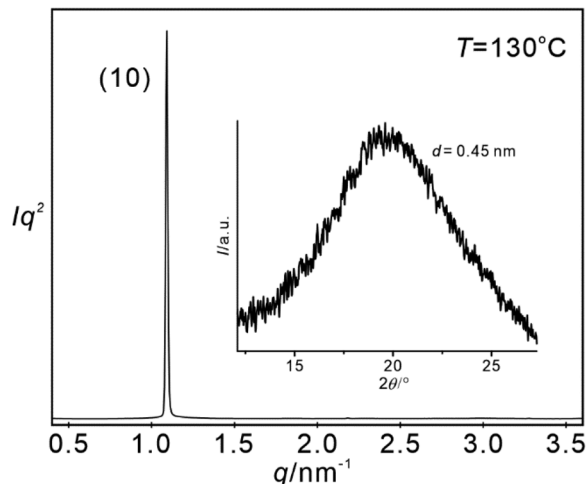


Fig. 6 Small X-ray diffractogram (SAXS) of **B6/12** on heating at 130 °C in the SmA phase. The insets show the wide-angle diffraction patterns (WAXS).

To further investigate the LC phases observed in **B6/n** series and to get more insights about the complex nanostructured 3D mesophases observed in this series, we performed XRD investigations for some selected examples.

As shown in Fig. 6, in the entire range of the LC phase exhibited by **B6/12** and at  $\sim 130$  °C one sharp Bragg reflection in the small angle region corresponding to  $d = 5.75$  nm is observed, while a diffuse scattering is observed in the wide-angle region. This indicates a smectic phase without in-plane positional order.

The maximum of the diffuse scattering in the wide-angle region is perpendicular to the small angle reflections, meaning an on average non-tilted arrangement of the molecules in layers *i.e.* a SmA phase in agreement with the observed optical textures (Fig. 4a and b). The experimental  $d$ -value  $\sim 5.75$  nm is significantly larger than the molecular length of a single

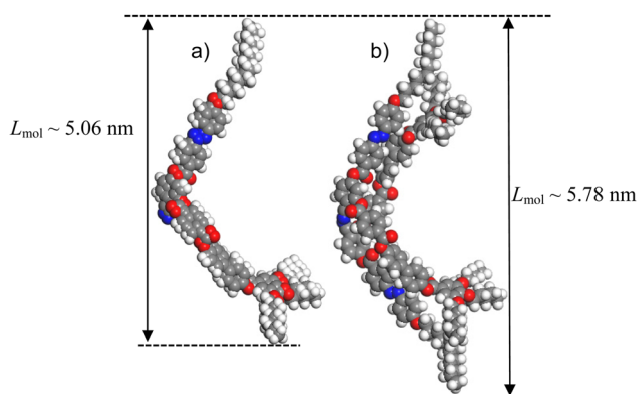


Fig. 7 Space-filling models of **B6/12** representing the possible modes of self-assembly in the SmA layers (one layer is represented): (a) parallel organization of the molecules with complete segregation of chains and cores and (b) intercalated bilayer structure with antiparallel (up-down symmetric) organization of the molecules with partial interdigitation of the alkyl chains and aromatic cores. Colour code: Gray = C; white = H; red = O and blue = N.

molecule ( $L_{\text{mol}} = 5.06$  nm) calculated with Materials Studio, for a V-shaped conformation with bending angle of 120° and all-*trans* stretched alkyl chains (Fig. 7a). This confirms an antiparallel side-by-side packing of the molecules in layers with partial interdigitation of the single alkyl chains and aromatic cores (Fig. 7b), whereas the non-interdigitated triple chain ends form the nano-segregated lipophilic layers.

Compound **B6/14** with three different LC phases was also investigated with XRD. In the lower temperature birefringent LC phase, a completely diffuse scattering with a maximum around 0.40 nm is observed in the wide-angle region (the inset in Fig. 8a). This indicates the presence of LC phase without fixed positions of the individual molecules. In the same LC phase, several sharp reflections are observed in the SAXS diffractogram (Fig. 8a), which could not be indexed to either Cub or tetragonal phase. Therefore, this LC phase is assigned as M phase. To get a clear picture about the exact structure of M phase additional investigations with resonant soft X-ray scattering (RSoXS) would be required.<sup>21,23</sup>

In the higher temperature LC crystalline phase one sharp Bragg reflection in the small angle region corresponding to  $d = 4.82$  nm is recorded (Fig. 8b), confirming the presence of SmA phase like that observed for the lower homologue **B6/12**. However, the molecular length ( $L_{\text{mol}} = 5.22$  nm), determined for a V-shaped conformation with bending angle of 120° and all-*trans* stretched alkyl chains is longer than the experimental  $d$ -value  $\sim 4.82$  nm, which differs from the SmA phase of **B6/12**. This indicates another way of arrangement of the molecules within the layers, confirming parallel organization of the molecules with complete segregation of chains and cores with additional tilt within the layers. This means that the SmA phase of **B6/14** is most likely to be of the de Vries type.<sup>68,69</sup> Obviously, the segregation of the alkyl chains (both at the single and triple chain ends) becomes sufficiently strong to remove the inter-coalition of the single-end alkyl chain and the aromatic core. In this way the large distance shrinks and the interfacial curvature between the aliphatic chains and aromatic cores increases.

In the LC phase below the SmA phase, several sharp reflections are observed. The most intense peaks can be indexed to the (211) and (220) reflections (Fig. 8c) of the bicontinuous cubic phase with  $Ia\bar{3}d$  lattice ( $\text{Cub}_{\text{bi}}/Ia\bar{3}d$ )<sup>21</sup> in agreement with the observed optical textures. The calculated lattice parameter  $a_{\text{cub}}$  is 11.30 nm, which is in the expected range of this type of cubic phase.<sup>11,14,15,27,28</sup> The additional small reflection peaks could be also indexed to  $\text{Cub}_{\text{bi}}/Ia\bar{3}d$  phase (see Table S1 in the ESI†). The reconstructed electron density map based on the obtained diffraction patterns, shows the double gyroid network structure of the  $Ia\bar{3}d$  phase (Fig. 8d), which further confirms the actual space group.

### 3.2. Hockey-stick polycatenars **B10/n**

To stabilize the cubic phase observed for the longest homologue **B6/16** from series **B6/n** series, the three terminal hexyloxy chains in compounds **B6/n** were replaced with decyloxy chains (**B10/n** series). The phase behaviour and types of LC phases formed by **B10/n** homologues are given in Table 1 and



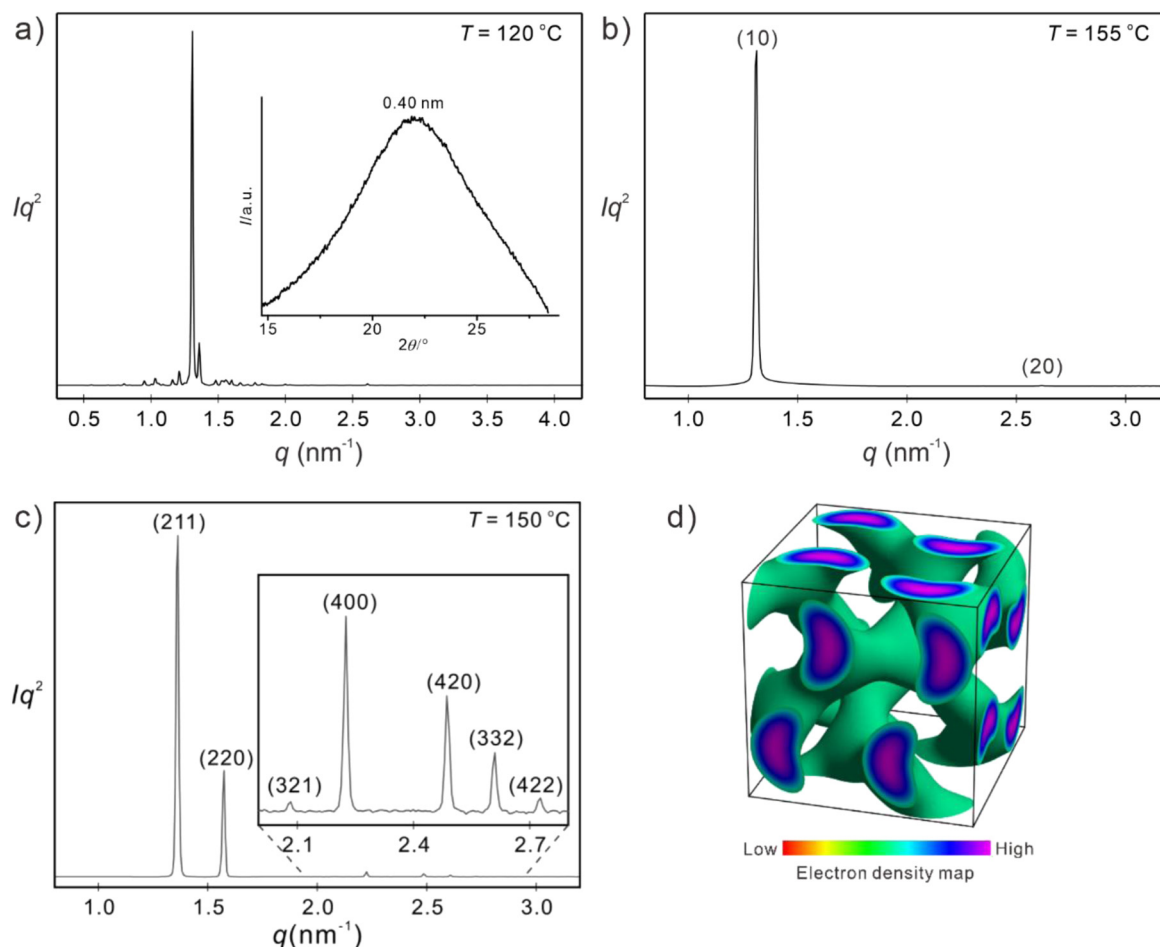


**Fig. 8** SAXS diffractogram of **B6/14** on heating: (a) in the M phase at 120 °C; (b) in the SmA phase at 155 °C; (c) at 150 °C in the  $\text{Cub}_{\text{bI}}/1a\bar{3}d$  phase ( $a_{\text{cub}} = 11.30$  nm) and (d) the electron density map of the  $1a\bar{3}d$  phase reconstructed from the diffraction data in (c); the inset in (a) shows the WAXS in the M phase. For numerical XRD data, see Table S1 (ESI†).

represented graphically in Fig. 3b. As can be seen from Table 1 and Fig. 3b, like **B6/6** the shortest compound **B10/6** also displays SmA phase but in this case, it is not a room temperature LC phase. Both compounds **B6/6** and **B10/6** exhibit almost the same melting temperatures but on cooling, compound **B10/6** crystallizes at  $\sim 54$  °C. Moreover, the Iso<sub>1</sub> phases are observed for all homologues with  $n \leq 10$  with an increasing range on chain elongation ( $n = 6 \rightarrow 10$ , see Fig. 3b and 5b). The M phase is also observed for **B10/8** as metastable mesophase as indicated from the texture under POM (Fig. 4d).

To check if the SmA phases displayed by either **B6/n** or **B10/n** are polar or not, some selected examples were further investigated by electro-optical experiments using a triangular wave voltage. For all investigated compounds from both series of materials no current peak could be observed in the SmA phases up to a voltage of 200 V<sub>pp</sub> in a 10 μm or 6 μm ITO cell, indicating the non-polar nature of the SmA phase. This behaviour is similar to that observed for the related analogues **A6/n** and **A10/n** (see Fig. 2).<sup>51</sup> The reason for this behaviour, could be also explained based on the XRD results of **B6/12** (Fig. 7). The arrangement of molecules in the SmA phase with an antiparallel side-by-side packing of the molecules (Fig. 7b)

in layers and partial interdigitation of the alkyl chains and aromatic cores results in removing the polar order. As known for BCLCs, the polar order could be expected if the molecules are preferred packed in layers with the BC molecules well organized in layers with a uniform bend-direction (Fig. 7a), which is not the case. This further indicates that these HS polycatenars behave typically like other HS molecules.<sup>52–66</sup> In the case of the **B6/14**, where the molecules are parallelly packed, the loss of polar order could be due the bulky end caused by alkyl chain intercoalition, which allows an easy rotation of the molecules around their long axis.

For all **B10/n** compounds with  $n \geq 10$  the achiral  $\text{Cub}_{\text{bI}}/1a\bar{3}d$  is formed as an enantiotropic mesophase, which is not crystallized on cooling except for the longest derivative (**B10/22**). For all  $\text{Cub}_{\text{bI}}/1a\bar{3}d$  phases there is  $\sim 6$ –12 K supercooling of the Iso– $\text{Cub}_{\text{bI}}$  transition compared to the  $\text{Cub}_{\text{bI}}$ –Iso transition temperature on heating (see Table 1 and Fig. 3b), which is a typical feature of such nanostructured 3D mesophase. More interesting, almost all the  $\text{Cub}_{\text{bI}}/1a\bar{3}d$  phases of **B10/n** series and **B6/16** are room temperature mesophases with wider ranges compared to their related analogues **Am/n**, meaning that increasing the chain volume at the crowded end of this type

of HS molecules results in stabilization of  $Cub_{bi}$  phases. Such room temperature  $Cub_{bi}$  phases could be good candidates for applications. Compound **B10/22** (see Fig. S8 and S19, ESI†) was synthesized aiming to induce the chiral version of the cubic phases *i.e.*  $Cub^{[*]}$  with  $I23$  symmetry ( $Cub^{[*]}/I23$ ) as would be expected upon alkyl-chain elongation.<sup>14,15,28</sup> However, the type of the  $Cub_{bi}$  does not change with increasing the length of the terminal chains, indicating that the required chain volume is not achieved.

## 4. Comparison with related compounds

Comparing the newly reported HS polycatenar reported herein **B6/8** with the previously reported rod-like polycatenar **C6/8** (Fig. 9)<sup>24</sup> having also an extended aromatic core but with one benzene ring less and no bent 4-cyanoresorcinol unit, we can conclude that the types of mesophases observed in both compounds are totally different.

For the linear polycatenar a complex nanostructure 3D tetragonal (Tet) phase is observed followed by a chiral isotropic liquid ( $Iso_1^{[*]}$ ) phase, while for the HS polycatenar **B6/8** only a SmA phase is observed without the formation of 3D or chiral mesophases. The reason for this different phase behaviour is the incorporation of 4-cyanoresorcinol bent-core unit into the molecular structure of **C6/8**. The chirality is induced in **C6/8** and similar related linear hydrogen-bonded supramolecular polycatenars as a result of the steric crowding of the three alkyl chains at one end of the rod-like cores.<sup>12</sup> This prevents the exact parallel organization of the rods and leads to a slight angle between the rods giving rise to a helical twist along the networks. The formation of such helical networks could be observed either in the isotropic liquid state or in the chiral

bicontinuous cubic phases with  $I23$  symmetry ( $Cub_{bi}^{[*]}/I23$ ). The bend of the 4-cyanoresorcinol unit ( $<120^\circ$ ) obviously distorts the helical packing and the large core of **B6/8** stabilizes the lamellar phase. To check if the 4-cyanoresorcinol unit is responsible for the disappearance of  $Cub_{bi}^{[*]}/I23$  and  $Iso_1^{[*]}$  phases and to avoid the formation of SmA phase, compound **D6/8** with a shorter core unit compared to **B6/8** (Fig. 9) was synthesized as described in detail in the ESI† (Scheme S1). The new compound **D6/8** was designed to have the same number of benzene rings as those of **C6/8** but with the 4-cyanoresorcinol unit more shifted toward the triple substituted end of the molecule.

As can be seen from the optical textures in Fig. 10, neither the SmA phase nor the Tet or  $Iso_1^{[*]}$  phases are observed. Instead, three different LC phases are formed by **D6/8** as indicated from POM and the DSC heating and cooling curves (see Fig. S20, ESI†). The higher LC phase is a nematic phase based on the texture shown in Fig. 10a. It is likely to be a cybotactic nematic phase with SmC type ( $N_{Cybc}$ ) clusters as supported by the appearance of the SmC phase below the nematic one (Fig. 10b).<sup>65,66</sup> The SmC phase has a birefringent texture in the homeotropic cell (Fig. 10b) and in the planar cell it displays a broken fan-shape texture with the dark extinctions inclined with the direction of the polarizers (Fig. 10e), confirming a synclinal tilt organization of the molecules in this SmC phase *i.e.* SmC<sub>s</sub> phase. The texture changes again at the transition to the lower temperature phase to unknown texture in both homeotropic and planar cells (Fig. 10c and f). Therefore, the lower temperature LC phase is assigned as SmX phase. No current peak could be observed under a triangular wave voltage in any of the LCs exhibited by **D6/8** up to a voltage of 200 V<sub>pp</sub> in a 6 μm ITO cell. This means that all LC phases are all non-polar. Based on these observations, it is obvious that the phase behaviour of **D6/8** is more related to conventional HSLCs<sup>63-66</sup> and not to linear polycatenars.<sup>24,27</sup> This not only confirms that the

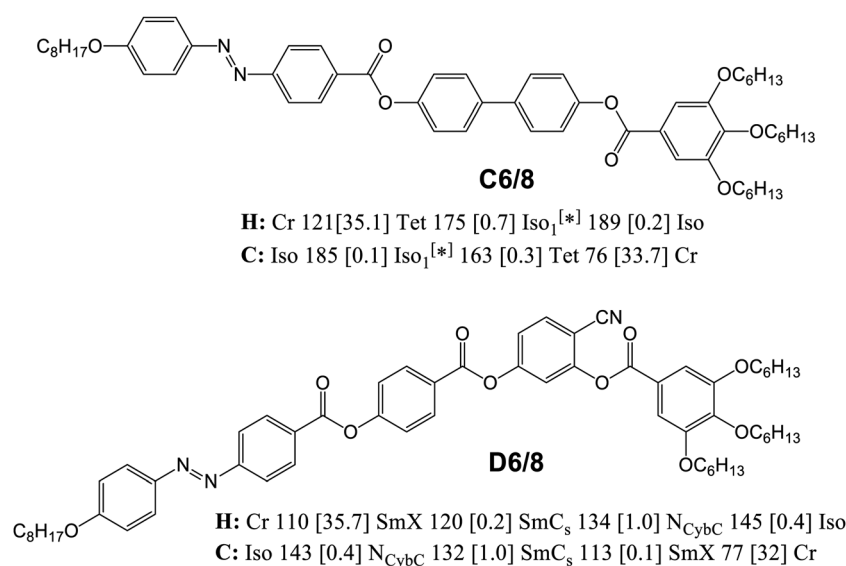
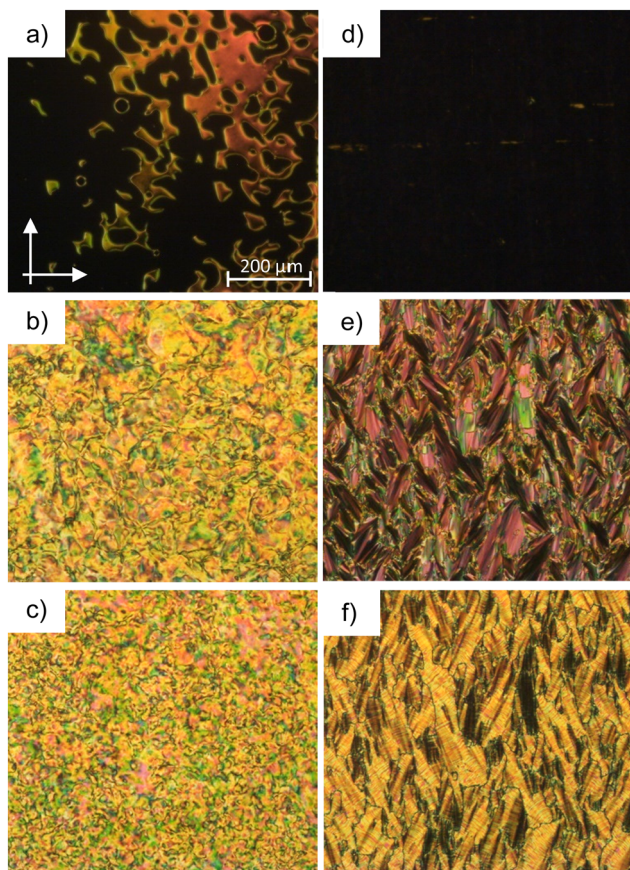


Fig. 9 Chemical structures, phase types, phase transition temperatures ( $T$  (°C)) and transition enthalpies [ $\Delta H$  (kJ mol<sup>-1</sup>)] on heating (H:) and cooling (C:) for the previously reported linear polycatenar **C6/8**<sup>24</sup> and the new related compound **D6/8**.



**Fig. 10** Optical micrographs observed for compound **D6/8** in a homeotropic cell (left column) and in a 6  $\mu\text{m}$  ITO planar cell (right column) as observed on cooling: (a and d) in the N phase at  $T = 140\text{ }^\circ\text{C}$ ; (b and e) in the  $\text{SmC}_s$  phase at  $T = 120\text{ }^\circ\text{C}$  and (c and f) in the  $\text{SmX}$  phase at  $T = 100\text{ }^\circ\text{C}$ . The direction of the polarizers and the scale bar for all textures are shown in (a).

4-cyanoresorcinol unit is responsible for the disappearance of chiral mesophases in these HS molecules, but also indicates that the type of LC phases depends strongly on the position of the 4-cyanoresorcinol unit. Therefore, if it is located at terminal position of the rod-like core N and  $\text{SmC}$  phases are formed and if shifted to an inner position,  $\text{SmA}$  and  $\text{Cub}$  phases could be induced. Moreover, depending on the chain volume used at the crowded end the stability of the  $\text{Cub}$  phases could be increased, where more stable  $\text{Cub}$  phases were observed in the new HS **Bm/n** compared to their related analogues **Am/n**.

#### 4.1. Photoisomerization in solution

To investigate the photoisomerization of the new HS polycatenars UV-vis absorption spectroscopy was performed on **B6/16** dissolved in chloroform solution as a representative example. As shown in Fig. 11 the UV-vis absorption spectra were measured at three different states (a–c). For a freshly prepared solution a maximum absorption at  $\sim 368\text{ nm}$  is observed, which is attributed to the  $\pi\text{-}\pi^*$  transition of the chromophore (Fig. 11a). This indicates the presence of the molecules in the more stable *trans* isomer. The second measurement was performed after irradiation of the solution with 365 nm light for

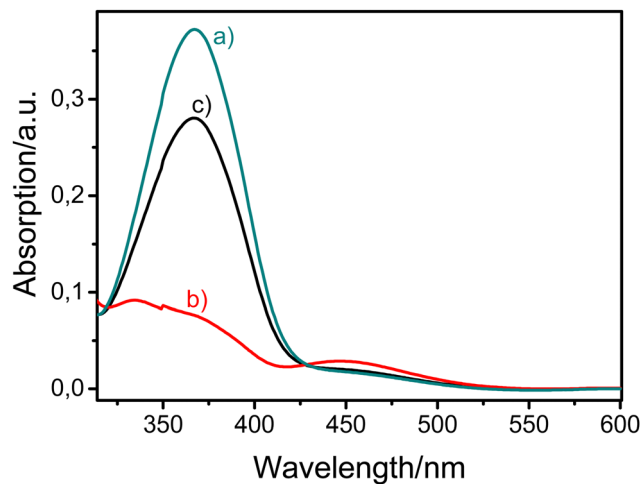


**Fig. 11** UV-Vis spectra (absorbance vs. wavelength) of **B6/16** dissolved in chloroform at room temperature. (a) Freshly prepared sample; (b) after irradiation for one hour with 365 nm light and (c) after keeping the sample in dark overnight.

one hour (Fig. 11b), where the absorption peak observed at  $\sim 368\text{ nm}$  almost disappears and another broad band at  $\sim 453\text{ nm}$  starts to appear. This indicates a photoisomerization from the more stable *trans*-isomer to the less stable *cis* isomer upon photo-irradiation. Finally, after storing the same solution in dark overnight and measuring it the peak at  $\sim 368\text{ nm}$  appears again, and that one at  $\sim 453\text{ nm}$  disappears (Fig. 11c). This confirms a reversible transformation to the *trans* isomer again, which means that the *trans-cis* photoisomerization is a reversible process.<sup>70</sup> To investigate the effect of the alkyl chain length on the photoisomerization, compound **B10/22** with longer chains at both ends of the aromatic core compared to **B6/16** was also investigated in a similar manner (Fig. S21, ESI<sup>†</sup>). The photoisomerization in both cases is very similar, indicating that the reversible *trans-cis* photoisomerization in such HS polycatenars does not depend on the terminal chain length. The detailed photo switching investigation in the bulk state *i.e.* in the LC phases is currently under investigation and will be published in a forthcoming paper.

## 5. Summary and conclusions

In summary, we reported the design, synthesis, and liquid crystal self-assembly of two new series of photoresponsive HS polycatenars. The new HSLCs are derived from 4-cyanoresorcinol as the bent-core unit connected to one short azobenzene-based wing and a long biphenyl-based side arm (**Bn/6** and **Bn/10**). In the first series (**Bn/6**) three hexyloxy chains are connected to positions 3, 4 and 5 in the terminal benzene ring of the long wing, while in the second series (**Bn/10**) they are replaced by three decyloxy chains. Depending on the alkyl chain length and temperature a transition from a non-tilted  $\text{SmA}$  phases to complex 3D nanostructured phases was observed. The 3D phases include the bicontinuous cubic phase with  $1a3d$  symmetry ( $\text{Cub}_{\text{bi}}/1a3d$ ) and an unknown mesophase assigned as M phase.

Also, network formation was detected in the achiral liquid phase (Iso<sub>1</sub>) for some compounds as confirmed by DSC investigations. The stabilization of the cubic phases was successfully achieved by increasing the chain volume at the crowded end of the aromatic core, where room temperature Cub<sub>bi</sub>/Ia $\bar{3}$ d phases were exhibited by all medium and long chain homologues of the B10/*n* series, making them good candidates for applications. The absence of chiral mesophases in the new HS polycatenars in comparison with related linear molecules was discussed based on the phase behaviour of a new compound having the 4-cyanoresorcinol unit at terminal position of the rod-like core. The results indicated that the 4-cyanoresorcinol bent unit distorts the helical packing and therefore suppress the formation of any chiral mesophase. Finally, the reversible *trans-cis* photoisomerization for two selected examples with short and long terminal chains was investigated in chloroform solution.

## Conflicts of interest

There are no conflicts to declare.

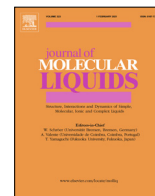
## Acknowledgements

Special thanks to Prof. Dr Carsten Tschierske for helpful discussion and reading of the manuscript. M. Alaasar acknowledges the German Research Foundation (DFG) for the financial support (AL2378/1-1, 424355983). The authors are grateful to Beamline BL16B1 at SSRF (Shanghai Synchrotron Radiation Facility, China) for providing the beamtime.

## References

- V. Luzzati, A. Tardieu, T. Gulik-Krzywicki, E. Rivas and F. Reiss-Husson, *Nature*, 1968, **220**, 485.
- S. Hyde, Z. Blum, T. Landh, S. Lidin, B. Ninham, S. Andersson and K. Larsson, *The language of shape: the role of curvature in condensed matter: physics, chemistry and biology*, Elsevier, 1996.
- A. J. Meuler, M. A. Hillmyer and F. S. Bates, *Macromolecules*, 2009, **42**, 7221.
- L. Han and S. Che, *Adv. Mater.*, 2018, **30**, 1705708.
- T. Kato, J. Uchida, T. Ichikawa and T. Sakamoto, *Angew. Chem., Int. Ed.*, 2018, **57**, 4355.
- S. Poppe, X. Cheng, C. Chen, X. Zeng, R.-B. Zhang, F. Liu, G. Ungar and C. Tschierske, *J. Am. Chem. Soc.*, 2020, **142**, 3296.
- T. Ichikawa, M. Yoshio, A. Hamasaki, S. Taguchi, F. Liu, X.-B. Zeng, G. Ungar, H. Ohno and T. Kato, *J. Am. Chem. Soc.*, 2012, **134**, 2634.
- E. J. W. Crossland, M. Kamperman, M. Nedelcu, C. Ducati, U. Wiesner, D. M. Smilgies, G. E. Toombes, M. A. Hillmyer, S. Ludwigs, U. Steiner and H. J. Snaith, *Nano Lett.*, 2009, **9**, 2807.
- O. Kwon, X. Cai, W. Qu, F. Liu, J. Szydłowska, E. Gorecka, M. J. Han, D. K. Yoon, S. Poppe and C. Tschierske, *Adv. Funct. Mater.*, 2021, **31**, 2102271.
- C. Dressel, T. Reppe, M. Prehm, M. Brautzsch and C. Tschierske, *Nat. Chem.*, 2014, **6**, 971.
- C. Dressel, F. Liu, M. Prehm, X. Zeng, G. Ungar and C. Tschierske, *Angew. Chem., Int. Ed.*, 2014, **53**, 13115.
- M. Alaasar, S. Poppe, Q. Dong, F. Liu and C. Tschierske, *Chem. Commun.*, 2016, **52**, 13869.
- O. Kwon, X. Cai, W. Qu, F. Liu, J. Szydłowska, E. Gorecka, M. J. Han, D. K. Yoon, S. Poppe and C. Tschierske, *Adv. Funct. Mater.*, 2021, **31**, 2102271.
- M. Alaasar, A. F. Darweesh, X. Cai, F. Liu and C. Tschierske, *Chem. – Eur. J.*, 2021, **27**, 14921.
- T. Reppe, C. Dressel, S. Poppe, A. Eremin and C. Tschierske, *Adv. Opt. Mater.*, 2021, **9**, 2001572.
- R. A. Reddy, U. Baumeister, C. Keith, H. Hahn, H. Lang and C. Tschierske, *Soft Matter*, 2007, **3**, 558.
- S. Kang, M. Harada, X. Li, M. Tokita and J. Watanabe, *Soft Matter*, 2012, **8**, 1916.
- J. Matraszek, J. Zapala, J. Mieczkowski, D. Pocięcha and E. Gorecka, *Chem. Commun.*, 2015, **51**, 5048.
- J. Matraszek, D. Pocięcha, N. Vaupotič, M. Salamończyk, M. Vogrine and E. Gorecka, *Soft Matter*, 2020, **16**, 3882.
- W. Weissflog, in *Handbook of Liquid Crystals*, ed. J. W. Goodby, J. P. Collings, T. Kato, C. Tschierske, H. F. Gleeson and P. Raynes, Wiley-VCH, Weinheim, 2nd edn, 2014, vol. 5, pp. 89–174.
- Y. Cao, M. Alaasar, A. Nallapaneni, M. Salamończyk, P. Marinko, E. Gorecka, C. Tschierske, F. Liu, N. Vaupotič and C. Zhu, *Phys. Rev. Lett.*, 2020, **125**, 027801.
- X. Zeng and G. Ungar, *J. Mater. Chem. C*, 2020, **8**, 5389.
- Y. Cao, M. Alaasar, L. Zhang, C. Zhu, C. Tschierske and F. Liu, *J. Am. Chem. Soc.*, 2022, **144**, 6936.
- M. Alaasar, M. Prehm, Y. Cao, F. Liu and C. Tschierske, *Angew. Chem., Int. Ed.*, 2016, **128**, 320.
- M. Alaasar, S. Poppe, Q. Dong, F. Liu and C. Tschierske, *Angew. Chem., Int. Ed.*, 2017, **56**, 10801.
- M. Alaasar, S. Poppe, Y. Cao, C. Chen, F. Liu, C. Zhu and C. Tschierske, *J. Mater. Chem. C*, 2020, **8**, 12902.
- M. Alaasar, J. C. Schmidt, X. Cai, F. Liu and C. Tschierske, *J. Mol. Liq.*, 2021, **332**, 115870.
- M. Alaasar, X. Cai, F. Kraus, M. Giese, F. Liu and C. Tschierske, *J. Mol. Liq.*, 2022, **351**, 118597.
- S. C. Lee, S. H. Lee and O. P. Kwon, *J. Mater. Chem. C*, 2016, **4**, 1935.
- T. Ikeda, J. Mamiya and Y. Yu, *Angew. Chem., Int. Ed.*, 2007, **46**, 506.
- E. V. Fleischmann and R. Zentel, *Angew. Chem., Int. Ed.*, 2013, **52**, 8810.
- M. Kondo, Y. Yu and T. Ikeda, *Angew. Chem., Int. Ed.*, 2006, **45**, 1378.
- H. K. Bisoyi and Q. Li, *Chem. Rev.*, 2016, **116**, 15089.
- M. Alaasar, *Liq. Cryst.*, 2016, **43**, 2208.
- D. Jágerová, M. Šmahel, A. Poryvai, J. Macháček, V. Novotná and M. Kohout, *Crystals*, 2021, **11**, 1265.

- 36 N. Gimeno, I. Pintre, M. Martínez-Abadía, J. L. Serrano and M. B. Ros, *RSC Adv.*, 2014, **4**, 19694.
- 37 M. V. Srinivasan, P. Kannan and P. Roy, *New J. Chem.*, 2013, **37**, 1584.
- 38 N. G. Nagaveni, A. Roy and V. Prasad, *J. Mater. Chem.*, 2012, **22**, 8948.
- 39 N. Trišović, M. Salamoneczyk, J. Antanasijević, S. Sprunt, T. Tóth-Katona, A. Jákli, M. Kohout and K. Fodor-Csorba, *RSC Adv.*, 2015, **5**, 64886.
- 40 M. Horčić, V. Kozmik, J. Svoboda, V. Novotná and D. Pocięcha, *J. Mater. Chem. C*, 2013, **1**, 7560.
- 41 M. Alaasar, M. Prehm and C. Tschierske, *RSC Adv.*, 2016, **6**, 82890.
- 42 M. Alaasar, M. Prehm, M. Nagaraj, J. K. Vij and C. Tschierske, *Adv. Mater.*, 2013, **25**, 2186.
- 43 M. Alaasar, M. Prehm, K. May, A. Eremin and C. Tschierske, *Adv. Funct. Mater.*, 2014, **24**, 1703.
- 44 M. Alaasar, M. Prehm, M.-G. Tamba, N. Sebastian, A. Eremin and C. Tschierske, *Chem. Phys. Chem.*, 2016, **17**, 278.
- 45 C. Tschierske, *Liq. Cryst.*, 2022, DOI: [10.1080/02678292.2021.2010142](https://doi.org/10.1080/02678292.2021.2010142).
- 46 I. Wirth, S. Diele, A. Eremin, G. Pelzl, S. Grande, L. Kovalenko, N. Pancenko and W. Weissflog, *J. Mater. Chem.*, 2001, **11**, 1642.
- 47 L. Kovalenko, M. W. Schröder, R. A. Reddy, S. Diele, G. Pelzl and W. Weissflog, *Liq. Cryst.*, 2005, **32**, 857.
- 48 C. Keith, A. Lehmann, U. Baumeister, M. Prehm and C. Tschierske, *Soft Matter*, 2010, **6**, 1704.
- 49 E. Westphal, H. Gallerdo, G. F. Caramori, N. Sebastian, M.-G. Tamba, A. Eremin, S. Kawauchi, M. Prehm and C. Tschierske, *Chem. – Eur. J.*, 2016, **22**, 8181.
- 50 H. Ocak, M. Poppe, B. Bilgin-Eran, G. Karanlık, M. Prehm and C. Tschierske, *Soft Matter*, 2016, **12**, 7405.
- 51 M. Alaasar and S. Poppe, *J. Mol. Liq.*, 2022, **351**, 118613.
- 52 G. Pelzl and W. Weissflog, in *Thermotropic Liquid Crystals: Recent Advances*, ed.: A. Ramamoorthy, Springer; Amsterdam, 2007, pp. 1–58.
- 53 D. Pocięcha, E. Gorecka, M. Čepić, N. Vaupotić and W. Weissflog, *Phys. Rev. E: Stat., Nonlinear, Soft Matter Phys.*, 2006, **74**, 021702.
- 54 A. Eremin, M. Floegel, U. Kornek, S. Stern, R. Stannarius, H. Nadasi, W. Weissflog, C. Zhu, Y. Shen, C. S. Park, J. MacLennan and N. Clark, *Phys. Rev. E: Stat., Nonlinear, Soft Matter Phys.*, 2012, **86**, 051701.
- 55 V. Gude, K. Upadhyaya, G. Mohiuddin and V. S. R. Nandiraju, *Liq. Cryst.*, 2013, **40**, 120.
- 56 F. C. Yu and L. J. Yu, *Chem. Mater.*, 2006, **18**, 5410.
- 57 S. Kang, Y. Saito, N. Watanabe, M. Tokita, Y. Takanishi, H. Takezoe and J. Watanabe, *J. Phys. Chem. B*, 2006, **110**, 5205.
- 58 K. M. Fergusson and M. Hird, *J. Mater. Chem.*, 2010, **20**, 3069.
- 59 A. S. Matharu, C. Grover, L. Komitov and G. Anderson, *J. Mater. Chem.*, 2000, **10**, 1303.
- 60 W. Weissflog, U. Dunemann, S. F. Tandel, M. G. Tamba, H. Kresse, G. Pelzl, S. Diele, U. Baumeister, A. Eremin, S. Stern and R. Stannarius, *Soft Matter*, 2009, **5**, 1840.
- 61 M. Monika, V. Prasad and N. G. Nagaveni, *Liq. Cryst.*, 2015, **42**, 1490.
- 62 R. Deb, R. K. Nath, M. K. Paul, N. V. S. Rao, F. Tuluri, Y. Shen, R. Shao, D. Chen, C. Zhu, I. I. Smalyukh and N. A. Clark, *J. Mater. Chem.*, 2010, **20**, 7332.
- 63 D. K. Yoon, R. Deb, D. Chen, E. Korblova, R. Shao, K. Ishikawa, N. V. S. Rao, D. M. Walba, I. I. Smalyukh and N. A. Clark, *Proc. Natl. Acad. Sci. U. S. A.*, 2010, **107**, 21311.
- 64 R. K. Nath, D. D. Sarkar, D. S. S. Rao and N. V. S. Rao, *Liq. Cryst.*, 2012, **39**, 889.
- 65 M. Alaasar, S. Poppe and C. Tschierske, *Liq. Cryst.*, 2017, **44**, 729.
- 66 M. Alaasar, S. Poppe, C. Kerzig, C. Klopp, A. Eremin and C. Tschierske, *J. Mater. Chem. C*, 2017, **5**, 8454.
- 67 K. Miyasato, S. Abe, H. Takezoe, A. Fukuda and E. Kuze, *Jpn. J. Appl. Phys.*, 1983, **22**, L661.
- 68 J. P. F. Lagerwall and F. Giesselmann, *Chem. Phys. Chem.*, 2006, **7**, 20.
- 69 M. Alaasar, M. Prehm, S. Poppe and C. Tschierske, *Chem. – Eur. J.*, 2017, **23**, 5541.
- 70 J. M. Shivanna, M. Alaasar and G. Hegde, *J. Mol. Liq.*, 2021, **341**, 117341.



# Hockey-Stick Polycatenars: Network formation and transition from one dimensional to three-dimensional liquid crystalline phases

Mohamed Alaasar<sup>a,b,\*</sup>, Silvio Poppe<sup>a</sup>

<sup>a</sup> Institute of Chemistry, Martin Luther University Halle-Wittenberg, Kurt Mothes Str. 2, D-06120 Halle (Saale), Germany

<sup>b</sup> Department of Chemistry, Faculty of Science, Cairo University, Giza, Egypt



## ARTICLE INFO

### Article history:

Received 12 December 2021

Revised 17 January 2022

Accepted 24 January 2022

Available online 29 January 2022

### Keywords:

Polycatenar liquid crystals

Bent-core liquid crystals

Hockey-stick

Azobenzenes

Cubic phases

Photo switching

## ABSTRACT

Photo switchable liquid crystalline (LC) materials are of great interest for optical and photonic applications. Herein we report the design, synthesis, and molecular self-assembly of the first examples of photosensitive hockey-stick (HS) polycatenars. Therefore, two new series of HSLCs derived from 4-cyanoresorcinol bent-core unit connected to a short azobenzene-based side arm with one variable alkoxy chain and a long ester-based wing terminated with two alkoxy chains at 3 and 5 positions of the terminal benzene ring are reported. They differ from each other in the length of the terminal chains connected to the long arm. The LC self-assembly of these HSLCs was investigated by polarized optical microscopy (POM), differential scanning calorimetry (DSC), X-ray diffraction (XRD) and electro optical investigations. Depending on length of terminal chains a transition from one dimensional (1D) tilted and non-tilted smectic phases to three dimensional (3D) achiral bicontinuous cubic phases with  $1a3d$  symmetry ( $Cub_{bi}/1a3d$ ) upon chain elongation is observed. Moreover, achiral isotropic liquid networks were observed for medium and long chain homologues. Most of mesophases are room temperature LCs phases with wide ranges as observed in the cooling cycles, where once they are formed on heating, no sign of crystallization is detected down to ambient temperature. Finally, UV light irradiation results in fast and reversible photoinduced transformation between different types of LCs phases as well as between LC phase and isotropic liquid.

© 2022 The Author(s). Published by Elsevier B.V. This is an open access article under the CC BY license (<http://creativecommons.org/licenses/by/4.0/>).

## 1. Introduction

Designing materials with potential nano-technological applications is of great interest. Liquid crystals (LCs) represent one class of such materials which are widely applied nowadays in electronic and optoelectronic devices [1,2]. LCs have not only been applied in liquid crystals displays (LCDs) but also as organic semiconductors in organic field effect transistors (OFETs) [3], organic light emitting diodes (OLEDs) [4], and organic photovoltaic cells (OPV) [5]. Besides conventional rod-like LCs, bent-core liquid (BCLCs) represent an interesting class of nonconventional LCs, which exhibit unique and fascinating mesophases ranging from polar smectic to non-polar smectic phases known to be formed by rodlike LCs [6–11]. More interesting, BCLCs can form spontaneously mirror symmetry broken mesophases such as the helical nanofilament phase (B4 phase) [12,13] and dark conglomerate phases (DC phases) [14,15], though the molecules themselves are achiral. BCLCs can

also display cybotactic and paraelectric nematic phases [16,17] in addition to their potential to form biaxial nematics.[18–22]. Due to their reversible *trans-cis* photoisomerization upon light irradiation azobenzene-based BCLCs have attracted the attention of many researchers [11,23–29]. The presence of the azobenzene unit in the molecular structure provides an efficient way to photocontrol the molecular structure and to modulate the physical properties toward applications [30]. Therefore, azobenzene based LCs have been applied in optoelectronic sensing devices [31] and organic light-driven actuators [32–34]. Recently, we have reported different classes of azobenzene containing BCLCs derived from 4-substituted resorcinol core unit that exhibit mirror-symmetry breaking in helical nano-crystallite phases (HNC) [11,15] as well as in fluid smectic C phases depending on the type of the substituent used [35–38]. One of the most promising central core units is 4-cyanoresorcinol, which is known to induce LC mesophases at the border line between rod-like and bent-core molecules [36–43]. A breakthrough came with the discovery of mirror-symmetry breaking in the liquid networks known as Iso<sub>1</sub><sup>[\*]</sup> formed by polycatenars [44,45]. Polycatenars represent another class of nonconventional LCs consisting of a long aromatic rod-like core

\* Corresponding author at: Institute of Chemistry, Martin Luther University Halle-Wittenberg, Kurt Mothes Str. 2, D-06120 Halle (Saale), Germany.

E-mail address: [mohamed.alaasar@chemie.uni-halle.de](mailto:mohamed.alaasar@chemie.uni-halle.de) (M. Alaasar).

decorated with multiterminal flexible chains [46]. Due to nanosegregation of the aromatic rigid core and the terminal flexible chains, polycatenars can display different types of LCs mesophases including nematic, smectic, bicontinuous cubic ( $\text{Cub}_{\text{bi}}$ ), micellar cubic and columnar phases depending on the number of the terminal chains.  $\text{Cub}_{\text{bi}}$  phases are three dimensional LCs phases, which represent an intermediate state between the one dimensional (1D) lamellar and the two dimensional (2D) columnar mesophases and are very interesting for a wide range of applications e.g. as 3D conducting or photonic materials [47,48], and for optical band-gap materials [49–51]. These 3D phases with cubic symmetry are rarely observed in bent-core molecules [52–55], while they are known to be formed by polycatenars having terminal chains non-symmetrically distributed at both ends of the long aromatic core [44,45,56–59]. There are two types of  $\text{Cub}_{\text{bi}}$  formed by such polycatenars, the first one is achiral  $\text{Cub}_{\text{bi}}$  with  $Ia\bar{3}d$  symmetry ( $\text{Cub}_{\text{bi}}/Ia\bar{3}d$ ) [60], and the second type is chiral  $\text{Cub}_{\text{bi}}$  with  $I23$  symmetry ( $\text{Cub}_{\text{bi}}^*/I23$ ) [61]. The two different types are characterized by their high viscosity and can be distinguished by XRD investigations [60,61]. Under POM with crossed polarizers both of them appear totally isotropic, while under slightly uncrossed polarizers dark and bright areas could be only observed in the case of the chiral  $\text{Cub}_{\text{bi}}^*/I23$ . These domains invert their signs by inverting the direction of rotation of the analyzers, confirming the chirality of this  $\text{Cub}_{\text{bi}}^*/I23$  phase. The  $\text{IsoI}^*$  phase was found to be formed beside either the chiral  $\text{Cub}_{\text{bi}}^*/I23$  or the achiral  $\text{Cub}_{\text{bi}}/Ia\bar{3}d$  phases in most cases [44,45,56,57,58,59,62]. However, we have also reported recently the first example of an  $\text{IsoI}^*$  phase occurring beside a Smectic A (SmA) phase exhibited by azobenzene-based tricatenars [63]. The latter was also able to form the achiral version of the 3D  $\text{Cub}_{\text{bi}}$  phases i.e.  $\text{Cub}_{\text{bi}}/Ia\bar{3}d$  beside SmA and other different types of smectic phases depending on the length of the terminal alkyl chain [64]. Therefore, the question arose if the LC phases of polycatenars still show chiral mesophases if a bend is induced in its molecular structure by using 4-cyanoresorcinol as central bent unit (see scheme 1), which known to have low bend angle  $< 120^\circ$  [36,37,38,39,40,41,42,43]. Moreover, would this molecular structure exhibit banana-mesophases or other LCs phases that are displayed by HS molecules?

To answer these two questions, herein we report the synthesis and investigation of the liquid crystal self-assembly of a new family of polycatenars in the form of hockey-stick (HS) molecules derived from 4-cyanoresorcinol connected to two side arms, where one arm is much longer than the other (**A6/n** and **A10/n**, Scheme 2). HSLCs represent materials that could display mesophases at the cross over between BCLCs and rod-like molecules which could also lead to new mesophases [65–79]. The new HS molecules represent

tricatear systems having two terminal alkyl chains attached to the long side arm at positions 3 and 5 on the terminal benzene ring and one alkyl chain attached to the azobenzene-based short side arm. Therefore, two different series of these HS molecules **A6/n** and **A10/n** (see Scheme 2 and Fig. 1) were designed and synthesized, where in the first series the double chain on the long side arm are kept fixed with 6 carbon atoms in each chain i.e. hexyloxy chains and in the second series they are replaced by decyloxy chains. In both series of compounds, the number of carbon atoms in terminal chain attached to the azobenzene-based wing i.e. the short arm was varied between  $n = 6 \rightarrow 16$ . To the best of our knowledge **A6/n** and **A10/n** compounds are the first examples of photosensitive hockey-stick polycatenars reported up to date. The mesophase behaviour of these new HS has been investigated by polarizing optical microscopy (POM), differential scanning calorimetry (DSC), X-ray diffraction (XRD) and electro optical measurements.

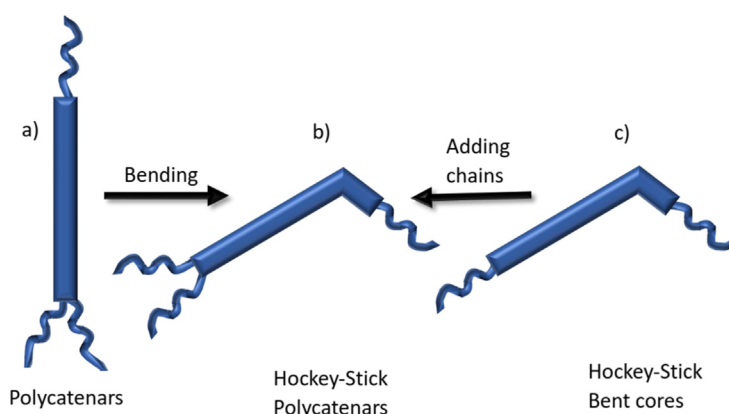
## 2. Experimental

### 2.1. Synthesis

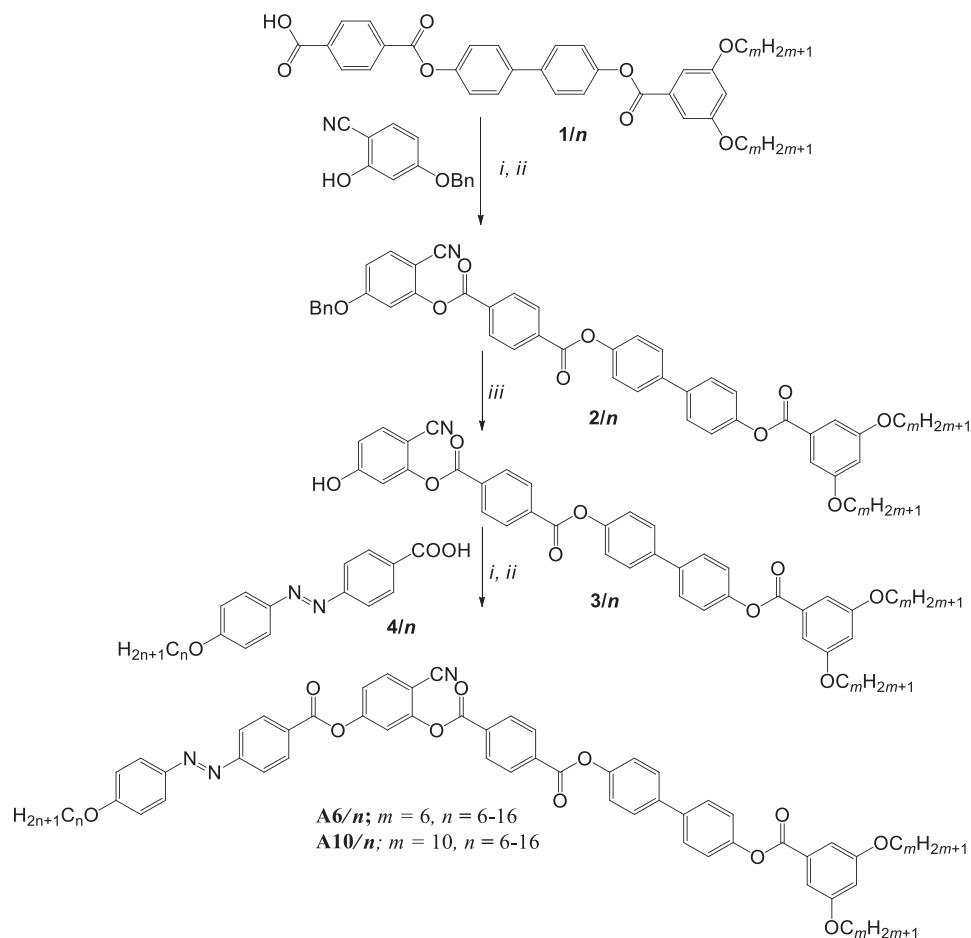
The synthesis of the target HS polycatenars **A6/n** and **A10/n** was performed as shown in Scheme 2. The azobenzene containing benzoic acids derivatives (**1/n**) were prepared as described before [35], while the synthetic procedures for the benzoic acid derivatives terminated with double chains are recently reported elsewhere [80]. All final HS molecules were synthesized by acylation reaction of the hydroxy compounds **3/n** with one equivalent of the acid chloride derived from azobenzene-based benzoic acid derivatives **4/n**. The acylation reactions were carried out in presence of triethylamine as a base and a catalytic amount of pyridine. The crude final materials were purified firstly by column chromatography using dichloromethane as an eluent followed by recrystallization from ethanol/chloroform (1:1) mixture to yield the target HS polycatenars. The synthesis details of all intermediates as well as the final materials and the analytical data are reported in the Electronic Supporting Information (ESI). All compounds are thermally stable as proved by the reproducibility of DSC thermograms in repeated heating and cooling cycles.

### 2.2. Methods

The thermal behaviour of all synthesized compounds was studied by polarizing optical microscopy (POM) and differential scanning calorimetry (DSC). For polarizing microscopy a Mettler FP-82 HT hot stage and control unit in conjunction with a Nikon



Scheme 1. Molecular design principle of the new hockey-stick polycatenars.



**Scheme 2.** Synthesis of the target HS polycatenars **A6/n** and **A10/n**. Reagents and conditions: i) DMF,  $\text{SOCl}_2$ , reflux 1 hr.; ii) dry  $\text{CH}_2\text{Cl}_2$ , dry TEA, dry pyridine, reflux for 6 hr; iii)  $\text{H}_2$ , Pd/C-10%, dry THF, stirring 24 hr.

Optiphot-2 polarizing microscope was used. DSC-thermograms were recorded on a Perkin-Elmer DSC-7 with heating and cooling rates of  $10 \text{ K min}^{-1}$ . Electro-optical switching characteristics were examined in  $6 \mu\text{m}$  polyimide coated ITO cells (EHC Japan) using the triangular-wave method [81]. XRD patterns were recorded with a 2D detector (Vantec-500, Bruker). Ni filtered and pin hole collimated  $\text{CuK}_\alpha$  radiation was used. The exposure time was 15 min and the sample to detector distance was 27.4 and 9.5 cm for small angle and wide angle scattering experiments, respectively. Alignment was attempted by slow cooling (rate:  $1 \text{ K min}^{-1}$  to  $0.1 \text{ K min}^{-1}$ ) of a small droplet on a glass plate.

### 3. Results and discussion

#### 3.1. Hockey-stick polycatenars **A6/n**

Compounds **A6/n** having two hexyloxy chains attached at position 3 and 5 in the terminal benzene ring of the long side arm of the HS molecules form two different types of enantiotropic mesophases (see Table 1 and Fig. 1).

The shortest compound **A6/6** with  $n = 6$  forms tilted and non-tilted smectic phases. On cooling **A6/6** from the isotropic liquid a transition to a highly birefringent phase with a fan shaped texture associated with dark areas are observed at  $T \sim 142 \text{ }^\circ\text{C}$  as typically observed for non-tilted smectic A (SmA) phases. Therefore, the higher temperature LC phase of **A6/6** is assigned as SmA phase. On further cooling and at  $T \sim 99 \text{ }^\circ\text{C}$ , a weak birefringence is induced in the dark areas observed in Fig. 2a, while the fan

shaped textures are not altered and the directions of the dark extinctions observed in Fig. 2a and b are the same, confirming a transition from SmA phase to the rarely observed anticlinic tilted SmC phase i.e.  $\text{SmC}_a$  [79], which remains without crystallization till room temperature. The crystallization is only observed on heating cycle and the same phase sequence is observed on heating and cooling scans confirming the enantiotropic nature of these LCs phases. The  $\text{SmC}_a$ -SmA phase transition could be also detected by DSC investigations (see Table 1 and Fig. 3a). On chain elongation the  $\text{SmC}_a$  phase is removed for all longer homologues with  $n \geq 8$ , where SmA is the only observed mesophase (see Table 1 and Fig. 1).

For all medium chain compounds with  $n = 8-12$ , the SmA remains till room temperature on cooling without crystallization, which is only observed for longer homologues with  $n \geq 14$ . Another interesting feature of compounds **A6/n** is the observation of a broad peak in the DSC curves in the isotropic liquid range for compounds **A6/12** - **A6/16** (see Fig. 3b). This broad feature is observed on cooling cycle only for **A6/12** and on both heating and cooling cycles in case of **A6/14** and **A6/16**. By rotating one of the analyzers from the crossed position in the temperature range of this isotropic liquid phase for any of **A6/12** - **A6/16** compounds no dark and bright domains could be observed indicating that this isotropic liquid is not chiral as reported before for related linear tricatensars.[63,64] Therefore, this achiral isotropic liquid phase is designated as  $\text{Iso}_1$  without asterisk. As can be seen from Table 1, the enthalpy value of LC-Iso transition either on heating or cooling is relatively large, indicating a significant packing density of the



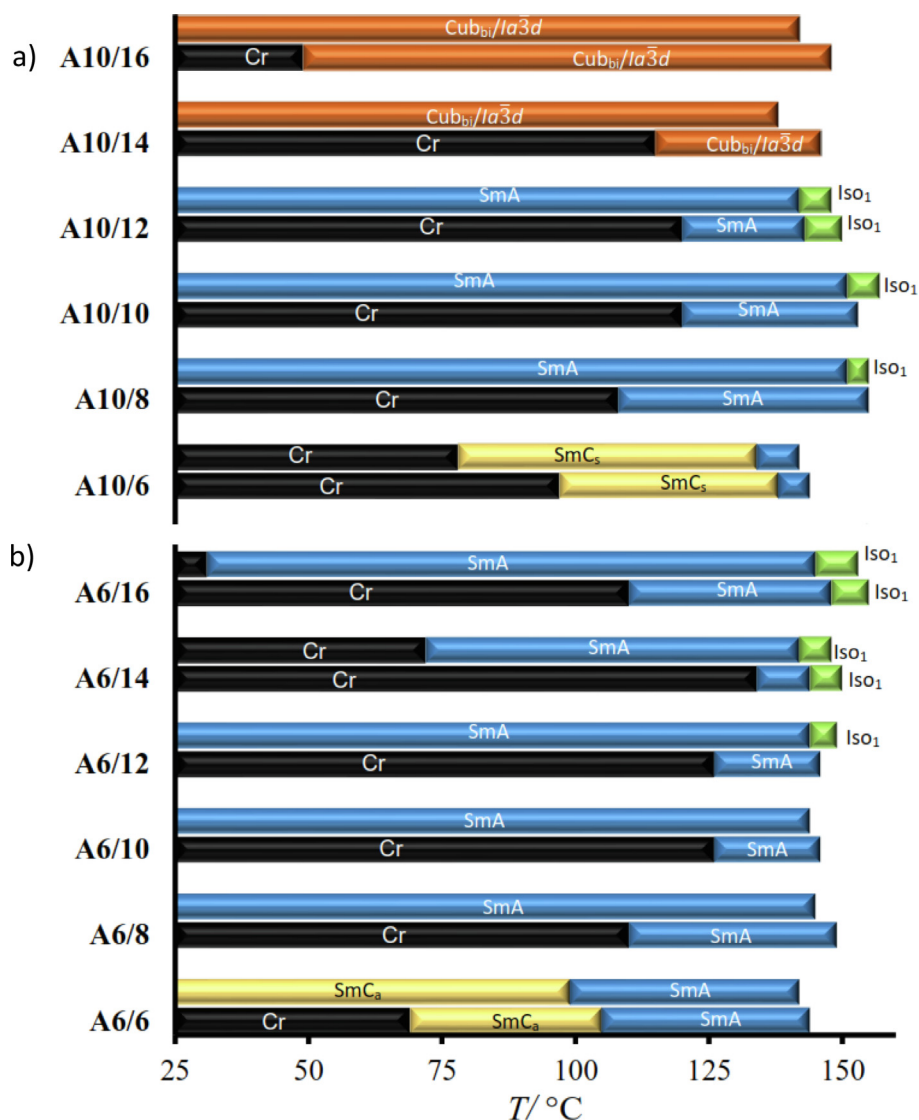


**Fig. 1.** Phase behaviour of the investigated new polycatenars on heating (lower bars) and on cooling (upper bars) for: a) series **A10/n** and b) series **A6/n**. For abbreviations see Table 1.

long aromatic cores, which simultaneously stabilizes the smectic phases and thus lead only to the formation of SmA phases in most cases.

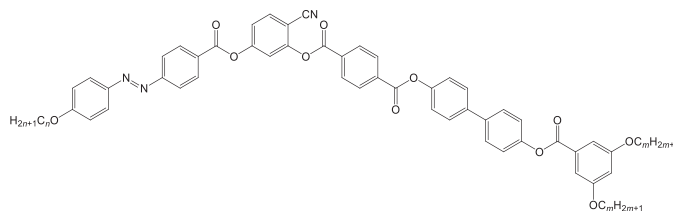
To confirm the type of the smectic phases formed by **A6/n** compounds, we performed X-ray diffraction (XRD) investigations for some selected examples. In the higher temperature smectic phase of compound **A6/6** at 120 °C a diffuse scattering is observed in the wide-angle region, while one sharp Bragg reflection in the small angle region (see Fig. 4a) corresponding to  $d = 5.63$  nm is observed. This indicates that this phase represents a smectic phase without in-plane positional order. The maximum of the diffuse scattering in the wide-angle region is perpendicular to the small angle reflections, which confirms an on average non-tilted organization of the molecules in the layers i.e. a SmA phase in agreement with the observed optical texture in this LC phase. The experimental  $d$ -value is larger than the molecular length of a single molecule ( $L_{\text{mol}} = 4.44$  nm), determined with Materials Studio for a V-shaped conformation with bending angle of 120° and all-trans stretched alkyl chains (see Fig. 5). This indicates an antiparallel side-by-side packing of the molecules in layers with partial interdigitation of the alkyl chains and aromatic cores (Fig. 5a).

In the temperature range of the other smectic phase and at  $T = 60$  °C, the  $d$ -value decreases only slightly to be  $d = 5.55$  nm (Fig. 4b), in line with a tilted organization of the molecules and indicated by the weak birefringence texture in this LC phase (Fig. 2b). Based on the small difference between layer spacing in SmA and SmC phases, it is likely that the SmA phase is of the de Vries type [82,83]. It should be noted that XRD measurements cannot precisely differentiate between the synclinal and anticlinal SmC phases [79,84]. However, based on the XRD results and the textural observations of **A6/6** at  $T = 60$  °C, this phase is assigned as a anticlinal tilted smectic C phase i.e. SmC<sub>a</sub>.

### 3.2. Hockey-stick polycatenars A10/n

Replacing the two terminal hexyloxy chains in compounds **A6/n** with two longer decyloxy chains leads to the formation of series **A10/n**. The phase sequence and types of mesophases formed by **A10/n** derivatives are given in Table 1 and represented graphically in Fig. 1a. As can be seen from Table 1 and Fig. 1a, the shortest homologue **A10/6** exhibit SmA and SmC phases as observed for the related analogue **A6/6**. However, the SmA phase range of

**Table 1**  
Phase transition temperatures ( $T/^\circ\text{C}$ ), mesophase types, and transition enthalpies [ $\Delta H/k\cdot\text{mol}^{-1}$ ] of compounds **A6/n** and **A10/n**.<sup>a</sup>



Cpd.	<i>m</i>	<i>n</i>	Transition Temp.
<b>A6/6</b>	6	6	<b>H:</b> Cr 69 [9.5] SmC <sub>s</sub> 105 [0.6] SmA 144 [2.4] Iso <b>C:</b> Iso 142 [2.2] SmA 99 [0.8] SmC <sub>s</sub> < 20 Cr
<b>A6/8</b>	6	8	<b>H:</b> Cr 110 [32.7] SmA 149 [3.2] Iso <b>C:</b> Iso 145 [3.1] SmA 96 < 20 Cr
<b>A6/10</b>	6	10	<b>H:</b> Cr 126 [36.4] SmA 146 [2.6] Iso <b>C:</b> Iso 144 [2.6] SmA < 20 Cr
<b>A6/12</b>	6	12	<b>H:</b> Cr 126 [38.3] SmA 146 [3.7] Iso <b>C:</b> Iso 149 [0.1] Iso <sub>1</sub> 144 [2.4] SmA < 20 Cr
<b>A6/14</b>	6	14	<b>H:</b> Cr 134 [52.0] SmA 144 [1.2] Iso <sub>1</sub> 150 [1.0] Iso <b>C:</b> Iso 148 [2.1] Iso <sub>1</sub> 142 [1.2] SmA 72 [16.0] Cr
<b>A6/16</b>	6	16	<b>H:</b> Cr 110 [25.6] SmA 148 [0.8] Iso <sub>1</sub> 155 [1.3] Iso <b>C:</b> Iso 153 [0.9] Iso <sub>1</sub> 145 [0.8] SmA 31 [5.6] Cr
<b>A10/6</b>	10	6	<b>H:</b> Cr 97 [25.6] SmC <sub>a</sub> 138 [0.5] SmA 144 [4.8] Iso <b>C:</b> Iso 142 [4.6] SmA 134 [0.6] SmC <sub>a</sub> 78 [24.8] Cr
<b>A10/8</b>	10	8	<b>H:</b> Cr 108 [27.0] SmA 155 [2.3] Iso <b>C:</b> Iso 155 [2.4] Iso <sub>1</sub> 151 [1.6] SmA < 20 Cr
<b>A10/10</b>	10	10	<b>H:</b> Cr 120 [38.8] SmA 153 [2.0] Iso <b>C:</b> Iso 157 [7.3] Iso <sub>1</sub> 151 [1.8] SmA < 20 Cr
<b>A10/12</b>	10	12	<b>H:</b> Cr 120 [29.8] SmA 143 [0.8] Iso <sub>1</sub> 150 [2.0] Iso <b>C:</b> Iso 148 [3.0] Iso <sub>1</sub> 142 [0.8] SmA < 20 Cr
<b>A10/14</b>	10	14	<b>H:</b> Cr 115 [39.4] Cub <sub>bi</sub> /Ia $\bar{3}d$ 146 [1.3] Iso <b>C:</b> Iso 138 [0.5] Cub <sub>bi</sub> /Ia $\bar{3}d$ < 20 Cr
<b>A10/16</b>	10	16	<b>H:</b> Cr 49 [43.8] Cub <sub>bi</sub> /Ia $\bar{3}d$ 148 [2.2] Iso <b>C:</b> Iso 142 [1.7] Cub <sub>bi</sub> /Ia $\bar{3}d$ < 20 Cr

Notes: <sup>a</sup>Transition temperatures and enthalpy values were taken from the second DSC heating scans (**H**) and cooling scans (**C**) with 10 K min<sup>-1</sup>; abbreviations: Cr = crystalline solid; SmC<sub>s</sub> = synclincic smectic C phase; SmC<sub>a</sub> = anticlinic smectic C phase; SmA = orthogonal non-tilted smectic A phase; Cub<sub>bi</sub>/Ia $\bar{3}d$  = achiral cubic phase with Ia $\bar{3}d$  lattice; Iso<sub>1</sub> = achiral isotropic liquid; Iso = isotropic liquid.

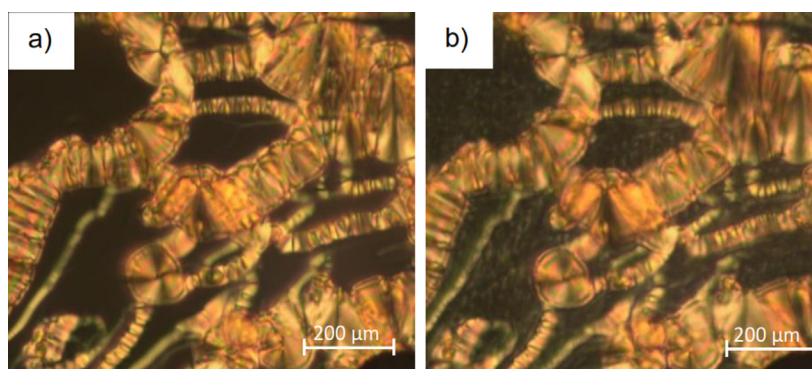


**Fig. 2.** Optical micrographs observed for compound **A6/6** in a homeotropic cell (ordinary non-treated microscopy slides) on cooling in: a) in the SmA phase at  $T = 130^\circ\text{C}$  and b) in the SmC<sub>a</sub> phase at  $T = 60^\circ\text{C}$ .

**A10/6** is narrower as would be expected by chain elongation and the SmC phase is crystallized on cooling and not a room temperature LC phase as that exhibited by **A6/6**.

More interesting, the SmC phase of **A10/6** is synclinically tilted and not anticlinically tilted as that of **A6/6**. The synclincic tilt is confirmed by the high birefringence of the SmC exhibited by **A10/6** compared to the weak birefringence of that of **A6/6** (compare Fig. 6a and the homeotropic regions in Fig. 2b). Moreover, a schlieren texture with four brush disclinations could be observed, which also confirms the presence of a synclincic SmC i.e. SmC<sub>s</sub> mesophase [79]. To further confirm the SmC<sub>s</sub>-SmA transition, the optical

textures were recorded in a planar 6 μm ITO cell, where the fan textures observed in the SmA phase became broken in the SmC<sub>s</sub> phase accompanied by increasing of birefringence (Fig. 6c, d).

To test if the smectic phases formed by **A6/6** and **A10/6** are polar or not, electro-optical experiments were performed using a triangular wave voltage for these two compounds. For both materials no current peak could be observed neither in the SmA, nor in the SmC<sub>s</sub> phases of these two materials up to a voltage of 200 V<sub>pp</sub> in a 6 μm ITO cell, indicating the non-switching behaviour and the non-polar nature of these two phases. The loss of polar order in these smectic phases indicate that they are different from those

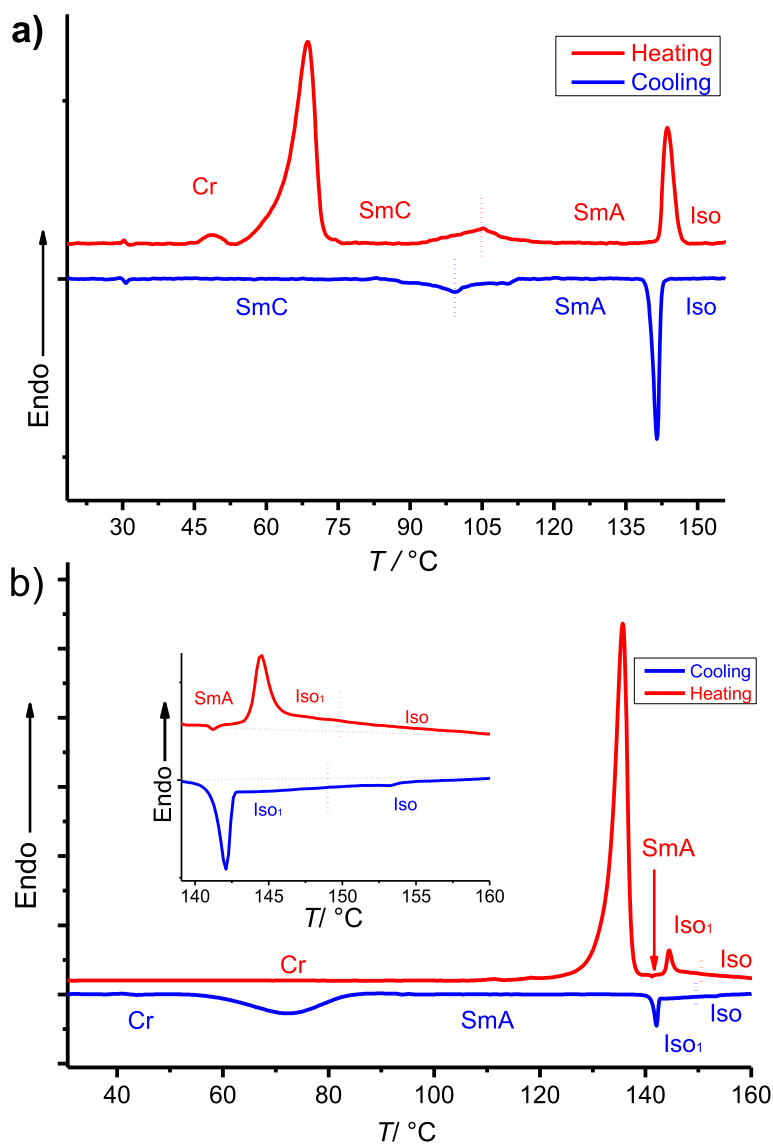


**Fig. 3.** DSC thermograms obtained for: a) compound **A6/6** and b) **A6/14**; with  $10 \text{ K min}^{-1}$  heating and cooling rates. The inset in b) represents an enlarged range ( $138 \text{ }^\circ\text{C}$ - $160 \text{ }^\circ\text{C}$ ) showing the Iso<sub>1</sub>-Iso broad transition peaks on heating and cooling cycles of **A6/14**.

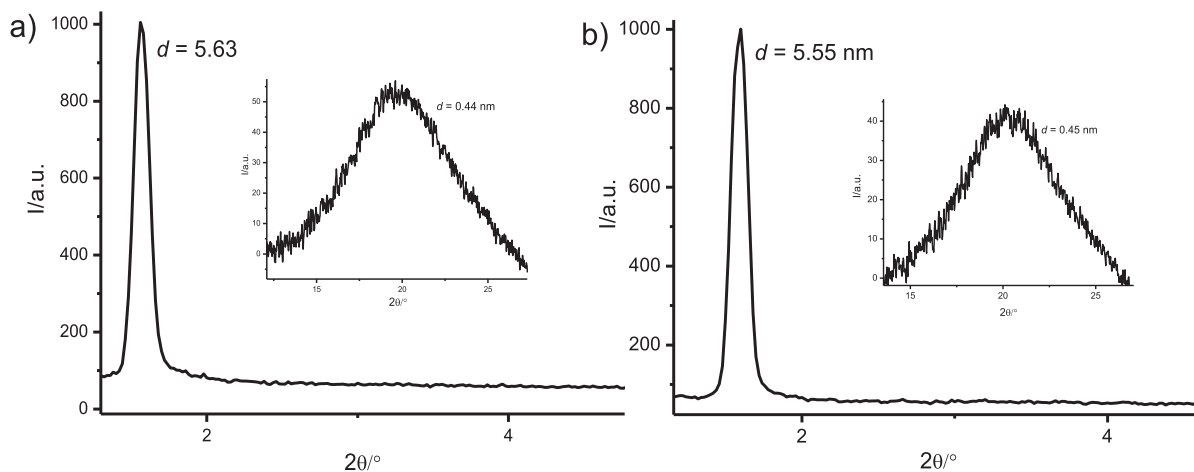


**Fig. 4.** Small X-ray diffraction (SAXD) patterns of **A6/6** at: a)  $T = 120 \text{ }^\circ\text{C}$  in the SmA phase and b)  $T = 60 \text{ }^\circ\text{C}$  in the SmC<sub>3</sub> phase. The insets show the wide-diffraction patterns (WAXD).

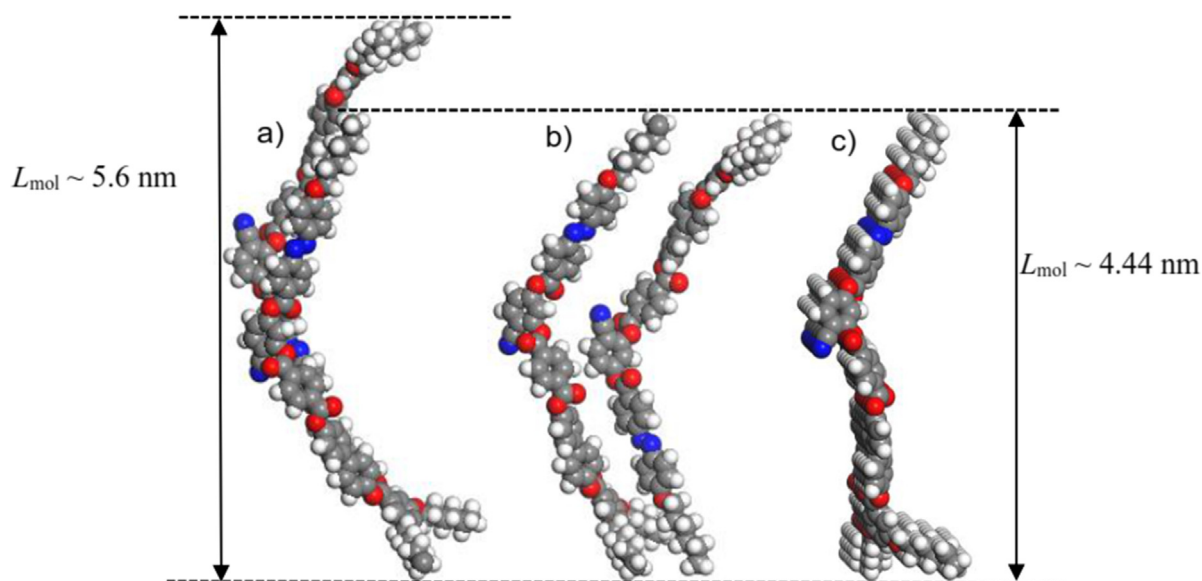


**Fig. 5.** Space-filling models of **A6/6** showing the distinct modes of self-assembly in the SmA layers (one layer is represented): a) intercalated bilayer structure with antiparallel (up-down symmetric) arrangement of the molecules, b) antiparallel arrangement of the molecules with complete segregation of aromatic cores and aliphatic chains and c) parallel organization of the molecules with complete segregation of chains and cores.

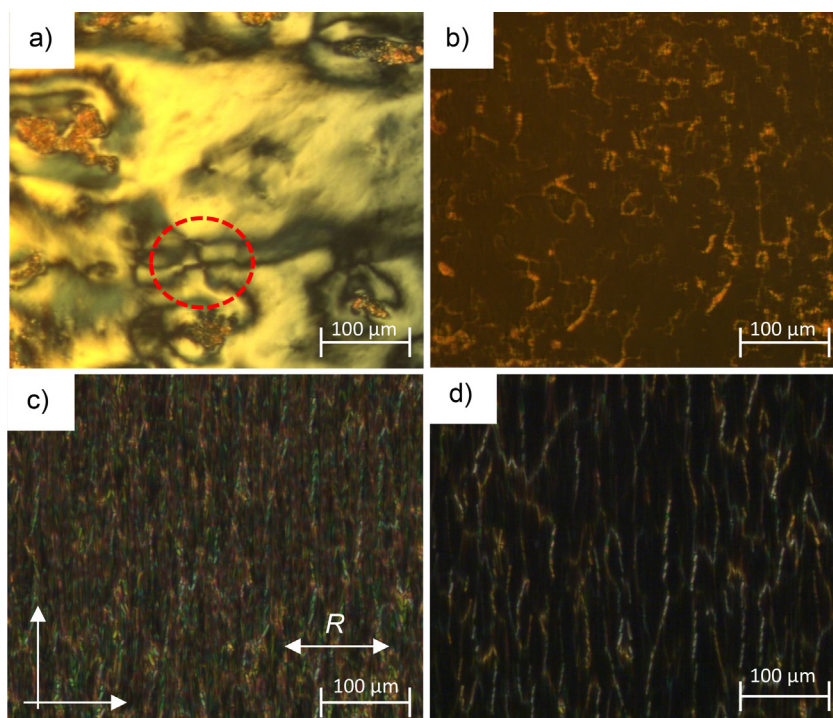


**Fig. 6.** Optical micrographs observed for compound **A10/6** in: a, b) a homeotropic cell (ordinary non-treated microscopy slides) in the SmC<sub>s</sub> phase at  $T = 100\text{ °C}$  a); in the SmA phase at  $T = 110\text{ °C}$  b); The red dashed circle in a) indicates the four brush defects, which confirm the presence of SmC<sub>s</sub> phase; c), d) in a planar  $6\text{ }\mu\text{m}$  ITO cell c) the SmC<sub>s</sub> phase at  $T = 100\text{ °C}$  and d) the SmA phase at  $T = 110\text{ °C}$ . The directions of polarizers and analyzer and the rubbing direction (R) are indicated in c).

usually observed in BCLCs, which might be attributed to the distorted packing of the molecules as described above giving rise to a significant distortion for the directed packing of the bent directions of the cores (see Fig. 5). A polar order could be expected if a uniform bend-direction with preferred packing of the bent-core molecules with parallel organization could be achieved (Fig. 5c), which is not the case in our molecules. This behaviour is like other

previously reported HS molecules, which also exhibit non-polar smectic phases in most cases.[65–79]

On chain elongation the SmC<sub>s</sub> phase is removed and the SmA phases are formed beside the liquid networks i.e. Iso<sub>1</sub> phases for all medium chain derivatives with  $n = 10\text{--}12$  (see Fig. 1b). The Iso<sub>1</sub> phase is formed as a metastable phase for **A10/8** and as enantiotropic one for **A10/10** and **A10/12**. Moreover, the SmA phases of

these medium chain compounds are stable down to room temperature as once they formed on heating, they do not show any sign of crystallization on cooling cycles (Fig. 1a). On further chain elongation and with  $n \geq 14$  the SmA phase is replaced by another highly viscous phase, which is characterized by its isotropic appearance under crossed polarizers as observed in POM investigations. This indicates the formation of a cubic liquid crystalline phase which is not exhibited by any other homologues of **A6/n** or **A10/n** derivatives. On rotation one of the analyzers from the crossed position with a small angle either in clockwise or anti clockwise direction no dark and bright domains could be seen, indicating that this phase is of achiral nature. Also, for this LC phase there is  $\sim 6$  K supercooling of the Iso-LC transition compared to the LC-Iso transition temperature on heating (see Table 1 and Fig. 1b) which is a typical feature of cubic LC phases.

These observations are all typically observed for the achiral bicontinuous cubic phase with  $1a\bar{3}d$  space group ( $\text{Cub}_{\text{bi}}/1a\bar{3}d$ ) [45,59,64]. This cubic phase is formed for both **A10/14** and **A10/16** as an enantiotropic phase with very wide temperature range on heating for the longest homologue **A10/16**, which became

even room temperature stable phase for both materials on cooling from the isotropic liquid phase (see DSC traces of **A10/14**, Fig. 7b). Compound **A10/14** was further investigated with XRD investigation to confirm the type of the  $\text{Cub}_{\text{bi}}$  phase (Fig. 8). The two most intense peaks in the SAX pattern (Fig. 8) can be indexed to the (211) and (220) reflections, confirming a  $\text{Cub}_{\text{bi}}$  phase with  $1a\bar{3}d$  lattice with a calculated lattice parameters  $a_{\text{cub}}$  of 13.3 nm, which is also in the expected range.

### 3.3. Photosensitivity

The HS polycatenars **A6/n** and **A10/n** were designed to be photo switchable by incorporation of the photosensitive azo unit in their molecular structures. Therefore, the geometry of the azo unit could be changed by UV/Vis light irradiation due to *trans-cis* photoisomerization, which leads to breaking of the supramolecular order, and thus to phase modulation. Recently, interesting photoswitching properties were reported for azobenzene-based polycatenars [85–88] as well as for azobenzene-based BCLCs [23–29,35,36]. The new HS polycatenars reported herein except **A10/14** and

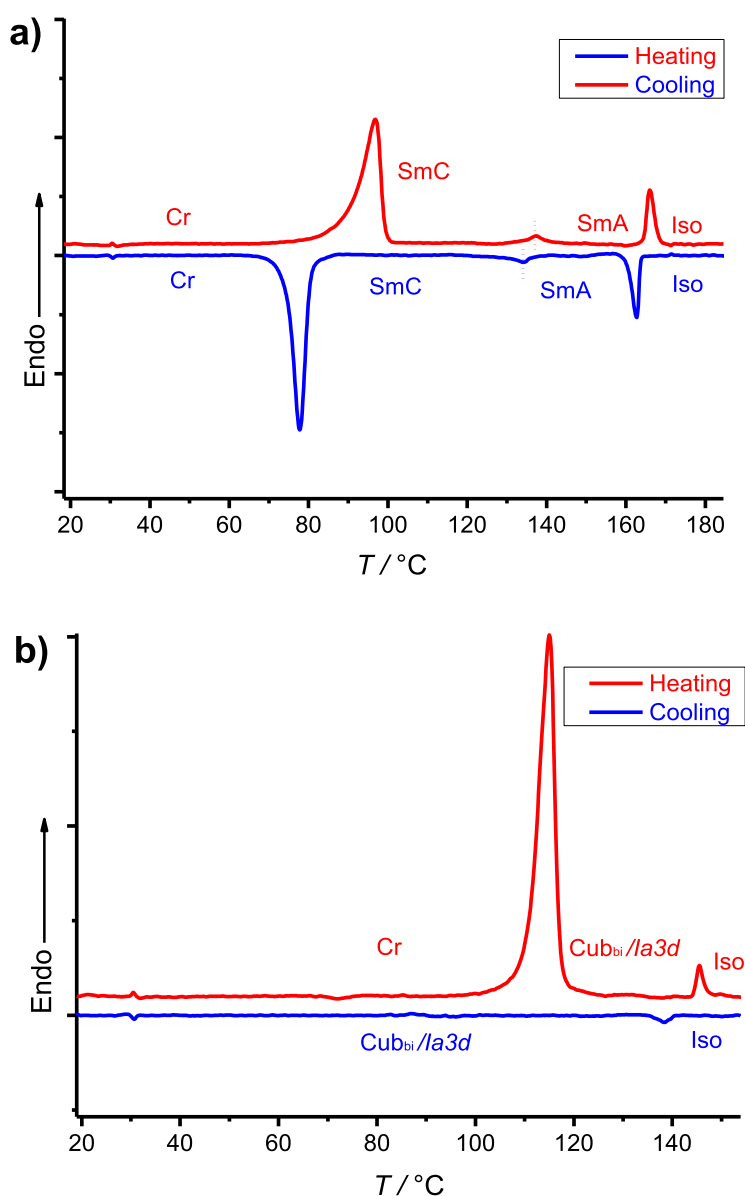
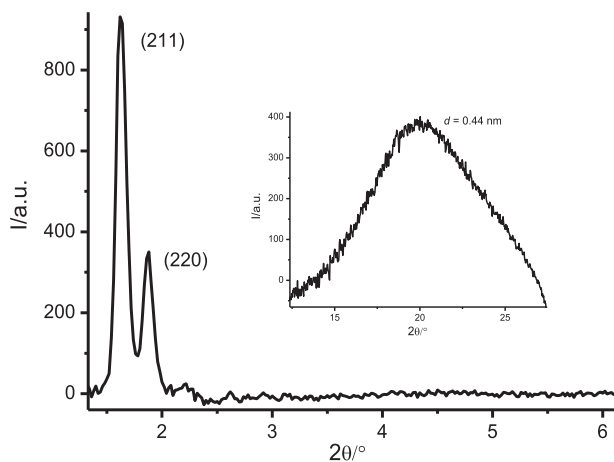


Fig. 7. DSC thermograms obtained for: a) compound **A10/6** and b) **A10/14**; with  $10 \text{ K min}^{-1}$  heating and cooling rates.



**Fig. 8.** Small X-ray diffraction (SAXD) patterns of **A10/14** at  $T = 110$  °C in the  $Cub_{bi}/Ia\bar{3}d$  phase. The inset shows the wide-diffraction patterns (WAXD) at the same temperature.

**A10/16** undergo a fast and reversible isothermal phase transition upon illumination with UV laser pointer (405 nm, 5 mW/mm<sup>2</sup>). As a representative example, Fig. 9 shows the results observed for compound **A10/6** under POM. Fig. 9a shows the birefringent texture of the  $SmC_s$  phase at  $\sim T = 100$  °C prior to light irradiation, which upon light illumination changes to the oily streak characteristic texture of the  $SmA$  phase, coexisting with homogeneously aligned regions which appear black under crossed polarizers (Fig. 9b). On switching off the light source, the  $SmA$  phase transforms back in <3 s to the  $SmC_s$  phase. Similar observation was also observed in the  $SmA$  phase, where a transformation to the isotropic liquid was achieved upon light irradiation of the  $SmA$  phase within <3 s (Fig. 9b, c), which also relaxes back to the  $SmA$  texture very quickly on removing the light source. These observations indicate a fast and an efficient photoinduced phase transition between

different types of LCs phases as well as between  $SmA$  and isotropic liquid i.e. isothermal photoinduced phase transitions as a result of *trans*-*cis* photoisomerization of the azobenzene units.

#### 3.4. Comparison with related linear polycatenars

By comparing the phase behaviour of the newly reported HS polycatenars reported herein **A6/n** and **A10/n** with the recently reported rod-like polycatenars **Bn** (Scheme 3) [63,64] having also an extended aromatic core but missing the central 4-cyanoresorcinol core which induces bending of the molecule we can reach the following conclusions.

Depending on the terminal chain length in case of linear polycatenars **Bn** a rich variety of LCs phases were observed, including hexatic phases ( $HexI_s$ ,  $HexB$ ), non-tilted smectic A ( $SmA$ ), synclonic and anticlinic tilted smectic C phases ( $SmC_s$ ,  $SmC_a$ ), a long pitch helical smectic C phase as well as  $Cub_{bi}/Ia\bar{3}d$  in addition to the chiral  $Iso_1^{*|}$  and the achiral  $Iso_1$  isotropic liquid mesophases. The formation of the rare anticlinic  $SmC_a$  phases is a characteristic feature of HS molecules, which notably formed by the linear tricateenars **Bn** and only for the new HS molecule **A10/6**. This means that **Bn** compounds combine the properties of conventional HS materials and those of nonsymmetric polycatenars. On the other hand, for the HS **A6/n** and **A10/n** such rich mesomorphism was not observed and no chiral mesophases were formed as those exhibited by **Bn** materials. Obviously, the introduction of the central bent-core unit in the structure of the rod-like polycatenars **Bn** retain some mesophases formed by the nonsymmetric polycatenars such as the achiral  $Iso_1$  and  $Cub_{bi}/Ia\bar{3}d$  phases but at the same time suppress the formation of any chiral phases and any of the known banana mesophases as one would expect. This might be explained by removing the polar order in **A6/n** and **A10/n** HS polycatenars because of the antiparallel organization of the molecules with partial interdigitation of the alkyl chains in the aliphatic layers (Fig. 5a). Another possible explanation could be the low bending angle provided by the 4-cyanoresorcinol core unit, resulting in the formation of LCs phases at the border line between conventional rod-like molecules

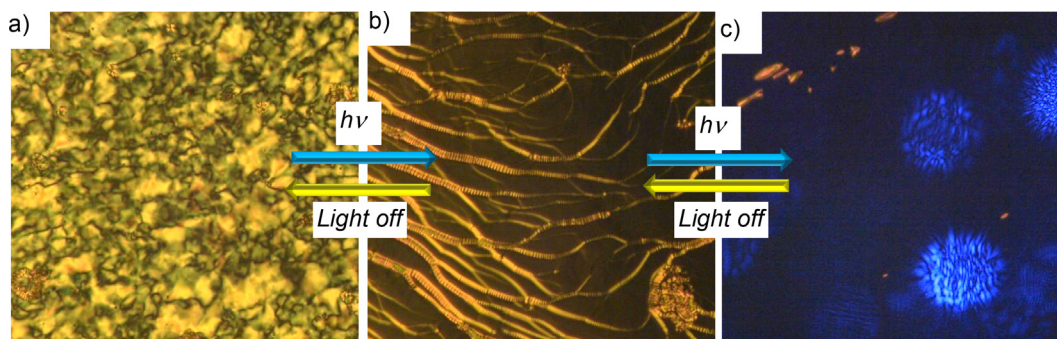
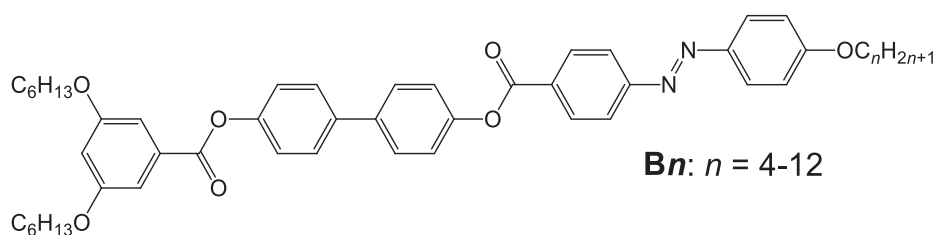


**Fig. 9.** Optical textures observed on heating for compound **A10/6** under crossed polarizers: a) in the  $SmC_s$  phase at  $T = 100$  °C before irradiation with UV light and b) after irradiation with UV light showing the transformation from the  $SmC_s$  phase to the  $SmA$  phase and c) in the isotropic liquid phase after light irradiation of the  $SmA$  phase at 140 °C. The blue dots in c) are due to UV light.



**Scheme 3.** Previously reported rod-like polycatenars **Bn** [63,64].

and BCLCs. This needs further investigation and synthesis of related materials using different types of central core units to reach the right core unit able to combine the LCs mesophases of both BCLCs and polycatenars. However, notably the SmA phases exhibited by all **A6/n** homologues and the short and medium chain homologues of **A10/n** series represent room temperature LC phases as observed on cooling cycles for all materials (Fig. 1), whereas no ambient temperature LCs phases were formed by any of **Bn** compounds. Moreover, the  $Cub_{bi}/Ia\bar{3}d$  phases formed **A10/14** and **A10/16** are more stable compared to those formed by **Bn** derivatives, where no crystallization is detected down to room temperature for **A6/14** and **A10/16**, making them good candidates for applications.

#### 4. Summary and conclusions

In summary, we reported the design, synthesis, and molecular self-assembly of the first example of photo switchable HS polycatenars derived from 4-cyanoesorcinol central core unit connected to one short azobenzene-based side arm and a long ester-based wing (**An/6** and **An/10**). The two series differ from each other in the length of the terminal chains at position 3 and 5 in the terminal benzene ring of the long arm. For the shortest homologues of both series (**A6/6** and **A10/6**) non-tilted SmA and tilted SmC phases were observed. The type of tilt in the SmC phases changes from anticlinic ( $SmC_a$ ) in **A6/6** to synclinic ( $SmC_s$ ) in **A10/6** with chain elongation. In electro optical investigations of both phases no current peak could be detected, indicating the non-polar nature of these two phases. This behaviour is explained based on the experimental results of the XRD investigations, which confirms an antiparallel side-by-side packing of the molecules in layers with partial interdigitation of the alkyl chains in the aliphatic layers. Such arrangement results in removing the polar order in these smectic phases. On chain elongation in both series the SmC phases are removed and only SmA phases are observed, which once formed on heating do not show any sign of crystallization on cooling down to room temperature in most cases. In addition to SmA phases achiral liquid networks ( $Iso_1$  phases) are detected by DSC investigation. On further chain elongation a transition from the one-dimensional smectic phases to three dimensional achiral bicontinuous cubic phase with  $Iadla\bar{3}d$  symmetry ( $Cub_{bi}/Ia\bar{3}d$ ) is observed for the longer homologues of **A10/n** series i.e. **A10/14** and **A10/16** as indicated from POM and XRD investigations. These cubic phases are also stable down to ambient temperature, which could be of interest for technological applications. The photoisomerization of the synthesized materials was investigated by UV light irradiation, where a fast and reversible isothermal photo switching between SmC and SmA as well as between SmA and the isotropic liquid phase could be achieved.

#### CRedit authorship contribution statement

**M. Alaasar:** Conceptualization, Data curation, Funding acquisition, Investigation, Methodology, Project administration, Supervision, Writing-original draft, Writing-review and editing. **S. Poppe:** Investigation.

#### Declaration of Competing Interest

The authors declare that they have no known competing financial interests or personal relationships that could have appeared to influence the work reported in this paper.

#### Acknowledgements

We thank Prof. Dr. Carsten Tschierske for helpful discussion and reading of the manuscript. M. Alaasar acknowledges the German Research Foundation (DFG) for the financial support (AL2378/1-1, 424355983).

#### Appendix A. Supplementary material

Supplementary data to this article can be found online at <https://doi.org/10.1016/j.molliq.2022.118613>.

#### References

- [1] T. Kato, J. Uchida, T. Ichikawa, T. Sakamoto, *Angew. Chem. Int. Ed.* 57 (2018) 4355.
- [2] C. Tschierske, *Angew. Chem. Int. Ed.* 52 (2013) 8828.
- [3] C.L. Wang, H.L. Dong, W.P. Hu, Y. Liu, D. Zhu, *Chem. Rev.* 112 (2012) 2208.
- [4] M. Ghedini, D. Pucci, A. Crispini, A. Bellusci, M.L. Deda, I. Aiello, T. Pugliese, *Inorg. Chem. Commun.* 10 (2007) 243.
- [5] A. Hayer, V. De Halleux, A. Köhler, A. El-Garouhy, E.W. Meijer, J. Barberá, J. Tant, J. Levin, M. Lehmann, J. Gierschner, J. Cornil, Y.H. Geertset, *J. Phys. Chem. B.* 110 (2006) 7653.
- [6] T. Niori, T. Sekine, J. Watanabe, T. Furukawa, H. Takezoe, *J. Mater. Chem.* 6 (1996) 1231.
- [7] R.A. Reddy, C. Tschierske, *J. Mater. Chem.* 16 (2006) 907.
- [8] H. Takezoe, Y. Takanishi, *Jpn. J. Appl. Phys.* 45 (2006) 597.
- [9] A. Eremin, A. Jáklí, *Soft Matter* 9 (2013) 615.
- [10] J. Etxebarria, M.B. Ros, *J. Mater. Chem.* 18 (2008) 2919.
- [11] M. Alaasar, *Liq. Cryst.* 43 (2016) 2208.
- [12] T. Sekine, T. Niori, J. Watanabe, T. Furukawa, S.W. Choi, H. Takezoe, *J. Mater. Chem.* 8 (1997) 1309.
- [13] L.E. Hough, M. Spannuth, M. Nakata, D.A. Coleman, C.D. Jones, G. Dantlgraber, C. Tschierske, J. Watanabe, E. Körblová, D.M. Walba, J.E. MacLennan, M.A. Glaser, N.A. Clark, *Science* 325 (2009) 452.
- [14] M. Nagaraj, *Liq. Cryst.* 43 (2016) 2244.
- [15] M. Alaasar, M. Prehm, C. Tschierske, *Chem. Eur. J.* 22 (2016) 6583.
- [16] G. Shanker, M. Nagaraj, A. Kocot, J.K. Vij, M. Prehm, C. Tschierske, *Adv. Funct. Mater.* 22 (2012) 1671.
- [17] O. Francescangeli, V. Stanic, S.I. Torgova, A. Strigazzi, N. Scaramuzza, C. Ferrero, I.P. Dolbnya, T.M. Weiss, R. Berardi, L. Muccioli, S. Orlandi, C. Zannoni, *Adv. Funct. Mater.* 19 (2009) 2592.
- [18] C. Tschierske, D.J. Photinos, *J. Mater. Chem.* 20 (2010) 4263.
- [19] L.A. Madsen, T.J. Dingemans, M. Nakata, E.T. Samulski, *Phys. Rev. Lett.* 96 (2006).
- [20] G.S. Lee, J.S. Cho, J.C. Kim, T.-H. Yoon, S.T. Shin, *J. Appl. Phys.* 105 (2009).
- [21] R. Stannarius, A. Eremin, M.-G. Tamba, G. Pelzl, W. Weissflog, *Phys. Rev. E: Stat., Nonlinear, Soft Matter Phys.* 76 (2007).
- [22] V. Prasad, S.-W. Kang, K.A. Suresh, L. Joshi, Q. Wang, S. Kumar, *J. Am. Chem. Soc.* 127 (2005) 17224.
- [23] D. Jágerová, M. Šmahel, A. Poryvai, J. Macháček, V. Novotná, M. Kohout, *Crystals* 11 (2021) 1265.
- [24] N. Gimeno, I. Pintre, M. Martínez-Abadía, J.L. Serrano, M.B. Ros, *RSC Adv.* 4 (2014) 19694.
- [25] M.V. Srinivasan, P. Kannan, P. Roy, *New J. Chem.* 37 (2013) 1584.
- [26] N.G. Nagaveni, A. Roy, V. Prasad, *J. Mater. Chem.* 22 (2012) 8948.
- [27] N. Trišović, M. Salamonczyk, J. Antanasijević, S. Sprunt, T. Tóth-Katona, A. Jáklí, M. Kohout, K. Fodor-Csorba, *RSC Adv.* 5 (2015) 64886.
- [28] M. Horčič, V. Kozmík, J. Svoboda, V. Novotná, D. Pocięcha, *J. Mater. Chem. C* 1 (2013) 7560.
- [29] M. Alaasar, M. Prehm, C. Tschierske, *RSC Adv.* 6 (2016) 82890.
- [30] H.K. Bisoyi, Q. Li, *Chem. Rev.* 116 (2016) 15089.
- [31] S.C. Lee, S.H. Lee, O.P. Kwon, *J. Mater. Chem. C* 4 (2016) 1935.
- [32] T. Ikeda, J. Mamiya, Y.Yu, *Angew. Chem. Int. Ed.* 46 (2007) 506.
- [33] E.V. Fleischmann, R. Zentel, *Angew. Chem. Int. Ed.* 52 (2013) 8810.
- [34] M. Kondo, Y. Yu, T. Ikeda, *Angew. Chem. Int. Ed.* 45 (2006) 1378.
- [35] M. Alaasar, M. Prehm, M. Nagaraj, J.K. Vij, C. Tschierske, *Adv. Mater.* 25 (2013) 2186.
- [36] M. Alaasar, M. Prehm, K. May, A. Eremin, C. Tschierske, *Adv. Funct. Mater.* 24 (2014) 1703.
- [37] M. Alaasar, M. Prehm, M.-G. Tamba, N. Sebastian, A. Eremin, C. Tschierske, *Chem. Phys. Chem* 17 (2016) 278.
- [38] M. Alaasar, M. Prehm, S. Belau, N. Sebastián, M. Kurachkina, A. Eremin, C. Chen, F. Liu, C. Tschierske, *Chem. Eur. J.* 25 (2019) 6362.
- [39] I. Wirth, S. Diele, A. Eremin, G. Pelzl, S. Grande, L. Kovalenko, N. Pancenko, W. Weissflog, *J. Mater. Chem.* 11 (2001) 1642.
- [40] L. Kovalenko, M.W. Schröder, R.A. Reddy, S. Diele, G. Pelzl, W. Weissflog, *Liq. Cryst.* 32 (2005) 857.
- [41] C. Keith, A. Lehmann, U. Baumeister, M. Prehm, C. Tschierske, *Soft Matter* 6 (2010) 1704.

- [42] E. Westphal, H. Gallerdo, G.F. Caramori, N. Sebastian, M.-G. Tamba, A. Eremin, S. Kawachi, M. Prehm, C. Tschierske, *Chem. Eur. J.* 22 (2016) 8181.
- [43] H. Ocak, M. Poppe, B. Bilgin-Eran, G. Karanlık, M. Prehm, C. Tschierske, *Soft Matter* 12 (2016) 7405.
- [44] C. Dressel, T. Reppe, M. Prehm, M. Brautzsch, C. Tschierske, *Nat. Chem.* 6 (2014) 971.
- [45] C. Dressel, F. Liu, M. Prehm, X. Zeng, G. Ungar, C. Tschierske, *Angew. Chem. Int. Ed.* 53 (2014) 13115.
- [46] W. Weissflog, in: J. W. Goodby, J. P. Collings, T. Kato, C. Tschierske, H. F. Gleeson, P. Raynes (Eds.) *Handbook of Liquid Crystals*, Wiley-VCH, Weinheim, 2nd edn, vol. 5, 2014, pp. 89–174.
- [47] L. Han, S. Che, *Adv. Mater.* 30 (2018) 1705708.
- [48] G. Ungar, F. Liu and X. B. Zeng, in: W. Goodby, P. J. Collings, T. Kato, C. Tschierske, H. Gleeson, P. Raynes (Eds.) *Handbook of Liquid Crystals*, Wiley-VCH, Weinheim, Germany 2014.
- [49] N. Marets, D. Kuo, J.R. Torrey, T. Sakamoto, M. Henmi, H. Katayama, T. Kato, *Adv. Healthcare Mater.* 6 (2017) 1700252.
- [50] K. Bisoyi, T.J. Bunning, Q. Li, *Adv. Mater.* 30 (2018) 1706512.
- [51] H.-Y. Hsueh, Y.-C. Ling, H.-F. Wang, L.-Y.C. Chien, Y.-C. Hung, E.L. Thomas, R.-M. Ho, *Adv. Mater.* 26 (2014) 3225.
- [52] R.A. Reddy, U. Baumeister, C. Keith, H. Hahn, H. Lang, C. Tschierske, *Soft Matter* 3 (2007) 558.
- [53] S. Kang, M. Harada, X. Li, M. Tokita, J. Watanabe, *Soft Matter* 8 (2012) 1916.
- [54] J. Matraszek, J. Zapala, J. Mieczkowski, D. Pocięcha, E. Gorecka, *Chem. Commun.* 51 (2015) 5048.
- [55] J. Matraszek, D. Pocięcha, N. Vaupotič, M. Salamończyk, M. Vogrine, E. Gorecka, *Soft Matter* 16 (2020) 3882.
- [56] M. Alaasar, S. Poppe, Q. Dong, F. Liu, C. Tschierske, *Chem. Commun.* 52 (2016) 13869.
- [57] O. Kwon, X. Cai, W. Qu, F. Liu, J. Szydłowska, E. Gorecka, M.J. Han, D.K. Yoon, S. Poppe, C. Tschierske, *Adv. Funct. Mater.* 31 (2021) 2102271.
- [58] M. Alaasar, A.F. Darweesh, X. Cai, F. Liu, C. Tschierske, *Chem. Eur. J.* 27 (2021) 14921.
- [59] T. Reppe, C. Dressel, S. Poppe, A. Eremin, C. Tschierske, *Adv. Optical Mater.* 9 (2021) 2001572.
- [60] Y. Cao, M. Alaasar, A. Nallapaneni, M. Salamończyk, P. Marinko, E. Gorecka, C. Tschierske, F. Liu, N. Vaupotič, C. Zhu, *Phys. Rev. Lett.* 125 (2020).
- [61] X. Zeng, G. Ungar, *J. Mater. Chem. C* 8 (2020) 5389.
- [62] M. Alaasar, M. Prehm, Y. Cao, F. Liu, C. Tschierske, *Angew. Chem. Int. Ed.* 128 (2016) 320.
- [63] M. Alaasar, S. Poppe, Q. Dong, F. Liu, C. Tschierske, *Angew. Chem., Int. Ed.* 56 (2017) 10801.
- [64] M. Alaasar, S. Poppe, Y. Cao, C. Chen, F. Liu, C. Zhu, C. Tschierske, *J. Mater. Chem. C* (2020) 12902.
- [65] G. Pelzl, W. Weissflog, in: A. Ramamoorthy (Ed.) *Thermotropic Liquid Crystals: Recent Advances*, Springer, Amsterdam, 2007, pp. 1–58.
- [66] D. Pocięcha, E. Gorecka, M. Čepič, N. Vaupotič, W. Weissflog, *Phys. Rev. E* 74 (2006).
- [67] A. Eremin, M. Floegel, U. Kornek, S. Stern, R. Stannarius, H. Nadasi, W. Weissflog, C. Zhu, Y. Shen, C.S. Park, J. MacLennan, N. Clark, *Phys. Rev. E* 86 (2012).
- [68] V. Gude, K. Upadhyaya, G. Mohiuddin, V.S.R. Nandiraju, *Liq. Cryst.* 40 (2013) 120.
- [69] F.C. Yu, L.J. Yu, *Chem. Mater.* 18 (2006) 5410.
- [70] S. Kang, Y. Saito, N. Watanabe, M. Tokita, Y. Takamishi, H. Takezoe, J. Watanabe, *J. Phys. Chem. B* 110 (2006) 5205.
- [71] K.M. Fergusson, M. Hird, *J. Mater. Chem.* 20 (2010) 3069.
- [72] A.S. Matharu, C. Grover, L. Komitov, G. Anderson, *J. Mater. Chem.* 10 (2000), 1303.
- [73] W. Weissflog, U. Dunemann, S.F. Tandel, M.G. Tamba, H. Kresse, G. Pelzl, S. Diele, U. Baumeister, A. Eremin, S. Stern, R. Stannarius, *Soft Matter* 5 (2009) 1840.
- [74] M. Monika, V. Prasad, N.G. Nagaveni, *Liq. Cryst.* 42 (2015) 1490.
- [75] R. Deb, R.K. Nath, M.K. Paul, N.V.S. Rao, F. Tuluri, Y. Shen, R. Shao, D. Chen, C. Zhu, I.I. Smalyukh, N.A. Clark, *J. Mater. Chem.* 20 (2010) 7332.
- [76] D.K. Yoon, R. Deb, D. Chen, E. Korblova, R. Shao, K. Ishikawa, N.V.S. Rao, D.M. Walba, I.I. Smalyukh, N.A. Clark, *Proc. Nat. Acad. Sci.* 107 (2010) 21311.
- [77] R.K. Nath, D.D. Sarkar, D.S.S. Rao, N.V.S. Rao, *Liq. Cryst.* 39 (2012) 889.
- [78] M. Alaasar, S. Poppe, C. Tschierske, *Liq. Cryst.* 44 (2017) 729.
- [79] M. Alaasar, S. Poppe, C. Kerzig, C. Klopp, A. Eremin, C. Tschierske, *J. Mater. Chem. C* 5 (2017) 8454.
- [80] M. Alaasar, X. Cai, F. Kraus, M. Giese, F. Liu, C. Tschierske, *J. Mol. Liq.* (2022), <https://doi.org/10.1016/j.molliq.2022.118597>, In press.
- [81] K. Miyasato, S. Abe, H. Takezoe, A. Fukuda, E. Kuze, *Jpn. J. Appl. Phys.* 22 (1983) L661.
- [82] J.P.F. Lagerwall, F. Giesselmann, *Chem. Phys. Chem.* 7 (2006) 20.
- [83] M. Alaasar, M. Prehm, S. Poppe, C. Tschierske, *Chem. Eur. J.* 23 (2017) 5541.
- [84] E. Enz, S. Findeisen-Tandel, R. Dabrowski, F. Giesselmann, W. Weissflog, U. Baumeister, *J. Mater. Chem.* 19 (2009) 2950.
- [85] M. Alaasar, M. Prehm, Y. Cao, F. Liu, C. Tschierske, *Angew. Chem. Int. Ed.* 128 (2016) 320.
- [86] M. Alaasar, J.-C. Schmidt, X. Cai, F. Liu, C. Tschierske, *J. Mol. Liq.* 332 (2021).
- [87] M. Alaasar, S. Poppe, C. Tschierske, *J. Mol. Liq.* 277 (2019) 233.
- [88] J.M. Shivanna, M. Alaasar, G. Hegde, *J. Mol. Liq.* 341 (2021).





# Nematic phases driven by hydrogen-bonding in liquid crystalline nonsymmetric dimers

Mohamed Alaasar <sup>a,b</sup> and Carsten Tschierske<sup>b</sup>

<sup>a</sup>Department of Chemistry, Faculty of Science, Cairo University, Giza, Egypt; <sup>b</sup>Institute of Chemistry, Martin Luther University Halle-Wittenberg, Halle (Saale), Germany

## ABSTRACT

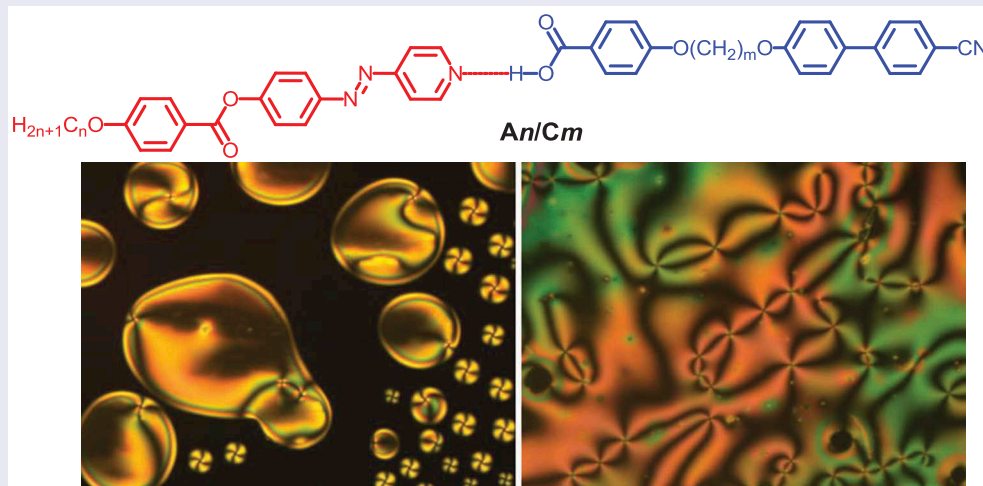
A new type of supramolecular liquid crystalline complexes formed by intermolecular hydrogen bond formation between rod-like 4-(4'-pyridylazophenyl)-4"-alkoxybenzoates as proton acceptors and 4-[5-(4'-cyanobiphenyl-4-yloxy)alkyloxy]benzoic acids as proton donors have been designed and prepared. The benzoic acids derivatives consist of two variable aliphatic spacers with odd number of carbon atoms and terminated with the highly polar cyano group. The liquid crystalline behaviour of the new complexes has been characterised using polarised light microscopy (POM) and differential scanning calorimetry (DSC). It was found that regardless the terminal alkyl chain lengths at the pyridine-based component or the length of the flexible spacer on the benzoic acid derivatives; all of the prepared complexes exhibit only enantiotropic nematic phases over a broad temperature range.

## ARTICLE HISTORY

Received 19 April 2018  
Accepted 11 May 2018

## KEYWORDS

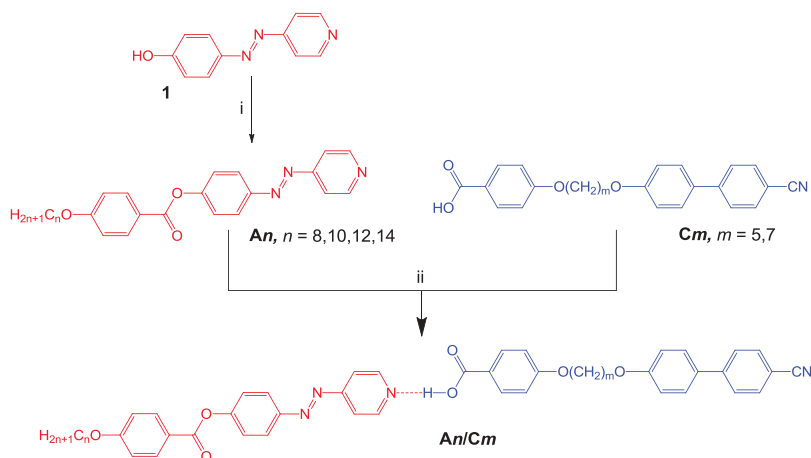
Azopyridine; hydrogen bonding; dimers; nematic phase; liquid crystals



## 1. Introduction

The liquid crystal display (LCD) technology, the main consumer of liquid crystalline materials, is continuously searching for new materials with improved physical properties compared to the currently used LCs. Therefore, the markets of laptops, TV sets and other modern devices using LCD are growing. The mostly used LCs materials for this purpose are low melting point nematogenic or chiral smectic LCs. One of the most promising tools that have been used for creating order and complexity is non-covalent interaction, such as hydrogen or halogen bonding. Hydrogen bonding, especially between pyridines moieties

and benzoic acid derivatives, was previously used to design nematic, smectic and columnar mesomorphic materials [1–6] and more recently in inducing twist-bend phases ( $N_{tb}$ ) in LCs dimers or by mixing achiral components [7,8]. Hydrogen bonding was even used in induction of chirality in isotropic liquid phases, as well as bicontinuous cubic phases [9]. The role of hydrogen bonding in the formation of liquid crystallinity in supramolecular aggregates has been well investigated by temperature-dependent Fourier transform infrared (FTIR) spectroscopy [10–12]. LCs dimers represent a class of compounds containing two mesogenic units that might be symmetric or non-



**Scheme 1.** (Colour online) Synthetic route to the hydrogen-bonded complexes **An/Cm**. Reagents and conditions: (i) 4-*n*-alkoxybenzoic acids, DCC, DMAP, dichloromethane/THF mixture, stirring at room temperature, 48 h; (ii) melting with stirring.

symmetric linked by a flexible spacer. Most of the LC dimers have usually different LC properties differing from those of the individual mesogenic parts and therefore they have been used as a rich source for the discovery of new LC phases [13,14]. On the other hand, azo functionalised materials are one of the most frequently used photochromes for the manufacture of light-addressable materials due to their unique *trans-cis* isomerisation upon photo irradiation [15–20]. The incorporation of azo units into LCs results in photoresponsive materials with potential applications, such as molecular scissors [21], photo-oscillators [22,23], and optogenetics [24]. Due to similar molecular structures azopyridine derivatives with one carbon atom replaced by nitrogen atom exhibit related photosensitivity to azobenzenes [25,26]. Moreover, azopyridines have the advantage of combining the photoresponsive nature with the capability of self-assembly through intermolecular interactions [27,28].

Herein, we report how hydrogen bonding can be used for the formation of LC nonsymmetric dimers exhibiting broad ranges of enantiotropic nematic phases. For this purpose we designed and prepared the hydrogen-bonded supramolecular complexes shown in Scheme 1. The building blocks for these complexes represent 4-(4'-pyridylazo-phenyl)-4'-alkoxybenzoates (**An**) [29] as the proton acceptors with different terminal alkyl chain lengths ( $n = 8, 10, 12, 14$ ) and benzoic acid derivatives (**Cm**) as the proton donors. The acids **Cm** consist of a cyanobiphenyl unit connected to a benzoic acid fragment by an aliphatic spacer with two different chain lengths consisting of odd number of carbon atoms ( $m = 5$  or  $7$ ) to induce bending of the formed dimers. The link used to connect the benzoic acid to the cyanobiphenyl unit is an ether linkage at both sides of the chain. These two acids were used recently to prepare polycatenars materials with

nematic phases [30] and the acid **C5** analogue with the oxygen atoms in the ether linkages replaced by methylene links was reported before to exhibit the  $N_{tb}$  phase beside the conventional nematic phase [7]. It should be mentioned that  $N_{tb}$  phase was reported for some LCs dimers formed by covalent bonds and consisting of ether linkages at both sides of the aliphatic spacer [31,32]. Therefore, it was interesting for us to check if the  $N_{tb}$  phase could be also induced by intermolecular hydrogen-bond formation in supramolecular LCs incorporating ether linkages at both terminals of the aliphatic spacers.

## 2. Characterisation

Thin layer chromatography (TLC) was performed on aluminium sheet precoated with silica gel. Analytical quality chemicals were obtained from commercial sources and used as obtained. The solvents were dried using the standard methods when required. The purity and the chemical structures of all synthesised materials were confirmed by the spectral data. The structure characterisation of the prepared materials is based on  $^1\text{H-NMR}$  (Varian Unity 500 and Varian Unity 400 spectrometers, in  $\text{CDCl}_3$  solutions, with tetramethylsilane as internal standard). Microanalyses were performed using a Leco CHNS-932 elemental analyser.

The mesophase behaviour and transition temperatures of the supramolecular complexes were measured using a Mettler FP-82 HT hot stage and control unit in conjunction with a Nikon Optiphot-2 polarising microscope. The associated enthalpies were obtained from DSC-thermograms, which were recorded on a Perkin-Elmer DSC-7, heating and cooling rate:  $10 \text{ K min}^{-1}$ .

### 3. Results and discussion

#### 3.1. Synthesis

The synthesis of the supramolecular aggregates under discussion (**An/cm**) is shown in Scheme 1. The pyridine-based components (**An**) were synthesised according to the procedure described before [29] by the esterification between 4-(4'-pyridylazo)-phenol (**1**) and 4-n-alkoxybenzoic acids. For example, the synthesis details and analytical data of the non-reported compound **A8** is described below. The synthesis steps for 4-[5-(4'-cyanobiphenyl-4-yloxy)alkoxy]benzoic acids (**Cm**) is described in details in our recent publication [30].

##### 3.1.1. 4-(4'-pyridylazophenyl)-4''-octyloxybenzoate (**A8**)

4-(4'-Pyridylazo)-phenol (0.30 g, 1.35 mmol) with octyloxybenzoic acid (0.34 g, 1.35 mmol), DCC (0.28 g, 1.35 mmol), and few crystals of 4-dimethylaminopyridine (DMAP) as a catalyst, were dissolved in 50 mL (0.75:0.25) mixture of CH<sub>2</sub>Cl<sub>2</sub> and THF; the mixture was stirred at room temperature for 48 h. The solid materials were filtered off, washed with 20 mL CH<sub>2</sub>Cl<sub>2</sub>, and the solvent was removed under vacuum. The obtained crude product was purified first by column chromatography using CH<sub>2</sub>Cl<sub>2</sub> as an eluent followed by recrystallisation from ethanol to give the pure material as orange crystals. The analytical data are as follow:

**A8.** Orange crystals; yield (0.40 g, 61.6%). <sup>1</sup>H NMR (400 MHz, CDCl<sub>3</sub>) δ 8.82 (d, *J* = 8.5, 2H, Ar-H), 8.16 (d, *J* = 8.5, 2H, Ar-H), 8.05 (d, *J* = 8.3, 2H, Ar-H), 7.71 (d, *J* = 8.7, 2H, Ar-H), 7.41 (d, *J* = 8.7, 2H, Ar-H), 6.99 (d, *J* = 8.3, 2H, Ar-H), 4.06 (t, *J* = 6.6 Hz, 2H, Ar-OCH<sub>2</sub>CH<sub>2</sub>), 1.91 – 1.77 (m, 2H, Ar-OCH<sub>2</sub>CH<sub>2</sub>), 1.58 – 1.19 (m, 10H, CH<sub>2</sub>), 0.90 (t, *J* = 6.9 Hz, 3H, CH<sub>3</sub>). Elemental Analysis: Calc. for C<sub>26</sub>H<sub>29</sub>N<sub>3</sub>O<sub>3</sub> C, 72.37; H, 6.77; N, 9.74. Found C, 72.30; H, 6.77; N, 9.72%.

##### 3.1.2. Preparation of the supramolecular complexes (**An/Cm**)

The supramolecular aggregates (**An/Cm**) were prepared by mixing equimolar amounts of **An** and **Cm** and melting them together in DSC pans with stirring. After crystallisation the materials were grinded, and this process were repeated two times to obtain a homogeneous mixture. For example, to prepare the supramolecular complex **A8/C5** (0.10 g, 0.231 mmol) of **A8** was mixed together with (0.09 g, 0.231 mmol) of **C5** as described above.

#### 3.2. Mesomorphic properties

Before discussing the phase behaviour of the new supramolecular complexes we should mention the LC

properties of the individual components. The phase transitions temperatures and phase types of the acids **Cm** and pyridine based **An** materials are collected in Table 1. The transition temperatures of the acid **C5** are in good agreement with those reported in reference [7]. The two acids prepared for this study (**C5** and **C7**) were found to exhibit an enantiotropic nematic phase (see Table 1).

The formation of the nematic phases in these acids is attributed to the dimerisation of the acid molecules as a result of intermolecular hydrogen bond formation between the two free carboxylic groups yielding supramolecular LC trimers consisting of three mesogenic fragments connected by two flexible spacers (Figure 1) [7]. The transition temperatures of the pyridine-based components (**A10-A14**) were found to be slightly different from those reported in reference [29], therefore the new transition temperatures are reported in Table 1 in addition to those of the non-reported shortest homologue **A8**. The shorter homologues **A8** and **A10** were found to be dimesomorphic materials exhibiting SmA and N phases and the nematic phase range is decreasing with chain elongation as one would expect for a homologues series of compounds. Therefore, for the next two longer homologues **A12** and **A14** the nematic phase is removed and only SmA phases are observed.

The transition temperatures (°C) and the associated enthalpies (kJ mol<sup>-1</sup>) obtained from DSC thermograms of the prepared complexes **An/Cm** are given in Table 2 and represented graphically in Figure 2. The DSC thermograms obtained for the supramolecular complex **A14/C5** as a representative example is shown in Figure 3. Homogenous melting and reproducible transition temperatures were observed for all supramolecular complexes **An/Cm**.

As can be seen from Table 2 and Figure 2 the formation of the supramolecular 1:1 complexes between the pyridine-based compounds **An** and benzoic acid derivatives **Cm** is clearly indicated from the disappearance of the transition temperatures of the individual components (compare Tables 1 and 2). The formation of the intermolecular hydrogen bonding between the base and acid components leads to the suppression of the SmA phases of the pyridine-based derivatives **An** and induction of broad nematic LC phase ranges for all hydrogen bonded complexes as determined by differential scanning calorimetry (DSC) (see Figure 3 as an example) and by polarised light microscopy (POM) (see Figure 4).

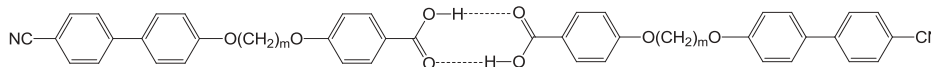
As a common feature for all complexes on heating and cooling cycles, three endotherms were observed (see Figure 3). The lower-temperature endotherm represents a crystal-crystal transition, the next endotherm which is the strongest endotherm representing a crystal-nematic

**Table 1.** Transition temperatures of the acids (**Cm**) and the azopyridine based derivatives (**An**).<sup>a</sup>

Comp.	<i>m</i>	<i>n</i>	Heating	Cooling
C5	5	-	Cr 197 [152.7] 209 [6.0] Iso	Iso 208 [5.9] N 124 [151.7] Cr
C7	7	-	Cr 172 [130.8] N 201 [6.2] Iso	Iso 199 [6.0] N 88 [86.8] Cr
A8	-	8	Cr 112 [98.8] SmA 128 [2.0] N 141 [1.2] Iso	Iso 139 [1.3] N 126 [2.1] SmA 86 [82.2] Cr
A10	-	10	Cr 94 [157.9] SmA 134 [5.0] N 139 [2.3] Iso	Iso 135 [2.5] N 131 [5.0] SmA 75 [137.7] Cr
A12	-	12	Cr 96 [188.8] SmA 134 [13.4] Iso	Iso 132 [13.8] SmA 75 [185.9] Cr
A14	-	14	Cr 97 [190.7] SmA 133 [13.6] Iso	Iso 132 [14.6] SmA 78 [192.2] Cr

Cr: crystalline solid; N: nematic phase; SmA: smectic A phase; Iso: isotropic liquid.

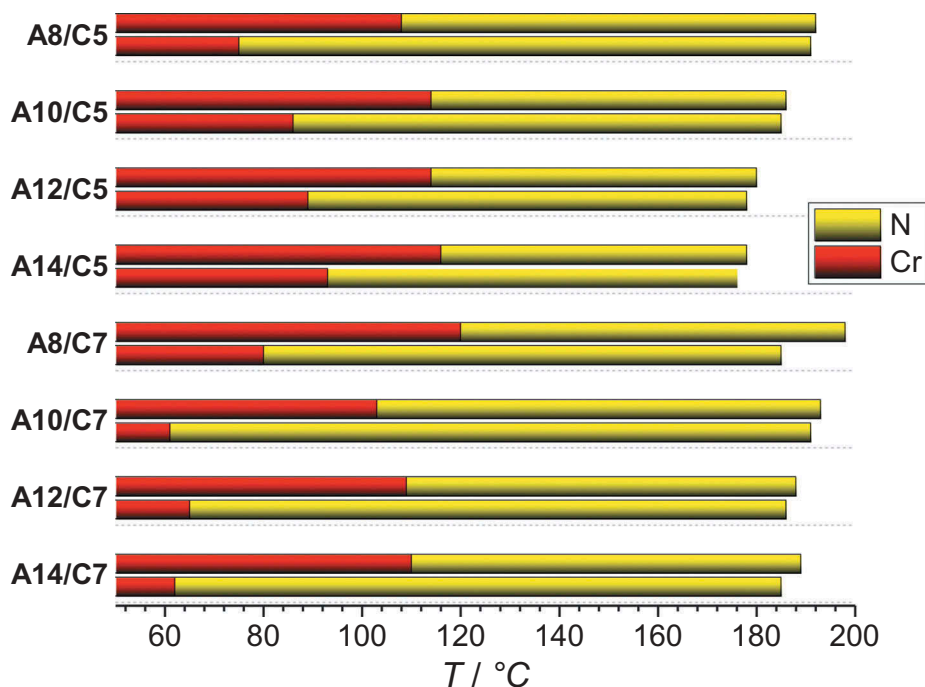
<sup>a</sup>Transition temperatures and enthalpy values were taken from the second DSC heating scans (10 K min<sup>-1</sup>).

**Figure 1.** The hydrogen-bonded supramolecular liquid crystalline trimers of the benzoic acid derivatives (**Cn**).**Table 2.** Transition temperatures of the supramolecular complexes **An/Cm**.<sup>a</sup>

An/Cm	<i>m</i>	<i>n</i>	Heating	Cooling
A8/C5	5	8	Cr 108 [50.5] N 192 [4.5] Iso	Iso 191 [5.7] N 75 [58.3] Cr
A10/C5	5	10	Cr 114 [50.1] N 186 [3.7] Iso	Iso 185 [5.3] N 86 [56.3] Cr
A12/C5	5	12	Cr 114 [47.7] N 180 [3.2] Iso	Iso 178 [4.2] N 89 [50.7] Cr
A14/C5	5	14	Cr 116 [50.1] N 178 [3.4] Iso	Iso 176 [3.6] N 93 [58.4] Cr
A8/C7	7	8	Cr 120 [34.9] N 198 [5.6] Iso	Iso 185 [6.3] N 80 [45.0] Cr
A10/C7	7	10	Cr 103 [34.2] N 193 [5.1] Iso	Iso 191 [6.7] N 61 [33.1] Cr
A12/C7	7	12	Cr 109 [33.8] N 188 [4.2] Iso	Iso 186 [4.1] N 65 [37.5] Cr
A14/C7	7	14	Cr 110 [39.6] N 189 [4.4] Iso	Iso 185 [5.3] N 62 [41.3] Cr

For abbreviations see Table 1.

<sup>a</sup>Transition temperatures and enthalpy values were taken from the second DSC heating scans (10 K min<sup>-1</sup>).

**Figure 2.** (Colour online) Phase transitions of the complexes **An/Cm** as determined from 2nd heating (upper columns) and 2nd cooling DSC scans (lower columns) with rate 10 K min<sup>-1</sup>; abbreviations: N = nematic phase; Cr = crystalline solid; for numerical data and transition enthalpies see Table 2.

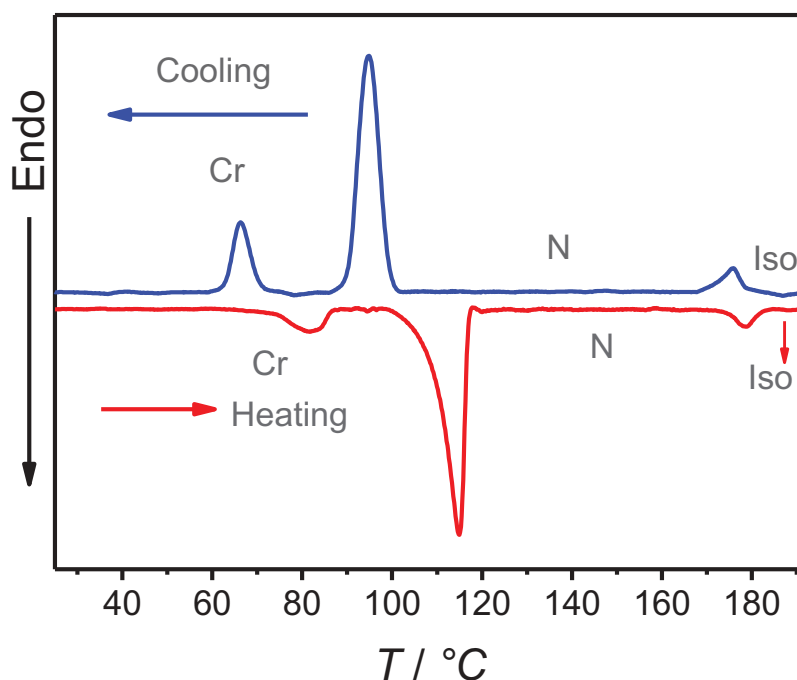


**Figure 3.** (Colour online) DSC thermograms obtained for the complex **A14/C5**; heating and cooling rates are  $10 \text{ K/min}^{-1}$ .

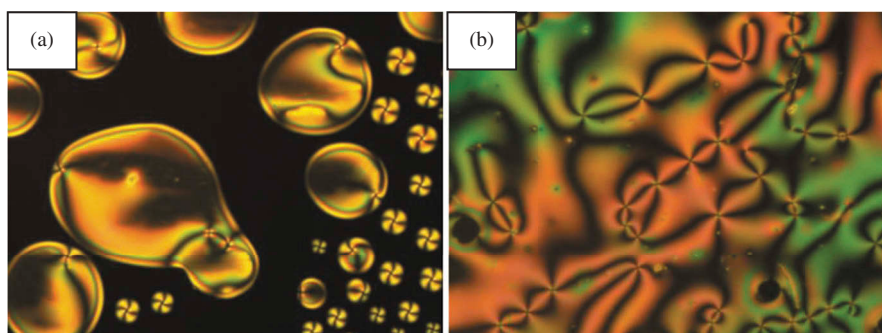


**Figure 4.** (Colour online) Optical micrographs observed for the nematic phase of the supramolecular complex **A8/C5** in homeotropic cell: (a) nematic droplets at the transition from the isotropic liquid at  $T = 191^\circ\text{C}$ ; (b) schlieren texture of the nematic phase showing four-brush defects at  $T = 150^\circ\text{C}$ .

transition, and the last endotherm at the highest temperature is for the nematic–isotropic transition. Under the POM, a characteristic schlieren textures with four-brush defects and which flashed when subjected to mechanical stress were observed as typically observed for nematic phases indicating that the LC phase exhibited by the prepared complexes is the nematic one. For all complexes the nematic phases could be supercooled prior to crystallisation with the lowest value  $\sim 23 \text{ K}$  for **A8/7** and the highest value  $\sim 48$  for **A14/7** (see Table 2

and Figure 2). We emphasise here that nematic phases exists for short ranges for the pure individual acids **Cm** and the shorter pyridine-based derivatives **A8** and **A10**, whereas interestingly, the nematic phase exhibited by all supramolecular complexes extends over a broad temperature range, even exceeding  $\sim 75 \text{ K}$  for most of the complexes and reaches  $\sim 90 \text{ K}$  for **A10/7**. This implies the importance of the hydrogen bonding in stabilising the nematic phases in such types of supramolecular structures.

#### 4. Summary and conclusions

In summary, we have designed and prepared new type of supramolecular liquid crystalline nonsymmetric dimers via intermolecular hydrogen bonding interaction between benzoic acid derivatives and azopyridine-based homologues. The formation of these complexes was confirmed by DSC and POM investigations. All of the prepared dimers were found to exhibit nematic phases as the only mesophase. Interestingly, regardless the terminal alkyl chain lengths on the pyridine-based components or the number of carbon atoms on the aliphatic spacer the nematic phases exist over a broad temperature range for all members of the supramolecular dimers. Moreover, no indication of any nematic–nematic transition or twist bend nematic phase formation was found in any of the prepared materials.

#### Disclosure statement

No potential conflict of interest was reported by the authors.

#### ORCID

Mohamed Alaasar  <http://orcid.org/0000-0003-4155-8644>

#### References

- [1] Kato T, Fréchet JMJ. A new approach to mesophase stabilization through hydrogen bonding molecular interactions in binary mixtures. *J Am Chem Soc.* 1989;111:8533–8534.
- [2] Wallage MJ, Imrie CT. Supramolecular dimeric liquid crystals. The liquid crystalline behaviour of mixtures of alpha-(4-pyridyloxy)-omega-4-(4-butylphenylazo) phenoxy alkanes and 4-octyloxybenzoic acid. *J Mater Chem.* 1997;7:1163–1167.
- [3] Friot B, Boyd D, Willis K, et al. Hydrogen-bonded polycatenar mesogens. *Liq Cryst.* 2000;27:605–611.
- [4] Paleos CM, Tsiourvas D. Supramolecular hydrogen-bonded liquid crystals. *Liq Cryst.* 2001;28:1127–1161.
- [5] Kato T, Kamikawa Y. Handbook of liquid crystals. In: Goodby JW, Collings PJ, Kato T, et al., Eds.. Vol. 5. Weinheim: Wiley-VCH; 2014. p. 513–540.
- [6] Alaasar M, Tschierske C, Prehm M. Hydrogen-bonded supramolecular complexes formed between isophthalic acid and pyridine-based derivatives. *Liq Cryst.* 2011;38:925–934.
- [7] Jansze SM, Martínez-Felipe A, Storey J, et al. A twist-bend nematic phase driven by hydrogen bonding. *Angew Chem Int Ed.* 2015;54:643–646.
- [8] Walker R, Pocięcha D, Abberley JP, et al. Spontaneous chirality through mixing achiral components: a twist-bend nematic phase driven by hydrogen-bonding between unlike components. *Chem Commun.* 2018;54:3383–3386.
- [9] Alaasar M, Poppe S, Dong Q, et al. Mirror symmetry breaking in cubic phases and isotropic liquids driven by hydrogen bonding. *Chem Commun.* 2016;52:13869–13872.
- [10] Martínez-Felipe A, Imrie CT. The role of hydrogen bonding in the phase behaviour of supramolecular liquid crystal dimers. *J Mol Stru.* 2015;1100:429–437.
- [11] Martínez-Felipe A, Cook AG, Abberley JP, et al. An FT-IR spectroscopic study of the role of hydrogen bonding in the formation of liquid crystallinity for mixtures containing bipyridines and 4-pentoxybenzoic acid. *RSC Adv.* 2016;6:108164–108179.
- [12] Paterson DA, Martínez-Felipe A, Jansze SM, et al. New insights into the liquid crystal behaviour of hydrogen-bonded mixtures provided by temperature-dependent FTIR spectroscopy. *Liq Cryst.* 2015;42:928–939.
- [13] Imrie CT, Henderson PA. Liquid crystal dimers and higher oligomers: between monomers and polymers. *Chem Soc Rev.* 2007;36:2096–2124.
- [14] Imrie CT, Henderson PA, Yeap G-Y. Liquid crystal oligomers: going beyond dimers. *Liq Cryst.* 2009;36:755–777.
- [15] Bandarab HMD, Burdette SC. Photoisomerization in different classes of azobenzene. *Chem Soc Rev.* 2012;41:1809–1825.
- [16] Alaasar M. Azobenzene-containing bent-core liquid crystals: an overview. *Liq Cryst.* 2016;43:2208–2243.
- [17] Alaasar M, Prehm M, Nagaraj M, et al. A liquid crystalline phase with uniform tilt, local polar order and capability of symmetry breaking. *Adv Mater.* 2013;25:2186–2191.
- [18] Alaasar M, Poppe S, Dong Q, et al. Isothermal chirality switching in liquid-crystalline azobenzene compounds with non-polarized light. *Angew Chem Int Ed.* 2017;56:10801–10805.
- [19] Alaasar M, Prehm M, Tschierske C. Influence of halogen substituent on the mesomorphic properties of five-ring banana shaped molecules with azobenzene wings. *Liq Cryst.* 2013;40:656–668.
- [20] Paterson DA, Xiang J, Singh G, et al. Reversible isothermal twist-bend nematic-nematic phase transition driven by the photoisomerization of an azobenzene-based non-symmetric liquid crystal dimer. *J Am Chem Soc.* 2016;138:5283–5289.
- [21] Zaremba M, Siksnys V. Molecular scissors under light control. *Proc Natl Acad Sci USA.* 2010;107:1259–1260.
- [22] Lee KM, White TJ. Photomechanical response of composite structures built from azobenzene liquid crystal polymer networks. *Polymers.* 2011;3:1447–1457.
- [23] Garcia-Amorós J, Reig M, Castro MCR, et al. Molecular photo-oscillators based on highly accelerated heterocyclic azo dyes in nematic liquid crystals. *Chem Commun.* 2014;50:6704–6706.
- [24] Fehrentz T, Schönberger M, Trauner D. Optochemical genetics. *Angew Chem Int Ed.* 2011;50:12156–12182.
- [25] Chen Y, Yu H, Quan M, et al. Photothermal effect of azopyridine compounds and their applications. *RSC Adv.* 2015;5:4675–4680.
- [26] Garcia-Amorós J, Reig M, Cuadrado A, et al. A photo-switchable bis-azo derivative with a high temporal resolution. *Chem Commun.* 2014;50:11462–11464.
- [27] Chen Y, Yu H, Zhang L, et al. Photoresponsive liquid crystals based on halogen bonding of azopyridines. *Chem Commun.* 2014;50:9647–9649.
- [28] Pfltscher M, Wölper C, Gutmann JS, et al. A modular approach towards functional supramolecular aggregates - subtle structural differences inducing liquid crystallinity. *Chem Commun.* 2016;52:8549–8552.

- [29] Naoum M, Fahmi A, Alaasar M. Supramolecular hydrogen-bonded liquid crystals formed from 4-(4'-pyridylazophenyl)-4''-alkoxybenzoates and 4-substituted benzoic acids. *Mol Cryst Liq Cryst.* **2008**;487:74–91.
- [30] Alaasar M, Tschierske C. Non-symmetric ether-linked liquid crystalline dimers with a highly polar end group. *Liq Cryst.* **2017**;44:387–393.
- [31] Mandle RJ, Davis EJ, Voll -C-CA, et al. The relationship between molecular structure and the incidence of the NTB phase. *Liq Cryst.* **2015**;42:688–703.
- [32] Mandle RJ. The dependency of twist-bend nematic liquid crystals on molecular structure: a progression from dimers to trimers, oligomers and polymers. *Soft Matter.* **2016**;12:7883–7901.



# Azobenzene-based supramolecular liquid crystals: The role of core fluorination

Mohamed Alaasar<sup>a,b,\*</sup>, Jaques-Christopher Schmidt<sup>b</sup>, Ahmed F. Darweesh<sup>a</sup>, Carsten Tschierske<sup>b</sup>

<sup>a</sup> Department of Chemistry, Faculty of Science, Cairo University, Giza, Egypt

<sup>b</sup> Institute of Chemistry, Martin Luther University Halle-Wittenberg, Kurt Mothes Str. 2, D-06120 Halle (Saale), Germany

## ARTICLE INFO

### Article history:

Received 24 March 2020

Received in revised form 23 April 2020

Accepted 28 April 2020

Available online 03 May 2020

### Keywords:

Supramolecular liquid crystals

Azobenzene

Hydrogen-bonding

Nematic

Fluorination

Photosensitivity

## ABSTRACT

The impact of core fluorination on the phase behaviour of supramolecular hydrogen-bonded liquid crystals (HBLCs) is investigated in detail. Therefore, different types of HBLCs were synthesized using two benzoic acid derivatives as proton donors, namely, 4-octyloxybenzoic acid and octylbenzoic acid. The two acids were combined through intermolecular hydrogen-bonding with alkoxyazopyridine derivatives as proton acceptors. Three different types of azopyridines were used either without fluorine substitution or with one lateral fluorine substituent at different positions. The study proved the importance of using core fluorination as a significant tool to modify the liquid crystalline behaviour of HBLCs, where all azopyridines are non-mesomorphic and almost all their complexes exhibit enantiotropic mesophases. The formation of the hydrogen bond between the complementary components was confirmed using FTIR and <sup>1</sup>H NMR spectroscopy, while the liquid crystalline self-assembly of the HBLCs was investigated in detail using polarized light microscope (PLM) and differential scanning calorimetry (DSC). Depending on the type of the terminal chain on the benzoic acid derivative and on the position of the lateral fluorine substituent different types of mesophases including nematic (N), smectic A (SmA) and smectic C (SmC) phases were observed. Finally, under UV light illumination all the prepared HBLCs show *cis-trans* photoisomerization resulting in tuning the liquid crystalline phases, which is of importance for industrial applications.

© 2020 Elsevier B.V. All rights reserved.

## 1. Introduction

Liquid crystalline (LC) materials are of special interest for the display technology due to their molecular self-assembly which can be tuned under the effect of external stimuli, temperature or light. Since the first discovery of LC, different classes of molecular structures have been designed to produce several LCs with fascinating properties. A huge number of LCs have been reported using different synthetic methods, however the design of supramolecular liquid crystals by intermolecular interaction between complementary components is of great importance. The intermolecular interactions could be either halogen-bonding [1–6], or hydrogen-bonding [7–9], and both have the advantage of the ease accessibility compared to covalently bonded LCs. Kato et al. reported the first examples of hydrogen bonded liquid crystals (HBLCs) designed by hydrogen-bond formation between pyridine-derivatives and benzoic acid derivatives [10,11] later several HBLCs were designed using different types of proton donors and proton acceptors to produce wide varieties of molecular architectures such as rod-

like HBLCs [12,13], bent-shaped LCs [14–18] polymeric framework [19], modular hierarchical [20], non-symmetric dimers having conventional nematic phases [21] or exhibiting the heliconical twist-bend nematic phase ( $N_{TB}$ ) [22] and supramolecular polycatenars capable of displaying chiral isotropic liquids beside chiral cubic phases [23]. One class of the commonly used proton acceptors is azopyridine-derivatives [12,13,16,20,21,23–26]. Azopyridines are interesting because they combine the possibility of self-assembly through intermolecular hydrogen- or halogen-bond formation together with the unique phenomenon of *trans-cis* photoisomerization under light irradiation due to the presence of the azo linkage. Azo functionalized LCs are of special interest for the manufacture of light responsive materials for the technological applications such as molecular scissors [27] and photo-oscillators [28,29]. In recent years different types of azobenzene-based LCs with fascinating properties were reported [30–32]. One way to modify the liquid crystalline behaviour is aromatic core fluorination [33–40]. This is caused by the unique combination of high polarity and low polarizability of the fluorine atom, as well as steric and conformational effects. Due to its small size fluorine atom can be accommodated by the molecular core affecting the strength of the electrostatic and  $\pi$ -stacking core-core interactions. In 2003 X. Song et al reported HBLCs between 4-octyloxybenzoic acid and 4-(alkoxyphenylazo) pyridines with

\* Corresponding author at: Department of Chemistry, Faculty of Science, Cairo University, Giza, Egypt.

E-mail address: [malaasar@sci.cu.edu.eg](mailto:malaasar@sci.cu.edu.eg) (M. Alaasar).



**Table 1**  
Phase transition temperatures (T/°C), mesophase types, and transition enthalpies [ $\Delta H$  (J/g)] of the supramolecular HBLCs **An**, **A3Fn** and **A2Fn**<sup>a</sup>.

Complex	n	X	Y	Phase sequence (T/°C [ $\Delta H$ (J/g)])
<b>A10</b> [41]	10	H	H	<b>H:</b> Cr 88 [62.2] SmC 128 [22.0] Iso <b>C:</b> Iso 126 [−19.5] SmC 89 [−70.8] Cr
<b>A12</b> [41]	12	H	H	<b>H:</b> Cr 92 [40.2] SmC 128 [22.0] Iso <b>C:</b> Iso 126 [−19.5] SmC 82 [−43.3] Cr
<b>A14</b> [41]	14	H	H	<b>H:</b> Cr 90 [82.3] SmC 127 [25.5] Iso <b>C:</b> Iso 126 [−23.5] SmC 82 [−39.3] Cr
<b>A3F8</b>	8	F	H	<b>H:</b> Cr 93 [75.2] N 113 [5.9] Iso <b>C:</b> Iso 111 [−5.3] N 92 [−1.8] SmC 84 [−73.4] Cr
<b>A3F10</b>	10	F	H	<b>H:</b> Cr 84 [46.8] SmC 98 [11.2] <sup>b</sup> N 115 [11.2] <sup>b</sup> Iso <b>C:</b> Iso 110 [−10.0] <sup>b</sup> N 95 [−10.0] <sup>b</sup> SmC 64 [−53.0] Cr
<b>A3F12</b>	12	F	H	<b>H:</b> Cr 87 [59.7] SmC 111 [16.2] <sup>b</sup> N 116 [16.2] <sup>b</sup> Iso <b>C:</b> Iso 114 [−14.8] <sup>b</sup> N 108 [−14.8] <sup>b</sup> SmC 73 [60.6] Cr
<b>A3F14</b>	14	F	H	<b>H:</b> Cr 88 [73.6] SmC 115 [18.9] Iso <b>C:</b> Iso 111 [−17.6] SmC 73 [−73.5] Cr
<b>A2F8</b>	8	H	F	<b>H:</b> Cr 96 [51.2] SmC 107 [3.6] N 116 [0.3] Iso <b>C:</b> Iso 110 [−0.2] N 105 [−2.1] SmC 88 [−50.6] Cr
<b>A2F10</b>	10	H	F	<b>H:</b> Cr 86 [80.5] SmC 102 [2.0] N 113 [5.3] Iso <b>C:</b> Iso 111 [−5.5] N 100 [−1.8] SmC 79 [−47.6] Cr
<b>A2F12</b>	12	H	F	<b>H:</b> Cr 93 [85.6] SmC 108 [16.4] <sup>b</sup> N 114 [16.4] <sup>b</sup> Iso <b>C:</b> Iso 110 [−14.4] <sup>b</sup> N 106 [−14.4] <sup>b</sup> SmC 79 [−49.8] Cr
<b>A2F14</b>	14	H	F	<b>H:</b> Cr 85 [66.7] SmC 110 [18.2] Iso <b>C:</b> Iso 108 [−15.4] SmC 75 [−48.5] Cr

<sup>a</sup> Peak temperatures as determined from 2nd heating (**H**) and 2nd cooling (**C**) DSC scans with rate 10 K min<sup>−1</sup>; abbreviations: Cr = crystalline solid; SmC = smectic C phase; SmA = smectic A phase; N = nematic phase; Cr = crystalline solid; Iso = isotropic liquid.

<sup>b</sup> The enthalpy value of Iso-N phase transition could not be separated from that of the N-SmC phase transition (see Fig. S5 in the SI).

variable chain lengths (the supramolecules **A10–A14** in Table 1) [41] and it was found that all of **An** complexes exhibit smectic C (SmC) phases regardless the alkoxy chain lengths in the proton acceptor. It was interesting for us to check how lateral fluorine substitution could affect the liquid crystalline behaviour of **An** complexes. To answer this question, we prepared different types of azopyridine derivatives without any fluorine substitution (**Hn**) [23] or with one fluorine substituent either at ortho position with respect to the terminal alkoxy chain (**3Fn**) [42] or at meta position with respect to the terminal alkoxy chain (**2Fn**) (see Scheme 1). All of the synthesized azopyridine derivatives (**Hn**, **3Fn** and **2Fn**) were found to be non-mesomorphic and were used as proton acceptors to prepare new fluorinated HBLCs by intermolecular H-bond formation with the mesomorphic 4-octyloxybenzoic acid (**A3Fn** and

**A2Fn**) to compare it with the previously reported **An** complexes. Moreover, the effect of removing the oxygen atom connecting the terminal chain on the benzoic acid on the LC behaviour of the synthesized HBLCs was investigated systemically by preparing other types of H-bonded aggregates (**Bn**, **B3Fn** and **B2Fn**) using the nematogenic 4-octylbenzoic acid as the proton donor instead of 4-octyloxybenzoic acid.

## 2. Experimental

### 2.1. Synthesis

The synthesis of the HBLCs is shown in Scheme 1. The benzoic acid derivatives are commercially available, while the azopyridine

**Table 2**  
Phase transition temperatures (T/°C), mesophase types, and transition enthalpies [ $\Delta H$  (J/g)] of the supramolecular HBLCs **Bn**, **B3Fn** and **B2Fn**<sup>a</sup>.

Complex	n	X	Y	Phase sequence (T/°C [ $\Delta H$ (J/g)])
<b>B8</b>	8	H	H	<b>H:</b> Cr 100 [48.5] SmA 124 [23.7] Iso <b>C:</b> Iso 121 [−23.4] SmA 88 [−47.4] Cr
<b>B10</b>	10	H	H	<b>H:</b> Cr 89 [35.7] SmC 105 [−] SmA 123 [24.8] Iso <b>C:</b> Iso 119 [−23.6] SmA 104 [−] SmC 77 [−34.9] Cr
<b>B12</b>	12	H	H	<b>H:</b> Cr 90 [33.4] SmC 119 [−] SmA 124 [27.6] Iso <b>C:</b> Iso 121 [−25.8] SmA 115 [−] SmC 81 [−16.6] Cr
<b>B14</b>	14	H	H	<b>H:</b> Cr 88 [30.7] SmC 122 [−] SmA 124 [28.1] Iso <b>C:</b> Iso 121 [−28.8] SmA 119 [−] SmC 89 [−8.4] SmX 79 [−13.3] Cr
<b>B3F8</b>	8	F	H	<b>H:</b> Cr 88 [47] SmC 102 [11.7] Iso <b>C:</b> Iso 99 [−11.7] SmC 71 [−43.6] Cr
<b>B3F10</b>	10	F	H	<b>H:</b> Cr 87 [53.2] SmC 101 [9.5] Iso <b>C:</b> Iso 96 [−10.9] SmC 72 [−55.3] Cr
<b>B3F12</b>	12	F	H	<b>H:</b> Cr 83 [49.2] SmC 106 [16.3] Iso <b>C:</b> Iso 102 [−14.9] SmC 68 [−52.2] Cr
<b>B3F14</b>	14	F	H	<b>H:</b> Cr 89 [64.1] SmC 106 [19.4] Iso <b>C:</b> Iso 103 [−18.0] SmC 74 [−63.8] Cr
<b>B2F8</b>	8	H	F	<b>H:</b> Cr 94 [53.4] Iso <b>C:</b> Iso 94 [−7.7] SmA 80 [−36.1] Cr
<b>B2F10</b>	10	H	F	<b>H:</b> Cr 90 [42.0] SmA 106 [19.6] Iso <b>C:</b> Iso 102 [−17.5] SmA 72 [−45.3] Cr
<b>B2F12</b>	12	H	F	<b>H:</b> Cr 84 [45.7] SmC 93 [−] SmA 108 [22.8] Iso <b>C:</b> Iso 105 [−21.6] SmA 92 SmC [−] 70 [−41.5] Cr
<b>B2F14</b>	14	H	F	<b>H:</b> Cr 83 [43.0] 95 SmC [−] SmA 108 [19.1] Iso <b>C:</b> Iso 104 [−20.6] SmA 94 SmC [−] 68 [−37.9] Cr

<sup>a</sup> Peak temperatures as determined from 2nd heating (**H**) and 2nd cooling (**C**) DSC scans with rate 10 K min<sup>−1</sup>; abbreviations: SmA = smectic A phase; SmX = unidentified smectic phase. For other abbreviations see Table 1.

derivatives with or without fluorine substitution were synthesized as described in the supporting information (SI) by a coupling reaction between the diazonium salt of 4-aminopyridine and phenol, 2-fluorophenol or 3-fluorophenol followed by etherification of the resulting azo dyes with different alkyl bromides to give the target proton acceptors. The analytical data for 4-(3-fluoro-4-dodecyloxyphenylazo)pyridine **3F12** and 4-(2-fluoro-4-dodecyloxyphenylazo)pyridine **2F12** are given below as representative examples. The supramolecular HBLCs (**An**, **A3Fn**, **A2Fn**, **Bn**, **B3Fn** and **B2Fn**) were prepared by mixing equimolar amounts of each of the azopyridine derivatives (**Hn**, **3Fn** or **2Fn**) and each of the benzoic acid derivatives (**OC8** or **C8**) and melting them together in a DSC pan with stirring to give an intimate blend then cooling to room temperature. The obtained crystals were then melted, and the process was repeated two additional times. Homogenous melting and reproducible phase transition temperatures were observed for all complexes (Table 1).

#### 2.1.1. 4-(3-Fluoro-4-dodecyloxyphenylazo)pyridine, **3F12**

Orange crystals. Melting point: 66 °C, 0.58 g, 68% yield.  $^1\text{H NMR}$  (500 MHz,  $\text{CDCl}_3$ )  $\delta$  8.86–8.68 (m, 2H, Ar–H), 7.82 (ddd,  $J = 8.7, 2.4, 1.3$  Hz, 1H, Ar–H), 7.72 (dd,  $J = 11.9, 2.3$  Hz, 1H, Ar–H), 7.69–7.63 (m, 2H, Ar–H), 7.09 (t,  $J = 8.6$  Hz, 1H, Ar–H), 4.14 (t,  $J = 6.6$  Hz, 2H, O–CH<sub>2</sub>), 2.07–1.70 (m, 2H, O–CH<sub>2</sub>–CH<sub>2</sub>), 1.55–1.15 (m, 18H, CH<sub>2</sub>), 0.88 (t,  $J = 6.9$  Hz, 3H, CH<sub>3</sub>).  $^{13}\text{C NMR}$  (126 MHz,  $\text{CDCl}_3$ )  $\delta$  157.07, 153.86, 151.88, 151.30, 151.24, 151.15, 146.23 (d,  $J = 5.6$  Hz), 124.28 (d,  $J = 2.9$  Hz), 116.15, 113.39 (d,  $J = 2.3$  Hz), 107.89 (d,  $J = 19.5$  Hz), 69.57, 31.89, 29.63, 29.55, 29.51, 29.32, 29.30, 29.01, 25.86, 22.66, 14.09.  $^{19}\text{F NMR}$  (470 MHz,  $\text{CDCl}_3$ )  $\delta$  –132.38 (dd,  $J = 11.9, 8.4$  Hz). **MS (ESI)**:  $m/z$  (%): positive: 408.2421 ( $[\text{M} + \text{Na}]^+$ ,  $\text{C}_{23}\text{H}_{32}\text{FN}_3\text{O} + \text{Na}^+$ , calc.:  $m/z = 408.24$ ).

#### 2.1.2. 4-(2-Fluoro-4-dodecyloxyphenylazo)pyridine, **2F12**

Orange crystals. Melting point: 67 °C, 0.50 g, 56% yield.  $^1\text{H NMR}$  (500 MHz,  $\text{CDCl}_3$ )  $\delta$  8.91–8.61 (m, 2H, Ar–H), 7.81 (m, 1H, Ar–H), 7.71–7.62 (m, 2H, Ar–H), 6.88–6.62 (m, 2H, Ar–H), 4.04 (t,  $J =$

6.5 Hz, 2H, O–CH<sub>2</sub>), 1.82 (m, 2H, O–CH<sub>2</sub>CH<sub>2</sub>), 1.51–1.42 (m, 2H, CH<sub>2</sub>), 1.41–1.21 (m, 16H, CH<sub>2</sub>), 1.05–0.73 (m, 3H, CH<sub>3</sub>).  $^{13}\text{C NMR}$  (126 MHz,  $\text{CDCl}_3$ )  $\delta$  164.46, 164.37, 163.37, 161.30, 157.47, 151.27, 134.74 (d,  $J = 7.0$  Hz), 118.66, 116.22, 111.61 (d,  $J = 2.7$  Hz), 102.33 (d,  $J = 23.3$  Hz), 68.98, 31.89, 29.63, 29.61, 29.55, 29.51, 29.32, 29.29, 28.95, 25.90, 22.66, 14.09.  $^{19}\text{F NMR}$  (470 MHz,  $\text{CDCl}_3$ )  $\delta$  –116.75 to –121.48 (m). **MS (ESI)**:  $m/z$  (%): positive: 408.2422 ( $[\text{M} + \text{Na}]^+$ ,  $\text{C}_{23}\text{H}_{32}\text{FN}_3\text{O} + \text{Na}^+$ , calc.:  $m/z = 408.24$ ).

### 3. Characterization

Thin layer chromatography (TLC) was performed on aluminium sheet precoated with silica gel. Analytical quality chemicals were obtained from commercial sources and used as obtained. The solvents were dried using the standard methods when required. The purity and the chemical structures of all synthesized materials were confirmed by the spectral data. The structure characterization of the prepared materials is based on  $^1\text{H NMR}$ ,  $^{13}\text{C NMR}$ ,  $^{19}\text{F NMR}$  (Varian Unity 400 spectrometers, in  $\text{CDCl}_3$  solution, with tetramethylsilane as internal standard) and high resolution mass spectroscopy.

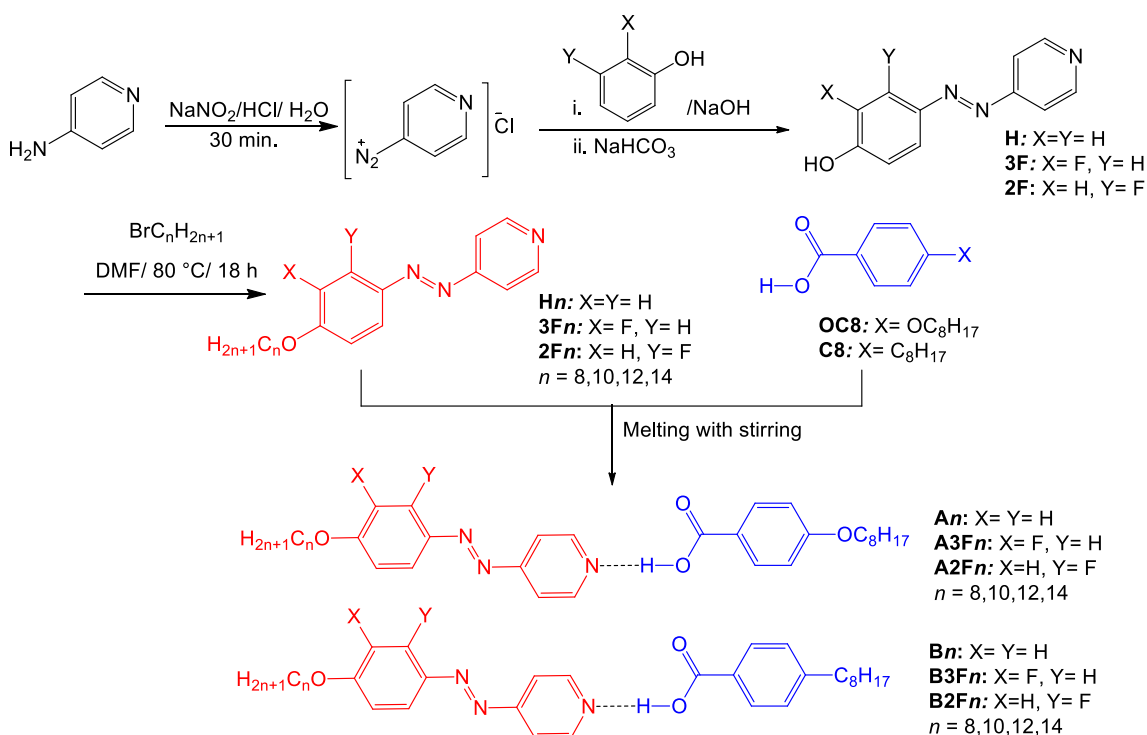
Infrared absorption spectra were measured in dry KBr with a Perkin-Elmer B25 spectrophotometer.

The mesophase behaviour and transition temperatures of the supramolecular complexes were measured using a Mettler FP-82 HT hot stage and control unit in conjunction with a Nikon Optiphot-2 polarizing microscope. The associated enthalpies were obtained from DSC-thermograms which were recorded on a Perkin-Elmer DSC-7, heating and cooling rate: 10 K min<sup>-1</sup>.

### 4. Results and discussion

#### 4.1. FTIR and NMR measurements

As an effective tool to investigate the intermolecular interactions [43,44,16], FTIR spectroscopy was performed for the supramolecule



**Scheme 1.** Synthesis of the azopyridines (**Hn**, **3Fn** and **2Fn** and **23F8**) and the hydrogen-bonded supramolecules (**An**, **A3Fn**, **A2Fn**, **Bn**, **B3Fn** and **B2Fn**).

**B2F14** as a representative example for the prepared HBLCs in crystalline state (KBr) at room temperature to prove the formation of the hydrogen-bond between the benzoic acid derivatives and the azopyridines. Fig. 1a, b shows the IR spectra of **B2F14** and its complementary components the azopyridine derivative **2F14** and the proton donor **C8** at two different regions (see Figs. S1–S3 in the SI for the complete range of spectra).

The absence of a band at around  $3000\text{ cm}^{-1}$  together with the appearance of two bands at around  $2479\text{ cm}^{-1}$  and  $1888\text{ cm}^{-1}$  (black curve in Fig. 1a) clearly indicate the formation of 1:1 hydrogen-bonded complex between the azopyridine derivative **2F14** and the benzoic acid **C8** [26,31]. Moreover, the carbonyl stretching vibration band of the pure benzoic acid **C8** which is present in a dimeric form as a result of the intermolecular hydrogen-bond formation between the free carboxylic groups is observed at around  $1680\text{ cm}^{-1}$  (blue curve in Fig. 1b) and upon complexation with the proton acceptor **2F14** it is shifted to higher value  $\sim 1693\text{ cm}^{-1}$  (i.e. blue shifted, black curve in Fig. 1b). This indicates the formation of another intermolecular hydrogen bond between the monomeric form of **C8** and the pyridine based derivative **2F14** which also confirms the formation of the supramolecule **B2F14** [26,31,45].

Whereas IR confirms complex formation in the solid state,  $^1\text{H}$  NMR spectroscopy was used to prove the hydrogen-bond formation in solution. Fig. 2 shows the  $^1\text{H}$  NMR spectroscopy in the aromatic region of the supramolecule **A3F14** and its complementary components the proton donor **OC8** and the proton acceptor **3F14** as representative examples (See Fig. S4 for the complete  $^1\text{H}$  NMR spectra).

The spectra of the proton acceptor **3F14** shows that the signal corresponding to the hydrogen atoms at ortho positions to the nitrogen atom in the pyridine ring appears at  $\delta$  8.86–8.68 ppm (red curve in Fig. 2) and upon hydrogen bond formation it becomes broad and shifted to  $\delta$  8.89–8.74 ppm (black curve in Fig. 2). Also, the signal appearing at  $\delta$  7.68 ppm in the pure azopyridine-based component **3F14** which corresponds to the protons at meta positions to the nitrogen atom in the pyridine ring is slightly low field shifted and overlaps with the hydrogens at the fluorinated ring after complexation and become more closer to each other's (compare the red and black curves in Fig. 2).

#### 4.2. Liquid crystalline behaviour of **An**, **A3Fn** and **A2Fn**

The phase transition temperatures and types of LC phases of the prepared HBLCs are revealed based on DSC measurements and textural observations under PLM. The obtained data for **An**, **A3Fn** and **A2Fn** are summarized in Table 1 and represented graphically on Fig. 3a–c, while those of **Bn**, **B3Fn** and **B2Fn** are collected in Table 2 and plotted on Fig. 3d–f. As representative examples the DSC traces of **A3F14** and **B14** are shown in Fig. 4.

The benzoic acid derivative used to prepare the first type of the HBLCs i.e. 4-octyloxybenzoic acid forms smectic C (SmC) and nematic (N) phases in the following sequence: Cr  $101^\circ\text{C}$  SmC  $107^\circ\text{C}$  N  $147^\circ\text{C}$  Iso, while all of the individual azopyridine derivatives are nonmesomorphic and melts directly to isotropic liquids (see Table S1 in the SI). As can be seen from Table 1 the nonfluorinated HBLCs (**An**) exhibit only SmC phases as enantiotropic mesophases and the nematic phase is not observed for any of **An** derivatives [41].

The HBLCs **A3Fn** having a fluorine atom at ortho position next to the terminal chain at the azopyridine derivatives show different phase behaviour (Fig. 3b). For the shortest complex **A3F8** an enantiotropic LC phase is observed over  $\sim 20\text{ K}$ , which show typical observation of the conventional nematic phase (N) with a characteristic schlieren texture containing two- and four-point brush singularities in untreated cells (Fig. 5a). On cooling **A3F8** from the isotropic liquid the nematic phase is observed followed by a monotropic SmC phase (Fig. 5b). This transition is accompanied by an enthalpy transition value in the DSC cooling curve of **A3F8** indicating a first order transition (Table 1). On chain elongation and for the next homologue (**A3F10**) the SmC phase becomes an

enantiotropic LC phase with wider range compared to that observed for **A3F8** and on further chain elongation the range of the SmC phase becomes more wider on the expense of the nematic phase. For the supramolecules with  $n = 10$  and  $12$  the transition enthalpy values for the SmC–N and N–Iso transitions on heating and cooling scans cannot be separated from each other's (see Table 1 and Fig. S5 in the SI). For the longest complex **A3F14** the nematic phase is totally removed and the SmC phase is the only observed mesophase. The range of the SmC phase of **A14** is wider than that of the fluorinated supramolecules **A3Fn**. This also applies for all **An** complexes compared to **A3Fn** irrespective of the terminal chain length on the azopyridine segment.

Changing the position of the lateral fluorine atom from ortho position with respect to the terminal chain on the proton acceptors i.e. the azopyridine derivatives to be at meta position leads to the **A2Fn** complexes. The phase behaviour of **A2Fn** complexes is very similar to that of **A3Fn** complexes (Fig. 5c and Fig. S6 in the SI), however the SmC phase is more stabilized and is observed as enantiotropic phase starting from the shortest homologue **A2F8**.

#### 4.3. Liquid crystalline behaviour of **Bn**, **B3Fn** and **B2Fn**

In order to investigate the effect of removing the oxygen atom connecting the terminal octyl chain to the benzoic acid on the

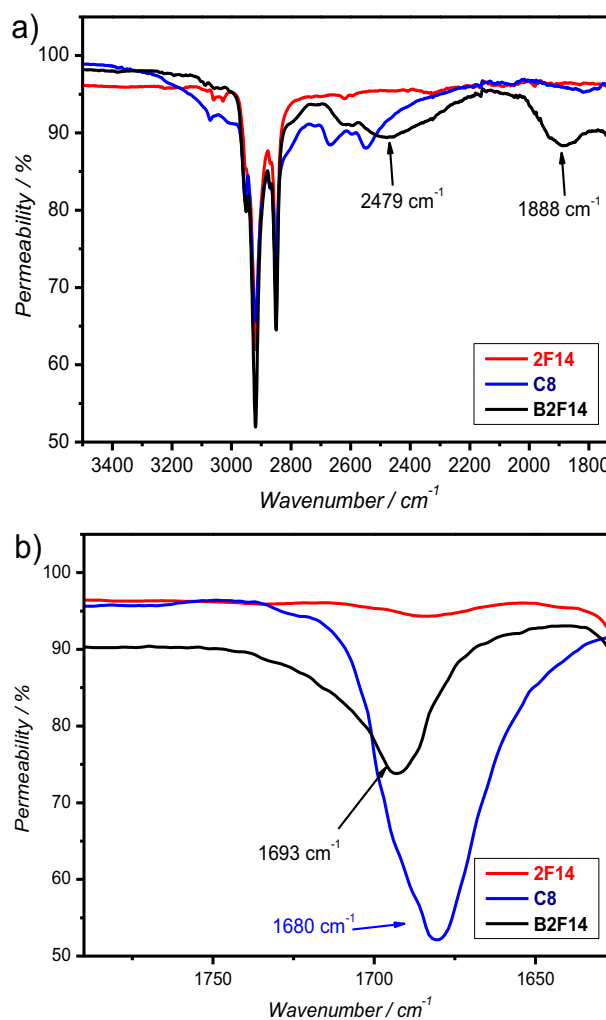


**Fig. 1.** FTIR spectra of the supramolecule **B2F14** (black) and its complementary components **C8** (blue) and **2F12** (red) in the crystalline state (KBr) at room temperature: a) enlarged area between  $1700\text{ cm}^{-1}$  and  $3500\text{ cm}^{-1}$ ; b) enlarged area between  $1630\text{ cm}^{-1}$  and  $1790\text{ cm}^{-1}$ . (For interpretation of the references to colour in this figure legend, the reader is referred to the web version of this article.)

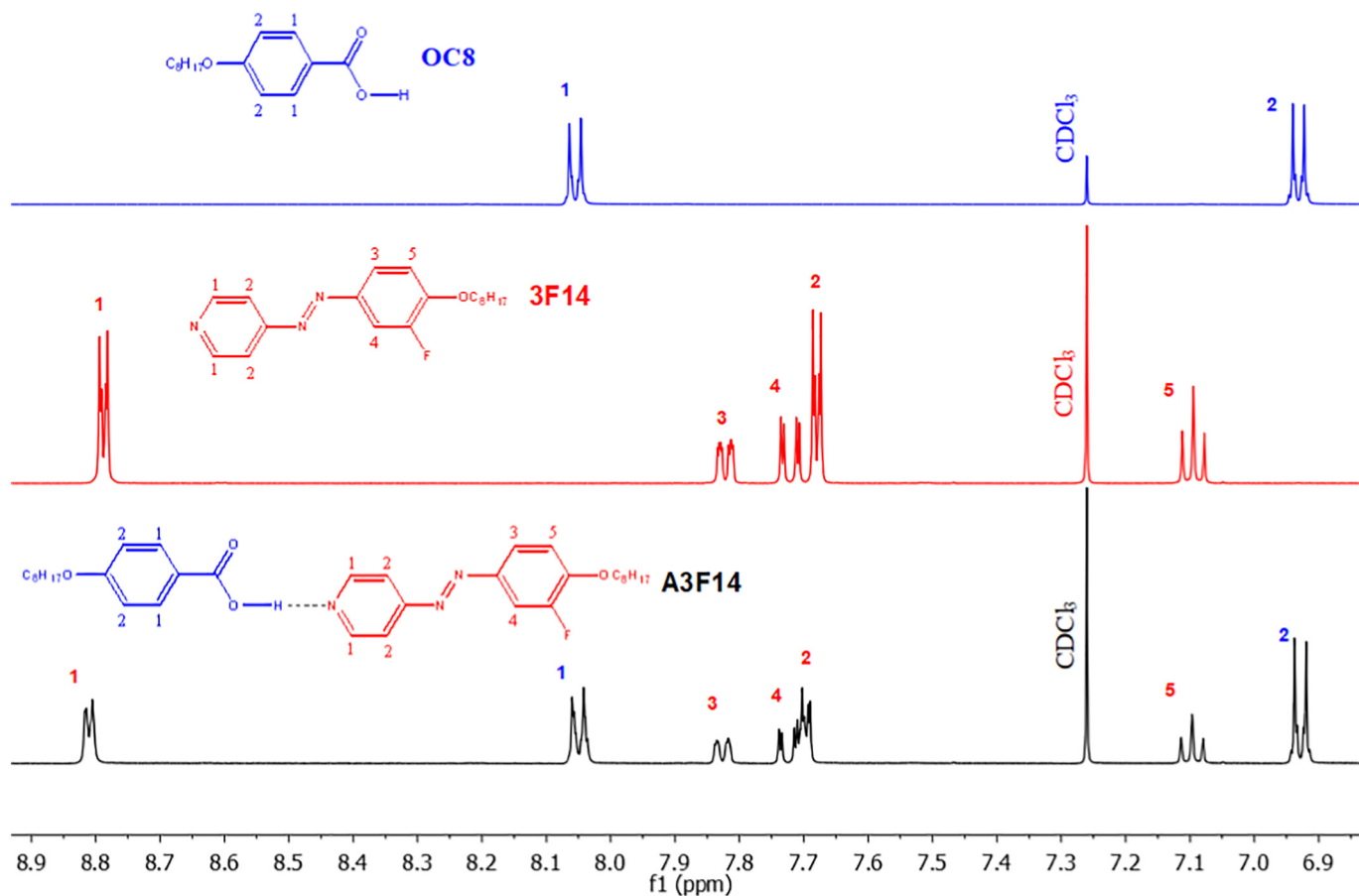


**Fig. 2.**  $^1\text{H}$  NMR spectra (500 MHz,  $\text{CDCl}_3$ ) in the aromatic region of the supramolecule **A3F14** (black) and its complementary components **OCS** (blue) and **3F14** (red). The blue numbers are for the benzoic acid **OCS** protons and the red numbers are for the azopyridine **3F14** protons before and after complexation. (For interpretation of the references to colour in this figure legend, the reader is referred to the web version of this article.)

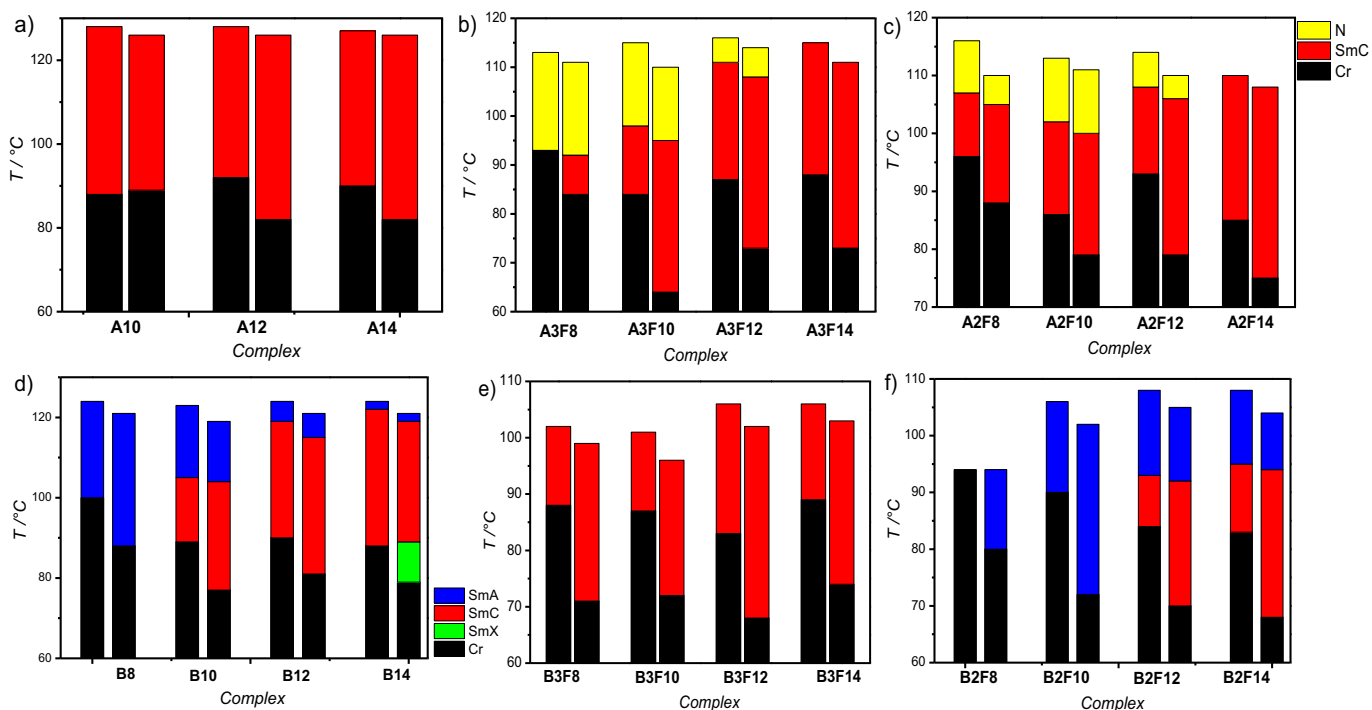


**Fig. 3.** Phase diagrams of the supramolecular HBLCs: a) **A1n** [41], b) **A3Fn**, c) **A2Fn**, d) **Bn**, e) **B3Fn** and f) **B2Fn**. The phase types are shown in c) and d).

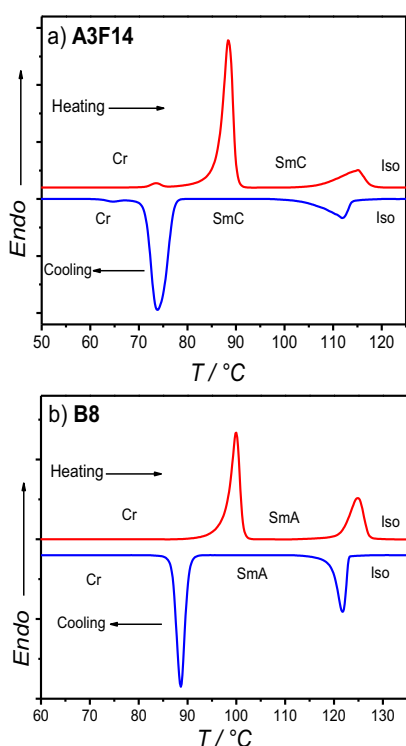


Fig. 4. DSC traces of a) **A3F14** and b) **B8** with heating and cooling rates 10 K/min.

mesophase behaviour of the HBLCs **An**, **A3Fn** and **A2Fn** we prepared another related H-bonded complexes (**Bn**, **B3Fn** and **B2Fn**) using 4-octylbenzoic acid as the proton donor instead of 4-octyloxybenzoic acid. The results prove that this slight modification has a great effect on the liquid crystalline behaviour of the HBLCs. The pure 4-octylbenzoic acid (**C8**) exhibits only a nematic phase in the following sequence: Cr 100 °C N 109 °C Iso, while all of the HBLCs do not exhibit N phases and form different types of mesophases.

As can be seen from Table 2 and Fig. 3d–f the nonfluorinated HBLCs (**Bn**) exhibit three different types of mesophases depending on the chain length and temperatures. For the shortest homologue **B8** only SmA phase is observed based on the textural observations (see Fig. 6 as an example), where totally isotropic texture is observed on the homeotropic cell and a truncated focal conic fan texture is observed in the planar cell confirming the presence of a SmA phase. For the next longer homologues **B10–B14** (with  $n \geq 10$ ) SmC phase starts to appear below the SmA phase as indicated from the DSC traces (Table 1) and the change in the optical textures under the PLM. The range of the SmC phase increases with chain elongation, while that of the SmA phase is suppressed (see Fig. 3d).

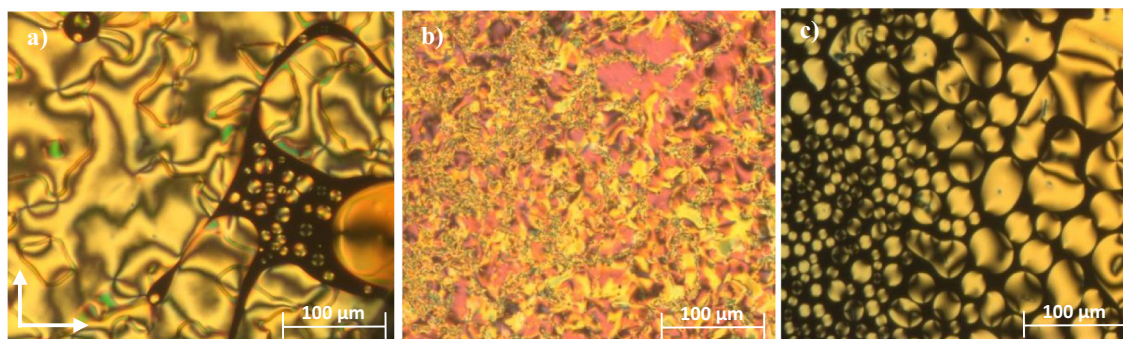


Fig. 5. Photomicrographs of: **A3F8** in a) the N phase at 108 °C and in b) the SmC phase at 89 °C and c) **A2F10** in the N phase at 110 °C. The direction of the polarizers is shown in a).

As shown in Fig. 6a, b at the transition to the SmC phase from the SmA phase the birefringence in the homeotropic cell suddenly increases indicating the tilt of the molecules, while in the planar cell the fan shaped textures become broken as typically observed for SmC phases. The orientation of the extinctions becomes inclined with the directions of polarizer and analyzer indicating a synclinc SmC phase. On further cooling **B14** from the SmC phase the birefringence changes again at ~89 °C on both homeotropic and planar cells indicating the transition to another LC phase (Fig. 6c, f). The formation of this phase is associated with a large enthalpy change ~8.4 J/g (Table 2), indicating the formation of additional monotropic highly ordered unidentified smectic LC phase assigned as SmX phase below the SmC phase for the longest homologue. As the inclination of the extinctions is retained a transition to a tilted low temperature hexatic (HexI) or crystalline mesophases (CrI/G) is likely. The schlieren texture in Fig. 6c is in favour for a HexI phase, whereas the CrI/G phases are known to prefer moasic like textures [46].

Using 4-(3-fluoro-4-alkoxyphenylazo)pyridines (**3Fn**) as proton donors leads to **B3Fn** HBLCs having a fluorine substituent at ortho position with respect to the terminal alkoxy chain at the azopyridine side. All derivatives of **B3Fn** complexes show only enantiotropic SmC mesophases with comparable melting and clearing temperatures. Changing the position of the fluorine atom to be in meta position leads to the formation of **B2Fn** complexes. The shortest complex **B2F8** melts directly to the isotropic liquid on heating from the crystalline solid and on cooling it exhibits short range of the SmA phase. The SmA phase converts to an enantiotropic phase for all next longer homologues (with  $n \geq 10$ ) which appears as the only mesophase for the complex **B2F10** and beside SmC phases for **B2F12** and **B2F14**.

The results obtained for the prepared supramolecular aggregates indicate that for both types of complexes **An** or **Bn** without fluorine substitution core fluorination leads to lower clearing temperatures (Fig. 3) i.e. lower mesophase stability. However, the type of the mesophases exhibited by HBLCs could be modified by fluorination. Therefore, for the fluorinated complexes **A3Fn** and **A2Fn** nematic and SmC phases were observed, while the nonfluorinated supramolecules **An** exhibit only SmC phases. The same effect was also observed for the other types of the complexes **Bn**, **B3Fn** and **B2Fn**, where the SmA phases are exhibited by the HBLCs or suppressed depending on the position of the fluorine substitution (Fig. 3d–f).

## 5. Photosensitivity

The prepared supramolecular complexes were designed to be photosensitive due to the presence of the azopyridine segments in its molecular structures. We found that all of the prepared HBLCs are photosensitive and undergo a fast and reversible isothermal phase transition upon illumination with a UV laser pointer (405 nm, 5 mW/mm<sup>2</sup>). This is due to the *trans-cis* photoisomerization of the azo unit upon photo illumination. The photosensitivity of the supramolecule **B10** will be discussed here in details as a representative example (see Fig. S7 in

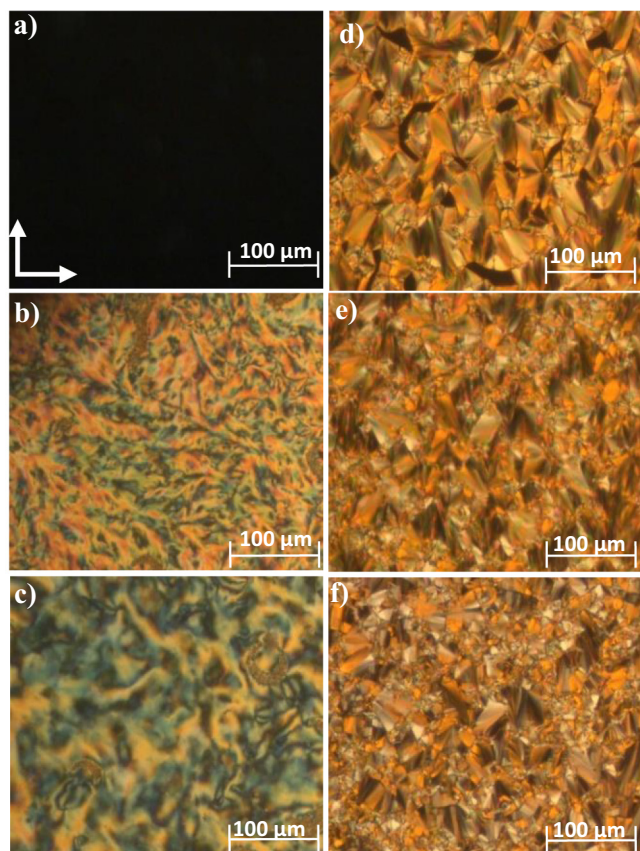


**Fig. 6.** Optical textures of the supramolecular complex **B14** a–c) in homeotropic cell and d–f) in 10 μm ITO coated cell: a, d) in SmA phase at 120 °C; b),e) in SmC phase at 95 °C and c, f) in the SmX phase at 88 °C. The direction of the polarizers is shown in a).

the SI for UV–Vis spectroscopy in solution). **B10** exhibits enantiotropic SmC and SmA phases, therefore we investigated the photoinduced SmC–SmA and SmA–Iso phase transitions in homeotropic cells. The SmC phase has a birefringent homeotropic texture under crossed polarizers prior to the UV illumination (Fig. 7a). Under UV irradiation and at 5 K below the SmC–SmA transition temperature i.e. ~99 °C the birefringent textures disappeared and converts within 3 s into the totally dark homeotropic texture of the uniaxial SmA phase (Fig. 7b). On removing the UV source, the dark texture relaxes back to the original SmC texture in few seconds, indicating a fast and reversible photoinduced phase transition between the SmC and SmA phases. Similar photoinduced phase transition was also achieved between the SmA phase

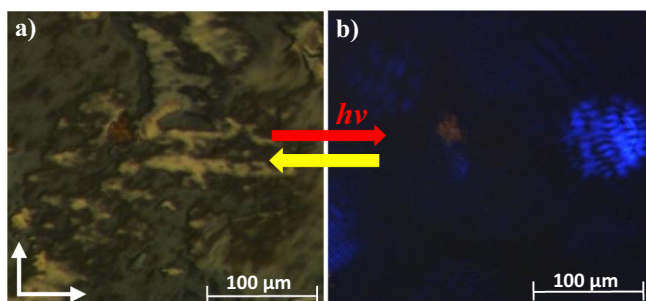


**Fig. 7.** Textures of the supramolecular complex **B10** under crossed polarizers: a) in the homeotropic aligned SmC phase at  $T = 99$  °C before UV irradiation and b) after UV irradiation indicating the transformation from the biaxial SmC phase to the uniaxial SmA phase. The blue colour in b) is due to the UV light. (For interpretation of the references to colour in this figure legend, the reader is referred to the web version of this article.)

and the isotropic liquid phase. Therefore, the SmC–SmA or SmA–Iso transitions achieved upon UV irradiation both resulting from *trans*–*cis* photoisomerization between the more stable *trans* form of the azopyridines before light irradiation and the less stable *cis* form after irradiation [4].

## 6. Summary and conclusions

In summary, we have reported herein the design and synthesis of new azopyridine derivatives which have been used to prepare new photosensitive supramolecular liquid crystals via intermolecular hydrogen bond formation with two different types of benzoic acid derivatives. The formation of the supramolecular HBLCs was confirmed by FTIR,  $^1\text{H}$  NMR, DSC and PLM. Where all the azopyridine derivatives are crystalline solids, all their H-bonded aggregates exhibit LCs phases. They show rich mesomorphism depending on the position of the lateral fluorine substituent, on the terminal chain length and on the type of the proton donor. The supramolecules derived from 4-octyloxybenzoic acid and non-fluorinated azopyridines exhibit only SmC phases irrespective of the terminal chain length (**An** complexes). Using fluorine substituted azopyridines either at ortho or meta positions with respect to the terminal chains as the proton acceptors with 4-octyloxybenzoic acid (**A3Fn** and **A2Fn** complexes) results in additional nematic phases beside the SmC phases for short and medium chains supramolecules (with  $n = 8$ –12). Removing the oxygen atom connecting the terminal octyl chain to the benzoic acid results in the related HBLCs **Bn**, **B3Fn** and **B2Fn** constructed using 4-octylbenzoic acid as the proton donor instead of 4-octyloxybenzoic acid. The later complexes do not exhibit nematic phases but form SmA, SmC phases, and in one case of a non-fluorinated complex an additional unidentified low temperature smectic phase assigned as SmX. The effect of changing the position of the lateral fluorine substituent was found to be more pronounced in these types of complexes, where ortho fluorinated complexes (**B3Fn**) exhibit SmC phases and their related meta fluorinated complexes (**B2Fn**) exhibit SmA and SmC phases. Moreover, all of the prepared complexes show fast and reversible photoinduced LCs phase transitions under UV irradiation due to *trans*–*cis* photoisomerization of the azopyridine units. Therefore, the transition between different types of LCs phases or between the LCs phases and the isotropic liquid could be affected with UV light, which provide additional possibility of phase modulation by interaction with light.

## CRedit authorship contribution statement

**Mohamed Alaasar:** Conceptualization, Supervision, Writing - original draft, Writing - review & editing. **Jaques-Christopher Schmidt:** Investigation. **Ahmed F. Darweesh:** Investigation. **Carsten Tschierske:** Writing - review & editing.

## Declaration of competing interest

The authors declare no conflict of interest.

## Acknowledgements

Ahmed F. Darweesh acknowledges the support by the Alexander von Humboldt Foundation for the research fellowship at Martin Luther University Halle-Wittenberg, Germany.

## Appendix A. Supplementary data

Supplementary data to this article can be found online at <https://doi.org/10.1016/j.molliq.2020.113252>.

## References

- [1] H.L. Nguyen, P.N. Horton, M.B. Hursthouse, A.C. Legon, D.W. Bruce, Halogen bonding: a new interaction for liquid crystal formation, *J. Am. Chem. Soc.* 126 (1) (2004) 16–17.
- [2] P. Metrangolo, C. Prasang, G. Resnati, R. Liantonio, A.C. Whitwood, D.W. Bruce, Fluorinated liquid crystals formed by halogen bonding, *Chem. Commun.* (2006) 3290–3292.
- [3] Prasang, H.L. Nguyen, P.N. Horton, A.C. Whitwood, D.W. Bruce, Trimeric liquid crystals assembled using both hydrogen and halogen bonding, *Chem. Commun.* (2008) 6164–6166.
- [4] M. Alaasar, S. Poppe, C. Tschierske, Photoresponsive halogen bonded polycatenar liquid crystals, *J. Mol. Liq.* 277 (2019) 233–240.
- [5] H. Wang, H.K. Bisoyi, L. Wang, A.M. Urbas, T.J. Bunning, Q. Li, Photochemically and thermally driven full-color reflection in a self organized helical superstructure enabled by a halogen-bonded chiral molecular switch, *Angew. Chem. Int. Ed.* 57 (2018) 1627–1631.
- [6] M. Saccone, L. Catalano, Halogen bonding beyond crystals in materials science, *J. Phys. Chem. B* 123 (2019) 9281–9290.
- [7] C.M. Paleos, D. Tsiourvas, Supramolecular hydrogen-bonded liquid crystals, *Liq. Cryst.* 28 (2001) 1127–1161.
- [8] T. Kato, in: D. Demus, J.W. Goodby, G.W. Gray, H.-W. Spiess, V.V. Vill (Eds.), *Handbook of Liquid Crystals*, 2B, Wiley-VCH, Weinheim 1998, p. 969.
- [9] T. Kato, T. Uryu, F. Kaneuchi, C. Jin, J.M.J. Frechet, Hydrogen-bonded liquid crystals built from hydrogen-bonding donors and acceptors infrared study on the stability of the hydrogen bond between carboxylic acid and pyridyl moieties, *Liq. Cryst.* 33 (2006) 1434–1437.
- [10] T. Kato, J.M.J. Frechet, A new approach to mesophase stabilization through hydrogen bonding molecular interactions in binary mixtures, *J. Am. Chem. Soc.* 111 (1989) 8533–8534.
- [11] U. Kumar, T. Kato, J.M.J. Frechet, Use of intermolecular hydrogen bonding for the induction of liquid crystallinity in the side chain of polysiloxanes, *J. Am. Chem. Soc.* 114 (1992) 6630–6639.
- [12] Naoum, A. Fahmi, M. Alaasar, Supramolecular hydrogen-bonded liquid crystals formed from 4-(4'-Pyridylazophenyl)-4"-substituted benzoates and 4-alkoxy benzoic acids, *Mol. Cryst. Liq. Cryst.* 482 (2008) 57–70.
- [13] H.A. Ahmed, M. Hagar, M. Alaasar, M. Naoum, Wide nematic phases induced by hydrogen-bonding, *Liq. Cryst.* 46 (2019) 550–559.
- [14] M.B. Ros Gimeno, J.L. Serrano, M.R. De la Fuente, Hydrogen-bonded banana liquid crystals, *Angew. Chem. Int. Ed.* 43 (2004) 5235–5238.
- [15] M. Gimeno, B. Ros, J.L. Serrano, Noncovalent interactions as a tool to design new bent-core liquid-crystal materials, *Chem. Mater.* 20 (2008) 1262–1271.
- [16] M. Alaasar, C. Tschierske, M. Prehm, Hydrogen-bonded supramolecular complexes formed between isophthalic acid and pyridine-based derivatives, *Liq. Cryst.* 38 (2011) 925–934.
- [17] J. Wang, Y. Shi, K. Yang, J. Wei, J. Guo, Stabilization and optical switching of liquid crystal blue phase doped with azobenzene-based bent shaped hydrogen-bonded assemblies, *RSC Adv.* 5 (2015) 67357–67364.
- [18] M.K. Paul, P. Paul, S.K. Saha, S. Choudhury, Bent shaped H-bonded mesogens derived from 1,5-bis(4-hydroxyphenyl) penta-1,4-dien-3-one: synthesis, photophysical, mesomorphism and computational studies, *J. Mol. Liq.* 197 (2014) 226–235.
- [19] B. Korkmaz, N.C. Yilmaz, Z.G. Özdemir, M. Okutan, Y.H. Gursel, A. Sarac, B.F. Senkal, Synthesis and electrical properties of hydrogen bonded liquid crystal polymer, *J. Mol. Liq.* 219 (2016) 1030–1035.
- [20] M. Pfletscher, C. Wölper, J.S. Gutmann, M. Mezger, M. Giese, A modular approach towards functional supramolecular aggregates - subtle structural differences inducing liquid crystallinity, *Chem. Commun.* 52 (2016) 8549–8552.
- [21] M. Alaasar, C. Tschierske, Nematic phases driven by hydrogen-bonding in liquid crystalline nonsymmetric dimers, *Liq. Cryst.* 46 (2019) 124–130.
- [22] R. Walker, D. Pocięcha, J.P. Abberley, A. Martinez-Felipe, D.A. Paterson, E. Forsyth, G.B. Lawrence, P.A. Henderson, J.M.D. Storey, E. Gorecka, C. Imrie, Spontaneous chirality through mixing achiral components: a twist-bend nematic phase driven by hydrogen-bonding between unlike components, *Chem. Commun.* 54 (2018) 3383–3386.
- [23] M. Alaasar, S. Poppe, Q. Dong, F. Liu, C. Tschierske, Mirror symmetry breaking in cubic phases and isotropic liquids driven by hydrogen bonding, *Chem. Commun.* 52 (2016) 13869–13872.
- [24] H. Yu Chen, M. Quan, L. Zhang, H. Yang, Y. Lu, Photothermal effect of azopyridine compounds and their applications, *RSC Adv.* 5 (2015) 4675–4680.
- [25] J. Garcia-Amorós, M. Reig, A. Cuadrado, M. Ortega, S. Nonell, D. Velasco, A photoswitchable bis-azo derivative with a high temporal resolution, *Chem. Commun.* 50 (2014) 11462–11464.
- [26] H. Yu Chen, L. Zhang, H. Yang, Y. Lu, Photoresponsive liquid crystals based on halogen bonding of azopyridines, *Chem. Commun.* 50 (2014) 9647–9649.
- [27] M. Zaremba, V. Siksnys, Molecular scissors under light control, *Proc. Natl. Acad. Sci. U. S. A.* 107 (2010) 1259–1260.
- [28] K.M. Lee, T.J. White, Photomechanical response of composite structures built from azobenzene liquid crystal polymer networks, *Polymers* 3 (2011) 1447–1457.
- [29] J. Garcia-Amorós, M. Reig, M.C.R. Castro, A. Cuadrado, M.M.M. Raposo, D. Velasco, et al., Molecular photo-oscillators based on highly accelerated heterocyclic azo dyes in nematic liquid crystals, *Chem. Commun.* 50 (2014) 6704–6706.
- [30] M. Alaasar, Azobenzene-containing bent-core liquid crystals: an overview, *Liq. Cryst.* 43 (2016) 2208–2243.
- [31] H.K. Bisoyi, Q. Li, Light-driven liquid crystalline materials: from photo-induced phase transitions and property modulations to applications, *Chem. Rev.* 116 (2016) 15089–15166.
- [32] B.N. Sunil, M.K. Srinatha, G. Shanker, G. Hegde, M. Alaasar, C. Tschierske, Effective tuning of optical storage devices using photosensitive bent-core liquid crystals, *J. Mol. Liq.* 304 (2020) 112719.
- [33] M. Hird, Fluorinated liquid crystals - properties and applications, *Chem. Soc. Rev.* 36 (2007) 2070–2095.
- [34] C. Tschierske, Fluorinated liquid crystals: design of soft nanostructures and increased complexity of self-assembly by perfluorinated segments, *Liq. Cryst.* 318 (2011) 1–108.
- [35] M. Alaasar, M. Prehm, C. Tschierske, Influence of halogen substituent on the mesomorphic properties of five-ring banana-shaped molecules with azobenzene wings, *Liq. Cryst.* 40 (2013) 656–668.
- [36] M. Saccone, K. Kuntze, Z. Ahmed, A. Siiskonen, M. Giese, A. Priimagi, Orthofluorination of azophenols increases the mesophase stability of photoresponsive hydrogen-bonded liquid crystals, *J. Mater. Chem. C* 6 (2018) 9958–9963.
- [37] M. Saccone, M. Pfletscher, E. Dautzenberg, R.Y. Dong, C.A. Michal, M. Giese, Hydrogen-bonded liquid crystals with broad-range blue phases, *J. Mater. Chem. C* 7 (2019) 3150–3153.
- [38] M. Alaasar, M. Prehm, C. Tschierske, Mirror symmetry breaking in fluorinated bent-core mesogens, *RSC Adv.* 6 (2016) 82890–82899.
- [39] M. Alaasar, M. Prehm, S. Poppe, C. Tschierske, Development of polar order by liquid-crystal self-assembly of weakly bent molecules, *Chem. -A Eur. J.* 23 (2017) 5541–5556.
- [40] M. Alaasar, M. Prehm, Y. Cao, F. Liu, C. Tschierske, Spontaneous mirror-symmetry breaking in isotropic liquid phases of photoisomerizable achiral molecules, *Angew. Chem. Int. Ed.* 128 (2016) 320–324.
- [41] X. Song, J. Li, S. Zhang, Supramolecular liquid crystals induced by intermolecular hydrogen bonding between benzoic acid and 4-(alkoxyphenylazo)pyridines, *Liq. Cryst.* 30 (2003) 331–335.
- [42] M. Spengler, R.Y. Dong, C.A. Michal, W.Y. Hamad, M.J. MacLachlan, M. Giese, Hydrogen-bonded liquid crystals in confined spaces-toward photonic hybrid materials, *Adv. Funct. Mater.* 28 (2018) 1800207–1800217.
- [43] D. Bruce, P. Metrangolo, F. Meyer, C. Prasang, G. Resnati, G. Terraneo, A. Whitwood, Mesogenic, trimeric, halogen-bonded complexes from alkoxystilbazoles and 1,4-diiodotetrafluorobenzene, *New J. Chem.* 32 (2008) 477–482.
- [44] A. Martinez-Felipe, G. Cook, J.P. Abberley, R. Walker, J.M.D. Storey, C.T. Imrie, An FT-IR spectroscopic study of the role of hydrogen bonding in the formation of liquid crystallinity for mixtures containing bipyridines and 4-pentoxibenzoic acid, *RSC Adv.* 6 (2016) 108164–108179.
- [45] Y. Arakawa, Y. Sasaki, K. Igawa, H. Tsuji, Hydrogen bonding liquid crystalline benzoic acids with alkylthio groups: phase transition behavior and insights into the cybotactic nematic phase, *New J. Chem.* 41 (2017) 6514–6522.
- [46] G.W. Gray, J.W. Goodby, *Smectic Liquid Crystals*, Leonard Hill, Glasgow, 1984.

## Hydrogen-bonded supramolecular complexes formed between isophthalic acid and pyridine-based derivatives

Mohamed Alaasar<sup>a\*</sup>, Carsten Tschierske<sup>b</sup> and Marko Prehm<sup>b</sup>

<sup>a</sup>Department of Chemistry, Faculty of Science, Cairo University, Giza, Egypt; <sup>b</sup>Institute of Chemistry, Martin-Luther-University Halle-Wittenberg, Halle, Germany

(Received 23 June 2010; final version received 7 May 2011)

Two types of supramolecular liquid crystals were prepared through the formation of double hydrogen-bonded complexes between isophthalic acid (**A**) and two different groups of pyridine-based derivatives (**In** and **I<sub>a-e</sub>**). The first group of the base, **In** (molecular formula 4-C<sub>n</sub>H<sub>2n+1</sub>OC<sub>6</sub>H<sub>4</sub>COOC<sub>6</sub>H<sub>4</sub>-N=N-C<sub>5</sub>H<sub>4</sub>N) homologues differ from each other by the number of carbon atoms (*n*) in the alkoxy chain, which varies between 8, 10, 12 and 14 carbons. The second group of the pyridine-based derivatives, **I<sub>a-e</sub>** (molecular formula 4-X-C<sub>6</sub>H<sub>4</sub>COOC<sub>6</sub>H<sub>4</sub>-N=N-C<sub>5</sub>H<sub>4</sub>N) analogues differ from each other by the terminal polar substituent, X, that changes between OCH<sub>3</sub>, CH<sub>3</sub>, H, NO<sub>2</sub> and Br groups. In this manner two different groups of complexes are formed, one of them is **A** : 2**In**, (Group **A**), and the other is **A** : 2**I<sub>a-e</sub>**, (Group **B**). All complexes were investigated for their mesophase behaviour by differential scanning calorimetry and polarised light microscopy. The formation of 1:2 hydrogen-bonded complexes was confirmed by FTIR spectroscopy and binary phase diagrams. Most complexes **A** and **B** show nematic and/or SmA phases. X-ray diffraction of the SmA phase of a representative complex of type **A** indicates a layer distance corresponding to only half of the length of the H-bonded complexes which is interpreted by a phase structure where these complexes adopt a U-shape which intercalate and form non-polar SmA phases.

**Keywords:** isophthalic acid; hydrogen bonding; supramolecular LCs; 4-(4'-pyridylazo)phenyl benzoates; binary mixtures; bent-core mesogens

### 1. Introduction

The current demand in highly ordered solid-state  $\pi$ -conjugated materials for application in electronic devices, e.g. organic field-effect transistors and organic solar cells [1–3], constitutes a touchstone for supramolecular chemistry that has stimulated several groups to synthesise receptor-functionalised chromophores and to control their solid-state organisation by means of intermolecular forces [1–5]. For most examples, this interaction relies on hydrogen bonding, which is a directional–reversible interaction with adjustable binding strength [4, 5]. Within the family of hydrogen-bonded systems, aromatic carboxylic acids are the first compounds that exhibit liquid crystalline behaviour due to hydrogen bond formation [6–10].

In recent years, supramolecular liquid crystals (LCs) have been synthesised through hydrogen bonding of complementary molecules in a large number [11–19]. Recently, we have prepared a novel family of liquid crystalline materials involving intermolecular hydrogen bonding between mesogenic compounds [20, 21], between mesogenic and non-mesogenic compounds [22, 23], or between non-mesogenic compounds [24]. In 1992, the Kato group used isophthalic acid to prepare hydrogen-bonded complexes

with trans-4-alkoxy-4'-stilbazole [25]. Since 2004, hydrogen bonding has also been used to design bent-core liquid crystals [26].

The present work deals with the synthesis of new supramolecular liquid crystalline materials incorporating a bend between two mesogenic or non-mesogenic fragments connected to a single bifunctional proton donor, namely isophthalic acid (**A**). The hydrogen-bonded supramolecular complexes were prepared from a mixture (1:2 molar ratio) of isophthalic acid and two different groups of pyridine-based derivatives **In** and **I<sub>a-e</sub>** according to Scheme 1.

### 2. Experimental

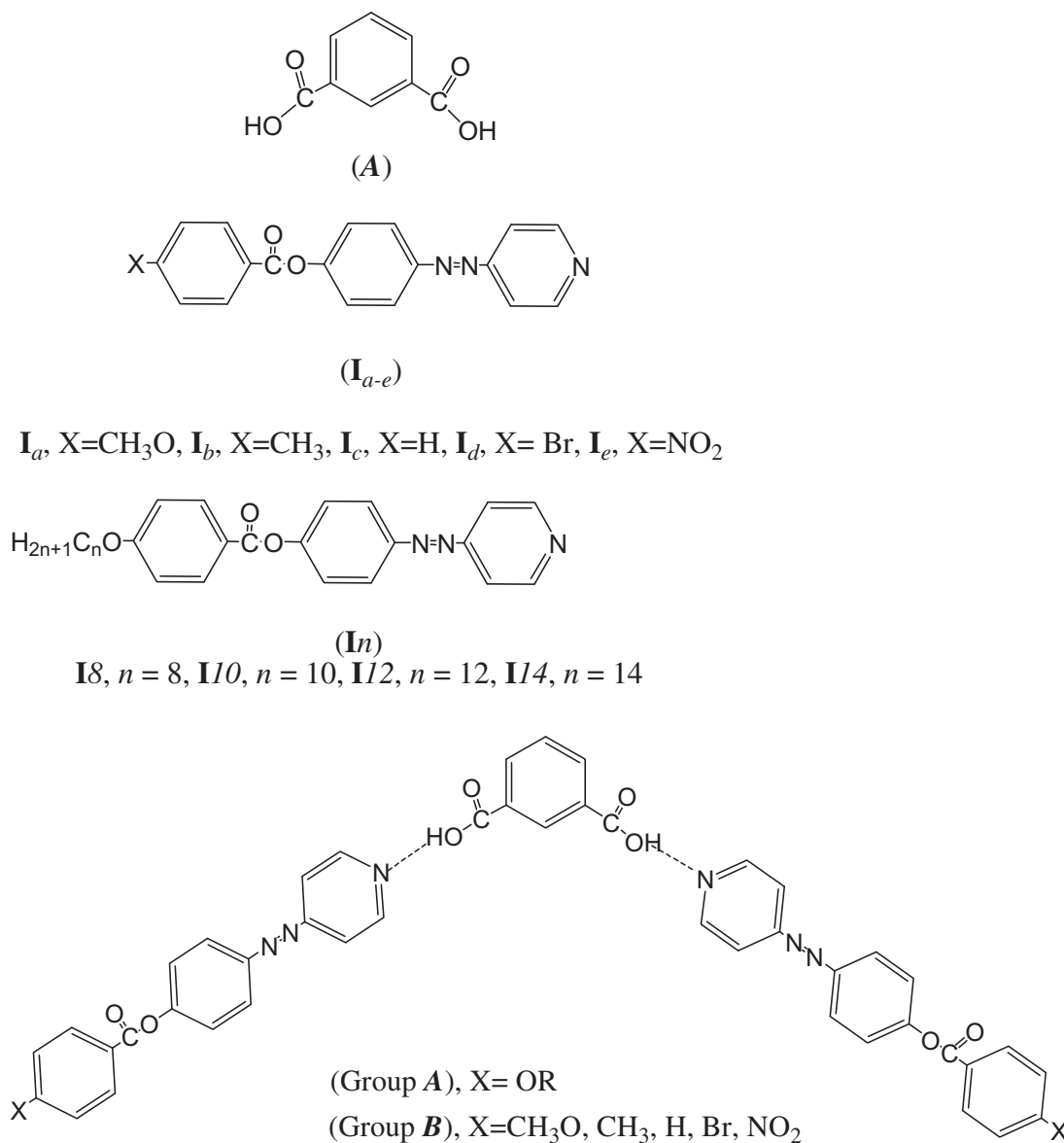
Chemicals were purchased from the following companies: Fluka, Buchs, Switzerland; BDH, Poole, UK; Aldrich, Wisconsin, USA; and E. Merck, Darmstadt, Germany.

#### 2.1 Preparation of materials

All alkoxybenzoic acids were prepared according to methods described previously [27]. The transition temperatures of all the acids agreed with those reported before [28]. The pyridine-based azo dyes

\*Corresponding author. Email: m\_alasaar@yahoo.com





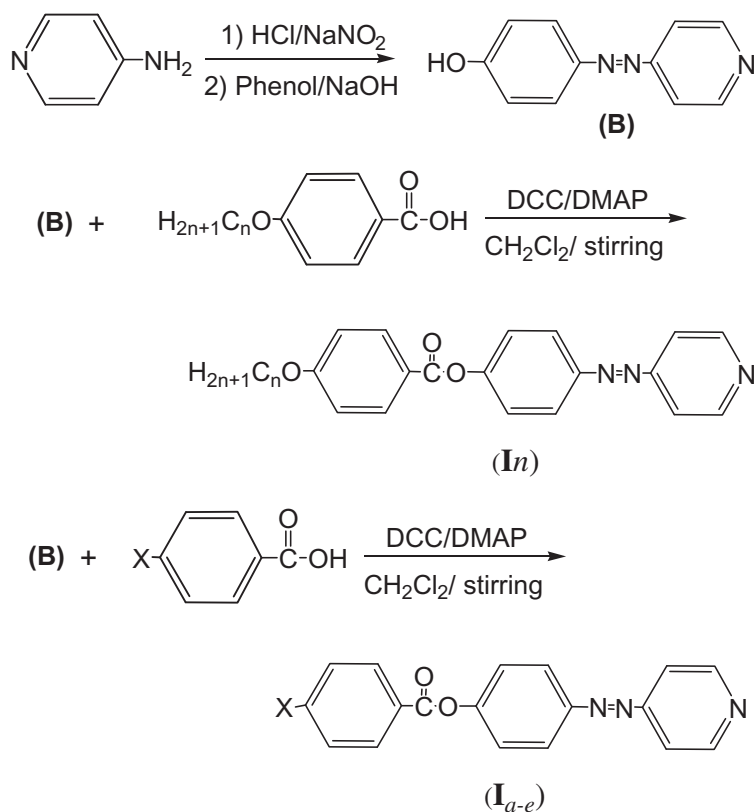
Scheme 1. Proposed structures of the angular liquid crystalline supramolecular hydrogen-bonded complexes.

(4-(4'-pyridylazo)phenyl 4'-alkoxybenzoates **I<sub>n</sub>** and 4-(4'-pyridylazo)phenyl benzoates **I<sub>a-e</sub>**) were prepared as described previously [20], according to Scheme 2.

The solids obtained were crystallised twice from ethanol and found to be pure by thin layer chromatography (TLC) performed with TLC-sheets coated with silica gel (E. Merck), whereby spots were detected by ultraviolet (UV) irradiation. The compounds possessed sharp melting temperatures as measured by differential scanning calorimetry (DSC) and are given in Tables 1 and 2 for **I<sub>a-e</sub>** derivatives and for **I<sub>n</sub>** homologues, respectively. In the tables, the symbols *Cr*, *SmA*, *N*, and *I* denote crystal, smectic A, nematic mesophases and isotropic

liquid, respectively. It can be seen from Tables 1 and 2 that all the pyridine-based homologues (**I<sub>n</sub>**) investigated are mesomorphic, while the analogues (**I<sub>a-e</sub>**) are not. Elemental analyses for **I<sub>n</sub>** homologues and **I<sub>a-e</sub>** derivatives are given in Tables 3 and 4, respectively.

Supramolecular complexes, in the 1:2 molar ratios of any two complimentary components, were prepared by melting the appropriate amounts of each component, stirring to give an intimate blend, and then cooling with stirring to room temperature. For example, to prepare the supramolecular complex **A/2I/2**, 0.0166 mg of isophthalic acid was melted together with 0.0974mg of 4-(4'-pyridylazo)phenyl 4'-dodecyloxybenzoates in the same way.

Scheme 2. Steps for the synthesis of pyridine-based derivatives. **In** and **I<sub>a-e</sub>**.Table 1. Melting points (°C) and melting enthalpies (kJ/mol) of the pyridine-based azo dyes, **I<sub>a-e</sub>**.

Compound	X	$T_{Cr-I}$	$\Delta H_{Cr-I}$
<b>I<sub>a</sub></b>	OCH <sub>3</sub>	170	32.3
<b>I<sub>b</sub></b>	CH <sub>3</sub>	162	31.5
<b>I<sub>c</sub></b>	H	178	20.1
<b>I<sub>d</sub></b>	Br	186	11.3
<b>I<sub>e</sub></b>	NO <sub>2</sub>	205	65.9

Table 2. Transition temperatures (°C) and transition enthalpies (kJ/mol) of the pyridine-based azo dyes, **In**.

Compound	<i>n</i>	$T_{Cr-SmA}$	$\Delta H_{Cr-SmA}$	$T_{SmA-N}$	$\Delta H_{SmA-N}$	$T_{SmA-I}$	$\Delta H_{SmA-I}$	$T_{N-I}$	$\Delta H_{N-I}$
<b>I<sub>8</sub></b>	8	117	32.6	129	0.4	-	-	142	0.9
<b>I<sub>10</sub></b>	10	97	26.9	-	-	129	1.7	-	-
<b>I<sub>12</sub></b>	12	104	43.7	-	-	136	4.9	-	-
<b>I<sub>14</sub></b>	14	96	31.0	-	-	130	4.3	-	-

Table 3. Elemental analyses of pyridine-based azo dyes, **I<sub>n</sub>**.

Compound	<i>n</i>	Calculated (found)		
		% C	% H	% N
<b>I8</b>	8	72.38 (72.42)	6.72 (6.75)	9.74 (9.71)
<b>I10</b>	10	73.2 (73.25)	7.19 (7.24)	9.15 (9.11)
<b>I12</b>	12	73.92 (73.89)	7.59 (7.53)	8.62 (8.59)
<b>I14</b>	14	74.56 (74.58)	7.96 (7.99)	8.15 (8.10)

Table 4. Elemental analyses of pyridine-based azo dyes, **I<sub>a-e</sub>**.

Compound	X	Calculated (found)			
		% C	% H	% N	%Br
<b>I<sub>a</sub></b>	OCH <sub>3</sub>	68.64 (68.51)	4.50 (4.48)	12.61 (12.59)	-
<b>I<sub>b</sub></b>	CH <sub>3</sub>	71.92 (71.88)	4.73 (4.70)	13.24 (13.26)	-
<b>I<sub>c</sub></b>	H	71.28 (71.32)	3.96 (3.94)	13.86 (13.83)	-
<b>I<sub>d</sub></b>	Br	56.69 (56.72)	3.15 (3.11)	11.02 (11.00)	20.73 (20.75)
<b>I<sub>e</sub></b>	NO <sub>2</sub>	62.06 (62.03)	3.45 (3.47)	16.09 (16.11)	-

The prepared mixtures were investigated for their mesophase behaviour by differential scanning calorimetry (DSC) and the phase was identified by polarising light microscopy (PLM). The transition temperatures obtained for the prepared complexes, as measured by both DSC and PLM, agreed within 2–3°C. The phase transition temperatures of the synthesised groups of complexes are given in Tables 5 and 6 for group **A** and group **B** complexes, respectively.

## 2.2 Physical characterisation

Infrared absorption spectra were measured in dry KBr with a Perkin-Elmer B25 spectrophotometer. Calorimetric measurements were carried out using a PL-DSC of Polymer Laboratories, England. The instrument was calibrated for temperature, heat and heat flow according to the method recommended by Cammenga *et al.* [29]. DSC measurements were carried out for small samples (2–3 mg) placed in sealed aluminium pans. All the thermograms were achieved

Table 5. Transition temperatures (°C), transition enthalpies (kJ/mol) and entropies of transitions for the hydrogen-bonded complexes formed between isophthalic acid and 4-(4'-pyridylazo)phenyl 4''-alkoxybenzoates (group **A**).

Complex	$T_{Cr-SmA}$	$\Delta H_{Cr-SmA}$	$T_{SmA-N}$	$\Delta H_{SmA-N}$	$T_{N-I}$	$\Delta H_{N-I}$	$\Delta S/R$
<b>A/2I8</b>	114	17.6	-	-	145*	4.4*	1.26
<b>A/2I10</b>	104	16.7	133	0.9	139	1.2	0.35
<b>A/2I12</b>	101	16.0	134	0.9	155	0.7	0.20
<b>A/2I14</b>	100	14.5	142	0.8	159	0.7	0.19

Note: \*Transition from SmA to isotropic.

Table 6. Transition temperatures (°C), transition enthalpies (kJ/mol) and entropies of transitions of hydrogen-bonded complexes **B**.

Complex	X	$T_{Cr-SmA}$	$\Delta H_{Cr-SmA}$	$T_{Cr-N}$	$\Delta H_{Cr-N}$	$T_{SmA-N}$	$\Delta H_{SmA-N}$	$T_{N-I}$	$\Delta H_{N-I}$	$\Delta S/R$
<b>A/2I<sub>a</sub></b>	OCH <sub>3</sub>	-	-	191	11.7	-	-	231	1.0	0.23
<b>A/2I<sub>b</sub></b>	CH <sub>3</sub>	-	-	179	9.7	-	-	213	0.8	0.25
<b>A/2I<sub>c</sub></b>	H	107	16.6	-	-	129	1.3	150	0.4	0.17
<b>A/2I<sub>d</sub></b>	Br	210	12.8	-	-	248	1.7	254	0.6	0.13
<b>A/2I<sub>e</sub></b>	NO <sub>2</sub>	-	-	172	9.5	-	-	286	0.7	0.15

at a heating rate of 10 °C/min in an inert atmosphere of nitrogen gas (flow rate: 10 ml/min).

Transition temperatures were checked and the types of mesophases identified for the prepared mixtures and their pure components with a standard polarised light microscope (Wild, Germany) attached to a home made hot-stage. The temperatures were measured just under the sample by a thermocoupler attached to Brookfield temperature programme.

X-ray diffraction (XRD) was performed using a two-dimensional (2D) detector (HI-Star, Siemens). Uniform orientation was achieved by slowly cooling a drop of the compound on a glass surface. The X-ray beam was applied parallel to the substrate (exposure time 30 min).

### 3. Results and discussion

#### 3.1 IR spectra

To confirm the formation of intermolecular hydrogen bonding between the isophthalic (**A**) and pyridine-based derivatives (**In** or **I<sub>a-e</sub>**), Fourier transform infrared (FTIR) spectroscopy was chosen because it is sensitive to the change of molecular conformation, inter- and intramolecular interactions [30, 31]. As an example, the FTIR spectra of **A**, **I10** and **A/2I10** are shown in Figure 1.

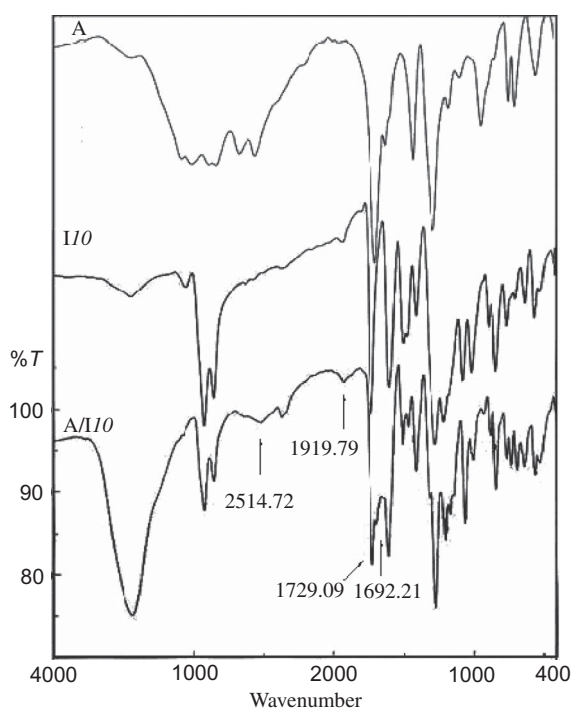


Figure 1. FTIR of isophthalic acid (**A**), 4-(4'-pyridyl-lazo)phenyl 4'-decyloxybenzoate **I10**, and the supramolecular complex **A/2I10**.

The peak of the carboxylic carbonyl band of **A** is 1691.27  $\text{cm}^{-1}$ ; this band shows that the carboxylic acid dimer occurs by means of intermolecular hydrogen bonding [32]. The spectrum of **I10** has an ester carbonyl band at 1724.20  $\text{cm}^{-1}$ . In the IR spectrum of complex **A/2I10**, the ester carbonyl band changes from 1724.20  $\text{cm}^{-1}$  to 1729.09  $\text{cm}^{-1}$  due to the complexation of **A** with **I10**, and the carboxylic carbonyl peak changes from 1691.27  $\text{cm}^{-1}$  to 1692.21  $\text{cm}^{-1}$ . These results mean that the intermolecular hydrogen bonding between carboxylic groups of the acids has been replaced by an intermolecular hydrogen bonding between the pyridyl and the carboxylic acid moieties.

The two new bands centred at 2514.72  $\text{cm}^{-1}$  and 1919.79  $\text{cm}^{-1}$  are taken as strong evidence of the intermolecular hydrogen bonding, which is of a unionised type between the pyridyl and the carboxylic acid [33, 34]. The formation of hydrogen bonding between isophthalic acid and each of the pyridine-based derivatives is also confirmed by the strong broad frequency at  $\approx 465.5 \text{ cm}^{-1}$  exhibited by all the supramolecular complexes investigated [35–37]. This band lies in the frequency range of stretching –OH group involved in the hydrogen bonding. All the remaining complexes **A : 2In**, (Group **A**), and **A : 2I<sub>a-e</sub>**, (Group **B**), similarly showed the same characteristic FTIR spectra. The main differences between the prepared complexes are the changes occurring in the frequency of the ester carbonyl of the pyridine-based derivatives in its free and complexed states (Table 7).

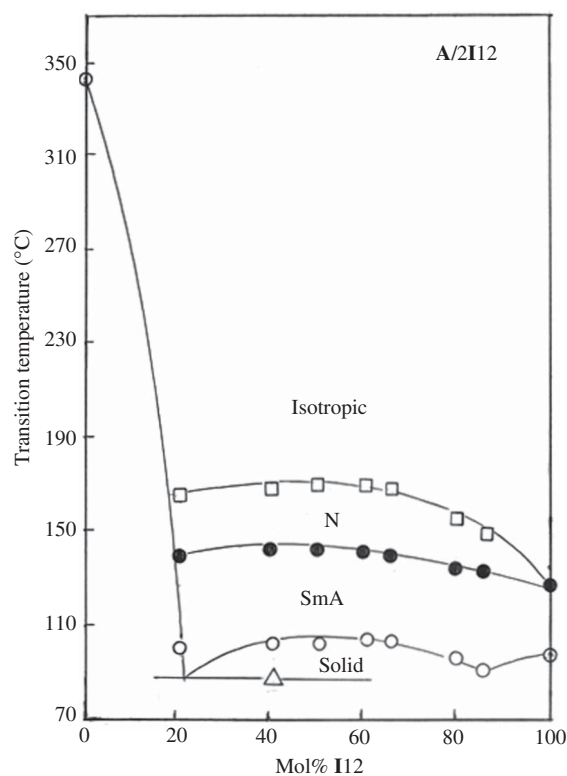
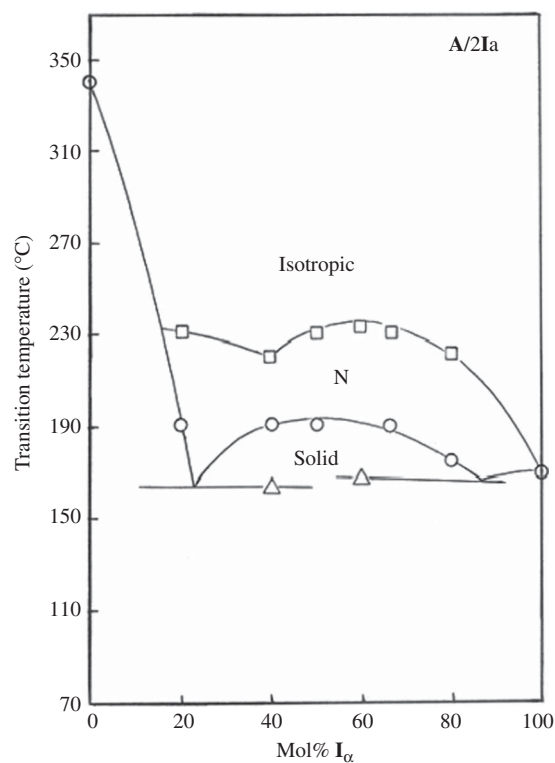
The formation of intermolecular hydrogen bond between the acid (**A**) and the pyridine-based derivatives was also confirmed from the observed increase in the carbonyl frequency of the acid (**A**) by  $\approx 2\text{--}3 \text{ cm}^{-1}$ , as well as in the ester carbonyl frequency of both pyridine-based derivatives (**In** or **2I<sub>a-e</sub>**) (see Table 7).

#### 3.2 Thermal and phase behaviour

The formation of the hydrogen-bonded complexes was further confirmed by constructing the binary phase diagrams of both acid and base components, covering the whole composition range. Figures 2 and 3 represent the phase diagrams for the two types of complexes, namely **A/2I12** and **A/I<sub>a</sub>** as examples, respectively. In the phase diagrams, which were constructed by plotting transition temperatures *versus* mixture composition, the symbol ‘o’ denotes solid-mesophase, ‘□’ mesophase-isotropic transitions, ‘●’ transitions between mesophases and ‘Δ’ eutectic temperature. As can be deduced from

Table 7. Ester (**I<sub>n</sub>** or **I<sub>a-e</sub>**) and isophthalic acid (**A**) carbonyl stretching frequencies ( $\nu_{\text{C=O}}/\text{cm}^{-1}$ ) in their free and complexed states for the prepared supramolecular complexes.

	Complex	X	Free ester	Complexed ester	Free acid	Complexed acid
Group <b>A</b>	A/2 <b>I</b> 8	OC <sub>8</sub> H <sub>17</sub>	1723.09	1727.91	1691.27	1692.21
	A/2 <b>I</b> 10	OC <sub>10</sub> H <sub>21</sub>	1724.20	1729.09	1691.27	1692.21
	A/2 <b>I</b> 12	OC <sub>12</sub> H <sub>25</sub>	1723.91	1727.91	1691.27	1692.23
	A/2 <b>I</b> 14	OC <sub>14</sub> H <sub>29</sub>	1724.50	1728.09	1691.27	1692.23
Group <b>B</b>	A/2 <b>I</b> <sub>a</sub>	OCH <sub>3</sub>	1728.00	1730.94	1691.27	1692.50
	A/2 <b>I</b> <sub>b</sub>	CH <sub>3</sub>	1730.00	1732.73	1691.27	1693.19
	A/2 <b>I</b> <sub>c</sub>	H	1728.00	1730.80	1691.27	1692.01
	A/2 <b>I</b> <sub>d</sub>	Br	1743.00	1745.81	1691.27	1694.16
	A/2 <b>I</b> <sub>e</sub>	NO <sub>2</sub>	1747.00	1749.55	1691.27	1692.23

Figure 2. Binary phase diagram of the pyridine-based derivative (**I/2**) with isophthalic acid (**A**).Figure 3. Binary phase diagram of the pyridine-based derivative (**I<sub>a</sub>**) with isophthalic acid (**A**).

Figures 2 and 3, independent of the type of proton acceptor used (**I/2** or **I<sub>a</sub>**), hydrogen bond formation is revealed from the enhanced mesophase stability and the formation of solid complexes evidenced by the two eutectic points one preceding and the other following  $\approx 60$  mol% concentration of the proton acceptor (**I**), whereby an enhancement of the mesophase stability around the 1:2 (**A** : **I**) molar ratio was observed in each case.

The textures observed under the polarised microscope for the complex **A/2I/2** are shown in Figure 4 as a representative example. All the

prepared complexes of group **A** are dimorphic exhibiting smectic A (**SmA**) and nematic mesophases, apart from the complex **A/2I/8** which is monomorphic possessing only the nematic mesophase. On the other hand, all group **B** complexes exhibit nematic phases except the complexes **A/2I<sub>c</sub>** and **A/2I<sub>d</sub>** which are dimorphic possessing both **SmA** and nematic phases. Microscopic studies also indicated that none of the mesophases for group **A** or group **B** complexes shows textural features as typical for bent-core liquid-crystalline phases; this was confirmed by XRD investigations.

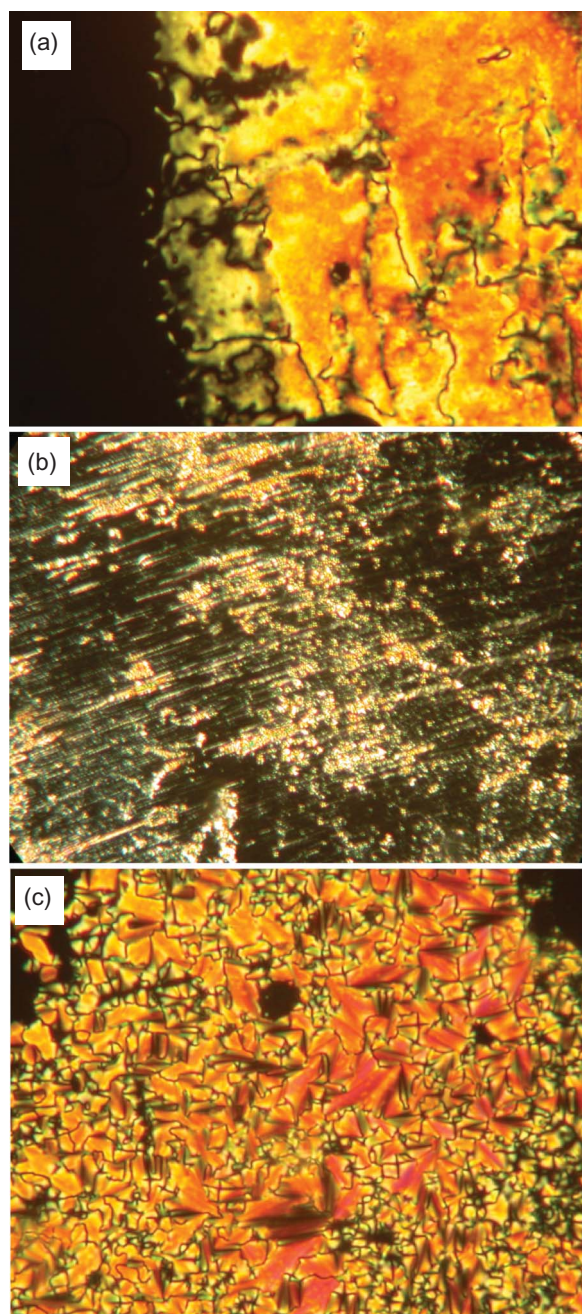


Figure 4. Optical microscopic textures (crossed polarisers) of the complex A/2II2 (a) at the I–N transition at  $T = 155^\circ\text{C}$ ; (b) in the SmA phase at  $T = 130^\circ\text{C}$  showing oily streaks texture and homeotropically aligned regions; and (c) in a region with fan texture.

### 3.3 X-ray diffraction and molecular self-assembly in the LC phases

In order to investigate the phase structures, X-ray diffraction (XRD) of a surface aligned sample of the A/2II2 complex was examined as a representative example (Figure 5). The diffuse wide angle scattering

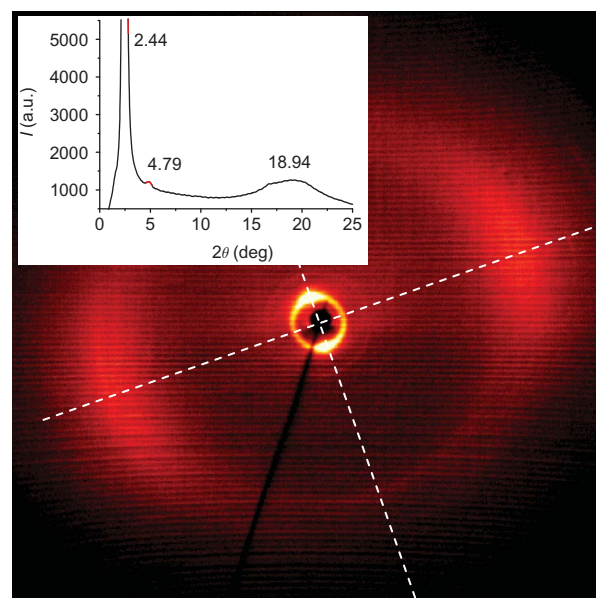


Figure 5. X-ray diffraction pattern of an aligned sample of the complex A/2II2 in the SmA phase at  $T = 120^\circ\text{C}$ . The inset shows the  $\theta$  scan indicating the positions of the first and second order layer reflection.

at  $d = 0.45$  nm confirms the presence of a LC phase. It has maxima perpendicular to the direction of the layer reflection, indicating a non-tilted organisation of the molecules in the LC phase. In the small angle region, the layer reflection corresponding to  $d = 3.62$  nm and the corresponding weak second order reflection can be found. Interestingly, the measured layer distance does not correspond to the length of the expected bent-core complex shown in Figure 6(a) which has a length of  $L = 6.7$ – $6.8$  nm, but it is slightly larger than the length of a single pyridine-based unit II2, with  $L = 3.4$ – $3.5$  nm in the most extended conformation with all-*trans* conformation of the alkyl chains. The fact that  $d$  exceeds the length of the uncomplexed pyridine compound II2 indicates that hydrogen bonded complexes should be formed. However,  $d$  is only about half of the size of a bent-shape 1:2 complex. This could be explained by an intercalation of the bent-core complexes, leading to a B6-type bent-core mesophase (Figure 6(b)).

However, the optical textures observed for the LC phase of the A/2II2 complex are quite distinct from those typically observed for B6 type phases. The smectic phase of the A/2II2 complex predominantly appears with a homeotropic texture which is completely dark between crossed polarisers, indicating an optically uniaxial SmA phase. In contrast, B6 phases form exclusively fan-like textures and, if homeotropic alignment could be achieved, these areas show a birefringent schlieren texture. In

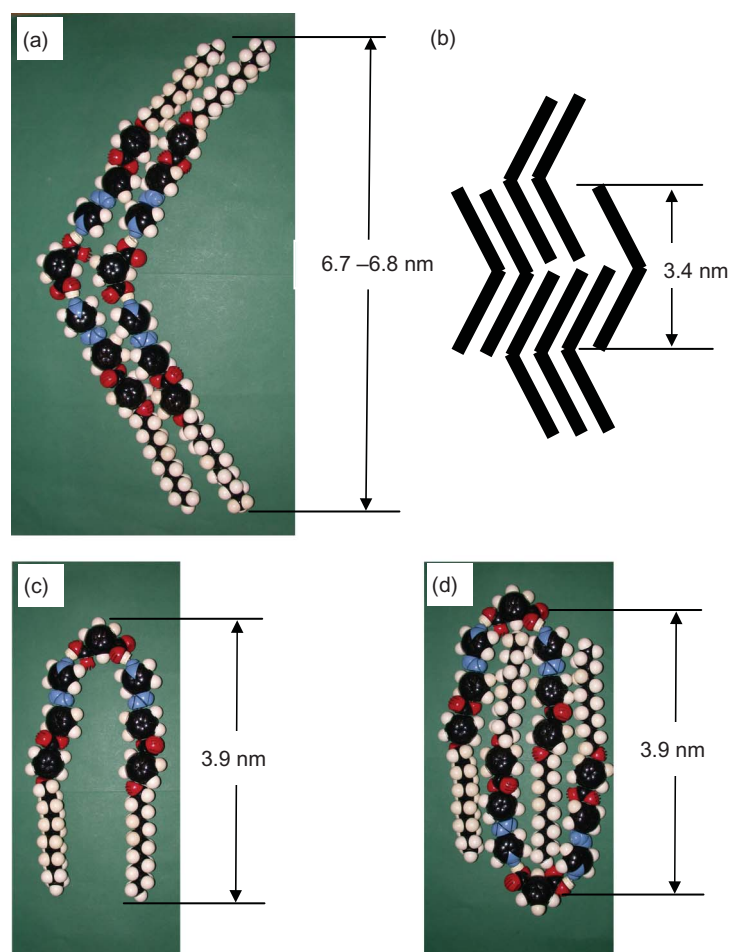


Figure 6. CPK molecular models of the hydrogen-bonded complex A/2I12 and possible arrangements in the formed smectic phases: (a) chevron-shaped complex as expected for polar smectic phases of bent-core mesogens (B2 phases); (b) arrangement with complete intercalation of the rod-like wings as typical for B6 phases; (c) U-shaped conformation; and (d) two intercalated U-shaped complexes as proposed for the SmA phase of A/2I12 (colour version online).

addition, such an intercalated smectic phase is unlikely for the hydrogen-bonded complexes under investigation as it requires a mixing of the polar hydrogen bonding with the lipophilic alkyl chains. In addition, for previously reported linear and only slightly bent pyridine–benzoic acid complexes, XRD investigations indicated non-intercalated monolayer structures with layer spacings in the range of the length of the hydrogen-bonded complexes [38]. Hence, a phase structure similar to the B6-phases of bent-core mesogens can be excluded and the formation of a U-shaped hydrogen-bonded complex (shown in Figure 6(c)) could be considered as an alternative possibility. A smectic phase composed of U-shaped A/2I12 complexes (all-*trans* conformation of the alkyl chains) and completely intercalated rod-like wings, as shown in Figure 4(d), leads to a layer distance of 3.9 nm. Though this is slightly larger than the experimentally observed *d*-value, it is in a good

agreement with the experimental *d*-value, considering that chain folding in the LC state leads to an effective reduction of the molecular length by about 10%. In this SmA phase, the polar regions of the isophthalic acid–pyridine hydrogen bonding form distinct layers which are separated by the intercalated rod-like cores and the alkyl chains.

Further evidence for the formation of U-shaped conformations can be found in the entropies associated with the nematic–isotropic transitions obtained for the prepared supramolecular complexes; see Tables 5 and 6, respectively. From the tables it can be seen that the nematic–isotropic entropies are of low values and fall between 0.13 and 0.35. This is because, in the U-shaped complexes, the molecular biaxiality will be high and this reduces the entropy of transition [39–44].

The ability of the isophthalic acid–pyridine complexes to adopt a U-shaped instead of the expected

chevron-like conformation was not discussed in previous studies [25] and is of general interest for the design of bent-core mesogens [45–50] by using hydrogen bonding. It also explains why such simple complexes have so far been unsuccessful in the design of supramolecular bent-core mesogens [26, 51–55]. It seems that the flexibility around the hydrogen bonding could not only lead to linear molecular conformation as discussed in previous work [51–55] but, as shown here, it can also adopt U-shaped conformations, leading to the loss of typical bent-core liquid crystalline phases. To avoid formation of these U-shaped conformers the hydrogen-bonds should be placed at the periphery of the bent cores; however, formation of polar switching bent-core mesophases seems to require, in addition, that there is only one hydrogen bonding site in these mesogens [51–54]. It is also worth mentioning that the layer distance in smectic phases formed by supramolecular complexes between stilbazoles and thiophene-2,5-dicarboxylic acid, having a reduced bending angle around 150°, were found to match the calculated molecular lengths [38]. Hence, it seems that the larger bend (120°) of the isophthalic acid is responsible for the change to the U-shaped conformation. This prevents the polar packing required for the formation of bent-core mesophases.

#### 4. Conclusions

In this paper, novel liquid crystalline hydrogen-bonded supramolecular complexes were prepared. Isophthalic acid (**A**) was taken as the proton donor and the proton acceptor is a pyridine-based derivative. Two different groups of supramolecular complexes (group **A** and group **B**) were prepared through intermolecular hydrogen bond formation between each of the pyridine-based components (**In** or **I<sub>a-e</sub>**) and isophthalic acid (**A**). The intermolecular hydrogen bonding interactions between each of the components were confirmed by FTIR spectroscopy and their binary phase diagrams.

The mesomorphic behaviour of the complexes was characterised through differential scanning calorimetry, polarised light microscopy and X-ray diffraction. The results revealed the following:

(1) All the prepared group **A** complexes, which are formed between the mesomorphic components **In** and the non-mesomorphic isophthalic acid, exhibited smectic A and induced nematic mesophases – except for complex **A/2I8** which showed only the smectic A mesophase. In addition, almost all of group **A** complexes showed

wider liquid crystalline ranges compared with the pure components **In**.

- (2) None of the mesophases observed for group **A** or group **B** complexes were identified as any of the typical bent core liquid-crystalline phases. This is attributed to the flexibility of the hydrogen bond compared with covalent bonds, which could give rise to different conformations of the hydrogen bonded complexes. It was deduced from XRD data and molecular modelling that a U-shape conformation is dominating in the case of isophthalic acid complexes.
- (3) With respect to group **B** complexes, which are formed between the two non-mesomorphic components, **I<sub>a-e</sub>** and isophthalic acid **A**, and exhibit induced enantiotropic liquid crystalline properties, the complexes bearing the terminal OCH<sub>3</sub>, CH<sub>3</sub> or NO<sub>2</sub> groups are monomorphic possessing nematic mesophases. The complex bearing a Br group as well as the unsubstituted analogue are dimesomorphic, possessing smectic A and nematic phases.

#### References

- [1] Cornil, J.; Beljonne, D.; Calbert, J.P.; Brédas, J.L. *Adv. Mater.* **2001**, *13*, 1053–1067.
- [2] Würthner, F. *Angew. Chem., Int. Ed. Engl.* **2001**, *40*, 1037–1039.
- [3] Brabec, C.J.; Sariciftci, N.S.; Hummelen, J.C. *Adv. Funct. Mater.* **2001**, *11*, 15–26.
- [4] Schenning, A.P.H.J.; Jonkheijm, P.; Peeters, E.; Meijer, E.W. *J. Am. Chem. Soc.* **2001**, *123*, 409–416.
- [5] Würthner, F.; Thalacker, C.; Sautter, A.; Schärtl, W.; Ibach, W.; Hollricher, O. *Chem. Eur. J.* **2000**, *6*, 3871–3886.
- [6] Gray, G.W. *Molecular Structure and the Properties of Liquid Crystals*; Academic Press: London, 1969; p 163.
- [7] Kelker, H.; Hatz, R. *Handbook of Liquid Crystals*; Verlag Chemie: Weinheim, 1980; p 59.
- [8] Vorländer, D. *Ber. Deutsch. Chem. Ges.* **1908**, *41*, 2033–2052.
- [9] Gray, G.W.; Jones, B. *J. Chem. Soc.* **1954**, 683–686.
- [10] Gray, G.W.; Jones, B. *J. Chem. Soc.* **1954**, 1467–1470.
- [11] Paleos, C.M.; Tsiourvas, D. *Angew. Chem., Int. Ed. Engl.* **1995**, *34*, 1696–1711.
- [12] Paleos, C.M.; Tsiourvas, D. *Liq. Cryst.* **2001**, *28*, 1127–1161.
- [13] Prade, H.; Miethchen, R.; Vill, V. *J. Prakt. Chem.* **1995**, *337*, 427–440.
- [14] Kato, T. In *Handbook of Liquid Crystals*; Demus, D., Goodby, J., Gray, G.W., Spiess, H.W., Vill, V., Eds.; Wiley-VCH: Weinheim, 1998; pp 969–979.
- [15] Kato, T.; Frechet, J.M.J. *Macromol. Symp.* **1995**, *98*, 311–326.
- [16] Kato, T. *Supramol. Sci.* **1996**, *3*, 53–59.
- [17] Kato, T.; Frechet, J.M.J. *J. Am. Chem. Soc.* **1989**, *111*, 8533–8534.



- [18] Kato, T.; Norihiro, M.; Kenji, K. *Angew. Chem., Int. Edn. Engl.* **2006**, *45*, 1390–1393.
- [19] Kato, T.; Fukumasa, M.; Fréchet, J.M.J. *Chem. Mater.* **1995**, *7*, 368–372.
- [20] Naoum, M.M.; Fahmi, A.A.; Alaasar, M.A. *Mol. Cryst. Liq. Cryst.* **2008**, *487*, 74–91.
- [21] Magdi, M.M.; Fahmi, A.A.; Mohammady, S.Z.; Abaza, A.H. *Liq. Cryst.* **2010**, *37*, 475–486.
- [22] Magdi, M.M.; Fahmi, A.A.; Alaasar, M.A. *Mol. Cryst. Liq. Cryst.* **2008**, *482*, 57–70.
- [23] Magdi, M.M.; Fahmi, A.A.; Almlal, W.A. *Mol. Cryst. Liq. Cryst.* **2010**, *518*, 109–128.
- [24] Magdi, M.M.; Fahmi, A.A.; Alaasar, M.A. *Mol. Cryst. Liq. Cryst.* **2009**, *506*, 22–33.
- [25] Kato, T.; Adachi, H.; Fujishima, A.; Fréchet, M.J. *Chem. Lett.* **1992**, 265–268.
- [26] Gimeno, N.; Ros, M.B.; Serano, J.L.; De La Fuente, M.R. *Angew. Chem., Int. Ed.* **2004**, *43*, 5235–5238.
- [27] Naoum, M.M.; Saad, G.R.; Nessim, R.I.; Abdel Aziz, T.A.; Seliger, H. *Liq. Cryst.* **1997**, *23*, 789–795.
- [28] Prade, H.; Miethchen, R.; Vill, V. *J. Prakt. Chem.* **1995**, *337*, 427–440.
- [29] Cammenga, H.K.; Eysel, W.; Gmelin, E.; Hemmiger, W.; Hoehne, G.W.H.; Sagre, S.M. *Thermochim. Acta*, **1993**, *219*, 333–342.
- [30] Ghanem, A.; Noel, C. *Mol. Cryst. Liq. Cryst.* **1987**, *150*, 447–472.
- [31] Benedetti, E.; Galleschi, F.; Chiellini, E.; Galli, G.; Lenz, R.W. *J. Polym. Sci.* **1989**, *B27*, 25–37.
- [32] Kato, T.; Uryu, T.; Kaneuchi, F.; Jin, C.; Fréchet, M.J. *Liq. Cryst.* **1993**, *14*, 1311–1317.
- [33] Johnson, S.L.; Rumon, K.A. *J. Phys. Chem.* **1965**, *69*, 74–86.
- [34] Odinokov, S.E.; Iogansen, A.V. *Spectrochim. Acta*, **1972**, *A28*, 2343–2350.
- [35] Silverstein, R.M.; Bassler, G.C.; Morrill, T.C. *Spectroscopic Identification of Organic Compounds*, 5th ed.; Singapore: Wiley, 1991.
- [36] Carpaneto, I.; Peluffo, C.; Piaggio, P.; Valenti, B. *J. Chem. Soc., Faraday Trans.* **1997**, *93*, 1095–1100.
- [37] Vijayalakshmi, K.; Sastry, S.S. *Acta Physica Polnica A* **2009**, *115*, 742–744.
- [38] Lin, H.C.; Ko, C.W.; Guo, K.; Cheng, T.W. *Liq. Cryst.* **1999**, *26*, 613–618.
- [39] Imrie, C.T. *Liq. Cryst.* **1989**, *6*, 391–396.
- [40] Attard, G.S.; Imrie, C.T.; Karasz, F.E. *Chem. Mater.* **1992**, *4*, 1246–1253.
- [41] Attard, G.S.; Imrie, C.T. *Liq. Cryst.* **1992**, *11*, 785–789.
- [42] Donaldson, T.; Staesche, H.; Lu, Z.B.; Henderson, P.A.; Achard, M.F.; Imrie, C.T. *Liq. Cryst.* **2010**, *37*, 1097–1110.
- [43] Blatch, A.E.; Fletcher, I.D.; Luckhurst, G.R. *J. Mater. Chem.* **1997**, *7*, 9–17.
- [44] Yeap, G.Y.; Hng, T.C.; Yeap, S.Y.; Gorecka, E.; Ito, M.M.; Ueno, K.; Okamoto, M.; Mahmood, W.A.K.; Imrie, C.T. *Liq. Cryst.* **2009**, *36*, 1431–1441.
- [45] Pelzl, G.; Diele, S.; Weissflog, W. *Adv. Mater.* **1999**, *11*, 707–724.
- [46] Tschierske, C.; Dantlgraber, G. *Pramana J. Phys.* **2003**, *61*, 455–481.
- [47] Walba, D.M. *Topics Stereochem.* **2003**, *24*, 457–518.
- [48] Ros, M.B.; Serrano, J.L.; De la Fuente, M.R.; Folcia, C.L. *J. Mater. Chem.* **2005**, *15*, 5093–5098.
- [49] Reddy, R.A.; Tschierske, C. *J. Mater. Chem.* **2006**, *16*, 907–961.
- [50] Takezoe, H.; Takanishi, Y. *Jpn. J. Appl. Phys.* **2006**, *45*, 597–625.
- [51] Gimeno, N.; Ros, M.B.; Serrano, J.L. *Chem. Mater.* **2008**, *20*, 1262–1271.
- [52] Pérez, A.; Gimeno, N.; Vera, F.; Ros, M.B.; Serano, J.L.; De La Fuente, M.R. *Eur. J. Org. Chem.* **2008**, 826–833.
- [53] Wang, L.-Y.; Chiang, I.-H.; Yang, P.-J.; Li, W.S.; Chao, I.-T.; Lin, H.-C. *J. Phys. Chem. B* **2009**, *113*, 14648–14660.
- [54] Wang, L.-Y.; Tsai, H.-Y.; Lin, H.-C. *Macromolecules* **2010**, *43*, 1277–1288.
- [55] Martin, P.J.; Bruce, D.W. *Liq. Cryst.* **2007**, *34*, 767–774.

# Condensed Curriculum Vitae

## 1) General Information

Name Dr. Mohamed Alaasar  
Date of birth 02.05.1980  
Place of birth Egypt  
Marital status Married  
Citizenship German

## 2) Scientific Degrees

- B.Sc. (Very Good), Major Chemistry, Faculty of Science, Cairo University (2002), Egypt.
- M.Sc. (Organic Chemistry), Cairo University (2006), Egypt.
- Ph.D. (Organic Chemistry), Cairo University (2009), Egypt.

## 3) Professional Career from Graduation

- Since** Post-Doc at Institute of Chemistry – Organic Chemistry, Martin-Luther University  
**04.2020** via temporary position funded by DFG Foundation “einge Stelle”
- 12.2017-** Post-Doc at Institute of Chemistry – Organic Chemistry, Martin-Luther University  
**03.2020** via temporary position funded by DFG Foundation
- 04.2017-** Associate professor of Organic chemistry, Chemistry Department, Faculty of  
**11.2017** Science, Cairo University
- 02.2015-** Post-Doc at Institute of Chemistry – Organic Chemistry, Martin-Luther University  
**03.2017** via temporary position funded by DFG Foundation
- 09.2014-** Lecturer in Organic chemistry, Chemistry Department, Faculty of Science, Cairo  
**01.2015** University
- 08.2012-** Post-Doc at Institute of Chemistry – Organic Chemistry, Martin-Luther University  
**08.2014** via Alexander von Humboldt Foundation
- 01.2012-** Lecturer in Organic chemistry, Chemistry Department, Faculty of Science, Cairo  
**07.2012** University
- 07.2011-** Post-Doc at Institute of Chemistry – Organic Chemistry, Martin-Luther University  
**01.2012** via DAAD Fellowship
- 09.2009-** Lecturer in Organic chemistry, Chemistry Department, Faculty of Science, Cairo  
**07.2011** University
- 07.2006-** Assistant Lecturer of Organic Chemistry, Chemistry Department, Faculty of  
**09.2009** Science, Cairo University
- 12.2002-** Instructor of Organic Chemistry, Chemistry Department, Faculty of Science, Cairo  
**07.2006** University

## **Erklärung**

Hiermit erkläre ich, dass ich die vorliegende Arbeit selbständig und ohne fremde Hilfe verfasst, andere als die angegebenen Quellen und Hilfsmittel nicht benutzt und die den benutzten Werken wörtlich oder inhaltlich entnommenen Stellen als solche kenntlich gemacht wurden.

Die Arbeit wurde nur an der Naturwissenschaftlichen Fakultät II der Martin-Luther-Universität Halle-Wittenberg vorgelegt.

Mohamed Alaasar

Halle Saale, February 2023